The sedimentology and diagenesis of the Raisby Formation (Z1 carbonate), northern England.

This thesis is submitted in fulfillment of the requirements for the Degree of Doctor of Philosophy in the Department of Geology

Martin R. Lee

Department of Geology
April 1990

University of Newcastle upon Tyne
Newcastle upon Tyne NE1 7RU

TEXT BOUND CLOSE TO THE SPINE IN THE ORIGINAL THESIS

ORIGINAL COPY TIGHTLY BOUND

The sedimentology and diagenesis of the Raisby Formation (Z1 carbonate), northern England

Volume 1

Abstract

The Raisby Formation is the basal Zechstein (Upper Permian) carbonate, that crops out in northeast England. It was deposited in environments ranging from shallow water, above wave base, into a deeper water carbonate slope. The shallow water sediments are skeletal wackestones and packstones which contain some sandstone horizons, whereas those deposited in deeper waters are mudstones, incorporating resedimented carbonates of variable thickness and extent. Many slope sediments were lithified early, forming nodular horizons. These cements, dominantly high magnesian calcite and aragonite, also occluded intra-skeletal pores, and were followed by the precipitation of framboidal pyrite. Early lithification of slope sediments had a significant influence on their stability, and response to resedimentation. Much of the Raisby Formation which was deposited on lower parts of the slope, was removed during an episode of catastrophic slope failure close to the end of first cycle carbonate deposition.

During early burial, some sediments which were lithified early, neomorphosed to low-magnesian calcite microspar, which at a few localities was accompanied by the formation of coarsely crystalline calcite concretions. At the same time, or slightly earlier, sediments which did not lithify early, and some of those which did, were dolomitized and replaced by gypsum and anhydrite. Replacement by both dolomite and calcium sulphates was directly related to the deposition of the Hartlepool Anhydrite Formation.

During burial, following calcium sulphate precipitation, the formation was relatively diagenetically inactive. Patchy Cu-Pb-Zn mineralization may have resulted from thermochemical reduction of anhydrite, in association with methane, and base metal-rich fluids derived from the Palaeozoic basement.

During Tertiary uplift of the formation, a meteoric aquifer was established, which led to dissolution and calcitization of dolomite, anhydrite, and gypsum, and the precipitation of calcite cements. The calcite cements are associated with different types of iron and clay minerals and internal sediments. Luminescence petrography and stable isotope geochemistry demonstrate that most calcitization and calcite cementation was concentrated in two areas of the aquifer; a distal zone where fluids of elevated temperatures calcitized dolomite, gypsum and anhydrite, and precipitated pyrite, marcasite, barite and fluorite, and a proximal zone in which calcite cementation and dolomite calcitization was driven by CO_2-degassing of calcite saturated, oxic groundwaters.

Acknowledgements.

I would like to thank my supervisor, Gill Harwood, for constructing the original research project, and for supervision throughout my research and writing up. This work was carried out mainly during the tenure of a research studentship from the Natural Environment Research Council (no. GT4/GS/86/133).

Numerous people have helped me with my research, including Denys Smith, who assisted me with some aspects of the fieldwork, and obtained borehole cores on my behalf. I am also grateful to Stuart Kearns and Pete Hill (Edinburgh) for help with the microprobe, Pete Greenwood and Mike Fowler (BGS) for assistance with stable isotope analyses, the staff at Royal Holloway and Bedford New College for help with ICP analyses, and technical staff at the department of Metallurgy, Newcastle University for their help with the SEM. I am also very grateful to the late Peter Oakley for his invaluable help and guidance with chemical analyses, and encouragement during my research. I also acknowledge the technical staff of the geology department for their help; Len Rhodes, Ann Meldrum, Rob Hunter (especially, for continual mending of the dental drill), Trevor Whitfield, and Ann Thwaites (for her invaluable secretarial and organizational skills).

Many of the research students in the department have made my time at Newcastle an enjoyable experience, especially Ivan Sansom, Smail Belaribi, Bryn Jones, and Meng Fang Chen and Said Benzagouta, with whom sharing an office has been a privilege. Other people have been a source of great inspiration throughout my university career, including Andrew Hutchins, Ian Fowler, Robert Dallimer, John Marret, Beatrice Roberts, and Simon Best.

I would especially like to thank Maxine Akhurst, and Pearl, for their ceaseless help and encouragement, and in providing a sanctuary from work.

This thesis is dedicated to my parents and my sister, without whom none of this would have been possible.

Contents

Chapter 1

Introduction

1.1. Introduction to the Raisby Formation

The Raisby Formation (formerly Lower Magnesian Limestone of Durham) comprises the lowermost division of a sequence of cyclic carbonate and evaporite sediments deposited in the Upper Permian Zechstein Sea. It crops out in northeast England from just north of the River Tyne in Northumberland, as far south as north Yorkshire (Fig. 1.1). The Raisby Formation is overlain by the Ford Formation, which together comprise the first cycle Zechstein carbonate of northeast England (Fig. 1.2). The Raisby Formation is of considerable economic importance in the northeast, being extensively quarried for road aggregate, especially in Co. Durham. Carbonates equivalent to the Raisby Formation locally form significant reservoir rocks for Coal Measure-sourced gas in the southern North Sea, The Netherlands, Poland and West Germany. They may also provide a productive source of gas in yet unexplored parts of eastern England (Clark, 1986). Small oil fields have also been discovered in Zechstein carbonates of West Germany and the Southern North Sea Basin.

In comparison to many English carbonates, the Raisby Formation together with the Zechstein carbonates and evaporites in general, have received little attention from geologists, apart from where they are of economic importance. This is mainly due to the multiphase, obliterative diagenesis the carbonates and evaporites have undergone. Exposure is also poor because these carbonates are not strongly resistant to erosion, nor have they undergone much structural deformation.

1.2. Previous work on the first cycle Zechstein carbonates of northeast England.

The first comprehensive study of the Zechstein in eastern England was by Sedgwick (1829). Considerable work followed on the palaeontology of the first cycle carbonates in the mid to late nineteenth century by Howse (1848 & 1857), King (1850) and Kirkby (1858 & 1867), although much of this inevitably concentrated on abundant faunas within reef carbonates of the overlying Ford Formation. The first serious studies of the stratigraphy and composition of the Raisby Formation were published by Woolacott (1903, 1905, 1912, 1914, 1919a & b) and Trechmann (1913, 1914, 1921, 1925, 1931, 1941 & 1954). These provided the basis for the most recent and widely accepted interpretations of the stratigraphy of the first cycle Zechstein carbonates in northeast England, which have been progressively improved over the last 25 years (Magraw *et al.*, 1963; Smith and Francis, 1967; Smith 1970a, b & c; Smith 1971; Pattison *et al.*, 1973; Smith *et al.*, 1974; Magraw, 1975 & 1978; Mills and Hull, 1976; Smith 1979, 1980a & b). The most recent interpretations of Zechstein stratigraphy and sedimentology of northeast England are in papers in Smith and Harwood (1986), principally Smith *et al.*, (1986).

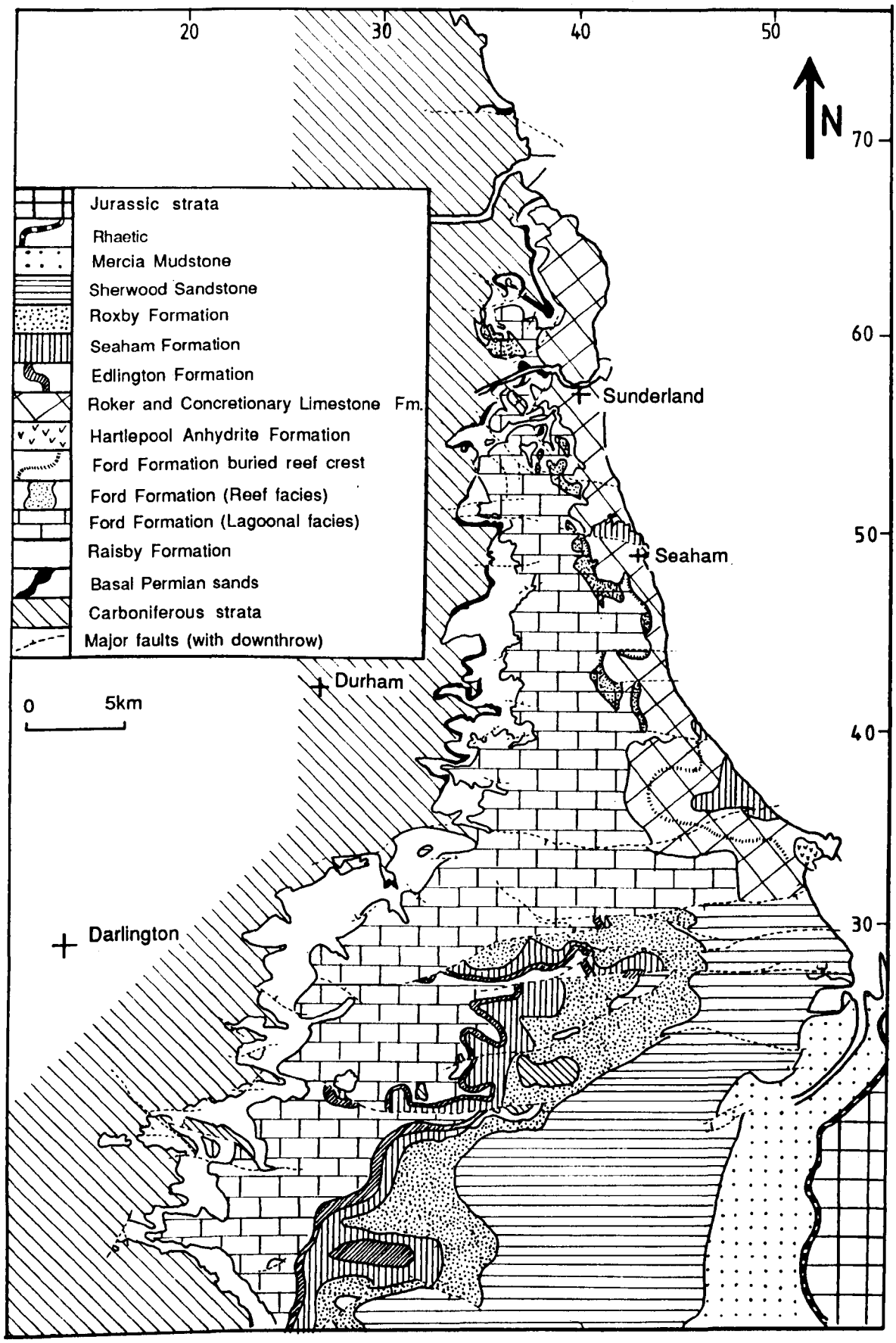

Fig. 1.1. Geological map of northeast England (compiled from British Geological Survey maps, and memoirs (Smith and Francis, 1967; Mills and Hull, 1976)).

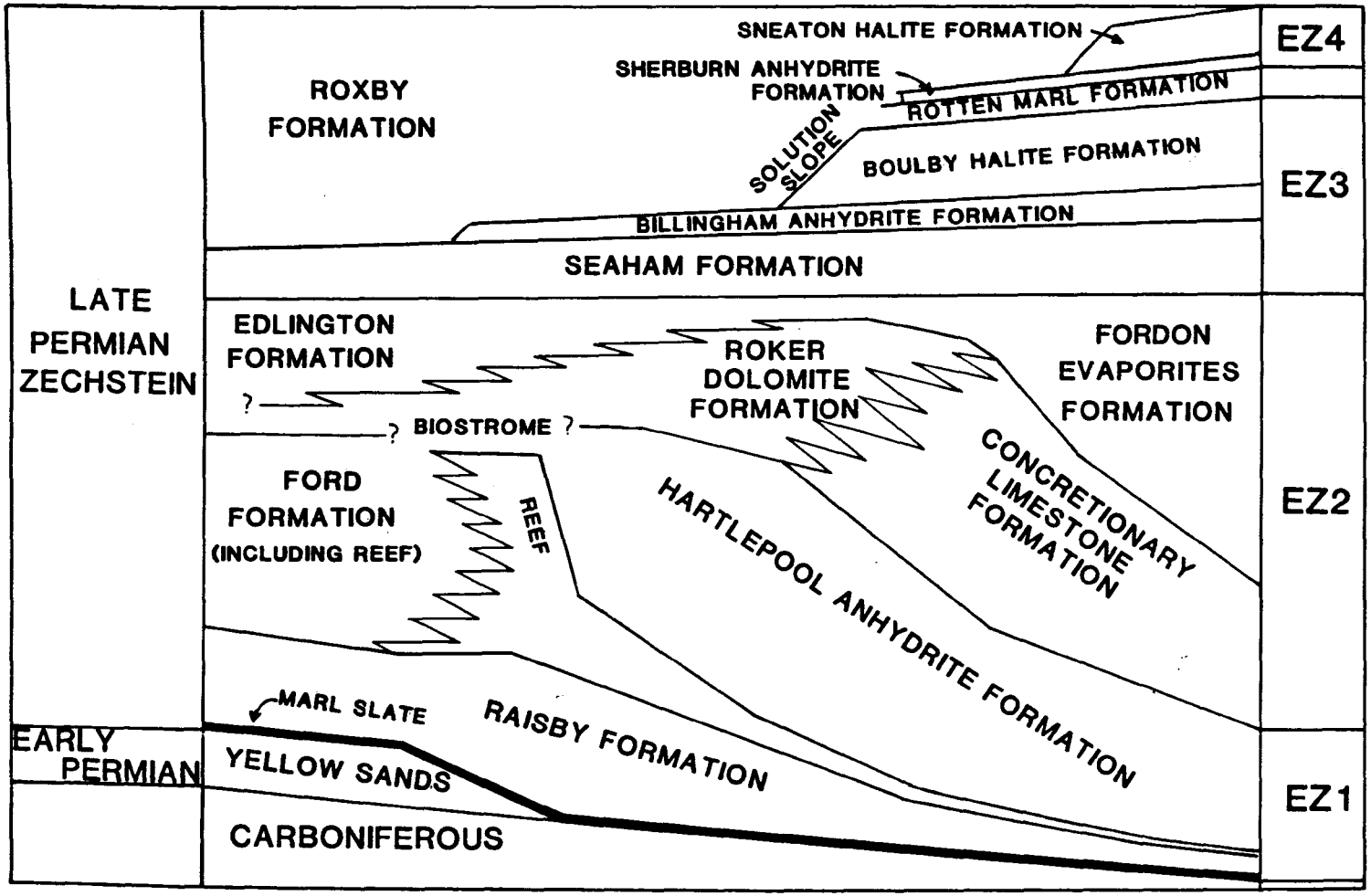

Fig. 1.2. Diagramatic stratigraphy of the Permian in northeast England (modified from Smith and Taylor, 1990).

Very little detailed work has been conducted on the sedimentology and diagenesis of Raisby Formation. Some aspects of its mineralogy have been covered by Trechmann (1914), Woolacott (1919a & b), Raymond (1962) and Jones (1969) and of base metal mineralization by Fowler (1943 & 1957), Jones and Hirst (1972) and Hirst and Smith (1974). The only detailed diagenetic work has been published is by Lee and Harwood (1989). Some aspects of the sedimentology of the Raisby Formation, concentrating on resedimentation, have been published in Smith (1970b & 1986), Land (1974) and Magraw (1975 & 1978).

In contrast, the sedimentology and especially the diagenesis of carbonates immediately underlying and overlying the Raisby Formation has been studied in great detail. A plethora of papers has been written on the Marl Slate, which concentrate on mineralization and geochemistry. These include Hirst and Dunham (1963), Turner and Vaughan (1977), Gibbons (1978), Turner *et al.*, (1978), Magaritz and Schulze (1980), Vaughan and Turner, (1980), Magaritz *et al.*, (1981), Magaritz and Turner (1982), Turner and Magaritz (1986) and Magaritz *et al.*, (1987). In addition to faunal studies already mentioned, considerable recent work has also been done on the Ford Formation reef, concentrating on diagenesis (Aplin 1981, 1985) and palaeontology with diagenesis (Smith, 1981; Tucker and Hollingworth, 1986; Hollingworth, 1987; Hollingworth and Tucker, 1987). Recently, work has also been completed on the sedimentology and diagenesis of the Edlington Formation (first and second cycle) of Teesside (Goodall, 1987). The sedimentology and diagenesis of the first cycle Zechstein carbonate (Cadeby Formation) of Yorkshire has recently been studied by Kaldi (1980a & b, 1986a & b), Kaldi and Gidman (1982) and Harwood (1981, 1986a & b).

1.3.1. Permo-Carboniferous tectonic evolution of northwest Europe

The Southern North Sea Permian basin in which the English Zechstein sequence was deposited, formed following the Upper Carboniferous Variscan orogeny. The Variscan orogeny was the result of continent-continent collision between Laurasia (northern Europe, North America, Asia) and Gondwanaland (South America, Africa, Antarctica, Australia). This collision was caused by closure of the Proto-Tethys Ocean which formed the supercontinent of Pangaea (Fig. 1.3). The continent-continent collision may have started as early as the Visean and orogenic activity persisted until the late Westphalian to early Stephanian (Glennie, 1984a). The resultant Variscan fold belt had a west-east trend, from Brittany to Romania, dissecting Pangaea (Fig. 1.3).

Following, and due to erosion and isostatic uplift of the Variscan fold belt in the early Permian (Saxonian), extensive downwarping took place in the northern Variscan foreland. Two major east-west orientated collapse basins were formed, called the Northern and Southern Permian basins (Fig. 1.4). The Southern basin, much larger than the Northern, is now 1500km east to west (however, owing to later extension, the North Sea basins are now wider than they were during the Upper Permian). These two basins were separated by the fragmented mid North Sea-Ringkøbing-Fyn system of highs (Ziegler, 1982) (Fig. 1.4). These highs were exempt from the general subsidence of the northern Variscan foreland and were

initiated as an area of east-west aligned updoming during the Stephanian-Autunian before substantial subsidence took place (Ziegler, 1982). A number of smaller Permian basins are also probably attributable to the regional downwarping, such as the Moray Firth Basin (a sub-basin of the Northern Permian Basin) and the Manx-Furness, Solway and Ulster basins (Glennie, 1984a) (Fig. 1.4).

Soon after cessation of north-south compression of the Variscan orogeny, northern Europe was subject to east - west orientated tension. This stress field was most likely linked to a failed rifting attempt of the proto-Atlantic between North America and Eurasia which may have started as early as the late Dinantian (Glennie, 1986). This tension led to the formation of a number of north-south orientated grabens which cut the Northern and Southern Permian basins as well as the intervening highs (Fig. 1.4). The largest of these grabens are the Central Graben and its northwards extension the Viking Graben, and the Horn Graben which extends northwards into the Oslo Graben (Fig. 1.4). A number of smaller fault-bounded structures also cut the Mid North Sea-Ringkøbing-Fyn highs such as the Grinsted Graben east of the Horn Graben (Glennie, 1986), and two small structures west of the Central Graben, one identified by Jenyon *et al.* (1984) and another tentatively identified by Smith and Taylor (1990) adjacent to the coast of northeast England.

1.3.2. Permian climate of northwest Europe

During the Upper Carboniferous, northwest Europe was in an equatorial position, but following the Variscan orogeny the supercontinent of Pangaea drifted northwards into the northern Trade Wind belt (Ziegler, 1982). In the Lower Permian, Durham was in an area just to the south of 10° north latitude (Glennie, 1982) (Fig. 1.3). Position and climate of the Permian basins was very similar to the present-day Arabian and North African deserts (Glennie, 1984b). Eustatic sea level fall accompanying the Gondwanaland glaciation gave the Pangaean supercontinent a very dry, continental climate with any rain precipitating long before it reached the Permian basins (Ziegler, 1982). The winds in the basin were strong, dry, desiccating and even cold as a result of compressed climatic belts produced by the southern hemisphere glaciation (Glennie, 1982). The Permian basins themselves had a hot, dry, arid climate.

On the basis of cross bedding orientations in Lower Permian Rotliegendes dunes, Glennie (1982) and Yardley (1984) suggest that the Durham area had a prevailing wind to the southwest (normal to the shoreline of the Zechstein Sea in Durham). The wind directions in the Northern and Southern Permian basins were not unidirectional, but 'wheel round' a barometric high situated over the Mid North Sea high (Glennie, 1984a). Sneh (1988) however, from a reinterpretation of Rotliegendes dune morphology suggests that throughout the North Sea basins the prevailing winds were unidirectional from north to south and so oblique to the shoreline of the Zechstein Sea in Durham. This interpretation however is still consistent with location of the North Sea basins in the trade wind belt (Sneh 1988). Wind velocity at least is suggested to have declined following transgression of the

Zechstein Sea. Glennie and Buller (1983) suggest that both processes were due to melting of the southern hemisphere ice sheets.

1.4.1. Lower Permian sedimentation in the North Sea basins.

Uplift of the northern Variscan foreland accompanied the final stages of the Variscan orogeny, which led to the development of a pronounced erosional unconformity between the Carboniferous and Permian. This is termed the Saalian unconformity (Ziegler, 1982). In southern Co. Durham, up to 910m of Carboniferous strata has been removed by erosion (Smith, 1970a). The top few meters of the Carboniferous are also often reddened, testifying to weathering in an arid environment (Anderson and Dunham, 1953).

The first sediments, of pre-Zechstein age in the North Sea basins are termed 'Rotliegendes'. The 'Yellow sands' of Durham are Rotliegendes aeolian sediments. Glennie (1984b) subdivides the Rotliegendes into two informal units, the Lower and Upper. The Lower Rotliegendes is mainly characterized by calc-alkaline volcanics and volcanic-associated sediments. These are restricted to tectonically active areas of the basins. The volcanism was most likely the product of east-west tension and so synchronous with graben formation (Glennie, 1984b).

The Lower Rotliegendes are at least partly coeval with Upper Rotliegendes sediments. Four distinct facies associations of Upper Rotliegendes can be defined in the Southern Permian Basin (Glennie *et al.*, 1978; Glennie, 1984b); fluvial (wadi), aeolian (sand dune), marginal dune-lacustrine sabkha, and basin centre lacustrine (muds and silts with non-marine halite and anhydrite [Ziegler, 1982]) (Fig. 1.5). Wadi sands and conglomerates are concentrated along the southern margin of the Southern Permian Basin. Clastic influx was northwards from the Variscan highlands. Decrease in sediment supply over time may reflect movement of the Variscan highlands from the fringes of the equatorial into the arid trade wind belt (Ziegler, 1982) and/or gradual denudation of the landscape. The areal extent of dune sands and the basin centre lake varied over time, in relation to climatic changes (Glennie, 1984b). In the Northern Permian and Moray Firth basins, these facies are less well developed (Fig. 1.5).

Thicknesses of Rotliegendes sediments in the Moray Firth and Northern Permian basins are similar (600m and 500m respectively) although the center of the Southern Permian Basin contains over 1km Rotliegendes (Glennie, 1984b). In the Moray Firth Basin sedimentation kept pace with subsidence, but this was not the case in the Northern and Southern Permian basins such as by the end of the Rotliegendes the bottoms of both were at least 200-300m below the level of surrounding oceans (Smith, 1979, Glennie, 1984b). The nature of the Rotliegendes in northeast England will be discussed in chapter 2.

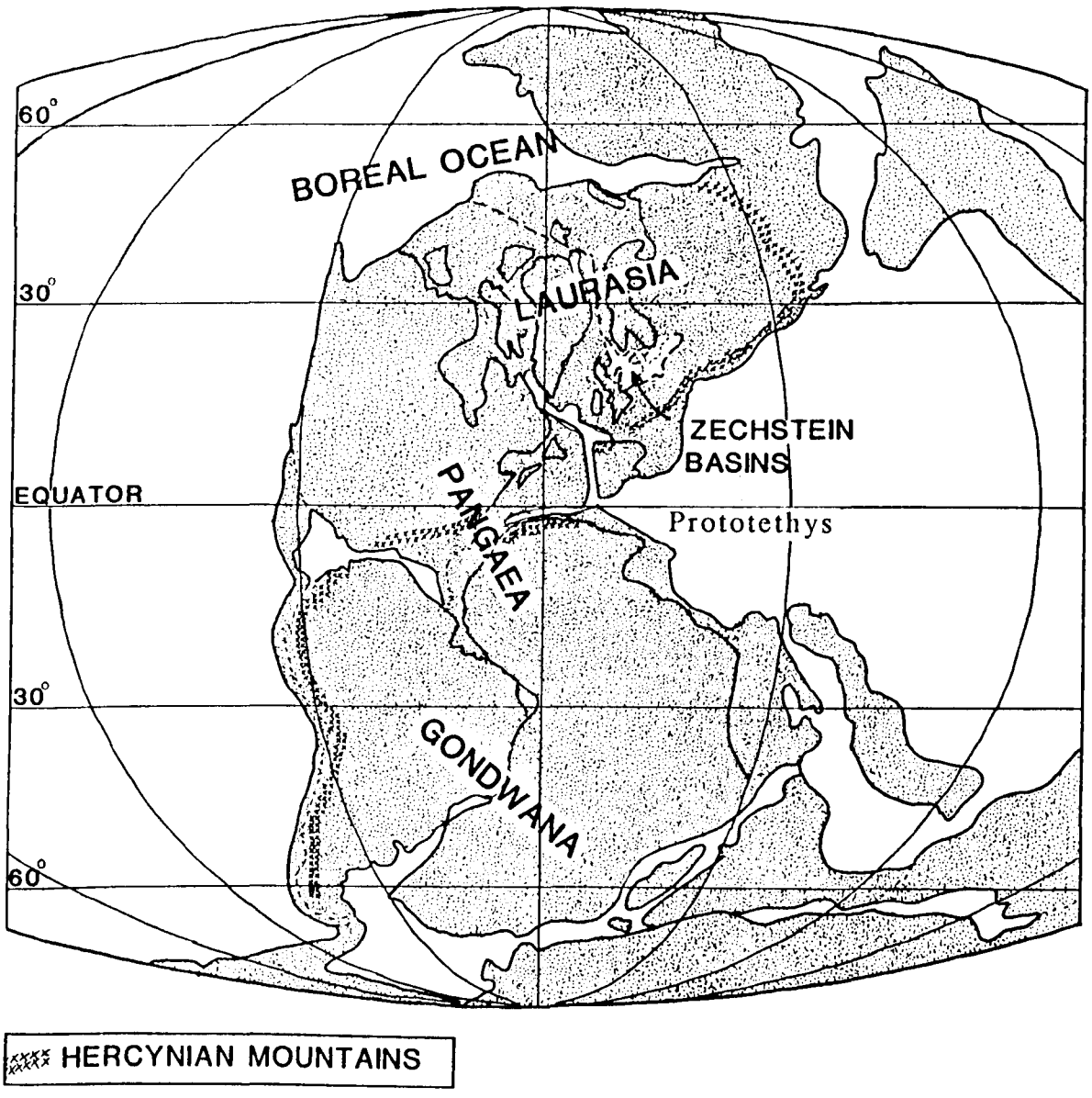

Fig. 1.3. Upper Permian palaeogeographic map (modified from Glennie, 198 6).

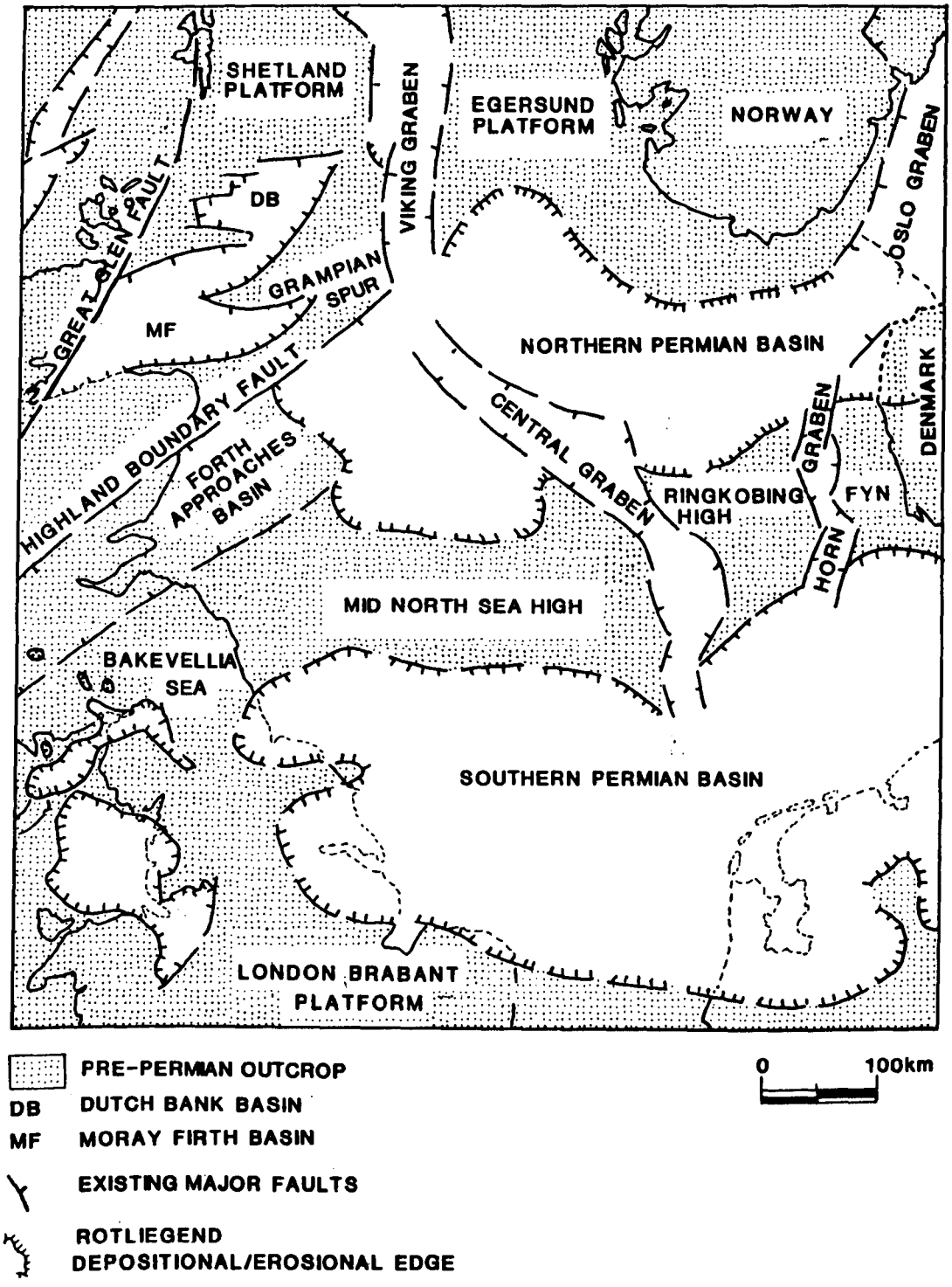

Fig. 1.4. Structural elements of the North Sea and adjacent areas during the Upper Permian (modified from Glennie, 1984b).

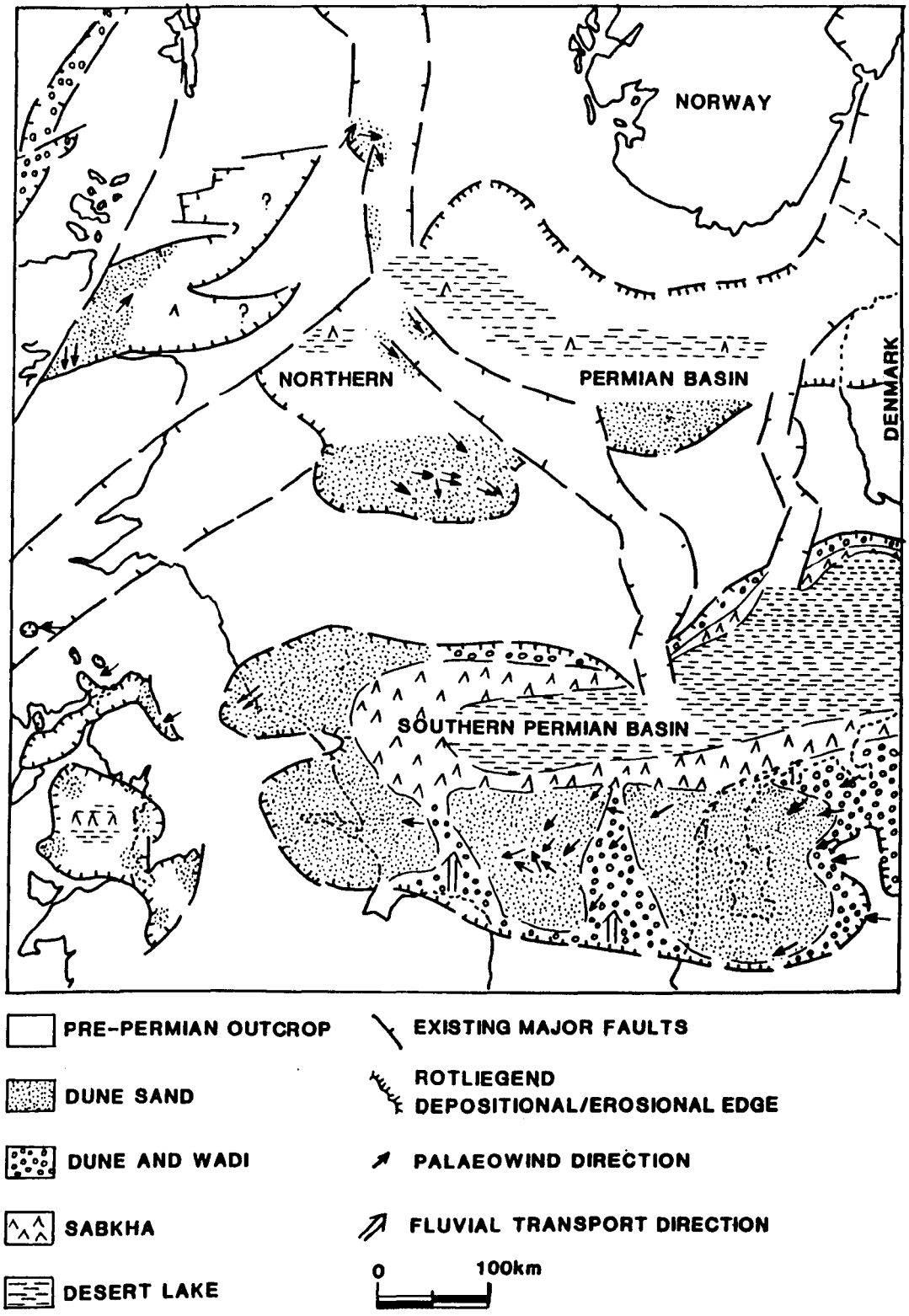

Fig. 1.5. Lower Permian, Rotliegendes facies of the Northern and Southern Permian Basins and adjacent areas (modified from Glennie, 1984b).

1.4.2. Transgression of the Zechstein Sea.

The Rotliegendes basins were inundated by seawater from the Boreal Ocean to the north as evidenced by fauna (Pattison, 1970; Pattison *et al.*, 1973). It is widely suggested that the filling of the North Sea Permian basins was geologically more or less instantaneous, giving rise to the hypothesis of the 'instant Zechstein' (Smith, 1970a & c; Smith, 1979). Some of the main supporting evidence for the rapidity of the transgression is in the preservation of Rotliegendes dunes which show minimal marine reworking (Smith, 1970a & c; Smith, 1979). Reworking of the dunes is normally restricted to the top few tens of centimeters to few meters, which is commonly represented by parallel-bedded (beach?) sands, well cemented, with marine fossils such as *Lingula credneri* (Bell *et al.*, 1979; Glennie and Buller, 1983). Rapidity of the transgression is also supported by liquefaction structures in the upper parts of Rotliegendes dune sands produced by rapidly rising water table levels (Glennie and Buller, 1983).

The conduit between the Boreal Ocean and Northern and Southern Permian basins was provided by the proto-Atlantic rift and Viking-Central Graben systems (Smith, 1980; Glennie and Buller, 1983) (Fig. 1.3 & 1.4). This is supported by recent work by Surlyk *et al.*, (1986) who describe a sequence of Permo-Carboniferous sediments in central east Greenland. These sediments record an episode of extensive proto-Atlantic rifting from the start of the Upper Carboniferous (310Ma) to the end of the Lower Permian (Autunian) (280Ma). Clastic syn-rift sediments are overlain by marine Upper Permian carbonates and evaporites with a European Zechstein fauna. This strongly suggests the path of the Boreal floodwaters was between Greenland and Norway. The initial trigger for the flooding is widely suggested to have been a glacio-eustatic sea level rise following total, or partial melting of the Gondwanaland ice caps (Smith, 1970a & c and 1979; Glennie and Buller, 1983). To fill the Northern and Southern Permian basins would have required 110,000km^3 of water. Smith (1970c) suggests a timescale for infilling of the basins of weeks or months. Glennie and Buller (1983) have calculated that to fill the basins in 6 years would need a supply rate of 50km^3 day^{-1}. Such a flow rate could be achieved if the floodwater channel was 10km wide, 20m deep and the water was flowing at a rate of 3m s^{-1} (Glennie and Buller, 1983). These floodwaters would have inundated sand dunes such as those recorded in Durham in 8 months (Glennie and Buller, 1983). This is a very reasonable rate considering their amount of apparent reworking.

1.4.3. Upper Permian sedimentation in the Southern Permian Basin.

Following inundation of the Lower Permian basins, marine sedimentation in the Zechstein Sea reflected the balance between degree of connection with the Boreal Ocean, rate of evaporative loss of seawater and basin subsidence. Periods of good oceanic connection saw deposition of carbonates, whereas when restricted, or isolated, precipitation of evaporites was dominant. The deposition of carbonates and evaporites is characteristically cyclic and the cycles can be traced from eastern England to Poland. This allows correlation of Zechstein sediments across the basin, on the assumption that each cycle was synchronous basin-wide.

In eastern England, five cycles (four major, one minor) are developed (Smith, 1980b). Each cycle was initiated by a fresh influx from the Boreal Ocean (depositing carbonates), and ended with extensive desiccation of the basin (depositing evaporites). The controls of this cyclicity are uncertain, although one of the most widely accepted mechanisms is glacio-eustatic fluctuation in ocean levels due to advance and retreat of the Gondwanaland ice caps (Smith, 1970a). However, glacio-eustatic fluctuation of the Boreal Ocean was probably not the only factor (Smith, 1979) and most likely operated together with basin subsidence, fluctuation in levels of the barrier with the Boreal Ocean, sedimentary filling of the basin and climatic changes (Smith, 1979; Smith, 1980; Taylor, 1980 & 1984). Glennie and Buller (1983) suggested that during the Rotliegendes, fluctuation in Gondwanaland ice had a direct effect on climate in the North Sea basins.

Within both carbonate and evaporite member of each cycle, smaller scale, short term cyclicity may be recognized (Smith, 1985). Such sub-cycles have been described within first cycle carbonates from Yorkshire (Smith, 1968), West Germany (Paul, 1986a & b) and Poland (Peryt and Wazny, 1980; Peryt, 1986). Sedimentation of the Hartlepool Anhydrite Formation is also suggested to have been influenced by a basin-wide cyclicity imposed by interaction of barrier levels with glacio-eustatic fluctuations in the level of the Boreal Ocean (Taylor, 1980 & 1984). Local tectonic and sedimentological processes may also have played an important role within small sub-basins (Smith, 1985).

Superimposed on sedimentological cyclicity within the Zechstein Basin is a secular change of an increase in salinity of the Zechstein Sea over time. A truly marine fauna is only seen in the first cycle carbonates, whereas in carbonates of later cycles even the initial seawater was well above normal salinity (Smith, 1980b). A marine biota is not seen above carbonates of cycle 3. The reasons for the secular increase in salinity are probably a combination of mixing of transgressing seawater with residual evaporitic brines from the previous cycle and dissolution of evaporites deposited during the previous cycle (Smith, 1980b). Sedimentation rate of the first couple of cycles greatly outstripped subsidence rate, such that by the end of the second cycle, the English sub-basin was almost completely infilled (Smith, 1970a & c). Thus interconnection of the Zechstein Sea in succeeding cycles was limited, and various sub-basins became increasingly isolated. Carbonates and evaporites of cycles 3, 4 and 5 were accommodated by a slow, basin-wide subsidence (Smith, 1970a).

The English sub-basin of the Southern Permian Basin was a marginal embayment approximately 250km north-south and 300km east-west (Smith, 1980b). The sedimentary sequence deposited in the sub-basin is illustrated in table 1.1 and Fig. 1.2. This demonstrates another control on development of the cyclic sedimentation in that the cycles are only well developed away from the palaeoshoreline (Durham and Yorkshire subsurface). This is further complicated by dissolution of evaporitic units at outcrop in Yorkshire and Durham. To the west of the Zechstein outcrop in northeast England the presence of a permanent land barrier is suggested which separated the English sub-basin from the *Bakevellia* Sea that stretched from northwest England to northeast Ireland (Smith, 1970c).

Group	Cycle	Yorkshire Province (outcrop)	Yorkshire Province (subsurface)	Durham Province (outcrop and subsurface)	North Sea, Germany, The Netherlands
ESKDALE	EZ5	ROXBY FORMATION	ROXBY FORMATION LITTLEBECK FORMATION SLEIGHTS (SILTSTONE) FORMATION	ROXBY FORMATION	ZECHSTEINLETTEN GRENZANHYDRIT
STAINTONDALE	EZ4		SNEATON (HALITE) FORMATION: including SNEATON POTASH MEMBER SHERBURN (ANHYDRITE) FORMATION UPGANG FORMATION CARNALLITIC MARL FORMATION	SHERBURN (ANHYDRITE) FORMATION	ALLER HALIT and EQUIVALENTS PEGMATITANHYDRIT and EQUIVALENTS ROTER SALZTON
TEESSIDE	EZ3	BROTHERTON (MAGNESIAN LIMESTONE) FORMATION	BOULBY (HALITE) FORMATION: including BOULBY POTASH MEMBER BILLINGHAM (ANHYDRITE) FORMATION BROTHERTON (MAGNESIAN LIMESTONE) FORMATION	BILLINGHAM (ANHYDRITE) FORMATION SEAHAM FORMATION	LEINE HALIT and EQUIVALENTS HAUPTANHYDRIT PLATTENDOLOMIT GRAUER SALZTON
AISLABY	EZ2	EDLINGTON FORMATION	FORDON (EVAPORITE) FORMATION KIRKHAM ABBEY FORMATION	East of province: FORDON (EVAPORITE) FORMATION and SEAHAM RESIDUE ? ROKER (DOLOMITE) FORMATION ? CONCRETIONARY LIMESTONE FORMATION South of province: EDLINGTON FORMATION	STASSFURT SALZE HAUPTDOLOMIT
DON	EZ1	CADEBY (MAGNESIAN LIMESTONE) FORMATION { SPROTBROUGH MEMBER; WETHERBY MEMBER	HAYTON (ANHYDRITE) FORMATION CADEBY (MAGNESIAN LIMESTONE) FORMATION MARL SLATE FORMATION	HARTLEPOOL (ANHYDRITE) FORMATION FORD (MAGNESIAN LIMESTONE) FORMATION RAISBY (MAGNESIAN LIMESTONE) FORMATION MARL SLATE FORMATION	WERRAANHYDRIT WERRADOLOMIT and ZECHSTEINKALK KUPFERSCHIEFER

Table 1.1. Stratigraphy and correlation of the Zechstein throughout eastern England (modified from Smith *et al.*, 1986).

1.5.1. Correlation of Zechstein deposits.

No precise correlation exists for the European Zechstein sequence in relation to marine Permian sequences internationally. The problems in correlation are due to the combination of a number of factors (Smith *et al.*, 1974; Kozur, 1981a; Holser *et al.*, 1986):

1. There is no internationally accepted marine Permian standard section,
2. Sediments underlying the European Zechstein are mainly arid continental,
3. The Zechstein Sea only had an intermittent connection with the Boreal Ocean, and truly marine sediments are only seen in the first cycle,
4. There is a lack of biostratigraphically useful fossils such as ammonoids and fusilinaceans,
5. Biostratigraphically useful fauna is often facies controlled,
6. Many potentially useful taxa are stenohaline,
7. Most Zechstein carbonates have been pervasively dolomitized.
8. Difficulties in recognizing paraconformities where stages may be missing in marine sections.

There are two current correlations for the European Permian. The most widely accepted one (Smith *et al.*, 1974; Harland *et al.*, 1982) (Table 1.2) gives the first cycle Zechstein carbonates an Ufimian age (basal Upper Permian). The base of the upper Permian lies at 258Ma (Harland *et al.*, 1982) or 251Ma (Van Eysingia, 1978). The Ufimian correlates with the Guadalupian in a carbonate-evaporite sequence of the Delaware basin U.S.A. (similar in character to the European Zechstein). This is supported by Surlyk *et al.*, (1986) who suggest that the Zechstein transgression in central eastern Greenland occurred at the Lower-Upper Permian boundary.

However, Kozur (1981a & b) suggests a different correlation for the European Zechstein, whereby, on the basis of conodont faunas he correlates Zechstein cycles 1 - 3 with his Abadehian stage. The Abadehian he correlates with the lower Tatarian of the Urals and the lower Ochoan of the Delaware basin (Table 1.3). The conodont *Merrillina divergens* occurs in the Abadehian stratotype of central Iran and early cycle Zechstein carbonates including the Raisby Formation (Swift, 1986). Such an age for the lower part of the Zechstein sequence is possibly supported by the miospore genus *Luekisporites* (Smith *et al.*, 1974; Holser *et al.*, 1986) and correlations by carbon stable isotopes by Holser *et al.*, 1986. The similarity of carbon isotope profiles between the Guadalupian-Ochoan contact in the Delaware basin and carbonates at the base of the Zechstein sequence has led Holser *et al.*, (1986) to suggest a globally synchronous positive excursion in the carbon isotopic composition of shelf marine carbonates. The positive excursion is recorded in the upper part of the Bell Canyon Formation in the Delaware basin and in the Kupferschiefer of the Zechstein Basin continuing throughout most of the remaining Upper Permian at these localities. This would place the base of the Zechstein sequence at the Capitanian-Abadehnian stage boundary (Table 1.3). However, there are considerable problems with this global carbon isotope correlation, which will be discussed further in chapter 3.

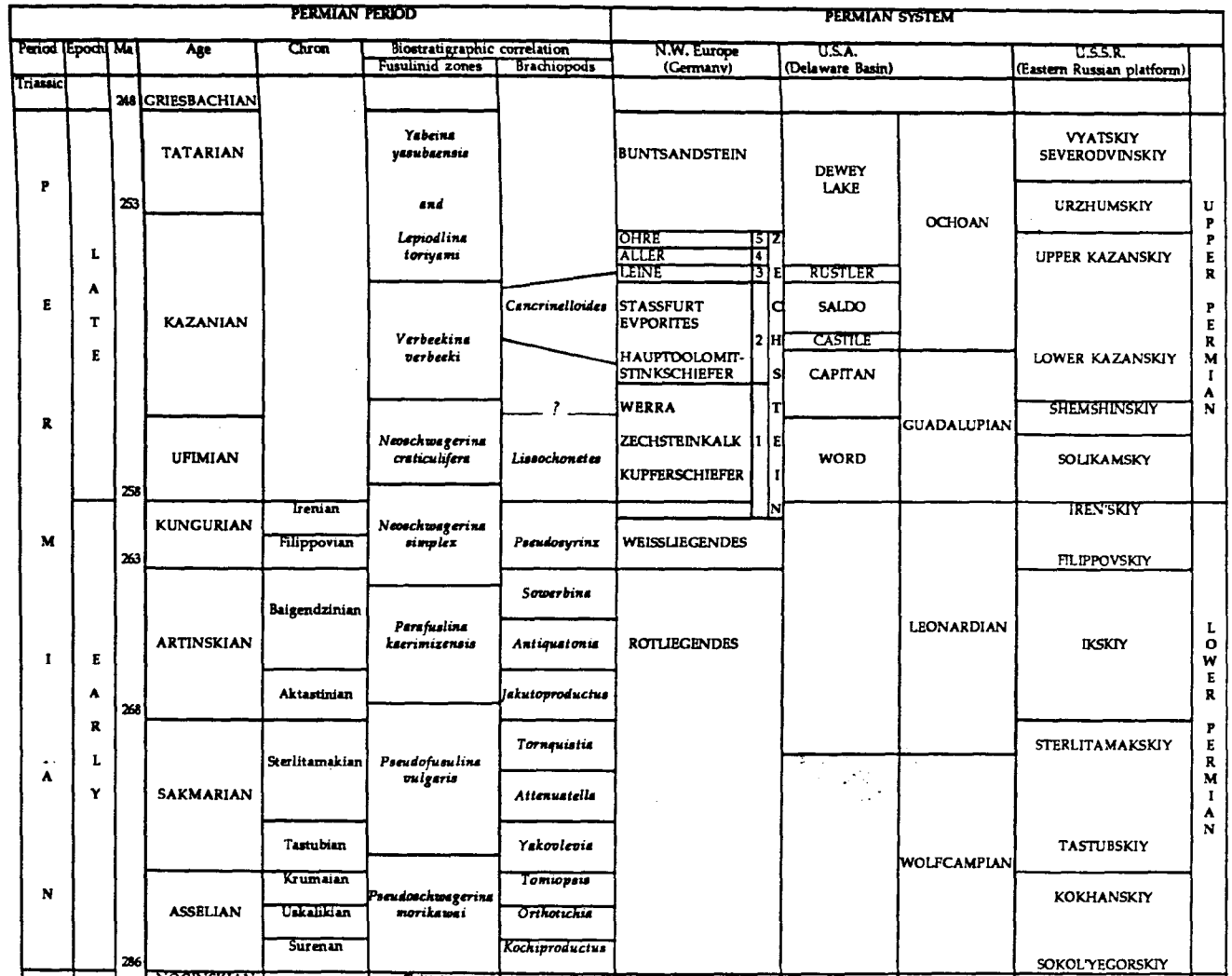

Table 1.2. Sratigraphy and correlation of the Permian in N.W. Europe, U.S.A., and U.S.S.R. The Raisby Formation is time-equivalent to the Zechsteinkalk (modified from Harland *et al.*, 1982).

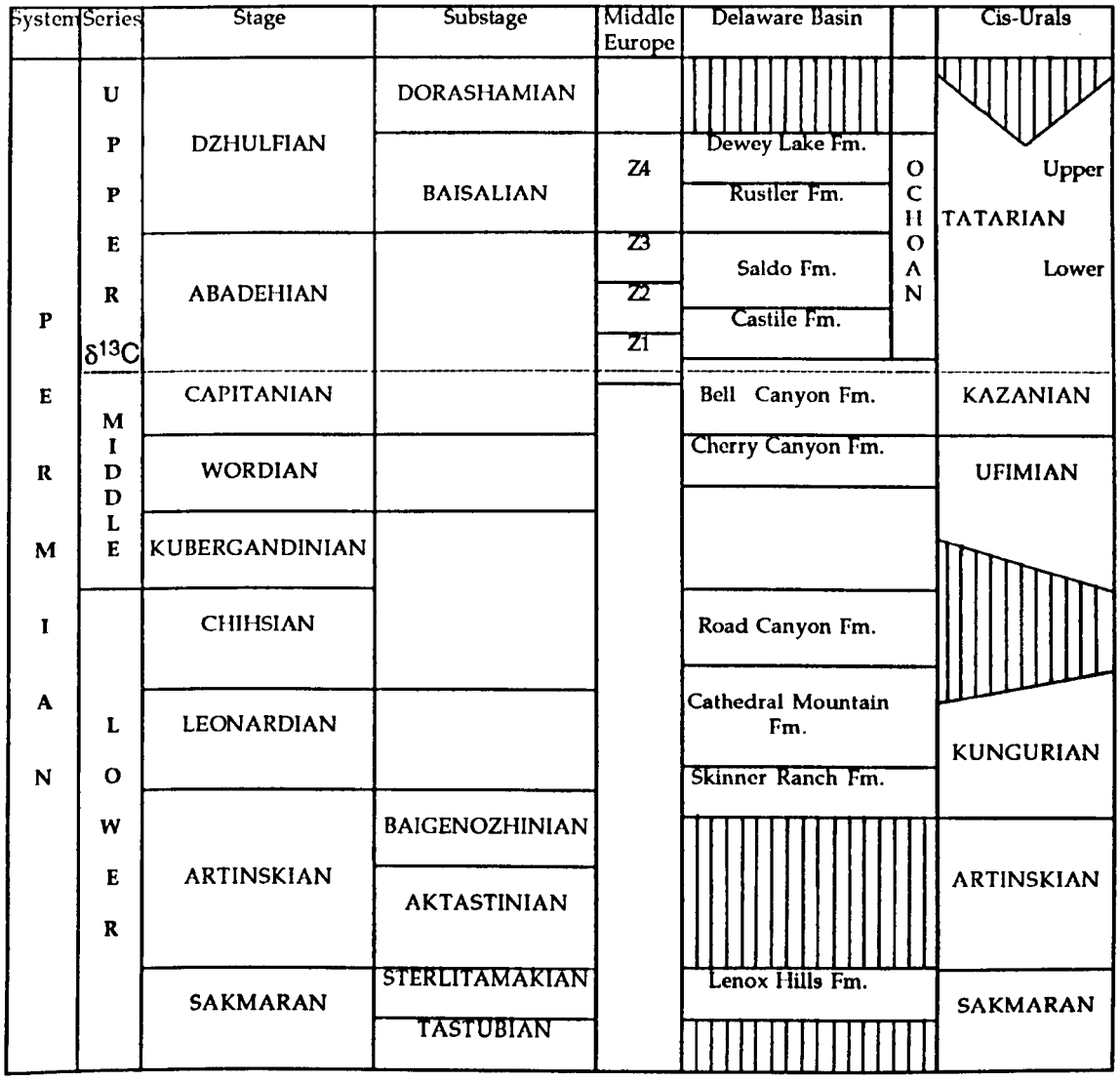

Table 1.3. Stratigraphy and correlation of the Permian in Europe, U.S.A. (Delaware Basin), and U.S.S.R. (Cis-Urals) (after Kozur, 1981a & b), with the proposed carbon isotope correlation (δ^{13} C) of Holser *et al.*, (1986).

Therefore, there is considerable disagreement as to the precise age and correlation of the European Zechstein sequence which will probably only be resolved by use of higher resolution biostratigraphic tools, such as palynomorphs.

1.6.1. The Raisby Formation in northeast England.

The Zechstein sediments in eastern England outcrop along a narrow N-S belt from just north of the Tyne in Northumberland, south to near Nottingham (Fig. 1.6). To the east the Permian is underlain dominantly by Carboniferous, and in Yorkshire and Nottinghamshire is overlain by a Mesozoic cover. The Zechstein sequence commonly has a gentle eastwards dip.

As table 1.1 illustrates, the Zechstein within the English sub-basin is subdivided itself into two provinces, Durham and Yorkshire, which were separated by the east-west trending Cleveland High. The Raisby Formation is thus approximately coeval with the Wetherby member of the Cadeby Formation in Yorkshire. The Raisby Formation is defined as "Upper Permian marine strata from the latitude of Catterick (north Yorkshire) northwards, lying between the Marl Slate....and the Ford (Magnesian Limestone) Formation...." (Smith *et al.*, 1986, p.13). The formation is generally 20-50m thick. It is thickest in Co. Durham (73m) and thins sharply into the basin (Smith *et al.*, 1986). Although the base of the Raisby Formation is generally taken as the top of finely laminated Marl Slate, where absent the Raisby Formation rests directly on an eroded Carboniferous surface, or Rotliegendes sands. The top of the Raisby Formation in the west is marked by the incoming of oolitic or reef carbonates of the Ford Formation, whereas in the east it is at the base of a thin sequence of transitional strata (Magraw *et al.*, 1963) or the top of the Trow Point bed (Smith, 1986; Smith *et al.*, 1986). Details of the upper and lower contacts of the Raisby Formation will be discussed in chapter 2.

The Raisby Formation outcrops on a more or less continuous, narrow, NNE - SSW tract (Fig. 1.6.). The trend of the outcrop is at an angle to the depositional strike (approximately north-south). In the Durham area between Ferryhill and Hetton-le-Hole the Raisby Formation forms a 30-60m high escarpment (Smith & Francis, 1967), although to the north and south it has a much more subdued topographic expression.

The Raisby Formation at outcrop has a gentle (average 1°-3°) eastwards dip. This is partly sedimentological, inherited from the Carboniferous peneplain and syn-Zechstein subsidence accompanying the deposition of later cycles, and partly tectonic with gentle tilting accompanying Tertiary uplift (Smith and Francis, 1967; Mills and Hull, 1976). Dips are locally increased adjacent to major faults (Mills and Hull, 1976). In the Ferryhill area, axes of anticlines within the Raisby Formation parallel anticline axes in the underlying Carboniferous (Smith and Francis, 1967). The Raisby Formation is cut by a few east-west trending faults, most of which formed due to reactivation of pre-Permian structures which cut the underlying Carboniferous, during the Tertiary (Clarke, 1962). Ratios of pre-Permian to post-Permian movement varies from 5:2 to 0:1 (Clarke, 1962). One dyke (56±1Ma [Green,

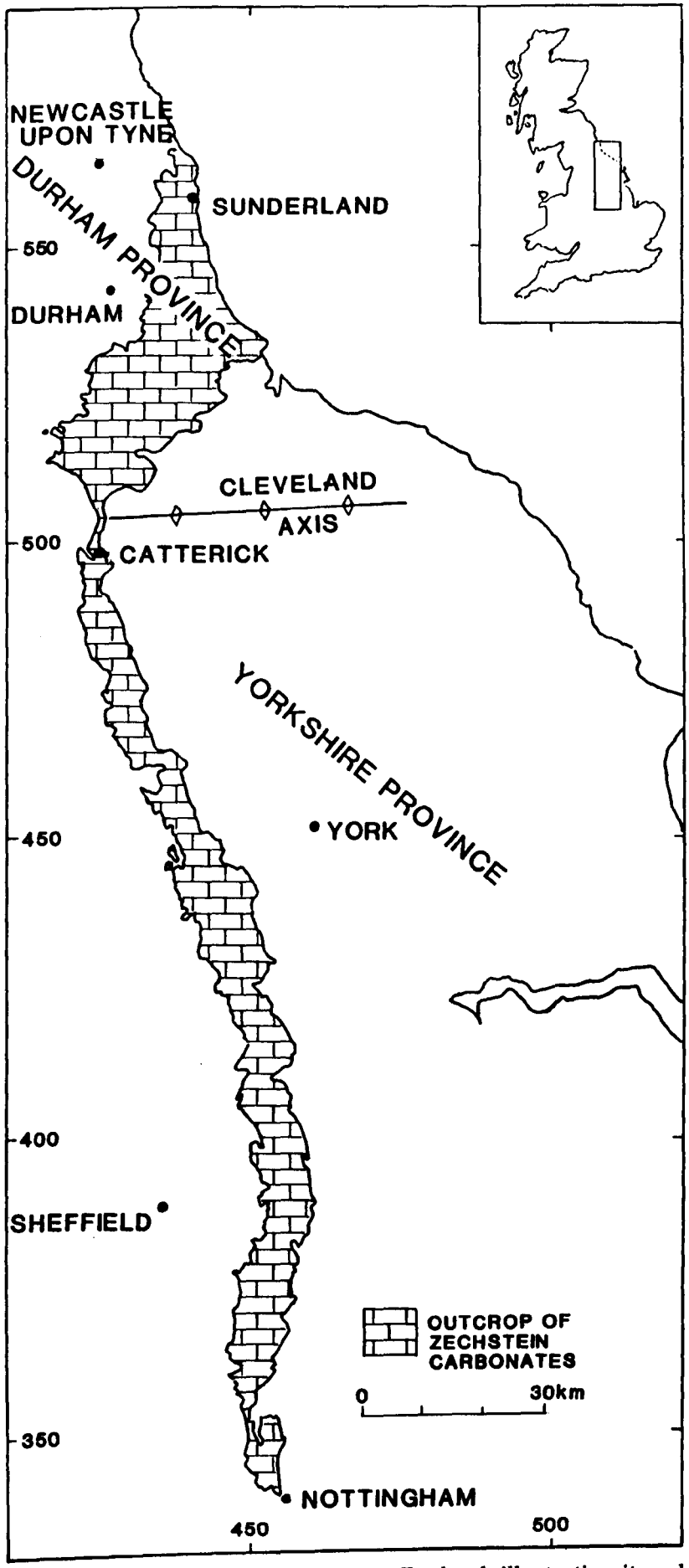

Fig. 1.6. Outcrop of the Permian through eastern England, illustrating its subdivision into two provinces by the Cleveland axis (modified from Smith *et al.*, 1986).

1989]), the Cleveland dyke cuts the Permian, and is most likely of a similar age to uplift, tilting and folding (Mills and Hull, 1976).

1.7.1. Objectives of the study.

The original aims of this research project were to fully describe and asses both the sedimentological and diagenetic histories of the Raisby Formation from outcrop and borehole data. However, in common with the other English Zechstein carbonates, the Raisby Formation has suffered a pervasive, multiphase, obliterative diagenetic overprint. This renders any detailed sedimentological analysis difficult. In the north of the outcrop the Raisby Formation was deposited in a carbonate slope environment with a very sparse pelagic/hemipelagic microfauna, and an even less abundant macrofauna. Where the Raisby Formation does attain a reasonably shallow water facies, in the south of the outcrop it is very poorly exposed, and pervasively dolomitized. The lack of any biostratigraphical correlation within the formation also makes correlation even between adjacent quarry sections difficult.

The aforementioned factors mean that the work presented in this thesis has inevitably concentrated on the diagenetic history of the formation, although diagenesis cannot be considered in isolation from sedimentology. No previous detailed work has been done on the diagenesis of the formation, and there is clearly a great potential. Zechstein carbonates below (Marl Slate [Sweeney *et al.*, 1987]), above (Ford Formation [Aplin, 1985; Tucker and Hollingworth 1986]; Edlington Formation [Goodall, 1987]) and laterally equivalent to the Raisby Formation (Cadeby Formation [Harwood, 1981 & 1986; Kaldi, 1980 & 1986b]) have been recently studied in great detail, and so give an excellent framework into which the diagenesis of the Raisby Formation may be placed. This may help lead to an integrated model for the diagenesis of Zechstein carbonate - evaporite sequences (e.g. Lee and Harwood, 1989).

1.8.1. Organization and subdivision of the thesis

This thesis is structured broadly according to the order of events in the Raisby Formation. It starts with sedimentology; the nature of upper and lower contacts, and depositional environments of the Raisby Formation (Chapter 2). It is necessary to consider the Permo-Carboniferous unconformity, the Basal Permian Sands and Breccias and Marl Slate in the beginning of chapter 2, as all three substrates have influenced deposition of the Raisby Formation, and may help to ascertain the palaeo-bathymetry of the Zechstein Sea during Raisby Formation deposition. Likewise, the sedimentology of the Ford Formation is very important for determining the reasons for cessation of deposition of the Raisby Formation, and so it is also discussed in chapter 2. Early, post-depositional diagenesis of the Raisby Formation is discussed in chapter 3. Initially in chapter 3, the principles of trace and minor element geochemistry is outlined, as it is used throughout the rest of this thesis. The primary isotopic composition of the Zechstein Sea is included in chapter 3, as it is an original feature, and a baseline for interpretation of the stable isotope geochemistry of Raisby

Formation carbonates. Chapter 4 deals with the petrography and geochemistry of limestones and calcite concretions. These are intimately related, both spatially and geochemically and so are considered together. Generally, although not exclusively, later diagenetic dolomitization and precipitation of calcium sulphate evaporites is discussed in chapter 5. They are treated together as dolomitization and the precipitation of sulphate evaporites took place at a similar time, and from fluids of a similar composition and derivation. All late, uplift-related diagenesis is bought together in chapter 6. All aspects of telogenesis (calcitization of evaporites and dolomite, calcite cementation, and iron and clay mineral diagenesis) are closely spatially and genetically interrelated. Epigenetic mineralization, of a variable timing relative to other diagenetic events, is discussed separately in chapter 7. Both the depositional and diagenetic histories of the Raisby Formation are summarized and concluded in chapter 8. Geochemical results (electron microprobe, AAS and ICP, and stable isotopes) are presented in the chapters to which the results refer. Details of all analytical techniques, outcrop and borehole logs and geochemical results are given in the appendices.

Chapter 2

Sedimentology

2.1.1. Sedimentology of the Raisby Formation - Introduction.

Very little detailed work has been completed on the sedimentology of the Raisby Formation. Smith (1970a) focussed on evidence for resedimentation, which was also briefly mentioned in Smith and Taylor (1990). Some sedimentology was included by Magraw *et al.*, (1963), Smith and Francis (1967), Land (1974), Magraw (1975 & 1978) and Mills and Hull (1976). These previous studies have established that the formation is largely featureless and sparsely fossiliferous, with horizons of resedimented carbonates concentrated in the north of the outcrop, and within offshore boreholes. These studies identified depositional environments for the Raisby Formation, ranging from outer shelf, through slope and into basin. Onshore, the Raisby Formation is overlain by shallower water sediments of the Ford Formation, deposited in lagoonal and reef environments (Fig. 1.2). The Raisby Formation also passes laterally southwards into shallower water (shelf) sediments of the Yorkshire Province (Wetherby Member of the Cadeby Formation).

In the study area, the Raisby Formation conformably overlies the Marl Slate Formation, or unconformably overlies Rotliegendes (Basal Permian) Sands or Breccias, or an eroded Carboniferous surface. All three substrates have strongly influenced sedimentation of the Raisby Formation. The conditions of deposition of the overlying Ford Formation, and especially the nature of the Raisby-Ford Formation contact, are also of importance for an understanding of depositional history of the Raisby Formation. Therefore, before considering the sedimentology of the Raisby Formation, the nature of the directly underlying and overlying sediments will be discussed, specifically with reference to indicators of palaeoenvironment and/or palaeobathymetry.

2.1.2. Permo-Carboniferous unconformity.

Between the late Carboniferous and the base of the Zechstein, the study area was exposed, and experienced erosion for at least 28 million years, with little or no evidence now remaining for sedimentation. At least 380m of Coal Measures were removed in the north (Magraw, 1975), and up to 910m of Carboniferous sediments were eroded from the south of the area (Smith, 1980a). The Permo-Carboniferous erosional unconformity thus oversteps progressively older Carboniferous sediments from Westphalian, through Namurian, into Dinantian from north to south. In addition, as the Carboniferous in Durham forms a broad syncline, Upper Coal Measures crop out in the center of the area, becoming progressively older to the north and south (Anderson and Dunham, 1953).

This eroded Carboniferous surface was bordered to the west by the Pennine massif and to the south by the Cleveland High, a large Carboniferous anticlinal ridge (Fig. 1.6). The Carboniferous palaeo-surface dips a few degrees gently eastwards, some of which is a later tectonic overprint. It had considerably less relief in the north of the area than the south, related both to more intense Hercynian faulting and folding, together with a greater resistance to erosion of the southern Namurian and Dinantian sediments, especially the limestones. The dividing line between the two palaeotopographical provinces runs approximately ENE-WSW through Trimdon (Smith, 1970a). However, at least one palaeotopographical eminence has been described in the north of the area at Newbottle (NZ 345, 517) (Smith 1970a) (no longer exposed), over which the Raisby Formation developed a 'littoral' facies (D.B. Smith *pers. comm.*, 1987). However, in general, the palaeotopography of the south of the area immediately prior to the Zechstein transgression was more undulate than the north, with hills up to 200m above the surrounding land surface in the south (Smith, 1980a).

From the distribution of Zechstein sediments, it is clear that the north of the study area was well below the level of the Zechstein Sea, whereas the south was shallower, and included small islands, or palaeohighs, of Carboniferous sediments, the largest of which was the Cleveland High. Another Carboniferous palaeohigh, centered on Billingham, has been described by Napier (1948), Wood (1950) and Raymond (1960). This palaeohigh had a significant affect on Zechstein sedimentation, especially that of early cycles, with all of the Raisby and Ford Formations being cut out on its flanks, and overlapped by progressively younger Zechstein sediments (Raymond, 1960, figure 2). In the Billingham area, the flanks of the palaeohigh dip generally eastwards at between 5° and 18°, with its culmination centered on Billingham (Wood, 1950; Raymond, 1960). Wood (1950) inferred the palaeohigh to represent a discontinuous ridge (an erosional scarp) with a N-S to NE-SW trending axis, and margins sloping off to the east and west (Fig. 2.1). However, Raymond (1960) reinterpreted the structure as a plateau extending from Billingham westwards towards Gt. Stainton (NZ 338, 220), with an eastwards-dipping margin in the Billingham area. The margin of the plateau, he suggests, may have been purely erosional, or an eroded, fault-bound block. This early work was confirmed by Goodall (1987) who shows (from unpublished seismic data), that the Carboniferous surface in this area was broken up into a series of en echelon, normal fault-bounded, NNE-SSW orientated horsts and grabens approximately 10km in size, which demarcated a number of small sub-basins. Goodall (1987, fig. 1.11) figures three main palaeohighs within the area covered by seismic data; one of a NNE-SSW orientation west of the Billingham area, another between Gt. Stainton and Sedgfield and a third slightly to the east of Newton Aycliffe (Fig. 2.1). Goodall (1987) also recognises the NE-SW orientated palaeohigh in the Billingham area identified by Napier (1948), Wood (1950) and Raymond (1960) (Fig. 2.1). The position of the Billingham

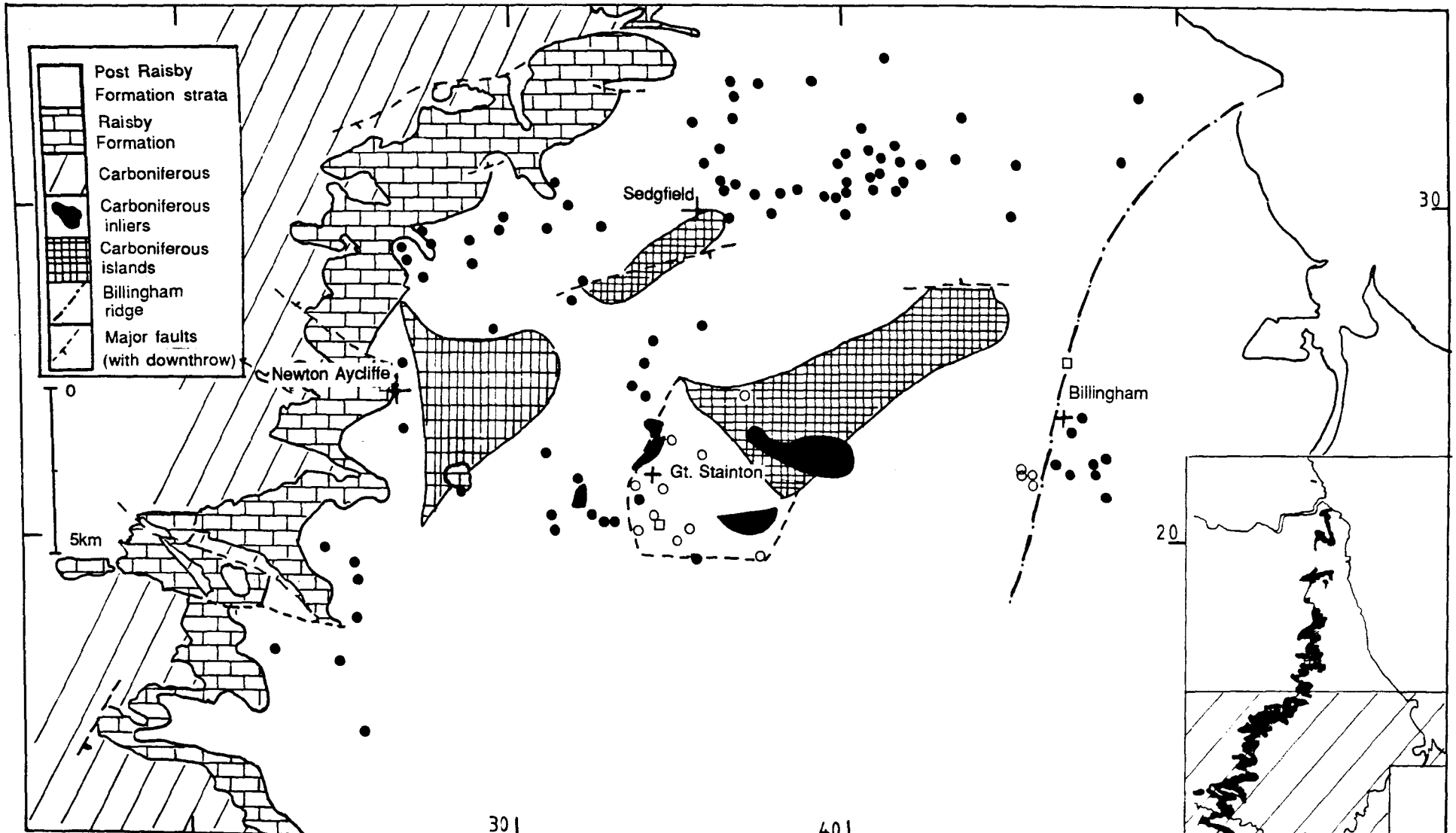

Fig. 2.1. Map of the southern part of the study area, showing the Carboniferous palaeohighs identified seismically by Goodall (1987), and the position of the Billingham Ridge (Wood, 1950 & Raymond, 1960). The locations of boreholes which proved substantial Raisby Formation (●), thinned Raisby Formation (□), and no Raisby Formation (○) are also plotted. Borehole data from Mills and Hull (1976), Goodall (1987), and unpublished data courtesy

palaeohigh, and those identified seismically by Goodall (1987), in general agree well with borehole data for present, absent, and thin Raisby Formation in that area (Fig. 2.1). This borehole data also suggests that the central and largest palaeohigh extended further southwest, at least during deposition of the Raisby Formation (Fig. 2.1). The most westerly palaeohigh identified by Goodall, cuts across an inlier of Raisby Formation on its southern margin (Fig. 2.1), suggesting the margins of that palaeohigh changed with time. These palaeohighs had a significant influence on the deposition of the Edlington Formation (Goodall, 1987), so a similar influence on the sedimentation of the Raisby Formation is likely. Goodall (1987) suggests that the palaeohighs were transgressed prior to the end of Zechstein cycle 1 by collapse of bounding normal faults. Smith and Moore (1973) also identify a 'buried hill' of Carboniferous rocks at the site of the Hurworth Place borehole (NZ 2902, 0953).

The uppermost surface of the Carboniferous Coal Measures has been diagenetically reddened by *in situ* oxidation of pyrite and siderite, and the introduction of iron oxides along joints and into pore spaces (Anderson and Dunham, 1953). The reddening, in general, extends to a depth of 7.6m, although occasionally reaches up to 15.2m below the Permo-Carboniferous unconformity (Anderson and Dunham, 1953). In the north of the study area, the land surface of exposed Carboniferous rocks was fissured owing to desiccation. Basal Permian Sands fill these fissures, forming neptunean dykes commonly extending for up to 0.5m below the Permo-Carboniferous unconformity (Magraw, 1975; Gibbons, 1978).

2.1.3. Basal Permian Sands and Breccias.

Between the Zechstein marine sediments (most commonly the Marl Slate) and the eroded Carboniferous surface, sandstones and/or breccias of very variable thickness are common (Fig. 2.2). The sands, partially equivalent to the Rotliegendes of the Southern North Sea Basin are locally known as the Yellow Sands or Basal Permian Sands. They are thought to be almost exclusively of Lower Permian age (Smith and Francis, 1967), although complete absence of fossils hinders precise dating. Laterally equivalent to, although spatially distinct from these sands are the Basal Permian Breccias, in general considerably thinner than the sands.

The Basal Permian Sands, which are thickest in the north and center of the study area, are generally considered to be of aeolian origin, deposited in an arid, desert environment (Smith, 1970a; Steel, 1981; Yardley, 1984). Pryor (1971) however, suggested that the sands were deposited subaqueously as tidal current ridges, and Magraw (1975) invokes deposition as beach dunes on a series of NE-SW aligned coastlines. The sands themselves are mineralogically mature, with greater than 85% quartz and quartzite, less than 5% feldspar, less than 5% rock fragments, and negligible mica (Smith and Francis, 1967; Smith, 1980; Smith, 1984). The sands are also texturally mature, with grain sizes in the range of 0.063mm-1mm (Magraw, 1975), which are sometimes unimodally distributed, but most

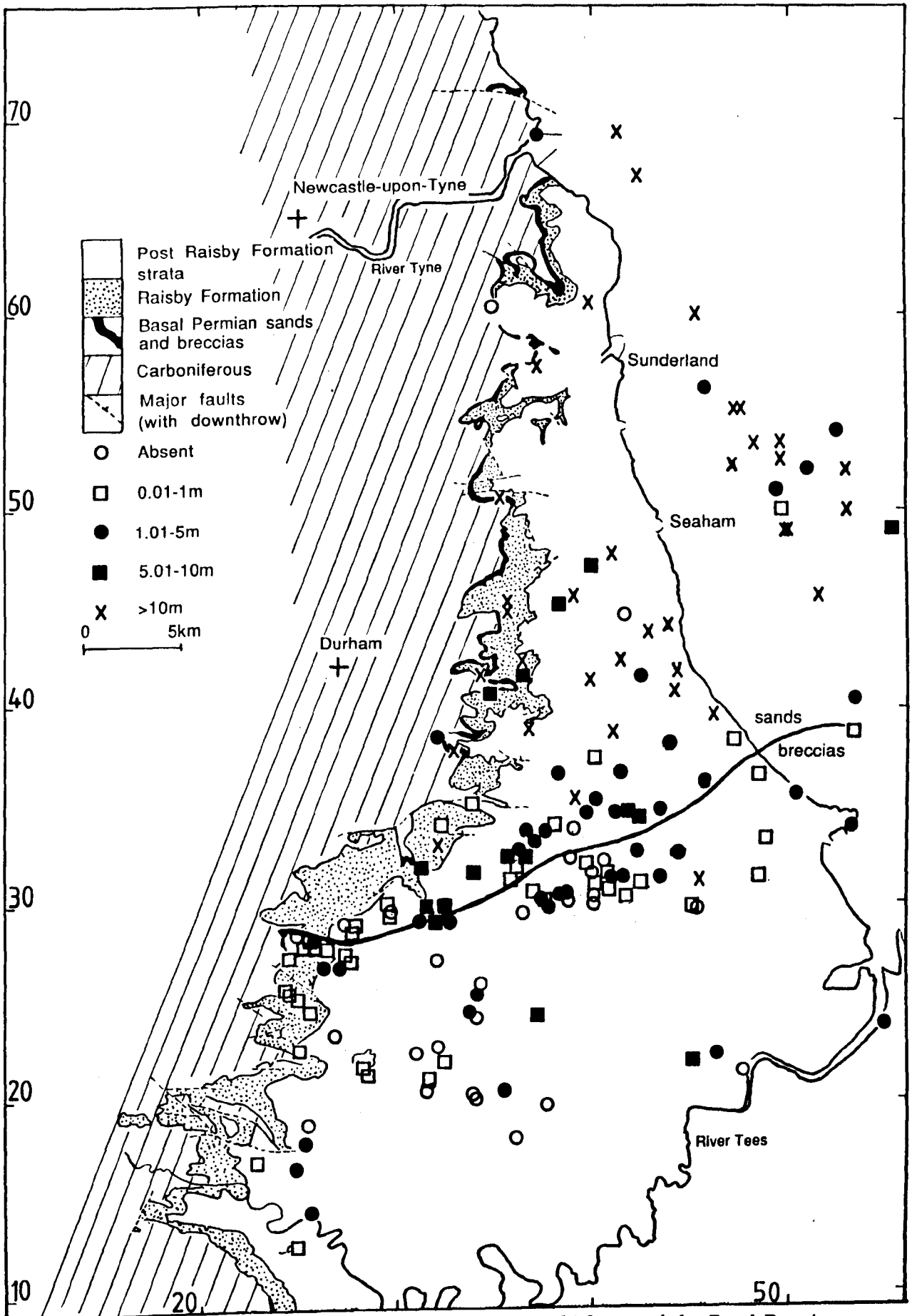

Fig. 2.2. Map of the study area, showing the variation in thickness of the Basal Permian Sands and Breccias, and the division between the area dominated by sands, and that dominated by breccias (after Smith, 1990). Data from this study, Magraw *et al.*, (1963), Smith and Francis (1967), Mills and Hull (1976), Goodall (1987), and unpublished borehole data courtesy of D.B. Smith. The area dominated by breccias was of higher elevation than that dominated by sands, owing to a Dinantian and Namurian substrate, which was more resistant to erosion.

commonly bimodal (Smith, 1970a). Analysis of cumulative percentage curves for samples from one borehole, suggests possibly a dual sorting agency (i.e., aeolian and fluvial) (Magraw, 1975). Using heavy mineral analysis, Hodge (1932 [in: Smith and Francis, 1967]) concluded that the sands were derived in part from local Carboniferous rocks and in part from a source to the north, where sandstones, granitic and metamorphic rocks were undergoing erosion. The sand grains themselves are well rounded (commonly 'millet seed' grains) and frosted, with microscopic surface textures indicative of an aeolian depositional environment (Krinsley and Smith, 1981). At outcrop, the sands are largely unlithified, or cemented by coarse, poikilitic calcite. Most samples analysed during this study show evidence for minimal compaction or diagenetic alteration. This suggests the former presence of an early diagenetic cement which has since been dissolved, such as gypsum/anhydrite or calcite. Smith (1984) suggests that sulphates may have formed early cements from evidence of red Basal Permian Sands within an offshore borehole.

The Basal Permian Breccias are concentrated in the south of the study area (Fig. 2.2), where they are patchily distributed, covering 1/3 to 2/3 of the former land surface (Smith, 1970a). They are in general between 0.6 and 1.8m thick, exceptionally reaching 13.4m (Smith, 1970a). The breccias comprise angular to subangular, poorly sorted, centimetre-sized rock fragments in a matrix of poorly sorted, frosted sand grains with occasional lenses of clay and dolomitic marl (Smith, 1970a; Mills and Hull, 1976). Some of the clasts are of dreikanter form, with a desert varnish (Smith and Francis, 1967). Most rock fragments are Carboniferous limestone (Dinantian/Namurian) with subordinate sandstone and shale (Smith, 1970a). Smith (1980a) suggests that the breccias represent a desert lag, or piedmont gravels with thin sandstone horizons being the relics of small migrating dunes. From an exposure at Cleasby cutting (NZ 246, 124), Mills and Hull (1976, fig. 15) demonstrate that the 1.1m of Basal Permian Breccias infill a hollow in the top of the Carboniferous, and were deposited in a watercourse. Bell *et al.*, (1979) suggest that the Basal Permian Breccia exposed at Middridge Quarry was deposited rapidly from periodic sheet floods across the desert surface, and Goodall (1987) recognizes small alluvial fans of Basal Permian Breccias overlying the Carboniferous surface in the Teesside area.

It is commonly suggested that the Basal Permian Sands form a number of elongate, ENE-WSW orientated ridges (8-9 [Yardley, 1984]; 11 [Smith, 1980a]), 1-2km wide and up to 60m high in north Durham. They are separated by parallel belts where the sands are thin or absent (Smith, 1980a). These elongate ridges are interpreted as the variably-preserved relics of primary aeolian bedforms, possibly transverse draas (Yardley, 1984) or seif dunes (Smith, 1970a; Magraw, 1975), which developed under a prevailing northeasterley wind. In order for the primary dune features to be preserved (albeit eroded to possibly one third of their original height), Smith (1970a & 1979) has invoked a very rapid marine transgression of the Zechstein basin (the 'instant Zechstein' hypothesis) (1.4.2). However, a number of authors have suggested that the Basal Permian Sands partly or wholly occupy hollows or gullies cut

into the otherwise peneplained Carboniferous surface (Lebour, 1886; Armstrong and Price, 1954; Hopkins, 1954 (in: Magraw, 1975); Woolacott, 1912; Trechmann, 1921 & 1931; Clarke, 1962; Gibbons, 1978; Magraw, 1978). This has been recorded with regard to the Basal Permian Breccias at Cleasby (Mills and Hull, 1976, fig. 15). Magraw (1978) further documents two offshore boreholes (D8 [NZ 4966, 5257] and D8a [NZ 4969, 5257]), positioned 30m apart, between which the base of the Carboniferous surface dropped in elevation by 14.1m, and the thickness of the Basal Permian Sands correspondingly increased by 11.8m. Clarke (1962) documents a similar Basal Permian Sand-filled gully of a ENE-WSW orientation between Mainsforth and Thrislington, south Durham, which Magraw (1978) suggests may be of wadi origin. It is also likely that thick Basal Permian Sands exposed at Quarrington Quarry occupy hollows in the Coal Measures surface (J. Bell, *pers comm.*, 1987). Therefore, it is probable that the recorded thickness of Basal Permian Sands is a combination of relic primary relief, and occupancy of erosional hollows in the Coal Measures surface.

The upper surface of the Basal Permian Sands and, occasionally, that of the Basal Permian Breccias may be planar laminated, with a sparse brackish marine fauna indicative of reworking during the Zechstein transgression (Trechmann, 1921; Smith, 1970a; Bell *et al.*, 1979). However, the upper surface of the Basal Permian Sands was not uniformly flat, as evidenced by the pinching out of Marl Slate and the basal Raisby Formation on the margins of mounds or dunes (Fig. 2.3a). However, much of this attenuation may be due to differential compaction of the semi-lithified Raisby Formation carbonate muds over lithified Basal Permian Sands (which are minimally compacted), and both Marl Slate and Raisby Formation may be continuous over the relic dunes (Fig. 2.3b). However, the relic dunes may have played a minor role in determining the nature of succeeding carbonate sedimentation.

Thus, two facies of Lower Permian continental clastics underlie the Marl Slate and/or Raisby Formation in northeast England. The breccias developed in the south of the area on an eroded Carboniferous surface, probably an upland setting, whereas the sands are thickest in the north and east of the study area and were deposited on a lower relief surface with numerous erosional gullies and hollows. Only the thickest Basal Permian Sands retained some positive relief (on the scale of a few metres) above the eroded Carboniferous surface, and had limited influence over sedimentation of the Marl Slate and Raisby Formation. The influence is mainly by lower Raisby Formation beds being cut out laterally by onlap onto the relic dunes. Slumping off the margins of dunes was suggested by Magraw (1975 & 1978) to be very important with regard to resedimentation of the Raisby Formation in Durham, although there is no evidence for this.

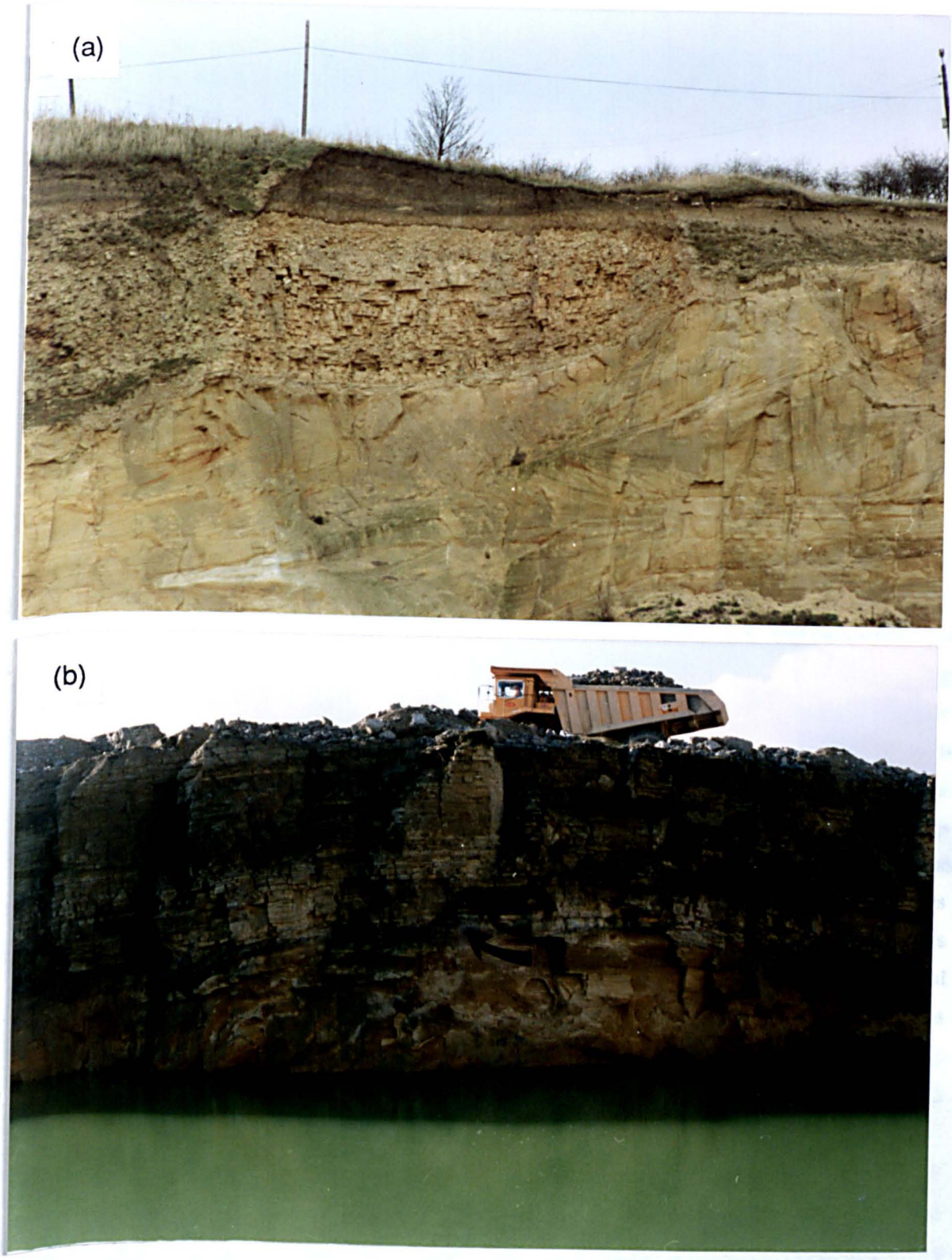

Fig. 2.3. Outcrop photographs of Basal Permian Sands and lowest Raisby Formation; (a) Crime Rigg Quarry, (b) Raisby Quarry. In (a), the basal Raisby Formation is being cut out on the margins of a relic 'dune'; much of this is probably due to differential compaction, although the Marl Slate is absent. By contrast, in (b), both the Marl Slate (arrowed) and lower Raisby Formation are continuous over a small dune of Basal Permian Sands, whose axis trends WSW - ENE.

2.1.4. Deposition of the Marl Slate.

The Marl Slate Formation (or Kupferschiefer in continental Europe and the North Sea basin) was first defined, in northeast England, by Sedgwick (1835). It is a thin, silty, sapropelic dolostone or limestone, the first truly marine deposit of the Zechstein Sea. It can be traced almost uninterrupted for 400,000km^2 through eastern England, the Northern and Southern Permian basins (although locally absent over the Mid North Sea High), and eastwards into Denmark, Germany and Poland. The Marl Slate is characterized both by being organic-rich, and containing high concentrations of stratabound Cu-Fe-Pb-Zn sulphides, commonly considered to be syngenetic (Sedgwick, 1835), and precipitated as a part of the biogeochemical cycle during sedimentation of the Marl Slate (Turner and Magaritz, 1986). The Marl Slate unconformably overlies Carboniferous sediments or Basal Permian Sands/Breccias, and grades upwards into first cycle carbonates. It is present throughout most of the study area, although locally absent in the south (Fig. 2.4).

Turner and Magaritz (1986) define three lithotypes of Marl Slate from a borehole offshore northeast England (VT8 [NZ 4862 5095]), also recognised in core during this study, although with difficulty from outcrop. As defined by Turner and Magaritz (1986), the silty sapropelic dolostone (sapropel) lithotype characteristically contains 8-10% organic carbon and 25-30% quartz. It is finely laminated, on a 60-80μm scale, and comprises alternating carbonate- and organic-rich laminae. The laminite lithotype contains less than 6% organic carbon, approximately 10% quartz, and has a higher percentage of carbonate. This lithotype is again laminated, although laminae are farther apart and more distinct than those of the sapropel lithotype. The massive finely crystalline dolostone lithotype contains generally less than 3% organic carbon and slightly more carbonate than the laminite lithotype. Organic matter is unevenly distributed as discontinuous laminae and flakes (Turner and Magaritz, 1986). In this study of the Raisby Formation, and most previous works, repeated cycles of lithotypes, from sapropel to laminite to dolostone, or a general trend for an upward decrease in the amount of organic carbon and increase in carbonate can be recognized (Fig. 2.5). In nearly all cases, the initial Marl Slate is a sapropel, which passes up into laminites and dolostones in various proportions, with thinner or no sapropel horizons (Fig. 2.5).

The Marl Slate contains an abundant, well-preserved biota dominated by nektonic fishes, with land and marine plants, foraminifera and a species of nautiloid (Smith, 1980b). The excellent preservation of fossils, and general absence of a sessile benthonic fauna or bioturbation, indicates stagnant bottom conditions. Pettigrew (1985) recognizes three ecological assemblages; offshore, nearshore and derived terrestrial within the Marl Slate of Co. Durham. The offshore assemblage is characterized by a nektonic fauna (dominantly palaeoniscid fishes) which lived in upper, oxic levels of the Zechstein Sea. The nearshore assemblage (less common) contains a more varied fish fauna, some of which lived in lower

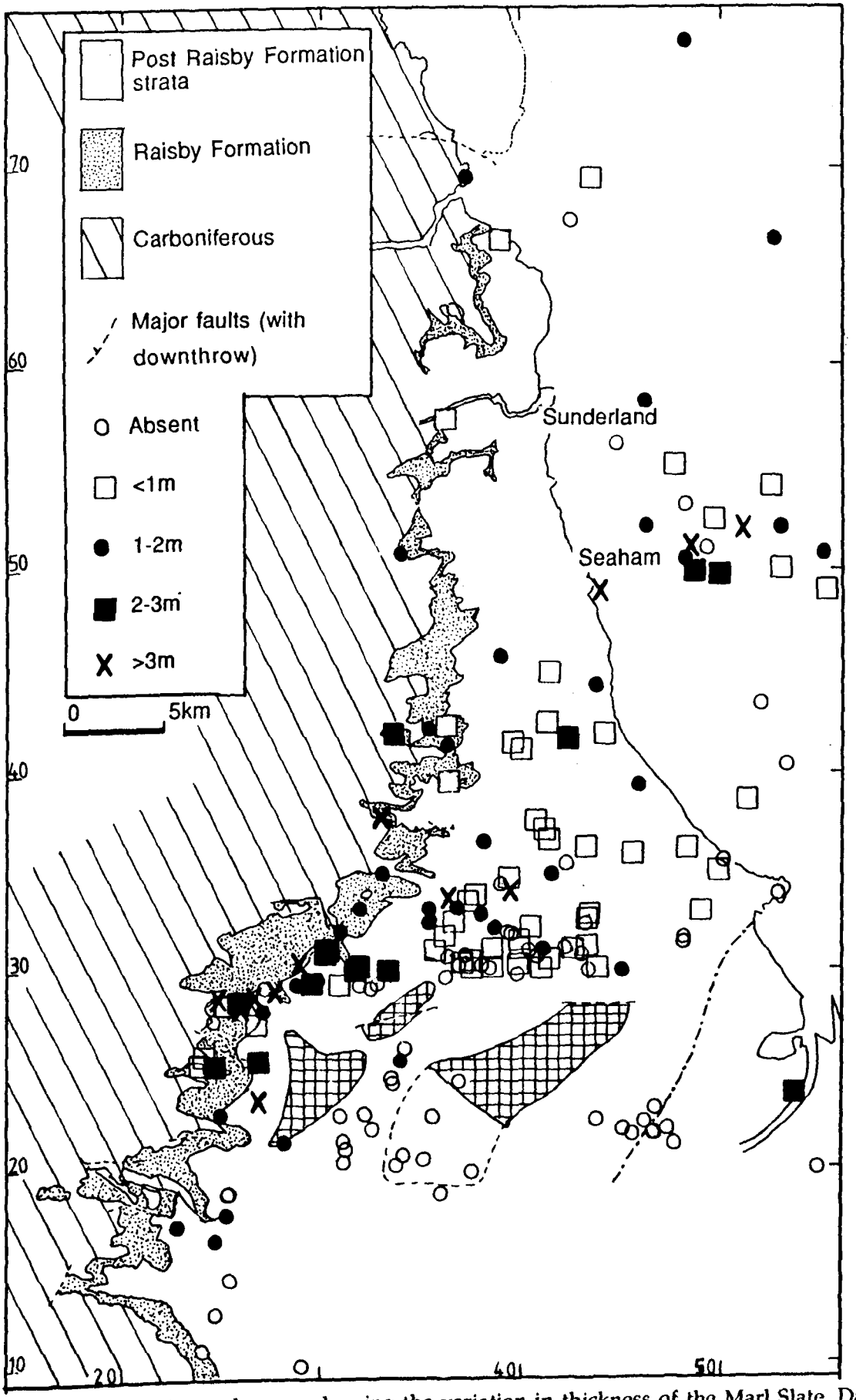

Fig. 2.4. Map of the study area, showing the variation in thickness of the Marl Slate. Data from this study, Hirst and Dunham (1963), Magraw *et al.*, (1963), Smith and Francis (1967), Mills and Hull (1976), Gibbons, (1978), Goodall (1987), and unpublished borehole data courtesy of D.B. Smith. Palaeohighs are shown in cross-hatched shading

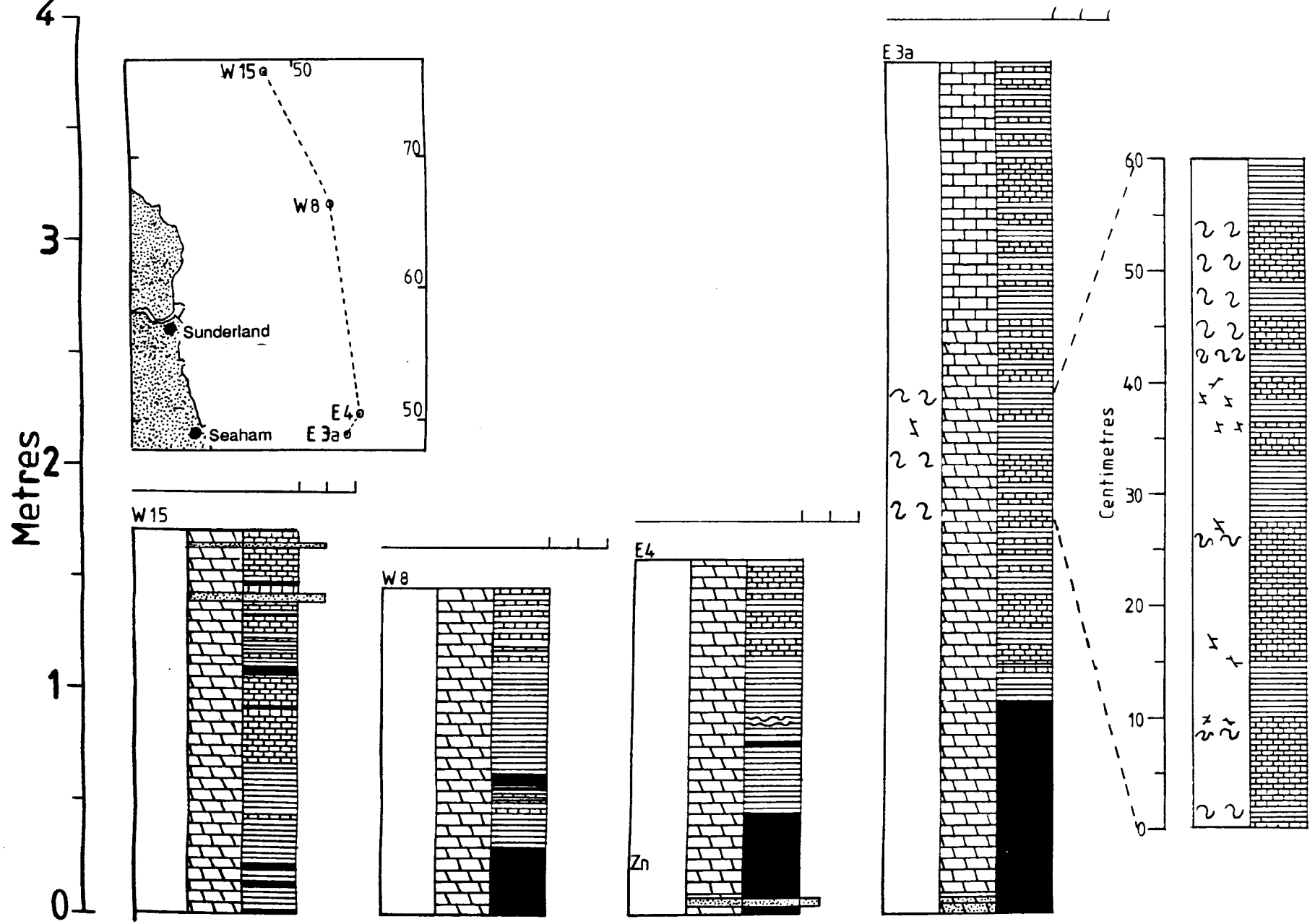

Fig. 2.5. Logs of the Marl Slate from four offshore boreholes examined during this study. Details of slumping and microfaults within borehole E3a are also illustrated. For legend see appendix XII.

levels of the Zechstein Sea and fed on shelly invertebrates. Rare horizons containing a sessile benthonic fauna including bivalves, brachiopods, bryozoans, foraminifers, and ostracodes, are recorded within unlaminated Marl Slate in this nearshore position (i.e., Middridge Quarry (NZ 249, 252) [Bell *et al.*, 1979]). The terrestrial assemblage includes land plants and reptiles derived from the coast marginal to the Zechstein Sea, or small islands of Carboniferous rocks. This assemblage is only recorded from south Durham (Pettigrew, 1985).

At a number of localities at outcrop and in core, the Marl Slate is disturbed by small slumps, synsedimentary faults, and neptunean dykes. The slumps are represented as contorted laminites of a very small scale (centimetres in thickness). The throws of synsedimentary faults are likewise small (millimetres) and most recorded in this study were indicative of extensional movement. At Frenchmans Bay (NZ 3890, 6615), the Marl Slate, as well as the basal metre of the Raisby Formation, is cut be three thin neptunean dykes of Basal Permian Sands, intruded along joints of a consistent orientation. Gibbons (1978) records neptunean dykes and sills within the Marl Slate from borehole S1 [NZ 3799, 5777] (onshore Durham). He relates dyke intrusion to fracturing of the Marl Slate allowing overpressurized fluids within the Basal Permian Sands to escape through the otherwise impermeable Marl Slate seal. The dykes at Frenchmans Bay, are a few metres below a major slide plane, which suggests that large scale resedimentation triggered the fracturing. Likewise, fracturing is common within the Marl Slate directly underlying the slide plane at Claxheugh Rock (NZ 363, 575), although not associated with sandstone dyke intrusion. Borehole S1 which contains neptunean dykes and sills is only 1.5km east of Claxheugh Rock, and is thus probably related to the same episode of resedimentation.

Thin redistributed beds of Basal Permian Sands are also common within the Marl Slate, either concentrated within its basal few centimetres adjacent to the Basal Permian Sands, or as discrete lenses throughout. Such lenses, centimetres in thickness, were recorded within the Marl Slate at Quarrington Quarry (NZ 327, 379) where they were directly related to the margins of ridges of Basal Permian Sands. An extreme development of these sands has been described by Magraw (1978, plate 4) from offshore borehole W2 (NZ 4405 7385), whereby Marl Slate and reworked Basal Permian Sands alternate over a vertical distance of 2.4m. In this case, the sand lenses were probably derived by avalanching down the margins of sand ridges from higher levels, where shallower, more energetic water conditions prevailed. The presence of these current-deposited sands within basal sapropels shows that the environment during sapropel deposition was not completely stagnant.

The Marl Slate thickens westwards in the study area, from the basin floor, where it is commonly less than 0.8m thick, up to a maximum of 6m in a belt a few kilometres wide, some distance from the inferred shoreline (Smith, 1980b), in the Ferryhill, Quarrington and Middridge areas. The Marl Slate is widely absent in the south of the area (Fig. 2.4), and has not been recorded south of the River Tees (Mills and Hull, 1976). Turner *et al.*, (1978, fig. 1)

have constructed a Marl Slate isopach map which defines NE-SW trending areas, along the axes of which the Marl Slate is thin (less than 0.5m), and between which it is thicker. This parallels the trends of presumed buried ridges of Basal Permian Sands. However, no such trends can be defined from figure 2.4, although constructed from considerably more data points. Thickness variations of the Marl Slate are also accompanied by a change in the dominant lithotypes, from basinal Marl Slate which is mainly sapropelic (Sweeney *et al.*, 1987), to a shallower-water Marl Slate (that outcrops in Co. Durham), which is thicker, with a more extensive development of the laminite and dolostone lithotypes. In the shallower-water areas, the thicknesses of individual laminae also tends to be greater (Smith, 1980b).

Early work suggested that the Marl Slate was deposited in an estuarine (Lebour, 1905) or lagoonal environment (Hirst and Dunham, 1963). However, it is now well established that the Marl Slate sea was relatively deep, greater than 200m in the basin (Smith, 1970a), although probably less in the area of present day outcrop. From the evidence of high organic carbon contents and palaeoecology, it is generally considered that the Marl Slate was deposited in a stratified sea, the lower part of which was at least partly anoxic. Its high organic content appears to be the by-product of high phytoplankton productivity in oxic surface waters, which may well have been seasonal as blooms. From these seasonal layers, Oelsner (1959 [In: Turner and Magaritz, 1986]) suggests that the Marl Slate was deposited in less than 20,000yrs.

In marginal, shallower water areas, the Marl Slate was either not deposited and is represented by time-equivalent normal Raisby Formation lithologies, or was deposited with intercalations of normal marine, fossiliferous carbonates (Bell *et al.*, 1979). This suggests that the oxic-anoxic interface within the then stratified Zechstein Sea was relatively static, at a given depth, and so the presence or absence of the Marl Slate can be used as a crude palaeo-bathymetric indicator. This trend is further borne out by the observation that where the Marl Slate is absent, the Raisby Formation is of a relatively shallow water facies. A shelly coquina at the base of boreholes W.O.17 (NZ 3253, 2191), W.O.18 (NZ 3121, 2085), and the Hurworth Place borehole (NZ 2902, 0953) (Fig. 2.9.a), time equivalent to the Marl Slate, is analogous to the fossiliferous 'Mutterfloz' (Thuringia, West Germany), present on the slopes of palaeohighs where the Kupferschiefer is absent (Paul, 1986a). The Marl Slate is absent from the Yorkshire Province at outcrop (only recorded in the subsurface), where the carbonates were deposited in much shallower waters than those of the Raisby Formation (cf. Harwood, 1981; Kaldi, 1986a). Smith (in Bell *et al.*, 1979) suggests that the Marl Slate dies out at approximately 15-20km from the palaeo-shoreline of the Zechstein Sea in Durham.

Marl Slate thickness data defines three distinct areas of deposition in the southern part of the study area (Fig. 2.4). In the south-central part of the study area the Marl Slate is widely absent. This passes westwards into a NE-SW trending zone in which the Marl Slate is thickest (in general greater than 2m), and northwards into a central area in which the Marl

Slate is of variable thickness, in general less than 2m. As the Marl Slate is present, even in the center of the Zechstein Basin, the area in which it is widely absent is interpreted to reflect the position of palaeohighs and islands of Carboniferous rocks, where the sea floor was too shallow for the Marl Slate to be deposited (i.e., above the oxic-anoxic interface) or emergent. This area corresponds to that in which Carboniferous palaeohighs were identified by Goodall (1987) (Fig. 2.7), and where the Raisby Formation is of a shallow water facies (Fig. 2.7.). Where the Marl Slate is thickest, in the southwest of the study area, the sea floor was clearly below the oxic-anoxic interface and, accordingly, the Marl Slate is overlain by relatively deeper water carbonates (Fig. 2.7). Thus, from east to west in the southernmost part of the study area, an abrupt thickening of the Marl Slate is recorded, suggesting a fairly abrupt deepening of the Zechstein Sea (i.e., lowering of elevation of the sea floor). This is in the opposite sense to the regional, E-W palaeoslope, although explicable by the presence of Carboniferous palaeohighs and islands. The eastwards thinning of the Marl Slate from generally greater than 2m to less than 2m in the central part of the study area is interpreted to reflect a progressive deepening of the sea, in accordance with the regional palaeoslope. There is possibly an overprint on this data by isolated submarine highs or emergent islands of Basal Permian Sands. A crude, although by no means universal inverse correlation has been suggested between thickness of the Basal Permian Sands and thickness of the Marl Slate in the study area (Turner *et al.*, 1978). Gibbons (1978) suggests that the Marl Slate is commonly atypically thin or absent where Basal Permian Sands are greater than 30m thick.

The vertical contact of the Marl Slate with the Raisby Formation is the source of considerable controversy. Hirst and Dunham (1963) took the top of the Marl Slate as the top of the last bituminous (sapropel?) layer, whereas other workers (Kirkby, 1867; Magraw, 1975) have recognized a gradational contact between the Marl Slate and Raisby Formation via the 'passage beds'. The lower part of the passage beds has also been termed the 'transition zone' (Sweeney *et al.*, 1987). However, Smith *et al.*, (1986) have suggested that a gradational unit be disregarded, and the top of the Marl Slate defined at the top of the uppermost finely laminated (laminite) unit (Fig. 2.6), a definition which is adopted in this thesis. However, there is a gradual change in the composition of the Marl Slate, commonly represented by a decrease in the thickness of sapropel units in favour of laminites, which in turn grade up into Marl Slate dominated by dolostones (Fig. 2.5).

Despite the large number of papers written on the Marl Slate, few if any suggest why the Zechstein Sea became stratified, with an anoxic lower layer, almost immediately after it had formed. This lack of understanding, in turn, hinders any interpretation of conditions which led to the change from deposition of Marl Slate to Raisby Formation carbonates.

The three lithotypes which comprise the Marl Slate represent, from sapropel to laminite to dolostone, a relative decrease in the rate of input and/or preservation of organic matter and/or an increase in the rate of carbonate sedimentation. As both sapropels and

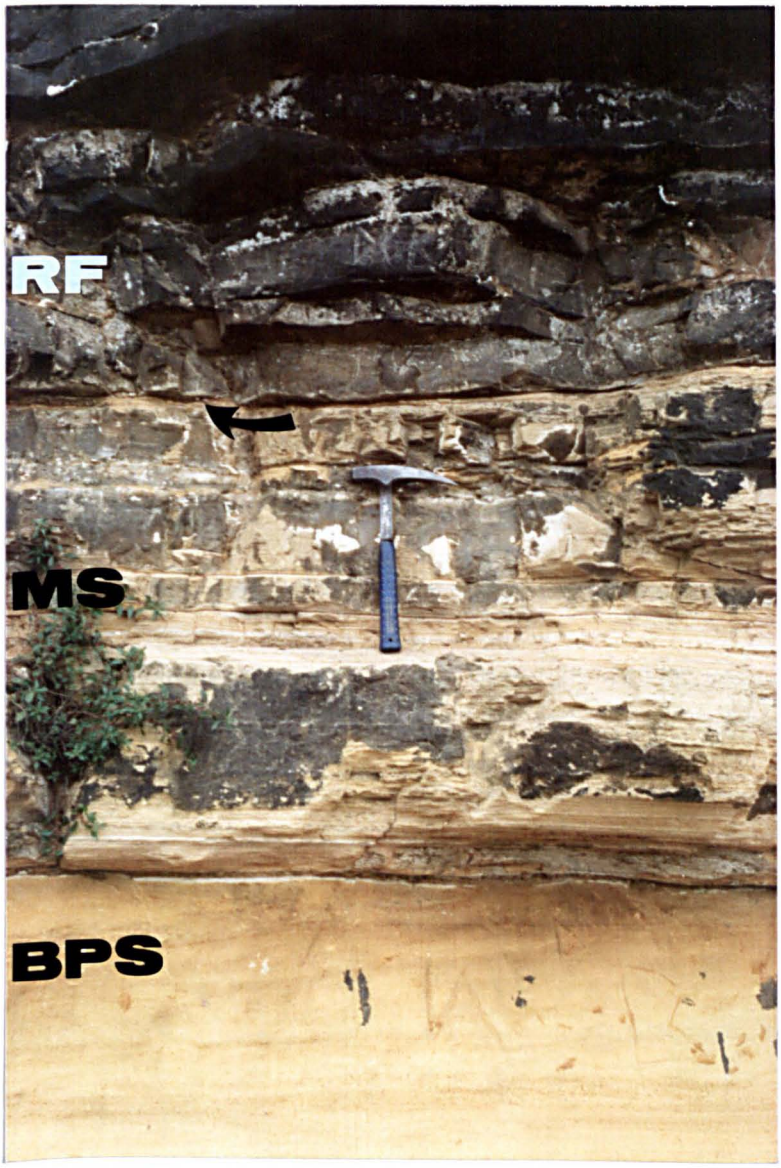

Fig. 2.6 Outcrop photograph of the contact of Basal Permian Sands (BPS) with Marl Slate (MS), which is overlain by the Raisby Formation (RF), Claxheugh Rock. The precise contact of Marl Slate with Raisby Formation at this locality is demarcated by a thin brown clay (arrowed). Hammer is 32cm long.

laminites contain preserved ?annual layers, thicker within the laminites than sapropels, this suggests that the vertical and lateral transition from sapropel to laminite represents an increase in the rate of deposition of carbonate over that of organic matter (i.e., any one area was closer to the locus of carbonate production [shallow waters]). The dolostone horizons are thus interpreted to reflect uniformly high rates of carbonate sedimentation, whereby organic matter was highly diluted. Thus, the rate of carbonate input at any one locality was a factor of proximity to shallow waters where carbonate production (by biological and abiological precipitation) was at a maximum. The variation in proximity to shallow waters at any one locality was, in turn, a product of fluctuation in the level of the Zechstein Sea, which may have been climatically controlled (Sweeney *et al.*, 1987). That the initial Marl Slate is nearly always a sapropel, could suggest that sea level was initially higher than during the deposition of succeeding Marl Slate. Another factor may have been that it took some time, after the initial Zechstein transgression, for carbonate production on the shelves to become established, and so sapropelic Marl Slate was initially deposited. This model readily explains a number of key features of the Marl Slate;

1. The basinal Marl Slate is almost entirely sapropelic, as it is distant from the major source of carbonate (shallow water),
2. The Marl Slate becomes thicker shorewards, reflecting more rapid carbonate sedimentation rates. Accordingly, it is dominated by laminites and dolostones,
3. Fossiliferous horizons within laminated Marl Slate represent cessation of anoxic bottom water conditions (Bell *et al.*, 1979), which suggest a lower sea level and lower height of the oxic-anoxic boundary.

Stratification within the Zechstein Sea was most likely the result of establishment of a mid-water halocline, restricting vertical water movement, eventually leading to anoxity in lower water layers owing to oxygen consumption by decomposing organic matter. Initial high bioproductivity within the newly-formed Zechstein Sea may have facilitated rapid eutrophication (Smith, 1985). Haloclines in the Black Sea result from the intrusion of dense, saline water into the basin across a shallow sill (Degens and Stoffers, 1980). The Zechstein Sea was connected to the Boreal Ocean via a narrow, shallow sill (1.4.2), and a similar mechanism may well have acted here. The very early onset of stratification can be accounted for if a considerable quantity of the inflowing water from the Boreal Ocean was saline. In this model, the transition from Marl Slate to Raisby Formation deposition, probably resulted from destruction of the halocline, eliminating anoxic bottom water conditions, accompanying a much freer interchange with the Boreal Ocean. An improvement in circulation of the ocean waters, in turn, probably resulted from a eustatic sea level rise, thus improving water movement over the sill (Smith, 1980a). Such a sea level rise at the end of Marl Slate deposition is suggested by Taylor and Coulter (1975) to have been responsible for the overlap of the Marl Slate by first cycle marine carbonates towards the basin margins.

2.2.1. Sedimentology and correlation of the Ford Formation.

The Ford Formation at outcrop and in core in northeast England is divided into three facies; lagoonal, reef, and fore-reef talus and basin (Smith, 1970a).

2.2.1.1. Lagoonal facies.

Over most of its outcrop and subcrop onshore, the Raisby Formation is overlain by the lagoonal facies of the Ford Formation. Carbonates of this facies, which are almost exclusively dolostones, are up to 91m thick, and form a belt greater than 24km wide in south Durham (Smith, 1970a). The westerly limit of the lagoonal facies is not exposed in south Durham, and the amount of lagoonal facies which is exposed decreases northwards along the Ford Formation erosional edge (Fig. 1.1). The lagoonal facies lies to the west of the Ford Formation reef; sedimentation within the lagoon was largely controlled by reef development (Smith and Francis, 1967). Smith (1980a) distinguishes two subfacies within Ford Formation lagoonal deposits; a 3 to 10km wide belt immediately to the west of the reef, comprising cross-laminated oolitic dolostones with a sparse fauna of small gastropods, bivalves, and locally abundant foraminifers. This passes westwards into a finer-grained dolostone with characteristic 'felted' calcium sulphate replacement texture, and locally abundant burrows. Although most lagoonal sediments accumulated in fairly shallow agitated waters, only during the latter stages of development of the reef, when it built up close to sea level, did the area to the west of the reef become a truly lagoonal environment (i.e., with a restricted connection to the Zechstein Sea).

2.2.1.2. Reef facies.

The growth of a large, shelf-edge, bryozoan-algal reef is a prominent feature of the deposition of the Ford Formation. As with the lagoonal facies, the Ford Formation reef has been almost completely dolomitized, apart from small areas, such as the reef base coquina at Tunstall Hills (NZ 392 545) (Tucker and Hollingworth, 1986). The reef has a generally linear, albeit slightly sinuous outcrop, greater than 30km long although commonly only 400-800m wide (Smith *et al.*, 1986) (Fig. 1.1). It is up to 120m thick, being thickest in the south (Smith, 1981).

Reef growth was established on patchy, early marine-cemented shelly coquinas, and progressed by the baffling action of bryozoans and algae, further aided by early high magnesian calcite and aragonite cementation (Smith, 1980a; Aplin, 1985; Tucker and Hollingworth, 1986). Tucker and Hollingworth (1987) distinguish five sub-facies within the reef; reef-base coquina, reef core, reef flat, fore-reef talus, and backreef with patch reefs, each characterized by a different faunal assemblage. The reef is suggested to have grown along the shelf break provided by the uppermost Raisby Formation, at a distance of 20-30km from the then contemporaneous shoreline, initially in waters 20-50m deep which progressively

shallowed as the reef aggraded towards sea level (Smith, 1981). However, Tucker and Hollingworth (1986) suggest that the reef base coquina at least, was deposited in waters less than 2-3m deep, possibly with periodic emergence. Reef growth probably terminated owing to an increase in seawater salinity, possibly followed by exposure accompanying evaporative drawdown of the Zechstein Sea immediately preceding deposition of the Hartlepool Anhydrite Formation (Smith, 1981; Tucker and Hollingworth, 1986; Hollingworth and Tucker, 1987).

2.2.1.3. Fore-reef talus and basinal facies.

In comparison to the thickness of sediment deposited in the lagoonal and reef environments, that deposited basinwards of the reef is extremely thin. To the east of the reef is a talus deposit comprising allochthonous reef material intermixed with indigenous organisms (Smith, 1980a). The talus deposit, which thins and fines abruptly into the basin, was partly overstepped during reef growth (Smith, 1980b). At distances greater than 5km from the reef front (i.e., from Seaham northwards), Smith (1970a & 1980a) suggests that reef- and reef-talus-equivalent sediments are less than 1-2m thick. Although generally poorly exposed, this unit is seen extensively along the South Shields coastal section between Trow Point (NZ 384, 667) and Frenchmans Bay (NZ 3890, 6615). Smith (1986) has adopted this as the type locality for this facies of the Ford Formation, the Trow Point Bed. At the type locality, the Trow Point Bed comprises oncoids, peloids, and columnar stromatolites up to 60cm thick, which patchily overlie an irregular upper surface of resedimented Raisby Formation carbonates (Smith, 1986). Smith (1986) suggests that this bed is time equivalent to fossiliferous and pisoid-rich horizons at the top of the first cycle carbonates described from the Southern North Sea Basin (Taylor and Colter, 1975), West Germany, and Poland. Smith (1986) concludes that, at the type locality, the Trow Point Bed was deposited on a basin margin slope in quiet, slightly saline, oxic waters at a water depth of 25-100m. If the Trow Point Bed is the equivalent of the Ford Formation, this bed, a maximum of 0.6m thick at the type locality (Smith, 1986), accumulated during the same time as up to 91m of lagoonal sediments and 120m of reef sediments which lay, at the least, only 3 to 5km west.

2.2.2. Contact of the Raisby with Ford Formations.

The contact of the Raisby Formation with lagoonal and reef facies of the Ford Formation is very poorly exposed, and so has been defined mainly from boreholes east of the outcrop of the Raisby Formation in central and south Durham. The contact of Raisby Formation with lagoonal Ford Formation is commonly described as being gradational, via a group of transitional beds 0.9 to 12m thick (Magraw *et al.*, 1963). These transitional beds are characteristically coarse-grained, locally cross-stratified dolostones containing a sparse shelly fauna, characterized by the small lamellibranch *Astartella vallisneriana* (King) (Magraw *et al.*,

1963). Smith and Francis (1967) suggest that the transitional beds reflect a period of progressively decreasing seawater salinity following from more saline conditions in which the uppermost Raisby Formation was deposited.

The contact of the Raisby Formation with the Ford Formation reef facies is even less well exposed. Where seen at Claxheugh Rock (NZ 363, 575) and Down Hill Quarry (NZ 3485, 6012), the base of the reef is strongly erosive, cutting out most or all of the Raisby Formation. This relationship appears to characterize much of the contact in the north of the study area. Where the sub-reef surface is not a slide plane, it may be sharply delineated by the reef base coquina, which Tucker and Hollingworth (1986) hypothesize accumulated on an irregular surface resulting from an episode of regional resedimentation at the end of the deposition of the Raisby Formation. However, such a relationship is not exposed, nor has been encountered in core, and is unlikely to have existed. The contact of a patch reef with the possible top of the Raisby Formation is exposed is at Gilleylaw Plantation Quarry (NZ 376, 537). The base of the patch reef is conformable on well bedded, poorly fossiliferous/unfossiliferous dolostones, which may either be Ford Formation backreef facies or uppermost Raisby Formation. Thus, the boundary between the Raisby and Ford Formations remains poorly defined.

2.3.1. Sedimentology of the Raisby Formation.

Four lithofacies have been delineated within the Raisby Formation;

1. Skeletal wackestone/packstone lithofacies
2. Nodular wackestone/mudstone lithofacies
3. Resedimented wackestone/mudstone lithofacies
4. Resedimented mudstone lithofacies

The boundaries between these lithofacies are gradational, although each is identified by a characteristic suite of textures and structures. Lithofacies 2, 3 and 4 contain resedimented carbonates, but which distinctly change in character between each lithotype. The spatial distribution of the four lithotypes is illustrated in figure 2.7, and recorded thicknesses of the Raisby Formation throughout the study area in figure 2.8.

2.3.2. Skeletal wackestone/packstone lithofacies - Description.

Raisby Formation carbonates belonging to this lithofacies are distinguished on the basis of the type of constituent allochems, presence of sandstone horizons, and the absence of features typical of carbonates belonging to the other lithofacies, especially evidence for resedimentation. The Raisby Formation comprising this lithofacies is mainly between 10m and 20m thick, although it thins, and may disappear over palaeohighs, and thickens to the north and west (Fig. 2.8). This lithofacies has only been recorded from the south of the study area, although Smith (1970a) has described a shelly packstone facies in the Raisby Formation overlying a submarine high at Newbottle (NZ 345 517) (2.1.2.). In the southern part of the study area, islands of Carboniferous rocks were common, emergent during all, or part of deposition of the Raisby and Ford Formations (Fig. 2.1). The Raisby Formation is absent, or atypically thin over these palaeohighs, as is the Marl Slate and, commonly, only thin Basal Permian Sands/Breccias are present (Figs. 2.1, 2.2 & 2.4). Raisby Formation carbonates deposited on the flanks of these islands, or over submarine highs, have developed the skeletal wackestone/packstone lithofacies. These areas, however, are very poorly exposed, and known mainly from boreholes. The scarcity of examples of this lithofacies, albeit probably widespread, mitigates against a discussion of its general characteristics, in favour of detailed analysis of the few examples recorded. All known examples of this lithofacies have been completely dolomitized and, commonly, extensively replaced by sulphates.

Most carbonates belonging to this lithofacies comprise skeletal wackestones and packstones. The fauna is dominated by abundant, broken bryozoan fronds, shell and echinoderm fragments, and relatively large, articulated foraminifers (Fig. 3.3a) and ostracodes. Plant fragments are also locally abundant. Skeletal fragments are commonly distinguishable at both outcrop and in core owing to their selective replacement by sulphates (now open or calcite-cemented pores).

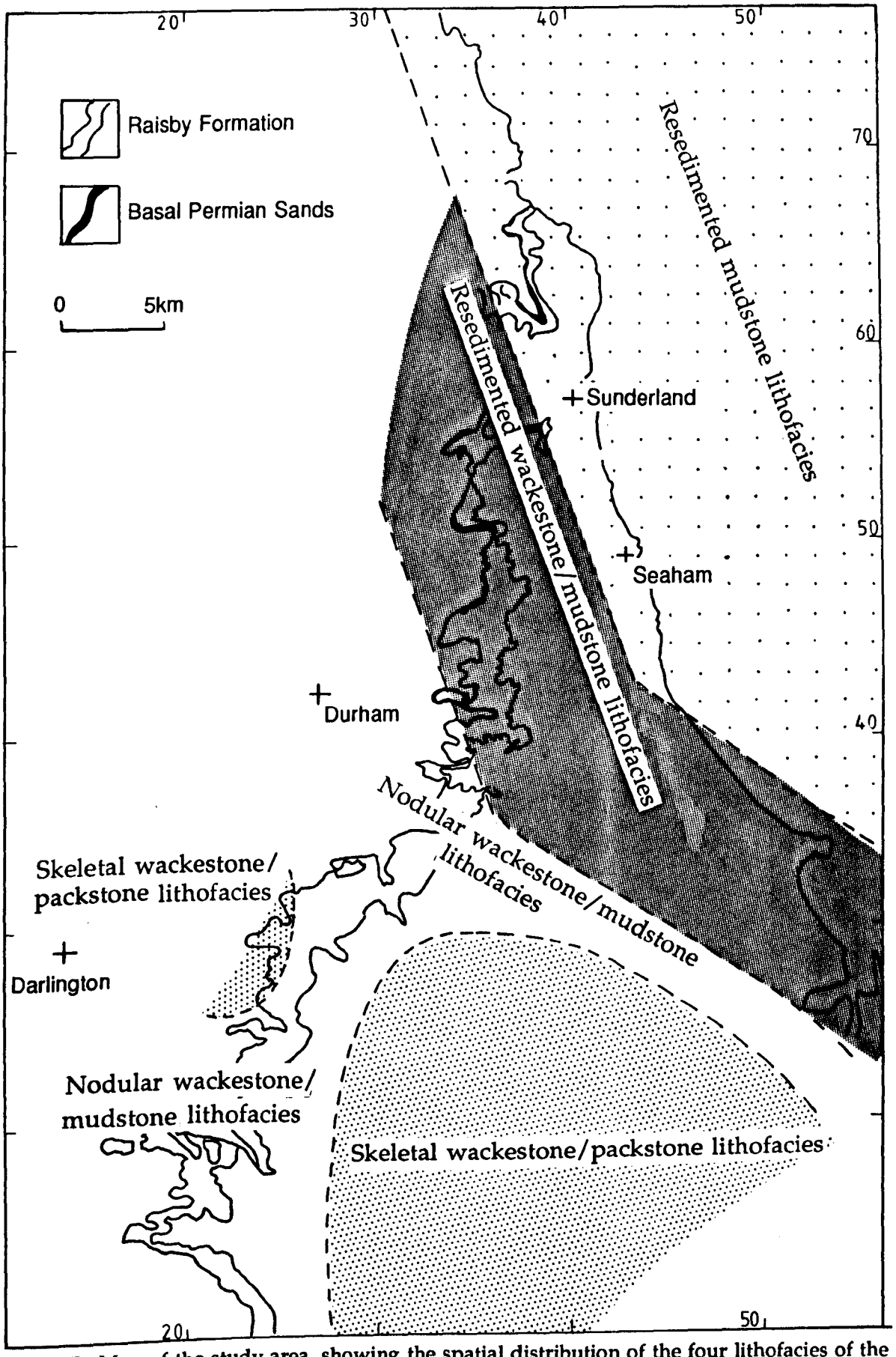

Fig. 2.7. Map of the study area, showing the spatial distribution of the four lithofacies of the Raisby Formation identified in this study.

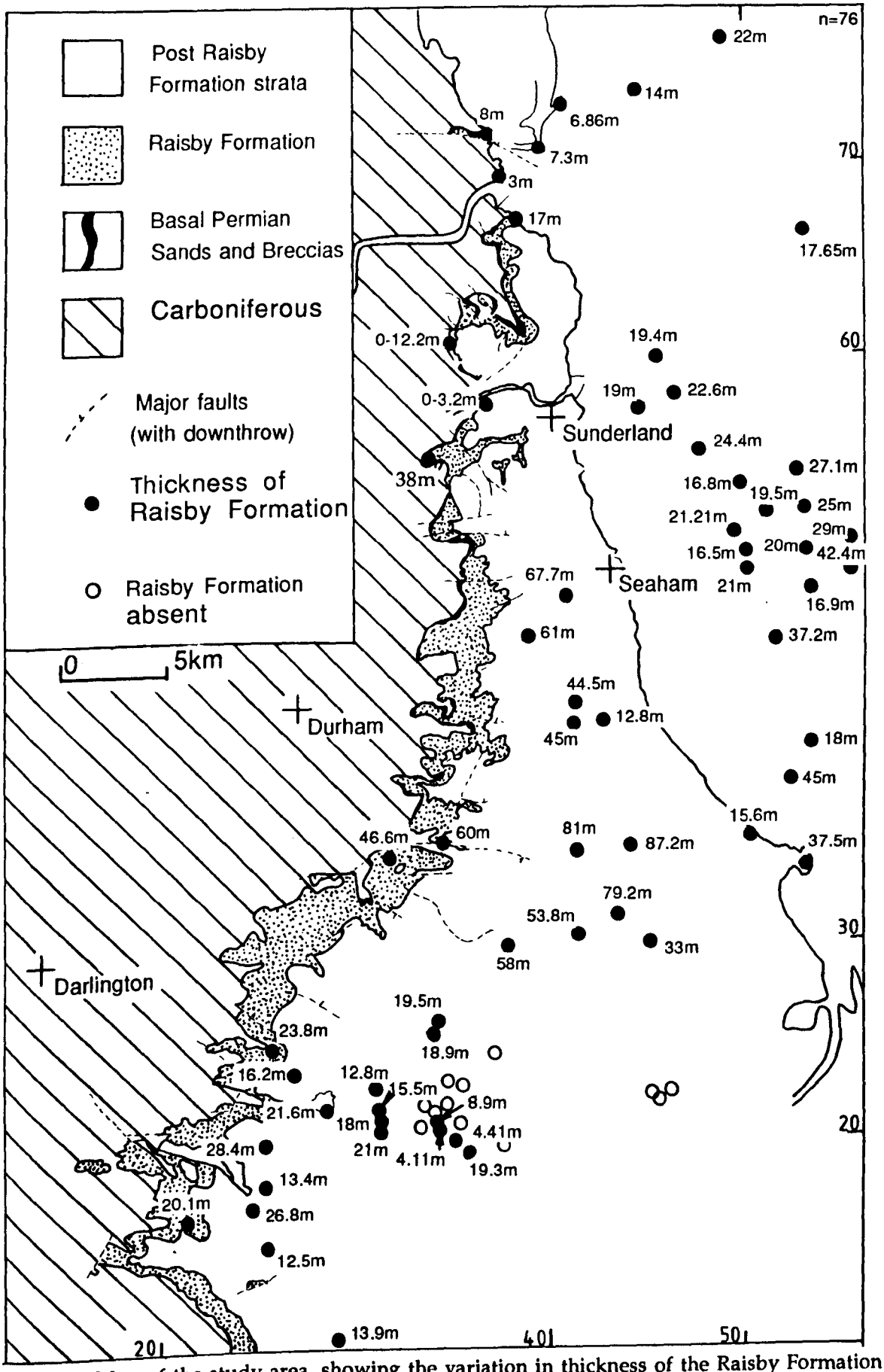

Fig. 2.8. Map of the study area, showing the variation in thickness of the Raisby Formation. Data from this study, Magraw *et al.*, (1963), Smith and Francis (1967), Mills and Hull (1976), Goodall (1987) and unpublished borehole data courtesy of D.B. Smith.

In the Hurworth Place borehole (NZ 2902, 0953), the base of the Raisby Formation is a packstone of algal -coated shell fragments, plus reworked clasts of the underlying Basal Permian Breccias (Fig. 2.9a). This shelly packstone passes up into a well sorted, skeletal peloid grainstone (Fig. 5.10), itself overlain by typical fossiliferous wackestones and packstones. The grain size of the skeletal material decreases up through the borehole as its degree of disarticulation increases. Skeletal packstone/grainstones, incorporating reworked fragments of Carboniferous limestone, have also been recorded close to the bases of boreholes W.O. 17 and W.O. 18, which again pass up into relatively uniform, finer skeletal wackestone/packstones. All of these boreholes grade vertically into lagoonal facies of the Ford Formation.

Sandstone horizons have been recorded within this lithofacies from Eldon Hill (NZ 242 272) and Morton Limekilns (NZ 190, 205) Quarries. The sandstone at Eldon Hill is 1.6m thick. It abruptly, although conformably, overlies thinly-bedded carbonate mudstones/wackestones, and is overlain by a thickly-bedded, sandy, shelly coquinoid grainstone (Fig. 2.9b). The sandstone is structureless and very poorly sorted, comprising angular to sub-rounded quartz and feldspar grains with abundant mica flakes. The silicate grains are in places supported within a dolomitized carbonate mud matrix (Fig. 6.69b). Larger shale, fine siltstone/fine sandstone, dolostone, and rare coal clasts also occur. The sandstone is unfossiliferous. Overlying coquinoid grainstones contain articulated shell fragments, bryozoans, and algal fronds. The algae in places encrust shale clasts. Quartz grains, similar to those within the sandstone are common within the basal part of this coquina, although sharply decrease in abundance upwards over a distance of several centimetres. The coquina is itself overlain by a few decimetres of more finely-fossiliferous packstones/grainstones containing an abundant, less well intact bryozoan and shelly fauna to the top of the exposure. Mills and Hull (1976) record twenty species of fossils from Eldon Hill, including an unusual faunal assemblage dominated by the bryozoa *Batostomella crassa* and fragments of *Acanthocladia* or *Thamniscus*. This bryozoan fauna is probably representative of that within the grainstones above the sandstone. This locality also contains *Lingula credneri* (Mills and Hull ,1976; Bell *et al.*, ,1979), which Bell *et al.*, (1979) describe as being 'common'. The dolomitic sandstone at Morton Limekilns Quarry is considerably more texturally and mineralogically mature than that at Eldon Hill, although its field relations are uncertain owing to poor exposure.

2.3.3. Skeletal wackestone/packstone lithofacies - Interpretation.

The abundance of skeletal material within this lithofacies, albeit most commonly comminuted, is indicative of a fairly diverse faunal assemblage which probably accumulated within relatively shallow waters, where subject to disarticulation and reworking by wave and current action. Mills and Hull (1976) also describe nearshore shell banks, in which

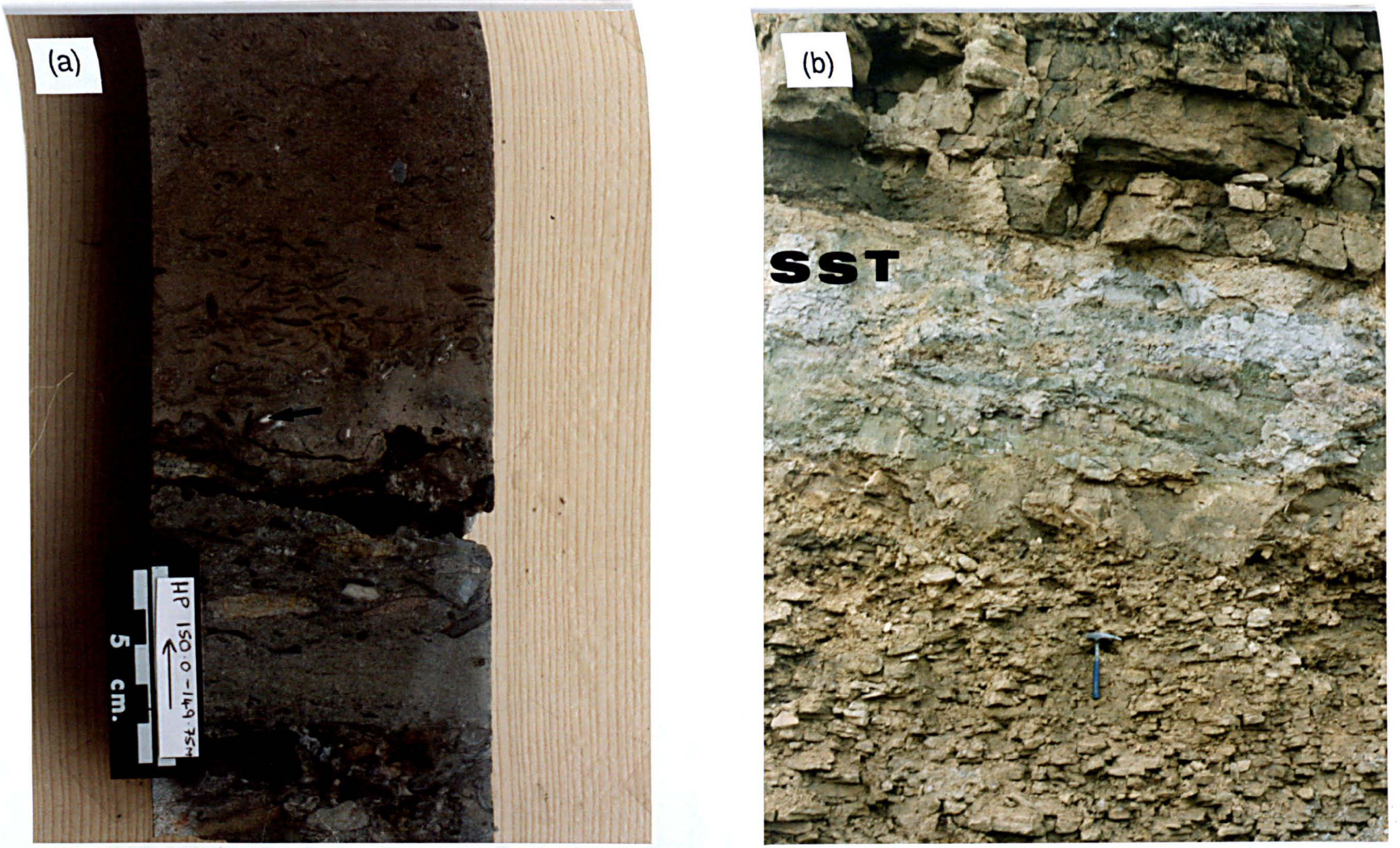

Fig. 2.9. Photographs showing characteristics of the skeletal wackestone/packstone lithofacies; (a) base of the Hurworth Place borehole, (b) most of the exposed Raisby Formation at Eldon Hill Quarry. (a) illustrates an algally-coated shelly packstone incorporating reworked clasts of Basal Permian Breccias. Note barite mineralization within some shell fragments (arrowed). (b) illustrates a sandstone (SST) horizon between thin bedded mudstone/wackestones below, and thicker bedded skeletal grainstones above. Hammer is 32cm long.

Horridonia horrida and *Strophalosia morrisiana* are particularly common at Hobgate Quarry (NZ 1646 1888). That these shelly coquinas are overlain by comminuted fossiliferous packstones is suggestive of a progressively increasing sea level during deposition of the lower part of the Raisby Formation. This is supported by limited overlap of lower Raisby Formation sediments onto the eroded Carboniferous surface in the southeast of the area, where the sea bed was uneven adjacent to the Middleton-Tyas anticline (Mills and Hull, 1976).

The coarsest, and most abundant faunal assemblages normally occur at the base of the Raisby Formation. These most likely reflect shallow water conditions at the beginning of first cycle carbonate deposition, and may be time-equivalent to the Marl Slate in deeper waters, thus analogous to the Mutterfloz of West Germany (2.1.4.). The importance of algae during deposition of the basal Raisby Formation in these areas is illustrated both by algal coatings on shell fragments, and the occurrence of peloid grainstones at the base of the Hurworth Place borehole. The peloid grainstones themselves, are current-swept accumulations, as they are well sorted, containing only coarse skeletal material.

Rapid deposition of the sandstone at Eldon Hill, locally increased the elevation of the sea floor (before burial compaction, the sandstone would have been considerably thicker than it is currently recorded to be), such that conditions were more favorable to the establishment of benthic faunal communities than they had previously been. The coarseness of the fossiliferous grainstones, and the abundance of algae, attest to agitated, current-swept waters, of probably only a few metres depth. Paul (1986a) suggests that wave base during deposition of the Kupferschiefer in West Germany was 10 to 50m. A water depth in this area, of ≤10m to 15m, would be in accordance with the winnowed nature of the sediments and information from palaeoecology, such as the common occurrence of *Lingula credneri*. The vertical change from coquinoid grainstone to skeletal packstone at Eldon Hill, demonstrates that conditions did not remain so favorable for benthic faunal communities for long, possibly again reflecting a sea level rise.

The textural and mineralogical immaturity, and composition of both sandstones, suggests a source from Westphalian Coal Measures. The sandstones may have been deposited by the redistribution of fluvially-derived sediments, or could have been reworked from submarine exposed Coal Measures by wave and current action. The former possibility is favoured here. If wave and current action in the Zechstein Sea was sufficiently energetic to erode, transport, and deposit lithified sandstones in this area, it is unlikely that carbonate mudstone/wackestones underlying these sandstones would have been deposited, or preserved. Sourcing of the sands from a nearby river could explain why they form distinct units, representing a temporary change in the site of fluvial input to deposit sands in that place at that time.

Meteoric (river) water input from marginal continental areas into the Zechstein Sea has been hypothesized by Magaritz and Turner (1982) and Turner and Magaritz (1986) on the basis of stable isotope data of authigenic carbonates, and the presence of detrital quartz within the Durham Marl Slate. A sandstone unit, of presumed fluvial derivation, has also been described by Sherlock (1911) from the Wetherby Member of the Cadeby Formation, near Mansfield. Given the high initial relief of parts of the south of the study area, and the presence of emergent Carboniferous islands, the sourcing of sands from ephemeral, braided (?) rivers or wadis is likely, in a similar environment to that in which the Basal Permian Breccias were deposited (2.1.3.). The absence of sands at higher levels of the Raisby Formation in this area probably reflects progressive drowning of Carboniferous islands, the source area of the sands, during deposition of the first cycle carbonate. It is also possible that the sands were genetically related to active fault movement along the margins of small horsts and grabens, as described by Goodall (1987) from this area.

2.3.4. Skeletal wackestone/packstone lithofacies - Summary.

Skeletal wackestones and packstones, deposited in relatively shallow waters, accumulated in the southern part of the study area on the margins of emergent islands and over submarine highs of Carboniferous rocks. The sea floor topography was very irregular, giving rise to laterally variable sedimentation. That these sediments were deposited over submarine highs is supported by the absence of both Basal Permian Breccias and Marl Slate in those areas. It is possible that the influx of sands into the Zechstein Sea was due to active movement along bounding faults of horsts and grabens.

2.4.1. Nodular wackestone/mudstone lithofacies - Description.

This is a broad, poorly defined lithofacies belt, which covers most of the southern part of the outcrop of the formation, extending northwards into north Durham (Fig. 2.7). Features of this lithofacies include widespread limestones, nodules and nodular bedding, local evidence for resedimentation, and a characteristic macrofossil, microfossil, and ichnofaunal assemblage. The Raisby Formation of this lithofacies varies from 20m-30m in the southern part of the area, thinning eastwards into the shallow water skeletal wackestone/packstone lithofacies near to islands and palaeohighs, and thickening to the northeast (Fig. 2.8).

Limestones and dolostones of this lithofacies are dominantly mudstones and wackestones. The palaeontological content of the limestones at Thickley and Raisby Quarries can be used as a guide for an interpretation of the depositional environment of this lithofacies. A well-preserved brachiopod fauna, dominated by *Horridonia horrida*, has been described by Trechmann (1921) from Thickley Quarry. He figures articulated brachiopods, lying more or less in life position, supported by large, intact spines, onto which smaller brachiopods have attached themselves. Microscopically, the Thickley limestone is a wackestone containing a relatively abundant microfauna dominated by intact foraminifers (Fig. 3.11a), ostracodes, calcispheres, and larger fragments of brachiopods and bryozoans. Much of the coarser skeletal material has been finely comminuted. The Raisby Quarry limestone is considerably less fossiliferous than that at Thickley (also noted by Trechmann, 1921), and is almost exclusively a mudstone, containing scattered skeletal material. Rare brachiopods, similar to those at Thickley, have been recorded, which were again supported on the sediment surface by large spines. Microscopically, the sparse fauna is dominated by small intact microfossils. Some laminae within the limestones have noticeably higher concentrations of microfossils than others. Millimetre-thick layers, hosting well sorted concentrations of broken bryozoan fragments, aligned with long axes horizontal, and orientated in the same direction, are relatively common. In these bryozoan-rich layers, microfossils are virtually absent, although coarse silt-grade quartz and muscovite are common. A very similar bed, a few centimetres in thickness, has been recorded from close to the base of the Raisby Formation in Quarrington Quarry (NZ 327, 379) (Fig. 6.31a). Again the fauna is dominated by disarticulated, aligned bryozoan fronds up to 5mm long, and also contains some disarticulated bivalves. The limestone at Raisby Quarry is also intensely bioturbated. All burrows are horizontal, with near circular cross sections, approximately 4mm in diameter. They are all straight or slightly sinuous, and occasionally bifurcate. One example was recorded where burrows branched out from a central point (Fig. 2.10). This ichnofauna resembles *Chondrites*, or possibly, *Planolites*.

Fig. 2.10. Photograph of a bedding surface, Raisby Quarry. The branching burrow system on this bed surface is attributable to *Chondrites* or *Planolites*.

Most limestones and dolostones of this lithofacies are evenly bedded on a centimetre to decimetre scale. Few, if any, sedimentary structures can be defined within these beds, although wavy and nodular bedding is a very important feature of this lithofacies. It has been recorded from a number of localities within the Raisby Formation, mainly in the nodular wackestone/mudstone and resedimented wackestone/mudstone lithofacies. Nodules and nodular bedding are commonly associated with bedded limestones. The characteristics of nodules of all lithofacies will be considered here.

2.4.1.1. Nodules - Description.

Three different types of nodules have been defined within the Raisby Formation, although gradational types exist;

1. Isolated nodules; (High Moorsley [NZ 334, 455], Old Towns [NZ 257 246] and Raisby [NZ 338, 354 - 352, 352] Quarries),
2. Nodular bedding structures; (Chilton [NZ 302, 246], High Moorsley, Middridge [NZ 249, 252], Thickley [NZ 2408, 2564] and West Cornforth [NZ 318, 345] Quarries),
3. Microstylolitized nodules; (Cotefield Close borehole [Woolacott, 1919a], Hartlepool Lighthouse borehole [NZ 3519, 3387] [Smith and Francis, 1967], Penshaw Hill Quarry [NZ 3365, 5460], Tinkler's Gill borehole [NZ 4157, 3054], W8 borehole [NZ 52688, 66339], W15 borehole [4809, 7622]).

Isolated and microstylolitized nodules commonly occur in direct association with limestones, whereas nodular bedding structures are more numerous within dolostones.

Isolated nodules are best developed above, and to a lesser extent below, the limestone at Raisby Quarry (Fig. 2.11), above the limestone at Old Towns Quarry, and within dolostones at the top of High Moorsley Quarry (Fig. 2.12a). At Old Towns and Raisby Quarries, the nodules comprise limestone, and lie within a partially to completely dolomitized matrix (Fig. 2.11), whereas at High Moorsley Quarry both nodules and matrix have been completely dolomitized (Fig. 2.12a). However, in all cases, centimetre- to decimetre-sized oval nodules can be defined within a matrix of different character. The nodules may be completely isolated within the matrix, or laterally-linked, forming a continuous bed with undulate upper and lower surfaces (Figs. 2.11 & 2.12a). At Old Towns and Raisby Quarries the abundance of nodules decreases with height above the underlying bedded limestone (Fig. 2.11a), and at Raisby Quarry the thickness of the nodular horizon decreases from 6.5m at the southeast end (Fig. 2.11a) of the main face to 1.5m at its northwest end, approximately a distance of 500m. Thus, to the northwest, nodules pass laterally into bedded dolostones with no nodules. The nodules at High Moorsley Quarry are distinguished from their matrix by being lighter coloured, more brittle, and heavily dissected by autobreccia-like fractures (Fig. 2.12a), which in turn correlates with a difference in dolomite texture.

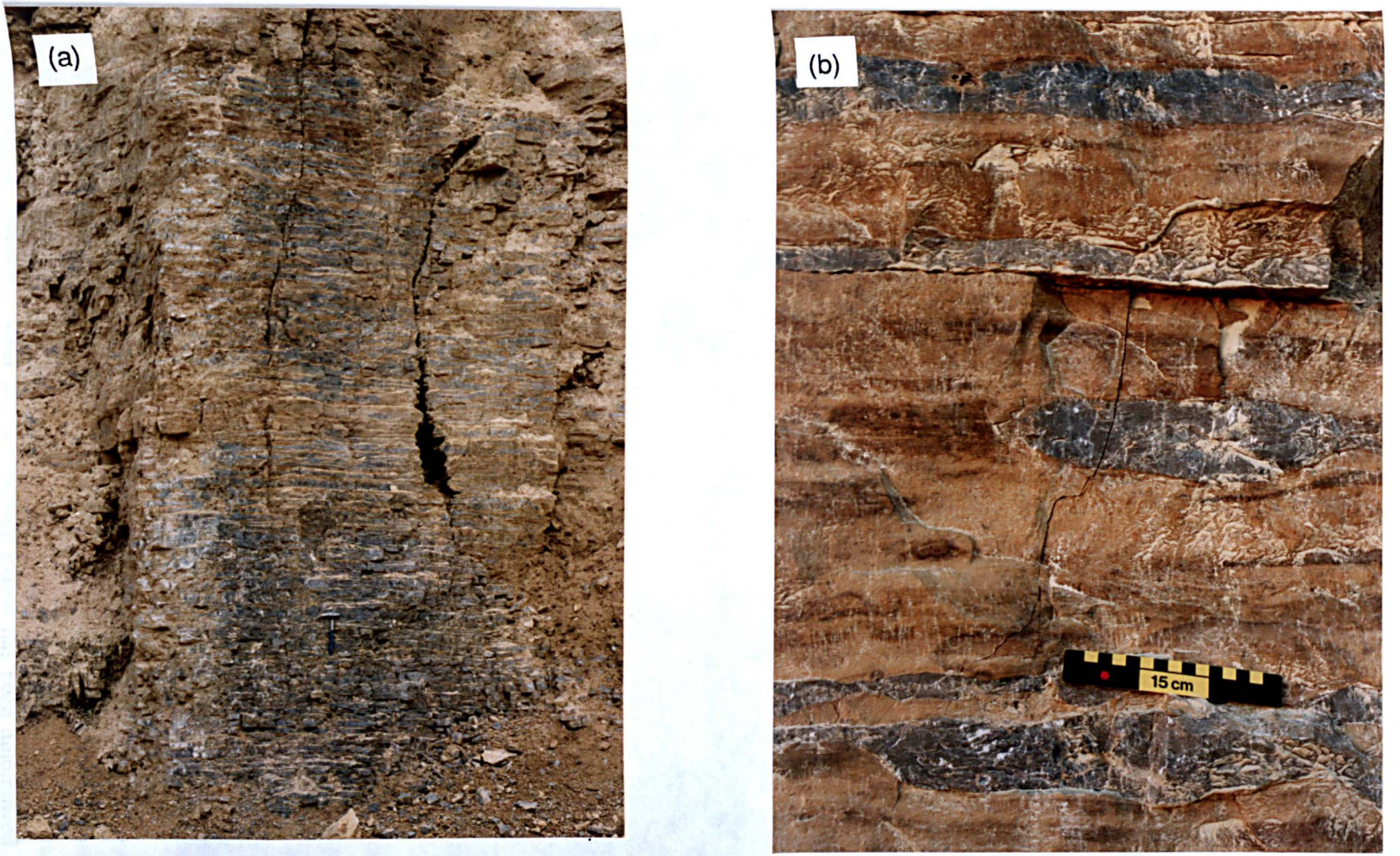

Fig. 2.11 Photographs of isolated limestone nodules, Raisby Quarry. (a) shows detail of the transition from bedded limestone at the base, into nodular limestones within partially dolomitized limestones above. The nodules are shown in detail in (b). Hammer in (a) is 32cm long.

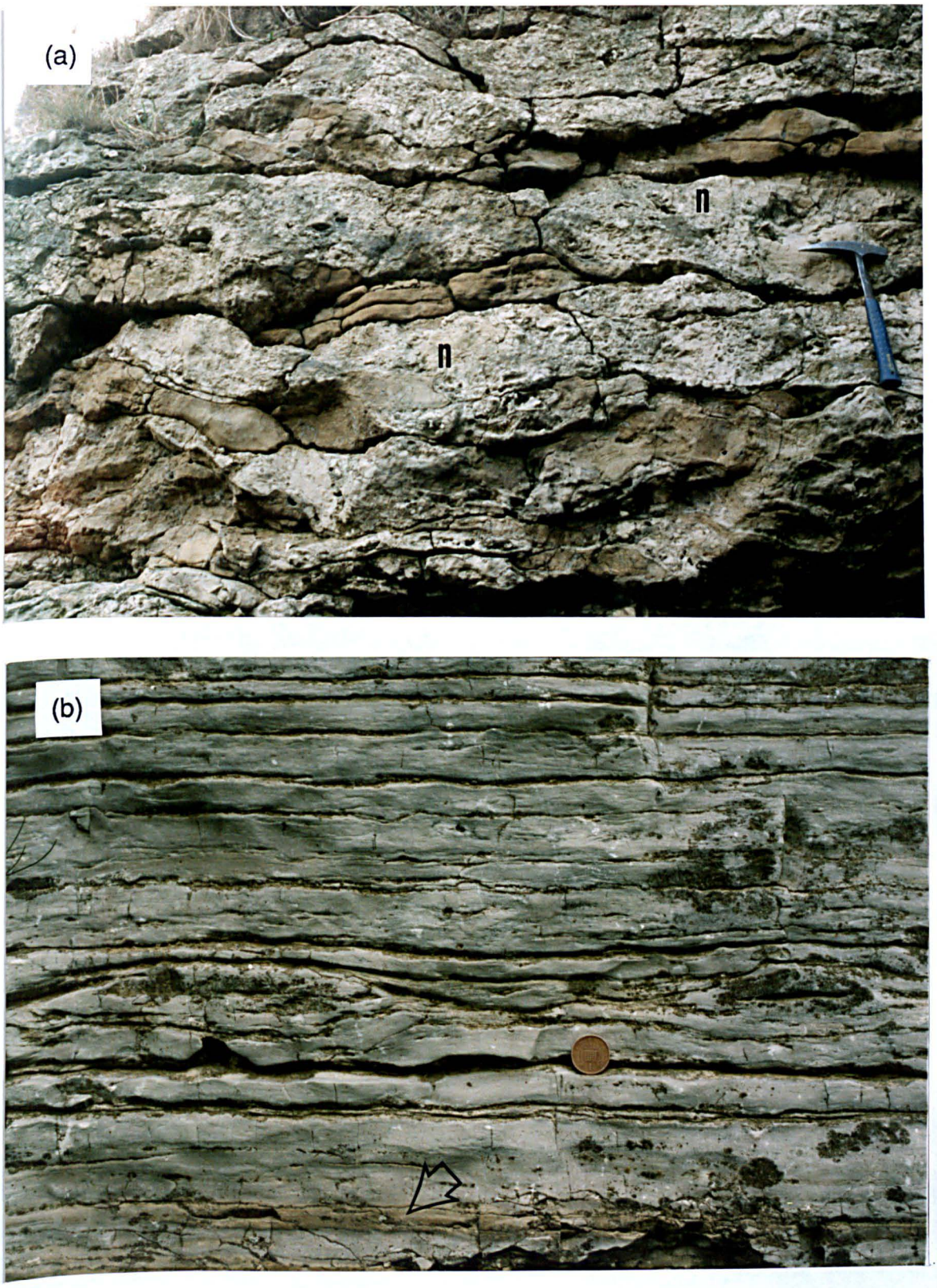

Fig. 2.12. Photographs of nodules; (a) High Moorsley Quarry, (b) Penshaw Hill Quarry. In (a), both nodules (n) and inter-nodule carbonate have been completely dolomitized. Hammer is 32cm long. (b) illustrates the discrete development of two nodules within an otherwise bedded limestone. Limestone either side of bedding planes has been dolomitized during microstylolitization (arrowed). Vertical fractures are also numerous within this limestone.

Fig. 2.13. Photograph of microstylolitized nodules from borehole W15, 252.97m. Note colour variation within the nodules, and the very different character of the microstylolitized inter-nodule matrix (m).

The Raisby Quarry isolated nodules are commonly cut by small (millimetres to few centimetres long), downward-tapering, V-shaped regularly spaced fractures on their upper surfaces. These fractures may be unoccluded, filled by former marine cements (Figs. 3.4 & 3.5), or partially occluded by former marine cements and partially by host dolostone which has been injected into the fractures. The Raisby Quarry nodules are also radially-zoned geochemically, with Sr decreasing from nodule core to margins (Fig. 4.11). This is mainly a diagenetic effect, although may in part reflect an original compositional gradient (4.3.2).

Nodular bedding is very widespread within the formation at outcrop, and most common within the upper parts of Raisby Formation sections. The nodules are most commonly indistinct, and represented by a low amplitude undulation of bedding surfaces. Stronger development of this undulation, whereby individual beds pinch and swell, leads to the development of nodular bedding. These nodules were recorded within dolostones at a number of localities, although within limestones only from High Moorsley Quarry. Nodular bedding is characterized by an interlocking mosaic of nodules, with the convex part of one nodule interlocking into the thinned area between two nodules above and below (Fig. 2.16). Most nodules are laterally interlinked, and it is rare for the bedding surfaces to be deformed to such a degree that nodules are completely isolated from each other. Faint fleck lamination within nodular bedded dolostones demonstrates that all of the bed has been deformed internally in order to form the nodular structure.

Microstylolitized nodules have been recorded from limestones in boreholes, and at one locality from outcrop (Penshaw Hill Quarry) (Fig. 2.12b). Dolomitized equivalents have been recorded within borehole W8, and by Smith and Francis (1967, plate VIIIB) from the Hartlepool Lighthouse borehole. Very similar structures have also been recorded by Fusezy (1980) and Kaldi (1980) from boreholes to the east of the outcrop of the Cadeby Formation. Raisby Formation microstylolitized nodules are characteristically elongate, generally ovoid in shape, a few centimetres in height, and up to 10-20 centimetres in length (Figs. 2.12b & 2.13). Most nodules are delineated by a distinctive matrix which has suffered intense microstylolitization, giving it a very dark colour in hand specimen (Fig. 2.13). On rare occasions where the nodules are in contact, their junction is delineated by coarser, sutured seam stylolites. Many nodules display abundant, V-shaped, downwards-tapering fractures, a few millimetres to centimetres in length, and whose long axes are normal to the upper external surface of the nodule. The fractures may be occluded by gypsum/anhydrite, or former marine cements. Sutured seam stylolites postdate formation and cementation of the fractures. The nodules comprise featureless, virtually unfossiliferous, finely-crystalline calcite or dolomite mudstone, whereas the microstylolitized inter-nodule matrix is commonly more coarsely crystalline and contains a greater abundance of skeletal material, together with fine-grained detrital siliciclastic grains. In limestones from outcrop and core, the microstylolitized matrix has commonly been partially dolomitized (Fig. 2.12b), although

host limestone nodules are completely unaffected. Nodules characteristically have variable colours in hand specimen, becoming lighter towards their margins (Fig. 2.13). In limestone nodules, this correlates with a radial variation in trace element geochemistry, especially a decrease in Sr. In the W15 and Tinkler's Gill boreholes, some nodule layers have been heavily contorted during slumping (Fig. 2.31b).

2.4.1.2. Resedimentation - Description.

Evidence for large-scale resedimentation was recorded at two localities within this lithofacies; Old Towns (NZ 257, 246) and Summerhouse (NZ 2100, 1966) Quarries, with lesser developments at Chilton (NZ 302, 341) and Thickley (NZ 2408, 2564) Quarries. In one part of Chilton Quarry, close to its base, bedding was contorted into a number of interfering tight overfolds, suggestive of soft sediment deformation, although here, no reliable palaeoslope indices could be measured. The stratigraphic position of this unit is uncertain, although probably close to the base of the formation. Two resedimented horizons are exposed at Summerhouse Quarry, one approximately 0.4m thick close to the base of the section, and one 3.2m thick near to its top (Appendix XII). The lower unit is characterized by a concentration of large (up to 10cm long) cavities after sulphates. The unit has an uneven, undulate, erosive base on an underlying dolostone bed, although an even top. Its upper surface may have been planed off prior to deposition of the overlying bed. The thickness of the resedimented horizon is inversely proportional to that of the underlying eroded bed. The upper horizon of Summerhouse Quarry is characterized by large-scale deformed and contorted bedding, with a few smaller-scale tight anticlinal folds. The intensity of deformation is greatest within a 0.75m thick unit at the top of the horizon. This horizon has a planar contact with underlying dolostones.

A small overfold, similar to those in the upper unit of Summerhouse Quarry, has been recorded 0.5m below the top of the exposure, within slightly deformed nodular dolostones at Thickley Quarry. The axial plane of this fold is horizontal and trends approximately north-south. Much more intense deformation occurs at a similar horizon in Old Towns Quarry nearby, where a thick resedimented unit can be traced throughout the quarry. In the southernmost part of the exposure, a thick basal limestone is gradationally overlain (via isolated nodular limestones) by dolostones. Immediately to the north of this, the top of the limestone has been abruptly eroded off in a northwesterly direction (Fig. 2.14). The erosion surface trends 041°/26°NW such that 3.5m, at least, of limestone has been eroded within approximately 14m from southeast to northwest (Fig. 2.14). Relic blocks of limestone at the base of the major erosion surface have been rotated. The erosion surface is overlain by a coarse, mixed dolostone and limestone breccio-conglomerate. The breccio-conglomerate at the foot of the main erosion surface is 2.6m thick, with a very poor internal structure. Coarse, 0.3m-0.5m angular to subrounded, jumbled blocks of dolostone and

Fig. 2.14. Photographs showing the main erosion surface, Old Towns Quarry. A thick limestone (lst) is strongly eroded off from SE to NW. At the NW end, only rotated blocks of relic limestone remain (arrowed).

Fig. 2.15. Photograph showing the exposed Raisby Formation in the NW end of Old Towns Quarry. At the base of the exposure is a large translational slide, 3.2m thick, inside which bedding is heavily contorted, including tight slump folds (arrowed). This translational slide unit is laterally-equivalent to, and to the NW of, the large erosion surface in figure 2.14.

limestone lie in a matrix of finer dolomite. The breccio-conglomerate passes northwestwards into a 3.6m thick unit of heavily contorted dolostones with minor slump overfolds and fine conglomeratic layers which rests on a planar erosion surface (Fig. 2.15). The internal structure of this unit is extremely similar to the upper resedimented horizon in Summerhouse Quarry. At Old Towns Quarry, breccio-conglomerate and slump movement directions parallel that of the main erosion surface, from southeast to northwest.

2.4.2. Nodular wackestone/mudstone lithofacies - Interpretation.

That skeletal material is supported within the carbonate mudstone matrix of limestones, demonstrates that they were originally deposited as fine carbonate muds. The absence of an obvious abundant macrofauna, apart from large epifaunal brachiopods, suggests an environment of low faunal diversity. A low current strength is also attested to by the dominance of a pelagic microfauna, which would not be deposited in an energetic sedimentary environment. However, pulses of energetic current activity are evidenced by layers of concentrated macrofauna fragments at Raisby and Quarrington Quarries. The absence of finer skeletal material in these layers shows that the currents were too energetic to deposit entrained microfauna. The allochthonous, shallow-water fauna, suggests that current movement was downslope, from a shallower water environment, rather than as contour currents. Thus, quiet periods (depositing carbonate mud and microfossils), alternated with episodes of more energetic current activity, depositing coarse skeletal material and winnowing carbonate mud, forming concentrated microfossil-rich layers. The restriction of sessile benthonic fauna to spinose brachiopods also suggests that the bottom sediments were soft. That smaller brachiopods have attached themselves to the spines of *Horridonia horrida* (Trechmann, 1921, fig. 2), further supports this assertion, such that the spines were the only rigid attachment surfaces available. The burrowing ichnofauna likewise suggests a soft sea floor sediment. Burrows from Raisby Quarry are systematic feeding traces, and possibly attributable to the *Cruziana* or, more likely, the *Zoophycus* ichnofacies (Frey and Pemberton, 1984). Both ichnofaunal assemblages are indicative of relatively deep, quiet water environments in the shelf or slope areas respectively (Frey and Pemberton, 1984). Thus, evidence from structures within the limestones, and their palaeontological content, suggest deposition in a moderately deep water, quiet environment, occasionally disturbed by more energetic current activity. This suggests water depths of ≥50m, taking 50m to be maximum wave base (Paul, 1986a) (2.3.3).

2.4.2.1. Nodules - Interpretation

The three types of nodular structures described are interpreted as being of marine eogenetic origin, most likely accompanying sediment lithification slightly below the sea floor. The evidence for such an origin includes;

1. Distortion of sedimentary laminae within nodules and nodular beds, paralleling nodule margins,

2. V-shaped fractures, indicating compaction of a lithified or semi-lithified body within a less lithified, more ductile host sediment. Very similar fractures are common cutting limestone clasts within debris flows of the resedimented wackestone/mudstone lithofacies, which are directly related to early lithostatic compaction (Fig. 2.22). Fractures were occluded by seawater-derived cements, demonstrating that the nodules were at least semi-lithified when within, probably, a few centimetres to decimetres of the sea floor. Other fractures, cemented by calcium sulphates, possibly formed later, or calcium sulphate may have selectively replaced an earlier marine cement,

3. Semi-lithified nodules were incorporated into synsedimentary slumps in borehole W15 of the resedimented mudstone lithofacies,

4. The limestone composition of the nodules suggests a relatively early lithification, prior to dolomitization (2.4.2.2.).

The three different nodule types are thus of a similar origin (Fig. 2.16). The isolated and microstylolitized types represent the discrete growth of nodules within a host sediment which remained unlithified until considerably later, and so was more prone to later diagenetic alteration (dolomitization and/or microstylolitization) (Fig. 2.16). The greater susceptibility to alteration of the matrix was probably a function of a greater porosity and permeability resulting from less extensive early cementation. These ductile host sediments also deformed around more competent nodules, and were injected into fractures during early burial compaction. Even where the nodule and matrix have both been completely dolomitized, such as High Moorsley Quarry, original textural differences remain, with nodules being more brittle and less permeable than their matrix. The apparent concentration of skeletal and siliciclastic grains in the matrix of microstylolitized nodules may be a real effect, such that nodules did not form within relatively coarse skeletal layers. However, it is more likely due to the partial destruction of skeletal material during early cementation and nodule formation, plus the accentuation of skeletal and siliciclastic grains by microstylolitization. Microstylolitization is very important for the recognition of these nodules. Thus, nodular bedding may represent microstylolitized-type nodules whose matrix has not been microstylolitized. Furthermore, as microstylolitized nodules have been mainly recognized from boreholes, it may well be that outcrop weathering obscures the differences between nodules and their microstylolitized host. Nodular bedding represents a very extensive form of nodule development whereby almost all beds were cemented early. The

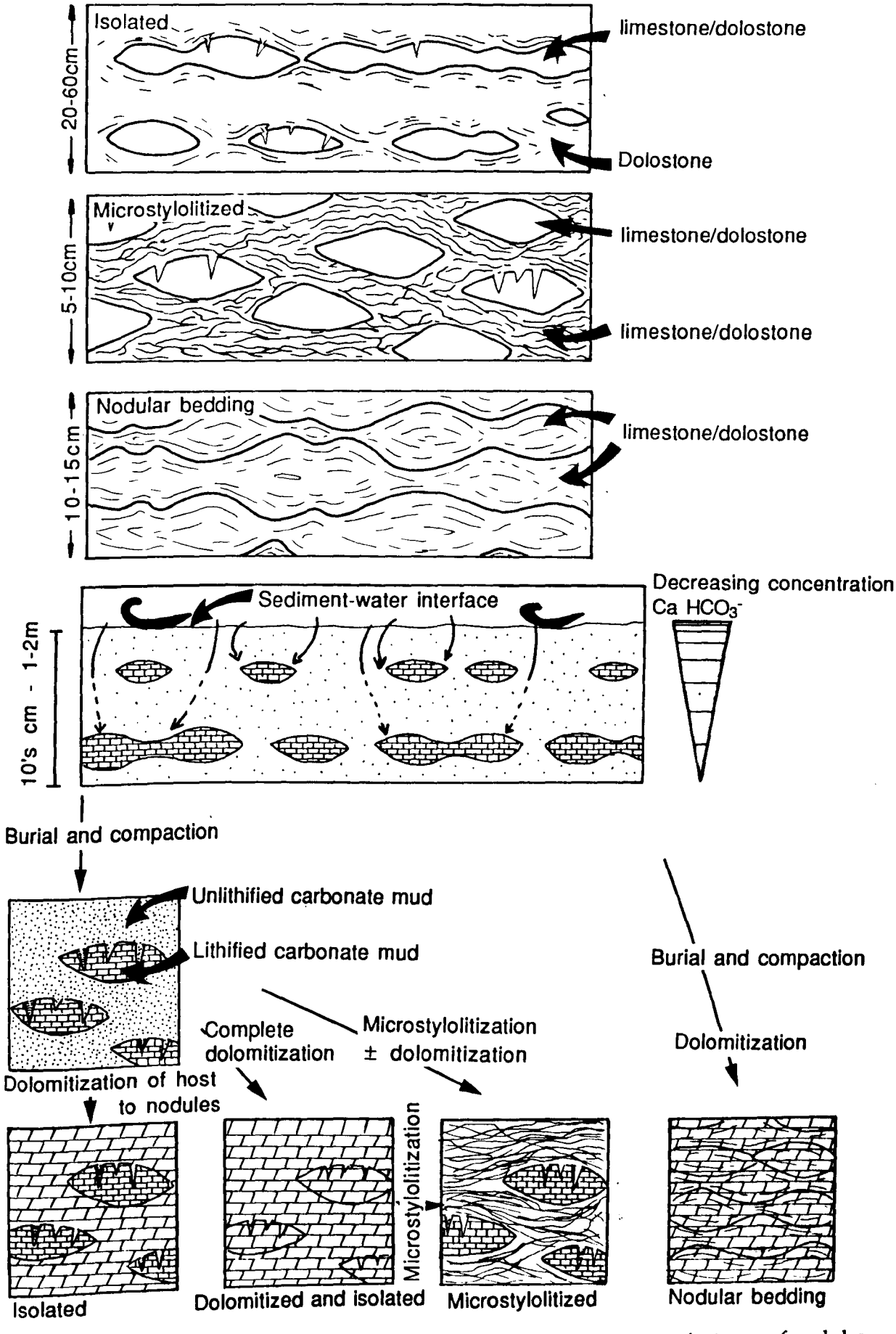

Fig. 2.16. Schematic diagram showing the characteristics of the three main types of nodules identified (upper diagram), and the different diagenetic processes which have gone to produce those nodules (lower diagram).

common dolomitization of nodular bedding nodules may reflect a less intense early cementation than with the other types of nodules, which are more normally still limestone.

Nodules within the Raisby Formation, probably very similar to the microstylolitized type, were interpreted by Trechmann (1914) to represent the concentration of calcite within the nodules, whereas Woolacott (1919a) interpreted nodules from the Cotefield Close borehole to have formed as a result of pressure solution, a hypothesis also favoured by Smith and Francis (1967). The position of nodule-rich localities within the Raisby Formation, relative to the estimated contemporaneous shoreline of the Zechstein Sea, is very similar to that of analogous structures described from slope carbonates of the Cadeby Formation by Fuzesy (1980) and Kaldi (1980) (Fig. 2.17). This suggests that nodule formation may well be a feature of slope carbonates, and, in turn, be restricted to certain areas of the slope.

Kaldi (1980) relates nodule formation in the Cadeby Formation to early diagenetic cementation of carbonate sediment below the floor of the Zechstein Sea, followed by pressure solution during burial. He suggests that slow sedimentation rates are very important contributing factors to nodule growth. Very early diagenetic formation is strongly supported by the occurrence of slumped and resedimented nodules interbedded with undeformed nodules in a borehole described by Kaldi (1980), similar to resedimented and slumped nodules in Tinkler's Gill and W15 boreholes (Fig. 2.31b). Fuzesy (1980) also favours an origin by selective early cementation, but in micro-environments created by ammonia generated from decomposing organic matter. Kaldi (1980), however, suggests that the necessary ions were derived by diffusion from the overlying Zechstein Sea through unconsolidated sediments.

Nodules from Jurassic pelagic carbonates (Ammonitico Rosso) of the Mediterranean area (Jenkyns, 1974), are very similar to those from the Cadeby Formation, and Raisby Formation microstylolitized nodules in size, shape and facies in which they occur (deep water sediments dominated by a pelagic and nektonic fauna). Jenkyns (1974) also stresses the importance of very slow sedimentation rates, plus the availability of metastable aragonite, which is dissolved at the sea floor and reprecipitated as a cement within the shallow subsurface. The growth of the Ammonitico Rosso nodules was thus a factor of the rates of diffusion of Ca^{2+} and HCO_3^- from the sea floor to sites of nodule growth, inversely proportional to the thickness of overlying sediments (i.e., sedimentation rates). With sea floor aggradation, new nodules formed when the previous set were too far from the sediment-water interface for diffusion to be effective (Jenkyns, 1974). This model is mostly, although not wholly applicable to the Raisby Formation, as the Zechstein Sea was an 'aragonite sea' and so aragonite would not have been so unstable on the sea floor. Stable isotope compositions of nodules and limestones (very similar to Zechstein seawater) do not support substantial involvement of organic matter in supplying bicarbonate (4.3.2).

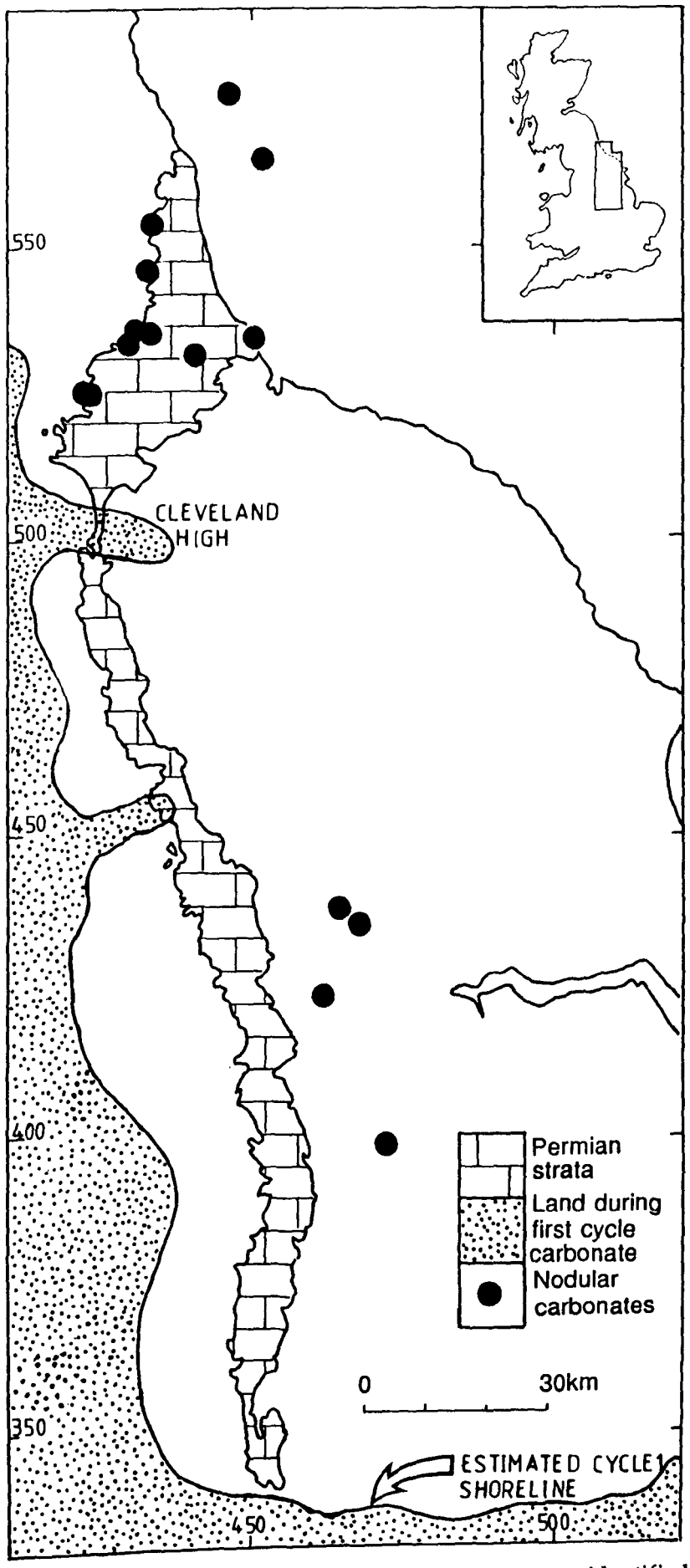

Fig. 2.17. Map showing the location of nodule-rich exposures identified from the Raisby Formation during this study, and nodules proved in boreholes east of the outcrop of the Cadeby Formation (Fuzesy, 1980 and Kaldi, 1980). The reason for the relative scarcity of nodule localities in the Yorkshire Province is due to the small number of boreholes studied by Fuzesy and Kaldi, which were only from one area.

However, there is abundant evidence for the cementation of macro- and microfossil intraskeletal porosity by aragonite/high magnesian calcite during early marine diagenesis of Raisby Formation limestones (3.3.2). The cement for nodule growth was thus probably seawater-derived, and most likely precipitated as overgrowths on micron-sized carbonate mud grains.

Nodules within the Raisby Formation are largely restricted to quiet, relatively deep water environments, and so formed by processes not operative in shallower waters (i.e., skeletal wackestone/mudstone lithofacies). This is interpreted to reflect the importance of slow sedimentation rates and low current activity, thus giving sediments ample time to become cemented, in common with the ideas of Jenkyns (1974), and Kaldi (1980). As the host sediments are dominantly mudstones and wackestones, bottom current activity, and thus winnowed sediment movement, must have been negligible.

Limestones - Interpretation

Limestones are almost exclusive to the nodular wackestone/mudstone and resedimented wackestone/mudstone lithofacies of the Raisby Formation, and are more common within the former than the latter. Their patchy development within these lithofacies is in part a function of the spatial variation in the intensity of dolomitization, in part due to synsedimentary erosion of the limestones (i.e., figure 2.14), but possibly also related to primary sedimentological factors. Although the conditions necessary for limestone formation may have occurred elsewhere within the Raisby Formation and have since been obliterated by later dolomitization, the localities where limestones have been recorded are clear evidence for the occurrence, or non-occurrence of specific diagenetic processes.

Limestones have a number of features in common with nodules, including abundant V-shaped, downwards-tapering fractures. In the Penshaw Hill limestone, fractures are especially numerous and regular (Fig. 2.12b), although those within Raisby Quarry are less regular and tend to be concentrated in association with burrows, often cutting them. At both of these localities, the fractures are unoccluded, as are similar-sized pseudomorphs after anhydrite within the limestones, suggesting that the fractures were originally filled by sulphate. The fractures are again interpreted to have formed by the compaction of brittle, lithified limestones over more ductile sediments, later dolomitized. *Planolites/Chondrites* burrows within the Raisby Quarry limestone are near-circular in cross section (perpendicular to burrow long axis). The long (horizontal) axes of the burrow cross sections vary from 4mm-5mm and the short (vertical) axes range from 3mm-4mm in diameter. From the 'Carbonate Compaction Law' of Ricken (1987) (and assuming the burrows were originally circular in cross section), their calculated maximum amount of compaction is 25%, less than 5% for most samples. Minimal burrow compaction is further supported by the deformation

of sparse skeletal material around the burrows (although this may in part be a by-product of burrow formation). These data suggests that, in the limestones, burrows were lithified very early, before significant compaction. Absence of detrital clay minerals within the limestones means that an estimation of the amount of compaction of the host limestones after burrow lithification is not possible (Ricken, 1987). Although their preservation is most likely due to petrophysical differences with surrounding sediments, the very fact that limestones are preserved, shows that their early diagenesis was somewhat different from that of host dolostones. The close spatial association of bedded limestones with isolated and microstylolitized nodules (Figs. 2.11a & 2.12b) implies a genetic link, and thus a common origin by early submarine cementation.

The bedded limestones may reflect more widespread sea floor lithification than do associated isolated nodules. The occurrence of microstylolitized nodules and nodular bedding within the limestones (Fig. 2.12b), in turn, suggests that limestones may accrete via lateral coalescence of nodules. The vertical transition from bedded limestone into isolated nodules (Fig. 2.11a) suggests the two may have been laterally equivalent, or it may simply represent a vertical decrease in the intensity of early sea floor cementation.

Submarine hardgrounds, possibly analogous to the Raisby Formation limestones, are widespread on the upper parts of Bahamian carbonate slopes at the present day (Mullins *et al.*, 1980). They pass downslope into nodular limestones. On the Bahamian slopes, submarine hardground formation is due to a combination of winnowing of carbonate muds by bottom currents, and bioturbation (Mullins *et al.*, 1980). Within the Raisby Quarry limestone, bioturbation was clearly effective in promoting early cementation, at least for the burrows themselves. There is also good evidence for bioturbation within other Raisby Formation limestones, although not as distinctive as at Raisby Quarry. There was some current action during deposition, but most limestones are mudstones or wackestones, deposited with insignificant current action. However, some of the more energetic currents may have winnowed away the uppermost layer of unconsolidated carbonate muds, exposing the lower layers to form submarine hardgrounds. A slow sedimentation rate and quiet bottom water conditions may have been equally as favorable for submarine lithification, with seawater circulation assisted by bioturbation. Therefore, the upwards change from bedded, to isolated nodular limestones, to homogeneous dolostones may reflect an increase in sedimentation rate with a concurrent, and possibly related, decrease in bioturbation. This could, in turn, have been due to a larger scale, basin-wide event such as a fall in sea level, although there is no evidence for such a regression in the shallower water skeletal wackestone/packstone lithofacies. Thus, the reason for attenuation of nodule growth is unclear. The absence of bedded limestones in upper parts of the Raisby Formation may be wholly diagenetic in origin, or due to a cessation of conditions suitable for widespread early submarine lithification.

2.4.2.2. Resedimentation - Interpretation.

Although evidence for resedimentation in this lithofacies is not abundant, it has been recorded on three scales;

1. Millimetre- to centimetre-scale

Individual beds of allochthonous, aligned bryozoans and concentrated, microfossil-rich layers whose carbonate mud matrix has been winnowed away,

2. Decimetre- to metre-scale,

Rare horizons of erosive-based resedimented carbonates (whose exact nature is obscured by sulphate replacement), plus erosive-based coarse breccio-conglomerates,

3. Metre-scale,

Deformed and contorted bedded dolostones with variable amounts of internal deformation. These are the down-flow equivalents of erosive-based breccio-conglomerates,

The millimetre- to centimetre- and decimetre-scale resedimented units reflect sporadic downslope currents, possibly triggered by increased water pressure due to storm build up on the shelf of the Raisby Formation. Their origin from shallower waters is demonstrated by an allochthonous fauna. The absence of coarse clasts in these beds suggests that the currents were of a low velocity, that these beds were deposited from waning currents produced by the passage of a more energetic density current, and/or that the source area contained only unlithified carbonate muds.

Metre-scale deformation structures at Chilton, Old Towns and Summerhouse Quarries are very similar to translational slides described by Cook (1979). In these, discrete packages of sediment, metres in thickness, move downslope along a horizontal basal shear plane. Internal disruption of bedding is often limited, especially in the central parts of the slide, and rupture strength is only exceeded along its margins. Thus, the majority of deformation is plastic in nature, with small overfolds being characteristic. These are very similar to the Raisby Formation examples, although in those described by Cook (1979), the translational slides were commonly remoulded in their lateral and distal parts into debris flows. In the Raisby Formation, translational slides appear to have been triggered by large-scale slope failure with attendant deposition of minor breccio-conglomerates. The consistent thickness (a few metres) of the translational slides, is probably a function of the depth at which underlying beds are reasonably well lithified, and so act as a decollement plane for the overlying, less well-lithified sediments to slide and deform. This is supported at Old Towns Quarry by occurrence of a limestone directly underlying the translational slide. Thus, the nature of resedimentation may have been largely controlled by early marine diagenesis.

The scarce palaeoslope orientation data from resedimented units of this lithofacies differs from the regional palaeoslope (NE) and the slope on the Permo-Carboniferous unconformity in this area documented by Smith (in press). The direction of movement of the slump fold at Thickley Quarry (from east to west) is broadly in agreement with the

regional palaeoslope, although the NW-directed erosion surface at Old Towns Quarry is not. The dip of the Permo-Carboniferous in the area of Old Towns Quarry (from data in Smith, in press), is 1.4° N.E. This may suggest the presence of a locally abnormal palaeoslope at Old Towns Quarry, owing to a thick accumulation of Basal Permian Breccias or, more likely, the margins of a Carboniferous palaeohigh. Old Towns Quarry lies close to the western margin of the most westerly palaeohigh identified by Goodall (1987) (Fig. 2.1). The resedimented carbonates at Old Towns may, in turn, have been triggered by fault movements along the margins of the adjacent palaeohigh.

2.4.3. Nodular wackestone/mudstone lithofacies - Summary and conclusions.

Most of this lithofacies was deposited in a relatively quiet, deep water environment, probably >50m. Sea floor sediments were soft and heavily bioturbated, although became lithified a few centimetres to decimetres below the sediment-water interface. At least some sediments were deposited by density currents derived from shallower water environments.

Resedimented carbonates of this lithofacies lie a few kilometres to the west of localities in which the shallower water skeletal wackestone/packstone lithofacies of the Raisby Formation is developed (Fig. 2.7), in association with Carboniferous palaeohighs and islands (Fig. 2.18). Therefore, in the southern part of the study area, the regional palaeoslope was locally reversed. The relative rapidity of facies changes, from shallow water skeletal wackestones and packstones to deeper water nodular and resedimented wackestones and mudstones, suggests moderately steep slopes to the palaeohighs and islands; Wood (1950) and Raymond (1960) document slopes of 5° to 18° for the margins of the Billingham palaeohigh. These facies changes are represented schematically in figure 2.18. Such rapid lateral facies changes are very similar to those recorded on the margins of palaeohighs in the first cycle carbonates of West Germany, where a basin and swell bathymetry was developed (Paul, 1986a). The palaeohighs described by Paul (1986a) were not fault-controlled, but those within the Raisby Formation may well have been (Fig. 2.18). In addition, a distinct thickening of the Marl Slate is recorded from the area where Carboniferous palaeohighs and islands were present, westwards into the area in which the nodular wackestone/mudstone lithofacies of the Raisby Formation is developed (Fig. 2.4), further supporting the interpretation of a basin and swell bathymetry.

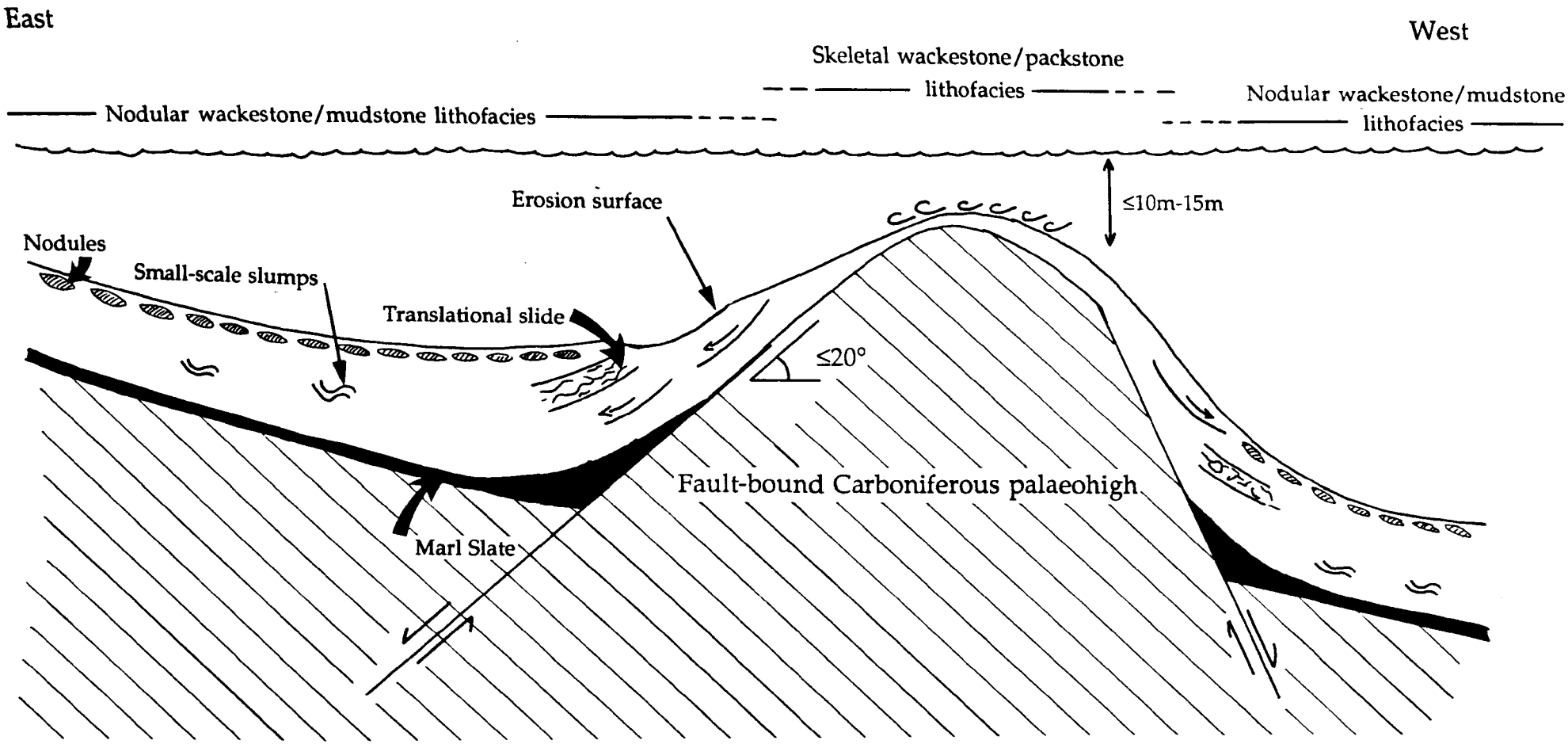

Fig. 2.18. Summary of the relationships between lithofacies of the Raisby Formation in the southern part of the study area. The skeletal wackestone/mudstone lithofacies, developed over palaeohighs, passes both west and east into deeper water nodular wackestone/mudstone lithofacies, deposited in a slope environment. Diagram is not to scale.

2.5.1. Resedimented wackestone/mudstone lithofacies - Description.

In common with the nodular wackestone/mudstone lithofacies, the resedimented wackestone/mudstone lithofacies contains planar to nodular, centimetre- to decimetre-scale bedded dolostones, locally with minor limestones near to the base of the formation. Nodules and nodular bedding is less common than within the nodular wackestone/mudstone lithofacies, although limestones are equally as abundant. This lithofacies is distinguished from the nodular wackestone/mudstone lithofacies by a distinctive suite of sedimentary structures relating to both erosion and resedimentation.

Fossils are very sparse within limestones of this lithofacies, and less common than within those of the nodular wackestone/mudstone lithofacies. The limestones, and probably most dolostones, were deposited as mudstones, with thin wackestone horizons. Fossils within the limestones are normally restricted to small calcispheres, foraminifers and ostracodes. Occasional peloids also occur. Rare, centimetre-sized articulated brachiopods, some with spines still attached were recorded from High Moorsley and Houghton Quarries, and also from a dolostone at Crime Rigg Quarry (NZ 341, 416) (Fig. 5.29a). In limestones at these localities, skeletal material is also concentrated in distinct horizons, millimetres to centimetres in thickness. One wackestone horizon at Houghton Quarry contained a well-sorted assemblage of large articulated foraminifers and ostracodes, with brachiopod and bryozoan fragments (Figs. 4.3a & 4.5a), all aligned with long axes horizontal, and parallel to each other. Relatively large (300μm), monocrystalline quartz grains were also common in this assemblage. No fine microfossils, characteristic of the host limestones, were recorded within these skeletal wackestones. Branching, horizontal burrow systems very similar to *Chondrites* (from Raisby Quarry [Fig. 2.10]) were also recorded at Houghton Quarry. Most other burrow systems, although less clear, were straight to sinuous and horizontal. The only exception was a number of sub-vertical, sinuous burrows recorded from Low Moorsley and Penshaw Hill Quarries.

Evidence for erosion, resedimentation, and slump folding of limestones and dolostones within this lithofacies was recorded at four main localities; Dawsons Plantation (NZ 337, 548), High Moorsley (NZ 334, 455), Houghton (NZ 341, 506) and Penshaw Hill (NZ 3365, 5460) Quarries, with lesser developments at Haswell Moor Farm (NZ 352, 426) and Pittington (NZ 332, 447) Quarries. It is possible that abundant joints, of a distinctive listric geometry have also influenced erosion and resedimentation in this lithofacies.

2.5.1.1. Erosion surfaces - Description.

Erosion surfaces were recorded cutting bedded carbonates on a centimetre- to metre-scale. Erosion surfaces at Haswell Moor Farm and Pittington Quarries were of similar form, comprising a few dolostone beds, which thinned abruptly laterally, and were unconformably overlain by slightly inclined beds. At High Moorsley Quarry, the contact of

dolostones with an underlying nodular limestone is strongly erosive. The erosion surface is planar, and dips to the north east. Eroded limestone blocks have been rotated, dipping at angles of up to 26°, although in different directions in different parts of the exposure. Erosion of the limestone postdated the formation of nodules within it. Large, angular slabs of dolostone up to 6 metres in length, although only a few centimetres to decimetres in thickness, overlie the erosion surface. The slabs are of all orientations, although most commonly sub-parallel to the erosion surface. The slabs themselves are overlain by normally-bedded dolostones. This erosion surface cannot be recognized at Low Moorsley Quarry, 1km to the northeast, where the contact of limestone and overlying dolostone is again exposed.

At Houghton Quarry, an erosion surface was recorded underlying an autobrecciated dolostone in the middle of the exposed Raisby Formation sequence. The erosion surface marks the abrupt junction between a decimetre-scale bedded dolostone and a metre-scale bedded autobrecciated dolostone. This erosion surface is not smooth, but stepped (Fig. 2.19). The intensity of erosion differs between quarry faces, describing a broad channel form, with the direction of erosion to the south or southeast (Fig. 2.19). Two parallel channels have been identified in the south of this quarry, although throughout most of the exposure, the contact of bedded with autobrecciated dolostone is parallel to bedding.

2.5.1.2. Resedimentation - Description.

Two lithotypes of resedimented carbonates can be defined within this lithofacies; the conglomerate lithotype (Dawsons Plantation, High Moorsley, and Penshaw Hill Quarries) and the breccia lithotype (Houghton Quarry).

Conglomerate lithotype - Description.

The conglomerate lithotype comprises one or more, predominantly fining-upwards units, composed of a calcirudite grainstone overlain by calcarenite grainstone/packstone. As an example, a conglomerate at High Moorsley Quarry lies a few metres above a limestone erosion surface, and is interbedded with slump-folded dolostones (Appendix XII). It comprises a completely-dolomitized, clast-supported, poorly-sorted calcirudite, capped by a thinner, poorly-laminated, fining-upwards calcarenite. Calcirudite clasts are rounded to sub-rounded, commonly tabular, 2-10cm long and 2-4cm thick (Fig. 2.20). The long axes of most clasts are sub-horizontal, although orientations approaching vertical may occur (Fig. 2.20). Although heavily obscured by dolomitization, relatively abundant bryozoan fragments occur within the inter-clast matrix. The calcirudites may be structureless, or faint coarsening-and fining-upwards sequences can be distinguished. The base of the calcirudite is bed-parallel, although commonly with a centimetre-scale relief owing to nodularity of the underlying dolostones. The upper surface of the calcirudite is

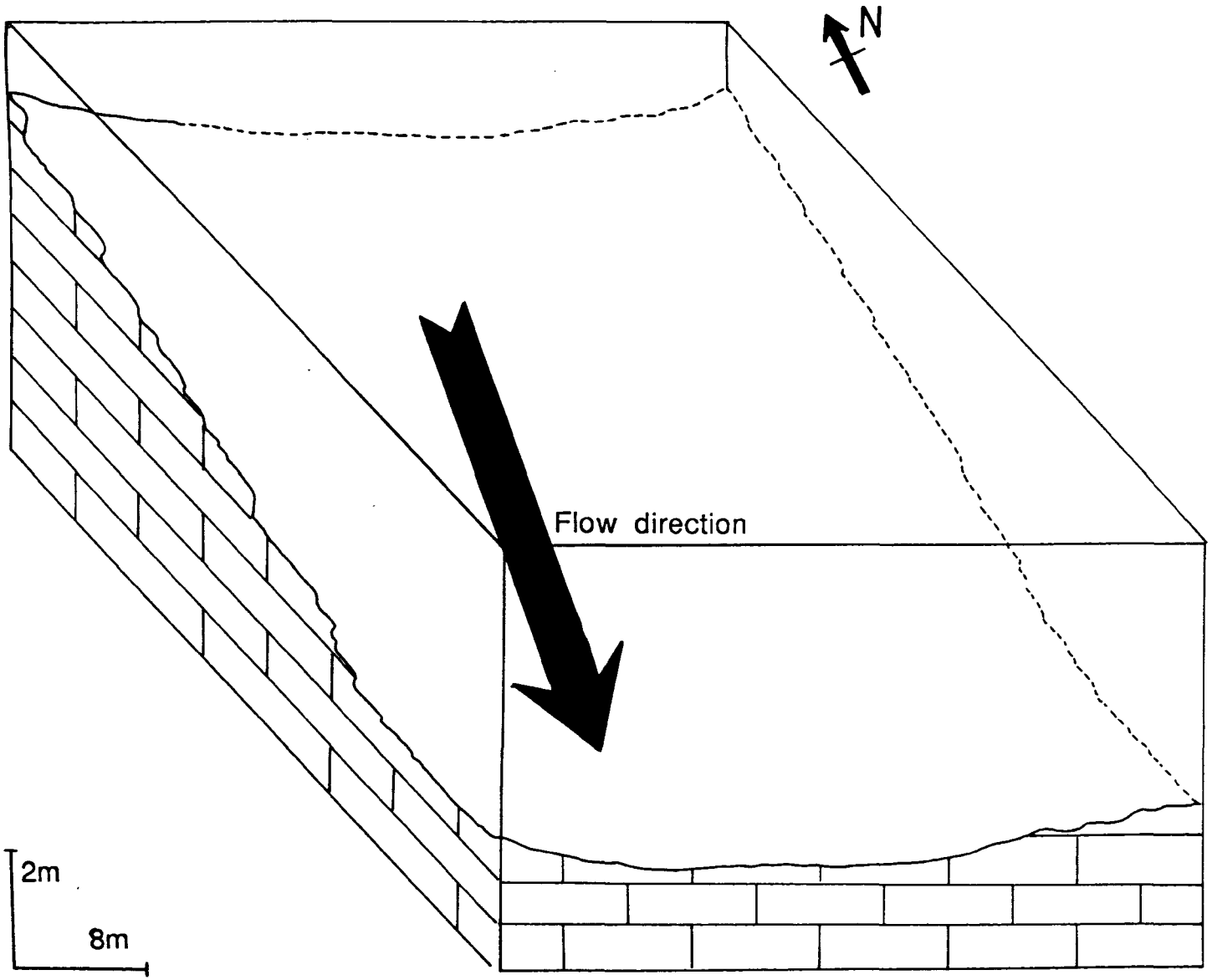

Fig. 2.19. Block diagram showing the three-dimensional structure of the erosion surface below an autobrecciated dolostone in the middle of the exposed Raisby Formation sequence, Houghton Quarry. Dashed parts of the erosion surface are inferred.

Fig. 2.20. Hand specimen of the conglomerate lithotype, High Moorsley Quarry. Tabular dolostone clasts lie in a matrix (m) which has been selectively replaced by calcium sulphate (now cemented by calcite). The dolostone clasts are, however, completely unaltered.

more irregular, the irregularities being infilled by overlying calcarenites. Tops of the calcarenites are flat and planar. The thickness of the calcarenite is roughly inversely proportional to that of calcirudite. The conglomerate at High Moorsley is of a constant character east-west, although varies abruptly north-south, eventually thinning and fining out towards the south.

A more complex example of the conglomerate lithotype occurs at Dawsons Plantation. A large resedimented unit can be traced for 243m along a northeast-southwest aligned quarry face. Its internal structure is complex, and laterally variable. Six units can be distinguished (Fig. 2.21):

1. Clast-supported calcirudite of well-rounded, grey lime mudstone clasts. This has a planar base, and abruptly varies in thickness laterally (0-20cm),

2. Deformed bedded calcite- interbedded with dolomite-mudstones (0-40cm). This unit varies from slightly contorted beds, with deformation greatest at the top of the unit, through a more deformed sediment where limestone layers exhibit sedimentary boudinage, into a sediment which has undergone complete disruption, with *in situ* formation of clasts. Some beds within this unit were deposited as matrix-supported calcirudites. This unit can be traced throughout most of the exposure,

3. One, or more, patchily developed, fining-upwards fine calcirudites/calcarenites, with strongly erosive bases into unit 2 (0-20cm),

4. Coarse, poorly-sorted, poorly-structured calcirudite (Fig. 2.22). Clasts range from subspherical to tabular, and comprise unfossiliferous lime mudstone. Clast sizes of 2-4mm are by far the most abundant. Tabular clasts are locally imbricate. Thickness (0-40cm) is broadly inversely proportional to that to unit 2, and so very variable along the outcrop (Fig. 2.21)

5. One to three units of erosive- or conformably-based, fining-upwards fine calcirudites/pebbly calcarenites (Fig. 2.22), which can be traced throughout most of the exposure. Well developed planar lamination is defined by layers of coarser and finer lime mudstone clasts (Fig. 2.22). Occasional outsized (up to 16cm long by 4cm thick) tabular clasts occur within the calcarenite. These calcarenites infill the uneven upper surface of the underlying unit 4, or that of contorted unit 2 limestones, although the junction is very abrupt (Fig. 2.22). The calcarenites also infiltrate the upper few centimetres of the unit 4 calcirudite (Fig. 2.22). The uppermost part of this unit grades conformably into calcite, and then dolomite mudstone (Fig.2.22) (0-40cm),

6. One, or more, conformably-based, laterally continuous, fining-upwards calcarenites, above unit 5, and interbedded with host lime mudstones (0-4cm).

These six units are best developed where the conglomerate as a whole is thickest (80-90cm) at the northeast end of the exposure (Fig. 2.21). At the far southwest, only thin, fine calcirudites

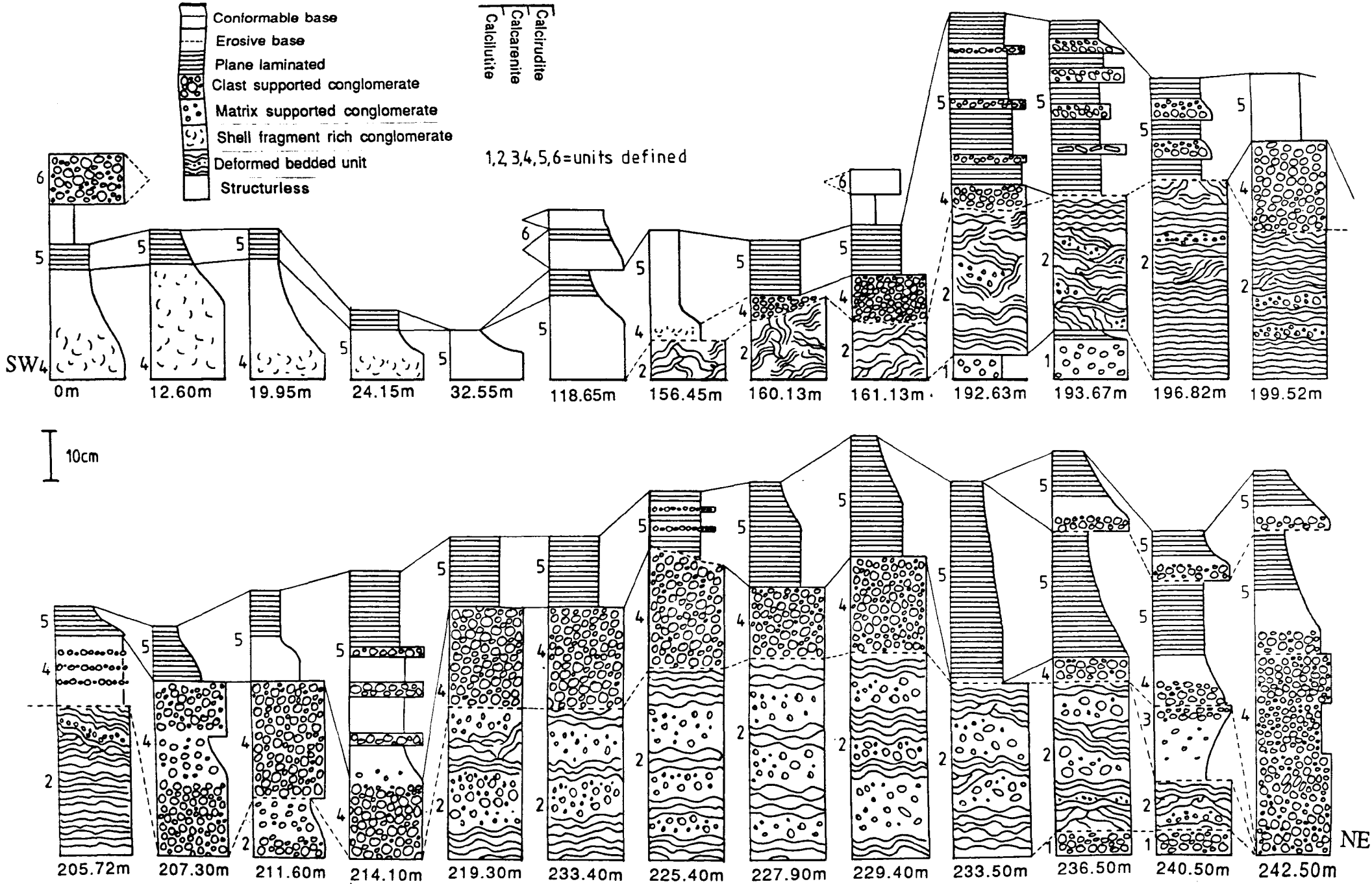

Fig. 2.21. Log sections of the conglomerate lithotype, Dawsons Plantation from various localities along the quarry face.

Fig. 2.22. Hand specimen of the unit 4 calcirudite overlain by unit 5 calcarenite, Dawsons Plantation. The unit 4 conglomerate is abruptly overlain by the calcarenite, which has also infiltrated the upper parts of the conglomerate. Part of a *Horridonia* valve is incorporated into the conglomerate (arrowed), and many limestone clasts have V-shaped fractures, into which matrix has been injected (arrowed).

and calcarenites can be recognized. At most points in the exposure, only units 2, 4 and 5 are present (Fig. 2.21).

Conglomerate clasts within unit 4 comprise uniform, unfossiliferous lime mudstones, very similar in composition to the host bedded limestones. The amount of inter-clast matrix increases up through unit 4, with basal clasts having stylolitic contacts (Fig. 2.22). Numerous V-shaped fractures cut tabular clasts, into which matrix has been injected (Fig. 2.22). The matrix contains abundant, well-articulated fossil material, including intact, centimetre-sized *Horridonia horrida* at the base, with abundant brachiopod, bryozoan and echinoderm fragments, and articulated foraminifers and ostracodes throughout. The abundance and size of skeletal fragments correlates well with the size of clasts within the calcirudite of unit 4 and calcarenite of unit 5. Skeletal material is concentrated within the finer calcirudite and calcarenite layers, where it is of a similar size to clasts.

Breccia lithotype - Description.

The breccia lithotype, only recorded from Houghton Quarry, is very different in structure and composition to the conglomerate lithotype. The breccias at Houghton Quarry overlie an erosion surface which cuts into the underlying limestones, and the thickness of the breccia is inversely proportional to that of the limestones below, with no resedimented breccias where the limestone is thickest. The limestone erosion surface is extremely irregular, and characterized by deep scours in the form of gullies (Fig. 2.23a), and larger scale erosion surfaces where up to 4.2m of the limestone has been removed, scouring off to the N or NNE. The gullies have roughly E-W orientated axes. At least one scour has formed along the upper part of a large listric joint (Fig. 2.23b). Scour surfaces are always smooth (Fig. 2.23a), and the underlying limestone, in places, shows some deformation around scour margins. The inner surfaces of some scours have small, parallel groove casts orientated ENE-WSW. The points of initial and complete erosion of the limestone within the quarry lie along parallel E-W lineations, suggesting that erosion was from the south, northwards.

The breccias which infill scour hollows are up to 4m thick, and consist of coarse, angular platy dolostone clasts within a brown clayey dolomitic matrix, and are clast-supported (Fig. 2.24). Fossils are extremely rare both within matrix and clasts. Decimetre-sized subangular to subrounded clasts of dolostone and limestone also occur within the breccias. These larger clasts commonly comprise finely bedded dolostones, in which every gradation, from unaltered dolostones, through stretched and boudinaged dolostone layers (Fig. 2.25), through layers broken into clasts, into completely disrupted and rotated dolostone layers can be recognized. The intact dolostone layers are identical to the platy dolostone clasts (Fig. 2.25). Also, the ductile, interbedded dolostone within which the lithified dolostone layers have deformed, is identical to the debris flow matrix (Fig. 2.25). The breccias, as a

Fig. 2.23. Two outcrop photographs of the limestone erosion surface and breccia fill, Houghton Quarry. (a) shows a section through a large gully cut into the grey limestone, and breccia fill. Detail of one part of the margins of the breccia fill (arrowed) is shown in figure 2.24. Approximately 1.5m of limestone is exposed. (b) shows clear evidence for an erosional gully (arrowed) being controlled by a listric joint (arrowed).

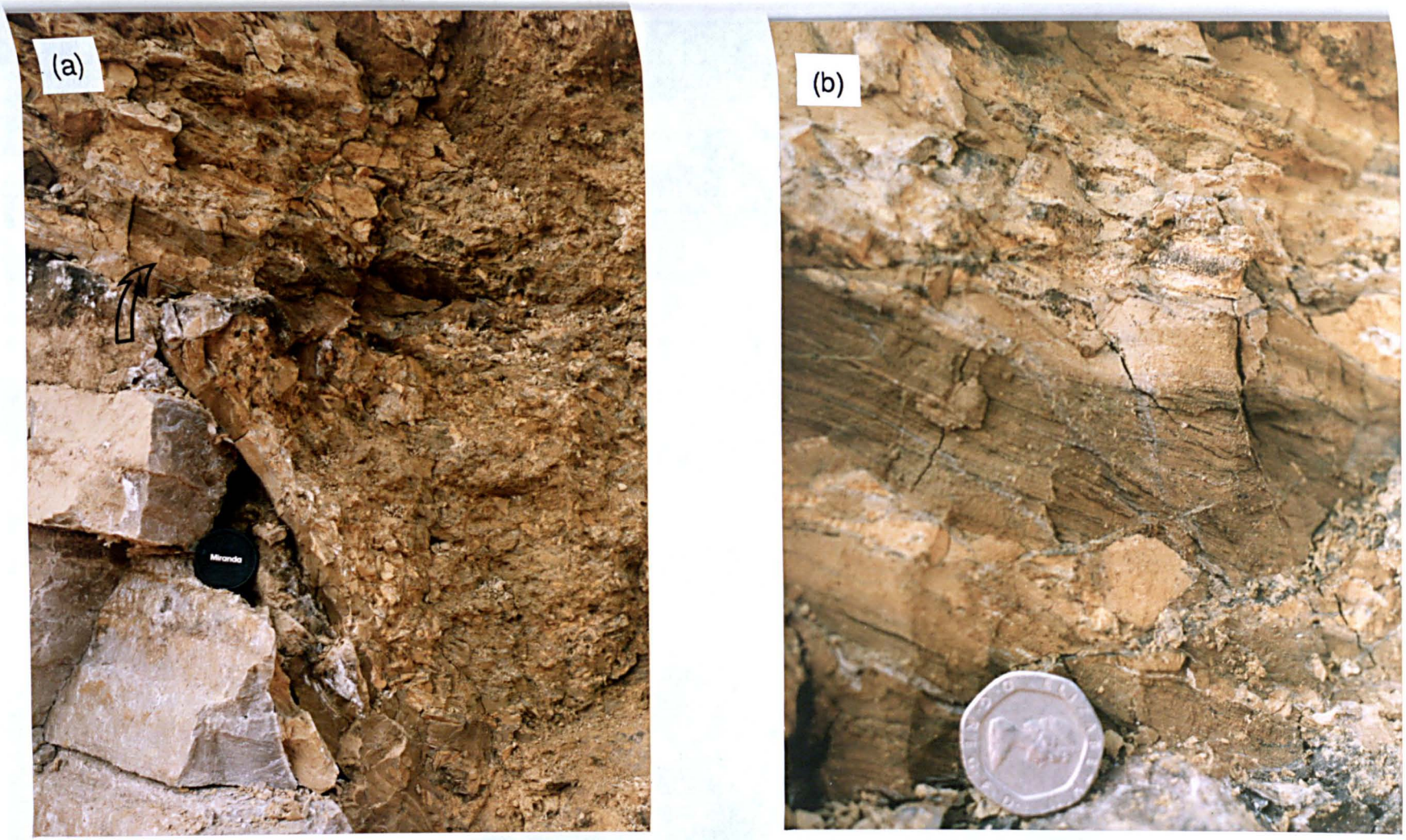

Fig. 2.24. Details of the margins of a large breccia-filled gully (figure 2.23a), Houghton Quarry. (a) shows the basal contact of the breccia with gully walls. A brown dolomitic clay lines gully margins, thickening into the axis of the gully. Lense cap is 5.5cm in diameter. Detail of the clay (arrowed) is shown in (b), which illustrates the well-laminated nature of the clay, and incorporation of layers of abraded dolostone clasts.

Fig. 2.25. Hand specimen of part of a dolostone clast within the resedimented breccia lithotype, Houghton Quarry. The clast comprises a laminated dolostone. Some layers were semi-lithified, when others were still ductile. This has led to sedimentary boudinage and incipient brecciation of some dolostone layers (arrowed).

whole, are extremely poorly sorted, and the majority of clasts are of a random orientation. However, within a few decimetres of the base of the breccia, clasts become well-orientated, with long axes parallel to both each other, and to the limestone erosion surface. These clasts dip towards the NNE/NE and SE/SSW. In most locations however, the basal few centimetres to decimetres of the resedimented unit comprises a clast-free, laminated, organic-rich, brown dolomitic clay, interbedded with thin horizons of fine subrounded dolostone clasts (Fig. 2.24a & b). The dolomitic clay lines gully margins inclined at angles of up to 70°, with lamination of the clay being parallel to gully margins (Fig. 2.24a & b). Thus, most commonly, the breccia is laminated and inversely graded at its base, and structureless in its center (Fig. 2.24a). The breccia contains evidence for considerable compaction, as the dolomitic clay is injected into joints within the underlying, much more rigid limestone. Furthermore, many of the platy dolostone clasts are cut by V-shaped fractures, into which breccia matrix has been injected.

The contact of the resedimented breccia with overlying bedded dolostones is extremely irregular, with large brecciated blocks of the dolostone within the upper parts of the resedimented breccia. Where the resedimented breccia is absent, and the dolostone directly overlies un-eroded limestone, there is no brecciation, and the bedded dolostone may onlap steep erosion surfaces within the limestone. The thickness of the brecciated bedded dolostone is broadly proportional to that of the resedimented breccia. The fractured and brecciated bedded dolostones may grade both vertically and laterally into un-fractured bedded dolostones.

2.5.1.3. Slump folds - Description.

Slump folds were recorded from High Moorsley and Houghton Quarries. In both, bedded dolostones, a few decimetres in thickness, have been deformed into small folds. At High Moorsley these are asymmetric anticlines (Fig. 2.26), whereas at Houghton the folds are symmetrical anticlines although commonly, with one limb fractured away from the other. The folds at High Moorsley are present both above and below the conglomerate lithotype (Appendix XII), whereas at Houghton Quarry, they occur within bedded dolostones directly underlying the breccia lithotype and limestone erosion surface. Of four folds at High Moorsley, three have an axial plane with a similar NW-SE strike (149°-329°, 165°-345°, 128°-308°) whereas one has a NE-SW strike (025°-308°) although the axial trend itself was curved. The facing directions of the folds show movement was from SW to NE. One fold at Houghton Quarry had a NNW-SSE strike, with facing direction suggesting movement from SSW to NNE.

Fig. 2.26. Photograph of an asymmetrical anticline, High Moorsley Quarry. Notebook is 19cm long.

2.5.1.4. Listric joints - Description.

Large-scale listric joints have been recorded from Cobblers Quarry (NZ 345, 499), Dawsons Plantation, Houghton (Fig. 2.23b), and Penshaw Hill Quarries within this lithofacies, and from a number of localities within the resedimented mudstone lithofacies. These listric joints are characteristically en-echelon, or form a conjugate pair which converge downwards, and may be up to 5m in height. Although curved in cross section, most appear to be planar along strike. They are near-vertical upwards, curving downwards to near-horizontal at their base, passing into bedding planes. Dip directions of joints measured from four localities within this lithofacies are shown in figure 2.27. There are no clear examples of synsedimentary movement along listric joints in this lithofacies, although listric joints at Houghton Quarry have influenced the shape and orientation of the limestone erosion surface (Fig. 2.23b).

2.5.2. Resedimented wackestone/mudstone lithofacies - Interpretation.

Carbonates of this lithofacies are similar, in a number of respects, to those of the nodular wackestone/mudstone lithofacies, especially with regard to the abundance of bedded limestones, and nodular limestones and dolostones, again indicative of widespread early submarine cementation. Such features, in turn, are also suggestive of slow sedimentation rates and, possibly, significant bioturbation. From the paucity of sedimentary structures, it is possible that most sediments of this lithofacies have been homogenized by bioturbation. The limestones of this lithofacies, and, by extension, dolostones as well, accumulated as fine grained hemipelagic/pelagic-derived carbonate muds containing a sparse planktonic microfauna. The only autochthonous fauna was small epifaunal brachiopods. Skeletal material is less abundant than in limestones of the nodular wackestone/mudstone lithofacies, although discrete, coarse, fossiliferous horizons again indicate input from density currents flowing from shallower water environments. In the skeletal wackestones of this lithofacies, the relative proportion of large bryozoans is less than within those of the nodular wackestone/mudstone lithofacies. This could be due to a greater distance from the shallow water source area, or more dilution of the shallower water fauna by other skeletal material entrained during flow. This evidence suggests that for most of the time, the depositional environment was one of low energy, and had a low faunal diversity. The resedimented wackestone/mudstone lithofacies was deposited lower down the depositional slope than the nodular wackestone/mudstone lithofacies.

2.5.2.1. Erosion surfaces - Interpretation.

Erosion within this lithofacies appears to have been volumetrically as significant, if not more so than resedimentation. The large scale, channelized erosion surfaces underlying autobrecciated dolostones at Houghton Quarry (Fig. 2.19), are very

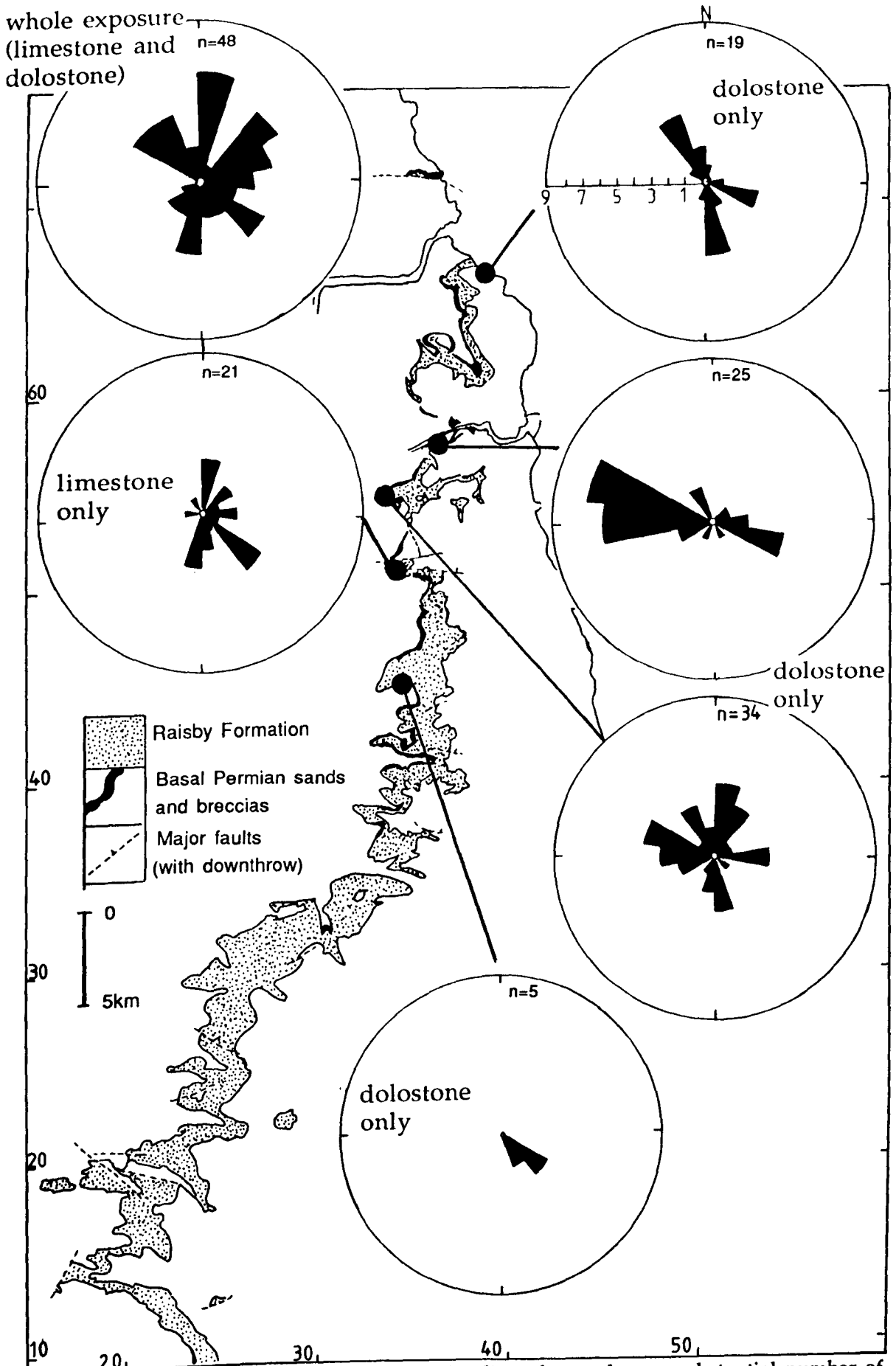

Fig. 2.27. Map of the study area, showing localities from where a substantial number of listric joints have been recorded, and their directions of dip (relative to true north). The localities, from north to south are; South Shields coastal section, Claxheugh Rock, Dawsons Plantation, Houghton Quarry, Cobblers Quarry.

similar to low angle, intraformational truncation surfaces commonly described from ancient carbonate slopes (cf. Cook, 1983). The origin of many such surfaces previously described is unclear, and may be purely erosional, or due to slope failure along discrete slide planes (Cook, 1983). An erosive origin is favoured for the Houghton Quarry structures, owing to their channeled form, consistent orientation, stepped profile, and lack of evidence for deformation of immediately underlying dolostones. The palaeoflow direction of the erosive currents (to the south or southeast) is at an angle (approximately 45°) to the regional palaeoslope inherited from the Permo-Carboniferous unconformity (northeast) in this area. Such deviation could be explained by local modification of the regional palaeoslope. Smith (1970a) records a palaeohigh of Carboniferous sandstone at Newbottle, 1km north (2.1.2). The deviation could also have resulted from the deflection of erosive currents by a north-south flowing contour current. The minor erosion surfaces recorded at Haswell Moor Farm and Pittington Quarries are smaller examples of similar submarine erosion. Thus, current strength in this lithofacies was variable, ranging from sufficiently energetic to produce large-scale erosion, to much lower velocity, probably decelerating currents which deposited layers of fine macro- and microfossils, and locally winnowed away carbonate muds.

The erosion surfaces cutting into limestones in the lower parts of High Moorsley and Houghton Quarries are clearly the product of more energetic, wholesale sediment failure. Their geometry is very similar to that of the major erosion surface at Old Towns Quarry within the nodular wackestone/mudstone lithofacies, with erosion again cutting into a limestone (Fig. 2.14). The reason for preferential development of massive failure surfaces in limestones is a factor of the rheology of the limestones, in comparison to their associated dolostones. As the limestones lithified early, they were more prone to brittle failure, whereas the associated sediments (now dolostones) were less well-consolidated, and so dissipated stress by intra-sediment, inter-bed deformation (i.e., slump folding). At all three localities where limestones have undergone large-scale failure (High Moorsely, Houghton and Old Towns Quarries), underlying, overlying, and laterally equivalent dolostones are contorted and slump folded. Orientation of the slump folds at High Moorsley and Houghton Quarries show that soft sediment movement was broadly parallel to palaeoslope (northeast), confirming that the stress was predominantly gravitational.

The limestone erosion surfaces at Houghton Quarry reflect movement along concave planes, which is supported by deformation of limestones marginal to them. These large failure surfaces have a common east-west strike, dipping northwards. Thus, they appear to have been controlled, at least in part, by failure along listric fault surfaces which dip in a similar direction (Fig. 2.27). The origin of the smaller scours at this locality is less clear, although they too were at least in part controlled by east-west striking listric joints (Fig. 2.23b).

2.5.2.2. Resedimentation - Interpretation.

The two lithotypes of resedimented carbonate clearly reflect contrasting conditions of transportation and deposition.

Conglomerate lithotype - Interpretation.

Deposition of the conglomerate lithotype was multiphase, although preservation of these individual phases is variable between localities. The most complex sequence, at Dawsons Plantation, represents three main episodes of resedimentation, interspersed with erosion. The first episode of resedimentation (unit 1) deposited a clast-supported fine calcirudite on a planar erosion surface or un-eroded bed surface. This calcirudite was partially or completely eroded, and then overlain by a sequence of carbonate mudstones interbedded with fine matrix-supported calcirudites (unit 2). Locally extensive soft sediment deformation of the upper part of this unit occurred during erosion, and later emplacement of the overlying coarse calcirudite (unit 4). Erosion of unit 2, preceding emplacement of the calcirudite was very irregular. The geometry of the erosion surfaces suggest that channels were cut into the unit 2 sediments, with their axes oblique to the NE-SW trend of the present day outcrop. Minor resedimentation, associated with some further erosion (unit 3), predated emplacement of the main calcirudite (unit 4), but these sediments are only preserved along channel axes. Deposition of the main calcirudite (unit 4) was largely controlled by the pre-existing channelized erosion surfaces. The succeeding fine calcirudite and calcarenites (unit 5) blanketed the channels and interfluves, demonstrating that, by this time, the flow was not channelised, perhaps because it was much less dense, or the channels had been infilled. The last sediments (unit 6) reflect minor density flows eroding into the top of the preceding calcarenite, and interbedding with background carbonate mudstones. They probably reflect the final pulses of the preceding resedimentation episodes.

The coarse grain size, and poor sorting and internal structure of the main calcirudite (unit 4), suggests deposition from a high density, and/or energetic flow. Transportation and deposition may have been from a high density turbidity current, or debris flow. A turbidity current is suggested by rounding of the clasts (indicative of turbulence within the flow), grading of skeletal material, and a low percentage of matrix (although this may have been substantially modified by later pressure solution). However, resedimentation by debris flow is possibly evidenced by coarse clasts, poor internal structure, and the abrupt transition into the overlying calcarenite (unit 5). Resedimentation by dilute debris flow is favoured here, although a continuum may exist between dilute debris flow and concentrated turbidity current flow. This interpretation is also valid for the conglomerates at Penshaw Hill and High Moorsley Quarry.

The fine calcirudite/calcarenite (unit 5) which caps the coarse calcirudite (unit 4) at Dawsons Plantation, and at High Moorsley and Penshaw Hill Quarries, is more clearly the product of deposition from a waning turbidity current, being normally-graded and parallel-laminated. Only Bouma divisions A, B, E(t) and E(h) have been distinguished, with B dominant (Fig. 2.22). The absence of the cross-laminated C division reflects the unsuitability of the carbonate mudstone clasts to form cross-bedding structures (they were probably too coarse). At all three localities, a relatively lower velocity, and/or density than the flow which deposited the preceding conglomerate, is indicated by the finer grain sizes, lamination, blanketing of irregularities of the upper surface of the calcirudite, and a flat, even top. The invariable occurrence of laminated calcarenites overlying poorly-structured calcirudites, with no sediments preserved between the two, suggests a genetic link. It is probable that movement of the dilute debris flow downslope generated turbidity currents. Such a process was first invoked experimentally by Hampton (1972) and has been described from ancient carbonate slopes by Krause and Oldershaw (1979).

A moving debris flow has been shown experimentally to generate turbulence in the directly overlying water mass (Hampton, 1972) (Fig. 2.28). Owing to water resistance at its leading edge, an area of reversed shear is established at the nose of the debris flow, which transports sediment backwards towards an area of fluid turbulence above the flow where sediment is kept in suspension (Fig. 2.28). Thus, as it moves downslope, the debris flow generates a considerable volume of turbulent, sediment-laden water which itself moves downslope under the influence of gravity (turbidity current). This will deposit a sequence of finer-grained sediments directly above the debris flow which record deposition from waning currents. This process can account for all of the features observed within the conglomerate lithotype of the resedimented wackestone/mudstone lithofacies. The thickness of laminated calcarenite, together with its relative coarseness, favours a low density precursor debris flow in which, as illustrated experimentally by Hampton (1972), areas of reversed shear develop through a large part of the nose of the debris flow. This reversed shear increases the relative size of the turbulent cloud, and also increases turbulence within the debris flow itself, leading to greater clast rounding. Furthermore, this process can also explain the presence of anomalous, outsized, tabular clasts within the laminated calcarenite. Hampton (1972) observed that, in both high and low density experimentally-produced debris flows, coherent lumps of sediment were occasionally ripped from the front of nose of the debris flow and tossed into the overlying turbulent cloud.

Clasts of the conglomerate lithotype are all very similar, tabular, unfossiliferous mudstones. They are almost identical in composition to the non-resedimented carbonates of this lithofacies, and so most clasts were probably derived by rip-up of semi-lithified sea floor material, probably analogous to the early diagenetic nodular limestones. This further suggests that the onset of early cementation was at relatively shallow depths below the sea

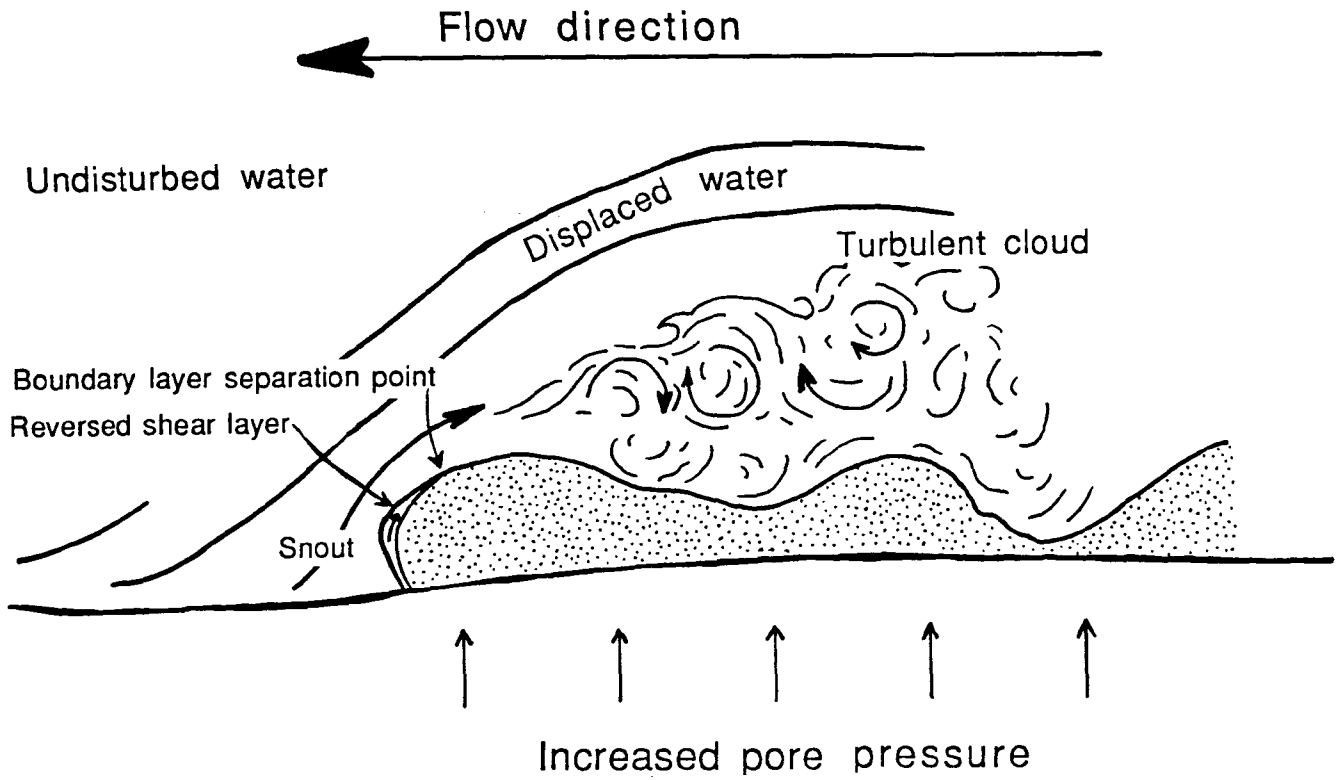

Fig. 2.28. Schematic diagram showing the most important features relating to down-slope movement of a debris flow (modified from Krause and Oldershaw, 1979). The main body of the debris flow (stippled) deposits coarse conglomerates, whereas the entrained turbulent cloud deposits finer clastic layers (turbidity current deposits).

floor, although the lithified layers could have been exposed on the sea floor following winnowing of overlying unconsolidated carbonate muds to form submarine hardgrounds. Clast formation by the rip-up of early cemented layers is further confirmed by the extensive sedimentary boudinage and semi-brittle deformation of bedded limestones at Dawsons Plantation (unit 2), where semi-lithified limestone layers have deformed within a considerably more ductile matrix, now dolomite. Therefore, the debris flow conglomerates originated on the slope, possibly from large-scale failure surfaces, such as exposed in Old Towns and High Moorsley Quarries. Old Towns Quarry is equivalent to approximately 11km upslope of Dawsons Plantation. Cook (1983) favours an origin for debris flows composed primarily of slope-derived carbonate by the re-moulding of submarine slides. As there is good evidence for translational slides in the nodular wackestone/mudstone lithofacies, debris flow generation was, thus, probably linked to the formation of submarine slides, themselves generated by large scale slope failure.

Palaeoflow directions for the conglomerate lithotype are difficult to determine. The debris flow conglomerate at High Moorsley Quarry indicates an eastwards palaeoflow, because its exposure on the north-south orientated quarry face is strongly irregular in thickness, a common characteristic of debris flows seen in section normal to palaeoflow (Hiscott and James, 1985). Smith and Taylor (1990) suggest, on the basis of clast imbrication, that palaeoflow at Dawsons Plantation was to the northeast, parallel to palaeoslope. However, at this locality, much of the flow was channelized, and the orientations of the axes of these erosive channels cannot be accurately determined. In spite of this, an eastwards palaeoflow would be in broad agreement with geometry of the channelization.

Breccia lithotype - Interpretation.

The breccia lithotype at Houghton Quarry was deposited under very different conditions than was the conglomerate lithotype. The Houghton Quarry breccia has more abundant matrix, and the clasts are angular and tabular, and show minimal abrasion and little internal structure. There is also no evidence for a finer-grained capping turbidite deposit, although this may have been obscured by later brecciation of the overlying dolostones, or eroded off before sedimentation of overlying dolostones. It is most likely that the breccia lithotype was deposited as a viscous, subaqueous debris flow, channelized within the irregular, eroded surface of the underlying limestone.

In subaqueous debris flows, clasts are supported by the strength and buoyancy of a dense fluid matrix. They move slowly and, commonly, intermittently. During their movement, two rheological zones are developed; a narrow basal, and an upper zone characterised by laminar shear, and a central area where no movement takes place, and which is rafted along as a rigid plug (Fig. 2.29). The debris flow moves by laminar shear in its basal part where in contact with the substrate. Development of the upper laminar shear zone

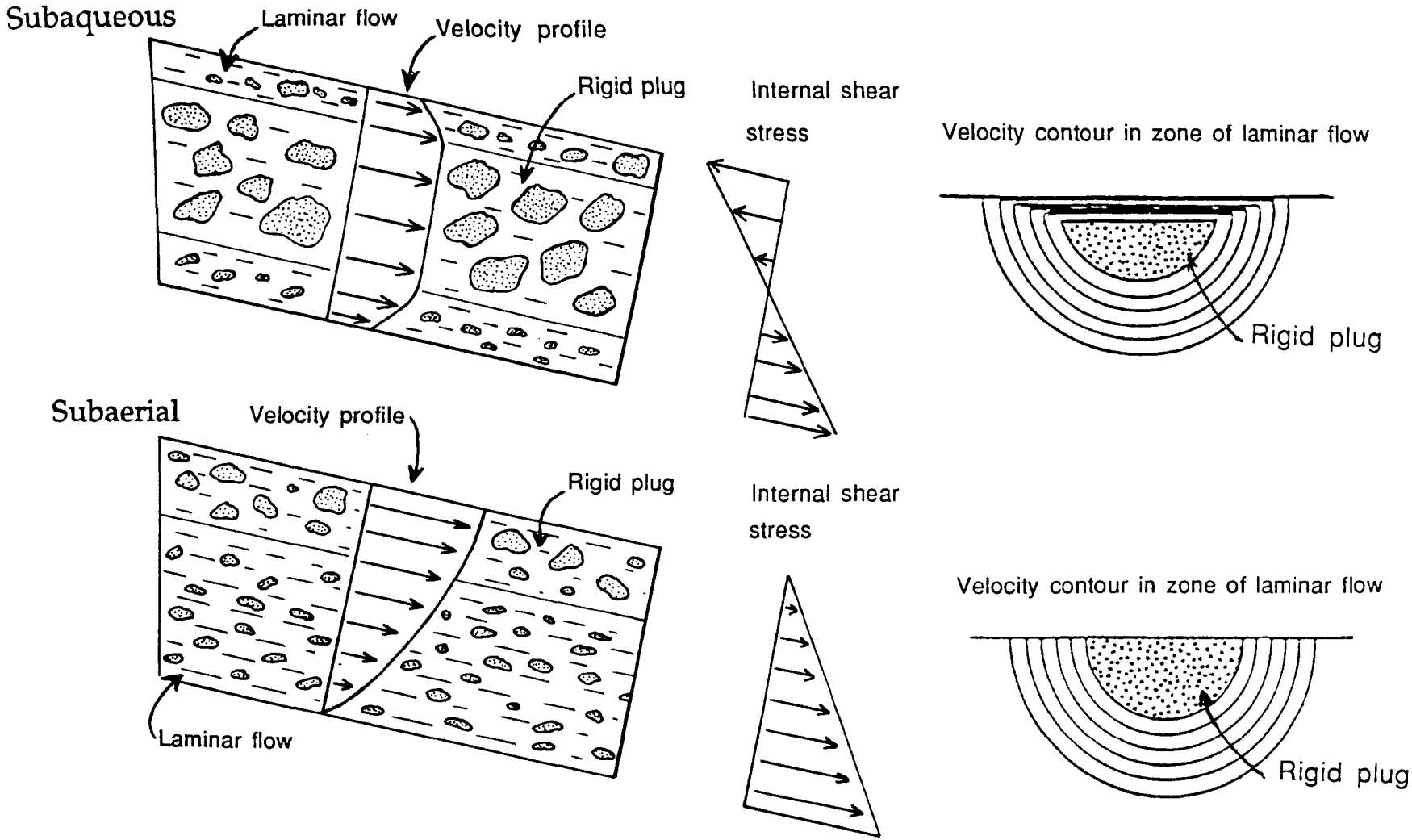

Fig. 2.29 . Schematic diagrams illustrating the different rheological zones and movement characteristics within subaqueous and subaerial debris flows. Modified from Carter (1975), Middleton and Hampton (1976), and Stow (1986).

is in response to friction from the overlying water column. In the Houghton Quarry example, which probably moved erratically and very slowly, the upper laminar zone is unlikely to have developed, and thus the velocity profile through the flow may have been analogous to that characteristic of subaerial debris flows (Fig. 2.29). Debris flows move in response to gravity, but only when shear strength owing to gravity exceeds total yield strength of the debris. Yield strength is not exceeded in the central plug. Deposition from debris flow occurs by mass emplacement, whereby the debris flow abruptly stops moving (or 'freezes') when the matrix strength of the lower parts of the flow are not exceeded by gravitationally-induced shear, i.e., the rigid plug expands to the whole flow.

The predicted patterns of movement (Fig. 2.29), accord exceptionally well with structures within the Houghton Quarry breccia. Most significantly, the inverse grading at its base, where finely laminated dolomitic clays are interbedded with abraded, subrounded dolostone clasts (Fig. 2.24) and parallel-aligned platy dolostone clasts, is exactly what would be expected within the basal shear zone of such a debris flow. This is further confirmed by the presence of laminated dolomitic clay lining near-vertical scour walls (Fig. 2.24), a feature difficult to account for apart from by viscous debris flow deposition in channels. Laminar shear circumferential to the whole flow is the predicted and observed pattern for channelized debris flow (Carter, 1975; Middleton and Hampton, 1976) (Fig. 2.29). Hampton (1975) suggests that fine grained materials tend to be transported in the basal and lateral shear zones of the flow, rather than in the rigid plug, as is observed at Houghton Quarry. Inverse grading from the laminated clay into structureless platy breccia reflects the gradation from laminar into plug flow. Alignment of basal platy clasts suggests movement of the Houghton Quarry debris flow to the NNE/NE.

The distinctive clasts of the Houghton Quarry breccia very closely resemble finely bedded dolostones within Houghton Quarry, and dolostone clasts showing signs of incipient brecciation are common (Fig. 2.25). This suggests that the whole debris flow has formed by local disaggregation of a carbonate, originally containing semi-lithified layers, interbedded with a much more ductile sediment. Disruption and brecciation of the finely-bedded dolostone, and large-scale failure of the underlying limestone, were probably genetically related. The stresses imparted on the sediment pile by large scale slope failure along listric faults may have triggered disaggregation of the laterally equivalent and overlying dolostones, owing to pore water expulsion. Rapid, upwards expulsion of pore waters caused fluidization of overlying sediments, decreasing their static yield strength, thus enabling them to flow. Sands are commonly recorded to temporarily fluidize (become 'quick') following rapid pore water expulsion associated with earthquake shocks (Carter, 1975; Middleton and Hampton, 1976). The same process may have been operative within finely bedded dolostones at Houghton Quarry, albeit only momentarily, sufficient to cause mobilization and instability enough to form debris flow.

The coarse, angular dolostone breccias overlying the debris flow breccia are considered to have formed during early burial in response to intense compaction of the debris flow breccia in contrast to that of the host rigid limestones. As the debris flow is not continuous, abruptly thinning and thickening, compaction during burial would have been uneven, leading to brecciation of dolostone overlying the thickest parts of the debris flow. As the debris flow was still partially ductile during burial, the large dolostone clasts may have become further rotated within the debris flow, producing the complex structures now seen.

2.5.2.3. Listric joints - Interpretation.

Listric joints measured at Houghton Quarry, and other localities, have variable orientations (Fig. 2.27). This variability is probably the combination of three factors:

1. The joints may be curved parallel to strike on a large (metre) scale, such that the orientation measured along one part of the joint surface at outcrop is not necessarily representative of the overall trend,
2. Formation of the joints may not have been controlled solely by palaeoslope,
3. Conjugate pairs of joints dip in opposite directions, thus imparting a strong bimodality of orientations.

However, at Houghton Quarry at least, listric joints played a significant role in determining the geometry of the major erosion surfaces and smaller scours. That listric joints occur within non-deformed Raisby Formation sequences, shows that they formed independently of distinct resedimentation episodes, although were activated during slope failure. Movement along listric faults is discussed further with regard to the resedimented mudstone lithofacies (2.6.4.1).

2.5.3. Resedimented wackestone/mudstone lithofacies - Summary and conclusions.

Non-resedimented carbonates of this lithofacies were deposited as mudstones and wackestones. At least some of the skeletal material for wackestone horizons was derived from shallower waters by downslope-moving currents, but most sedimentation was probably by slow settling out of carbonate mud and fine skeletal material derived from the Raisby Formation shelf.

The resedimented wackestone/mudstone lithofacies is characterized by both erosion and resedimentation. Erosion by downslope-moving currents was channelized, or controlled by slope failure along listric faults with strike directions normal to the slope. However, where the sediment was un-lithified or partly lithified, it responded to this gravitational stress by soft-sediment deformation rather than brittle failure. In the cases where resedimentation followed erosion, the resedimented carbonates were channelized. Where not preceded by erosion, they were deposited as laterally extensive sheets, probably kilometres in extent. The agents by which the resedimented carbonates were deposited were

not sufficiently energetic to substantially erode sea floor sediments themselves. The coarser resedimented carbonates were sourced from further up the carbonate slope, such as in the nodular wackestone/mudstone lithofacies, or within the resedimented wackestone/mudstone lithofacies itself. Finer fossiliferous resedimented units may have been sourced from the uppermost slope, or outer shelf. Resedimentation in this lithofacies was volumetrically more important than within the nodular wackestone/mudstone lithofacies, suggesting a higher depositional gradient. Thus, this lithofacies is considered to have been deposited in a slope environment, lower down the slope from the nodular wackestone/mudstone lithofacies where erosion was of much less significance, and controlled by sea floor irregularities. In detail, styles of erosion and resedimentation of the nodular and resedimented wackestone/mudstone lithofacies is directly related to the intensity of early cementation of sea floor sediments (Fig. 2.30).

Water depths in this area, of 60m to 90m have been suggested by Smith (1980a). However, on the basis that parts of this lithofacies were deposited probably ≥15km from the contemporaneous shoreline, water depths of ≥200m are more realistic.

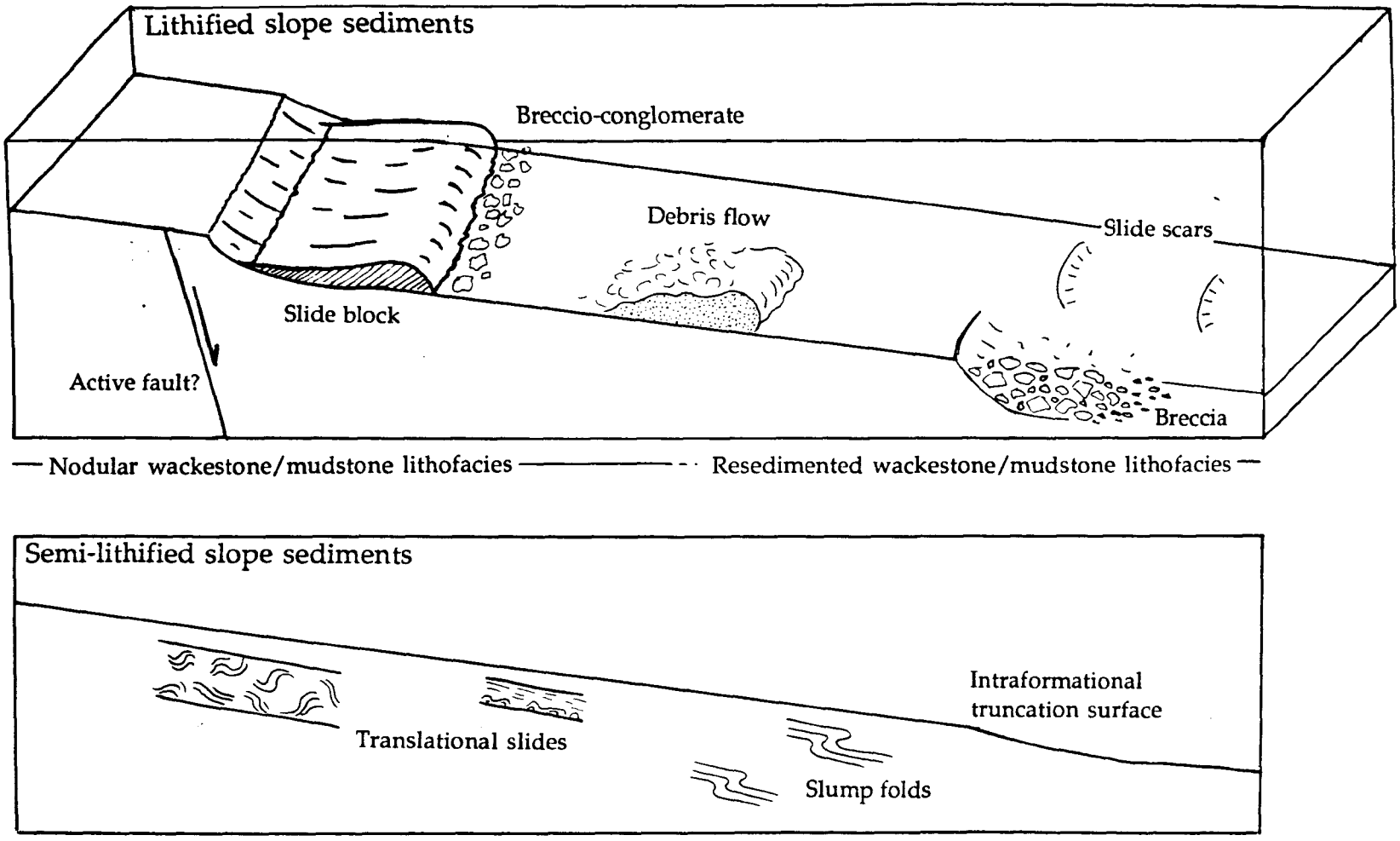

Fig. 2.30. Schematic diagram illustrating the different styles of failure between lithified (above) and semi-lithified (below) slope sediments in the Raisby Formation. Some of the sediments which were lithified when resedimented are now limestones, whereas all of those which were semi-lithified during resedimentation are now dolostones.

2.6.1. Resedimented mudstone lithofacies - Introduction.

The resedimented mudstone lithofacies is distinguished from the resedimented wackestone/mudstone lithofacies by its composition, and in being affected by large-scale resedimentation, which took place close to the end of deposition of the Raisby Formation of this lithofacies. The resedimented wackestone/mudstone lithofacies is overlain by lagoonal facies of the Ford Formation, whereas this lithofacies is overlain by reef facies of the Ford Formation, and coeval sediments which were deposited to the east of the reef.

Much of the resedimented mudstone lithofacies has been removed at outcrop by large-scale resedimentation, such that little of this lithofacies, as it was originally deposited, is preserved. Thus, the original nature of the resedimented mudstone lithofacies will be discussed firstly, mainly from offshore borehole data, followed by the nature of large scale resedimentation, mainly recorded from outcrop.

2.6.2. Resedimented mudstone lithofacies not affected by large scale resedimentation - Description.

Raisby Formation carbonates of this lithofacies at outcrop, are exclusively evenly-bedded dolostones. Owing to texture-destructive dolomitization, little can be deduced of their depositional environment from palaeontology or palaeoecology. Undisturbed dolostones of this lithofacies crop out below resedimented carbonates along the Trow Point to Man Haven coastal section, South Shields. These dolostones are evenly-bedded and uniform, although have been intensely bioturbated. Most burrows are tubular, a few millimetres in diameter, elongate, slightly sinuous and occasionally branching, a few centimetres in length. In the northern part of Grahams Sand (NZ 3850, 6650) distinctive, radiating star-shaped trace fossils have also been recorded, very similar to *Lorenzinia* (cf. Frey and Pemberton, 1984). These dolostones are almost completely undisturbed, apart from sedimentary boudinage of some thin beds where close to thick resedimented units, plus the development of abundant listric joints.

The Raisby Formation within offshore boreholes is variable in thickness, an average of 20m. Most boreholes record a more complete sequence of this lithofacies than do onshore exposures. The boreholes comprise uniform bedded dolostones, with limestones recorded at the base of E3a, and throughout most of W15. Poorly-preserved fossils from the dolostones are mainly calcispheres and small foraminifers. Likewise, most of borehole W15 comprised a mudstone, with a sparse fauna of small intact microfossils, and some broken shell fragments. However, one horizon within W15 comprised a packstone of large, algal —coated shell fragments and coated grains, all extensively replaced by sulphates (Fig. 5.23).

Within most of the boreholes, few, if any, primary sedimentary structures could be discerned. However, very finely crystalline dolostones close to the base of the Seaham borehole contained numerous, thin (millimetre- to centimetre-sized), graded units. The

main constituent of the graded units are millimetre-sized flecks of organic matter. These graded units are both slumped and microfaulted, and have been bioturbated to a greater or lesser extent (Fig. 2.31a). Microstylolitized nodules were also recorded from a number of boreholes, including W8, W15 (Fig. 2.13), and the Hartlepool Lighthouse borehole (NZ 5319, 3387) (Smith and Francis, 1967).

Resedimented horizons were recorded from most boreholes, and concentrated a few metres above the base of the formation, and at its top. The uppermost unit within the Seaham and W15 boreholes comprises large-scale slumped and contorted dolostones, whereas the lower unit comprises conglomerates in E3a, and conglomerates plus slump folds in W15 (Appendix XII). The conglomerates are made up of well-rounded to angular, mudstone clasts supported within a mudstone matrix. The conglomerate clasts within W15 are very similar in appearance to the microstylolitized nodules with which they are interbedded, and many of the small slump folds in the lower part of borehole W15 have deformed both conglomeratic layers and nodules. The nodule layers have been fractured during slumping (Fig. 2.31b), and show signs of incipient brecciation.

2.6.3. Large scale resedimentation within the resedimented mudstone lithofacies - Description.

Undisturbed carbonates of the resedimented mudstone lithofacies are unconformably overlain by large-scale resedimented carbonates in all localities at outcrop. These exposures are all very different, and so will be described individually.

2.6.3.1. Claxheugh Rock (NZ 363, 575).

At this exposure, approximately 180m long (Fig. 2.32), the Basal Permian Sands and first cycle carbonates are exposed from the Marl Slate, through the Raisby Formation (Fig. 2.6), to the reef facies of the Ford Formation (Fig. 2.32). The base of the Ford Formation reef is strongly unconformable, overlying progressively older sediments from the Raisby Formation, through the Marl Slate, and onto the Basal Permian Sands from SW to NE. Here, the Raisby Formation is very thin, reaching a maximum of 3.2m at the SW end of the exposure. Smith (1970b) suggests that 18m to 25m of Raisby Formation has been removed from this locality.

Where the Ford Formation reef overlies the Raisby Formation, their contact is gently erosional along a smooth plane. The erosion surface dips towards the SE, as does bedding in the Marl Slate, Raisby and Ford Formations, at a similar angle. At the SW end of the exposure, where the reef rests on Raisby Formation, two large groove casts are developed on the basal surface of the reef. Although they are similar in form they are not parallel. The largest strikes 058°-238°. Where the Raisby Formation is absent, the reef rests on the Basal Permian Sands, and the erosion surface is much more irregular and pitted. Large, metre-

Fig. 2.31. Photographs showing different styles of resedimentation within the resedimented mudstone lithofacies; (a) Seaham borehole, 116.40m, (b) borehole W15, 264.60m. (a) shows organic fleck-rich graded beds which have been microfaulted and partially bioturbated (arrowed) (scale in centimetres). (b) illustrates part of a slump fold which has deformed a conglomeratic horizon. Semi-lithified layers have also been fractured. The fractures are now cemented by gypsum. Arrow indicates way up. Scale in centimetres.

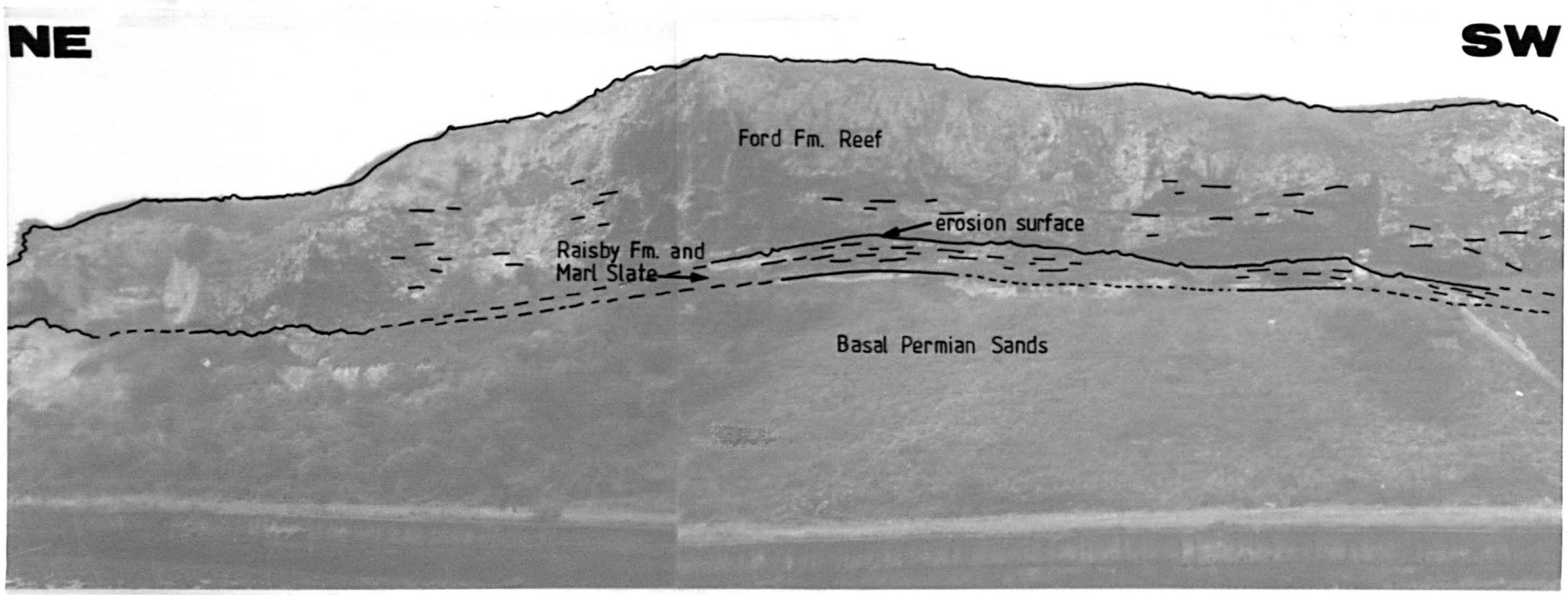

Fig. 2.32 Photographs showing the section exposed at Claxheugh Rock. Most of the exposure comprises the Ford Formation reef, which rests on progressively older sediments from SW to NE (details on overlay).

sized gouges are filled by a coarse (10-25cm), clast-supported breccia comprising angular, grey, porous reef and ?Raisby Formation dolostone clasts in a sand- and clay-rich matrix. Although the lower surfaces of the hollows are irregular, their upper surfaces have been planed by the reef base erosion surface. Where the breccia is absent, a 3cm-thick brown clay demarcates the Basal Permian Sand-Ford Formation reef junction.

Listric joints are extremely abundant within the Raisby Formation and Marl Slate at this exposure, although absent from the Basal Permian Sands and Ford Formation reef. The Basal Permian Sands are heavily fractured at this locality, although the fractures do not have a listric geometry. The listric joints are very similar in structure to those of the resedimented wackestone/mudstone lithofacies. Joint orientations are strongly bimodal (Fig. 2.27), reflecting the dominance of conjugate joint pairs. Most joints show no evidence for movement along their surfaces. However, in the SW end of the exposure, two listric faults were recorded, trending 168°/52°NE and 179°/41°NE downthrowing 29cm and 5cm respectively to the NE. The former fault displaced the base of the reef whereas the latter was truncated against it.

A very similar section was formerly exposed at Down Hill (NZ 3485, 6012) (2.5km NW). Here, the Raisby Formation was 0m-12.2m thick (Woolacott, 1914), and the Ford Formation reef rested unconformably on the Raisby Formation or Basal Permian Sands (Woolacott, 1914; Trechmann, 1954; Smith, 1970b). A dolostone breccia or brown clay was patchily developed between the reef and Basal Permian Sands. In one exposed face, the Raisby Formation was progressively cut out from south to north (Smith, 1970b). Woolacott (1914) and Trechmann (1954) also describe a very uneven, irregular contact of the Raisby Formation with Ford Formation reef at Hylton Castle, Sunderland (approximately NZ 350, 588), and Woolacott (1914) describes a similar irregular contact at West Boldon, Sunderland (approximately NZ 357, 612).

2.6.3.2. South Shields coastal section.

The Raisby Formation is exposed discontinuously along an approximately 2km-long coastal section to the south and east of South Shields. The top of the Raisby Formation is widely exposed, although its basal contact with the Marl Slate is only seen in the southern corner of Frenchmans Bay (NZ 3900, 6610). The Raisby Formation comprises well-bedded dolostones, abruptly overlain by a complex sequence of resedimented dolostones, a few metres in thickness. These in turn are patchily overlain by a centimetre- to decimetre-thick bed of algal stromatolites or oncoid packstone (the Trow Point Bed [Smith, 1986]). The uppermost resedimented carbonates, or Trow Point Bed, are overlain by a centimetre-thick, clayey residue of the Hartlepool Anhydrite Formation and calcitized, collapse brecciated, cycle two carbonates (Appendix XII).

Resedimented dolostones are present throughout the coastal exposure, from Trow Point (NZ 384, 667) to Man Haven (NZ 3461, 6601), and are laterally highly variable in thickness. Their contact with the undisturbed, bedded Raisby Formation is generally sharp, planar, and bed-parallel, although with local scouring on the scale of a few decimetres. The position of the Marl Slate relative to the top of the Raisby Formation throughout most of the exposure cannot be determined. Smith (unpublished field guide, 1989) estimates that the top of the Raisby Formation is up to 17m above the Marl Slate at Trow Point. In Frenchmans Bay, where the Marl Slate is exposed, the top of the Raisby Formation is approximately 9.8m-13.55m above the Marl Slate, although much of this thickness is accommodated by a large displaced block. The basal erosion surface of this block comes within a few metres of the top of the Marl Slate. Most of the thickness variation of the resedimented Raisby Formation is accommodated by variation in relief of its upper surface.

Within the Raisby Formation along the South Shields coastal section, three lithotypes of resedimented carbonates may be defined:

1. Structureless lithotype.

This is volumetrically very significant. The dolostones are characteristically unbedded, and have been intensely replaced by large sulphate nodules (now calcite-lined cavities after sulphates) (Fig. 2.33a). Rounded, centimetre-sized, tabular dolostone clasts are common, supported within a structureless matrix, and larger, decimetre- to metre-sized blocks of bedded dolostones also occur,

2. Bedded lithotype

This lithotype is volumetrically of equal importance as the structureless lithotype. It passes laterally and vertically into the structureless lithotype, gradationally by a decrease in the definition of beds, or abruptly, with truncation of the beds along a planar or slightly undulate erosion surface (Fig. 2.33b). Characteristically, beds are thicker and less well-defined than those of the undisturbed Raisby Formation below, and may incorporate decimetre-sized blocks of bedded dolostone. In almost all cases, beds gently onlap the uppermost surface of the undisturbed, bedded Raisby Formation (Fig. 2.35a). Bedding within this lithotype itself may vary from near horizontal or slightly inclined, to strongly contorted (Figs. 5.26b & 2.34b). In any one area, the bedded lithotype onlaps the upper surface of the undisturbed Raisby Formation with a consistent orientation. The most common strike direction of the bedded units throughout the coastal exposure is NNE/NE - SSW/SW, dipping either SE or NW (Fig. 2.35a).

3. Conglomerate lithotype.

Conglomerates are relatively rare. They are most commonly matrix supported, containing centimetre-sized tabular clasts. Most conglomerates are 10cm-20cm thick, but may reach up to a maximum of 70cm in thickness. Typically, they are very poorly sorted, with

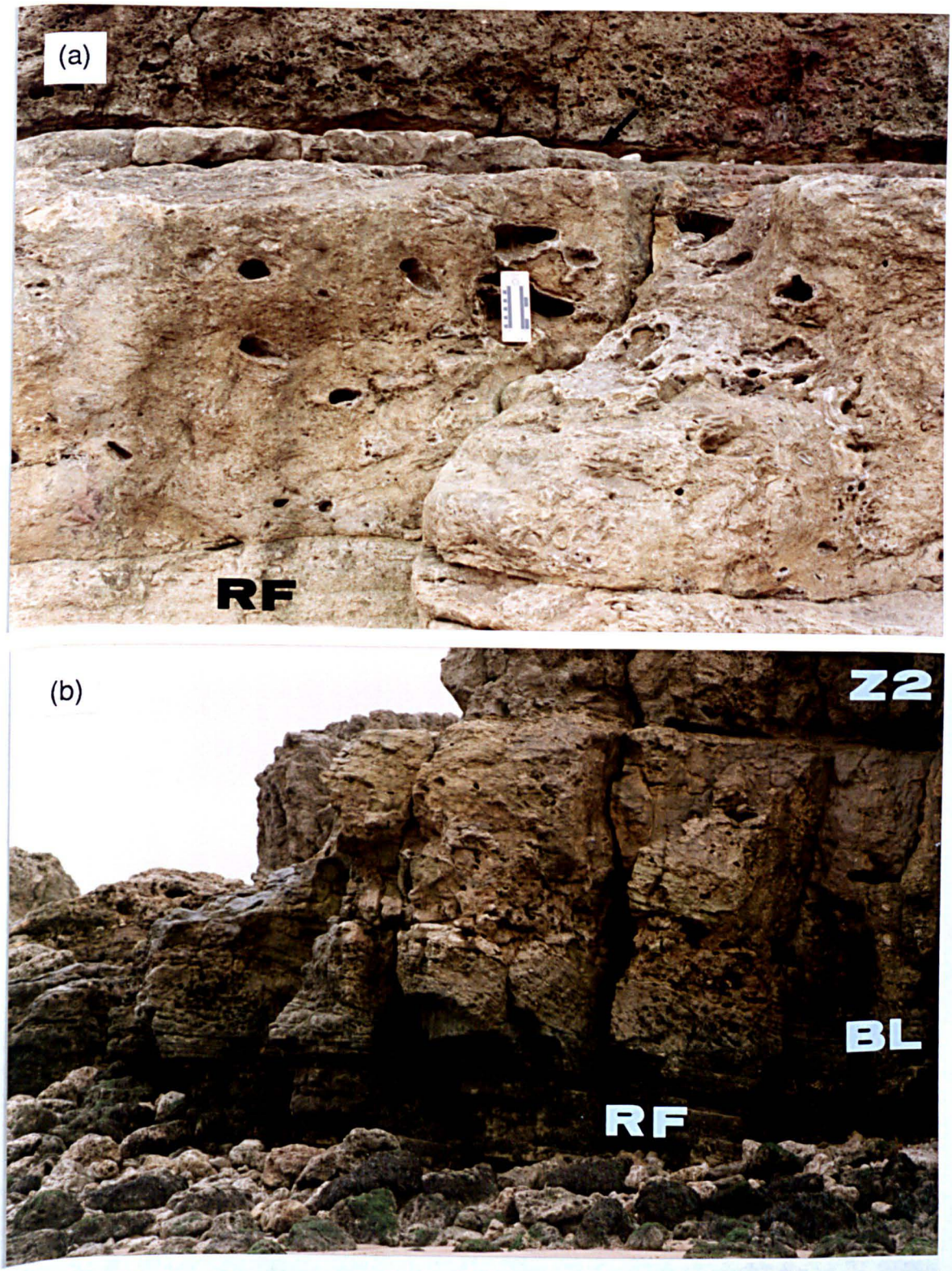

Fig. 2.33 Photographs of the resedimented Raisby Formation along the South Shields coastal section. (a) the structureless lithotype where it directly overlies undisturbed Raisby Formation (RF), in the northernmost part of Graham's Sand. This unit has been heavily replaced by gypsum/anhydrite, now cavities after sulphates. It is overlain by one bed of Raisby Formation, followed by the residue of the Hartlepool Anhydrite Formation (arrowed) and Z2 collapse breccias (Z2). Scale is 16cm long. The same sequence, from Trow Point is shown in (b), although the structureless is overlain by bedded lithotype (BL), which unconformably overlies Raisby Formation (RF). The cliff face is approximately 5m high.

Fig. 2.34. Two photographs of the bedded lithotype (a) shows a well-developed bedded unit in the southernmost part of Target Rocks, South Shields. The bedded lithotype overlies undisturbed Raisby Formation, and is itself overlain by calcitized Trow Point Bed (tp) and Z2 collapse breccias. Tape is 1m long. (b) illustrates a very large, internally-deformed bedded lithotype, Trow Point. Bedding is accentuated by calcitization along bedding planes. Cliff face is approximately 5m high.

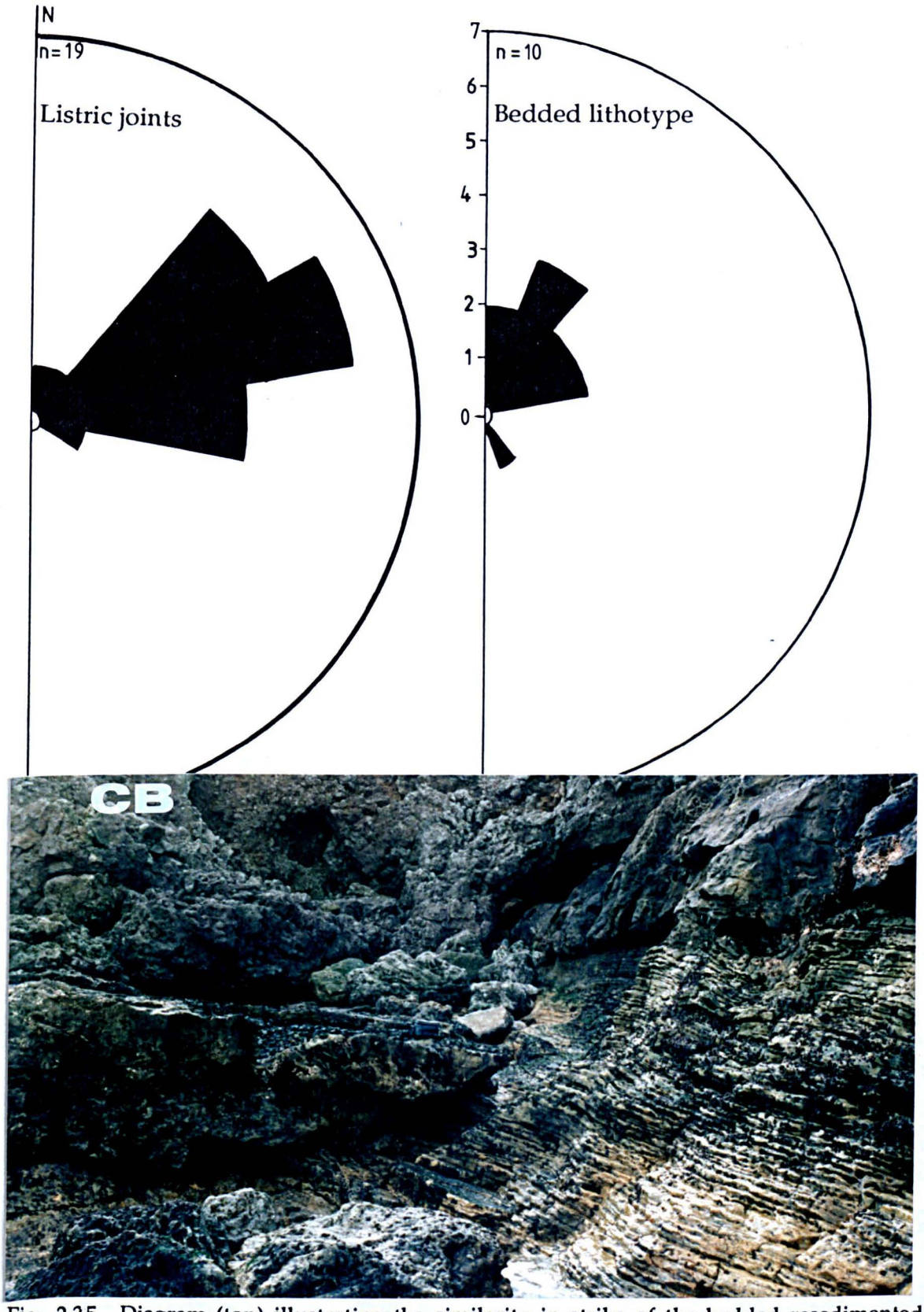

Fig. 2.35 Diagram (top) illustrating the similarity in strike of the bedded resedimented lithotype, and listric joints along the South Shields coastal section. The photograph below is of a listric fault, Man Haven. The whole of the exposed Raisby Formation (approximately 6m) is cut, although Z2 collapse breccias (CB) are not.

with little internal structure; they have been intensely replaced by sulphates, and the sulphates themselves locally replaced by barite (Fig. 7.3a). Conglomerates may occur within the uppermost, undisturbed Raisby Formation, or along the contact of resedimented with un-disturbed dolostones (Fig. 7.3a). A conglomerate is incorporated into a large slump fold in one part of Frenchmans Bay, and has acted as a decollement surface for the basal slide plane of a large block in another part of the same locality.

Most typically, the resedimented sequence comprises a few metres of the bedded lithotype overlain by an equal or lesser thickness of the structureless lithotype (Fig. 2.33b) which may, or may not, contain blocks and conglomeratic layers. Where the bedded lithotype is thick, the structureless lithotype is thin or absent (Fig. 2.34b). Thickness variations within the resedimented dolostones, as a whole, reveal no systematic trends, although they are thickest in the northern part of Trow Point.

Listric joints are very common along this coastal section. Some cut both undisturbed and resedimented carbonates, whereas others only cut the undisturbed dolostones. None of the joints cut the Z2 collapse breccias. The joints commonly occur in conjugate pairs, breaking the rock up into wedge-shaped units. The joints have a predominant NNW and SSE dip (Fig. 2.27). The strike of the joints is, in turn, very similar to the strike of the beds within the bedded resedimented lithotype (Fig. 2.35a). In nearly all cases, apart for one example at Man Haven (Fig. 2.35b), displacement along joints was small or negligible, although with some post-lithification reactivation in places. The listric surface at Man Haven downthrows the Raisby Formation by 5.5m to the southeast (Fig. 2.35b). It predates formation of the Z2 collapse breccias (Tertiary in age ([Smith, 1972]), although could have formed after deposition of the Hartlepool Anhydrite Formation. One listric joint had a large cavity after sulphate developed along its surface, suggesting that it predated precipitation of sulphate evaporites. Small neptunean dykes of Basal Permian Sands cut the Marl Slate and undisturbed Raisby Formation in Frenchmans Bay. The sandstone was intruded along non-listric vertical joints of consistent orientation.

A few decimetres of horizontally bedded dolostones, typical Raisby Formation mudstone/wackestones, commonly overlie the resedimented Raisby Formation (Fig. 2.33a). These beds partly infill relief of the irregular upper surface of the resedimented units. The Trow Point Bed overlies these dolostones, or encrusts irregularities in the uppermost surface of the resedimented Raisby Formation (c.f. Smith, 1986). The Trow Point bed was the final carbonate to be deposited at this locality prior to the Hartlepool Anhydrite Formation.

2.6.3.3. Tynemouth Castle Cliff (NZ 375, 696).

In common with other exposures of this lithofacies, the thickness of the Raisby Formation at this locality is very attenuated. Quoted thicknesses for the Raisby Formation in the northern part of the exposure vary from 3.8-3.9m (Smith, 1970b) to 2.4-3m

(Land, 1974). The Raisby Formation is underlain by 1.7m of Marl Slate which overlies 5m of Basal Permian Sands in the northeastern part of the locality (Smith, 1970b). The prominent feature of the Raisby Formation is that most of its thickness comprises a thick dolomitic sandstone. This sandstone coarsens and thickens from a 0.6-0.7m thick, structureless fine/medium sandstone in the southwestern part, to a 1.2m thick, planar-laminated coarse sandstone containing centimetre-sized dolostone clasts in the south of the exposure. Where coarsest, the sandstone displays a broad fining-upwards trend, superimposed on an irregular alternation of fine and coarser laminae. Overall, the sandstone coarsens and thickens from west to east. This coarsening and thickening accompanies a slight thinning of the Basal Permian Sands. In the southwestern part of the exposure, the lowermost Raisby Formation onlaps the top of the Basal Permian Sands.

Dolostone clasts within the sandstone range from subspherical to tabular, rounded to well rounded, with all clast long axes horizontal. They are supported within the coarse sandstone matrix. The siliciclastic component of this sandstone is texturally and mineralogically very mature. In addition to being well sorted, all sand grains are well rounded (Fig. 5.7). King (1850) recorded 21 species of fossils from this sandstone, although in thin section only bryozoans and foraminifers (Fig. 5.6) have been identified, owing to texture-destructive dolomitization.

The Raisby Formation is also attenuated in two offshore boreholes east of Tynemouth; OB14 (approximately NZ 396, 708) and OB16 (approximately NZ 404, 703) in which it is 7.32m and 6.86m thick respectively, and further north, in offshore boreholes Mill 10 (NZ 3879, 8431) and Mill 11 (NZ 3824, 8421) where it is 1.98m and 0.27m thick respectively (Land, 1974). In Mill 10, 1.37m of dolomitic conglomerate with quartz grains is overlain by 0.61m of dolostone containing aeolian-derived sand grains (Land, 1974).

2.6.3.4. Cullercoats (NZ 3671, 7116).

Bedded and resedimented Raisby Formation dolostones are exposed on a wave cut platform at Cullercoats. Land (1974) records a total of 6.1m of Raisby Formation at this locality, although during the present study 8.02m of Raisby Formation was measured, with the top not seen.

These dolostones are very similar in nature to those exposed along the South Shields coastal section, being predominantly uniform and planar bedded on a centimetre to decimetre scale. Small scale contorted bedding and larger, well-defined slump folds occur throughout the exposure, although most are poorly defined. One large slump anticline (Fig. 2.36) has a N-S orientated axial plane. Facing direction of the fold shows that movement was from east to west. Synsedimentary faults, with throws of a few centimetres are widespread.

Fig. 2.36. Photograph of a well-preserved slump fold on the Cullercoats foreshore. The axial plane of the fold strikes north-south. Hammer is 32cm long.

2.6.4. Resedimented mudstone lithofacies not affected by large scale resedimentation - Interpretation.

The scarcity of limestones, and large scale removal of sediments within this lithofacies, hinders interpretation of the depositional environment of non-resedimented carbonates. The scarce fauna of the lime mudstones within borehole W15, is suggestive of deposition in moderately deep, quiet waters with most fauna and carbonate derived from a slow pelagic rain. Locally abundant algal—coated shell fragments and coated grains suggest some transport from a shallower water area containing a more diverse benthos, and which was shallow enough for algal growth. Recognizable burrows within undisturbed bedded dolostones at Grahams Sand (*Lorenzinia*) are typical of the quiet and relatively deep water *Zoophycus* and *Nereites* ichnofacies (Frey and Pemberton, 1984). Most carbonates appear to have been intensely bioturbated, such that both original sedimentary structures, and the burrows themselves, are unrecognizable. The thin slumped, microfaulted, and graded beds from the Seaham borehole (Fig. 2.31a), partly obscured by bioturbation, possibly represent the form in which much of the resedimented mudstone lithofacies Raisby Formation was initially deposited. In most cases, these structures have been obscured by the combined effects of bioturbation and texture-destructive dolomitization.

The resedimented mudstone lithofacies is characterized by large-scale resedimentation, removing or reworking much of the Raisby Formation at outcrop. However, in offshore boreholes, the Raisby Formation is more complete, and demonstrates that resedimentation was active throughout its deposition, although in general concentrated a few metres above its base and at its top. The lower resedimented horizons are characteristically poorly structured, matrix-supported conglomerates of local derivation, probably by reworking of semi-lithified (nodular) carbonates. This reworking, in turn, may have been the by-product of the breakup of slump folds. Those folds preserved within W15 show good evidence for fracturing, and incipient breakup of semi-lithified layers (Fig. 2.31b). Magraw (1978, plate 4) describes the direct association of slumps with limestone breccias from an offshore borehole of the Raisby Formation. Cook and Taylor (1977) describe the remoulding of slumps into high viscosity sediment gravity flows, once the shear strength of the slumped lithologies had been exceeded. Matrix support, absence of fossils, and autochthonous derivation of the conglomerates, suggests movement by viscous debris flow. Conglomerates with more angular clasts, probably represent debris flows which have moved only a very short distance following remoulding from slumps. Similar conglomerates occur interbedded with undisturbed dolostones at Frenchmans Bay (Fig. 7.3a) and Down Hill Quarry (where 3.2m above the Marl Slate [Smith, 1970b]). Horizons within borehole W15 which contain a shallow water-derived fauna, and coated grains, were most likely transported and deposited by downslope-moving currents. This, in turn, may suggest that the Raisby Formation in the area of the W15 borehole was deposited in shallower waters

than the rest of this lithofacies, thus explaining the abundance of early diagenetic nodules, typical of the shallower water nodular and resedimented wackestone/mudstone lithofacies.

Data from the undisturbed sediments of this lithofacies therefore suggests that they were deposited in a quiet, relatively deep water environment, in a similar manner to those of the resedimented wackestone/mudstone lithofacies. The anomalously well-preserved graded beds from the Seaham borehole possibly suggest that a considerable proportion of this lithofacies was deposited from frequent, low-energy currents. It is likely that these beds are preserved in the Seaham borehole because the bottom waters and/or shallow intra-sediment pore waters at this locality were anomalously anoxic, thus preserving the organic laminae, and limiting bioturbation. Local, small scale resedimentation is also demonstrated by thin conglomeratic and slumped horizons, but resedimentation was not on the scale of the resedimented wackestone/mudstone lithofacies, possibly suggesting a lower depositional gradient. The general paucity of limestones and nodules in this lithofacies also suggests that early cementation was not as significant in this lithofacies as the others. D.B. Smith (unpublished field guide, 1989) suggests that the Raisby Formation at Trow Point was deposited in water depths of greater than 100m. On the basis of the distance of this lithofacies from the presumed shoreline (≥20km), and the dip of the Permo-Carboniferous unconformity, water depths in the Trow Point area of ≥250-300m are assumed (during normal sedimentation of the resedimented mudstone lithofacies), increasing eastwards into the basin.

2.6.4.1. Large scale resedimentation within the resedimented mudstone lithofacies - Interpretation.

The uppermost slumped and deformed sediments within the W15 and Seaham boreholes, mark the end of first cycle carbonate deposition. They can be directly correlated with the resedimented units at the top of the Raisby Formation along the South Shields coastal section. Furthermore, the similarity of resedimented sequences at Claxheugh Rock and Down Hill with the South Shields, Tynemouth, and Cullercoats sections, suggests they are also contemporaneous. Smith (1970b) likewise interprets this as a single episode, marking the end of deposition of the Raisby Formation, although predating deposition of the Ford Formation. Critical to this interpretation is the Claxheugh Rock exposure, where the Raisby and Ford Formations are most clearly juxtaposed. Woolacott (1912 & 1914) and Trechmann (1954) interpret this Raisby-Ford Formation contact as a thrust fault, along which up to 31m of the basal part of the reef has been removed. However, Smith (1970b & 1981) interprets the section to represent large-scale downslope removal of the Raisby Formation at the end of Raisby Formation deposition, followed by growth of the reef within the resultant hollow.

From the evidence presented in this study, the Claxheugh Rock section is re-interpreted to represent short distance downslope movement, from roughly west to east, of the Ford Formation reef, associated with erosion of the underlying Raisby Formation. The reef may have eroded the Raisby Formation itself, or may have moved downslope over, and planed off already substantially-eroded Raisby Formation. This was suggested, although rejected by Trechmann (1954) and Smith (1970b). There are a number of lines of evidence which support this interpretation in favour of that of Smith (1970b & 1981):

1. Woolacott (1914) and Trechmann (1954) record Raisby Formation dolostones mixed up with, thrust into, and over the reef,
2. Trechmann (1954) records Basal Permian Sands intermixed with reef dolostones,
3. Sub-reef breccias containing reef dolostone clasts are truncated by the sub-reef erosion surface,
4. No basal coquina has been recorded at Claxheugh Rock or Down Hill, thus supporting the suggestion, by Trechmann (1954), that the basal part of the reef has been removed,
5. No other resedimented carbonates lie at the contact of the Raisby Formation with the reef,
6. It is unlikely that a bryozoan-algal reef would have selectively grown in a hollow, probably greater than 20m deeper than the surrounding sea floor,
7. No evidence has been recorded during this study for resedimentation of uppermost Raisby Formation slope carbonates where overlain by lagoonal facies of the Ford Formation,
8. Tucker and Hollingworth (1986) suggest water depths during formation of the reef base coquina were possibly as low as 2-3m, which would mean that most of the surrounding Raisby Formation would have been exposed, for which there is no evidence.

Carbonates in the upper part of the South Shields section, interpreted to be synchronous with resedimentation at Claxheugh Rock, attest to multiphase erosion and redeposition. Throughout most of the exposure, resedimented carbonates were deposited on planar, to slightly undulate erosion surfaces. The amount of Raisby Formation removed by erosion is difficult to estimate, but is most likely a few metres. Stresses and elevated pore pressures created during erosion and resedimentation led to fracturing and neptunean dyke intrusion (also recorded close to Claxheugh Rock (2.1.3) and sedimentary boudinage with local breakup of underlying bedded carbonates.

The mode of emplacement of resedimented carbonates along this section is unclear. Smith (1970b & 1986) suggests that the sequence is dominated by displaced blocks of bedded Raisby Formation, formed by its breakup along listric faults. These slide blocks have come to rest after movement along a basal slide plane. However, in a number of cases (e.g., figure 2.34b), the packages of bedded resedimented Raisby Formation lithotype have substantially deformed internally, and so cannot be interpreted as wholly rigid slide blocks. The bedded lithotype also incorporates large clasts, again at variance with the rigid block interpretation. Smith's model also cannot explain why the bedded lithotype onlaps underlying undisturbed

carbonates with consistent orientations (Fig. 2.35a). The close similarity between the orientation of listric joints, and bedding within the bedded resedimented lithotype, suggests a genetic link. Strike directions of listric joints at Claxheugh Rock and the South Shields section, are approximately normal to palaeoslope, and thus failure along their surfaces would lead to movement of sediment parallel to the palaeoslope. A model for slope failure along listric faults, with attendant deformation of sediment packages, has been described by Gawthorpe and Clemmey (1985). In their model, packages of sediment separate out along listric fault surfaces and move downslope in a direction normal to the strike of the fault (Fig. 2.37). The leading edge of the sediment package comes to rest on a planar surface at a distinct angle (Fig. 2.37). The slide sheets can show variable degrees of deformation, and their leading margin may break up into blocks, generating debris flows (Fig. 2.37). This model adequately explains many features of the South Shields resedimented carbonates. Most importantly, the bedded lithotype is very similar to the inclined leading edge of rotated sediment packages (Fig. 2.37). This also explains the consistent orientation of the inclined bedded resedimented units, whose strike is approximately parallel to that of the listric joints (Fig. 2.35). In detail, many features of resedimented carbonates along the South Shields section are readily explicable in terms of the varying competence of the sediment packages rotating along listric faults.

Although listric joints are widespread within the resedimented wackestone/mudstone and resedimented mudstone lithofacies, they rarely show good evidence for displacement of host sediments. This could be due to deformation and destruction of the listric surfaces themselves during resedimentation, as proposed by Gawthorpe and Clemmey (1985) (Fig. 2.37). Smith (1970b) suggests that the listric joints formed in response to earthquake shock. However, they are recorded throughout some exposures, such as Houghton Quarry where they are present both above and below a major resedimented horizon. The joints more likely developed in response to gravitational instability within the sediment pile throughout deposition of the Raisby Formation. However, only during large scale sediment failure did the listric surfaces become active.

The structureless lithotype of the resedimented Raisby Formation was probably emplaced by debris flow. This is supported by its lack of internal structure, matrix-support of clasts, and inclusion of large rotated blocks of bedded Raisby Formation. The debris flows probably moved slowly, and possibly intermittently, as a viscous sludge, in a similar manner to those exposed at Houghton Quarry, although the source material for the debris flows was probably not as well-lithified. The conglomerate lithotype represents a more far-travelled, less viscous, smaller-volume debris flow. Within such flows, shearing within the flow may account for clast rounding, as observed within the resedimented mudstone/wackestone lithofacies conglomerate lithotype (Fig. 2.28).

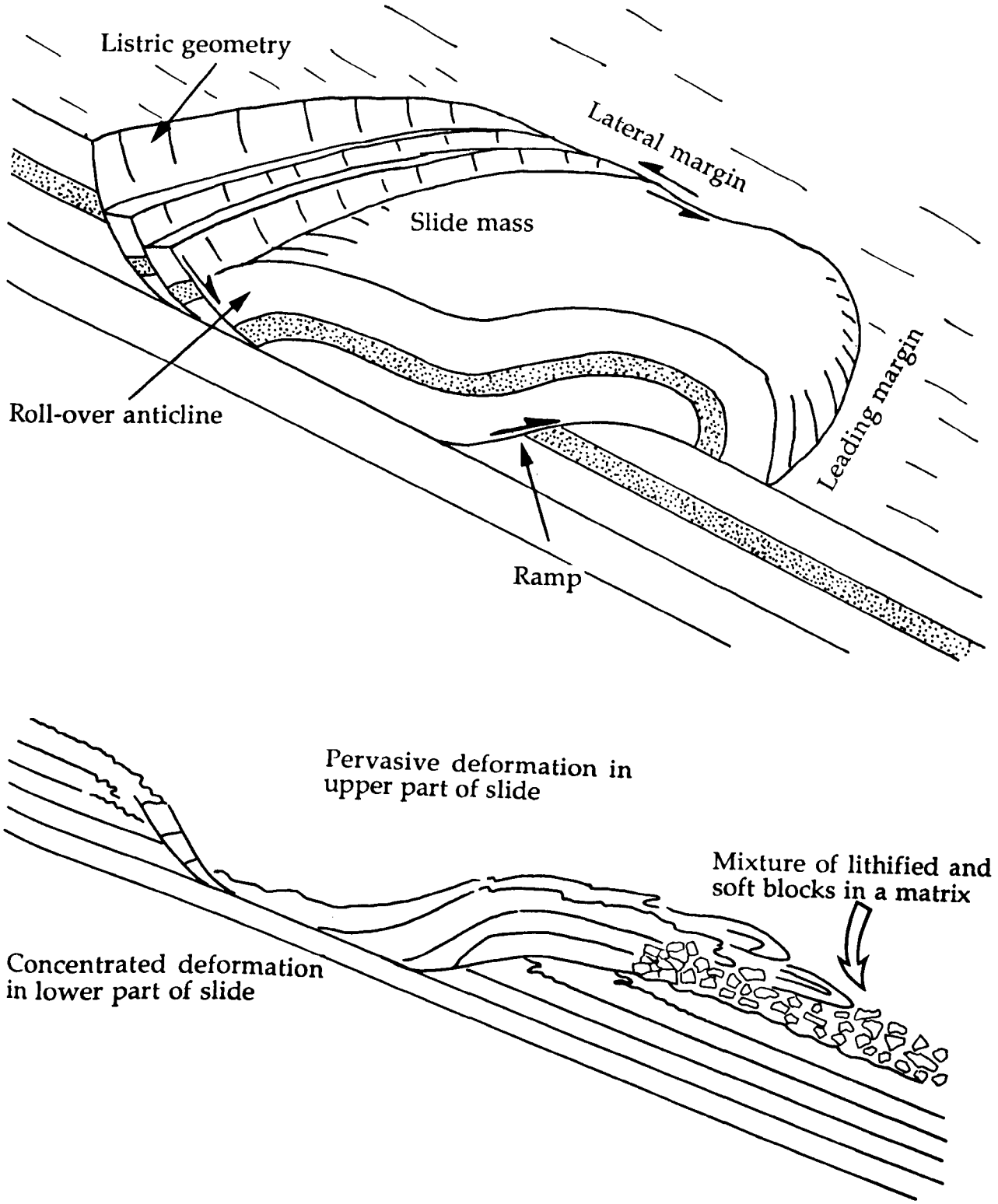

Fig. 2.37. Schematic diagrams showing the nature of sediment failure along submarine listric faults (modified from Gawthorpe and Clemmey, 1985). The upper diagram shows an idealized situation, with onlap of the leading margin of the slide mass onto undisturbed sediments. The lower diagram shows a more realistic case, in which the leading margin of the slide mass is re-moulded into a debris flow, and the listric fault plane itself is also deformed.

The South Shields coastal section was therefore the locus of both erosion and resedimentation, with resedimentation being of a greater volumetric significance. The source material was almost exclusively Raisby Formation carbonates, most likely derived upslope in an area of large scale erosion, such as represented by Claxheugh Rock and Down Hill. The few decimetres of apparently normal Raisby Formation dolostone overlying resedimented units may be a peri-platform ooze, or could have been deposited from small turbidity currents which marked the end of resedimentation.

At Tynemouth Castle Cliff, and in nearby offshore boreholes, the Raisby Formation is considerably more attenuated than at South Shields. This is interpreted to reflect the near-total erosion of the Raisby Formation, coeval with erosion/resedimentation at South Shields. Small-scale resedimentation at Tynemouth Castle Cliff is represented by the sandstone unit. Textural and mineralogical maturity of the sands suggests they were sourced from the Basal Permian Sands, although re-sorted during transport and resedimentation, such that only the coarser, and mineralogically more stable fraction of the sand was redeposited. Raisby Formation dolostone clasts within the sandstone further confirm that the Basal Permian Sands were exposed by submarine erosion. The sandstone was probably deposited by one, or a series, of turbidity currents. Lateral variability in thickness and composition of the sands possibly reflects the lateral variation through a ?channelized deposit, rather than a down-flow grading.

From the South Shields section to Tynemouth, the nature of resedimentation varies greatly, from substantial erosion and redeposition, to large-scale erosion with minor redeposition respectively. At Cullercoats, both erosion and resedimentation were less extensive than at Tynemouth. This abrupt variation parallel to depositional strike suggests that erosion and resedimentation were concentrated within laterally-restricted areas orientated normal to depositional strike, possibly large gullies. Smith (1970b, fig. 8) suggests that large, SW-NE orientated gullies formed during this phase of erosion and resedimentation, delineated by steep sided inter-gully areas, the margins of which were controlled by failure along large listric faults. At both Claxheugh Rock and South Shields, measured listric joint orientations differ from those suggested by Smith's model (which should strike approximately east-west), although there is a better correspondence of joint orientations at South Shields than Claxheugh Rock with those suggested by Smith (1970b). Thus, listric joints did have an important control on resedimentation, by generating slope failure and sediment movement parallel to palaeoslope, as also demonstrated from Houghton Quarry. These areas of slope failure were, however, concentrated in discrete, palaeoslope-parallel zones.

2.6.5. Resedimented mudstone lithofacies - Summary and conclusions.

The definition of this lithofacies is complicated by large scale sediment removal, and is, in part, due to the presence of these large scale resedimented carbonates. However, the nature of the undisturbed sediments of this lithofacies does differ from that of the resedimented wackestone/mudstone lithofacies, principally in the paucity of early cementation features, skeletal wackestone horizons, and large debris flow conglomerates. This would be in accordance with a deeper water depositional environment, and probably a shallower depositional gradient, farther down the depositional slope from the resedimented wackestone/mudstone lithofacies. The occurrence of large-scale resedimented carbonates in this lithofacies is due to the presence of the reef, as the reef itself was responsible for triggering, or accentuating the extent of the resedimentation episode. However, it is probable that the trigger for large-scale resedimentation was related to external factors, such as the sea level fall at the end of first cycle carbonate deposition, and not normal deep-water sedimentation processes. Such a sea level fall, accompanying evaporative drawdown of the Zechstein Sea preceding deposition of the Hartlepool Anhydrite Formation, could have made the reef and underlying slope carbonates unstable. Gawthorpe and Clemmey (1985) cite instability of sedimentary buildups as being a significant mechanism in producing large-scale episodes of resedimentation. Cook *et al.*, (1987) describe Late Cambrian/Early Ordovician large scale resedimentation in slope carbonates in response to eustatic sea level falls, correlatable between USA, China and Russia. They conclude ".... during the initial phases of a sea-level lowering, slope and/or platform-margin failure can occur, owing to gravitational instability of partially cemented carbonates". Cook *et al.*, (1987) further state that, at these times, segments of the platform margins and upper slopes fail catastrophically, producing boulder-bearing debris sheets of a very large size. This is in very good agreement with resedimentation structures recorded to the east of the reef.

2.6.6. Reinterpretation of the Raisby - Ford Formation contact.

Exposures at Claxheugh Rock, South Shields, and Tynemouth, and the W15 and Seaham boreholes, clearly demonstrate that large scale resedimentation took place at close to the end of deposition of the first cycle carbonate. At Claxheugh Rock, this episode of resedimentation postdated formation of at least a large part of the reef, whereas at South Shields, it predated deposition of the Trow Point Bed. Resedimented carbonates in coastal exposures are thus the direct, or indirect, by-products of the major sub-reef erosion higher up on the slope. Slumped and contorted carbonates at the top of the Raisby Formation in W15 and Seaham boreholes are therefore the distal products of this resedimentation episode. It cannot be unequivocally demonstrated that all of these resedimented carbonates were the result of one episode of slope failure, but it is considered likely owing to the lack of evidence for large scale resedimentation at any other horizons. One possible difficulty with this re-interpretation is with the apparent absence of Ford Formation reef debris within coastal resedimented carbonates. However, owing to the highly diagenetically altered, and strongly weathered nature of Raisby Formation dolostones exposed along the coast, reef debris would be difficult to recognize.

If the hypothesis of Smith (1970b & 1981) is accepted, the Trow Point Bed is time-equivalent to the Ford Formation (Smith, 1986). However, the major resedimentation episode postdated deposition of the reef, but predated deposition of the Trow Point Bed. That the Trow Point Bed, or an equivalent facies to it, can be traced into continental Europe, suggests that the deposition of algal carbonates reflects a period of anomalous, basin wide conditions. The Zechstein Sea at this time was probably restricted and saline owing to evaporative drawdown immediately preceding deposition of the Hartlepool Anhydrite Formation. Therefore, it is suggested here, that, from a re-interpretation of the timing of a large scale resedimentation episode, the Raisby Formation, as developed in coastal exposures and offshore boreholes, is at least partly equivalent to the Ford Formation reef and lagoonal facies. The Trow Point Bed represents an altogether different episode of sedimentation, related to evaporative drawdown of the Zechstein Sea. That the Trow Point Bed is not equivalent to the Ford Formation would be a better explanation for the very abrupt thinning of the Ford Formation sequence, from up to 120m in the reef facies, to only a few metres in the Trow Point Bed.

This type of re-interpretation of Zechstein carbonate stratigraphy is not without comparison. One of the greatest problems with Zechstein stratigraphy is the absence of biostratigraphic markers, and so most correlation is on the basis of basin-wide events, most importantly sea level falls. The onset of deposition of the Ford Formation in the west of the study area is marked by the incoming of reef and lagoonal carbonates. This change in sedimentation is commonly interpreted to have resulted from a basin wide regression on the scale of a few metres (Smith, 1980b & 1985; Paul, 1986b). This sea level fall correlates with the Hampole Discontinuity of the Yorkshire Province which delineates the Wetherby and

Sprotborough Members of the Cadeby Formation (Smith, 1968; Smith *et al.*, 1986). In relatively shallow-water environments (such as the skeletal wackestone/packstone and nodular wackestone/mudstone lithofacies of the Raisby Formation), the regression led to a considerable change in sedimentation. However, that this change cannot be recognized in the Durham Province east of the reef, led Smith (1986) to define the Trow Point Bed as the Ford Formation equivalent. The reason why the change cannot be easily recognised in this area is probably because the Zechstein Sea was too deep for a low amplitude fluctuation in sea level to have a noticeable effect on sedimentation.

Peryt (1986) defines three glacio-eustatic controlled sub-cycles within the Polish first cycle carbonate (Fig. 2.38). In addition, he recognizes two broad lithological associations within first cycle carbonates of Poland, Denmark and West Germany; a micritic complex (mudstones and wackestones) and a supramicritic complex (packstones, grainstones and boundstones) (Fig. 2.38). The supramicritic complex is the shallower water, lateral equivalent of the micritic complex, and also overlies it following sea level falls. Peryt (1986) recognizes that the occurrence of these complexes, at any one locality, is related to its position on the shelf, slope or basin (Fig. 2.38). Within shelf carbonates, only the supramicritic complex is developed, and eustatic sea level changes may be recognized, whereas in basinal carbonates only the micritic complex is developed, and eustatic sea level changes are hard to define (Fig. 2.38). The English first cycle carbonates at outcrop can be directly related to this model (Fig. 2.38). Therefore, the basinal micritic complex in Durham (Raisby Formation) is laterally diachronous with the micritic complex (Raisby Formation) overlain by supramicritic complex (Ford Formation) deposited in shallower waters up slope (Fig. 2.38). On this basis, the Ford Formation should be redefined as the reef and lagoonal, shallower-water member, of the Raisby Formation. The skeletal wackestone/packstone lithofacies of the Raisby Formation is a supramicritic complex which accumulated over submarine highs. It is thus an anomalous feature lying within deeper water micritic Raisby Formation carbonates. The skeletal wackestone/packstone lithofacies is conformably overlain by the supramicritic Ford Formation lagoonal facies, but should, in places, also pass laterally into it from the margins of submarine highs.

First cycle carbonates deposited in the Yorkshire Province also fit in well with this revised stratigraphic model. Both the Wetherby and Sprotborough Members were deposited in relatively shallow water shelf and lagoonal environments, and thus comprise the platform supramicritic complex in Yorkshire. In keeping with the shallow water environment of deposition, the mid first cycle regression is very clearly defined in the Yorkshire Province at outcrop (Hampole Discontinuity). Deeper water slope and basinal carbonates (i.e., micritic complex) do not crop out in the Yorkshire Province, although resedimented and nodular slope carbonate muds have been described by Kaldi (1980) to the east of the outcrop.

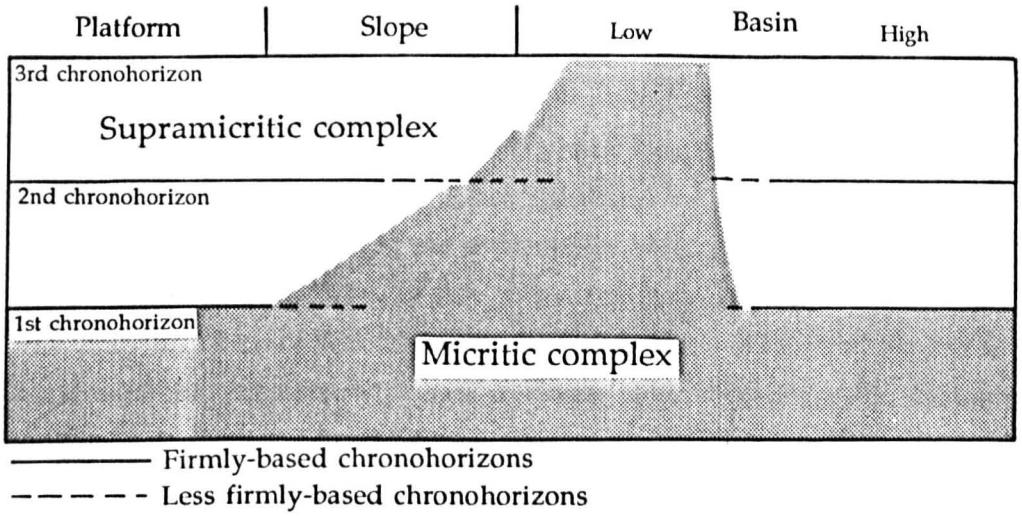

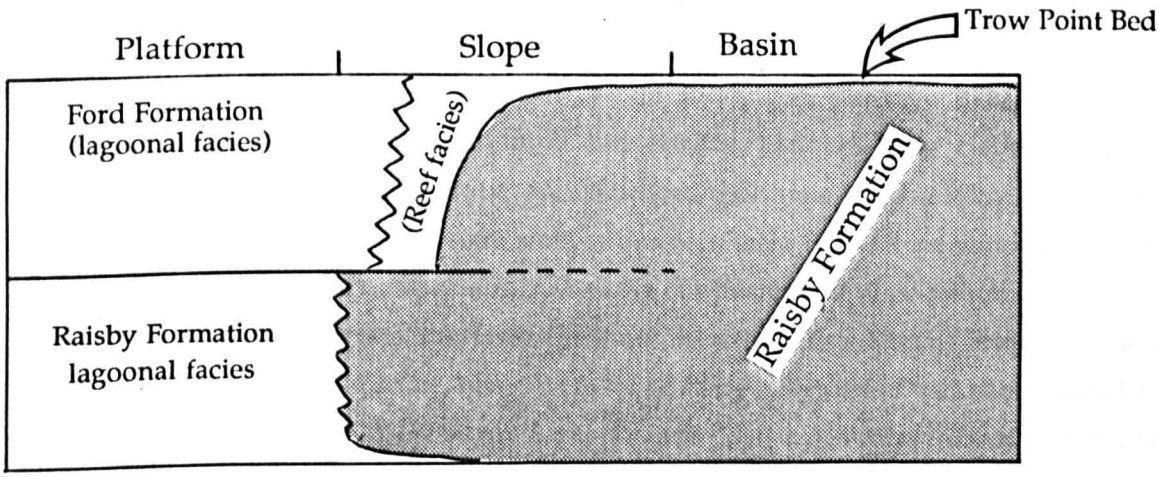

Fig. 2.38. Diagrams showing the spatial and temporal relationships between micritic and supramicritic complexes from the first cycle carbonates of Poland (modified from Peryt, 1986), and applied to the first cycle carbonates of northeast England. In northeast England, the Raisby Formation is here interpreted to be the diachronous, basinal equivalent of the Ford Formation reef and lagoonal facies, as the mid first cycle eustatic sea level fall chronohorizon cannot be identified in lower slope and basinal environments. The Raisby Formation lagoonal facies has been eroded off, although the skeletal wackestone/packstone facies is probably similar to it.

2.7.1. Deposition of the Raisby Formation - Conclusions

Most of the non-resedimented Raisby Formation carbonates at outcrop and in core comprise uniform bioturbated mudstones and wackestones. Bedding may be planar or nodular. Nodular bedding is a primary feature produced by marine lithification of shallow sub-surface carbonate muds. Such nodules are typical of carbonate slopes and are commonly used as a criteria for their identification (Mullins *et al.*, 1980). The presence of limestones within the Raisby Formation is also evidence for early, sea floor cementation. Most smaller scale sedimentary structures, which may have been present within Raisby Formation carbonates, have been obliterated by the combined effects of bioturbation and dolomitization. The ichnofauna, together with sparse macro- and microfauna are indicative of quiet, moderately deep water environments. The sea floor sediments were soft muds, although commonly lithified a few decimetres below the sediment surface. Most primary sedimentation was from combined pelagic (planktonic microfossils) and hemipelagic (carbonate mud winnowed off the shelf with fine fossil fragments) input (peri-platform sedimentation).

The style of resedimentation of Raisby Formation carbonates was both spatially and temporarily variable. Spatially, large translational slides pass through debris flow and turbidite deposits associated with slumps and erosion surfaces, into carbonate muds intercalated with small conglomeratic and slumped horizons (Fig. 2.39). Most of the resedimented mudstone lithofacies sediments at outcrop, were themselves removed close to the end of first cycle carbonate deposition by a phase of catastrophic slope failure.

Smith (1970b) suggests that resedimentation within the Raisby Formation was concentrated in two discrete phases, one after 3-7m of Raisby Formation had been deposited, and the other at its top. Both, he suggests, were generated by sudden episodes, such as earthquakes, possibly related to movement along the Ninety Fathom Fault, just north of the Tyne. There is evidence, especially in the resedimented wackestone/mudstone and resedimented mudstone lithofacies for most resedimentation to be concentrated in a zone between a few metres and less than ten metres above the Marl Slate. This episode may have been triggered by earthquake shock (as suggested by Smith [1970b]), for which there is some evidence, especially at Houghton Quarry. However, the sediment pile did not all fail at once. Earthquake shock may have served to weaken (decrease shear strength) of the slope carbonate muds, thus facilitating a later phase of gravitational instability.

Also, during initial deposition of the Raisby Formation, the sea floor topography may have been considerably irregular, owing to combined effects of elevated areas and islands of Basal Permian Sands and Carboniferous rocks. This irregularity was superimposed on the regional slope, thus locally producing areas of elevated slope angles of variable direction. This irregularity was especially important in the south of the area, for example at Old Towns Quarry, where the orientation of the erosion surface is not parallel to regional palaeoslope.

These irregularities would have been smoothed out during progressive sedimentation of the Raisby Formation.

The upper phase of catastrophic resedimentation, which only affects lower slope carbonates, is here considered to have been generated by the initial phases of evaporative drawdown of the Zechstein Sea, preceding deposition of the Hartlepool Anhydrite Formation. This lowering is considered to have made the lower slope carbonates and the reef itself unstable, promoting downslope movement.

The Raisby Formation carbonate slope is best classified as a 'slope apron' (cf. Mullins and Cook, 1986). Slope aprons develop immediately adjacent to shallow water platforms, on gentle (less than 4°) platform margin slopes. The source of carbonate is along a line rather than from a point, thus fans do not form. The composition of Raisby Formation resedimented carbonates, furthermore, show that material being resedimented was sourced mainly on the slope, rather than from the platform margin and shelf. Geometry of the Raisby Formation slope apron was laterally variable, and passes into relatively shallower water sediments and emergent islands southwards along strike. The Raisby Formation contains a considerably smaller proportion of obviously resedimented carbonates than other slope aprons in the geological record (cf. Mullins and Cook, 1986). This may be due to stabilization of slope sediments by widespread submarine cementation, with the apron sediments only becoming unstable in response to external stimulus (i.e., earthquake shock). In accordance with the morphology of such aprons, resedimented carbonates were deposited as sheets, and were only channelized where controlled by previous erosion, or local failure of listric faults. A model, showing the spatial variation in resedimentation styles on the Raisby Formation slope, and relative positions of the Raisby Formation lithofacies on that slope is illustrated in figure 2.39. On the basis of Raisby Formation lithofacies, it is possible that the Ford Formation reef did not develop on the Raisby Formation shelf break, but slightly downslope of the shelf break, such as described for Z1 reefs in Denmark (Clark, 1986).

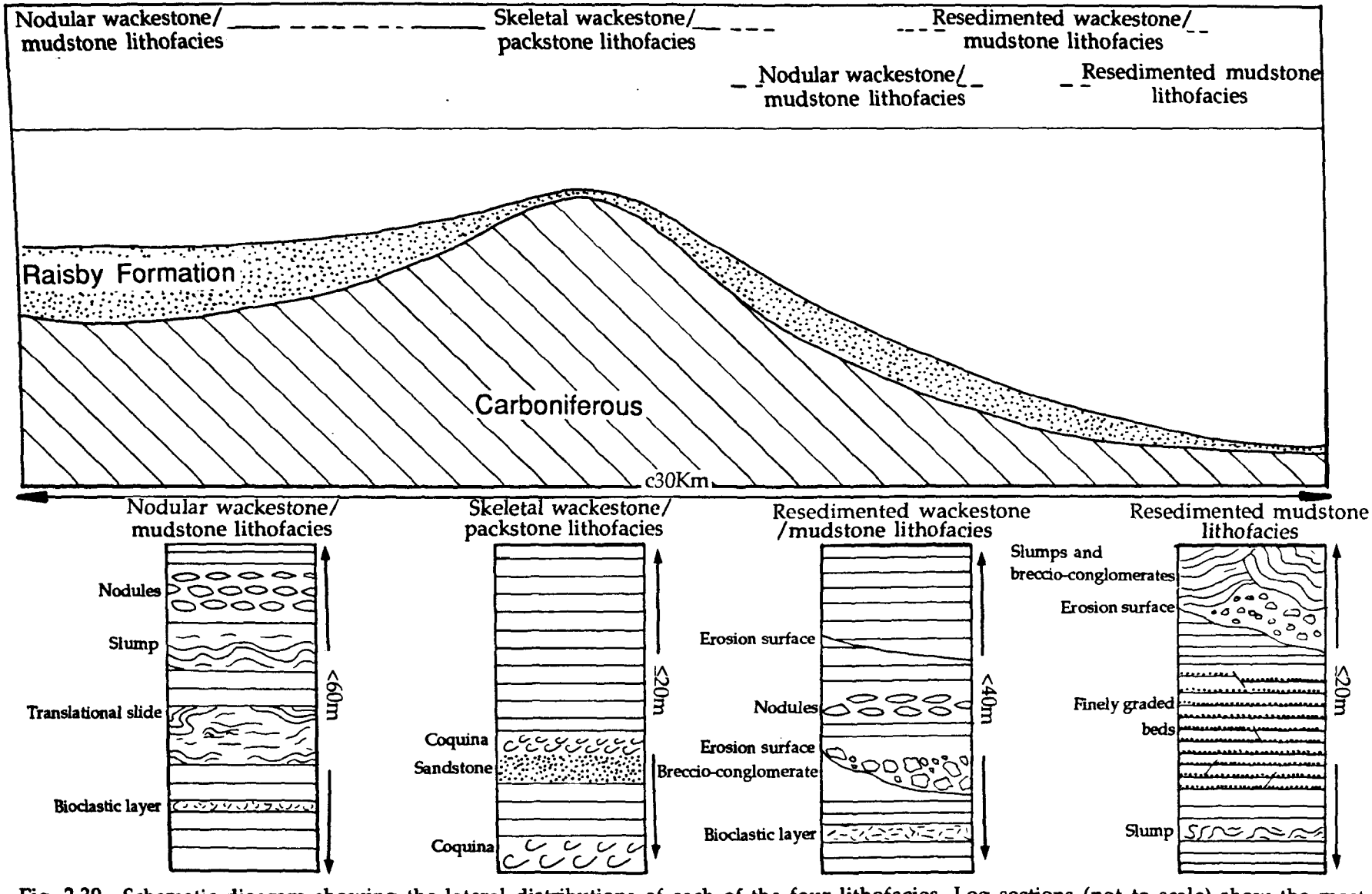

Fig. 2.39. Schematic diagram showing the lateral distributions of each of the four lithofacies. Log sections (not to scale) show the most diagnostic sedimentological characteristics of each lithofacies.

Chapter 3

Principles of trace and minor element geochemistry
Marine eogenesis,
Original isotopic composition of Zechstein seawater

3.1.1. Principles of trace and minor element geochemistry.

Trace and minor element geochemistry can be extremely useful in determining the diagenetic environment of precipitation of carbonate minerals. Trace and minor elements may occur in one or more settings within the carbonate phase (Veizer, 1983a):

1. Substituting for Ca^{2+} and/or Mg^{2+} within the carbonate lattice,
2. Interstitially between lattice planes,
3. Occupying lattice positions free due to crystal defects,
4. Absorbed due to remnant ionic charges,
5. Present within non-carbonate inclusions such as fluid inclusions.

In general, only factors 1, 5 and possibly 3 are significant, or can be considered in most carbonate studies. Factors 2 and 4 may well be of importance, but it is not possible to measure the amount of trace and major elements occupying those positions within the crystal during routine chemical analysis. Factor 5 may be taken into account by studying the statistical correlations between the amount of insoluble residue and trace/minor elements. In a recent study, Pingitore and Eastman (1986) defined a control of Sr, Ba and Na concentration in calcite as density of defect sites (factor 3), in turn a function of precipitation rates (see later).

The concentration of trace/minor element divalent cations substituting for major elements (Ca^{2+} and/or Mg^{2+}) within the carbonate lattice (factor 1) is, at low trace element concentrations and high water-rock ratios, directly related to the composition of the solution from which the carbonate phase precipitated via partition coefficients. This is outlined in the homogeneous distribution law (after McIntire, 1963):

$$\left(\frac{mT^{2+}}{mMe^{2+}}\right)_{Carbonate} \qquad K.\left(\frac{mT^{2+}}{mMe^{2+}}\right)_{Solution}$$

where:

mT^{2+} = moles of trace element

mMe^{2+} = moles of major element (Ca and/or Mg in this case)

K = partition coefficient for the specific minor/trace element at the appropriate temperature.

Details of the calculation of fluid and precipitate compositions from this expression are presented in appendix VIII.

Each cation has a different, temperature-dependant partition coefficient and most are very poorly understood. The partition coefficient for a given ion may also vary according to the phase being precipitated. The most important coefficients for carbonate studies are detailed below (modified from Veizer, 1983a):

Calcite

Sr	Direct precipitation	= 0.13
	Aragonite - dLMC	= 0.05
	HMC - dLMC	= 0.05
	LMC - dLMC	= 0.03
	Calcite = 0.04-0.2 (Pingitore and Eastman, 1986)	
Na	0.00002 - 0.00003	
Mg	0.013 - 0.06	
	0.0172 ± 0.0022 to 0.023 ± 0.0026 (Mucci *et al.*, 1989)	
Fe	Greater than 1	
	4 (in meteoric aquifers [Veizer, 1983b])	
Mn	Direct precipitation = 6	
	15 (in meteoric aquifers [Veizer, 1983b])	
	Aragonite - dLMC	= 15
	HMC - dLMC	= 15
	LMC - dLMC	= 30
Ba	0.06 ± 0.02	(Pingitore and Eastman, 1984).

Aragonite

Sr	0.9 - 1.2
	0.97 ± 0.08 to 1.05 ± 0.09 (Mucci *et al.*, 1989)
Mg	0.0006 - 0.005
Mn	0.86

Dolomite

Sr	0.025 - 0.06
Fe	Greater than 1
Mn	Greater than 1
Na	0.00002-0.00003
	0.00014 (at the point of gypsum precipitation [Sass and Bein, 1988]).

Partition coefficients assume that the precipitate is at, or near, thermodynamic equilibrium with the solution from which it is precipitating at a given time. Owing to very slow reaction rates characteristic of most diagenetic environments in nature, equilibrium conditions are most likely (E. Sass *pers. comm.*, 1989). Implicit in the homogeneous

distribution law is that an equilibrium also exists between the precipitate and the bulk aquifer solution (Morrow and Meyers, 1978) - 'bulk solution equilibrium'. However, bulk solution equilibrium is unlikely to exist with most diagenetic regimes, unless aquifer flow rates are slow in relation to reaction rates. Dolomitization is an example of a reaction whereby bulk solution equilibrium is approached (Machel, 1988). A converse view, expressed in various ways by Kinsman (1969), Bathurst (1975), Veizer (1978), Brand and Veizer (1980) and Pingitore (1976, 1978 & 1982), is that of bulk solution disequilibrium, where variable degrees of isolation exist between the fluid from which carbonate minerals are precipitating and the bulk aquifer. Thus, all of the aforementioned studies consider that relatively limited amounts of liquid are directly involved in precipitation (Pingitore, 1982).

In a completely closed system (total bulk solution-disequilibrium) with a low water-rock ratio, the composition of the fluid from which the carbonate is precipitating and the composition of the carbonate itself, changes in response to ions being removed from the solution during precipitation. In this situation, the (mT/mMe) ratio of the precipitate as a whole will not be proportional to that of the solution at any one time. The homogeneous distribution law will only apply to the very outermost layer of the crystal, which is in equilibrium with the solution from which it is growing at that time. The changing composition of the fluid is described by the 'Doerner-Hoskins' heterogeneous distribution law (after Doerner and Hoskins, 1925):

$$\text{Log}\left(\frac{mT_o^{2+}}{mT_f^{2+}}\right) \quad K \,.\, \text{Log}\left(\frac{mMe_o^{2+}}{mMe_f^{2+}}\right)$$

where:

mT^{2+} = moles of trace element

mMe^{2+} = moles of major element (Ca and/or Mg in this case)

K = partition coefficient for the specific minor/trace element at the appropriate temperature.

o = original concentration of trace or major element in solution

f = final concentration of trace of major element in solution

Doener-Hoskins behaviour assumes that the diffusion of ions within a solid crystal away from the original attachment sites will be very slow under most geological conditions, and there is no recrystallization. Continued precipitation in such a closed system produces a radial concentration gradient in the precipitate(s) whereby trace and minor elements are distributed in a logarithmic manner (Machel, 1988).

Most diagenetic environments lie between totally closed and totally open systems. This is because diagenetic reactions are considered to take place within a micron thick aqueous film, the 'reaction zone' (Pingitore, 1982). This reaction zone may have; (1) a composition identical to that of the bulk aquifer (bulk solution-equilibrium), (2) a

composition completely different from the bulk aquifer and controlled entirely by the dissolving (and precipitating) phases (bulk solution-disequilibrium) or, (3) more commonly a composition derived from the interaction of cations moving between the proximal bulk aquifer, the dissolving phase and the precipitating phase. Reaction zone processes are most easy to model with regard to the neomorphism of aragonite and high-magnesian calcite (HMC) to diagenetic low-magnesian calcite (dLMC). During these reactions, the composition of diagenetic fluids can be accurately calculated by comparing the composition of the dissolving aragonite and HMC to the measured composition of the dLMC precipitate. Such processes are considered in more detail in 4.3.2.1.

Thus, the chemical composition of a crystal will be related to that of the solution via a partition coefficient. If the solution has a constantly changing (mT/mMe) ratio, the (mT/mMe) ratios of the precipitate will likewise change. The partitioning of cations between solution and precipitate will however, be affected by factors such as temperature, pressure, pH, Eh (important with regard to Fe^{2+} and Mn^{2+}), complexing with other ions (especially marked with the hydration of Mg^{2+}) and reaction kinetics (most significantly crystal growth rates). Katz *et al.*, (1972) reported a temperature-dependance on K^{Sr}_{dLMC} for calcite replacing aragonite, with K^{Sr}_{dLMC} 0.055 at 40°C and 0.058 at 98°C. Stoessell *et al.*, (1987) likewise reported a temperature-dependance of $K^{Sr}_{Calcite}$ for calcite replacing dolomite, with $K^{Sr}_{Calcite}$ ranging from 0.027±0.008 at 100°C, through 0.048±0.017 at 150°C, to 0.063±0.013 at 200°C. However, as most diagenetic reactions considered in this thesis took place at temperatures of less than 100°C, the temperature-dependance of $K^{Sr}_{Calcite}$ is probably unimportant.

Kitano *et al.*, (1971) observed an increase in $K^{Sr}_{Calcite}$ and $K^{Ba}_{Calcite}$ with increasing precipitation rates. Lorens (1981) further demonstrated that cations with partition coefficients greater than 1 and less than 1 were depleted and enhanced respectively with increasing rates of precipitation ($K^{Sr}_{calcite}$ increased from 0.035 to 0.1 with a doubling of precipitation rate). Recent work by Pingitore and Eastman (1986) has integrated such data into a comprehensive model for Sr partitioning behavior into calcite, in Mg-free systems (Fig. 3.1). They showed that the observed $K^{Sr}_{Calcite}$ was a function of incorporation of the ion both into lattice sites (substituting for Ca) and into defect sites. The defect sites were considered less abundant than lattice sites, although the former increased in number with increasing rate of precipitation. In solutions with a low (Sr/Ca) ratio, defect site $K^{Sr}_{Calcite}$ may comprise a significant proportion of overall $K^{Sr}_{Calcite}$ and so give a higher value for $K^{Sr}_{Calcite}$ than that achieved simply by lattice substitution. Conversely, in solutions with a high initial (Sr/Ca) ratio, defect site $K^{Sr}_{Calcite}$ will of much less importance to total Sr partitioning, such that overall $K^{Sr}_{Calcite}$ is mainly lattice $K^{Sr}_{Calcite}$. Also, slow crystal growth will produce fewer defect sites and so lead to a lower overall $K^{Sr}_{Calcite}$ than rapidly growing crystals within a precipitating liquid of the same initial Sr concentration (Fig. 3.1). Other cations such as Ba and Na may also fill the defect sites, such that growing crystals within a solution containing Ba or Na will have a lower overall $K^{Sr}_{Calcite}$ than one within a solution of the same initial Sr concentration and no Ba and Na (Fig. 3.1). Experimental work by Mucci

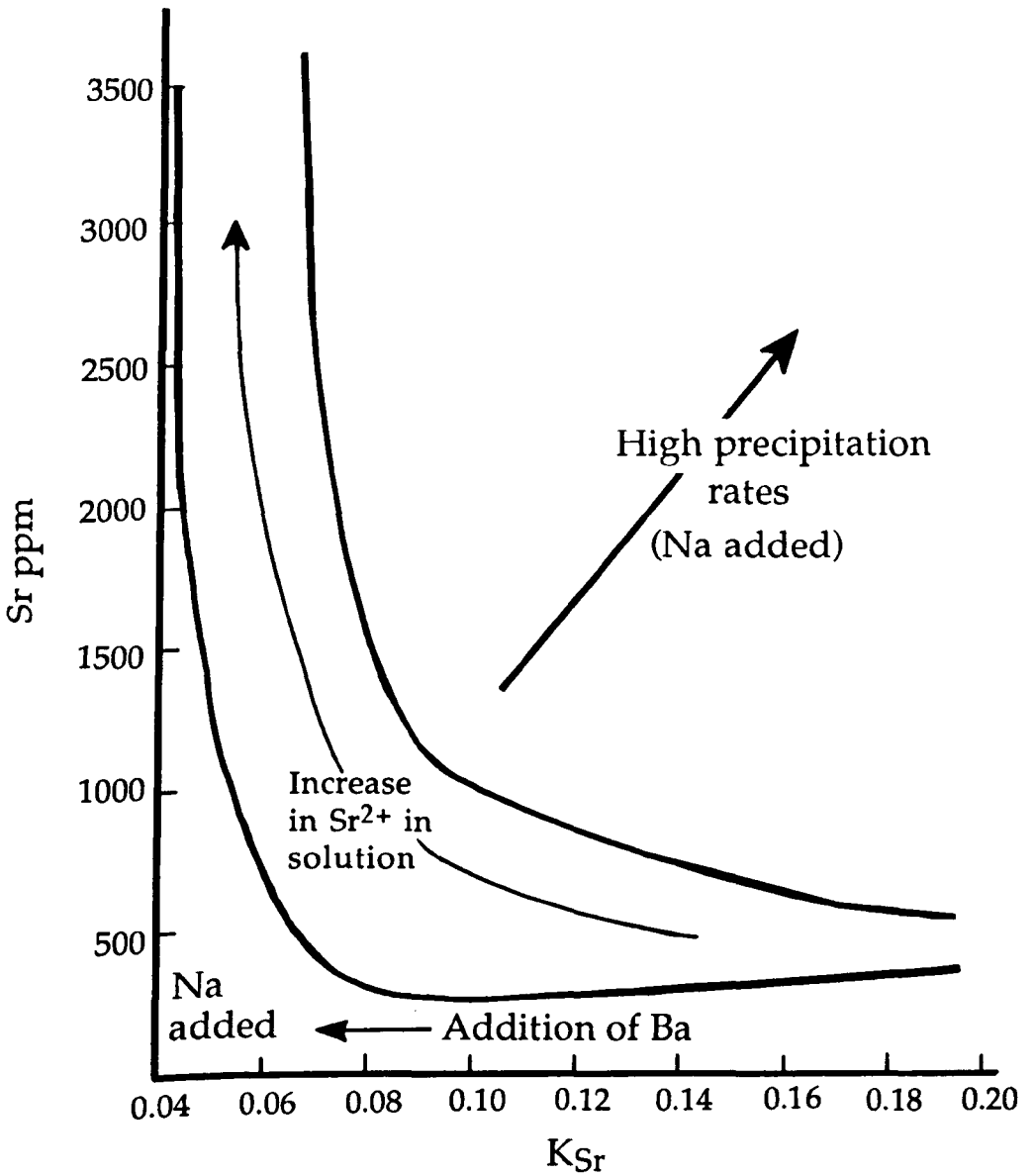

Fig. 3.1. Graph showing the main controls on the partition coefficient of Sr between a fluid and calcite, experimentally determined by Pingitore and Eastman (1986) (graphs slightly modified after Fairchild *et al.*, 1988). Two trends are clearly shown, of the partition coefficient decreasing with increasing concentration of Ba and Na in the fluid (preferentially incorporated into defect sites), and the partition coefficient increasing with precipitation rate (density of defect sites increases with precipitation rate).

and Morse (1983) and Takano (1985) has further demonstrated that $K^{Sr}_{Calcite}$ will increase with greater concentrations of Mn and Mg in the calcite precipitate. $K^{Mg}_{Calcite}$ was shown by Mucci and Morse (1983) to decrease with increasing Mg/Ca ratio in the solution. The partitioning behavior of Mg and Sr into calcite and aragonite overgrowths respectively has further been demonstrated by Mucci *et al.*, (1989) to be related to the SO_4^{2-} concentration of seawater solutions. In sulphate-free seawater, the $K^{Sr}_{Aragonite}$ and $K^{Mg}_{Calcite}$ are 8% and 32% greater respectively that in seawater of 'normal' sulphate concentrations.

There is a body of opinion which suggests that the experimental work on which most of the partition coefficient determinations are based is invalid, as partition coefficients will decrease with decreasing growth rates of the experimentally precipitated crystals (G.M. Harwood, *pers. comm.*, 1989). However, because at present it is difficult to derive partition coefficients in any other way than than from relatively rapidly experimentally grown crystals, this assumption cannot be validated.

Owing to the uncertainties outlined above, detailed quantitative geochemical modelling in ancient carbonates is problematical. Thus, in general, carbonate diagenetic studies are only concerned with; (1) the sign (less or greater than 1), and (2) the relative magnitudes of partition coefficients (in open to partially closed diagenetic systems). Cations which have a partition coefficient of less than 1, under equilibrium/near-equilibrium conditions will precipitate into a mineral phase with a (mT/mMe) ratio less than that of the solution, whereas cations with a partition coefficient of greater than 1 will be enriched into the precipitate relative to their (mT/mMe) concentration in the solution. Cations with a partition coefficient of 1 will have the same (mT/mMe) ratio in the precipitate as the solution at the time of precipitation.

3.2.1. Preservation and diagenesis of skeletal material and marine cements - Introduction.

Petrographic and geochemical study of Raisby Formation limestones, and dolostones which retain some original textures, can greatly elucidate upon early marine diagenesis (marine eogenesis). However, in common with many ancient marine carbonates, both fossil material and marine cements in the Raisby Formation have been variably altered, thus complicating interpretation of early diagenesis. The alteration has involved mobility of trace elements and isotopes, and commonly partial or complete destruction of original textures. Owing to its positive partition coefficient, Mn is a particularly sensitive element to this alteration (Mn increasing with recrystallization during burial diagenesis). As luminescence is largely activated by the presence of Mn (Appendix I), it is a very useful technique for assessing alteration in marine cements and fossil material, especially brachiopods. Following the work of Popp *et al.*, (1986), non-luminescent brachiopods are recognized as having undergone little diagenetic alteration, whereas those which have been altered, luminesce, rendering them unsuitable for geochemical analysis to determine information such as the original geochemical composition of seawater (3.4.1).

3.2.2. Preservation of skeletal material - Description

In contrast to most dolostones, fossil material within Raisby Formation limestones and partially dolomitized limestones is well preserved. Thick-walled, originally low-magnesian calcite (LMC) fossils such as brachiopods and bryozoans in general show excellent preservation of their original skeletal microstructure (Figs. 3.6 & 3.10). In one example from the debris flow conglomerate at Dawsons Plantation however, the internal structure of a *Horridonia horrida* valve has been obliterated by recrystallization, evident in both plane light and luminescence (Fig. 3.2). This recrystallization is also demonstrated by trace element geochemical differences:

Non-luminescent area:

$Ca_{(99.26)}(Mg_{(0.70)}Fe_{(0.01)}Mn_{(0.03)})CO_3$

n=2

Luminescent area:

$Ca_{(99.35)}(Mg_{(0.49)}Fe_{(0.04)}Mn_{(0.12)})CO_3$

n=3

Recrystallization was also identified within brachiopods from the Raisby Formation by stable isotope data (3.4.1).

In general, thin walled originally LMC fossil fragments (ostracodes, foraminifers and calcispheres) are less well preserved, and commonly have evidence for corrosion of shell material by calcite microspar (Fig. 3.11b). Such fossils are hard to differentiate from microspar in plane light, although in general luminesce a brighter orange. Some shell fragments and foraminifers have had their shell material completely dissolved out and cemented by coarse

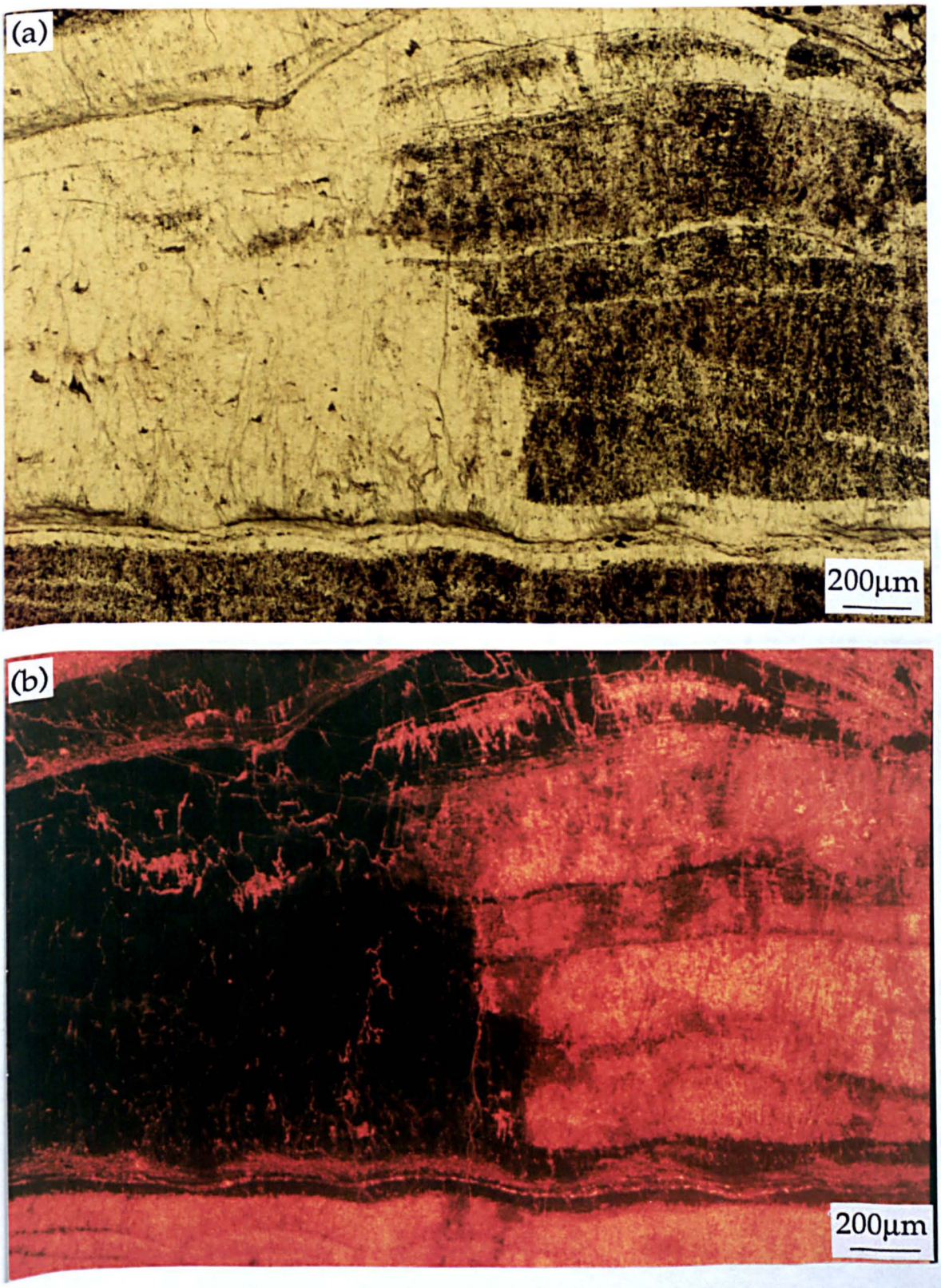

Fig. 3.2. Thin section photomicrographs of part of a large, semi-articulated Horridonia horrida from unit 4 of the debris flow, Dawsons Plantation; (a) plane light, (b) luminescence. An abrupt recrystallization front is seen in the middle of the field of view.

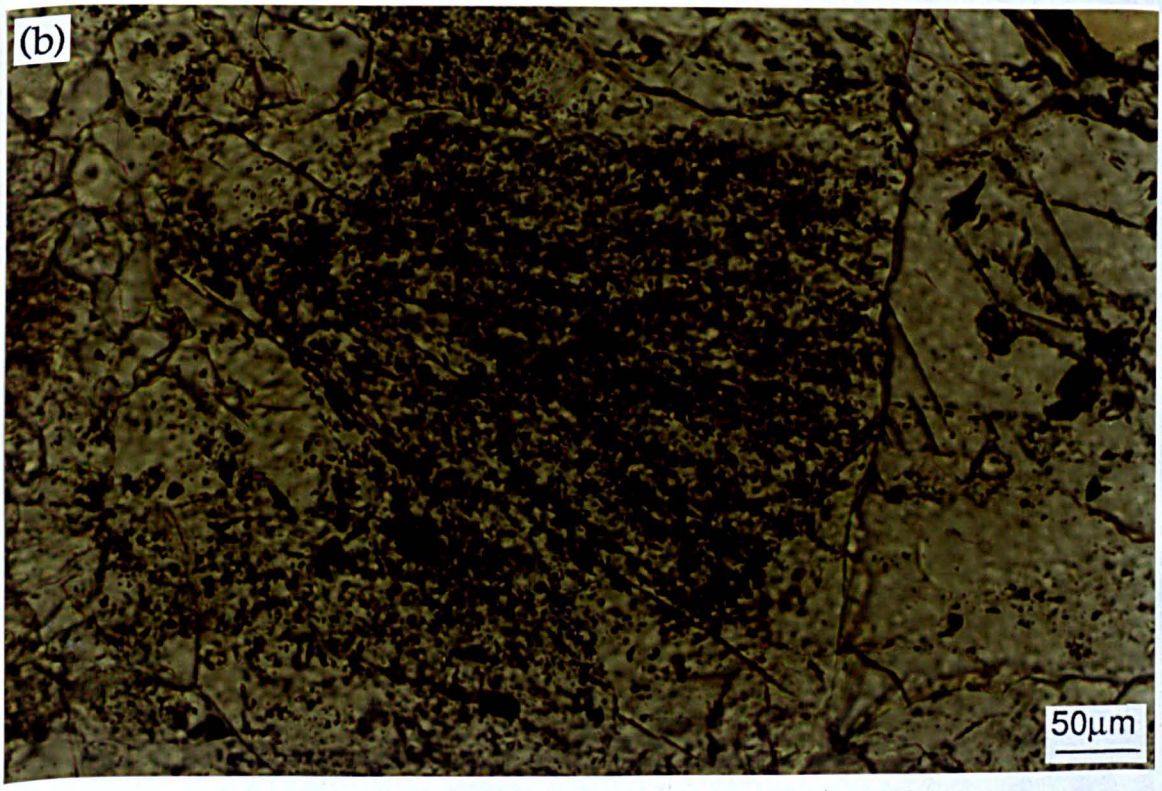

Fig. 3.3. Thin section, plane light photomicrographs of (a) a large phosphatized foraminifer, WO10 borehole 82.1m, and (b) a former marine cement bundle defined by the alignment of inclusions within replacive calcite. The former marine cement bundle lines an early diagenetic fracture cutting an isolated limestone nodule, Raisby Quarry.

calcite, or remain as voids. Skeletal material has also often been preferentially replaced by sulphates, which are preserved in core and represented by calcite cemented pores after leached sulphates at outcrop.

In one sample from borehole W.O.10, phosphatized foraminifers were recorded within a dolostone host rock. The dolostone has abundant evidence of being formerly fossiliferous, containing moulds, or coarse calcite cemented moulds after complete foraminifers, ostracodes and shell fragments. The foraminifers and ostracode skeletal moulds may contain mimic dolomitized former marine calcite cements which precipitated around the inner surfaces of intraskeletal pores. Most large foraminifers in this sample have had their shell material replaced by a mineral which is medium brown coloured in transmitted light, but has a poorly defined extinction position, suggesting that is comprises a mass very fine crystals. This mineral pseudomorphs skeletal material as a whole, although the microstructure is not preserved (Fig. 3.3a). The large foraminifers have commonly been fractured following burial compaction (Fig. 3.3a). The fracturing postdates replacement of the foraminifers, but predates dolomitization. The dolostone also hosts abundant amorphous light brown to black (in transmitted light) organic material represented as thin streaks between dolomite crystals. The pseudomorphed foraminifers have themselves been partially replaced by large equant calcite crystals which partly occlude dissolution porosity within the dolostone.

3.2.3. Preservation of skeletal material - Interpretation

Preservation of skeletal microstructure is to be expected, if the host limestones formed by aggrading neomorphism of originally less stable material (aragonite and high-magnesian calcite [HMC]) (Chapter 4). In such a diagenetic environment, LMC is the stable phase and so, originally LMC skeletal material should not be altered, although in the Raisby Formation limestones it was only the thicker LMC shell material which escaped most, although not all alteration. One isotope analysis of a brachiopod from High Moorsley Quarry suggests that the alteration of skeletal LMC took place during burial from fluids of elevated temperature (3.4.2.2). In this sample there is no textural evidence for alteration (Fig. 3.6), and so it may have mainly been via cementation of pores within the skeletal microstructure by burial calcites, as described by Al-Aasm and Veizer, (1986a) for Cretaceous Rudists, although minor dissolution - reprecipitation of LMC may also have been active (i.e., LMC - dLMC neomorphism [Veizer, 1983a]). The poorer preservation of thin walled LMC skeletal material most likely reflects some dissolution of the LMC during neomorphism. Some completely dissolved shell fragments and possibly some calcite cemented foraminifer moulds identified within limestones were probably originally aragonite (Fig. 3.11a).

The mineral replacing foraminifers from borehole W.O.10 is interpreted to be a phosphate, possibly apatite ($Ca_5(F,Cl)(PO_4)_3$) or a mineral of similar composition. Although

no analytical data is available, the petrographic characteristics of this material, and the extreme similarity of the replaced foraminifers to phosphatized foraminifers documented by Prevot and Lucas (1986) suggests it is apatite. The only other possibility, on petrographic grounds, is a very finely crystalline iron oxide/hydroxide, but that is considered unlikely given the very specific nature of the replacement. To the authors knowledge, no phosphatized skeletal material has previously been recorded within the English Zechstein sequence, despite recent comprehensive studies of the very fossiliferous Ford Formation Main Reef complex. The process of phosphatization is considered similar to that described by Prevot and Lucas (1986) from experimental work, and their study of Tertiary phosphatized foraminifers within dolostone host rocks from Morocco. They consider that phosphatization is an early diagenetic reaction within interstitial waters of sea floor muds. Bacteria break down long chain organic molecules, which creates phosphoric acid. The acid attacks shell calcite, liberating Ca which combines with organic-derived phosphate to form the apatite. Phosphatization is thus a dissolution-reprecipitation reaction. Its fairly coarse scale explains poor microstructure of the foraminifer skeletal material. Phosphate may have been derived both from soft tissues of the foraminifers, and the abundant amorphous organic residues recorded within the dolostone. The very finely crystalline apatite is interpreted as pseudomorphing bacteria (cf. Prevot and Lucas, 1986). Although this sample does contain abundant organic matter, the reason why phosphatization has only been recorded from one locality is not known.

3.3.1. Petrography and geochemistry of marine cements - Description

Within limestones, primary porosity has been occluded by a number a phases of marine-related carbonate cements. These cements are interpreted to have been precipitated by marine pore waters on the basis of their crystal form, trace element composition, luminescence characteristics and the nature of the primary porosity which they occlude. Such cements have not previously been recorded from the Raisby Formation, although they have been comprehensively documented from the undolomitized reef base coquina of the Ford Formation at Tunstall Hills, Sunderland (Tucker and Hollingworth, 1986; Hollingworth and Tucker, 1987).

Primary porosity-occluding cements occur in three major locations within Raisby Formation carbonates:

1. Fracture-fill cements
2. Macrofossil intra-skeletal porosity occluding cements
3. Microfossil intra-skeletal porosity occluding cements, and cement fringes on microfossils and macrofossil fragments.

These cements have only been recorded from primary limestones and calcite concretions within the Raisby Formation, although some have been partially preserved within dolostones by mimic dolomitization (5.2.1).

3.3.1.1. Fracture-fill cements.

These were recorded from both Raisby Quarry and borehole W15. The fractures were produced by compaction of early diagenetic limestone nodules. Two phases of fracture-fill calcite can be recognized:

1. Inclusion-rich coarse columnar calcite crystals. The crystals are elongate normal to fracture walls (250-400μm), with a unit extinction and elongate inclusions that describe a radiating fabric away from the pore walls (Figs. 3.3b; 3.4 & 3.5). The calcite is non-ferroan, with a blotchy luminescence comprising irregular bright orange- and non-luminescent areas (Fig. 3.4).
2. Where phase 1 does not completely occlude porosity, it is overlain by clear, coarse (mean 150μm), blocky, non-ferroan calcite, commonly in optical continuity with phase 1 columnar crystals. These cements are zoned dull-bright orange (Fig. 3.5b).

Geochemical analysis shows that fracture filling cements from Raisby Quarry comprise low-magnesian calcite, with low concentrations of Fe and Mn (Table 3.1). One ICP analysis is in accordance with the microprobe data, although greater Fe and Mn concentrations represent contamination from luminescent areas of the cements not analysed by microprobe. Sr is also high; this may represent contamination from host calcite

3.3.1.2. Macrofossil intraskeletal porosity-occluding cements.

These were recorded from High Moorsley (Fig. 3.6) and Raisby Quarries. A further sample from the Ford Formation reef base coquina at Tunstall Hills was analysed for comparison (Fig. 3.7). In these samples, a clear cement stratigraphy is developed:

1. Very finely crystalline, acicular, inclusion-rich calcite crystals normal to pore walls, (mean 50μm). Characterised by a blotchy bright/dull orange-luminescence.
2. Columnar, non-luminescent inclusion free calcite, coarser than phase 1 (70-100μm). Again normal to pore walls.
3. Coarsely crystalline (mean 1.7mm), equant, inclusion-free calcite cements with well-developed zoning. They have no crystallographic relation to the underlying calcite.

Both phases 1 and 2 encrust the whole inner surface of the macrofossil porosities. The junction between phases 2 and 3 is commonly marked by an abrupt increase in crystal size (generation boundary [Marshall, 1981]) (Figs. 3.6 & 3.7), although there may be an intermediate luminescent cement phase overlying and of similar size to the non-luminescent calcite (Fig. 3.6b). In a brachiopod from Raisby Quarry, only the phase 2 non-luminescent calcite, and a small amount of phase 3 luminescent calcite was present. The

Fracture filling cements		
Raisby Quarry		
-Microprobe (n=10)		
Non-luminescent cement		$Ca_{(98.13)}(Mg_{(1.79)}Fe_{(0.04)}Mn_{(0.04)})CO_3$
-ICP (n=1)		
Non-luminescent cement		$Ca_{(98.15)}(Mg_{(1.59)}Fe_{(0.13)}Mn_{(0.08)}Sr_{(0.06)})CO_3$
Brachiopod intra-skeletal porosity occluding calcite cements		
Ford Formation		
-Microprobe		
Acicular cement *(n=6)*		$Ca_{(96.48)}(Mg_{(3.29)}Fe_{(0.13)}Mn_{(0.10)})CO_3$
Non-luminescent cement *(n=9)*		$Ca_{(99.01)}(Mg_{(0.95)}Fe_{(0.02)}Mn_{(0.01)})CO_3$
Luminescent cement *(n=12)*		$Ca_{(98.79)}(Mg_{(0.80)}Fe_{(0.18)}Mn_{(0.23)})CO_3$
-ICP (n=3)		
Inter-skeletal cement		$Ca_{(98.53)}(Mg_{(0.98)}Fe_{(0.20)}Mn_{(0.23)}Sr_{(0.06)})CO3$
High Moorsley Quarry		
-Microprobe		
Brachiopod shell *(n=4)*		$Ca_{(99.20)}(Mg_{(0.51)}Fe_{(0.17)}Mn_{(0.13)})CO_3$
Acicular calcite *(n=8)*		$Ca_{(98.55)}(Mg_{(1.14)}Fe_{(0.16)}Mn_{(0.16)})CO_3$
Non-luminescent cement *(n=5)*		$Ca_{(98.89)}(Mg_{(1.07)}Fe_{(0.02)}Mn_{(0.03)})CO_3$
Coarse zoned luminescent cement *(n=8)*		$Ca_{(98.24)}Mg_{(0.90)}Fe_{(0.55)}Mn_{(0.32)}CO_3$
-ICP & stable isotope		
Coarse zoned luminescent		$Ca_{(98.48)}(Mg_{(0.77)}Fe_{(0.39)}Mn_{(0.35)}Sr_{(0.01)})CO_3$
cement *(n=1)*	$\delta^{13}C = 2.4‰$	
	$\delta^{18}O = -9.7‰$	
Brachiopod shell *(n=1)*	$\delta^{13}C = 1.8‰$	
	$\delta^{18}O = -5.0‰$	
3. Raisby Quarry		
-Stable isotope (n=2)		
Brachiopod shell	$\delta^{13}C = 4.0‰$	
	$\delta^{18}O = -3.2‰$	
Cements coating shell fragments		
Dawsons Plantation		
-Microprobe		
Brachiopod shell fragment *(n=2)*		$Ca_{(98.93)}(Mg_{(1.02)}Fe_{(0.02)}Mn_{(0.04)})CO_3$
Acicular calcite *(n=7)*		$Ca_{(97.83)}(Mg_{(2.02)}Fe_{(0.09)}Mn_{(0.06)})CO_3$
Luminescent calcite *(n=2)*		$Ca_{(98.44)}(Mg_{(1.09)}Fe_{(0.29)}Mn_{(0.19)})CO_3$
Non-luminescent calcite *(n=2)*		$Ca_{(97.80)}(Mg_{(2.15)}Fe_{(0.04)}Mn_{(0.02)})CO_3$

Table 3.1. Summary of the geochemistries of various marine cement phases identified. Where more than one sample was analysed, values presented are arithmetic means.

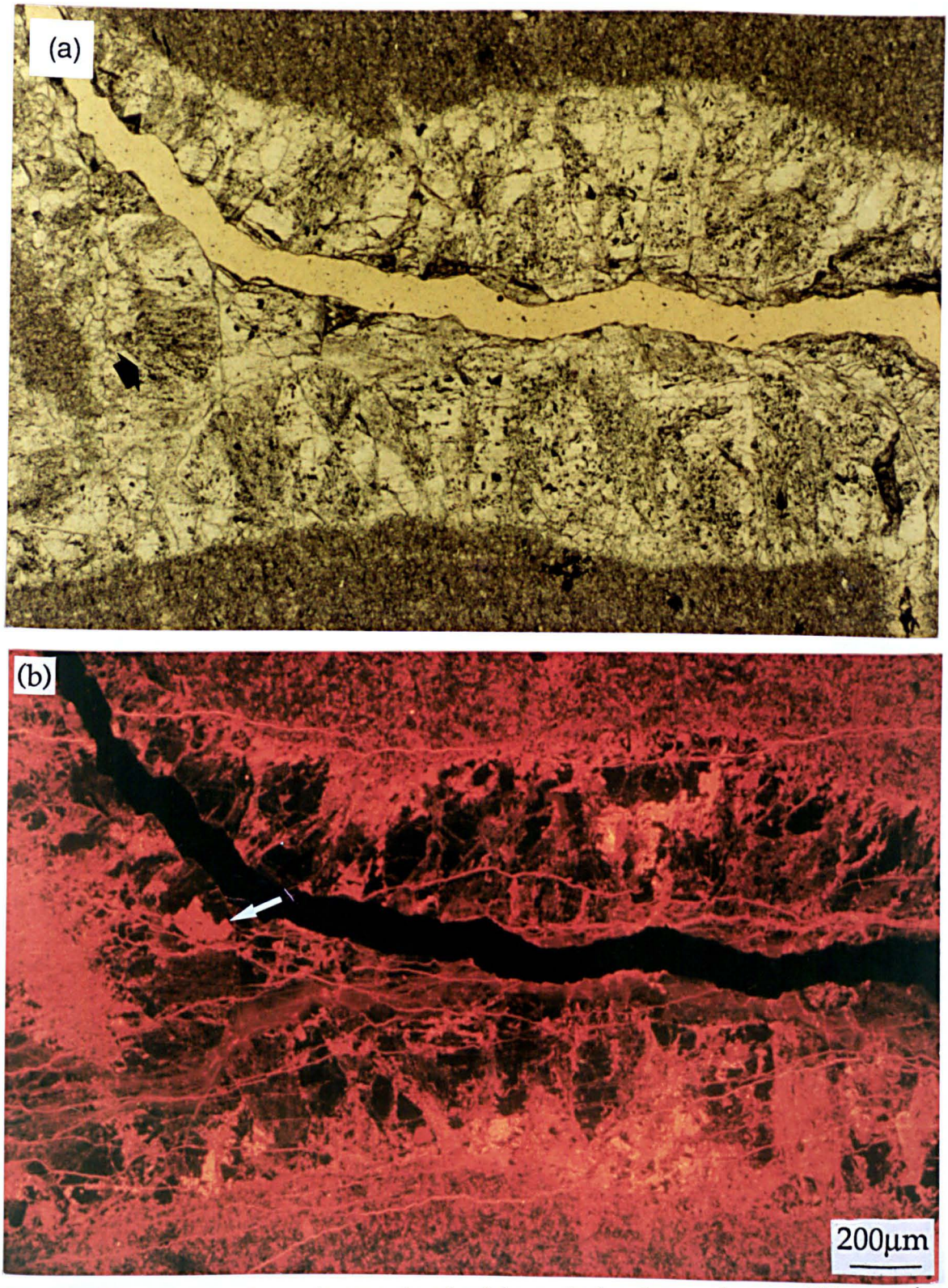

Fig. 3.4. Thin section photomicrographs of calcite replacing former fracture-filling marine cements within an isolated limestone nodule, Raisby Quarry; (a) plane light, (b) luminescence. Detail of one former cement bundle (arrowed) is shown in fig. 3.3b. The replacive calcites have a blotchy luminescence, partly due to the formation of numerous small fractures along the line of the original fracture, but also due partly to the replacement of dolomite (?microdolomite) by bright orange-luminescent calcite (arrowed).

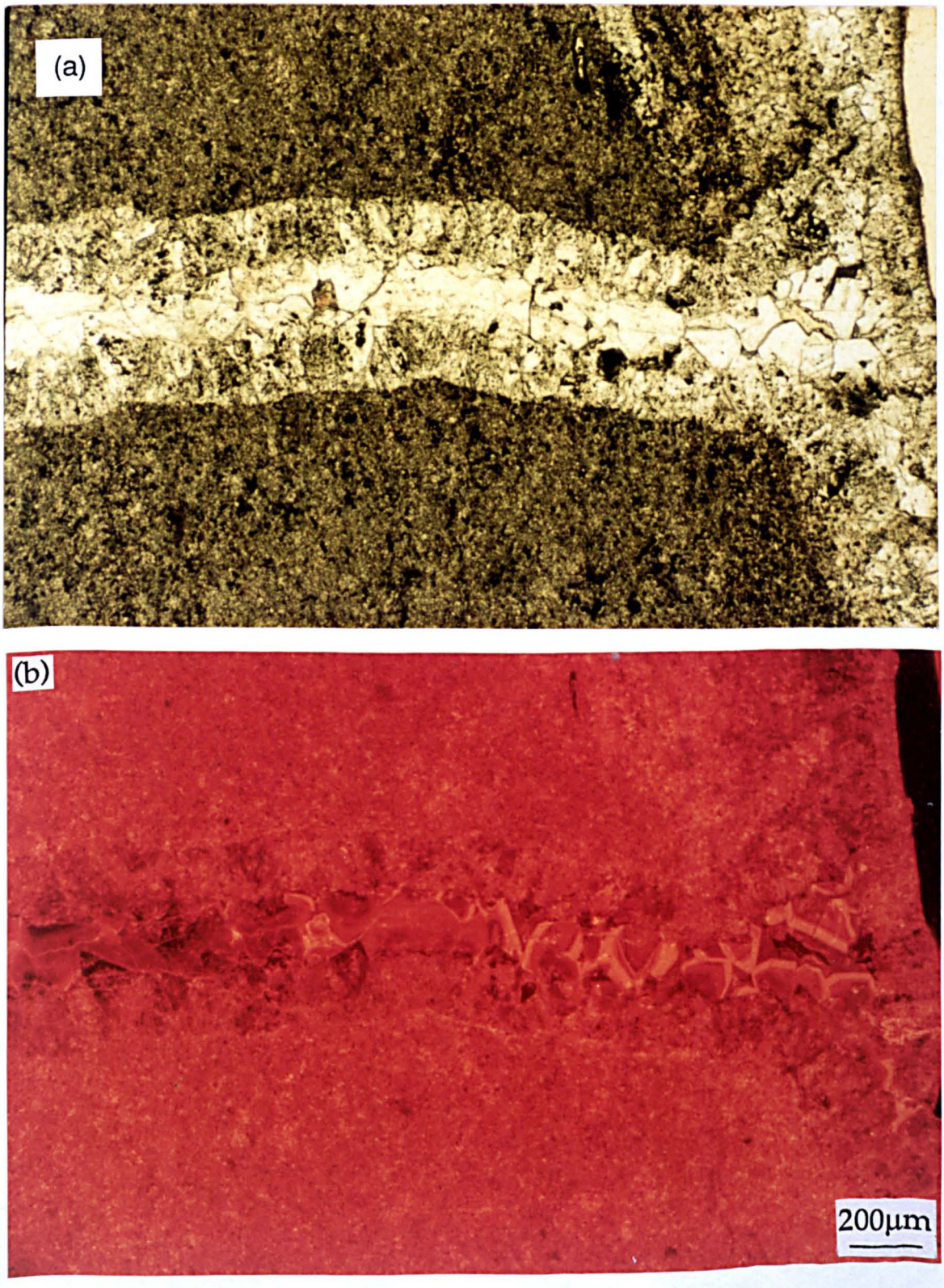

Fig. 3.5. Thin section photomicrographs of calcite, replacive of former fracture filling marine cements within an isolated limestone nodule, Raisby Quarry; (a) plane light, (b) luminescence. In contrast to fig. 3.4, marine cements incompletely occluded the fracture. Replacive calcite continued growing into unoccluded porosity as a zoned cement (b).

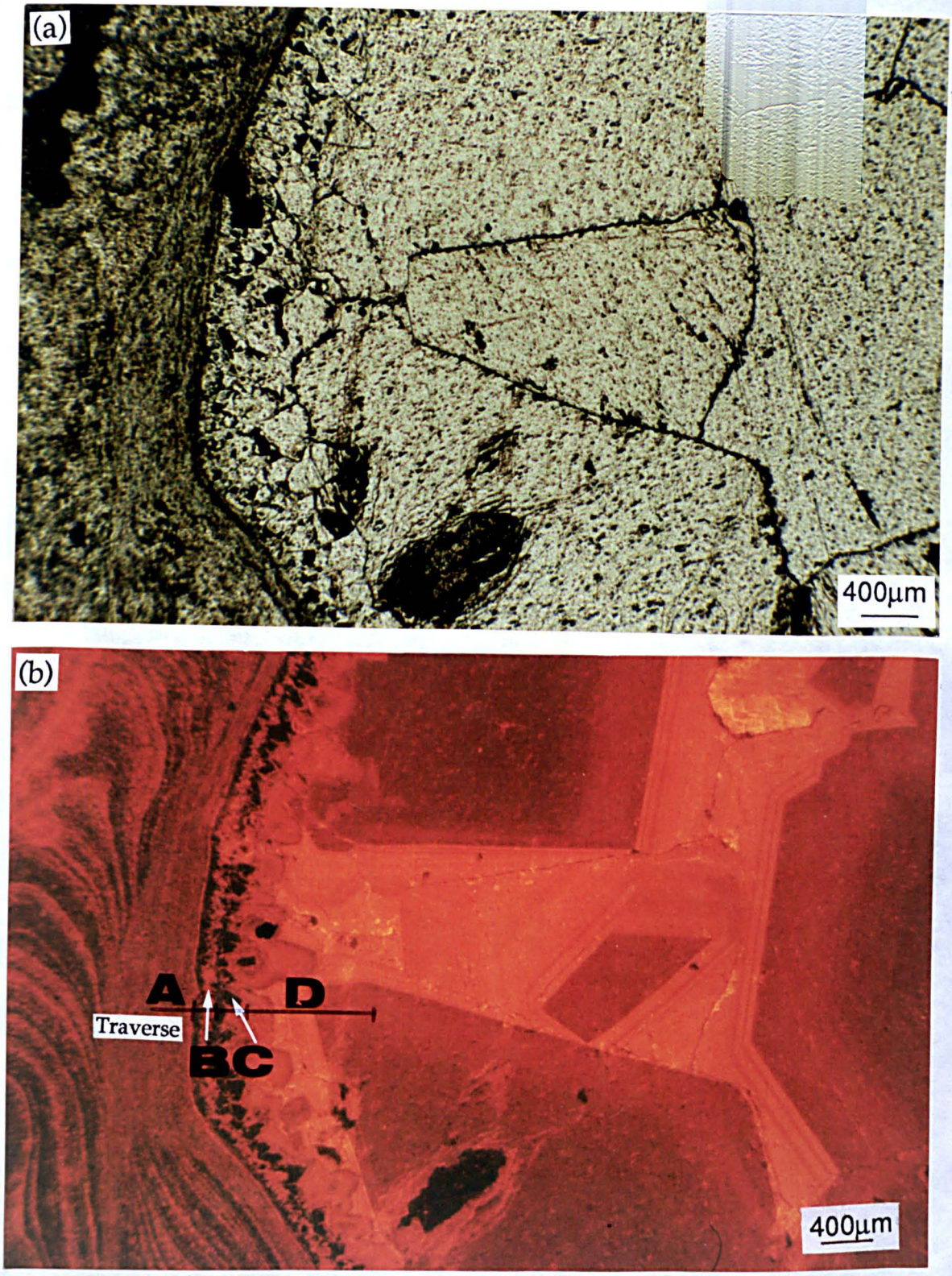

Fig. 3.6. Thin section photomicrographs of the calcite cement fill of an articulated brachiopod within the limestone at High Moorsley Quarry; (a) plane light, (b) luminescence. Four cement phases are developed, from very finely crystalline bright orange- into coarser non-luminescent calcite. Between the non-luminescent and coarse equant zoned calcite is an intermediate zoned orange-luminescent sub-equant calcite.

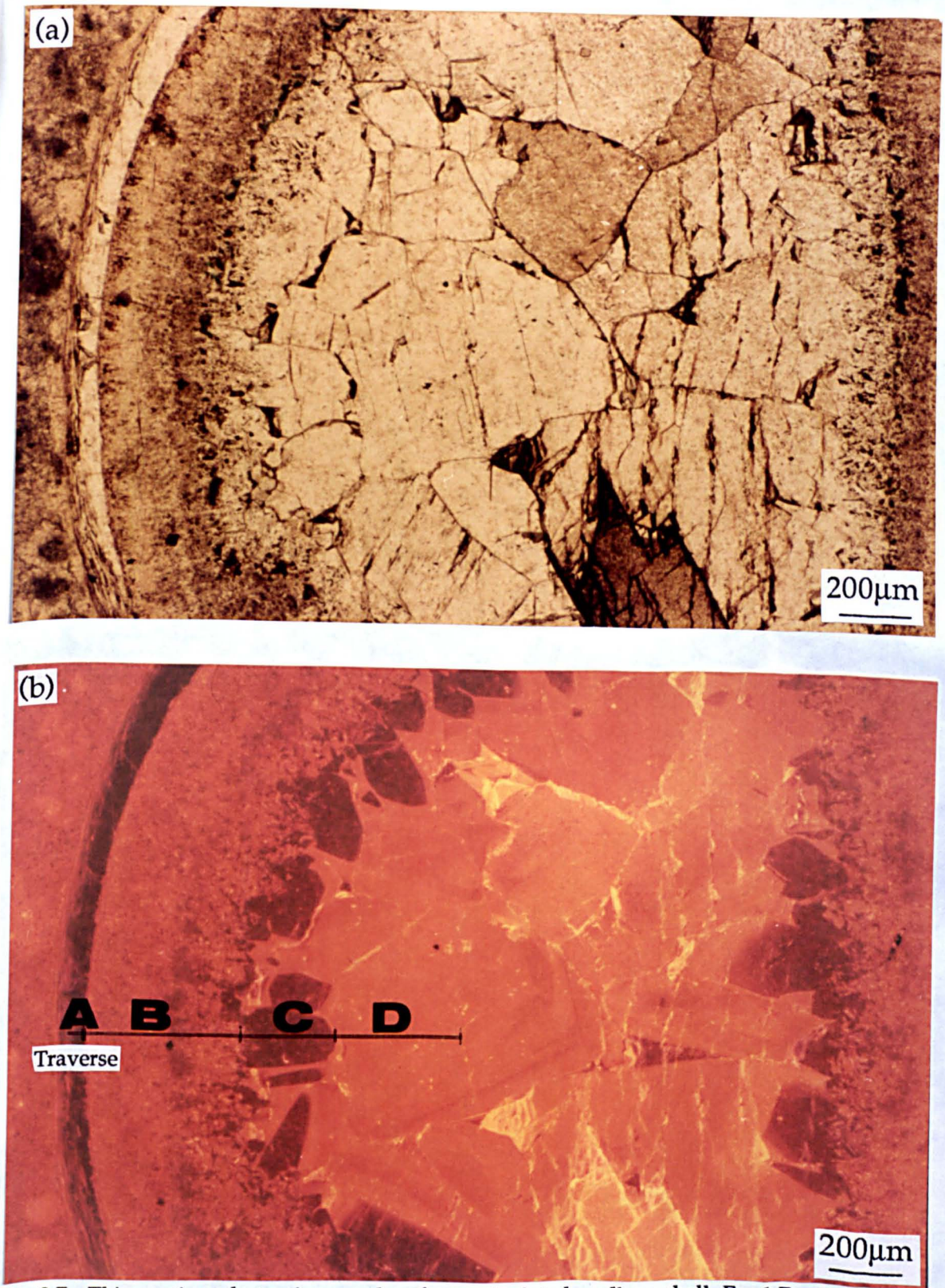

Fig. 3.7. Thin section photomicrographs of an articulated mollusc shell, Ford Formation reef base coquina, Tunstall Hills; (a) plane light, (b) luminescence. Although very much coarser, the cement evolution sequence is very similar to fig. 3.6, apart for the absence of an intermediate bright orange-luminescent cement. The mollusc shell wall was dissolved, and porosity cemented by non-luminescent calcite.

stratigraphy of the coarse, luminescent cement in this sample was the same as that of zoned cements postdating inclusion rich, fracture filling calcite from the same specimen (Fig. 3.5). Geochemical variation within these cements shows a similar pattern, with good correspondence between geochemistry and luminescence (Figs. 3.8 & 3.9). One analysis of the coarse luminescent zoned cement from High Moorsley Quarry by ICP and for carbon and oxygen stable isotopes, is characterized by very low Sr relative to host limestones and a considerably depleted oxygen isotope value (Table 3.1). Three ICP analyses of general interskeletal porosity occluding cements from Tunstall Hills had high Sr values, comparable to primary limestones from the Raisby Formation (Table 3.1). None of these cements were recorded coating the external surfaces of macrofossils from the Raisby Formation, although they are abundant on both inner and outer surfaces (intra- and inter-skeletal porosity) in the reef base coquina.

3.3.1.3. Cements associated with macrofossil fragments and microfossils - Description

These cements are by far the most common in any one sample, owing to the relative abundance of microfossils and macrofossil fragments. The nature of cements is specific to certain taxa. In general, bryozoan fragments are not associated with any cements, whereas cements are well-developed coating brachiopod shell fragments. Cements are also abundant coating, and occluding intra-skeletal porosity of ostracodes, foraminifers and calcispheres. Two phases of calcite may be distinguished:

1. Circumgranular, acicular, inclusion-rich calcite normal to growth surface (Fig. 3.10a). Commonly occurs as a fringe 50-90μm wide. Where the skeletal substrate comprises large single crystals, groups of needles are in optical continuity with the crystals off which they grew. Commonly, crystals encrust both the upper and lower surface of skeletal material (Fig.3.10a) and the inner and outer surfaces of ostracodes, foraminifers and calcispheres. Where pores are spherical (i.e., calcispheres), the acicular cements show a pseudo-uniaxial extinction cross. They range from non- to blotchy orange-luminescent.
2. Equant to columnar, inclusion-free luminescent zoned calcite cements (60-70μm) (Fig. 3.10b). These fill intra-skeletal porosity not previously occluded by the acicular calcite, and rarely occur as spire-like syntaxial overgrowths on circumgranular acicular cements coating the external surfaces of fossils (Fig. 3.10b).

Although the acicular calcites commonly encrust both inner and outer surfaces of microfossils, they are generally thicker on internal than external surface. Where the skeletal material has been fractured during compaction, the acicular cements predate this fracturing. The acicular cements may themselves be mimically dolomitized (5.2.1). In a sample from Houghton Quarry, the mimic dolomite was itself replaced by microspar in optical continuity with the original cement (Fig. 4.5). Echinoderm fragments in Raisby Formation limestones are generally overgrown by a single, syntaxial calcite crystal, which extends only a small

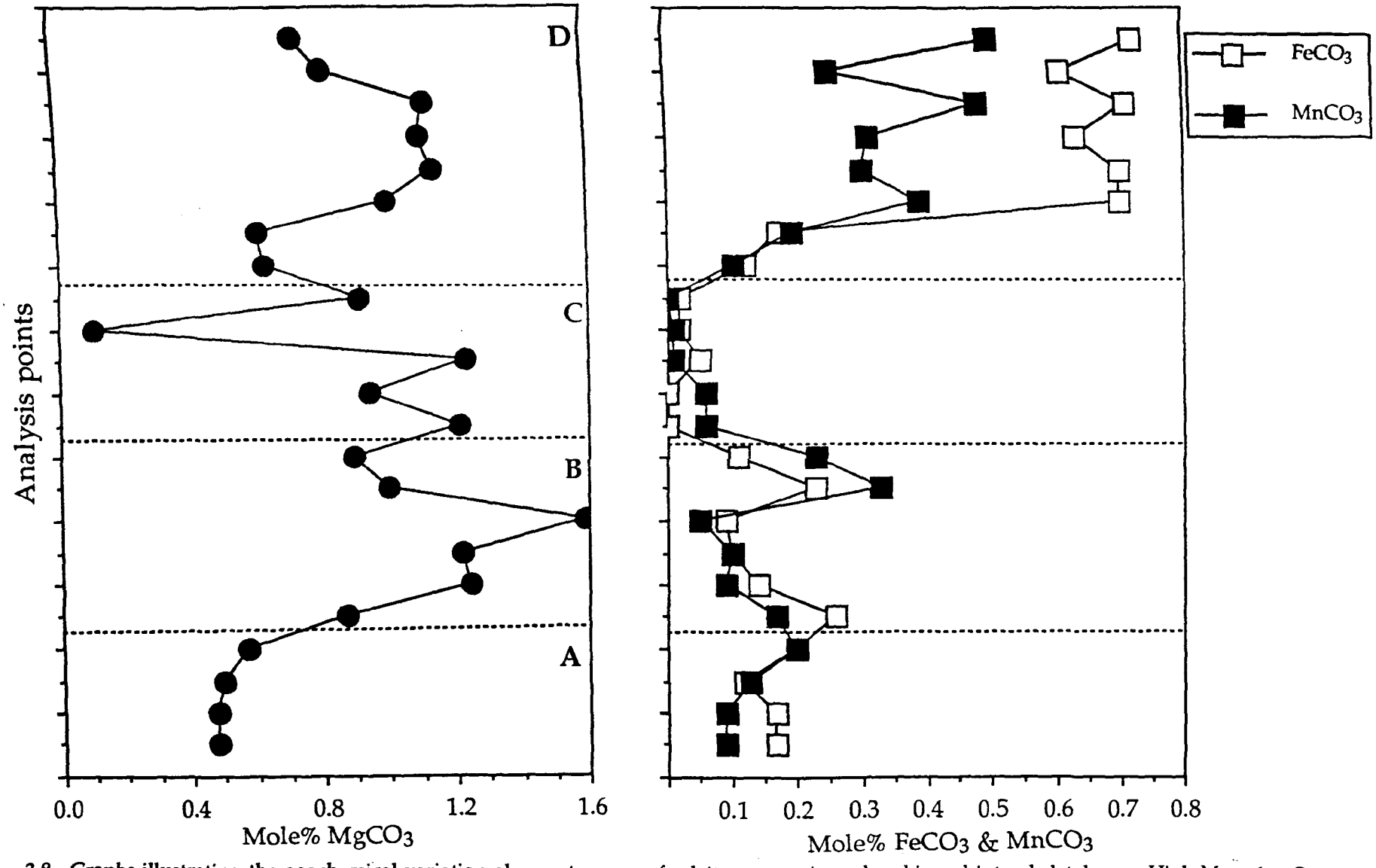

Fig. 3.8. Graphs illustrating the geochemical variation along a traverse of calcites cementing a brachiopod intraskeletal pore, High Moorsley Quarry (Fig. 3.6). A = shell wall, B = inclusion-rich former marine cement fringe, C = non-luminescent calcite, D = zoned luminescent cement.

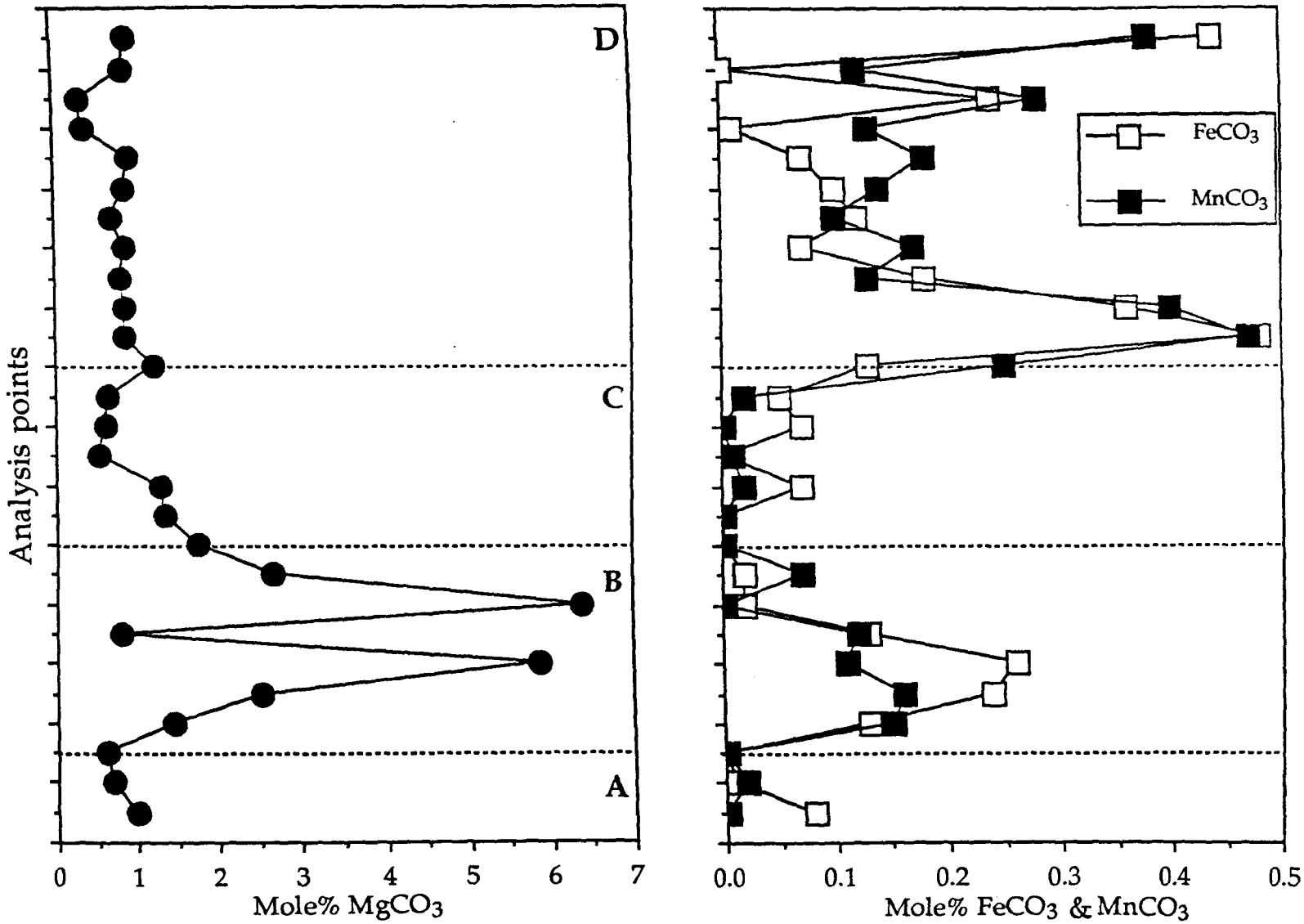

Fig. 3.9. Graphs illustrating the geochemical variation along a traverse of calcites cementing an intraskeletal pore within the Ford Formation reef base coquina, Tunstall Hills (Fig. 3.7). A = non-luminescent calcite filling the dissolved skeletal material, B = inclusion-rich former marine cement fringe, C = non-luminescent calcite, D = zoned orange-luminescent cement.

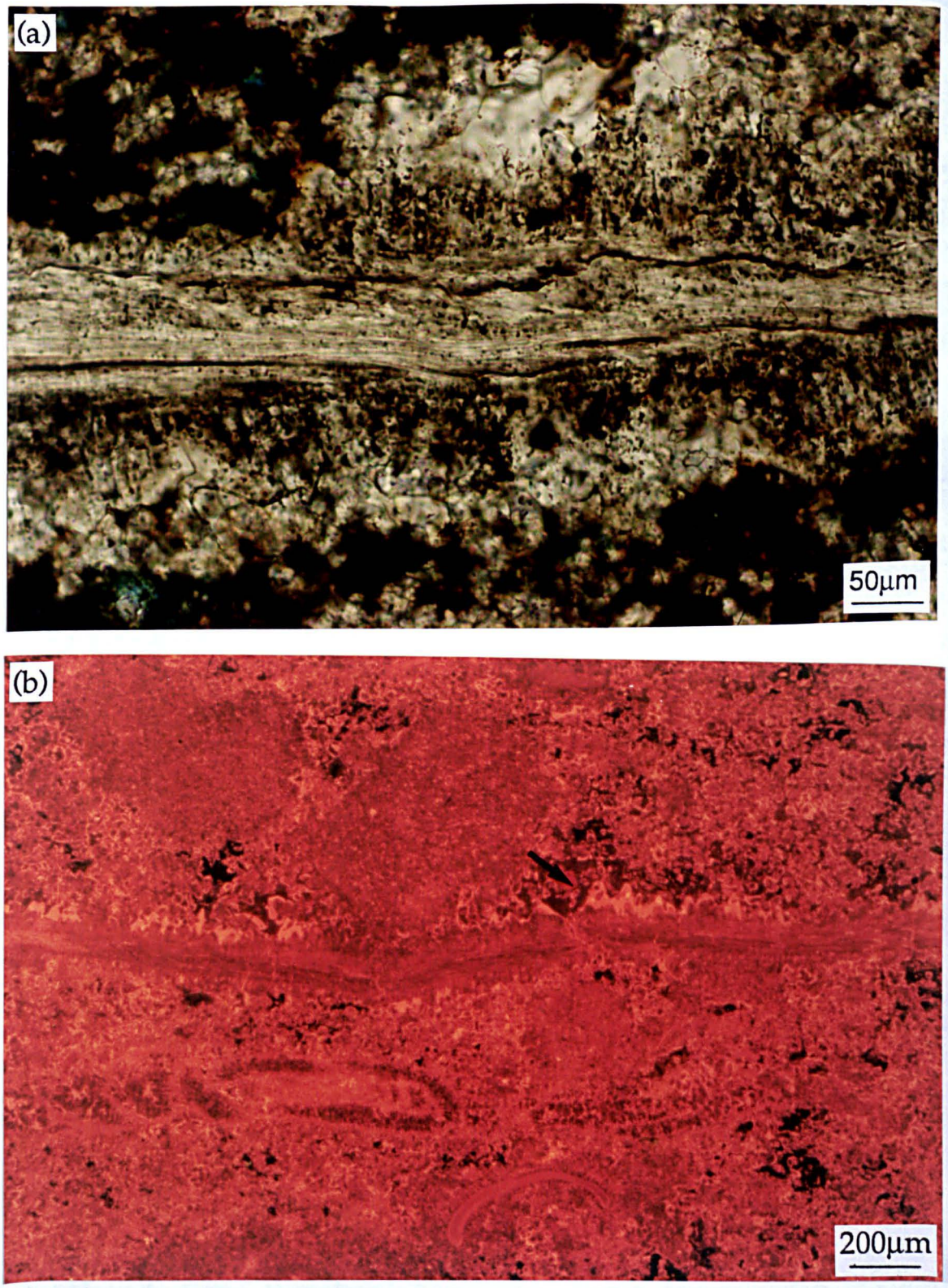

Fig. 3.10. Thin section photomicrographs of former marine cements lining brachiopod shell material, unit 4 of the debris flow, Dawsons Plantation. (a) detail of the cement fringe, plane light, (b) lower magnification view of the same brachiopod shell fragment, luminescence. Although marine cements originally precipitated on both sides of the shell fragment, bright orange- followed by non-luminescent pore filling calcite cements have only grown into inter-clast shelter pores (arrowed).

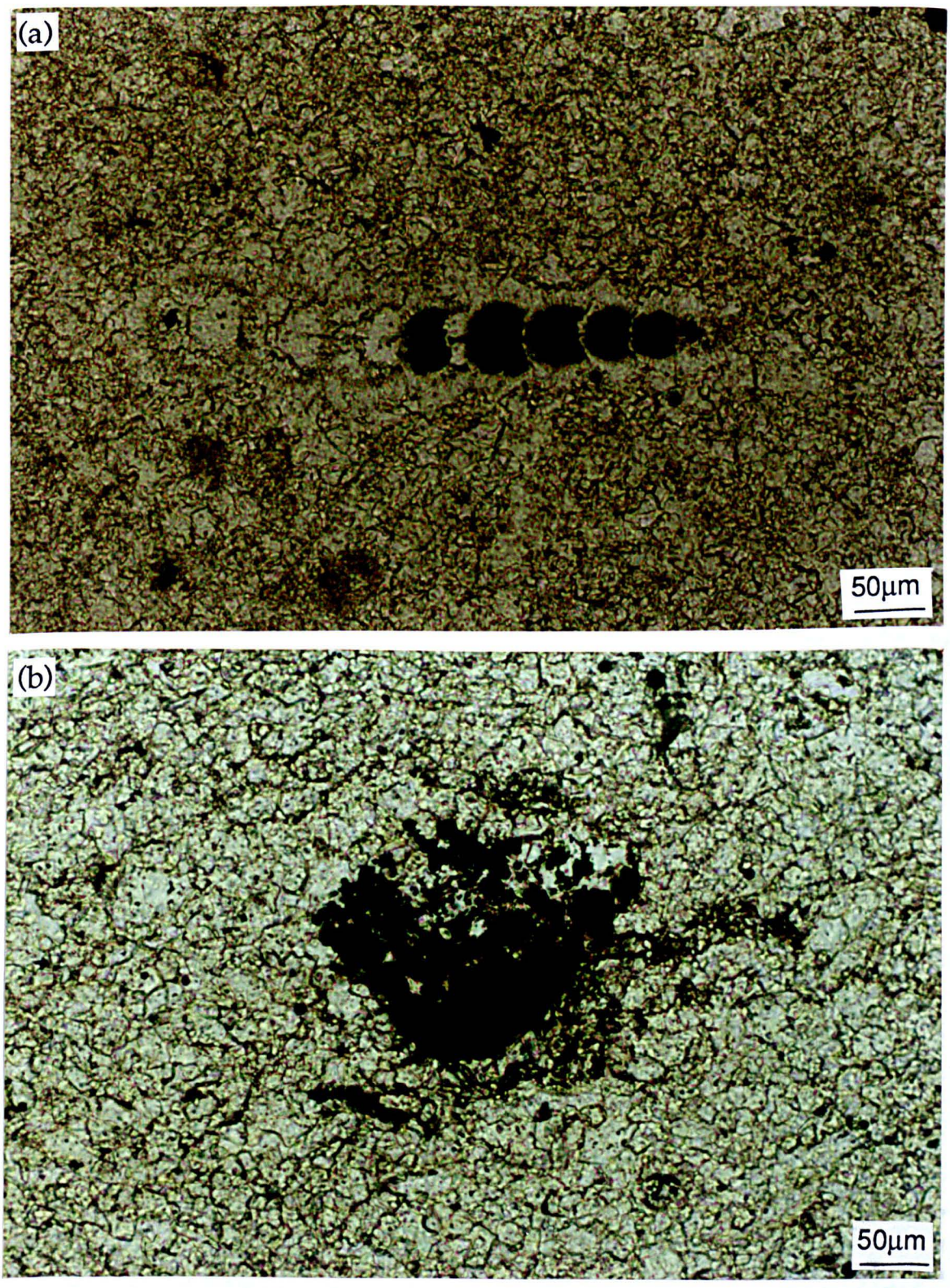

Fig. 3.11. Plane light thin section photomicrographs of pyrite framboids within intraskeletal pores in limestones. (a) pyrite occluding chambers within a large foraminifer, Thickley Quarry. The outer surface of the foraminifer is lined by acicular isopachous cements. (b) pyrite partially filling intraskeletal porosity, W15 borehole, 199.87m. The shell wall has either dissolved (was originally aragonite or HMC), or has been replaced by calcite microspar.

distance into the host microspar. No luminescence zonation can be detected in those cements.

Very commonly, microfossil intra-skeletal porosity has been partially occluded by geopetal pyrite framboids. They either rest on the internal shell wall or overlie the first phase acicular cements (Fig. 3.11a & b). Within multi-chambered foraminifers, the pyrite framboids are more common within the smaller chambers (Fig. 3.11a). Framboids have been recorded from every primary limestone and Raisby Quarry concretion sample. They have not been recorded within brachiopod intra-skeletal porosity, and are rare where not in association with microfossils within limestones.

One microprobe transect of cements coating a brachiopod shell fragment from the Dawsons Plantation debris flow showed a good correspondence of luminescence with geochemistry, which is similar to that of the intraskeletal porosity occluding cements (Table 3.1).

3.3.2. Petrography and geochemistry of marine cements - Interpretation.

Cement sequences developed are similar between the three porosity types, each showing an evolution from an initial fine acicular or columnar blotchy orange-/non-luminescent cement to a final luminescent, blocky, pore filling calcite. The initial, acicular-columnar calcites are interpreted as altered marine cements. This interpretation is based on their size and shape, their occurrence as the initial precipitate within primary pores, and their strong similarity to both ancient and modern marine cements commonly described. Acicular carbonate crystals are indicative of high supersaturation with respect to $CaCO_3$, resulting in rapid growth rates, most rapid parallel to the c-axis. In the marine diagenetic environment, high supersaturation is normally the product of a decrease in solubility of CO_2 in response to heating and/or agitation (Given and Wilkinson, 1985). The coarse fracture-fill calcites are simply much larger versions of the fine acicular cements associated with skeletal material. The fracture-filling, inclusion-rich calcite is interpreted as neomorphosed bundles of acicular cements. The radiating inclusion patterns are very similar to those figured by Kendall (1977) and interpreted by him as representing the remnants of bundles of marine cements (HMC or aragonite) replaced by low-magnesian calcite. Very similar inclusion-rich cement fringes have also been described by Marshall (1981) encrusting the internal surfaces of Jurassic ammonite chambers, and interpreted as replaced HMC cements.

The fracture-fill calcites are also almost identical to, albeit slightly smaller than, originally HMC cements from the Tunstall Hill reef base coquina (Tucker and Hollingworth, 1986). The fracture fill calcites however lack any clear petrographic evidence for microdolomites, commonly cited as indicative of replaced HMC (Lohmann and Meyers, 1977) and recorded from Tunstall Hills (Tucker and Hollingworth, 1986). However, one sample of fracture fill calcite from Raisby Quarry does show evidence for replaced finely

crystalline dolomite in luminescence, which could be a calcitized microdolomite (Fig. 3.4b), and some microprobe points do have elevated Mg concentrations (4.18 mole% $MgCO_3$ from inclusion rich cement, Dawsons Plantation (Appendix VII). However, there is no definitive evidence that the dolomite is genetically related to the HMC - dLMC transformation. The fracture-filling calcites also do not exhibit curved cleavages, or divergent/convergent optic axes, commonly cited as indicative of neomorphosed radiating marine cements (Kendall and Tucker, 1973; Kendall, 1977). However, both discrepancies may be reconciled if the replacement of HMC by dLMC was not crystallographically ordered, and occurred in a relatively open diagenetic system. Thus, little of the precursor mineralogy or geochemistry would be retained. Although ICP analyses of one fracture-filling cement have a high Sr, this may well reflect contamination from aragonite and HMC during their neomorphism to dLMC microspars, possibly synchronous with neomorphism of the host ADP muds to dLMC microspar (Chapter 4). Cements from Tunstall Hills (now altered HMC and aragonite, dominated by altered aragonite) have relatively high Sr concentrations, similar to the fracture filling calcite from Raisby Quarry (Table 3.1). However, that the Ford Formation examples have a low Sr relative to the original phases (7000 - 9400 ppm $Sr_{aragonite}$ [Veizer, 1983a]) demonstrates that neomorphism must also have been in fairly open system diagenetic conditions. The Raisby Formation neomorphic calcites still retain an element of original crystallography in that they form columnar crystals of a similar size and shape to original HMC bundles (Figs. 3.4 & 3.5). The neomorphism took place during early burial, when pore waters became undersaturated with respect to HMC and supersaturated with respect to LMC. On the basis of luminescence and geochemistry, this may have taken place during precipitation of overlying non-luminescent and luminescent calcites.

That the acicular cements encrust both the upper and lower surfaces of skeletal fragments shows that they were not cementing a shelter porosity (3.10a). Nearly all of the limestones studied were deposited as wackestones or, more commonly, mudstones so that little grain-supported inter-skeletal porosity existed. The grain-rimming cements could have formed in shallow waters, before resedimentation of the skeletal material, although there is no evidence for cement abrasion, and the cements are very similar to those which have precipitated on the internal surfaces of autochthonous brachiopods. Therefore, the grain-rimming acicular cements must have been at least partly displacive of the host carbonate muds. Kaldi (1980) figures similar displacive isopachous radial-acicular carbonate cement on a foraminifer from the Cadeby Formation. Displacive precipitation of calcite has been recorded (Folk, 1965) and is being increasingly widely recognized (Maliva, 1989).

Where developed, the succeeding inclusion-free, non-luminescent calcites were precipitated as LMC. The low concentrations of iron and manganese in these cements (Table 3.1; figs. 3.8 & 3.9) suggests precipitation from oxic fluids, but which were not of 'pure' open ocean seawater composition so that HMC or aragonite was not precipitated. This

suggests precipitation most likely a few tens of centimetres below the sediment-water interface where pore fluids were supersaturated with respect to LMC.

The precipitation of pyrite framboids occurs at the generation boundary between acicular (marine phreatic) or non-luminescent, and coarse, luminescent cements. Framboids are formed as a by-product of the activity of sulphate-reducing bacteria during sediment burial. Pyrite framboids are not a direct precipitate, but result from the recrystallization of iron monosulphides (see review in Raiswell, 1982). Necessary conditions for the formation of pyrite via sulphate-reducing bacteria are negative Eh conditions, abundant suitable organic matter, supply of sulphate (i.e., good connection with seawater) and supply of iron. Sulphate reduction may be active in well aerated sediments however, as long as suitable reducing micro-environments exist (Hudson, 1982). This appears to have been the case within the Raisby Formation limestones, as they were bioturbated and aerated, and at times did support a benthic fauna (Chapter 2). If the pore waters within the sediment were reducing, pyrite would be expected throughout the sediment (such as the Marl Slate) and not within intra-skeletal porosity (Hudson, 1982).

Sulphate reduction within intraskeletal micro-environments commonly takes place in two stages, with bacterial oxidation of organic matter followed by anaerobic sulphate reduction (Fig. 3.12). Bacterial oxidation serves to consume dissolved molecular oxygen so that sulphate reduction can begin (Irwin *et al.*, 1977). This can only take place where there is an abundant supply of organic matter, and the diffusion of dissolved molecular oxygen from overlying seawater is retarded, such as within microfossil intraskeletal porosity. Once such reducing micro-environments have established, dissolved iron (Fe^{2+}) and seawater sulphate migrate preferentially to those areas. In the Raisby Formation examples, iron must have been introduced into the pores by diffusion through shell walls (i.e., pyrite did not form by in-situ sulphidization of detrital iron oxides), because the framboids may be as large as the pores themselves (Fig. 3.11a). The source of iron was most likely detrital iron oxides and iron adsorbed onto clays. However, in order for the iron to be reduced (to allow it to be taken up into solution) the sediment pore waters in immediate contact with the iron oxides and clays must have been reducing, although not too reducing (probably only in localized microenvironments) such that the iron immediately combined with available sulphide to form pyrite. Sulphate reduction within intraskeletal porosity, such as in the Raisby Formation limestones, was most likely limited by the availability and quality of organic matter (cf. Raiswell, 1982). The absence of pyrite within macrofossil intraskeletal voids is most likely due to a more open system interchange with dissolved molecular oxygen within the host sediment.

Pyrite framboids are in general less common within Raisby Formation dolostones, compared to their abundance in the limestones. Thus, either the sediments which were later dolomitized went through a different early diagenetic history, or dolomite precipitation

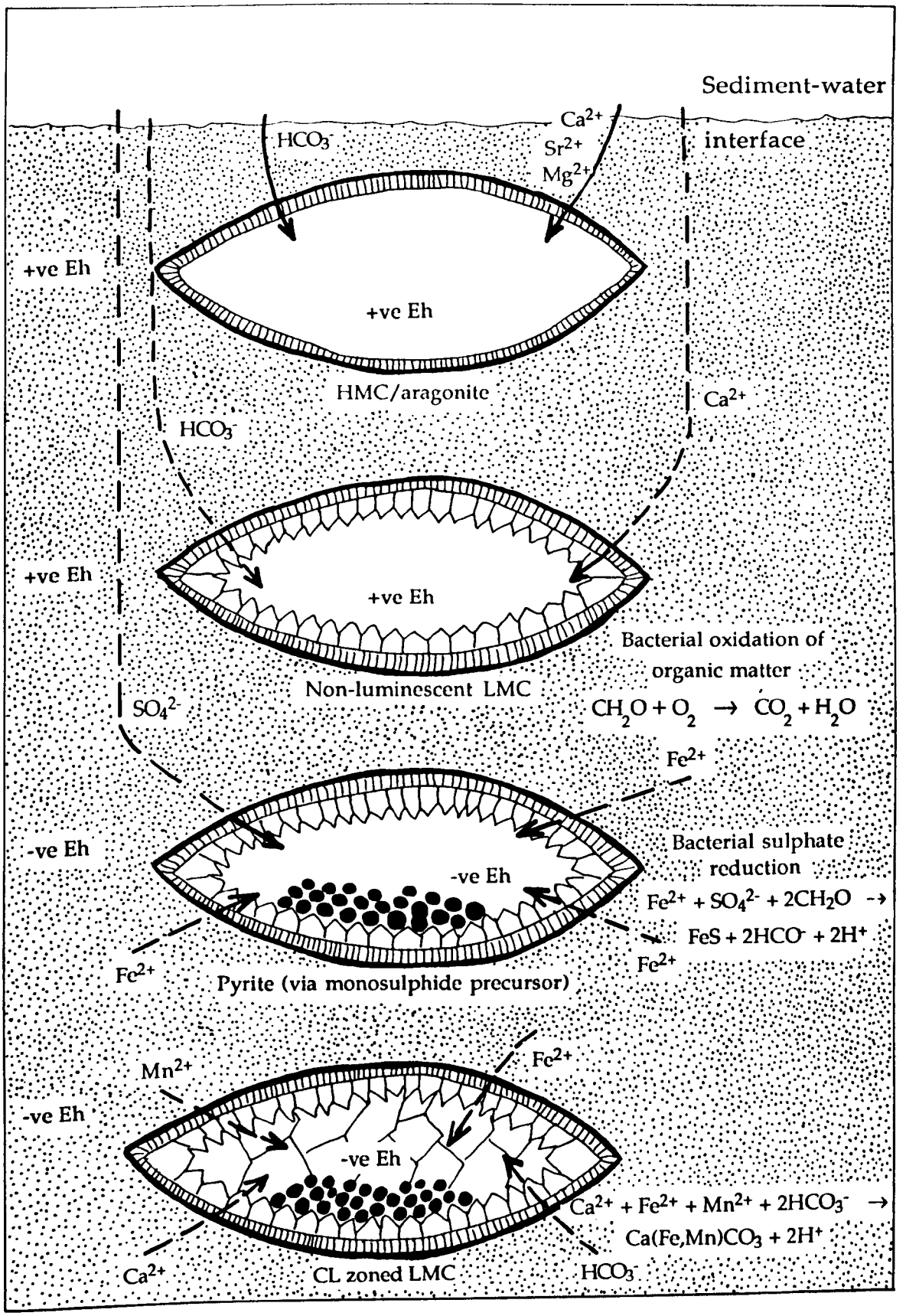

Fig. 3.12. Summary diagram illustrating the main episodes of marine diagenesis, related to progressive burial below the sediment-water interface of a hypothetical intraskeletal pore. No vertical scale is implied, but stage three is probably tens of centimetres to a few metres below the sediment-water interface. Hundreds of metres of burial separates stages 3 and 4.

destroyed the framboids, through oxidation or dissolution via reducing dolomitizing fluids. At one locality in the formation (the dolomitic debris flow at Houghton Quarry [Chapter 2]), the sediment itself is extremely rich in pyrite framboids. This debris flow is very dark, fine-grained and organic-rich, suggesting that, due to the rapid burial, organic matter was preserved (isolated from seawater-derived oxygen) which allowed much more extensive sulphate reduction to take place than is commonly recorded within the formation.

The transition from non-luminescent cement precipitation (positive Eh) to sulphate reduction (negative Eh) was abrupt. The non-luminescent cement must have been precipitated before significant aerobic bacterial oxidation (the succeeding precipitation of pyrite suggests lack of iron and manganese in the diagenetic system was not the cause of incorporation of no Fe and Mn into the non-luminescent calcite). Thus, at least in some intra-skeletal pores, bacterial oxidation and bacterial sulphate reduction all took place between non-luminescent and coarse luminescent cement precipitation. The generally large size difference between the acicular (= marine phreatic) and later luminescent calcite cements is indicative of a considerable hiatus in calcite precipitation. During coarse luminescent calcite precipitation, pore fluids were reducing (allowing Fe and Mn coprecipitation), of a low supersaturation, and possibly of an elevated temperature, based on a single oxygen isotope analysis from High Moorsley Quarry. These features are typical of burial cements.

The history of primary porosity occlusion within the Raisby Formation limestones, is very similar to that documented by Miller (1986) from Waulsortian mud mounds of Ireland. He described a cement sequence from marine (radiaxial-fibrous calcite) through non-luminescent cements (high Eh marine phreatic) into coarse, luminescent, burial calcites. Pyrite framboids occur at the contact of non-luminescent with luminescent cements. The proposed early diagenetic pore water evolution within Raisby Formation sediments is illustrated in fig. 3.12. This represents only the cement sequences developed in the lower part of the Raisby Formation (where the limestones are preserved), although these are in general similar to cements precipitated during deposition of the Ford Formation reef base coquina, and so may be taken as representative of the Raisby Formation as a whole. This is further supported by similar intraskeletal cements to those described, preserved by mimic dolomitization within the Raisby Formation (5.2.1).

3.3.3. Summary and conclusions.

Skeletal material within the Raisby Formation is in general well preserved. Originally LMC fossils most commonly remain as LMC, although alteration is apparent in some samples, illustrated by luminescence and oxygen stable isotope analyses. Originally aragonite/HMC fossils were dissolved out during early burial diagenesis and, locally, some foraminifers were phosphatized. Early marine diagenesis (marine eogenesis) in the Raisby Formation involved precipitation of aragonite/HMC cements within fractures, intraskeletal

pores, and as a displacive circumgranular coating on shell fragments. With further burial, those pores not completely occluded by the marine cements saw further precipitation of non-luminescent LMC cements followed by coarse, zoned pore-filling calcites with ^{18}O-depleted oxygen isotope ratios. Pyrite framboids mark an episode of bacterial oxidation followed by sulphate reduction between marine eogenetic cements and coarse burial calcites. This evolution path is illustrated below:

Acicular cements

Oxidizing marine pore waters

↓

Non-luminescent cements

Oxidizing pore waters, modified from marine composition such that crystal growth was slower, an HMC or aragonite was not precipitated.

↓

Framboidal pyrite

Reducing pore waters. Still close enough to the sediment-water interface for sulphate to be derived from sea water.

↓

Zoned luminescent equant cements

Reducing pore waters with no seawater influence. Two phases of zoned equant cements in some samples (i.e., Fig. 3.6b) reflect progressively increasing depth of burial with an attendant decrease in supersaturation, and so increase in crystal size.

The small size of marine eogenetic cements within intraskeletal porosity of the Raisby Formation, in comparison to those of the Ford Formation reef base coquina, suggest that rates of advection of seawater through sea floor sediments was much slower within the Raisby Formation than during early stages of deposition of the Ford Formation reef. This, in turn, is probably related to contrasting water depths and so turbulence between the basal Ford Formation (shallow water) and Raisby Formation (deep water).

These cements described, which precipitated during burial, are distinguished from calcite cements precipitated during uplift of the Raisby Formation (telogenesis) mainly on the basis of different luminescence sequences (burial shows a non-luminescent to luminescent evolution, whereas uplift is characterized by a luminescent to non-luminescent sequence [Chapter 6]). Burial calcites are also only seen within primary pores (i.e., intraskeletal pores), whereas uplift calcites occur within secondary pores. Burial calcites also lack intracrystalline iron oxides, characteristic of those precipitated during uplift (Chapter 6).

3.4.1. Primary isotopic composition of Zechstein seawater - Description

The isotopic compositions of limestones, dolostones and brachiopods within the Raisby Formation may be used to infer the isotopic composition of Zechstein seawater. Raisby Formation limestones and dolostones have mean carbon isotopic compositions of $\delta^{13}C$ 5.5‰ to 6.0‰ (Fig. 3.13). The carbon isotopic compositions of matrix replacive dolostones from the Ford Formation main reef (Aplin, 1981) also have a mean in the same group (Fig. 3.13). Oxygen isotopic compositions of limestones and dolostones from the Raisby and Ford Formations do not show such a tight grouping, although all analyses have low negative $\delta^{18}O$, with a peak for Raisby and Ford Formation dolostones in the -1.0‰ to -1.5‰ group (Fig. 3.14). Analyses of two non-luminescent brachiopods, from within the limestones at Raisby and High Moorsley quarries gave $\delta^{13}C$ 3.9‰ and 4.1‰, $\delta^{18}O$ -3.1‰ and -3.2‰ (for two samples of the same brachiopod) and $\delta^{13}C$ 1.8‰, $\delta^{18}O$ -5.0‰ respectively (Appendix IX). None of the brachiopod calcite was visibly altered in plane light or luminescence, although their host limestones have been neomorphosed (Chapter 4). There was insufficient shell material for ICP trace element analyses which could have helped ascertain whether or not alteration had taken place. One sample of an un-dolomitized brachiopod from within the Cadeby Formation near Ripon, analysed by Aplin (1985), had $\delta^{13}C$ 2.9‰ and $\delta^{18}O$ -5.2‰. Magaritz (1987, fig. 2) presents data for dolostones within an offshore borehole of the Hartlepool Anhydrite Formation which have a mean $\delta^{18}O$ -1.0‰ and more widely scattered $\delta^{13}C$ values of 3.0‰ to 5.8‰.

3.4.2. Primary isotopic composition of Zechstein seawater - Interpretation

3.4.2.1. Carbon.

The carbon isotopic compositions of Raisby Formation limestones and dolostones, and Ford Formation dolostones give very consistent results of $\delta^{13}C$ 5.5‰ to 6.0‰, considerably greater than that of the brachiopods. Owing to the small number of brachiopod samples, the limestone and dolostone analyses are a more reliable index of primary marine compositions. Geochemistry of the Raisby Formation limestones has shown that $\delta^{13}C$ decreases with progressive diagenetic alteration (Chapter 4). This trend is commonplace in carbonate diagenesis (Brand and Veizer, 1980; Veizer, 1983a), as there are more abundant sources of ^{12}C than ^{13}C in most diagenetic systems. Therefore, the most positive $\delta^{13}C$ values will be the most reliable, and the least altered. However, as both dolomitization and limestone neomorphism are considered to have been affected by modified Zechstein seawater, carbon isotope ratios would be expected to change little from their original values.

The Permian is now recognized as a time of unparalleled enrichment of marine carbonates in ^{13}C, with mean Upper Permian values of $\delta^{13}C$ 5.0‰ to 8.0‰ (Beauchamp *et al.*, 1987). A number of workers have documented ^{13}C enrichment in calcite and dolomite within the Marl Slate throughout the Zechstein Basin. This is suggested to have been due to

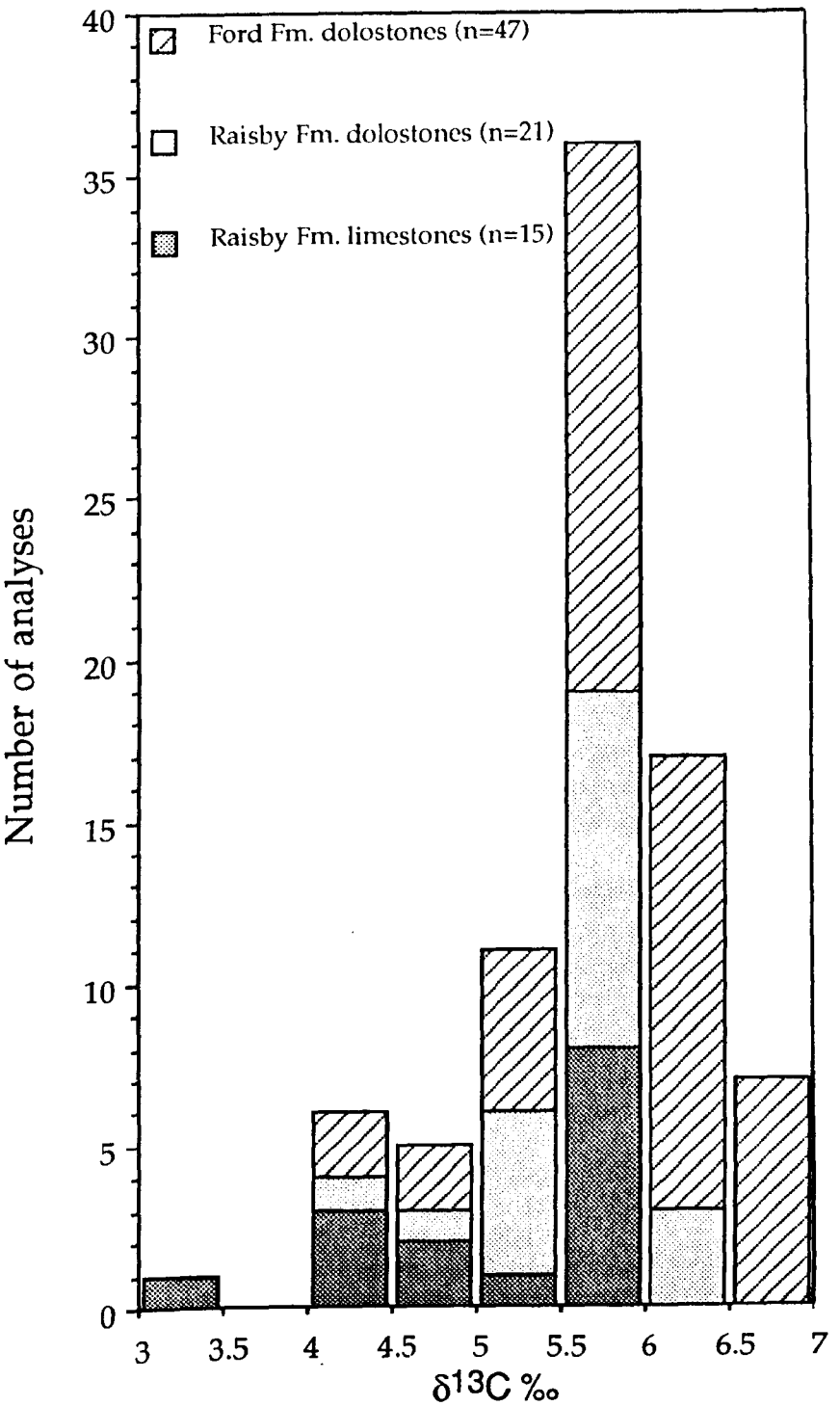

Fig. 3.13. Histogram showing the distribution of carbon isotope results from Raisby Formation limestones and dolostones, and Ford Formation dolostones (analysed by Aplin, 1981). Only analyses of massive replacive dolostones are plotted.

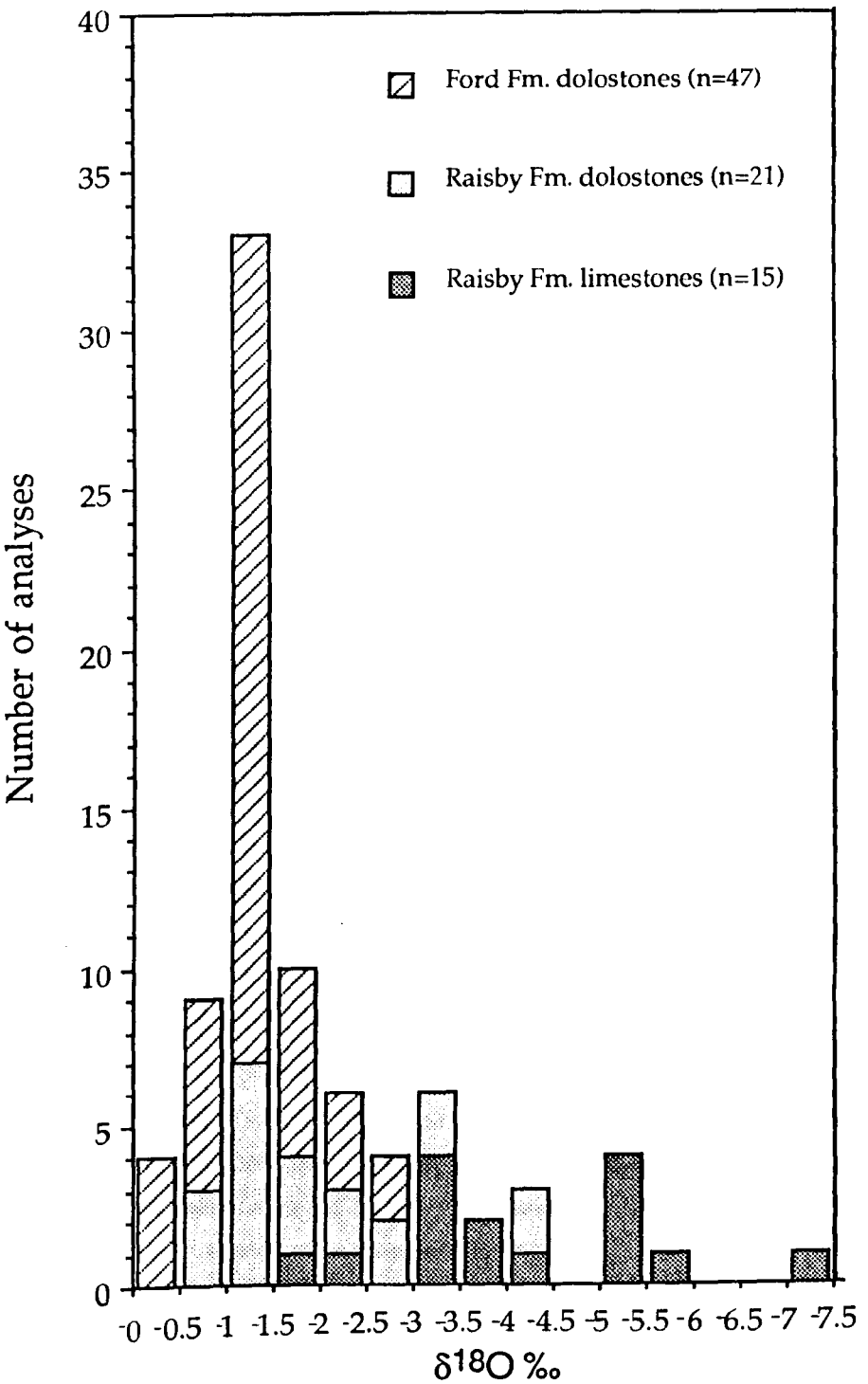

Fig. 3.14. Histogram showing the distribution of oxygen isotope results from Raisby Formation limestones and dolostones, and Ford Formation dolostones (analysed by Aplin, 1981). Only analyses of massive replacive dolostones are plotted.

burial of large quantities of organic matter within sapropels worldwide, especially those of the Marl Slate and Kupferschiefer (Magaritz and Schulze, 1980; Magaritz *et al.*, 1981; Magaritz and Turner, 1982; Turner and Magaritz, 1986; Sweeney *et al.*, 1987). Progressive increase in the $\delta^{13}C$ of carbonates within the Marl Slate has been identified, with amplitudes of up to 0‰ at the base to 6‰ at the top (Magaritz and Schulze, 1980) representing a duration of about 18,000yrs (on the basis of laminae counting) (Magaritz and Turner, 1982). The enrichment continues into the third cycle carbonate, from when on truly marine conditions were not re-established (Chapter 1). Although ^{13}C-enriched carbonates are characteristic of a total of six Upper Permian basins (such as the Delaware Basin = $\delta^{13}C$ 5.2‰ [Given and Lohmann, 1985]), ^{13}C enrichment of a similar amplitude has also been reported widely within Upper Carboniferous and Lower Permian carbonates, and in brachiopod calcite (Compston, 1960; Davies, 1977a; Popp *et al.*, 1986; Veizer *et al.*, 1986; Beauchamp *et al.*, 1987). Clearly, carbon isotope enrichment was a characteristic feature of the late Upper Palaeozoic, with a rapid rise from the Devonian and Lower Carboniferous to the Upper Carboniferous and Permian (Popp *et al.*, 1986; Veizer *et al.*, 1986). Lower Triassic carbonates have $\delta^{13}C$ values close to unity (Holser *et al.*, 1986). The enrichments recorded within the Marl Slate may represent a fluctuation towards ^{13}C-enrichment from a low point (near unity) at the end of the Lower Permian (Holser *et al.*, 1986). Holser *et al.*, (1986) also suggest that this upturn may have been synchronous globally (1.5.1.).

The reasons for the global ^{13}C enrichment of Upper Carboniferous and Permian marine carbonates are uncertain. Saporopel deposition during Marl Slate times cannot explain Upper Carboniferous or Lower Permian enrichments. Beauchamp *et al.*, (1987) have concluded that the ^{13}C enrichment of carbonates in the Upper Carboniferous to Upper Permian Sverdrup Basin, Arctic Canada, was due to a combination of high marine bioproductivity with burial of large quantities of marine organic matter, and nonequilibrium gas transfer isotope fractionation in evaporating seawater. These dual processes of ^{13}C concentration may well have been operative within the Zechstein Basin which also has organic-rich carbonates and abundant evidence of evaporative concentration. Implicit in the model of Beauchamp *et al.*, (1987) is that ^{13}C concentration is restricted to one or more basins and not necessarily a global feature, although episodic connection with larger oceans may contaminate their carbon isotopic ratios. One of the most important parts of their model, is that restricted basins can become isolated centers of ^{13}C enrichment, not immediately (on a geological timescale) equilibrating with the global CO_2- HCO_3 reservoir. Holser *et al.*, (1986) invoke very rapid global equilibration of the atmosphere-hydrosphere carbon budget to explain apparently globally-correlatable $\delta^{13}C$ excursions (1.5.1). Beauchamp *et al.*, (1987) suggest the reasons for the hypothesized reduced rates of carbon exchange in the Upper Permian, in comparison to the present day, was due to the combination of an arid to semi-arid climatic setting and low PCO_2 in the atmosphere, possibly a significant feature of

Upper Palaeozoic in general. However, the burial of vast quantities of organic matter in Upper Carboniferous coals of Europe and Lower Permian coals of Australasia must have had profound influences on the global carbon budget, and may have preconditioned the global carbon system for overprinting by ^{13}C enrichment in isolated, stagnant, hypersaline basins during the Upper Permian.

3.4.2.2. Oxygen

The oxygen isotopic composition of carbonates in general decreases with progressive diagenesis during burial. The oxygen isotope distribution of limestones and dolostones from the Raisby Formation, and dolostones from the Ford Formation, show that the least negative results cluster around $\delta^{18}O$ -0.5‰ to -3.5‰ (Fig. 3.14). The Raisby Quarry brachiopod sample is within this range ($\delta^{18}O$ -3.1‰ and -3.2‰) although oxygen isotope results for the brachiopod from High Moorsley Quarry ($\delta^{18}O$ -5.0‰) and the Cadeby Formation ($\delta^{18}O$ -5.21‰) suggest alteration from fluids of elevated temperature. A value of -0.5‰ to -3.5‰ is consistent with reported Permian marine carbonate values of -2.5 ± 1.5‰ (Veizer *et al.*, 1986) and -2.8‰ (Given and Lohmann, 1985). Popp *et al.*, (1986) suggest that seawater precipitated calcite of $\delta^{18}O$ -2‰ from the Early Carboniferous to Upper Permian. If the Permian seas did have a $\delta^{18}O$ (SMOW) value of 0‰ (in accordance with recent oceans), then they would have had a temperature of between 18.1° and 32.0°C to precipitate carbonate of $\delta^{18}O$ -0.5‰ and -3.5‰ (PDB) respectively. This is very unlikely on palaeontological grounds (Veizer *et al.*, 1986), and difficult to invoke for the lower slope facies Raisby Formation, from where some of the samples come. ^{18}O depletion probably represents depleted isotope ratios of Permian, as compared to recent seawater (Given and Lohmann, 1985; Veizer *et al.*, 1986).

If the Zechstein Basin was at least partly evaporitic during deposition of the Raisby Formation, $\delta^{18}O$ values of Raisby Formation carbonates would be expected to be enriched in ^{18}O owing to non-equilibrium gas transfer isotope fractionation during evaporation, as has been suggested for carbon isotope enrichment (see above). Carbonates should have been even more enriched during deposition of the Hartlepool Anhydrite Formation, although again, this is not supported by the data (Magaritz, 1987). The reason for this discrepancy is unclear. The anomalous oxygen isotope values of dolostones within the Hartlepool Anhydrite Formation may be due to dolomite neomorphism (5.3.4). However, if normal marine Zechstein carbonates did have a $\delta^{18}O$ of -2.5‰ to -2.8‰ (in accordance with Permian seawater values of Veizer *et al.*, (1986) and Given and Lohmann (1985) respectively), evaporative concentration would have altered the value, at most, to around -1.0‰ to 0.0‰, broadly in accordance with the least-altered Raisby and Ford Formation samples. The Raisby Quarry brachiopod data may reflect partial recrystallization at elevated temperatures, or more likely, normal marine lower Raisby Formation seawater $\delta^{18}O$, with the $\delta^{18}O$ increasing

through deposition of the Raisby Formation, in response to progressive evaporative concentration, as has been suggested on faunal grounds by Smith and Francis (1967).

The depleted oxygen isotope ratios of Upper Permian oceans thus reflect a change in seawater isotopic composition, rather than elevated temperatures. Lohmann and Walker (1989) and Walker and Lohmann (1989) suggest that throughout the Phanerozoic, such differences in isotope ratios to those of present-day oceans reflect changes in global scale processes. Oxygen isotope fluctuation from the largest amplitude of glaciation can only account for 1.6‰ of variation (Lohmann and Walker, 1989). From mass-balance calculations, Lohmann and Walker (1989) suggest that $\delta^{18}O$ changes of the magnitude which have been recorded, could only result from pulses of tectonism or sea floor spreading which modify mass-transfer of oxygen between the lithosphere and hydrosphere. Low temperature continental and marine weathering depletes the reactive waters in ^{18}O whereas high temperature water-rock interaction at mid ocean ridges increases ^{18}O of reactive waters. Thus, Lohmann and Walker (1989) and Walker and Lohmann (1989) conclude that the general decrease in $\delta^{18}O$ of marine waters throughout the Phanerozoic is related to the tectonic evolution of the earth, with more continental weathering and less important sea floor spreading (possibly the spreading ridges were above sea level) in the past.

3.4.3. Primary isotopic composition of Zechstein seawater - Conclusions.

Isotope data from the Raisby Formation is consistent with data from other Upper Permian basins, showing enriched carbon and depleted oxygen isotope ratios of marine carbonates relative to those precipitated within present day seawater. The extreme ^{13}C enrichment is most likely the product of a global depletion of ^{12}C owing to burial of large quantities of organic matter in Carboniferous and Lower Permian coals, overprinted by burial of considerable quantities of organic matter in organic rich horizons within Upper Permian marine basins and possibly, on a more local scale, by non-equilibrium gas transfer isotope fractionation during evaporation in semi-restricted basins. Evaporative concentration of ^{13}C may have been aided by limited equilibration of carbon isotopes between global hydrosphere and atmosphere reservoirs. There is no evidence to support the hypothesis of Holser *et al.*, (1986) that there was an abrupt, globally-synchronous enrichment in ^{13}C of marine waters at the base of the Zechstein sequence. It is much more reasonable to assume that Upper Permian marine basins were isolated in their carbon isotope evolution than to invoke deposition of the Marl Slate at the same time as a global carbon isotope shift, when such a correlation cannot be corroborated by biostratigraphy (1.5.1). Depletion in oxygen isotope ratios of the Zechstein Sea is a part of the general trend for ^{18}O-depletion throughout the Phanerozoic, possibly overprinted, in the Zechstein Basin, by non-equilibrium gas transfer isotope fractionation, enriching seawater in ^{18}O such that the negative oxygen isotope trend was subdued, and $\delta^{18}O$ values were closer to unity.

Chapter 4

Limestones

Calcite concretions.

4.1.1. Limestones - Introduction

The presence of limestones in the Raisby Formation has previously been reported by a number of authors (Trechman, 1914, 1921 & 1925; Woolacott, 1914, 1919a & b; Fowler, 1943; Magraw *et al.*, 1963; Smith and Francis, 1967) although no detailed studies have hitherto been carried out. Published hypotheses for their lack of dolomitization range from a hiatus in the precipitation of dolomite in the Zechstein Sea, thus allowing limestone deposition (Woolacott, 1919b), to preferential non-dolomitization after deposition (Trechman, 1914). Limestones have a very uneven spatial distribution within the Raisby Formation, although are most abundant within the upper and middle slope facies (Chapter 2) (Fig. 4.1). Limestone units at outcrop commonly thin and thicken abruptly laterally, such that a limestone in one quarry cannot be identified in an adjacent one at the same stratigraphic level. Nowhere have the limestones been seen to conformably pass into dolostones laterally. At High Moorsley, Houghton and Old Towns Quarries, the lateral transition from limestone into bedded dolostone is marked by an abrupt, synsedimentary erosion surface (Chapter 2). Limestones are usually both overlain and underlain by dolostones. The nature of the contact may be gradational, via an alternation of nodular limestone with dolostone, or, more rarely, sharp. All limestones at outcrop have been recorded towards the base of the formation, although limestone units may range from a few centimetres to 20m thick; they comprise almost the entire thickness of the Raisby Formation (approximately 20m) in some offshore boreholes such as W15. The petrography and geochemistry of the limestones is described in the following sections.

4.2.1. Petrography of limestones - Description.

Most limestones are hard, brittle, and well lithified. Colours range from 'medium dark grey' (N4) to 'medium light grey' (N6), becoming increasingly orange-brown with progressive dolomitization. Petrographically, the limestones comprise unimodal, 10-20μm non-ferroan, low-magnesian calcite crystals, classified as microspars (Folk, 1965) (Fig. 4.2a & b). No micrite (1-4μm) has been recorded. The microspar crystals are anhedral, with irregular, non-compromise intercrystalline boundaries (Figs. 3.11a, b & 4.2a). These textures are classified as 'mosaic' (Moshier, 1989), and accordingly have less than 5% intercrystalline porosity (Fig. 4.2a). Intermixed with the microspar is variable amounts of quartz and muscovite (less than 50μm), skeletal material, and authigenic pyrite framboids. Only rarely is skeletal material sufficiently abundant to produce a packstone/grainstone texture; most allochems 'float' within the microspar matrix (wackestone/mudstone textures). Microspar

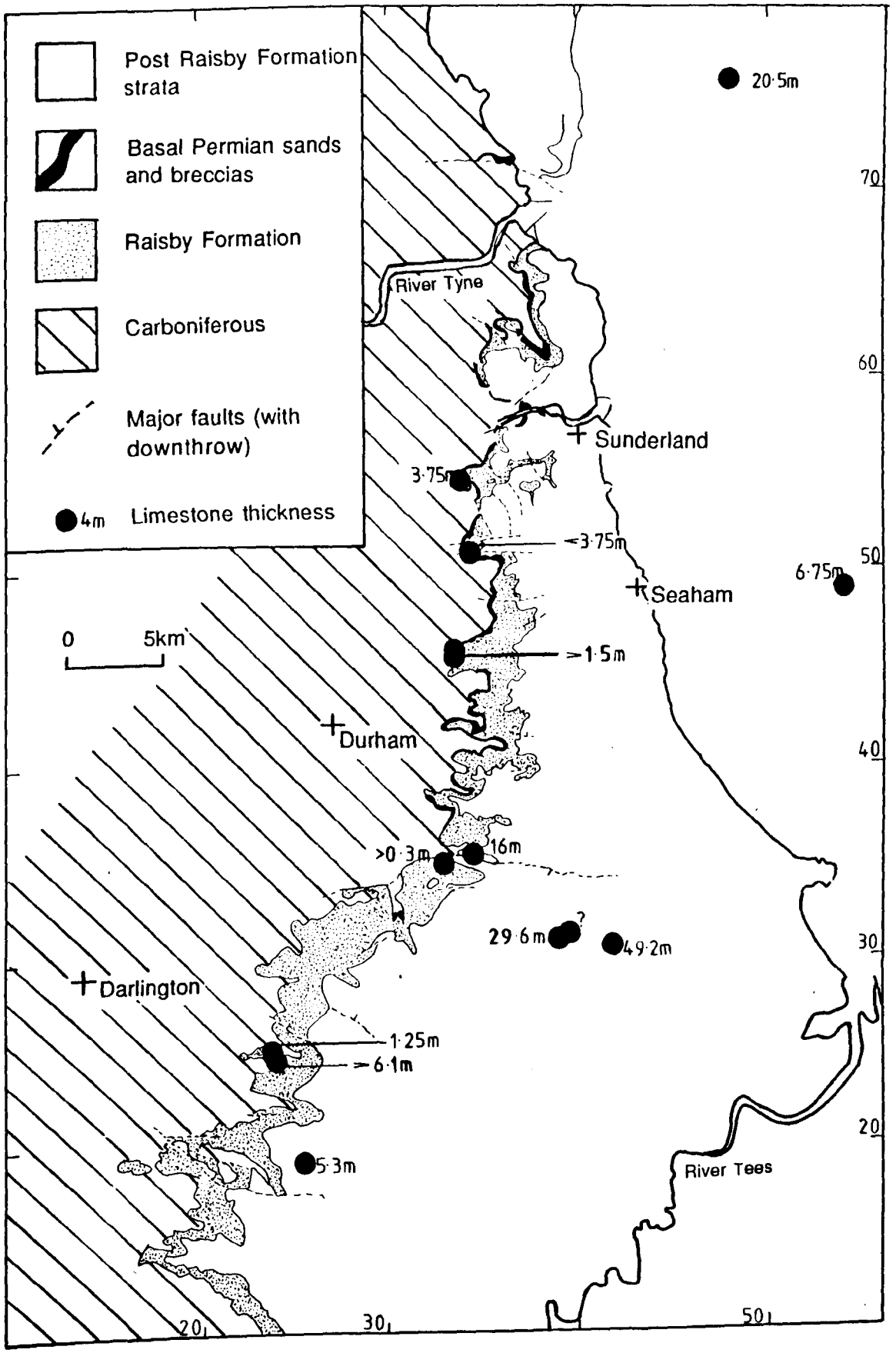

Fig. 4.1. Map showing the spatial distribution and thicknesses of limestones within the Raisby Formation. Data from this study, Smith and Francis (1967) and Mills and Hull (1976).

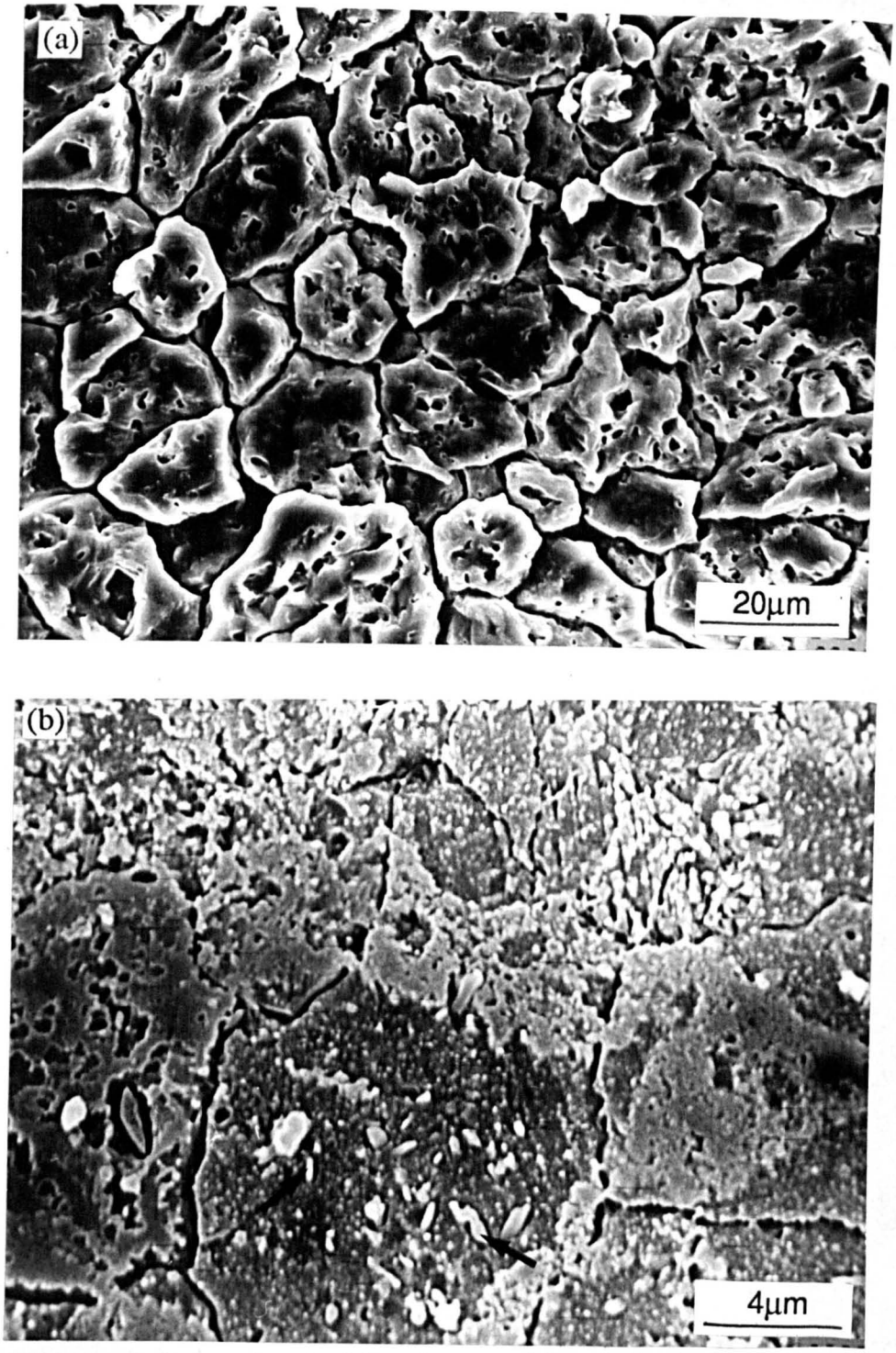

Fig. 4.2. SEM photomicrographs of calcite microspar. (a) typical microspar, Houghton Quarry (etched in hydrochloric acid), (b) microspar hosting relics of aragonite (arrowed), from the core of an isolated limestone nodule, Raisby Quarry (etched in formic acid). The pitting of the microspar surface in (a) is probably due to preferential attack of microspar by acid along cleavage planes and crystal imperfections. Most pits have straight sides with angular junctions, thus suggestive of a cleavage control. The relics in (b) are identified as aragonite both because they etch proud of the calcite microspar, and because the core of the limestone nodule from where the sample was taken is Sr-rich relative to margins of the same nodule, which lacks aragonite relics.

crystals in one limestone from Raisby Quarry contained very small, elongate inclusions of aragonite which etched out of the calcite after etching with 0.1% formic acid for 20 seconds (Fig. 4.2b). They comprise less than 5% of the surface area of any microspar crystal.

Limestones from all outcrop and core samples stain pink. They have a speckled, irregular dull/bright orange- and non-luminescence, with in general, dull/bright orange-luminescence predominant. In one sample from Houghton Quarry, 20-40μm microspar crystals within a fossiliferous limestone turbidite were zoned orange-luminescent, and grade out into pore-filling, zoned orange-luminescent calcite cements (Fig. 4.3b). These zoned microspar crystals commonly have planar intercrystalline boundaries.

Limestones at outcrop and in core have undergone varying degrees of partial replacement by dolomite. Limestones may be dolomitized along bedding-parallel, millimetre-to-centimetre thick bands. This dolomite is genetically associated with microstylolite swarms, and considered to postdate most of the dolomite in the formation, related to its pressure solution upon burial (5.4.3). More commonly, limestones pass into dolostones via an intermediate, partially dolomitized limestone, which comprises euhedral dolomite rhombs (mean 40μm) within calcite microspar. The contact of the partially dolomitized limestone with undolomitized limestone is abrupt, although the contact of partially dolomitized limestone with pure dolostone is gradational on a scale of hundreds of microns. At outcrop, this is represented by alternating nodules of limestone with partially dolomitized limestones, passing into dolostones over centimetres to metres.

Where limestones have been partially dolomitized (not microstylolite-associated), the isolated euhedral dolomite rhombs commonly have irregular, corroded edges. The margins of the dolomite crystals are often embayed and replaced by anhedral microspar, which is selective to zones within the dolomite (Fig. 4.4a). At Houghton Quarry, microspar replaces dolomitized early marine cement fringes on skeletal material (Fig. 4.4b & 4.5b). The replacive microspar is in optical continuity with the dolomite, which itself has replaced probable former circumgranular HMC cements, preserving their crystallographic orientation (Fig. 4.5b). Only in the Houghton Quarry example however, is the microspar coarse enough for the extinction position of individual crystals to be determined.

In contrast to the dolostones, limestones provide very little evidence of replacement by sulphates. Where the limestone has been replaced, replacement is commonly in the form of millimetre-sized lath-shaped crystals. Large, centimetre-sized evaporite clusters are uncommon. In cases where limestone nodules are interbedded with partially dolomitized limestones, sulphate replacement is often preferential to the partially dolomitized limestones.

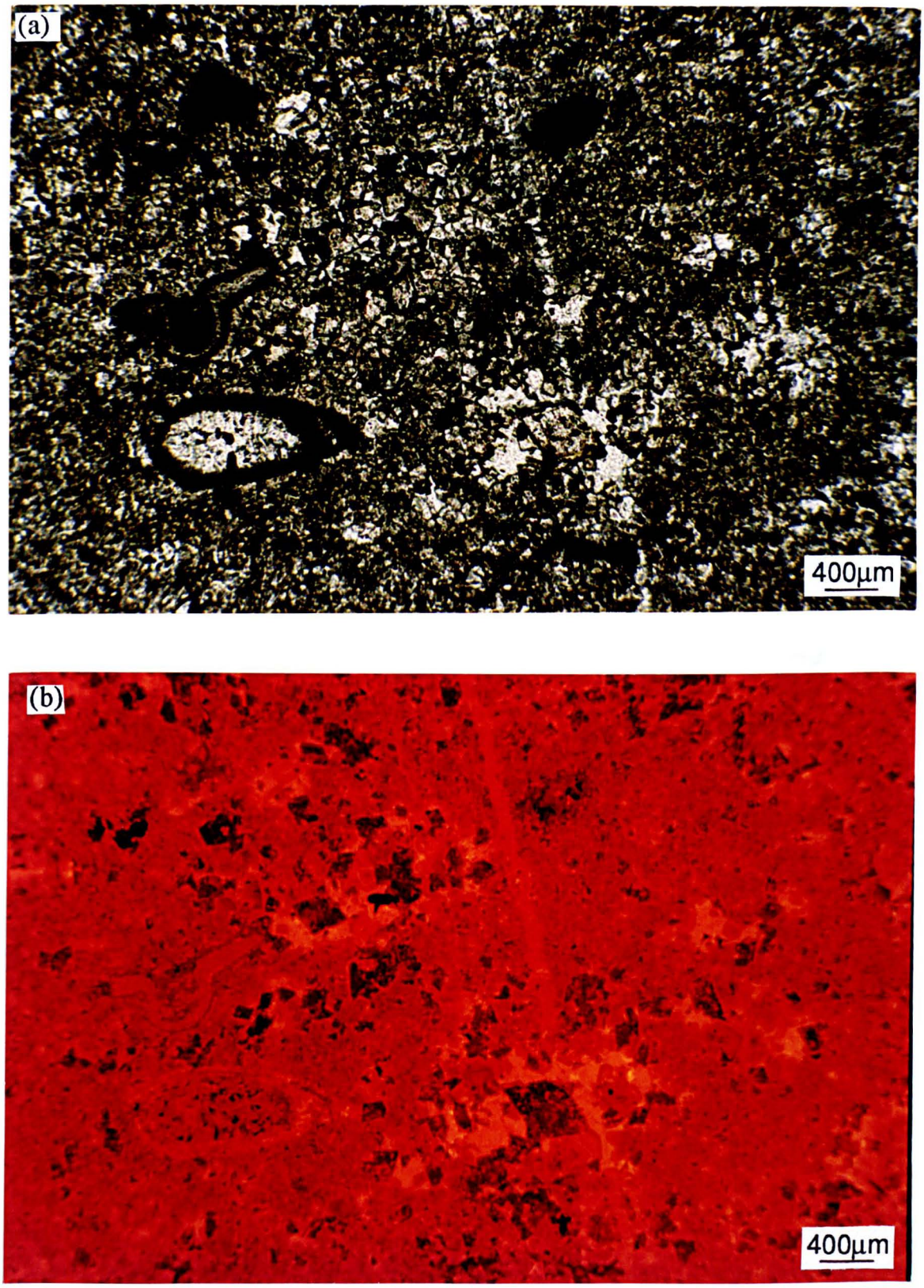

Fig. 4.3. Thin section photomicrographs of a fossiliferous limestone, Houghton Quarry; (a) plane light, (b) luminescence. Microspar crystals are zoned dull to bright orange-luminescent, passing into zoned bright orange-luminescent cements. Note the orange-luminescent speckling within some non-luminescent dolomite rhombs, suggestive of partial replacement of dolomite by calcite microspar.

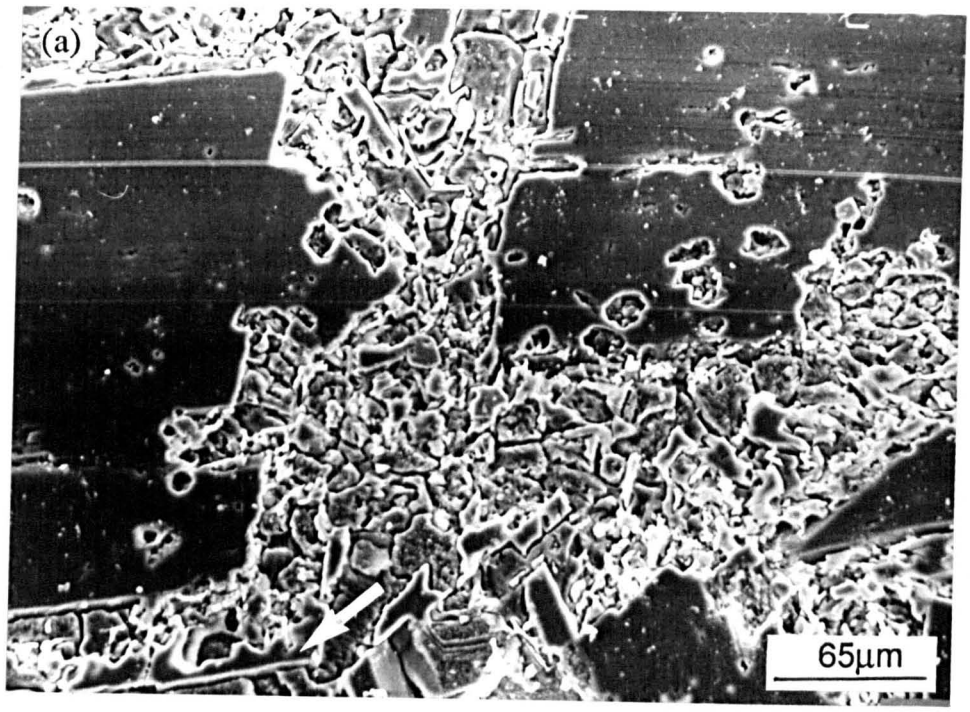

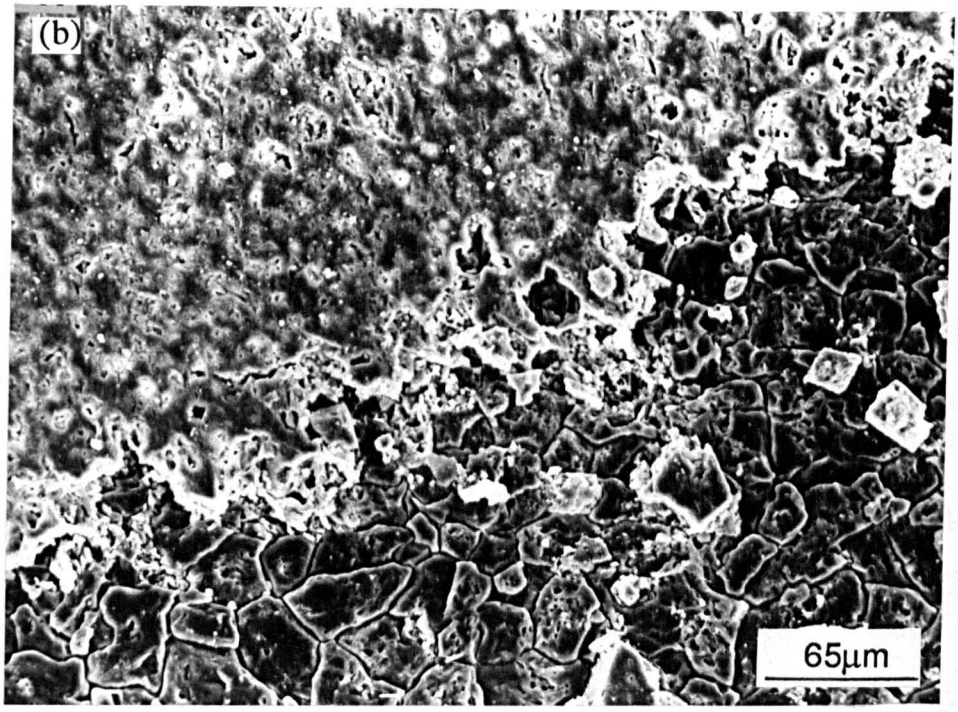

Fig. 4.4. SEM photomicrographs of dolomite replaced by calcite microspar. (a) Raisby Quarry, margin of an isolated limestone nodule, (b) Houghton Quarry, fossiliferous limestone (see fig. 4.3). The isolation of fragments of dolomite zones within microspar (a) (arrowed) demonstrates conclusively that dolomite was replaced by calcite. The embayed nature of the margins of a dolomitized echinoderm fragment (b) is also strongly suggestive of partial replacement. The isolated dolomite zone (arrowed in (a)) cannot result from incomplete dolomitization of microspar. Both samples were etched in hydrochloric acid.

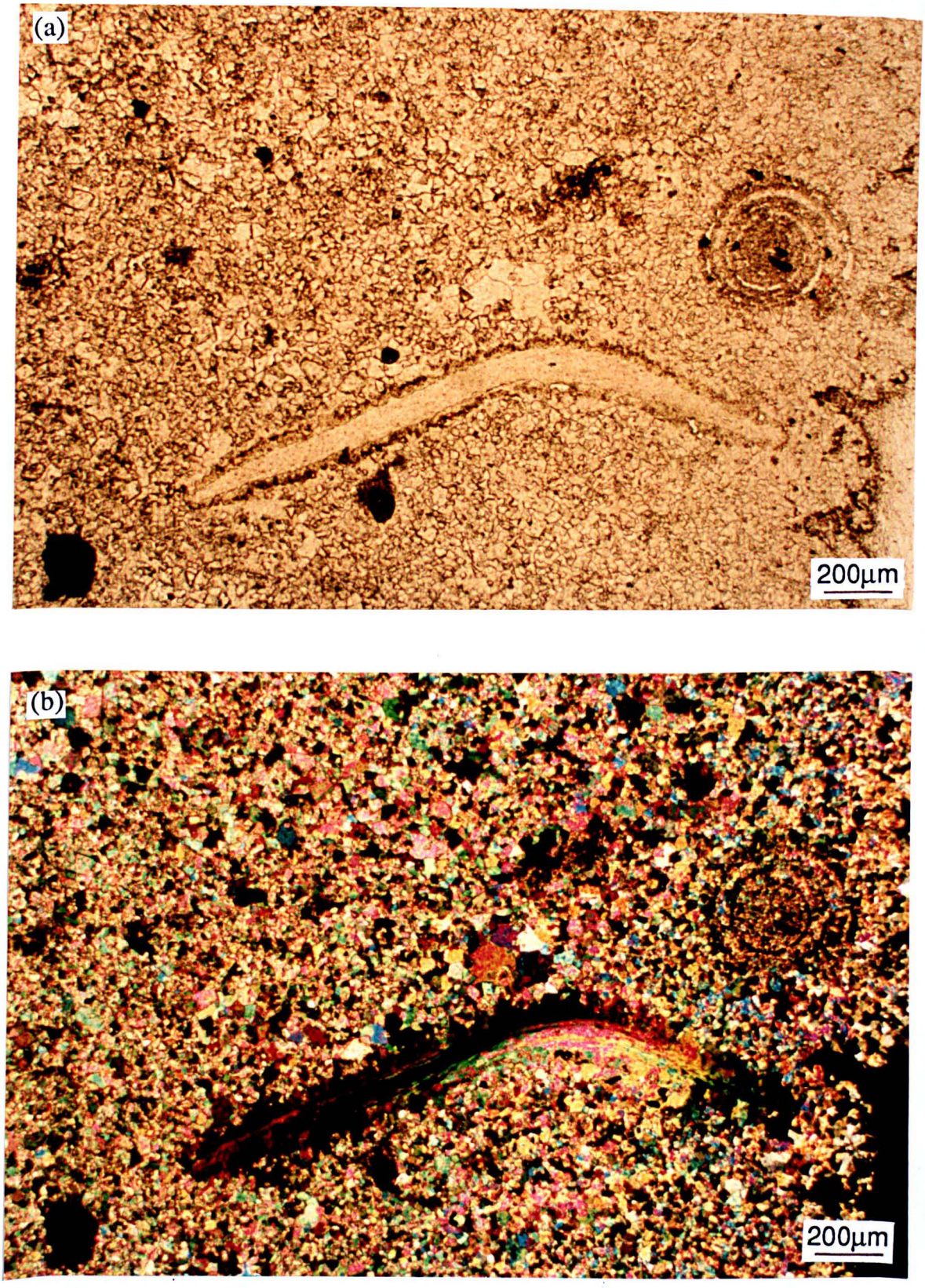

Fig. 4.5. Thin section photomicrographs of a fossiliferous limestone, Houghton Quarry; (a) plane light, (b) crossed polars. Note, in crossed polars, microspar adjacent to the dolomite rim of a brachiopod shell fragment goes into extinction at the same time, producing spire-like structures suggestive of a former marine cement fringe.

4.2.2. Petrography of limestones - Interpretation.

The Permian oceans were 'aragonite seas' (Sandberg, 1983) and so similar to those of the present-day. Thus, most or all of the carbonates comprising the Raisby Formation were originally deposited as a very fine-grained mixture of aragonite and high-magnesian calcite (HMC) with variable, although generally little of aragonite, HMC, or LMC skeletal material (Chapter 2). The sediment probably comprised mainly aragonite needles, which were perhaps similar to those of Recent carbonate muds, less than 4μm in length (Moshier, 1989). From work on the sedimentology of the Raisby Formation (Chapter 2), it is clear that sedimentation was very variable in character, in accordance with facies. The shallower water facies had a higher input from autochthonous and allochthonous skeletal material, whereas deeper water sedimentation was characterized by fine pelagic and hemipelagic carbonate muds. Modern shallow water carbonates are dominated by aragonite, with lesser amounts of HMC and LMC (Moshier, 1989), and Recent carbonate muds seawards of the Florida reef tract (possibly analogous to the Raisby Formation) comprise 61-80% aragonite (Lasemi and Sandberg, 1984). An average composition for the Raisby Formation upper and middle slope facies (in which most limestones occur [Fig. 4.1]) of 65% aragonite, 30% HMC and 5% LMC is assumed for the purpose of discussion (termed an aragonite-dominated precursor [ADP] carbonate mud [Lasemi and Sandberg, 1984]).

An aragonite and HMC-dominated mineralogical assemblage will become unstable if conditions change from those under which it was deposited, and will alter to a more stable form (diagenetic low-magnesian calcite [dLMC] or dolomite). The Raisby Formation limestones are interpreted to be neomorphosed ADP muds (Raisby Formation dolostones are likewise recrystallized ADP muds [Chapter 5]). Neomorphism is commonly accompanied by an increase in crystal size (aggrading neomorphism) and is a wet dissolution - reprecipitation reaction (Bathurst, 1975). In general, ADP muds neomorphose to microspars whereas CDP (calcite-dominated precursor) muds neomorphose to micrite, owing to a greater density of potential dLMC nucleation sites (Lasemi and Sandberg, 1984; Moshier, 1989). The uniform, finely crystalline microspars of Raisby Formation limestones (Fig. 4.2a) suggest numerous centres of crystal nucleation and even growth rates. Preservation of floating LMC skeletal material within microspars shows that no vuggy porosity was created during microsparitization. Rare, zoned microspars from Houghton Quarry (Fig. 4.5b) suggest LMC nuclei were further apart in those samples, allowing coarser crystals to grow and continue growing, as zoned cements, into any intercrystalline porosity. Zonation of these microspars also demonstrates that fluid composition changed during microspar growth. Zoned microspars may have developed in this sample because it was bioclastic, and so possibly able to form a skeletal framework, thus producing larger pores than normal.

When not exposed to aragonite and HMC-undersaturated meteoric-derived fluids, the catalyst for aragonite and HMC neomorphism is combined elevated lithostatic temperatures and pressures upon burial. These increase solubility of aragonite and HMC to

the point of dissolution (Veizer, 1983a). Thus, when buried with marine pore fluids, the aragonite and HMC may remain unaltered for a considerable time before neomorphism (Tucker, 1986).

The corrosive texture of dLMC with dolomite in partially dolomitized limestones from Houghton and Raisby Quarries (Figs. 4.4a, 4.4b & 4.5) suggest that dLMC is replacing dolomite and, in these cases, partial dolomitization of limestones predated their neomorphism to dLMC. Partial replacement of dolomite by dLMC has not, to the author's knowledge, been previously described. The textures cannot result from selective non-dolomitization of certain microspar crystals. Both examples studied in detail testify to a slow, mineralogically and crystallographically ordered style of replacement, always incomplete. During microspar growth, pore fluids would have been supersaturated with respect to LMC and, assuming 65% aragonite (containing 1000ppm Mg) and 30% HMC (containing 11 to 17mole% $MgCO_3$) were in solution during neomorphism, and the diagenetic system was relatively closed, the pore fluids would have had a Ca/Mg ratio of approximately 28.2-39.4, and so undersaturated with respect to dolomite. The distribution of dLMC nucleation sites was probably such that only the margins of the dolomite crystals could be replaced. Within the dolomite crystals, there would have been no drive for dLMC precipitation owing to the absence of dLMC nuclei, especially if the dolomite was relatively inclusion free. Aragonite relics within microspar crystals also testify to a very fine scale of dissolution-reprecipitation accompanying neomorphism to dLMC. The relics may have additionally been protected from replacement by organic coatings (Lasemi and Sandberg, 1984; Sandberg and Hudson, 1983), or neomorphism in the presence of highly saline pore fluids (McKenzie, 1985).

Although some limestones have been partially dolomitized, in which dolomite crystals have been partially replaced by dLMC microspar, most limestones have been minimally replaced by dolomite or gypsum/anhydrite. This is interpreted to be indicative of permeability differences between limestones and dolostones. Limestones, before neomorphism, were much more strongly cemented, probably close to the sea floor, than those carbonate muds which were later dolomitized (2.4.2.1). This is demonstrated by the common occurrence of limestone nodules alternating with (non stylolite-associated) partially dolomitized limestones. The nodules are interpreted as being formed by early-diagenetic, sea floor aragonite/HMC cementation of carbonate muds, whereas the host inter-nodule carbonate would have been less well lithified. This is supported by evidence from Raisby Quarry of early diagenetic fractures cutting the nodules into which the less brittle, still soft (un-dolomitized) inter-nodule carbonate was injected (2.4.2.1.). Thus, carbonates which are now dolostones and partially dolomitized limestones, were less strongly lithified than the limestones immediately before dolomitization, and thus were more susceptible to dolomitization and later replacement by sulphates. This original permeability difference is largely retained to the present-day. Overprinted on local permeability differences between

the two lithologies, which controlled the intensity of dolomitization, limestone preservation is also related to stratigraphic position within the formation. Dolomitized early diagenetic nodules, again lithified close to the sea floor, have been recorded from the Raisby Formation (2.4.1.1.), and described by Kaldi (1980) from the Cadeby Formation. Thus, only near to the base of the formation, furthest from the source of dolomitizing fluids (Chapter 5), were the dolomitizing brines of a sufficiently low dolomite supersaturation that nodules and bedded limestone units could remain un-dolomitized. In these areas, local (metre-scale) permeability differences controlled the extent of dolomitization.

4.3.1. Geochemistry of limestones - Description

Limestones from eight localities were analysed for major, minor and trace elements, and from six of those localities some of the samples were also analysed for carbon and oxygen stable isotopes. Most AAS and ICP analyses show that limestones are compositionally fairly pure low magnesian calcite, with less than 4% stoichiometric dolomite. The mean Mg contents of limestones analysed by AAS and ICP, and by microprobe from High Moorsley and Raisby Quarries are very similar (Table, 4.1). This confirms that most of the AAS and ICP limestone samples are, on average, fairly pure calcite microspar, with limited inclusion of dolomite within the samples. There is an abrupt compositional division between limestones, and partially dolomitized limestones which contain 20% to 60% stoichiometric dolomite (5.2.1).

The Fe and Mn concentrations of limestones are all low, and none are ferroan, in accordance with luminescence and staining (Table 4.1). The Fe, and especially Mn concentrations in the limestones correlate very well with Sr and Sr/Ca ratios; limestones with high Sr and Sr/Ca ratios have low Fe and Mn and vice versa (Fig. 4.6). Limestones have a maximum Sr concentration of 3200ppm and a mean of 1088ppm Sr from Raisby Quarry, although limestones from other localities contain less than 600ppm Sr (Fig. 4.6 & Table 4.1). These values are much higher than all dolostone analyses (Chapter 5), and significantly above average pre-Cretaceous values of 320ppm Sr (Veizer, 1977). Limestones contain very little insoluble residue and insoluble residue-associated trace elements (Al, Na, K, V, Y) relative to dolostones (5.3.3).

The carbon and oxygen stable isotope compositions of the limestones are, in general, comparable to those of the Raisby Formation dolostone samples analysed, although the dolostones on average have slightly higher carbon and oxygen values (Fig. 4.7). The limestone data shows a considerable scatter of values, although from any one locality, individual samples give comparable results (Fig. 4.8). The carbon and oxygen isotope results show a statistically significant correlation to Sr, Mn and to a lesser extent Fe, especially within Raisby Quarry (Fig. 4.9). Both carbon and oxygen isotope values become more negative with increasing Mn and Fe and decreasing Sr (Fig.4.9). This same antipathy between

Dawsons Plantation and Offerton Quarry		
-AAS & ICP (n=7)		$Ca_{(97.72)}(Mg_{(1.92)}Fe_{(0.23)}Mn_{(0.08)}Sr_{(0.06)})CO_3$
-Isotope (n=1)	$\delta^{13}C = 5.4‰$	
	$\delta^{18}O = -2.0‰$	
High Moorsley Quarry		
-AAS & ICP (n=3)		$Ca_{(98.60)}(Mg_{(0.88)}Fe_{(0.27)}Mn_{(0.20)}Sr_{(0.05)})CO_3$
-Isotope (n=1)	$\delta^{13}C = 3.3‰$	
	$\delta^{18}O = -5.1‰$	
High Moorsley Quarry		
-Microprobe (n=8)		$Ca_{(98.64)}(Mg_{(0.95)}Fe_{(0.24)}Mn_{(0.18)})CO_3$
Houghton Quarry		
-AAS & ICP (n=18)		$Ca_{(98.09)}(Mg_{(1.59)}Fe_{(0.16)}Mn_{(0.14)}Sr_{(0.03)})CO_3$
-Isotope (n=2)	$\delta^{13}C = 4.3‰$	
	$\delta^{18}O = -5.3‰$	
Penshaw Hill		
-ICP (n=2)		$Ca_{(97.67)}(Mg_{(2.09)}Fe_{(0.12)}Mn_{(0.12)}Sr_{(0.03)})CO_3$
Raisby Quarry		
-AAS & ICP (n=43)		$Ca_{(98.52)}(Mg_{(1.16)}Fe_{(0.10)}Mn_{(0.09)}Sr_{(0.12)})CO_3$
-Isotope (n=7)	$\delta^{13}C = 5.3‰$	
	$\delta^{18}O = -4.7‰$	
Raisby Quarry		
-Microprobe (n=13)		$Ca_{(98.55)}(Mg_{(1.15)}Fe_{(0.21)}Mn_{(0.09)})CO_3$
Thickley Quarry		
-AAS & ICP (n=2)		$Ca_{(96.39)}(Mg_{(2.95)}Fe_{(0.47)}Mn_{(0.13)}Sr_{(0.07)})CO_3$
-Isotope (n=1)	$\delta^{13}C = 5.8‰$	
	$\delta^{18}O = -3.1‰$	
W15 borehole		
-ICP (n=6)		$Ca_{(97.54)}(Mg_{(2.21)}Fe_{(0.15)}Mn_{(0.03)}Sr_{(0.06)})CO_3$
-Isotope (n=3)	$\delta^{13}C = 5.7‰$	
	$\delta^{18}O = -3.0‰$	

Table 4.1. Summary of the mean chemical compositions of limestones analysed from eight localities within the Raisby Formation. Where more than one sample was analysed, the value given is an arithmetic mean. The distribution of limestone isotope values is also shown in figures 3.13 and 3.14.

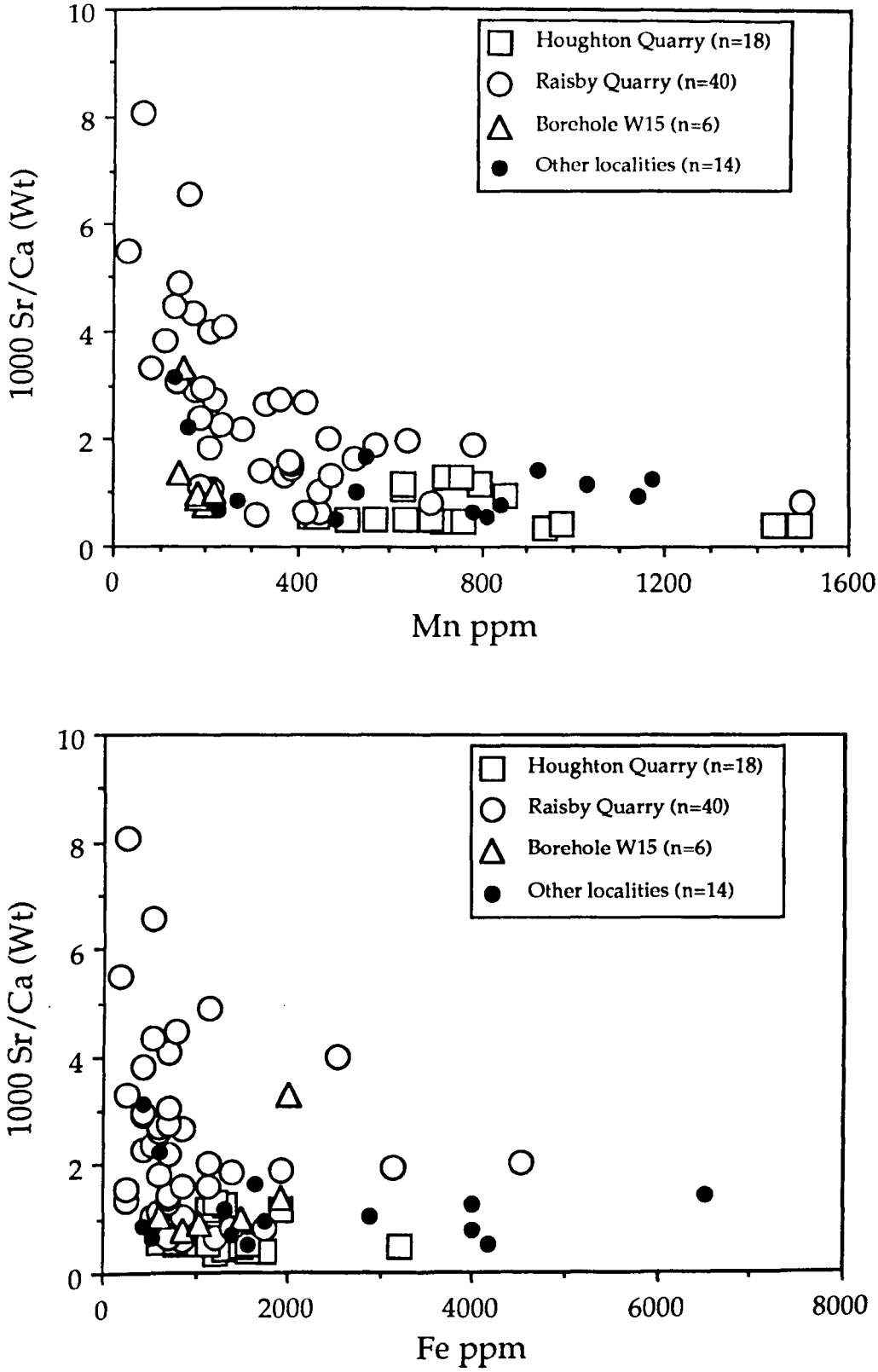

Fig. 4.6. Graphs showing the relationship between the Sr/Ca ratio of limestones from the Raisby Formation and their Fe and Mn contents. Analysed by ICP.

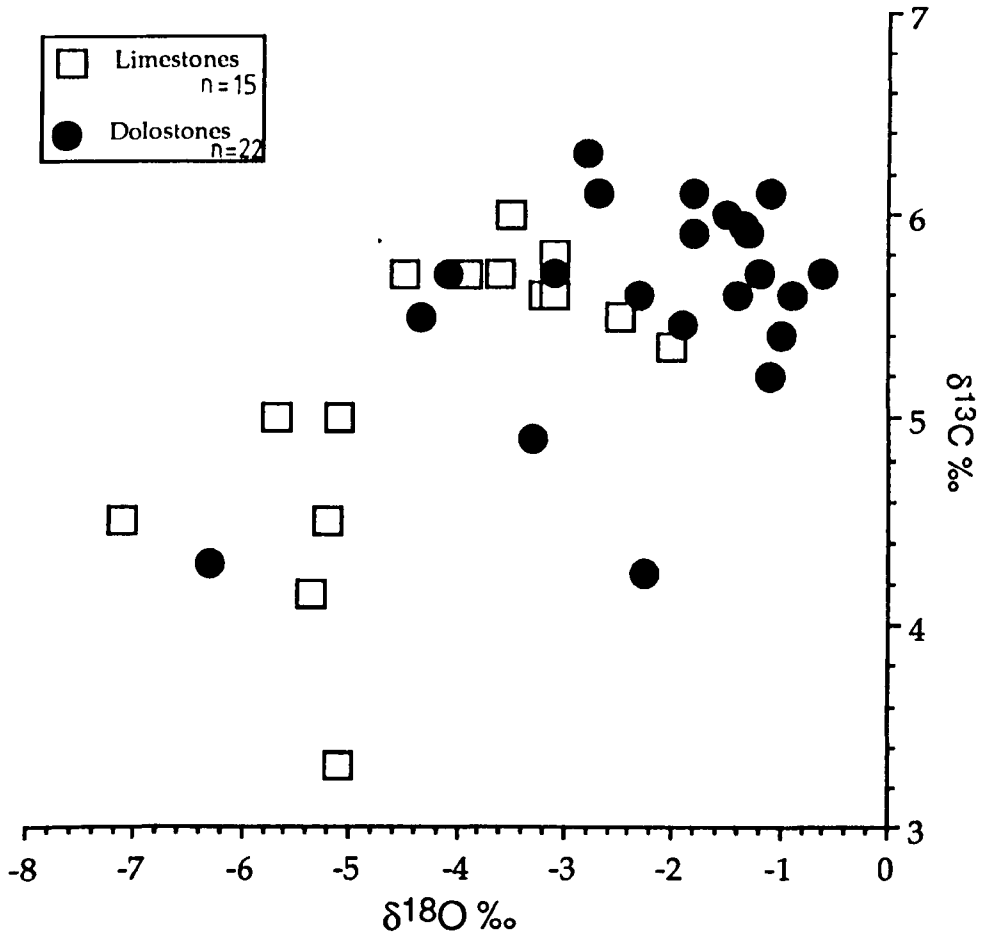

Fig. 4.7. Graph illustrating the slight isotopic differences between Raisby Formation limestones and dolostones.

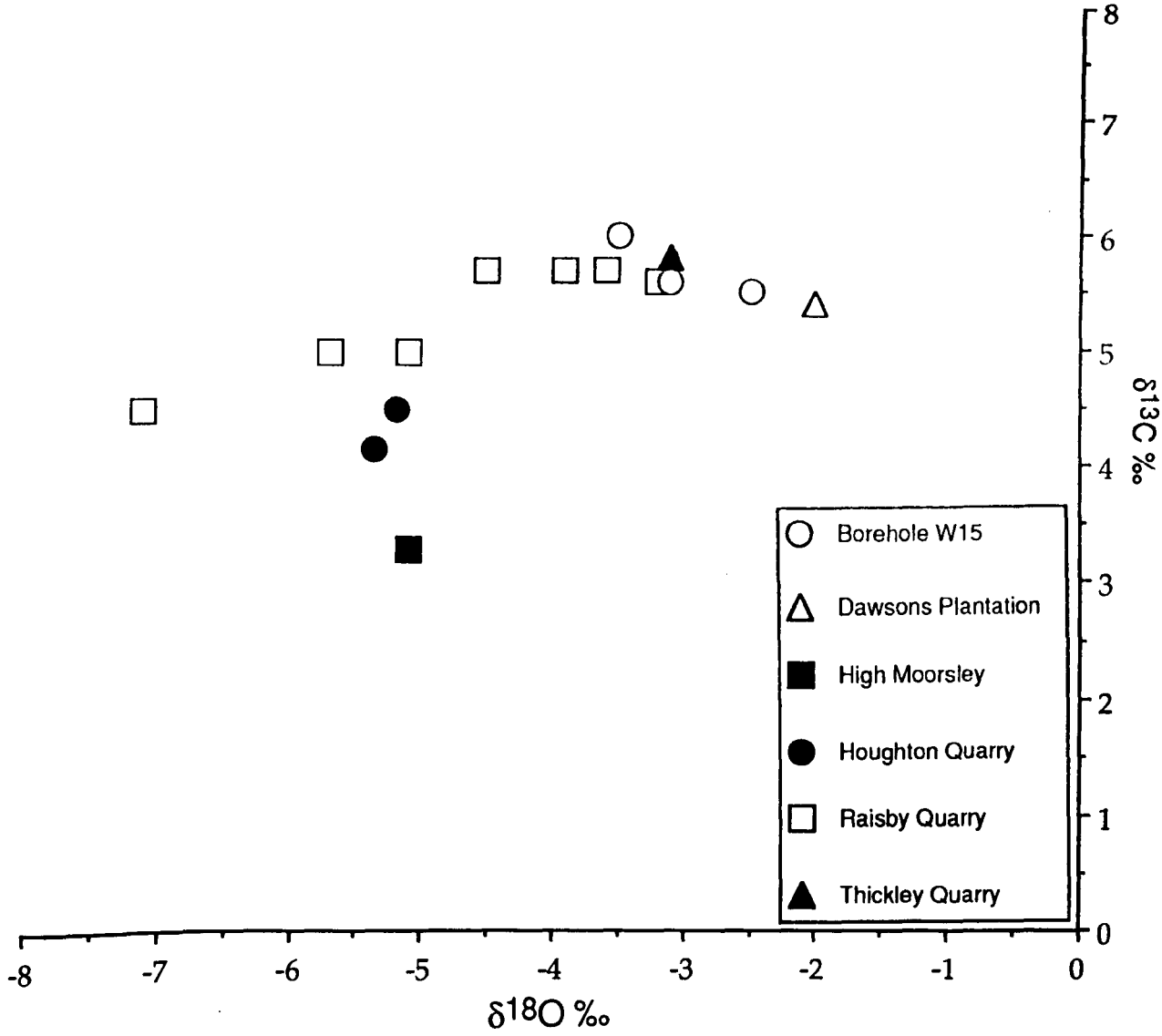

Fig. 4.8. Graph showing the isotopic composition of limestones from different localities within the Raisby Formation. Note the consistency of results from any one locality.

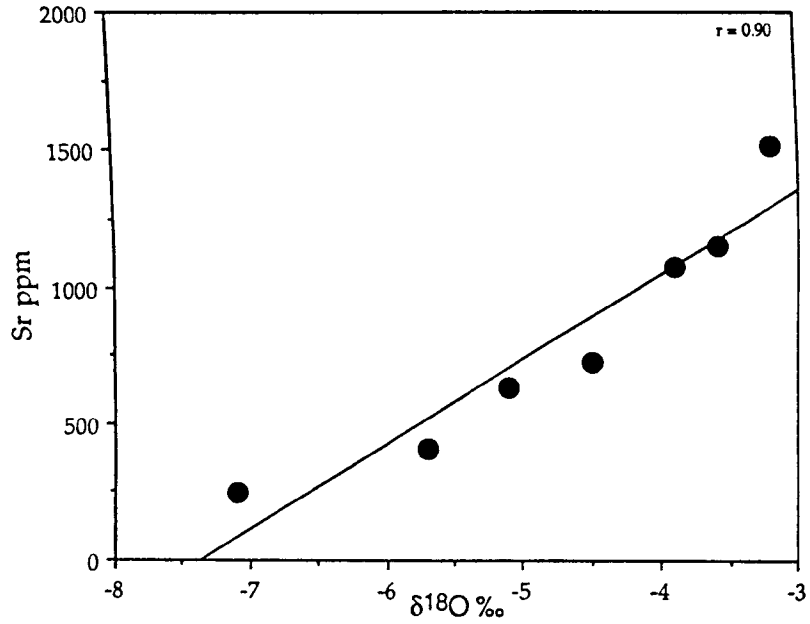

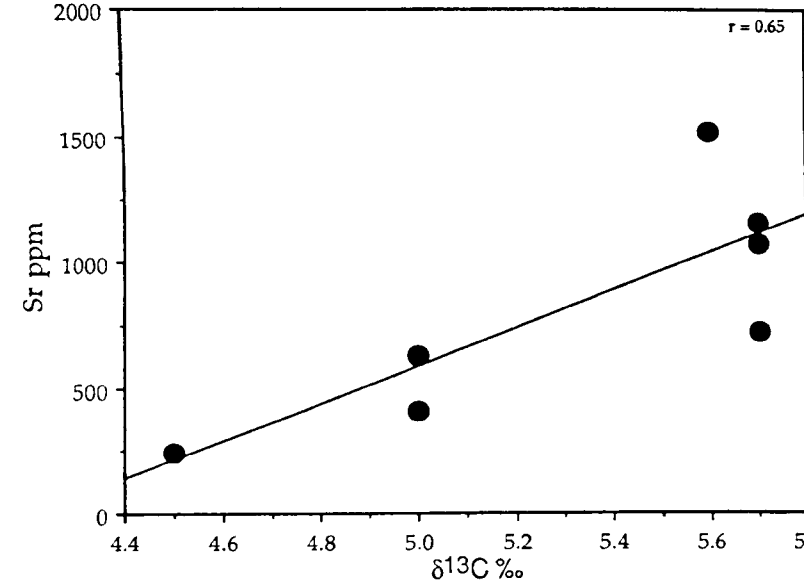

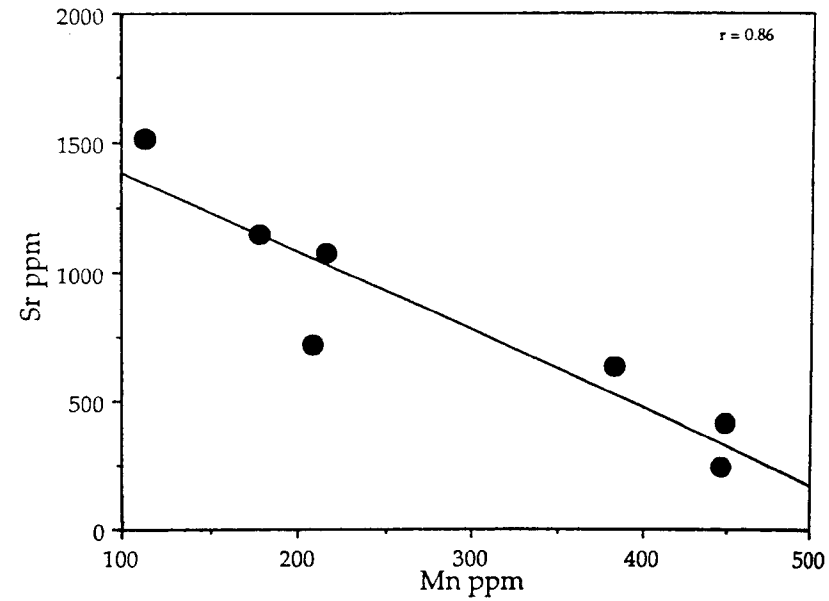

Fig. 4.9. Graphs illustrating the correlations between the trace element and isotopic composition of the Raisby Quarry limestone. Trace elements analysed by ICP.

Sr, and Mn and Fe can also be recognized in relation to position within the Houghton and Raisby Quarry limestone units (Fig. 4.10). These trends have been recognized on a smaller scale, from geochemical transects through an isolated limestone nodule from Raisby Quarry (Fig. 4.11) and microstylolitized limestone nodule from W15 borehole. In both cases, limestones with the highest Sr and lowest Fe and Mn occur in the center of limestone units and nodules. Limestones with the highest Sr, lowest Fe and Mn and least-negative $\delta^{13}C$ and $\delta^{18}O$ are considered to be the least altered, and so closest in composition to carbonates originally precipitated within the Zechstein Sea (3.4.1).

4.3.2. Geochemistry of limestones - Interpretation.

Petrography of the limestones has demonstrated that they now comprise dLMC microspar, which formed by aggrading neomorphism of ADP carbonate muds. Neomorphism of aragonite and HMC is a wet dissolution-reprecipitation reaction, which is accompanied by exchange of trace and minor elements and isotopes between the dissolving phase(s), pore fluids and authigenic dLMC. As documented by numerous studies (Morrow and Meyers, 1978; Pingitore, 1978 & 1982; Veizer, 1978 & 1983a; Brand and Veizer, 1980 & 1981; Moshier, 1989), it is possible to comprehensively model the geochemistry of aragonite/HMC - dLMC neomorphism using trace elements with a partition coefficient of less than 1 (i.e., Sr) and more than 1 (i.e., Mn).

The Sr content of dLMC after aragonite may, in part, reflect relic aragonite inclusions within dLMC (Sandberg and Hudson, 1983; Lasemi and Sandberg, 1984; Sandberg, 1985). Plio-Pleistocence ADP microspars at outcrop in Florida, contain an average of 5-10% relic aragonite (Lasemi and Sandberg, 1984), and Sandberg and Hudson (1983) reported 12-15% from neomorphosed originally aragonitic Jurassic bivalves. McKenzie (1985) recorded calcite after aragonite with more than 35% of the original aragonite preserved in Miocene limestones from Sicily, although such high concentrations are rare. Aragonite inclusions have been recorded from a number of samples of Raisby Formation microspar (Fig. 4.2b). Aragonite precipitated in equilibrium with seawater should contain 7000-9400ppm Sr (assuming $K^{Sr}_{Aragonite}$ 0.9 and 1.2 respectively [Veizer, 1983a]). Thus, 5% aragonite would contribute 350-470ppm Sr to a limestone analysis. Given the average Sr concentration of pre-Cretaceous limestones (320ppm), the maximum value of 3200ppm Sr from Raisby Quarry could be achieved by end-member combinations of:

1. 57% of 320ppm Sr_{dLMC} with 43% of 7000ppm $Sr_{Aragonite}$
2. 95% of 3000ppm Sr_{dLMC} with 5% of 7000ppm $Sr_{Aragonite}$

The second mixture appears most likely, given the reported small concentrations of aragonite relicts in ancient limestones (Sandberg and Hudson, 1983; Lasemi and Sandberg, 1984; Sandberg, 1985), and the density of aragonite relics identified by SEM within limestones at Raisby Quarry (Fig. 4.2b). The other possibility is that the high Sr values of Raisby

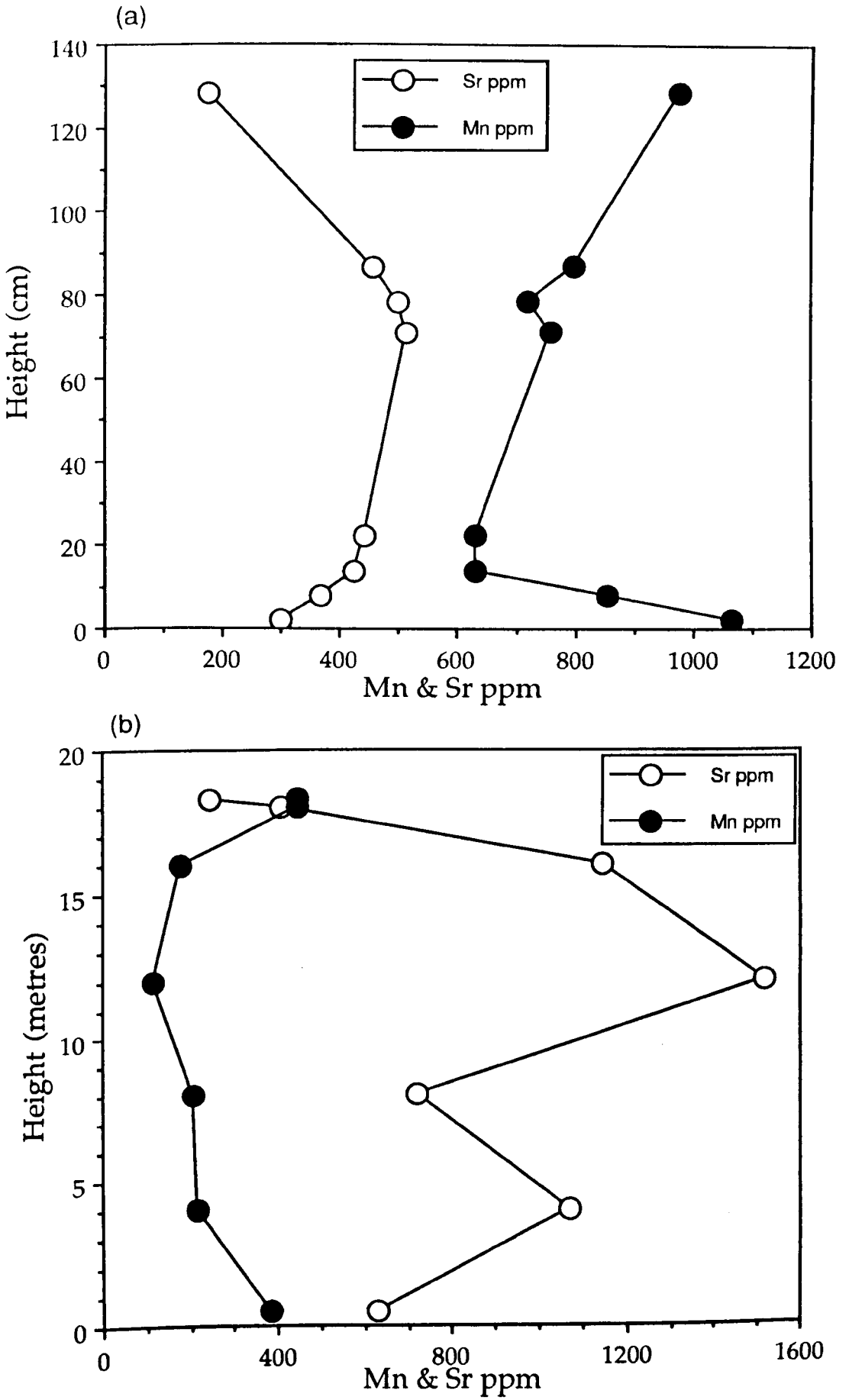

Fig. 4.10. Graphs showing the variation in geochemistry of limestones from Houghton (a) and Raisby (b) Quarries in relation to stratigraphic position within the limestones.

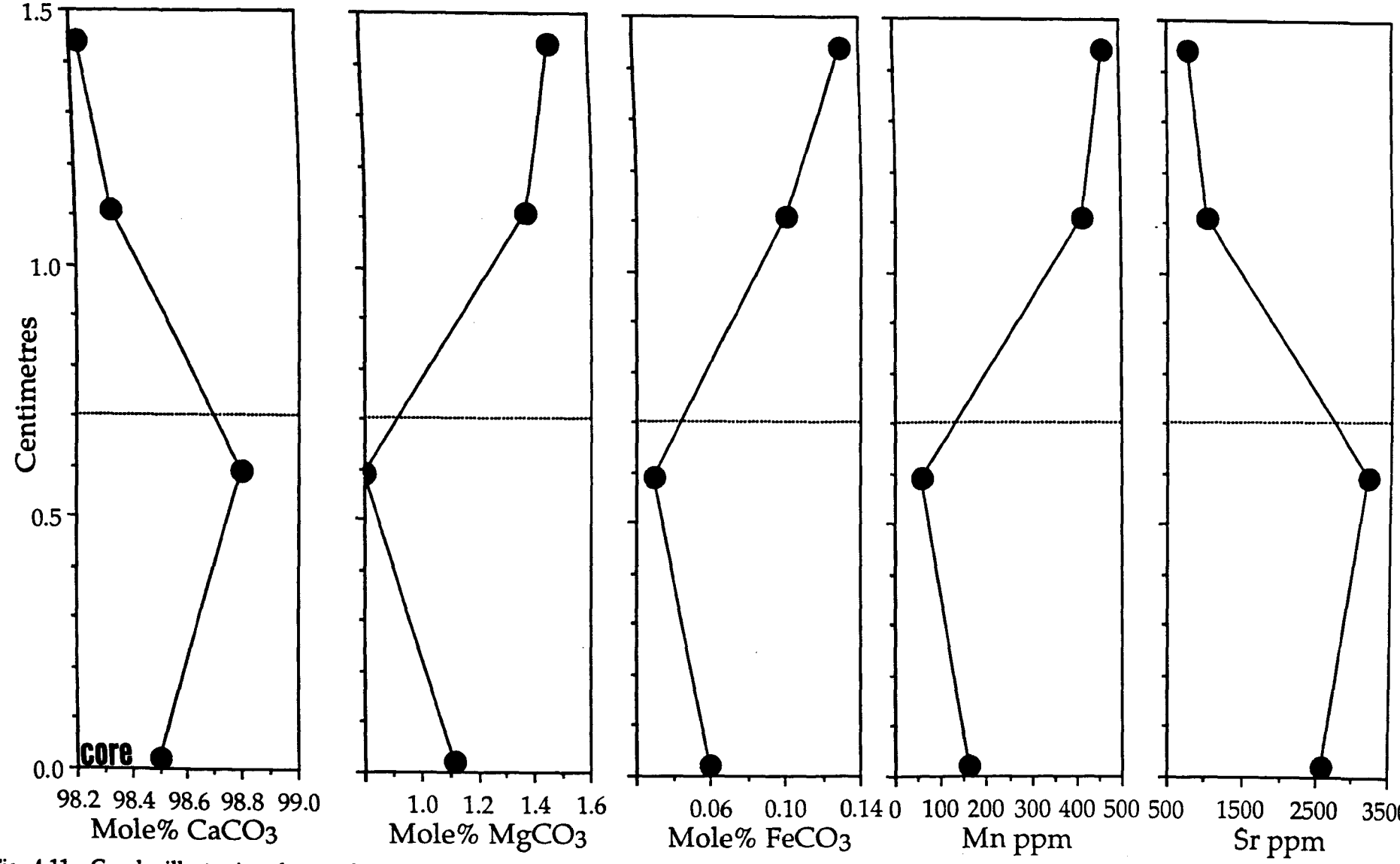

Fig. 4.11. Graphs illustrating the geochemical variation of limestone in a radial traverse from the core to the margin of an isolated limestone nodule, Raisby Quarry. The lowest point on the graphs is the core of the nodule. The line at 0.7cm separates the dark blue core and lighter blue margin of the nodule.

Formation limestones are due to contamination from Sr-rich minerals such as celestite ($SrSO_4$) and/or strontianite ($SrCO_3$). Both have been reported in association with neomorphosed aragonites (McKenzie, 1985; Decima *et al.*, 1988; Nickless *et al.*, 1976; Wood and Shaw, 1976). These minerals have not been recorded from the Raisby Formation during this study. However, Sedgwick (1835) reported celestite from near Hartlepool, and Fowler (1956) and Smith and Francis (1967) have identified celestite within first cycle carbonates of Co. Durham. The precise locations and diagenetic interrelations of this celestite is not known, although Fowler (1957) suggests that it is of epigenetic origin, possibly related to base metal mineralization. The complete absence of any dolostone analyses with greater than 160ppm Sr (5.3.3) lends support to the suggestion that the high Sr is contained mainly within dLMC microspars with or without relic aragonite inclusions.

Limestones analysed from the Raisby Formation therefore appear to be anomalously enriched in Sr relative to many ancient limestones. Even if all limestone samples contain 5% of 9400ppm $Sr_{Aragonite}$ (= 470ppm Sr), a considerable percentage of samples from the Raisby Formation would need to comprise dLMC microspar with more than 320ppm Sr. Anomalously Sr-enriched dLMC after aragonite has commonly been reported (Mazullo, 1980; Sandberg and Hudson, 1983; Tucker, 1986; Wiggins, 1986). Sandberg and Hudson (1983) recorded neomorphic calcite after originally aragonitic Jurassic bivalves with 1200-1350ppm Sr, and Davies (1977) reported neomorphosed Permian aragonite botryoids containing 7000-8000ppm Sr. Although these observations could be taken to suggest that all of the Sr of the limestones is within the calcite lattice, the aragonite relics from Raisby Quarry demonstrate, conclusively, that a proportion of the Sr, in at least one locality, comes from aragonite.

Fundamental to this discussion of the geochemistry of neomorphic calcite is that the dLMC itself has not been neomorphosed during later burial diagenesis. Such neomorphism, to a more stable form of dLMC under the new conditions, would undoubtedly involve trace element and isotope exchange with the ambient pore fluids. Most studies, however, suggest that dLMC is stable (Sandberg and Hudson, 1983; Lasemi and Sandberg, 1984; Sandberg, 1985; Moshier, 1989). At Houghton Quarry, there is some evidence for partial alteration of dLMC microspar during later, post-neomorphism, partial dolomitization associated with microstylolitization (pervasive pressure solution dolomitization [5.4.3]). Analyses of the partially dolomitized limestone and associated undolomitized limestone show two distinct groups, one of high Sr and low $MgCO_3$ (limestone) and another of lower Sr and higher $MgCO_3$ (partially dolomitized limestone), with one outlier of a more strongly dolomitized limestone (Fig. 4.12). The loss of Sr in a limestone analysis due to replacement of limestone by dolomite of a lower Sr content explains most of the difference. However, regression lines fitted to each set of points describe a much more rapid decrease in Sr (mean 32ppm Sr per 1% stoichiometric dolomite) than would be expected (1-3ppm Sr per 1% stoichiometric dolomite [assuming Sr_{Dol} = 100-300ppm]) (Fig. 4.12). This discrepancy is best explained by leaching of Sr

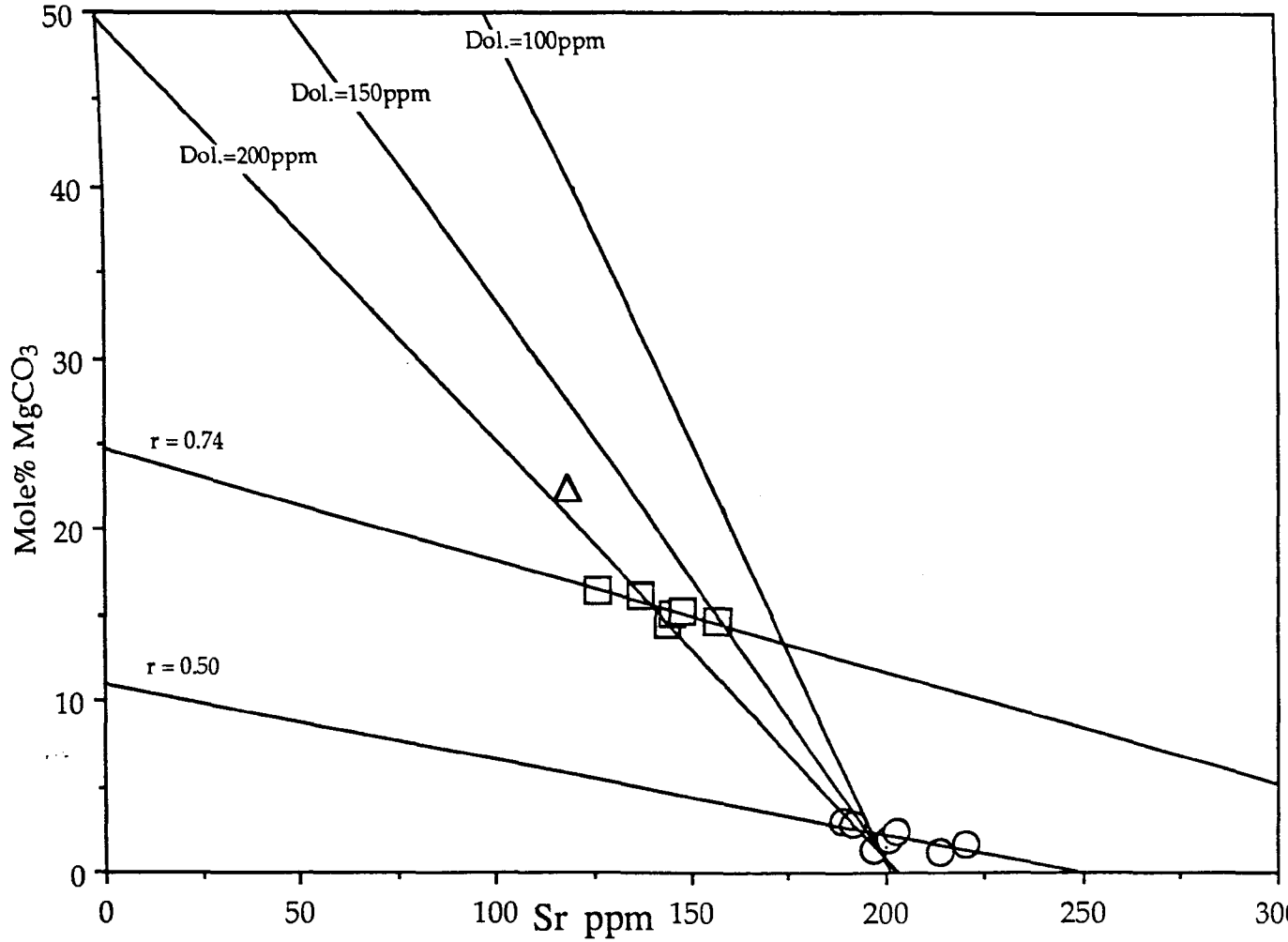

Fig. 4.12. Graph illustrating the composition of limestones and partially dolomitized limestones from the ribbon limestone, Houghton Quarry. The partially dolomitized limestones are associated with pressure solution. The two sub-horizontal lines are regression lines fitted to undolomitized (○) and partially dolomitized limestones (□). The three sub-vertical lines describe the change in composition of the undolomitized limestone which should be recorded with progressive replacement by dolomite of varied composition. That the partially dolomitized limestones do not fit the predicted trends suggests partial recrystallization of microspar has taken place. (△) is a more strongly dolomitized sample.

from the host microspar (i.e., partial neomorphism of dLMC) during dolomitization (1.5ppm Sr_{dLMC} leached per 1% stoichiometric dolomite). This leaching, however, only occurs where the limestones have been dolomitized after neomorphism, which is most likely rare in the Raisby Formation (5.4.3).

Both petrographic and geochemical evidence support limestone formation by aggrading neomorphism of an ADP carbonate mud. Three end products of the alteration may be defined:

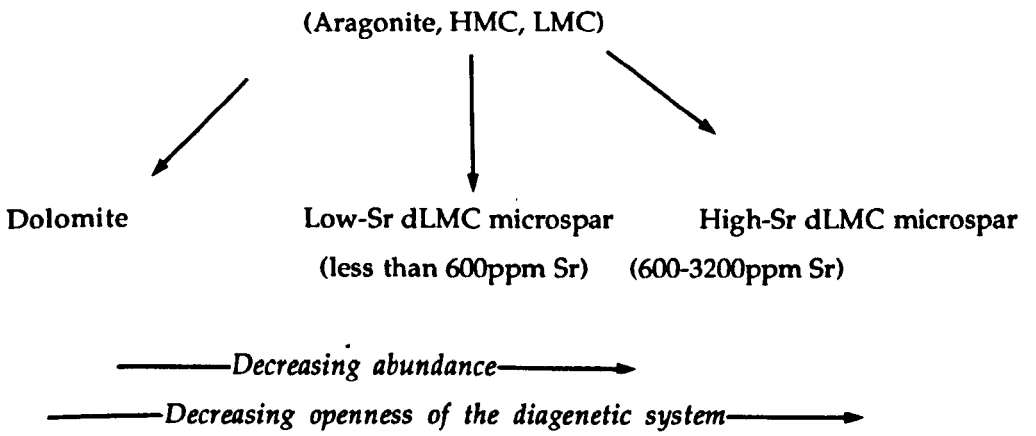

Most of the formation is now dolomite. Most of the undolomitized limestones comprise low-Sr dLMC with a few, at specific localities, comprising high-Sr dLMC. Although the Sr content of most dolomite is less than that of most low-Sr dLMC, that may be due to later neomorphism (5.3.1.1).

4.3.2.1. Trace element and isotope mobility during neomorphism

The chemistry of neomorphism of aragonite and HMC to dLMC is very complex, and has been most intensively studied with reference to meteoric aquifers (Brand and Veizer, 1980 & 1981; Veizer, 1983a; Pingitore, 1978 & 1982; Al-Aasm and Veizer, 1986a & b). Pingitore (1982) lists five factors which control the chemistry of the alteration process:

1. Chemical composition of aragonite and HMC,
2. Partition coefficients for the relevant species at relevant temperatures,
3. Externally-fixed chemistry of the diagenetic solution,
4. Openness of water flow or diffusion gradients to and from the site of diagenesis,
5. Non-carbonate chemical reactions.

The theoretical composition of aragonite and calcite precipitated in equilibrium with marine waters is tabulated below (after Veizer, 1983a).

	Marine calcites (ppm)	Aragonite (ppm)
Mg	16300-75400	750-6300
Fe	2-39	-
Mn	1	0.1-0.6
Sr	1000	7000-9400
Ba	0.2-0.8	2-4

Partition coefficients (only at 25°C) for the main trace elements in carbonates are discussed in 3.1.1. The influence of non-carbonate chemical reactions is hard to determine, although bacterial sulphate reduction (extracting Fe^{2+} and SO_4^{2-} from the diagenetic system) must have been significant during early diagenesis (3.2.2). The externally-fixed chemistry of the diagenetic solution and degree of openness of the diagenetic system (factors 3 and 4 respectively) are the most important variables in the present context. The positive $\delta^{13}C$ of the dLMC means that the externally-fixed chemistry of the diagenetic solution is very unlikely to have been solely of a meteoric-derivation and was, most probably, altered connate Zechstein seawater, modified from interaction with dolomitizing brines.

The openness of water flow, and diffusion gradients to and from the diagenetic site (factor 4) relates to the nature of solute transport and the interaction between grain surfaces undergoing dissolution with the bulk aquifer. Solute transport may be via diffusion, or advection (free fluid flow in response to hydraulic head and permeability). In the reaction zone model of Pingitore (1982), transfer of ions between the crystal surface undergoing dissolution and the growing surface of dLMC is via diffusion through a reaction zone (possibly only 0.05μm wide [Martin *et al.*, 1986]). Solute movement within bulk aquifer waters is by advection whereas solutes migrate between the reaction zones and bulk aquifer water via diffusion (Fig. 4.13). The openness of a diagenetic system (degree of bulk solution-equilibrium) is a function of the rate of diffusion transfer between the reaction zone and bulk aquifer which is a function of a number of variables (Pingitore, 1982):

$$\frac{dq}{dt} = D\,(C_r - C_a)\;A/l$$

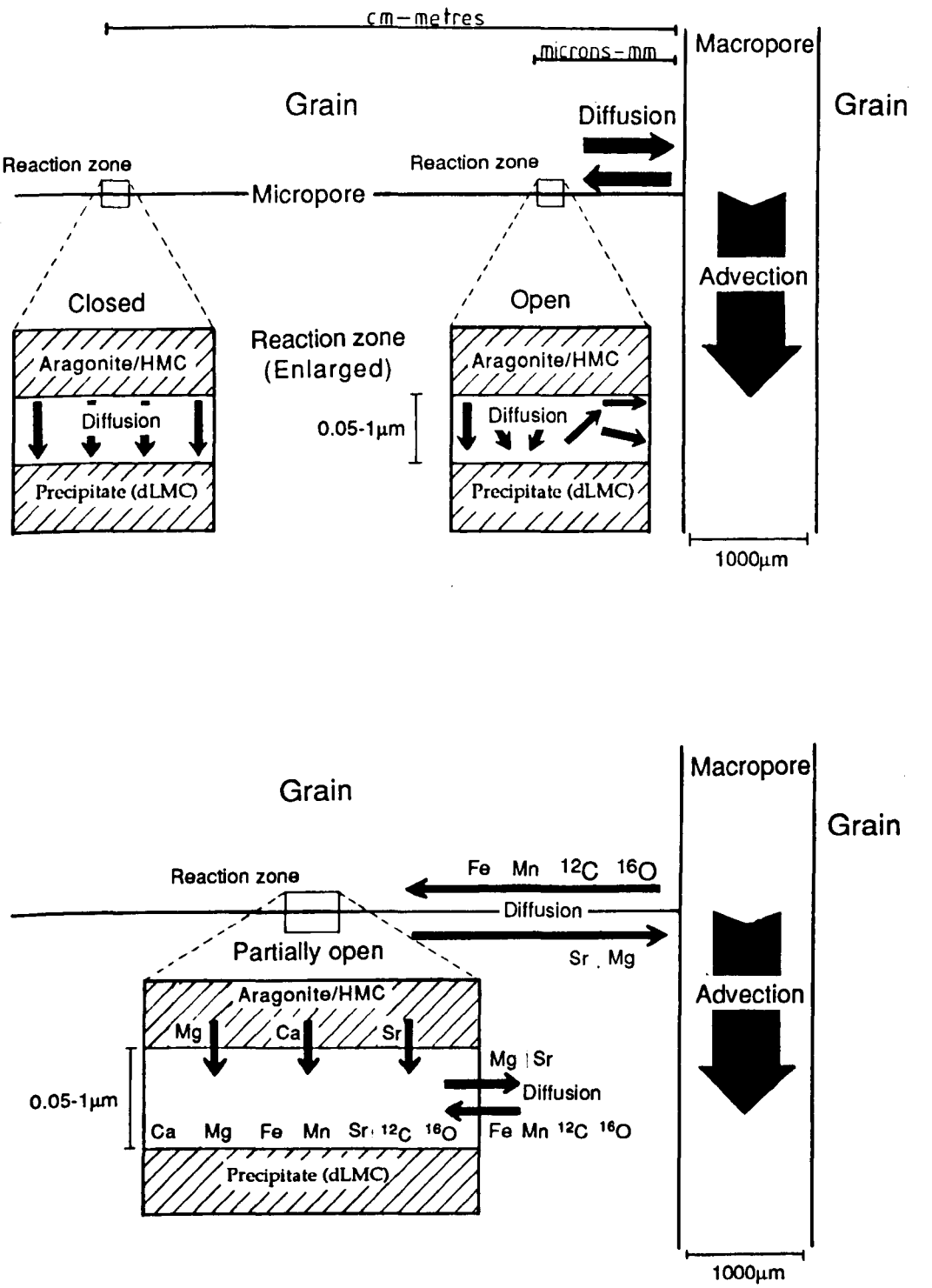

Fig. 4.13. Simplified models of a reaction zone between dissolving aragonite or HMC and precipitating dLMC microspar (modified from Pingitore, 1982 and Veizer, 1983a). The lower diagram illustrates the movement of ions and isotopes between the dissolving, precipitating phases, and the bulk aquifer, as deduced from the geochemistry of Raisby Formation limestones.

Where:

q = quantity of material

t = time

D = diffusion coefficients for specific ions

C_r = ion concentration at the reaction zone

C_a = ion concentration in the aquifer

A = effective pore area

1 = distance from reaction zone to aquifer in cms

Diffusion coefficients for most ions considered in carbonate diagenetic studies are similar, less than $1cm^2\ day^{-1}$ at 25°C. Diffusion rates also increase with temperature. In most systems, diffusion rates will be less than rates of aquifer advection (in the order of metres per year in confined aquifers [Veizer, 1983a]). The magnitude of the difference in concentration of solutes between the reaction zone and proximal bulk aquifer controls the rate of diffusion, with diffusion rates increasing with a greater concentration difference. Concentration gradients are, in general, the most important variables of diffusion, with pore path and geometry of secondary importance (Pingitore, 1982). The importance of pore path and pore geometry is that, in low permeability lithologies (i.e., lithified/semi-lithified carbonate muds), solutes have to diffuse further (centimetres to metres) to reach the bulk aquifer than in more permeable lithologies such as grainstones, where the bulk aquifer is in almost direct contact with the reaction zones (micron to millimetres long diffusion paths). Clearly therefore, it may take years for an ion to diffuse from the reaction zone to proximal bulk aquifer in a low permeability lithology (small pore area and tortuous pore path).

4.3.2.2. Geochemistry of Raisby Formation limestones related to reaction zone processes

The Raisby Formation limestones show a progressive depletion with respect to Sr (K <1) and enrichment in Fe and Mn (K >1). The samples with highest Sr, $\delta^{13}C$, $\delta^{18}O$ and lowest Mn and Fe are interpreted to represent least interaction with the bulk aquifer (i.e., closest in composition to the original carbonate mud). The systematic decrease in Sr, $\delta^{18}O$ and $\delta^{13}C$, and increase of Mn and Fe towards the margins of (a) limestone bodies on a scale of metres (Fig. 4.10) and (b) individual limestone nodules on a scale of centimetres (Fig. 4.11), suggests that the intensity of bulk solution-equilibrium during neomorphism was a function of permeability within the limestones (i.e., pore path and geometry) and proximity to the bulk aquifer (which was probably within the dolostones). Dolostones at the present day are considerably more permeable than the limestones (if the limestones did have a reasonable permeability they would have been dolomitized [4.2.2]), and may still have been, even if limestone neomorphism postdated sulphate precipitation within the dolostones.

Thus, where isolated from the bulk aquifer, diffusion paths would have been long and so the fluid from which the dLMC was precipitating would have been enriched in Sr (i.e., a relatively closed diagenetic system in bulk solution-disequilibrium). Diffusion paths from the bulk aquifer to reaction zones for Fe and Mn would also have been long, explaining their relative depletion within high Sr dLMC microspars. Thus, position within isolated limestone bodies controlled proximity to the bulk aquifer (i.e., openness of the diagenetic system), and so chemical composition of the dLMC. The lowest Sr, $\delta^{13}C$, $\delta^{18}O$ and higher Fe and Mn values, at the margins of nodules and limestone units represent near-equilibrium values with the bulk aquifer.

Within early diagenetic limestone nodules, there may have been an overprint on the aforementioned permeability difference in that, as the nodules were primary sea floor features, their cementation may be expected to have been greatest in their centers, decreasing outwards. This trend is very common with respect to carbonate concretions within shales, where the percentage of carbonate cement progressively decreases outwards. Pore water chemistry may also have changed during cementation, although this is unlikely, as the source of ions was seawater, of invariant composition. During neomorphism of the cemented carbonate mud, permeability would have been lowest and rock/water ratio highest in the most tightly cemented centers of the nodules (therefore the microspar there has highest Sr values). Variable neomorphism may be reflected by colour variation within Raisby Quarry and W15 borehole nodules. The core of Raisby Quarry nodules is commonly darker in colour ('dark grey' [N4]) than their margins ('medium grey' [N5]). Geochemical transects across such nodules (Fig. 4.11) show that the colour variation corresponds to an abrupt geochemical change and is interpreted to represent an 'alteration front'. Martin *et al.*, (1986) document similar inward-migrating neomorphic fronts within fossil fragments of grainstones from Florida. That this concentric colour and compositional variation is a neomorphic effect, is also vividly illustrated by limestone clasts within a middle slope calcirudite from Dawsons Plantation. Some of the component limestone pebbles have a pronounced concentric colour banding which parallels the outer margin of the pebbles. Such a colour variation cannot be due to a cementation gradient, as the limestone had been cemented, close to the sea floor prior to resedimentation (2.4.2.2). As concentric colour variation of the nodules is directly related to geochemistry, and the geochemistry is certainly of secondary origin, by extension, the concentric colour zonation must also be secondary in origin. The original, pre-neomorphism mineralogy of the nodules may have varied from core to margin in response to a cementation gradient, but this would tend to overprint, not counteract the geochemical gradients imposed by neomorphism, as much of the early cement may well have been aragonite. It is not possible that colour variation in nodules is a telogenetic weathering feature, as colour banding is seen in nodules from W15 (Fig. 2.13).

It appears that limestones most isolated from the bulk aquifer during neomorphism, may owe some of their high Sr to the presence of aragonite relics. Thus, the dissolution of

aragonite relics may have been a function of the water/rock ratio during neomorphism. In a high water/rock system, the diagenetic fluids would have been more undersaturated with respect to aragonite than in a more closed system. Accordingly, a higher density of aragonite relics has been recorded from the core than margin of a nodule from Raisby Quarry (Fig. 4.2).

The bulk aquifer must have been enriched in Mn and Fe and depleted with respect to Sr relative to the reaction zones, therefore developing concentration gradients, although in opposite directions. This may be due to the original chemical composition of the bulk aquifer, or it may have been modified during progressive diagenesis, dependant on the rate of advection of the bulk aquifer. Most studies of aragonite neomorphism have dealt with meteoric diagenetic fluids which have large concentration gradients of Sr, Mn and Fe with aragonite reaction zones. In the present context, it is likely that concentration gradients were much smaller, especially for Sr. Dolomitizing brines within the Raisby Formation would have been very Sr-rich owing to the low $K^{Sr}_{Dolomite}$, very open system conditions of dolomitization and the high-Sr aragonite-rich precursor. The brines themselves probably originally contained significant Sr owing to evaporative concentration of Zechstein seawater (Chapter 5). Fe and Mn concentrations in the aquifer were probably low relative to those of meteoric groundwaters. The generally low Fe and Mn of microspars (mean 0.21mole% $FeCO_3$, 0.11mole% $MnCO_3$ [all limestone AAS and ICP analyses (Table 4.1.)]) and low Fe/Mn ratios (1 to 5) suggest minor Fe and Mn sources (probably iron oxides, iron sulphides, and clays). They also indicate that the aquifer fluids originated within the Zechstein sediments, with little or no communication with aquifers in the Carboniferous, where many more abundant Fe and Mn sources would have been available. The aquifer fluids must have been reducing, in order to coprecipitate limited amounts of Fe and Mn within the calcite microspars. It is doubtful, however, if bacterial sulphate reduction was operative to remove iron during this time, (as suggested for Jurassic non-ferroan microspars by Hudson and Andrews, 1987), as sulphate reduction took place earlier in the diagenesis of the Raisby Formation limestones, producing framboidal pyrite (3.3.2). Although bacterial sulphate reduction predated the time during which neomorphism is considered to have taken place, it may have acted to reduce the potential iron supply by scavenging all easily available iron and locking it in pyrite, which was unreactive during neomorphism.

Within the limestones analysed, there will be some dolomite and insoluble residues (mainly detrital siliciclastics and authigenic iron/manganese oxide/hydroxides) within the samples, which may add 'contaminant' ions to the analyses. Both dolomite and authigenic iron/manganese oxide/hydroxides increase in abundance within the limestones towards their margins, towards contact with the dolostones, where the limestone has (and had) its greatest permeability. The relatively low Sr and high Fe & Mn concentrations of dolomite (5.3.2) will amplify the trends of decreasing Sr and increasing Fe and Mn towards the margins of the limestone units (Fig. 4.10). Brand and Veizer (1980) demonstrate that laboratory leaching during sample preparation of non-carbonate phases will tend to produce

similar trends for Fe and Mn and for Fe and Al. Although this will affect the degree of covariance between Fe and Mn, it will not affect the covariance of Sr and Mn, or Sr and Fe. Thus, contamination of limestone samples by dolomite and non-carbonate material will not alter the overall geochemical trends described.

4.3.2.3. Diagenetic model for limestone neomorphism.

From an understanding of reaction zone mechanics, and partition coefficients of relevant ions, it may be possible to model the expected composition of dLMC during neomorphism. This use of partition coefficients is based on the assumption that thermodynamic equilibrium is approached or reached during diagenetic reactions (3.1.1), which is likely, owing to the slowness of most burial diagenetic processes. This is also assumed in the very extensive literature on the modelling of carbonate diagenesis, which directly uses partition coefficients to predict fluid geochemistries (Pingitore, 1978 & 1982; Veizer, 1983a & b [and references therein]). Owing to the low partition coefficient of Sr, the Sr/Ca ratio in the reaction zone must have been considerably greater than that in the dLMC. The Sr/Ca ratio of a reaction zone solution may vary from $Sr/Ca_{Dissolving\ phase}$ in an open system (assuming a "geologically reasonable composition" of the bulk aquifer [Pingitore, 1982]) to $\frac{Sr/Ca_{Dissolving\ phase}}{K^{Sr}_{dLMC}}$ in a closed system (Pingitore, 1982). Both values represent a steady state which has been reached after a period of dissolution-reprecipitation. Firstly, aragonite is taken as the only dissolving phase and is assumed to have a composition of 7000-9400ppm Sr (Veizer, 1983a). K^{Sr}_{dLMC} is taken as 0.05, which is reasonable for neomorphism of a high Sr/Ca ratio precursor (Pingitore and Eastman, 1986) (3.1.1; Fig. 3.1). The reaction zone in the open system will have a Sr/Ca ratio of 0.0175-0.0235 and that in the closed system 0.35-0.47 (Fig. 4.14). If these ratios are substituted into the homogeneous distribution law (3.1.1), the dLMC precipitating during steady state conditions (and assuming all Ca liberated by dissolution is reprecipitated as dLMC, which is likely, as neomorphism is conservative with respect to Ca [Veizer, 1983a; Martin *et al.*, 1986]) will have a composition of 352-472ppm Sr in the open system and 7000-9400ppm Sr in the closed system (i.e., the composition of the dissolving aragonite) (Fig. 4.14). The second part of this calculation assumes that the homogeneous distribution law may be applied to this diagenetic environment. As outlined in 3.1.1, the homogeneous distribution law only applies to fluids which do not change in composition over time. However, in this model, the composition of dLMC in a steady state reaction zone is being considered (i.e., one of a stable, relatively invariant composition), and so the homogeneous distribution law may be used. The calculations outlined here give identical results for closed system dLMC after aragonite as presented by Pingitore (1982).

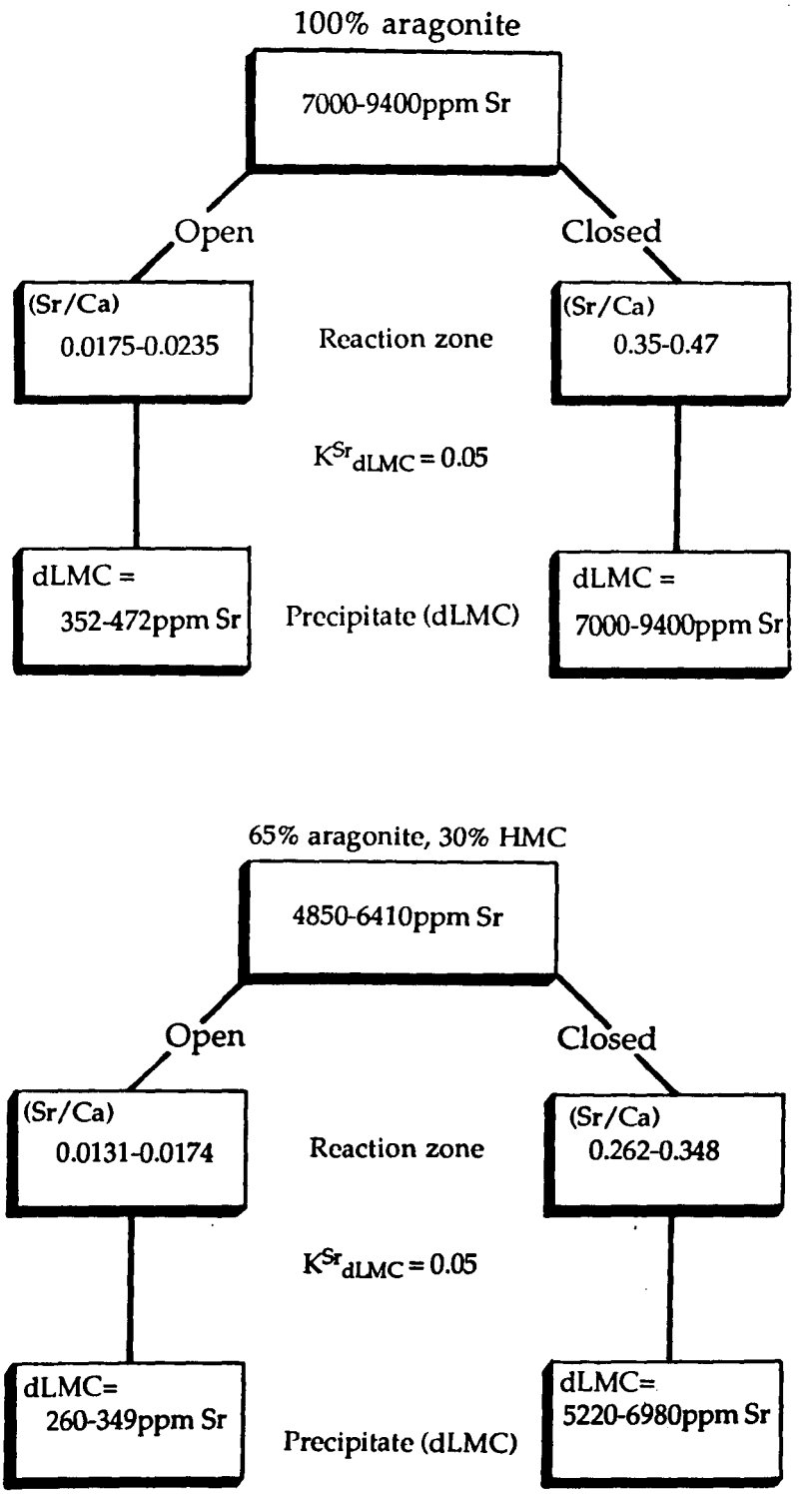

Fig. 4.14. Flowchart showing the calculations for the Sr composition of dLMC given open and closed diagenetic systems and different initial mineralogical assemblages. These calculations assume that equilibrium is reached or approached during neomorphism, such that the homogeneous distribution law may be applied.

If a more realistic starting composition for the dissolving phase of 65% aragonite and 30% HMC is assumed (the 5% LMC being stable), the predicted dLMC composition will be different from that for aragonite precursor. In this model, the HMC is assumed to contain 1000ppm Sr (Veizer, 1983a) and 11-17 mole% $MgCO_3$ (Bathurst, 1975), which results in less Ca is going into solution than from pure aragonite. If the influence of Mg on the reaction and dLMC composition is ignored, by repeating the calculations as for pure aragonite, in an open system the precipitating dLMC will have a lower Sr composition than that derived from pure aragonite (Fig. 4.14).

On the basis of the above principles, it is possible to model the Mg content of dLMC in open and closed system conditions at steady state. Both the Mg content of the aragonite (1000ppm [Veizer, 1983a] and HMC [11-17 mole% $MgCO_3$]) may be taken into account. Again the mixed assemblage of 65% aragonite and 30% HMC is assumed, with the LMC stable. The precipitating dLMC will have an open system composition of 203-280ppm Mg (0.0835-0.1152 mole% $MgCO_3$) and in closed system 10,148-14,220ppm Mg (4.18-5.85mole% $MgCO_3$) (Fig. 4.15). These calculations assume that the dLMC will be pure $CaCO_3$. Although it will not be, the role of other ions coprecipitated with it do not make a significant difference to the calculations. If only aragonite is the dissolving phase the precipitated dLMC will have a composition of 20ppm in open system and 1003ppm Mg in a closed system at steady state (Fig. 4.15).

When the results from this modelling are plotted against recorded values, Raisby Formation limestones lie between closed and open diagenetic systems for Mg (Fig. 4.16 & 4.17). This suggests that neomorphism took place in a diagenetic environment between fully open and fully closed with respect to Mg, and that 30% HMC, 65% aragonite is a reasonable estimate for the original sediment (on the basis of Mg data) (Fig. 4.17). Limestone Sr values, especially from Houghton Quarry, lie very close to the open system diagenesis, and below it (Fig. 4.16). This could imply recrystallization of dLMC, that the original sediment had a greater quantity of relatively low Sr HMC than suggested, or that the bulk aquifer was very depleted with respect to Sr and, at least at times, was advecting faster than input rate of Sr from the dissolving phases, such that a steady state could not be achieved. That the diagenetic system was apparently more closed for Mg than Sr however, suggests that the carbonate mud precursor had less Mg than the assumed 65% aragonite and 30% HMC. This would be consistent with a higher original aragonite/HMC ratio carbonate mud. There may be an overprint on some of the limestone analysis results (especially from Raisby Quarry) by inclusion of aragonite relics. However, as the quantity of relic aragonite is not known for most samples, it is difficult to correct for.

Solutes during neomorphism must maintain electroneutrality (Pingitore, 1982). Thus, cations being exchanged (Ca^{2+}, Mg^{2+}, Fe^{2+}, Mn^{2+}, Sr^{2+}) combine with CO_3^{2-} (the most abundant divalent anion in this diagenetic environment). Therefore, the large volume of

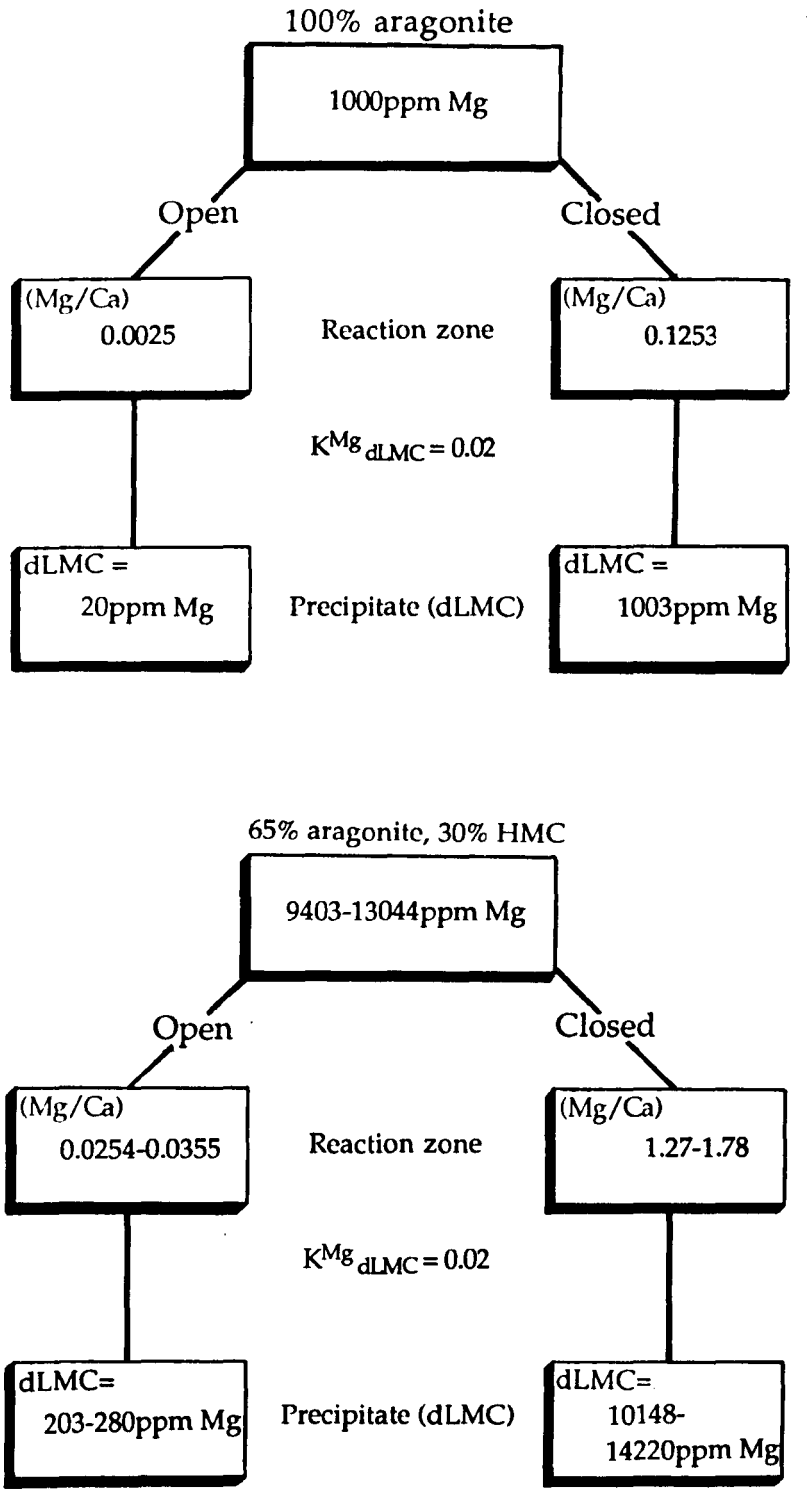

Fig. 4.15. Flowchart showing the calculations for the Mg composition of dLMC given open and closed diagenetic systems and different initial mineralogical assemblages. These calculations assume that equilibrium is reached or approached during neomorphism, such that the homogeneous distribution law may be applied.

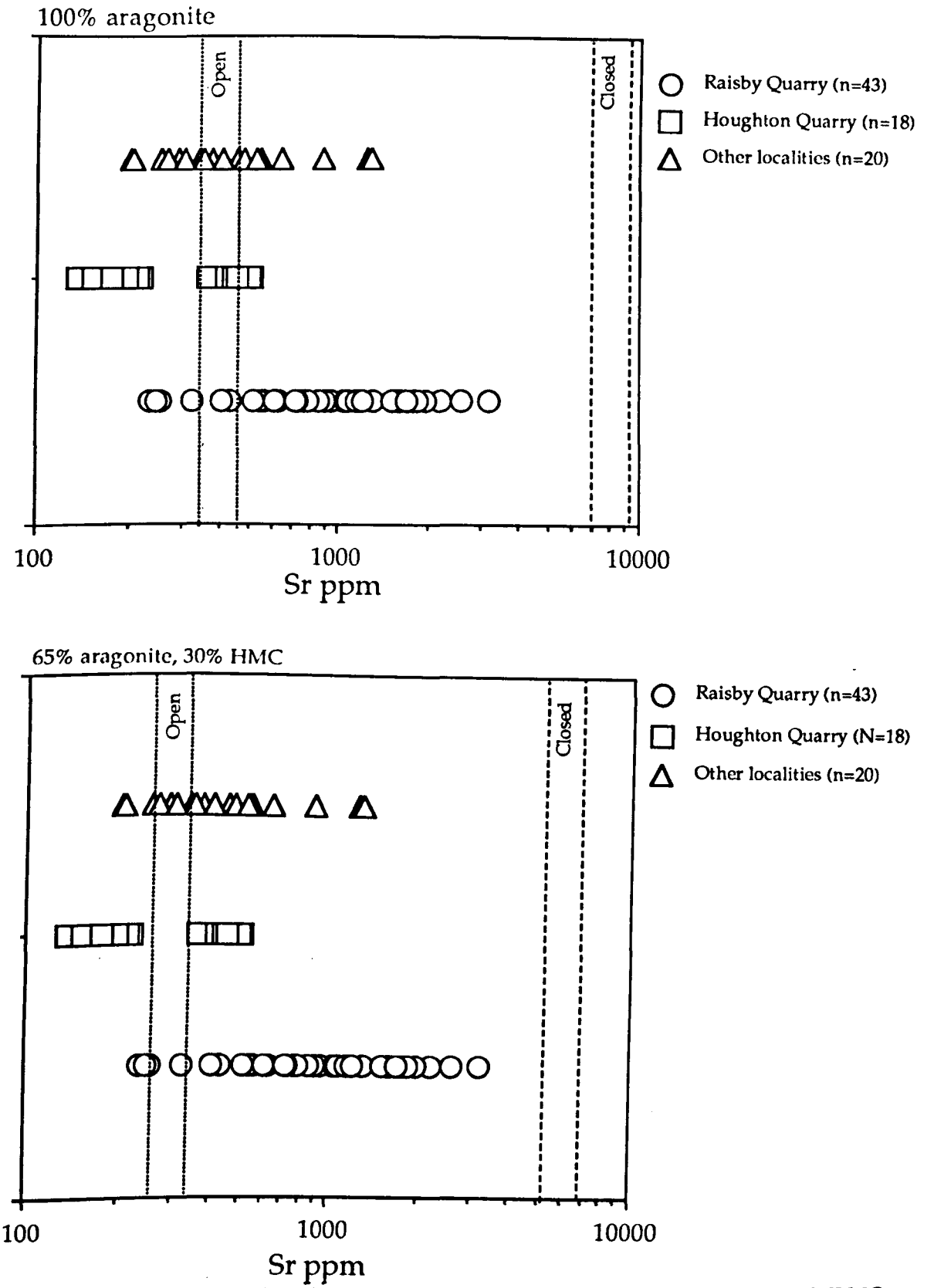

Fig. 4.16. Graphs showing the relationship between the modelled Sr compositions of dLMC microspar and the recorded values for Raisby Formation limestones. Note, the mixed aragonite - HMC combination gives more realistic results, and that most limestones lie at the open end of the diagenetic system. The two populations of limestones from Houghton Quarry represent the division between those recrystallized and those unaltered during pervasive pressure solution dolomitization.

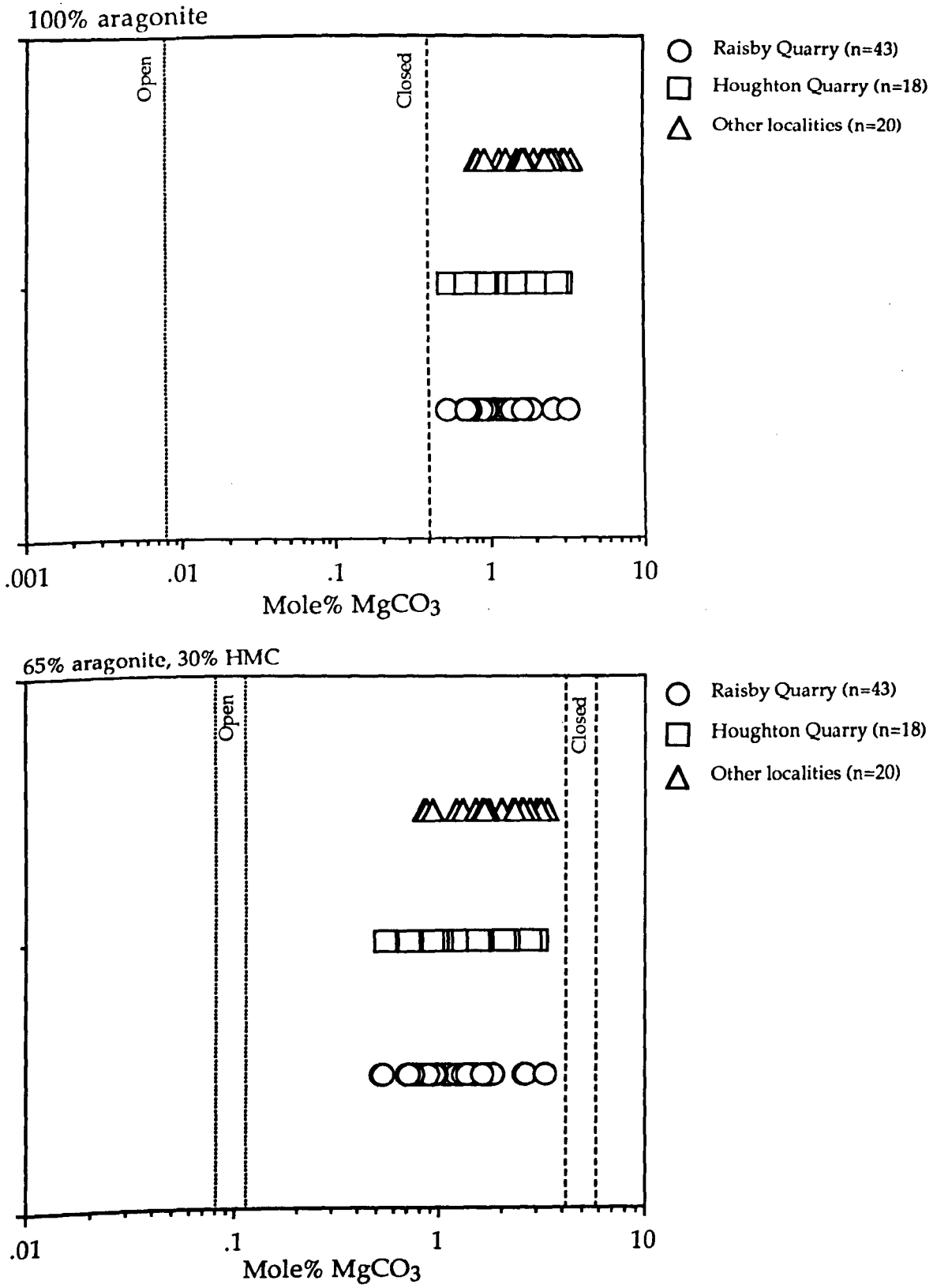

Fig. 4.17. Graphs showing the relationship between the modelled Mg compositions of dLMC microspar and the recorded values for Raisby Formation limestones. As with Sr results, on the basis of Mg data, the mixed aragonite - HMC assemblage is again more likely. That the limestones plot closer to the closed end of the diagenetic system suggests the aragonite to HMC ratio of the precursor carbonate mud may have been slightly higher than used in the model.

trace element movement demonstrated, suggests that there was an equally extensive interchange of CO_3^{2-}. That the interchange of CO_3^{2-} between the dissolving phases and bulk aquifer has given little change in $\delta^{13}C$ (approximately 1.5‰) showing that either the bulk aquifer was modified Zechstein seawater, or that the original bulk aquifer fluids had already been inundated with Zechstein seawater CO_3^{2-} from aragonite and HMC dissolution elsewhere within the system. Veizer (1983a) suggests that, in most diagenetic systems, the amount of oxygen derived from dissolution of $CaCO_3$ is negligible in comparison to that derived from the pore waters. Oxygen released as HCO_3^- has a half-life of exchange with oxygen in H_2O of approximately 470 seconds (Veizer, 1983a). Thus, for the isotopic identity of the dissolving phase to be retained, reprecipitation would have to occur within one hour. However, this does not take into account the openness of the system. In a relatively closed system (in which some limestones, in the centre of limestone units were demonstrably neomorphosed) with a large number of active sites of dissolution, the pore waters would be inundated with isotopes from the dissolving phase and so its isotopic identity would be retained. This would, however, be much more apparent for carbon than oxygen isotopes, owing to much greater abundance of oxygen than carbon in most diagenetic pore waters.

The carbon and oxygen stable isotope values for the neomorphosed limestones are not markedly different from those of the dolostones (Fig. 4.7). The only source of ^{13}C - enriched fluids in this context will be Zechstein seawater. Depleted oxygen isotope values of the limestones relative to dolostones and presumed seawater values (around -2.5‰) suggest neomorphism occurred at elevated temperatures. When the presumed temperature difference between the lowest and highest $\delta^{18}O$ limestones in Raisby Quarry is calculated, this represents approximately 25°C. If complete dissolution-reprecipitation has taken place in all samples (i.e., without the preservation of aragonite relics) this cannot be a real effect, as oxygen isotope fractionation due to temperature will be operative throughout, no matter how closed the diagenetic system. It could, however, represent numerous dissolution - reprecipitation events for the limestones, with the greatest number of events being in the limestones closest to the bulk aquifer and so recording the lowest $\delta^{18}O$. This is considered unlikely owing to the aforementioned relative diagenetic stability of dLMC. It could also reflect relatively large scale preservation of aragonite (with a low-negative $\delta^{18}O$) in limestones with the least negative $\delta^{18}O$. However, Sr values of these limestones, although relatively high, do not indicate preservation of sufficient aragonite to make a measurable difference in oxygen isotope values.

Thus, the bulk aquifer must have been depleted in ^{18}O relative to Zechstein seawater values, with a uniform overprint due to elevated temperatures. If the sample with $\delta^{18}O$ of -3.2‰ (Appendix IX) represents the least contribution from bulk aquifer ^{18}O, with the contribution from elevated temperatures, the most altered sample from Raisby Quarry (-7.1‰), (which is assumed to be closest to equilibrium with bulk aquifer oxygen isotopes),

suggests that the bulk aquifer was depleted by at least 3.9‰ relative to reaction zones from which the most isolated dLMC was precipitated. These differences in oxygen isotopic composition could, however, simply be due to an evolving pore water composition, towards lower $\delta^{18}O$ with time. However, this is unlikely, because, as neomorphism would be expected to start from the margins of limestone units, working inwards, microspars in the center of limestone units would be in equilibrium with the later, more evolved pore waters, not those on the margins, as is recorded.

The trends of trace element depletion and enrichment, especially curves on Sr/Ca - Mn plots are extremely similar to those described for meteoric aquifers by Brand and Veizer (1980) and Veizer (1983a) (Fig. 4.18). The trends of decreasing ^{18}O and ^{13}C with increasing interaction with the bulk aquifer are also similar to those described by McKenzie (1985) and Decima *et al.*, (1988) from the Miocene of Sicily. The limestones with highest $\delta^{18}O$ values were interpreted by McKenzie (1985) to be the least altered (closest to seawater oxygen isotope values). The source of ^{13}C and ^{18}O depleted fluids during neomorphism of Raisby Formation limestones is unclear. Meteoric interaction within the bulk aquifer is unlikely, owing to the paucity of evidence for late Permian/early Mesozoic uplift of the Raisby Formation. However, owing to the similarity of Raisby Formation limestone geochemical plots with those from meteoric-influenced neomorphosed limestones (Fig. 4.18), and the covariance of Sr with $\delta^{18}O$ and $\delta^{13}C$, meteoric water input into the diagenetic system cannot be discounted.

4.3.3. Summary and conclusions.

Raisby Formation limestones represent anomalously un-dolomitized carbonates, concentrated towards the base of the formation. Although originally precipitated as a fine grained mixture of aragonite, HMC and LMC, they were cemented, probably when just a few decimetres below the sea floor. This early cementation helped prevent access of dolomitizing fluids. During burial, the aragonite and HMC became unstable, and neomorphosed to dLMC, the stable carbonate phase in the burial diagenetic environment. Neomorphism took place by dissolution-reprecipitation, although locally was incomplete, leaving aragonite relics possibly protected by sheaths of organic matter. Spatial variation in the geochemistry of limestones relates directly to the openness of the diagenetic system during neomorphism, in turn controlled by porosity and permeability of the limestones. Modelling of the expected geochemical composition of the dLMC microspar, from an assumed average starting composition of the carbonate mud, agrees well with a dominantly open to semi-open system diagenesis. Carbon and oxygen isotope trends, although well defined, are difficult to account for within the framework of progressive post-depositional burial of the Raisby Formation up to the Tertiary (Appendix X) and may suggest some meteoric water influence on the isotopic composition of neomorphic fluids.

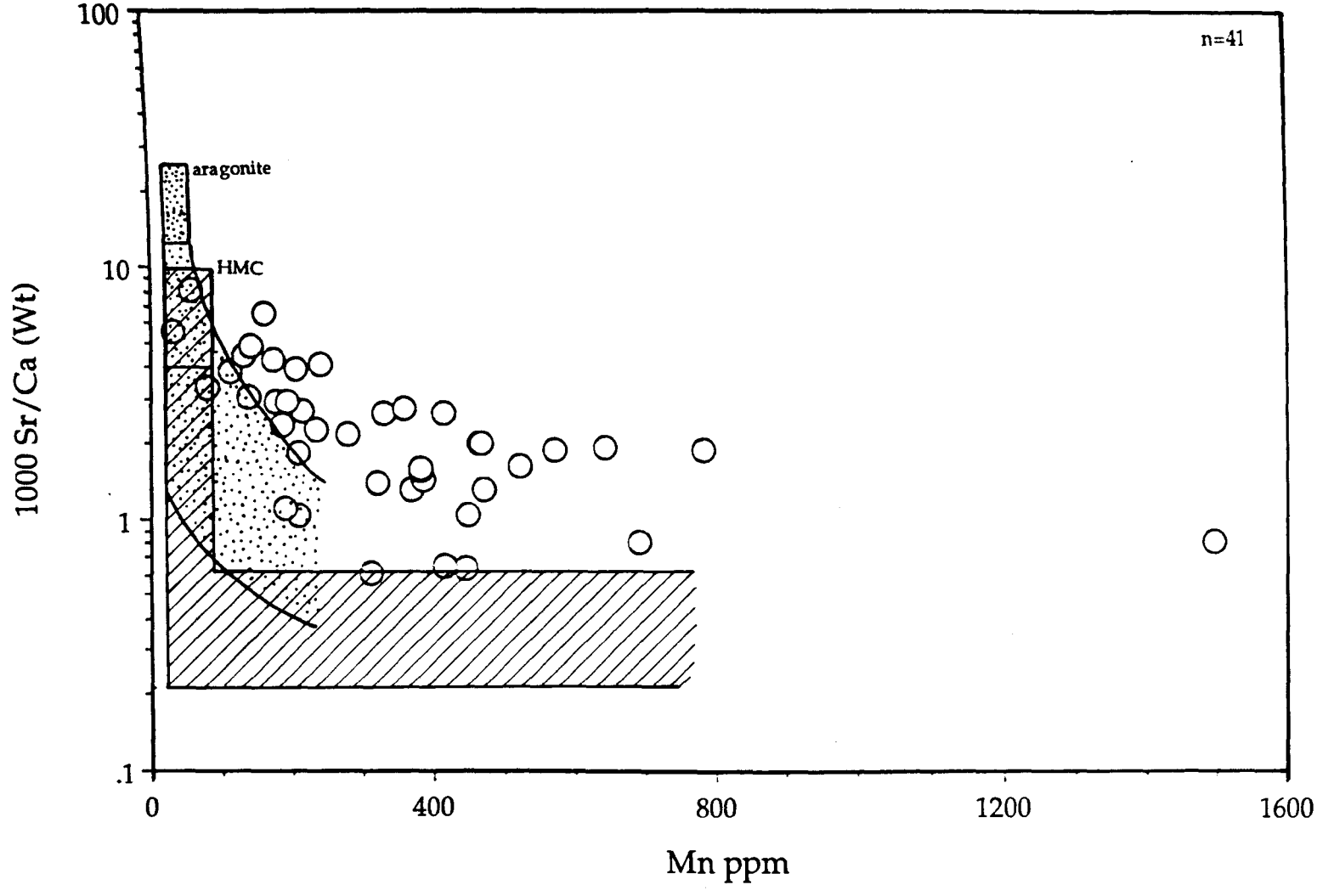

Fig. 4.18. Graph showing the comparison between the composition of limestone from Raisby Quarry and the predicted geochemical changes during progressive neomorphism in a meteoric diagenetic system (after Veizer, 1983a).

4.4.1. Petrography and geochemistry of calcite concretions - Introduction.

In Raisby and Old Towns Quarries, coarsely crystalline calcite concretions occur, which bear a strong petrographic and geochemical similarity to calcite concretions described from higher Zechstein formations of England and Europe. No such concretions have, however, previously been documented from the Raisby Formation, although Magraw (1978) described structures which may be concretions from offshore boreholes. Calcite concretions are distinguished from nodular limestones, with which they may be spatially associated in the Raisby Formation, and to which they are superficially similar in form, by petrography and geochemistry of their very much coarser component calcite crystals.

From Raisby and Old Towns Quarries, two types of concretion have been defined:

Type 1 concretions (Limestone concretions [LC])

LC concretions are present throughout most of the limestone unit at both Raisby and Old Towns Quarries. They are subcircular in plan view (a few centimetres to approximately 20cm in diameter) (Fig. 4.19a), and hemispherical to subspherical in cross section (from millimetres to centimetres in cross-sectional thickness) (Figs. 4.19b & 4.20a). All concretions have grown outwards from limestone nodules or limestone bedding planes (Fig. 4.20a). They are similar in colour to the limestones (mid way between 'medium dark grey' [N4] and 'dark grey' [N3]) and are commonly almost indistinguishable from them in hand specimen (Figs. 4.19b & 4.20a). Concretionary calcite crystals characteristically contain abundant lenses of black organic matter.

Type 2 concretions (Upper nodular limestone concretions [UNL])

UNL concretions were only recorded within the upper nodular limestone unit of Raisby Quarry. The size of UNL concretions is again variable, from a few centimetres up to 17cm in diameter and no greater than 10cm in cross-sectional thickness. They may be hemispherical in cross-section growing off limestone nodules, and are commonly oblate in overall shape. Their colour is distinctive (mid way between 'moderate yellowish brown' [10 YR 4/2] and 'dark yellowish orange' [10 YR 6/6]). Horizontal stringers of dark organic matter are also common.

4.4.1.1. Petrography of calcite concretions - Description.

Petrographically, both types of concretion comprise coarse, equant to columnar calcite crystals. In LC concretions, 4mm by 0.6mm columnar crystals dominate, associated with minor equant calcites (150-300μm), and radiate out over 180° from a central point at the base of the concretion (Fig. 4.20b & 4.21a). Although individual crystals are small, the overall structure of LC concretions is of large, radiating columnar calcites, centimetres in length. UNL concretions comprise radiating columnar calcites (1000μm by 600-800μm) alternating with columns, of similar size to the columnar crystals, composed of equant calcite (60-270μm) (Fig. 4.21b). Both concretion types have a gradational contact with

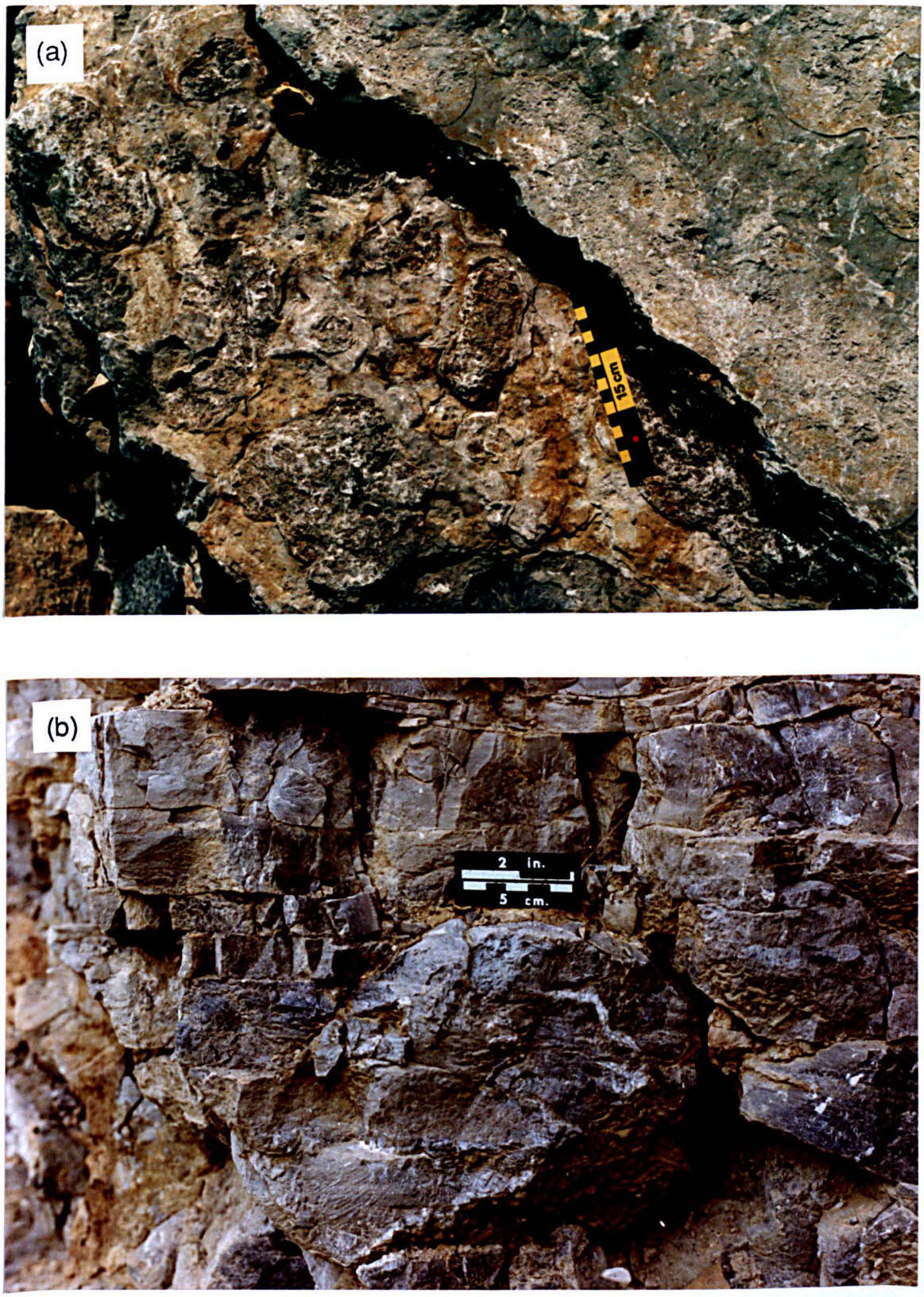

Fig. 4.19. Photomicrographs of LC concretions at outcrop; (a) Raisby Quarry, (b) Old Towns Quarry. (a) shows a plan view of a limestone bedding surface covered in very thin, flat, LC concretions. (b) is a side view of a much larger, sub-spherical concretion within limestone. Note fracturing of the concretion.

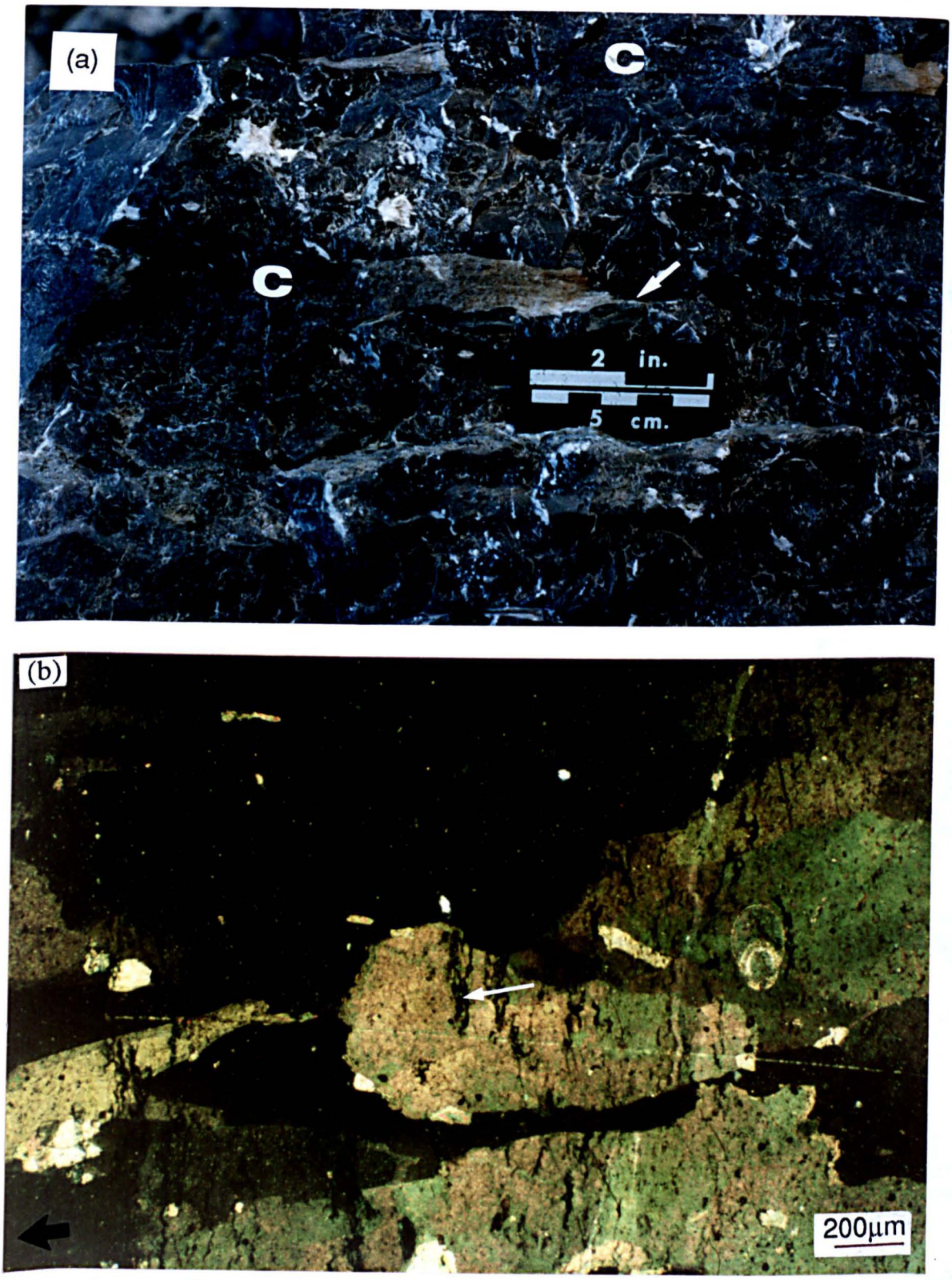

Fig. 4.20. Photomicrographs of LC concretions. (a) side view of concretions within limestone, Raisby Quarry. The concretions (C) are almost indistinguishable from their host limestone. They pass laterally into porous dolostones (brown coloured), which themselves pass into thick stylolites (arrowed). (b) photomicrographs of an LC concretion, thin section crossed polars. Note abundant streaks of organic matter (arrowed) and a foraminifer, all enclosed by coarse concretion calcite crystals (arrow indicates way up).

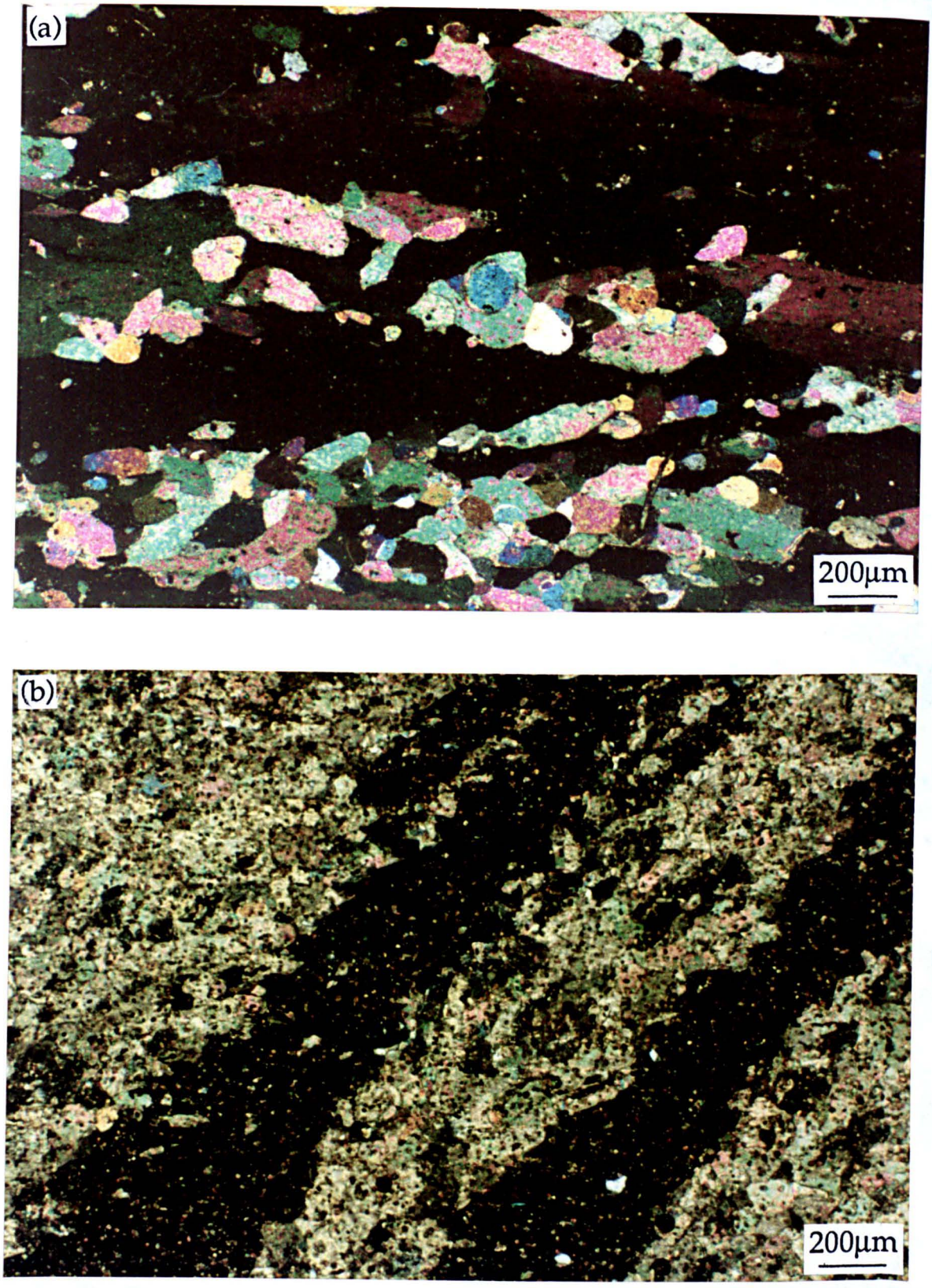

Fig. 4.21. Thin section photomicrographs of concretions, crossed polars; (a) an LC concretion, Raisby Quarry, (b) a UNL concretion, Raisby Quarry. (a) shows numerous equant calcite crystals inbetween coarser columnar calcites (in extinction). The basic structure is similar in (b) although the distinction between single columnar calcite crystals and columns of equant calcites is more strongly developed.

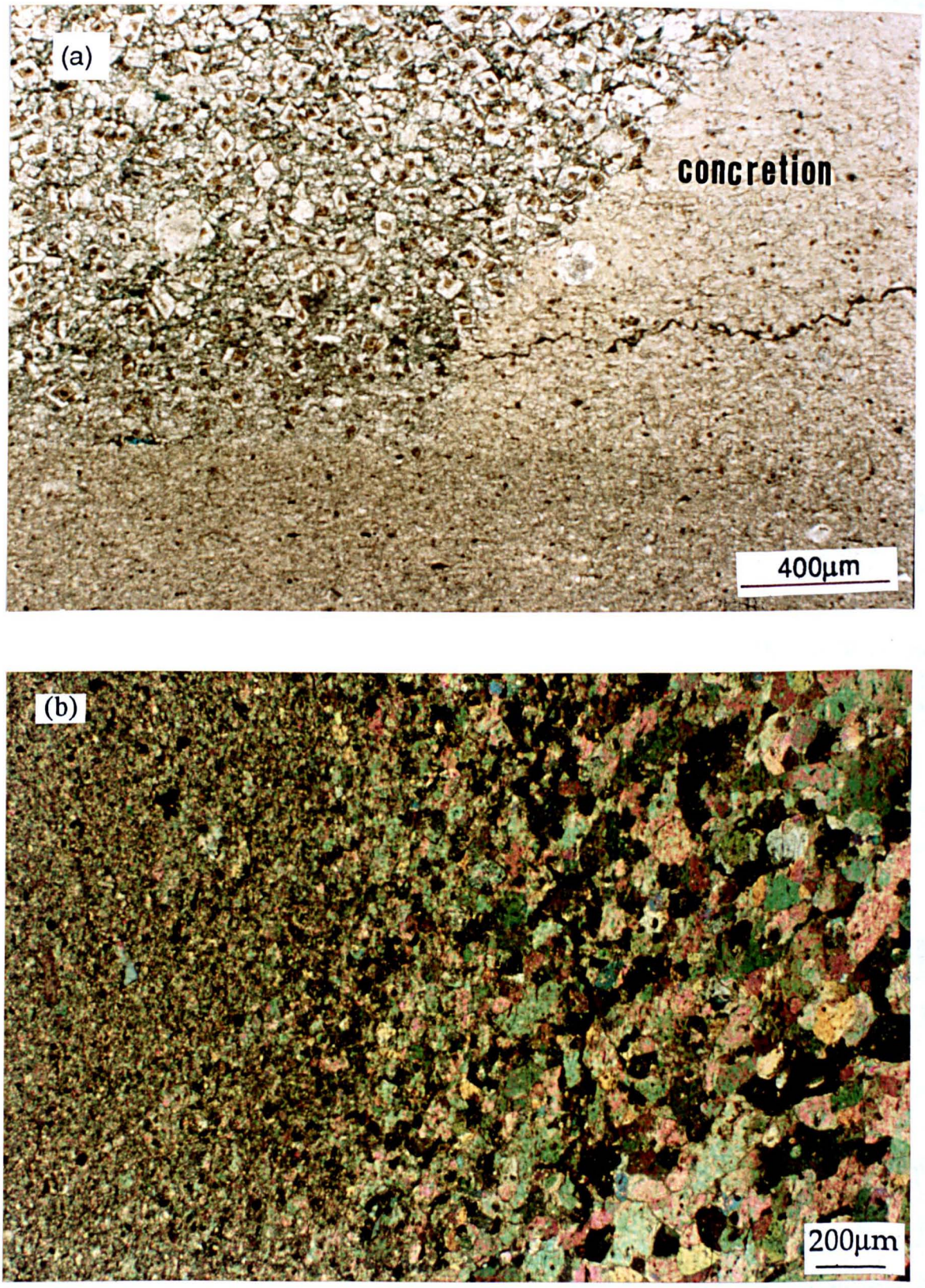

Fig. 4.22. Thin section photomicrographs of the contact between an LC concretion and underlying limestone nodule; (a) plane light, (b) crossed polars. (a) illustrates the contact between concretion, limestone nodule and dolostone. (b) shows the gradational nature of this contact between equant calcite at the base of the concretion and calcite microspar of the limestone nodule. Note, both concretions are stylolitized close to their base.

the underlying limestone via a decrease in crystal size from columnar to coarse equant, to finer equant (Figs. 4.22a & b). The calcite of both types is light brown in transmitted light and pseudo-pleochroic. Individual columnar crystals show a weak undulose extinction and adjacent columnar crystals have a similar extinction position (Fig. 4.21a & b), producing a sweeping extinction pattern within a concretion overall. The equant crystals show no such preferred crystallographic orientation. The calcite stains pink and luminesces a blotchy dull orange with no zonation. LC concretion calcite crystals luminesce brighter orange than their host limestone.

Calcite crystals of both concretion types poikilitically enclose numerous inclusions. Dolomite is most common, and considerably more abundant within UNL than LC concretions (Figs. 4.21a & b, 4.24a & b). In both types, dolomite inclusions have a planar-P texture and are 15-30μm in size. In LC concretions, the dolomite is commonly corroded and hollow centred , although not in UNL concretions (Fig. 4.24b). There is negligible dolomite in limestones adjacent to the concretions (Fig. 4.22a).

Fossils are common within both types of concretion, in a similar diversity and abundance as in associated limestones (Chapter 2). Skeletal structures of originally LMC fossils (brachiopod and bryozoan fragments, calcispheres and ostracodes) are well preserved, commonly better so than in adjacent limestones. Intraskeletal porosity-occluding calcite cements are also preserved intact, together with intraskeletal pyrite framboids (Figs. 4.23a & b). Within some fossils, intraskeletal cements are replaced by inclusion-rich concretionary calcites, although pyrite framboids normally remain floating. Echinoderm fragments retain their original inclusion-rich texture and are commonly enclosed by a single concretionary calcite crystal, with which they are in optical continuity. Foraminifers (probably originally aragonitic) have had their skeletons dissolved, and the resultant porosity cemented by coarse, zoned, inclusion-free calcite with a different trace element composition to host concretionary calcite (Figs. 4.24a & b, 4.25a & b). However, carbonate mud originally filling intraskeletal pores of the foraminifers has been preserved, neomorphosing to microspar (Figs. 4.24a & b). Skeletal material within concretions, including calcite cemented pores after foraminifers are commonly draped by original sediment laminae, suggesting considerable compaction predated concretion formation (Fig. 4.24b).

Non-carbonate inclusions within concretion calcite comprise fine-grained siliciclastic material, including quartz (mean 20μm) and muscovite (mean 100μm), the latter in original bed parallel orientation. Non-fossil associated pyrite framboids are common in bed parallel layers. Black, isotropic organic matter also occurs in thin, bed parallel 'streaks' up to 850μm long (Fig. 4.26). All of this material is also very common within limestones at Raisby Quarry, with the exception of the organic matter which is considerably more abundant within the concretionary calcite.

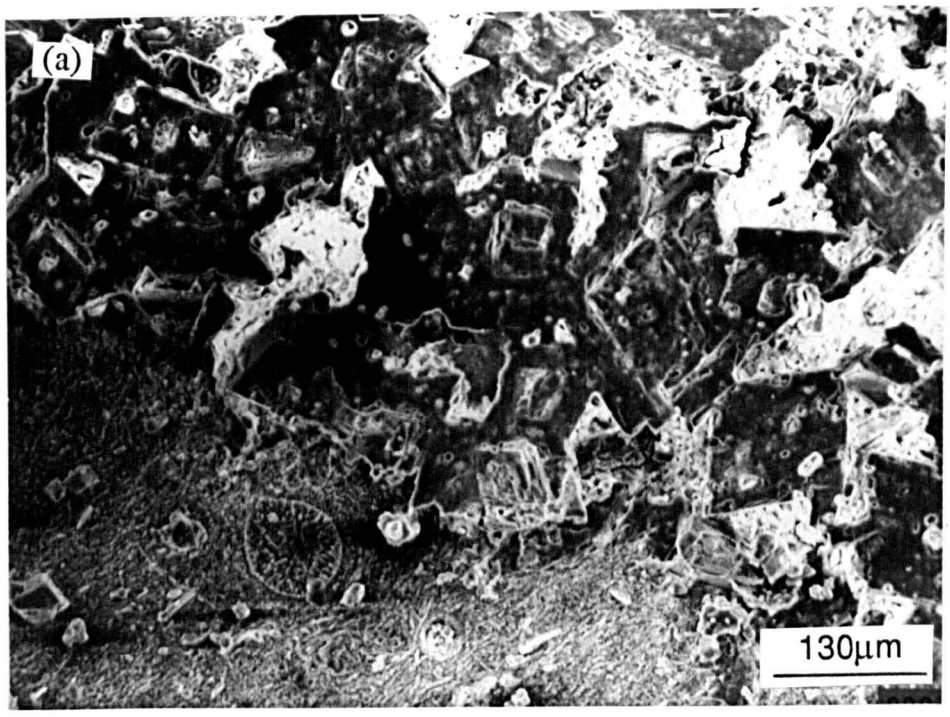

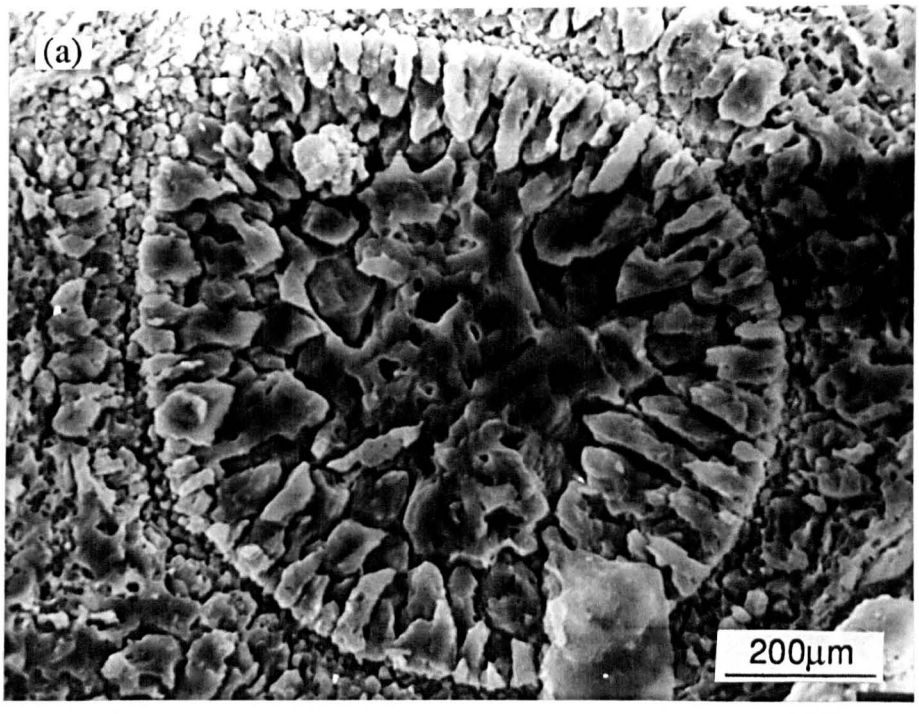

Fig. 4.23. SEM photomicrographs of the margin of an LC concretion, Raisby Quarry (etched in hydrochloric acid). An ostracode is enclosed close to the contact of the concretion with host dolostone (a), shown in detail in (b). The calcite which occludes the ostracode intraskeletal porosity has well developed para-axial cement fabrics (b).

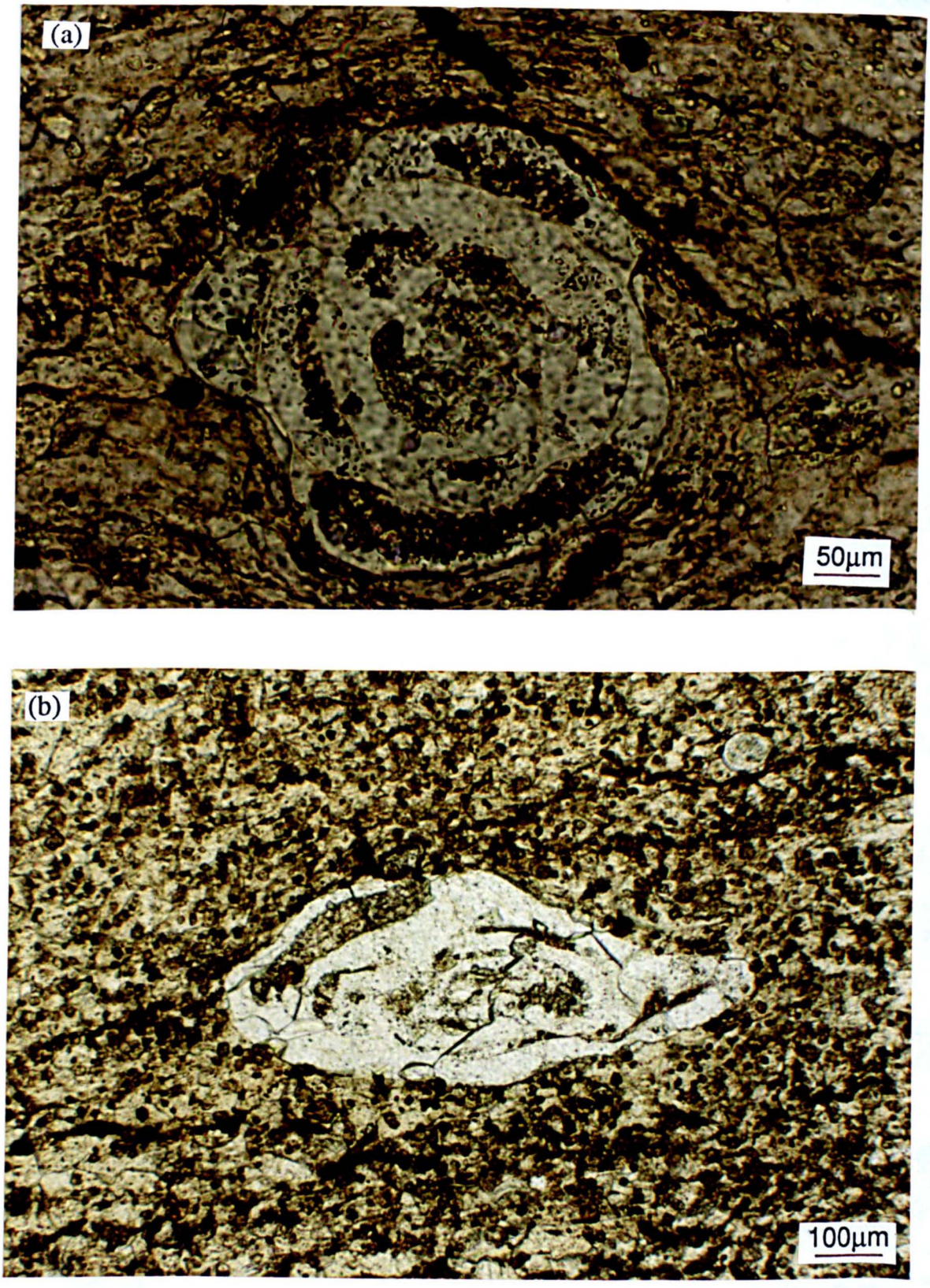

Fig. 4.24. Plane light, thin section photomicrographs of foraminifer moulds within an LC concretion (a) and UNL concretion (b), Raisby Quarry. In both, carbonate mud which filled original intraskeletal pores has neomorphosed to microspar. Original sediment laminae have compacted around the fossils, much more marked in (a) than (b).

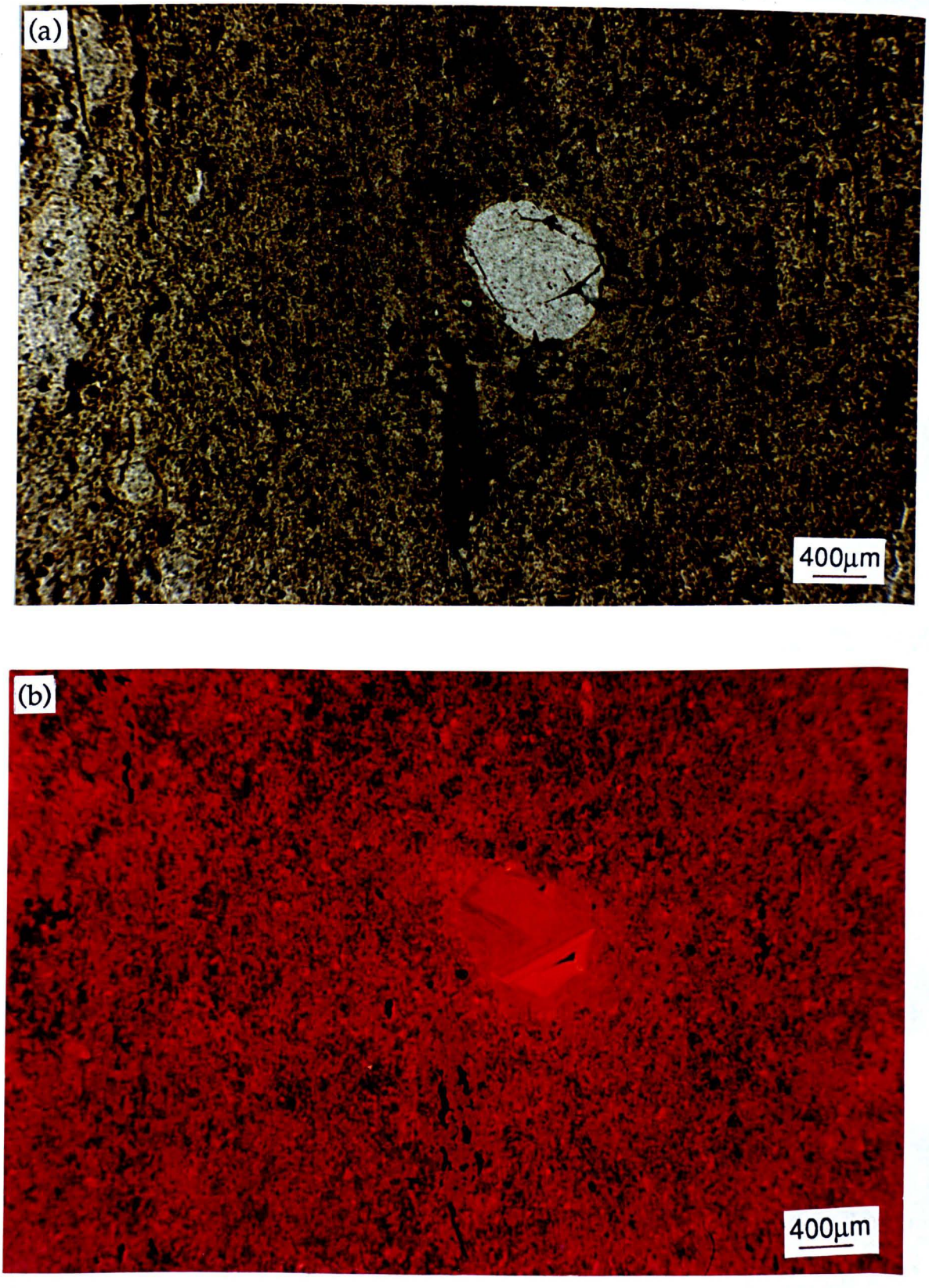

Fig. 4.25. Thin section photomicrographs of a foraminifer mould within an LC concretion, Raisby Quarry; (a) plane light, (b) luminescence. Note the very speckled luminescence of concretion calcite which contrasts with clear zoned cements filling the foraminifer mould.

Fig. 4.26. Plane light thin section photomicrograph of streaks of organic matter within an LC concretion, Raisby Quarry.

4.4.1.2. Geochemistry of calcite concretions - Description

Geochemically, both concretion types comprise low magnesian, non-ferroan calcite (Table 4.2). The elevated Mg content of UNL concretions (Table 4.2) reflects inclusion of 7.1% to 44.5% stoichiometric dolomite. The Mg content of LC concretions also probably reflects minor dolomite inclusion, although comparison of mean microprobe and ICP data (Table 4.2) suggests that this is less than a total 0.6% of stoichiometric dolomite on average. The mean Sr content of LC and UNL concretions (Table 4.2) is less than that of Raisby Quarry limestones, although values are similar to limestones from other localities within the Raisby Formation (Table 4.1). The low Sr content of UNL concretions in part reflects inclusion of dolomite with a lower Sr concentration than the concretionary calcite. If a stoichiometric dolomite of 100ppm Sr is assumed to be that in the UNL concretions, the pure UNL concretion calcite would then contain a mean of 257ppm Sr (Appendix VII). Both the Fe and Mn concentration of LC concretions is greater than Raisby Quarry limestones and most analyses from other localities within the formation. Correction of the Mn content of UNL concretions for Mn in the dolomite (assuming a mean dolomite composition of 330ppm Mn) gives similar concentrations to Mn in the LC concretions.

When plotted against Sr and Mn, Raisby Quarry LC concretions lie almost exactly along the geochemical trends described by increasing openness of the diagenetic system during limestone neomorphism (Fig. 4.27). They plot in the low Sr, high Mn part of the graphs, interpreted to represent most open system neomorphism for the limestones. A traverse through an LC concretion shows a well developed trace element and isotope zonation, with decreasing Mg, Sr and Mn away from the limestone substrate (Fig. 4.28). No clear zonation was recorded within UNL concretions, owing to heterogeneties imposed by dolomite inclusion. In one UNL concretion sample, an increase in the concentration of dolomite was recorded from limestone nodule through concretion into host partially dolomitized limestone (Fig. 4.29). Non-carbonate trace elements occur in similar concentration between the two concretion types, although UNL concretions have greater Al_2O_3 than LC (Appendix VII). The non-carbonate trace element and insoluble residue values for concretions are in turn similar to those within limestones (Appendix VII).

Carbon and oxygen stable isotope analyses are similar between the two concretion types, clustering around an area with moderate positive $\delta^{13}C$ and moderate negative $\delta^{18}O$ (Fig. 4.30). These values are in turn similar to those from the Raisby Quarry limestone, and other concretions analysed from Zechstein carbonates at outcrop in northeast England by Clark (1980) and the Ford Formation main reef by Aplin (1981) (Fig. 4.30). When compared to isotope data of enclosing limestones from Raisby Quarry, LC concretions plot very close to the limestones for Sr versus $\delta^{13}C$ and $\delta^{18}O$ (Fig. 4.31).

LC concretion		
-ICP (n=7)		$Ca_{(97.96)}(Mg_{(1.55)}Fe_{(0.24)}Mn_{(0.21)}Sr_{(0.05)})CO_3$
-Isotope (n=3)	$\delta^{13}C = 4.8‰$	
	$\delta^{18}O = -5.9‰$	
LC concretion		
-Microprobe (n=14)		$Ca_{(98.22)}(Mg_{(1.28)}Fe_{(0.37)}Mn_{(0.14)})CO_3$
UNL concretion		
-ICP (n=22)		$Ca_{(92.16)}(Mg_{(7.45)}Fe_{(0.25)}Mn_{(0.12)}Sr_{(0.03)})CO_3$
-Isotope (n=2)	$\delta^{13}C = 4.7‰$	
	$\delta^{18}O = -5.8‰$	
Scalenohedral calcite		
-ICP (n=1)		$Ca_{(98.67)}(Mg_{(0.99)}Fe_{(0.15)}Mn_{(0.19)}Sr_{(0.01)})CO_3$
-Isotope (n=1)	$\delta^{13}C = 2.9‰$	
	$\delta^{18}O = -11.3‰$	
Dull orange-luminescent scalenohedral calcite		
-Microprobe (N=5)		$Ca_{(98.03)}(Mg_{(0.92)}Fe_{(0.72)}Mn_{(0.33)})CO_3$
Bright orange-luminescent scalenohedral calcite		
-Microprobe (n=6)		$Ca_{(98.52)}(Mg_{(1.04)}Fe_{(0.14)}Mn_{(0.3)})CO_3$
HC dolomite		
-Microprobe (n=7)		$Ca_{(53.8)}(Mg_{(43.3)}Fe_{(2.7)}Mn_{(0.2)})CO_3$
SO dolomite		
-Microprobe (n=7)		$Ca_{(53.4)}(Mg_{(38.7)}Fe_{(7.3)}Mn_{(0.6)})CO_3$
Inter-concretion dolomite (HC and SO)		
-ICP (n=1)		$Ca_{(53.53)}(Mg_{(39.1)}Fe_{(6.17)}Mn_{(0.19)}Sr_{(0.01)})CO_3$
-Isotope (n=1)	$\delta^{13}C = 4.3‰$	
	$\delta^{18}O = -6.3‰$	
Partially calcitized inter-concretion dolomite		
-ICP (n=1)		$Ca_{(67.24)}(Mg_{(29.04)}Fe_{(3.18)}Mn_{(0.57)}Sr_{(0.01)})CO_3$

Table 4.2. Summary of the mean chemical compositions of Raisby Quarry concretions and associated diagenetic components. Where more than one sample was analysed, the value given is an arithmetic mean.

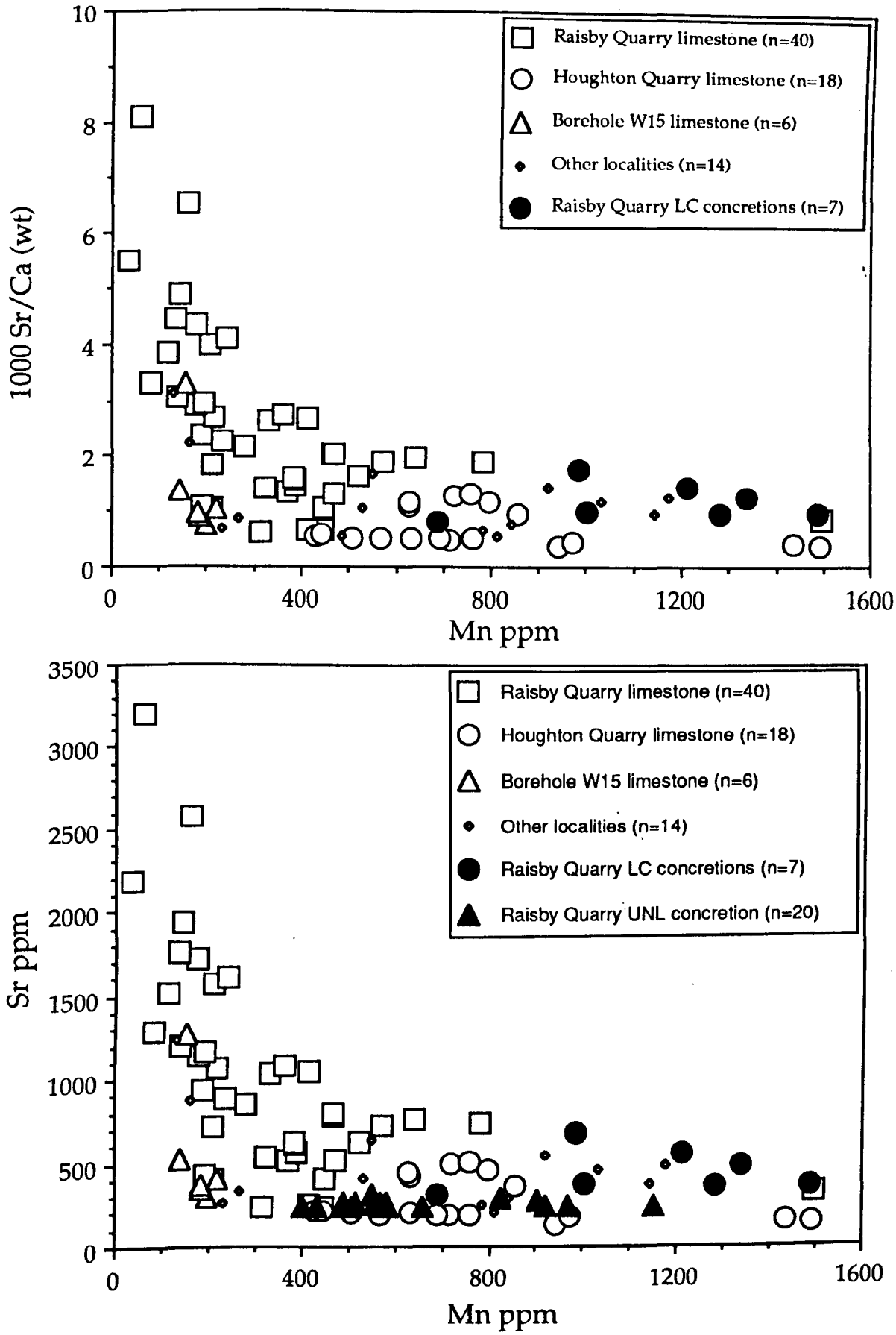

Fig. 4.27. Graphs illustrating the geochemistry of LC and UNL concretions related to the composition of limestones within the Raisby Formation. The Sr and Mn data for UNL concretions is corrected for dolomite content. Analysed by ICP.

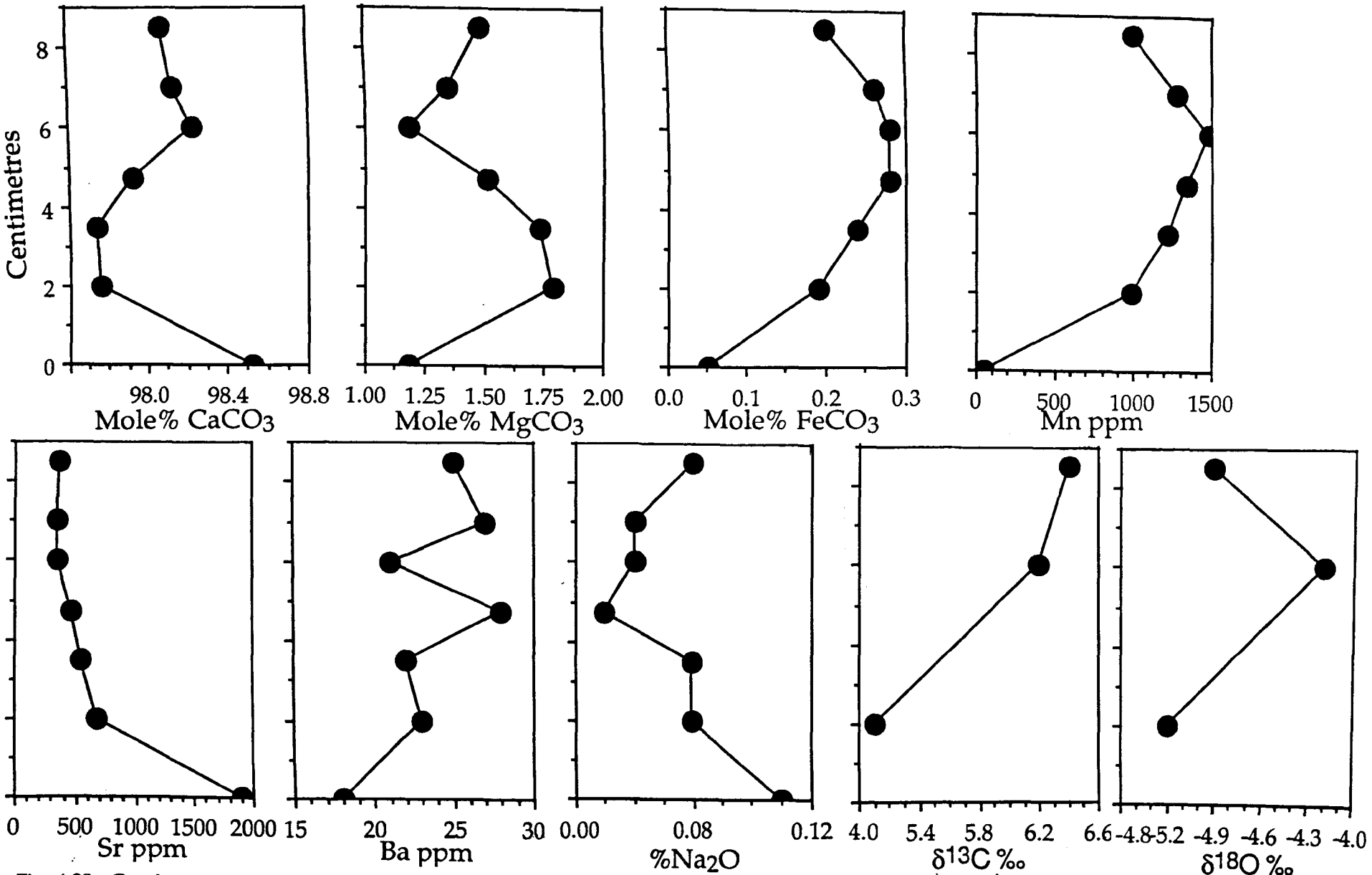

Fig. 4.28. Graphs showing the geochemical variation along a traverse from the base (0cm) to the margin (8.8cm) of a hemispherical LC concretion, Raisby Quarry. Analysed by ICP.

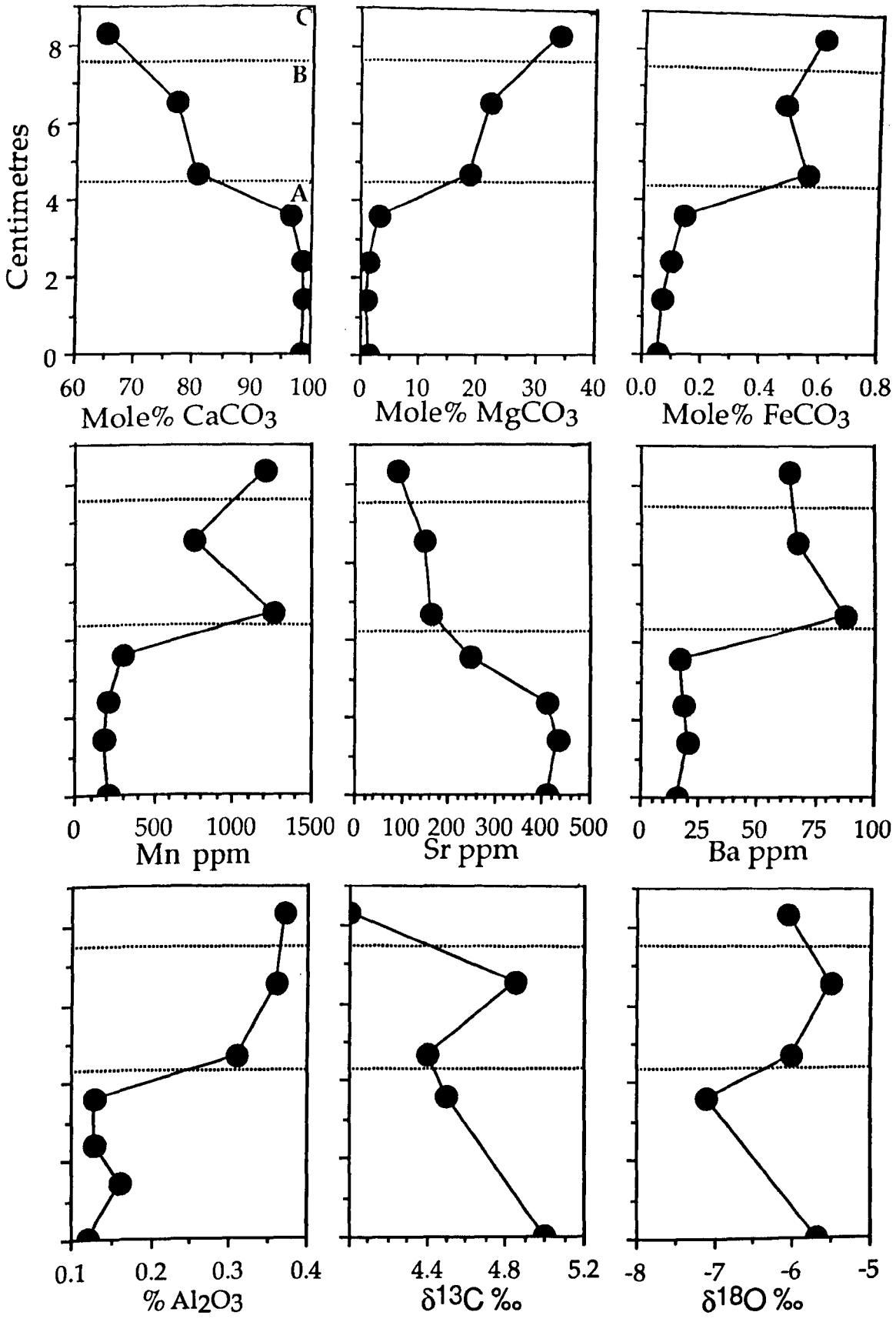

Fig. 4.29. Graphs illustrating the geochemical variation along a traverse from a limestone nodule (A) through UNL concretion (B) into partially dolomitized limestone (C), Raisby Quarry. Analysed by ICP.

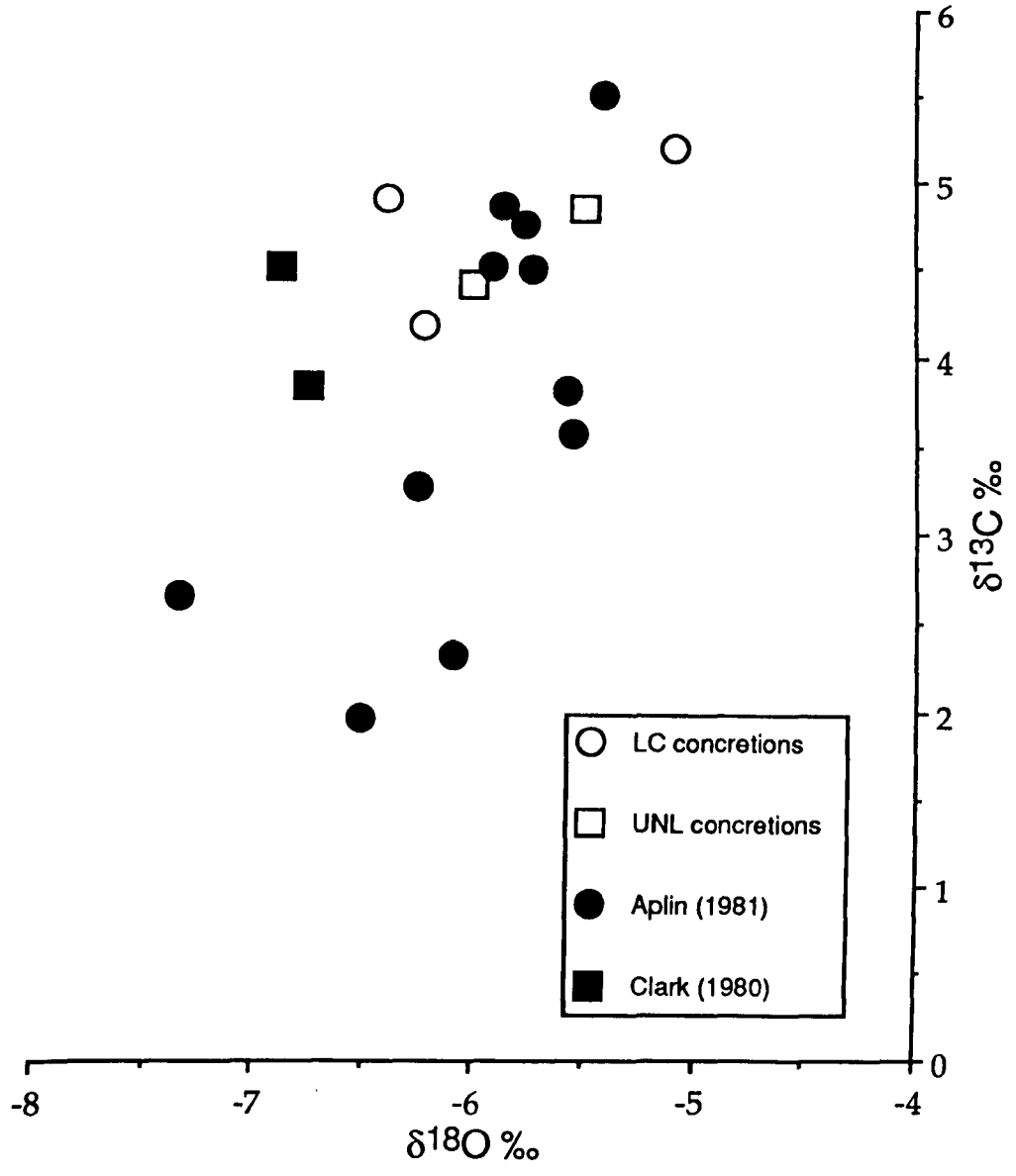

Fig. 4.30. Graph comparing the isotopic composition of Raisby Formation LC and UNL concretions with concretions analysed from within Z2 and Z3 carbonates at outcrop in northeast England (Clark, 1980) and the Ford Formation main reef (Aplin, 1981).

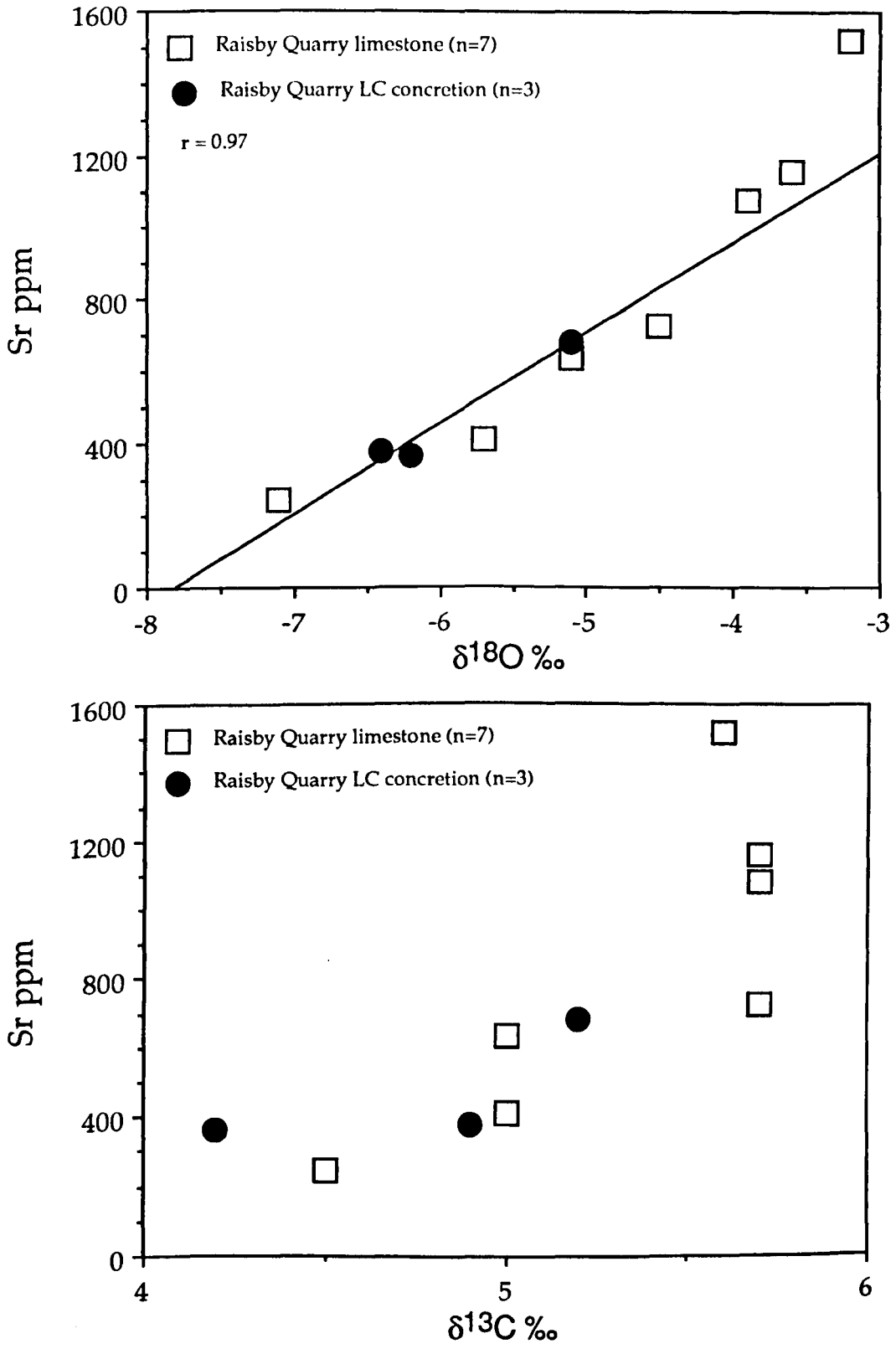

Fig. 4.31. Graphs showing the geochemical correlation between LC concretions and limestones from Raisby Quarry (compare fig. 4.9). Although a regression line has been fitted to the upper graph, the correlation is better represented as a curve rather than a straight line. The same is true for the lower graph.

4.4.1.3. Petrography and geochemistry of concretion-associated diagenetic components - Description.

LC concretions are commonly fractured (Fig. 4.19b), and those from Raisby Quarry are associated with two fracture episodes. The first phase of fracturing cuts limestone nodules normal to their outer surface. The fractures are occluded by former marine (probably HMC) cements (3.3.2), and formed by compaction of brittle limestone nodules within more ductile host carbonates during early burial. The lower part of concretions or overlying dolomite may occupy the upper part of fractures. Isolated limestone nodules, LC concretions and phase 1 fractures are all cut by a second phase of randomly orientated, angular fractures. They are partly cemented by coarse ferroan dolomite and partly by coarse, zoned inclusion-free calcite cements (Fig. 4.32), whose zonation pattern is similar to that of calcite which occludes foraminifer moulds (Figs. 4.25b & 4.32b). Sutured seam stylolites (up to 2mm amplitude) dissect concretions (commonly along their contact with limestone) (Fig. 4.22a & b) and also cut phase 2 fractures.

The contact of both concretion types with host dolostones is frequently abrupt with little evidence for replacement of concretion by dolomite, or dolomite by concretionary calcite (Figs. 4.22a & 4.34). The host dolostone at Raisby Quarry has a planar-S texture with 300μm crystals and stains a strong turquoise blue. The dolomite crystals themselves were precipitated in two distinct phases (Fig. 4.33a & b). Phase 1 (hollow centered [HC]) dolomite crystals are isolated, planar-P (mean 20μm), brown in colour, dully luminescent, and commonly hollow centred (Fig. 4.33a & b). They are similar petrographically to dolomite within LC and UNL concretions. HC dolomite is syntaxially overgrown, and poikilitically enclosed by coarse (mean 260μm), inclusion-poor, planar-P, non-luminescent dolomite crystals (syntaxial overgrowth [SO] dolomite) (Fig. 4.33a & b). Leaching of HC dolomite predated the precipitation of SO dolomite (Fig. 4.33b). SO dolomite also partially occludes phase 2 fractures cutting concretions. It shows concentric zoning in backscattered electron imaging. The dolostone adjacent to a concretion may be tightly interlocking or have an appreciable intercrystalline porosity, in general adjacent to the larger concretions (Fig. 4.34a & b).

The two dolomite phases are geochemically distinct (Table 4.2). SO dolomite is considerably more ferroan than HC, some zones reaching ankerite in composition, and is classified as a 'ferroan dolomite cement' (5.2.3). HC dolomite has a higher Fe/Mn ratio than SO dolomite, and is classified as a ferroan 'finely crystalline replacive' (FCR) dolomite (5.2.1). Both dolomite types are non-stoichiometric (Table 4.2). One ICP analysis (which mainly comprised the SO dolomite) showed low Sr relative to most dolostones within the formation (Table 4.2) (5.3.3). The $\delta^{13}C$ of the dolomite (again mainly SO) is similar to that of the concretions, Raisby Formation limestones and dolostones, although the $\delta^{18}O$ is considerably depleted (Table 4.2).

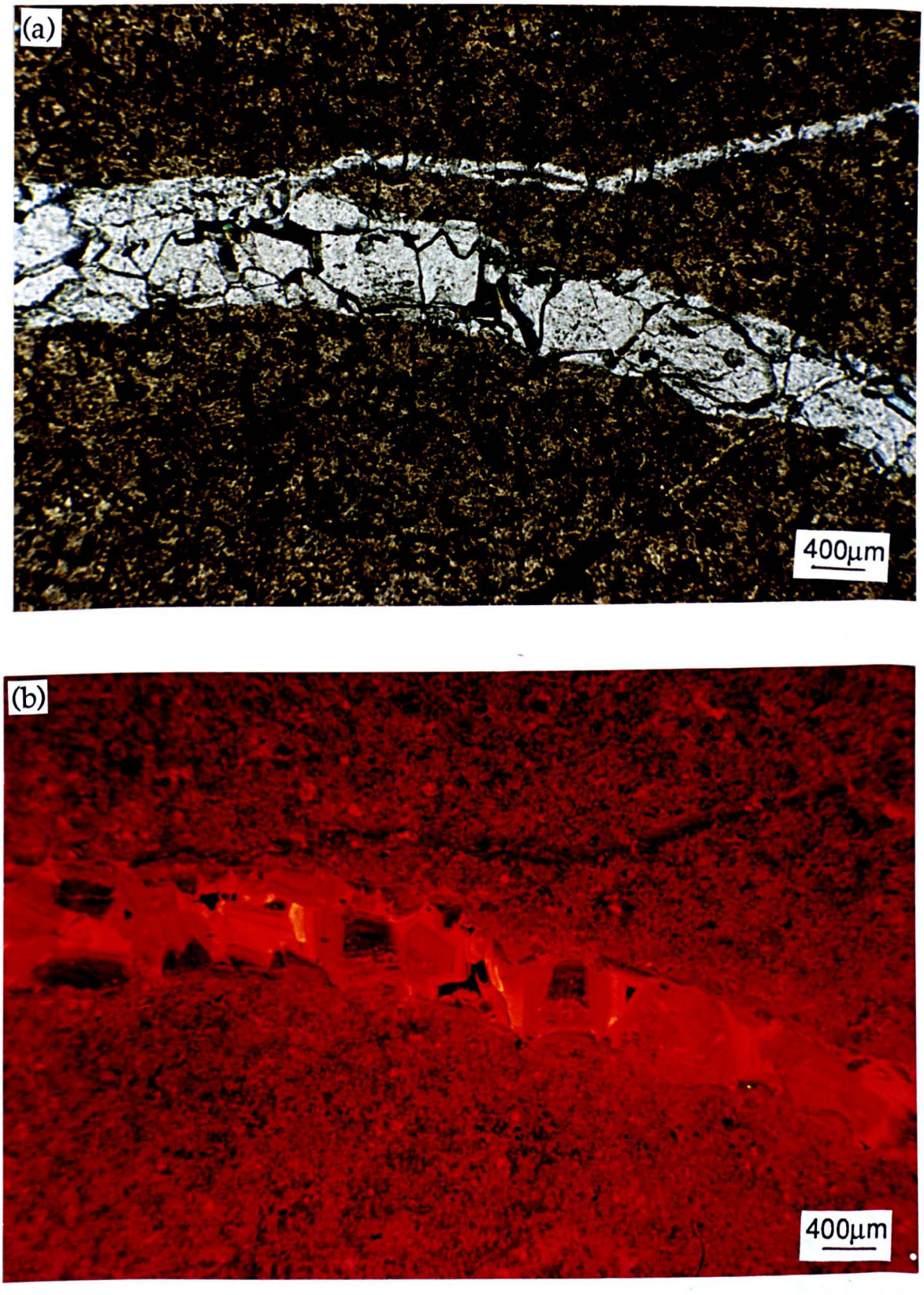

Fig. 4.32. Thin section photomicrographs of a phase 2 fracture cutting an LC concretion, Raisby Quarry; (a) plane light, (b) luminescence. Note the similarity of luminescence stratigraphy of the fracture-filling calcite cement with that occluding a foraminifer mould (Fig. 4.25).

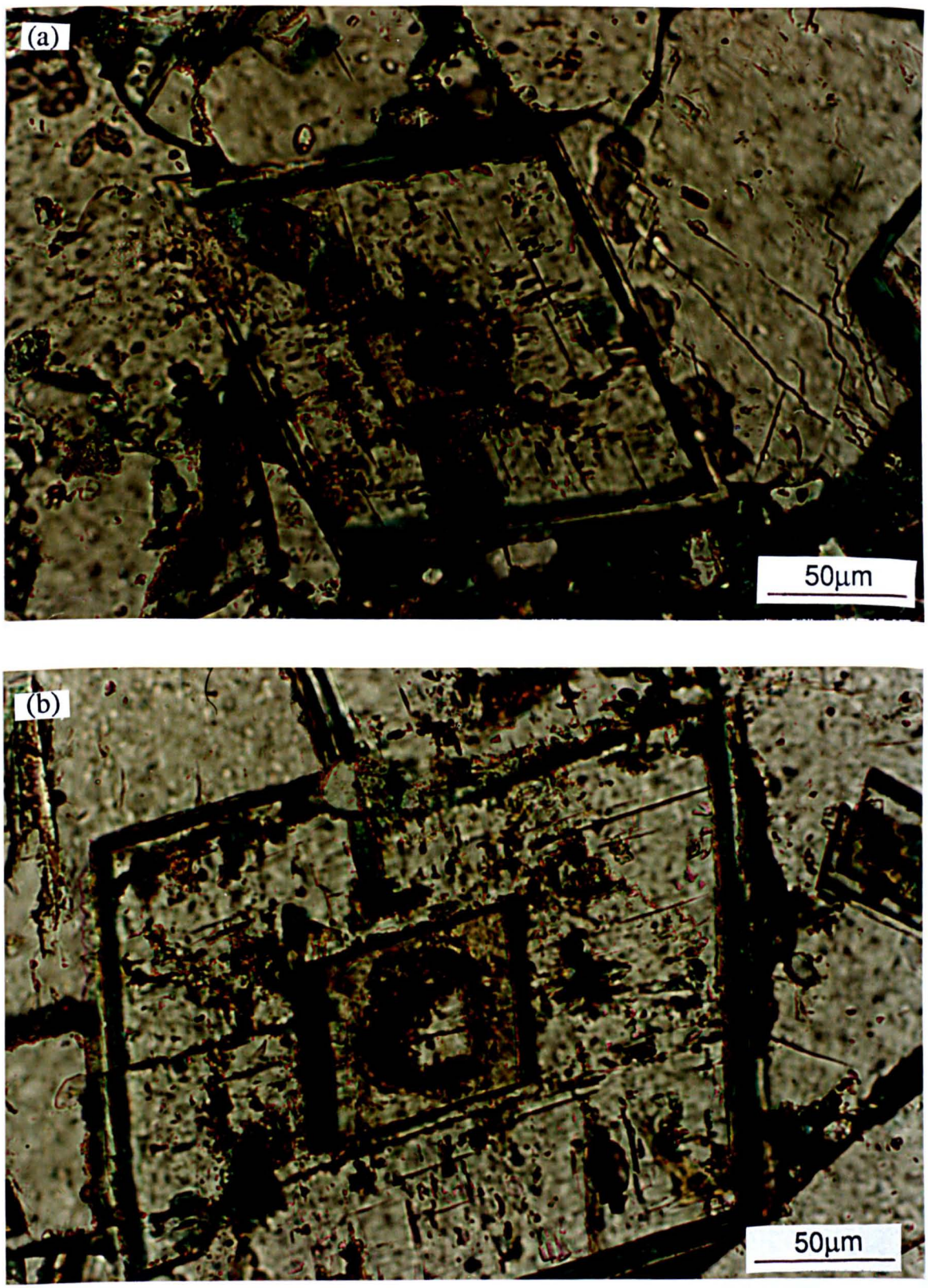

Fig. 4.33. Plane light thin section photomicrographs of dolomite adjacent to an LC concretion, Raisby Quarry. Two phases of dolomite are clearly developed, with a clear overgrowth enclosing hollow centred brown-coloured dolomite crystals.

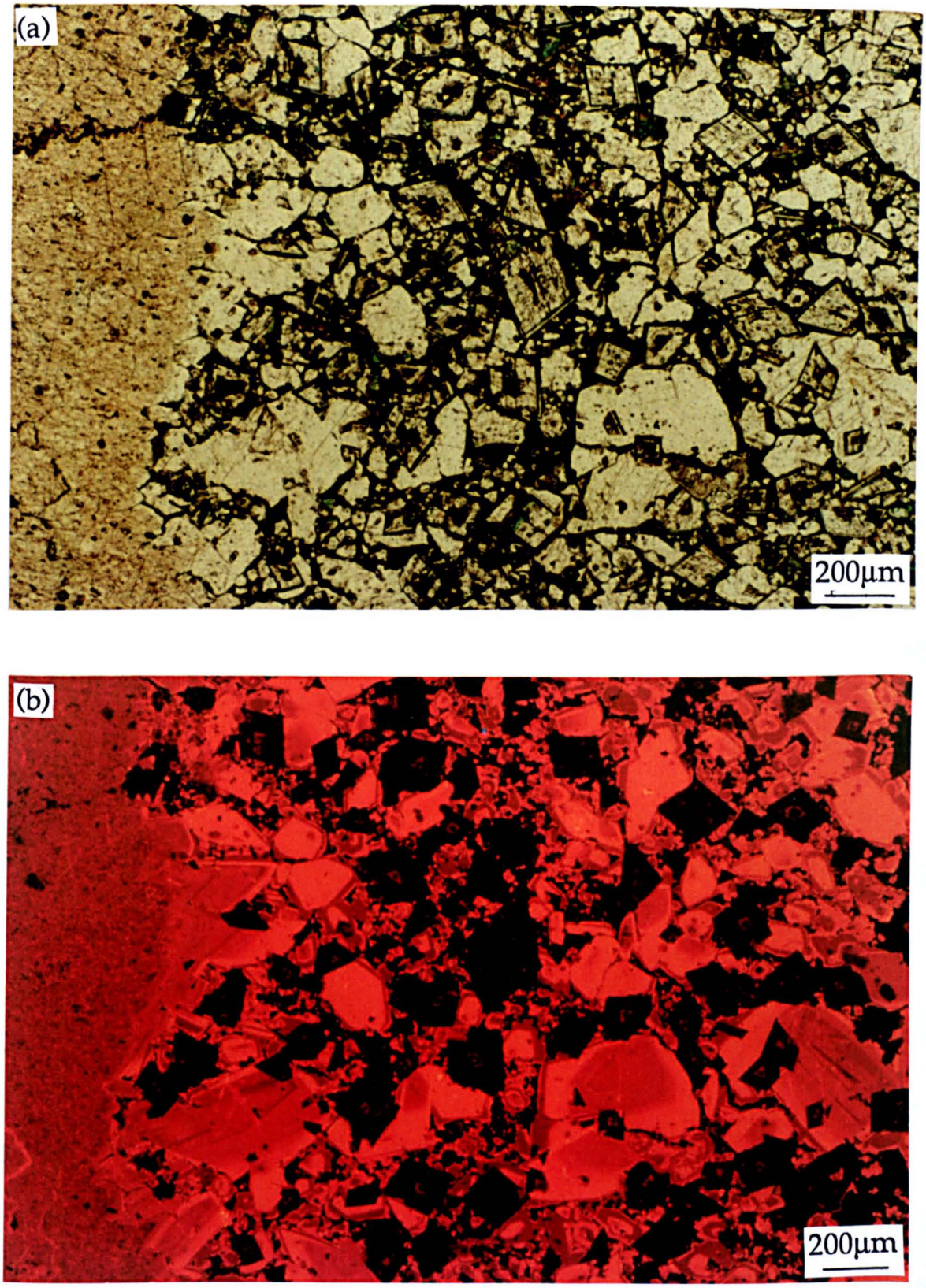

Fig. 4.34. Thin section photomicrographs of calcite adjacent to an LC concretion, Raisby Quarry; (a) plane light, (b) luminescence. Coarse zoned scalenohedral calcite has both overgrown the terminations of concretion calcite crystals and has also grown from within the dolostone itself. Note, the dolomite is zoned in luminescence (b).

At the contact of some LC concretions with dolostones of a high intercrystalline porosity, a very complex diagenetic history is evident. The terminations of columnar concretion crystals are syntaxially overgrown by clear, coarse calcite (up to 400μm), concentrically zoned (Fig. 4.34a & b). The zonation pattern is comparable to that of calcite cements which occlude phase 2 fractures and foraminifer moulds (Figs. 4.25b & 4.32b). The geochemistry of these cements correlates well with luminescence, and shows that most luminescence variation is due to variation in Fe content of the cements (Table 4.2). One ICP analysis showed that the calcite has a moderate Sr (greater than dolomite, less than concretions) (Table 4.2). Isotopic data showed a similar $\delta^{13}C$ to that of the concretions and dolomite, although a considerable depletion in $\delta^{18}O$ (Table 4.2). The zoned calcite also occurs as isolated crystals within the host dolostones adjacent to concretions (Fig. 4.34b). They are of a highly variable size (20-700μm) and the larger crystals have a scalenohedral habit. There is a gradation from dolostones adjacent to concretions with no intercrystalline calcite (Fig. 6.33b) through dolostones with common intercrystalline calcite (as just described) (Fig. 4.34) through to areas which solely comprise an interlocking mosaic of coarse scalenohedral calcite with no dolomite. The contact between SO dolomite and scalenohedral calcite may be passive or interpenetrative. Where interpenetrative, the contact may be smooth, or more commonly step-like, controlled by the cleavage pattern within the dolomite (Fig. 4.35a). Heavily corroded dolomite crystals may also be completely enclosed within coarse scalenohedra. In all cases, the interpenetration and corrosion preferentially affects the SO over HC dolomite crystals.

Independent of its association with zoned scalenohedral calcite, the SO dolomite may also have an extensive dissolution porosity. The leaching postdates scalenohedral calcite precipitation. It may just affect one zone within the dolomite, or be of a much larger scale with in places, nearly the entire crystal being dissolved (Fig. 4.35b). SO dolomite was considerably more susceptible than enclosed HC crystals and the surrounding scalenohedral calcite to leaching (Fig. 4.35b). HC dolomite inclusions may be internally sedimented after intense leaching of the enclosing SO dolomite (Fig. 4.35b). Within tightly interlocking dolostones adjacent to concretions, the dolomite has not been leached, but iron oxide/hydroxides have precipitated along cleavages within the SO dolomite (Fig. 6.33 b). Again, the HC dolomite is largely unaffected. This process is most intense adjacent to pores within the dolostone, commonly after inclusions of organic matter (Fig. 6.33b).

Within porous dolostones, pyrite framboids, original detrital quartz and muscovite, well preserved microfossils, and organic lenses are common intercrystalline material. Authigenic clay minerals are also abundant. The clay forms bundles of relatively coarse, square-ended lath or platy-shaped crystals (Fig. 4.36) with low-order interference colours. Analysis by EDAX showed the clay is dominated by Si and Al, with minor K. Clay minerals postdate dolomite cementation and possibly some calcite precipitation. Small (less than

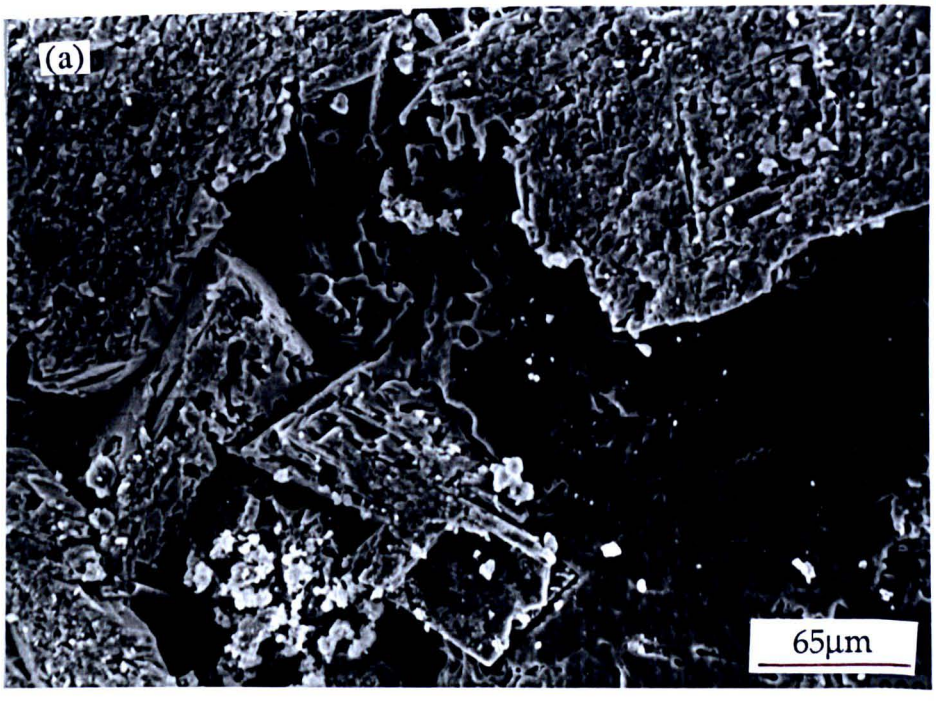

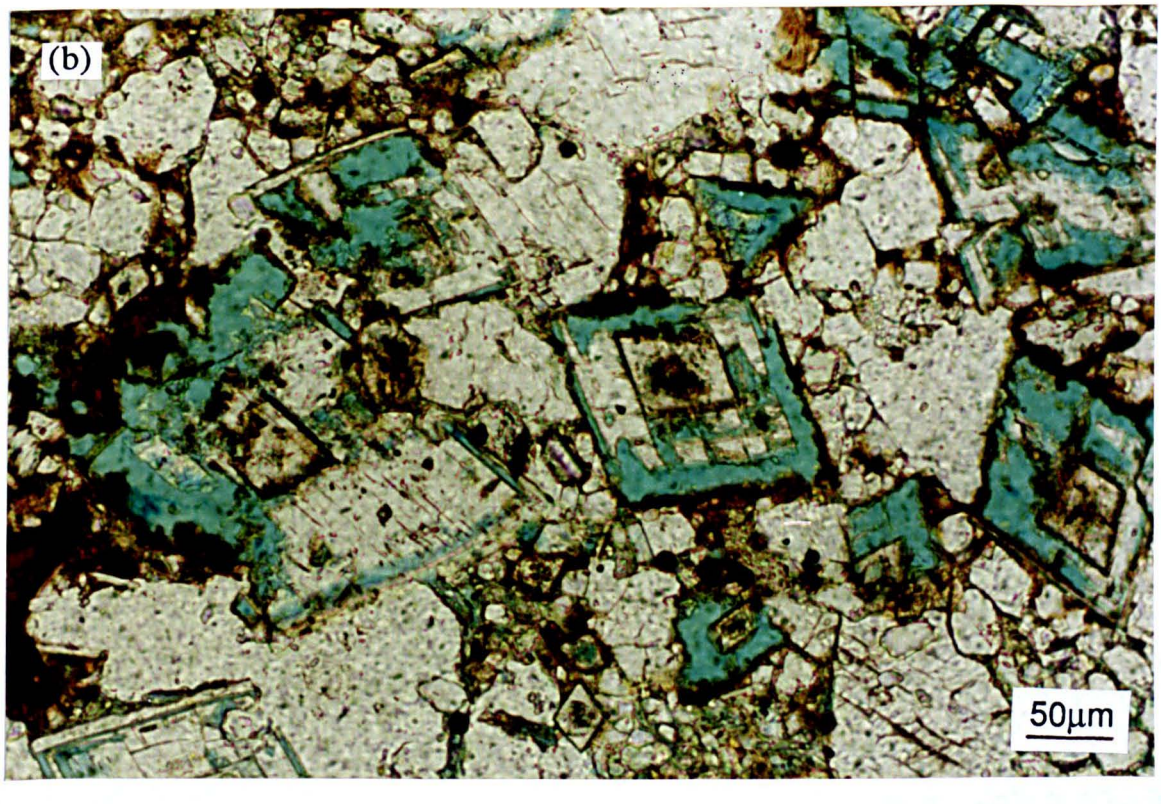

Fig. 4.35. Photomicrographs of dolomite marginal to an LC concretion, Raisby Quarry; (a) hydrochloric acid-etched SEM sample of clear zoned calcite overgrowing concretionary calcite and partially replacing zoned dolomite, (b) heavily leached dolomite rhombs within unaltered scalenohedral calcite crystals (blue is resin-filled porosity). Note that most dissolution has concentrated along zone and cleavage traces within the ferroan dolomite cement, although the less ferroan dolomite crystals are largely unaltered.

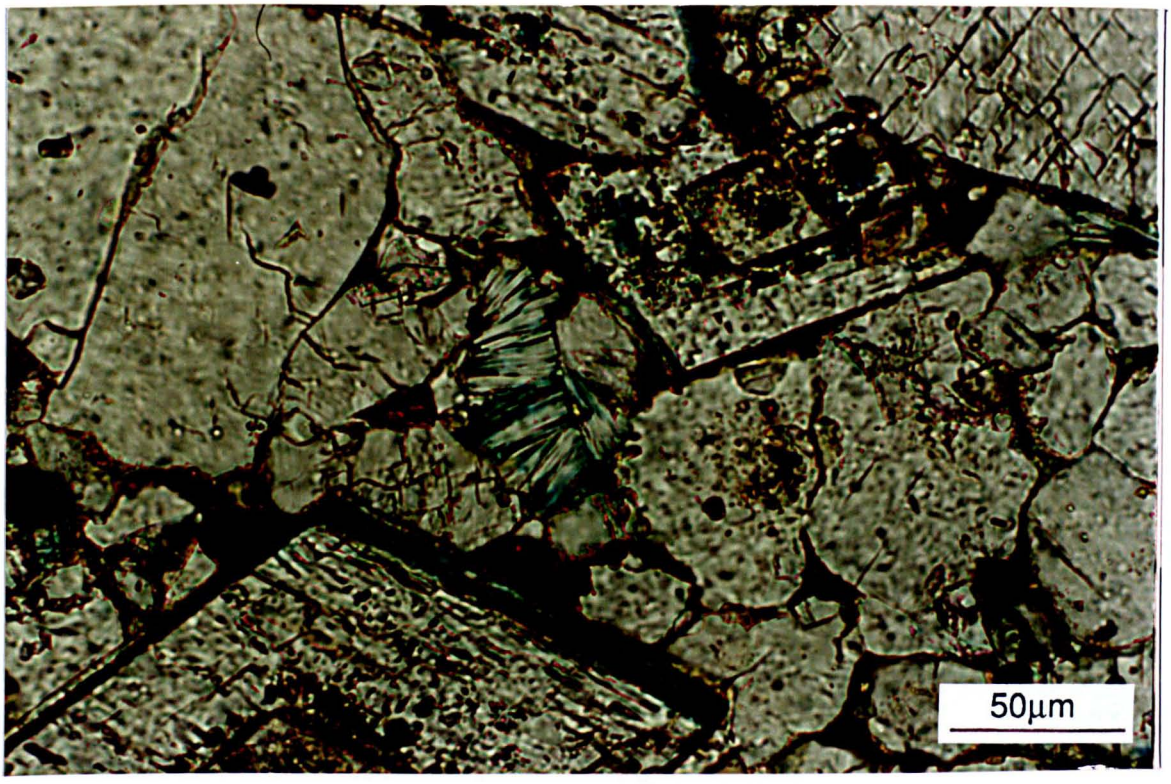

Fig. 4.36. Plane light thin section photomicrographs of kaolinite plates inbetween zoned scalenohedral calcite crystals, marginal to an LC concretion, Raisby Quarry.

20μm) crystals of authigenic hematite after euhedral pyrite/marcasite are also abundant. The crystals are rusty-brown in transmitted light, silver in reflected light, with small inclusions of relic gold-reflecting pyrite/marcasite. Most hematite crystals have hollow centers.

4.4.2. Petrography and geochemistry of calcite concretions - Interpretation

The origin of concretionary structures within Z2 and Z3 carbonates, very similar to those of the Raisby Formation have been ascribed to many different origins. These include calcitization of gypsum (Al-Rekabi, 1982), anhydrite (Shearman, 1971), calcitization of dolomite (Woolacott, 1919a; Clark, 1980; Tucker and Hollingworth, 1986; Braithwaite, 1988), and varied processes relating to recrystallization of calcite more or less in situ (Sedgwick, 1835; Garwood, 1891; Trechmann, 1914; Holmes, 1931; Tarr, 1933 and Aplin, 1985). Suggested timings for their formation are also diverse, from burial between 300-600m and 800-1200m (Clark, 1980), to uplift in the Permian (Aplin, 1985), Triassic (Braithwaite, 1988), or late Cretaceous/Tertiary (Tucker and Hollingworth, 1986). Morphologically very similar structures have also been described from the Carboniferous of Wales (Dixon and Wright, 1983), where they were interpreted as speleothem deposits, and of Belgium (Swennen *et al.*, 1981) where they were interpreted as calcitized gypsum. As they are geochemically and morphologically so similar, any interpretations of the concretions from the Raisby Formation cannot be divorced from those within other carbonates units.

The Raisby Quarry LC and UNL concretions formed within carbonates adjacent to limestone nodules and beds. These carbonates were ductile during at least some burial compaction, being injected into brittle fractures which cut limestone nodules, and also compacting around skeletal material. Concretion formation also postdates precipitation of marine cements within intraskeletal pores and early fractures, and postdates framboidal pyrite precipitation, both marine eogenetic (3.3.2). Some dolomitization (HC dolomite) also predated concretion formation, as unequivocally demonstrated by corroded HC dolomite rhombs incorporated within LC concretion calcite. Dolomitization was not total, and avoided skeletal material, as evidenced by the well preserved fossils. Aplin (1985) similarly explained well-preserved bryozoans within Ford Formation concretions. The intensity of dolomitization in pre-concretion carbonates was probably similar to that within partially dolomitized limestones adjacent to nodules in Raisby Quarry today (4.2.1). It is very unlikely that the precursor carbonate to concretions could have been near completely dolomitized except for the fossils. In the Raisby Formation and many other dolomite units, dolomitization is either partial (less than 30%) or total, very rarely nearly total (5.4.2). Stable isotopes do not allow differentiation of replaced dolomite from limestone in this case, as both Raisby Formation limestones and dolostones have very similar isotopic compositions. That the Sr concentration of concretions is higher than dolostones, and similar to some neomorphosed limestones however, suggests an aragonite/HMC precursor. To produce a

secondary, replacive precipitate with a higher Sr/Ca ratio than the original phase (dolomite), and given the very low partition coefficient of Sr into calcite, an almost/completely closed diagenetic system would be needed, or a more open system with a substantial concentration gradient of Sr from the bulk aquifer to concretionary calcite-dolomite reaction zones. This would be unlikely, as during limestone neomorphism at least, dLMC precipitated closest to equilibrium with the bulk aquifer only contained a few hundred ppm Sr (i.e., showing the bulk aquifer did not have very high Sr concentrations).

As the concretions did not wholly form by replacement of dolomite (dolomite in UNL concretions is well preserved), they must have formed by the replacement of partially dolomitized and non-neomorphosed carbonate. This pre-concretionary carbonate must have been uncemented when the associated limestone nodules were lithified, as it was injected into brittle fractures cutting the limestone. For the partially dolomitized carbonate to recrystallize, it must have been unstable, which suggests by analogy with the limestones, it was a mixture of aragonite and HMC carbonate mud. Formation of concretions by aragonite and HMC neomorphism would explain the well preserved LMC skeletal material, and the presence of still-aragonite foraminifers (Figs. 4.24 & 4.25). Garwood (1891) suggested that concretions in Z2 and Z3 carbonates originated by a solution-reprecipitation reaction analogous to molecular re-arrangement accompanying the transformation of aragonite to calcite in a mollusc shell. Tarr (1933) invoked fine scale solution-reprecipitation for the formation of Z2 and Z3 concretions in Sunderland, with calcite preferentially dissolving and reprecipitating over less soluble associated dolomite. However, although all of the Raisby Formation limestones have undergone extensive aggrading neomorphism to dLMC microspar, for some reason a concretionary texture has only been developed at Raisby and Old Towns Quarries.

That the concretions replaced only partially dolomitized carbonates also demonstrates a possible permeability control on their formation. As outlined in 4.2.2, the extent of dolomitization in the Raisby Formation was largely controlled by differential permeability of carbonate muds, the partially dolomitized muds representing less well-lithified carbonates. Partial dolomitization would accentuate any already-established permeability difference. This would explain why the junction of host limestone microspar with concretion calcite is gradational via a progressive increase in crystal size.

That the concretions comprise coarse calcite crystals poikilitically enclosing inclusions, suggests that they grew under conditions of low supersaturation, with growth faster than nucleation rates (Clark, 1980; Aplin, 1985; Braithwaite, 1988). Precipitation of the columnar calcite was most likely along a migrating solution film, a process outlined by Bathurst (1975). This produces no macroscopic porosity and so original textures are preserved. Different components of the limestone would have had different solubilities such that aragonite/HMC mud was most soluble, dolomite was relatively insoluble, as were

coarsely-crystalline LMC fossil fragments. Within concretions, equant crystals are common, much more so in UNL than LC. Where equant calcites occur isolated within LC concretion columnar crystals, they commonly surround fossil fragments (Fig. 4.21a), indicating that they were sites of preferential nucleation. The abundance of equant crystals in UNL concretions is probably due to the much higher density of dolomite inclusions (potential nucleation sites). Dixon and Wright (1983) describe petrographically extremely similar concretions, dominated by coarse columnar crystals, between which smaller equant calcites were common. They interpreted the equant calcites to be the products of dynamic recrystallization leading to crystal diminution (degrading neomorphism) along columnar crystal boundaries during burial diagenesis. Although this process cannot be ruled out, it is considered unlikely that the equant crystals formed later than columnar ones because:

1. Luminescence (and therefore Fe and Mn geochemistry) is identical between the two calcite crystal types,
2. Recrystallization would not be expected to retain inclusions (i.e., the equant calcite should be clear) unless dissolution and reprecipitation was on a very fine scale,
3. Equant crystals at the base of the concretions are identical to those within columnar crystals and conformably grade down into limestone nodule microspars.
4. Dixon and Wright (1983) suggest that these crystal dimminution features may be specific to fossil speleothems; the Raisby Quarry concretion are, without doubt, not fossil speleothems.

Formation of the radiating columnar habit of Raisby Formation concretions is problematical. The absence of regular inclusions shows that the columnar crystals are not after radial-acicular precursors. Bathurst (1975) describes 'radial fibrous' neomorphic calcite from the Dinantian of North Wales, comprising sub-spherical clusters of columnar neomorphic crystals which radiate out from a central mass of microspar. He attributes the coarse, radiating habit to preferential growth outwards, into as yet un-neomorphosed micrite. Braithwaite (1988) suggests that a radial columnar structure can be produced by competitive growth, with those crystals normal to the core body (i.e., bivalve) growing faster that tangential ones. However, such crystal growth processes are only operative during para-axial cement precipitation, not neomorphism (Kendall and Broughton, 1978).

Columnar crystals may also form owing to elevated growth rates on faces normal to the C- axis (Lahann, 1978). This may be due to lateral growth poisoning of faces parallel to the C - axis by Mg^{2+} (Folk, 1974), SO_4^{2-} or organic matter (Searl, 1989), or due to relatively elevated growth rates parallel to the C - axis. Given and Wilkinson (1985) suggest that elevated growth rates parallel to the C - axis are achieved by increased CO_3^{2-} or HCO_3^- supply in diagenetic environments where Ca^{2+} is normally more abundant that CO_3^{2-} or HCO_3^-. In the context of the Raisby Quarry concretions, elevated CO_3^{2-} may have come from reactions with organic matter, which is suggested as important in Z2 and Z3 concretion formation (Garwood, 1891; Trechmann, 1913, 1914, 1931; Woolacott, 1912, 1919a; Clark, 1980;

Braithwaite, 1988; A.C. Kendall and G.M. Harwood, *pers. comm.*, 1989). There are two possible processes:

1. Bacterial sulphate reduction or fermentation reactions with organic matter. Both Clark (1980) and Braithwaite (1988) invoke fermentation and sulphate reduction to supply bicarbonate anions to catalyse concretionary calcite precipitation. Carbon isotope values for the concretions however do not support these processes, which should produce extreme positive or negative values (Hudson, 1977). Less extreme isotopic values could result from buffering of organic-derived carbon by carbon from the dissolution of host limestones/dolostones. However, if buffering was important, by definition, organic-derived carbon would be of less importance than carbon from other sources, and so would not have a significant influence on calcite crystal growth.

2. Another anion may have substituted for CO_3^{2-}. One possible source is carboxylate anions ($RCOOH^-$) which are capable of bonding with Ca^{2+} (Mitterer and Cunningham, 1985). This mechanism is speculative. Carboxylate anions are the most likely interactive group of aspartic acid, which is the most common amino acid in modern carbonate sediments. Amino acids in turn, comprise more than 50% of organic carbon in modern carbonates (Mitterer and Cunningham, 1985). It is not known if the same was true in the Permian, although it is considered likely. Unfortunately, the isotopic composition of carboxylate anions is not known, although it could possibly be strongly negative.

Carbon isotope data for the concretions thus largely discounts extensive involvement of organic-derived carbon. The mean carbon isotope composition of the Raisby Quarry limestone samples is 5.3‰, whereas it is 4.75‰ for both types of concretions. Such a difference could be reconciled by incorporation of 1.75% of -25‰ $\delta^{13}C_{Org.}$ with 98.25% of 5.3‰ $\delta^{13}C_{Carbonate}$, which is probably insufficient to generate the columnar crystal growth. Carbon isotopes therefore suggest that the majority of concretion CO_3^{2-} was host rock-derived, which would be expected for a neomorphic calcite.

The exact reasons for the initiation of the radial-columnar fabric are therefore not known. Once the columnar crystals had started growing, however, they would have to continue growing radially outwards into the partially dolomitized carbonate mudstones, as that would be where the remaining aragonite/HMC was still located (Bathurst, 1975). Such a process would also tend to promote the growth of elongate crystals, as both cations and anions were being supplied to the C - axis face much faster than the side faces which were essentially enclosed within other columnar crystals.

The trace element geochemistry of the concretions is, in general, very similar to that of limestones from the Raisby Formation (Figs. 4.27 & 4.31). Graphs of Raisby Quarry concretions and Raisby Quarry limestones for Sr, Mn, $\delta^{13}C$ and $\delta^{18}O$ show a very good correlation, with the concretions at the 'most altered' end (Fig. 4.31). Likewise, if plotted against all Raisby Formation limestone Sr and Mn data, the concretions lie in the area of

most open system neomorphism of aragonite/HMC (Fig. 4.27). This suggests that the concretions formed in a geochemical environment similar to that of the Raisby Formation limestones, from a similar precursor, and probably at a similar time. However, location of the concretions at the low Sr/Ca, $\delta^{13}C$ and $\delta^{18}O$, high Mn (and Fe) area of the graphs suggests precipitation near to equilibrium with with the bulk aquifer fluids in a high water-rock ratio diagenetic environment. The trace element trends do not unequivocally demonstrate a close genetic and temporal association between concretion growth and limestone neomorphism, although the correspondence of isotope data with the more altered Raisby Quarry limestones, especially $\delta^{18}O$ (which should decrease in value with time [burial]), is extremely strong evidence for precipitation at a similar time to neomorphism from similar fluids. As with Raisby Formation limestone data (4.3.2.2), it is recognized that elevated Mn concentrations in the concretionary calcite could be due to contamination of the samples by pyrite, iron/manganese oxide/hydroxides and, possibly, organic matter. Although ICP data for LC concretions has a greater Fe concentration than microprobe analyses, it has a lower Mn concentration than microprobe (Table 4.2). Also, although the highest Mn concentration data may reflect contamination of pure concretionary calcite, this cannot explain the statistically significant correlations of Sr, $\delta^{13}C$ and $\delta^{18}O$ of Raisby Quarry LC concretions with Raisby Quarry limestones (Fig. 4.31).

4.4.2.1. Petrography and geochemistry of concretion-associated diagenetic components - Interpretation.

The association of Raisby Quarry LC concretions with a porous, leached dolostone surrounding the concretion, is a feature very common to English Z2 and Z3 concretions at outcrop. The presence of scalenohedral calcite spar within pores of the Z2 and Z3 inter-concretion dolostones, very similar to calcite associated with Raisby Quarry concretions, has been described by Garwood (1891), Trechmann (1914), Tarr (1933) and Braithwaite (1988). Clark (1980), also describes coarsely crystalline, luminescent calcite occluding fractures which cut calcite concretions in the subsurface Z2 and Z3 of northern Europe. The scalenohedral calcite spar has been suggested to be of a variety of origins. Tarr (1933) related it to slow addition of calcite after concretion growth, whereas Braithwaite (1988) suggested that the scalenohedral calcite was of meteoric vadose origin, precipitated during Triassic uplift. However, it is very unlikely that meteoric vadose cements would be luminescent, as they commonly are in Z2 and Z3 concretions (Braithwaite, 1988, fig. 10).

The porous, inter-concretion dolostone associated with Z2 and Z3 concretions has been assigned to a number of origins. The most common (Trechmann, 1914; Tarr, 1933), is that it is due to the dissolution of more soluble calcite associated with dolomite between concretions. Woolacott (1919a) suggested that the dissolution may have been by $CaSO_4$ -rich solutions. Braithwaite (1988) however, suggests that the inter-concretion porous dolomite is

an internal sediment, deposited near-surface during Triassic uplift, completely at odds with field evidence such as sedimentary laminae traceable from concretions through the surrounding porous dolostones. A.C. Kendall and G.M. Harwood (*pers. comm.*, 1989) suggest that the porous dolostones are the result of dissolution of former halite which plugged inter-concretion porosity following the dissolution of metastable carbonate phases.

After Raisby Quarry LC concretion growth, the carbonate above and to the sides of concretions, not replaced or enclosed by concretionary calcite, was in a corroded, mechanically unstable state. This suggests that original aragonite/HMC surrounding the concretions, but not replaced by them, had been dissolved out, leaving dolomite, pyrite framboids, fine siliciclastic material and fossil fragments, in a similar manner as suggested by Trechmann (1914) and Tarr (1933) for Z2 and Z3 concretions. This compacted about the concretions. In general, the more corroded carbonate occurs adjacent to the larger concretions. The resultant porosity was completely, or partially cemented by dolomite, depending on the extent of corrosion. Where tightly cemented, dolomitization was more or less the last diagenetic event associated with LC concretions. Precipitation of dolomite demonstrates that the inter-concretion porosity was not immediately plugged by halite or calcium sulphates. The dolomite was probably precipitated from fluids of relatively low supersaturation at elevated temperatures (shown by oxygen isotope data). The low Sr of the dolomite is possibly indicative of slow precipitation, and a solution of low supersaturation would explain why this dolomite nucleated off precursor corroded HC dolomite as an overgrowth cement and not replacive of the concretionary calcite.

The origin of the necessary cations and anions for the SO dolomite is problematical, especially considering the very low porosity and permeability of the host limestones to the concretions. A certain amount of Ca, Mg and Fe could have been derived from the corrosion of HC dolomite. Other possible sources include Zechstein seawater, brines from the first dolomitization episode or fluids as the by-product of large scale replacement of dolomite by calcium sulphates. The most likely source in a burial diagenetic environment, however, is chemical compaction of surrounding dolostones (Hudson, 1975). The concretions and associated dolomite all occur along bedding planes within the Raisby Quarry limestone, which has been intensively stylolitized (Lee and Harwood, 1989) (Fig. 4.20a). This stylolitization probably started at burial depths of greater than 1km. It is logical that stylolitization would begin along bedding surfaces, where the dolomite was concentrated (although this has all since been removed apart from where associated with concretions). It is thus likely that pressure solution of this dolomite, (and, inevitably, some calcite) would provide sufficient ions in solution. At elevated temperatures (as suggested by oxygen isotope data for the dolostones), the inhibition of a high Ca^{2+}/Mg^{2+} ratio (probably slightly greater than 1) and Ca^{2+}/CO_3^{2-} ratio (less than 2) would be largely overcome (5.4.4). The carbon isotope value for this dolomite, which is depleted relative to most Raisby Formation

dolomites, would be consistent with some bicarbonate being supplied by dissolution of more highly altered Raisby Quarry limestones and/or the concretions.

The timing of the precipitation of succeeding scalenohedral calcite cements, iron sulphides, and clay minerals is problematical. They may all be, (a) of mesogenetic origin, following dolomite cementation, or (b) telogenetic precipitates following uplift and dissolution of possible post-SO dolomite pore filling halite or calcium sulphates. The scalenohedral calcites themselves, however, may well have been of mesogenetic origin. Some of the main evidence for this is their low positive $\delta^{13}C$ and strongly negative $\delta^{18}O$ values. Although $\delta^{18}O$ is similar, $\delta^{13}C$ is very different from that of any meteoric-derived cements within the Raisby Formation (6.5.12).The $\delta^{18}O$ of scalenohedral calcite (-11.3‰) is considerably lower than that for the SO dolomite (-6.3‰). This could suggest a substantial time gap between precipitation of the two mineral phases. However, as the difference in oxygen isotope incorporation between coprecipitated calcite and dolomite may be as high as 3.8‰ (Land, 1985), the oxygen isotope difference is probably of much less significance.

With progressive pressure solution, most of the available dolomite could have been dissolved, and so the limestone was extensively attacked. This may have led to supersaturation with respect to calcite, and precipitation of the scalenohedral calcite cements. In this scenario, both the calcite and dolomite were reprecipitated adjacent to the concretions, as these represented a significant barrier to pressure solution, being much more coarsely crystalline, and so less soluble than host limestones. This in effect produced a 'pressure shadow' adjacent to the concretions, decreasing solubility of both calcite and dolomite, thus leading to precipitation of SO dolomite and probably also scalenohedral calcite. It is very common to see LC concretions passing laterally into coarse dolomite and calcite, and then, laterally, into thick stylocumulates (Fig. 4.20a). The areas around the concretions thus acted as a sink for ions produced by pressure solution.

Scalenohedral calcite started to precipitate both within porous dolomite, and overgrow the terminations of columnar concretion crystals adjacent to the porous dolomite. The coarsely crystalline poikilitic habit, and low Sr concentrations of the scalenohedral calcites, strongly indicates slow growth from fluids of low supersaturation (cf. Scholle and Halley, 1985). That the first, dull orange-luminescent calcite zone is relatively iron-rich is possible evidence that the calcite precipitated soon after the ferroan dolomite from fluids of a similar derivation (similar to calcite and dolomite cements described by Wong and Oldershaw, 1981). The calcite grew both as a cement phase and at the expense of dolomite. The textures observed could not have been produced by dolomite passively growing up against earlier calcite, as unequivocally evidenced by corroded parts of HC and SO dolomite crystals poikilitically enclosed within calcite. The irregular contacts between calcite and dolomite could have been the result of corrosion of dolomite and precipitation of calcite, separated by a very short time gap (i.e., calcitization of dolomite) or by different fluids with a

longer time gap and an intermediate porosity. However, as SO dolomite crystals are only corroded in the manner of those in contact with the scalenohedral calcite, where the calcite is present, this suggests that the fluids which precipitated the scalenohedral calcite cements, were responsible for the corrosion. Thus, scalenohedral calcite at least partly replaces SO dolomite (6.3.2.3).

The oxygen isotope value of one sample of scalenohedral calcite is consistent with precipitation from fluids of elevated temperatures at considerable burial depths whereas the carbon value suggests that most carbonate was derived from host limestones and/or replacement of dolomite cements (Table 4.2). The solutions precipitating scalenohedral calcite are suggested to have been undersaturated with respect to dolomite, as most of the ions for the calcite were derived by dissolution of limestones which would produce a solution of Ca/Mg ratio of 63. Although the dolomite is iron-rich, much of the partially-replacive scalenohedral calcite is not. This suggests that Fe^{2+} was being removed from the solution, especially during precipitation of bright orange-luminescent calcite. The most likely reason for this is that the precipitating fluids were either of a high Eh (partly oxidizing the Fe), or more likely, a very low Eh, so that the Fe^{2+} combined with H_2S or S^- generated from the bacterial reduction of Zechstein seawater-derived sulphate to precipitate euhedral pyrite. Euhedral pyrite is commonly recognized as a burial diagenetic phase, formed by slow precipitation from solutions of low iron sulphide saturation, and commonly associated with nearly exhausted (for bacteria) organic matter (Hudson, 1982; Raiswell, 1982). Minor input of HCO_3^- from bacterial sulphate reduction may explain why the $\delta^{13}C$ of the scalenohedral calcite is lower than host limestones.

The consistency of zonation patterns of scalenohedral calcites between samples is apparently incompatible with an origin by chemical compaction, during which the input of ions would be highly variable. This problem was addressed by Wong and Oldershaw (1981), who concluded that chemical and/or Eh changes producing cement zonation were controlled by bulk aquifer processes. Stylolite input causes local supersaturation, but this is overprinted by larger scale fluid changes, as long as crystal growth is slow enough to record bulk aquifer changes. As the size of the concretion-associated scalenohedral crystals are variable but zonation is constant, growth rates, although not duration of growth were very variable, although all relatively slow.

The final precipitates, in remaining dissolution porosity around the concretions were clay minerals (Fig. 4.36). The clays bear a strong resemblance to stacks of vermicular kaolinite (Welton, 1984), although EDAX identified some K along with Al and Si. This could represent a contaminant mineral within the kaolinite (i.e., illite), or K anomalously substituting into the kaolinite lattice. The diagenetic relationship between scalenohedral calcite and clay is ambiguous, although clay mineral precipitation probably postdates most or all of the scalenohedral calcite. Ions for the clays may have been derived by pressure

solution. Although iron minerals and siliciclastics (quartz and mica) are relatively insoluble, they are not completely so, and are commonly recorded to be dissolved by pressure solution within carbonates (Scholle and Halley, 1985). Clays may thus represent the final stages of pressure solution, possibly when the accumulated insoluble residues began to be attacked. However, the origin of the clays may also be similar to that of kaolinite booklets precipitated during telogenesis, in association with meteoric-derived calcite cements (6.5.7).

The last phases of diagenesis (dolomite leaching, dolomite oxidation to iron oxides and pyrite/marcasite oxidation to hematite) occurred after Tertiary uplift of the formation and contact with oxic meteoric-derived fluids (6.6.1).

4.4.3. Summary and conclusions.

Calcite concretions have been identified in association with limestones from two localities within the Raisby Formation. The only main similarity between these localities is the presence of a thick limestone unit, within which the concretions occur. Raisby and Old Towns Quarries host the two thickest limestones within the formation recorded during this study. These are very similar in appearance to calcite concretions reported widely within second and third cycle Zechstein carbonates at outcrop and in the subsurface. Characteristic features of the concretions include coarse, columnar calcite crystals with inclusions of dolomite, well preserved skeletal material, and amorphous organic matter. Geochemically, the concretions are very similar to their host limestones.

The mode of formation of the concretions is very problematical. One of the major difficulties is that although organic matter appears to have been very important in their formation, this is not reflected in their carbon isotope geochemistry. The organic matter may however only have had a passive, catalytic effect, which did not involve carbon isotope exchange. Another problem is that few if any published examples exist of coarse, columnar calcite crystals which have formed as a replacive phase. The origin of the Raisby Formation concretions appears to be related to neomorphism of their host limestones, mainly on the basis of trace element and stable isotope geochemistry. However, such an origin is difficult to apply to concretions within the Ford Formation (hosted within massive dolostones) and Z2 and Z3 carbonates at outcrop in northeast England where they are hosted in dolostones or calcitized dolostones. At these localities limestones are absent, although concretions were never recorded independently of limestones within the Raisby Formation.

Secondary porosity created within host sediments during concretion growth, is a very common feature to concretions in general. In Raisby Quarry, the secondary porosity was occluded by a complex sequence of calcite, dolomite, iron sulphides, and kaolinite. It is most likely that the dolomite cement, at least, formed during burial diagenesis (mesogenesis). Therefore, the concretions must have formed during eogenesis of earlier mesogenesis. They cannot be of telogenetic origin. However, although it is probable that similar concretions throughout Zechstein carbonates formed in response to similar processes, it is extremely unlikely that they formed at the same time. The diagenetic history of calcite concretions and associated dolostones is summarized in table 4.3.

	Marine eogenetic	Mesogenetic	Telogenetic
Deposition	–		
Lithification (of limestone)	-----		
Marine (?HMC) cementation	--------		
Compaction	------		
Fracturing	----	--------	
Pyrite/marcasite precipitation	----	----	
HC dolomitization		----	
Limestone neomorphism		----	
LC & UNL concretion growth		-----	
Foraminifer aragonite dissolution		---	
Stylolitization		----------	
SO dolomite cementation		---	
Scalenohedral calcite precipitation		----	
Kaolinite precipitation		?-----	?---
Pyrite/marcasite oxidation			—
Ferroan (SO) dolomite oxidation			---
SO dolomite leaching			-----

Table 4.3. Summary of the diagenetic history of Raisby Formation concretions.

Chapter 5

Dolomitization

Sulphate evaporites

5.1. Dolomitization - Introduction.

Dolomite is the single most important mineralogical component of the Raisby Formation, and many other English Zechstein carbonate units. Much controversy still surrounds the origins of dolomite both in the Recent, and the geological record. The essence of this 'dolomite problem' is that it is very difficult to precipitate dolomite from natural solutions at 25°C and 1 atm pressure in the laboratory, and so observe directly the physio-chemical controls on its formation. Another aspect of the problem is that few, if any, modern analogues exist for large scale pervasive dolomitization such as has occurred throughout ancient sediments, including the Raisby Formation.

Dolomite is a calcium-magnesium carbonate mineral which belongs to the trigonal subsystem of the hexagonal crystal system. Its formula may be written as:

$$Ca_{(1+x)}(Mg_{(1-x)}Fe_{(0+x)}Mn_{(0+x)})(CO_3)_2$$

This reflects the common substitution of Ca^{2+}, Fe^{2+} and Mn^{2+} ions for Mg^{2+} ions in the dolomite lattice. An 'ideal' or stoichiometric dolomite crystal comprises alternating sheets of pure Ca, pure Mg and pure CO_3^{2-} ions, normal to the C-axis of the crystal (Morrow, 1982a). It is this very ordered crystal structure which probably makes dolomite such a difficult mineral to experimentally precipitate.

5.1.1 Classification of dolomite.

In this thesis, the term 'dolomite' refers to individual crystals of the mineral dolomite, whereas 'dolostone' refers to a body of rock whose main constituent is the mineral dolomite. Petrographic description and classification of dolostones here is slightly modified from the textural-based system of Gregg & Sibley (1984) and Sibley & Gregg (1987) (Fig. 5.1). All crystal sizes are quoted in microns (μm), and the distribution of crystal sizes may be unimodal, or polymodal. The terms 'calcitic dolomite' and 'dolomitic limestone' are not used in this thesis as the petrographic classification adopted provisions for partially dolomitized carbonates. No widely accepted classification exists for the geochemistry of dolomite and ferroan dolomite. A ferroan dolomite is taken here as a dolomite incorporating more than 2 mole% $FeCO_3$. An ankerite is defined as a calcium magnesium carbonate whose Mg/(Fe+Mn) ratio is less than 4:1 (Deer *et al.*, 1962).

Planar dolomite

Rhombic shaped euhedral to subhedral crystals

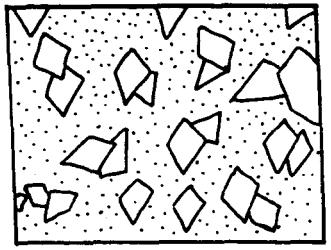

Planar-E (Euhedral)
Almost all dolomite crystals are euhedral rhombs. Crystal supported, with intercrystalline area filled by another mineral or porous (sucrose).

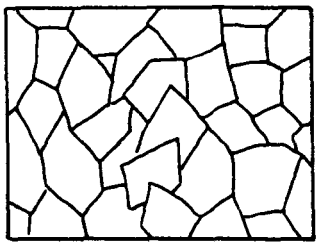

Planar-S (Subhedral)
Subhedral to anhedral dolomite crystals with low porosity and/or low intercrystalline matrix. Common straight compromise boundaries, and many crystals have preserved crystal face junctions.

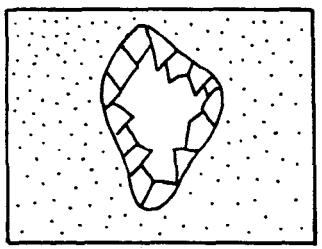

Planar-C (Cement)
Euhedral dolomite crystals lining or filling large pores, or surrounding patches of another mineral such as gypsum/anhydrite.

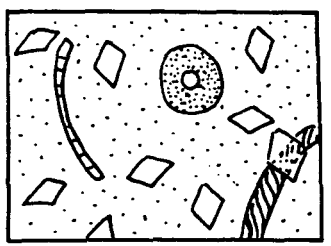

Planar-P (Porphyrotopic)
Euhedral dolomite crystals floating in a matrix, such as limestone or gypsum. Crystals are matrix-supported.

Non-planar dolomite

Non-rhombic, usually anhedral crystals

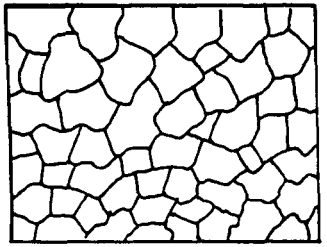

Non-Planar-A (Anhedral)
Tightly packed anhedral dolomite crystals. Mostly curved, lobate, or otherwise irregular or indistinct intercrystalline boundaries. Preserved crystal face junctions rare. Crystals often have an undulose extinction.

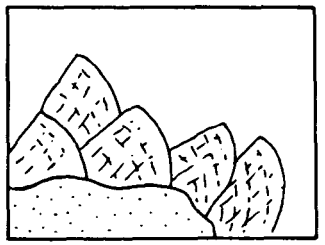

Non-Planar-C (Cement)
Pore lining or filling saddle shaped dolomite crystals characterised by scimitar-like terminations and sweeping extinction.

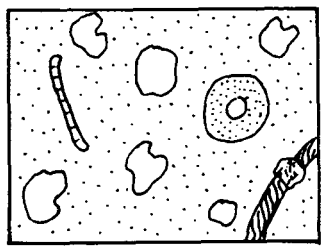

Non-Planar-P (Porphyrotopic)
Single anhedral dolomite crystals or patches of anhedral dolomite crystals floating in a matrix such as limestone or gypsum. Crystals usually have an undulose extinction.

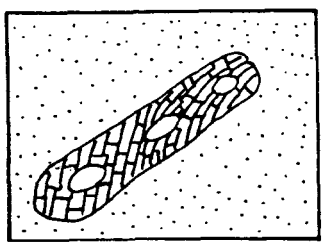

Non-Planar-M (Mimic)
Anhedral dolomite crystals, often finely crystalline, which preserve textures and/or crystallographic orientations of precursor carbonate, most commonly skeletal material.

Fig. 5.1. Classification of dolomite texture used in this thesis (modified from Gregg and Sibley, 1984 and Sibley and Gregg, 1987).

5.1.2 Methods of study.

Nearly all petrographic descriptions are from thin sections. Stained acetate peels were found unsuitable for the study of the finely crystalline dolostones which are characteristic of the Raisby Formation (Appendix III). Little information could also be gained from cathodoluminescence, as nearly all dolostones did not appreciably luminesce. S.E.M. petrography was of some use where the dolomite crystals were poikilitically enclosed within a calcite or gypsum/anhydrite matrix and so stood proud after etching.

A proportion of the dolostones examined petrographically were analysed by electron microprobe for Ca, Mg, Fe and Mn. A large number of samples from outcrop and core were further analysed for trace elements by AAS and ICP, and some of those were also analysed for carbon and oxygen stable isotopes. No X-Ray diffraction work was conducted, as reliable stoichiometry data could be obtained from electron microprobe analyses, and substantial Fe and Mn (more than a few mole percent), common in Raisby Formation dolostones, produces a peak shift similar to Ca-excess (Sperber *et al.*, 1984).

5.1.3. Limitations of the study.

This study of dolostones draws information from both outcrop and core material. This is necessary as, although outcrop gives a much better idea of the lateral relations of dolostone types, late-diagenetic interaction with meteoric-derived fluids has often altered the dolostones at outcrop (Fig. 5.3). Dolostones at outcrop also contain variable amounts of intercrystalline calcite cements and clay minerals, which can lead to anomalous geochemical results. Limitations on the study were imposed by the number of thin sections which could be made for petrographic study prior to chemical and isotopic analysis.

Examination of Raisby Formation dolostones has concentrated in two areas, considered to be potentially the most rewarding:

1. Dolomite textures in resedimented and bioclastic carbonates,
2. Areas of contact of dolostones and limestones.

Very little textural information could be gained from massive, uniform homogeneous dolostones which were sampled from both outcrop and core and which characterize most of the Raisby Formation. Sampling is therefore necessarily biased towards dolostones within the aforementioned two areas.

5.2. Types of dolomite recognized in the Raisby Formation - Description.

Four different types of dolomite have been recognized in the Raisby Formation on the basis of textural and geochemical criteria:

1. Finely crystalline replacive (FCR) dolomite,
2. Pervasive pressure solution-associated replacive (PPS) dolomite,
3. Ferroan dolomite cements,

4. Dolomitized anhydrite.

Finely crystalline replacive (FCR) dolomite is volumetrically by far the most important type, and constitutes almost all dolostones at outcrop and in core. The other three dolomite types have a much more localized occurrence, but are important in regard to evaluating the diagenetic history of the formation. Table 5.1 gives a summary of the petrographic and geochemical characteristics of each dolomite type.

5.2.1 Finely crystalline replacive (FCR) dolomite.

This type of dolomite forms nearly all of the dolostones in both core and outcrop. In core, the dolostones are dark (commonly 'medium grey' [N4]) whereas at outcrop they are all much lighter in colour ('very pale orange' [10YR 8/2] to 'pale yellowish orange' [10YR 8/6]). The dolomite crystals are on average 10μm to 50μm in size, unimodal in any one thin section and with textures ranging from planar-P through planar-E to planar-S and non-planar-A (Figs. 5.2 & 5.3). Commonly, a gradation in texture exists from planar-S/non-planar-A to planar-E to planar-P from a dolostone into a gypsum/anhydrite nodule or calcite lined cavity resulting from sulphate dissolution. Internally, the dolomite crystals may be inclusion-free, have uniform scattered inclusions, or contain an inclusion-rich core and inclusion-free (limpid) rim (Fig. 5.2b). The inclusions themselves are mainly carbonate, with some pyrite framboids and indeterminate clay minerals. At Houghton and Raisby Quarries, where the contact of FCR dolostones with limestones is gradational, the microspar of the limestones has partially replaced the dolomite (4.2.2., fig. 4.4). The contact of limestones with FCR dolostones in the field is commonly by interbedding of dolostones with isolated nodular limestones (4.2.1).

In nearly all examples, FCR dolostones contain very little or no vestige of the original, pre-dolomitization texture (texture-destructive or obliterative dolomitization). This is partly because most of the formation was deposited as a poorly-fossiliferous carbonate mud, and there were very few depositional textures or structures to preserve. Thus, little variability in the replacive dolomite would be expected. Where allochems did exist in the precursor carbonate, they are petrographically almost indistinguishable from the matrix-replacive dolomite, even in luminescence or blue light fluorescence. Some are distinguished by having a slightly smaller inclusion density that the matrix-replacive dolomite types (Fig. 5.4). However, larger macrofossil fragments, coated grains and clasts within bioclastic and resedimented carbonates do tend to be replaced by slightly finer dolomite crystals than their matrix.

Where dolostones have been partly leached at outcrop, or partly replaced by sulphate, fossil fragments are invariably selectively replaced and/or leached or, alternatively, selectively not affected (Figs. 6.31 & 6.32). This is normally attributable to the allochems originally being replaced by a more finely crystalline dolomite than the host carbonate.

1. *Finely crystalline replacive (FCR) dolomite.*

1a. Petrography

- 10-50μm, unimodal
- Planar-P/planar-E/planar-S/non-planar-A/non-planar-M
- Inclusion free/uniform inclusion density/inclusion rich core
- Allochems dolomitized, texture destructive/non-mimic/mimic
- Non-luminescent/dull red luminescence

1b. Geochemistry

- Non-ferroan, near stoichiometric/ferroan, non-stoichiometric
- $\delta^{13}C$ = 5.0‰ to 6.0‰ $\delta^{18}O$ = -2.0‰ to -0.5‰

2. *Pervasive pressure solution (PPS) dolomite*

2a. Petrography

- 20μm, unimodal
- Planar-E/planar-P
- Few inclusions
- Allochems selectively not dolomitized

2b. Geochemistry

- Non ferroan, non-stoichiometric/ferroan, non-stoichiometric

3. *Ferroan dolomite cements*

3a. Petrography

- 70-1000μm, polymodal
- Planar-C/non-planar-C
- Inclusion free
- Overgrow mimic dolomitized echinoderm fragments
- Non-luminescent

3b. Geochemistry

- Ferroan, non-stoichiometric
- $\delta^{13}C$ = 4.3‰, $\delta^{18}O$ = -6.3‰

4. *dolomitized anhydrite*

4a. Petrography

- 40-80μm, polymodal
- Non-planar-M
- Few inclusions
- Allochems dolomitized by same non-planar-M dolomite
- Dull red luminescent

4b. Geochemistry

- Non ferroan, near stoichiometric
- $\delta^{13}C$ = 5.5‰ to 5.6‰, $\delta^{18}O$ = -1.4‰ to -1.9‰

Table 5.1. Summary of the main petrographic and geochemical characteristics of the four dolomite types identified.

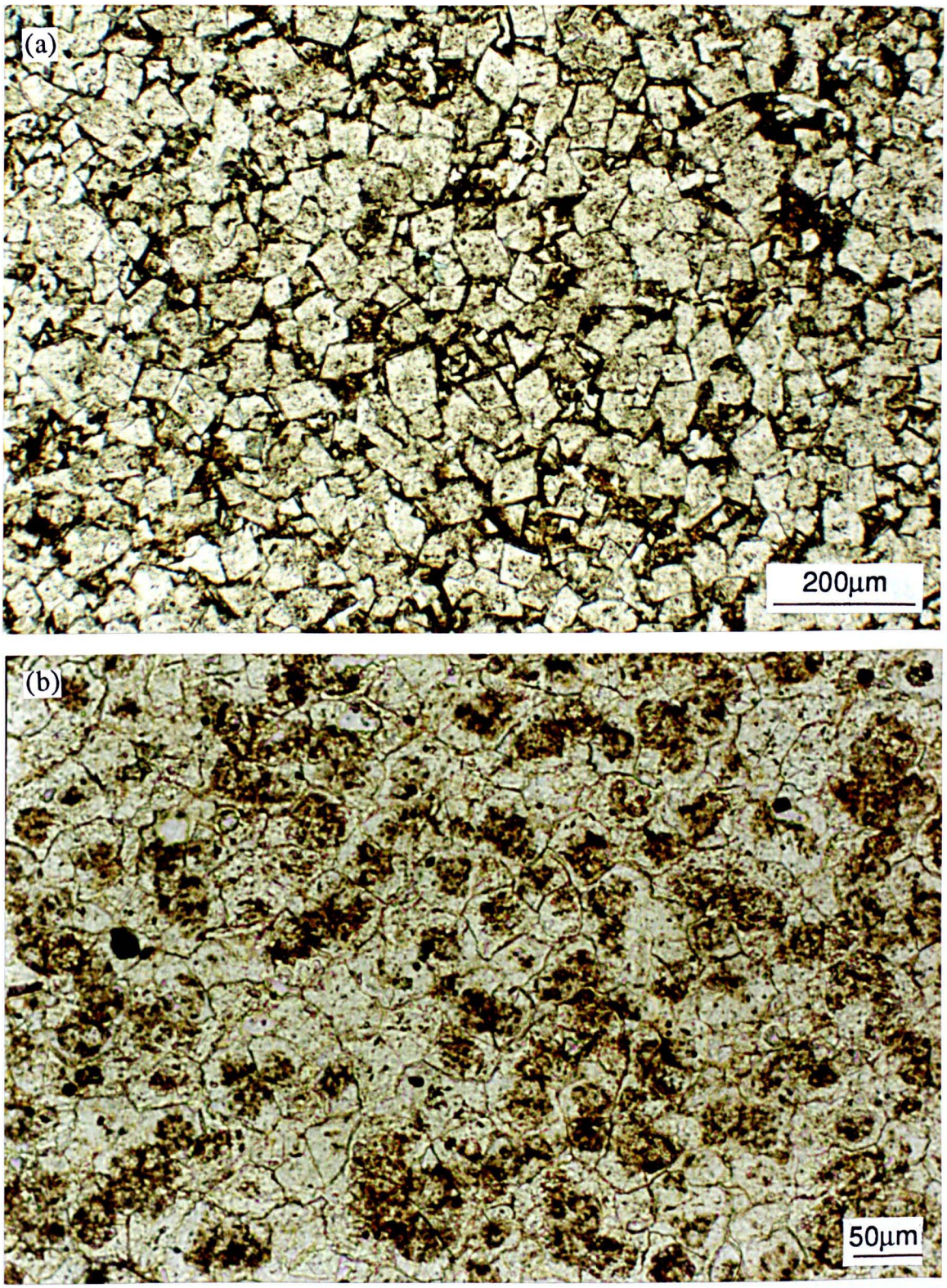

Fig. 5.2. Thin section, plane light photomicrographs of contrasting FCR dolostone textures; (a) basal dolostone, Raisby Quarry, (b) upper, autobrecciated dolostone, High Moorsley Quarry. (a) shows planar-S dolomite associated with calcite and iron hydroxide-cemented intercrystalline porosity, whereas (b) shows non-planar-A dolomite with inclusion-rich cores and inclusion-free rims.

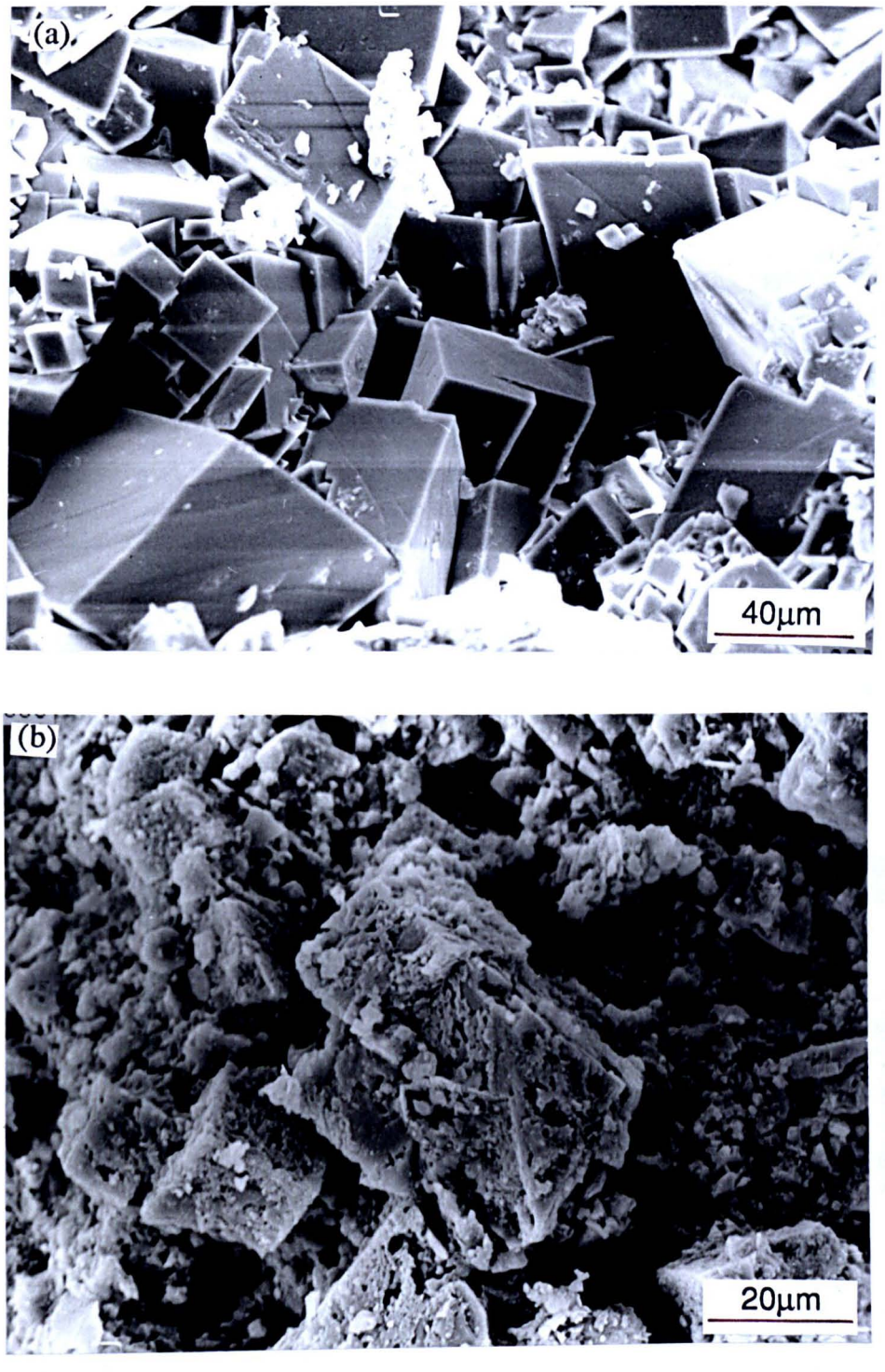

Fig. 5.3. SEM photomicrographs of un-etched fracture surfaces of FCR dolostones from borehole E3a, 351.0m (a), and the basal dolostone at Houghton Quarry (b). The dolomite in (a) is planar-S and polymodal. Note the heavy leaching of dolomite in (b) in contrast to (a), due to outcrop weathering.

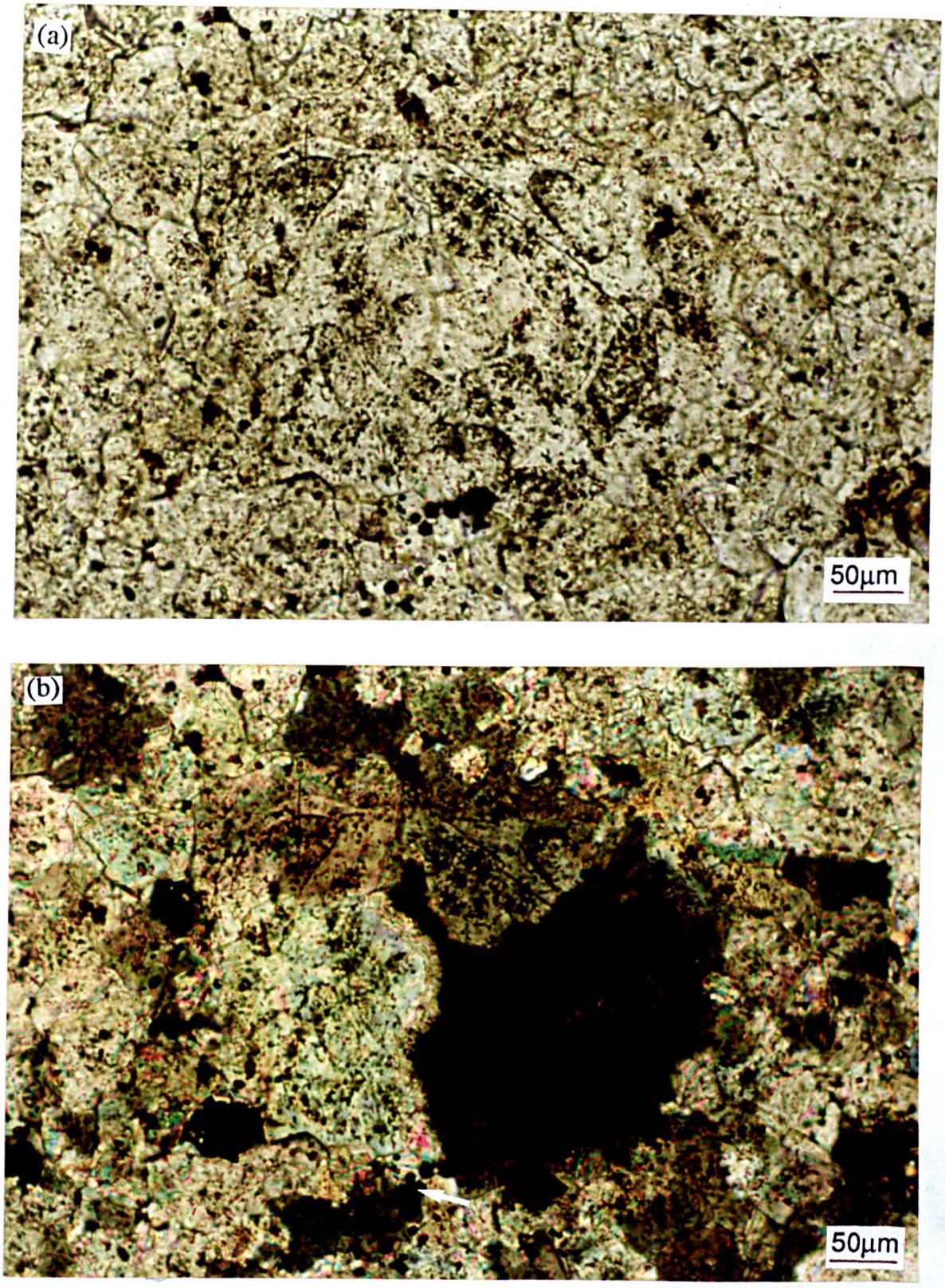

Fig. 5.4. Thin section photomicrographs of the ghost of a foraminifer (in the middle of the field of view) within ferroan FCR dolostones, Thickley Quarry; (a) plane light, (b) crossed polars. The foraminifer is only visible owing to a subtle contrast in inclusion density. The dolomite also encloses pyrite framboids (now oxidized to hematite) (arrowed).

Rarely, the original skeletal microstructure of faunal fragments has been preserved by non-Planar-M dolomitization (Fig. 5.5). In a few examples, non-Planar-M dolomitization has also preserved traces of early diagenetic, intraskeletal porosity-occluding calcite cements (Fig. 5.6). This may be represented by anomalously inclusion-free dolomite crystals with long axes normal to pore walls, or by finely crystalline dolomite which retains the original undulose extinction typical of elongate calcite crystals orientated with their long axes perpendicular to pore walls (Fig. 5.6). Echinoderm fragments are commonly mimicked by large, single dolomite crystals.

FCR dolomite is either non-luminescent, or luminesces a very dull red. Normally, no zoning can be detected within the crystals, although where their cores are rich in carbonate inclusions, they luminesce a lighter red-orange than inclusion-free rims (Fig. 5.7). Initially distinguished by staining, and later supported by trace element geochemistry, FCR dolostones can be subdivided into ferroan (stain turquoise-blue) non-stoichiometric, and non-ferroan (no stain) and stoichiometric (Table 5.2).

5.2.2 Pervasive pressure solution (PPS) dolomite.

Within the Raisby Formation in and around Houghton, High Moorsley, Offerton and Penshaw Hill Quarries, most limestones are interlaminated with dolostones on a fine, centimetre to millimetre scale. These are here termed ribbon and mottled limestones. In the Raisby Formation, the ribbon limestones contain horizontal bands of dolomite, centimetres in thickness, which are laterally continuous for decimetres to metres (Fig. 5.8a). The mottled limestones contain irregular, elongate areas of dolomite, millimetres in thickness, which are laterally discontinuous, commonly inclined to the horizontal. In both types, dolomitization is partial (rarely exceeding 30% dolomite), and crystal sizes are an average of 20μm and unimodal. The intensity of dolomitization decreases from the center of the dolomitized area to its contact with unaltered limestone, and the dolomite texture grades from planar-E to planar-P, although crystal size does not vary (Fig. 5.8b). The contact of limestone with dolostone is frequently sharp, gradational over only a few hundred microns. Fine siliciclastic material (quartz and mica), authigenic iron oxides and microfossils are frequently concentrated in the partially dolomitized areas (Fig. 5.8b). Fine microstylolite swarms are also very common. The partially dolomitized limestone is of very different colour ('dark yellowish orange' [10YR 6/6] to the limestone at outcrop (Fig. 5.8a). Where exposure is sufficiently extensive, such as Houghton Quarry, a lateral transition may be recorded from ribbon through mottled into pure undolomitized limestones. Another occurrence of dolomitization adjacent to stylolites is found in the W8 borehole, where a calcitized dolomite has been partially redolomitized for a few hundred microns either side of a few millimetres thick black stylolite. This is a 'sutured seam' type of stylolite (Wanless, 1979).

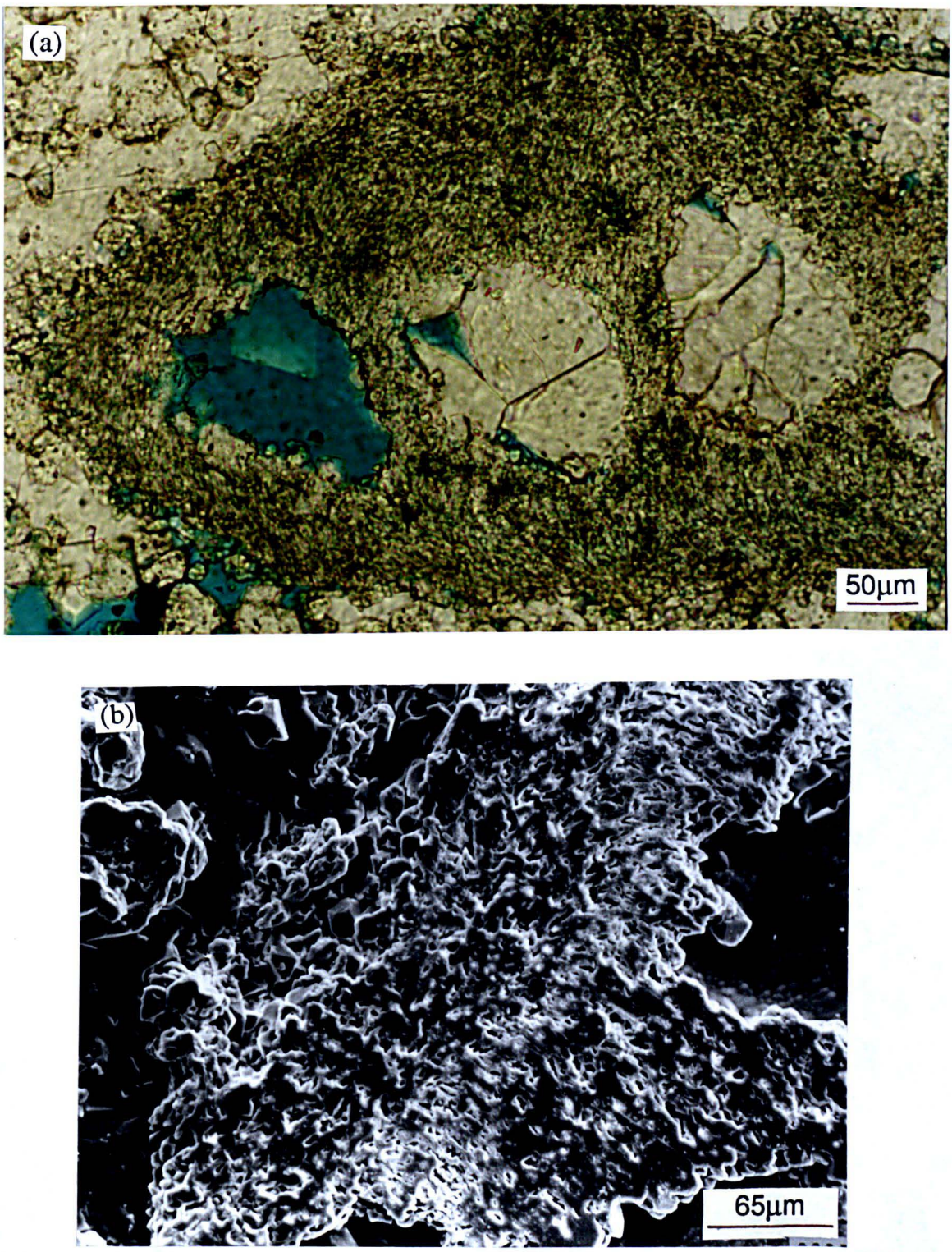

Fig. 5.5. Photomicrographs of a mimic-dolomitized bryozoan, Quarrington Quarry; (a) plane light (blue is resin-impregnated porosity), (b) polished and etched SEM sample. The original skeletal microstructure of the bryozoan has been near perfectly preserved by dolomite. Each original fibrous calcite crystal corresponds to an individual crystal of dolomite. The host dolomite to the bryozoan has been leached and resultant porosity partially occluded by zoned calcite cement (see fig. 6.31).

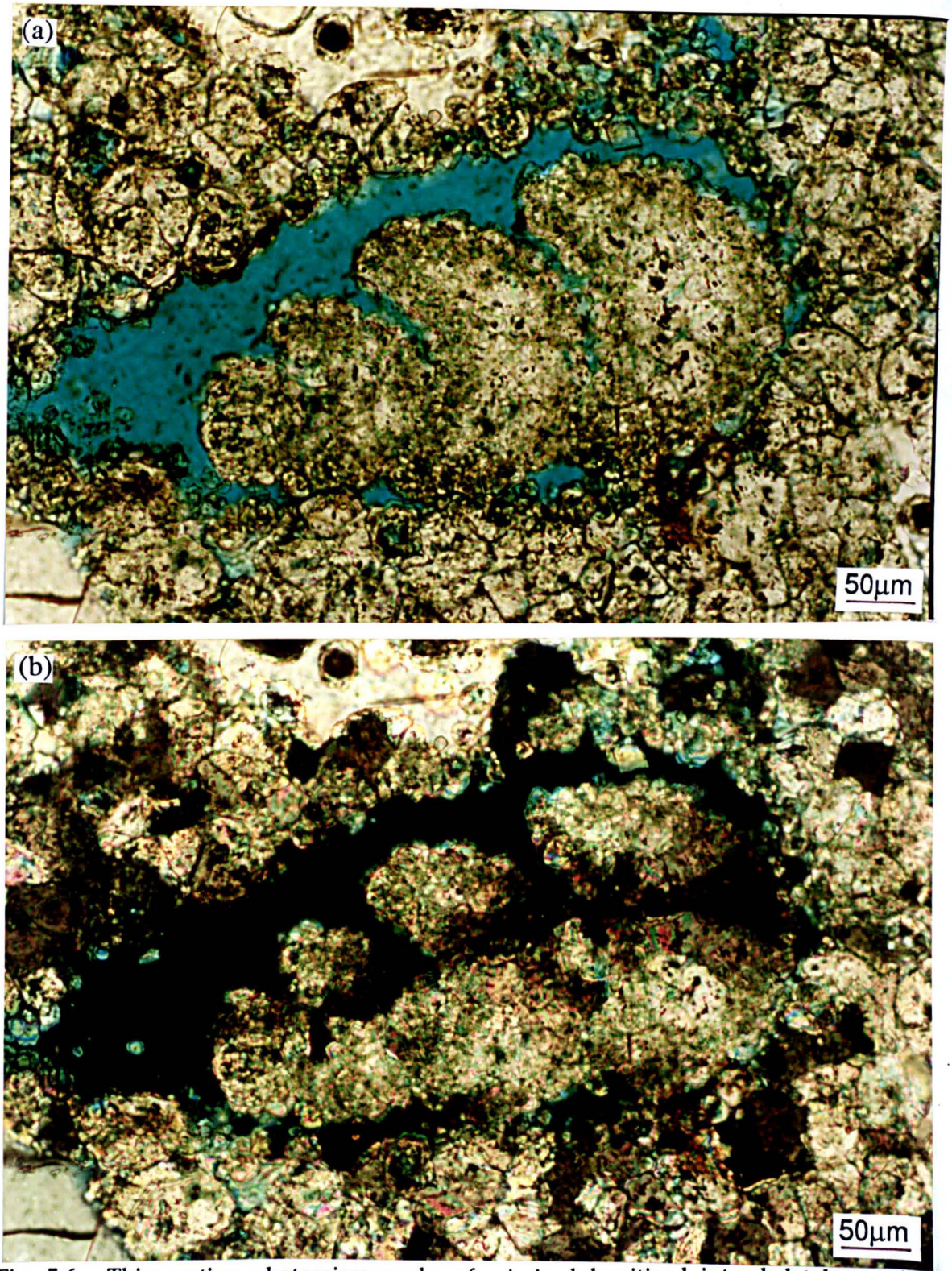

Fig. 5.6. Thin section photomicrographs of mimic dolomitized intraskeletal porosity-occluding cements originally within a foraminifer, Tynemouth Castle Cliff sandstone; (a) plane light, (b) crossed polars. The original shell wall has either been leached during recent outcrop weathering, or more likely was replaced by sulphates, which themselves have been leached, resulting in internal sedimentation of the dolomitized marine cements. Common crystallographic orientation of the replacive dolomite crystals is demonstrated by their sweeping extinction pattern in (b). Porosity is filled by blue resin.

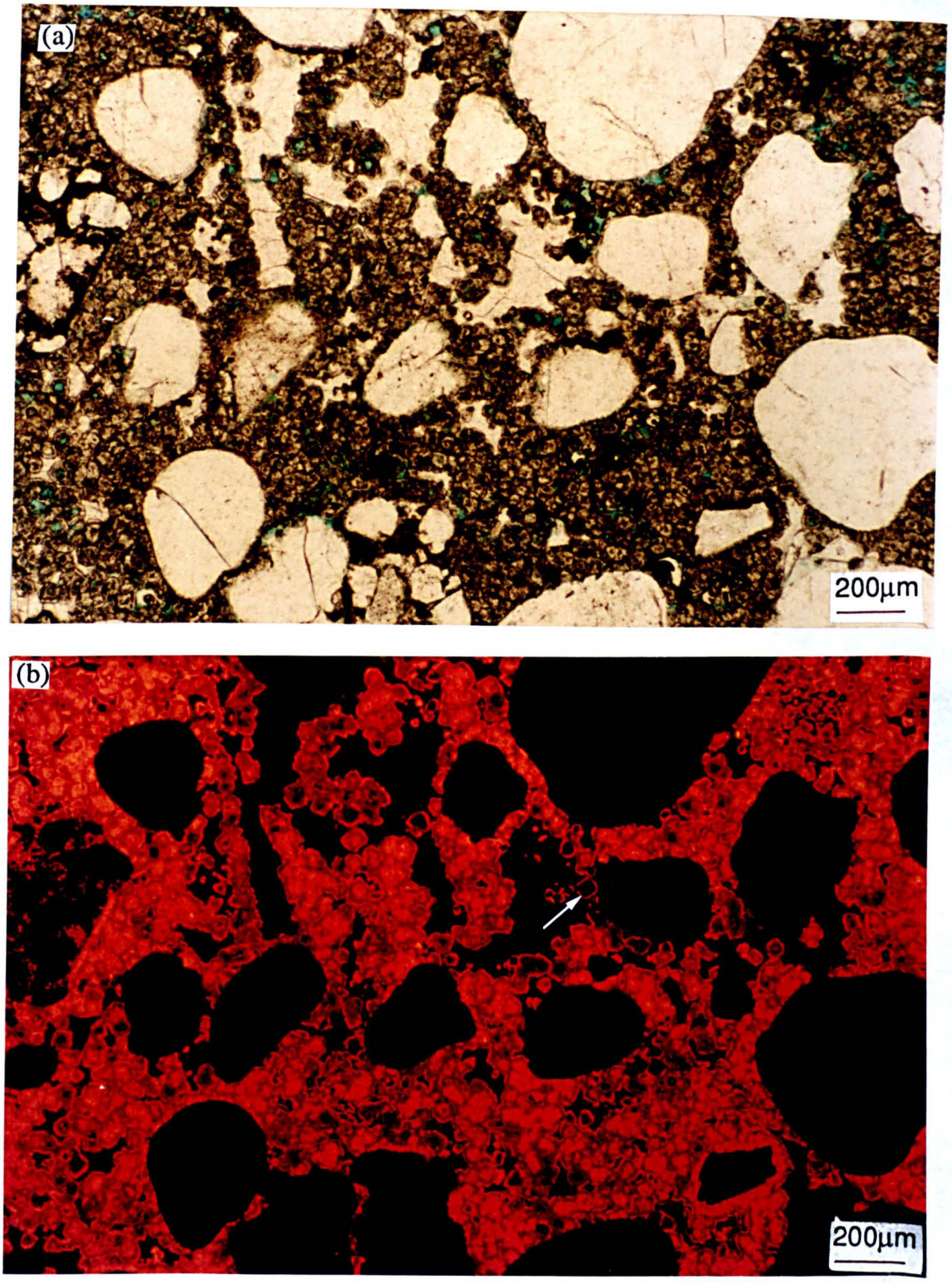

Fig. 5.7. Thin section photomicrographs of a dolomite-cemented sandstone, Tynemouth Castle Cliff; (a) plane light, (b) luminescence. The dolomite which replaces an original carbonate mud matrix of the sandstone is zoned bright to dull to bright orange-luminescent. In crystals which have been leached, and cemented by non-luminescent calcite (arrowed), the outermost bright orange-luminescent zone is most commonly preserved.

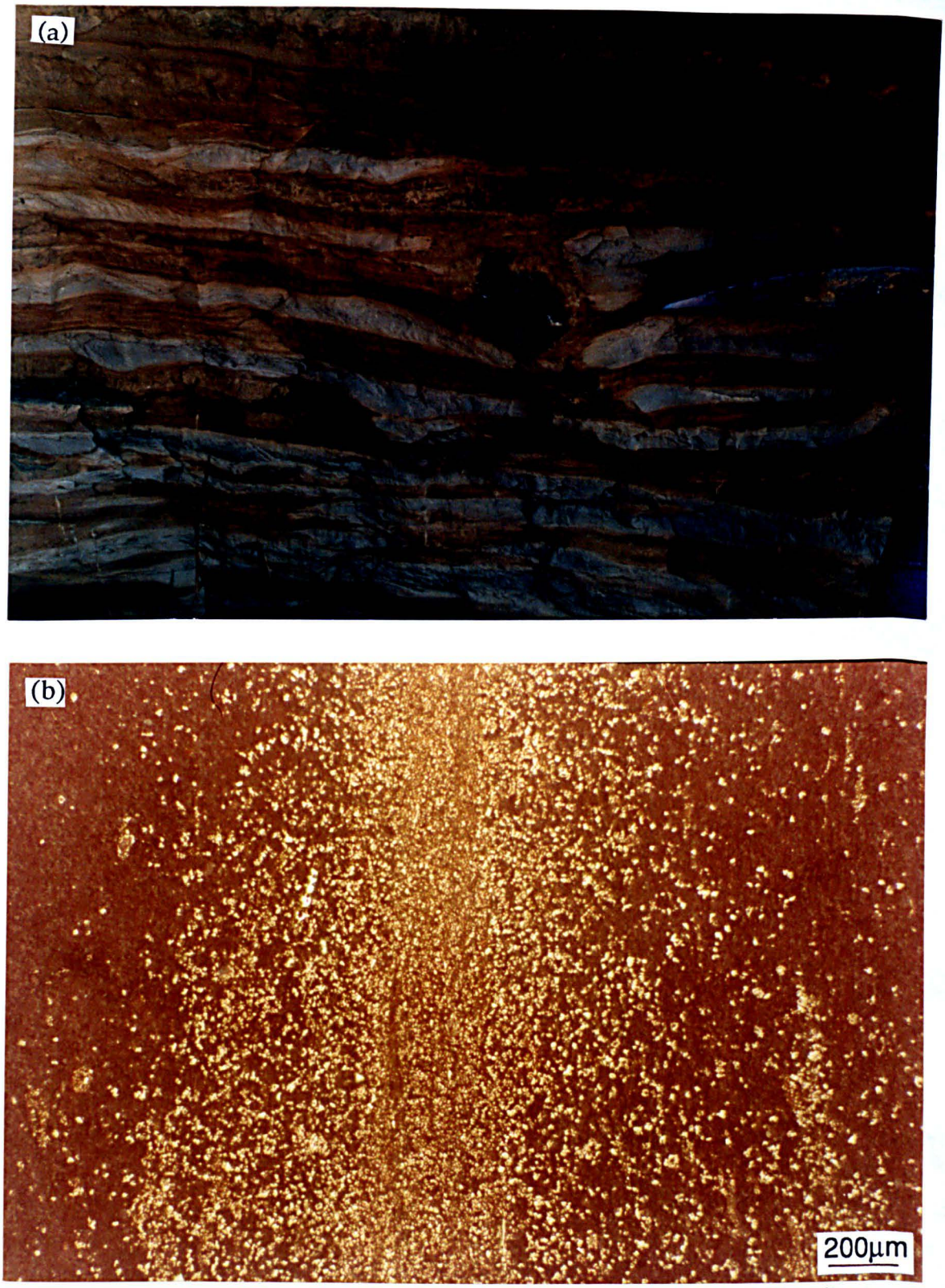

Fig. 5.8. Photographs of pervasive pressure solution dolomitization; (a) ribbon limestone at outcrop, Houghton Quarry, (b) stained thin section, reflected light photomicrograph of a mottled limestone, Offerton Quarry. In (a), some grey limestone layers are interrupted by a cavity after sulphate, possibly suggesting that it influenced later dolomitization. Dolomitization is concentrated in a central band in (b), along which microstylolites also occur.

The dolomite occurs as small rhombs, planar-E in form. Stylolitization and dolomitization in this example, postdate replacement by sulphates.

The small number of analyses of PPS dolomite does not allow any firm conclusions, but PPS dolomite is generally more ferroan and less stoichiometric than FCR dolomite (Table 5.2). These partially dolomitized limestones also have greater insoluble residues than do the host limestones.

5.2.3. Ferroan dolomite cements.

In a number of FCR dolostone samples, coarse dolomite crystals partially occlude a secondary porosity (which may be later filled by calcite cements). Two types of dolomite can be defined; ferroan pore filling cements, and ferroan cement overgrowths on allochems.

Ferroan pore filling dolomite cements range in size from 150μm to 1mm, are commonly polymodal and planar-C to non-planar-C in form. The FCR dolomite with which the dolomite cements are associated is occasionally corroded and always ferroan. At Thickley Quarry, non-planar-C dolomite cements line a cavity now occluded by coarse, zoned calcite cements (Figs. 6.34 & 6.35), and also fill fractures cutting the host FCR ferroan dolostone. These crystals have curved cleavages and sweeping extinction typical of saddle dolomite (cf. Radke and Mathis, 1980). The dolomite is directly associated with, although predates, sphalerite mineralization at Thickley Quarry. Other ferroan dolomite cements at Raisby Quarry, directly associated with calcite concretions, syntaxially overgrow earlier, corroded FCR dolomite crystals (Fig. 4.33). This type of ferroan dolomite cement stains turquoise-blue, is non-luminescent, non-stoichiometric, and enriched in Fe relative to the host FCR dolomite (Table 5.2). The crystals are commonly strongly zoned in trace elements and some zones may reach ankerite in composition (Fig. 5.9).

In a peloid grainstone from the Hurworth Place borehole, dolomite cements occur nucleating from dolomitized peloids and echinoderm fragments (Fig. 5.10). The crystals are an average of 70μm and are planar-C. The cement crystals are largest where in optical continuity with mimic dolomitized echinoderm fragments (Fig. 5.10). This dolomite is considered to be a primary, para-axial cement, and shows no evidence for being replacive of an original calcite overgrowth cement. The cements are non-luminescent, and ferroan in composition. Both the dolomitized peloids and their rimming cements have a similar composition (Table 5.2).

5.2.4. Dolomitized anhydrite.

A very anomalous dolomite texture occurs with otherwise uniform dolostones at High Moorsley and Rough Furze Quarries. The texture is characterized by a poorly interlocking mosaic of elongate, rod-shaped dolomite crystals of random orientation (Fig. 5.11). The crystals are 40-80μm long, 10-15μm wide and commonly polymodal. They have

Formula	Ca/(Mg+Fe+Mn)	Crystal Form	Locality
FCR dolomite			
$Ca_{(49.1)}(Mg_{(50.4)}Fe_{(0.3)}Mn_{(0.2)})CO_3$	0.97 (n=7)	Planar-S 80μm	Tynemouth Castle TS 38
$Ca_{(49.2)}(Mg_{(48.9)}Fe_{(1.6)}Mn_{(0.3)})CO_3$	0.97 (n=12)		E4 borehole ICP Analysed
$Ca_{(49.6)}(Mg_{(50.1)}Fe_{(0.2)}Mn_{(0.1)})CO_3$	0.98 (n=11)	Planar-S 55μm	Raisby Quarry TS8
$Ca_{(50.0)}(Mg_{(49.7)}Fe_{(0.2)}Mn_{(0.1)})CO_3$	1.00 (n=12)	Planar-S 200μm	Raisby Quarry TS 7
$Ca_{(50.3)}(Mg_{(49.5)}Fe_{(0.2)}Mn_{(0.0)})CO_3$	1.01 (n=8)	Planar-S 250μm	Raisby Quarry TS 8
$Ca_{(50.9)}(Mg_{(46.2)}Fe_{(2.6)}Mn_{(0.3)})CO_3$	1.04 (n=5)	Planar-S 60μm	Thickley TS 64
$Ca_{(51.1)}(Mg_{(47.8)}Fe_{(5.1)}Mn_{(0.2)})CO_3$	1.05 (n=8)	Planar-S 30-50μm	Hurworth Place Core TS 58
$Ca_{(51.3)}(Mg_{(47.3)}Fe_{(1.2)}Mn_{(0.2)})CO_3$	1.05 (n=6)	Non-Planar-M 500μm	Houghton Quarry TS 23
$Ca_{(51.3)}(Mg_{(47.9)}Fe_{(0.7)}Mn_{(0.1)})CO_3$	1.05 (n=8)		Seaham borehole ICP Analysed
$Ca_{(53.1)}(Mg_{(46.4)}Fe_{(0.4)}Mn_{(0.1)})CO_3$	1.13 (n=4)	Planar-E 70μm	W8 borehole AA 28
$Ca_{(53.2)}(Mg_{(37.9)}Fe_{(8.3)}Mn_{(0.6)})CO_3$	1.14 (n=7)	Non-Planar-A 20μm	E3a borehole 11m
$Ca_{(53.8)}(Mg_{(43.3)}Fe_{(2.7)}Mn_{(0.2)})CO_3$	1.16 (n=7)	Planar-E 70μm	Raisby Quarry TS 74
PPS dolomite			
$Ca_{(51.0)}(Mg_{(42.0)}Fe_{(7.4)}Mn_{(0.6)})CO_3$	1.04 (n=12)	Planar-E 40 μm	Raisby Quarry TS 1
$Ca_{(52.1)}(Mg_{(46.8)}Fe_{(1.0)}Mn_{(0.1)})CO_3$	1.09 (n=4)	Planar-E 40μm	W8 borehole AA 28
Ferroan dolomite cements			
$Ca_{(50.4)}(Mg_{(44.3)}Fe_{(5.1)}Mn_{(0.2)})CO_3$	1.02 (n=4)	Planar-C 70μm	Hurworth Place TS 58
$Ca_{(51.3)}(Mg_{(39.3)}Fe_{(8.5)}Mn_{(0.9)})CO_3$	1.05 (n=10)	Planar-E 150μm	Houghton Quarry TS 23
$Ca_{(52.3)}(Mg_{(42.4)}Fe_{(4.9)}Mn_{(0.4)})CO_3$	1.10 (n=21)	Planar-C 600μm	E3a borehole 11m
$Ca_{(53.4)}(Mg_{(38.7)}Fe_{(7.3)}Mn_{(0.6)})CO_3$	1.15 (n=7)	Planar-E 260μm	Raisby Quarry TS 74
$Ca_{(53.6)}(Mg_{(43.7)}Fe_{(2.5)}Mn_{(0.2)})CO_3$	1.15 (n=3)	Planar-C upto 1mm	Thickley Quarry TS 64
Dolomitized anhydrite			
$Ca_{(49.3)}(Mg_{(50.1)}Fe_{(0.5)}Mn_{(0.1)})CO_3$	0.97 (n=3)	Non-Planar-M	High Moorsley 15m
$Ca_{(49.4)}(Mg_{(50.3)}Fe_{(0.2)}Mn_{(0.1)})CO_3$	0.98 (n=17)	Planar-C 120μm	High Moorsley 15m

Table 5.2. Summary of the mean geochemistries and stoichiometries of the four dolomite types.

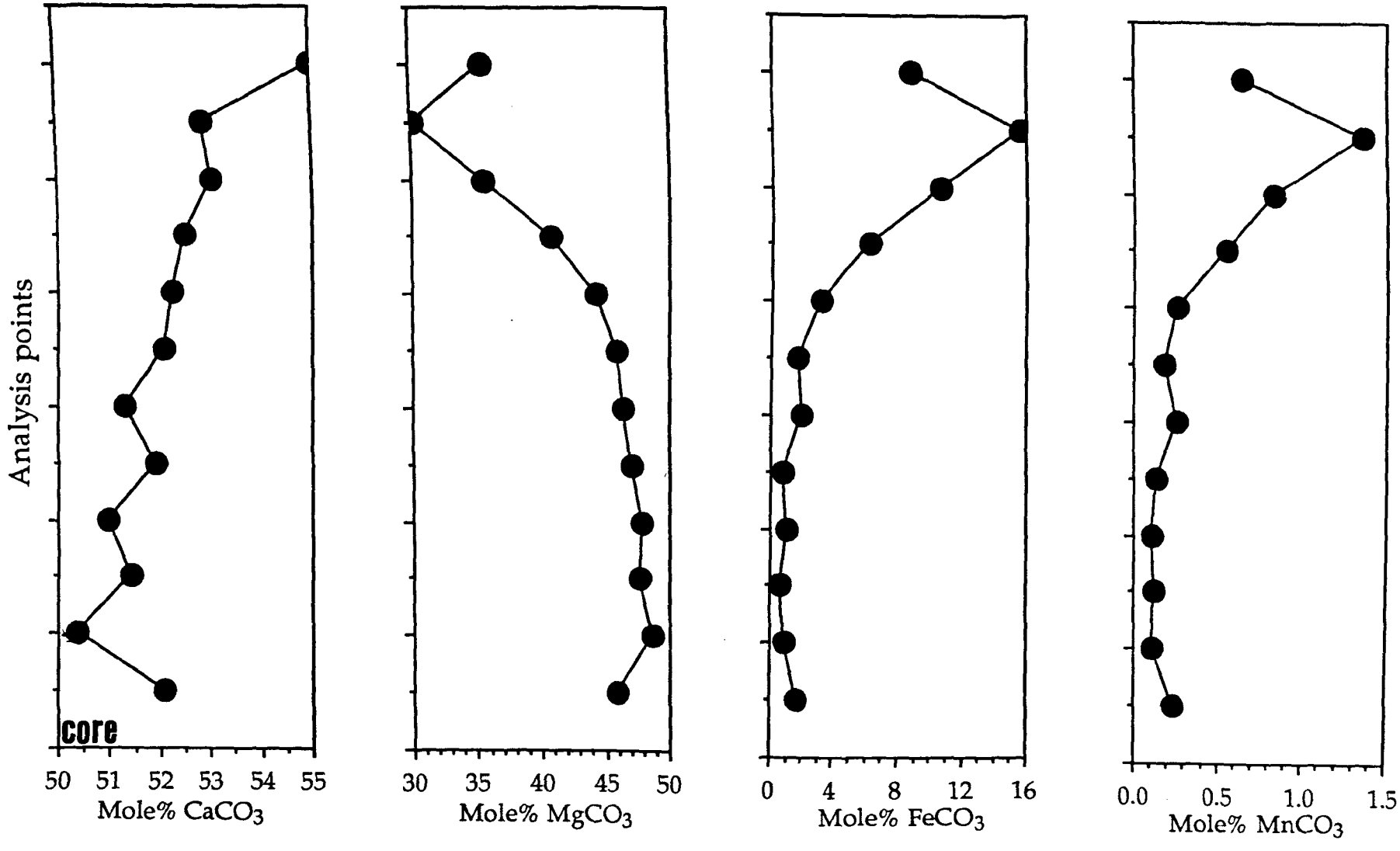

Fig. 5.9. Microprobe traverse from the core to the margin of a large ferroan dolomite cement crystal, borehole E3a, 352.70m.

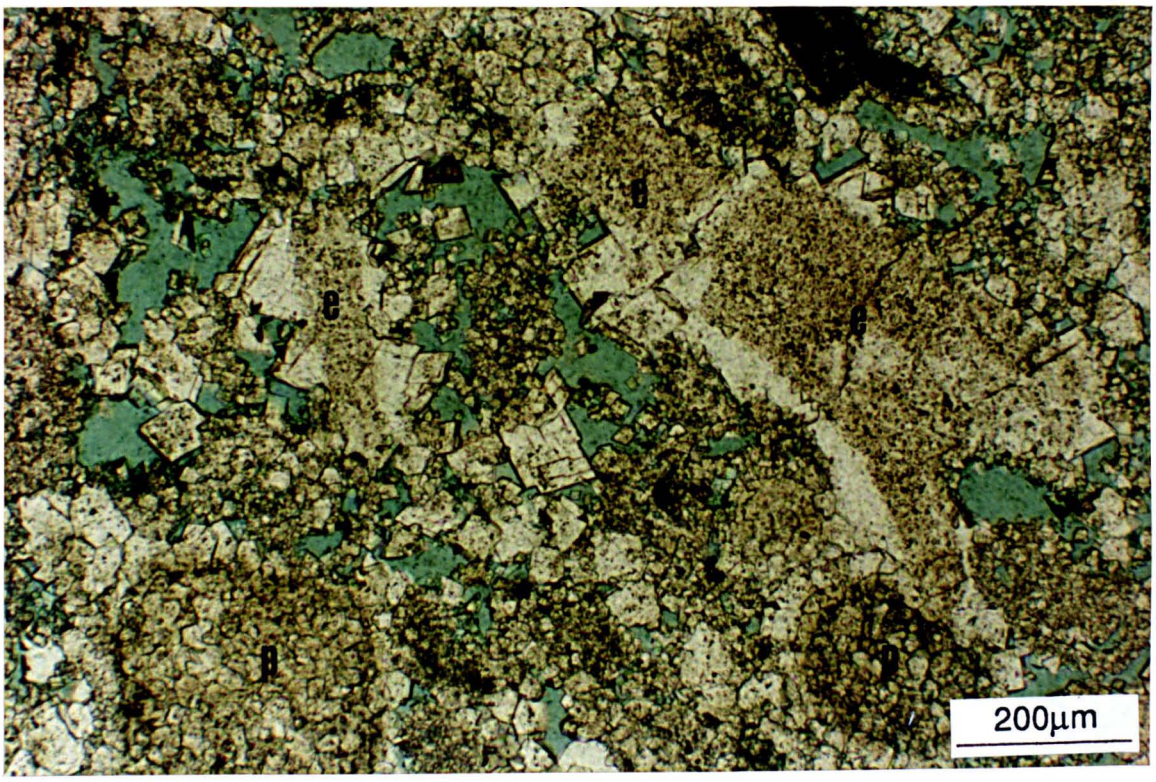

Fig. 5.10. Thin section, plane light photomicrograph of ferroan dolomite cements, Hurworth Place borehole, 148.98m. Most of the cements overgrow echinoderm fragments [e] which retain their original inclusion-rich texture. Dolomitized peloids [p] are again lined by ferroan dolomite cements, although they are smaller than those syntaxially overgrowing echinoderm fragments. Porosity is filled by blue resin.

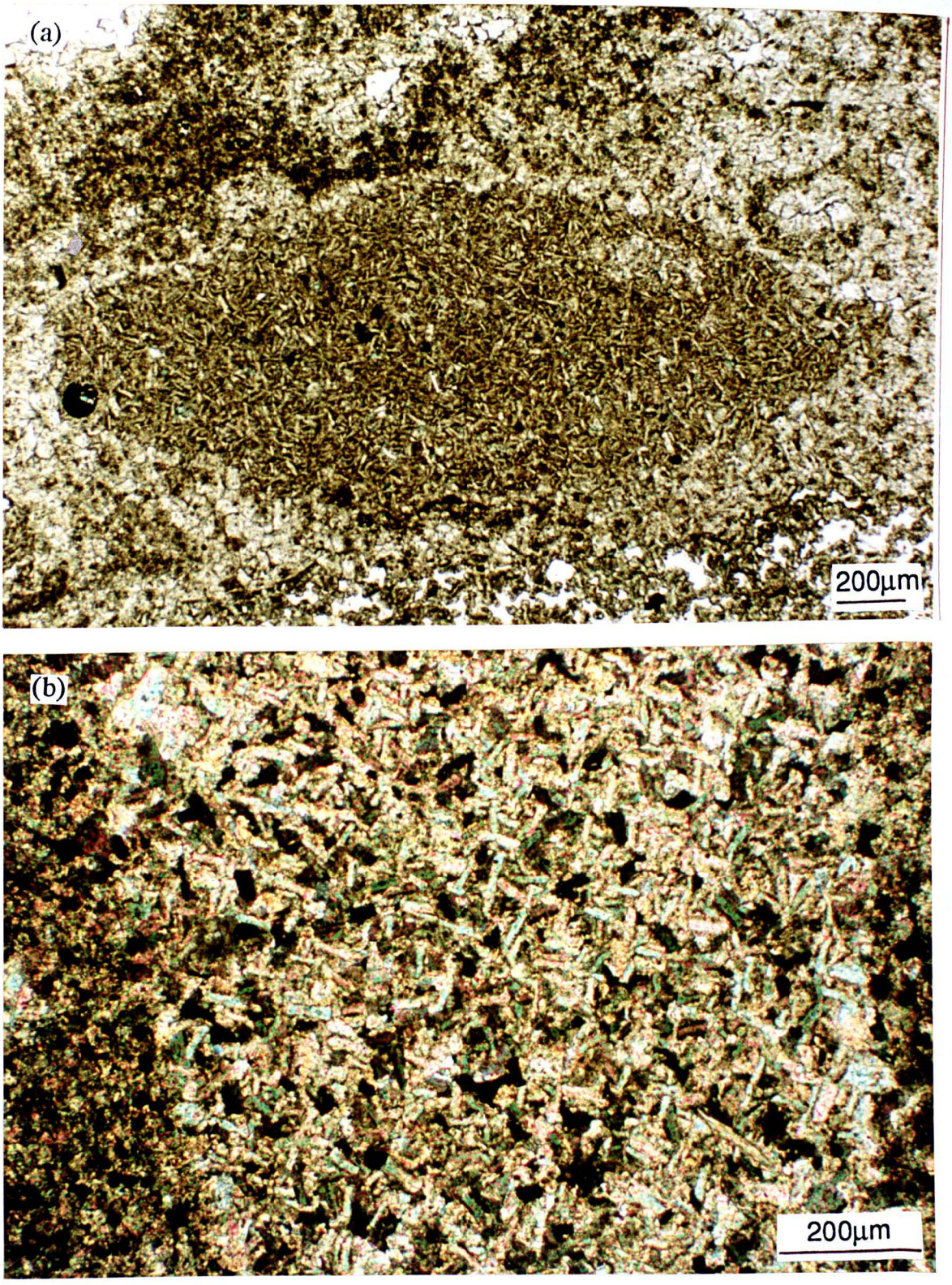

Fig. 5.11. Thin section photomicrographs of dolomitized anhydrite within a debris flow conglomerate, High Moorsley Quarry; (a) plane light, (b) crossed polars. (a) shows a euhedral gypsum pseudomorph hosting dolomitized anhydrite crystals, which are shown in detail in (b). Note, in (b), each lath corresponds to a single dolomite crystal.

straight sides and rounded ends. The dolostone is very similar in colour to FCR dolostones at outcrop (greyish orange [10YR 7/4]). In High Moorsley Quarry this dolomite only occurs apparently replacing lithoclasts, bioclasts and gypsum crystal pseudomorphs within a debris flow (Fig. 5.11a). Within the debris flow, a complete gradation in texture can be demonstrated, from fully dolomitized clasts or gypsum crystal pseudomorphs (Fig. 5.11a) into clast and gypsum pseudomorphs now cemented by coarsely crystalline calcite and with a geopetal internal sediment of the rod-shaped dolomite crystals at their base (Fig. 5.27b). At Rough Furze Quarry, the dolomitized anhydrite texture comprises millimetre to centimetre sized areas of dolostone, and also occurs as a zone up to 800μm wide between planar-S/non-planar-A dolomite and a cavity, now occluded by barite and calcite. Dolomitized anhydrite at High Moorsley Quarry has trace element and isotopic compositions no different from most FCR dolostones within the formation (Tables 5.1 & 5.2).

At both High Moorsley and Rough Furze Quarries, this dolomite texture is closely associated with 'stubby' dolomite crystals which form a poorly developed clast and pore-rimming cement phase that commonly nucleates from the lath dolomite substrate (Fig. 7.9b). The crystals do contain inclusions, commonly concentrated along intracrystalline zone boundaries, and vary in texture from non-planar-A to planar-C. They are poorly zoned with respect to trace elements and unzoned in luminescence. In the debris flow conglomerate at High Moorsley Quarry, the 'cements' predate clast fracturing. They also predate fracturing and barite mineralization at Rough Furze (Fig. 7.9b). Both the 'cements' and the lath dolomite crystals have very low (Fe+Mn) concentrations and are near stoichiometric (Table 5.2). They all have a very dull red luminescence and do not stain.

5.3.1. Dolomitization - Chemical considerations.

Dolomite samples have been analysed for major and trace elements by microprobe, AAS and ICP, and for carbon and oxygen stable isotopes. As these techniques give different types of results, they will be treated separately. The microprobe analyses allow determination of the geochemistry of individual dolomite crystals, whereas AAS and ICP analyses are of dolostones and so do not record the compositions of single crystals.

Understanding of the dolomitization reaction is important for any assessment of geochemistry. Dolomitization is a wet chemical dissolution - reprecipitation reaction. Dolomite normally replaces pre-existing carbonates volume-for-volume. Morrow (1982a), suggests that the reaction to produce a pure, stoichiometric dolomite should be written thus:

$$(2\text{-}y)CaCO_{3(aq)} + Mg^{2+}{}_{(aq)} + {}_yCO_3^{2-}{}_{(aq)} \rightleftharpoons CaMg(CO_3)_{2(s)} + {}_{(1y)}Ca^{2+}{}_{(aq)}$$

Where, for dolomitization of aragonite y = 0.11, and for calcite y = 0.25. In this equation, all three constituent ions are exchanged between solution and reactants, and some Ca must be

removed as Mg^{2+} is added. However, for the precipitation of dolomite as a cement, all constituents must be introduced by the solution to the precipitation site, and so the reaction may be written;

$$(1+x)Ca^{2+}_{(aq)} + (1-x)Mg^{2+}_{(aq)} + 2CO_3^{2-}{}_{(aq)} \rightleftharpoons Ca_{(1+x)}\,Mg_{(1-x)}(CO_3)_{2(s)}$$

(from Hardie, 1987).

However, it must be recognized that numerous other equations for the dolomitization reaction have been proposed (see Machel and Mountjoy (1986) for review), and interpretation of the geochemistry of dolomitization will be strongly dependant on which form of reaction is accepted.

5.3.1.1 Limitations of dolomite geochemistry

It should be possible by using major, trace element and stable isotopic composition of dolostones, to model the nature and composition of fluids from which the dolomite precipitated. However, there are two major problems with this approach:

1. The partition coefficients of trace elements and isotopes between fluids and growing dolomite crystals under sedimentary conditions are poorly known. K^{Sr}_{Dol} has received most attention. It is most likely less than 0.07 (Land, 1980) and probably 0.025-0.06 (Machel, 1988) (3.1.1). However, the partitioning of Sr may also be influenced by other factors such as temperature, pressure, precipitation rate (K^{Sr}_{Dol} decreases with decreasing precipitation rate [Bein and Land, 1983]), precursor mineralogy (Veizer, 1978), the relative importance of surface processes versus bulk solution equilibrium (Holail *et al.*, 1988), and the extent to which thermodynamic equilibrium is attained or approached if bulk solution processes dominate (Machel, 1988). The partition coefficients for other common trace elements are even less well known, although K^{Fe}_{Dol} and K^{Mn}_{Dol} are believed to be greater than 1 (Veizer, 1983a; Machel, 1988). The partition coefficient for sodium has been suggested to be 0.00002-0.00003 (Veizer, 1983a), which would make it a very important progress variable for dolomitization (Machel, 1988). However, Sass and Bein (1988) demonstrate that K^{Na}_{Dol} is directly related to salinity, and is 0.00014 at the point of gypsum precipitation.

2. There is evidence to suggest that dolomite crystals neomorphose over time. Neomorphism is most likely a dissolution-reprecipitation reaction (Land, 1980 & 1985), and so may involve a wholescale change of dolomite composition and, possibly, texture. Many authors therefore suggest that the geochemical composition of dolomite crystals may be of little use in determining the nature of the original precipitating fluids (e.g., Land 1980 & 1985; Bein and Land, 1983; Gregg and Sibley, 1984; Sperber *et al.*, 1984; Hardie, 1987; Qing and Mountjoy, 1989). The suggestion of the importance of neomorphism is partly based on the

observation that Holocene dolomite occurs as micron-sized crystals with a poorly ordered structure and is calcium-rich, whereas ancient dolomite has a much more well ordered structure and is more stoichiometric. The most stable way of combining calcium and magnesium carbonate under sedimentary conditions is as an ideal or stoichiometric dolomite. Any dolomite which deviates from this composition has a higher free energy and so is less stable and more soluble than ideal dolomite. Therefore, Holocene dolomite is less stable than ancient dolomite, although ancient dolomite itself is rarely 'ideal' (Land 1985). This suggestion of neomorphism over time (with heat and burial) is reinforced by Sr trace element and oxygen isotope data, which shows that both are depleted in ancient, relative to Holocene dolomite (Land, 1980 & 1985). Calculation of seawater temperatures from oxygen isotope data for a large number of marine dolomite samples by Land (1980), shows that they predict seawater temperatures which are far higher than they could have been. Land (1980, 1985) interpreted this to represent neomorphism of dolomite under the influence of fluids which were meteoric-derived or of elevated temperatures. In this case, the geochemical composition of any dolomite would be related, via partition coefficients (and factors which influence them) to the combined effects of at least two, and possibly numerous fluids. With successive dissolution-reprecipitation reactions dolomite should be enriched in trace elements with $K_{Dol} > 1$ (Fe and Mn) and depleted in those with $K_{Dol} < 1$ (Sr, Na, Ba) (autoenrichment and autodepletion respectively (Pingitore, 1978)).

One difficulty with invoking neomorphism, is that the assumption is being made that Holocene dolomite is similar in composition and texture to ancient dolomite when it was precipitated. However, documented localities of Holocene dolomitization (mainly small-scale hypersaline environments), are almost certainly different to the conditions in which most ancient dolomite formed (i.e., massive, platform dolostones). Also, as Holocene dolomite is geologically a very recent precipitate, there probably has not been sufficient time for the system to have become stabilized. Near-stoichiometric dolomite has also been recorded from the recent (Shatkay and Magaritz, 1987). Thus, the true significance of neomorphism is still poorly understood, and numerous authors still interpret ancient dolostones in terms of original fluid compositions and flow patterns (e.g., Mattes & Mountjoy, 1980; Sears and Lucia, 1980; Sass and Katz, 1982; Veizer, 1983a; Machel, 1986b & 1988; Sass and Bein, 1988; Graber and Lohmann, 1989). The importance of neomorphism of Raisby Formation dolostones will be assessed during interpretation of the geochemical results.

5.3.2. Dolomite composition and stoichiometry - Discussion.

An ideal, stoichiometric dolomite has a composition $Ca_{(0.50)}Mg_{(0.50)}CO_3$. However, rarely in nature does dolomite attain this ideal composition (Land, 1980), and can be enriched in Ca, or rarely Mg, over stoichiometry in addition to containing other cations in

significant amounts. As many Raisby Formation dolomites contain appreciable Fe, stoichiometry is here represented by the Ca/(Mg+Fe+Mn) ratio. A stoichiometric dolomite should have a Ca/(Mg+Fe+Mn) ratio of 1, regardless of the amount of Fe and Mn which substitute for Mg. A value greater than 1 indicates Ca substitution for Mg lattice plane sites. This ratio however gives no idea of ordering within the crystal. One possible difficulty with this expression is that it is possible that some Fe and/or Mn may substitute for Ca lattice plane sites, as they do in calcites (although the ionic radii of Fe and Mn are both closer to that of Mg than Ca). However, as most iron-rich dolomites in nature and in this study are calcian, Fe and Mn substitution only for Mg is assumed here.

The stoichiometry and compositions of all Raisby Formation dolomites analysed by microprobe, and the mean compositions of dolomite in two borehole sections analysed by ICP are shown in table 5.2. A rough division exists between near-stoichiometric (mainly the FCR, PPS and dolomitized anhydrite) and non-stoichiometric dolomite (ferroan dolomite cements), although none of the samples attain a true stoichiometric composition (Fig. 5.12). There is an approximate relation between those with high Ca and low Mg. The Mg also correlates well with Fe, but the Fe shows a very poor correlation with Ca. This is consistent with Fe only substituting for Mg, and the excess Ca over stoichiometric composition also substituting into the Mg sites (Fig. 5.12).

Most FCR, PPS and dolomitized anhydrite is near-stoichiometric, with little Fe and Mn substitution. ICP analyses of 68 samples of FCR dolostones from outcrop and borehole showed that 92.6% had less than 2 mole% $FeCO_3$ (i.e., non-ferroan) and 67.6% had less than 1mole% $FeCO_3$ (Appendix VII). Mn concentrations were similarly depleted, with 79.7% of dolostones having less than 0.2 mole% $MnCO_3$ and 49.3% less than 0.1 mole%. Aplin (1985) found that replacive dolostones from the Ford Formation reef were similarly pure and near-stoichiometric (50.3 - 52.7 mole% $CaCO_3$). They were also structurally well-ordered, as shown by XRD analysis. Good ordering and stoichiometry may simply be the product of neomorphism (Land, 1980 & 1985; Sperber *et al.*, 1984). However, if no substantial recrystallization has taken place, a low dolomite Ca/Mg ratio may directly reflect a low Ca/Mg ratio of the dolomitizing fluids (Sass & Katz, 1982; Sass & Bein, 1988). A fluid of low Ca/Mg ratio may be indicative of derivation from an evaporitic environment with gypsum/anhydrite precipitation (Sass & Bein, 1988). Here, the low Fe and Mn concentrations of the FCR, PPS dolomite and dolomitized anhydrite are considered to be at least partly original, because both Fe and Mn should increase during neomorphism, owing to their positive partition coefficients.

Most ferroan dolomite cements are enriched in both Ca and Fe, although some FCR dolomites (those associated with the ferroan dolomite cements) have similar compositions (Table 5.2). Ca-rich dolomites are theoretically metastable, and hence more prone to neomorphose, although Ca-rich Precambrian dolomites have been recorded. That the

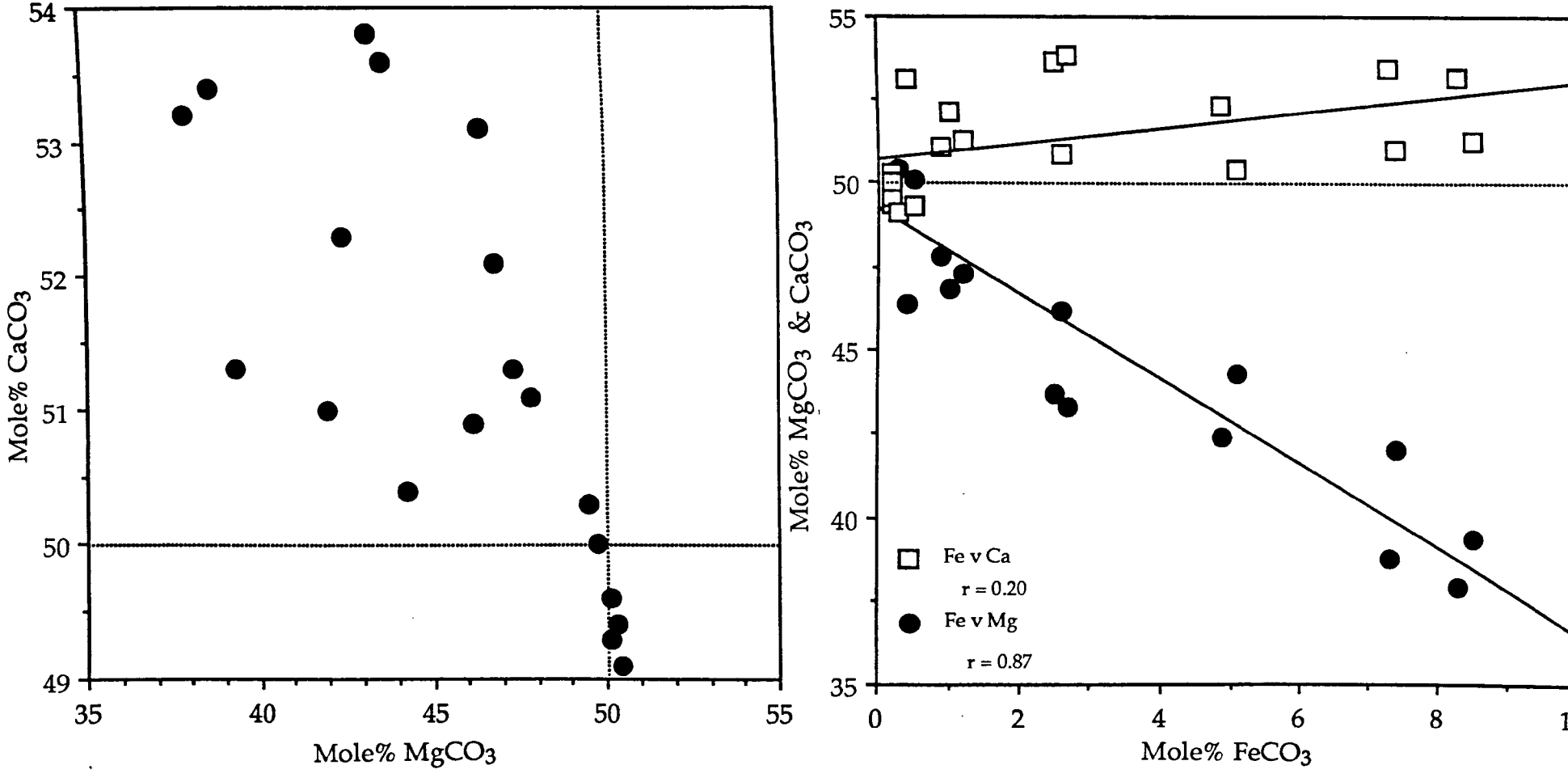

Fig. 5.12. Graphs showing the stoichiometry of dolomites analysed by microprobe (see table 5.2). Note the good correlation between Mg and Fe. Substitution of Mg by Fe explains the poor correlation between Mg and Ca, and Fe and Ca.

ferroan dolomite cements are still appreciably Ca-rich (although most FCR dolomites are near-stoichiometric) suggests the operation of a prohibiting factor. Sperber *et al.*, (1984) suggest that permeability of host rocks (and so access of Mg-rich, recrystallizing fluids) is the main limiting factor on neomorphism, but there is no such correlation in the Raisby Formation. It is possible that the concentration of Fe and Mn is an important controlling factor of susceptibility to neomorphism. As Fe and Mn occupy Mg lattice plane sites, without removing them, the dolomite cannot attain a fully ordered structure. For Fe and Mn to be removed, the ambient fluids during neomorphism would need to have considerably lower concentrations of Fe and Mn than those which originally precipitated the dolomite, and probably Mg/Ca ratios would have to be very much greater than Fe/Ca and Mn/Ca ratios in the neomorphosing fluid(s). Such conditions are unlikely within the burial environment. However, this does not discount the possibility of Mg 'displacing' Fe and Mn during neomorphism by some other mechanism.

5.3.3. Trace element geochemistry measured by ICP and AAS - Discussion.

Most ICP analyses were of FCR dolostones, as they are by far the easiest to sample and volumetrically the most important.

5.3.3.1. Strontium

Analysis of 65 FCR dolostone samples from core and outcrop shows a well defined distribution with a peak at 80-100 ppm Sr (Fig. 5.13). No dolostones were recorded with less than 50ppm Sr, and very few with more than 130ppm Sr. 93.8% of dolostones analysed contained between 50 and 130ppm Sr. There was no significant difference between the Sr content of dolostones between offshore boreholes (lower slope/basin) and outcrop (middle and upper slope) (5.13). No reliable Sr data could be obtained for PPS dolomite within partially dolomitized limestones. One analysis of a ferroan dolomite cement gave 69ppm, and two analyses of dolomitized anhydrite gave 138 and 148ppm Sr, in the upper range of FCR dolostones. The Sr content of dolostones from the Ford Formation reef range from 52-250ppm with most dolostones containing less than 100ppm Sr (Aplin, 1985).

One borehole (E4) was closely sampled in order to detect any vertical trace element variation (Fig. 5.14). Sr, Fe and Mn all show a general parallel decrease vertically, although Sr decreases in two 'steps'. With progressive dolomitization, a secular change in dolomite composition should be recorded, reflecting variation in the composition of the dolomitizing fluid. The nature of the change in Sr is dependant on the Sr/Ca ratio of the fluid in comparison to the Sr/Ca ratio of the precursor calcium carbonate being dolomitized (Sass and Katz, 1982; Machel, 1988). Dolomitization predated the neomorphism of ADP carbonate muds to dLMC microspar. The ADP muds (assumed to have originally comprised 65% aragonite, 30% HMC and 5% LMC [4.3.1]) would have a molar Sr/Ca ratio of 0.006 to 0.0076. This is slightly less

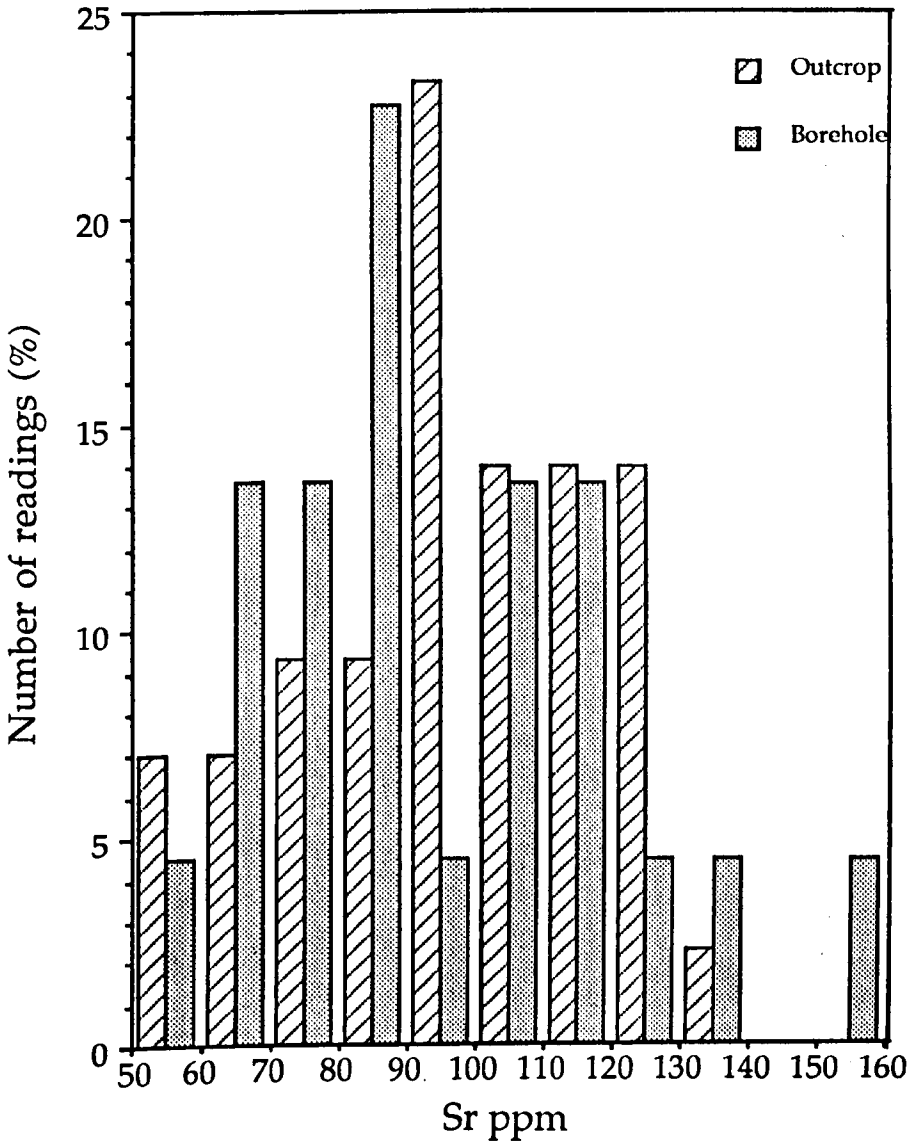

Fig. 5.13. Histogram showing the distribution of Sr concentrations of FCR dolostones, measured by ICP and AAS. The data is expressed as a percentage of the total number of analyses of borehole samples, and as a percentage of the total number of analyses of outcrop samples.

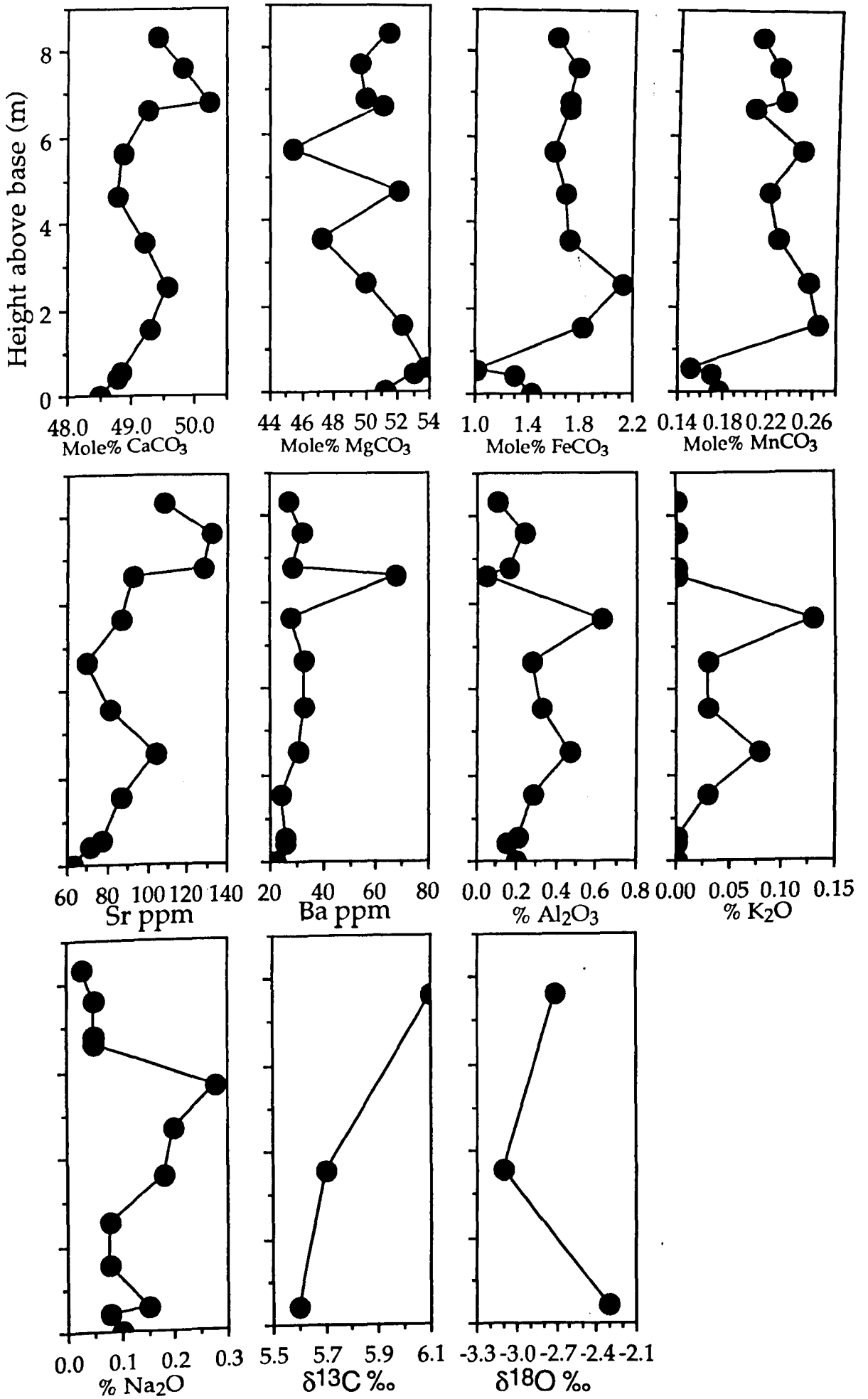

Fig. 5.14. Graphs showing an ICP geochemical traverse through borehole E4.

than the molar Sr/Ca ratio of seawater (0.0089). In this case, where the Sr/Ca ratio of the carbonate being replaced is slightly lower than that of the initial solution (assumed to have been normal seawater, although may well have been an evaporitically-concentrated brine of higher Mg/Ca and Sr/Ca ratio than seawater), during dolomitization in a closed, or partially closed system, the fluid Sr/Ca ratio should increase (cf. Sass and Katz, 1982, fig. 4). Thus, down-flow, dolomite crystals should become enriched in Sr, and the trends in the E4 borehole may reflect an upwards movement of dolomitizing brines. Given the very low initial concentrations of Fe and Mn expected for marine carbonates, and the positive partition coefficients of Fe and Mn, a down-flow decrease in the concentrations of both elements in the fluid and precipitate should be recorded. This suggests that the dolomitizing brines were moving downwards. The E4 section also shows a decrease in $\delta^{13}C$ downwards which could be due to the initial dolomitizing fluid having a heavier carbon isotopic value than the precursor carbonate, but with dolomitization, the dolomitizing fluid became progressively contaminated by the lighter carbon liberated from the limestone being dolomitized.

Owing to this contradictory data, fluid flow directions are uncertain, although a component of vertical movement is suggested. These trends may however just reflect differential neomorphism. If the factors which control trace element partitioning from fluid into dolomite during dolomitization are similar to those which control trace element partitioning during solution - reprecipitation neomorphism of dolomite, then the trace element gradients can be interpreted in the same way.

5.3.3.2. Barium

Most FCR dolostones contain between 10 and 50ppm Ba, with dolostones from outcrop having a peak (24.5%) in the 31-40ppm range, whereas those from core have a maximum in the 21-30ppm range (39.1%). The differences mainly reflect contamination due to barite mineralization which is more common in the dolostones from outcrop than core, and probably Ba associated with detrital and authigenic silicates. No significant differences were seen in the Ba contents of the other dolomite types.

5.3.3.3. Sodium

Sodium has long been recognized as potentially of importance with regard to dolomite geochemistry (Land and Hoops, 1973), although exactly what it shows is less clear. Raisby Formation samples have a mean of 519ppm Na [n=73], with a significant difference between core (mean 813ppm [n=25]) and outcrop samples (mean 359ppm [n=48]). The higher value of core samples is almost certainly due to contamination from evaporite minerals, and the highest Na values were recorded from the base of borehole E3a (Appendix VII), where both gypsum and anhydrite are preserved. Contamination from both liquid and solid, intra-

and intercrystalline inclusions, and laboratory preparation is commonly cited as a major problem with sodium analyses of carbonates.

Taking the partition coefficient of 0.00002-0.00003 (3.1.1) to represent normal marine salinity conditions, a marine dolomite should contain 105-157ppm Na. However, from their reinterpretation of salinity-dependant partition coefficients, Sass and Bein (1988) describe three fields of dolomite compositions;

Dolomitization by marine fluids	-	150-350ppm Na
Dolomitization associated with gypsum	-	400-2,700ppm Na
Dolomitization associated with halite	-	150-270ppm Na

The lower range of Raisby Formation samples (359ppm Na) (not contaminated by evaporites), falls just above the marine range of Sass and Bein (1988). However, Na contents of dolomites may be reset by neomorphism (Land and Hoops, 1973; Bein and Land, 1983), during which, owing to the low partition coefficient, Na would be expected to decrease.

5.3.3.4. Non-carbonate trace elements

All elements analysed by ICP, apart for Ca, Mg, Fe, Mn, Sr and possibly Na and Ba, were of little use in regard to assessing the diagenetic history of dolomite as they reflect partially hydrochloric acid-leached insoluble residues (clays, siliciclastics, and authigenic iron sulphides and oxides). These elements, notably Si, Al, K, V, Y and some Fe, Mn, Na and Ba generally correlate well with the percentage of insoluble residues. Of the ICP samples analysed, 61% of FCR dolostones, although only 22% of limestones, contained measurable insoluble residues. The poor accuracy of insoluble residue measurements (Appendix VII) mitigates against a quantification of this relationship.

In most FCR dolostones from offshore boreholes, insoluble residues identified petrographically comprise minor detrital quartz, micas (commonly 20μm in size), and authigenic iron sulphides. At outcrop, FCR dolostones contain detrital quartz and mica, plus authigenic iron oxide/hydroxides (hematite, goethite and iron-manganese dendrites), and authigenic clays. The authigenic clays comprise kaolinite, which partly occludes dissolution porosity, and smectite which encrusts dolomite crystals (6.5.6). There is negligible difference, however, in the Al contents between core (mean 0.193% Al_2O_3 [n=24]) and outcrop FCR dolostones (mean 0.153% Al_2O_3 [n=49]), although V and Y are greater in outcrop than core. There is also little difference in Al between limestones and FCR dolostones, despite the significant difference in insoluble residues. This suggests that the degree of acid leaching of the non-carbonate material during ICP sample preparation (Appendix VII) is insufficient to produce quantitatively significant Al variations. The greater insoluble residues of FCR dolostones than limestones may be due to preferential dolomitization of limestones which contain abundant siliciclastics, but it is more likely due to the preferential occurrence of authigenic clays and iron oxides in dolostones. Their greater abundance in dolostones

reflects both a greater porosity and permeability (due to sulphate dissolution and outcrop weathering) and partial breakdown of iron-rich dolomite during weathering (6.3.4.5). However, selective dolomitization of siliciclastic-rich carbonates cannot be discounted.

Analysis of 17 samples including limestones, dolostones and partially dolomitized limestones by AAS for elements including silica showed that Si is highest in partially dolomitized limestones from Raisby Quarry (3500-4620 ppm Si). In these and other samples, Si correlates very well with Al (r = 0.98 [n=17]) suggesting that during AAS sample preparation, most acid-leachable Si and Al are in aluminosilicate minerals such as detrital micas, feldspars, detrital and authigenic clays.

The PPS dolomites show considerable enrichment over their host limestones with respect to Mg, Fe, Mn, V, Ba, Na, Al and insoluble residues (Fig. 5.15). The Mg, Fe, Mn and Ba are in the dolomite, whereas the V, Na and Al enrichment is due to concentrated siliciclastics within the partial dolostones in the form of insoluble residues. This concentration is interpreted, from petrography, to be mainly due to concentration of insoluble material owing to pressure solution.

5.3.4. Carbon and oxygen stable isotopes - Discussion.

The carbon isotopic composition of dolomite mainly reflects the carbon isotopic composition of precursor carbonate with an overprint, should large enough quantities of carbon of a significantly different isotopic composition be introduced by the dolomitizing fluid (Land, 1980). As the carbonate anion is relatively diagenetically immobile, carbon isotope values should change little during neomorphism (Land, 1980). The partitioning of oxygen isotopes between fluid and dolomite depends on the oxygen isotopic composition of dolomite, and that of the precursor carbonate (whose influence is related to the openness of the system), plus temperature of the fluid (Land, 1980). The oxygen isotopic composition of the crystal will then only reflect that of the fluid if bulk solution-equilibrium exists, which it commonly may not (Mattes and Mountjoy, 1980), and whether or not the precipitation reaction reaches equilibrium, which again, it may not. The difference in oxygen isotopic composition between a calcite and a dolomite precipitated from an identical fluid under identical conditions is believed to be approximately 3‰ (Land, 1980 & 1985).

Most isotope analyses were of FCR dolostones. The results for FCR dolostones plot in an area of positive carbon and low-negative oxygen (Fig. 5.16). This is almost identical to the field described by dolostones from the Ford Formation (Aplin 1981 & 1985), and similar to analyses of general dolostones from the Zechstein of northeast England (Clark 1980), and dolostones within the Cadeby Formation of Yorkshire (Harwood and Coleman, 1983) (Fig. 5.16).

The carbon isotope composition of Raisby Formation limestones ($\delta^{13}C$ 3.0‰ to 6.0‰) is similar to that of the dolostones ($\delta^{13}C$ 5.0‰ to 6.0‰) (Fig. 4.7), suggesting little carbon isotope mobility during dolomitization. However, the limestones, as they are today,

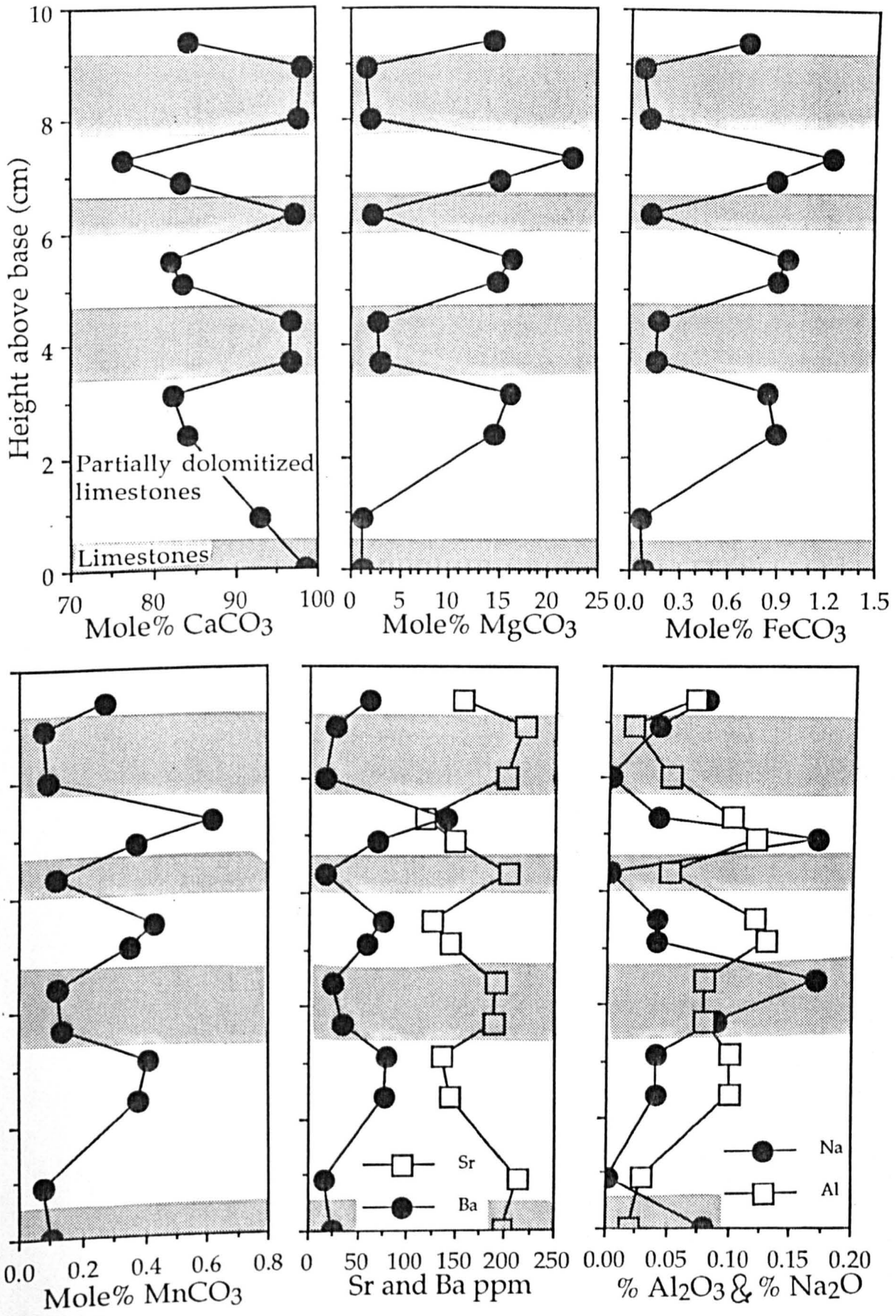

Fig. 5.15. Graphs showing an ICP geochemical traverse through a ribbon limestone, Houghton Quarry.

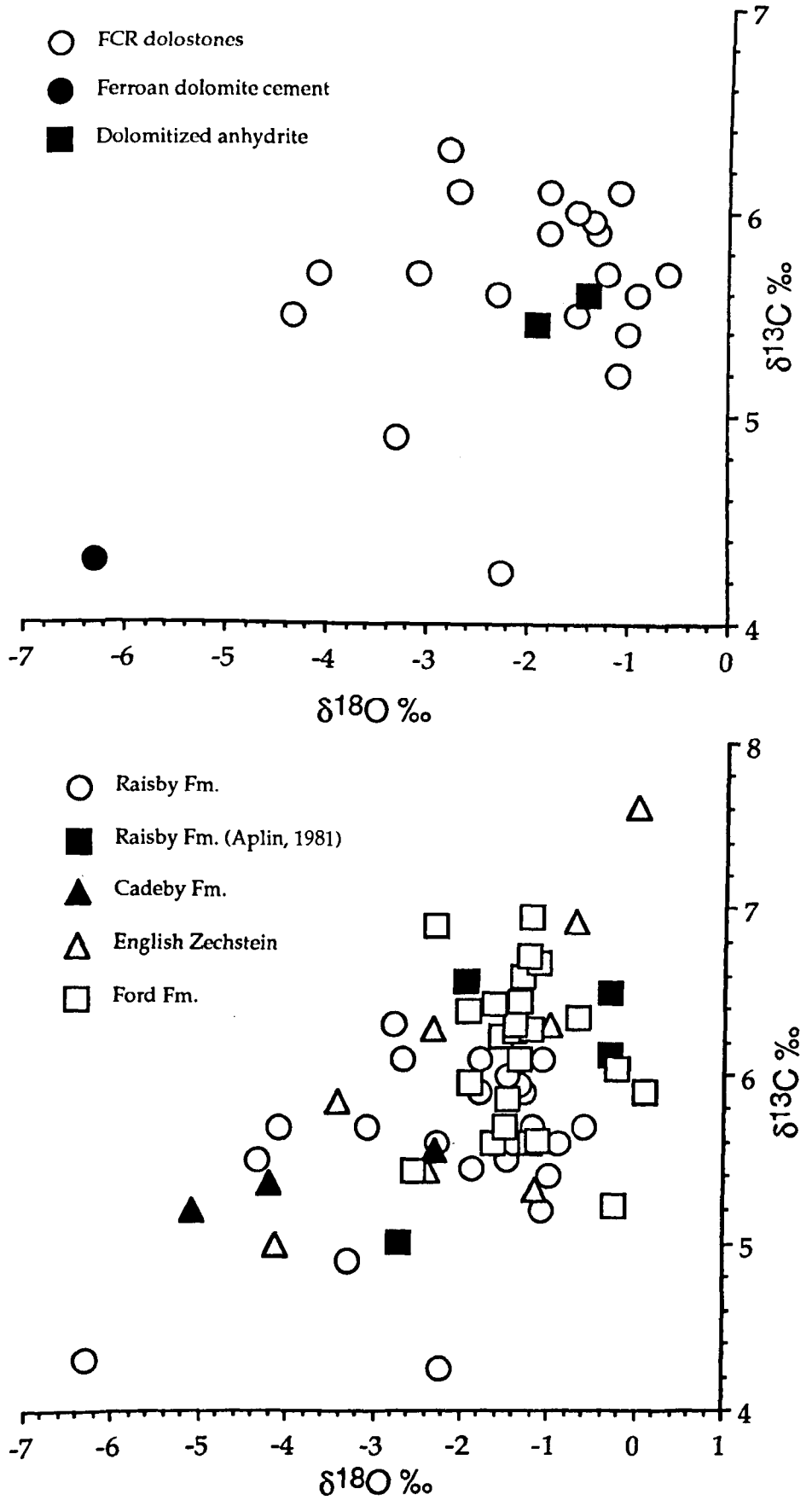

Fig. 5.16. Graphs showing the isotopic composition of Raisby Formation dolostones analysed in this study, and a comparison with other dolomite analyses (Cadeby Formation [Harwood and Coleman, 1983], English Zechstein carbonates [Clark, 1980], Ford Formation main reef [Aplin, 1981]).

have themselves been neomorphosed, probably following dolomitization, which has involved limited mobility of carbon isotopes (4.3.2.3). Thus, the $\delta^{13}C$ of present-day limestones is not necessarily an accurate reflection of the composition of the precursor carbonates when they were dolomitized. Nevertheless, the $\delta^{13}C$ of Raisby Formation FCR dolostones dominantly reflects the isotopic composition of the precursor limestone, although there may also be an overprint from a dolomitizing fluid of slightly different isotopic composition to that of the limestones. Taking the dolostones with the highest $\delta^{13}C$ as representing those with the least amount of possible dolomite neomorphism, these values are significantly higher than the limestones (Figs. 3.13 & 4.7). This could suggest that the dolomitizing fluid had a slightly elevated $\delta^{13}C$ above normal Zechstein seawater values (3.4.2.1). This fluid may have been evaporitically concentrated Zechstein seawater. ^{13}C enrichment was invoked by Aplin (1981 & 1985) to explain heavy $\delta^{13}C$ values of Ford Formation dolostones. Clark (1980) however, invoked fermentation of organic matter to explain the heavy $\delta^{13}C$ of Zechstein dolomites in general.

The oxygen isotope composition of most FCR dolostones ranges from $\delta^{18}O$ -4.5‰ to -0.5‰ (Fig. 5.16). Such a low negative value is common to many ancient dolostones. If the dolomite had been precipitated in equilibrium with Zechstein seawater (which precipitated calcite with $\delta^{18}O$ -2.5‰ ± 1.5‰) (3.4.2.2), given the assumed 3‰ fractionation between calcite and dolomite (Land, 1980), the dolomite should have $\delta^{18}O$ +0.5‰ ± 1.5‰. If the fluid was hypersaline, it would increase the $\delta^{18}O$, probably by 3-4‰ to +3.5‰ to +4.5‰ ± 1.5‰ (the enrichment from non-equilibrium evaporation to near gypsum saturation [Lloyd, 1966; Ruppel and Cander, 1988]). The observed much lower Raisby Formation values could then be achieved by a combination of one or more of the following:

1. Dolomitization at elevated temperatures,
2. Partly closed system or bulk solution disequilibrium dolomitization, thus enhancing precursor limestone influence (a more negative $\delta^{18}O$),
3. Neomorphism under the influence of meteoric fluids, or fluids at elevated temperatures.

It is very difficult to determine the relative importance of these factors in controlling the $\delta^{18}O$ of Raisby Formation dolostones. However, if the least negative $\delta^{18}O$ values are taken as representative of the least altered dolomite, these are less depleted than the least altered limestone samples (Figs. 3.13 & 4.7). This, together with the $\delta^{13}C$ data, could again suggest that the dolomitizing fluid was dominated by hypersaline Zechstein seawater, in which the heavier isotope (^{18}O) would be concentrated. Magaritz (1987) describes carbon and oxygen isotope data from dolomite laminae within anhydrite of the Hartlepool Anhydrite Formation from offshore borehole W5a. The dolomite has a fairly consistent $\delta^{18}O$ of -1‰ (Magaritz, 1987, fig. 2). Recognizing that hypersaline seawater should be enriched in ^{18}O by 3-4‰, he invokes large scale input of meteoric water into the basin to explain the recorded dolomite values. He does not recognize the possibility of neomorphism. In figure 5.16 there is possibly a trend of decreasing $\delta^{13}C$ with $\delta^{18}O$ of the dolostones. This trend may be suggestive of a change towards lower $\delta^{13}C$ and $\delta^{18}O$ values of dolomitizing or neomorphosing solutions over time, or in different parts of the formation.

There is no significant correlation between carbon and oxygen isotopic compositions and trace element geochemistry in the FCR dolostones. Some weak trends are evident in vertical traverses through FCR dolostones associated with limestones (Fig. 5.17). In all four examples, the $\delta^{18}O$ of dolostones is more negative below than above the interbedded limestone units from less than 0.5 to 2‰ (Fig. 5.17). This could be due to one or a combination of two possible processes:

1. The fluids which precipitated and/or neomorphosed the lower dolostones were relatively warmer,
2. As they were restricted by a low-permeability limestone, fluids which precipitated and/or neomorphosed the lower dolostones were less free-flowing and had restricted communication with the main body of fluids. This gave the isotopically lighter oxygen from the precursor limestones more time to be incorporated into the dolomite (i.e., a partially closed system not in equilibrium with the main body of fluids [bulk solution-disequilibrium]).

The amplitude of the isotopic difference is related to the thickness and impermeability of the limestones (the Raisby Quarry limestone is thickest, most impermeable, and shows the greatest isotopic shift). This would reinforce the observation that the limestone represented a barrier to free fluid flow; if it did not, the limestone itself should have been dolomitized.

A very weak, parallel decrease can be detected in both $\delta^{18}O$ and Sr values of FCR dolostones in a transect from upper slope (outcrop) into outer slope (borehole) carbonates (Fig. 5.18). The amplitude of the variation is small (5 ppm Sr and 1‰ $\delta^{18}O$), and may not be sufficiently significant, although 1‰ $\delta^{18}O$ is better than analytical accuracy (Appendix IX). If it is significant, it may reflect a greater neomorphism of dolomite in the basinal Raisby Formation (taking place during burial, at elevated temperatures, such that isotopically light dolomite was reprecipitated), or that dolomite further up the depositional slope precipitated from fluids enriched in ^{18}O and Sr over dolomite in the basin. Such trends could be expected if dolomitizing brines were hypersaline (containing evaporitically-concentrated ^{18}O and Sr), and sourced from the shelf area, flowing basinwards, and mixing with connate Zechstein seawater containing lesser amounts of ^{18}O and Sr (cf. Moore, 1989). The basinal area may also have been cooler than the shelf on which the dolomitizing brines may have been sourced. This would mean that basinal fluids with which the hypersaline, shelf-derived brines were mixing would tend to lower the temperature of the dolomitizing brines and so subdue the trends of decreasing $\delta^{18}O$ into the basin.

One sample of ferroan dolomite cement from Raisby Quarry, has a $\delta^{13}C$ of 4.3‰ and $\delta^{18}O$ of -6.3‰. The $\delta^{13}C$ value is depleted relative to nearly all Raisby Formation dolostones analysed (Fig. 5.16). The significance of this is uncertain, although clearly dolomitization/neomorphism was by different fluids to those which precipitated FCR

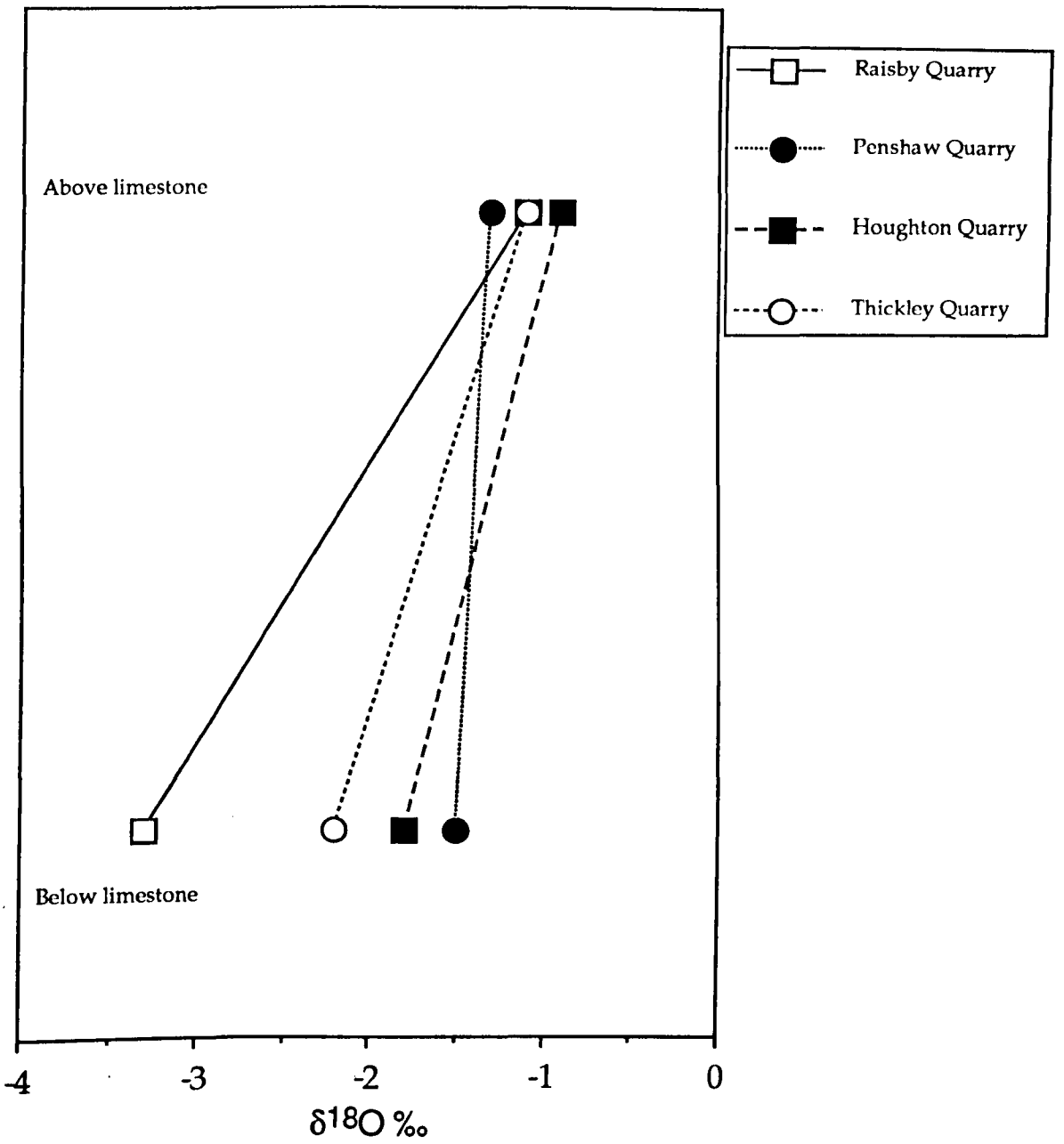

Fig. 5.17. Graph showing the difference in oxygen isotope composition of FCR dolostones analysed from directly above and directly below limestones close to the base of the Raisby Formation. No scale is implied on the vertical axis.

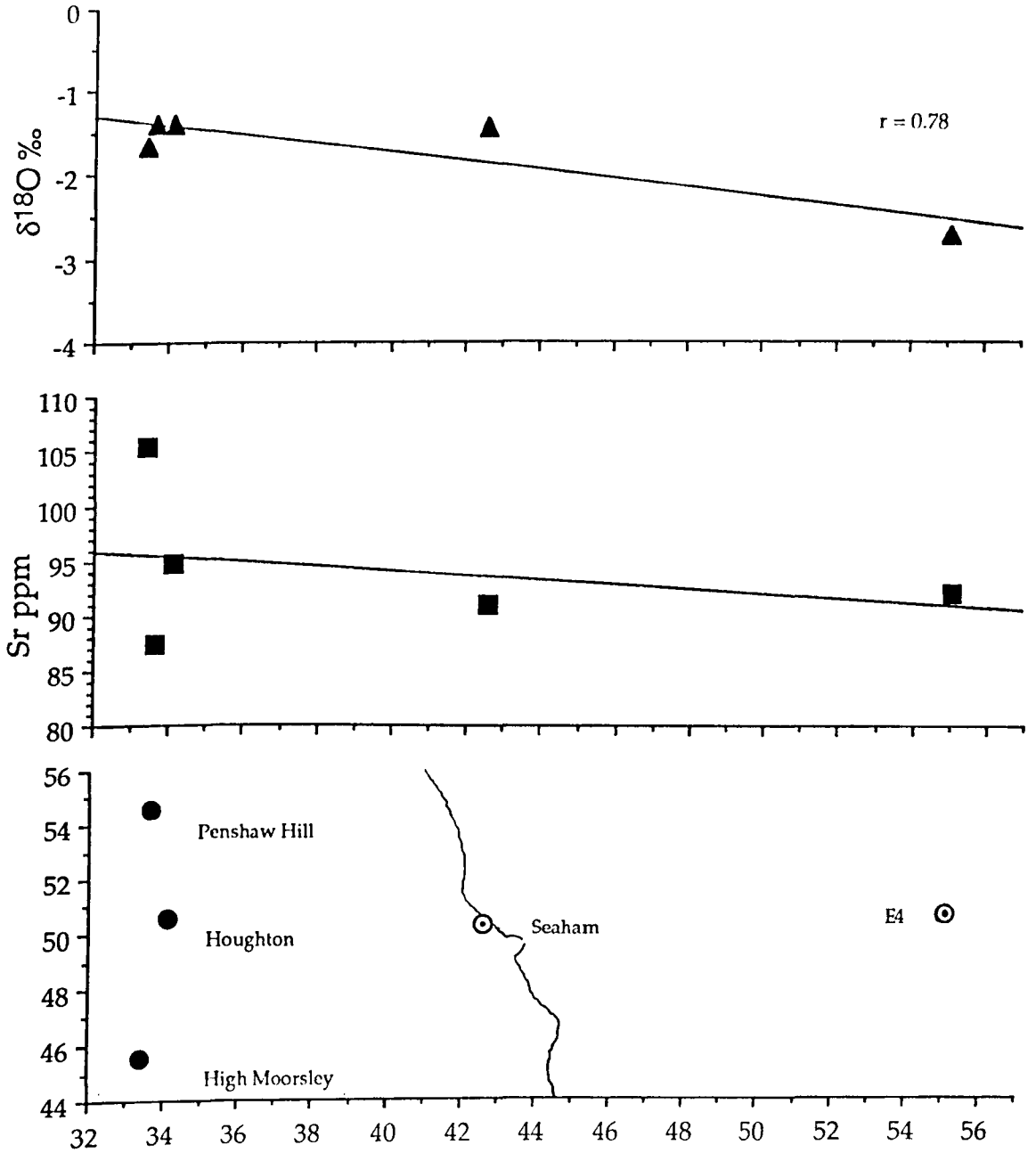

Fig. 5.18. Graphs showing the geochemical variation of the mean of FCR dolostone analyses in a traverse from outcrop into subsurface Raisby Formation. The values on the X and Y axes of the lower graph are national grid reference coordinates. The dolostone analyses are from throughout the Raisby Formation at the localities, and not one specific stratigraphic horizon.

dolomite. The $\delta^{18}O$ value is also depleted relative to FCR dolomite which is suggestive of precipitation from fluids of elevated temperatures (4.4.2.1).

Two samples of dolomitized anhydrite from High Moorsley Quarry gave carbon and oxygen isotope values more or less identical to FCR dolostones at High Moorsley Quarry (Fig. 5.16).

5.4.1. Petrography and geochemistry of dolomitization - Interpretation.

Four different types of dolomite have been distinguished within the Raisby Formation on the basis of petrography, later supported, to an extent, by trace element and stable isotope geochemistry. Owing to the aforementioned uncertainties of the partition coefficients of Fe, Mn, Sr and Na, and the question of neomorphism, trace element and stable isotope geochemistry is of questionable use in determining diagenetic environments of dolomitization, and origin and composition of dolomitizing fluids.

To be able to interpret the hydrological, geochemical and mineralogical environments under which dolomitization took place, the conditions which control dolomite precipitation need to be defined. The most important controlling (although not necessary) factors of large-scale dolomitization are summarized below:

Hydrologic

1. High enough permeability of carbonates to support a large scale fluid flow,
2. Effective and lasting hydrologic system to deliver Mg, CO_3 (? Fe, Mn & Na) and remove Ca and Sr,

Mineralogical

3. Suitably reactive substrate to be dolomitized (preferably finely crystalline),
4. Abundant HMC in the precursor will reduce the amount of Mg which has to be imported,

Thermodynamic

5. Low Ca/Mg ratio,
6. Low Ca/CO_3 ratio,
7. Elevated temperatures,

Kinetic

8. Low, as well as high salinities,
9. Slow crystallization to produce a well ordered dolomite
10. Reduced hydration of Mg ions,
11. Low dissolved SO_4 (less than 5% seawater),
12. Rapid dissociation of Ca, Mg and CO_3 ion complexes.

(compiled from Baker and Kastner, 1981; Bullen and Sibley, 1984; Machel and Mountjoy, 1986 & 1987; Hardie, 1987).

The geochemical conditions which promote and inhibit dolomitization are still very poorly understood, although in experimental work, the inhibition on dolomite precipitation (most likely kinetic) is greatly eased at elevated temperatures and given long reaction times (i.e., more realistic conditions for ancient dolostones). The presence of dissolved sulphate has been suggested to be the prime kinetic inhibitor to dolomitization (Baker and Kastner 1981; Morrow and Ricketts 1988), which indicates that dolomitization will be kinetically favoured in environments where sulphate is removed (i.e., hypersaline conditions with gypsum/anhydrite precipitation, or environments featuring sulphate reduction). This is supported by the very common association of large-and small-scale dolomitization with evaporitic environments. However, doubts have been raised concerning the universal applicability of sulphate inhibition (Machel and Mountjoy 1986; Morrow and Ricketts 1986; Hardie 1987). Although sulphate is removed from solution by the precipitation of sulphate evaporites, it commonly remains at high levels until near to the point of halite precipitation, and it is the availability of calcium which commonly limits the volume of evaporites precipitated in restricted evaporitic environments. E. Sass, (*pers. comm.*, 1989) suggests that the fluid Mg/Ca ratio is a more significant factor than is sulphate inhibition. The presence of dolomite in anoxic sediments featuring bacterial sulphate reduction has been suggested to be due not to sulphate removal, but to bicarbonate input as a by-product of the sulphate reduction reaction (Hardie, 1987; Sibley *et al.*, 1987; Shatkay and Magaritz, 1987). The increase in concentration of carbonate anions in solution means that relatively more anions have the energy to overcome the barrier of hydrated Mg ions on the surface of dolomite crystals (Morrow, 1982a; Machel and Mountjoy, 1986 & 1987; Hardie, 1987; Machel, 1987; Sibley *et al.*, 1987; Morrow and Ricketts, 1988). Supply of dissolved bicarbonate may thus be the single most important promoter of dolomitization in the sedimentary environment.

There are a large number of models which have been suggested to fulfill criteria for large-scale dolomitization (i.e., FCR dolostones). However, following a number of recent, contradictory reviews (Morrow, 1982a & b; Land, 1985; Machel and Mountjoy, 1986; Hardie, 1987), the applicability of these models is uncertain. Clearly, there is no one model to explain dolomitization; every occurrence is due to a unique juxtaposition of hydrological, mineralogical and geochemical processes. Broad-based models are of use to explain general hydrological and geochemical conditions. Currently, four main models are cited as able to account for massive dolomitization; meteoric-marine mixing, sabkha with reflux, seepage reflux, and 'seawater' models (Figs. 5.19 & 5.20). Most of these models, or variants of them, have been used at some time to explain dolomitization within the Zechstein Basin, and are illustrated, as may be applied to the Raisby Formation (Figs. 5.19 & 5.20).

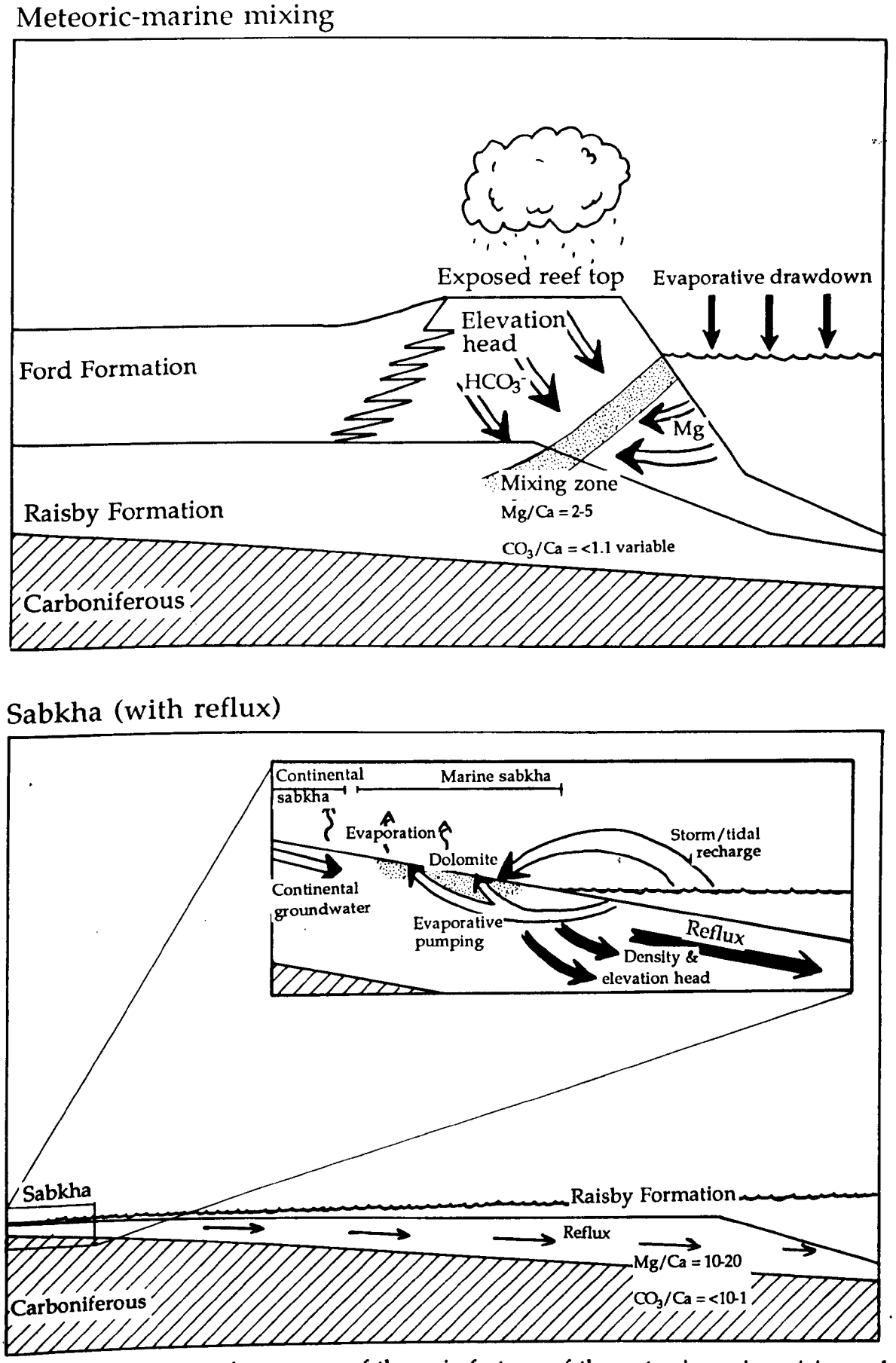

Fig. 5.19. Diagrammatic summary of the main features of the meteoric-marine mixing and sabkha dolomitization models, and how they could be applied to dolomitization of the Raisby Formation.

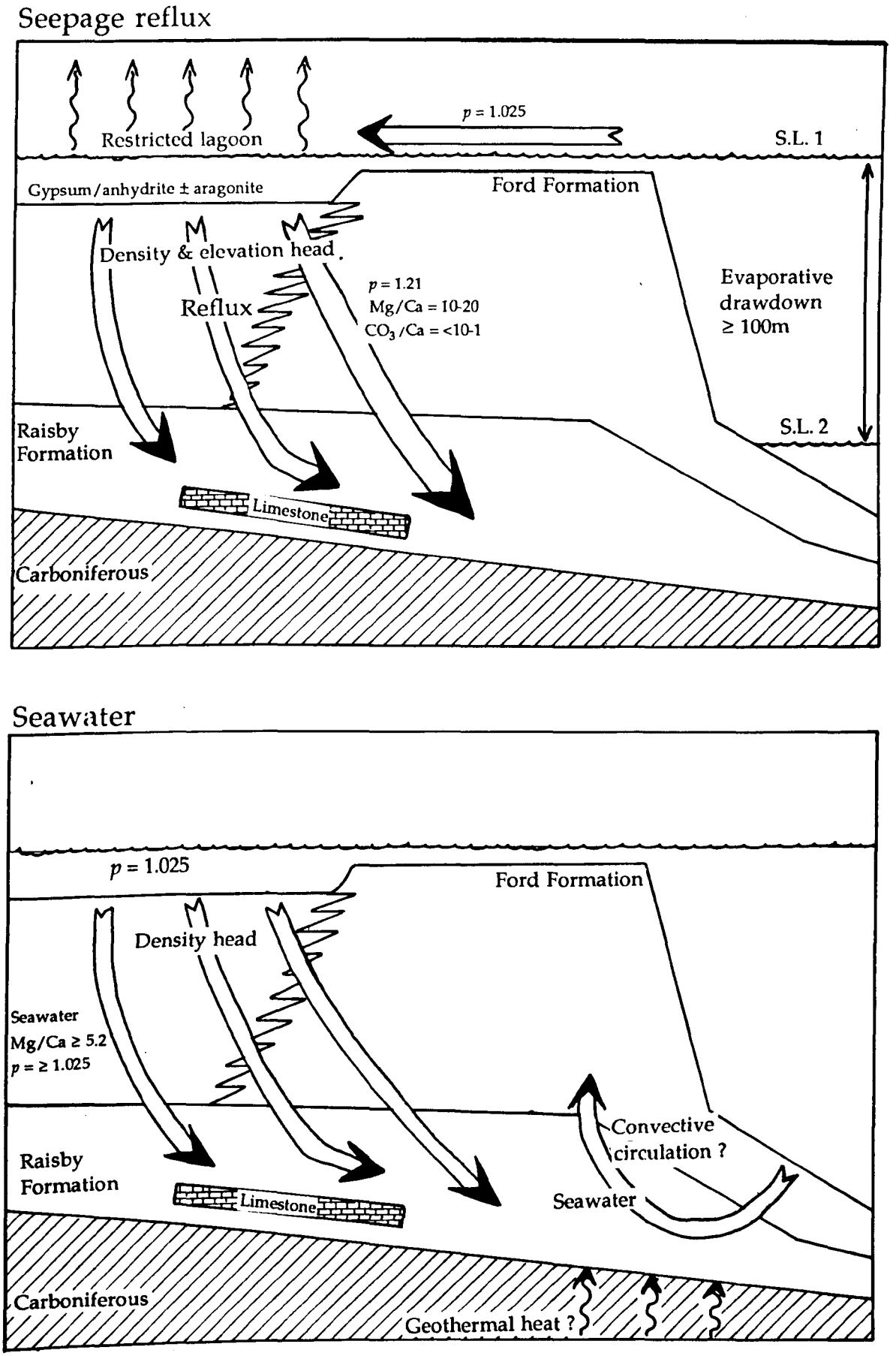

Fig. 5.20. Diagrammatic summary of the main features of the seepage reflux and seawater dolomitization models, and how they could be applied to dolomitization of the Raisby Formation.

A. Meteoric-marine mixing

This model was first applied by Badiozamani(1973) (Dorag model) and Land (1973) to the ancient following work by Hanshaw *et al.*, (1971), and further modified by Folk and Land (1975) (Schizohaline model). On the basis of thermodynamic calculations (Badiozamani, 1973), and kinetic considerations (Folk and Land, 1975), it is suggested that a mixed meteoric-marine solution would be simultaneously supersaturated with respect to dolomite and undersaturated with respect to calcite, plus have a low Ca/Mg ratio (it would also have a low Ca/CO_3 ratio [Morrow, 1982b]). Kinetic inhibitors to dolomitization decrease at lower salinities (Folk and Land, 1975; Machel and Mountjoy, 1986). Such dolomitization would be expected within coastal environments, in the marginal zone where meteoric aquifers interact with intruding seawater (such as coastal northeast England at the present day [Anderson, 1945]). Circulation of the mixed meteoric-marine solution is due to meteoric groundwater flow, itself commonly driven by an elevation head. To form extensive replacive dolostones, the narrow zone of mixing would have to migrate, probably very slowly, through the entire carbonate formation. Recently, doubt has been expressed as to the hydrologic and geochemical ability of mixing zones to form thick dolostone sequences (Machel and Mountjoy, 1986; Hardie, 1987; L.S. Land, *pers. comm.* to G.M. Harwood, 1988). Moreover, there is a lack of relevant modern examples where extensive mixing zone dolomitization has occurred, although this may be due to fluctuation in sea level during the Pleistocene and Recent (Land, 1985). In modern mixing zones, the rate of calcite dissolution usually greatly exceeds that of dolomite precipitation (Plummer, 1975). Where dolomitization has not taken place before uplift into the meteoric diagenetic environment, it may well be that the role of mixing zones is to 'precondition' the margins of carbonate platforms for later massive dolomitization, by providing dolomite nuclei together with high porosity and permeability, a result of dissolution (Plummer, 1975), thus promoting rapid advection rates of later dolomitizing solutions (Humphrey and Quinn, 1989).

A few previous authors have ascribed Zechstein dolomitization to mixing zone processes, most notably Kaldi and Gidman (1982) for localized dolomitization within the Cadeby Formation. Aplin (1985), suggested that dolostones of the Ford Formation reef may have been neomorphosed within a mixing zone during exposure of the reef associated with evaporative drawdown in the basin.

B. Sabkha dolomitization.

The occurrence of dolomite forming in recent, arid intertidal and supratidal plains was first described by Illing *et al.*, (1965) from the Qatar Peninsula of the Persian Gulf. Dolomite in modern sabkhas forms as finely crystalline (1-5μm), poorly ordered, calcian crystals (protodolomite) (Gaines, 1977; Morrow, 1982b). Dolomitization of aragonite muds is due to evaporation of marine floodwaters, commonly below the sabkha surface, so that

gypsum/anhydrite and aragonite are precipitated, which decreases fluid Ca/Mg and Ca/CO_3 ratios (Butler, 1969). Additional CO_3 may be provided by below-surface bacterial sulphate reduction (Machel and Mountjoy, 1986), and influx of continental groundwaters (Hardie, 1987). However, it is unlikely that sabkha dolomitization is effective on a large scale, as dolomite precipitation is restricted to a small area of the sabkha surface (McKenzie *et al.*, 1980; Morrow, 1982b; Machel and Mountjoy, 1986), and it may be that the dolomite which has been recorded is a cement, and not replacive at all (Hardie, 1987). It has however been suggested that a reflux (seawards flow) of slightly elevated, dense, evaporatively concentrated, magnesium-rich brines from on, or just below the sabkha surface, may produce regionally extensive dolomitization of laterally equivalent and underlying carbonates. Elevation head provided by storm recharge of marine waters is probably more important than the density head (Land, 1985). Such a reflux has, however, not been recorded more than a few metres below the sabkha surface, and so its importance is questionable, especially considering the relatively small volumes of fluids which can be sourced from the sabkha surface (Machel and Mountjoy, 1986). Another type of flow may also exist beneath sabkhas, termed 'evaporative pumping' by Hsu and Siegenthaler (1969). In this model, seawater is drawn landward due to intense evaporation and dessication on the sabkha surface. This flow is also capable of dolomitization, although again on a relatively small scale, and restricted to the sabkha itself (Fig. 5.19).

C. Seepage reflux.

In the seepage reflux model, as originally described by Adams and Rhodes (1960), the source of low Ca/Mg, low Ca/CO_3 ratio fluids is evaporatively concentrated seawater in large back-barrier lagoons. Seawater enters over a partial sill, becomes concentrated and increases in density, eventually refluxing seawards through underlying carbonates, displacing less dense marine pore fluids. Reflux may also be greatly enhanced by periodic eustatic falls in sea level (Fig. 5.20). Sulphate is precipitated within the lagoons, although as such sulphates are relatively porous, they would not completely seal off the lagoon floor. The principles of this process is similar to the seawards reflux of concentrated brines hypothesised for sabkhas, but clearly much larger volumes of brines can be generated over very much larger areas (tens to hundreds of square kilometres in the geological record). The difficulty with evaluating this model is the scarcity of adequate modern analogues, and so the scale and effectiveness of reflux cannot be quantified (Morrow, 1982b). One of the best documented reflux analogues to date is by Deffeyes *et al.*, (1965) from Bonaire. Implicit in the model of Adams and Rhodes (1960), is that reflux dolomites must be closely associated with large bodies of shallow water marine evaporites, and commonly also, replacive sulphates.

D. 'Seawater' models.

A number of models have been proposed in recent years whereby the dolomitizing agent is unmodified to slightly hypersaline seawater (Fanning *et al.*, 1981; Sass and Katz, 1982; Saller, 1984; Simms, 1984). Seawater has a high free energy drive to dolomitize carbonates (it has a molar Ca/Mg ratio of 0.19), and may cause dolomitization, providing a suitable hydrologic system is established (which in turn is partly dependant on the permeability of the sediments being dolomitized), and, more importantly, enough time is available (Morrow, 1982a; Land, 1985; Hardie, 1987). One of the most commonly cited mechanisms for driving large volumes of seawater through carbonates is 'Kohout convection' (Simms, 1984). This model, based on the margins of the Florida platform, suggests that seawater moves from the seaward margin into platform interior in response to thermal gradients between the geothermally heated shelf and cooler seawater. Therefore, seawater circulates owing to combined effects of the convection of buoyant, thermally heated seawater and interaction with meteoric waters driven by elevation head (Kohout, 1967). Analysis of the composition of fluids issuing from submarine springs on the margins of the Florida shelf by Fanning *et al.*, (1981), suggests that the brines were originally seawater, modified by dolomitization. However, it is probable that this seawater thermal convection model is only applicable to isolated banks and atolls (Hardie, 1987). Thus, thermal drive mechanisms are unlikely to have been of significance with regard to dolomitization of the Raisby Formation, owing to the relatively small size of the basin margin, not large enough for a substantial geothermal gradient to establish.

Simms (1984) describes a model ('plume reflux') for the dolomitization of Bahamian platform carbonates, whereby slightly hypersaline bank water is driven through hundreds of metres of underlying carbonates just by a density head. This should form dolostones which cross-cut several formation boundaries (Machel and Mountjoy, 1986). Within deep marine carbonates, it is possible that dolomitization may also be active, on a smaller scale, although seawater circulation would be limited by the low porosity and permeability of the sediments and the absence of significant density or thermal gradients. Graber and Lohmann (1989) describe dolostones within Permian basinal marine carbonates, where dolomitization was driven both by metastability of the aragonite-dominated sediments during early burial and diffusion of Mg from overlying seawater.

Clearly, hydrologic systems can be set up to drive large volumes of normal seawater through carbonate units. The seawater drive could be stable for geologically significant lengths of time, and so overcome kinetic and thermodynamic difficulties such as sulphate inhibition, and high Ca/CO_3 ratios. Given sufficient time, dolomitization may also be effective within fine, basinal carbonate sediments.

5.4.2. FCR dolostones - Interpretation.

Few major petrographic or geochemical subdivisions can be made within FCR dolostones, and so they are interpreted to be the product of the same episode of dolomitization, or later neomorphism, which has erased or subdued earlier compositional variation. That most dolomite crystals have planar faces and intercrystalline boundaries suggests a relatively low temperature dolomitization, probably below the critical roughening temperature (CRT) of 50-100°C (Gregg and Sibley, 1984; Sibley and Gregg, 1987), or ≤35°C (Shukla, 1986). As crystal sizes are due to an interplay between growth rate and nucleation rate, finely crystalline FCR dolomite suggests that nucleation rate outstripped growth rate. This could be indicative of a high density of nucleation sites, growth below 50-100°C, together with a relatively high dolomite supersaturation (Gregg and Sibley, 1986). Unimodal crystal size distributions suggest only one phase of nucleation (or a single phase of neomorphism) in any one place.

The common occurrence and restriction of inclusions to within dolomite crystal cores is taken to suggest that rates of dolomite precipitation over those of precursor carbonate dissolution were variable. The rates of dolomite crystal growth were initially relatively high, such that the dolomite was fully replacive of precursor carbonate, whereas later, carbonate dissolution was more rapid than dolomite crystal growth, and so the dolomite grew more by pore fill cementation. This in turn could suggest, with time, an increase in supersaturation with respect to dolomite and/or an increase in undersaturation with respect to the precursor carbonate. With progressive dolomitization, the fluid Ca/Mg ratio should increase overall (although the extent to which it increases depends largely on the openness of the diagenetic system). Such an increase may reduce supersaturation with respect to dolomite and so slow its growth, such that eventually, it is growing at a slower rate than the precursor carbonate is being dissolved. A slower, more ordered growth of the inclusion-free rim may explain why it is more stable (it has a lower free energy) during outcrop weathering, than the inclusion rich core. The relative rates of dolomite precipitation over those of carbonate dissolution are also suggested to have controlled the preservation, or not, of textures within precursor carbonates, especially fossil material. Furthermore, the retention of inclusion rich cores and relict textures within the dolomite suggests that neomorphism, if it did occur, did not alter textures (i.e., it was by fine scale dissolution-reprecipitation). Textural information thus suggests precipitation in a fairly low-temperature environment (shallow burial) with crystals having an ordered growth. The fluid was initially of a relatively high supersaturation with respect to dolomite, and at least at times reducing, allowing minor Fe and Mn coprecipitation.

The smaller crystal sizes of dolomite within dolomitized clasts of resedimented carbonates is most likely due to a combination of a higher density of nucleation sites, and a more tightly cemented precursor carbonate. Early cementation of carbonate muds at or close

to the sea floor, for which there is abundant evidence within the Raisby Formation, would generate a finely crystalline, tight limestone. As there is no evidence for cementation of intergranular porosity within carbonate muds by coarsely crystalline marine calcite, early cementation was most likely by add on growth of calcite onto fine carbonate grains. Therefore, the limestone would have been very finely crystalline, providing a high density of nucleation sites and so allowing no room, or time for large dolomite crystals to grow. The same explanation is true for the relatively small crystal sizes of dolomitized fossil fragments relative to their matrix. Mimic dolomitization is suggested by Bullen and Sibley (1984) to be indicative of abundant dolomite nuclei which result in relatively rapid crystal growth rates. This is in agreement with the fine crystal sizes of clasts and non-mimic dolomitized fossil fragments.

There is very little evidence for the timing of dolomitization in the Raisby Formation. As nearly all gypsum and anhydrite replaces dolostones, this suggests dolomitization predated extensive flow of calcium and sulphate-rich fluids, which was probably multiphase (5.7.1). The petrology and distribution of replacive gypsum and anhydrite does suggest it may have precipitated during, or shortly after dolomitization (5.7.1). In a number of samples, dolomitization postdates a phase of marine calcite cementation and pyrite framboid precipitation. At Houghton and Raisby Quarry, partial replacement of dolomite crystals in a partially dolomitized limestone by calcite microspar, suggests that, at least locally, dolomitization predated neomorphism of the aragonite-dominated carbonate mud to dLMC microspar. Dolomitization was therefore probably late eogenetic/early mesogenetic.

The trace element geochemistry of FCR dolomite is of little use in characterizing the dolomitizing fluid, although near-stoichiometric compositions may suggest evaporitically-concentrated fluids (i.e., high Mg/Ca ratio). The low Fe and Mn contents of the FCR dolomite also argue against significant involvement of meteoric fluids, as do the stable isotopes. Magaritz (1987) uses oxygen isotope compositions of dolostones from the Hartlepool Anhydrite Formation, similar in value to those of the Raisby Formation, to suggest meteoric water input into the basin. However, it is more likely that the deviation of Hartlepool Anhydrite Formation results from predicted values indicate neomorphism of dolostones during burial. That the carbon and oxygen isotope values of the least-altered Raisby Formation dolostones are both heavier than those of least-altered limestones, could suggest that hypersaline Zechstein seawater (concentrating ^{13}C and ^{18}O) was a major contributor to the dolomitizing fluid.

The petrographic and geochemical similarity of dolostones from the Ford and Raisby Formations suggest dolomitization and/or neomorphism by fluids of a similar nature, although not necessarily at the same time. The dolomitization of the Raisby Formation thus cannot be viewed in isolation. The ubiquitous occurrence of dolomitized carbonates

throughout the Zechstein Basin (Clark, 1980), implies dolomitization was a very common process operative throughout the basin and during most of its history.

Dolomitization by mixing zone processes is very unlikely to have occurred e:extensively within the Raisby Formation, which is mainly evidenced by the lack of lack of any evidence for extensive flow of meteoric-derived groundwaters (i.e., cavernous dissolution porosity). Kaldi and Gidman (1982) invoke marine-meteoric mixing to explain precipitation of early diagenetic dolomite cements within ooid shoals of the Cadeby Formation in Yorkshire. However, this is a localized occurrence, and the validity of their interpretation is questionable. Aplin (1985) suggested that a meteoric-marine mixing zone moved through the Ford Formation reef, leading to neomorphism of the earlier formed dolostones. Although the upper part of the Ford Formation was possibly exposed (Aplin, 1985), it is unlikely that it was exposed for long enough, or that there was a large enough meteoric input for meteoric-derived fluids to penetrate the 100m+ of overlying Ford Formation into the Raisby Formation (at least in those rocks exposed at outcrop) (Fig. 5.19). Lateral fluid advection from exposed shelf carbonates into slope and basinal Raisby Formation cannot be discounted.

Dolomitization of the Raisby Formation could have been achieved by circulation of normal seawater during deposition of the Ford Formation (Fig. 5.20). It is unlikely that thermally driven circulation would have been repeatedly operative throughout the Zechstein Basin during most of its history. This does not discount density-driven circulation of slightly hypersaline seawater from the back reef Ford Formation lagoon (Fig. 5.20). This process could have been operative widely through the Zechstein Basin. However, as the slope and basinal first cycle carbonates in Durham and Yorkshire are overlain by up to 180m of sulphates (Hartlepool Anhydrite Formation), this strongly suggests that dolomitization was associated with hypersaline fluids formed during deposition of the Hartlepool Anhydrite Formation (Lee and Harwood, 1989). This would be in accordance with petrographic evidence (late eogenetic/early mesogenetic dolomitization, a single nucleation event from fluids of low temperature, but relatively high supersaturation) and geochemical data (carbon and oxygen isotopes, and (Fe+Mn) suggest possibly hypersaline Zechstein seawater). Although they postdate dolomitization, replacive sulphates within the Raisby Formation clearly demonstrate that evaporitically-concentrated, seawater-derived fluids did move through the formation (5.7.1). Throughout the Zechstein Basin carbonate units are directly overlain by extensive bedded evaporites, and so dolomitization by hypersaline brines could have operated repeatedly throughout the basin, throughout its history.

All of the first cycle Zechstein carbonates in the English sub-basin have been pervasively dolomitized, from nearshore (Cadeby Formation) into slope and basin (Raisby Formation). The Cadeby Formation may be considered an analogue for the now eroded inner shelf Raisby and Ford Formations. If dolomitization was by fluids of the same origin,

they would have had to cover the area from nearshore to basin, over many tens of kilometres. Harwood (1981 & 1986) considers that most of the Cadeby Formation was dolomitized by hypersaline fluids originating from the deposition of overlying evaporites, although the most nearshore carbonates may have been dolomitized in a sabkha environment (Kaldi, 1986b). Aplin (1985) also considers that the source of hypersaline fluids which dolomitized the Ford Formation reef was in a semi-restricted back-reef lagoon. However, although dense, these fluids would not have had sufficient head to flow through great thicknesses of low permeability carbonate muds, and continually reinforce Mg to fluids down-flow (especially if the dolomitization reaction involved substantial liberation of Ca). The head in these back-barrier lagoons may have been greatly accentuated by falls in the level of the Zechstein Sea (Fig. 5.20). A fall of possibly greater than 100m, owing to evaporative drawdown of the basin, directly preceded the deposition of the Hartlepool Anhydrite Formation (Taylor, 1980 & 1984). Deposition of the Hartlepool Anhydrite Formation itself, was characterized by an oscillating brine level. Four to five cycles of basin recharge and evaporative drawdown can be detected in the basinal facies (Taylor, 1980), although to precipitate the observed thickness of anhydrite (relative to halite and bittern salts) there must have been many more episodes of partial flooding of the basin followed by evaporative drawdown, albeit of smaller amplitude. Such an oscillating brine level would have provided an effective pumping mechanism to force large volumes of Mg-rich hypersaline brines derived from back reef lagoon(s) through the first cycle carbonates (Fig. 5.20). Brines in these lagoons would have been recharged upon basin refilling, and then refluxed basinwards upon evaporative drawdown of the basin during progressive deposition of the Hartlepool Anhydrite Formation. This is supported by Goodall (1987), who shows that the Edlington Formation of Teesside was deposited in a system of shallow back-barrier lagoons, coeval with precipitation of the Hartlepool Anhydrite Formation in the basin. Flow of the Mg-rich brines through the first cycle carbonates would have been progressively aided by dolomitization which moved progressively deeper into the carbonate wedge, and so over time, the Mg-rich fluids could flow further and more easily (as dolostones had a relatively high porosity and permeability) before meeting any undolomitized limestones (Fig. 5.20). The main dolomitizing episode most likely took place relatively early in the history of deposition of the Hartlepool Anhydrite Formation, before the top of the first cycle carbonates were sealed by gypsum/anhydrite.

Support for the downwards-moving fluids from shelf to basin comes from the fact that limestones are only recorded within the first cycle carbonates of Durham in slope and basinal facies of the Raisby Formation far from the source of dolomitizing fluids (back-barrier lagoons), where they would have been least effective (Fig. 5.20).

5.4.3. PPS dolostones - Interpretation.

The crystal sizes and textures of these dolomites are very similar to type FCR, again suggesting a relatively low temperature, ordered growth from reducing fluids of relatively high dolomite supersaturation. Decreasing dolomitization away from the centre of dolomite-rich bands can be interpreted in terms of a gradient of decreasing dolomite supersaturation (Sibley and Gregg, 1987; Sibley *et al.*, 1987). Growth rate however, did not vary, and uniformity of crystal sizes suggests a single nucleation event in any one place (Sibley and Gregg, 1987). This dolomite is always associated with bedding-parallel swarms of microstylolites, which suggests an analogy with the pervasive pressure solution dolomitization model of Wanless (1979). In this model, fluids necessary for dolomitization are derived by flow along stylolites during pressure solution. This interpretation is supported by the lateral impersistence and high insoluble residue concentrations of the partially dolomitized limestones in the Raisby Formation. This style of dolomitization is only recognizable where it has been incomplete within limestones (Fig. 5.8a). It may have gone to completion elsewhere within the formation, but cannot be recognized.. No dolomitization was recorded along coarser sutured seam stylolites within limestones. The reason for the difference is not known. Redolomitization in the W8 borehole was along a sutured seam stylolite, although the stylolites themselves are anomalously thick, and in thin section comprise a concentrated mass of microstylolites. It is uncertain how large amounts of ions in solution can be transported along microstylolites, although it is a well documented phenomenon (Bathurst, 1975). It is possible that stylolites are open during a stage in their formation, facilitating relatively rapid rates of fluid advection.

There is no firm evidence concerning timing of this dolomitization. It most likely postdates FCR dolomite precipitation, as the PPS dolomitization may have resulted from partial redistribution of FCR dolomite. At Houghton Quarry, there is possible evidence for dolomitization postdating calcium sulphate precipitation, but it is certain in borehole W8. That, in W8, PPS dolomite is replacive of calcite, itself replacive of FCR dolomite, strongly suggests that PPS dolomite did postdate FCR dolomitization. The intimate association with stylolitization, suggests dolomitization during mesogenesis, following significant burial. Although, it is recognized that stylolites can form under relatively shallow burial conditions, it is most likely that they formed after more than 1km burial.

The Mg and CO_3 for dolomitization were most likely derived by dissolution of local (intra-formational) carbonates (cf. Wanless, 1979). It is commonly suggested that Mg from stabilization of HMC to dLMC is an important source (the 'solution-cannibalization' model [Morrow, 1982b]). However, such an early dolomitization is unlikely in the Raisby Formation. The host limestones at Houghton Quarry, following neomorphism, average 1 mole% $MgCO_3$ (4.3.2). PPS dolomitization at this locality postdated neomorphism of the host limestone, leading to further alteration (Fig. 4.12). To produce one unit of stoichiometric

dolomite, 49 units of this limestone would need to be dissolved, and the solution would have a Ca/Mg ratio of 99 and a Ca/CO_3 ratio of 0.99, which is not very conducive to dolomitization. Thus, dissolution of already-formed FCR dolomite is the most probable source. However, even with no contamination from dissolved limestone or sulphates (which is extremely unlikely), the solution would have a Ca/Mg ratio of 1 and Ca/CO_3 ratio of 0.5. However, with minimal gypsum/anhydrite dissolution the solutions would have very little dissolved sulphate to inhibit dolomitization. Given very long timescales and elevated temperatures of burial, dolomitization by pressure solution of FCR dolomite is likely. That the PPS dolomites appear to have a greater iron content than do precursor FCR dolomites, is also in support of the PPS dolomite postdating FCR dolomitization, iron being more concentrated in the later precipitate owing to its positive partition coefficient.

The fact that partial dolomites nearly all contain 28 to 30% dolomite, implies a limiting factor on pervasive pressure solution dolomitization. Sperber *et al.*, (1984) suggest that permeability is the major controlling factor restricting partial dolomitization of a limestone to 30%. In the Raisby Formation, the limiting factor may be a combination of very low permeabilities which characterize the limestones, coupled with an abrupt decrease in dolomite supersaturation away from the source (microstylolite swarm).

5.4.4. Ferroan dolomite cements - Interpretation.

All ferroan dolomite cements recorded were more coarsely crystalline than FCR and PPS dolomite, and have planar faces and intercrystalline boundaries. Their coarse crystal size is suggestive of relatively high temperature growth conditions (above CRT) and low dolomite supersaturation, whereby growth rate exceeds nucleation rate (Gregg and Sibley, 1984; Machel and Mountjoy, 1986; Zenger and Dunham, 1988). This is illustrated at Raisby Quarry whereby ferroan dolomites nucleate off some corroded dolomite crystals, although poikilitically enclose others. Thus, they indicate that some cement crystals grew substantially before others had time to nucleate (4.3.3). Dolomite growth above CRT would be expected to produce non-planar crystals. However, Gregg and Sibley (1984) show that dolomite cements commonly show faceted growth, even at temperatures above CRT, owing to impurities. The well developed cements syntaxially overgrowing echinoderm fragments in the Hurworth Place borehole, suggest that crystal growth rates were faster and more ordered where single crystals formed the substrate.

One isotopic determination of ferroan dolomite cements from Raisby Quarry with low $\delta^{18}O$ may support the suggestion of precipitation from fluids at elevated temperatures. Radke and Mathis (1980) suggest that saddle dolomite (as seen at Thickley), precipitates at temperatures of 50-130°C. The ferroan composition of all the dolomite cements shows that the dolomitizing fluids were reducing, and that the amount of iron and manganese in solution fluctuated significantly to produce trace element zonation (Fig. 5.10). Retention of

good crystal forms, together with corresponding trace element zonation suggests that the ferroan dolomite cements have undergone minimal, if any, neomorphism.

The reason for the relative scarcity of dolomite cements is that all of the Raisby Formation limestones and dolostones, throughout their diagenetic history up to the Tertiary, have had a very low porosity and permeability owing to 'plugging' by replacive and pore filling sulphates relatively early in their diagenetic history. The generation of porosity and permeability, facilitating such cement growth, came with mesogenetic fracturing and/or dissolution. The necessary cations and anions for dolomite precipitation may have been of very local derivation, by dissolution of ferroan dolomite host rocks, for example those from Raisby and Thickley Quarries and E3a borehole (cf. Radke and Mathis, 1980; Machel, 1987a). However, the association of ferroan cements with ferroan host dolostones could also be explained by neomorphism of the host FCR dolostones under the influence of Mg-, Fe-, and Mn - rich fluids which precipitated the ferroan dolomite cement. As K^{Fe}_{Dol} and K^{Mn}_{Dol} are greater than 1, such neomorphism should result in Fe and Mn autoenrichment. Alternatively, if not derived from dissolution of host rocks, the very small amounts of necessary Fe, Mn and Mg could also have been derived from illitization of smectite clays (cf. Schofield and Adams, 1986; Gawthorpe, 1987; Gregg, 1988), although this would only occur below 2km burial (Morrow, 1982b), which was reached in the late Mesozoic (Appendix X).

There are few problems in precipitating dolomite cements at elevated temperatures, especially in excess of 100°C, as most kinetic inhibitors to dolomitization become unimportant (Hardie, 1987). Saddle dolomite precipitation may have been further kinetically favoured by biological or thermochemical reduction of sulphate derived from dissolution of anhydrite within the dolostones to form sphalerite, a reaction which may also liberate carbonate anions (Radke and Mathis, 1980; Machel, 1987a) (7.2.3).

5.4.5. Dolomitized anhydrite - Interpretation.

These dolomite textures have not previously been described to the author's knowledge, although Stemmerik *et al.*, (1986) record similar, 500µm long dolomite needles within oncoids from Danish Zechstein carbonates. The needles, they suggest, are pseudomorphs after gypsum. The lath-shaped dolomite crystals in the Raisby Formation must have grown in an elongate form, most likely due to mimic replacement of a lath-shaped precursor. As the lath-shaped dolomite replaces material of different original mineralogies, there must have been a lath shaped intermediate phase - most likely anhydrite. Anhydrite nodules in the Raisby Formation commonly comprise a mass of small lath-shaped crystals. The variation of textures within the High Moorsley Quarry debris flow from interlocking and undisturbed dolomite laths (Fig. 5.11a & b) to internally sedimented crystals within debris flow clast and gypsum crystal pseudomorphs (Fig. 5.27b), is interpreted to represent variability in the intensity of replacement of the pre-existing anhydrite by

dolomite. The dolomite was internally sedimented where replacement of anhydrite had been incomplete, and so the dolomite laths could not form a self-supporting framework after sulphate dissolution.

To dolomitize anhydrite but still retain its original structure, a fine scale dissolution-reprecipitation reaction would be necessary and Mg and CO_3 would need to be imported and SO_4^{2-} exported by the solution. This is problematical considering the possible inhibiting effect of SO_4, and the necessity for large quantities of CO_3. Pierre and Rouchy (1988) describe dolomitized sulphates, characterized by strongly negative carbon isotope compositions, clearly indicating that the CO_3 was derived by bacterial reduction of the gypsum/anhydrite sulphate. Anderson and Garven (1987) also suggest that sulphates cannot be replaced by dolomite unless simultaneous bacterial sulphate reduction is taking place. Carbon isotope values for dolomitized anhydrite in the Raisby Formation do not indicate bacterial reduction, although the isotopic composition may have been reset by neomorphism. As the dolomite replaces anhydrite, although occurs within gypsum crystal pseudomorphs, dolomitization must have been at least after burial below the depth of dewatering of gypsum to anhydrite (5.7.2). The physico-chemical controls on the replacement of anhydrite by dolomite are thus unknown, and no explanation can be provided, given the apparent non involvement of organic matter and bacterial sulphate reduction. The significance of the dolomite cements associated with the lath-shaped dolomite texture is unclear. However, it may simply represent the form a dolomite cement takes when growing into a porosity filled by sulphate, as would have been the case in both of the examples.

5.5. Summary.

Replacive dolomite, which comprises almost all of the dolostones in the Raisby Formation, appears to be attributable to dolomitizing fluids which originated by evaporative concentration of Zechstein seawater, immediately preceding, and during precipitation of the Hartlepool Anhydrite Formation. The brines most likely moved from the shelf areas of the top of the first cycle carbonates, down-dip towards the basin. Reflux of these brines was facilitated by cycles of recharge and evaporative drawdown in the basin. Following burial and replacement by sulphates, some of the initial replacive dolomite was locally dissolved by pressure solution and redistributed along stylolites to form replacive dolomite (PPS dolomite) and ferroan dolomite cements which partly occlude secondary dissolution and fracture porosity. The origin of the dolomite which locally replaced anhydrite remains uncertain.

5.6.1. Sulphate evaporites - Introduction.

The former presence of considerable quantities of disseminated calcium sulphate evaporite minerals within the Raisby Formation was first noted by Woolacott (1919b), who described gypsum from within the limestone at Raisby Quarry, and recognized that numerous calcite-lined geodes at outcrop originally hosted gypsum and/or anhydrite. Raymond (1962) described the petrography of still-preserved gypsum and anhydrite from boreholes in the Raisby and Ford Formations of the Stainton and Billingham areas. Numerous other authors have noted the presence, and former presence of sulphates within the Raisby Formation (Magraw *et al.*, 1963; Smith and Francis, 1967; Jones, 1969; Jones and Hirst, 1972; Hirst and Smith, 1974; Mills and Hull, 1976), although no detailed work has hitherto been carried out. In addition to calcium sulphates, Raymond (1962) records very minor quantities of epsomite, magnesite and sylvite from within Raisby/Ford Formation dolostones in borehole G7 near Gt. Stainton. Still preserved and/or former sulphate evaporites have been described from the Ford Formation main reef (Smith, 1981; Aplin, 1985; Tucker and Hollingworth, 1986), and the Cadeby Formation (Harwood, 1981; Harwood and Coleman, 1983; Harwood, 1986; Kaldi, 1986b).

In the Raisby Formation at outcrop, virtually all pre-existing sulphates have been leached. Gypsum and anhydrite are currently preserved only where the Raisby Formation is overlain by considerable thicknesses of Zechstein sediments, in south Durham and off the Durham coast. Thus, most of this study on calcium sulphate precipitation and diagenesis is from pseudomorphs at outcrop, supplemented by data from still-preserved sulphates in offshore boreholes.

5.6.2. Gypsum and anhydrite within boreholes - Description.

Preserved gypsum and anhydrite was studied from three offshore boreholes; W15, W8 and E3a. No boreholes examined in the present study hosted unaltered anhydrite, and so only analysis of gypsum, forming by the hydration of anhydrite, and relics of anhydrite within secondary gypsum was possible. Two types of gypsum have been identified crystallographically; porphyroblastic and alabastrine. The mineralogy of the evaporites was obscured in some samples by partial dehydration of gypsum to acicular ?bassanite crystals, presumably during section making (G.M. Harwood, *pers comm.*, 1989).

Porphyroblastic gypsum is a very common rehydration product, whereby anhydrite has partially or completely converted to coarse, anhedral to sub-euhedral gypsum crystals. Porphyroblasts within the Raisby Formation are almost all elongate, from 500μm to 1.8mm in length, and most have curved, non-linear intercrystalline boundaries (Fig. 5.21a). In general, the largest porphyroblasts have straighter sides and are more euhedral. Within some samples, growth of porphyroblasts may in part have been controlled by the distribution of fine dolomite inclusions, inherited from former replacive sulphate. Most

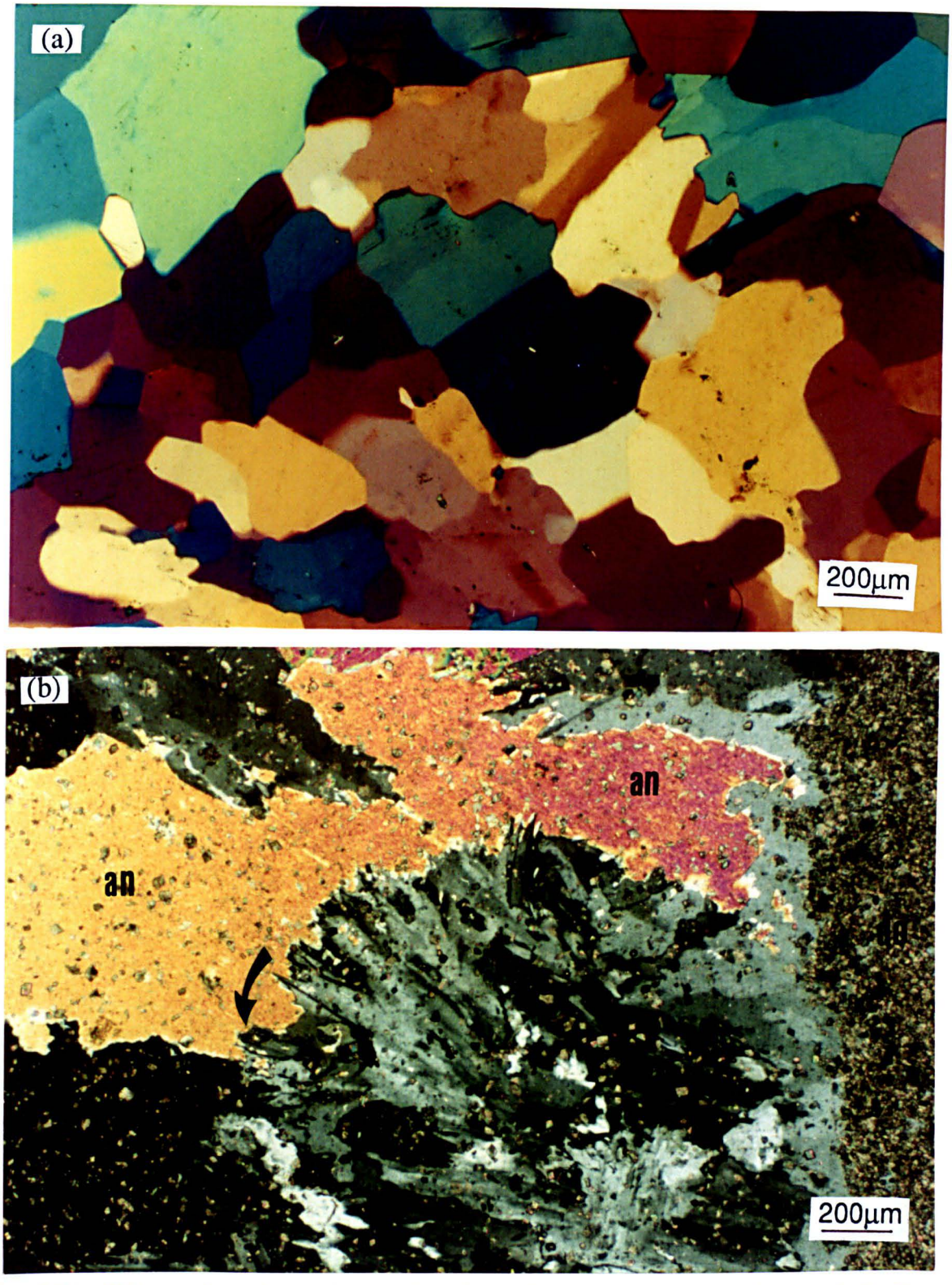

Fig. 5.21. Thin section photomicrographs of porphyroblastic gypsum; (a) borehole E3a, 354.33m, crossed polars with sensitive tint plate, (b) borehole W8, 277.60m, crossed polars. (a) shows the typical nature of porphyroblastic gypsum, which contains very few anhydrite or dolomite inclusions. In (b), anhydrite [an] is being replaced by a radiating array of gypsum crystals. Note the rectilinear terminations of the gypsum crystals (arrowed), and that there is no change in the density of dolomite inclusions between anhydrite and gypsum. Replacement of anhydrite in (b) has started from the margins of the host dolostone [do].

porphyroblasts have an irregular to undulose extinction, defining numerous poorly developed subcrystals. In any one area of a rehydrated sulphate nodule, component porphyroblasts commonly have a shared, preferential orientation, which produces a pallisade (long axes parallel), or radiating (rosette) texture in which porphyroblasts are orientated crystallographically, diverging from a central point which may, or may not, be the dolostone host. A variant of this fabric, recorded only from borehole W8, is where the radial splay is smaller (up to 1mm diameter) and composed of a number of poorly defined, elongate subcrystals which are actively growing at the expense of adjacent anhydrite (Fig. 5.21b). The contact of subcrystals with anhydrite defines tapered terminations which in detail are rectilinear, controlled by the crystallographic structure of the anhydrite being replaced (Fig. 5.21b).

Relic anhydrite occurs in one of two forms within porphyroblastic gypsum, depending on the intensity of hydration. Anhydrite relics most commonly occur as corroded, elongate crystals (up to 400μm), floating within the gypsum. Although they are corroded, each anhydrite relic is similar in size to the component crystals of unaltered anhydrite nodules (Fig. 6.16a). These relics are also of a similar size and shape to anhydrite preserved within calcitized sulphate nodules (Fig. 6.16a & b). Where replacement has been less intense, anhydrite is largely preserved, concentrated in the center of the former nodule/crystal (Fig. 5.21b). The gypsum porphyroblasts have grown inwards from the margins of the nodule/crystal, and the contact of gypsum with anhydrite broadly parallels the contact of nodule/crystal with host carbonate (Fig. 5.21b). These relatively large masses of relic anhydrite are commonly dissected by fine (40-50μm wide) gypsum-filled fractures. The fractures respect cleavages within the relic anhydrite. Gypsum occluding these fractures is free from dolomite or anhydrite inclusions. Similar fractures, cemented by fibrous gypsum were recorded from the basal Hartlepool Anhydrite Formation, being themselves replaced by coarse gypsum porphyroblasts.

There is no change in the density of dolomite inclusions from anhydrite to porphyroblastic gypsum, and none appear to have been rotated during recrystallization. The porphyroblasts commonly have diffuse, gradational contacts with host dolostones (Fig. 5.22a) via an increasing density of euhedral dolomite relics.

Alabastrine gypsum is uncommon, although recorded from two of the three boreholes. It occurs both within nodules, and selectively replaced fossil material in limestones and dolostones (Fig. 5.23). Most commonly, the alabastrine gypsum occurs as numerous elongate lath/acicular, poorly defined crystals/subcrystals with their long axes parallel to each other (Figs. 5.23a & b). Each elongate crystal has an undulose extinction, and individual crystals are commonly bent. Anhydrite relics are rare, and normally recorded in the centre of alabastrine gypsum-filled areas. The alabastrine gypsum may also enclose relics of the carbonate initially replaced by anhydrite/gypsum (Fig. 5.23b).

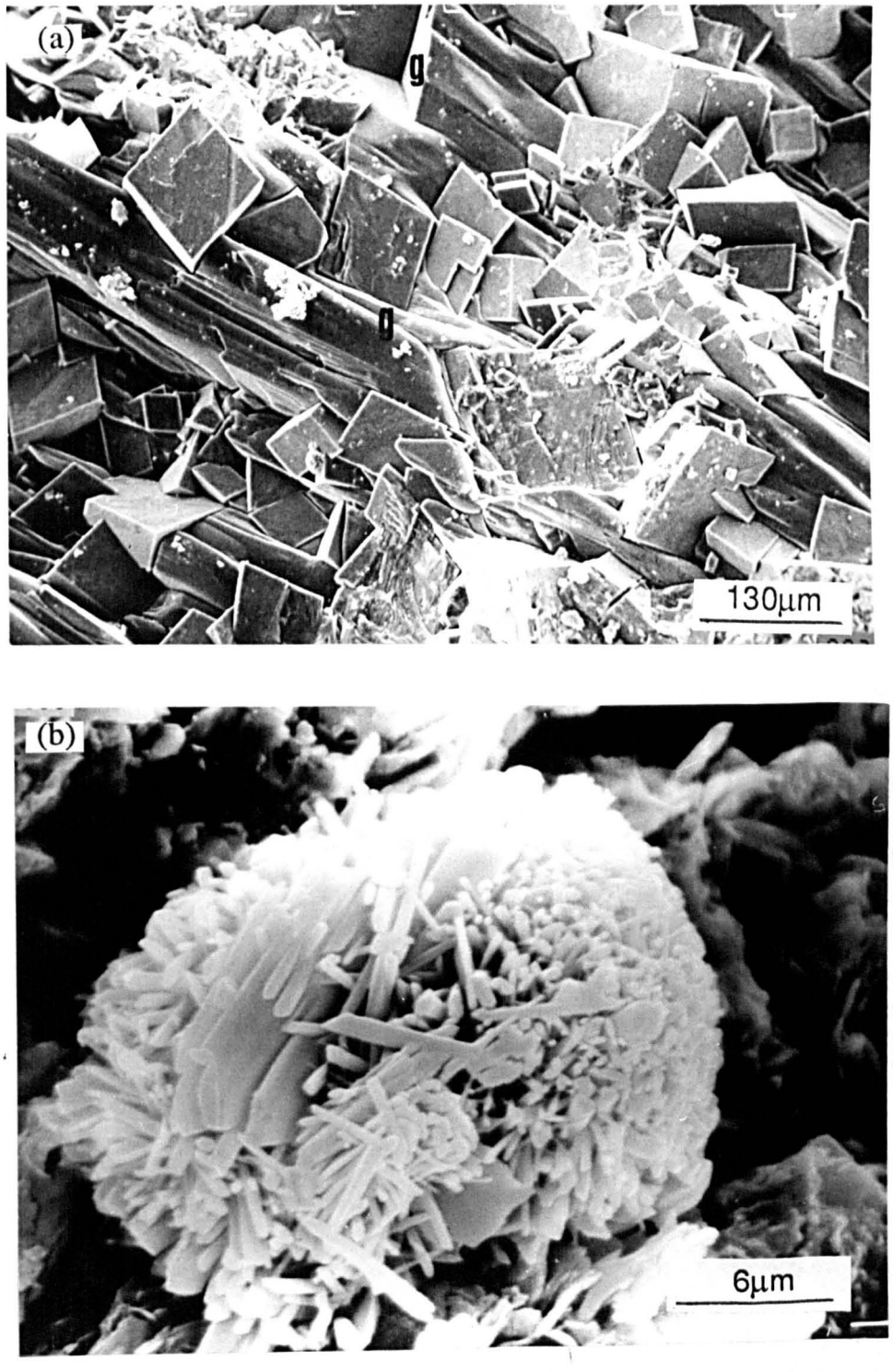

Fig. 5.22. SEM photomicrographs of fracture surfaces of gypsum. (a) the margin of a nodule of gypsum, borehole E3a, 351.0m. Isolated dolomite rhombs are poikilitically enclosed within porphyroblastic gypsum [g]. (b) a bundle of euhedral gypsum laths within a dark, organic-rich dolostone, borehole W8, 285.35m.

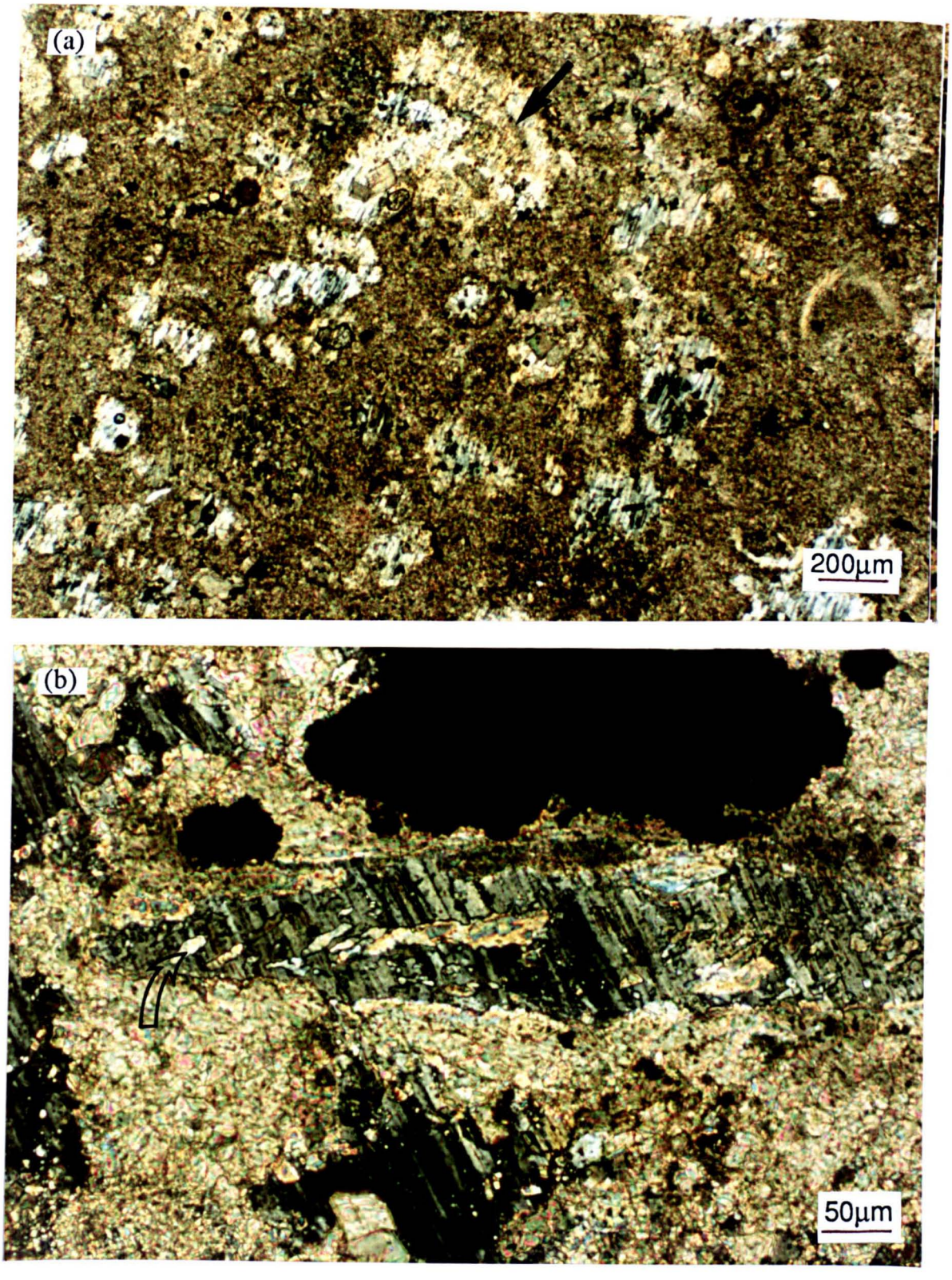

Fig. 5.23. Thin section photomicrographs, crossed polars, of a bioclastic limestone, borehole W15, 254.28m. Most of the replaced material in (a) is subspherical coated grains with some shell fragments (arrowed). Replacement of a shell fragments by alabastrine gypsum (b) has been near-complete, although some relics of the shell structure remain (arrowed),

Some very small crystals of gypsum have been recorded cementing intergranular porosity within borehole W8 (Fig. 5.22b). The gypsum may have formed as a by-product of anhydrite rehydration, or may be a very recent precipitate, postdating recovery of the core.

5.6.3. Pseudomorphs after calcium sulphate at outcrop and in shallow offshore boreholes - Description.

A number of different types of pseudomorph after calcium sulphates have been identified within the Raisby Formation at outcrop. Most pseudomorphs within dolostones are partially or completely filled by calcite, whereas those within limestones are in general unoccluded. Some of these types have been identified from offshore boreholes, still containing sulphates.

5.6.3.1. Nodular cavities after sulphates.

These are by far the most numerous and easily-recognized pseudomorphs after sulphate evaporites. They are millimetres to tens of centimetres in diameter (most a few centimetres in diameter), and subrounded to irregular in shape (Figs. 5.24a & 5.8a). They have been recorded from almost every locality at outcrop, and similar-sized nodules are abundant in offshore boreholes, now filled by gypsum with or without anhydrite. Such nodules have also been recorded, still filled by gypsum, from dolostones at West Cornforth Quarry and the limestone at Raisby Quarry (Fig. 5.24b). Nodular cavities are very common within dolostones although rare within limestones. The subrounded cavities may be subspherical or hemispherical in cross section (Fig. 5.25a). The hemispherical cavities have flat bases (normally along bedding planes) and convex-up tops (Fig. 5.25a). The external surfaces of subrounded cavities often have cauliflower-like rounded protuberances superimposed on their subrounded form. Where dolostones are finely laminated, laminae may be at least partly deformed around the cavities (Fig. 5.25a), although most commonly, they are completely cut by them. Some cavities are directly associated with networks of fine fractures which radiate out from them into host dolostones at all angles, although there is a tendency for them to be sub-horizontal (Fig. 5.25b). These fractures are occluded by the same generation of calcite which cements adjacent cavities.

Individual cavities are commonly divided into two or more sub-cavities by narrow stringers of dolomite. These divisions also occur within gypsum and anhydrite-filled nodules in core. At outcrop they may be preserved with calcite cements nucleating off them (Fig. 6.15), or internally sedimented during sulphate dissolution. In some dolostones, a distinct type of cavity is developed, comprising a number of individual cavities (which may or may not be internally divided into sub-cavities), aggregated into a vertical/sub-vertical 'string' up to 1m long (Fig. 5.26a). Details of the contact between former sulphate nodules and host dolostones is often obscured at outcrop owing to dissolution and calcitization of

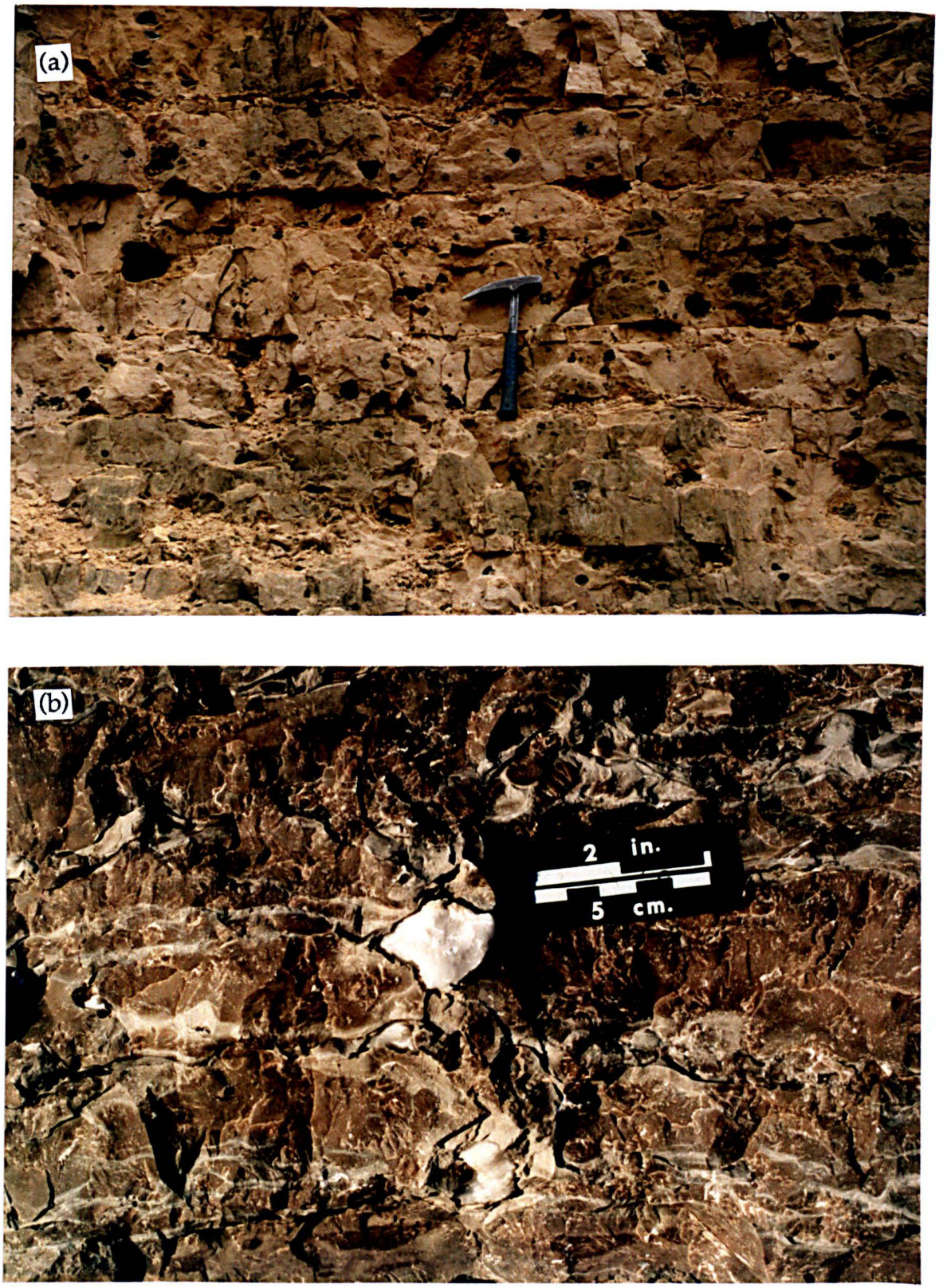

Fig. 5.24. Outcrop photographs of cavities after sulphates within dolostones at Houghton Quarry (a), and still-preserved gypsum nodules within the limestone at Raisby Quarry (b). Note the random distribution of cavities after sulphates in (a). Hammer in (a) is 32cm long.

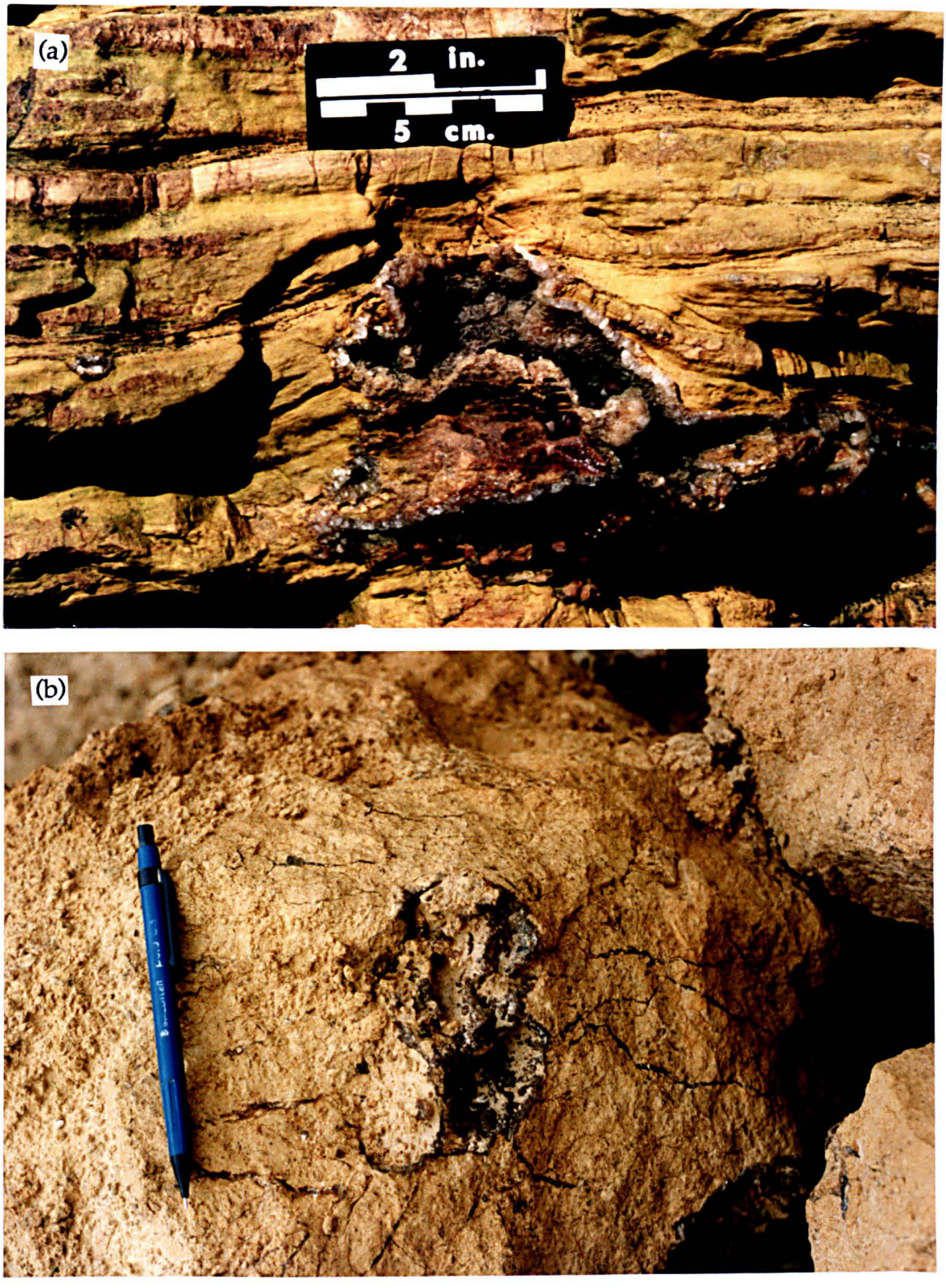

Fig. 5.25. Outcrop photographs of cavities after sulphates from Frenchmans Bay (a) and Eldon Hill Quarry (b). Some original sediment laminae in (a) are deformed around the cavity after sulphate, although most are cut by it. Fractures which radiate out from a large cavity after sulphate in (b) are clearly genetically related to it. Note, most, although not all fractures in (b) are sub-horizontal.

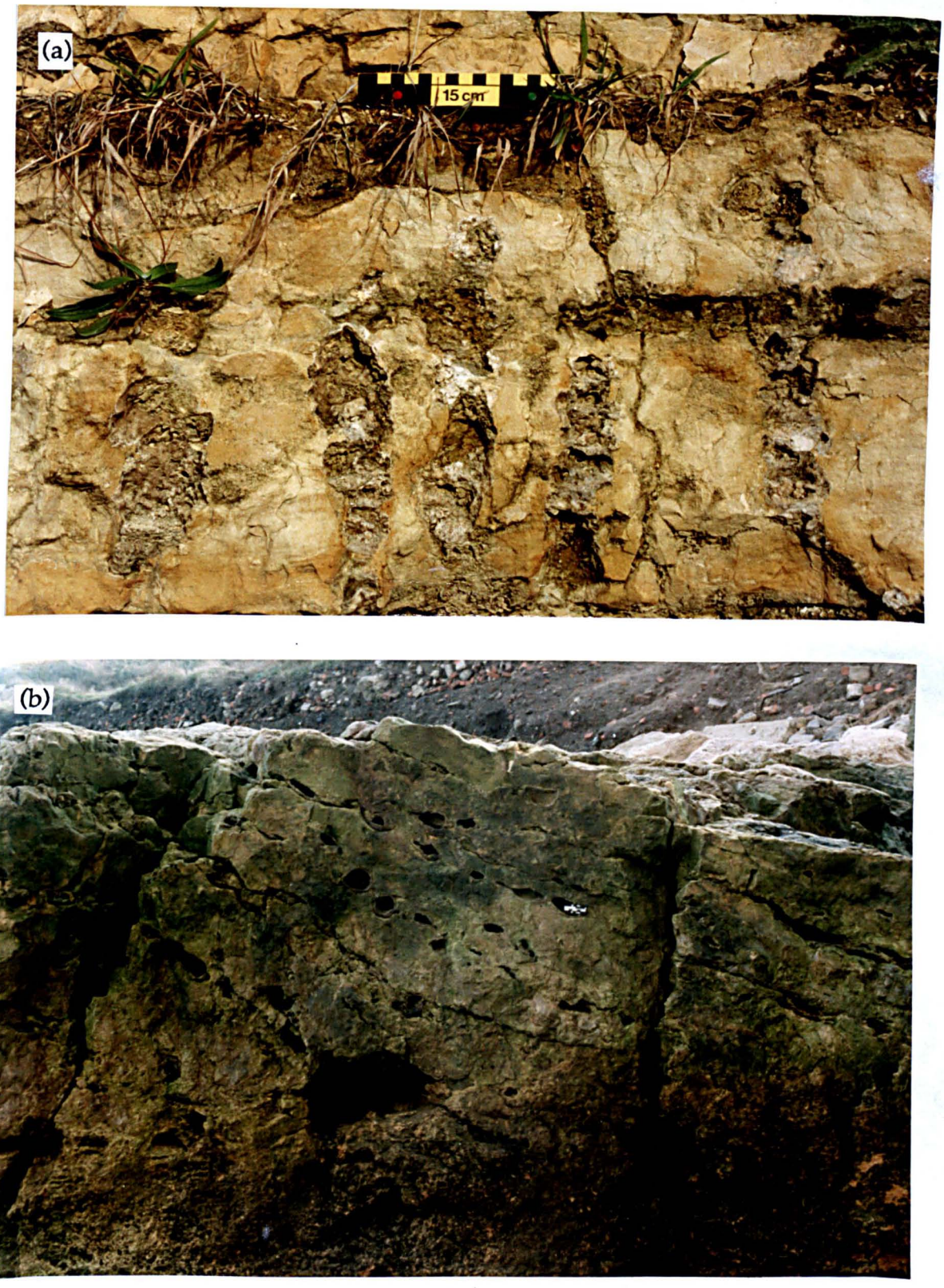

Fig. 5.26. Outcrop photographs of cavities after sulphates within dolostones from Crime Rigg Quarry (a) and Target Rocks, near Trow Point, South Shields (b). A number of vertical 'strings' of cavities are developed in (a), which bear no obvious relation to structure within the dolostone, although those in (b) all lie along bedding planes within the resedimented dolostones. Dolostones underlying this unit have very little evidence for replacement by sulphates. A 5cm scale is in the centre of the field of view in (b).

dolomite. However, at least some display small, elongate, lath-shaped re-entrants with rectilinear terminations, indicative of former anhydrite. This is further supported by the enclosed carbonate inclusion (ECI) texture developed within some calcitized sulphate nodules (Fig. 6.5), which demonstrates that the initial replacive mineral was anhydrite. However, with regard to most nodules, the original replacive mineralogy cannot be determined.

Cavities after nodular sulphates are rarely uniformly distributed within dolostones or limestones. In any one area, their abundance is related to lithology and structure. Cavities are commonly developed along specific bedding surfaces in limestones and dolostones, especially marked in exposures around Trow Point (Fig. 5.26b). Listric joints at this locality may also have cavities after sulphates developed along their length. Most debris flows (both limestone and dolomite) within the formation have been replaced by nodular sulphates, commonly to a greater degree than host bedded dolostones. The replacement may be selective to the resedimented carbonate in general, selective to the clasts, or selective to the matrix, leaving clasts intact.

On a large scale within the formation, there is a general, qualitative trend, for the intensity of replacement by nodular sulphate (and other forms of replacive sulphates) to increase upwards. This is especially marked where thick limestones are present, with the density of cavities after sulphates being considerably less within dolostones below than above the limestone. Large (tens of centimetres in diameter) cavities after sulphates have not been recorded within the basal few metres of the Raisby Formation, nor the Marl Slate. Both bedded and resedimented dolostones directly below the residue of the Hartlepool Anhydrite Formation have been heavily replaced by very large (some, metres in diameter) nodular sulphates (Figs. 5.25a & 5.26b). This is in part related to the disturbed nature of these carbonates, and in part to the proximity of the former Hartlepool Anhydrite Formation. There is also a possible trend for the intensity of replacement by nodular sulphates to be less in the south of the study area, although this may be a factor of poor exposure.

5.6.3.2. Pseudomorphs after radiating anhydrite clusters.

This specific type of pseudomorph after sulphate is common within the Raisby Formation, and even more abundant within lagoonal facies dolostones of the Ford Formation (Smith and Francis, 1967; Jones, 1969; Jones and Hirst, 1972 [who call the texture 'felted anhydrite']). It comprises subspherical/spherical millimetre-sized radiating aggregates of elongate, narrow, straight-sided lath-shaped crystal pseudomorphs. Each crystal pseudomorph increases in width from the core of the structure, and then decreases in width as it tapers to an irregular/rectilinear termination (Fig. 5.27a). The laths radiate out in all directions, apart from where they are in contact with heterogeneities within the dolostone such as debris flow clasts. The laths may or may not selectively replace these clasts. Where

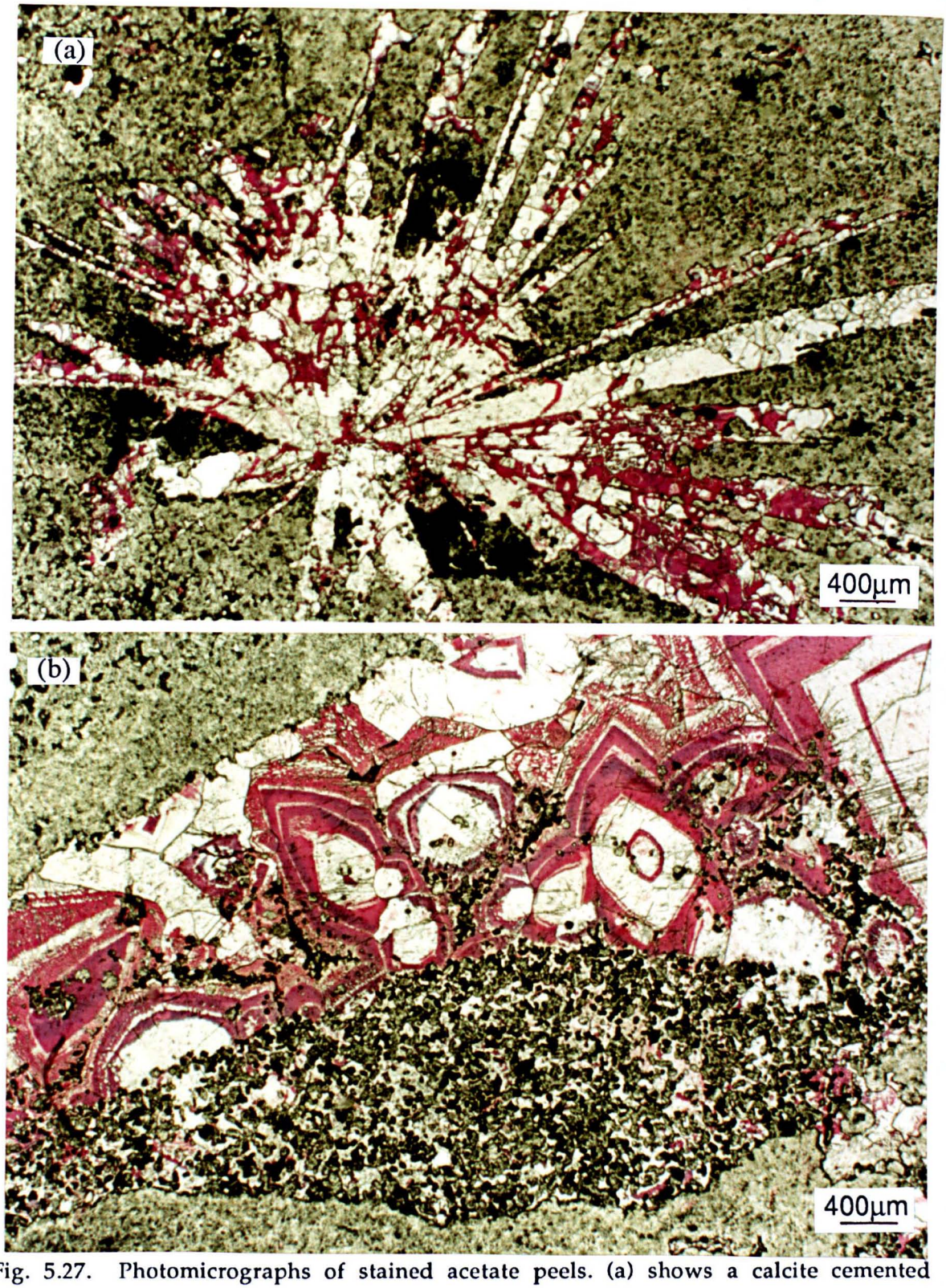

Fig. 5.27. Photomicrographs of stained acetate peels. (a) shows a calcite cemented pseudomorph after a radiating anhydrite cluster from High Moorsley Quarry. Note that each individual crystal increases in width out from the core of the structure. (b) illustrates a calcite cemented pseudomorph after a debris flow clast from High Moorsley Quarry. The clast was originally replaced by gypsum, which, after dehydration to anhydrite, was partially dolomitized. As dolomitization was only partial, upon rehydration and dissolution of the un-replaced sulphate, that which was dolomitized formed a geopetal internal sediment, later cemented by zoned calcite.

carbonate inclusions have been retained within calcite cementing the pseudomorphs, they define parallel-sided crystals or subcrystals with rectilinear terminations.

The radiating anhydrite cluster texture has been recorded within dolostones (although not limestones) from most localities within the formation. Its development varies from a few interfering laths, through isolated spherical arrays of numerous laths, into masses of spherical arrays which replace much of the host dolostone. These radiating anhydrite clusters do not in general show any fabric selectivity within the dolostones, although were most abundant within a debris flow at High Moorsley Quarry, and a dolomitic breccia (? synsedimentary resedimented) at Running Waters Quarry (Fig. 7.6b).

Smith and Francis (1967) suggest that this texture, in the lagoonal facies of the Ford Formation, has formed where dolomite has recrystallized into platy crystals up to 5mm across, arranged into sheath-like and semi-radial aggregates. Jones (1969) and Jones and Hirst (1972) however recognize that the pseudomorphs are filled by calcite and are most probably after anhydrite.

5.6.3.3. Gypsum pseudomorphs.

Within dolostones and some limestones, pseudomorphs after euhedral sulphate have been identified, which were originally precipitated as gypsum (Fig. 5.28). They are of a general blocky form, hundreds of microns to a few millimetres in length, and most commonly comprise sub-rectangular pseudomorphs with pointed terminations and well developed monoclinic habits (Fig. 5.11a & 5.28). These pseudomorphs have a strong tendency to occur in discrete clusters. They may or may not be closely spatially associated with pseudomorphs after radiating anhydrite clusters and/or large subrounded cavities after sulphates. However, where associated with pseudomorphs after radiating anhydrite clusters, diagenetic interrelationships are commonly unclear. Within the debris flow conglomerate from High Moorsley Quarry, gypsum has been partially or completely dolomitized (Figs. 5.11a & b). Dolomite defines former anhydrite laths, but these are considered to have formed from the dehydration of the original replacive gypsum. Following dissolution of the undolomitized sulphate, the dolomite anhydrite lath pseudomorphs have been geopetally internally resedimented (Fig. 5.27b).

5.6.3.4. Sulphates within limestones.

Limestones within the Raisby Formation are characterized by a much less intense sulphate replacement than dolostones. Some subrounded, centimetre-sized cavities have been recorded within limestones (a few of which still contain gypsum at Raisby Quarry) (Fig. 5.24b), but the dominant form is small (millimetre-sized) elongate pseudomorphs. These pseudomorphs are parallel-sided with tapered terminations. They characteristically contain a little calcite cement or are unfilled. They are most common

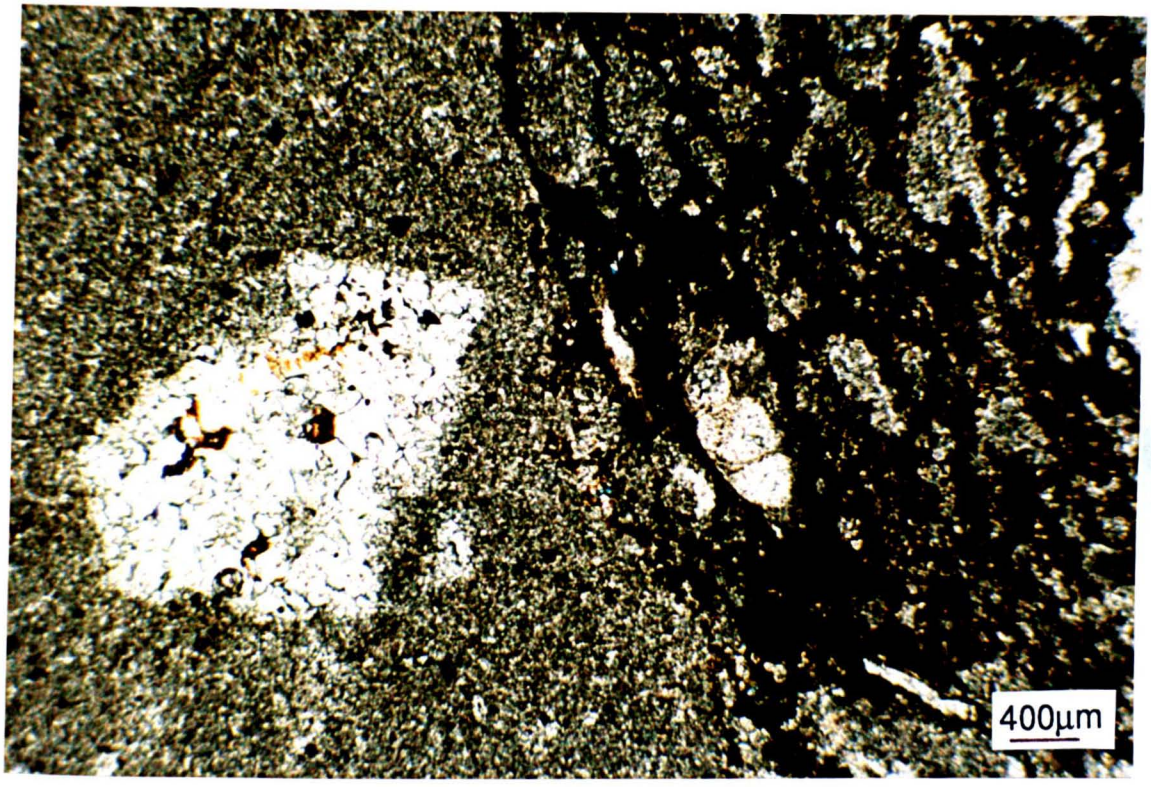

Fig. 5.28. Plane light, thin section photomicrograph of a calcite cemented pseudomorph after gypsum from the debris flow conglomerate, Dawsons Plantation. The pseudomorph is within a limestone clast.

within limestones at Houghton, Offerton, Penshaw Hill and Raisby Quarries. They are absent from the limestones at High Moorsley, Old Towns and Thickley Quarries to the south. Pseudomorphs within the Raisby Quarry limestone are substantially larger (up to 5mm long) than those of other localities (1-3mm long). The pseudomorphs may occur on their own, or as small groups of interfering crystals. They do not form ordered, spherical, radiating structures such as the radiating anhydrite clusters. At Raisby Quarry, these pseudomorphs occur selectively along bedding surfaces and in association with fossils.

Similar shaped sulphate crystals to those within Raisby Formation limestones were recorded from dolostones in W8 and W15 boreholes. They comprise millimetre-sized, euhedral, lath to acicular-shaped crystals which host gypsum and anhydrite containing abundant dolomite inclusions (Fig. 5.21b). The crystals are in general isolated from each other within the host rock, or occur along fractures, replacing dolostone marginal to the fracture. These crystals are cut by stylolites directly associated with pressure solution dolomitization. The habit of these crystals closely resembles that of 'axe head' anhydrite described by Clark and Shearman (1980). The similarity between these crystals and pseudomorphs within limestones suggests they too were originally precipitated as anhydrite.

Along small sub-vertical fractures within the limestone at Houghton Quarry, narrow pseudomorphs after sulphate spherulites (mean 5mm diameter) abundantly occur. They comprise a number of radiating, small (1-2mm long), elongate crystal pseudomorphs. Interference of separate crystal aggregates makes their precise form difficult to determine, although each component crystal widens outwards. In contrast to the radiating anhydrite cluster pseudomorphs, these crystal arrays only radiate in two dimensions, leaving very faint impressions on fracture surfaces. These are extremely similar to joint-coating, two-dimensional spherulites of gypsum, common within sulphate formations at outcrop (i.e., Harz mountains of West Germany). Thus, by analogy, the structures from Houghton Quarry are likewise interpreted as pseudomorphs after gypsum.

5.6.3.5. Fabric-selective replacive sulphates.

On a microscopic scale, sulphate replacement is often specific to certain components in the rock. Sulphates may precipitate as an intercrystalline cement within dolostones, represented by porosity, or calcite-cemented intercrystalline porosity at outcrop. Sulphates may also selectively replace the inclusion-rich core of dolomite crystals. Resultant calcite-cemented pores have been recorded from outcrop marginal to calcite lined cavities (hollow-centered dolomite textures [Fig. 6.30]).

Rare fossiliferous and ooid/pisoid-rich limestones and dolostones at outcrop and in core have commonly been selectively replaced by sulphates, facilitating their identification. Normally, only the allochems have been replaced (Figs. 5.23a & b), and isolated fossils may

be perfectly pseudomorphed by the sulphate (Fig. 5.29a). Pseudomorphs after needle or lath-shaped crystals commonly project from the selectively replaced fossils into host dolostones, suggesting that the original replacive phase was anhydrite. The skeletal structure of a fossil may be selectively replaced over its intraskeletal porosity-occluding cements, leading to internal sedimentation or rotation of the cements when the sulphate is dissolved at outcrop (Fig. 5.6). Commonly, relics of the skeletal microstructure remain floating within sulphate after replacement (Fig. 5.23b), which again will be internally sedimented following sulphate dissolution. The converse of this selectively has also been recorded from dolostones, whereby the matrix dolomite has been extensively replaced by sulphate, but allochems (skeletal material and ooids) replaced by more finely crystalline dolomite are unaltered (Fig. 6.31).

This fine-scale fabric-selectivity of replacement is analogous to the selective replacement of resedimented carbonates by nodular sulphates. The fabric-selectivity is also expressed in the much more intense replacement of oolitic Ford Formation lagoonal dolostones (one of their main distinguishing features in the field) than dolomitized Raisby Formation carbonate mudstones.

5.6.3.6. Late diagenetic anhydrite.

In a number of boreholes, selvages of calcium sulphate minerals have been recorded along stylolite surfaces and fractured/faulted stylolite surfaces. This sulphate has clearly precipitated after stylolitization, and is not replacive.

Early telogenetic anhydrite cements have been described from within coarse dolostone breccias at Raisby Quarry by Lee and Harwood (1989, figs 7 & 9). The anhydrite is now represented by calcite-filled pseudomorphs after radiating laths with rectilinear terminations, within coarse, equant calcite cements. No telogenetic replacive sulphates have been recorded during this study.

5.6.4. Autobrecciated dolostones. - Description

Large areas of upper Raisby Formation dolostones are irregularly fractured, with limited brecciation, giving them a characteristic hackly weathered surface (Fig. 5.29b). These are termed autobreccias (Smith and Francis, 1967). Autobrecciation may affect many metres of Raisby Formation dolostones vertically and hundreds of metres (entire quarry sections) laterally. The characteristic texture is due to dense, irregular, fine fractures (Fig. 5.29b). The fractures are at all angles, commonly irregular and bifurcating, a few centimetres long. Normally, no displacement of the host dolostone along fractures is evident, although minor rotation of centimetre- to millimetre-sized clasts in more heavily autobrecciated examples has been recorded. The fractures may be closed, or slightly open and cemented by coarse, zoned calcite. In association with the calcite, finely crystalline hematite after pyrite/marcasite

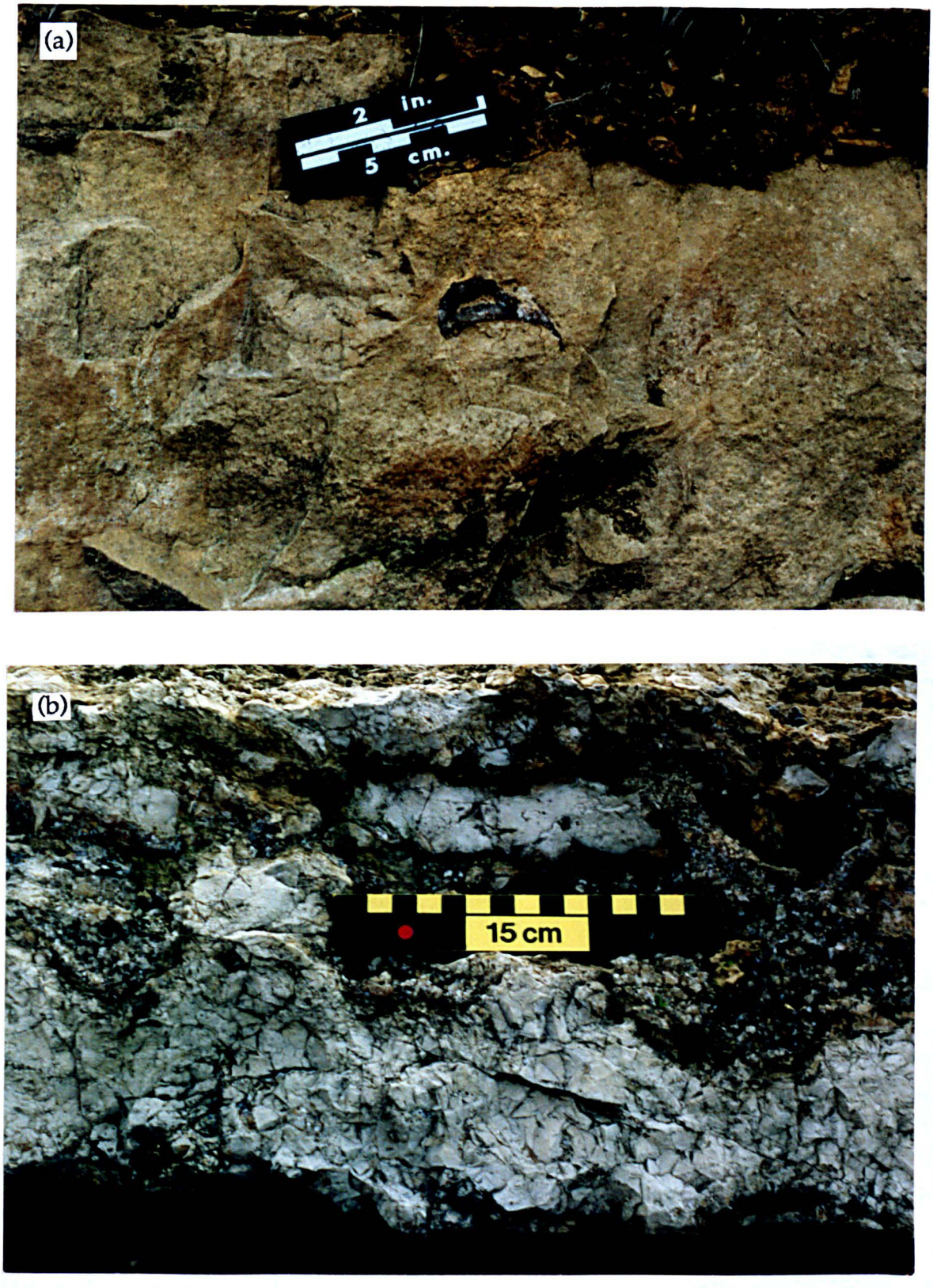

Fig. 5.29. Outcrop photographs. (a) shows a brachiopod within a dolostone, selectively replaced by sulphate (now a partially calcite cemented cavity after sulphate), Crime Rigg Quarry. (b) illustrates an autobrecciated dolostone, Haswell Moor Farm Quarry. Note that the brachiopod in (a) (probably *Horridonia* sp.) is not in life position and that the surrounding dolostones are completely unfossiliferous.

and kaolinite platelets may occur. Autobreccias have only been recorded from hard, brittle, finely crystalline dolostones. Neither dolostones in the basal few metres of the Raisby Formation, nor limestones are autobrecciated. There is also possibly a trend for autobrecciated dolostones to be less common in the south of the study area, although this again may be a factor of poor exposure.

The vertical contact of autobrecciated with non-autobrecciated dolostones is commonly gradational over a number of metres by a decrease in the intensity of fracturing. At Houghton Quarry, the contact is abrupt, and demarcated by a synsedimentary erosion surface. Autobrecciated dolostones commonly contain numerous cavities after nodular replacive sulphates. In quarries around Houghton-le-Spring, where autobrecciated dolostones are most common, the cavities after nodular sulphates are distinctive, being elongate (long axes horizontal) and ovoid in cross section. However, autobreccias may occur which are devoid of cavities after sulphates, and unfractured dolostones may host abundant cavities after nodular sulphates. Autobrecciated dolostones are distinct in their fracturing from fractures which surround large isolated cavities after nodular sulphates (Fig. 5.25b).

5.7.1. Sulphate precipitation within the Raisby Formation - Interpretation.

The precipitation of sulphate evaporites within the Raisby Formation was clearly multiphase. Four separate episodes may be distinguished:

1. Gypsum (euhedral crystals, ?nodules, fracture-lining spherulites).

   Occur within both limestones and dolostones. Timing relative to dolomitization of the Raisby Formation is uncertain.

2. Anhydrite (nodular, radiating lath cluster, axe-head, fabric-selective [within dolostones] and needle [within limestones]).

   Postdates dolomitization of the Raisby Formation.

3. Stylolite-associated anhydrite.

   Minor dissolution and reprecipitation of anhydrite related to stylolitization during burial. Continued precipitation of anhydrite of the above types during burial diagenesis cannot be discounted.

4. Anhydrite breccia cements.

   Anhydrite cements within coarse dolostone breccias probably precipitated during early uplift (Lee and Harwood, 1989). Volumetrically very minor.

Most gypsum and anhydrite within the Raisby Formation has directly replaced calcite or dolomite. During early burial, sulphate precipitation would involve partial replacement of carbonate, but also occlusion of intercrystalline porosity and larger (fracture/intraskeletal) porosities. The preservation of fine scale textures of the precursor carbonates (i.e., skeletal microstructure [Fig. 5.23b]) demonstrates that replacement did not

involve the development of a porosity greater than a few microns in size. This is consistent with near simultaneous dissolution of carbonate and precipitation of calcium sulphate within the resultant porosity, along a narrow aqueous film (reaction zone).

Clark and Shearman (1980) suggest that anhydritization of limestones is closed with respect to calcium (all calcium within anhydrite being derived from precursor calcite), but open with respect to sulphate, which results in a net volume increase. This process is considered highly unlikely to have been operative within the Raisby Formation, where the large quantities of replacive sulphates almost guarantee that the system was near to, or completely open with respect to all ions. The replacement reaction must have been driven by fluids simultaneously undersaturated with respect to calcite and/or dolomite and supersaturated with respect to gypsum or anhydrite. For replacement of dolomite, this would necessitate that the fluids be considerably depleted with respect to Mg^{2+} and/or CO_3^{2-}. As both ions would be liberated by the replacement reaction, an open diagenetic system, with maintained high concentration gradients of Mg^{2+} and CO_3^{2-} away from the reaction zones, and Ca^{2+} and SO_4^{2-} towards them would be necessary (anhydritization of dolomite molecule for molecule in a closed system with respect to Ca^{2+} would lead to a volume decrease, which is not recorded).

The main determinant on whether gypsum or anhydrite is precipitated from a calcium sulphate supersaturated brine is temperature, and the activity of water (which decreases with increasing salinity). In pure water, the gypsum-anhydrite transition temperature is approximately 42°C, decreasing with increasing salinity (Sonnenfeld, 1984). In brines of the salinity attained at gypsum saturation, the gypsum-anhydrite transition is at approximately 32-35°C (Sonnenfeld, 1984). Thus, during burial, gypsum will precipitate before anhydrite, if salinity remains reasonably constant. It is unlikely that the Zechstein Sea attained gypsum saturation during deposition of the Raisby Formation or most of the Ford Formation. This is evidenced both by the marine fauna of the Raisby and Ford Formations (albeit restricted at times), and that to reach gypsum saturation, seawater has to be concentrated approximately three-fold, for which there is no evidence during first cycle carbonate deposition in Durham. The minor fall in the level of the Zechstein Sea corresponding to the Hampole Discontinuity of the Yorkshire Province (Smith, 1968), and probably the Raisby-Ford Formation junction in Durham, was possibly a response to evaporative drawdown, although only on the scale of a few metres (G.M. Harwood *pers. comm.*, 1988), and thus insufficient to trigger gypsum precipitation. Replacive gypsum must therefore have precipitated after deposition of the first cycle carbonate, but before substantial burial. Assuming an average geothermal gradient of 25°C/km, and reasonable Zechstein surface temperatures, the gypsum-anhydrite transition would have been reached at a depth of 400-600m. In the area of the Raisby Formation where gypsum pseudomorphs have been described (upper/middle slope), such burial depths would have been attained shortly after

deposition of the Hartlepool Anhydrite Formation. It is probable, therefore, that gypsum precipitation was directly related to deposition of the Hartlepool Anhydrite Formation.

Gypsum may have precipitated directly from calcium sulphate-rich fluids refluxing out of the Zechstein Sea during deposition of the Hartlepool Anhydrite Formation (itself deposited as gypsum). Shearman (in Harwood, 1980) however, states that sulphates can only be precipitated in carbonates up to 50m below a bedded sulphate formation, which discounts such a mechanism for gypsum precipitation within the Raisby Formation where it is overlain by lagoonal and reef facies of the Ford Formation. However, the anomalously large, very abundant cavities after sulphates within the resedimented Raisby Formation along the South Shields coastal section (Fig. 5.25a & 5.26b), directly underlying the residue of the Hartlepool Anhydrite Formation, probably did precipitate by reflux of concentrated brines out of the Zechstein Sea. This may also explain the common deformation of host dolostones around these nodules (Fig. 5.25a), implying an early diagenetic precipitation, before dolomitization, and so lithification.

Alternatively, gypsum may have been precipitated as a direct by-product of dolomitization of the Raisby Formation, which itself most likely resulted from the reflux of concentrated brines produced during deposition of the Hartlepool Anhydrite Formation (5.4.2). Sulphate precipitation directly related to reflux dolomitization has been described by Adams and Rhodes (1960), Fusezy (1980), Kendall (1984 & 1989), and Maliva (1987). Both dolomitization and the precipitation of sulphates are considered to result from the reflux of Mg^{2+} and SO_4^{2-}-rich brines. If these brines are calcium sulphate-undersaturated (they should be calcium-depleted as, during gypsum precipitation, calcium in the brine is depleted before sulphate, which remains in solution or combines with other ions), they may become supersaturated with respect to gypsum by combining with calcium liberated during dolomitization (there are no autochthonous sources of sulphate within the Raisby Formation to supersaturate the fluids in calcium sulphate):

$$2CaCO_3 + Mg^{2+} \rightleftharpoons CaMg(CO_3)_2 + Ca^{2+}$$

$$Ca^{2+} + SO_4^{2-} + 2H_2O \rightleftharpoons CaSO_4.2H_2O$$

Thus,

$$Mg^{2+} + SO_4^{2-} + 2CaCO_3 + 2H_2O \rightleftharpoons CaMg(CO_3)_2 + CaSO_4.2H_2O$$

(after Braitch (1971) [in Kendall, 1989]).

However, gypsum precipitated by this process is a primary precipitate. For replacement, the reaction must be expressed differently:

$$2CaCO_3 + Mg^{2+} \rightleftharpoons CaMg(CO_3)_2 + Ca^{2+}$$

$$Ca^{2+} + SO_4^{2-} + CaMg(CO_3)_2 + 4H_2O \rightleftharpoons 2CaSO_4.2H_2O + Mg^{2+} + CO_3^{2-}$$

Or,

$$Ca^{2+} + SO_4^{2-} + CaCO_3 + 4H_2O \rightleftharpoons 2CaSO_4.2H_2O + CO_3^{2-}$$

In this situation, there will be a drive for the replacement of calcite by gypsum (calcite is undersaturated during dolomitization) but not of dolomite, the dolomite actively precipitating. For gypsum to be replacive of dolomite, the gypsum-precipitating fluids must be undersaturated with respect to dolomite, which suggests that dolomitization and gypsum replacement were not simultaneous. Gypsum precipitation thus occurred after dolomitization in an open diagenetic system where dolomite was maintained at undersaturation (Mg and CO_3 being removed). The extent of gypsum precipitation will also be dependant upon the initial concentration of Ca^{2+} and SO_4^{2-} in the refluxing brines (i.e., degree of saturation with respect to gypsum [the fluids should be deficient in Ca^{2+} otherwise dolomitization will be slow, or will not occur]) and the rate of dolomitization relative to the rate of sulphate-rich brine advection. Machel (1986b) suggests that dolomitization and the precipitation of replacive sulphates may fluctuate during the advanced stages of dolomitization, with gypsum precipitation decreasing the fluid Ca/Mg ratio, favouring dolomitization, and dolomitization increasing the fluid Ca/Mg ratio, thus favouring gypsum precipitation. As the Raisby Formation (and Ford Formation) is almost completely dolomitized, and the quantity of obvious gypsum is small, sulphate precipitation as a by-product of dolomitization is very attractive. Implicit in this process (occurring under low burial depths and in fluids of relatively low salinity), is that gypsum will most likely be the precipitate. The only difficulty with this mechanism is that the necessary high concentration of sulphate in the refluxing brines may inhibit dolomitization (Baker and Kastner, 1981). This could suggest that dolomitization and gypsum precipitation were near-simultaneous (unlikely owing to the aforementioned constraints), or that gypsum precipitated by the interaction of SO_4^{2-}-rich brines with connate calcium-rich fluids after dolomitization. Maliva (1987) however, states that in fluids of a high Mg/Ca ratio, sulphate inhibition to dolomitization is overridden.

Replacement of Raisby Formation carbonates by anhydrite most likely followed deposition of the Hartlepool Anhydrite Formation (and probably some or all of the higher cycle Zechstein carbonates), and postdated most dolomitization. However, temperatures

within the Raisby Formation during burial were a factor of the amount of overburden. Thus, if fluids of equivalent salinity are assumed, equilibrium conditions with respect to anhydrite would have been attained in outer shelf and slope facies of the Raisby Formation in which overburden was greatest, before it was attained in the basinal facies that was overlain by an overall thinner sequence of cycle 1 carbonates and evaporites. Anhydritization of Raisby Formation dolostones by refluxing sulphate-rich brines from deposition of the Hartlepool Anhydrite Formation in the deepest buried parts of the Raisby Formation cannot be discounted. However, the most widely suggested mechanism for anhydritization of Zechstein carbonates is by overpressured fluids, expelled from large sulphate formations during dewatering and pressure solution of gypsum during burial (Clark, 1980). Sulphate-rich fluids would have been driven out of the Hartlepool Anhydrite Formation in all directions during burial, including downwards (Clark, 1980). Implicit in this mechanism, is that anhydrite will precipitate from the fluids. The conversion of gypsum to anhydrite in theory involves a 38.5% reduction in volume of the solid phase (163 volumes of gypsum produce 100 volumes of anhydrite, with 78 volumes of structural water liberated [Kendall, 1975]). It is this structural water, together with calcium sulphate remobilized by pressure solution which would cause anhydritization. The vertical increase in intensity of sulphate replacement within the Raisby Formation would be consistent with the derivation of anhydrite-precipitating brines from burial dewatering of the Hartlepool Anhydrite Formation. The different crystal habits of replacive anhydrite may relate to separate episodes of fluid expulsion from the Hartlepool Anhydrite Formation (and to a lesser extent gypsum within the Raisby and Ford Formations) during burial (i.e., fluid expulsion by dewatering of gypsum followed by later pressure solution of anhydrite). A source of anhydrite-precipitating brines from the Hartlepool Anhydrite Formation may also help explain why the intensity of sulphate replacement decreases towards the south of the area, where the Hartlepool Anhydrite Formation was thinner.

Uncertainty about the original mineralogy of the very abundant irregular and subrounded cavities within the Raisby Formation, argues against any firm assessment of the importance of burial dewatering in supplying anhydritizing brines. From the abundance of replacive sulphate in the Raisby Formation (and Ford Formation), and the amount of anhydrite in solution liberated during burial dewatering of gypsum, it is unlikely that burial dewatering could be responsible for the majority of replacive sulphates within the Raisby Formation. Also, porosity and permeability within the Raisby Formation would have been undergoing a drastic reduction during this time (early mesogenesis), retarding the downwards advection of anhydritizing brines. Furthermore, fluid flow in compacting sedimentary basins is in general upwards, or laterally through permeable beds, not vertically downwards, further limiting the potential importance of burial fluids from the Hartlepool Anhydrite Formation. Therefore, it is most likely that at least some, and possibly the

majority of large subrounded cavities within the Raisby Formation were originally precipitated as gypsum, during and/or shortly after dolomitization.

Most anhydrite remained largely unaltered during burial until rehydration and dissolution upon uplift, as the diagenetic system was largely sealed after anhydrite precipitation. Minor diagenetic modifications of anhydrite during burial included small-scale pressure solution with reprecipitation along stylolites, dolomitization of anhydrite (5.4.3), and replacement of anhydrite by barite, fluorite and base metal sulphides (7.2.3). However, all of these processes were probably localized and of very minor extent.

During early uplift, minor calcitization of anhydrite/gypsum took place at a similar time to initial sulphate dissolution and calcite cementation (6.2.3). During sulphate dissolution, in certain microenvironments (such as the Raisby Quarry breccias) anhydrite was reprecipitated, with calcium and sulphate ions being derived from the dissolving gypsum during a period of elevated heat flow related to epigenetic mineralization (Lee and Harwood, 1989). There is no evidence for telogenetic precipitation of replacive gypsum or anhydrite. The hydration of anhydrite to gypsum does involve a substantial increase in volume of the solid phase. This calcium and sulphate may be reprecipitated close to the site of rehydration as a cement within formerly water filled pores (Mossop and Shearman, 1973) but there is no firm evidence for the replacement of carbonate host rocks to any substantial degree. The gypsum spherulites on fracture surfaces at Houghton Quarry probably do represent a late-stage gypsum cement, precipitated after anhydrite rehydration.

5.7.1.1. Fabric-selective anhydritization - Interpretation.

Much of the calcium sulphate precipitation within the Raisby Formation was clearly selective to certain components of the rock, normally inhomogeneities on a large scale (bed and joint planes, resedimented carbonates) and small scale (selectively replacing or not replacing coated grains, fossils, dolomite crystals). This is a common feature of replacement anhydrite within limestones and dolostones (Adams and Rhodes, 1960; Kendall and Walters, 1978; Clark, 1980). Most selectivity is directly related to permeability inhomogeneities. Fluid access will be easier where the rock is heterogeneous, such as along joint and bedding planes and through clastic carbonates. On a fine scale, this selectivity of replacement is controlled by differences in micro-scale permeability (i.e., inclusion rich core of a dolomite crystal versus the inclusion free outer part). Some selectivity of replacement to allochems may reflect the role of organic matter and preserved intraskeletal porosity in localizing initial calcium sulphate precipitation (Maliva, 1987), especially with regard to fossils and coated grains. By contrast, euhedral gypsum, anhydrite, and subrounded nodules will only form where the host rock is homogeneous, allowing an equal ease of replacement in all directions (Clark and Shearman, 1980), although the site of initial sulphate nucleation may be an inhomogeneity within the carbonate. Nodular sulphates within the Raisby

Formation probably formed by the growth of euhedral sulphate crystals (gypsum/anhydrite) in clusters.

The much greater intensity of replacement of dolostones than limestones by sulphate evaporites is another manifestation of the influence of porosity and permeability on localization of sulphate precipitation. This selectivity has also been demonstrated by Jones and Hirst (1972), who describe an antipathy between calcite (limestones) and calcium sulphate in the basinal Raisby Formation (calcite-rich lithologies containing little sulphate). They interpret this as representing calcitization of dolomite related to evaporite dissolution, although it is more likely that it represents the selective non-replacement of limestones by sulphates. However, a control on the intensity of replacement by mineralogy of the host rock cannot be discounted. Kendall and Walters (1978) describe preferential replacement of limestones over dolostones by metasomatic anhydrite, as the anhydrite-supersaturated fluids were not sufficiently undersaturated with respect to dolomite. The converse may have resulted in selective replacement of dolomite over limestone within the Raisby Formation. If calcium sulphate precipitation was genetically associated with dolomitization, this may also, in part, explain the selective intense replacement of dolomite by sulphate.

5.7.2. Anhydrite rehydration.

Most authors agree that the most important process of hydration of anhydrite to gypsum is by the dissolution of anhydrite with concurrent precipitation of calcium sulphate and water (Holliday, 1970). This is based both on the necessity to precipitate crystallographically well-ordered (i.e., porphyroblastic) gypsum crystals, and the lack of evidence for substantial volume increase (≥60% if hydration only involved the solid state addition of water [Mossop and Shearman, 1973; Sonnenfeld, 1984]). The excess calcium sulphate produced during hydration may be removed by advecting groundwaters (Mossop and Shearman, 1973). However, regardless of groundwater advection rates, Sonnenfeld (1984) states that at burial depths of greater than 60-75m, lithostatic pressures will be greater than hydration pressure, and so a volume increase should not occur. In northeast England at the present day the gypsum-anhydrite transition depth is at greater than 200m (Fig. 5.30), and so a volume increase should not have resulted from hydration. To rehydrate 100 volumes of anhydrite, 78 volumes of water are required, which necessitates an external source (Sonnenfeld, 1984). This is most commonly meteoric, although a small part may also be from formation waters.

Porphyroblastic gypsum is interpreted as a rehydration texture formed by slow crystal growth from a small number of nucleation sites (commonly inclusions within the anhydrite or the marginal host carbonate) (Holliday, 1970; Mossop and Shearman, 1973). Slow growth would be most likely in conditions close to equilibrium with respect to anhydrite (i.e., just below the anhydrite/gypsum transition temperature at a given fluid

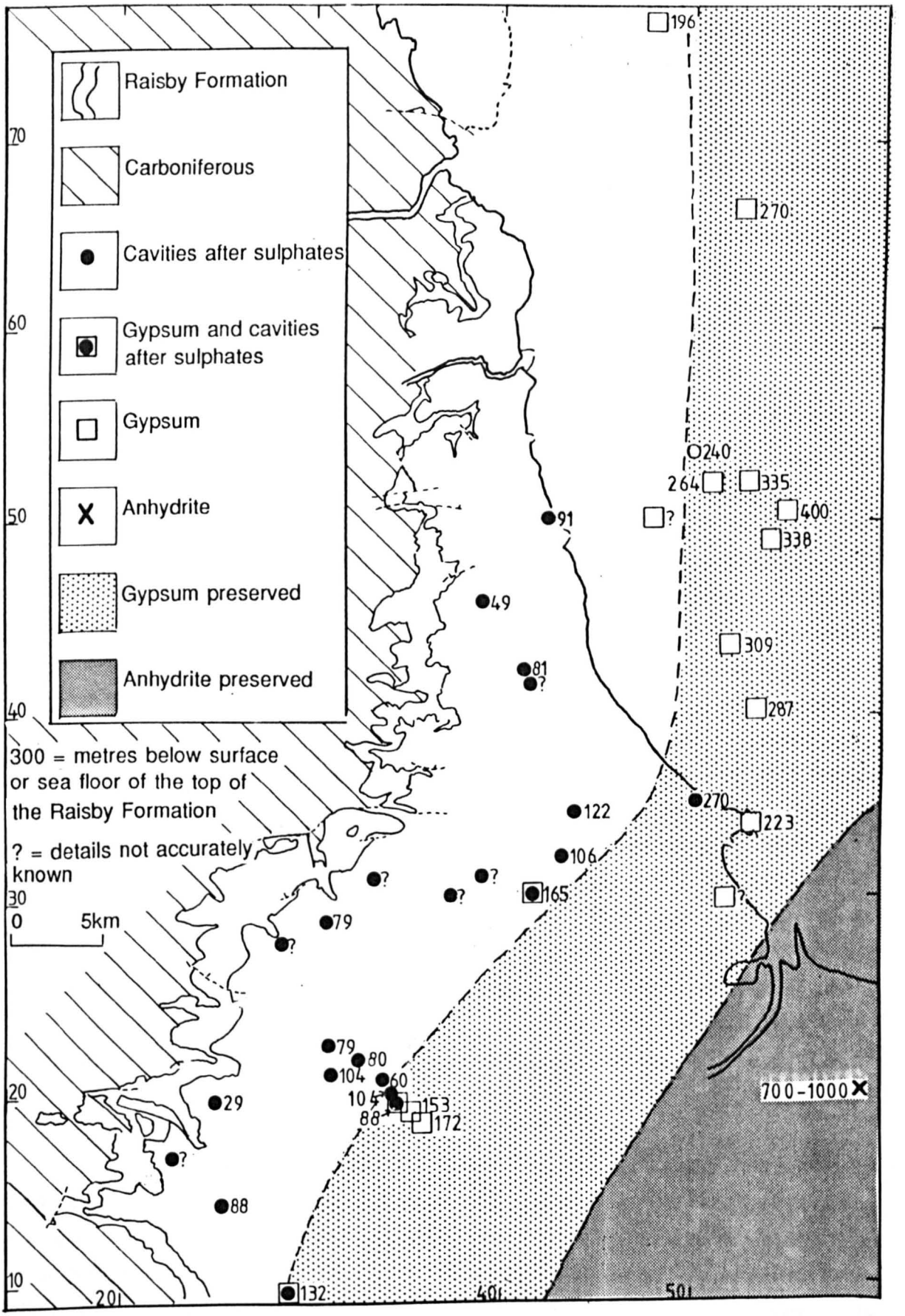

Fig. 5.30. Map showing the spatial distribution of calcite lined cavities after sulphates, gypsum-filled nodules, and anhydrite-filled nodules in the study area. Data compiled mainly from this study, and Woolacott (1919a), Raymond (1962), Magraw *et al.*, (1963) and Smith and Francis (1967). The exact details of some of the boreholes were not given in the relevant papers.

salinity [at depth] [Mossop and Shearman, 1973]). The pallisades and rosettes of porphyroblasts in Raisby Formation examples demonstrate that growth was relatively ordered from a given nucleation site. The common enclosure of dolomite and anhydrite relics, undisturbed from their original orientation suggests a fine scale of replacement, along a dissolution-precipitation front less a few microns wide. Both Holliday (1970) and Mossop and Shearman (1973) suggest that rehydration to porphyroblastic gypsum involves a negligible volume change and is achieved by dissolution-precipitation. However, narrow gypsum filled fractures cutting anhydrite relics testify to a minor volume increase accompanying hydration.

Alabastrine gypsum is commonly interpreted as a late stage product of the hydration of anhydrite (Holliday, 1970; Mossop and Shearman, 1973), postdating porphyroblastic gypsum. Within Raisby Formation examples, alabastrine and porphyroblastic gypsum were not recorded in contact with each other, although they were present within the same borehole (W8). Holliday (1970) defines two types of alabastrine gypsum, distinguished on the basis of definition and development of component gypsum crystals/subcrystals. Most alabastrine gypsum within the Raisby Formation corresponds to the more poorly crystalline variety described by Holliday (1970). Holliday (1970) suggests that alabastrine gypsum is formed by the direct addition of structural water to anhydrite, and so should be associated with a volume increase, although no expansion textures have been recorded within examples from the Raisby Formation (possibly owing to their depth of burial). Both Holliday (1970) and Mossop and Shearman (1973) suggest that hydration of anhydrite to alabastrine gypsum is probably rapid, under conditions far removed from equilibrium with respect to anhydrite and with free access of large volumes of hydrating water (i.e., shallow burial). The Raisby Formation alabastrine gypsum does not fully substantiate these conclusions, occurring at a similar stratigraphic level to porphyroblastic gypsum (although may have formed more recently than it). The horizons in which the alabastrine gypsum occur are commonly more porous than those hosting porphyroblastic gypsum, which may substantiate faster hydration by more rapidly advecting groundwaters.

5.7.3. Sulphate dissolution.

Following gypsification, nearly all sulphate has been dissolved from within the formation at outcrop and in shallow onshore boreholes. The distribution of boreholes containing gypsum, anhydrite and cavities after sulphates (Fig. 5.30) clearly demonstrates that the area of contact of Raisby Formation containing still-preserved sulphates, with Raisby Formation hosting dissolved sulphate parallels the trend of the present-day outcrop. The transition from gypsum to cavities after sulphates occurs at approximately 90-140m below surface onshore (Fig. 5.30). The gypsum-anhydrite transition depth is less well known, although appears to lie at greater than 700m onshore, and is very gradational. Assuming a

present day geothermal gradient in northeast England of 30°C/km (Appendix X), the gypsum-anhydrite transition should be approximately 1km depth, in agreement with the recorded values.

Rehydration of anhydrite and dissolution of sulphates is not only related to depth, and salinity of fluids, but also porosity and permeability of the Raisby Formation and overlying and underlying lithologies. Gypsification within the Raisby Formation in boreholes appears to have been more rapid than gypsification of the overlying Hartlepool Anhydrite Formation, presumably owing to differences in fluid access. The intensity of hydration of the basal Hartlepool Anhydrite Formation decreases with height above the top of the Raisby Formation in boreholes. Goodall (1987) noted that the intensity of hydration of anhydrite within the Edlington Formation of Teesside, increased towards its contacts with underlying and overlying carbonates, supporting the suggestion that groundwater advection during early stages of hydration is more rapid within carbonate than evaporite units.

The intensity and relative timing of the dissolution of gypsum from within the Raisby Formation was also strongly controlled by local porosity and permeability factors, often varying greatly within any one borehole (6.5.2.1). Preservation of gypsum within the highly impermeable Raisby Quarry limestone (Fig. 5.24b) supports this assertion. However, the spatial distribution of core containing cavities after sulphates (Fig. 5.30), demonstrates that differential porosity and permeability of the Raisby Formation does not markedly effect the overall trends of sulphate dissolution.

The rate of sulphate dissolution also appears to have been a factor of the intensity of sulphate replacement in any one area. Thus, where the Raisby Formation was heavily replaced by sulphates, their dissolution will eventually produce a higher secondary porosity than would be recorded in a less-intensely sulphate-replaced section. This higher secondary porosity in turn allows higher rates of groundwater advection and so more rapid sulphate dissolution. This is probably the reason why the Ford Formation, which has been very intensely replaced by sulphates (especially within the lagoonal facies), is a much better groundwater aquifer than the Raisby Formation in south Durham (Cairney, 1972).

It is probable that the rate of gypsum dissolution within Raisby Formation carbonates now at outcrop was much more rapid than the dissolution of gypsum in the subsurface at the present day. Many metre-thick sections of bedded Zechstein sulphates in continental Europe are commonly exposed at outcrop and may often still be partly anhydrite (i.e., in the Harz mountains area of West Germany). The climate is not considerably different between northeast England and northern Europe at the present day. Thus, a Tertiary pluvial episode, or glacial and periglacial conditions during the last ice age probably contributed to more rapid rates of gypsum dissolution than is currently recorded. This may have been especially so during glaciation, with low sea levels resulting in a much greater hydrostatic head. The present day contacts of gypsum with anhydrite and with cavities after sulphates

within the Raisby Formation in northeast England may thus be 'fossilized' products of a previous, more extensive groundwater aquifer.

5.7.4. Autobrecciated dolostones - Interpretation.

Woolacott (1919b) was the first to describe autobreccias (he termed them contemporaneous breccias), and suggested that they had formed by shrinkage of the host rock on drying. Magraw *et al.*, (1963) and Smith and Francis (1967) record common mechanical brecciation of Raisby Formation dolostones which they ascribe to collapse and fracturing following the removal of anhydrite formerly interbedded with the Raisby Formation. However, there are a number of possible processes which may have produced the autobreccia lithology:

1. Early mesogenetic,

   Veins of sulphate growing outwards into host dolostones from replacive sulphate nodules. Sulphate dissolution produces fractures following uplift,

2. Later mesogenetic,

   Compaction and fracture of brittle host dolostones following volume reduction owing to anhydritization of original replacive gypsum,

3. Telogenetic,

   Expansion of replacive calcium sulphate upon uplift and gypsification,

4. Telogenetic,

   Compaction and fracture of brittle host dolostones following dissolution of replacive sulphates.

One of the most widely suggested processes for the formation of veins of fibrous gypsum (satin spar) (to become fractures upon sulphate dissolution), is by fracturing followed by gypsum cementation. The gypsum is considered to be derived from the rehydration of anhydrite (mechanism 3 above). The stresses to generate fracturing may be related to volume increases upon gypsification, hydraulic fracturing by overpressured fluids injected into the rock during the initial stages of uplift, or tectonic compression (Shearman *et al.*, 1972). These processes produce distinctive, relatively large, not especially dense, subhorizontal fractures and so are unlikely to be of direct importance in forming autobreccias. However, they may well explain the fractures commonly associated with large cavities after nodular sulphates at outcrop (Fig. 5.25b). In support of this, Raymond (1962) records dolostones brecciated by fibrous gypsum-filled veins in the Raisby/Ford Formations within boreholes from the Gt. Stainton and Billingham areas. Raymond (1962) suggests that hydration pressures of the former anhydrite were responsible for the brecciation. Fracturing of host dolostones as a by-product of the hydration of anhydrite thus remains a possibility for localized fracturing as is recorded around large cavities after nodular sulphates.

It is more likely that autobreccias are a product of compactional fracturing, which would be more effective with regard to finely crystalline, brittle dolostones, and would better explain the observed density and distribution of fractures. The timing of compactional fracturing may have been after anhydritization of originally replacive gypsum, following dissolution of gypsum (when host rocks are still at considerable depths [some greater than 100m]), or both. The restriction of autobrecciation to upper parts of the Raisby Formation is thus explicable in terms of the greater density of replacive sulphates. The mechanism invoked for autobrecciation here is essentially a modification of that of Magraw *et al.*, (1963) and Smith and Francis (1967), although the sulphates are considered to be disseminated through the host rock, not interbedded within the Raisby Formation, and lithology of the host dolostone is an important determinant of autobrecciation.

5.8.1. Summary.

The Raisby Formation has very extensive evidence for the presence and former presence of replacive and partly displacive evaporite minerals. A number of different types of pseudomorphs of both anhydrite and gypsum have been identified at outcrop. However, owing to their small size, and dissolution and calcitization of dolostones hosting them, the original mineralogy of most pseudomorphs is uncertain. The spatial distribution of calcium sulphate pseudomorphs within the Raisby Formation is controlled both by proximity to the Hartlepool Anhydrite Formation on a large scale, and porosity and facies-related permeability of the host rocks on a smaller scale.

Different crystal habits represented by the pseudomorphs reflect different episodes of sulphate precipitation. Initially, gypsum precipitated synchronous with, or shortly after dolomitization, followed by anhydrite during later burial. During uplift, anhydrite was firstly rehydrated to gypsum when it was approximately 1km from the surface, and then dissolved when approximately 100m from the surface. The present day distribution of gypsum and anhydrite may largely reflect a once, more deeper-penetrating groundwater system than at present.

The sedimentology and diagenesis of the Raisby Formation (Z1 carbonate), northern England

Volume 2

ORIGINAL COPY TIGHTLY BOUND

TEXT BOUND CLOSE TO THE SPINE IN THE ORIGINAL THESIS

Chapter 6

Telogenesis.
Calcitization of sulphate evaporites and dolomite,
calcite cementation,
precipitation of iron oxides, and clay minerals.

6.1.1. Introduction.

This chapter deals with the precipitation of calcite, as a replacement of evaporite minerals (gypsum/anhydrite) and dolomite, and as a passive void-filling cement. Associated with these calcites are abundant iron minerals (goethite, hematite, pyrite/marcasite), and clay minerals. Most of these telogenetic minerals occur within cavities in dolostones, formed by the dissolution of replacive sulphate evaporites. The initial parts of calcite crystals within these pores may be replacive of sulphate evaporites and/or dolomite, and associated with hematite and pyrite/marcasite, whereas the later parts of calcite crystals are purely cements, in which iron oxide/hydroxides occur at specific levels. Clay minerals however, do not have a clearly defined relationship to pore occlusion.

6.2.1. Calcitization of evaporites - Introduction.

In this thesis, calcitized sulphate evaporites (gypsum/anhydrite) are interpreted to have formed by an almost simultaneous dissolution of gypsum/anhydrite, and precipitation of calcite in the resultant porosity. The process is thus analogous to that of calcitization of dolomite (6.3.1), and neomorphism (or calcitization) of aragonite (4.3.2.). Where floating relics, or textures of former gypsum/anhydrite can be identified within calcite, calcitization is considered to have taken place. However, it is recognized that there is a complete gradation in process between the two end-members of calcitized gypsum/anhydrite and total gypsum/anhydrite dissolution predating calcite pore fill cementation. A division between the two is, necessarily, arbitrary.

Calcite cements occluding, or partially occluding cavities after replacive/displacive evaporites are ubiquitous within the Raisby Formation (Lee and Harwood, 1989). In nearly all examples, the calcite is a pore filling cement and the precursor sulphate has been completely dissolved prior to the onset of cementation. However, in some examples, clear evidence of former gypsum/anhydrite remains within the calcite, demonstrating that precipitating calcite coexisted with dissolving sulphates, partially replacing them. Four types of calcitized sulphates may be defined (Fig. 6.1):

1. Poikilitically Enclosed Relic (PER).

Calcite crystals poikilitically enclosing relic anhydrite crystals, or calcite-filled pseudomorphs after relic anhydrite crystals,

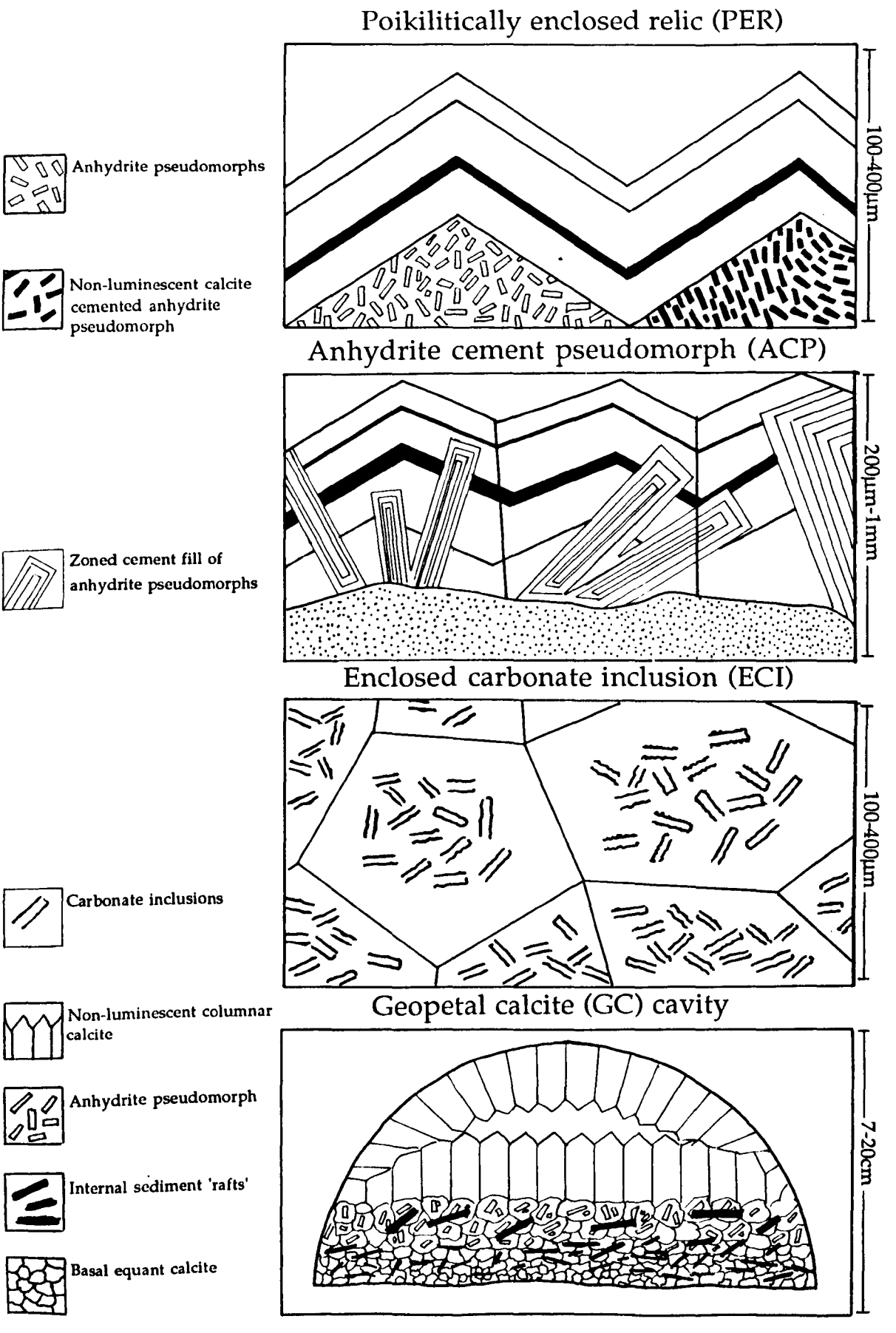

Fig. 6.1. Schematic diagram showing the petrographic characteristics of the main types of calcitized sulphates identified within the Raisby Formation.

2. Anhydrite Cement Pseudomorphs (ACP).

Large calcite crystals poikilitically enclosing large calcite-filled pseudomorphs after anhydrite. The anhydrite crystals were enclosed by calcite prior to their dissolution, and calcite cementation of the resultant pore,

3. Enclosed Carbonate Inclusions (ECI).

Calcite crystals poikilitically enclosing carbonate inclusions which define former anhydrite crystals,

4. Geopetal Calcite (GC).

Large cavities after sulphates, with finely crystalline equant calcite crystals geopetally arranged at their base.

There is no firm distinction between each type. Replacive textures developed in type 1 (PER) are similar to those of type 3 (ECI), and anhydrite pseudomorphs characteristic of types 1 (PER) and 2 (ACP) may occur within equant calcites of type 4 (GC).

6.2.1.1. Poikilitically enclosed relic (PER) - Description.

These textures have been identified within millimetre-sized equant calcite crystals lining cavities after sulphates from Eldon Hill, Field House, Haswell Moor Farm, Raisby, and Rough Furze Quarries. Evidence for calcitization is either as small (20-30μm), square-ended to irregular, lath-shaped anhydrite relics poikilitically enclosed within the core of a calcite crystal (Fig. 6.2a), or more commonly, as similar-sized pseudomorphs after anhydrite relics occluded by non-luminescent calcite within the core of a bright orange- to dull orange-luminescent calcite crystal (Figs. 6.2b, 6.3b & 6.8b). These two textures may occur, albeit rarely, within the cores of adjacent calcite crystals (Fig. 6.2). The anhydrite relics, and pseudomorphs after anhydrite relics may be randomly arranged within the calcite, or form a decussate texture. The contact of the calcitized anhydrite-bearing calcite with succeeding calcite cement is sometimes demarcated by a concentric zone boundary, and is always parallel to cement zonation (Figs. 6.2b, 6.3b & 6.8b). The succeeding cements have a variable bright/dull orange-luminescence, featuring concentric and occasional sector zonation, and pass into non-luminescent calcite with or without bright orange hairline subzones near the pore centre (Figs. 6.2b & 6.8b). This non-luminescent calcite, which also occludes pseudomorphs after anhydrite relics, contains negligible Fe or Mn, whereas the bright/dull orange-luminescent cements contain variable Fe and Mn in accordance with their luminescence intensity.

6.2.1.2. Anhydrite cement pseudomorphs (ACP) - Description.

These are rare, mainly recorded from dolostone breccias at Raisby Quarry (Lee and Harwood, 1989, figs. 7 & 9). The petrographic relationship between calcite and anhydrite is complex. Large (hundreds of microns to millimetre-sized) pseudomorphs after

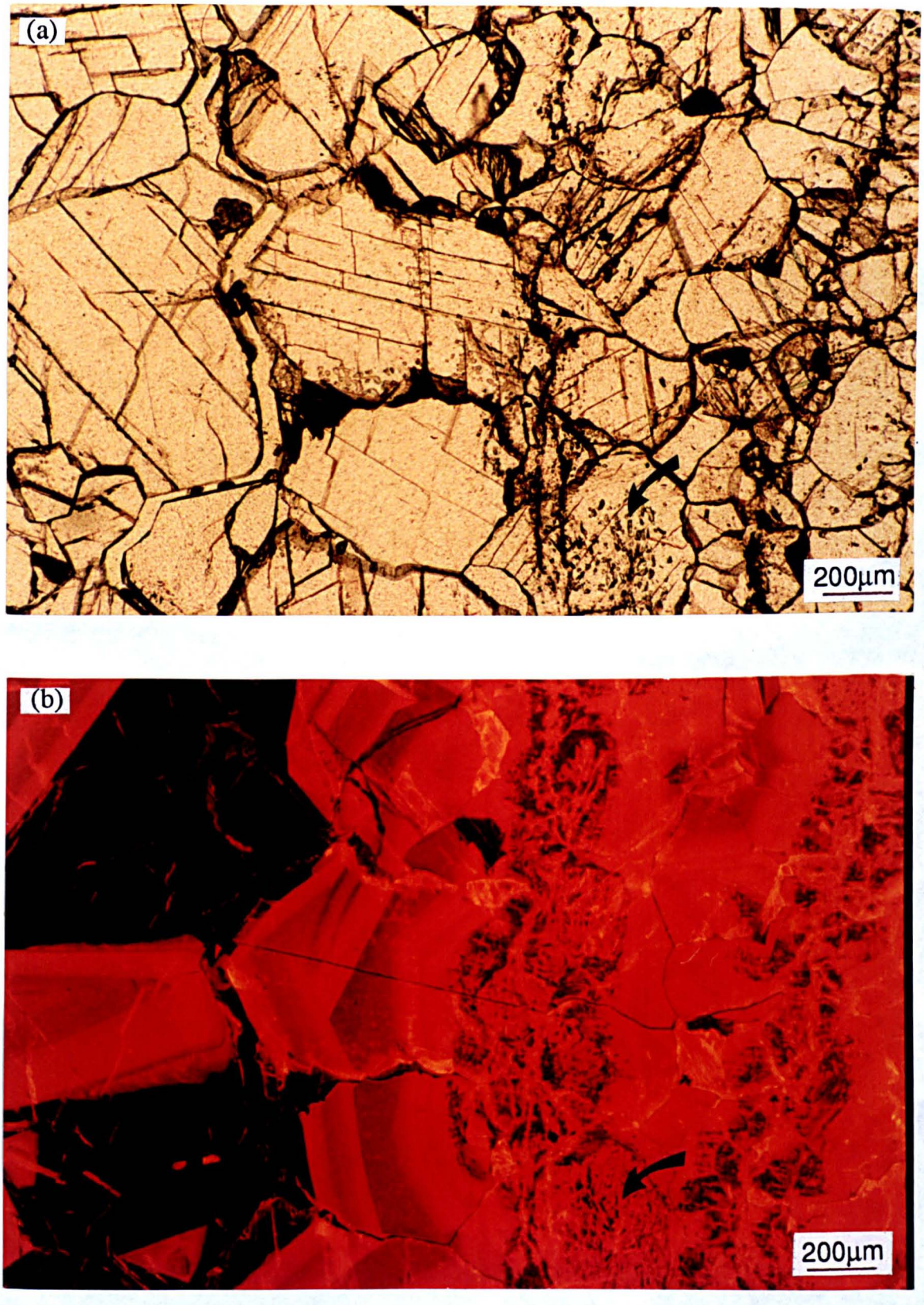

Fig. 6.2. Thin section photomicrographs of PER textures developed within calcite crystals lining a cavity after sulphate, Field House Quarry; (a) plane light, (b) luminescence. One crystal hosts relic anhydrite laths (arrowed), whereas the others contain non-luminescent calcite cemented pseudomorphs after anhydrite relics, invisible in plane light.

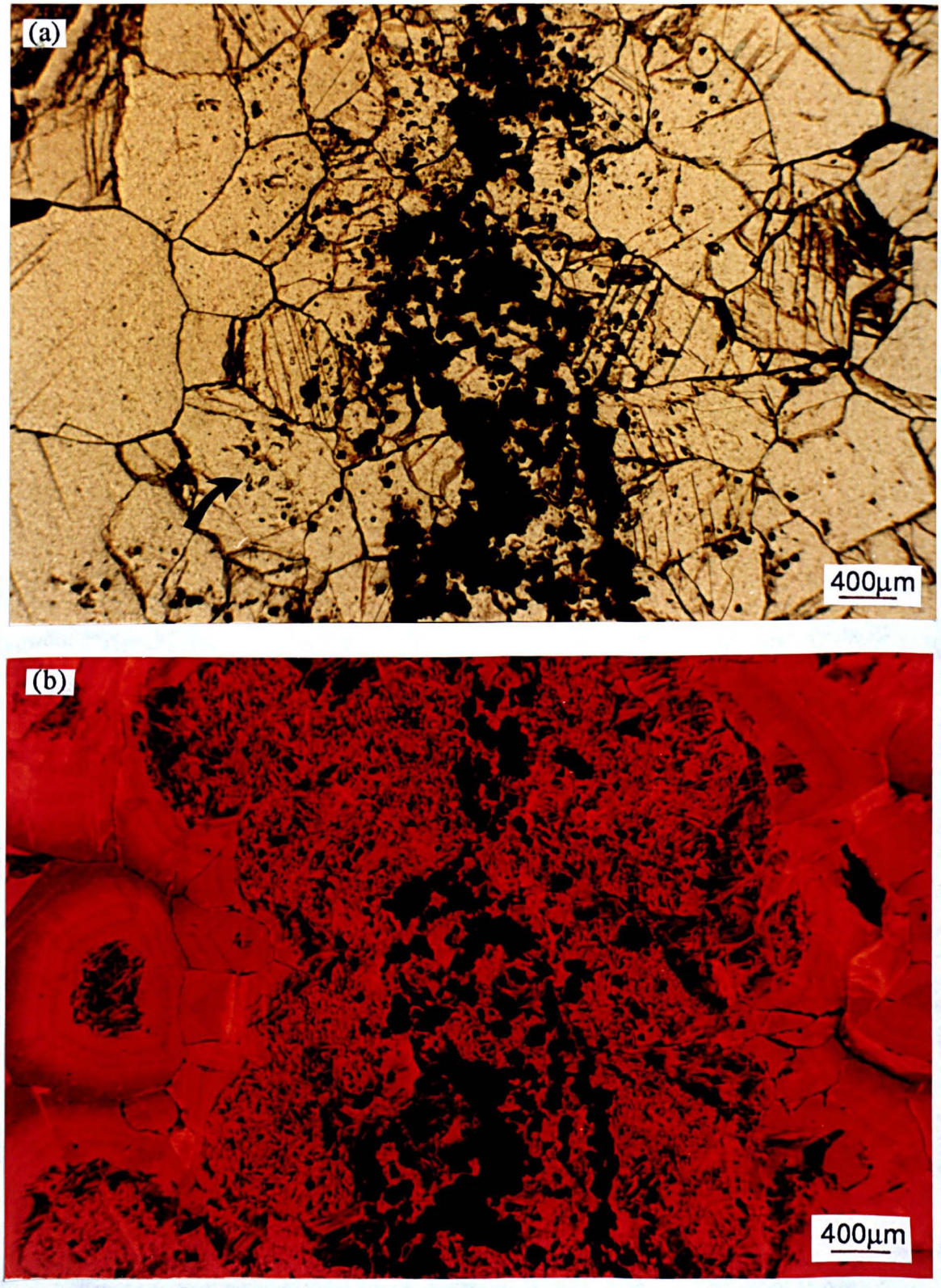

Fig. 6.3. Thin section photomicrographs of PER textures developed within calcite crystals lining a cavity after sulphate, Field House Quarry; (a) plane light, (b) luminescence. Most crystals have grown outwards from a vertically-orientated narrow stringer of dolomite, along which pyrite crystals (now hematite) nucleated. A few anhydrite relics remain (arrowed), but most have been dissolved, and the resultant pores cemented by non-luminescent calcite.

pore-filling anhydrite cements occur enclosed within large, millimetre-sized calcite crystals. The pseudomorphs after anhydrite are occluded by calcite of a similar luminescence character to that of the cements which encloses them. The concentric zonation of calcite which fills the pseudomorphs after anhydrite suggests that it is occluding porosity formed by the dissolution of anhydrite, after the anhydrite had been fully enclosed within the host calcite cement (Lee and Harwood, 1989, fig. 9). This close association of sulphate dissolution with calcite cementation is the basis for the identification of calcitization, although no relics of anhydrite remain. Lee and Harwood (1989) concluded that anhydrite within breccias at Raisby Quarry was a late diagenetic cement, in contrast to most other anhydrites within the Raisby Formation, which formed during early mesogenesis (5.7.1). This process of enclosure of anhydrite by calcite, and subsequent dissolution of anhydrite within the calcite is the same as that described for the non-luminescent pseudomorphs after anhydrite relics of the PER type. However, in contrast to PER, the anhydrite pseudomorphs are much larger, and the cement fill luminescent, thus petrographic textures are more easily discernable.

6.2.1.3. Enclosed carbonate inclusions (ECI) - Description.

This is the most common, and easily recognised type of calcitized evaporite. It has been recorded from Houghton road cut, Hetton-le-Hill, Raisby, Rough Furze, and Quarrington Quarries. The former evaporites commonly occur as subrounded nodules, a few centimetres in diameter, internally subdivided by thin stringers of dolomite. At Raisby Quarry, the former evaporite nodules are anomalous, being of metres in diameter (Fig. 6.4). Calcite completely, or near-completely fills the former evaporite nodules. The colour of the calcite in hand specimen is distinctive, varying from white to 'light olive grey' (5 Y 6/1). The colouration is due to inclusions, the replacive calcite becoming whiter with increasing inclusion density. Within the nodules, individual calcite crystals are 30μm-5mm in diameter, subrounded, and equant (Fig. 6.5a & b). They poikilitically enclose numerous very finely crystalline carbonate inclusions. The inclusions may occur throughout a calcite crystal, or, more commonly, be concentrated in its center (Fig. 6.5a). Rarely, ghosts of fossil fragments can be recognised, defined by the inclusions (Fig. 6.5b). Parallel-sided square-ended laths (mean 30μm in length) are also defined by the inclusions (Fig. 6.6a). They may be of random orientation, or, in any one area, have a common alignment, producing a decussate texture, or flow lineation. The inclusions define former anhydrite crystals within large, replacive anhydrite nodules. In contrast to the PER type, replacement of carbonate by anhydrite was incomplete, thus many carbonate inclusions remain. Within the large former evaporite nodules at Raisby Quarry, the calcite crystals grew from individual nucleation sites within the sulphate and carbonate (Fig. 6.5a), whereas, within smaller nodules, most calcites grew from nodule margins towards their center.

Fig. 6.4. A large isolated mass of ECI calcitized sulphate, Raisby Quarry (arrowed). This is very close to the top of the Raisby Formation, and cross-bedded ooid grainstones of the basal Ford Formation occur at the top of the quarry face.

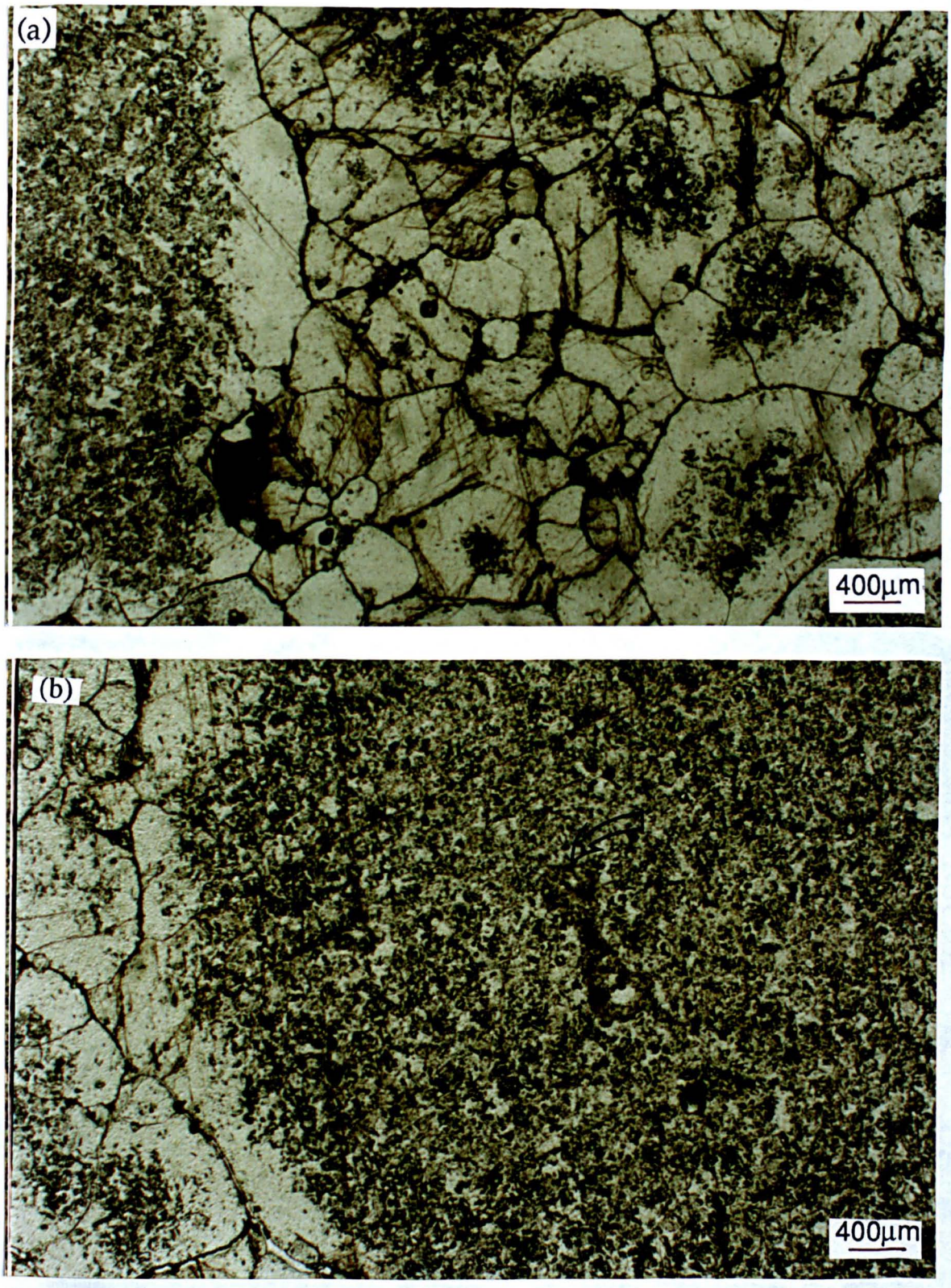

Fig. 6.5. Plane light thin section photomicrographs of a large ECI calcitized sulphate nodule from Raisby Quarry (very similar to that in fig. 6.4). Most carbonate inclusions, which defined the relic anhydrite, are concentrated in the cores of subrounded calcite crystals (a), clearly demonstrating the change in replacement style with time. That the carbonate inclusions have not been displaced during replacement, is illustrated by the ghost of a foraminifera within the replacive core of a large calcite crystal (b) (arrowed).

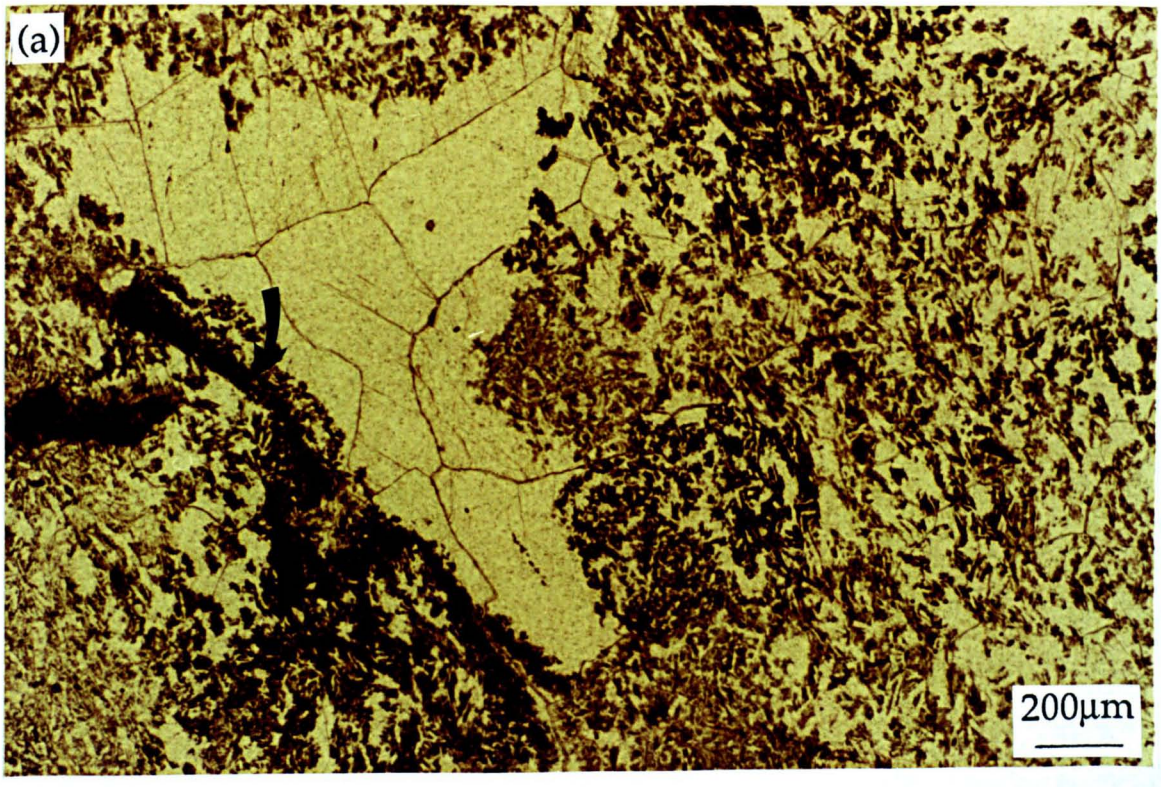

Fig. 6.6. Thin section photomicrographs of an ECI calcitized sulphate nodule, Quarrington Quarry; (a) plane light, (b) luminescence. At the junction of zoned orange-luminescent replacive calcite and pore filling non-luminescent cement is a geopetal internal sediment of carbonate inclusions (arrowed). Note, there are two separate phases of zoned, non-luminescent calcite cement (b). Arrow indicates way up.

The replacive calcite is bright orange- to dull orange-luminescent, and commonly concentrically zoned (Fig. 6.6b). The stratigraphy of the zonation is, in general, correlatable throughout any one sample (Fig. 6.6b). Inclusion-free cement, overlying the inclusion-rich calcite, is also concentrically zoned, and ranges from bright- to dull- to, most commonly, non-luminescent with bright orange hairline subzones (Fig. 6.6b). The calcite cement, at its junction with the replacive calcite, and at certain levels within it, commonly contains geopetal layers of internal sediments, petrographically identical to carbonate poikilitically enclosed within the replacive calcites (Fig. 6.6a). The thickness of the internal sediment layers decreases with precipitation of the inclusion free cement.

ICP analyses of replacive calcites from Raisby and Quarrington Quarries (Appendix VII) show they have a variable Mg content, up to 6.14 mole% $MgCO_3$, which correlates with inclusion density. They also have a low Fe/Mn ratio (less than 0.5) reflecting the dominance of bright orange-luminescent replacive calcite (Appendix I). Sr concentrations range from 70 to 147ppm. Non-carbonate trace element concentrations and insoluble residues are negligible. Two carbon and oxygen stable isotope determinations of a sample from Raisby Quarry gave results of $\delta^{13}C$ -6.1‰ & -12.1‰, and $\delta^{18}O$ -12.3‰ & -13.1‰, very similar to some pore filling cements from the same locality (Fig. 6.54).

6.2.1.4. Geopetal calcite (GC) - Description.

This type occurs within a very distinctive form of cavity after sulphate, easily recognizable in the field. GC cavities have been recorded from Crime Rigg, Field House, Haswell Moor Farm, Middridge, and Running Waters Quarries, and are especially abundant in and around Frenchmans Bay. They are commonly 5cm to 15 cm in diameter, hemispherical, with fine equant (50μm to 150μm) luminescent calcite geopetally arranged at the base of the cavity fill, grading into coarser non-luminescent (with bright orange hairline subzones) columnar calcite cement (2-4mm long) which encrusts both the upper surface of the equant calcite, and the roof of the cavity (Fig. 6.7). The columnar calcite may or may not occlude remaining porosity within the cavity.

The luminescent equant calcite crystals increase in size from the base to the top of the equant calcite layer. All GC cavities have abundant internal sediments within and between the equant calcite (Fig. A2.4a). The internal sediments comprise fine (less than 100μm) monocrystalline and polycrystalline subrounded to subangular quartz grains, and muscovite flakes within a clay-rich matrix. The internal sediments may also occur as large (hundreds of microns in length) tabular 'rafts' floating within the equant calcite. The rafts may be randomly orientated and subhorizontal, or form a decussate texture. Composition of the internal sediments from microprobe analysis shows that they are dominated by Si, Al and Ca, with minor Mg, Fe and Na (Appendix V).

Fig. 6.7. Polished hand specimen of a GC cavity, Frenchmans Bay. A clear change is evident, from basal finely crystalline calcite into coarser columnar cement. 'Rafts' of dolomitic clays (arrowed) occur throughout the cavity fill. Scale in millimetres. Arrow indicates way up.

Some GC cavities have abundant evidence for the former presence of sulphates, whereas others do not. Evidence of former sulphates is commonly as small (20-30μm), non-luminescent pseudomorphs after anhydrite relics (PER textures) in the core of equant calcites (Fig. 6.8b). In one cavity fill from Haswell Moor Farm Quarry, anhydrite lath pseudomorphs were much larger than normal, up to 1mm long (similar in texture to ACP). These pseudomorphs are represented as either porosity, are filled by a zoned bright orange-luminescent cement (ACP textures), or remain as corroded anhydrite crystals (Fig. 6.9b). In all cases, the anhydrite relics, or their pseudomorphs are restricted to the bright orange-luminescent core zone of the calcite crystals and abruptly terminate against the succeeding zone (Fig. 6.8b & 6.9b). One of the GC cavities from Frenchmans Bay provides indirect evidence for former anhydrite, via pseudomorphs (now calcite cemented) outlined by replacive barite (Fig. 7.2b).

Most GC cavities are associated with abundant hematite after pyrite/marcasite, or pyrite/marcasite itself. Hematite after pyrite/marcasite is concentrated along intercrystalline boundaries of the equant calcite (Figs. 6.10a & b) or partly replacing internal sediments, suggesting iron sulphide precipitation postdated calcite cementation. Unaltered pyrite/marcasite is only recorded where isolated in the centre of equant calcites (Fig. 6.10b). No pyrite/marcasite or hematite after pyrite/marcasite was recorded within non-luminescent columnar cements. The occurrence of pyrite/marcasite crystals within calcite cemented anhydrite pseudomorphs (Fig. 6.10b) could suggest that the iron sulphides have directly replaced anhydrite. However, this apparent selectivity may just be because calcite pseudomorphing the anhydrite was less resistant to replacement by iron sulphides.

Geochemistry of the calcite cements is variable. The common cement evolution sequence is from dull orange- to subzoned and sector zoned bright orange-, into non-luminescent calcite, correlating with an overall decrease in Fe, Mn and Sr, and increase in Mg (Figs. 6.11 & 6.12). A traverse through a GC cavity from Frenchmans Bay (Fig. 6.12), clearly shows these geochemical trends, along with an upwards decrease in trace elements not related to carbonate minerals, reflecting a decrease in the abundance of clay-rich internal sediments. Other type GC equant calcites are strongly depleted in Fe and are almost exclusively bright orange-luminescent (Mn-rich) (Fig. 6.13). These calcites are commonly directly associated with abundant pyrite/marcasite, and hematite after pyrite/marcasite (Fig. 6.10a & b). Sr concentrations for all type GC samples are low, and range from approximately 50 to 230ppm (Appendix VII).

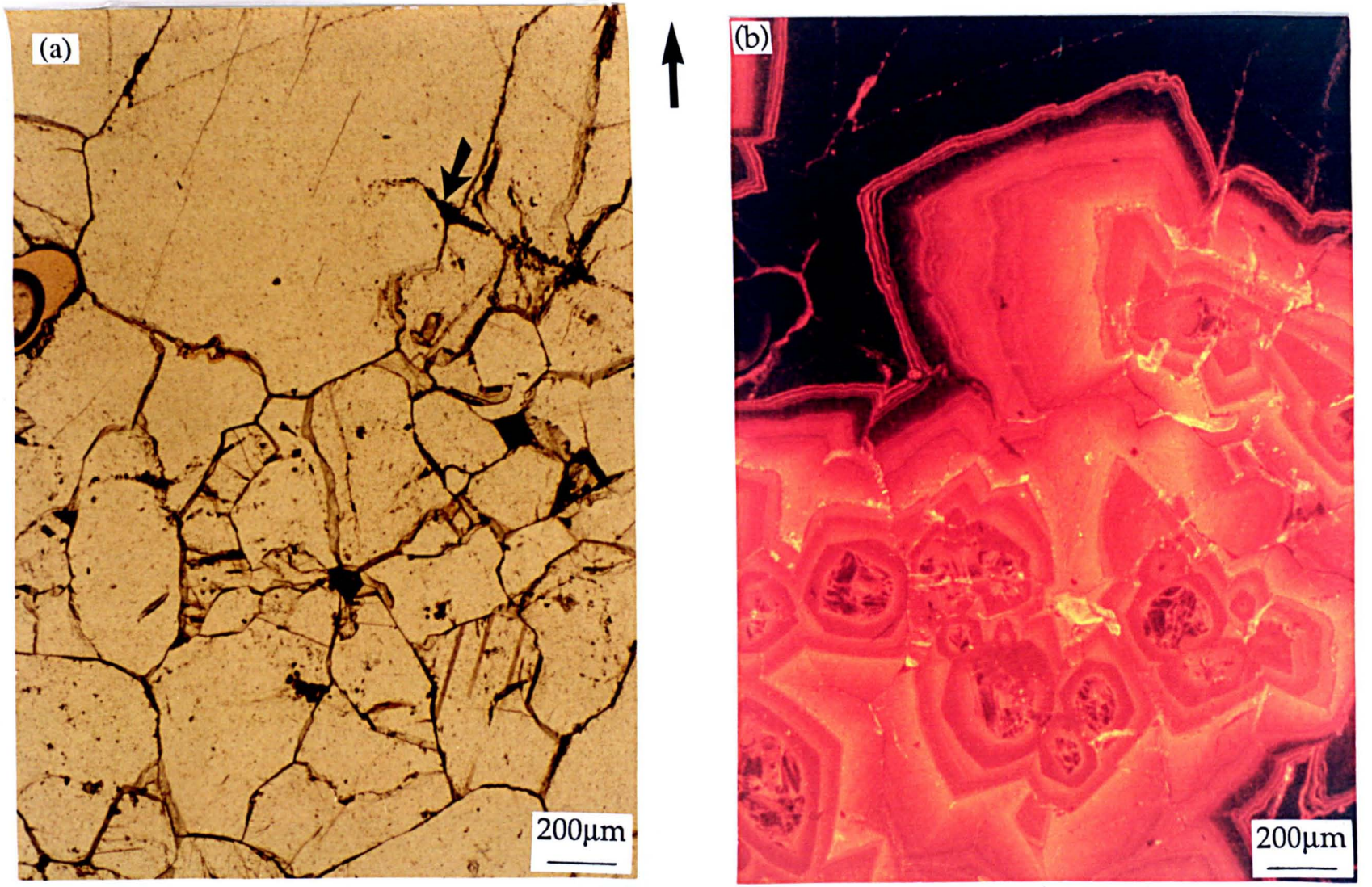

Fig. 6.8. Thin section photomicrographs of the contact of equant with columnar calcite within a GC cavity fill, Field House Quarry; (a) plane light, (b) luminescence. The cores of the luminescent equant crystals show PER replacement textures (b). A thin layer of dolomitic internal sediments lie at one of the luminescent calcite zone boundaries (arrowed). Arrow indicates way up.

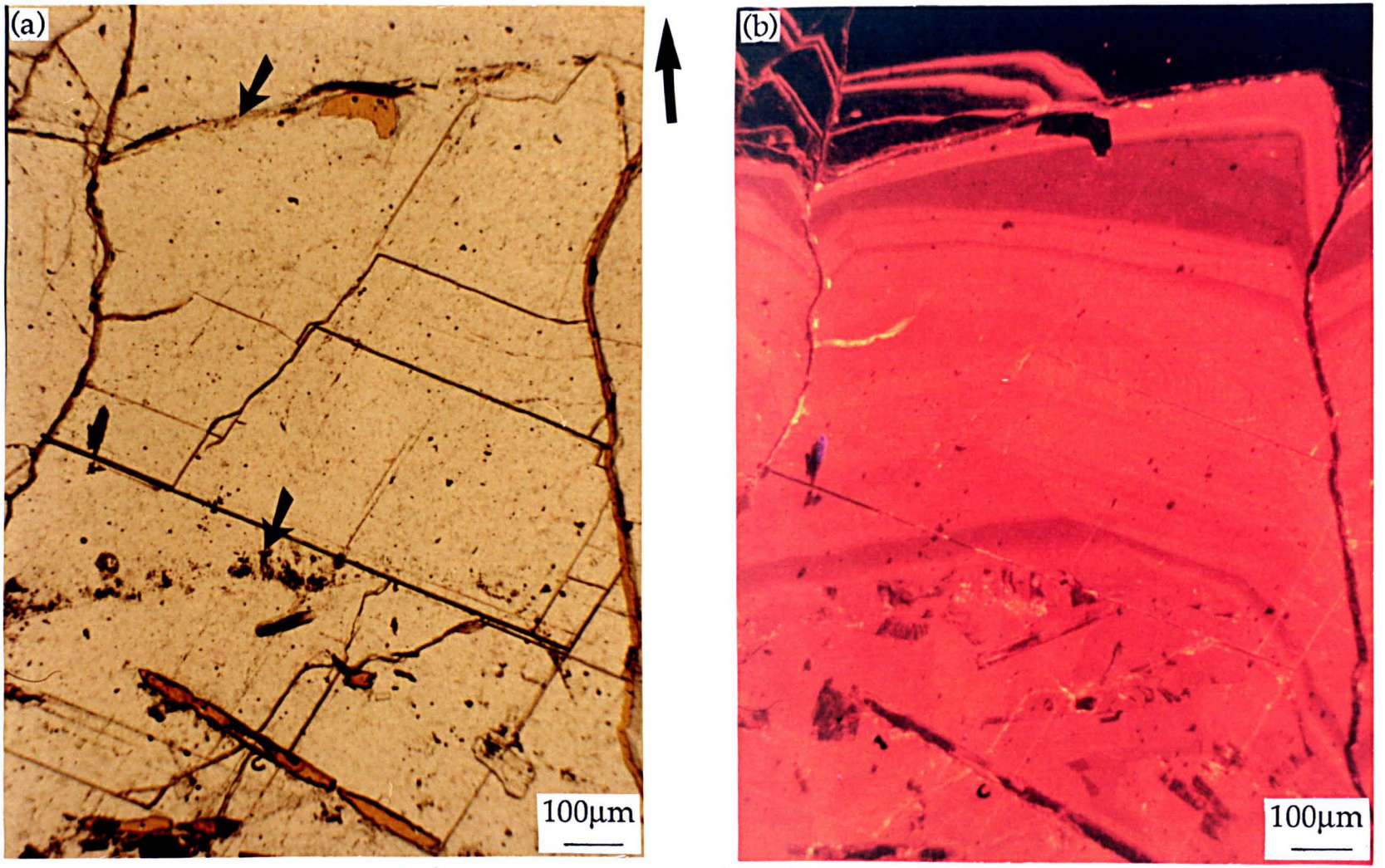

Fig. 6.9 Thin section photomicrographs of the contact between replacive and pore filling calcite within a GC cavity, Haswell Moor Farm Quarry; (a) plane light, (b) luminescence. The replacive part of the crystal hosts pores after and partially calcite cemented pores after, anhydrite laths. The contact of replacive and pore filling calcite is demarcated by a dull orange-luminescent zone. A thin layer of internal sediment lies close to the top of the replacive calcite (arrowed), and corrosion marks the junction of luminescent with non-luminescent cement (arrowed). Arrow indicates way up.

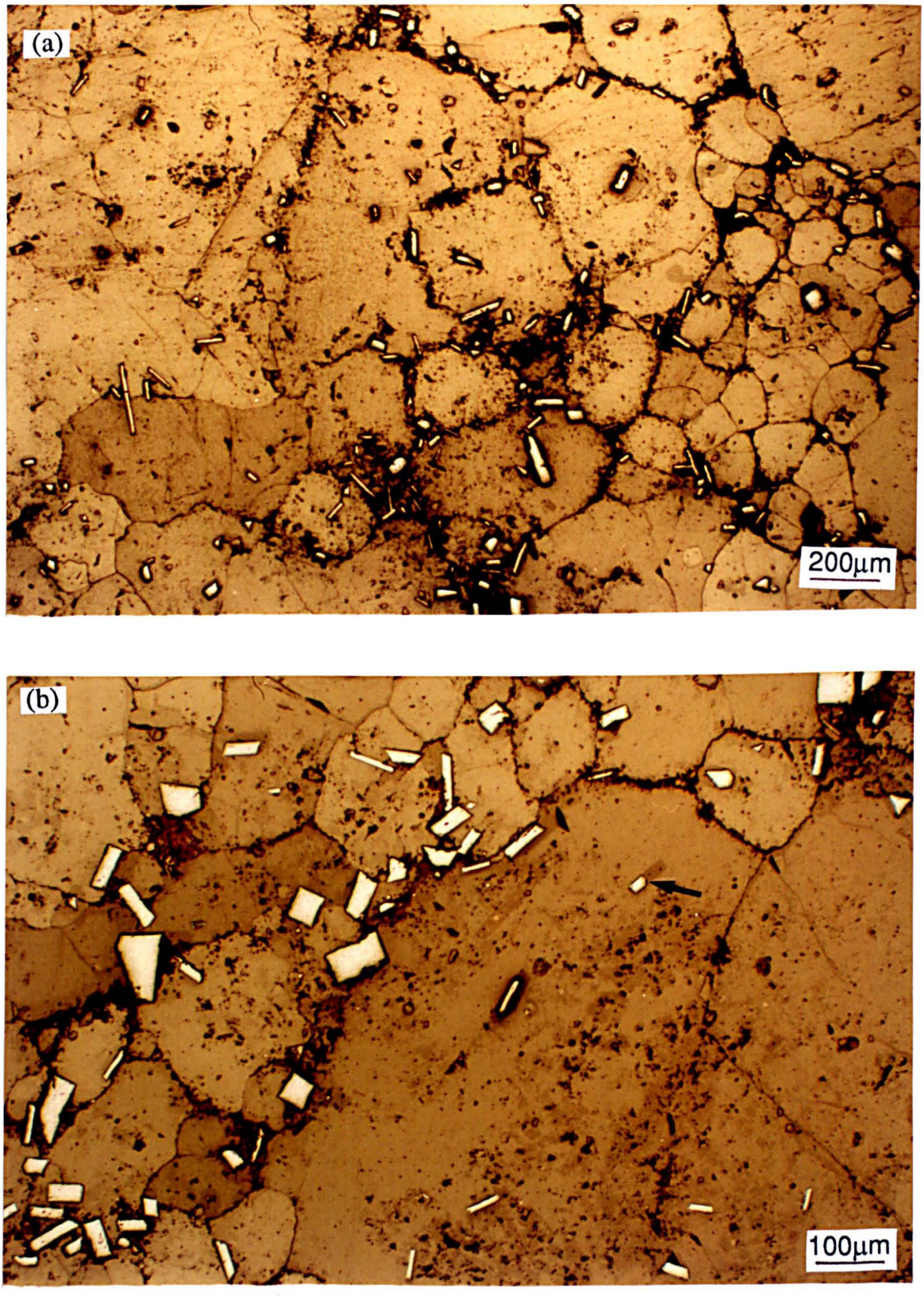

Fig. 6.10.. Thin section photomicrographs of the basal equant calcite within a GC cavity, Haswell Moor Farm Quarry. Both (a) and (b) are in reflected light. Hematite after marcasite is concentrated along intercrystalline boundaries between the equant calcite crystals. Unaltered marcasite (arrowed) is concentrated in the centers of equant crystals. One small hematite crystal in (b) (arrowed), is possibly partly replacive of an anhydrite lath.

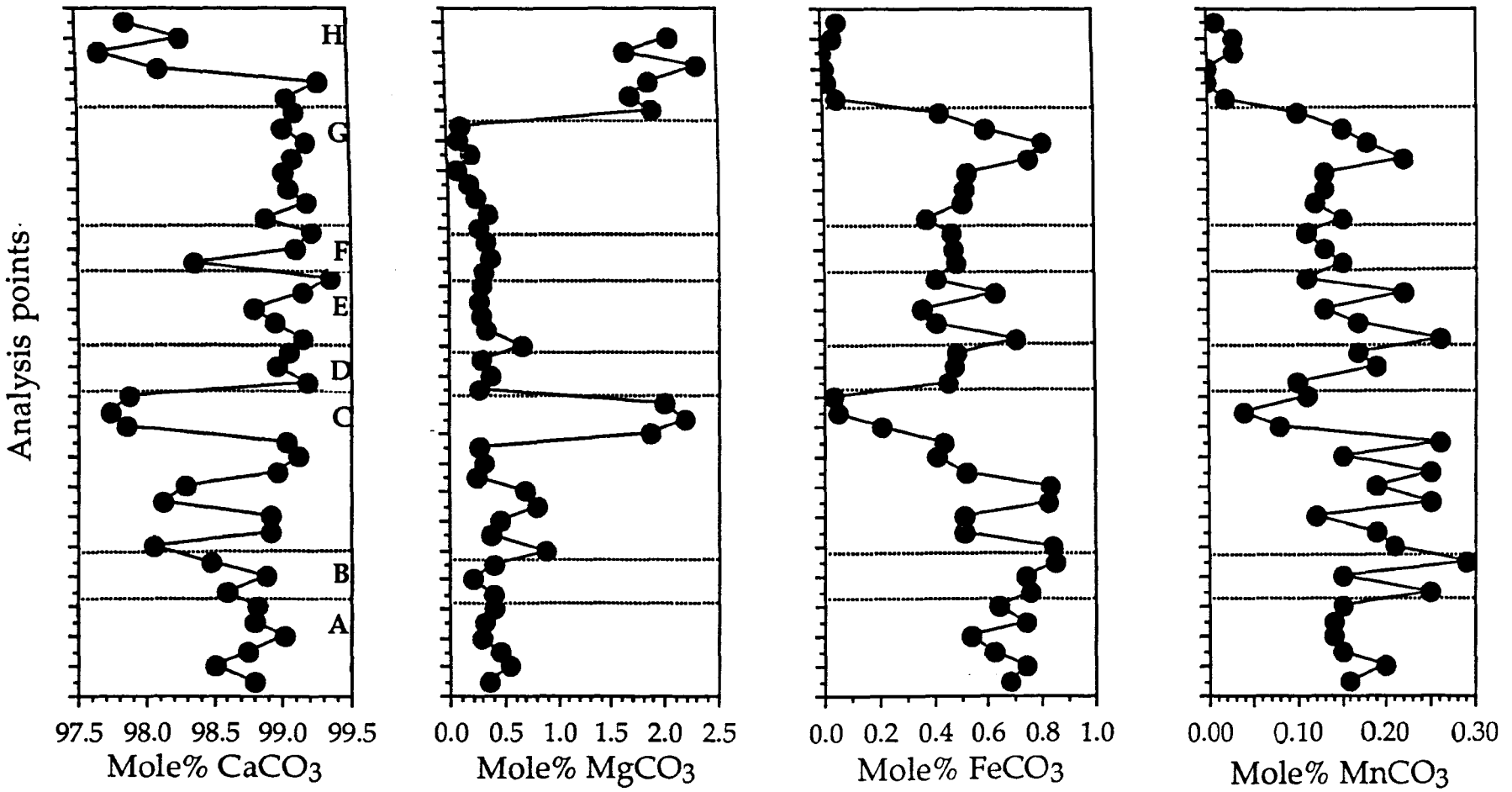

Fig. 6.11. Graphs illustrating the geochemical variation of calcites within a GC cavity fill, Frenchmans Bay, from basal equant (A) to non-luminescent columnar calcite (H). A = finely crystalline equant calcite, B = medium crystalline equant calcite, C = coarsely crystalline equant calcite, D = subzoned equant calcite, E = sector zone, F & G = subzoned equant calcite, H = non-luminescent calcite. Analysed by microprobe.

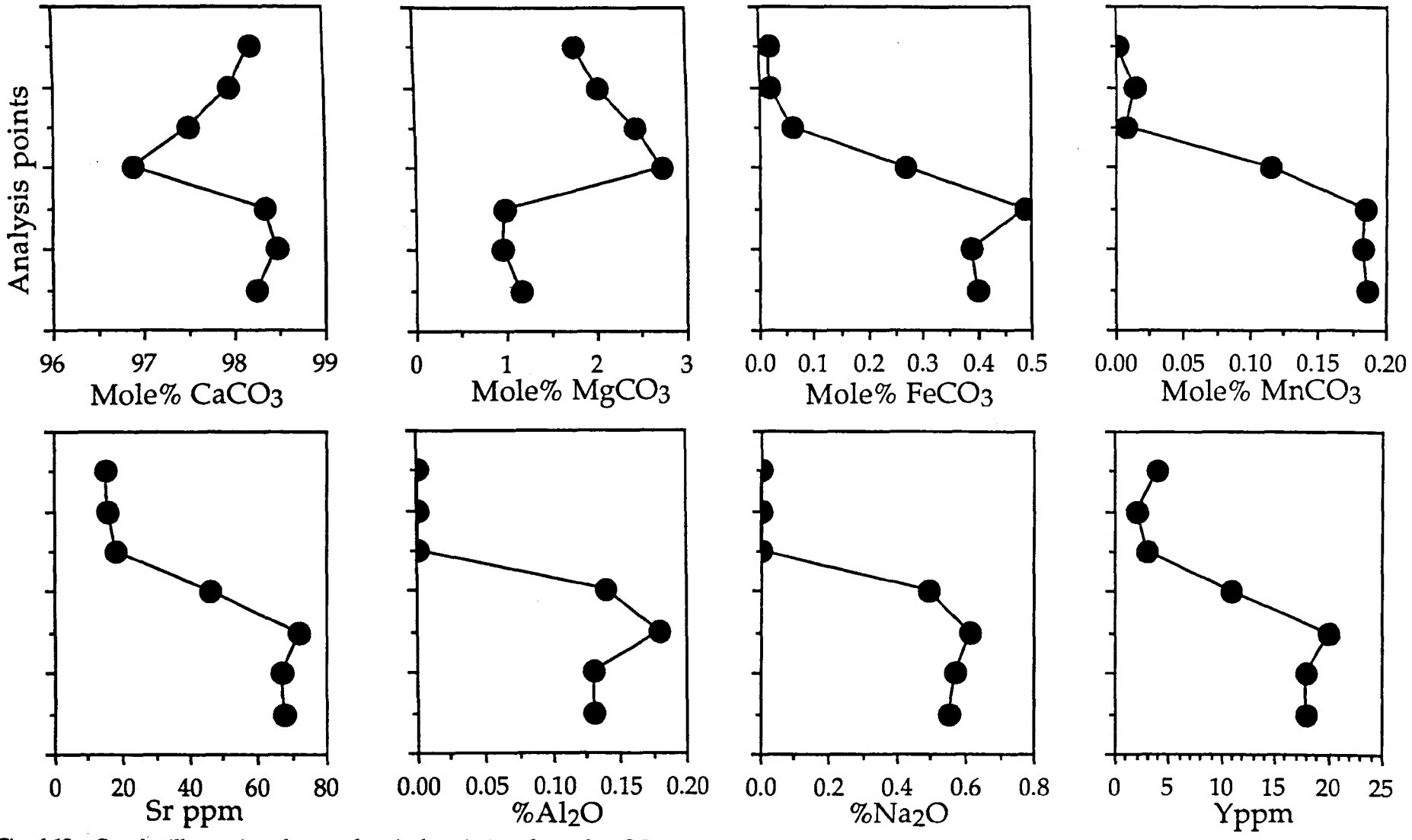

Fig. 6.12. Graphs illustrating the geochemical variation through a GC cavity fill, Frenchmans Bay, analysed by ICP. The lowermost analysis point of each graph corresponds to the base of the cavity fill. The vertical distance covered by the traverse is approximetely 5cm. The distinct change between the third and fifth analysis points corresponds to the boundary between basal equant and upper columnar calcite.

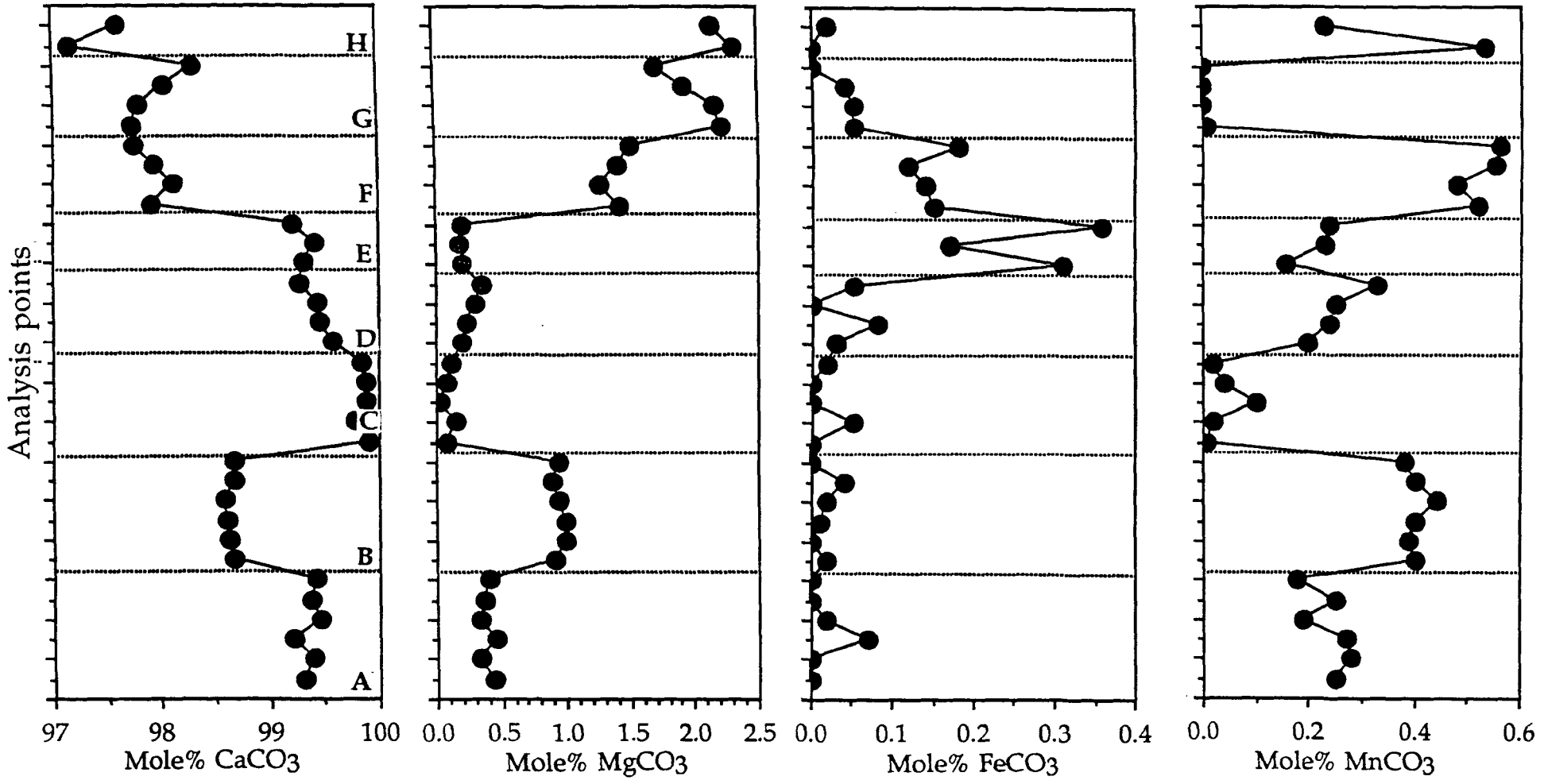

Fig. 6.13. Graphs illustrating the geochemical variation in a large calcite cement crystal (Figs. 6.10a & b, A2.1a & b), within a GC cavity fill, Haswell Moor Farm Quarry, from its replacive base (A) to non-luminescent top (H). A = bright orange-luminescent replacive calcite, B & D = medium orange-luminescent cement, C = fir-tree sector zone, E = dull orange-luminescent cement, F = bright orange-luminescent zone, G = non-luminescent calcite, H = bright orange-luminescent hairline subzone.

6.2.2. Calcitization of evaporites - Chemical considerations.

Although the calcitization of evaporites is probably a common diagenetic process, especially within dolomite-evaporite sequences, very few occurrences have been described in detail. Calcitization of Zechstein anhydrites have been documented by Turner *et al.*, (1978) and Turner and Magaritz (1982) (from the Marl Slate), Jones and Hirst (1972), Clark (1980), Harwood (1980), Harwood and Coleman (1983), Smith (1986), and Lee and Harwood, (1989). They have also been described from the Devonian (Shearman and Fuller, 1969) and Mississippian (Kaldi and Hartling, 1982) of Canada, the Permian of the Delaware Basin, U.S.A. (Kirkland and Evans, 1976), the Jurassic of Dorset (West, 1964; Holliday and Shephard-Thorn, 1974), and the Miocene of Egypt (Pierre and Rouchy, 1988). Only West (1964) and Harwood (1980) provide detailed petrographic descriptions. Suggested timings of calcitization vary from synsedimentary/early diagenetic, before significant lithification (Shearman and Fuller, 1969; Harwood, 1980; Pierre and Rouchy, 1988), to late diagenetic associated with uplift (West, 1964; Kirkland and Evans, 1976; Pierre and Rouchy, 1988).

The replacement of gypsum/anhydrite by calcite is not possible unless another simultaneous reaction consumes the acidity produced:

$$CaSO_4 + H_2CO_3 \rightleftharpoons CaCO_3 + SO_4^{2-} + 2H^+$$

$$2CaCO_3 + 4H^+ \rightleftharpoons 2Ca^{2+} + 2CO_2 + 2H_2O$$

(modified from Anderson and Garven, 1987).

A solution to this problem is that replacement is mediated by sulphate-reducing bacteria, which reduce the calcium sulphate and use organic matter (commonly liquid, or gaseous hydrocarbons such as methane [CH_4]) as a source of energy:

$$CaSO_4 + CH_4 \rightarrow H_2S + H_2O + CaCO_3 + \text{Energy}$$

(after Kirkland and Evans, 1976).

Bacteria cannot reduce the sulphate in its solid form, and so it has firstly to be in solution (Machel, 1987b). Many authors invoke meteoric-derived fluids as the agent by which bacteria can be juxtaposed with migrating (gaseous or liquid) hydrocarbons in reaction zones (Machel, 1987b). For bacteria to metabolize, the diagenetic environment needs to be anoxic and of a pH between 5 and 9 (Trudinger *et al.*, 1985). As the above equation illustrates, bacterial sulphate reduction is exothermic. The amount of heat produced is 10-30 Kcal $mole^{-1}$ $CaSO_4$ which, in a rock unit 1km thick containing 30% sulphate would, in 1Ma, produce a heat flux of the same order of magnitude to that of standard geothermal heat flow (Machel, 1987b).

Although the above formulae represent the straightforward recrystallization of one unit of anhydrite into one unit of calcite, it is unlikely that the reaction will proceed in such a manner. No net volume reduction is recorded within Raisby Formation samples, although this should occur on the basis of the previous reaction (the molar volume at standard state of gypsum is $74.31cm^3$/mole, anhydrite $45.94cm^3$/mole and calcite $36.94cm^3$/mole [Berner, 1971]). Thus, calcitization of sulphate is most likely to occur in a relatively open diagenetic system, with fluids close to saturation with respect to calcite. Ca input from gypsum dissolution and CO_3^{2-} provided by sulphate reduction supersaturate the diagenetic fluids with respect to calcite (common ion effect). Thus, in an open system, replacement will be volume-for-volume, although porosity may be created by dissolution of unreplaced sulphate (Kirkland and Evans, 1976). As bacterial sulphate reduction requires sulphate to be in solution, the calcitization process is probably analogous to wet dissolution-reprecipitation of aragonite along a narrow solution film (Fig. 6.17).

Hydrogen sulphide (H_2S) is an important by-product of the replacement reaction. It may migrate from the reaction site to the surface and be oxidized, producing elemental sulphur (Kirkland and Evans, 1976). If H_2S remains at the diagenetic site, it is available to combine with base metal ions in solution to form sulphide minerals such as pyrite/marcasite (FeS_2), sphalerite (ZnS) and galena (PbS). Such a process has been invoked by Harwood (1980) and Harwood and Coleman (1983) for Fe-Pb-Zn sulphide mineralization in association with calcitized anhydrite from the Cadeby Formation (7.2.4.1). However, if such mineralization takes place within the diagenetic site, it should inhibit calcitization of the sulphates, owing to an increase in acidity:

$$M^{2+} + H_2S \rightleftharpoons 2H^+ + MS$$

(M = any divalent metal ion (i.e., Fe^{2+}, Zn^{2+}). After Anderson and Garven, 1987).
Thus, the overall reaction will be:

$$CaSO_4 + CH_4 + 2M^{2+} \rightleftharpoons CaCO_3 + H_2O + 2H^+ + 2MS$$

$$CaCO_3 + 4H^+ \rightleftharpoons 2Ca^{2+} + 2CO_2 + 2H_2O$$

Therefore:

$$CaSO_4 + M^{2+} + CH_4 \rightleftharpoons MS + Ca^{2+} + CO_2 + 2H_2O$$

(modified from Anderson and Garven, 1987).

This defines an important problem with regard to calcitization of sulphates, in that, if metal ions are available in sufficient quantity at or near the reaction site, these equations predict that metal sulphides, and no replacive calcite will be precipitated. As the pore fluids at the reaction site by definition will be reducing, metal ions will be in solution if they are available (sourced from the dissolution of iron-rich dolomite and/or detrital/authigenic iron oxide/hydroxides by reducing pore fluids, or introduced by hot brines, upwelling from the Palaeozoic basement [i.e., Cu, Pb, Zn] [7.2.4.1]). If no such ions are available, H_2S will evolve as a gas phase and eventually migrate from the reaction site (Anderson and Garven, 1987).

Luminescence of replacive calcites and associated calcite cements can greatly help in defining pore fluid conditions during replacement and succeeding cementation. The luminescence intensity and colours of calcites are directly controlled by the relative concentrations of Fe and Mn substituting for Ca within the calcite lattice (Appendix I). Fe and Mn need to be in a reduced (divalent) state for incorporation into calcites, as only ions with the same valency state can substitute for Ca^{2+}. The exact redox conditions which control Fe and Mn reduction have recently been redefined (Barnaby and Rimstidt, 1989) (Fig. 6.14), although precise values are not as important as general trends in this study. Assuming both Fe and Mn are available within the pore fluids, at a constant pH, dull orange-luminescent calcite will be precipitated under lower Eh conditions than bright orange-luminescent calcite, which is itself precipitated by fluids of a lower Eh than non-luminescent calcite (Fig. 6.14). A further phase of bright orange-luminescent calcite may precipitate in very low Eh conditions during bacterial sulphate reduction and iron sulphide precipitation (Frank *et al.*, 1982). This is because iron forms a sulphide phase much more easily than Mn. MnS (alabandite) has a very small stability field, and will only precipitate from fluids of a negative Eh and a pH of between 8 and 9 (Garrels and Christ, 1965). Bacterial sulphate reduction is optimized at pH of 5 to 9, and so it is unlikely that bacterial sulphate reduction and MnS precipitation will be coincident. Pyrite/marcasite precipitation will further decrease the pH of the pore waters. Thus, in a fluid where H_2S is available together with Fe^{2+} and Mn^{2+}, and calcite is precipitating, Fe will precipitate as a sulphide phase (pyrite/marcasite), whereas Mn^{2+} will be available for incorporation into the calcite, leading to bright orange-luminescence.

6.2.3. Calcitization of evaporites - Interpretation.

Most of the calcitized sulphates described from the Raisby Formation provide direct evidence for precursor gypsum/anhydrite via relics or pseudomorphs which were poikilitically enclosed during calcite precipitation. Thus, the basis for the identification of calcitization is that enclosure occurs during the replacement process (i.e., calcitization is incomplete). The preservation of fine scale textures of the former sulphates demonstrates that no significant porosity (greater than a few microns), was created during calcitization,

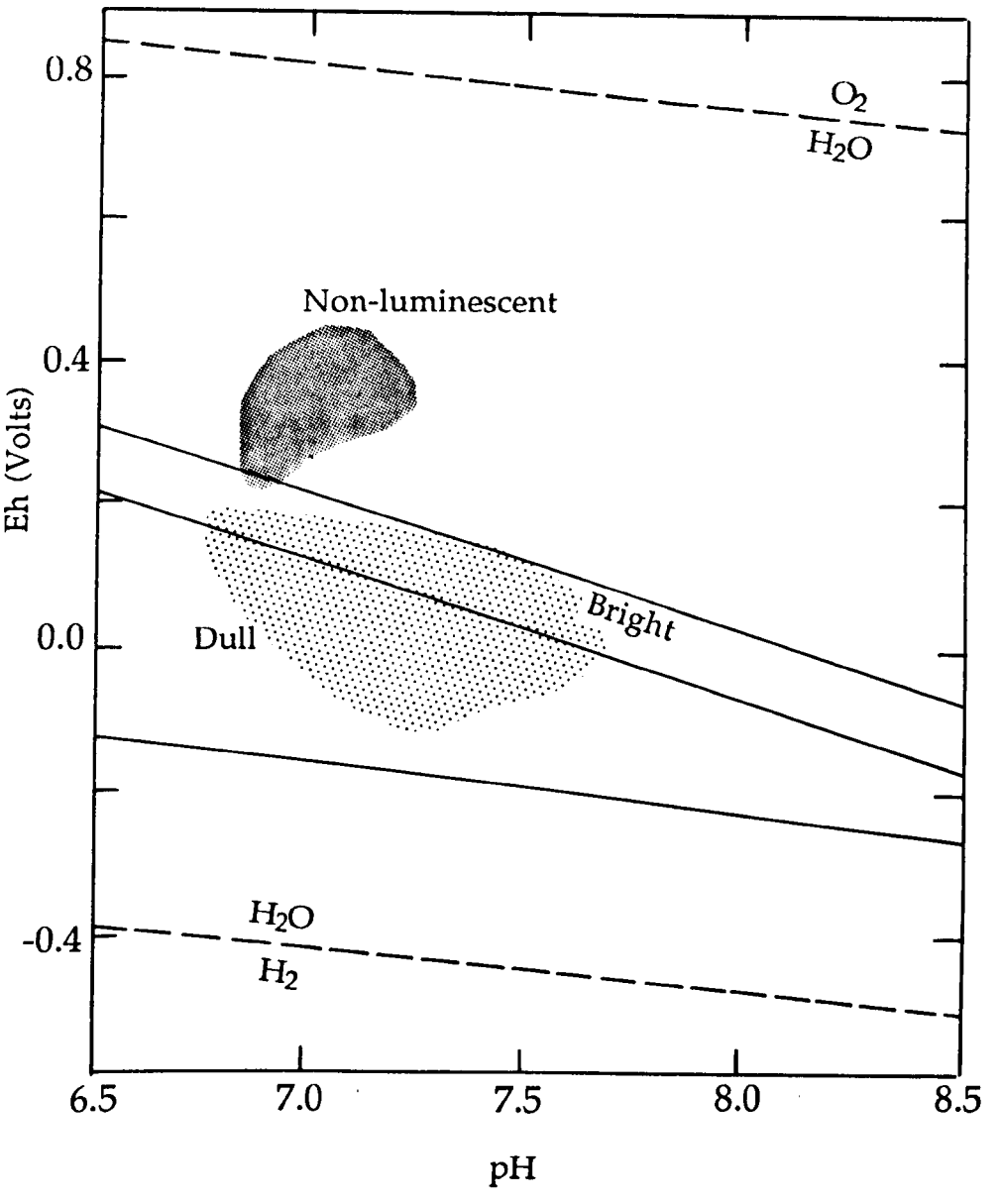

Fig. 6.14. Eh-pH diagram, defining the conditions under which dull, bright, and non-luminescent calcite should be precipitated within shallow, fresh water aquifers. The areas in dark and light stipple represent the actual Eh and pH conditions under which non-luminescent and bright/dull luminescent calcite respectively will be precipitated, on the basis of chemical analyses of recent groundwaters (Barnaby and Rimstidt, 1989, fig. 9). The areas in which bright orange-luminescent calcite is precipitated during bacterial sulphate reduction are not shown.

which suggests that the width of the reaction zones were probably of a similar magnitude as those involved in calcitization of aragonite (Fig. 6.17) (4.3.2.1). Types ACP and GC are not direct replacement textures (i.e., dissolution of sulphates and precipitation of calcite was not simultaneous), but sulphate dissolution did occur closely before/during (GC), or soon after (ACP) calcite precipitation, and, most likely, Ca derived from the dissolution of sulphate participated in precipitation of the associated calcites.

6.2.3.1. Petrography of calcitized evaporites - Interpretation.

Most of the replacive calcite crystals are large, equant, and poikilitically enclose anhydrite relics and/or pseudomorphs. This typical habit is indicative of a low density of nucleation sites and/or low supersaturation with respect to calcite. Replacement proceeded either within the original sulphate nodule from a small number of nucleation sites, or from nodule margins towards their centres (Fig. 6.15). Replacement style was, in part, controlled by the density of carbonate impurities (nucleation sites) within the precursor sulphate (Fig. 6.15). Both styles of replacement have also been recorded from silicified evaporites (Milliken, 1979). In GC cavities, strong upward gradients in size of the equant luminescent calcites, imply either a decrease in nucleation rate/density of nucleation sites, or a decrease in supersaturation with respect to calcite over time. The GC textures overall, are best interpreted in terms of the calcite growing within a 'sulphate mush' such that insoluble residues from the dissolving inclusion-rich sulphate nodule collected at the base of the cavity. The initial calcites grew within this dense mass of insoluble residues such that there was only a small distance between nucleation sites, leading to fine crystals. Higher up in the cavity, where the amount of insoluble residues were less, nucleation sites were further apart and so coarser equant calcites could grow. The final columnar cements grew after all sulphate had dissolved out. Thus, sulphate dissolution, producing internal sediments, was continuing during the period of equant cement precipitation, because the internal sediments within GC cavities are not solely concentrated at their base.

In types ACP, and some GC cavities, anhydrite was clearly the main sulphate evaporite coexisting with calcite during replacement. However, it is possible that gypsum was the dominant sulphate during the formation of types PER, and ECI. Although anhydrite was clearly the initial replacive phase of dolomite in type ECI, it may have rehydrated to gypsum prior to replacement, the rehydration process not disturbing carbonate inclusions. Similarly, the density of anhydrite relics within type PER calcites, is almost identical to the density of anhydrite relics where anhydrite has been partially rehydrated to gypsum in the Raisby Formation and Hartlepool Anhydrite Formation (Fig. 6.16a & b). Thus, in types PER and ECI, gypsum may have been replaced by calcite, although in PER, the less soluble anhydrite relics within the gypsum were more resistant to replacement. With regard to most

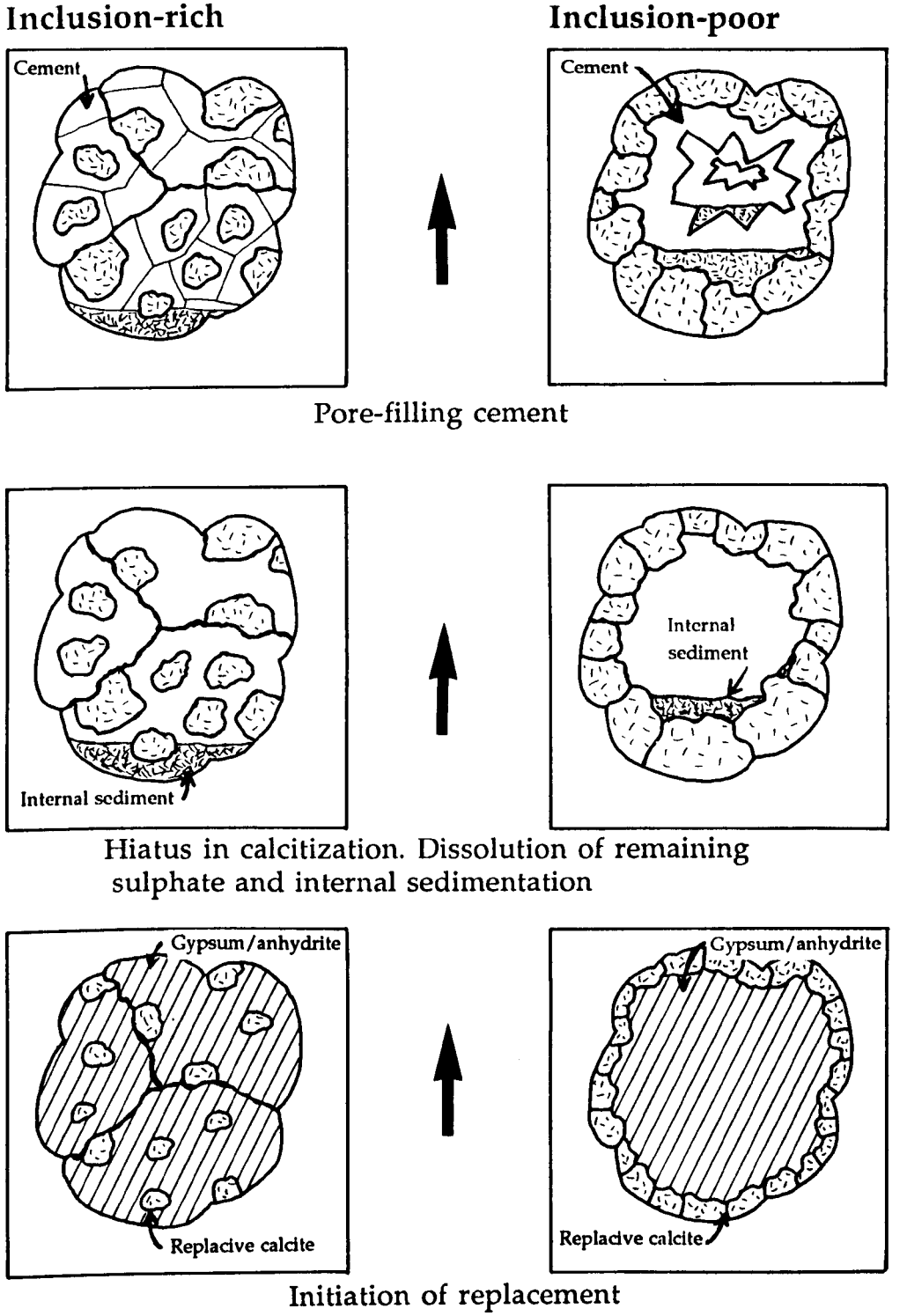

Fig. 6.15 . Schematic diagrams illustrating contrasting styles of calcitization between inclusion-rich and inclusion-poor sulphate nodules. Within inclusion-rich nodules, replacive calcite may nucleate and grow from many points, but calcite replacing inclusion-free sulphate nodules grows mainly from their outer margins, inwards.

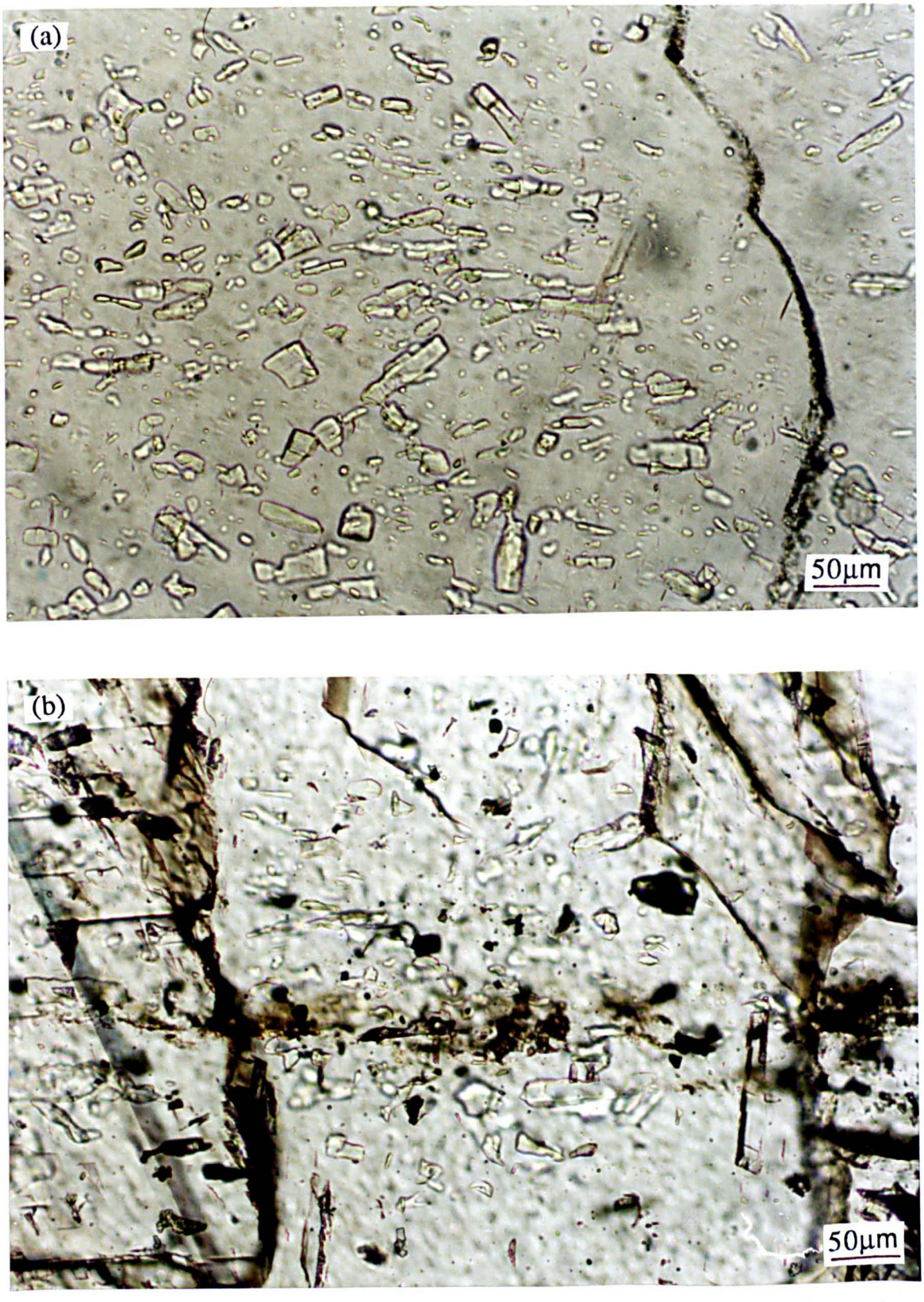

Fig. 6.16. Plane light, thin section photomicrographs showing a comparison between the density of anhydrite relics within a large gypsum porphyroblast from the base of the Hartlepool Anhydrite Formation, W15 borehole 194.50m (a), and within replacive calcite, Field House Quarry (b). The density of relics in the center of the field of view in (b) is comparable with the density of relics in (a).

PER and ACP textures, although anhydrite was enclosed by calcite, it was dissolved soon after enclosure (ACP), or later, during non-luminescent calcite precipitation (PER).

The well developed luminescence zonation of ECI replacive calcites questions whether the calcite is replacive, or pore filling (albeit with calcite precipitating only a short distance behind the sulphate dissolution front). Concentric luminescence zonation indicates variation in supply of Fe and/or Mn to growing crystal faces, and that all crystal faces were in contact with the same fluid. Such a widespread fluid communication suggests a relatively open diagenetic system, i.e., replacement did not take place along numerous small, isolated diagenetic fronts. This indicates that either there was a fairly large (microns to tens of microns) porosity along the diagenetic fronts and/or that crystal growth was very slow, thus allowing a full equilibration of diagenetic fronts with the bulk aquifer fluid. A combination of both processes was most likely responsible for the zonation, although the small size of inclusions poses stringent limits (a few microns) on the width of the dissolution - reprecipitation front (Fig. 6.17).

The restriction of most anhydrite relics, and pseudomorphs after anhydrite relics, to the cores of calcite crystals is interpreted in terms of a changing style of calcite precipitation. During initial replacement, the rate of sulphate dissolution was slightly slower than, or comparable to calcite precipitation, whereas beyond the replacive calcite, cement precipitation was much slower than sulphate dissolution (most likely the rate of sulphate dissolution had increased), such that no relics or pseudomorphs were preserved. A similar explanation has been given for analogous textures of euhedral megaquartz within silicified anhydrite nodules (Tucker, 1976; Milliken, 1979; Maliva, 1987). The transition from sulphate calcitization to sulphate dissolution and calcite pore fill cementation may have been due to an influx of strongly sulphate-undersaturated fluids, an increase in oxygenation (terminating bacterial sulphate reduction) or, more likely, a combination of both, with the invasion of the reaction site by sulphate-undersaturated, partly oxygenated meteoric-derived fluids. Apart from increasing the rate of sulphate dissolution, these fluids would also have greatly slowed calcite precipitation by decreasing the rate of bicarbonate input (previously partly derived as a by-product of bacterial sulphate reduction), and so decreasing overall supersaturation with respect to calcite. This is confirmed by the common occurrence of non-luminescent cements, directly overlying the luminescent replacive calcite (Fig. 6.6b). This type of transition suggests a catastrophic increase in oxygenation of the pore waters (Lee and Harwood, 1989), although there was probably a hiatus between precipitation of the two cement generations. Geopetal internal sediments of carbonate previously within the sulphate at the junction of orange- with non-luminescent calcites (Fig. 6.6), confirm that most or all of the sulphate had completely dissolved prior to the resumption of calcite precipitation.

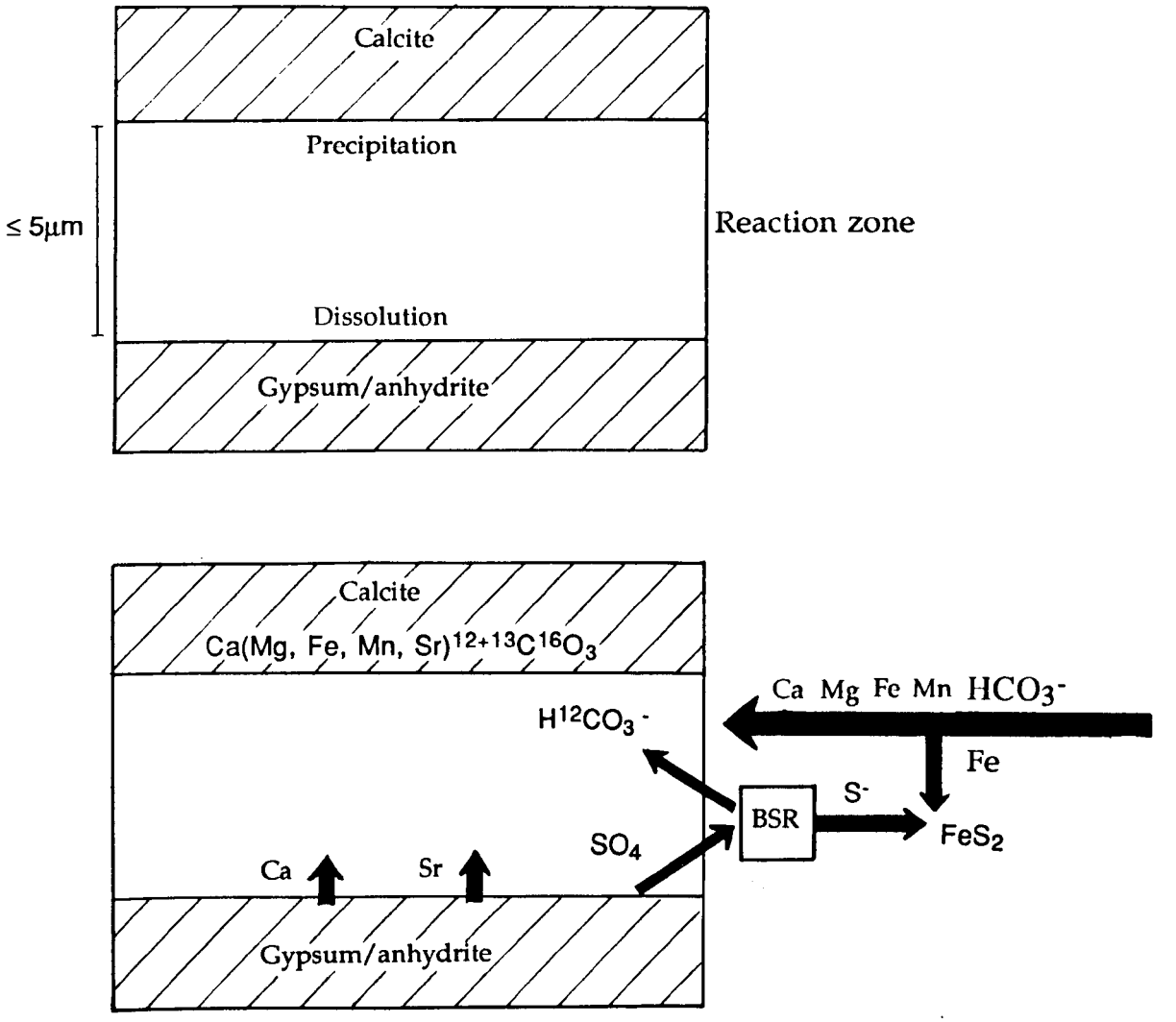

Fig. 6.17 . Schematic representation of ion movement within a reaction zone between dissolving gypsum/anhydrite and precipitating calcite during calcitization. The degree of movement of ions to and from the reaction zone will be a factor of the openness of the diagenetic system, and the concentration gradient of each ion between the reaction zones and proximal aquifer. Ion movement within the reaction zone is by diffusion.

In a GC cavity from Haswell Moor Farm Quarry, the junction of replacive with pore filling calcite is demarcated by a dull orange-luminescent cement zone which overlies the bright orange-luminescent replacive calcite associated with patchy internal sedimentation (Fig. 6.9a & b). The transition from bright orange- to dull orange-luminescent calcite correlates with an increase in Fe (although with little change in Mn [Fig. 6.13]), implying an increase in fluid Eh. This may suggest that bacterial sulphate reduction was active during bright orange-luminescent replacive calcite precipitation (the Fe^{2+} combined with H_2S to form pyrite/marcasite), but ceased abruptly, along with replacement, following input of more oxygenated fluids. In this example there is abundant pyrite/marcasite within the basal bright orange-luminescent replacive calcite (Figs. 6.10a & b), but not above that level. Overlying the dull orange-luminescent cement zone is a sector zoned bright orange-luminescent calcite, suggesting that sulphate reduction may have re-started, although calcite precipitation could no longer match the rate of sulphate dissolution. In a number of cases therefore, the cessation of calcitization was due to an increase in oxygenation of the pore fluids, which terminated or greatly slowed the rate of bacterial sulphate reduction, and increased the rate of sulphate dissolution.

Many type PER, ACP, and GC calcitized sulphates are directly associated with hematite after pyrite/marcasite, or pyrite/marcasite itself. The hematite is interpreted to have formed by oxidation of pyrite/marcasite, which precipitated during bacterial sulphate reduction (6.5.4.1). Accordingly, the associated calcites are bright orange-luminescent, containing Mn but negligible Fe (Figs. 6.9b & 6.13). However, precipitation of metallic sulphides should increase acidity, inhibiting precipitation of replacive/pore filling calcite (6.2.2). The calcites in which pyrite/marcasite do occur have no obvious corrosive textures. One possibility, suggested by Anderson and Garven (1987), is that silicate alteration may consume the acidity produced. The Raisby Formation in general contains very few detrital or authigenic silicates, although quartz and muscovite are fairly common within internal sediments of GC cavities. An alternative explanation is that the acidity is consumed by the replacement of calcite by pyrite/marcasite:

$$Fe^{2+} + 2H_2S + 3CaCO_3 + 2H^+ \rightarrow FeS_2 + 3Ca^{2+} + 3H_2O + 3CO_2$$

However, the magnitude of fall in pH of the diagenetic fluids accompanying metal sulphide precipitation will be proportional to the quantity of pyrite/marcasite precipitated, and the openness of the diagenetic system, i.e., the rate of bulk aquifer advection. In any one thin section, hematite after pyrite/marcasite occupies no more than 10% of the surface area (Fig. 6.10a & b). Also, from luminescence zonation of the replacive calcite, it has been argued that diffusion and advection rates of ions were relatively rapid in relation to calcite precipitation rates. Most iron sulphides are now hematite, and the oxidation reaction is also strongly acid-

producing (6.5.5.1), although again there is no evidence for extensive corrosion associated with this event. Thus, the small amount of iron sulphides precipitated, coupled with open diagenetic systems, strongly limited the build up of an acidic fluid, both during initial sulphide precipitation and oxidation of pyrite/marcasite to hematite.

6.2.3.2. Geochemistry of calcitized evaporites - Interpretation.

Trace element data of the replacive calcites, as with petrography, is suggestive of a relatively open diagenetic system, at least for the precipitation of type ECI and GC calcites. Gypsum and anhydrite contain approximately 1000 to 2000ppm Sr (Dunham, 1966; Ichikuni and Musha, 1978 [taking K^{Sr}_{Gypsum} as 0.21±0.01]), whereas the replacive calcites have approximately 50 to 230ppm Sr. Within an open diagenetic system, where the Sr/Ca ratio of dissolving phase equals the Sr/Ca ratio of the fluid from which the replacive calcite is precipitating (Pingitore, 1982), and given that the molar Sr/Ca ratio of gypsum is 1.56×10^{-3} to 3.10×10^{-3}, with K^{Sr}_{dLMC} of 0.05 to 0.1, the replacive calcite should have a composition of 68 to 271ppm Sr (by using the Homogeneous Distribution Law (3.1.1). This is in good agreement with recorded values, suggesting that most Sr was derived from the former sulphates. However, the presence of appreciable Fe and Mn (of a very low concentration in gypsum), demonstrates at least a limited communication with the bulk aquifer fluids. Thus, by analogy with calcitization of aragonite, there was a good communication between reaction zones and the bulk aquifer, with a relatively low concentration gradient with respect to Sr (i.e., reaction zones and bulk aquifer fluids had similar Sr concentrations), and high concentration gradients with respect to Fe and Mn (the reaction zones were greatly depleted with respect to Fe and Mn relative to the bulk aquifer) (Fig. 6.17).

Indications of the involvement of organic matter in calcitization, comes from two strongly negative carbon isotope analyses (ECI calcitized sulphate from Raisby Quarry). These $\delta^{13}C$ values are similar in magnitude to those quoted by Kirkland and Evans (1976) and Pierre and Rouchy (1988) for calcitized sulphates. If 50% of carbon is considered to have been derived from organic matter ($\delta^{13}C_{(CH_4)}$ -25‰), 30% from host dolostones ($\delta^{13}C$ 5.6‰) and 20% from meteoric waters ($\delta^{13}C$ -12.0‰), the diagenetic calcite would have a $\delta^{13}C$ -13.2‰, in good agreement with recorded values. It is unlikely that sufficient organic matter could have been transported to these reaction sites from the vadose zone by meteoric waters, and so it was most likely methane generated by maturation of Carboniferous Coal Measures. The possible timing of gas generation is not known, but is assumed to have been pre-uplift (pre late Cretaceous/Tertiary). The strongly negative $\delta^{18}O$ values of the replacive calcites are comparable to values for calcitized anhydrite quoted by Harwood and Coleman (1983) from the Cadeby Formation, and are suggestive of considerably elevated temperatures during calcitization. If oxygen from SO_4 is considered to not participate in calcite precipitation (even

if it did, it would be swamped by oxygen from pore fluids owing to open system diagenesis), pore water values of -5.0‰ (SMOW) (reflecting meteoric-derived fluids [6.5.3]) gives a temperature of 55.6°C in the diagenetic site for $\delta^{18}O_{dLMC}$ = -13.1‰ (using palaeotemperature equation in appendix IX). The similarity of the $\delta^{18}O$ values with those of luminescent calcite cements from numerous other localities within the Raisby Formation, including Raisby Quarry (Fig. 6.66), implies that depth of burial was the most important factor contributing to elevated fluid temperatures during calcitization, and input from exothermic bacterial sulphate reduction was of relatively minor importance. These calculated fluid temperatures are well below the upper limit of bacterial sulphate reduction of approximately 85°C (Machel, 1987b).

6.2.4. Calcitized evaporites - Summary and conclusions.

The calcitization of sulphate evaporites within the Raisby Formation is defined by three different petrographic textures:

1. Anhydrite crystal relics, or former anhydrite crystals defined by calcite of different luminescence character to that of the host cement (types PER and ACP),
2. Former anhydrite laths defined by carbonate inclusions within equant calcite crystals (type ECI),
3. Equant calcite partially filling cavities after sulphates which provide evidence for calcite precipitation during sulphate dissolution (type GC).

Typical PER and ECI replacement textures are illustrated in figure 6.18.

The distinction between these types is a function of the relative rates of sulphate dissolution and calcite precipitation, which increases from types PER/ACP through ECI to GC. The differences between types are gradational, and two end members exist of unaltered anhydrite and pore filling calcite within fully open cavities after sulphates. Each type of calcitized evaporite, in turn, also displays an evolution through time from replacive to pore filling calcite precipitation. The luminescence sequences developed within succeeding pore filling cements clearly demonstrate that calcitization took place during uplift of the Raisby Formation under the influence of meteoric-derived groundwaters (Lee and Harwood, 1989) (Table 6.1) (6.5.2.1). The co-existence of precipitating calcite and dissolving sulphate is most likely to occur in the lower parts of meteoric-derived aquifers, where groundwaters are slightly undersaturated with respect to gypsum and saturated or supersaturated with respect to calcite. The precipitation of calcite in conjunction with bacterial sulphate reduction in the distal parts of a groundwater aquifer have been described by Edmunds *et al.*, (1982). Such a distal location would also be in accordance with elevated fluid temperatures. The hydrogeochemical environments of calcitization of evaporites are integrated with those of calcitization of dolomite in 6.4.1.

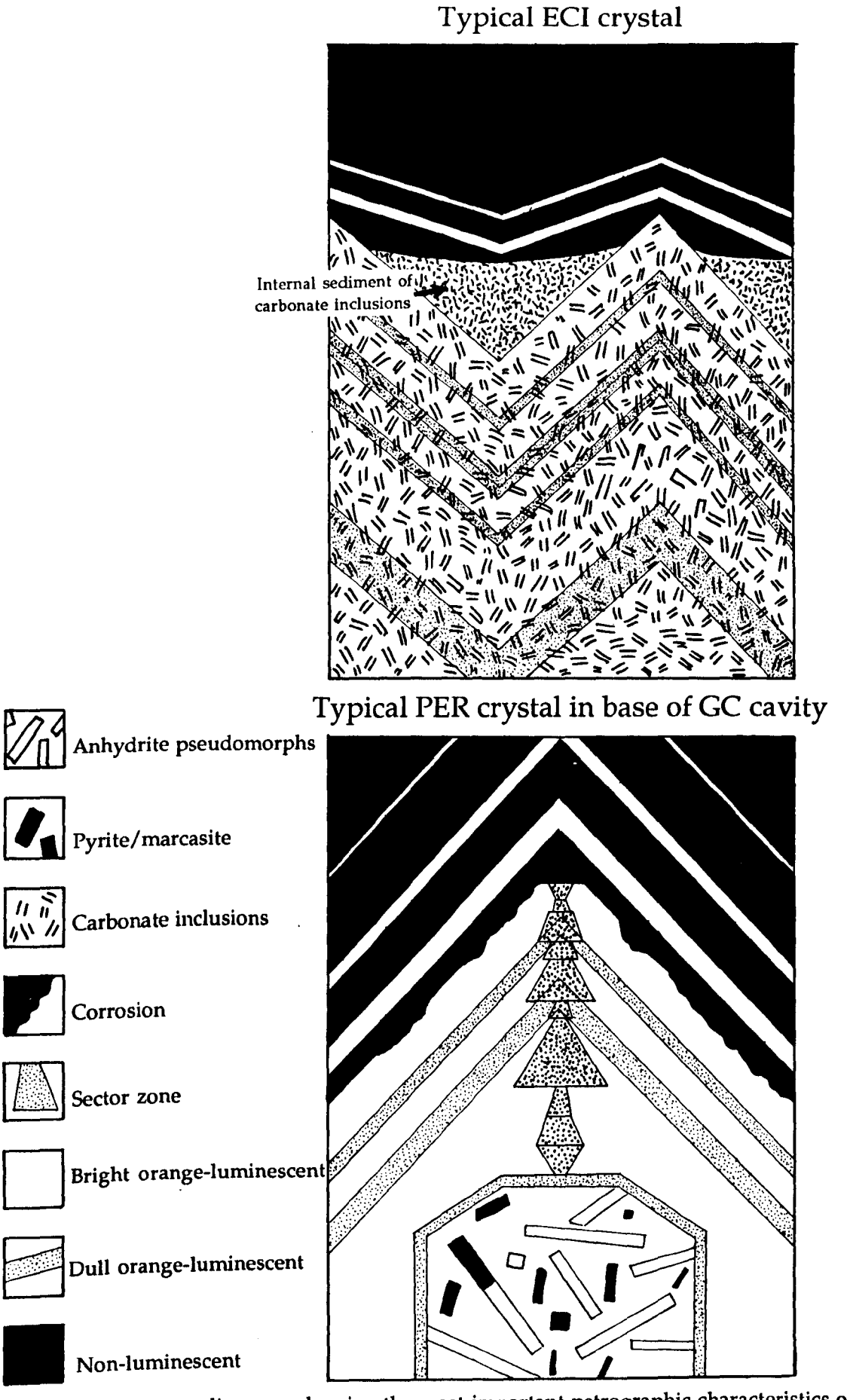

Fig. 6.18. Summary diagrams showing the most important petrographic characteristics of the two most easily recognized types of calcitized evaporites.

Enclosed carbonate inclusions (ECI)		Poikilitically enclosed relics (PER)/ anhydrite cement pseudomorphs (ACP) within geopetal calcite (GC) cavities	Diagenetic processes
Calcite cement Non-luminescent with bright orange hairline subzones Ca (Mg (Mn)) CO3 Internal sedimentation		Calcite cement Non-luminescent with bright orange hairline subzones Ca (Mg (Mn)) CO3 Relic anhydrite dissolution and pore fill cementation (Internal sedimentation)	Influx of oxic meteoric-derived fluids
Hiatus ?		Calcite cement Bright/Dull orange-luminescent Ca (Fe, Mn) CO3 Relic anhydrite dissolution and pore fill cementation	Reduction of meteoric-derived fluids
Replacive calcite Bright/Dull orange-luminescent Ca (Fe, Mn) CO3 Pyrite/Marcasite ?		Replacive calcite Bright orange-luminescent Ca (Mn) CO3 Pyrite & Marcasite	Bacterial sulphate reduction
Anhydrite/Gypsum		Anhydrite/Gypsum	

_ _ _ _ _ _ = Dissolution phase

Table 6.1. Summary of the relationships between calcitization, calcite cementation, and pore fluid evolution for calcitized sulphates within the Raisby Formation.

6.3.1. Calcitization of dolomite - Introduction and definition.

Calcitization of dolomite is the term used in this thesis to describe the simultaneous, or near-simultaneous dissolution of dolomite and precipitation of calcite. It is equivalent to 'dedolomitization' of other authors (e.g., De Groot, 1967), and its usage is analogous to that of calcitization of sulphate evaporites (6.2.1). In common with calcitization of sulphates, a continuum of processes exist:

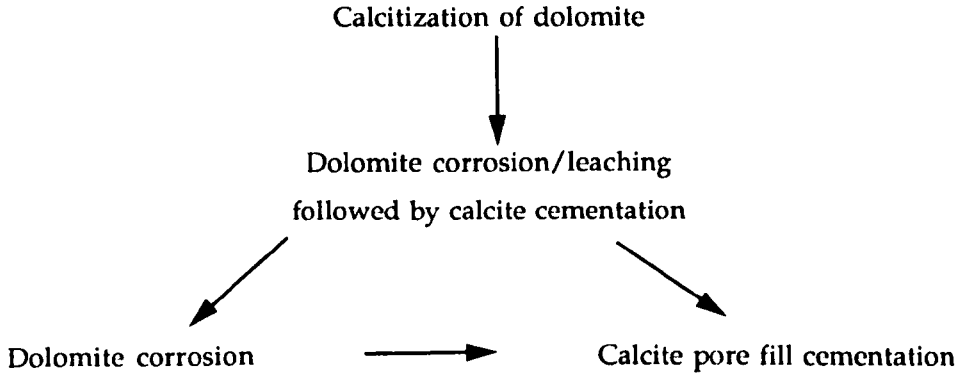

The distinction between dolomite calcitization, and dolomite leaching followed by calcite cementation of the resultant porosity, is essentially one of time, provenance of the diagenetic fluids, and origin of ions within the calcite. With calcitization of dolomite, dolomite dissolution should be nearly simultaneous with calcite precipitation (not necessarily in absolute time, but relative to the speed of associated diagenetic processes such as fluid flow), and achieved by the same fluids, whose composition (and thus the composition of the calcite) is influenced by the dissolving dolomite. If the composition of the diagenetic fluids changes between dolomite dissolution and calcite precipitation, such that no ions derived from dissolving dolomite directly enter the calcite lattice, then the process is not calcitization of dolomite. The proportion of ions incorporated into the calcite derived from the dissolving dolomite during calcitization will, however, be a function of the openness of the diagenetic system.

6.3.2. Recognition of calcitized dolomite.

A wide variety of textures have been suggested as indicative of the calcitization process:

1. Pseudomorphs of dolomite rhombs infilled by finely crystalline to coarsely crystalline calcite, or single calcite crystals (Evamy, 1967; Folkman, 1969; Chafetz, 1972; Longman and Mench, 1978; Hawkins, 1979; Wolfe, 1970; Clark, 1980; Purser, 1985 and Stoessell *et al.*, 1987).
2. Leached dolomite crystal cores (most commonly) and/or one or more zones of dolomite rhombs now filled by calcite (normally in optical continuity) (Evamy, 1963; Katz, 1968;

Longman and Mench, 1978; Wolfe, 1970; Budai *et al.*, 1984; Theriault and Hutcheon, 1987; Lee and Harwood, 1989).

3. Ghost textures indicative of former dolomite crystals (mineral or iron oxide inclusions) enclosed within calcite (Shearman *et al.*, 1961; Folkman, 1969; Chafetz, 1972; Al-Hashimi and Hemingway, 1973; Frank, 1981; Magaritz and Kafri, 1981; Stoessell *et al.*, 1987).

4. Strongly corroded, irregular relics of dolomite, poikilitically enclosed, and sometimes floating within calcite (Shearman *et al.*, 1961; Al-Hashimi and Hemingway, 1973; Longman and Mench, 1978; Clark, 1980; Land and Prezbindowski, 1980; Budai *et al.*, 1984; Stoessell *et al.*, 1987; Lee and Harwood, 1989),

5. The calcitized dolomite has a porous, vuggy appearance in hand specimen, commonly iron stained, and in the field or core passes laterally/horizontally into unaltered dolomite (Folkman, 1969; Magaritz and Kafri, 1981; Purser, 1985; Stoessell *et al.*, 1987; Theriault and Hutcheon, 1987).

It must be noted that, although most fine scale alternations of dolomite and calcite are the result of calcitization, some may be primary, reflecting alternating precipitation of calcite and dolomite from pore fluids of fluctuating composition (e.g., Zenger, 1973).

The consensus is that dolomite rhombs partially or completely filled by calcite, and corroded dolomite relics or other ghost textures poikilitically enclosed within calcite are the most diagnostic petrographic criteria for the identification of calcitization. However, few if any authors distinguish between dolomite corrosion followed by later calcite cementation, and calcitization of dolomite. This is exemplified by Budai *et al.*, (1984) "Regardless of fabric, if it is possible to demonstrate that dolomite dissolved and calcite precipitated in its place, then dedolomitization did occur". In this thesis, clear distinction is drawn between calcitization of dolomite on the basis of the aforementioned petrographic criteria, and dolomite dissolution followed by calcite cementation which previously may have been misidentified as calcitization.

On the basis of petrographic texture, three types of calcitized dolomite have been distinguished within the Raisby Formation (Fig. 6.19):

Type 1. Enclosed Dolomite Relic (EDR) calcitized dolomite.

Highly corroded relics of dolomite crystals poikilitically enclosed within calcite.

Type 2. Crystallographically selective (CS) calcitized dolomite.

Whole dolomite crystals, or certain zones within the crystals, replaced by calcite, normally in optical continuity with the precursor dolomite.

Type 3. Embayed Dolomite (ED) calcitized dolomite.

Dolomite rhombs partially 'eaten' into/embayed by calcite,

This textural-based classification broadly, although not wholly, correlates with different calcitization processes.

Enclosed Dolomite Relic (EDR)

A. Luminescent calcite poikilitically enclosing dolomite relics.
B. Luminescent calcite poikilitically enclosing dolomite relics and iron oxide /hydroxides, with an inclusion-free non-luminescent overgrowth.

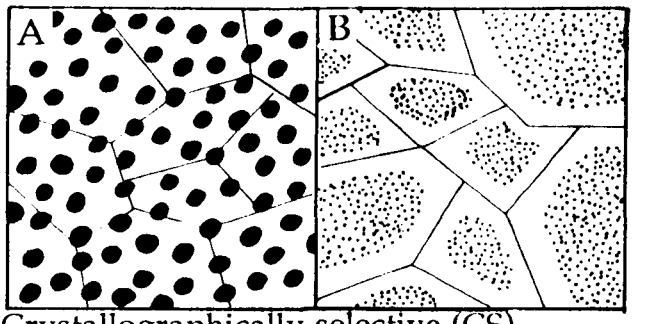

Crystallographically selective (CS)

A. Luminescent calcite poikilitically enclosing zone selective calcitized dolomite
B. Luminescent calcite poikilitically enclosing completely calcitized dolomite

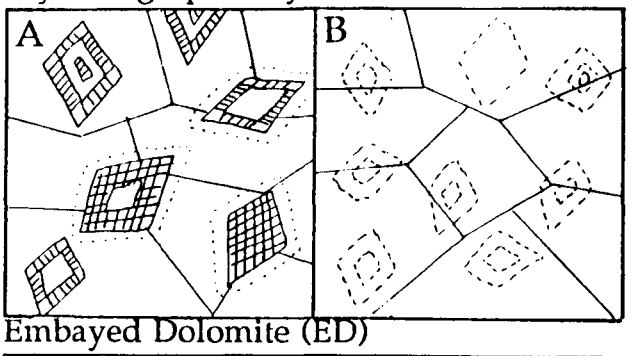

Embayed Dolomite (ED)

Dolomite crystals embayed by calcite

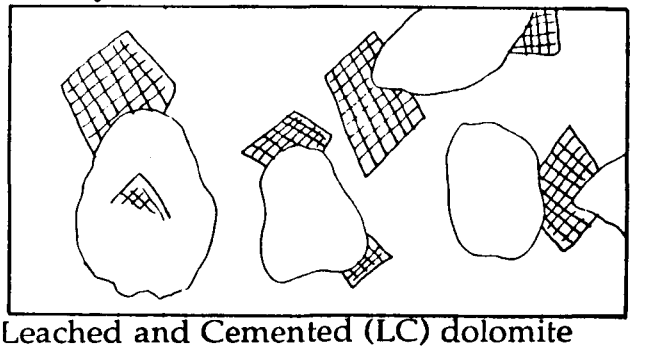

Leached and Cemented (LC) dolomite

A. Hollow dolomite rhombs poikilitically enclosed and cemented by coarse, luminescent/non-luminescent calcite, some with geopetal internal sediments
B. Leached and calcite cemented oolitic dolostones

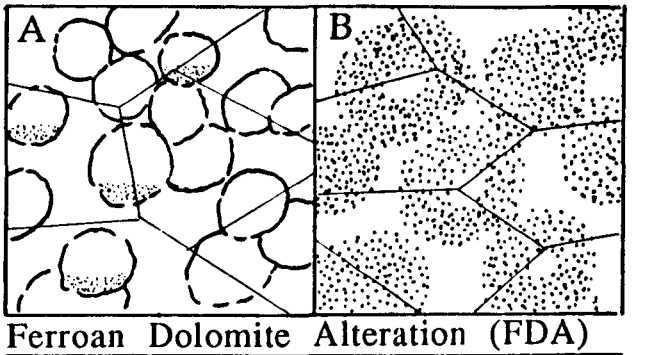

Ferroan Dolomite Alteration (FDA)

Ferroan dolomite alterted internally, with zone and cleavage-parallel aggregates of goethite needles enclosed within calcite cement

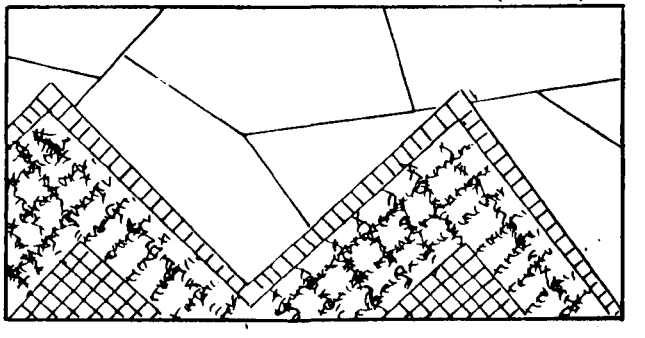

Fig. 6.19. Schematic diagram illustrating the most important petrographic characteristics of the different types of calcitized and altered dolomite recognized in the Raisby Formation.

In addition, two further types of corroded dolomite in association with calcite can be recognized, but which are unlikely to have been the direct result of calcitization:

Type 4. Leached and Cemented (LC) dolomite.

Corroded, commonly hollow-centered dolomite crystals, poikilitically enclosed within much larger coarse, zoned, equant calcites,

Type 5. Ferroan Dolomite Alteration (FDA).

Corroded dolomite crystals, partially filled by calcite which is associated with abundant zone- and cleavage-parallel aggregates of authigenic goethite.

6.3.2.1. Enclosed Dolomite Relic (EDR) calcitized dolomite - Description.

This represents the volumetrically most important style of calcitization within the Raisby Formation. It comprises corroded relics of dolomite crystals poikilitically enclosed within finely crystalline calcite. The size of dolomite relics varies from microns, to an appreciable fraction of the unaltered dolomite crystal (tens of microns). The replacive calcite forms an interlocking mosaic of unzoned equant crystals, from 50 to 200μm in size (Fig. 6.20a & b). Dolomite relics may be restricted to the centres of calcite crystals, or occur throughout. Most EDR examples studied are now composed principally of calcite.

EDR calcitization is extensively developed within second cycle carbonate (Z2) collapse breccias, which have been studied where they overlie the Raisby Formation between Trow Point (NZ 384, 667) and Man Haven (NZ 3461, 6601) South Shields, and at Marsden Bay (NZ 397, 655), South Shields. The calcitized collapse breccias have a characteristic 'light grey' colour (N7), and are almost pure calcite (less than 1.10 mole% $MgCO_3$ [Appendix VII]). The buff-coloured matrix associated with collapse breccias in Marsden Bay is less completely calcitized (Fig. 6.21). Thus, density of relic dolomite correlates to colour. The replacive calcite is finely crystalline (50μm), and dolomite relics occur throughout. Sr values are variable, from 32 to 556 ppm(n=5). One sample analysed for isotopes from the basal collapse breccias directly overlying calcitized uppermost Raisby Formation at Man Haven, gave $\delta^{13}C$ 0.2‰ and $\delta^{18}O$ -6.5‰.

Along the coastal section between Trow Point and Man Haven, the Raisby Formation has also been extensively calcitized, developing EDR textures similar to those of the overlying calcitized Z2 collapse breccias (Fig. 6.20a & b). Some of the apparent alteration is due to blue-grey coloured, geopetal, laminated, internal sediments derived from the collapse breccias infilling fractures/cavities within the uppermost few tens of centimetres of the Raisby Formation. Calcitization of the Raisby Formation itself is, in general, also restricted to its upper few tens of centimetres directly below the Z2 collapse breccias. The Trow Point Bed which locally caps the Raisby Formation along this section has been pervasively calcitized (Smith, 1986), and calcitization is commonly restricted to that bed. Locally, calcitization may extend down to 2m along bedding surfaces within large slumps

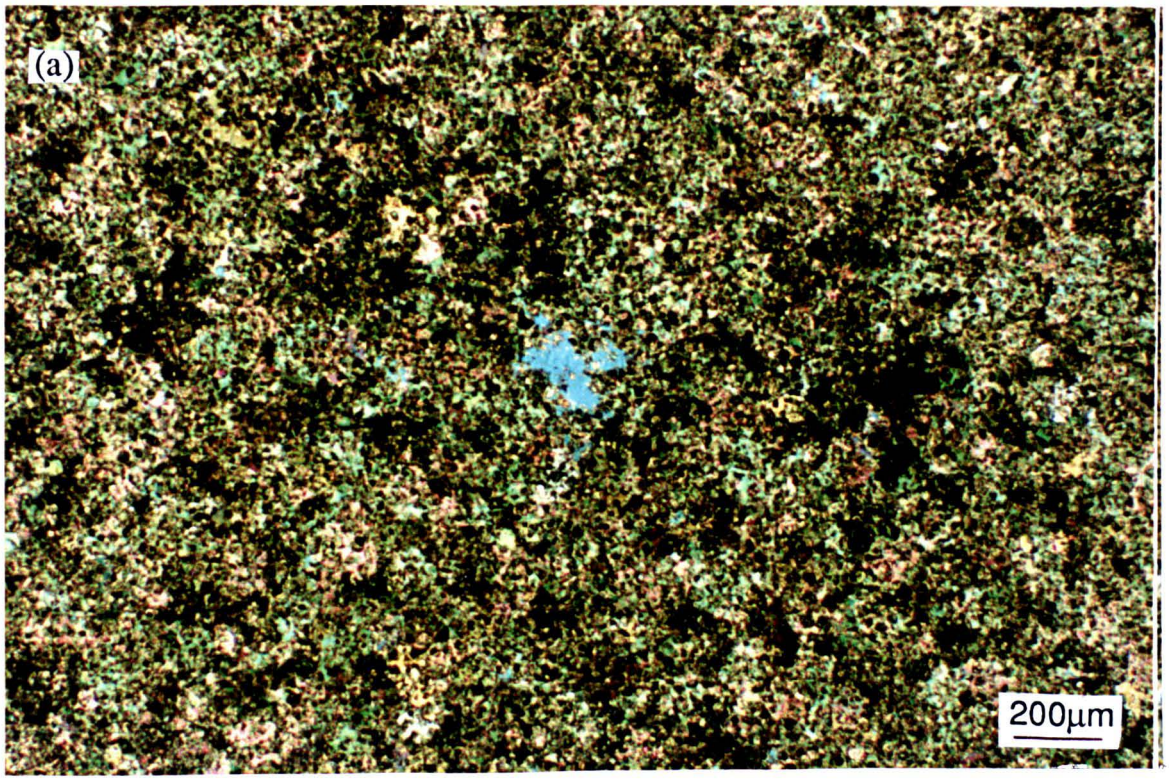

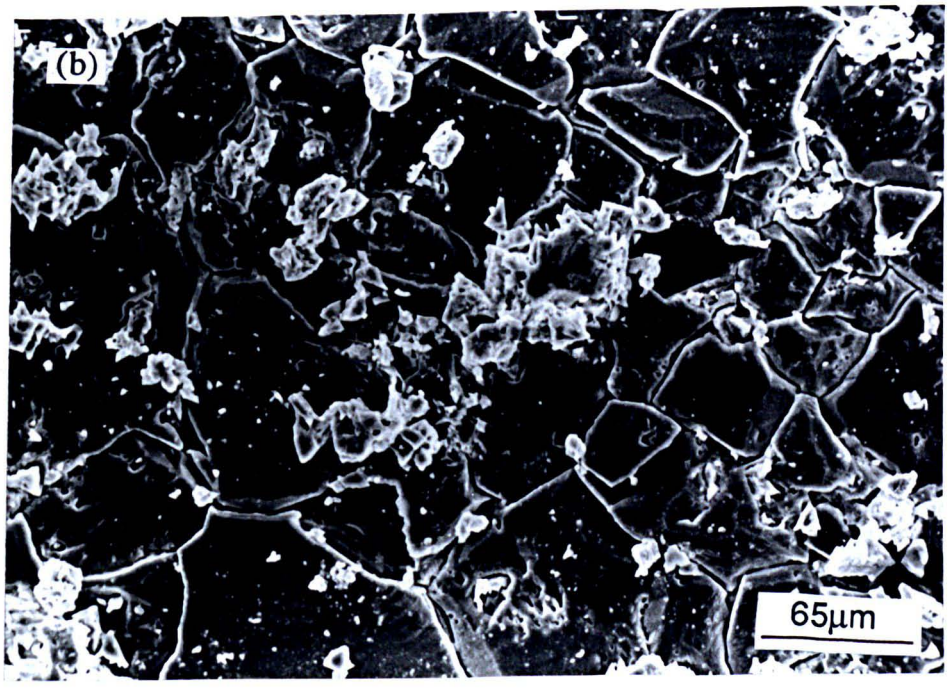

Fig. 6.20. Photomicrographs of EDR calcitized uppermost Raisby Formation dolostones, Trow Point; (a) thin section, crossed polars, (b) etched SEM sample. Both show corroded dolomite relics poikilitically enclosed within anhedral calcite crystals.

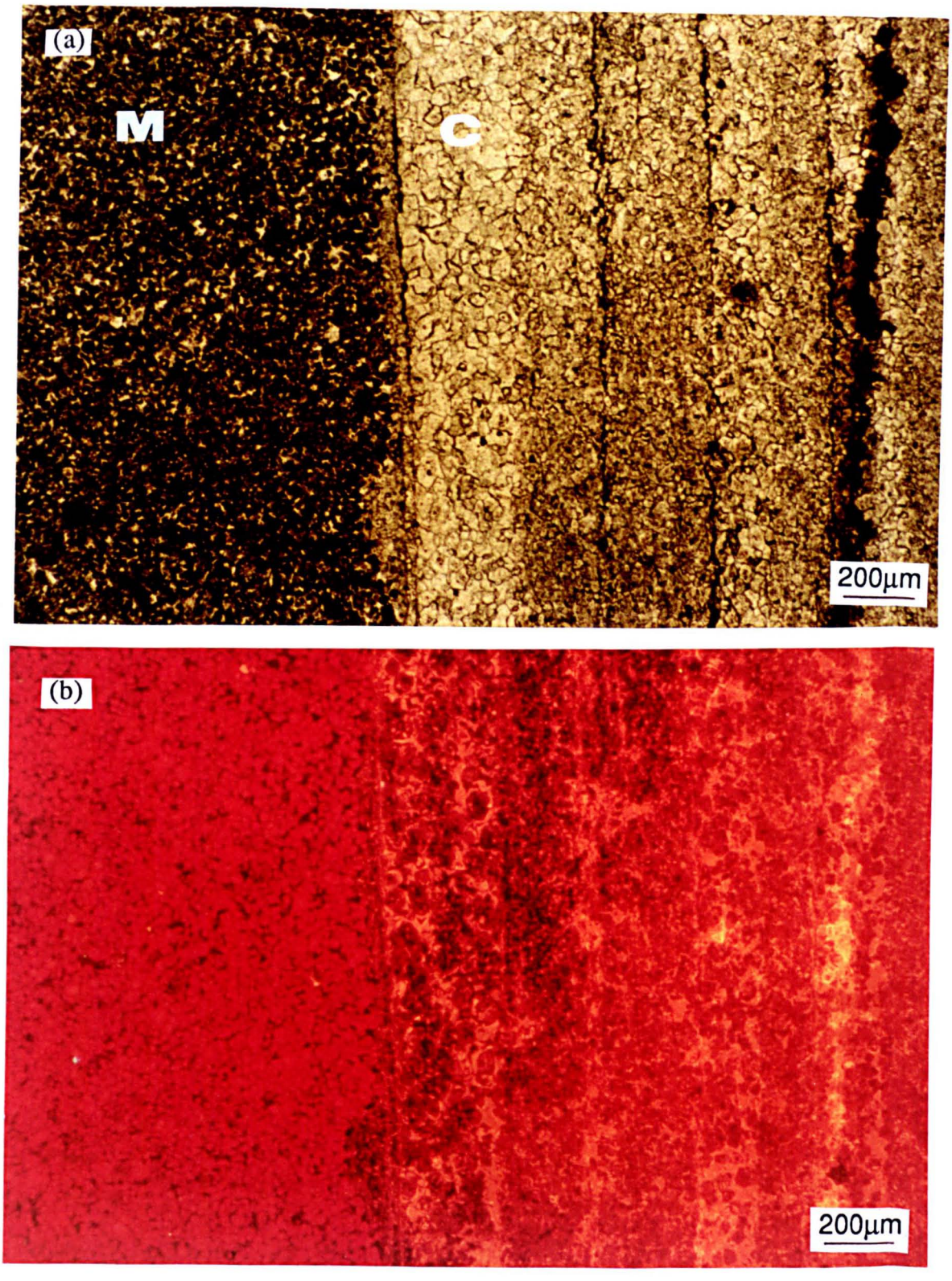

Fig. 6.21. Thin section photomicrographs of part of a clast (C) and enclosing matrix (M) of a Z2 collapse breccia, Marsden Bay; (a) plane light, (b) luminescence. The clast (originally a finely laminated dolostone) has been near-completely calcitized, although the matrix has been much less extensively replaced. Note, the calcite crystals which have replaced the clast are zoned, with a dull orange-luminescent core and bright orange-luminescent outer zone.

underlying resedimented carbonates (Fig. 2.34b). Dolomite rims a few centimetres thick which surround large cavities after sulphates, characteristic of the resedimented uppermost Raisby Formation along this section, have also been calcitized (Fig. 2.33a). In places, calcitization may extend into the well bedded Raisby Formation below the resedimented unit. This is most commonly represented by blue-grey selvages of calcitized dolomite a few centimetres wide along joints and bedding surfaces, especially well developed at Target Rocks (NZ 385, 665). In addition, larger areas, on the scale of whole beds may be calcitized adjacent to the joint and bedding plane selvages. These calcitized dolostones are indistinguishable on the basis of colour from unaltered dolostones, although they are fairly pure calcite.

The intensity of calcitization within the Raisby Formation along the Trow Point to Man Haven section is variable. Calcitized dolomites contain 0.65 - 0.95 mole% $MgCO_3$, 0.21-0.29 mole% $FeCO_3$ and 0.02-0.07 mole% $MnCO_3$, and 137-608ppm Sr (Appendix VII). The replacive calcite is dull orange-luminescent (Fe/Mn ratio = 1.38 to 2.32), although, where it cements fracture porosity, dull orange-luminescent calcite passes into bright orange- followed by non-luminescent cements (Fig. 6.22b). One carbon and oxygen isotope analysis of a sample of calcitized Raisby Formation directly below an isotope sample of the overlying Z2 collapse breccia gave an almost identical result ($\delta^{13}C$ -0.1‰, $\delta^{18}O$ -6.3‰).

EDR textures have been commonly recorded elsewhere within the Raisby Formation, although nowhere as extensively as along the Trow Point to Man Haven section. Calcitized clasts of dolostone breccias from Raisby Quarry have been described by Lee and Harwood (1989). Their petrographic textures are very similar to those described above, with fine dolomite relics poikilitically enclosed within calcite (Fig. 6.23a), although they differ in that the dolomite relics are restricted to the cores of orange-luminescent replacive calcites, and are associated with iron hydroxides such as goethite. Outer parts of the calcite crystals are inclusion-free and zoned non-luminescent with bright orange hairline subzones (Lee and Harwood, 1989, figure 5). Petrographic differences are supported by geochemical variations (Fig. 6.24). This differentiation between replacive core, and pore filling zoned cement overgrowth is very similar to textures of types PER and ECI calcitized sulphates (6.2.3.1). Within calcitized clasts of a compaction breccia overlying a debris flow breccia at Houghton Quarry (2.5.1.2), this differentiation of inclusion-rich core and inclusion-free overgrowth is more clearly developed (Fig. 6.23b). The calcite crystals are an average of 100μm in size. Their inclusion-rich cores are again associated with both dolomite relics (less than 10μm) and iron hydroxides, whereas clear parts of the same crystals have no inclusions apart for very fine layers of dolomite and iron hydroxide internal sediments (Fig. 6.23b). More extensive internal sediments (20-30μm thick) lie between the inclusion-rich cores and inclusion-free overgrowths, occasionally inhibiting growth of the inclusion-free calcite (Fig. 6.23b). Inclusion-free calcite crystals have euhedral faces into the adjacent, still unoccluded,

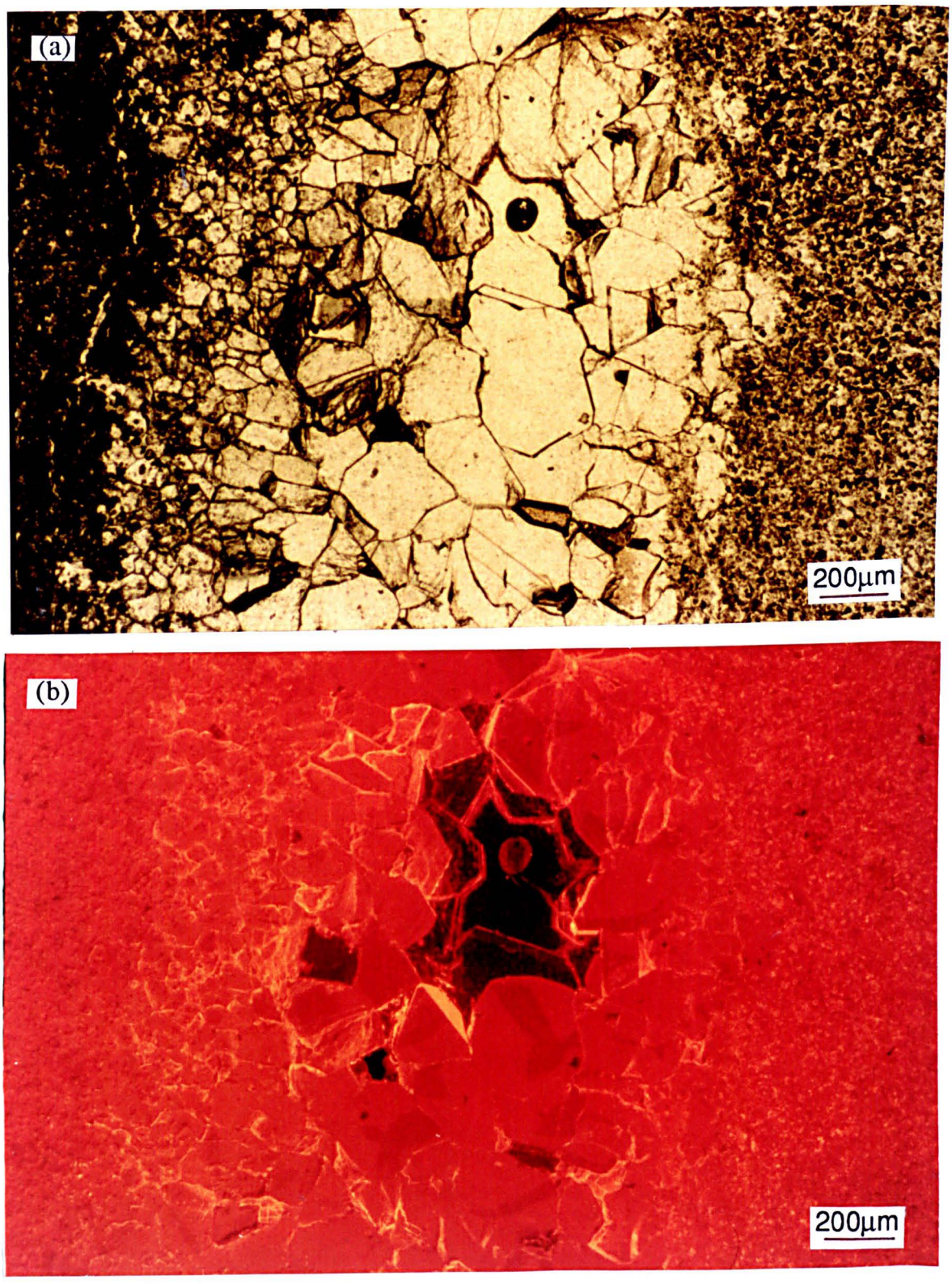

Fig. 6.22. Thin section photomicrographs of the uppermost calcitized Raisby Formation dolostones, Trow Point; (a) plane light, (b) luminescence. A fracture which cuts across the field of view has been cemented by a sequence of dull to bright orange- to non-luminescent calcite cement. The bright orange-luminescent zone is patchy and discontinuous. Some dull orange-luminescent crystals are sector zoned.

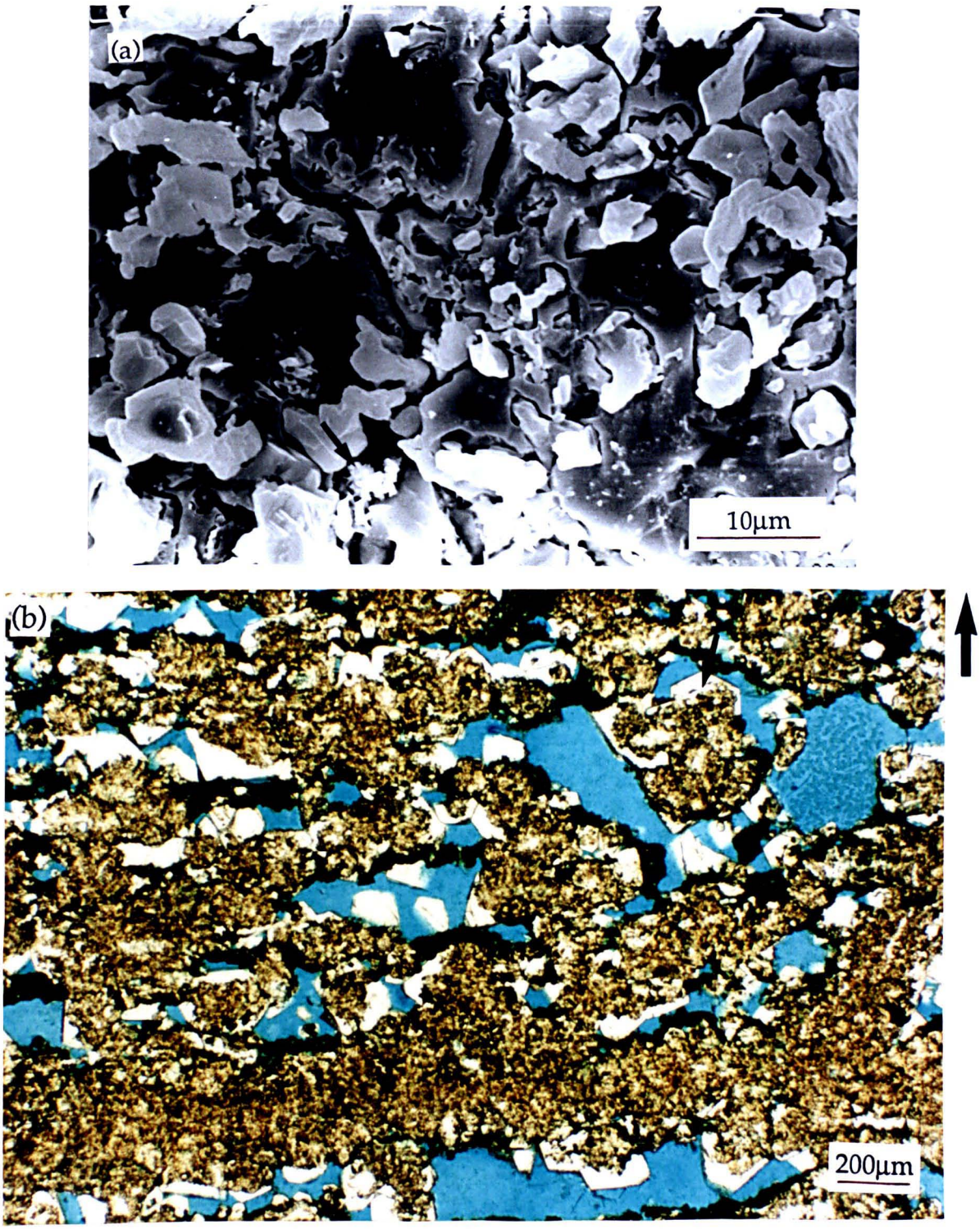

Fig. 6.23. Thin section photomicrographs of EDR textures; (a) etched SEM sample from a dolostone breccia, Raisby Quarry, (b) thin section of the compaction breccia from Houghton Quarry, plane light. Small goethite needle bundles (arrowed) are poikilitically enclosed within calcite together with dolomite (a). Two phases of internal sedimentation are evident in (b), one overlying the inclusion-rich replacive calcite crystals inhibiting growth of the inclusion-free overgrowth, and another within the inclusion-free calcite overgrowth (arrowed). Arrow indicates way up.

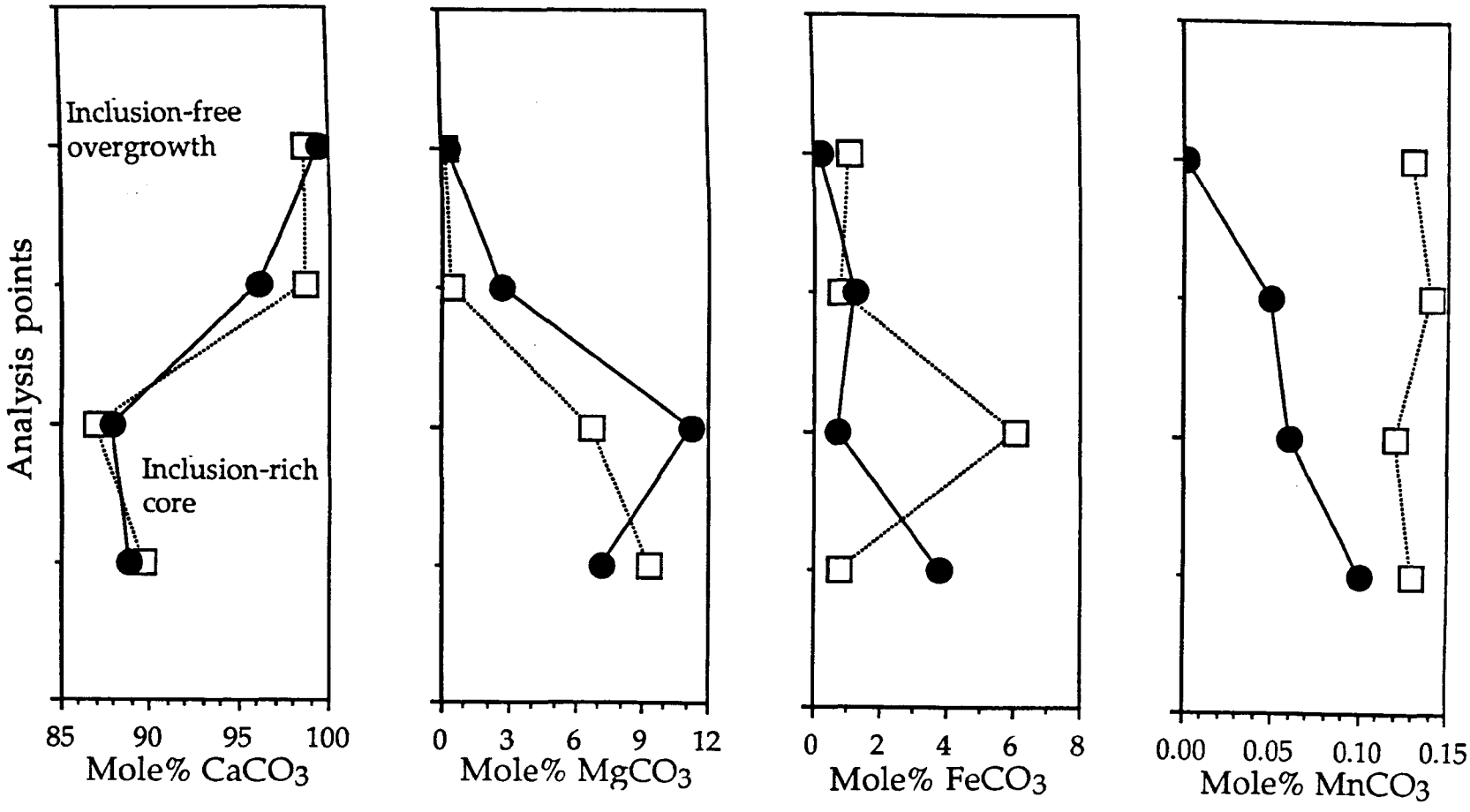

Fig. 6.24 . Graphs illustrating the geochemical variation in two microprobe traverses from the inclusion-rich core to the inclusion-free overgrowth of replacive calcite crystals within a calcitized clast of a dolostone breccia, Raisby Quarry. The inclusion-rich core is shown in fig. 6.26a.

porosity. All of the calcite is non-luminescent apart for a few bright orange-luminescent hairline subzones within the inclusion rich, replacive core.

Most other occurrences of EDR textures are small-scale and closely associated with cavities after sulphates. One sample from close to the top of the Raisby Formation at Raisby Quarry had calcitized dolomite and calcitized evaporite (type PER) within the same thin section, apparently related to the same generation of replacive calcite (Fig. 6.25). Coarse, barite-mineralized dolostone breccias from Running Waters Quarry have also been pervasively calcitized and are associated with abundant cavities and euhedral pseudomorphs after sulphates. The calcitization of dolomite is one part of a very complex diagenetic history (7.1.1.5). Calcitization postdates evaporite dissolution although predates barite mineralization (Fig. 7.5a). Samples from this quarry have slightly different textures, with the replacive calcite (dull to bright orange-luminescent) slightly more coarsely crystalline (100-200μm), and relic dolomite crystals better preserved (Fig. 6.26a), calcitization being preferential along zones and cleavages (Figs. 6.26a & b).

6.3.2.2. Crystallographically selective (CS) calcitized dolomite - Description.

This type is volumetrically much less important than EDR. It is characterized by partially to completely replaced dolomite rhombs, poikilitically enclosed within coarsely crystalline luminescent calcite cement, which occludes adjacent pores. Two end members may be distinguished:

CSa (zone-selective replacement). Calcitization selective to specific zones within dolomite crystals, most commonly the outermost zone and/or the core.

CSb (whole crystal replacement). Calcitization of the entire dolomite rhomb by part of a single calcite crystal.

A gradation exits between these two end members. With increasing intensity of replacement, CSa (zone-selective) passes into CSb (whole crystal) (Fig. 6.27). Distinction of the partially/completely replaced dolomite over host calcite is made on the basis of contrasting calcite luminescence characteristics and/or the presence of fine inclusions.

Zone-selective replacement (CSa) is best developed around the margins of calcite-filled cavities and fractures within coarse dolostone breccias at Raisby Quarry (Lee and Harwood, 1989, fig. 7). Here, the replaced zones (30μm wide) of euhedral dolomite rhombs (planar-P dolomite texture) luminesce brighter orange than the enclosing calcite (Lee and Harwood, 1989 fig. 7). Fine dolomite relics and iron oxide/hydroxides also demarcate the former outer margin of the replaced zone. The intensity of replacement varies from only the outermost zone of the dolomite crystal (most common) to near-complete calcitization, with every stage between (Fig. 6.27). The calcitized portions of the dolostone clasts are associated with high concentrations of euhedral hematite crystals after pyrite/marcasite. ICP analysis confirms that these areas are considerably more iron-rich than the host dolostone (Fig. 6.28),

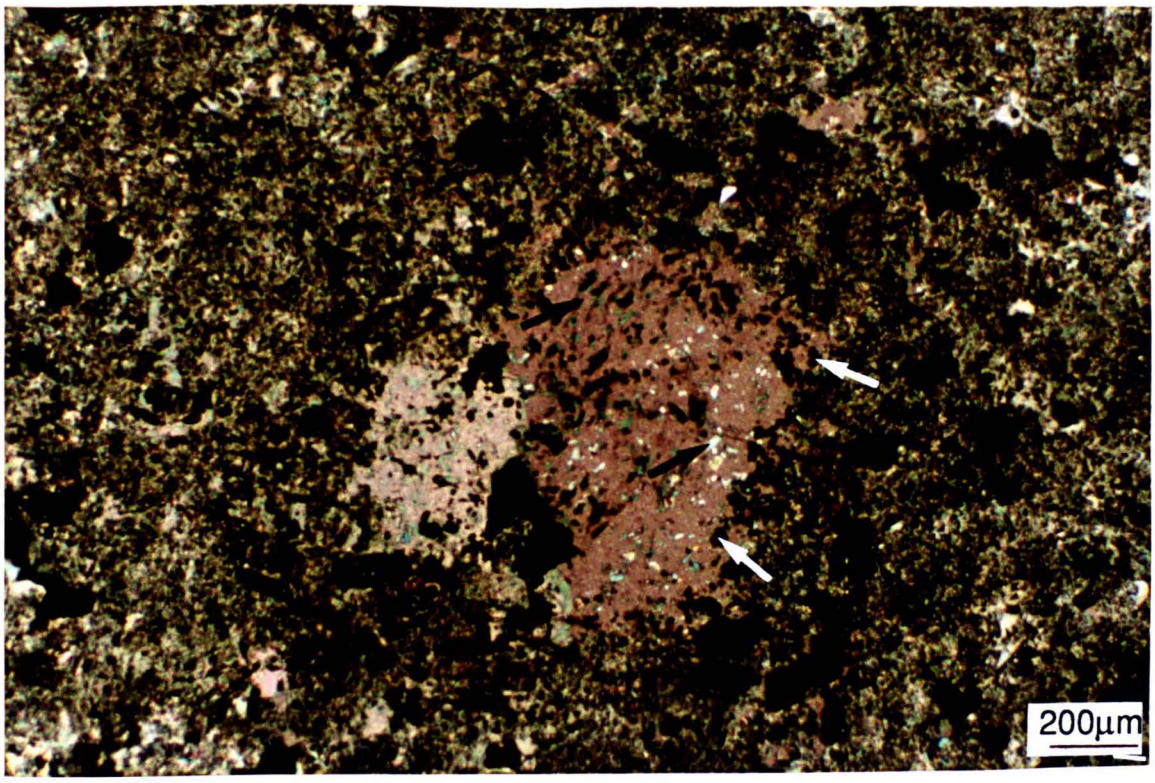

Fig. 6.25. Photomicrograph, crossed polars, of intimately associated PER calcitized evaporite and EDR calcitized dolomite, Raisby Quarry. Relic anhydrite crystals (black arrows) occur within replacive calcite, forming a decussate texture. Around the margins of the calcitized evaporite is hematite after pyrite/marcasite (white arrows). The surrounding calcitized dolomite comprises irregular dolomite relics, poikilitically enclosed within calcite.

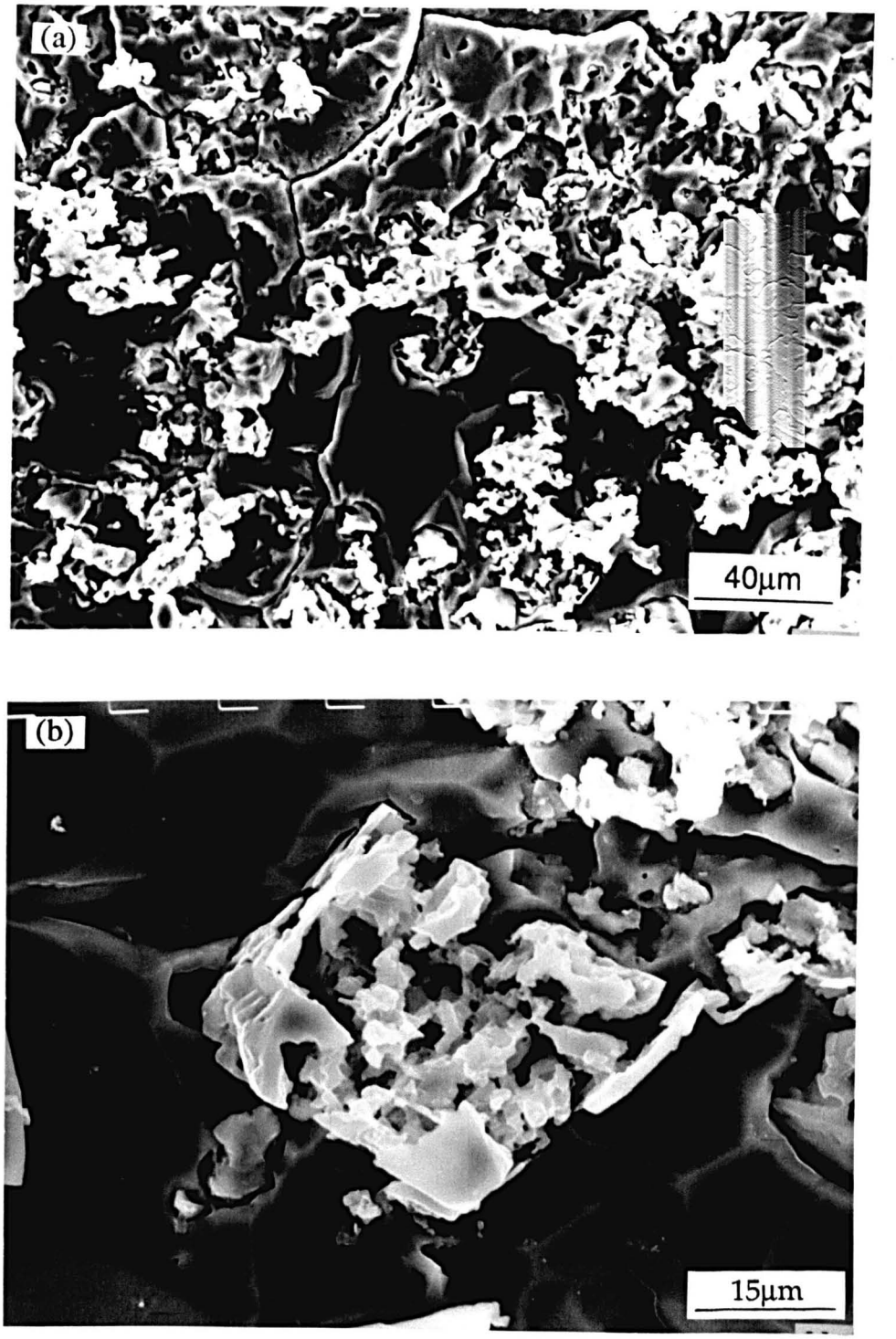

Fig. 6.26 . SEM photomicrographs of two etched EDR calcitized, and barite mineralized samples from Running Waters Quarry. In detail (b), replacement by calcite has concentrated along lines of weakness (zone and cleavage traces) within the dolomite.

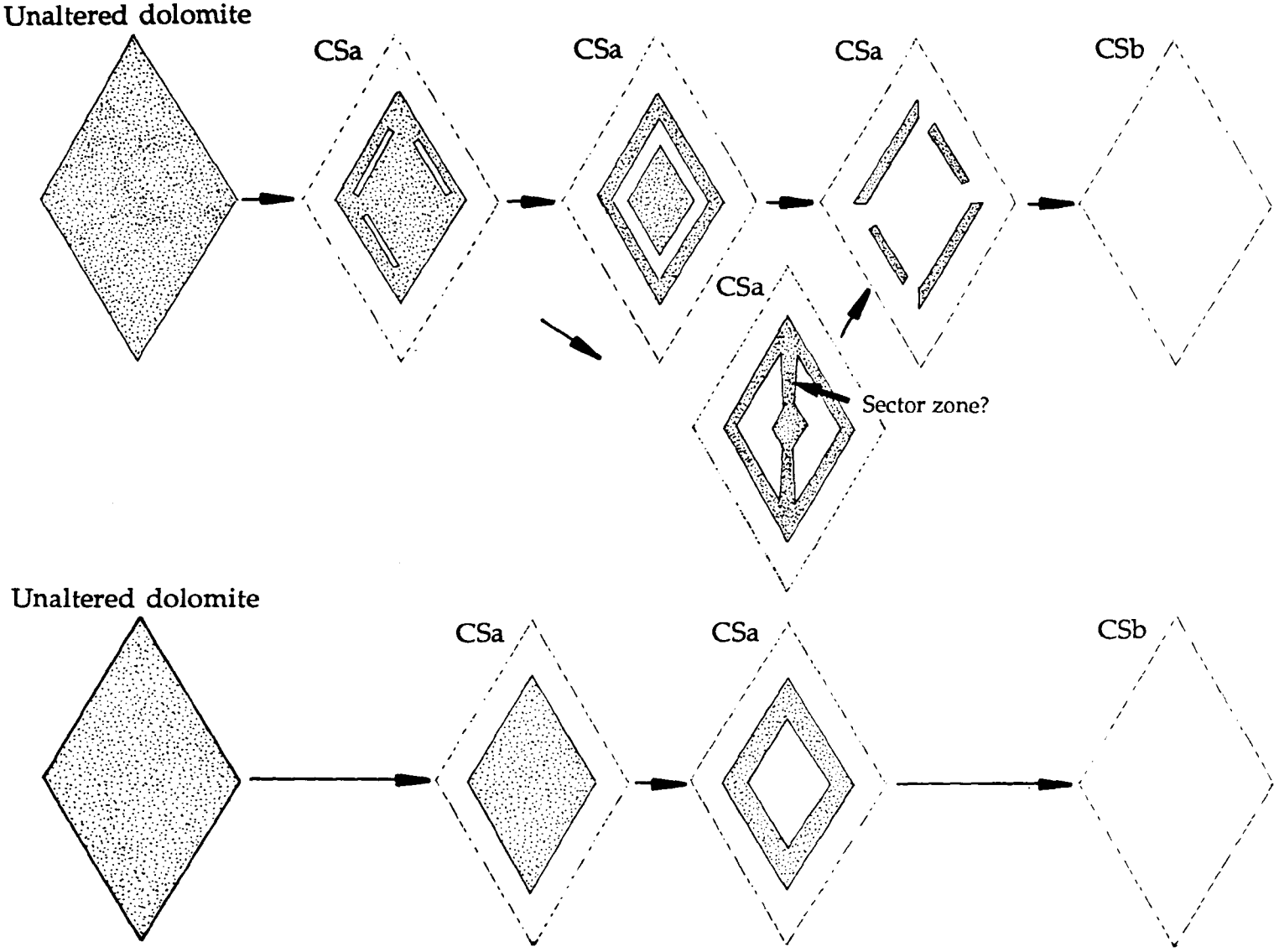

Fig. 6.27 . Schematic diagrams illustrating the variation in intensity of crystallographically-selective calcitization, and progression from zone-selective (CSa) to whole crystal (CSb) calcitization. The diagrams are based on a number of thin sections.

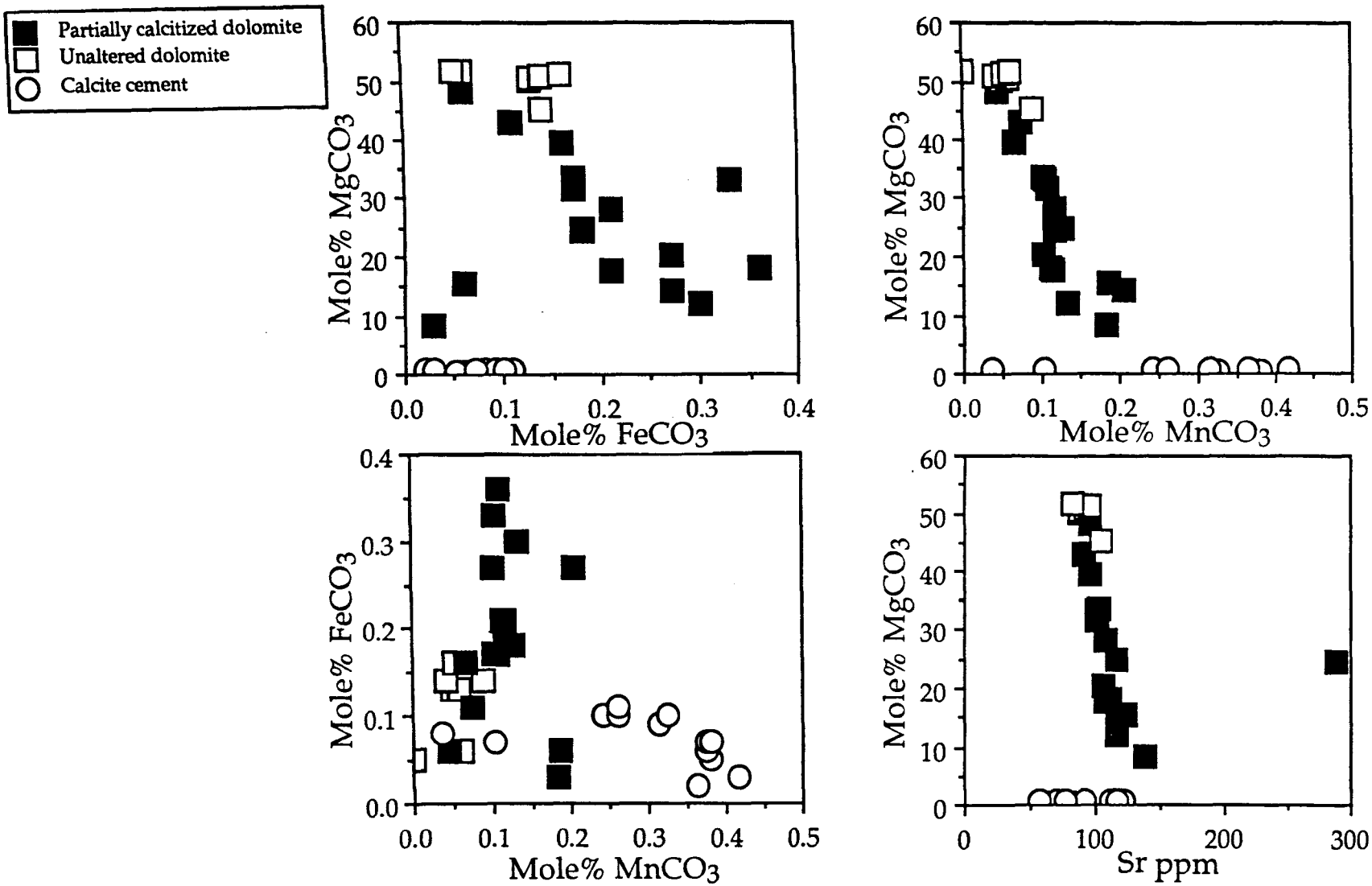

Fig. 6.28 . Graphs illustrating the geochemical variation along a traverse from unaltered dolomite, into partially zone-selective calcitized dolomite and host calcite cement. Sample from a dolostone breccia, Raisby Quarry, analysed by ICP. Note, the calcitized areas have much higher concentrations of iron than the unaltered dolomite.

although Mn and Sr are relatively invariant between the area of replacement and dolostone host (Fig. 6.28). Calcite cements adjacent to replaced dolomite are also associated with pseudomorphs after late diagenetic anhydrite (calcitized evaporite type ACP) (Lee and Harwood, 1989 fig. 7).

In most other examples of the CSa zone-selective replacement texture, calcitization was restricted to the outermost zone of dolomite crystals in contact with calcite which cements the adjacent pore. In these cases, zone-selective calcitization was mainly identified from concentrations of iron oxide/hydroxides or pyrite/marcasite at the contact of the former outer dolomite zone with calcite cement (Fig. 6.29a).

Whole crystal replacement (CSb) was only identified by luminescence contrasts with enclosing calcite cements. In common with zone-selective calcitization textures from Raisby Quarry, the replacive calcite is often brighter orange-luminescent than the enclosing calcite. In all examples where the whole crystal replacive texture has been identified, the dolomite pseudomorphs are within formerly unstable, now-calcitized minerals (e.g., evaporite minerals and former HMC marine cements [Fig. 3.4b]).

6.3.2.3. Embayed dolomite (ED) calcitized dolomite - Description.

This is a heterogeneous grouping of samples from a variety of diagenetic environments. This type is characterized by a partial, generally non zone-selective replacement, whereby dolomite crystals are 'embayed' by calcite. Three different occurrences have been recorded:

A. Neomorphic calcite microspar partially replacing dolomite within partially dolomitized limestones from Houghton and Raisby Quarries. The dolomite has been marginally replaced where in contact with host microspars (Figs. 4.4a & 4.5). At Houghton Quarry, the replacive microspar is in optical continuity with relic dolomite (Fig. 4.5), although no such relationship could be determined from Raisby Quarry. This replacive texture is restricted to partially dolomitized limestones.

B. A buff-coloured ('pale yellowish orange [10 YR 8/6]) calcitic lithology from borehole W8. This lithology passes sharply into dolomite both at its upper and lower margins (Appendix XII). It comprises lozenge- or 'batten'-shaped calcite crystals, 10μm in size, which have grown at the expense of dolomite. A few remaining relic dolomite crystals are strongly embayed by the calcite (Fig. 6.29b). This lithology is homogeneous dull orange-luminescent, and fairly pure calcite (1.62-4.79 mole% $MgCO_3$) with 266 to 276ppm Sr, and 2 isotope analyses gave $\delta^{13}C$ 5.0‰ and 5.5‰, $\delta^{18}O$ -4.4‰ and -4.5‰, very similar to Raisby Formation dolostones. This lithology has been strongly replaced by sulphates, now gypsum hydrating from anhydrite. The replacive calcite has itself been partially replaced by later, stylolite-fed dolomite (Pervasive Pressure Solution [PPS] dolomite [5.2.2]).

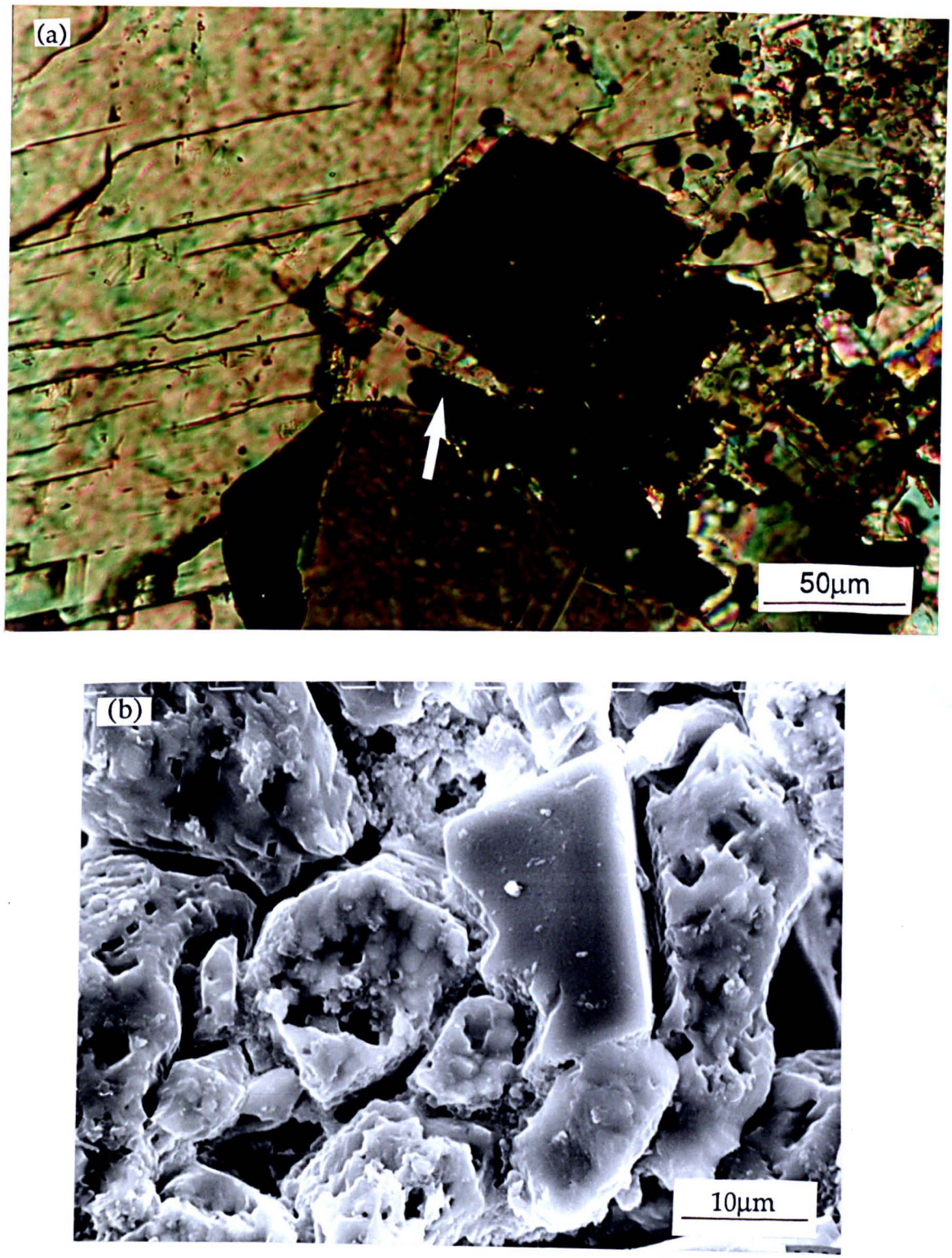

Fig. 6.29 . Photomicrographs of (a) a thin section of CSa, zone-selective calcitization, North Sands borehole, 274.30m (thin section, crossed polars) and (b) an etched SEM sample of embayed dolomite from W8 borehole. The outer margin of the replaced dolomite zone in (a) is encrusted by pyrite (arrowed).

C. Partially-calcitized coarsely crystalline ferroan dolomite in association with calcite concretions, Raisby Quarry (4.4.1.3). This dolomite is partially replaced by zoned dull to bright orange-luminescent, scalenohedral calcite. The calcite may abut dolomite with no replacement, or may embay the dolomite in an irregular manner, finally leading to relics of dolomite poikilitically enclosed and floating within calcite. The contacts between calcite and dolomite may be smooth surfaces, or cleavage-controlled (Fig. 4.35a).

6.3.2.4. Leached and Cemented (LC) dolostones - Description.

Corroded dolomite crystals poikilitically enclosed within coarse, equant, zoned calcites (LC textures) are a very common textural relationship between dolomite and calcite cement within the Raisby Formation. Textures similar to these have previously been attributed to calcitization by various authors, although it is considered unlikely in these Raisby Formation examples. This texture occurs on two scales:

LCa (hollow dolomite).

Heavily-corroded, hollow-centered dolomite crystals marginal to calcite lined/filled cavities after sulphates. Dolomite is enclosed within the basal parts of coarse pore filling calcite cements. The texture extends for hundreds of microns to millimetres into the host dolomite.

LCb. (leached dolostones).

Extensively-leached dolostones cemented by calcite. Large areas of rock are affected, from square centimetres, to bedded former dolostones of metres in thickness. Not necessarily associated with cavities after sulphates.

The most distinctive texture, type LCa (hollow dolomite) comprises formerly hollow-centred, 50-200μm, anhedral dolomite crystals now enclosed within large (greater than 300μm) calcite cements (Fig. 6.30a & b). One calcite crystal may enclose and infill numerous hollow centered dolomites (Fig. 6.30b). The leached anhedral crystals may, however, remain unoccluded by calcite. Very fine geopetal internal sediments of insoluble material formerly within the inclusion rich core of the dolomite, are present within some calcite cemented relic dolomite crystals. In one small replacive evaporite-dissolution collapse breccia from the uppermost part of Raisby Quarry, whole centimetre-sized dolomite clasts have had the centres of component dolomite crystals leached. Only the margins of clasts are cemented by coarse non-luminescent calcite, and the cement crystals present euhedral faces into the adjacent complex of unoccluded pores. Unaltered dolomite crystals in the centre of the clasts have inclusion-rich cores. Within a sandstone from Tynemouth Castle Cliff, the same hollow-centred dolomite texture is developed. Porosity is unoccluded, or filled by non-luminescent calcite. Dissolution was selective to the innermost inclusion-rich, bright orange luminescent dolomite zone (Fig. 5.7b). The outermost, inclusion-free narrow bright orange-luminescent zone is rarely altered (Fig. 5.7b).

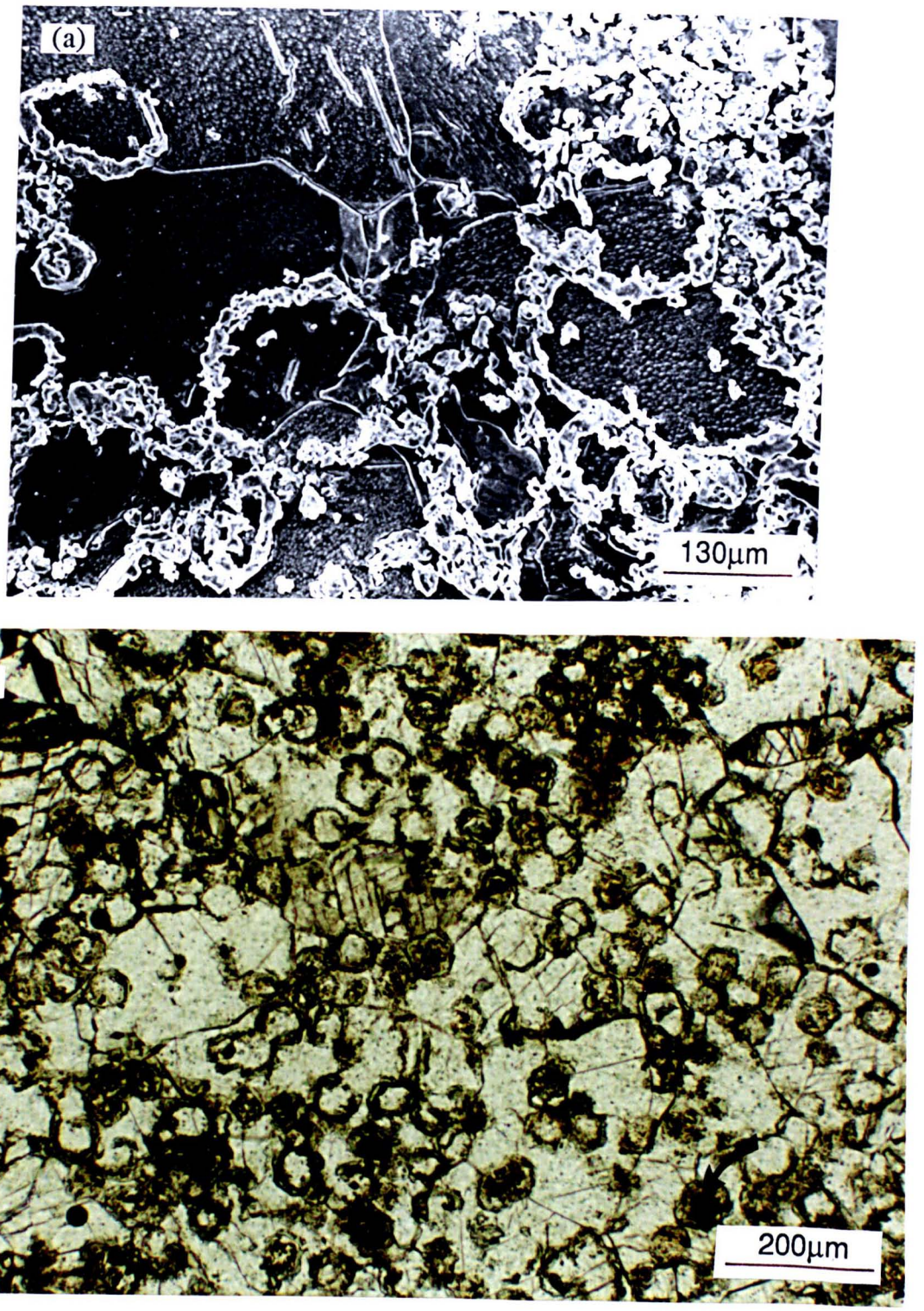

Fig. 6.30. Photomicrographs of leached and cemented dolomite textures marginal to calcite cemented cavities after sulphates; (a) an etched SEM sample from Raisby Quarry, (b) a thin section from Man Haven, plane light. In (b) some isolated, but internally unaltered dolomite crystals remain, which have inclusion-rich cores (arrowed).

The petrographic relationship between calcite and dolomite is very similar between LCa (hollow dolomite) and LCb (leached dolostone), although the hollow dolomite is rarely developed in LCb, possibly due to smaller dolomite crystal sizes. Cementation of large areas of former dolostone by zoned, luminescent calcite was only observed where the rock was originally coarse grained (i.e., oolitic or skeletal). Fig. 6.31 illustrates an originally bryozoan-rich dolostone, in which the matrix-replacive dolomite has been extensively leached, and poikilitically enclosed within coarsely crystalline bright/dull orange-luminescent zoned calcite. In contrast, the mimicly-dolomitized bryozoan fragments have been unaltered, although their original intraskeletal pores have been regenerated (Fig. 6.31). Within Raisby Quarry, oolitic grainstones of the basal Ford Formation have been pervasively leached and calcite cemented (Fig. 6.32), although are apparently unaltered in hand specimen. Corroded relics of dolomite crystals are poikilitically enclosed by zoned calcite (Fig. 6.32). The original ooids and some of their internal structure may be regenerated by dissolution and calcite cementation. The leached areas locally extend through the total thickness of Ford Formation (approximately 2m) at this locality.

6.3.2.5. Ferroan Dolomite Alteration (FDA) textures - Description.

This style of alteration has only been recorded from two localities within the formation (Raisby Quarry [NZ 338, 354 - 352, 352] and Thickley Quarry [NZ 2408, 2564]), although present in several different places at these localities. It is characterized by the precipitation of authigenic iron hydroxides, commonly goethite (Fig. 6.33a) as linear accumulations of needle-bundles accompanying extensive corrosion and calcite cementation of the dolomite crystal. Development of the texture is variable, from precipitation of iron hydroxides along etched zone and cleavage traces within otherwise unaltered dolomite crystals (Fig. 6.33b), to extensive growth of iron hydroxides and calcite precipitation within the interior of leached dolomite rhombs (Figs. 6.34 & 6.35). The alteration is always associated with pores, either still open (Fig. 6.33b) or now calcite cemented (Fig. 6.34). Alteration is also specific to ferroan dolomite (Raisby [Fig. 6.33b] = 7.3 mole% $FeCO_3$; Thickley [Fig. 6.34] = 2.6 mole% $FeCO_3$) and will selectively not affect less-ferroan dolomite within otherwise ferroan crystals (Fig. 6.33b).

At Thickley Quarry, alteration of the host dolomite is in a halo, a few centimetres wide, surrounding a calcite-filled cavity after sulphate (Fig. 7.11a). Coarsely crystalline calcite which occludes the cavity is bright orange-luminescent (with non-luminescent calcite-cemented fractures) (Fig. 6.34b), whereas that occluding porosity within altered dolomite is non-luminescent with bright orange hairline subzones (Fig. 6.34b), and in optical continuity with the relic dolomite. Isotopic analysis of the enclosing luminescent calcite gave $\delta^{13}C$ 0.6‰ and $\delta^{18}O$ -13.1‰.

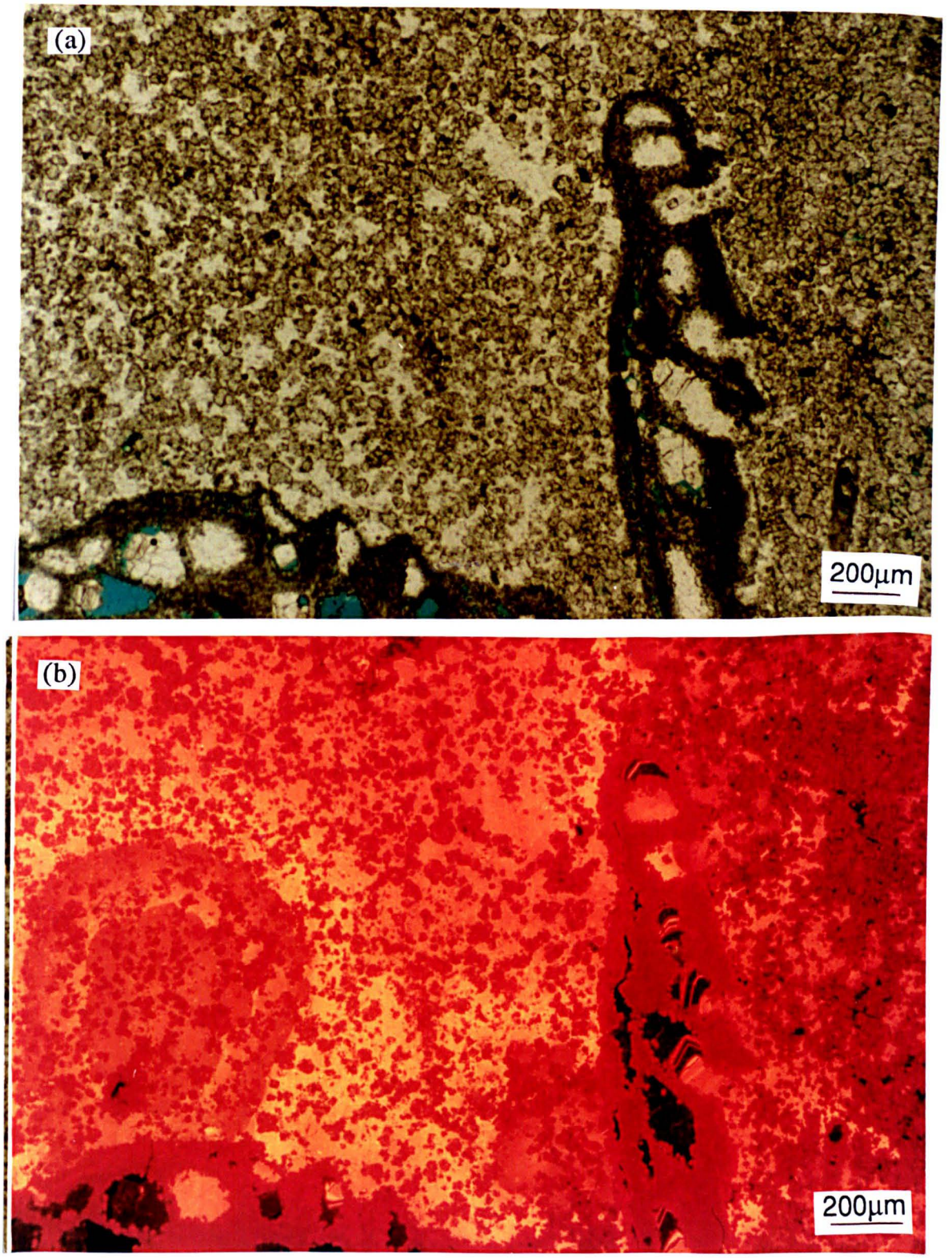

Fig. 6.31. Thin section photomicrographs of a leached and cemented bryozoan-rich dolostone, Quarrington Quarry; (a) plane light, (b) luminescence. The mimic dolomitized bryozoan fronds have been selectively preserved over the coarser, matrix-replacive dolomite, although original intra-skeletal pores within the bryozoa have been regenerated by dissolution and later calcite cementation. Note the cement evolution from dull to bright orange- to non-luminescence.

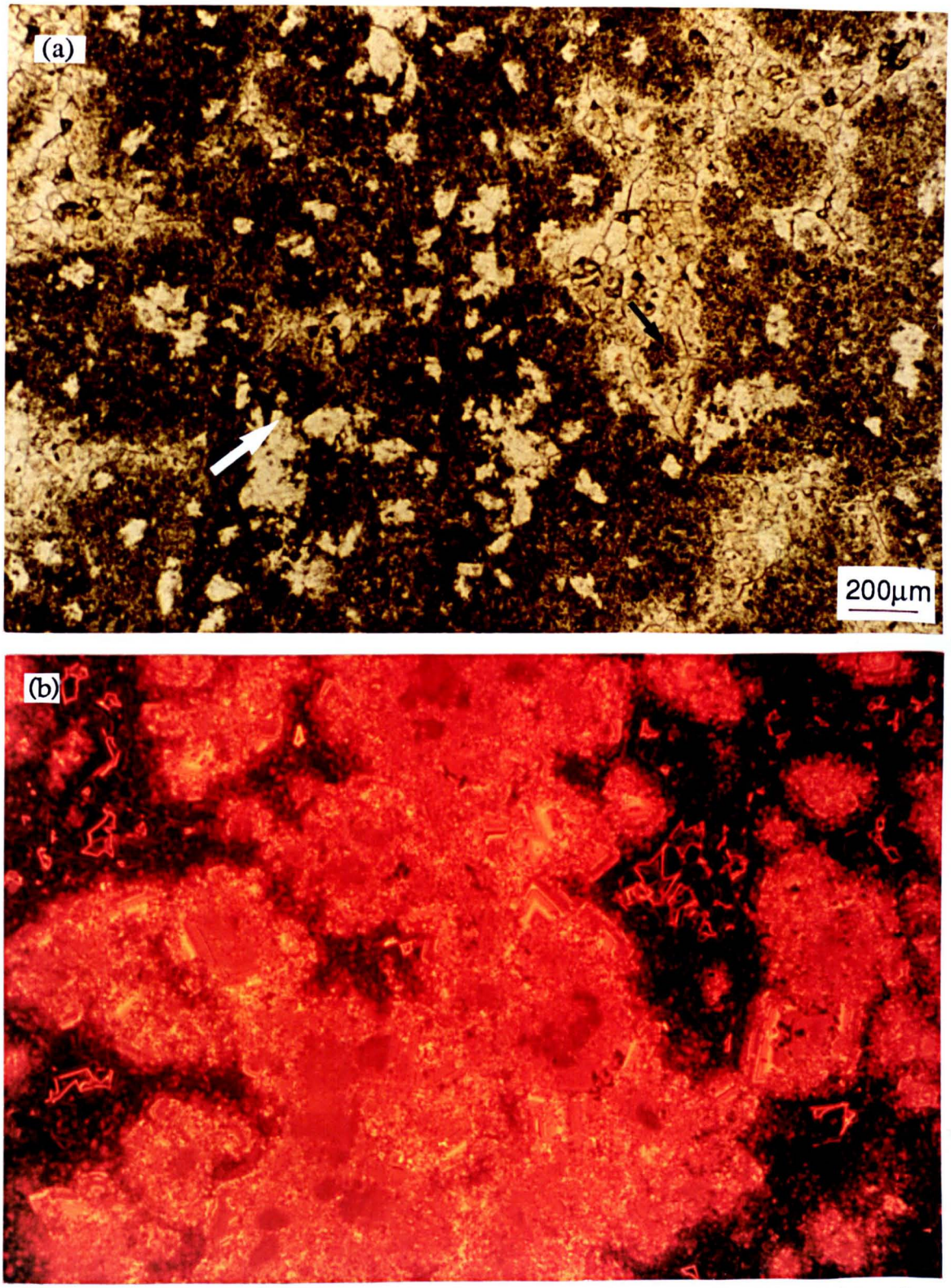

Fig. 6.32. Thin section photomicrographs of a leached and cemented ooid grainstone from the basal Ford Formation, Raisby Quarry; (a) plane light, (b) luminescence. Numerous fine, corroded dolomite relics have been enclosed within the zoned calcite cement.

The cores of most ooids have been replaced by anhydrite, now calcite cemented pseudomorphs (white arrow). Note, many calcite crystals have dolomite inclusions concentrated in their cores (black arrow), suggestive of a change in the style of calcite cementation, possibly demarcated by a phase of dissolution.

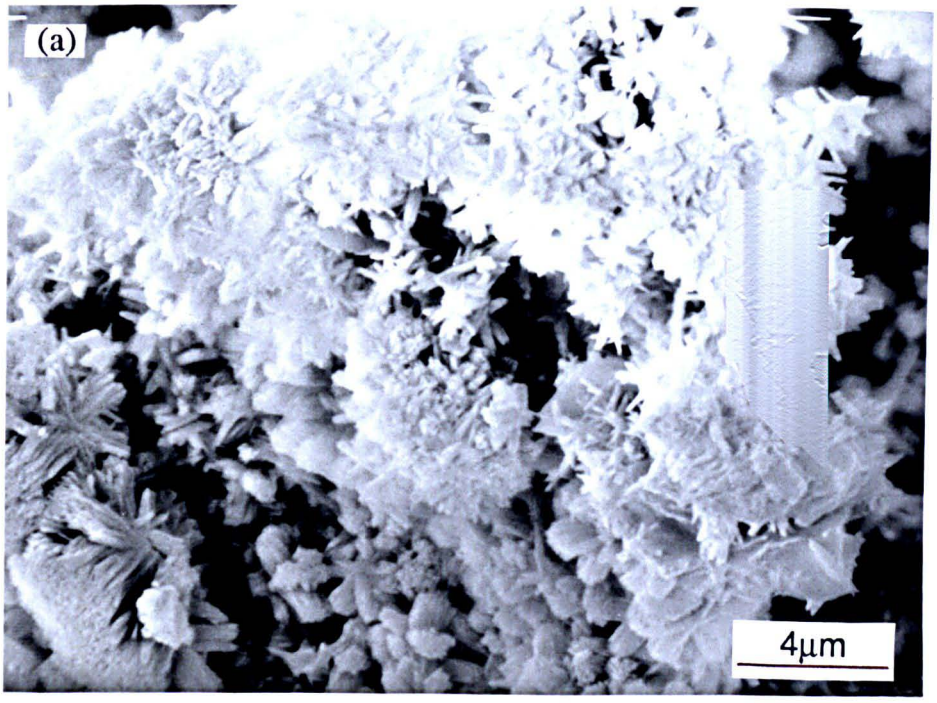

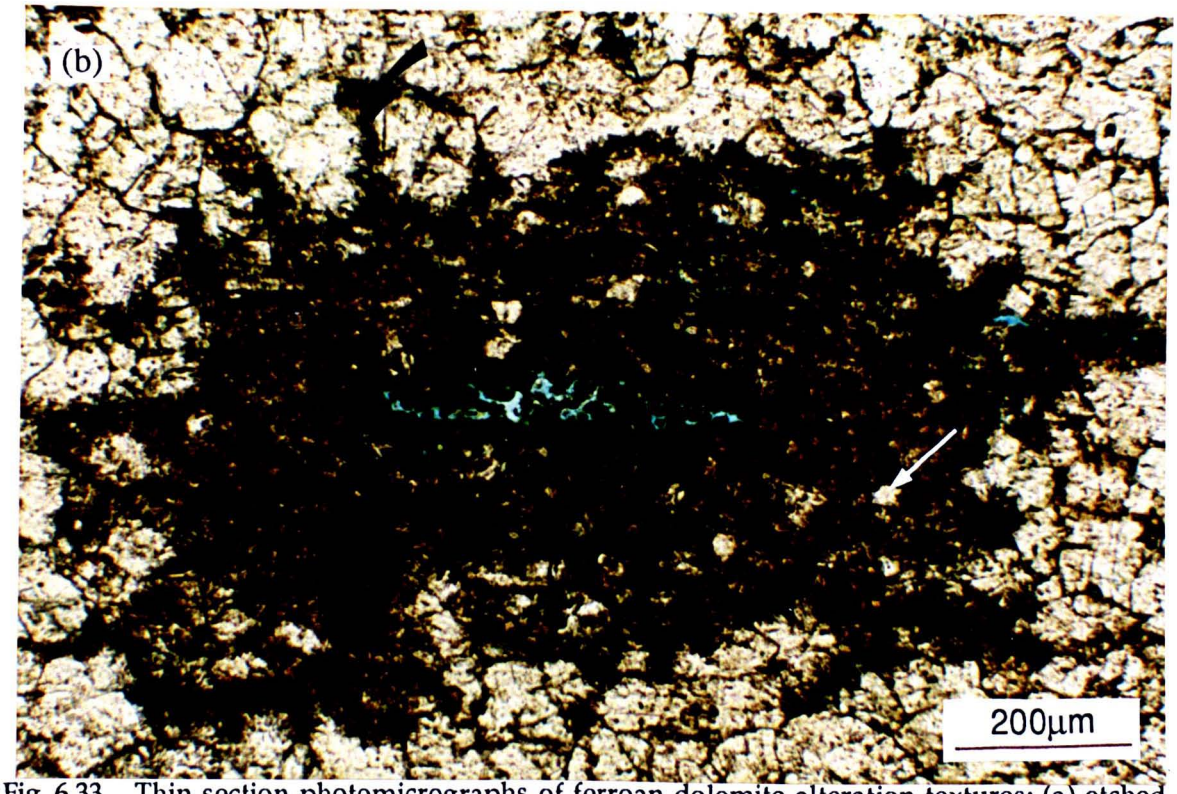

Fig. 6.33. Thin section photomicrographs of ferroan dolomite alteration textures; (a) etched SEM sample, (b) thin section, plane light. Bundles of goethite needles within leached ferroan dolostones marginal to a calcite-filled cavity after sulphate, Thickley Quarry (a), are characteristic of FDA textures. (b) shows alteration of ferroan dolomite marginal to a pore produced by the leaching of an inclusion of organic matter adjacent to an LC calcite concretion, Raisby Quarry. The alteration has progressed from intercrystalline boundaries, working inwards (black arrow). Less ferroan cores of the dolomite crystals (white arrow) remain unaltered.

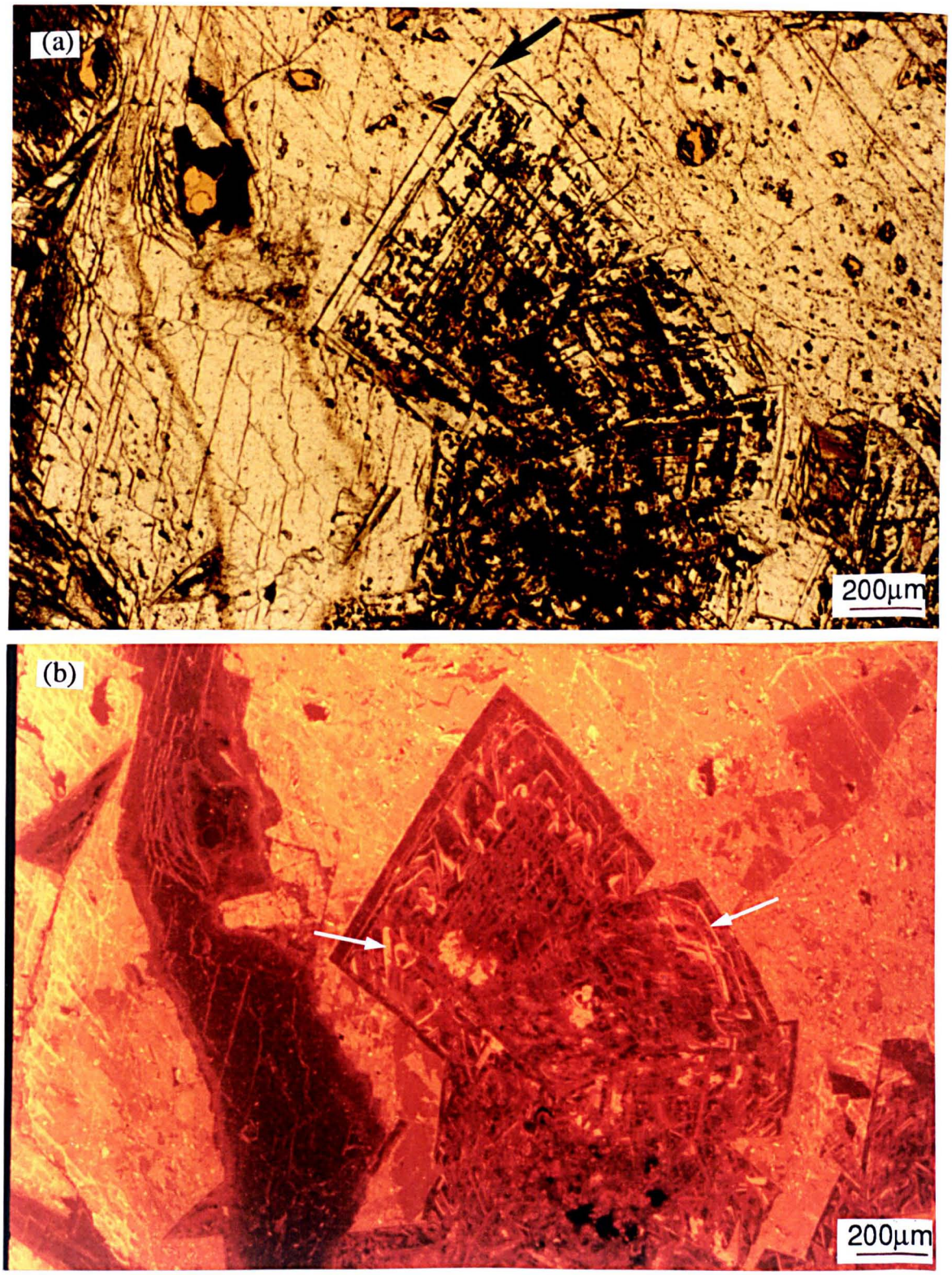

Fig. 6.34 . Thin section photomicrographs of altered pore-lining saddle dolomite, Thickley Quarry; (a) plane light, (b) luminescence. The outer zone of the dolomite rhomb (black arrow) is unaltered, although its inner parts have been completely leached, with goethite precipitating along zone and cleavage traces. The zoned calcite cement which occludes dissolution porosity (b) shows an approximate relation to the crystallographic structure of the former dolomite in some parts, but not in others (white arrows).

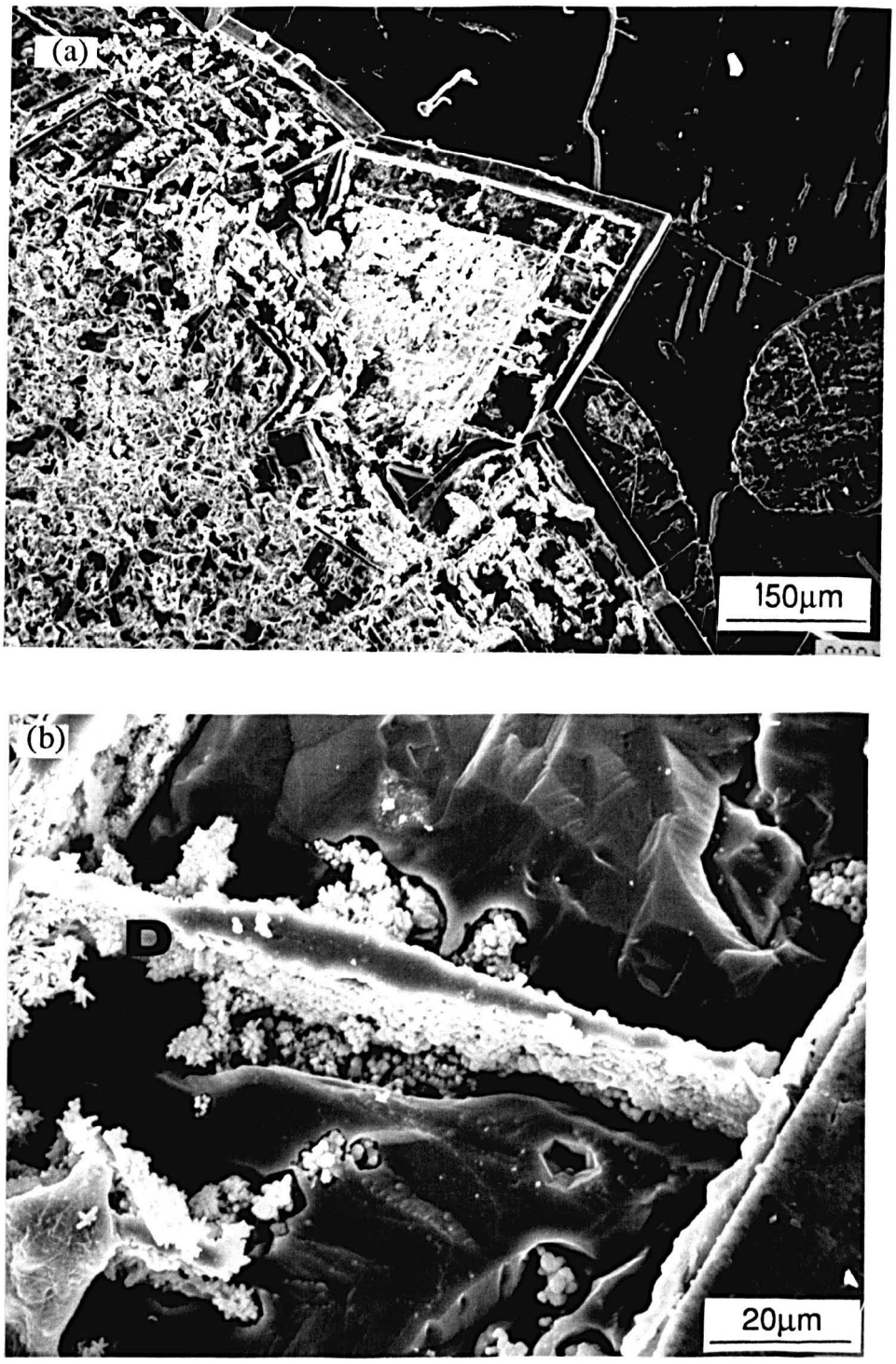

Fig. 6.35 . SEM photomicrographs of an etched sample of pore lining saddle dolomite, Thickley Quarry. Detail of the zone and cleavage-parallel aggregates of goethite (b) shows that goethite bundles encrust an upstanding ridge of dolomite (D).

6.3.3. Calcitization of dolomite - Chemical considerations.

Most authors call upon one or more of four processes to explain calcitization of dolomite:

1. The action of calcium sulphate-rich fluids derived from the dissolution of gypsum (Sorby (1856 (in: Woolacott, 1919b); Von Morlot, 1847; Woolacott, 1919b; De Groot, 1967; Goldberg, 1967; Folkman, 1969; Wolfe, 1970), burial dewatering of sulphate evaporites (Clark, 1980), or pyrite oxidation (Evamy, 1963; Folkman, 1969).
2. The natural instability of calcian dolomite (Katz, 1968) or ferroan dolomite (Katz, 1971; Chafetz, 1972; Al-Hashimi and Hemingway, 1973; Frank, 1981).
3. The action of fluids charged with CO_2 derived from the decomposition of organic matter during burial (Clark, 1980).
4. The action of Ca-rich meteoric groundwaters (± high Ca/Mg ratio) (Kastner, 1982; Budai *et al.*, 1984). These may be produced in early diagenetic mixed meteoric-marine water systems (Magaritz and Kafri, 1981) or ancient/present-day meteoric aquifers (Evamy, 1967; Abbott, 1974; Longman and Mench, 1978; Land and Prezbiowski, 1981; Edmunds *et al.*, 1982; Back *et al.*, 1983; Bath *et al.*, 1987; Theriault and Hutcheon, 1987; Holail *et al.*, 1988; Lee and Harwood, 1989).

Calcitization is essentially the incongruent dissolution of dolomite. In its simplest form, the reaction is expressed thus:

$$CaMg(CO_3)_2 \rightarrow CaCO_3 + Mg^{2+} + CO_3^{2-}$$

Dolomite breaks down to produce calcite, magnesium, and a carbonate anion. In a closed system, this reaction will lead to a net volume loss of 42.6%, although in an open system with respect to Ca and CO_3, volume-for-volume replacement occurs. Most calcitization is volume-for-volume (i.e., more calcite is precipitated than is liberated by dissolution). The drive for this reaction (dolomite is a relatively stable mineral under natural conditions) is commonly achieved by fluids which are simultaneously undersaturated with respect to dolomite and saturated or, more likely, supersaturated, with respect to calcite. Replacement is at least partly driven by the input of Ca^{2+} and CO_3^{2-} into the diagenetic fluids from the dissolving dolomite, which further supersaturates the fluids with respect to calcite. However, the importance of dolomite-derived Ca and CO_3 is dependant on the relative rates of dolomite dissolution and calcite precipitation, and openness of the diagenetic system. Dolomite will dissolve congruently however, if the diagenetic fluids are undersaturated with respect to both calcite and dolomite:

$$CaMg(CO_3)_2 \rightarrow Ca^{2+} + Mg^{2+} + 2CO_3^{-}$$

For incongruent dissolution to progress, Mg must be exported from the reaction site in order to maintain undersaturation with respect to dolomite. This necessitates that the diagenetic system is relatively open with respect to Mg (De Groot, 1967), as well as Ca and CO_3. The increase in concentration of Mg in diagenetic fluids is commonly used as a progress variable to identify calcitization of dolomite within modern aquifers (Land and Prezbindowski, 1981; Back *et al.*, 1983). The replacement reaction itself is considered to be by dissolution-reprecipitation, with exchange of ions through a narrow solution film (Stoessell *et al.*, 1987) (Fig. 6.36). De Groot (1967) suggests necessary factors for calcitization include a low PCO_2 (less than 0.5 atm) and temperatures of less than 50°C. However, calcitization has been recorded experimentally at 200°C (Kastner, 1982; Stoessell *et al.*, 1987).

For extensive calcitization of dolomite, a large and constant imbalance of calcite and dolomite saturation states must be maintained. The easiest way to produce this is by extensive dissolution of gypsum, which will give the diagenetic fluids a very high Ca/Mg ratio, generating supersaturation with respect to calcite (owing to the common ion effect), and undersaturation with respect to dolomite. Although dissolution of gypsum is the most effective source of high Ca/Mg ratio fluids in nature (De Groot, 1967), other sources have been invoked, most commonly dissolution of limestone in the groundwater recharge area (Abbott, 1974; Longman and Mench, 1978; Theriault and Hutcheon, 1987), and mixing of meteoric groundwater with seawater (Al-Hashimi and Hemingway, 1973; Kafri and Magaritz, 1981; Holail *et al.*, 1988). The most effective way of dissolving large quantities of gypsum and maintaining high fluid flow rates together with open system conditions, is within meteoric groundwater systems; groundwaters are commonly strongly undersaturated with respect to gypsum. In groundwaters, once gypsum dissolution creates a sufficient imbalance of saturation states, calcitization may often be very extensive (Back *et al.*, 1983).

The most widely quoted expression of calcitization in association with calcium sulphate dissolution is after Von Morlot (1847):

$$\underset{\text{Dolomite}}{CaMg(CO_3)_2} + \underset{\text{Anhydrite}}{CaSO_4} \rightarrow \underset{\text{Calcite}}{CaCO_3} + MgSO_4$$

Or,

$$\underset{\text{Dolomite}}{CaMg(CO_3)_2} + \underset{\text{Gypsum}}{CaSO_4 .2H_2O} \rightarrow \underset{\text{Calcite}}{2CaCO_3} + MgSO_4 + 2H_2O$$

(modified from Von Morlot (1847) [In: Goldberg, 1967]).

This expression has led to the erroneous belief that calcitization of dolomite is related to the action of sulphate ions. In fact, although calcitization is associated with dissolved sulphate, it

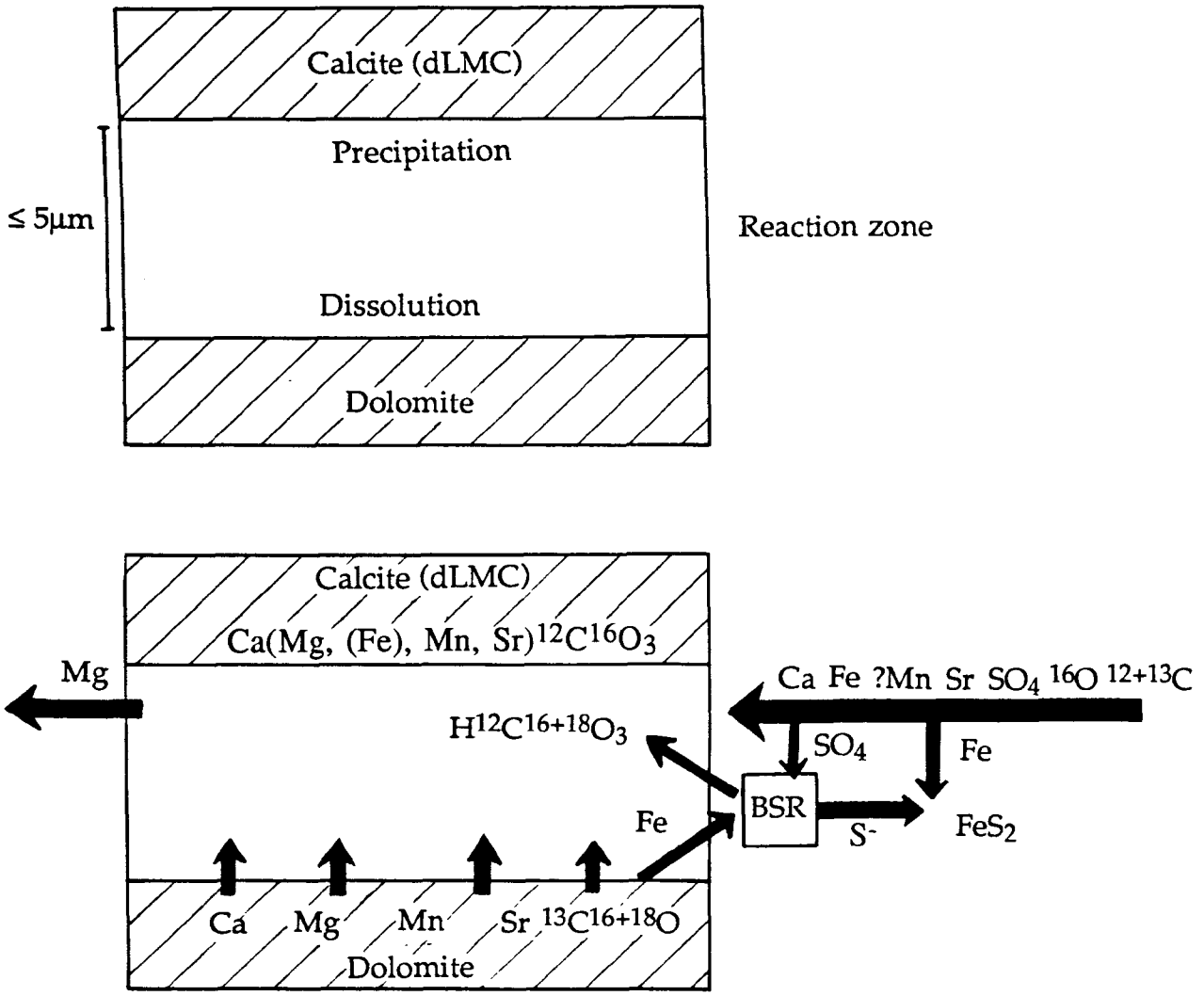

Fig. 6.36. Schematic representation of a reaction zone, along which the transfer of ions during calcitization is considered to take place by diffusion. The main directions of movement of ions and isotopes are indicated. There is a net export of Mg, and Fe derived from dolomite as well as in solution from groundwater. The Fe is scavenged during bacterial sulphate reduction (BSR) which also utilizes sulphate introduced by the groundwaters.

is simply a consequence of obtaining large quantities of Ca from gypsum (Back *et al.*, 1983). Thus, the oxidation of pyrite (Evamy, 1963) is not a significant mechanism of calcitization. The by-product of this reaction ($MgSO_4$) is highly soluble and so rarely recognized at outcrop.

Another major explanation for calcitization of dolomite concerns ferroan dolomite, which is naturally metastable especially under near-surface diagenetic conditions, and may dissolve incongruently:

$$4[Ca(Mg,Fe)(CO_3)_2] + 2H_2O + 1/2O_2 \rightarrow 4CaCO_3 + Fe_2O_3 + 2Mg^{2+} + 2CO_3^{2-} + 2H_2CO_3$$

Dolomite — Calcite — Hematite

$$Fe_2O_3 + H_2O \rightarrow 2FeOOH$$

Hematite — Goethite

(after Al-Hashimi and Hemingway, 1973).

With regard to this reaction, one of the most important by-products is iron oxide/hydroxides, which have previously been very widely recognized in association with calcitized dolomite. Implicit in this process, is that the reaction is near-surface (mediated by high Eh fluids). It has been suggested that oxidation of iron is the driving force for the reaction, and promotes centripetal breakdown of the dolomite crystal (Al-Hashimi and Hemingway, 1973). However, unless the ambient fluids are saturated or supersaturated with respect to calcite, incongruent dissolution is unlikely to occur, or the replacement reaction will involve a volume reduction (as expressed in the previous formula) which is not recorded.

Near-surface undersaturation with respect to dolomite and supersaturation with respect to calcite is common within meteoric-derived groundwaters during early groundwater evolution. Owing to their different solubilities, groundwaters will quickly attain saturation with respect to calcite by congruent dissolution, but not so quickly with respect to dolomite. This period of saturation with respect to calcite, and undersaturation with respect to dolomite will be characterized by incongruent dissolution of dolomite. As these processes are near surface, oxidised iron minerals (oxidized pyrite [Evamy, 1963], and goethite [only where the precursor contains significant iron] [Al-Hashimi and Hemingway, 1973; Frank, 1981]) will be common by-products. Reported occurrences of calcitized dolomite associated with iron oxide/hydroxides are of a much smaller extent than those which are associated with dissolution of sulphates, suggesting calcite and dolomite saturation states are not greatly imbalanced, and are imbalanced for a relatively short period of time in the upper parts of groundwater systems.

Other, less well defined environments of calcitization, occur during burial diagenesis (Clark, 1980; Budai *et al.*, 1984). Replacement is due to processes which lead to local undersaturation with respect to dolomite and supersaturation with respect to calcite, such as diagenesis of organic matter.

6.3.4. Previous work on calcitized dolomite within the Raisby Formation.

Calcitization of dolomite within the Zechstein of northeast England was first noted by Sorby (1856 [in: Woolacott, 1919b]) who suggested that, following the experimental work of Von Morlot in 1847, it was the product of calcium sulphate rich fluids. This was followed up by a number of other workers early this century who applied the process to the formation of calcite concretions within second and third cycle carbonates. One of the most thorough discussions of the process of calcitization following sulphate dissolution was by Woolacott (1919b), who invoked the action of gypsiferous fluids in conjunction with tectonism for much of the calcitization within Zechstein carbonates of northeast England.

More recently, calcitization within the Zechstein in general terms has been described by Clark (1980), and has been thoroughly investigated from the Ford Formation main reef by Smith (1981), Aplin (1985), Tucker and Hollingworth (1986) and Hollingworth and Tucker (1987). Again, there is a considerable overlap in these discussions with the formation of calcite concretions, invoked by these authors to be the product of dolomite calcitization, although concretions within the Raisby Formation are not the result of calcitization of dolomite (4.4.3). However, there is general agreement that sulphate dissolution is an important calcitization mechanism in the Zechstein of northeast England. Calcitization of dolomite within the Raisby Formation has been described by Lee and Harwood (1989).

6.3.4.1. Enclosed Dolomite Relic (EDR) calcitized dolomite - Interpretation.

Many of the EDR examples are genetically related to gypsum dissolution. This is demonstrated by their close association along the Trow Point to Man Haven section with the residue of the Hartlepool Anhydrite Formation, and association with pseudomorphs after evaporites at Running Waters Quarry and other localities. At South Shields, the greater porosity and permeability of the open-textured collapse breccias has lead to more pervasive calcitization than within the underlying, relatively impervious Raisby Formation, where dolomite was only calcitized along lines of preferential fluid movement (bedding planes and joints).

Petrographic textures of EDR calcitized dolomite associated with sulphate dissolution, suggest that the calcitizing fluids were of a relatively high supersaturation with respect to calcite, producing fine crystal sizes as a result of growth from numerous nucleation sites. The more pervasive calcitization of Z2 collapse breccias, implies that ease of fluid movement on a large scale was of greater significance in determining the intensity of calcitization than was supersaturation with respect to calcite.

Replacement of dolomite by dull orange-luminescent calcite (and positive Fe/Mn ratios of the calcites) demonstrates that the diagenetic fluids were reducing, containing Fe and Mn in solution. The most pervasively calcitized (least dolomitic) Z2 collapse breccias and underlying Raisby Formation samples at South Shields contain approximately 1 mole% $MgCO_3$. Calcitized Raisby Formation samples have up to 600ppm Sr (Appendix VII). The

calculations in figure 6.37, using the homogeneous distribution law (3.1.1), support the suggestion of a strong involvement of gypsum in calcitization. If only dolomite was the dissolving phase, the replacive calcite would contain more Mg and less Sr than measured values. Thus, a high Ca/Mg, low Ca/Sr ratio mineral (gypsum) was a significant contributor to the geochemistry of the calcitizing fluid (Fig. 6.37). The maximum Sr value of 600ppm does not agree with the calculations, suggesting a more closed diagenetic system, probably with more than 50% gypsum contribution.

The two isotope analyses from the calcitized Z2 collapse breccia and immediately underlying Raisby Formation plot very close together (Fig. 6.38), indicating a common source for the calcitizing fluids. These analyses differ from Raisby Formation limestones and dolostones, although are similar to calcite cements lining cavities after sulphates within the Raisby Formation (Fig. 6.66b). They also plot extremely close to the 'meteoric calcite line' as defined from non-luminescent columnar calcites within the Raisby Formation (Fig. 6.66b). This suggests that oxygen isotopes were largely derived from meteoric sources (open system, low rock/water ratio diagenetic environment), although carbon isotopes reflect an admixture from isotopically light (soil gas) and heavy (precursor carbonate) sources. There may have been some fractionation of oxygen isotopes owing to elevated temperatures. Assuming the fluids had a $\delta^{18}O$ -8.0‰ to -5.0‰ (SMOW) (reflecting dominantly meteoric sources [6.5.3]), the oxygen isotope results suggests temperatures of 10.1-22.5°C and 9.3-21.6°C for the Z2 and Raisby Formation respectively (using palaeotemperature equation in Appendix IX). Both Clark (1980) and Aplin (1981 & 1985) have described 'surface related secondary limestones' (calcitized dolostones) from outcrop in northeast England and the Ford Formation main reef respectively. Both authors relate calcitization to near-surface, calcite-saturated groundwater. Their isotope data supports that interpretation, and is in good agreement with the Z2 and Raisby Formation EDR calcitized dolostones (Fig. 6.38). The dull orange- to bright orange- to non-luminescent cement sequence, which occludes fracture pores within calcitized dolostones at South Shields (Fig. 6.22b), suggests an analogy with cement sequences developed during uplift of the Raisby Formation, whereby calcite was precipitated from progressively more oxidized fluids (Lee and Harwood, 1989) (6.5.2.1). This is good secondary evidence that calcitization along the Trow Point to Man Haven section, was fairly late diagenetic, and took place during uplift.

Some EDR examples are closely associated with non-luminescent calcite and iron oxide/hydroxides (those from breccia clasts at Houghton and Raisby Quarries). The similarity of petrographic textures with PER and ECI calcitized evaporites (Figs. 6.2, 6.3 & 6.5) suggests a similar replacement process. The inclusion-rich cores are thus interpreted to represent the precipitation of replacive calcite, whereas the inclusion-free overgrowths are interpreted as pore filling cements. A phase of dissolution between the core and overgrowth calcites,

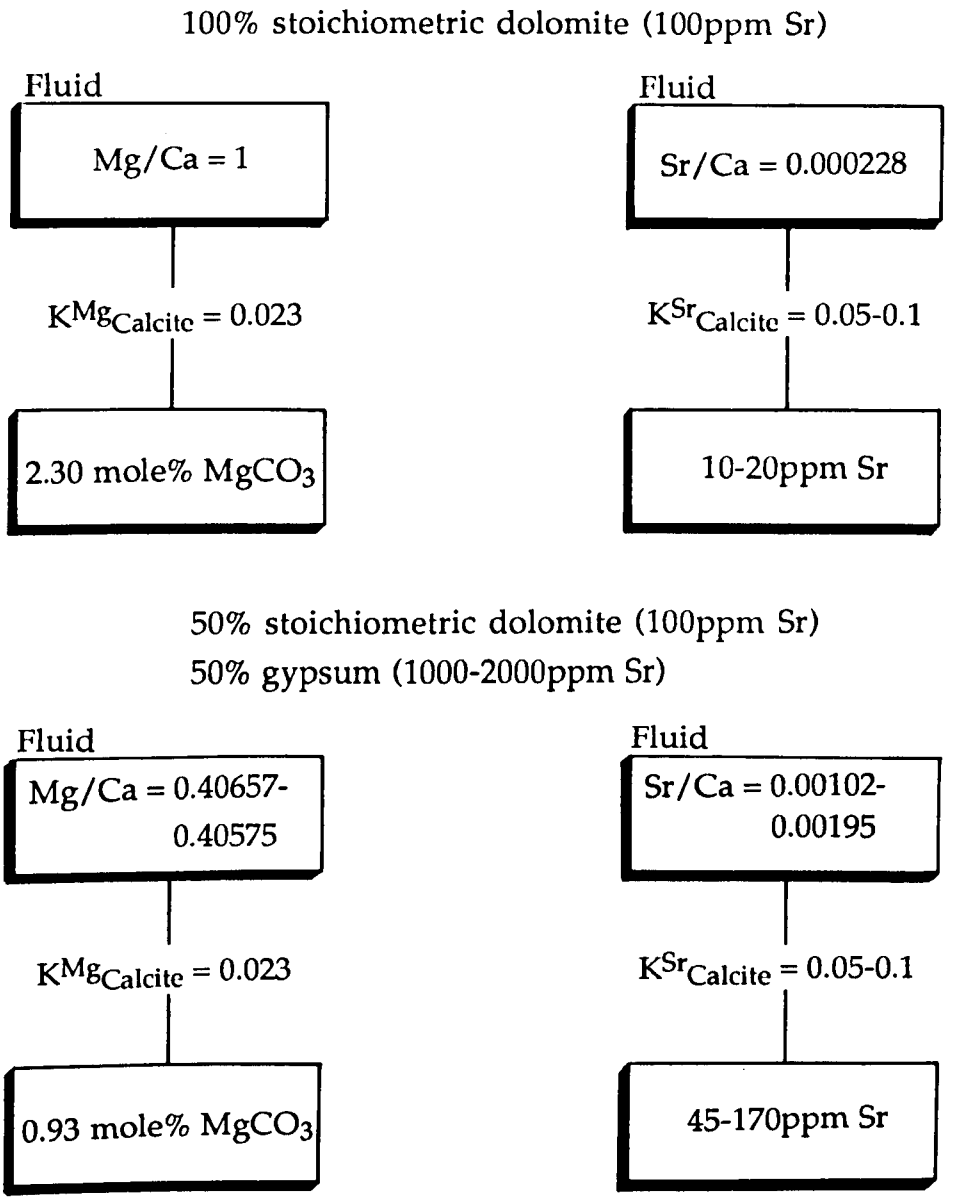

Fig. 6.37. Summary of calculations for the expected geochemical composition of replacive calcite, if all ions were derived from the dissolution of dolomite, or from a mixed dolostone and gypsum source. These calculations assume that during precipitation, equilibrium is approached or reached between the precipitate and the diagenetic fluid so that the homogeneous distribution law can be applied. The diagenetic system is also assumed to be fully open, and the replacement front has a reaction zone structure.

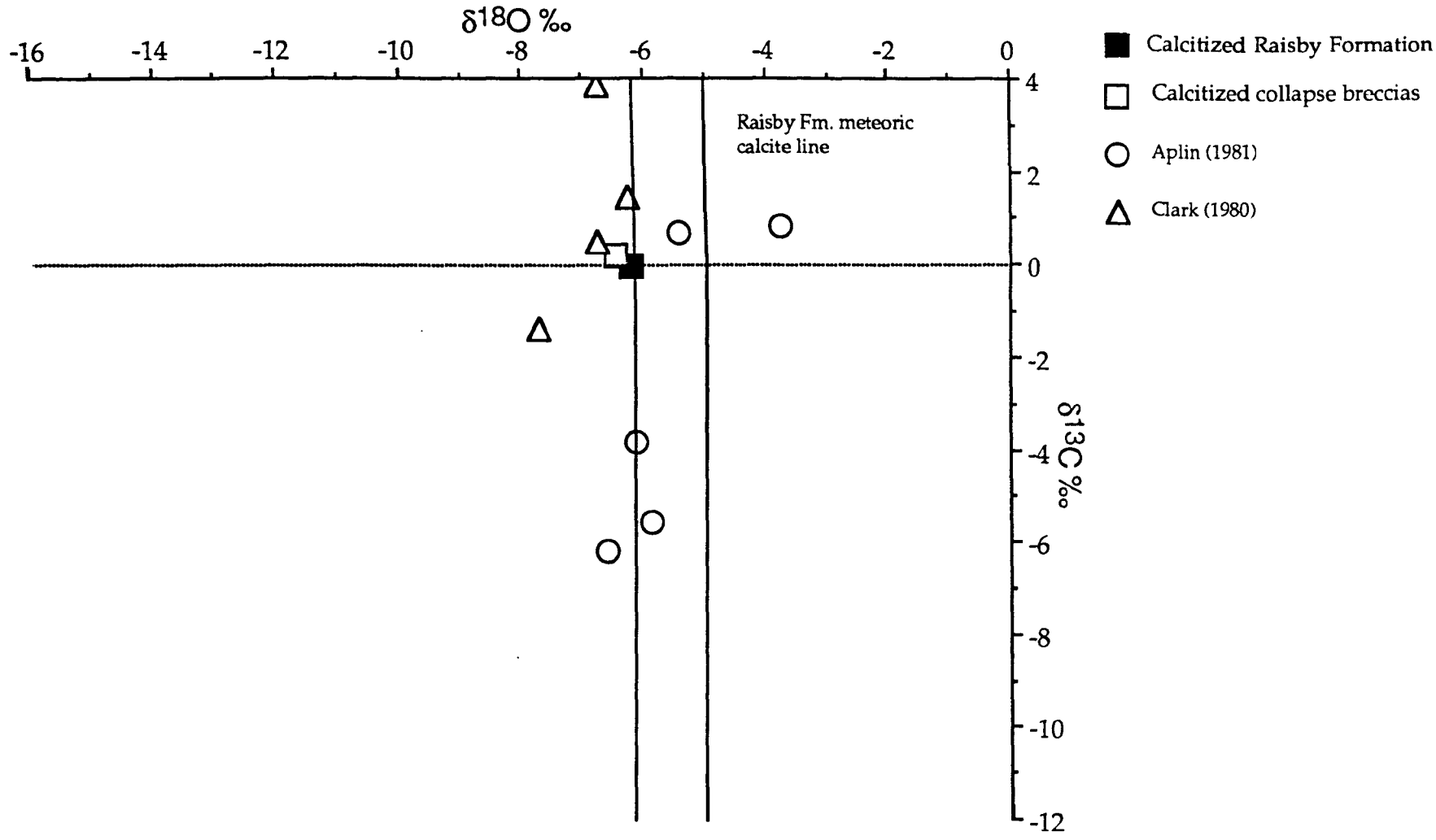

Fig. 6.38. Graph showing the relationship between the isotopic composition of EDR calcitized dolomite from the uppermost Raisby Formation and lowermost Z2 collapse breccias, Man Haven and 'surface-related secondary limestones' analysed by Clark (1980) and Aplin (1981). The Raisby Formation meteoric calcite line defines the oxygen isotopic composition of calcites precipitated in equilibrium with near-surface groundwaters.

is represented at Houghton Quarry by a geopetal internal sediment of corroded dolomite and insoluble residues (Fig. 6.23b), and in Raisby Quarry by calcite luminescence contrasts (Lee and Harwood, 1989 fig. 5). Late diagenetic, non-luminescent calcites in the Raisby Formation are suggested by Lee and Harwood (1989) to be indicative of precipitation from relatively near-surface oxygenated groundwaters. In such conditions, Fe^{2+} liberated during dolomite dissolution would oxidize, precipitating as oxide/hydroxides, and fluids would commonly fluctuate in calcite saturation levels owing to variation in the nature of aquifer recharge fluids (Lee and Harwood, 1989, fig. 16). Such variations in calcite saturation levels would lead to alternating episodes of incongruent and congruent dolomite dissolution, replacive and pore filling calcite precipitation.

The EDR calcitization textures therefore represent two similar replacement processes, although within different hydrogeochemical environments (Fig. 6.39). The Eh, saturation levels and advection rates of diagenetic fluids determined the extent of replacement, and the fate of Fe and Mn liberated from dolomite (and possibly other sources) during incongruent dissolution. One sub-type, characterized by iron hydroxides, represents calcitization from near surface, oxidizing fluids of fluctuating saturation states, whereas the other sub-type, associated with evaporite dissolution, reflects replacement at deeper levels where Fe and Mn were reduced. Some of the replacement of dolomite, and calcitization of gypsum/anhydrite took place at a similar point in the hydrogeochemical evolution of the Raisby Formation during uplift, as demonstrated by the rare juxtaposition of ECR calcitized dolomite and PER calcitized anhydrite (Fig. 6.25).

6.3.4.2. Crystallographically selective (CS) calcitized dolomite - Interpretation.

This is a partial, selective style of replacement, volumetrically less important than type EDR. Four processes have previously been proposed to explain zone-selective calcitization:

1. Selective to calcian zones in dolomite crystals (Katz, 1968),
2. Selective to iron-rich zones in dolomite crystals (Frank, 1981),
3. Selective to inclusion-rich parts of dolomite crystals (i.e., Theriault and Hutcheon, 1987),
4. Selective to crystal defects/imperfections (which may or may not parallel zone boundaries) (Stoessell *et al.*, 1987).

Katz (1968) suggested that dolomite zones with greater than 8% $CaCO_3$ over stoichiometric composition were especially susceptible to replacement, either because of their greater free energy, or owing to their relative ease of replacement (because the zones were already partly calcitic). Frank (1981) described dolomite zones with 3.48mole% $FeCO_3$ being partially altered whereas those with 4.56 mole% $FeCO_3$ were more pervasively altered. The composition of the partially calcitized dolomite crystals from Raisby Quarry shows that they are neither calcian nor ferroan $(Ca_{(49.6)}\ Mg_{(50.1)}\ (Fe_{(0.2)}\ Mn_{(0.1)})\ CO_3$ (n=11) [Appendix

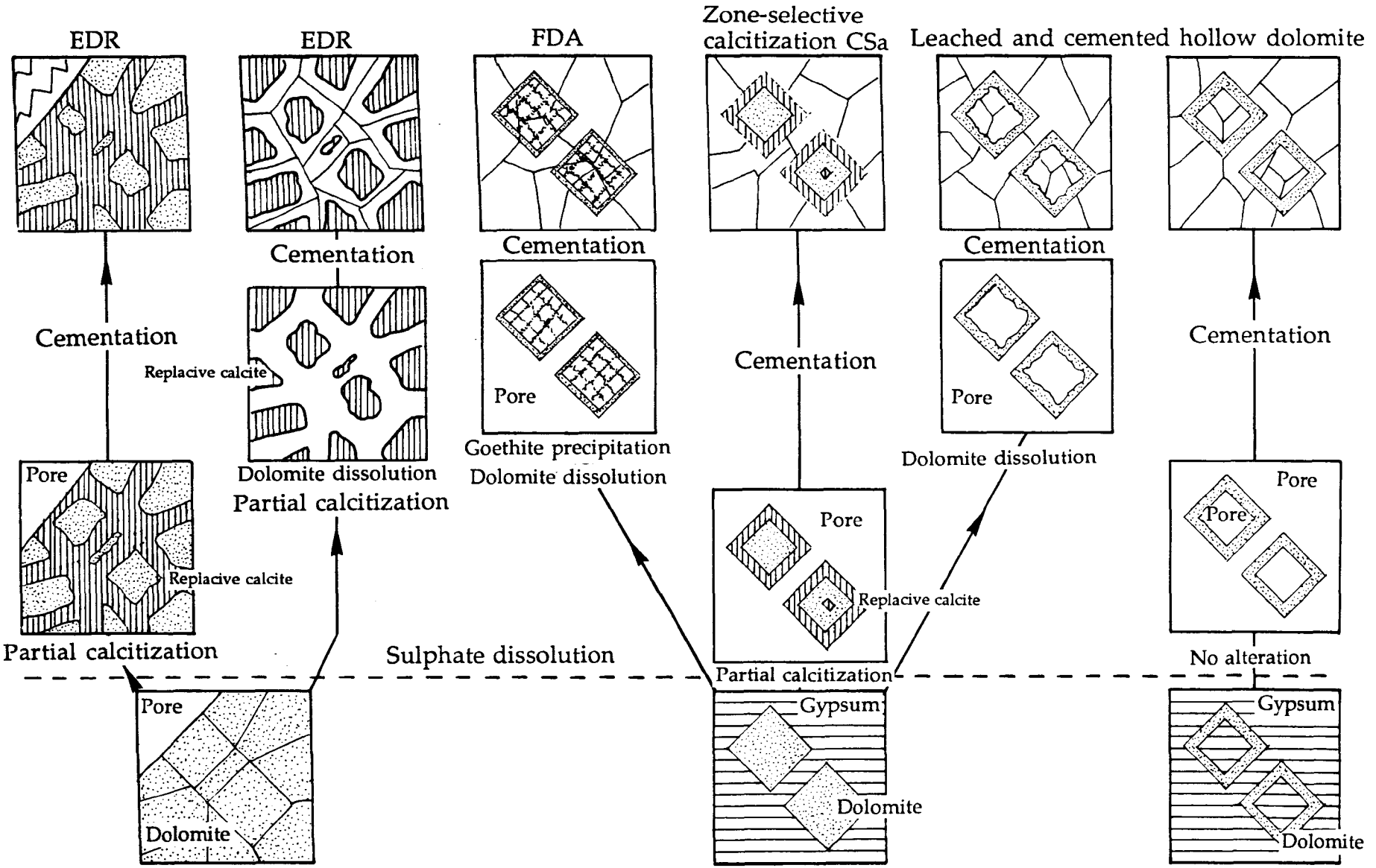

Fig. 6.39. Summary diagram showing textural and diagenetic interrelationships between the main types of calcitized and altered dolomites identified within the Raisby Formation.

V]). This does not rule out the possibility that the now-replaced zones were of a significantly different composition to those which have been preserved, but ICP, microprobe analyses, and luminescence of unaltered dolostones suggest that this is highly unlikely. The un-replaced dolomite does contain inclusions, but they are randomly scattered throughout the crystals.

The most likely processes leading to zone selective alteration is that proposed by Stoessell *et al.*, (1987), whereby imperfections within dolomite crystals calcitized experimentally (at elevated temperature [200°C] and pressure [300 bars] conditions) were picked out by the replacive calcite. The replacement was also concentrated at the external surfaces of the dolomite crystals, working inwards. Replacive calcite experimentally precipitated as euhedral rims 10μm to 20μm wide in optical continuity with the dolomite substrate. This is the best model to explain all the textural features of CSa, zone-selective calcitization.

The zone-selective calcitized dolomite and host calcite cements are commonly associated with pyrite/marcasite (in core) or hematite after pyrite/marcasite (at outcrop). This suggests that sulphate reduction was active during or after calcite cementation, although not necessarily synchronous with calcitization. However, in the example from North Sands borehole, pyrite only occurs in direct association with the calcitized dolomite zones, implying a genetic association (Fig. 6.29a). The pyrite may have formed by H_2S scavenging of Fe^{2+} within the pore waters. H_2S in turn may have been derived from bacterial reduction of sulphate liberated by the dissolution of gypsum. In such reducing pore waters, Fe^{2+} can be derived from the dissolution of detrital/authigenic iron oxide/hydroxides and/or the congruent/incongruent dissolution of dolomite. Analyses of calcitized dolomite from the Raisby Quarry breccias by ICP show that the calcitized areas have a much higher concentration of Fe that that within a similar volume of unaltered dolomite (Fig. 6.28). This may be explained by Fe^{2+} migrating preferentially towards microenvironments of active sulphate reduction, as is common during precipitation of framboidal pyrite (3.3.2). If sulphate reduction was in progress during dolomite calcitization, this may explain why the replacive calcite is bright orange-luminescent (Fe-depleted) within Raisby Quarry breccia samples (Fig. 6.24) (6.2.3.1). Furthermore, Kastner (1982) and Brauer and Baker (1984) suggest that significant quantities of SO_4 (considerably less than seawater concentrations) may effectively inhibit calcitization. Thus, iron sulphide precipitation may aid calcitization of dolomite.

Carbon and oxygen stable isotope analyses of coarsely crystalline, predominantly dull orange-luminescent calcite from within the calcitized Raisby Quarry breccia samples (although not necessarily the calcitizing phase) have a mean $\delta^{18}O$ of -11.4‰. This suggests elevated temperatures. If a fluid composition of $\delta^{18}O$ -5.0‰ to -6.0‰(SMOW) is assumed (reflecting a meteoric derivation [6.5.3]), they would precipitate a calcite of $\delta^{18}O$ -11.4‰ at

temperatures of between 42.2°C and 47.8°C respectively (Appendix IX for details of calculation). Both are well below the upper limit for bacterial sulphate reduction (approximately 85°C [Machel, 1987b]). The $\delta^{13}C$ values for these cements (mean -3.2‰ [n=3]) lie between those of luminescent calcites from the Raisby Formation and ECI calcitized evaporites from Raisby Quarry (which did have significant input of carbon from sulphate reduction [6.2.3.2]). Thus, on the basis of carbon isotope values, the identification of bacterial sulphate reduction is not certain, although a component from this source is likely.

Completely calcitized dolomite crystals (type CSb) have only been identified within minerals which became unstable during diagenesis, such as HMC marine cements and evaporites. This association implies that calcitization of the dolomite took place at a similar time to alteration of the unstable phases, in an environment of dissolution of Ca-rich precursor minerals and calcite cementation.

The CS textures thus represent partial to total calcitization at a similar time to calcite precipitation, and so may be understood in terms of pore fluids being supersaturated with respect to calcite but undersaturated with respect to dolomite. Although there is evidence for the indirect involvement of calcium sulphate in solution from iron sulphides, the driving force for calcitization (i.e., Ca/Mg ratio) was probably not strong and so recrystallization was partial. Both elevated temperatures (most likely from burial, possibly with locally elevated geothermal gradients in response to mineralization) and bacterial sulphate reduction (possibly itself catalysed by the elevated temperatures of the environment) may have played indirect roles in the calcitization process.

6.3.4.3. Embayed Dolomite (ED) calcitized dolomite - Interpretation.

This is a heterogeneous grouping of calcitized dolomites, all of which most likely formed during mesogenesis. Partially-calcitized dolomite in association with calcite microspar is only recorded where ADP carbonate muds were incompletely dolomitized prior to neomorphism. During neomorphism, pore fluids were supersaturated with respect to dLMC, although undersaturated with respect to dolomite (4.2.2). This locally created conditions favorable to dolomite replacement by microspar, although it was only effective where the diagenetic fluids were un-diluted by the bulk aquifer (i.e., relatively closed system conditions).

The calcitized dolomites from borehole W8 are very anomalous. Their petrographic textures, stable isotope and trace element geochemistry are very similar to limestones within the Raisby Formation, which could suggest an analogy with the calcitization of dolomite during neomorphism of ADP carbonate muds. However, the position of the calcitized dolomite within this borehole, and its very strong association with replacive sulphates suggests it is not a limestone. This lithology may represent localized calcitization of dolomite in response to the dewatering of replacive gypsum (the expelled water of crystallization

having a high Ca/Mg ratio) following burial (the process described by Clark, 1980), or concentrated Ca-rich fluids associated with the precipitation of replacive sulphates (much more abundant within this lithology than anywhere else in the core). Both the water of crystallization and sulphate-precipitating fluids would be expected to have an isotopic composition similar to the dolostones and limestones within the Raisby Formation (i.e., close to Zechstein seawater values).

The calcitized dolomites in association with calcite concretions at Raisby Quarry are difficult to explain, as there appears to have been no drive for replacement, other than calcite precipitation, and accordingly the dolomite is only calcitized adjacent to scalenohedral calcite crystals. Thus, the replacement mechanism was possibly similar to that of the calcitized dolomite within calcite microspars, and resulted from an environment of concentrated, albeit local, calcite supersaturation and dolomite undersaturation.

6.3.4.4. Leached and Cemented (LC) dolomite - Interpretation.

The isolated, corroded dolomite rhombs characteristic of this type superficially resemble zone-selective, CSa replacement textures. Although corroded dolomite rhombs lie within calcite, there is no direct evidence for replacement. Furthermore, the LC (hollow dolomite) textures support the interpretation of dissolution followed by later cementation via four petrographic features:

1. Numerous hollow centered dolomite crystals remain unoccluded by calcite,
2. Adjacent hollow crystals are commonly cemented by the same calcite crystal,
3. Calcite crystals presenting euhedral faces into rhomb center pores have been 'caught in the act' of cementing dolomite dissolution porosity,
4. Geopetal internal sediments of insoluble material formerly enclosed within the dolomite demonstrate that a distinct void stage occurred.

This evidence suggests that porosity existed between congruent dissolution of dolomite and passive calcite cementation, although does not discount minor calcitization of the relic dolomite accompanying later cementation. The hollow dolomite crystals may be a product of dolomite dissolution selective to crystal imperfections such as inclusion-rich cores. However, these textures may also represent the dissolution of calcium sulphates which selectively replaced the inclusion-rich cores of dolomite crystals. This would explain the common association of hollow dolomite crystals with cavities after sulphates, although dolomite crystal cores replaced by sulphate have not been recorded from the Raisby Formation in core. Ferroan dolomite cements surrounding calcite concretions at Raisby Quarry have been heavily leached (the ferroan dolomite selectively over the less iron-rich core crystals) (Fig. 4.35b), although not cemented by calcite. The leaching is selective to zone and cleavage traces, and also crystal imperfections such as fluid inclusions (Fig. 4.35b). This leaching is not the product of sulphate dissolution. The hollow dolomite texture is,

therefore most likely the product of congruent dolomite dissolution, although leaching of selectively replacive sulphates cannot be discounted.

Congruent dissolution of dolomite demonstrates that the ambient fluids were undersaturated with respect to dolomite. The fact that calcite cementation took place some time later than leaching suggests that fluid flow was relatively rapid, such that the dissolving dolomite (minor in overall volume) did not get the opportunity to supersaturate the local pore fluids with respect to calcite (i.e., the rate of dolomite dissolution was much slower than that of aquifer flow and/or calcite did not have enough time to concentrate in the solution [high water/rock ratio diagenetic environment]).

The probable cause of hollow dolomites most likely lies with all three processes outlined; dissolution of selective replacive sulphate, congruent dissolution of dolomite before calcite cementation and, possibly, late stage, near-exposure congruent dissolution of dolomite. The convergence of product, hollow dolomite reflects the selectivity of all three processes to inclusion rich cores. The larger scale, LCb (leached dolostone) texture most likely formed by dissolution of replacive evaporites with minor dolomite dissolution and possible minor calcitization, although petrographic textures are very similar to some ECI calcitized evaporites (Fig. 6.6b). Most of the dissolution predated luminescent calcite cementation. Sulphate replacement was selective, in this case, to clastic dolomite horizons with a marked heterogeneity in dolomite crystal sizes.

6.3.4.5. Ferroan Dolomite Alteration (FDA) textures - Interpretation.

These textures are extremely similar to those described by Evamy (1963), Chafetz (1972), Al-Hashimi and Hemingway (1973), Frank (1981), Harwood (1981), Elmore *et al.*, (1985), and Loucks and Elmore (1986) for calcitization of ferroan dolomite. In these examples, the definitive by-product of the process is abundant hematite and/or goethite along narrow bands parallel to zones and cleavages within the former dolomite crystals. The iron hydroxides were formerly considered to have been precipitated because the calcite could not accommodate Fe^{3+}/Fe^{4+} within its lattice (Evamy, 1963), but they are now recognized as oxidation products of Fe^{2+} (Al-Hashimi and Hemingway, 1973).

The characteristic textures of zone- and cleavage-parallel aggregates of goethite occur both within otherwise unaltered ferroan dolomites (Fig. 6.33b), and heavily leached and calcite cemented ferroan dolomites (Figs. 6.34 & 6.35). This suggests that, over time, alteration proceeds from lines of weakness (cleavages and zone boundaries), to alteration of the entire crystal. The precipitation of the iron hydroxides along zone and cleavage traces suggests that dolomite-undersaturated, oxygenated fluids attack the dolomite along those lines, the immediate consequence of which is the precipitation of iron hydroxides. The initial iron hydroxides must therefore have been derived from within only a few microns of the cleavages/zone boundaries. In more advanced stages of dissolution, iron hydroxides are

still only developed along the initial lines (Fig. 6.35b), suggesting that, with further dissolution of the dolomite, liberated Fe^{2+} preferentially precipitates with the already-formed iron minerals. Additional iron in solution may also have been introduced by reducing groundwaters. The preference of iron precipitation to already-formed nuclei is another explanation for the anomalously high concentrations of iron oxide/hydroxides in association with calcitized and leached dolomite.

The calcite within altered dolomite crystals from Thickley Quarry is in optical continuity with the relic dolomite, and also zoned (Fig. 6.34b). Some of the zonation suggests that calcite may have inherited the crystal form of precursor saddle dolomite, with calcite crystal growth being determined by the narrow bands of iron and dolomite which in turn mirror the former crystal structure. These features are interpreted to suggest that the calcite within altered dolomite rhombs is a pore filling cement rather than a replacive phase.

All of the host calcites to the altered rhombs at Thickley Quarry are either bright orange- or non-luminescent, containing less than 0.1 mole% $FeCO_3$. This would be in accordance with precipitation of the calcite within an partially oxidizing pore waters. However, the oxygen isotopic composition of the bright orange-luminescent pore filling calcite ($\delta^{18}O$ -13.1‰) is at variance with such an explanation, implying precipitation from fluids of considerably elevated temperatures. This bright orange-luminescent calcite however, is dissected by fractures cemented by non-luminescent calcite (Fig. 6.34b), which most likely represent conduits for later oxidizing fluids in the Thickley Quarry example. Thus, alteration of dolomite in this case was considerably later than cementation of adjacent porosity.

The evidence from the few Raisby Formation examples of the FDA texture therefore suggest that it is the product of congruent dolomite dissolution, which may be followed by calcite cementation. There is no *a priori* reason why a dolomite should be calcitized by oxidizing fluids simply because it is iron-rich (6.3.3), although its ferroan composition makes it more susceptible to congruent dissolution. Both the congruent dissolution of dolomite and calcite pore fill cementation most likely took place in near-surface oxidizing environments. There is clear evidence in some EDR calcitized dolomites for non-luminescent calcite pore fill cementation postdating congruent dissolution of dolomite; such an interplay of saturation states is common with the near surface oxidizing groundwater environment (Lee and Harwood, 1989). Furthermore, it is likely that the fundamental difference between FDA textures and some of the LC examples is the oxygenation of diagenetic fluids and iron content of the former dolomite. Thus, dolomite within the Tynemouth Castle Cliff sandstone has abundant evidence for late diagenetic dissolution associated with non-luminescent calcite cementation (Fig. 5.7), although it is not associated with iron oxide/hydroxides. This is because the unaltered dolomite contains negligible iron ($Ca_{(49.1)}Mg_{(50.4)}(Fe_{(0.3)}Mn_{(0.2)})\ CO_3$).

6.4.1. Dolomite and evaporite calcitization model.

For a meaningful interpretation, calcitization processes described have to be integrated into a larger scale model. The EDR, CS, LC, and FDA calcitized dolomites, and all calcitized evaporites are considered to have formed during regional uplift of the Zechstein sequence in northeast England during the late Cretaceous or early Tertiary (Tables 6.1 & 6.2). The calcitized dolomite ED and CSb textures represent a heterogeneous grouping of mesogenetic processes.

Uplift of the Raisby Formation exposed minerals, stable during burial diagenesis (calcite, dolomite and anhydrite/gypsum), to meteoric-derived fluids initially at least, undersaturated with respect to all three minerals (Lee and Harwood, 1989). Following penetration of the Raisby Formation by these fluids, when it was probably a few hundred metres from the earths surface [5.7.3], a meteoric groundwater system (aquifer) was established. Late diagenetic minerals in the Raisby Formation at outcrop represent the exposed products of that aquifer.

Within modern meteoric carbonate aquifers (Longman and Mench, 1978; Back *et al.*, 1983), and mixed carbonate-siliciclastic aquifers (Edmunds *et al.*, 1982; Bath *et al.*, 1987), distinct geochemical profiles may be defined which describe gradients in the saturation states of various minerals such as calcite, dolomite, and gypsum. Saturation with respect to all three in general increases down-flow, reflecting progressive rock-water interaction which corresponds to an increase in concentration of all major dissolved ions (Ca^{2+}, Mg^{2+}, SO_4^{2-}, HCO_3^- [Fe and Mn are redox-dependant]). In general, within any one meteoric groundwater system, equilibration with calcite and dolomite is achieved fairly early, following intense congruent dissolution by CO_2-charged vadose groundwaters (6.5.2.3). Major departures from equilibrium occur when the groundwaters encounter a new, soluble phase, such as gypsum in the lower levels of the aquifer (Back *et al.*, 1983). Less significant departures from equilibrium may result from cation exchange reactions (Drever, 1982).

Within meteoric aquifers there is also commonly a well defined decrease in the oxygenation of groundwaters from near-surface (unconfined) conditions to the more distal (confined) aquifer (Champ *et al.*, 1979; Barnaby and Rimstidt, 1989) (Fig. 6.40). This down-flow decrease in oxygenation may be abrupt and fault-related (Longman and Mench, 1978), or gradational (e.g., Edmunds *et al.*, 1982) (Fig. 6.40). If a gradational change is assumed, the oxidation states of iron minerals in association with authigenic mineral phases may be used to deduce palaeoredox conditions, and so relative position within the aquifer and, by extension, relative concentrations of dissolved ions (Lee and Harwood, 1989). Owing to uncertainties as to the climate during establishment of this aquifer, flow patterns of the present day can only be used as approximate indicators of groundwater movement in the past (5.7.3).

Crystallographically seclective, (CSa) zone-selective subtype	Evaporite dissolution-associated enclosed dolomite relic (EDR)	Goethite-associated enclosed dolomite relic (EDR) and ferroan dolomite alteration (FDA)	Diagenetic processes
No cementation Pyrite/marcasite oxidation	Calcite cement Non-luminescent ± bright orange hairline subzones Ca (Mg (Mn)) CO3	Calcite cement Non-luminescent ± bright orange hairline subzones Ca (Mg, Mn) CO3 Congruent dolomite dissolution Goethite Internal sedimentation Replacive calcite Non-luminescent/luminescent Ca (Mg (Mn)) CO3 Goethite	Influx of oxic meteoric-derived fluids
No cementation Calcite cement Dull orange-luminescent Ca (Fe, Mn) CO3	Calcite cement Bright orange-luminescent Ca (Mn) CO3 Replacive calcite Dull orange-luminescent Ca (Fe, Mn) CO3		Reduction of meteoric-derived fluids
Replacive calcite Bright orange-luminescent Ca (Mn) CO3 Pyrite/marcasite			Bacterial sulphate reduction

Table 6.2. Summary of the diagenetic interrelationships between the main types of calcitized dolomite, and nature of the ambient diagenetic fluids. Note the similarity with calcitized evaporites (Table 6.1).

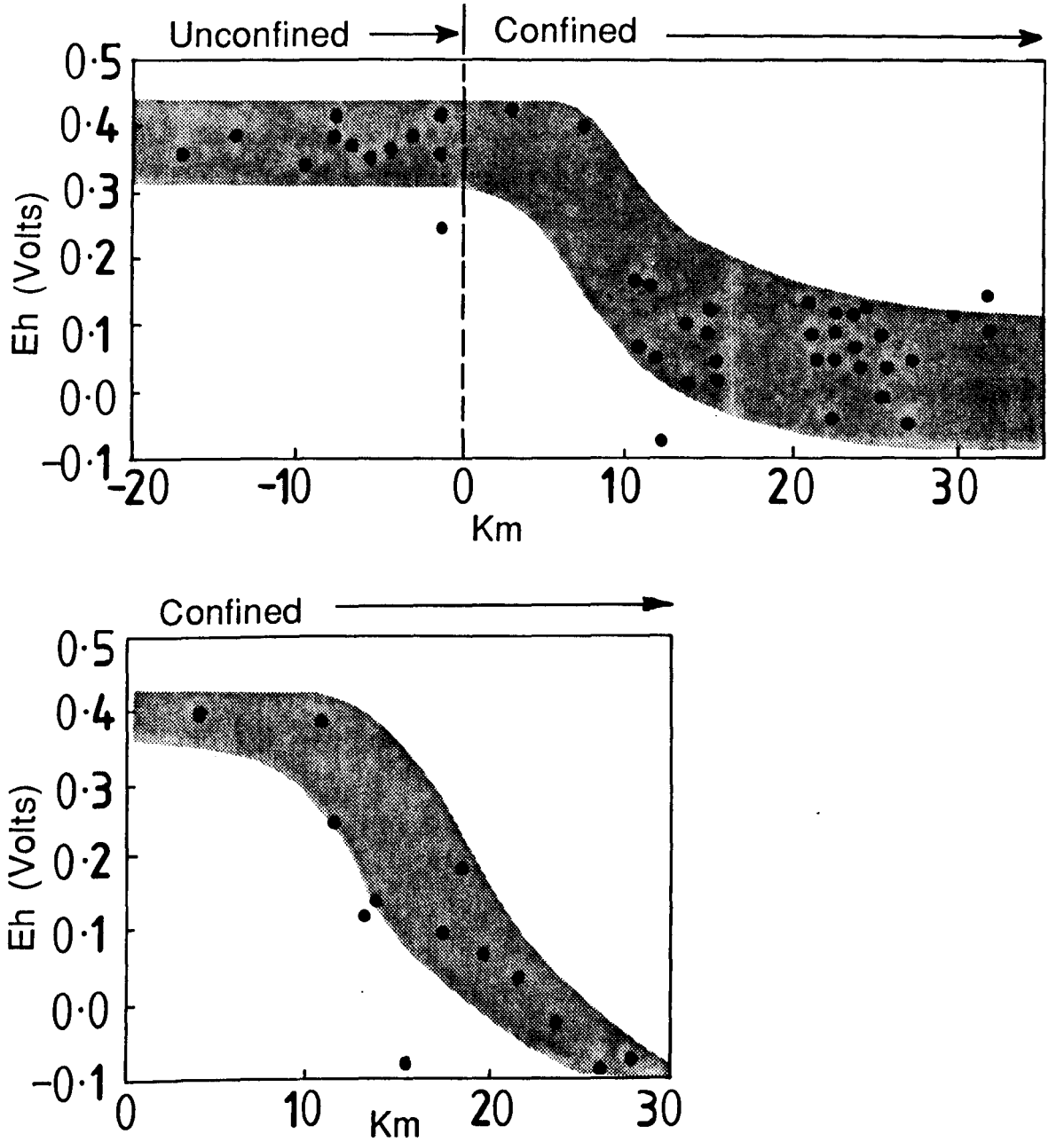

Fig. 6.40. Graphs illustrating profiles of decreasing Eh in groundwaters with distance from their recharge area (modified from Barnaby and Rimstidt, 1989).

Calcitized and altered dolomites, and calcitized evaporites within the Raisby Formation define three redox-related diagenetic environments (groundwater zones) from the oxidation states of associated iron minerals, and luminescence characteristics of authigenic calcites (Fig. 6.41):

6.4.1.1. Groundwater zone 1 (shallow aquifer).

Near-surface, unconfined aquifer. Characterized by the oxidation of iron and manganese to oxide/hydroxide minerals, and non-luminescent, with subordinate bright orange-luminescent pore filling calcites (fig. 6.41). Owing to their high solubility, all calcium sulphates have been dissolved out from this zone. Dolomite is undersaturated and may dissolve congruently (FDA and some LC textures), or incongruently (some EDR textures), depending on the saturation state of calcite within the same fluids. Calcitization of dolomite in the oxidizing, near-surface parts of meteoric aquifers has been described by Longman and Mench (1978) and Bath *et al.*, (1987). Congruent dissolution of dolomite in the same setting has been described by Edmunds *et al.*, (1982). Longman and Mench (1978) also describe coarse equant calcite cements in association with calcitized dolomite within the oxidizing part of a carbonate aquifer. The groundwater zone 1 reactions may be represented thus:

$$CO_2 + H_2O \rightarrow H_2CO_3$$

Carbonic acid

Incongruent dissolution of ferroan dolomite

$$CaMg(Fe,Mn)(CO_3)_2 + 2H_2CO_3 \rightarrow Ca(Mn)CO_3 + Mg^{2+} + 4HCO_3^- + Fe^{2+}$$

Dolomite — Calcite (luminescent)

$$Fe^{2+} + 1/2O_2 + 2H_2O \rightarrow Fe_2O_3 + 4H^+$$

Hematite

Congruent dissolution of ferroan dolomite

$$CaMg(Fe,Mn)(CO_3)_2 + H_2CO_3 \rightarrow Ca^{2+} + Mg^{2+} + 4HCO_3^- + Mn^{2+} + Fe^{2+}$$

Dolomite

$$Fe^{2+} + 1/2O_2 + 2H_2O \rightarrow Fe_2O_3 + 4H^+$$

Hematite

The proposed variations in saturation states with respect to calcite (producing some EDR textures) are most likely due to an input of CO_2-charged fluids (or organic matter) into areas undergoing calcite precipitation, possibly due to locally elevated aquifer flow rates or establishment of open system conditions with respect to CO_2 (6.5.2.3). The processes of iron,

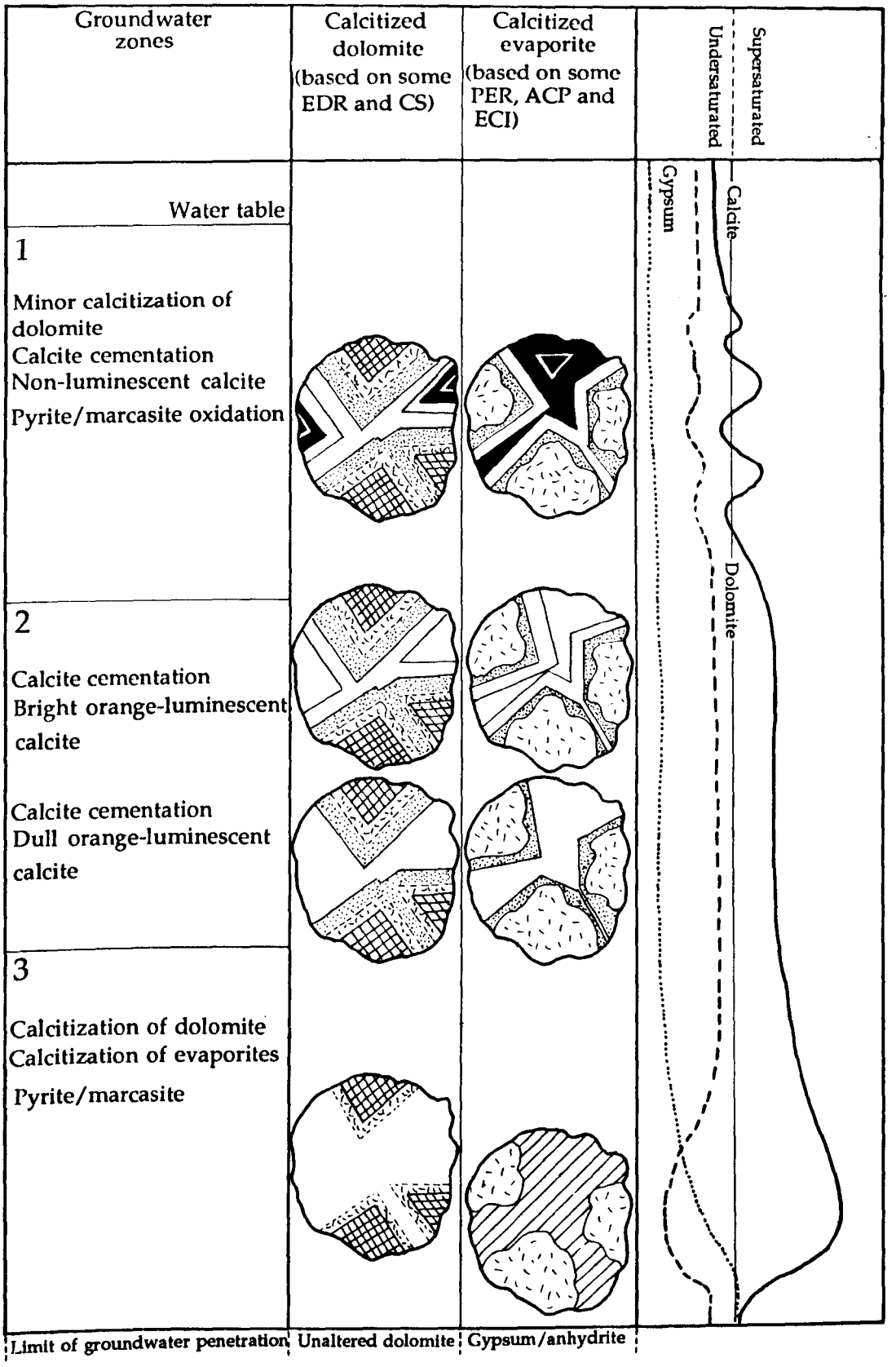

Fig. 6.41. Schematic diagram illustrating the textural changes in both calcitized dolomites and calcitized evaporites in relation to position within the Raisby Formation palaeoaquifer, and relative saturation states of calcite, dolomite and gypsum. Replacive calcite is denoted by flecks, dull orange-luminescent by stipple, bright orange-luminescent by plain white and non-luminescent calcite is black.

manganese and pyrite/marcasite oxidation are major oxygen-consuming reaction in this part of any aquifer (Edmunds *et al.*, 1982) (6.5.5.1).

6.4.1.2. Groundwater zone 2 (deeper aquifer).

The transitional area between groundwater zones 1 and 3 is characterized by passive pore fill non-luminescent/luminescent calcite cementation, with little calcitization of dolomite, in groundwaters close to saturation with respect to dolomite and slightly supersaturated with respect to calcite. Accordingly, most calcites are coarse and equant, suggestive of slow growth from fluids of relatively low supersaturation. Congruent dolomite dissolution to produce most LC textures, and gypsum dissolution may be operative in the lower parts of this zone.

6.4.1.3. Groundwater zone 3 (distal aquifer).

The transition into groundwater zone 3 is marked by an increase in fluid Ca/Mg ratio, undersaturation with respect to dolomite, supersaturation with respect to calcite (owing to calcium input from gypsum dissolution), and an approach towards saturation with respect to calcium sulphates (Fig. 6.41). With regard to calcitization of dolomite, although the end products are different (EDR and CSa calcitization textures), replacement was probably operative in the same, distal parts of the aquifer.

The most important style of dolomite calcitization (EDR) is directly related to the dissolution of calcium sulphates, producing, on a large scale, collapse breccias. Input of Ca, and so high fluid Ca/Mg ratios, are the most significant factors. Calcitization in such an environment has been thoroughly described by Back *et al.*, (1983):

$$CaCO_3 + H_2O + CO_2 \rightarrow Ca^{2+} + 2HCO_3^-$$

Calcite

$$CaSO_4.2H_2O \rightarrow Ca^{2+} + SO_4^{2-} + 2H_2O$$

Gypsum

$$CaMg(Fe,Mn)(CO_3)_2 + 2H_2O + 2CO_2 \rightarrow Ca^{2+} + Mg^{2+} + Fe^{2+} + Mn^{2+} + 4HCO_3^-$$

Dolomite

$$3Ca^{2+} + Fe^{2+} + Mn^{2+} + 6HCO_3^- \rightarrow Ca(Fe,Mn)CO_3 + 3HCO_3^- + 3H^+$$

Calcite

$$Mg^{2+} + SO_4^{2-} \rightarrow MgSO_4$$

(modified from Back *et al.*, 1983).

The end products are thus dull orange-luminescent calcite and Mg^{2+} with SO_4^{2-}, which may combine to form aqueous magnesium sulphate, a commonly suggested soluble by-product of dolomite calcitization associated with sulphate dissolution.

However, with CSa (zone selective) calcitization textures, the reaction is dominantly that of calcite cementation associated with pyrite/marcasite precipitation and minor dolomite calcitization. The presence/former presence of iron sulphides demonstrates involvement of SO_4^{2-} derived from gypsum dissolution with subsequent sulphate reduction. This is not a widespread process, and is most likely restricted to isolated microenvironments (such as the Raisby Quarry breccias) in the distal parts of the aquifer, possibly associated with fluids of elevated temperature. The expression of dolomite calcitization within fluids of elevated Ca/Mg ratios from calcite, dolomite and gypsum dissolution of Back *et al.*, (1983) may be modified for the isolated microenvironments of groundwater zone 3:

$$CaSO_4.2H_2O \rightarrow Ca^{2+} + SO_4^{2-} + 2H_2O$$

Gypsum

$$CaMg(Fe,Mn)(CO_3)_2 + 2H_2O + 2CO_2 \rightarrow Ca^{2+} + Mg^{2+} + Fe^{2+} + Mn^{2+} + 4HCO_3^-$$

Dolomite

$$2Ca^{2+} + Mn^{2+} + 4HCO_3^- \rightarrow 2Ca(Mn)CO_3 + 2HCO_3^- + 2H^+$$

Calcite

$$2SO_4^{2-} + Fe^{2+} + 2CH_2O + 6H^+ \rightarrow FeS_2 + 2HCO_3^- + 4H_2O$$

Pyrite/marcasite

Bacterial sulphate reduction, as expressed in the last line of the above formula, and as evidenced from CSa calcitized dolomites, requires strongly reducing conditions coupled with an input of organic matter and sulphate-reducing bacteria (6.2.2). In the distal parts of one mixed carbonate-siliciclastic aquifer described by Edmunds *et al.*, (1982), reduced sulphate was derived from the dissolution of gypsum, demonstrating that sulphate reduction was coincident with gypsum dissolution. Edmunds *et al.*, (1982) also showed that calcite cementation occurred in the same part of the aquifer.

The calcitization of dolomite in groundwater zone 3 most likely took place in a similar relative location as most calcitization of sulphate evaporites, although calcitization of gypsum/anhydrite took place prior to, and during sulphate dissolution. The diagenetic fluids during gypsum/anhydrite calcitization must have been supersaturated with respect to calcite, precipitating bright orange-luminescent replacive calcite in association with iron

sulphides during bacterial sulphate reduction (PER, ACP, and some ECI calcitized sulphates). However, the cessation of some calcitization immediately prior to non-luminescent calcite precipitation (although possibly separated by a substantial hiatus [some ECI textures and some GC cavities]) suggest that calcitization may have continued, at least locally, through a substantial part of groundwater zone 2. There are no equivalents to the near-surface style of dolomite calcitization, owing to the rapid decrease in gypsum saturation with depth (Fig. 6.41).

6.5.1. Pore filling calcite cements - Introduction.

Two types of late diagenetic calcite cements have been identified within the Raisby Formation, on the basis of their petrography and geochemistry:

1. Luminescent equant and non-luminescent columnar calcite cements occluding porosity formed by the dissolution of sulphates, and some breccia porosity,
2. Fine columnar speleothem calcites which coat joints and fractures, and cement interclast porosity within dolostone breccias.

The petrography and geochemistry of both types will be described in turn.

6.5.1.1. Petrography of luminescent equant and non-luminescent columnar calcite cements - Description

Calcite-lined and, less commonly, calcite-filled cavities after the dissolution of sulphate evaporites are ubiquitous within the Raisby Formation, and most other English Zechstein carbonates at outcrop. The porosity is most easily recognized as large cavities, millimetres to centimetres in size (Fig. 5.24a), although fracture porosity, and on a microscopic scale mouldic, intercrystalline, and intracrystalline porosity is equally as important. Locally, similar calcites occlude inter-clast porosity within dolostone breccias of various origins (Lee and Harwood, 1989). Sulphates have been almost completely dissolved from within Raisby Formation carbonates at outcrop and in shallow onshore boreholes (Fig. 5.30). The intensity of calcite cementation of these pores decreases with depth below the surface such that, within dolostones, cavities well cemented by calcite at outcrop pass into open cavities with no cement and into dolostones with gypsum remaining in shallow onshore boreholes (Fig. 5.30). The extent of calcite fill of cavities after sulphates is also commonly dependant on the nature of the host carbonate. Cavities after sulphates within porous dolostones at outcrop have a well developed, thick calcite rind, whereas those within less permeable limestones commonly do not contain calcite cements, and may even still host gypsum (Fig. 5.24b). The intensity of sulphate dissolution may also vary within one locality, for example the Hurworth Place borehole (NZ 2902, 0953) (Appendix XII), whereby the lower part of the Raisby Formation contains no sulphate, open pores and limited luminescent calcite cement, although upper levels of the core host nodules of gypsum.

Most calcite cements occluding sulphate dissolution porosity are equant (rhombohedral), dull/bright orange-luminescent, a few hundred microns in size, and present euhedral terminations into pores. The pores may be lined by only one generation of luminescent equant calcite, or the equant cements may be overlain by coarser (few millimetres in size), dominantly non-luminescent columnar calcites. Most cavities are completely lined by calcite, although, in some, the cements are thicker at the bases of the cavities. This may also be recognized from luminescence, with individual cement zones being considerably wider in lower parts of the cavities (Fig. 6.42b).

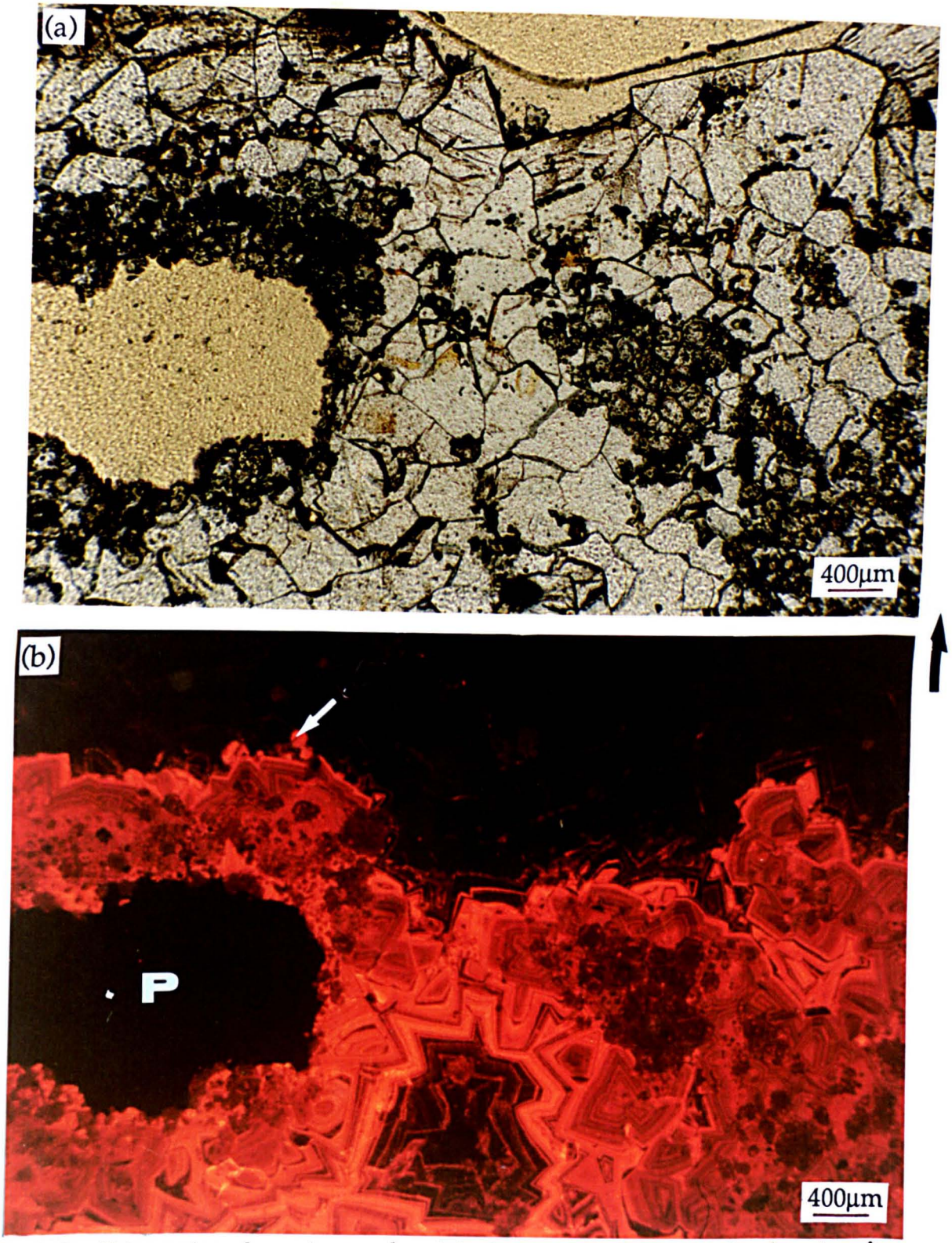

Fig. 6.42. Thin section photomicrographs of the lower part of a calcite lined cavity after sulphate, W.O.17 borehole, 83.52m; (a) plane light, (b) luminescence. The cement zones are considerably wider in the lower part of the cavity fill (b). Iron hydroxides encrust the junction of dull with bright orange-luminescent calcite in (a), either as a thin coating or a thicker crust comprising sub-spherical structures (arrowed). Bright orange-luminescent calcite fills the central pores of the spheres (arrowed). P denotes porosity. Arrow indicates way up.

Petrographically, the equant calcite cements are inclusion-free, apart from scarce dolomitic internal sediments at zone boundaries. Overlying columnar calcites commonly contain numerous layers of geopetal internal sediments, of greatly variable thickness (Fig. 6.43), and which in general, decrease in thickness through the growth of columnar crystals. Internal sediments are rarely randomly distributed through the columnar cements, and are commonly concentrated in discrete horizons, especially at their contact with equant calcite (Fig. 6.43), although by no means all equant-columnar crystal contacts are demarcated by internal sediments. Lee and Harwood (1989, figure 12b) describe internal sediments of fluorite at the contact of equant luminescent with non-luminescent columnar calcites from Chilton Quarry (NZ 302, 341). The internal sediment layers describe crystal faces, and are concentrated between crystal terminations. In most cases, sediment input disrupted crystal growth, although it did not alter the growth axes of the columnar calcites (Fig. 6.43).

Dissolution surfaces are also common within cement sequences. They may be irregular or undulate, unrelated to crystal structure, or parallel to zonation. The irregular or undulate surfaces commonly demarcate the contact of luminescent equant with non-luminescent columnar crystals (Fig. 6.44), whereas the zone-selective dissolution occurs within specific zones of luminescent calcites. Zone-selective dissolution porosity may or may not be occluded by a later calcite cement, commonly non-luminescent. The zone-selective style is similar to dissolution textures developed within zoned dolomite at outcrop.

Iron minerals are common within calcite cements, encrusting former crystal faces (which may or may not be corroded) (Fig. 6.44), and occurring along the contact of equant calcite cements with dolostone host rocks. Iron in association with equant calcites is most commonly pyrite/marcasite and/or hematite after pyrite/marcasite, whereas that encrusting former crystal faces (mainly equant luminescent with non-luminescent columnar calcites) comprises goethite and/or other finely crystalline iron hydroxides (6.44, 6.45 & 6.46a). Hematite after pyrite/marcasite is more common in calcites associated with calcitized dolomite/sulphate evaporites than passive pore filling cements.

Some non-luminescent columnar calcites contain small (10-50μm long) elongate, upwards-tapering fluid/gas-filled inclusions. The inclusions are parallel to the C-axis of their host crystal (Fig. 6.46b), and were only recorded where in direct association with fine dolomitic internal sediments. They appear to have 'grown' off the internal sediment grains into the host calcite (Fig. 6.46b).

On a broad scale, luminescence sequences of calcites which occlude sulphate dissolution porosity are very similar, with an evolution from luminescent equant to non-luminescent columnar calcite (Lee and Harwood, 1989). However, the outer parts of equant crystals are commonly non-luminescent, and the basal parts, and subzones within columnar calcites may be bright orange-luminescent, although no entirely luminescent columnar calcites were recorded. Where associated with extensive calcitization of dolomite or

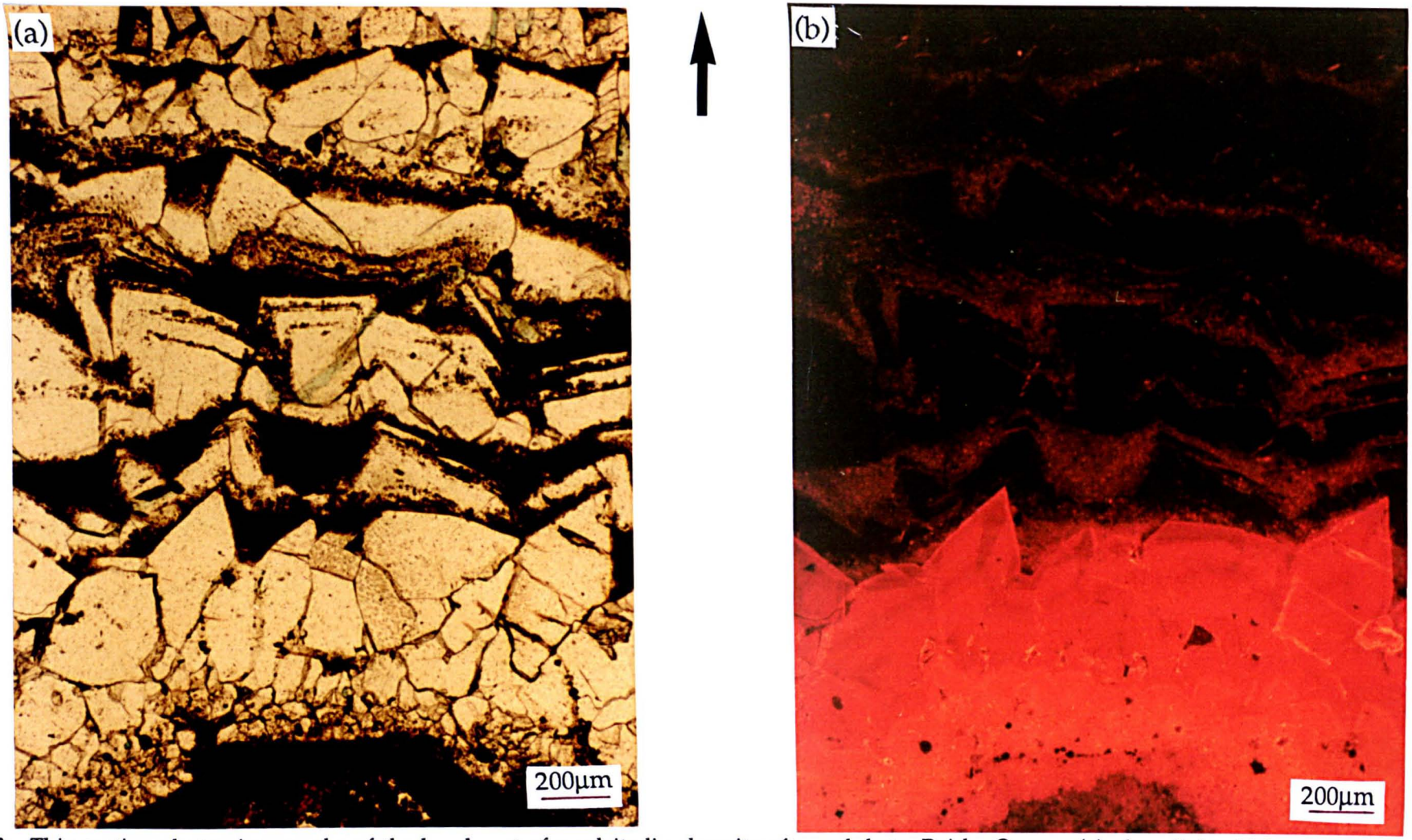

Fig. 6.43. Thin section photomicrographs of the basal part of a calcite-lined cavity after sulphate, Raisby Quarry; (a) plane light, (b) luminescence. The contact of luminescent with non-luminescent calcite is demarcated by the initial influx of geopetal dolomitic internal sediments. The contact is also encrusted by goethite (not shown). The internal sediments have disrupted the growth of columnar crystals, and internal sediment layers in general decrease in thickness upwards. Arrow indicates way up.

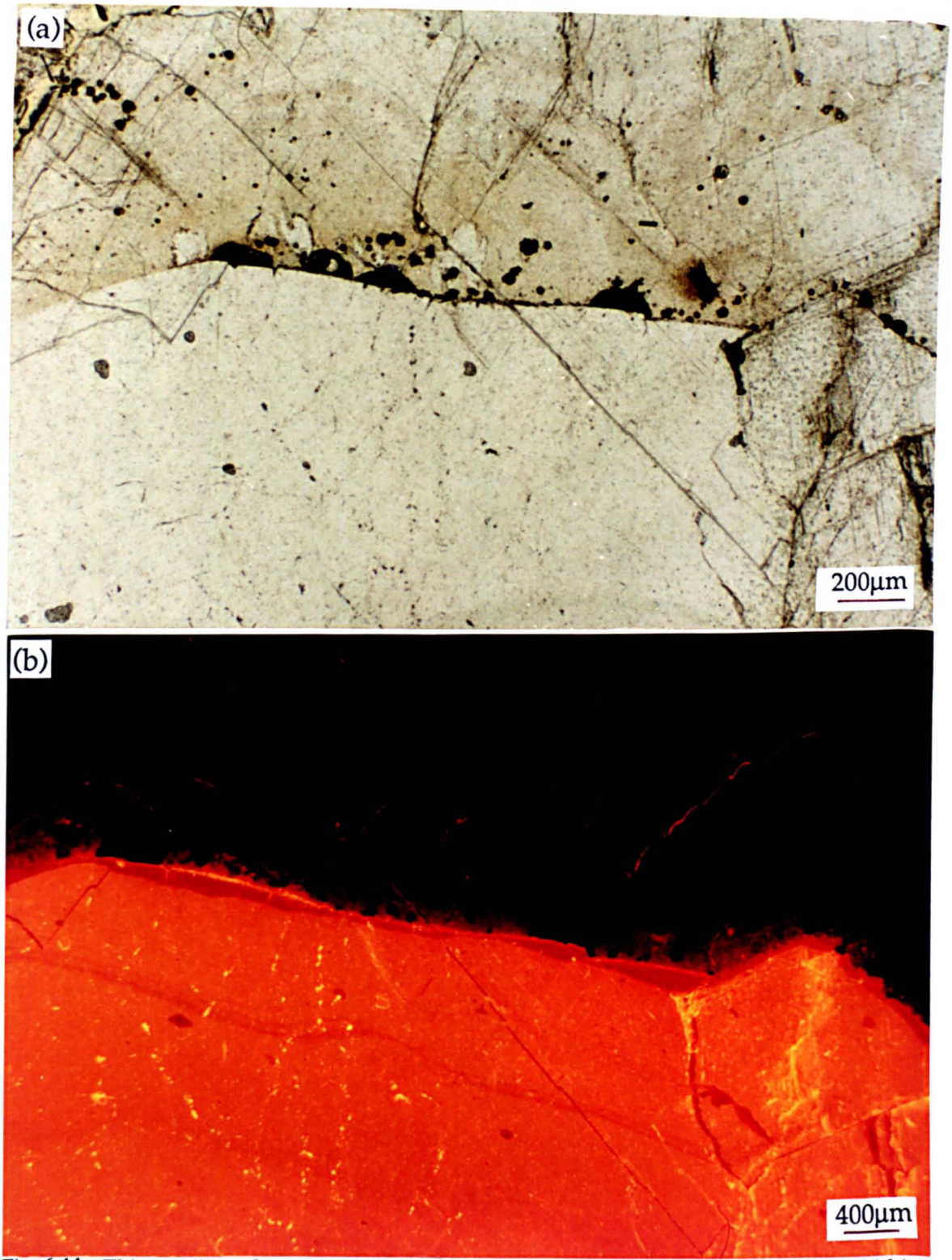

Fig. 6.44 . Thin section photomicrographs of calcite cementing inter clast porosity within a compaction breccia, Houghton Quarry; (a) plane light, (b) luminescence. There are two episodes of corrosion evident, one between bright and dull orange-luminescent calcite and the other between dull orange- and non-luminescent calcite cement. The contact of dull orange- with non-luminescent calcite is encrusted by hemispherical bundles of goethite needles. Note the distinct change in crystal habit between luminescent and non-luminescent calcite. The bright orange-luminescent calcite itself host iron sulphides (not shown) (Fig. 6.67a).

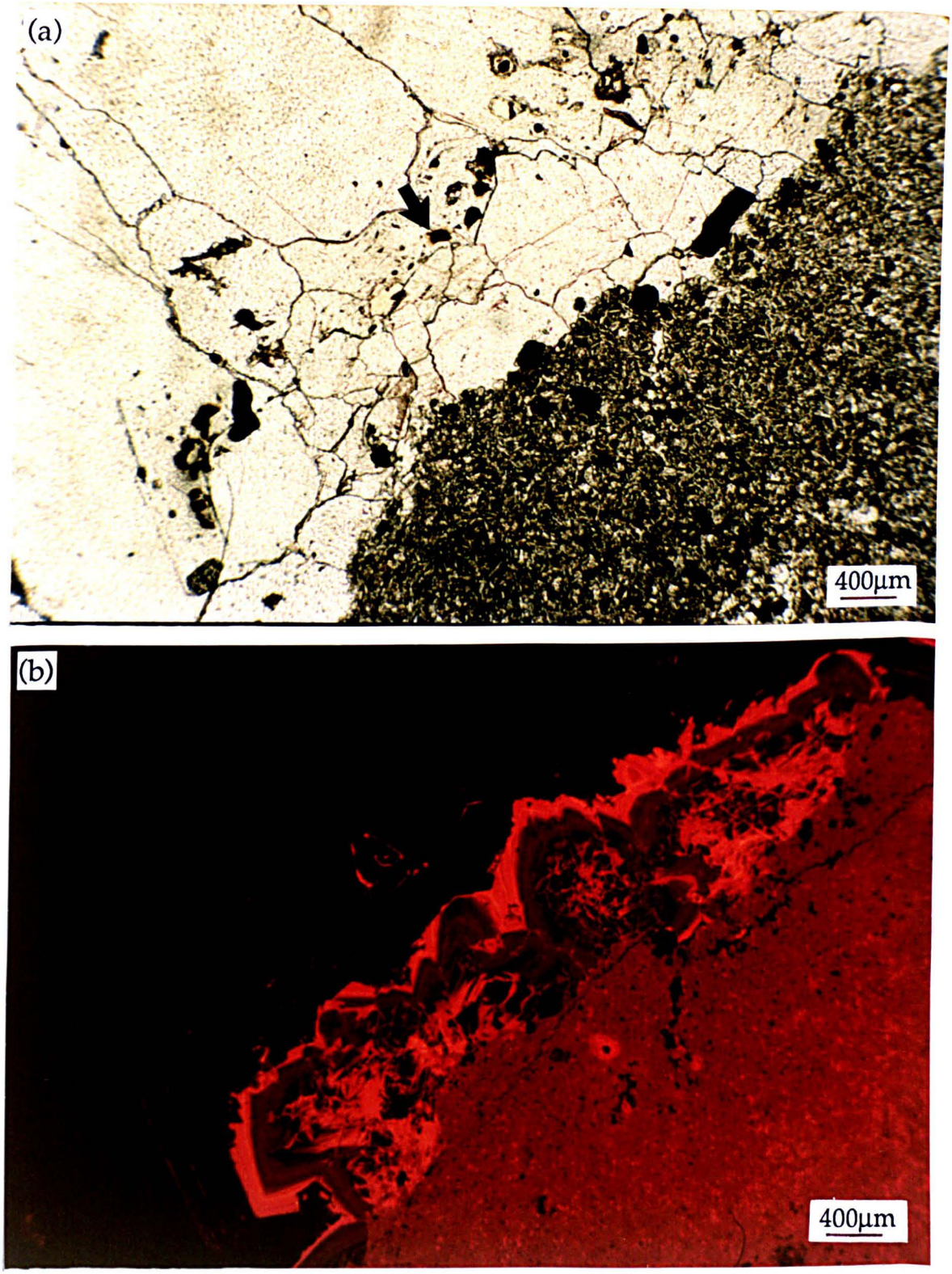

Fig. 6.45. Thin section photomicrographs of the contact between dolostone host rocks and calcite lining a cavity after sulphate, Rough Furze Quarry; (a) plane light, (b) luminescence. Hematite after pyrite/marcasite encrusts the dolostone-calcite cement contact, and goethite needle bundles occur at the corroded junction between bright orange- with non-luminescent calcite (arrowed). The core zone of the luminescent calcite is possibly replacive after anhydrite (PER) texture. A goethite bundle in the center of the field of view (arrowed) is illustrated in fig. 6.67b.

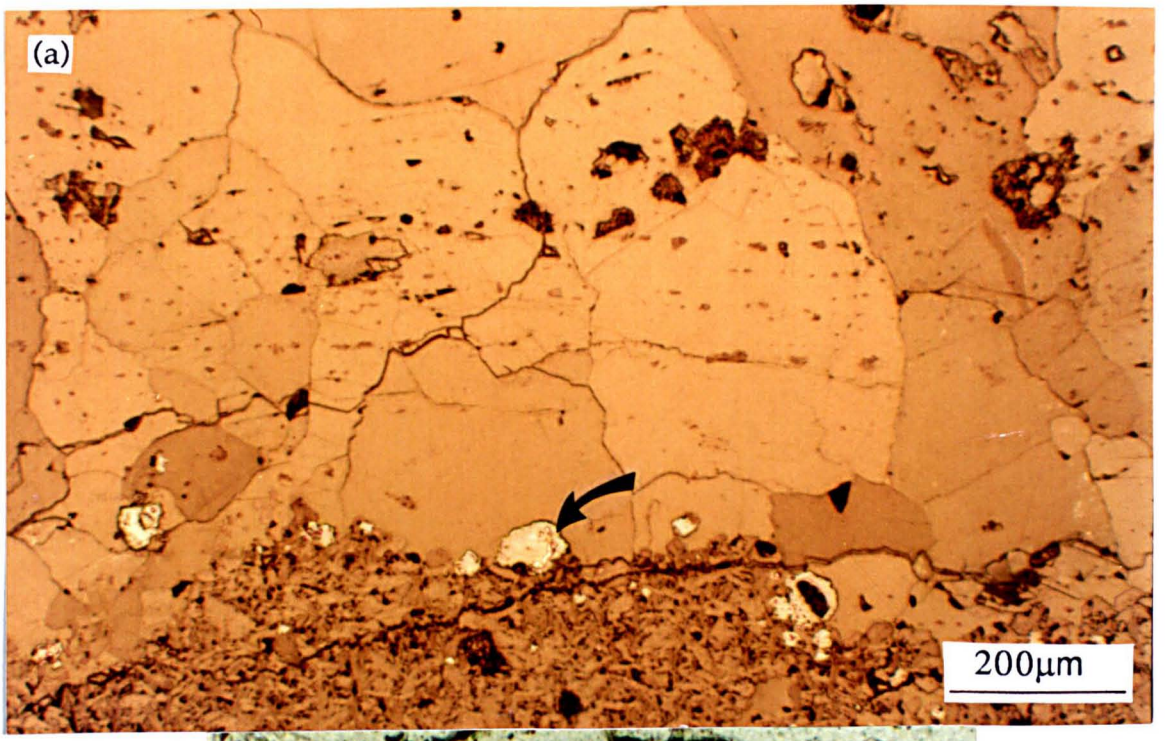

Fig. 6.46. Thin section photomicrographs of calcite cements within cavities after sulphates. (a) shows a field of view similar to fig. 6.45, in reflected light. Silver-reflecting hematite crystals contain inclusions of iron sulphides (arrowed). (b) illustrates thorn shaped fluid/gas filled inclusions within a non-luminescent columnar calcite crystal from a cavity after sulphate, Raisby Quarry. Plane light.

sulphates (and pyrite/marcasite), equant cements tend to be dominated by bright orange-luminescent calcite. Within cavities with no such processes, the cement stratigraphies show an evolution from dull orange- to bright orange- into non-luminescent equant calcite (Lee and Harwood, 1989, fig. 14). In detail, the exact sequence of cements, and the relative abundance of individual zones is variable, although the aforementioned evolution is dominant (Fig. 6.47). Hairline bright orange-luminescent subzones are abundant within non-luminescent calcites, and are concentrated close to the top of underlying luminescent cements, decreasing in abundance through the columnar crystals (Fig. 6.47). Boundaries between concentric luminescent cement zones may be gradational, or more commonly abrupt, whereas the contacts of luminescent with non-luminescent calcite is nearly always abrupt (Fig. 6.47). Sector zones are locally abundant within bright orange-luminescent zones of equant calcites, most commonly of the fir-tree type (Appendix II). The typical cement sequence within a cavity after sulphate is illustrated in figure 6.48.

6.5.1.2. Geochemistry of luminescent equant and non-luminescent columnar cements - Description.

Luminescent equant, and non-luminescent columnar calcite cements, plot within well constrained fields of Mg, Fe, Mn, and Sr. All cements analysed by microprobe contain less than 1.1 mole% $FeCO_3$ and 0.8 mole% $MnCO_3$, although Mg varies over a wider range, up to 4 mole% $MgCO_3$ (Figs. 6.49 & 6.50). In addition, Sr (analysed by ICP) varies from below detection limits up to 424ppm, although most analyses are below 200ppm Sr (Fig. 6.50). Non-luminescent calcites contain considerably less Fe, Mn and Sr than the luminescent, although are relatively enriched in Mg (Fig. 6.49 & 6.50) (Appendix I). Distinct compositional populations may also be defined within luminescent calcites, between which few cements occur (Fig. 6.49). These populations relate very well to luminescence characteristics (Appendix I). Microprobe traverses through two contrasting equant luminescent to non-luminescent columnar cement sequences are illustrated in figures 6.51 & 6.52. An ideal geochemical profile through an equant luminescent to columnar non-luminescent cement sequence is shown in figure 6.53.

Carbon and oxygen stable isotope data for all calcite cements within cavities after sulphates, plot into three well-defined groups, comprising two luminescent populations, and one population of wholly non-luminescent columnar calcite (Fig. 6.54a). One of the luminescent populations comprises three samples of dull and bright orange-luminescent cements from breccias at Raisby Quarry, which have highly negative carbon and oxygen values, and plot in a very similar area as ECI calcitized evaporites from the same locality (Fig. 6.54b). Non-luminescent columnar cements from these breccias, separated from luminescent calcite by multiple layers of dolomitic internal sediments, plot in an area of similar $\delta^{13}C$ although considerably lower $\delta^{18}O$ (Fig. 6.54a). This is in the same area as other

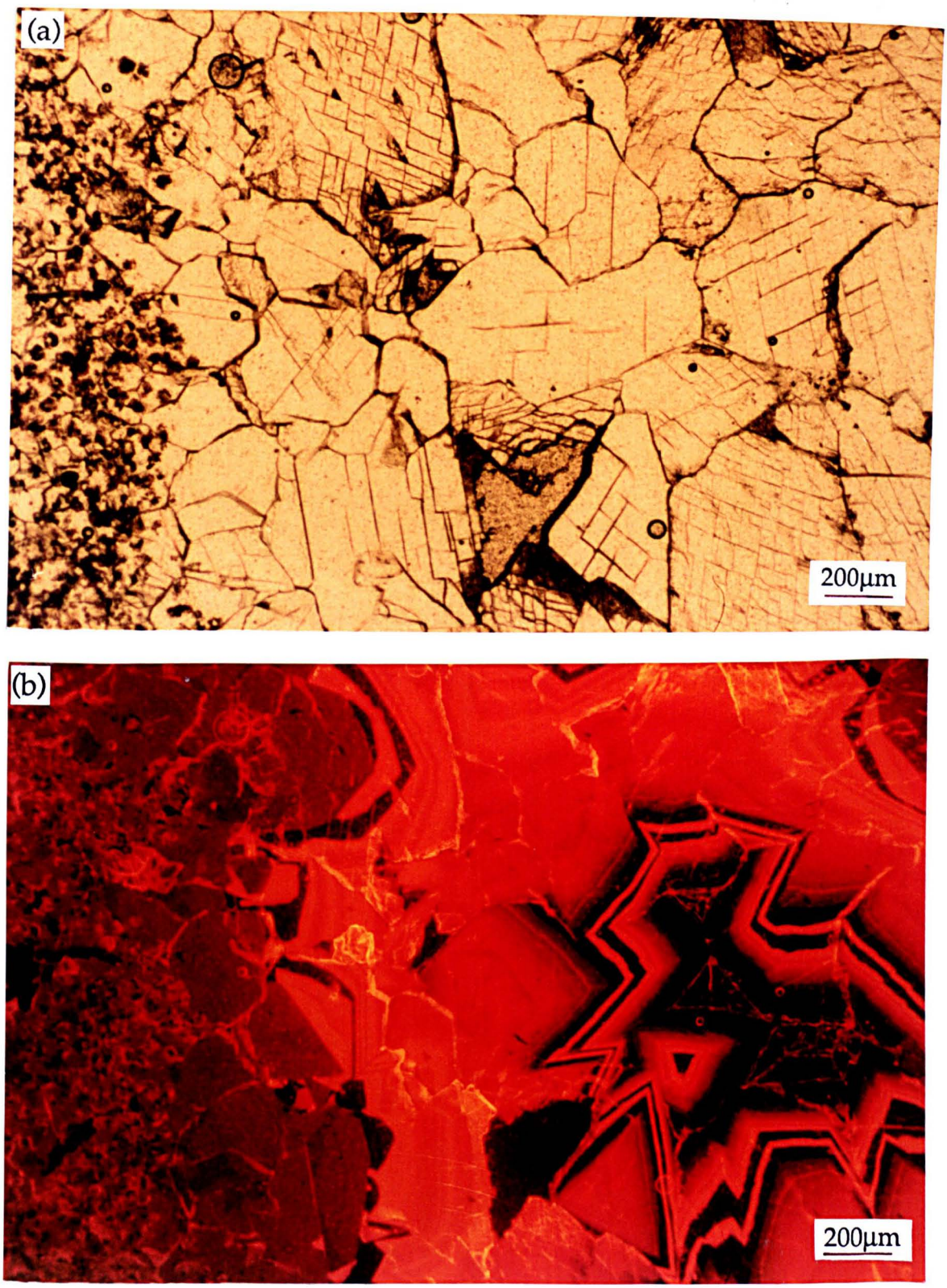

Fig. 6.47. Thin section photomicrographs of calcite lining a cavity after sulphate, Man Haven; (a) plane light, (b) luminescence. In this cavity, the bright orange-luminescent subzones are atypically thick and numerous at the contact of bright orange- with non-luminescent calcite.

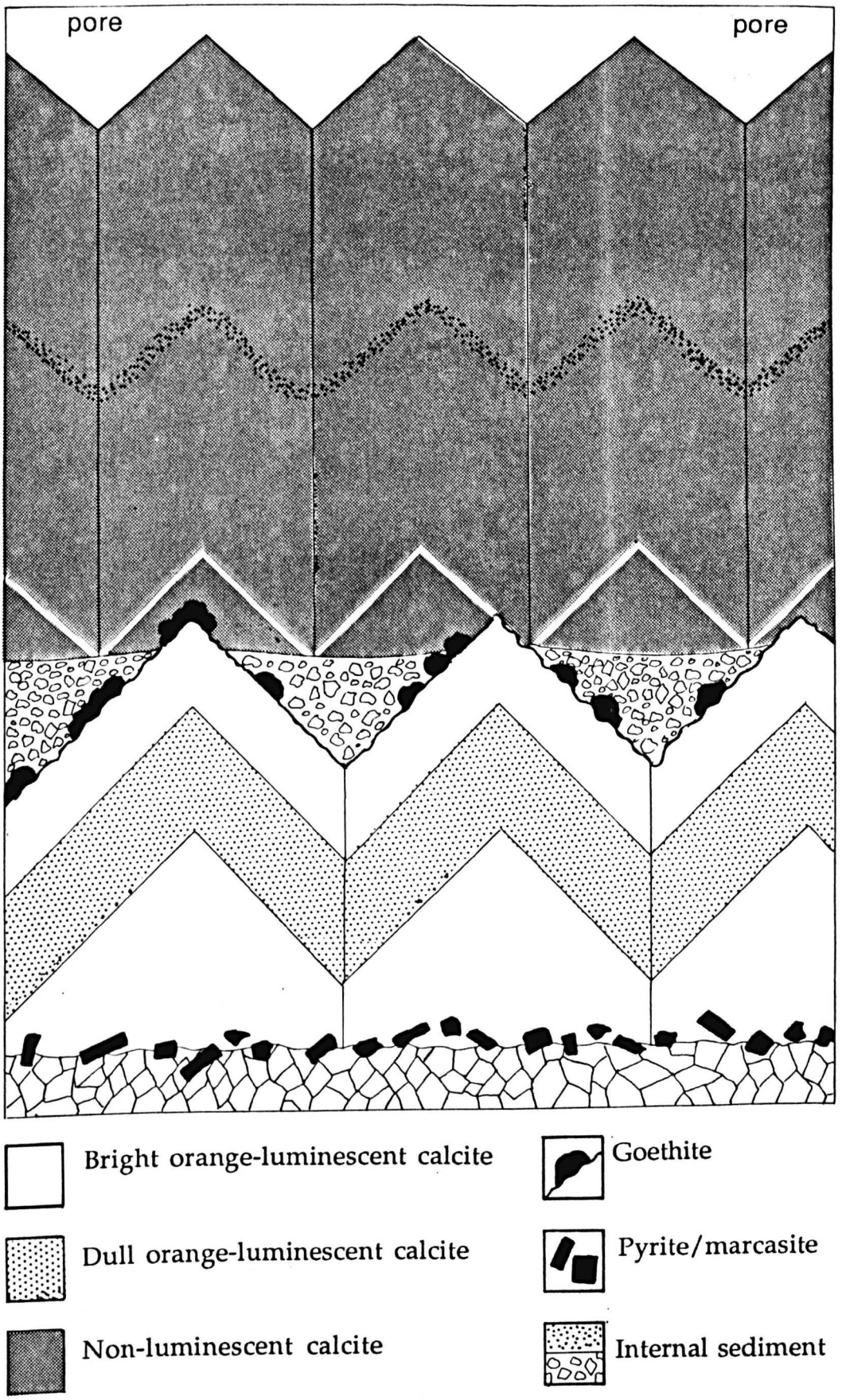

Fig. 6.48. Schematic diagram showing an ideal calcite cement sequence occluding a cavity after sulphate. In detail, very few cavity-fills have all of these features, although the luminescent to non-luminescent evolution is common to most.

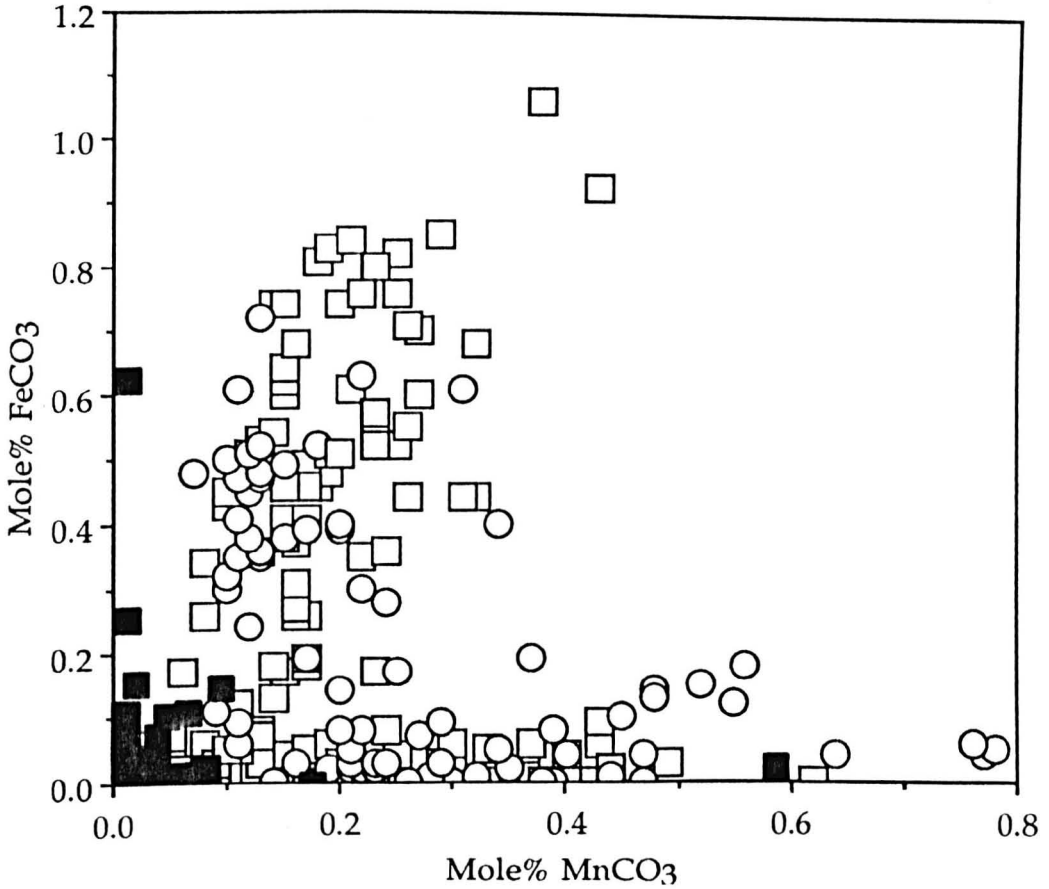

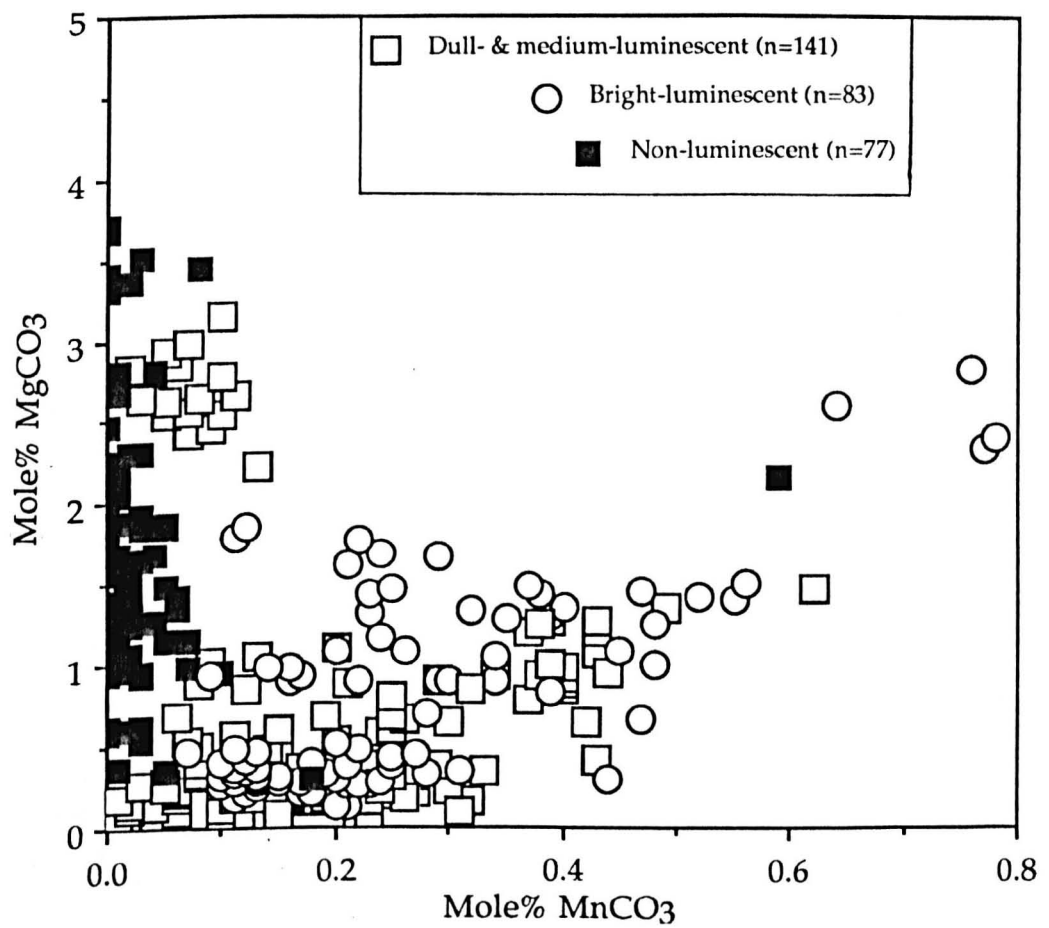

Fig. 6.49. Graphs illustrating all microprobe results for calcite cements analysed from within cavities after sulphates. The two populations of luminescent cements defined by Fe and Mn data correspond to medium and dull orange- and bright orange-luminescent calcite for the populations with positive and negative Fe/Mn ratios respectively. Bright orange-luminescent equant cements, and bright orange-luminescent hairline subzones within non-luminescent calcites are grouped together. See 6.5.2.4. for the distinction of these calcites.

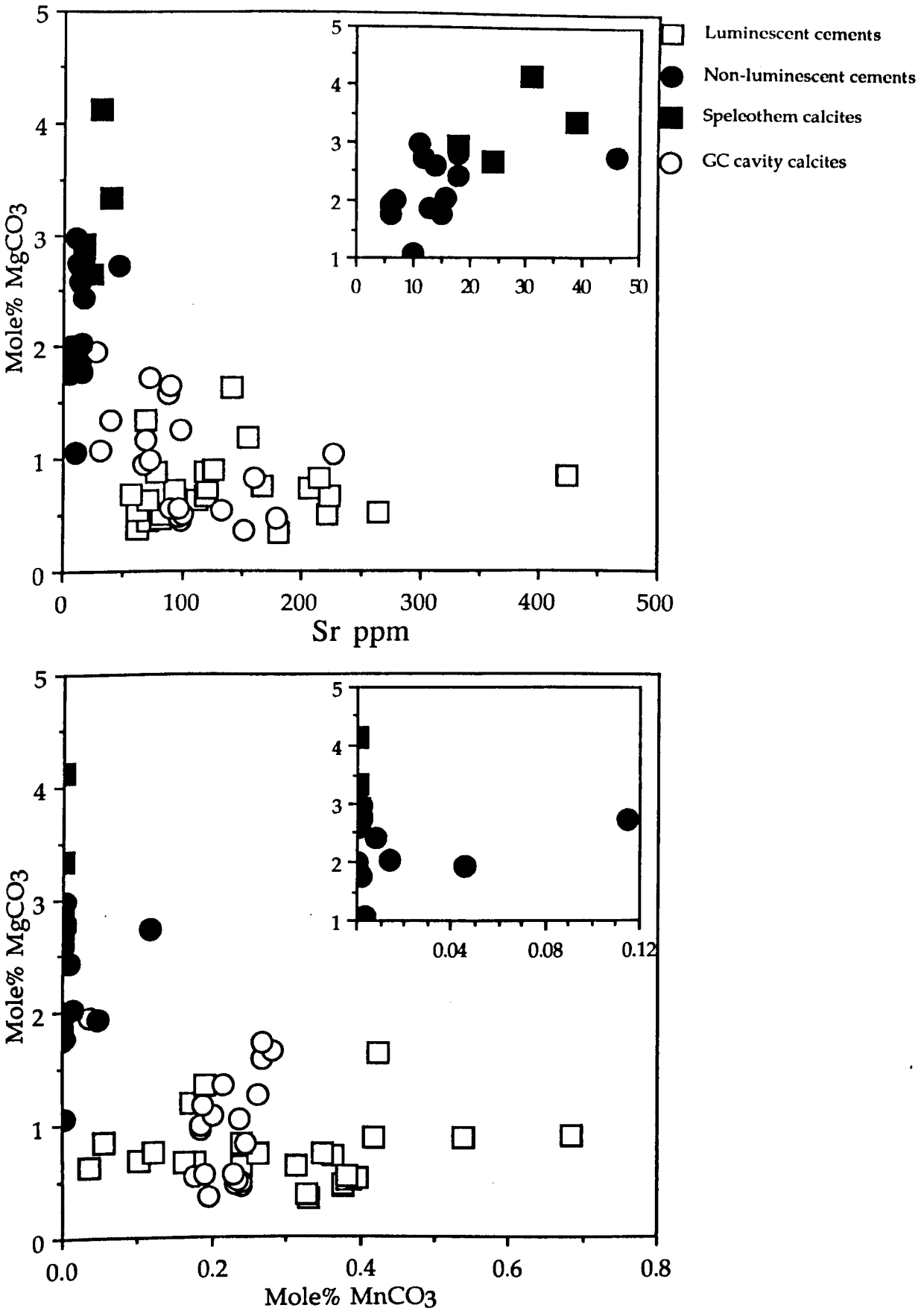

Fig. 6.50. Graphs illustrating all ICP results for calcites within cavities after sulphates and speleothem calcites. Insets show details of composition of non-luminescent columnar and speleothem calcites.

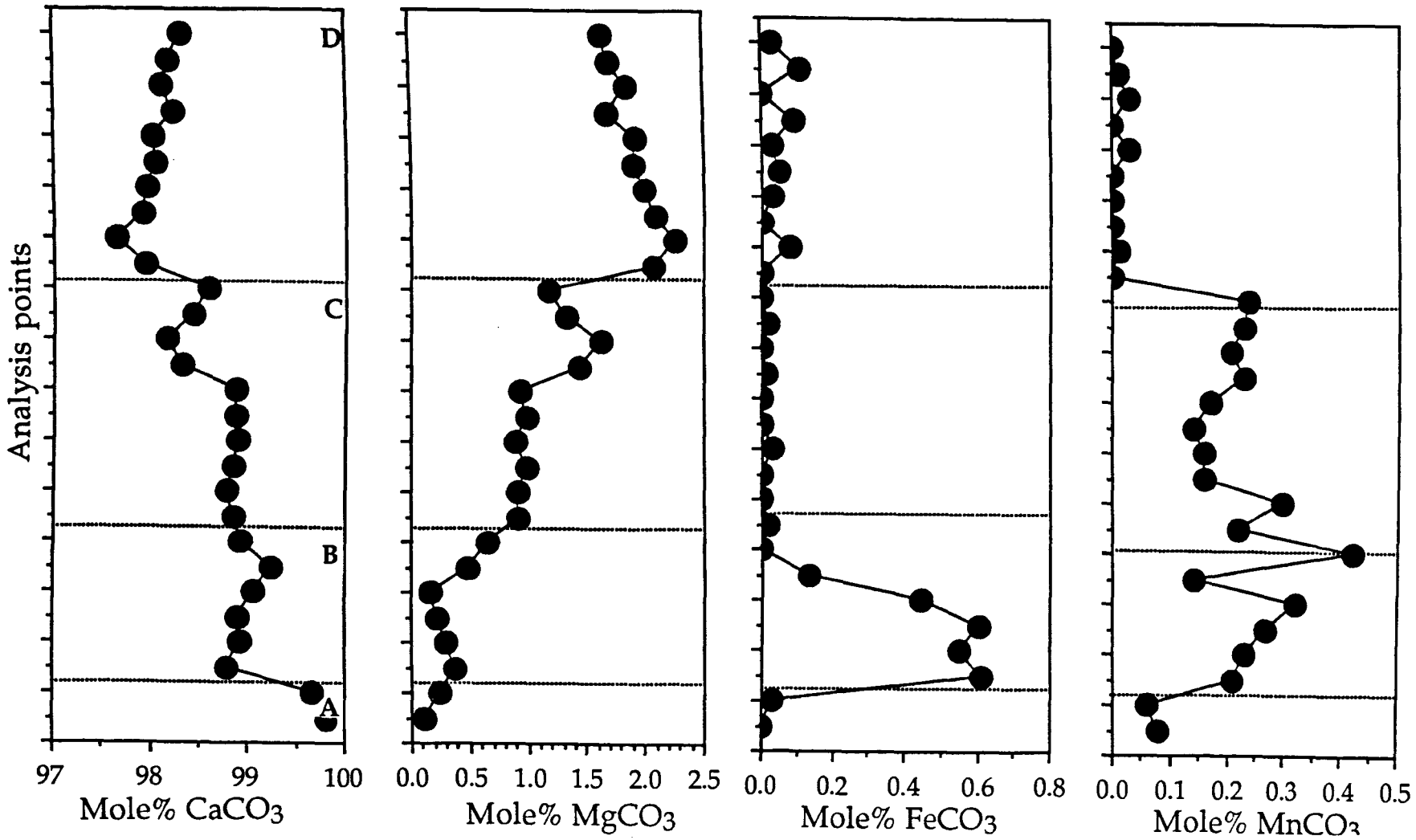

Fig. 6.51. Graphs illustrating the geochemical variation along a microprobe traverse from non-luminescent (A), through dull orange- (B), into bright orange- (B) and non-luminescent calcite (C). Sample from a calcite lined cavity after sulphate, Houghton Quarry (see Lee and Harwood, fig. 14). The basal non-luminescent calcite (A) is a cemented pore after dissolved relic dolomite or anhydrite.

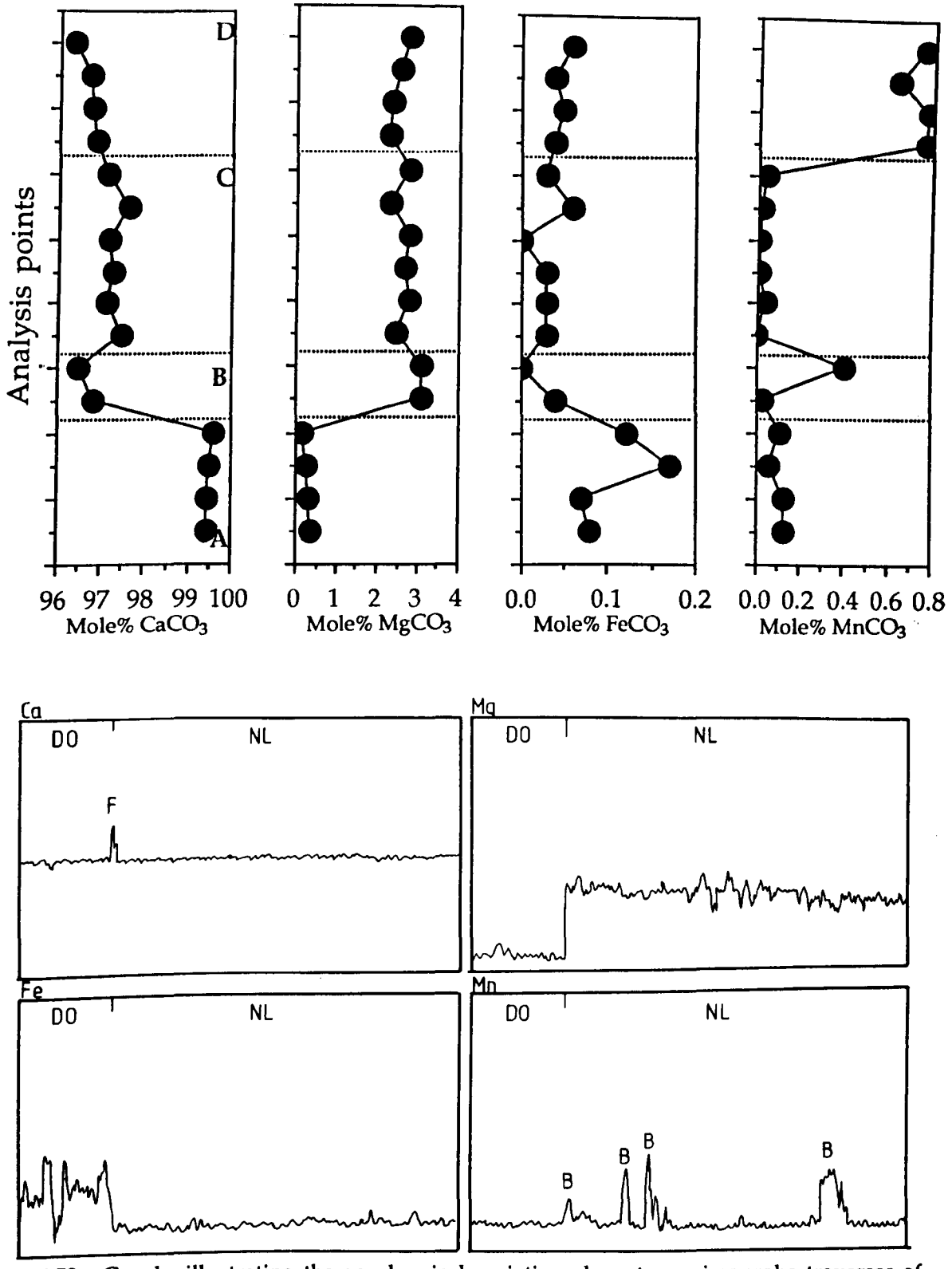

Fig. 6.52. Graphs illustrating the geochemical variation along two microprobe traverses of calcite lining a cavity after sulphate, Chilton Quarry. The upper four graphs are a point traverse from dull orange (A), through non-luminescent calcite with very abundant hairline bright orange-luminescent subzones (B), into non-luminescent columnar calcite (C), and a thick bright orange-luminescent hairline subzone (D). The lower four graphs illustrate a semi-quantitative line traverse through the same cement sequence, from dull orange- (DO) into non-luminescent calcite (NL). F denotes a breccia of fluorite at the contact of dull orange- with non-luminescent calcite, and B bright orange hairline subzones.

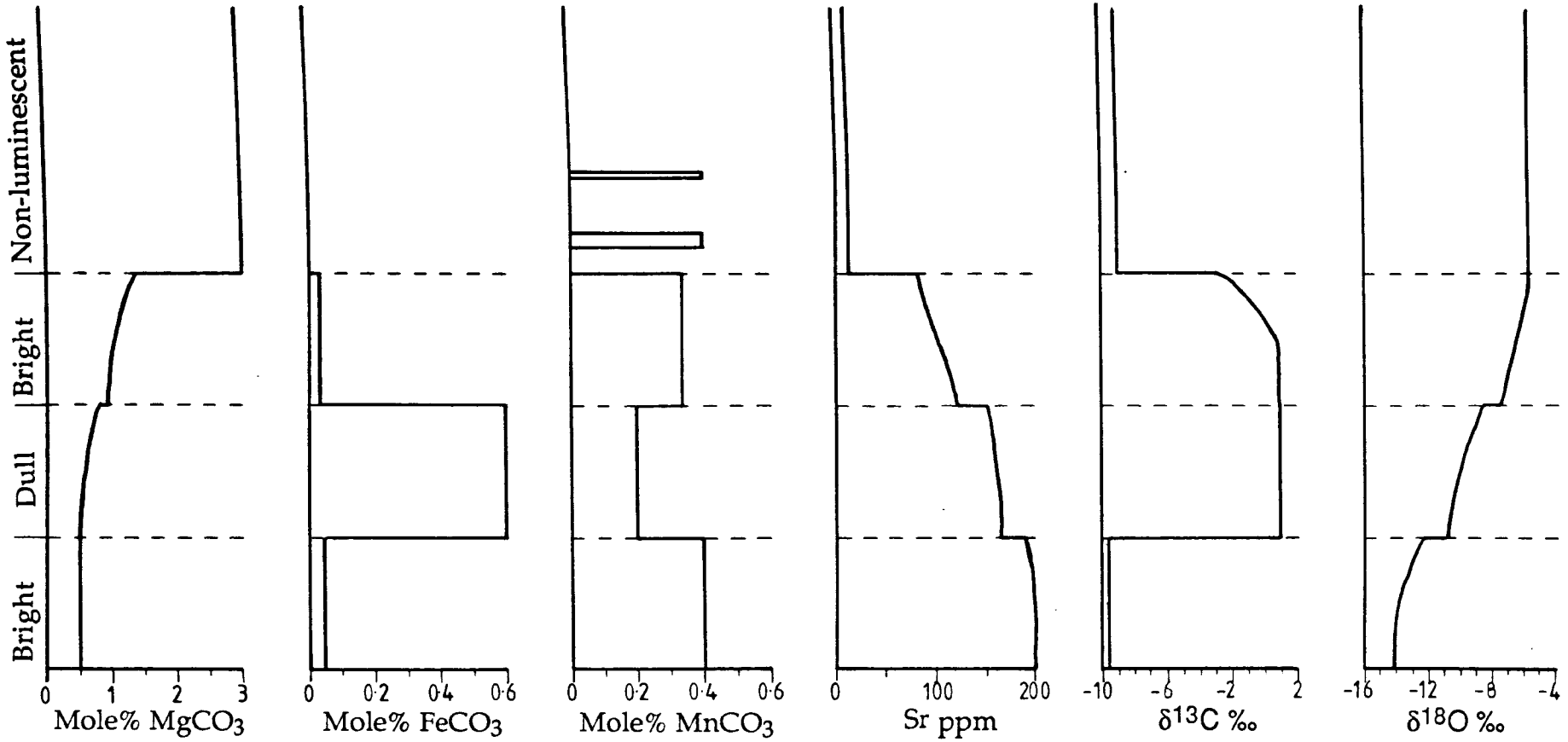

Fig. 6.53. Graphs illustrating the expected changes in geochemistry which would accompany a transect through an ideal calcite cement sequence lining a cavity after sulphate (Fig. 6.57). The values are based on measured cement geochemistries, but are not exact. Note, the geochemical variation is abrupt in steps, not gradational. Sr data is compiled from large, easily distinguished cements analysed by ICP, and not analysis of one cement sequence from a single pore.

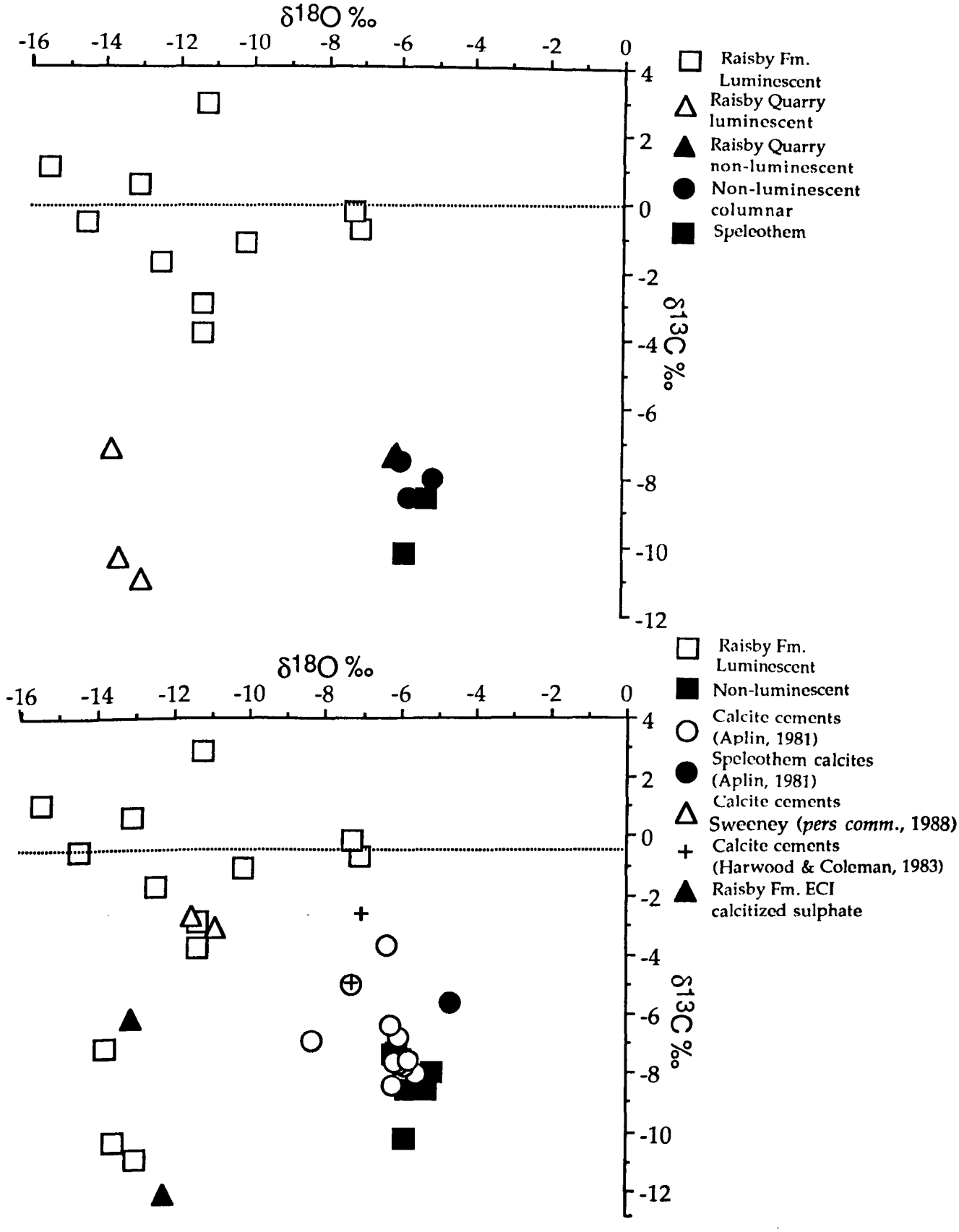

Fig. 6.54. Graphs showing the isotopic compositions of calcite cements within the Raisby Formation (top), and this data combined with the isotopic composition of calcitized evaporites within the Raisby Formation, other analyses of calcite cements from the Raisby Formation, and calcite cements from the Cadeby and Ford Formations (bottom).

Raisby Formation non-luminescent columnar calcites, which together define the second population. The third cement population is more diffuse, made up of equant luminescent cements with generally low negative $\delta^{13}C$ and variably negative $\delta^{18}O$ (Fig. 6.54a). At least part of the variability is due to the difficulties in separating dull and bright orange-luminescent zones of the equant cements. Isotope data from calcite cements filling cavities after sulphates within the Ford Formation main reef (Aplin, 1981) and from the Raisby Formation at Quarrington Quarry (NZ 327, 379) (M. Sweeney, *pers. comm.*, 1988) plot between the non-luminescent and the larger of the luminescent calcite populations (Fig. 6.54b).

6.5.1.3. Petrography and geochemistry of speleothem calcite cements - Description

All speleothem calcites occur within large, open pores. They are characterised by milky-white crusts on dolostone host rocks. Two types of speleothem calcite may be defined:

Type 1. Joint-coating

Encrusting vertical to sub-vertical joint/fracture surfaces,

Type 2. Breccia-cementing

Cementing coarse dolostone breccias which lie within large joints and fractures.

Joint-coating speleothem calcites are developed coating enlarged joints/fractures at Haswell Moor Farm (NZ 352, 246), Houghton (NZ 341, 506), Pittington (NZ 332, 447), and Running Waters (NZ 334, 404) Quarries. Speleothem calcites encrusting a joint face at Haswell Moor Farm Quarry have developed into spectacular stalactites (Fig. 6.55a). Internally, these stalactites are strongly colour banded, some layers incorporating thin (millimetre-scale) angular dolostone breccias with millimetre to sub-millimetre sized clasts. The dolostone breccias also incorporate fine quartz, and clasts of corroded, zoned luminescent calcite cements. However, most speleothem calcites form much thinner, centimetre-thick crusts. The sequence of calcites in any one sample is variable, owing to internal sedimentation and corrosion. Two subtypes of joint-coating speleothem calcites may be defined on the basis of the presence or absence of fluid/gas-filled thorn-shaped inclusions. In general, the inclusion-free calcites are coarser than those which contain inclusions, and commonly have well developed para-axial fabrics, with basal fine (tens of microns long) columnar calcites passing abruptly into coarser (commonly 1000μm long by 100-200μm wide) columnar calcites with planar compromise boundaries (Fig. 6.55b). Columnar crystals may incorporate fine (10-20μm) dolomitic internal sediments, randomly scattered through the calcites, or in specific layers. Small (tens of microns long) columnar crystals may grow off the dolomite internal sediments, but are soon engulfed by the larger host columnar calcites (Fig. 6.55b). These large columnar crystals commonly display an undulose extinction over approximately 15°. Any two adjacent columnar calcites go into

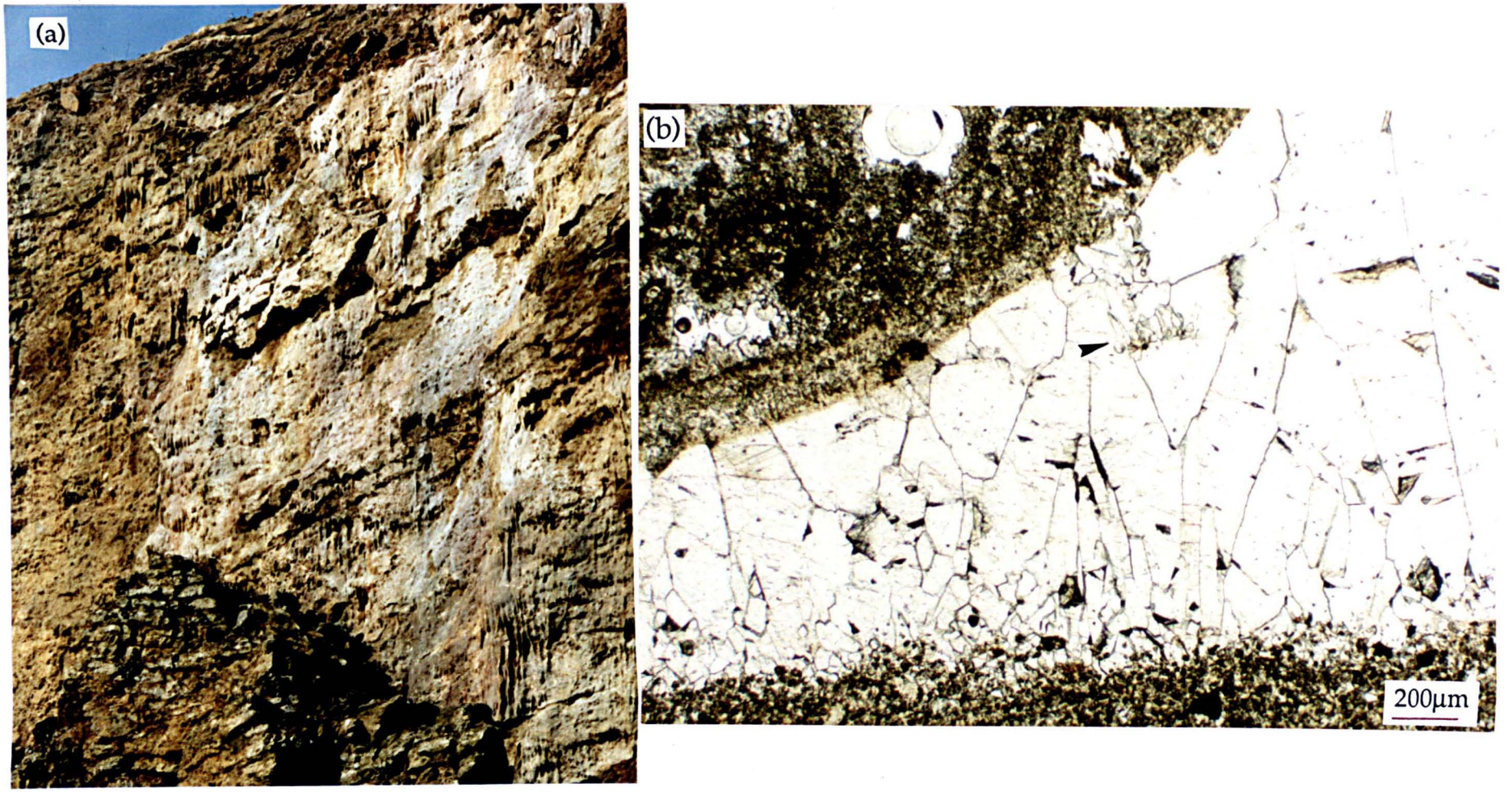

Fig. 6. 55. Joint-coating speleothem calcites. (a) stalactites encrusting a large solution-widened joint, Haswell Moor Farm Quarry. (b) inclusion-free coarse columnar calcites incorporating much smaller columnar calcite crystals which nucleated off fine dolomitic internal sediments (arrowed). The upper surface of the columnar crystals has been heavily corroded. Thin section, plane light, Houghton Quarry.

extinction at roughly the same point, which produces a sweeping extinction pattern overall. Along intercrystalline boundaries, small (mean 150μm) subequant calcites are common. They do not share the optic orientation of their host calcite, and two adjacent crystals do not have similar optic orientations. Similar crystals are also common in association with columnar calcites within concretions (Fig. 4.21a). These fluid/gas inclusion-free calcites are very similar to non-luminescent columnar calcites within cavities after sulphates. The fluid/gas inclusion-rich calcites are the last precipitates where recorded, although may be interlayered with numerous phases of dolomitic internal sediments. The fluid/gas-filled inclusions are very numerous, and elongate parallel to the C-axis of the host fine columnar calcite crystal. They are a few microns in length. Where present in sufficient density, they produce a distinct colour banding within the calcites (Fig. 6.56). Similar inclusions were recorded within coarse columnar calcites from cavities after sulphates associated with dolomitic internal sediments (Fig. 6.46b).

All speleothem calcites analysed were completely non-luminescent, although those encrusting a vertical joint face at Houghton Quarry, were underlain by a complex sequence of equant luminescent cements (Figs. 6.56 & 6.57). There are five cement phases developed, from fine (20-100μm) equant unzoned dull orange luminescent, through bright orange-luminescent calcite of similar size and shape, into non-luminescent equant calcite with bright orange hairline subzones, overlain by coarse (2-3mm) fluid inclusion-free columnar speleothem calcite, into layers of fluid inclusion-rich fine (300μm) columnar speleothem calcite alternating with internal sediments (Figs. 6.56 & 6.57). The dull, bright orange- and non-luminescent calcites have nucleated off brecciated dolostone and earlier luminescent cement clasts (Figs. 6.56b & 6.57b). The bright orange-luminescent calcite layer is abruptly overlain by non-luminescent calcite, although some non-luminescent calcite overgrows the outer parts of precursor bright orange-luminescent crystals (Fig. 6.56b). The non-luminescent equant calcite is distinctly brown stained and associated with very abundant intercrystalline iron hydroxides (Figs. 6.57a & 6.69a). Corrosion surfaces are common, and most pronounced between the coarse columnar non-luminescent calcite and a major phase of internal sediments (Fig. 6.55b).

The geochemistry of two joint-coating speleothem calcites, one from Haswell Moor Farm Quarry, the other from Houghton Quarry, were similar with 2.66-4.13 mole% $MgCO_3$, 18-39ppm Sr, and negligible Fe, Mn and non-carbonate trace elements (Fig. 6.50). Carbon and oxygen isotope analyses from the two localities gave comparable results, similar to speleothem calcites from the Ford Formation main reef, analysed by Aplin (1981) (Fig. 6.54b).

Breccia-cementing speleothem calcites were recorded from Cobblers Quarry (NZ 345, 449), Field House Quarry (NZ 354, 506), Haswell Moor Farm Quarry (NZ 352, 426), and Frenchmans Bay (NZ 3890, 6615). Dolostone clasts vary in size from millimetres to metres in diameter. They are very poorly sorted and angular. The breccias may have an open texture,

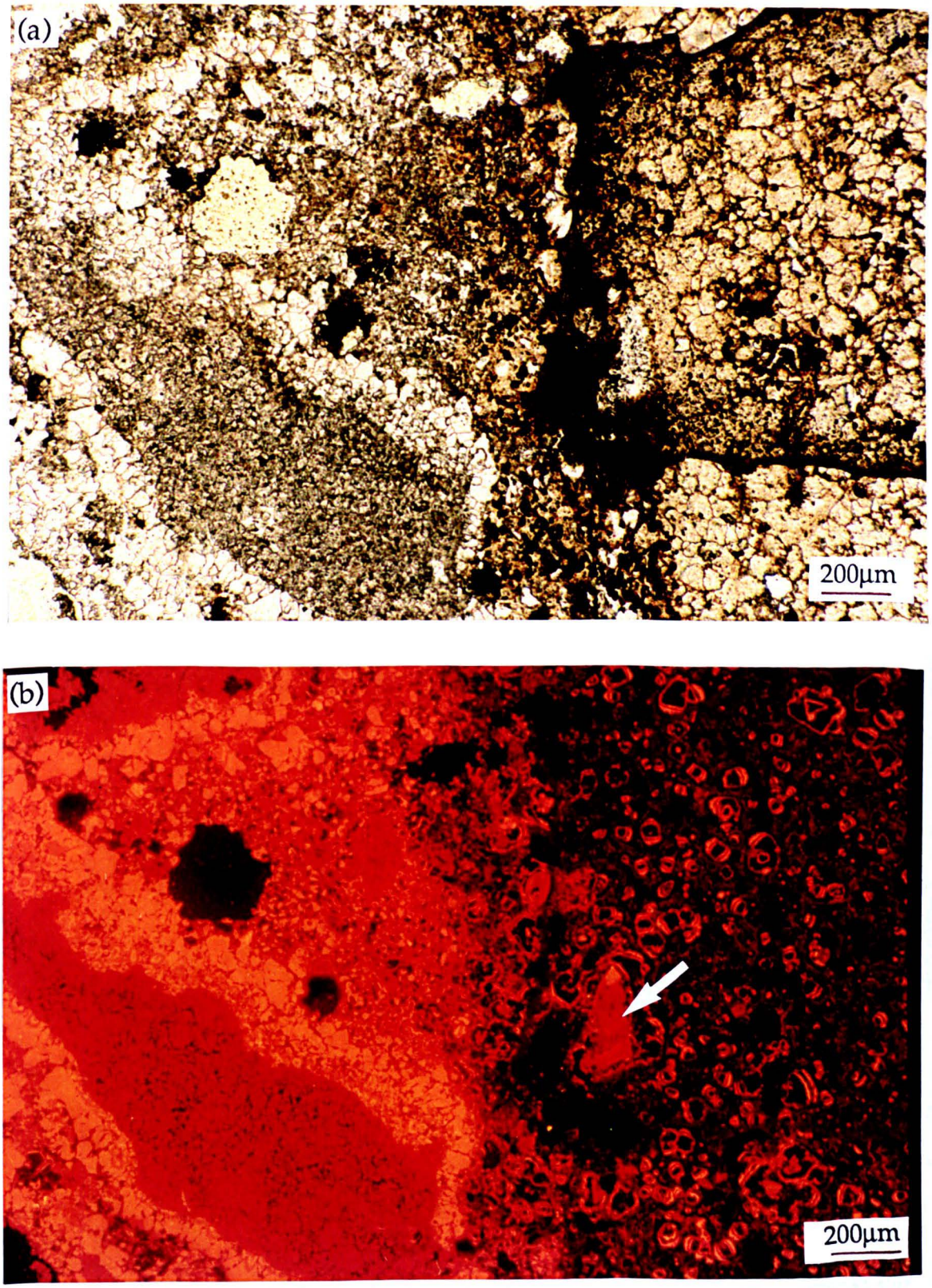

Fig. 6.56. Thin section photomicrographs of the inner part of a joint-coating calcite cement sequence, Houghton Quarry; (a) plane light, (b) luminescence. The cement sequence is from inclusion-rich dull orange through inclusion-free bright orange, into non-luminescent calcite with bright orange hairline subzones. Many of the non-luminescent crystals have grown off corroded luminescent cement crystal clasts (arrowed).

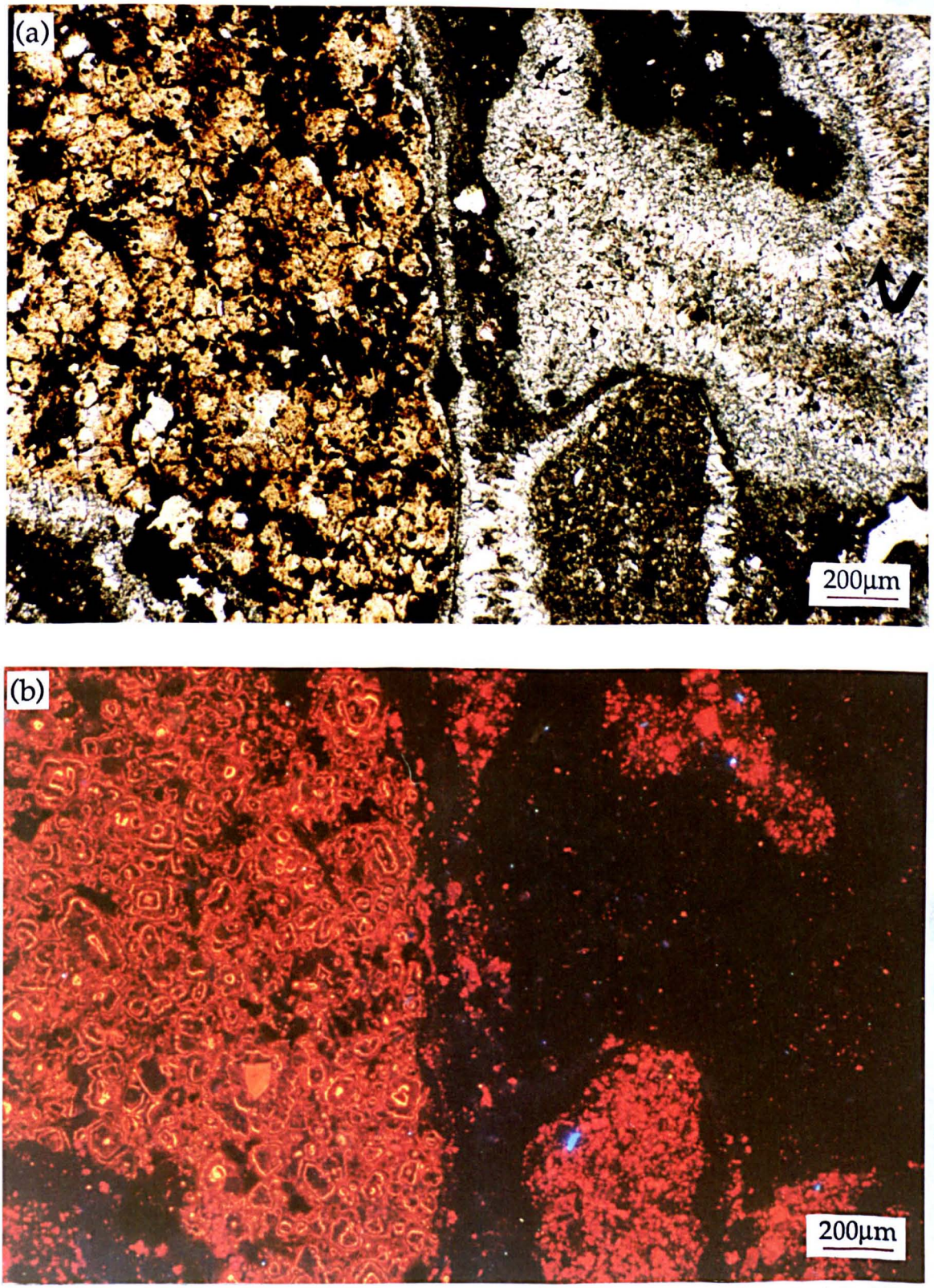

Fig. 6.57. Thin section photomicrographs of the outer part of a joint-coating calcite cement sequence, Houghton Quarry; (a) plane light, (b) luminescence. The non-luminescent equant crystals host abundant opaque iron hydroxides, and are overlain by fluid/gas thorn-shaped inclusion-rich fine columnar calcites. The density of inclusions imparts a distinct colour banding (arrowed). Some internal sediments interlayered with fine columnar calcites incorporate blue-luminescent quartz grains.

or inter-clast porosity is partially filled by much finer dolostone fragments. Most breccias are developed along dissolution-enlarged vertical to sub-vertical joints or fractures, although at Cobblers Quarry, the breccias coat a late stage reactivated listric joint. Coarse, columnar, circumgranular speleothem calcite encrusts the outer surfaces of the breccia clasts. Along a joint surface, immediately north of Frenchmans Bay, a coarse angular dolostone breccia has been cemented by speleothem calcite with a distinctive texture comprising horizontal sheets, ≤1mm thick of finely crystalline non-ferroan calcite.The upper and lower surface of each sheet is encrusted by fine rhombohedral/scalenohedral calcite crystals which present euhedral terminations into the adjacent voids. Larger (centimetre-sized) pores between calcite sheets are partially occluded by millimetre- to centimetre-sized upwards-branching calcite crystals which nucleated off the underlying sheet.

6.5.2. Pore filling calcite cements - Interpretation.

From the previous descriptions, it is clear that, although the petrography of the two calcite cement types is different, their geochemistries are similar. Thus, the petrography of the two cement types will be interpreted individually, followed by a discussion of their trace element and isotope geochemistries together.

6.5.2.1. Petrography of luminescent equant and non-luminescent columnar calcite cements - Interpretation.

Nearly all equant luminescent and non-luminescent columnar calcite cements described, occlude or partially occlude porosity produced by the dissolution of sulphate evaporites. The calcites cementing fractures most likely also postdate a fracture-filling phase of gypsum/anhydrite. The dissolution of evaporite minerals from within the Raisby Formation was in response to regional uplift, which started in the late Cretaceous/early Tertiary (Appendix X).

Dissolution of sulphate evaporites follows their hydration from anhydrite. Gypsum itself, dissolves congruently by molecular dissociation:

$$CaSO_4.2H_2O \rightleftharpoons Ca^{2+} + SO_4^{2-} + 2H_2O$$

(after Freeze and Cherry, 1979).

The kinetics of gypsum dissolution are a function of the degree of undersaturation of the fluids with respect to gypsum, salinity of the fluids, rates of groundwater advection, surface area of gypsum exposed to the fluids, and temperature. The dissolution rate is linearly dependant on undersaturation, and increases with temperature (James and Lupton, 1978). At 25°C, 1bar, pH 7 the solubility of gypsum is high (2400 mg l^{-1} [Freeze and Cherry, 1979]). In modern aquifers, where gypsum is actively being dissolved, the saturation of groundwaters with respect to gypsum increases down flow (Freeze and Cherry, 1979; Edmunds *et al.*, 1982; Back *et al.*, 1983). Gypsum saturation states may also vary in response to pyrite oxidation in upper aquifer levels, and bacterial sulphate reduction in lowest levels, although the influence of these diagenetic processes is a function of reaction rates, and the openness of the diagenetic system. Thus, as the Raisby Formation was penetrated by meteoric-derived groundwaters, the rate of gypsum dissolution would initially have been very slow (as the groundwaters would have been far from recharge area), but would have increased with time as overlying carbonates were eroded off and the surface was approached (Lee and Harwood, 1989). An increase in the saturation of groundwaters with respect to gypsum with depth has also been inferred from Raisby Formation calcitized dolomites and evaporites (Fig. 6.41).

Complete sulphate dissolution in any one part of the formation most probably took place when it was within a few hundred metres of the surface (Fig. 5.30), although the exact

timing of dissolution would have been strongly dependant on porosity and permeability of the host carbonates, and local groundwater regimes. The Tertiary climate may well have been considerably wetter than at present, with meteoric groundwaters penetrating relatively deeper into the Raisby Formation. Fluctuations in sea level would also have had a significant influence on groundwater movement. Thus, the depth of preservation of gypsum, and distribution of calcite cements in shallow onland boreholes at the present day (Fig. 5.30), is not a reliable indicator of the depth of groundwater movement during the Tertiary (5.7.3).

Although calcite cementation in general has followed complete sulphate dissolution, the initial parts of some calcite crystals provide evidence for the co-existence of precipitating calcite with dissolving gypsum/anhydrite, although the rate of sulphate dissolution soon outstripped that of calcite precipitation (6.2.3.1). Some types of calcitized dolomite, within basal parts of equant calcites, also formed at a similar time as sulphate dissolution (6.3.4.2). The common occurrence of pyrite/marcasite in association with bright orange-luminescent pore filling cements, also shows that there was a significent sulphate (and iron) source available, immediately preceding, and during, initial calcite cementation. The sulphate source was almost certainly dissolving gypsum.

That most luminescent calcites are coarse and equant suggests that they precipitated relatively slowly from fluids of a low supersaturation with respect to calcite. Although growth was slow, it was, in general, uninterrupted by episodes of corrosion or internal sedimentation, which suggests that the precipitating fluids were also of a relatively constant saturation with respect to calcite. The diagenetic system must also have been relatively open during the precipitation of luminescent calcite. If the calcites were growing within a closed diagenetic system, their trace element content would be variable in response to ion removal, such that they would have gradients of decreasing Fe and Mn and increasing Mg and Sr from base of the cement (Doerner-Hoskins behavior [3.1.1]).

The luminescence of equant calcites demonstrates that precipitating fluids were reducing for Fe and Mn, and that Fe and Mn (as well as Ca, Mg, and Sr) were available within the diagenetic system. Apart from Eh, Fe and Mn contents of calcites will also be influenced by fluid pH, although this should be generally invariant (6.5-8.5) within a carbonate diagenetic system (Barnaby and Rimstidt, 1989). Average northeast England Permian groundwater has a pH 7.6 (when measured in 1945 [Anderson, 1945]). Fe and Mn concentrations are also influenced by partition coefficients which may be affected by numerous factors such as fluid composition (i.e., Fe/Ca and Mn/Ca ratios), and growth kinetics (3.1.1).

The non-luminescent columnar calcites overlying luminescent equant cements commonly precipitated following a hiatus, during which the luminescent calcites suffered corrosion, dolomitic internal sediments were infiltrated, and goethite precipitated (Figs. 6.43, 6.44 & 6.45). This suggests a major change in pore water conditions towards temporary undersaturation with respect to calcite, and influx of fluids capable of transporting internal sediments. The internal sediments may also have been derived by corrosion of dolomite crystals away from pore walls by pore fluids undersaturated with respect to dolomite. This corrosion, and influx of rapidly moving fluids is suggestive of near surface conditions, where groundwaters often fluctuate between saturation and undersaturation with respect to calcite. Undersaturation is commonly in response to the influx of groundwaters which have not had the opportunity to dissolve calcite to saturation (i.e., their advection rate has been too rapid to dissolve enough calcite and/or there was insufficient carbonate in the recharge area). This was probably connected with an episode of more rapid groundwater recharge, probably due to climatic fluctuation and/or decrease in vegetation cover at the surface.

The size and shape of non-luminescent columnar calcites also suggests a change in the kinetics of calcite precipitation from equant cements. Elongate calcite crystal habits are common within near-surface diagenetic environments whereby fluids attain a high supersaturation with respect to calcite, and resultant high HCO_3^- concentrations generate rapid C-axis parallel crystal growth (Given and Wilkinson, 1985) (6.5.2.3). Non-luminescence of the columnar calcites, and encrustation of contacts between luminescent and non-luminescent calcites by iron hydroxides, also supports a near surface origin, with precipitation in oxic fluids. The absence of authigenic iron minerals within the non-luminescent calcites further demonstrates that little or no Fe was in solution during their precipitation. Bright orange-luminescent hairline subzones within the non-luminescent columnar calcites testify to temporary aquifer stagnation, allowing consumption of dissolved oxygen, and so reduction of $Mn^{3+/4+}$ to Mn^{2+}. However, the degree of stagnation was never sufficiently great for significant quantities of iron to be reduced.

The thorn-shaped fluid/gas-filled inclusions within columnar calcites are very similar to inclusions described from speleothem calcites by Kendall and Broughton (1978), and in this study. Kendall and Broughton (1978) suggest that the inclusions form in response to growth of columnar calcites in the vadose zone by lateral coalescence of numerous small crystallites growing off columnar crystals. Development of the fluid/gas-filled inclusions, which represent primary porosity between the crystallites, is dependant on the degree of crystallite coalescence. Therefore, thorn-shaped inclusions in columnar calcites within cavities after sulphates, attest to the temporary establishment of vadose conditions in those pores, which, in one case, was also associated with internal sedimentation (Fig. 6.46b).

The general Raisby Formation luminescence sequence of dull to bright orange-, to non-luminescent equant, overlain by non-luminescent columnar calcite can be interpreted

in terms of precipitation from fluids of a progressively increasing Eh (Fig. 6.58), and increasing saturation with respect to calcite (cf. Lee and Harwood, 1989). The variability of cements in detail from this general pattern reflects inhomogeneity within the aquifer. Thus, different cement zones may have been precipitated from groundwaters of a different derivation and dissolved ion concentrations, which were not necessarily of a progressively increasing Eh. Groundwaters may also have been modified by diagenetic processes such as bacterial sulphate reduction, oxidation and precipitation of iron minerals (6.5.5), calcitization of evaporites and dolomite (6.4.1), and clay mineral precipitation (6.5.7). The common occurrence of bright orange-luminescent calcite cementing pores associated with calcitized sulphates has already been demonstrated as being due to Fe removal during bacterial sulphate reduction (6.2.3.1). The sharpness of luminescent cement zone boundaries shows that changes in fluid Eh were abrupt (relative to the cement precipitation rate), and a lengthy time gap may have separated each phase of cementation. Thus, pore fluid evolution may not have been gradual in an evolving aquifer, but pulsed, although the overall trend was for each episode of cementation to be from fluids of higher Eh (Fig. 6.58).

6.5.2.2. Petrography of speleothem calcites - Interpretation.

Speleothem calcites have been described from the Ford Formation main reef by Aplin (1985). He records fissures lined with fibrous laminated calcite crusts 1cm to 25cm wide. The fissure-lining calcites are commonly associated with iron oxide/hydroxides (Aplin, 1985). Speleothems are precipitating at the present day from groundwaters in Permian carbonates at Knaresborough, Yorkshire.

Pallisade columnar calcites are characteristic precipitates of the uppermost phreatic/vadose zones, in locations such as caves (Kendall and Broughton, 1978). The variable nature of columnar pallisade calcites within the Raisby Formation (stalactites versus circumclast breccia cements) shows that they were precipitated in the vadose and phreatic zones respectively. The crystallography of speleothem calcites has been comprehensively documented by Kendall and Broughton (1978), who suggest that columnar calcites precipitated in the vadose zone grow by lateral coalescence of numerous small crystallites, producing distinctive textures such as non-compromise intercrystalline boundaries and thorn-shaped fluid/gas-filled inclusions. Non-competitive growth fabrics were observed within some speleothem calcites, and thorn-shaped fluid/gas-filled inclusions were locally common in joint-coating speleothem calcites as well as columnar cements within cavities after sulphates. Speleothem calcites precipitated in the upper phreatic zone should display more normal para-axial growth fabrics (Kendall and Broughton, 1978), which accords with the textures developed within breccia cements, and inclusion-free joint-coating calcites.

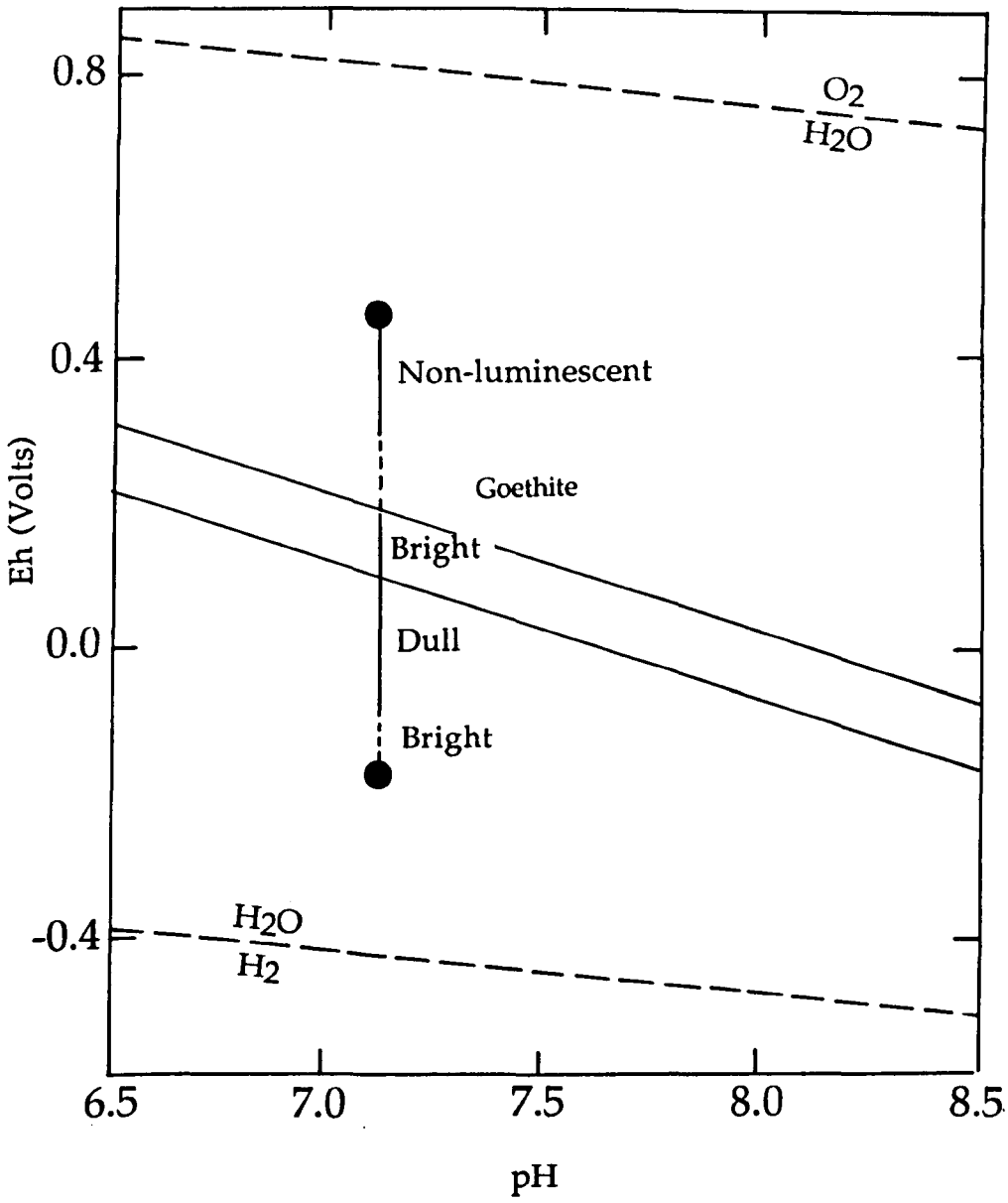

Fig. 6.58. Eh-pH diagram (from Barnaby and Rimstidt, 1989), showing the cement evolution trend developed within the Raisby Formation, related to groundwater Eh, assuming an invariant pH. The dashed parts of the line represent areas where the cements were commonly not precipitated.

The characteristic internal sediments and corrosion surfaces of speleothem calcites, in common with similar features of non-luminescent columnar cements, suggest near-surface conditions where fluid movement was relatively rapid, and groundwaters were periodically undersaturated with respect to calcite. The precipitation of iron oxide/hydroxides in association with non-luminescent speleothem calcites is in good agreement with high Eh fluid conditions.

The distinctive sheet-like speleothem breccia cements from Frenchmans Bay are extremely similar to 'calcite raft' travertines described by Folk *et al.*, (1985) from Italy. These rafts are interpreted to form by calcite precipitation on the surface of bodies of still water within enclosed cavities following CO_2-degassing. Folk *et al.*, (1985) also suggest that precipitation may be mediated by photosynthetic bacteria, one manifestation of which are millimetre- to centimetre-high bacterial shrubs growing from the upper surface of some rafts. Such shrubs (Folk *et al.*, 1985, figure 7b) are very similar to the branching calcite crystals which overlie sheets of calcite within the Frenchmans Bay breccias.

The occurrence of equant luminescent cements beneath joint-coating speleothem calcites was only recorded from Houghton Quarry (Figs. 6.56b & 6.57b). Both the luminescence character and crystal habit of the equant calcites, suggest precipitation from fluids of different geochemical and electrochemical characteristics than the speleothem calcites. Equant habit and unimodal crystal size distribution imply slow precipitation from fluids of a lower supersaturation with respect to calcite than succeeding columnar cements. Dull orange-luminescence of the first phase calcites shows that fluids were reducing enough to incorporate Mn^{2+} and Fe^{2+}, followed by bright orange-luminescent calcite (Mn but no Fe). The transition to non-luminescent calcites with bright orange hairline subzones is likewise interpreted to represent a further abrupt increase in fluid Eh, although it fluctuated across the Mn^{2+}-Mn^{3+} redox boundary, producing bright orange-luminescent hairline subzones. The inclusion-free and inclusion-rich pallisade columnar calcites are the final precipitates of this sequence, representing conditions of constant high fluid Eh. These cements provide good evidence for the movement of large volumes of fluids along joints and fractures during precipitation of calcites from progressively more oxic fluids. That these cement sequences are also very common within cavities after sulphates, suggests that the fluids which precipitated calcite within cavities after sulphates moved predominantly along joints and fractures. Most groundwater movement within Permian carbonates of northeast England at the present-day is also via joints and fractures (Jones and Hirst, 1972).

6.5.2.3. Precipitation of non-luminescent columnar and speleothem calcites - Summary.

Non-luminescent columnar cements within cavities after sulphates, and non-luminescent speleothem calcites are clearly very alike petrographically, suggesting precipitation within similar diagenetic environments. That they are both non-luminescent, and associated with iron oxide/hydroxides, demonstrates precipitation from high Eh (oxidizing for Fe and Mn), near-surface meteoric groundwaters. In such locations, the advection rate of oxygenated meteoric water outstrips the rate of consumption of dissolved molecular oxygen by processes such as the oxidation of organic matter and iron sulphides (6.5.5.1). Such a near-surface position is also supported by evidence for corrosion, internal sedimentation, and fluid/gas-filled thorn-shaped inclusions. Most speleothem calcites were precipitated within partly fluid-filled vadose pores, whereas columnar calcites were mainly precipitated in completely fluid-filled cavities after sulphates (phreatic environment).

Within the meteoric vadose and uppermost phreatic zones, calcite precipitation is induced by degassing of CO_2 and/or evaporation from meteoric-derived fluids supersaturated with respect to, normally, low-magnesian calcite. Rainwater, in equilibrium with atmospheric CO_2 (partial pressure (PCO_2) = $10^{-3.5}$ [Lohmann, 1988]) is undersaturated with respect to carbonate minerals and will congruently dissolve calcite and/or dolomite until saturation with respect to one or both is reached at the ambient PCO_2 and pH (Freeze and Cherry, 1979), after which dissolution is incongruent. In a soil environment, PCO_2 is elevated above atmospheric levels (up to $10^{-1.5}$ [Lohmann, 1988]) owing to oxidation of organic matter and the respiration of plant roots. Groundwaters in equilibrium with this soil atmosphere will be able to dissolve more carbonate than surfacial waters, because the higher the PCO_2 with which the fluids are in contact (and attempting to attain equilibrium), the more CO_2 will dissolve into the fluid, producing greater amounts of carbonic acid (H_2CO_3), thus effecting more carbonate dissolution. The dissolution reaction consumes carbonic acid:

$$CaCO_3 + H_2CO_3 \rightarrow Ca^{2+} + 2HCO_3^-$$

$$CaMg(CO_3)_2 + 2H_2CO_3 \rightarrow Ca^{2+} + Mg^{2+} + 4HCO_3^-$$

(after Freeze and Cherry, 1979).

The amount of carbonic acid available to vadose fluids is a function of the openness of the diagenetic system with respect to CO_2.

If carbonic acid-rich groundwaters are able to by-pass the soil zone with minimal carbonate dissolution (and so H_2CO_3-consumption) via fluid conduits (joints/fractures), or

due to absence of carbonate minerals in the soil zone, they may produce joint/fracture enlargement and karstification adjacent to the water table. Dissolution in this area may also result from transport of organic matter to lower levels of the vadose zone which, upon oxidation, may produce locally high local concentrations of CO_2 (Wood, 1985). Such dissolution (predating calcite cementation), is recorded along speleothem calcite-encrusted joint and fracture surfaces within Raisby Formation dolostones.

When calcite-saturated groundwaters from the soil zone enter an environment of lower PCO_2 (such as a pore which does not have open system exchange of CO_2 with the soil zone), calcite precipitation will occur. Precipitation results from CO_2-degassing as the groundwater tries to attain equilibrium with the lower PCO_2 in the pore. As the rate of degassing is faster than that of calcite precipitation, the groundwaters become supersaturated with respect to calcite, resulting in rapid precipitation (Freeze and Cherry, 1979). As the rate of degassing decreases (as does calcite precipitation), evaporation, in concentrating the fluid, may become a significant cause of calcite precipitation (Gonzalez and Lohmann, 1988).

Most speleothem and non-luminescent columnar calcites in the Raisby Formation are therefore considered to have been precipitated in response to CO_2-degassing (with or without associated evaporation), following extensive open system, near-surface dissolution by carbonic acid rich groundwaters. Rapid degassing generates large quantities of CO_3^{2-} anions from the dissociation of HCO_3^-, which, in response to high supersaturation, produces characteristic C-axis preferential crystal growth, i.e., columnar crystal habits (Given and Wilkinson, 1985; Lee and Harwood, 1989).

6.5.2.4. Trace and minor element geochemistry of calcite cements - Interpretation.

Distinct compositional populations are defined by trace element data, with a clear distinction between luminescent equant, and non-luminescent columnar and speleothem calcites, with regard to Mg, Fe, Mn, and Sr (Figs. 6.49 & 6.50).

Two clearly demarcated populations of luminescent calcites are defined by Fe and Mn (Fig. 6.49a). These populations, in turn, have distinct luminescent characteristics (Fig. A1.3). Very few luminescent calcites have Fe/Mn ratios of greater than 4, or between 1.1 and 0.35 (Fig. A1.3). The absence of high Fe/Mn ratio calcites is because at no time was the diagenetic system such that abundant Fe^{2+} was available, but not Mn^{2+}. Thus, the line Fe/Mn = 4 represents the greatest disparity between Fe and Mn concentrations which was attained within the precipitating fluids. Likewise, the line Fe/Mn = 1.1 (demarcating the lower limit of medium and dull orange-luminescent calcites) reflects the least disparity between Fe and Mn concentrations attained within the Raisby Formation palaeoaquifer during calcite cementation. The composition of fluids which would precipitate calcites of Fe/Mn 1.1 and Fe/Mn 4 (calculated using the homogeneous distribution law, and assuming the fluids have 70-100ppm Ca [Fig. 6.62]) would have Fe/Mn ratios of 2.9 to 6.02 and 15.2 to

22.4 respectively. If the Fe and Mn composition of the fluids was derived solely from the congruent dissolution of Raisby Formation ferroan dolomites, it would have a Fe/Mn ratio of approximately 5 to 15. This suggests that most Fe and Mn within the Raisby Formation aquifer during precipitation of dull and medium orange-luminescent cements could have been derived from dolomite, although it is likely that other sources such as Fe sulphides, and Fe and Mn oxide/hydroxides were probably also significant. However, the constant maximum and minimum Fe/Mn ratios of dull and medium orange-luminescent calcites does suggest that the aquifer was relatively well mixed, i.e., it did not locally stagnate during calcite precipitation such that Fe-rich sources (e.g., oxidizing iron sulphides) could inundate the diagenetic fluids.

The abundance of cements with Fe/Mn ratios ≤0.35 (bright orange-luminescent), represents the precipitation of calcites in semi-oxygenated fluids, oxidizing for Fe, but reducing for Mn. The line Fe/Mn = 0.35 therefore represents the maximum amount of Fe which could be incorporated into calcites precipitated in semi-oxygenated fluids. The line Fe/Mn = 0.35 is thus redox-controlled. The absence of cements between Fe/Mn = 0.35 and Fe/Mn = 1.1 is a reflection of the sharpness of the redox boundary between fluids reducing for Mn and fluids reducing for Fe and Mn. Thus, calcite-precipitating fluids were either only reducing for Mn or fully reducing for Fe and Mn, not semi-reducing for Fe. Those fluids fully reducing for Fe and Mn therefore contained the maximum amount of Fe and Mn available in the fluids at any one given time, which was, as stated, controlled by the Fe/Mn ratio of the source materials. These relationships are summarized in figure 6.59a.

The trends for Mg are more easy to interpret. When plotted against Mn, two trends are evident. The main one, of increasing Mg and Mn is because most analyses of calcites with high Mn were in bright orange-luminescent hairline subzones of columnar (Mg-rich) non-luminescent calcites. The second trend, of decreasing Mn with increasing Mg represents analyses of duller orange-luminescent zones within Mg-rich columnar calcites (Fig. 6.59b). However, that there are no low Mg/Mn ratio calcites, suggests that partition coefficients for Mn were greater during columnar calcite precipitation, possibly due to relatively rapid growth rates. No clear trends are evident for ICP-analysed Sr, although Sr concentrations are clearly higher within luminescent cements than non-luminescent calcites. That most Sr analyses of luminescent cements range between 50 and 250ppm Sr, clearly shows that the source of Sr for the cement-precipitating fluids must have had a higher Sr/Ca ratio than Raisby Formation dolomite, given the dominantly open diagenetic system during luminescent cement precipitation (Fig. 6.63). In the Raisby Formation such a high Sr/Ca ratio source was most likely gypsum.

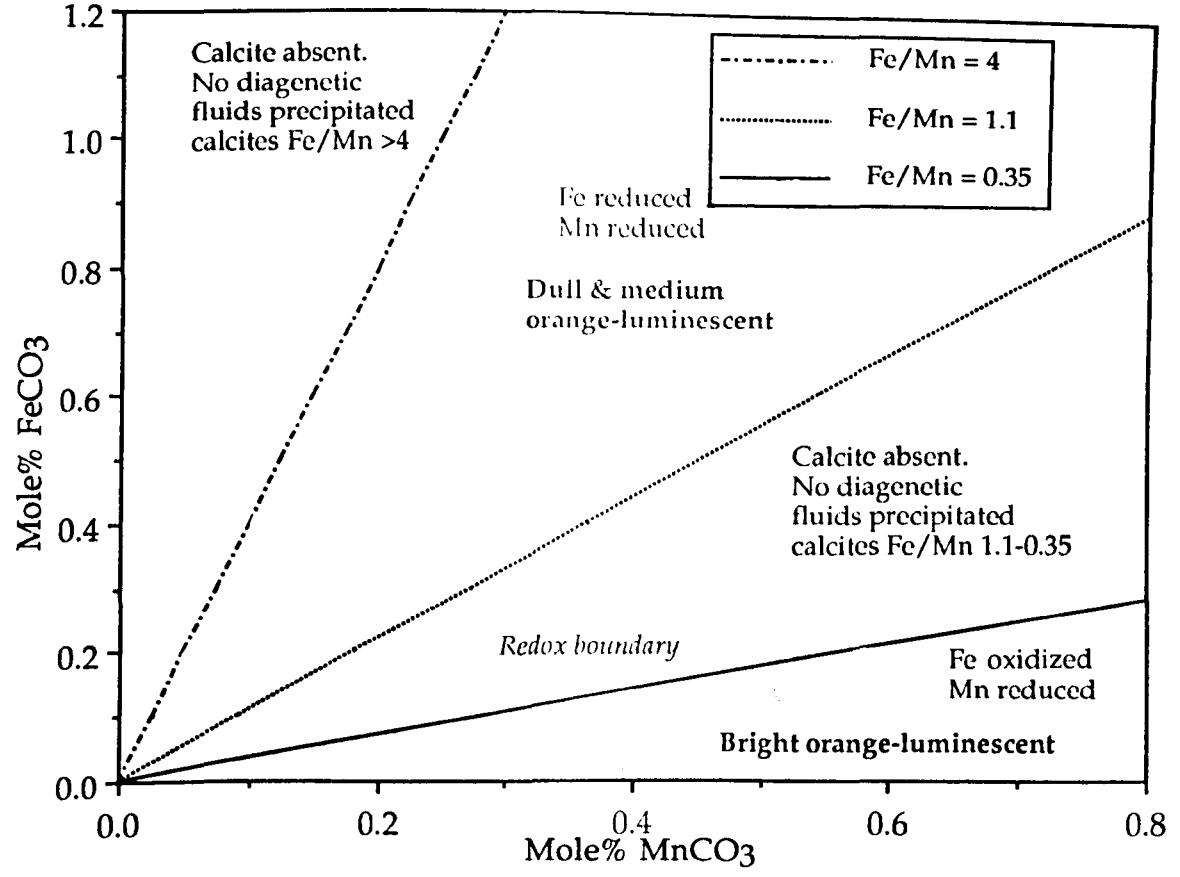

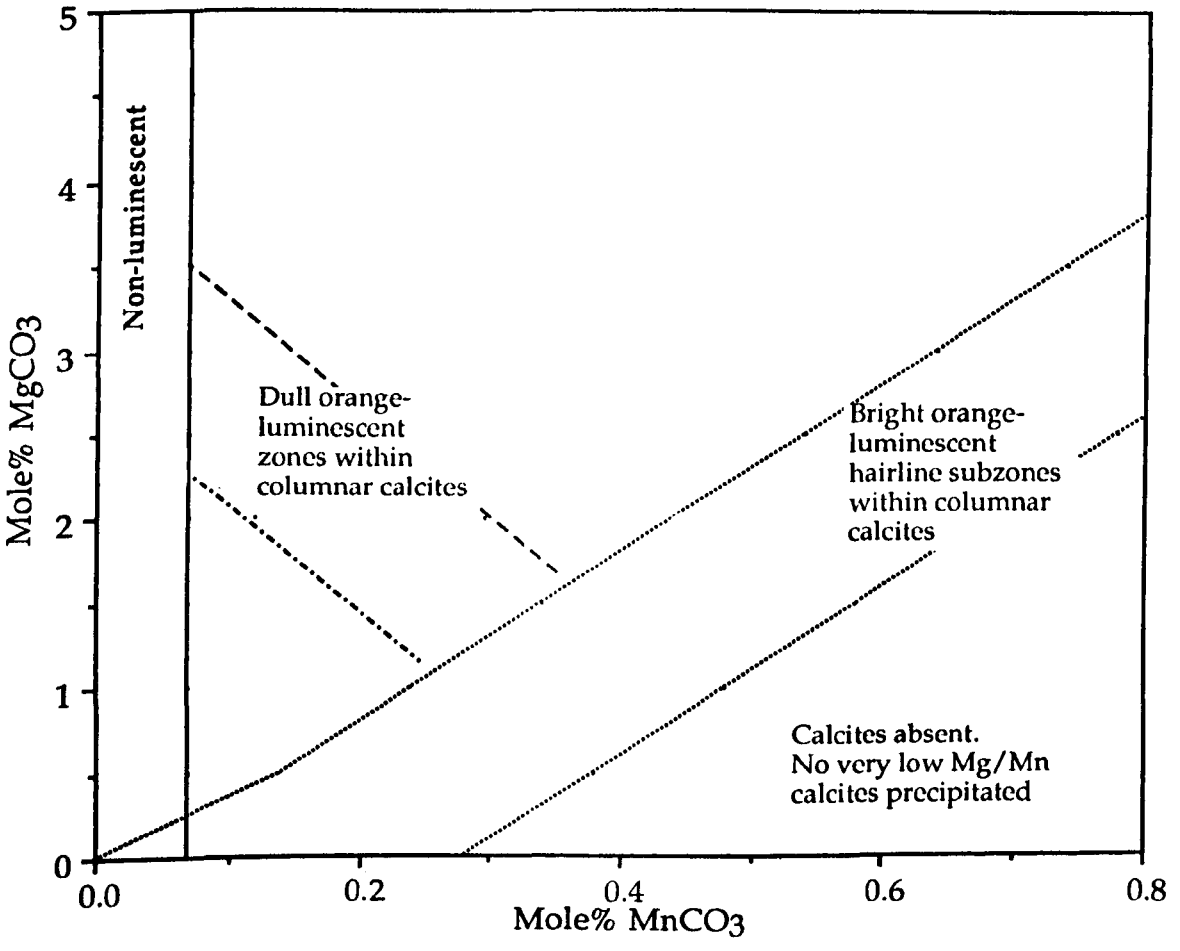

Fig. 6.59. Graphs showing the geochemical interpretation of cement populations defined in microprobe analyses (Fig. 6.58).

The trace element composition of fluids from which the luminescent calcites were precipitated may be calculated by using the homogeneous distribution law (3.1.1) (Appendix VIII), and assuming that the groundwater contained 70-100ppm Ca^{2+}, a reasonable value for meteoric carbonate aquifers (Niemann and Read, 1988; Barnaby and Rimstidt, 1989). Anderson (1945) gave average northeast England Permian groundwater values of 85.7ppm Ca. A sequence of dull to bright orange- to non-luminescent calcite cements from Houghton Quarry (Lee and Harwood, 1989, fig. 14) is taken as being representative of pore-filling calcite cements, as these are not associated with replaced dolomite, evaporites, kaolinite, pyrite/marcasite or any other iron minerals. Mean compositions of the cements, together with predicted fluid compositions are illustrated in figure 6.60. These calculations demonstrate that the concentration of Fe in the fluid was approximately 7 times greater than that of Mn during the precipitation of dull orange-luminescent calcite. However, Fe was completely removed by oxidation during bright orange-luminescent cement precipitation, whilst Mn stayed at a similar concentration. Mg was of a much greater concentration in the diagenetic fluids than Fe and Mn during precipitation of the dull orange-luminescent calcite, and was greatly elevated during precipitation of the bright orange-luminescent cement. However, this Mg change may, in part, reflect an increase in its partition coefficient, as is commonly recorded with respect to the precipitation of non-luminescent cements (see below). On a broader basis, most Raisby Formation calcites contain less than 0.8 mole% $FeCO_3$ and $MnCO_3$, less than 2 mole% $MgCO_3$, and 100-200ppm Sr. Predicted compositions of fluids which precipitated these cements are illustrated in figure 6.61.

The predicted Mg and Sr compositions of the diagenetic fluids are closely comparable to analyses of meteoric groundwaters from the Pahasapa aquifer (in mixed limestone, dolomite, gypsum) of Wyoming and Dakota (Back *et al.*, 1983), and Mg data is comparable to average Sunderland water described by Woolacott (1919b), and average Permian aquifer water described by Anderson (1945) (Fig. 6.62). These results are also comparable to fluid compositions calculated from the geochemistries of cements precipitated within other ancient meteoric aquifers (Fig. 6.62).

Precipitation of the equant luminescent cements was in response to supersaturation of diagenetic fluids with respect to calcite. Supersaturation was, in turn, due to the input of Ca and CO_3 from various sources, such as congruent dissolution of gypsum, dolostones, and limestones, and bacterial reduction of gypsum-derived sulphate. However, as near-surface aquifer fluids are, in general, close to saturation with respect to dolomite, and gypsum is only preserved in distal parts of meteoric aquifers, saturation with respect to calcite will, in general, increase with depth. Calculations of the abundance of Sr in diagenetic fluids clearly supports the suggestion that gypsum dissolution had an important influence on their chemistry. The evidence for a hiatus between luminescent and non-luminescent calcite cementation, suggests that groundwaters were not supersaturated with respect to calcite

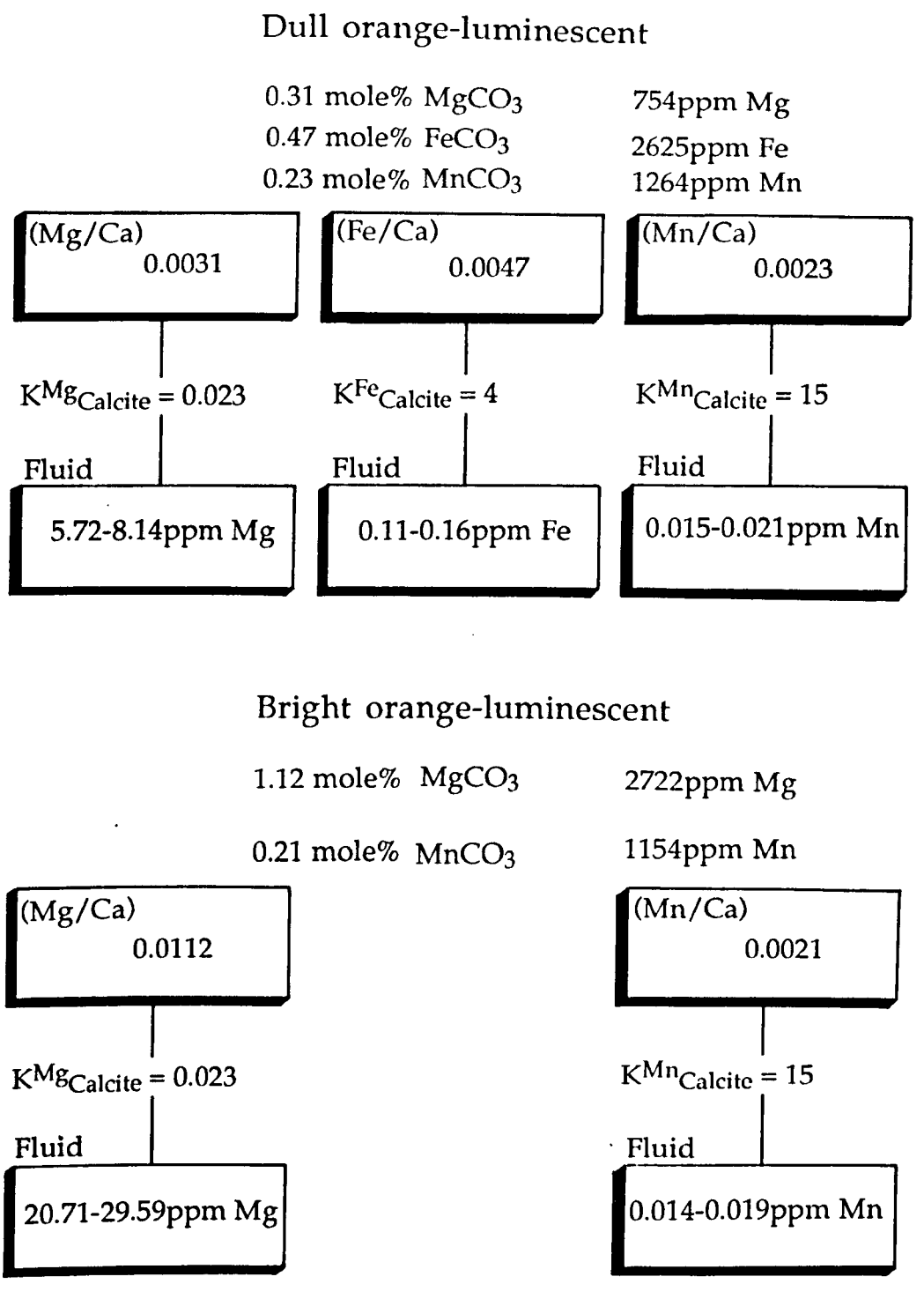

Fig. 6.60. Summary of the calculations of the composition of fluids which would precipitate dull and bright orange-luminescent calcite cements analysed from a single cavity after sulphate, Houghton Quarry (Lee and Harwood, 1989, fig. 14). These calculations assume that during precipitation, equilibrium is approached or reached between the precipitate and the diagenetic fluid so that the homogeneous distribution law can be applied. The diagenetic system is also assumed to be fully open.

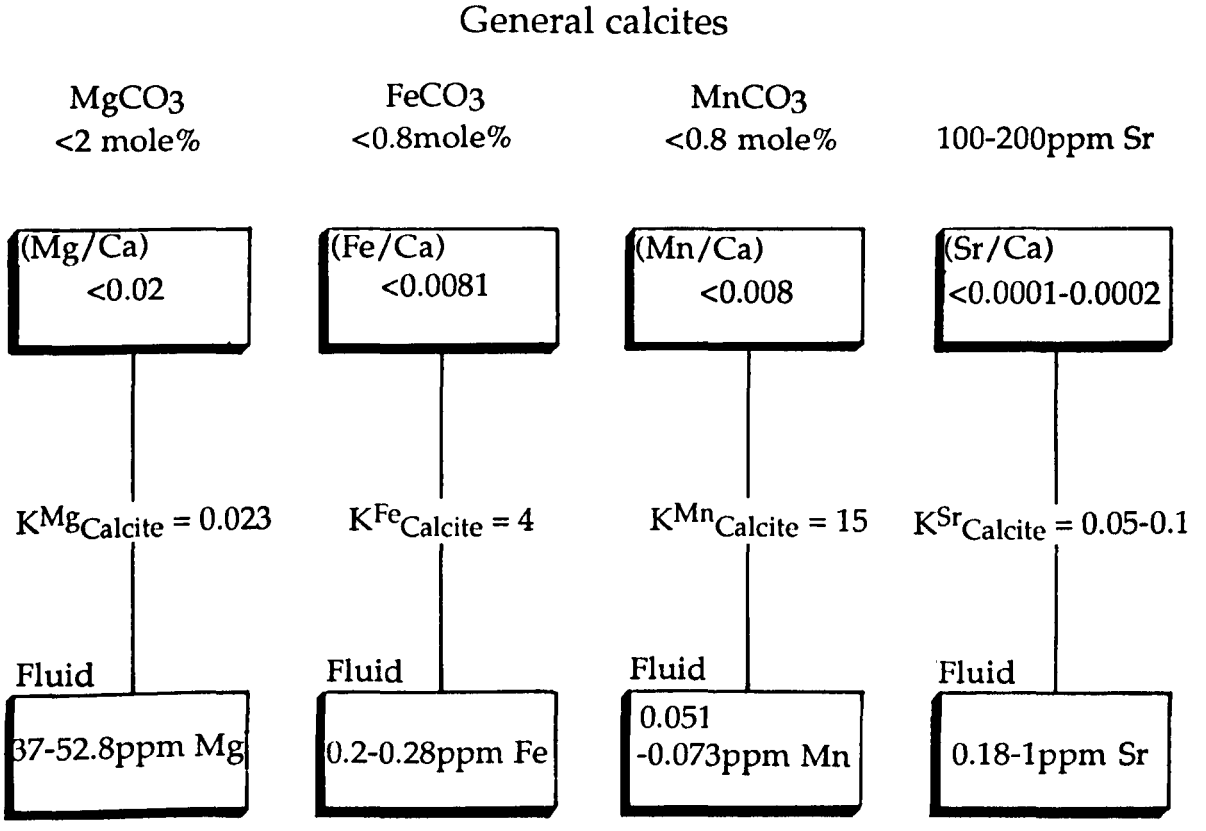

Fig. 6.61. Summary of calculations of the geochemistry of fluids which would precipitate most calcites analysed from within cavities after sulphates. These calculations assume that during precipitation, equilibrium is approached or reached between the precipitate and the diagenetic fluid so that the homogeneous distribution law can be applied. The diagenetic system is also assumed to be fully open.

	Mg ppm	Fe ppm	Mn ppm	Sr ppm
-Calcite lining of cavity after sulphate, Houghton Quarry				
Dull orange- luminescent zone	5.72-8.14	0.11-0.16	0.015-0.021	
Bright orange-luminescent zone	20.71-29.59		0.014-0.019	
-General Raisby Formation calcite cements	<37-52.8	<0.2-0.28	<0.051-0.073	<0.18-1
-Meteoric-related calcite cements (Niemann and Read, 1988):				
Dull orange-luminescent	4-7	<1	<0.1	
-Meteoric calcite cements, (Barnaby and Rimstidt, 1989)				
Dull orange-luminescent		0.0088-0.44	0.0012-0.035	
Bright orange-luminescent		<0.088	0.0047-0.105	
-Sunderland water (Woolacott, 1919b)	38.5			
-Mean northeast England Permian groundwater (Anderson, 1945)	36.2			
-Phasapa aquifer (Back *et al.*, 1983)	19-96			0.07-6.2
-Seawater (Drever, 1982)	1290	2	0.2	8

Fig. 6.62. Summary of the calculated compositions of groundwaters which would precipitate calcites within cavities after sulphates from the Raisby Formation, together with other published fluid calculations and the measured compositions of groundwaters.

throughout the aquifer. In the upper parts of the phreatic zone, supersaturation with respect to calcite would probably have been at a minimum, as all gypsum had been dissolved out, and dolomite was close to saturation following intense congruent dissolution in the vadose zone. Thus, in the upper phreatic zone, there were few autochthonous sources of Ca and CO_3.

The negligible Fe and Mn concentrations of non-luminescent calcite cements is due to oxic pore water conditions during cement precipitation. The amount of Sr (<50 ppm) in the non-luminescent columnar and speleothem calcites demonstrates the absence of significant Sr sources in uppermost aquifer levels. There are areas of overlap between luminescent equant and non-luminescent columnar cements, principally with some microprobe-analysed luminescent calcites containing high Mg (greater than 2 mole% $MgCO_3$) (Figs. 6.49b & 6.50a). These luminescent cements are mainly orange-luminescent subzones within columnar calcite crystals. They demonstrate that Mg-enrichment of columnar calcites is not related to luminescence, and that it is an intrinsic feature of columnar crystal growth.

The enrichment of Mg in columnar speleothem calcites, Carlsbad Caverns, U.S.A. was suggested by Gonzalez and Lohmann (1988) to be at least partly controlled by the enrichment of fluid Mg/Ca ratios owing to evaporation, and/or concentration of Mg in the precipitating fluid, owing to its low partition coefficient (i.e., closed system diagenetic processes). However, groundwaters within the upper parts of the Raisby Formation palaeoaquifer, would not have been isolated for long enough for appreciable Mg enrichment to occur as a result of precipitation (fluid flow rate was much faster than calcite precipitation rate). Also, an enrichment in Sr, at least twice as large as than for Mg should be recorded within speleothem calcites owing to the same processes of enrichment as a function of partition coefficients. Given these results, plus the fact that even a pure dolomite source rock will only precipitate a dLMC with 2.30 mole% $MgCO_3$ in an open diagenetic system (Fig. 6.63), another mechanism for Mg-enrichment is necessary. The most probable process is that outlined by Gonzalez and Lohmann (1988) and Lee and Harwood (1989) from the work by Given and Wilkinson (1985), whereby K^{Mg}_{dLMC} is elevated for rapidly-precipitating columnar calcites, owing to preferential incorporation of Mg^{2+} in the C-axis face of columnar crystals. On the basis of predicted and recorded compositions, K^{Mg}_{dLMC} ranged from 0.023 (value predicted by Mucci and Morse, 1983) (3.1.1) to 0.40 in rapidly-precipitating columnar speleothem calcites.

From an understanding of the geochemical environments of speleothem and columnar non-luminescent calcite cementation, it is possible to model the geochemical composition of the groundwaters from which the cements were precipitated. The roles of both Fe^{2+} and Mn^{2+} are ignored as these have negligible concentrations within the calcites. During congruent dissolution, trace, minor and major elements are stochiometrically

transferred from the dissolving phase(s) into the diagenetic fluid (Lohmann, 1988). The relative proportions of cations within the fluid will be identical to those within the dissolving phase prior to precipitation. The role of differential cation exchange with, for example clay minerals, in altering cation ratios (and so, possibly mineral saturation states), may be significant (Freeze and Cherry, 1979; Drever, 1982; Gonzalez and Lohmann, 1988; Lee and Harwood, 1989), but is difficult to quantify and so cannot be considered. During precipitation of dLMC (in response to CO_2 degassing), trace and minor elements will be removed from the fluid in accordance with their partition coefficients, although Ca^{2+} will stay at an approximately constant concentration. As the Raisby Formation columnar and speleothem calcites were precipitated in a nearly/completely open diagenetic system, the trace/minor element to Ca^{2+} ratios in the diagenetic fluids reflect those of the dissolving phase(s) (Pingitore,1982).

The calculations of fluid compositions (Fig. 6.63) show that the maximum amount of Mg which can be incorporated into the dLMC in an open system, is 2.30 mole% $MgCO_3$ whereas the Sr content is relatively invariant at around 15 to 40 ppm. These data agree well with recorded values (mean Sr of speleothem calcites = 28ppm, of columnar calcites = 12ppm), although $MgCO_3$ values recorded (especially for speleothem calcites) can be greater than 4 mole% $MgCO_3$ (Figs. 6.49b & 6.50a), further supporting the assumption of elevated partition coefficients for Mg into columnar calcites.

6.5.2.5. Isotopic composition of calcite cements - Interpretation.

The oxygen isotopic compositions of near-surface meteoric groundwaters are a function of the annual mean of rainwater composition in the recharge area, the amount of rock-water interaction (a factor of the openness of the diagenetic system), and the degree of mixing with waters of substantially different isotopic composition (difficult to evaluate in this context). Rainwater isotopic compositions are a function of latitude, altitude and temperature (Anderson and Arthur, 1983). With respect to ancient sequences, the isotopic composition of rainwaters will change with time, owing to secular variations in $\delta^{18}O$ of the oceans (Walker and Lohmann, 1989), and smaller amplitude fluctuations owing to glaciation (maximum of approximately 1‰ $\delta^{18}O$ amplitude [Anderson and Arthur, 1983] or 1.6‰ [Lohmann and Walker, 1989]). The longer time scale fluctuations are not relevant to this study, although those due to fluctuations in ice volume may well be. At the latitude of northern England today, the mean annual $\delta^{18}O$ of rainwater is -8‰ to -6‰ (SMOW) (Anderson and Arthur, 1983), which would have been increased by approximately 1.0‰ (to -7.0‰ to -5.0‰) if polar ice was absent. Edmunds *et al.*, (1982) and Bath *et al.*, (1987) record values of $\delta^{18}O$ -7.5‰ to -8.5‰, and -8.5‰, respectively, from shallow groundwaters in present day southern England aquifers. Only at very low water/rock ratios, in relatively closed diagenetic systems, does the oxygen isotopic composition of meteoric waters become significantly

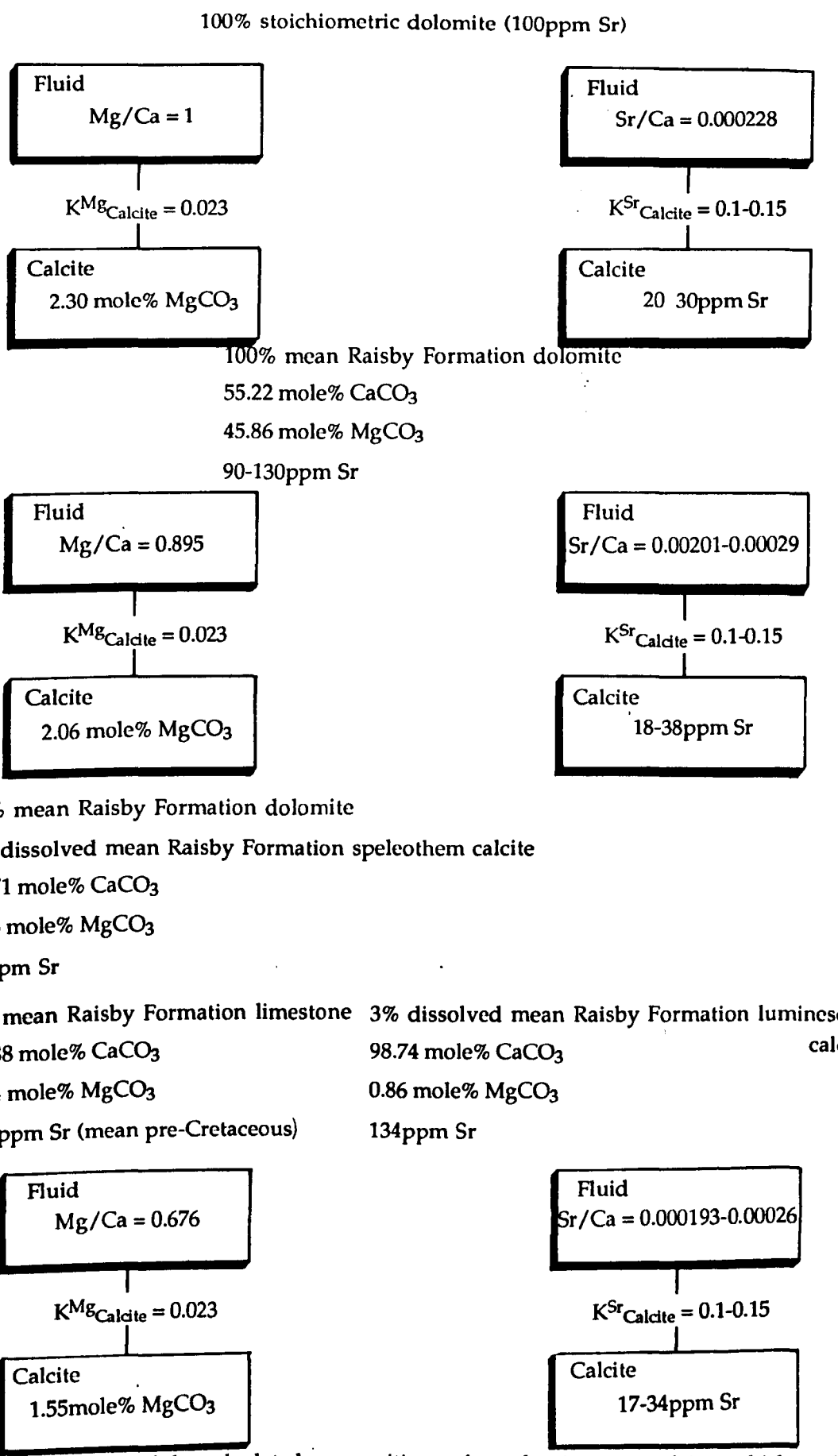

Fig. 6.63. Summary of the calculated compositions of non-luminescent calcites which could result from the near-surface congruent dissolution of various mineral assemblages. These calculations assume that during precipitation, equilibrium is approached or reached between the precipitate and the diagenetic fluid so that the homogeneous distribution law can be applied. The diagenetic system is also assumed to be fully open.

modified by oxygen isotopes derived from the dissolution of host rocks (Veizer, 1983a; Meyers and Lohmann, 1985).

The carbon isotopic composition of meteoric vadose groundwaters is highly variable, and a product of the interplay between four sources (Anderson and Arthur, 1983; Veizer, 1983b; Lohmann, 1988):

1. CO_2 from the oxidation of organic matter in the soil zone ($\delta^{13}C$ = -16‰ to -25‰),
2. Carbon isotopes from the dissolution of carbonates (positive $\delta^{13}C$),
3. Atmospheric CO_2 (water in equilibrium with atmospheric CO_2 at 25°C = $\delta^{13}C$ 1.0‰ to 2.0‰),
4. The extent of photosynthetic withdrawal of ^{12}C into C_{org}, producing heavier $\delta^{13}C$ of residual TDC reservoir.

In reality, the range of the carbon isotopic composition of groundwaters is -30‰ to 3‰, with a mean of -10‰ (Anderson and Arthur, 1983). From the upper levels of groundwaters in mixed siliciclastic-carbonate aquifers from southern England, Edmunds *et al.*, (1982) and Bath *et al.*, (1987) $\delta^{13}C$ values of -11.5‰ to -13.5‰ and -10.0‰ to -13.0‰ respectively.

The strongly negative $\delta^{18}O$ of both equant luminescent calcite populations (Fig. 6.54) implies precipitation from fluids of elevated temperatures. As the diagenetic system was relatively open, a meteoric fluid composition of $\delta^{18}O$ -6.0‰ to -5.0‰ (SMOW) may be assumed for the precipitation of luminescent cements (the value reflecting limited rock-water interaction). The mean $\delta^{18}O$ composition of Raisby Quarry luminescent calcites with very low $\delta^{13}C$ values, suggest precipitation from fluids of 55.7° to 62.0°C (Fig. 6.64). These calculated temperatures contrast with the non-luminescent calcites from the same sample, which give temperatures of 9.7°C to 22.0°C (Fig. 6.64). This suggests that the transition from luminescent to non-luminescent calcite in the Raisby Quarry sample is coincident with a fall in temperature of 33° and 52°C. However, as the luminescent cements sampled were mixed dull and bright orange-luminescent, the actual temperature drop may have been much less, as the two cement zones most likely have different isotopic compositions (the basal bright orange-luminescent calcite hosts anhydrite pseudomorphs, suggested by Lee and Harwood (1989) to have been precipitated from fluids of elevated temperatures during Ba-F mineralization). However, a significant hiatus, corresponding to internal sedimentation, is still evident.

The $\delta^{13}C$ values of the Raisby Quarry luminescent and non-luminescent cements, in being very similar and from the same sample suggest the same source, although the highly contrasting temperatures at which these cements precipitated makes that unlikely. The luminescent cements probably derived ^{12}C from bacterial sulphate reduction, whereas that for the non-luminescent calcites most likely came from the soil zone. As with the calcitized evaporites (ECI) from Raisby Quarry, the organic matter for sulphate-reducing bacteria was probably methane derived from the underlying Coal Measures.

Luminescent calcites	Non-luminescent calcites
Assumed fluid composition $\delta^{18}O$ -6.0 to -5.0‰ (SMOW) (Rainwater modified by interaction with isotopically heavier dolostones)	Assumed fluid composition $\delta^{18}O$ -8.0 to -5.0‰ (SMOW) (Full range of possible rainwater isotopic values)
Raisby Quarry breccia calcites	
Mean $\delta^{18}O$ = -13.5‰ Temperature = 55.7° to 62.0°C	Mean $\delta^{18}O$ = -6.2‰ Temperature = 9.7° to 22.0°C
Raisby Formation luminescent calcites	
Range $\delta^{18}O$ = -7.0‰ to -16.0‰ Temperature = 21.2° to 78.8°C	
Raisby Formation meteoric calcite line	
	Range $\delta^{18}O$ = -5.2‰ to -6.2‰ Temperature = 6.1° to 21.0°C

Fig. 6.64. Summary of calculated palaeotemperatures for the various calcite cements measured from the Raisby Formation.

The majority of luminescent cements (the low negative $\delta^{13}C$ population) (Fig. 6.54), are less well-constrained in their paragenesis. Some cement sulphate dissolution porosity, some cement breccia clasts, and yet others are associated with mineralization, although all probably postdate sulphate dissolution. Their $\delta^{13}C$ values are less-negative than those of non-luminescent calcites, suggesting a fairly high degree of buffering of meteoric waters by positive $\delta^{13}C$ rock sources. Their $\delta^{18}O$ values are again high, although variable, their temperatures of precipitation calculating at 21.2° to 78.8°C (Figs. 6.64 & 6.65a).

Thus, luminescent cements from the Raisby Formation describe two trends which meet at the non-luminescent cement population (Fig. 6.54a). The isotopic trends reflect processes such as bacterial sulphate reduction, mineralization, and elevated temperatures from burial. Although the sample of luminescent cements is small, and probably atypical, the data of Aplin (1981) for very similar calcites from the Ford Formation main reef, and Sweeney (*pers. comm.*, 1988) from Quarrington Quarry, confirms the dominant trends (Fig. 6.54b).

The non-luminescent columnar and speleothem calcites plot in a well-constrained grouping of invariant oxygen, although slightly more variable carbon (Fig. 6.54a). In meteoric vadose/upper phreatic environments, one of the most important influences on the carbon and oxygen isotopic composition of calcites is the extent of rock-water interaction (Meyers and Lohmann, 1985). Variation in the isotopic composition of meteoric-derived fluids in response to rock-water interaction is described by the 'inverted J curve' trend (Meyers and Lohmann, 1985; Martin *et al.*, 1986; Lohmann, 1988) (Fig. 6.66a). During most rock-water interaction, the $\delta^{18}O$ composition of meteoric fluids is relatively invariant, and describes the 'meteoric calcite line', whose position is controlled by the isotopic composition of rainwaters within the catchment area at any particular time (Fig. 6.66a). The invariance of $\delta^{18}O$ is due to the very large reservoir of oxygen isotopes within the fluid as opposed to those derived by interaction with the host rock (approximately $10^4/1$ water to rock oxygen isotope ratio [Al-Aasm and Veizer, 1986b]). The Raisby Formation meteoric calcite line lies at $\delta^{18}O$ -5.15‰ to -6.2‰ (Fig. 6.66a), corresponding to temperatures during precipitation of 6.1°C to 21.2°C, realistic near-surface values (Fig. 6.64). The invariance of the meteoric calcite line demonstrates little interaction with heavier $\delta^{18}O$, rock isotope sources. The carbon isotopic composition of meteoric vadose groundwaters reflect an interaction of light (soil-derived) with heavy (host rock derived) isotopes. At a very low rock-water ratio (open system), carbon isotopes reflect equilibration with soil ± atmospheric CO_2 whereas at high rock-water ratios (closed system), carbon isotopes are dominated by rock sources. During the typical carbonate dissolution reaction, half of the carbon isotopes are derived from soil gas CO_2 and half from the dissolving carbonate rock:

$$H_2{}^{12}C^{16}O_3 + Ca^{13}C^{18}O_3 \rightarrow Ca^{2+} + 2H^{12+13}C^{16+18}O_3$$

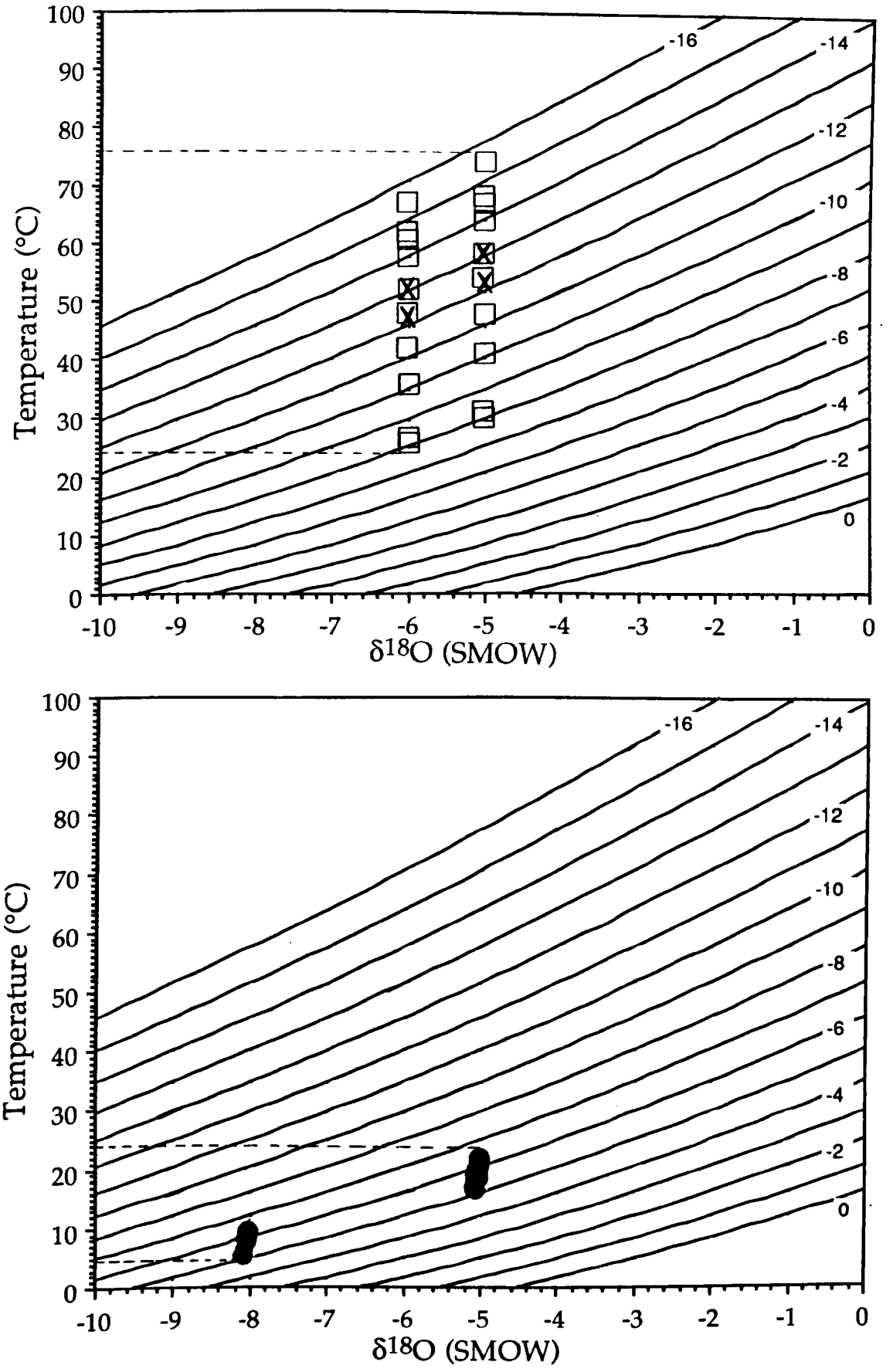

Fig. 6.65. Graphs showing the range of palaeotemperatures for luminescent calcite cements from the Raisby Formation (□), ECI calcitized evaporites, Raisby Quarry (X) and non-luminescent columnar cements from the Raisby Formation (O). The lines on the graph from -16 to 0 represent calcite isotope values in ‰ PDB.

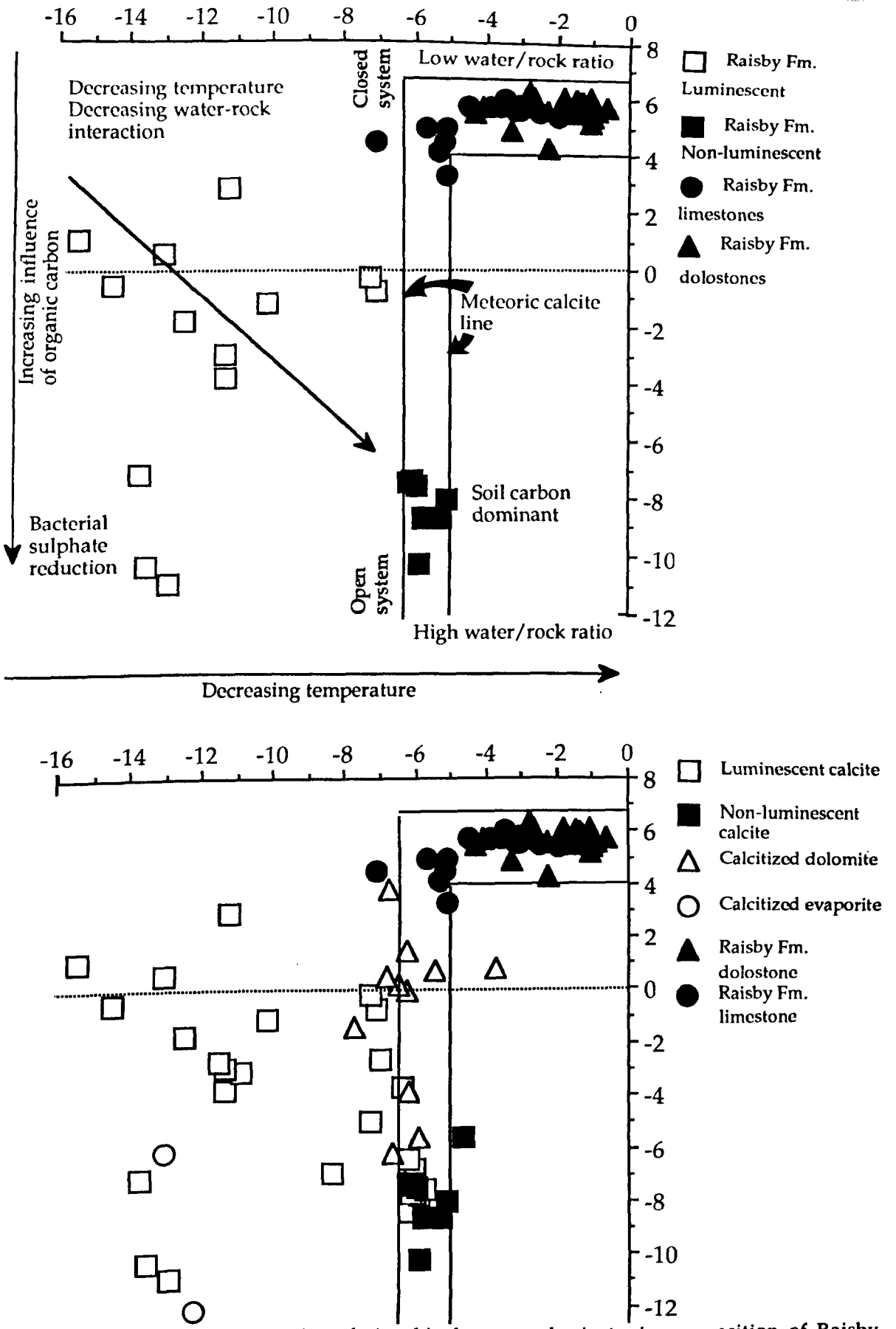

Fig. 6.66. Graphs showing the relationship between the isotopic composition of Raisby Formation calcite cements, and diagenetic processes which have influenced their carbon and oxygen isotope ratios (top). Note the correspondence of the isotopic composition of non-luminescent calcites to the open system end of the inverted J curve. In the lower graph, the isotopic composition of Raisby Formation calcite cements is combined with that of Raisby Formation calcitized evaporites and dolostones, calcite cements from the Cadeby and Ford Formations (see figure 6.54) and calcitized dolostones from the Ford Formation and Zechstein of northeast England (see figure 6.38).

If rock $\delta^{13}C$ = 5.6‰ to 6‰ (mean Raisby Formation limestone and dolostone) and soil gas CO_2 = -20‰, then $\delta^{13}C_{dLMC}$ = -7.2‰ to -7.0‰.These values are similar to those of the Raisby Formation speleothem and columnar calcites, suggesting a moderate degree of carbon isotopic buffering by rock sources.

Therefore, Raisby Formation speleothem and columnar cement isotope data show an excellent correlation with the low rock-water ratio (open system) end of the inverted J curve trend (Fig. 6.66a). Carbon isotopic compositions are typical of meteoric vadose calcites, with a dominance of soil gas-derived ^{12}C, although with some samples trending towards higher rock/water ratios. Raisby Formation limestone and dolostone samples plot at the uppermost end of the J curve trend, and possibly some limestones suggest limited, high rock/water ratio interaction with meteoric-derived fluids (Fig. 6.66a). When all available isotopic data for calcite cements, calcitized evaporites and dolomite, and host rocks are plotted (Fig. 6.66b), clear trends are apparent, demonstrating a very variable degree of rock-water interaction, modified by elevated temperatures during burial.

6.5.3. Pore filling calcite cements - Summary and conclusions.

Telogenetic calcite cements within the Raisby Formation record the geochemical evolution of the Raisby Formation palaeoaquifer, which developed following meteoric water penetration of the formation during uplift. Calcite cements were precipitated within two main zones of this aquifer; a distal zone characterized by calcium and sulphate-rich groundwaters from dissolving gypsum, and a proximal zone, where calcite precipitation was driven by degassing of carbon dioxide. Calcite which precipitated in the distal zone is luminescent, containing Fe, Mn, and Sr, whereas that precipitated close to the earth's surface, in the proximal zone, is non-luminescent, columnar, Mg-enriched, and associated with iron hyroxides and internal sediments.

Stable isotope data, supported by encrustation of calcite crystal faces by iron hydroxides, corrosion, and internal sedimentation, suggest that a relatively long time gap separated precipitation of luminescent and non-luminescent calcites. Thus, cement precipitation was not in a gradually evolving aquifer, but in one in which cementation was largely restricted to distinct areas, inbetween which there was no strong drive for calcite precipitation.

6.5.4. Diagenesis of iron minerals in association with calcite - Description.

Three types of iron minerals have been identified in association with calcitized evaporites and dolomites, and calcite cements within the Raisby Formation:

1. Pyrite/marcasite (FeS_2) and hematite (Fe_2O_3) after pyrite/marcasite
2. Goethite (FeOOH)
3. Very finely crystalline/amorphous iron/manganese hydroxides.

6.5.4.1. Pyrite/marcasite and hematite after pyrite/marcasite - Description.

Pyrite and marcasite are rare in the Raisby Formation at outcrop, although common within offshore boreholes. The difference between the generally buff Raisby Formation dolostones at outcrop, and their much darker colour in offshore boreholes is due to the absence and presence respectively of iron sulphides and organic matter, both being oxidized at outcrop. Framboidal, and coarser equant pyrite has been recorded from the Raisby Formation at outcrop within intraskeletal pores in limestones (3.3.1.3, fig. 3.11), and within coarse equant calcite crystals respectively.

Much of the evidence for precipitation of iron sulphides in association with diagenetic phases such as calcitized dolomite (6.3.4.2), sulphate evaporites (6.2.3), and bright orange-luminescent calcite cement (6.5.1.1) at outcrop, comes from the identification of hematite after pyrite/marcasite within calcite cements. Most hematite occurs either along the contacts of the dolostone host rock with calcite cements, and/or along intercrystalline boundaries of finely crystalline equant calcite (commonly bright orange-luminescent) (Figs. 6.10 & 6.46a). No authigenic hematite was recorded within non-luminescent calcite. Hematite crystals are anhedral to euhedral with, most commonly, elongate habits from rectangular to lensoid, and are 50μm to 500μm in size. The evidence that hematite is after iron sulphides comes from the presence of small (10-20μm) flecks of relic pyrite/marcasite contained within anhedral/euhedral hematite crystals (Fig. 6.46a). Craig and Vaughan (1981) describe replacement of pyrite and marcasite by iron oxides, the only evidence for the precursor phase being irregular blebs of iron sulphide remaining within the iron oxides (Craig and Vaughan, 1981, fig. 7b). The occurrence of unaltered euhedral pyrite/marcasite crystals close to and within the same cement phase as hematite, is also strong evidence that hematite is replacive of pyrite/marcasite in the Raisby Formation (Figs. 6.10 & 6.67a). The unaltered pyrite/marcasite crystals are of a similar habit to hematite, although often considerably smaller (Fig. 6.67a). Where seen together, pyrite/marcasite is isolated within the centre of calcite crystals, whereas hematite preferentially occurs along intercrystalline boundaries and host dolostone-cement contacts.

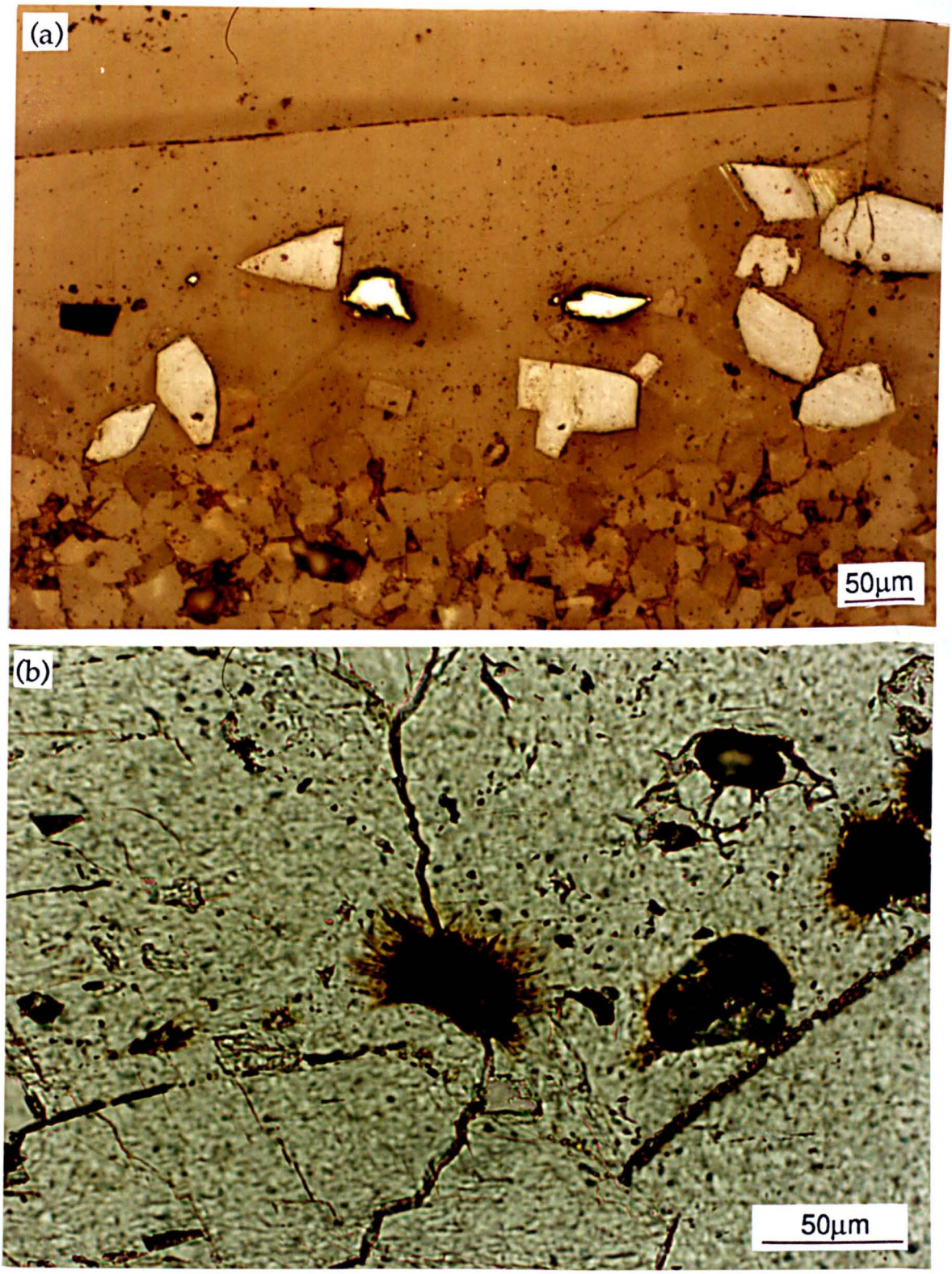

Fig. 6.67. Thin section photomicrographs of iron minerals within calcite cements. (a) shows the hematite and marcasite lined contact of bright orange-luminescent calcite with dolostone from the compaction breccia, Houghton Quarry. Note that the hematite crystals are substantially larger than their marcasite precursors. (b) illustrates a bundle of goethite needles encrusting a former calcite crystal face, Rough Furze Quarry. Another crystal face just below has a thin coating of iron hydroxide.

6.5.4.2. Goethite - Description

Goethite is commonly recorded from the same samples as hematite, although it only occurs within calcite cements and not along cement-host dolomite contacts (Fig. 6.45a). Goethites within calcite cements are very similar to those associated with altered ferroan dolomite (FDA textures) (6.3.2.5, Figs. 6.33a & 6.35b). The goethite occurs as large (up to 150μm diameter), hemispherical bundles of radiating, very fine (few microns long) acicular crystals (Fig. 6.67b). All goethites encrust specific calcite crystal growth faces, which most commonly directly correspond to a change in luminescence character from luminescent to non-luminescent (Figs. 6.44 & 6.45). These goethite-encrusted crystal faces may (Fig. 6.44), or may not (Fig. 6.45) be corroded.

6.5.4.3. Very finely crystalline/amorphous iron/manganese hydroxides - Description.

Finely crystalline/amorphous iron/manganese hydroxides are dark red-brown and semi opaque in transmitted light, and isotropic in crossed polars. Most hydroxides occur within calcite crystals, and are considerably more abundant than goethite. Iron hydroxides within a calcite-lined cavity after sulphate from borehole WO17 encrust a specific former crystal face (Fig. 6.68a). The hydroxides form sub-spherical, hollow-centred structures, 40-50μm in diameter with walls 5-10μm thick (Fig. 6.68a). Where they do not encrust the crystal face, it has a thin, light yellow-brown coloured crust (Figs. 6.42a & 6.68a). The iron-encrusted surface corresponds to the junction of dull orange- with subzoned bright orange-luminescent cement (Fig. 6.42b). The central pore of the iron hydroxide spheres is filled by bright orange-luminescent calcite (Fig. 6.42b). Within the overlying non-luminescent cement, geopetal internal sediments of broken iron hydroxide spheres occur (Fig. 6.68b). The presence at other localities of light yellow-brown coloured crusts on calcite crystals cementing cavities after sulphates is very common, and the encrusted growth face marks the junction of bright/dull orange- with non-luminescent calcite.

Finely crystalline/amorphous iron/manganese hydroxides may also encrust an irregular, corrosive contact between calcites of no specific luminescence character (Fig. 6.69a). The iron incrustation is mainly as a thin coating on the corroded calcite surface, although large acicular crystals have been recorded from one sample, possibly lepidocrocite (Fig. 6.69a). Dendritic hydroxide structures are also common, penetrating into calcite from open pores such as in the centers of leached dolomite rhombs, or intercrystalline boundaries. Iron/manganese hydroxides (and some minor hematite) also occur in association with completely or partially leached, now calcite-cemented silicate grains within siliciclastic dolostones (Fig. 6.69b). The iron hydroxide is exclusively associated with the former silicate grains, partially, or near completely, occluding dissolution porosity. These hydroxides are also commonly associated with kaolinites which again partly occlude the silicate dissolution porosity (Fig. 6.69b).

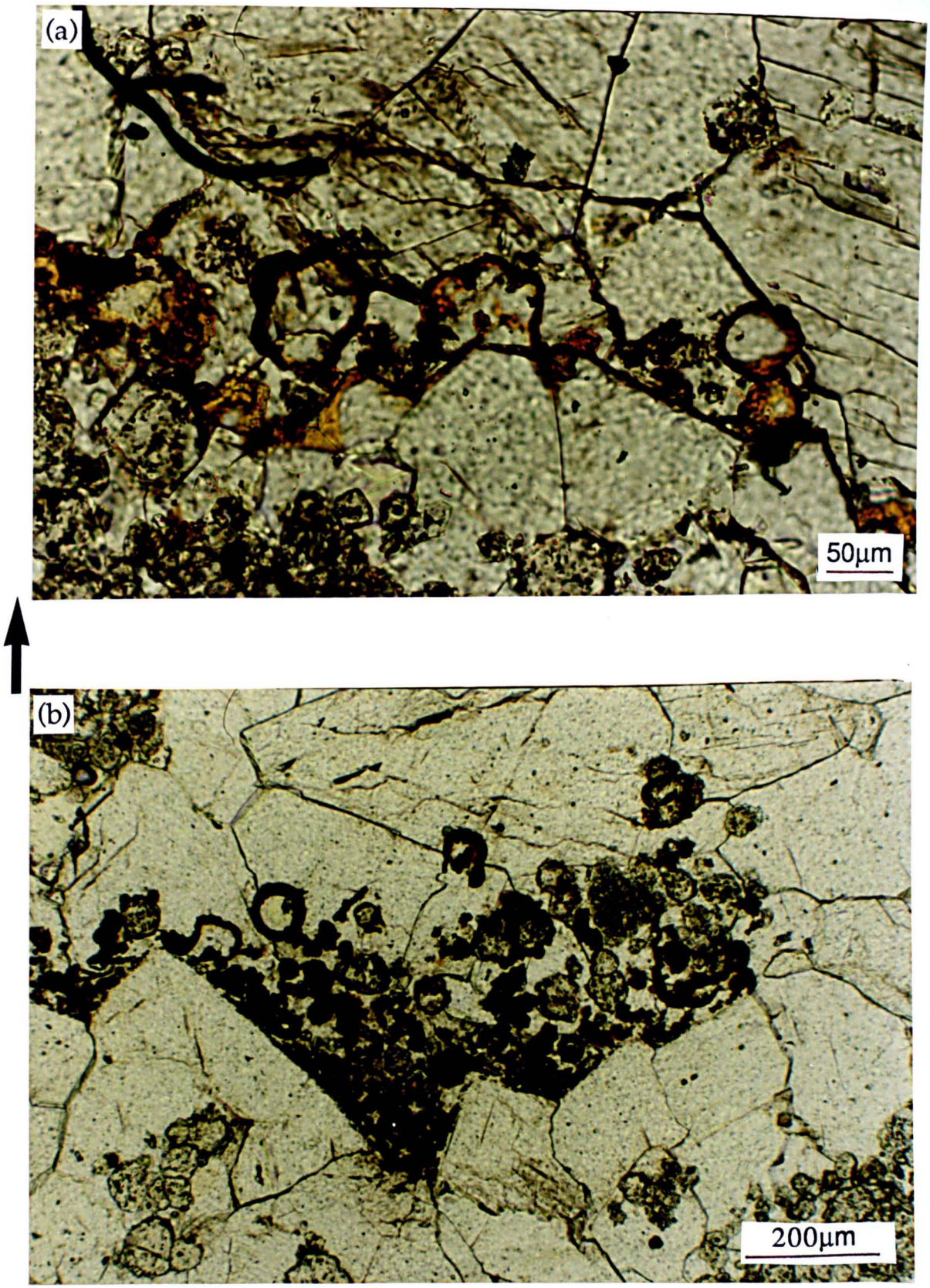

Fig. 6.68. Thin section photomicrographs of spherical iron hydroxide structures within a calcite lined cavity after sulphate, WO17 borehole. (a) shows detail of the crystal face which they encrust (junction of dull with subzoned bright orange-luminescent calcite) (see fig. 6.42b). (b) shows a geopetal internal sediment of iron hydroxide spheres within non-luminescent calcite. Arrow indicates way up.

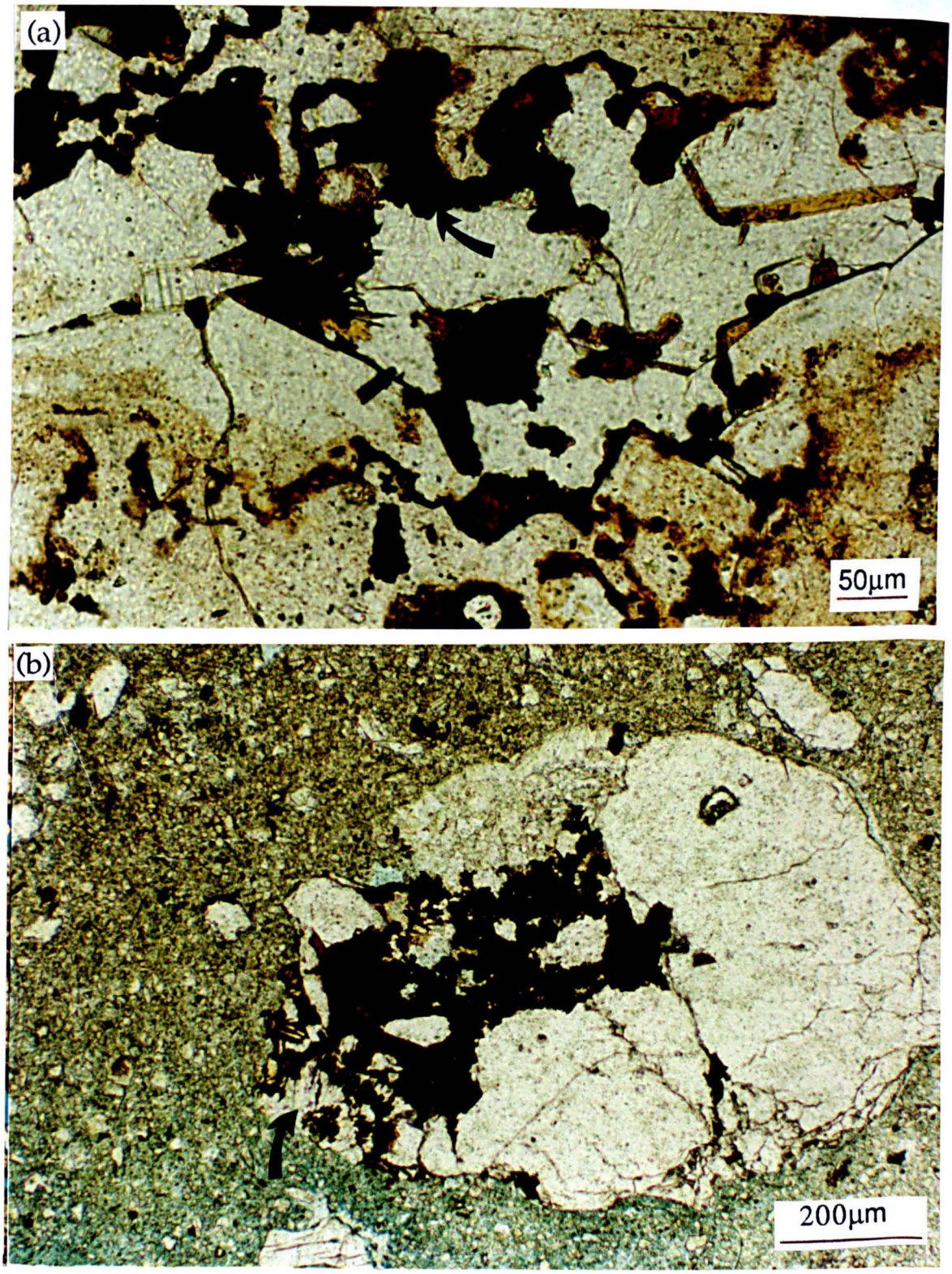

Fig. 6.69. Thin section photomicrographs of iron hydroxides. (a) shows two phases of iron hydroxide encrustation, one of an irregular corrosion surface and another of calcite cementing the dissolution porosity (arrowed). Acicular crystals of possibly lepidocrocite also partially occlude the dissolution porosity just left of the center of the field of view. All of the calcite is non-luminescent, and lines a joint in Houghton Quarry (Fig. 6.57). (b) illustrates a partially leached silicate grain, cemented by both iron hydroxide an kaolinite (arrowed) from a sandstone, Eldon Hill Quarry.

6.5.5. Diagenesis of iron minerals in association with calcite cements - Interpretation.

Three phases of iron mineral precipitation have been identified in association with late diagenetic calcite cements within the Raisby Formation. These minerals are also common within limestones and dolostones, especially the iron/manganese oxide/hydroxides which coat joint and bed surfaces in a dendritic (dendrite) or concentric (liesegang) form.

6.5.5.1. Pyrite/marcasite and hematite after pyrite/marcasite - Interpretation.

Hematite within calcite cements is clearly the earliest iron oxide phase, and most commonly predates calcite cementation. Much of the hematite has formed from the oxidation of pyrite/marcasite, and so its diagenetic relationship to the calcites reflects the timing of iron sulphide precipitation. Not all hematite is associated with definitive evidence for former pyrite/marcasite however, so it is possible that some is a primary precipitate. In this case, iron in solution may have been derived from outside the pore, or more likely, migrated a short distance from a site of nearby pyrite oxidation.

Iron sulphides are oxidized only at outcrop, demonstrating that oxidation postdates uplift, and is the product of relatively near surface diagenesis. Pyrite oxidation to goethite at outcrop has been described from the Raisby Formation at Chilton Quarry by Fowler (1957), and from the Marl Slate by Vaughan and Turner (1980). Natural remnant magnetism of these samples suggested the oxidation was Recent in age (Vaughan and Turner, 1980).

Within near-surface meteoric aquifers, iron sulphide oxidation is important both with regard to the position of the oxic-anoxic boundary within groundwaters (Morse *et al.*, 1987), and in the production of highly acidic groundwater conditions. Both effects may have been very important with regard to hydrogeochemical evolution of the Raisby Formation. The weathering of iron sulphides involves two steps, oxidation followed by dissolution. However, oxygen only plays an indirect role in this process, and Fe^{3+} is the most important oxidizing agent in pH ranges of 2 to 9 (Moses *et al.*, 1987):

$$FeS_2 + 14Fe^{3+} + 8H_2O \rightarrow 15Fe^{2+} + 2SO_4^{2-} + 16H^+$$

(after Moses *et al.*, 1987).

The role of dissolved molecular oxygen is to recycle Fe^{2+} into Fe^{3+}:

$$Fe^{2+} + 1/4O_2 + H^+ \rightarrow Fe^{3+} + 1/2H_2O$$

(after Moses *et al.*, 1987)

The rate determining step of iron sulphide oxidation, as expressed above, is the recycling of Fe^{2+} into Fe^{3+}, which is dependant on the supply of oxygen in the groundwaters

(Nordstrom, 1982). Fe^{2+} oxidation may be accelerated by iron-oxidizing bacteria (Nordstrom, 1982). Although iron sulphide oxidation is a strong acid-producing reaction, as shown in the preceeding formulae, the build-up of acidity in natural systems is a function of the rate of oxygen supply to the diagenetic site, iron sulphide abundance and crystal size, and carbonate alkalinity of the diagenetic fluids (in turn a function of PCO_2 and solubility of carbonates within the groundwater recharge area [Drever, 1982]). In natural systems, strongly acidic fluids as a by-product of pyrite oxidation are uncommon owing to an insufficient input rate of oxygen (i.e., slow groundwater advection rates) (Drever, 1982).

The fate of iron liberated during pyrite oxidation is largely a function of the pH of the ambient fluids (Loope and Watkins, 1989). If pyrite oxidation has produced an environment of low enough pH, iron can remain in solution (iron becomes more soluble in higher Eh fluids of a lower pH [Garrels and Christ, 1965]), but if not, it will oxidize and precipitate as hematite or oxidize and hydrolyze to an insoluble ferric hydroxide:

$$Fe^{2+} + 1/2O_2 + 2H_2O \rightarrow Fe_2O_3 + 4H^+$$

(hematite)

(after Loope and Watkins, 1989)

$$Fe^{2+} + 5/2H_2O + 1/4O_2 \rightarrow Fe(OH)_3 + 2H^+$$

(ferric hydroxide)

(after Drever, 1982)

The ferric hydroxide ($Fe(OH)_3$) may in turn dehydrate into goethite (FeOOH) and hematite (Nordstrom, 1982).

The autochthonous nature of hematite after iron sulphide in the Raisby Formation (i.e., hematite retains the crystal habit of the precursor sulphide phase), suggests that carbonate buffering prevented substantially acidic conditions from developing during pyrite oxidation, thus restricting iron mobility. However, there is little if any evidence of the host carbonate immediate to the pyrite being corroded (Fig. 6.67a). This suggests that most buffering was by dissolved carbonate within the groundwater. The increase in crystal size following oxidation could be explained by precipitating hematite crystals attracting iron in solution. However, if oxidation takes place with no net loss or gain of iron, a 26.5% increase in volume should be recorded following oxidation of pyrite to hematite (molar volume at standard state of pyrite is 23.94 cm^3/mole, and hematite is 30.28 cm^3/mole [Berner, 1971]). Both processes may well have been of significance.

Within the Raisby Formation, the main determinant of the intensity of pyrite oxidation was porosity and permeability of the host carbonates. Thus, early framboidal pyrite is commonly unaltered within relatively impermeable limestones, although completely

oxidized within adjacent dolostones, whereas euhedral pyrite/marcasite is preserved within the calcite crystals but oxidized along their intercrystalline boundaries. The complete preservation of pyrite/marcasite within a few tens to hundreds of microns of totally oxidized iron sulphide (Fig. 6.67a) is, however, anomalous.

Thus, pyrite/marcasite oxidation within the Raisby Formation was a significant process contributing to the precipitation of authigenic hematite, although usually only as pseudomorphs after iron sulphide minerals. Iron sulphide oxidation, along with the oxidation of organic matter, may have been important in contributing to the consumption of oxygen within groundwaters penetrating the Raisby Formation upon uplift. However, owing to the abundance of carbonate, and the relatively small quantities of iron sulphides, acidity generation was not a significant by-product of iron sulphide oxidation, especially as it took place in an open diagenetic system, necessary for oxidizing fluids. As iron was not taken up into solution, most iron sulphide oxidation must have taken place during or after precipitation of dull orange-luminescent calcite.

6.5.5.2. Goethite - Interpretation

All goethites described, as well as some finely crystalline/amorphous iron hydroxide coatings on calcite crystals, must have precipitated directly out of solution, most likely following a rise in Eh of the pore fluids (Lee and Harwood, 1989). This increase in Eh is also manifest in the transition in luminescence of the host cements, from dull or bright orange- to non-luminescent. Theoretically, iron should precipitate out of solution at a point marked by the transition from dull orange to bright orange-luminescent calcite (Frank *et al.*, 1982), whereas manganese should precipitate out at the point of transition between bright and non-luminescent calcite. As nearly all hydroxides are recorded at only one level, directly below the non-luminescent calcite, even where bright orange-luminescent calcite was present, Eh was probably not the only control on the kinetics of iron hydroxide precipitation. Possibly, considerable amounts of Mn hydroxides are intermixed with the iron minerals, and so Fe and Mn hydroxides precipitated out of solution together.

Goethite is also commonly associated with altered ferroan dolomite (FDA textures), again considered to precipitate by oxidation of Fe^{2+}, liberated during dolomite dissolution (6.3.4.5). The process is probably analogous to that described by Postma and Brockenhuus-Shack (1987) for the dissolution of amphiboles and pyroxenes, whereby Fe^{2+} released from the crystal lattice in dissolution cavities is transported to the surface of the crystal. Upon contact with oxidizing groundwaters the iron immediately precipitates as ferric hydroxides. This process in turn most likely explains the direct association of iron hydroxides with leached aluminosilicates (Fig. 6.69b).

The kinetics of iron hydroxide precipitation onto calcite surfaces has been studied by Clarke *et al.*, (1985) who suggest that iron precipitates by interaction with the calcite:

$$4Fe^{2+} + O_2 + 4CaCO_3 + 2H_2O \rightarrow 4FeOOH + 4Ca^{2+} + 4CO_2$$

(FeOOH = goethite/lepidocrocite)

$$3Fe^{2+} + 3CaCO_3 + 3H_2O \rightarrow 2Fe(OH)_3 + 3Ca^{2+} + 3CO_2$$

($Fe(OH)_3$ = amorphous ferric hydroxide)

(after Clarke *et al.*, 1985).

From their experimental work, Clarke *et al.*, (1985) record a progression from a yellow stain on the calcite surface to a dense brown crust during hydroxide precipitation. The iron hydroxides formed experimentally, precipitated both directly onto the calcite, and also as grains within the solution which settled onto the calcite surface, forming nuclei for further iron hydroxide growth. There is a suggestion in some calcite-lined cavities within the Raisby Formation that the iron hydroxide crusts are considerably thicker on upwards-pointing calcite surfaces in the bases of cavities (Fig. 6.42b) This implies that settling out from suspension of small hydroxide particles may have been an important process with regard to iron hydroxide nucleation and growth. In their experiments, Clarke *et al.*, (1985) found that the precipitation rate of iron hydroxides was controlled by the rate of Fe^{2+} oxidation, in turn influenced by pH (lower pH decreased the rate of Fe^{2+} oxidation), rate of aeration of the fluids and concentration of Fe^{2+}. Thus, iron hydroxides coating calcite surfaces within the Raisby Formation may be interpreted in terms of oxidation and hydrolysis of Fe^{2+} during an increase in Eh, although possibly, the exact timing of their precipitation was limited by a decrease in pH, accompanying further precipitation of bright orange-luminescent calcite.

Calcite crystal faces encrusted by goethite are common within a few hundred microns of hematite after pyrite/marcasite (Figs. 6.45a & 6.46a). This suggests both that different processes were involved in precipitation of the different iron minerals, and that possibly some Fe^{2+} liberated during pyrite/marcasite oxidation was able to enter solution (owing to a temporary reduced fluid pH accompanying closed system pyrite oxidation), and so create locally elevated Fe^{2+} concentrations within the fluid, therefore facilitating the precipitation of larger quantities of iron hydroxides than are otherwise recorded. It is also possible that hematite after pyrite/marcasite formed considerably earlier than iron hydroxides, and the hematite was itself derived from the dehydration and recrystallization of a precursor iron hydroxide (Durrance *et al.*, 1978; Postma and Brockenhuus-Shack, 1987). Goethite (especially where finely crystalline) is thermodynamically unstable and should convert to hematite within 10^5 to 10^6 years (Durrance *et al.*, 1978). Alternatively, the hematite after pyrite/marcasite may be a primary precipitate, reflecting different conditions from those during iron hydroxide precipitation, for example higher temperatures, which would favour a non-hydrated oxide.

6.5.5.3. Very finely crystalline/amorphous iron/manganese hydroxides - Interpretation.

Most finely crystalline/amorphous iron/manganese hydroxides either replace calcite, or encrust corroded calcite surfaces. Both are directly associated with calcite dissolution. Their common occurrence adjacent to pores demonstrates a permeability control on their precipitation. The non-specificity of the hydroxides for calcite luminescence types suggests that Eh did not directly control hydroxide precipitation, especially as they occur within non-luminescent calcites (Figs. 6.56, 6.57 & 6.69a). The hydroxides may have precipitated following a local decrease of Eh and/or pH, allowing Fe and Mn to enter solution and so be transported to the locus of precipitation. Such a decrease in Eh may have resulted from the local introduction of organic matter into the pores, which consumed available oxygen. A pH and Eh decrease may also have resulted from pyrite oxidation within the pore system. The Fe and Mn however, may also have been transported to the site of precipitation in the form of organo-metallic complexes, even within oxidizing groundwater (Van Straaten, 1978). Precipitation of the Fe and Mn as hydroxide phases can occur directly from the organo-metallic complexes in response to a decrease in pH, such as from calcite dissolution (Van Straaten, 1978). This readily explains many of the occurrences of Fe/Mn hydroxides both within the calcites, and coating joint and bed surfaces within limestones and dolostones of the Raisby Formation. Such complexes may also have been significant for the transportation of Al^{3+}, similarly insoluble in oxic groundwaters (6.5.7)

6.5.5.4. Diagenesis of iron minerals in association with calcite - Summary

Three phases of iron precipitation have been identified within the Raisby Formation, from precipitation of pyrite/marcasite and subsequent oxidation to hematite, precipitation of iron hydroxides following an increase in fluid Eh, to precipitation of organically-complexed iron and manganese in response to carbonate dissolution (Fig. 6.70). The precipitation of Fe/Mn oxide/hydroxides within calcite cements relates directly to groundwater redox conditions and to a lesser extent pH, within the narrow range allowed by carbonate buffering. The only exception is the most recent phase of hydroxide precipitation, which was independent of Eh, and which would give an erroneous interpretation of groundwater redox conditions if used to infer Eh of the diagenetic fluids. That goethite, which precipitated prior to non-luminescent calcite cementation, has not dehydrated to hematite, could suggest that goethite precipitation and all non-luminescent calcite cementation has taken place within the last 1 million years (Upper Pleistocene). Alternatively, the enclosure of goethite within calcite cements may have protected it from dehydration.

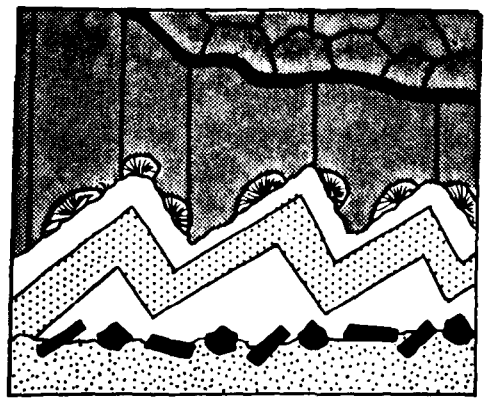

Non-luminescent calcite cementation. Cementation interrupted by phases of dissolution and precipitation of iron/manganese hydroxides from organo-metallic complexes.

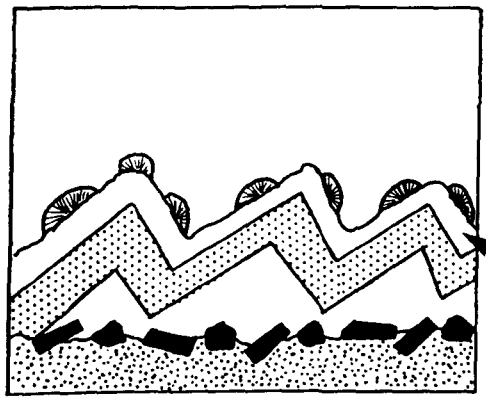

Hiatus in cementation. Luminescent calcite crystal faces corroded and encrusted by iron hydroxides, most commonly goethite.

Bright orange-luminescent

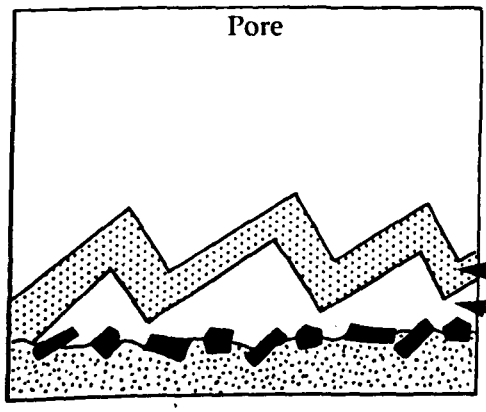

Calcite cementation. Iron sulphide oxidation begins after precipitation of bright orange-luminescent calcite.

Dull orange-luminescent

Bright orange-luminescent

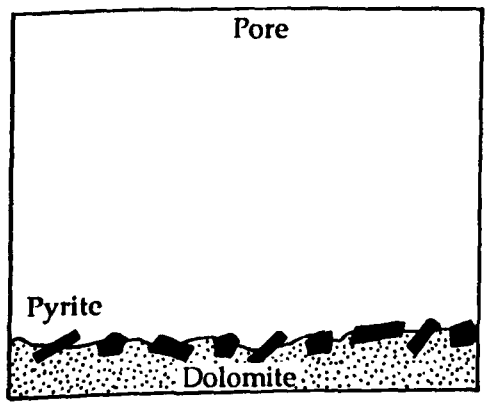

Sulphate dissolution. Iron sulphide precipitation around pore margins.

Fig. 6.70. Summary of the diagenetic relationships between iron minerals and calcite cements within a hypothetical cavity after sulphate.

6.5.6. Authigenic clay minerals - Description.

Three categories of predominantly late diagenetic clay minerals have been defined from the Raisby Formation, related to their mode of occurrence and, to a lesser extent, mineralogy.

6.5.6.1. Type 1, dolomite-encrusting clays.

Recorded encrusting etched dolomite crystal surfaces from the lowermost dolomite unit at Houghton Quarry. The most numerous clays identified by SEM are extremely small, six-armed stellate structures, approximately 1μm in diameter (Fig. 6.71a). They may coat the entire outer surface of dolomite rhombs. These closely resemble chlorites described by Ayalon and Longstaffe (1988), although EDAX analysis demonstrated the presence of Ca, Fe, Mg and Si (in that order), which could suggest smectite. Two types of more typical smectites were identified, one being very similar to 'webby' or 'highly crenulated' pore lining smectites figured by Welton (1984), and the other, more platy crystals (Fig. 6.71b), very similar to smectite figured by Goodall (1987) from the Edlington Formation. The well developed crystal form, and pore-lining nature of these clays suggests they are authigenic. Although only one sample was analysed, its very typical nature, and the common insoluble residues recorded from dolostones at outcrop (5.3.3.4), suggest that such clays are typical intercrystalline pore fills of Raisby Formation dolostones at outcrop.

6.5.6.2. Type 2, cavity filling clays

These are much more coarsely crystalline and occur in larger quantities than dolomite-encrusting clays. Characteristically, these clays occur within cavities after sulphates and/or dolostone intercrystalline porosity at outcrop and in shallow onshore boreholes. They may completely occlude porosity (Fig. 6.72a), or be enclosed within coarse equant calcite cement, which itself occludes the porosity (Fig. 6.72b). These clays are dominated by kaolinite, which occurs as individual plates up to 10μm long, or as 'booklets' of plates 20μm thick. Isolated plates of kaolinite are most widespread, and booklets are only common where clays almost completely occlude porosity (Fig. 6.72a). Calcite cementation postdates kaolinite precipitation. However, the exact timing of kaolinite precipitation relative to calcite cement luminescence development is difficult to determine, and the kaolinite may occur within bright to dull orange- to non-luminescent calcite. At Eldon Hill Quarry, kaolinite occurs within bioclastic dolostones which directly overlie a thick sandstone (2.3.2), and the abundance of kaolinite decreases with height above the sandstone. However, at other localities, there is no apparent immediate association of kaolinite with siliciclastic horizons. Pores within dolostones of the Hurworth Place borehole are completely occluded by kaolinite and lined by iron hydroxides, possibly goethite which most likely predates

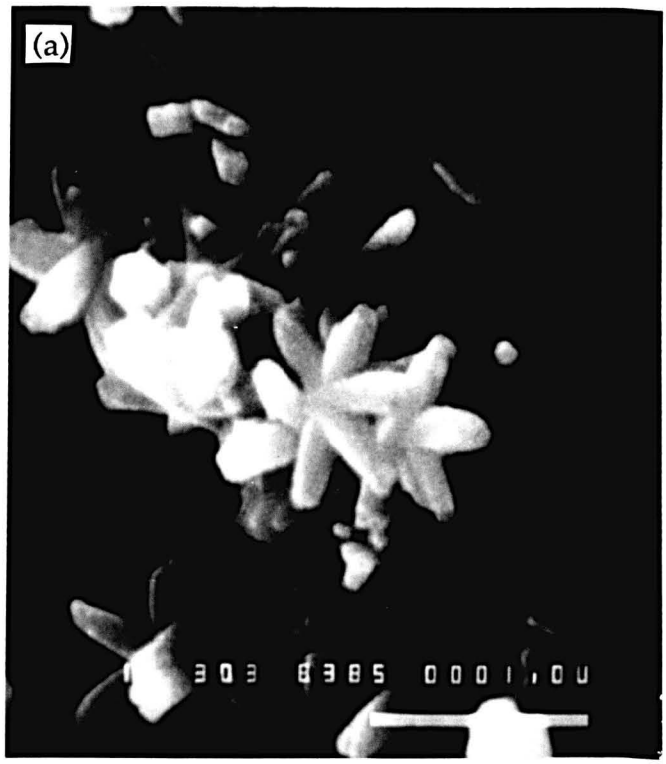

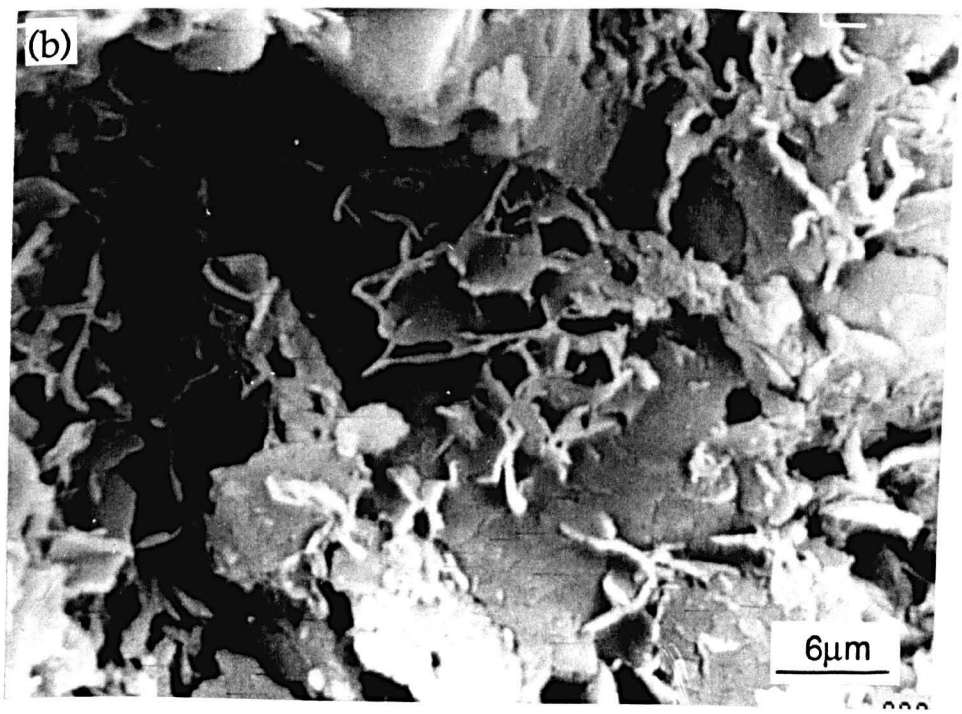

Fig. 6.71. SEM photomicrographs of dolomite encrusting clay minerals. (a) illustrates stellate crystals of ?chlorite and (b) platy crystals of smectite.

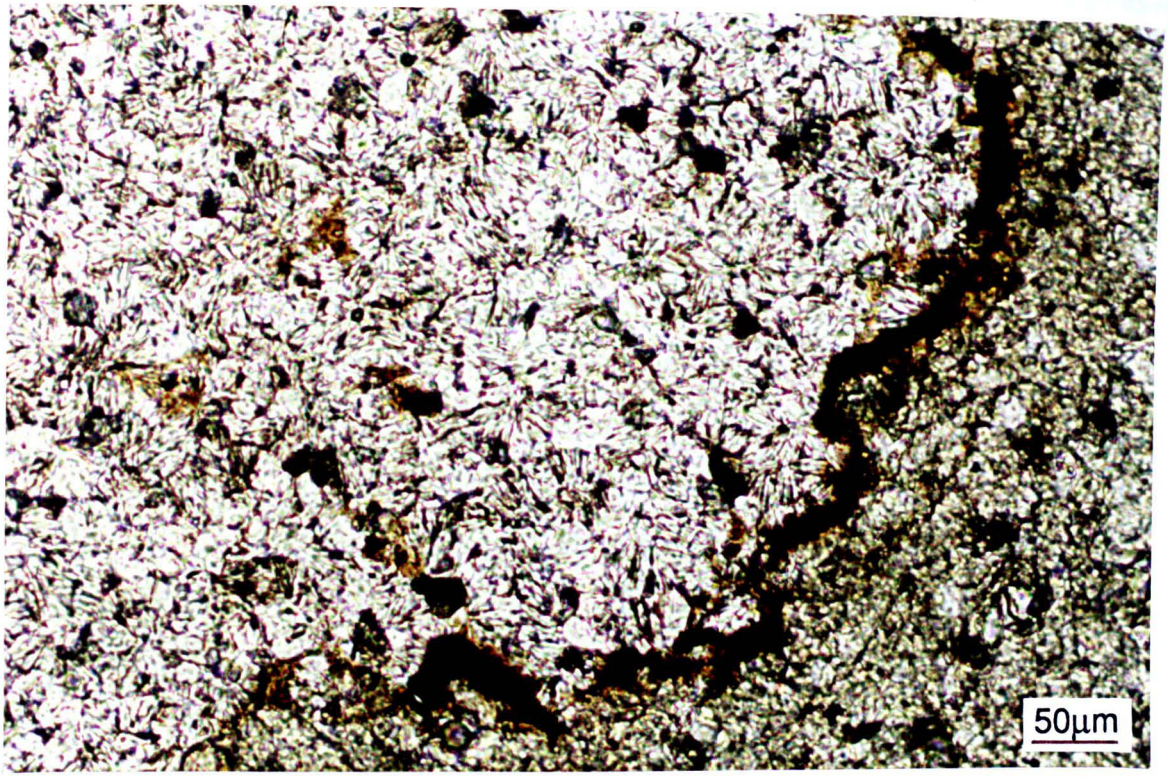

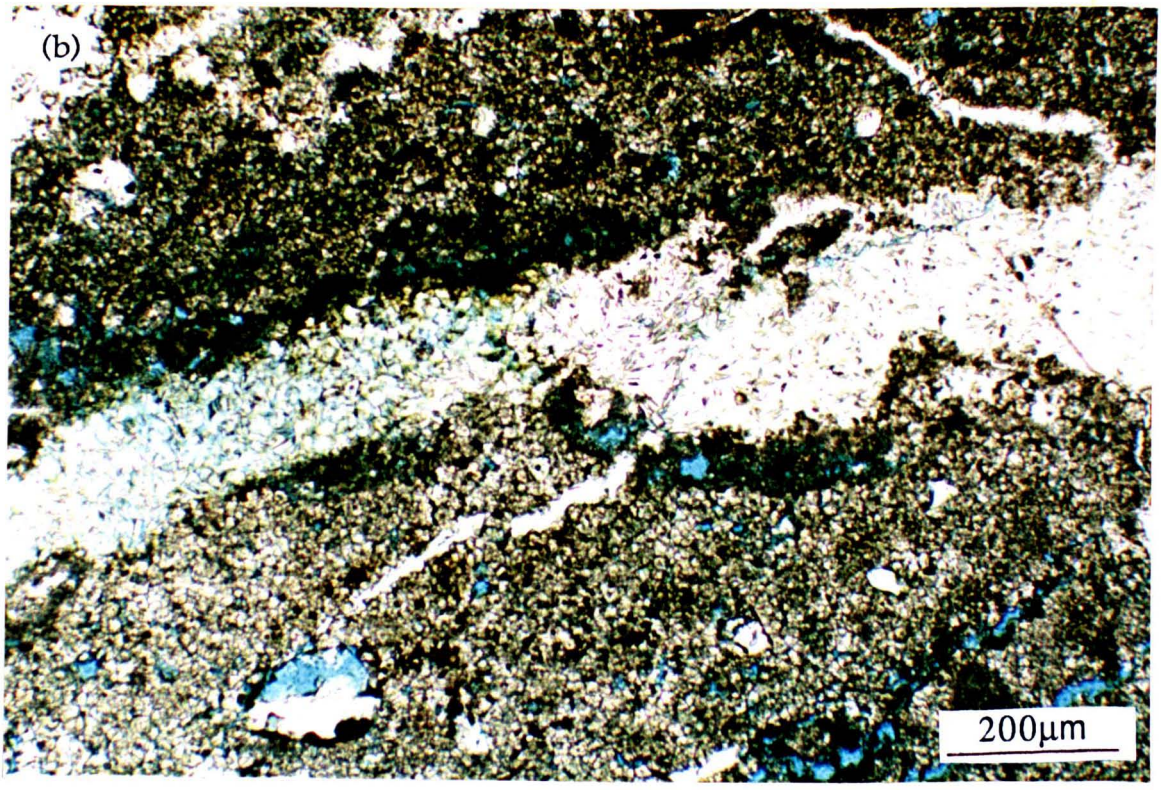

Fig. 6.72. Plane light, thin section photomicrographs of cavity-filling kaolinite, (a) the margin of a kaolinite-filled cavity, Hurworth Place borehole, 144.0m. The cavity is lined by iron hydroxides. (b) the transition within a pore from complete kaolinite cementation, to occlusion by calcite cement with kaolinite inclusions, Eldon Hill Quarry.

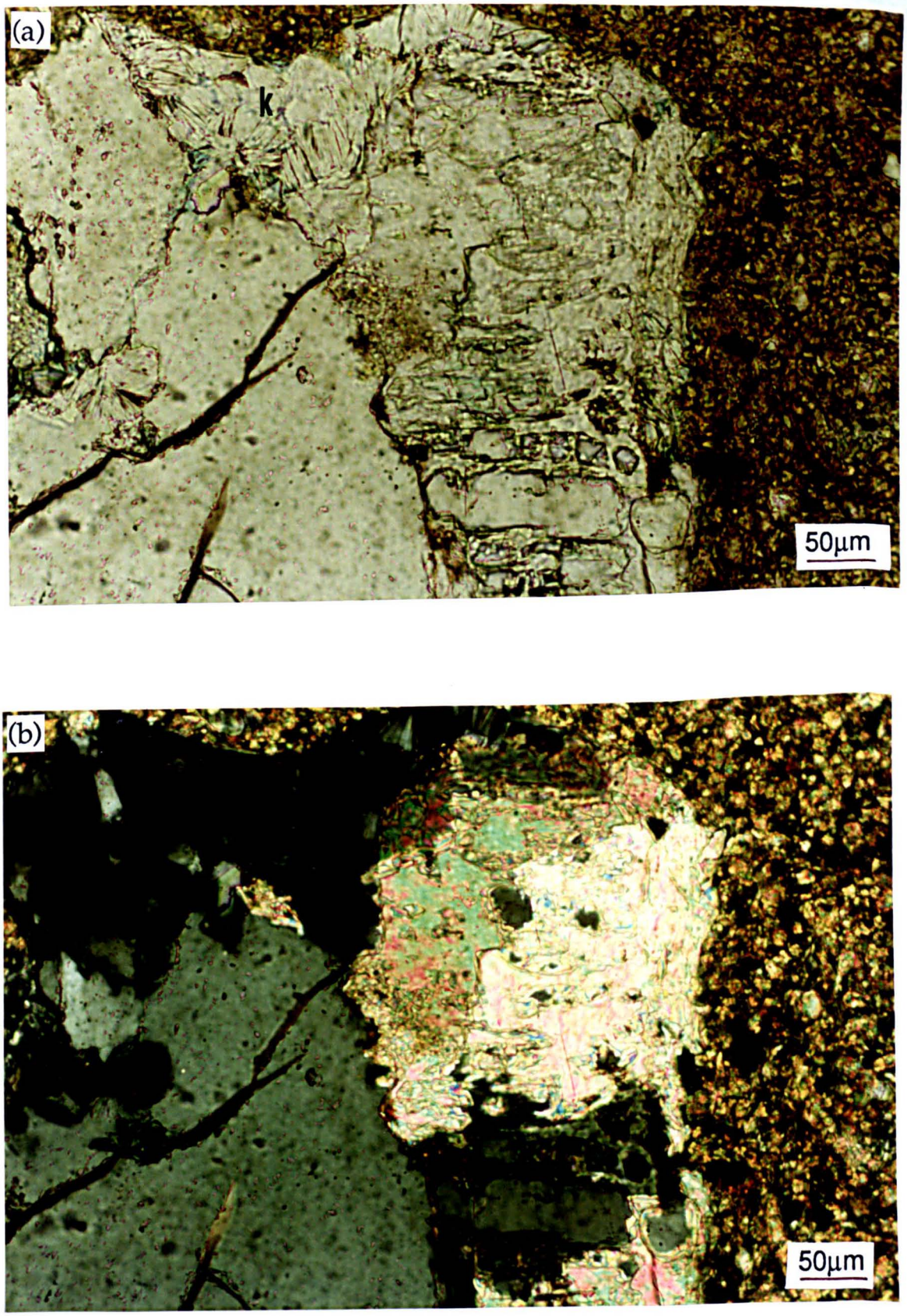

Fig. 6.73. Thin section photomicrographs of silicate-related kaolinite from part of a detrital silicate grain within a sandstone, Eldon Hill Quarry; (a) plane light, (b) crossed polars. In the upper part of the grain, dissolution porosity has been occluded by kaolinite booklets (K), whereas elsewhere it has been cemented by bright orange-luminescent calcite.

kaolinite precipitation (Fig. 6.72a). Other samples from the same borehole which retain gypsum have no pore filling kaolinite, or iron hydroxides.

6.5.6.3. Type 3, silicate-related clays.

These occur in direct association with partially leached silicates within siliciclastic dolostones. They are dominated by kaolinite, mainly as booklets, often tightly packed together (Fig. 6.73). The size and habit of this kaolinite is very similar to that of cavity-filling clays. The kaolinite may completely occlude dissolution porosity within silicate grains (where the volume of kaolinite precipitated is similar to the volume of aluminosilicate leached) (Fig. 6.73), may occur within calcite (bright to dull orange- to non-luminescent) occluding the dissolution porosity, or may occur cementing porosity between leached silicate grains. These kaolinites are also commonly associated with iron oxide/hydroxides, which are restricted in their occurrence within these dolostones to the leached silicates (Fig. 6.69b). The relative timings of kaolinite, calcite and iron oxide/hyroxide precipitation is difficult to assess, although all postdate silicate leaching.

6.5.7. Authigenic clay minerals - Interpretation.

A comprehensive study of the detrital clay mineralogy of the Raisby Formation is beyond the scope of this study. Work by Total oil company geologists (internal report, 1965) on exposures in Co. Durham, shows that the clay fraction of dolostones is dominated by kaolinite with subordinate montmorillonite, chlorite, and mixed layer clays. However, it is assumed that this data will reflect both authigenic and detrital components.

The precise timing of authigenic clay mineral precipitation is difficult to assess. However, the association of the clays with corroded dolomite crystal surfaces at outcrop (dolomite-encrusting clays), calcite cemented dolostone and evaporite dissolution porosity (cavity filling clays), and in some cases, still porous leached silicates (silicate-related clays), suggests that much clay mineral precipitation was telogenetic, postdating regional uplift and dissolution of gypsum by meteoric-derived groundwaters. Some kaolinite has been recorded occluding dolomite intercrystalline porosity from an offshore borehole (Fig. 6.74), although it is very rare.

The description of authigenic clays, in particular kaolinite within carbonates is uncommon. Kaolinites within carbonates have been described by Keller (1976), Longman and Mench (1978), Dickinson and Coleman (1980), and G. Darke (*pers. comm.*, 1989). Keller (1976) described kaolinites within limestones which have a pore filling geometry, occurring as 5μm to 15μm euhedral plates, singly or aggregated as books. However, no descriptions are known of the precipitation of kaolinite specifically during meteoric groundwater-influenced diagenesis of a carbonate sequence. The precipitation of kaolinite during meteoric diagenesis

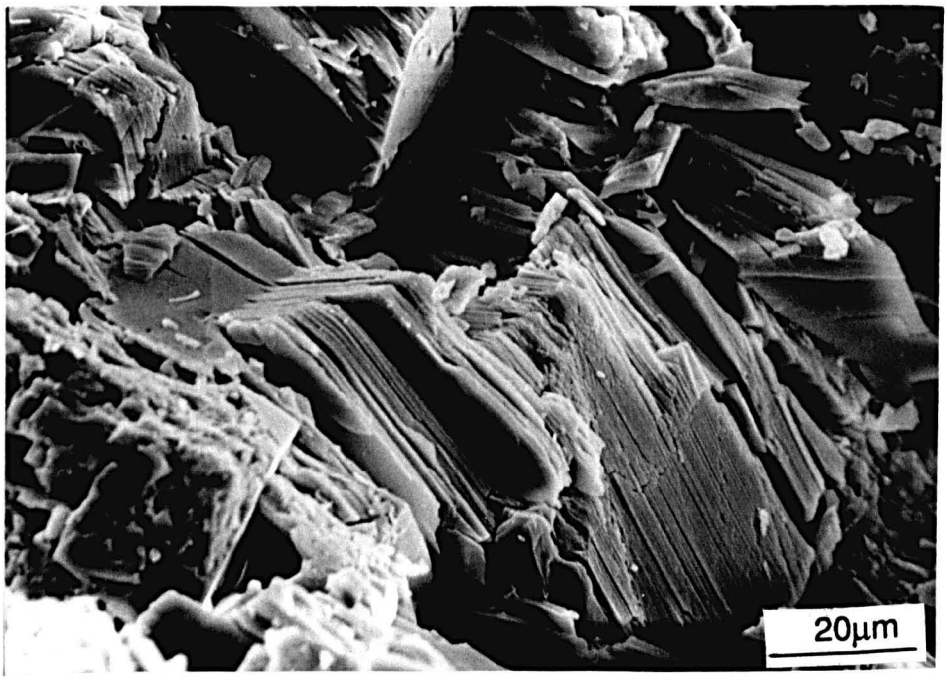

Fig. 6.74. SEM photomicrograph of a kaolinite booklet within a dolostone, E3a borehole, 351.0m.

of sandstones has been described by Walton (1982), Longstaffe (1984), Surdam *et al.*, (1984), Burley *et al.*, (1985) and Bjørkum and Gjelsvik, (1988).

In a meteoric-dominated diagenetic environment, aluminosilicate minerals (principally feldspars and micas) break down to produce clay minerals such as kaolinite. The dissolution of aluminosilicates is most commonly incongruent, owing to the very low solubility of Al and Si under normal (pH 6.5-8.5) carbonate groundwater conditions. A general expression of the reaction for microcline is:

$$2KAlSi_3O_8 + 2H^+ + H_2O \rightleftharpoons Al_2Si_2O_5(OH)_4 + 4SiO_2 + 2K^+$$

And for muscovite:

$$2KAl_3Si_3O_{10}(OH)_2 + 2H^+ + 3H_2O \rightleftharpoons 3Al_2Si_2O_5(OH)_4 + 2K^+$$

(after Bjørkum and Gjelsvik, 1988).

These reactions are not completely incongruent, and do release some cations into solution, including Na^+, K^+, Mg^{2+} and Ca^{2+}. Also, the reaction product (clay mineral) commonly has a higher Al/Si ratio than the precursor aluminosilicate (Freeze and Cherry, 1979). Dissolution is strongly influenced by carbonic acid, derived from carbon dioxide. The extensiveness of aluminosilicate dissolution is therefore largely a factor of the openness of the diagenetic system to a source of CO_2 (atmospheric/soil or reactions of organic matter at depth), and CO_2-charged groundwater advection rates

Incongruent dissolution of detrital feldspars and micas readily explains the occurrence of kaolinite in direct association with the leached aluminosilicates (silicate-related clays). Moreover, as the volume of authigenic kaolinite is approximately equal to the volume of aluminosilicate dissolved (Fig. 6.73), the source of kaolinite must be aluminosilicate dissolution (molar volumes at standard state of microcline =109.5cm^3/mole, kaolinite 99cm^3/mole [Berner, 1971]). That the aluminosilicates are leached, but adjacent kaolinites are unaltered, further supports the suggestion that the incongruent dissolution was relatively recent, otherwise the authigenic clays would be expected to have been corroded themselves during recent uplift diagenesis. Furthermore, the direct association of some cavity filling and silicate-related kaolinites with iron hydroxides, themselves considered to be derived from dissolution of aluminosilicates by high Eh fluids (6.5.5.2), supports the idea that both mineral phases were derived from the aluminosilicate minerals at a similar time.

Incongruent dissolution of aluminosilicates cannot explain dolomite-encrusting and cavity filling clay minerals, which are not directly associated with leached feldspars or micas.

As Al and Si are very insoluble under normal groundwater conditions, their transport to the sites of kaolinite precipitation is difficult to account for. One explanation is that Al, and possibly also Si were transported as soluble organic complexes (ligands) following aluminosilicate dissolution. Such complexing has been described from burial diagenetic environments in sandstones and near-surface, soil environments. In the burial environment, both CO_2 (to produce carbonic acid which leaches the aluminosilicates), and the organic complexing agents, are generated during the maturation of kerogen (decarboxylation) (Siebert *et al.*, 1984; Surdam *et al.*, 1984; Burley *et al.*, 1985). The congruent dissolution of aluminosilicates occurs in advance of migrating hydrocarbons. Within the soil and shallow vadose zones, Al and Si are complexed by autochthonously produced organic compounds such as the calcium oxylate anion ($2CaC_2O_4$) (Antweiler and Drever, 1983; Surdam *et al.*, 1984). Even small amounts of calcium oxylate may greatly enhance the solubility of Al (Surdam *et al.*, 1984). In the soil environment, organic acids as well as carbonic acid may leach aluminosilcates. The congruent dissolution reaction for an aluminium hydroxide is as follows:

$$3H^{+}_{(aq)} + Al(OH)_{3(s)} + 2CaC_2O_{4(s)} \rightarrow Al(C_2O_4)_{2(aq)} + 2Ca^{2+} + 3H_2O$$

(after Surdam *et al.*, 1984).

The clay minerals may be precipitated when organic complexes are destroyed or break down in response to changes in the geochemical environment (such as an increase of pH following carbonate dissolution) (Surdam *et al.*, 1984). As the organic complex is destroyed, Al precipitates as a hydroxide or clay mineral, incorporating other cations depending on the chemistry of the ambient groundwater (Antweiler and Drever, 1983). The effectiveness of near surface-derived organic matter will depend on the relative rates and spatial extents of its production and destruction. In soils, both production and destruction are at a maximum. However, it is possible for significant quantities of near surface-derived organic matter to be transported into the lower vadose/uppermost phreatic zones without consumption (Wood, 1985), where they could both complex insoluble ions and provide CO_2 for aluminosilicate dissolution.

Organic complexing was most likely important with regard to the transport and precipitation of late diagenetic iron/manganese hydroxides in the upper phreatic or vadose zones of the Raisby Formation palaeo-aquifer (6.5.5.3). Silicate-related kaolinite is directly associated with iron hydroxides, suggesting that aluminosilicate dissolution which produced both minerals was at least partly near surface in oxic groundwaters.

6.5.8. Authigenic clay minerals - Summary and conclusions.

In the absence of any other reasonable mechanism, carbonic acid derived from atmospheric/soil CO_2 in conjunction, in places, with oxylate anions likewise derived from the surface, were responsible for the precipitation of most late diagenetic kaolinite and smectite and within the Raisby Formation, as well as some iron/manganese hydroxides. Mesogenetic decarboxylation of organic matter may have been of some significance in the precipitation of authigenic clays currently seen in the subsurface (Fig. 6.74). However, during uplift diagenesis these would have been as prone to dissolution, if not more so, as the detrital aluminosilicates, and so are unlikely to be mis-identified as late diagenetic authigenic phases.

6.6.1. Telogenesis - Summary.

Uplift of the Raisby Formation, which started in the late Cretaceous/early Tertiary, was accompanied by a change of the ambient pore fluids, from being probably saturated with respect to calcite, dolomite, and anhydrite, to meteoric-derived fluids initially undersaturated with respect to all three. This change in conditions was the driving force for the pervasive alteration and precipitation of new mineral phases seen in the Raisby Formation at outcrop, and in shallow onshore boreholes.

In detail, the diagenesis was concentrated in two areas; distal meteoric aquifer (Raisby Formation being initially penetrated by groundwaters) and proximal meteoric aquifer (near-surface). The distal location was characterized by a low Eh, elevated fluid temperatures, and bacterial sulphate reduction. Precipitates included bright orange-luminescent calcite cements associated with calcitized dolomite and sulphate evaporites, and pyrite/marcasite. Migrating gaseous hydrocarbons derived from the underlying Coal Measures were important for catalysing bacterial sulphate reduction. The driving force for pervasive alteration within this zone was the high fluid Ca and SO_4 concentrations from gypsum dissolution, which caused a significant imbalance in the relative saturation states of calcite and dolomite. The upper limit of this zone of diagenesis is demarcated by a decrease in fluid Ca and SO_4 concentrations due to rapidly decreasing amounts of gypsum remaining, and more rapid groundwater advection rates.

The proximal aquifer area was characterized by high Eh fluids precipitating non-luminescent cements associated with oxidized Fe/Mn minerals. In this area of the aquifer, the driving force for diagenesis was degassing of CO_2 from calcite-saturated groundwaters. Some replacement was active in this zone, although diagenesis was dominated by congruent dissolution as groundwaters were undersaturated with respect to most mineral phases, especially dolomite and gypsum, and also, at times, calcite. Precipitation of authigenic kaolinite and smectite cements was of local significance in the upper parts of the aquifer.

The area between the two groundwater zones was characterized by limited diagenesis, mainly dull and bright orange-luminescent calcite cementation. However, the strong difference in palaeotemperature results between luminescent and non-luminescent calcites, suggests that the intermediate area may have been relatively diagenetically inactive, with fluids having a low supersaturation with respect to calcite. In this intermediate area, input into fluids of Ca and CO_3 was slow, as groundwaters were close to saturation with respect to dolomite following intense congruent dissolution in the vadose zone, and most gypsum had been dissolved out. Therefore, both calcite and dolomite were close to saturation. Thus, diagenesis was most important in lower and upper levels of the aquifer driven by variable saturation states of calcite, dolomite and gypsum. The main diagenetic zones, and characteristic precipitates of those zones within the Raisby Formation palaeoaquifer are illustrated in figure 6.75.

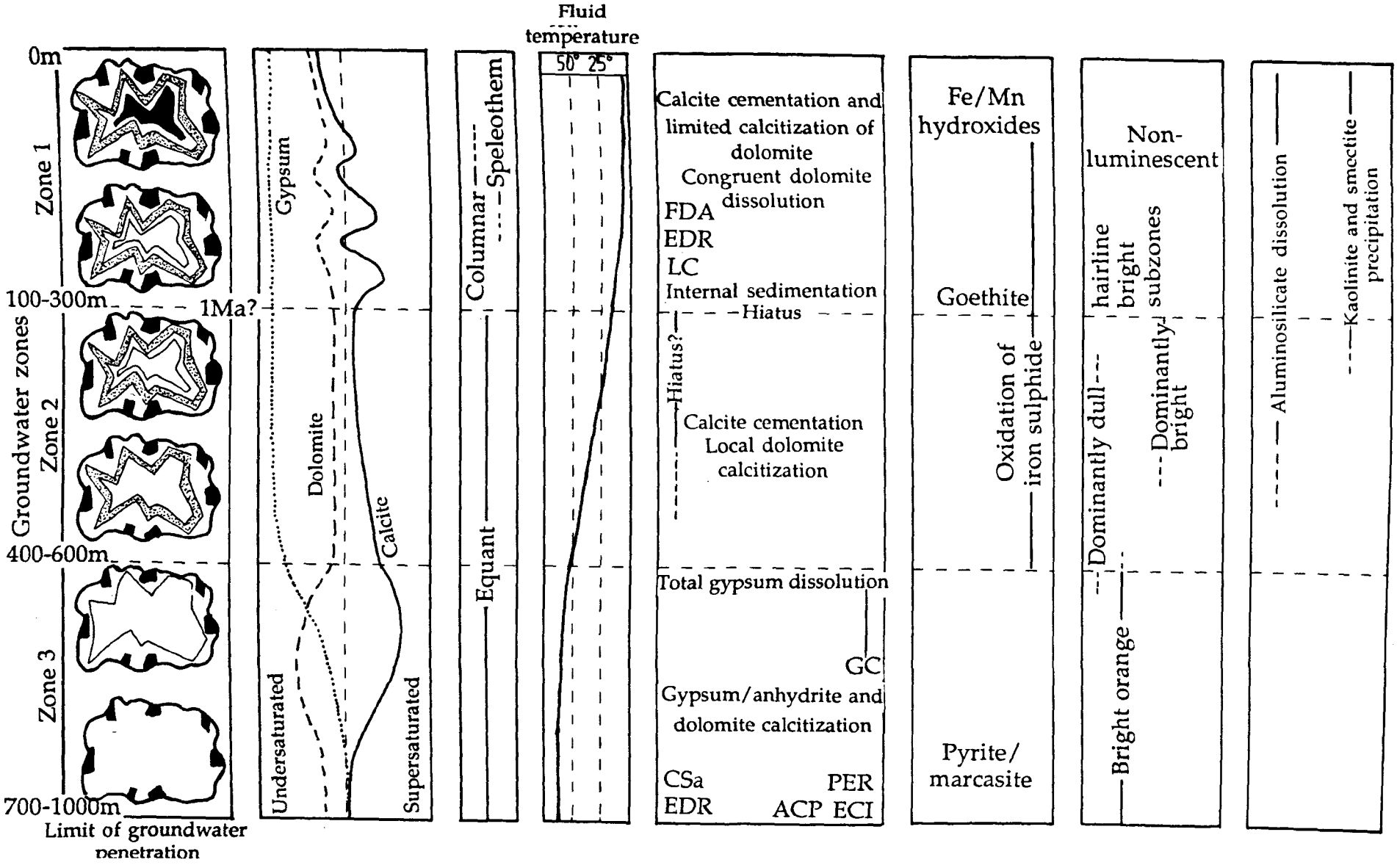

Fig. 6.75. Summary of the telogenetic evolution of the Raisby Formation, as defined from calcitized evaporites, calcitized dolomites, calcite cements, and authigenic iron and clay minerals.

Chapter 7

Mineralization.

7.1.1. Mineralization in the Raisby Formation - Description.

Mineralization of the Raisby Formation by barite, fluorite, galena, sphalerite, and copper minerals has been described throughout its outcrop, and in boreholes. The locations of the recorded mineralization are shown in figure 7.1, and tabulated in appendix XI. The paragenesis of mineralization recorded during this study is described below.

7.1.1.1. Borehole W8.

Small quantities of sphalerite, and less abundant barite were recorded within this borehole. Both were in direct association with gypsum and anhydrite, which is replacive of the distinct host lithology (a type ED mesogenetic calcitized dolomite).

Sphalerite occurs replacing anhydrite. It forms small (less than 1cm), anhedral crystals, blue-coloured in hand specimen, with a frosted surface texture, and commonly poorly-developed concentric light-dark blue colour zonation. It has been identified as sphalerite by XRD and chemical analysis. In hand specimen and thin section, the contact of sphalerite with host anhydrite is irregular, and demarcated by anhydrite cleavages (Fig. 7.2a). The sphalerite was recorded in two distinct areas of the core, from 276.44-276.03m and 274.00-273.77m.

Barite, likewise, occurs in direct association with the gypsum and anhydrite, although only where they have been leached out. The barite forms small (less than 1.1mm), water-clear euhedral crystals, partially occluding pores 2-3mm in size. This mineral has been identified as barite by SEM on the basis of crystal habit, although it could possibly be a related mineral, such as anglesite or celestite. Barite was concentrated in two zones within the core, from 280-278.73m and 276.44-276.03m, where approximately 50% of the sulphate had been dissolved out.

7.1.1.2. Frenchmans Bay.

Barite mineralization is abundant within the Raisby Formation at Frenchmans Bay, although absent in the extensively exposed Raisby Formation between the northern end of Frenchmans Bay and Trow Point. Barite occurs in four different paragenetic settings:

1. Cementing neptunean dykes of Basal Permian Sands within the lower Raisby Formation,
2. Partially replacing former sulphate evaporite nodules,
3. Partially occluding cavities formed by the leaching of clasts from within a debris flow,
4. Cementing fractures which cut the Marl Slate.

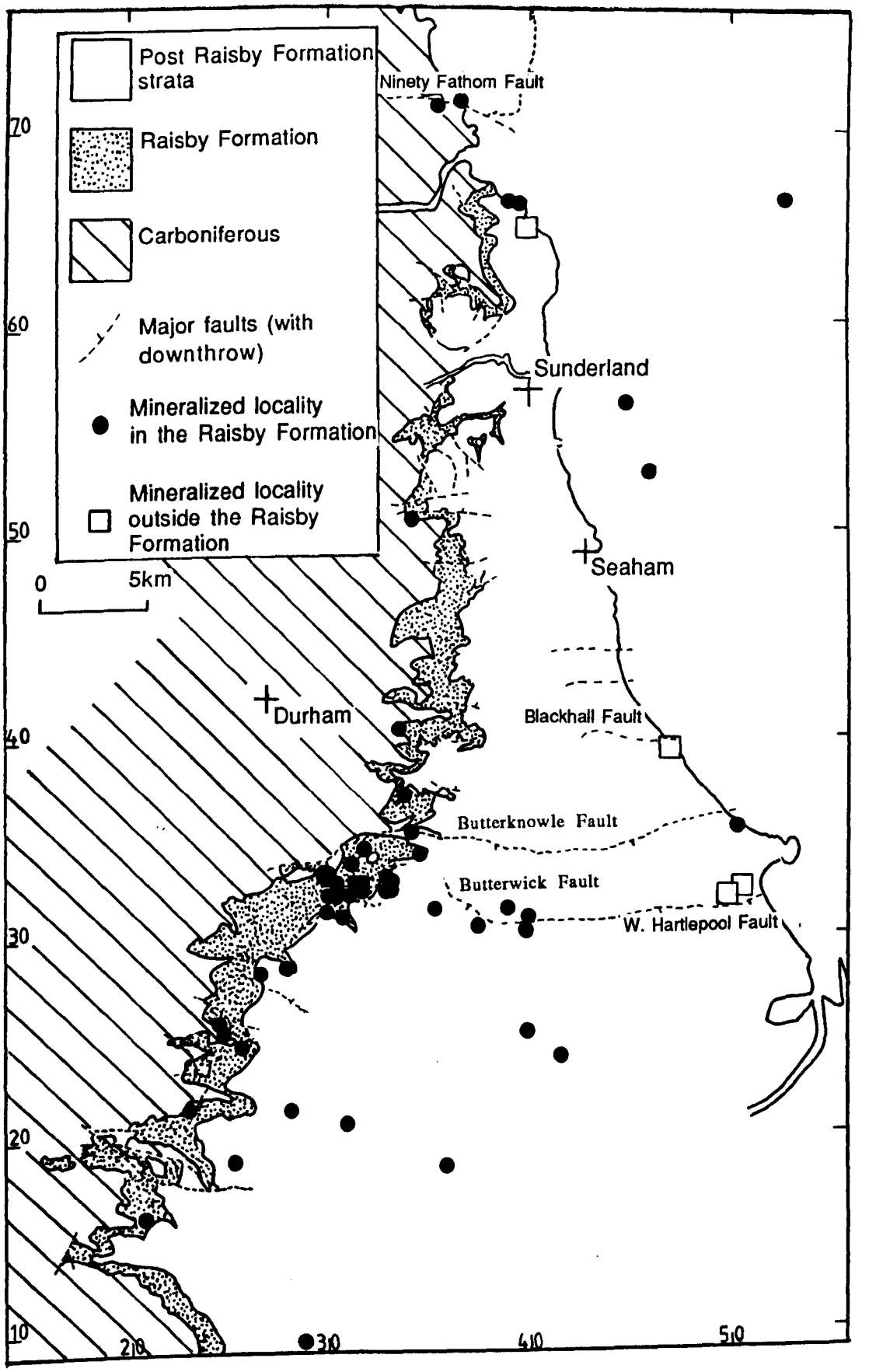

Fig. 7.1. Localities of mineralization within Zechstein carbonates of northeast England. Recorded from this study and previous works (tablulated in appendix XI).

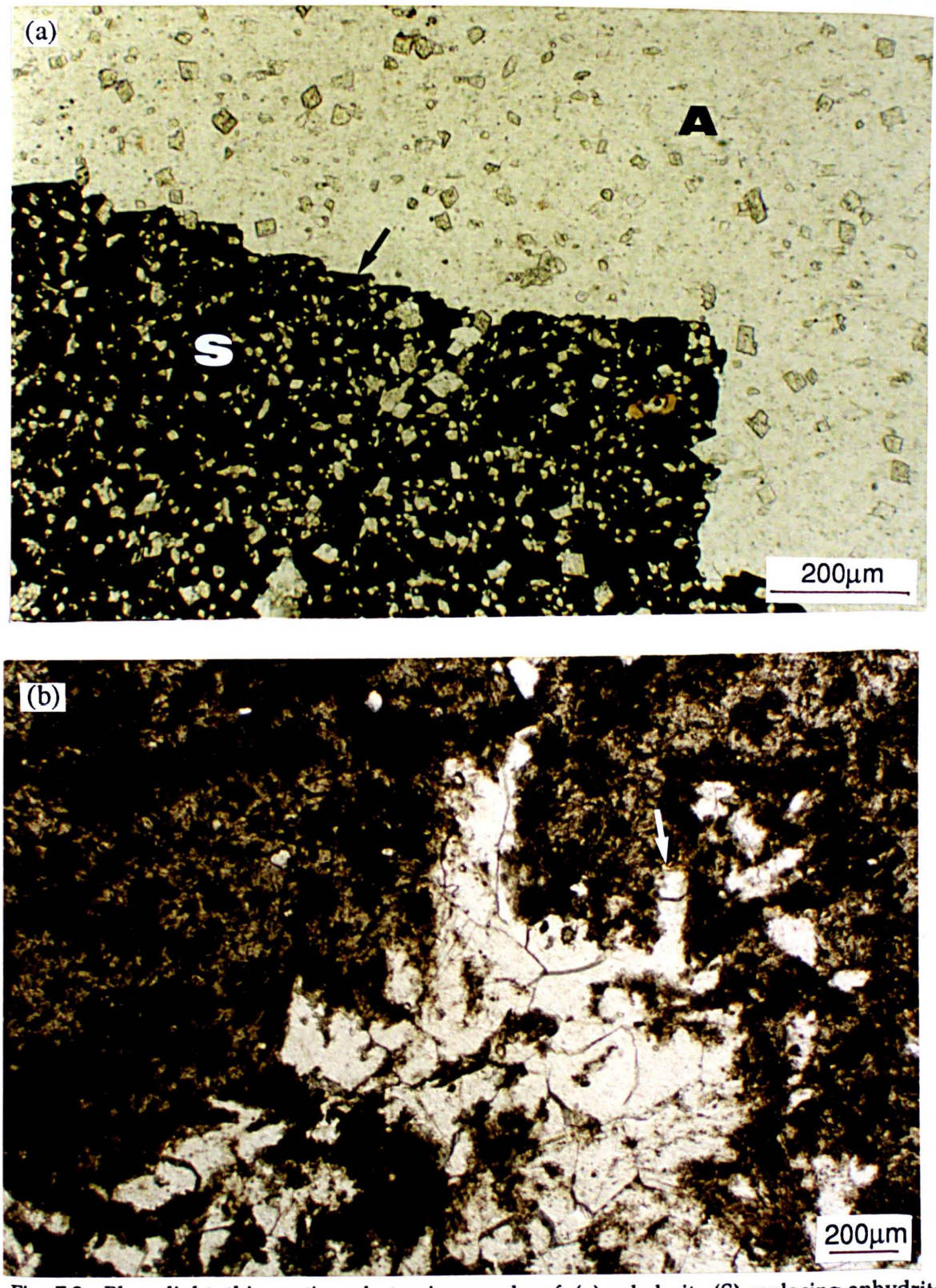

Fig. 7.2. Plane light, thin section photomicrographs of; (a) sphalerite (S) replacing anhydrite (A), borehole W8, 273.80m, (b) barite within a cavity after sulphate, Frenchmans Bay. The contact of sphalerite with anhydrite in (a) is controlled by cleavages within the anhydrite (arrowed). Note the very abundant dolomite inclusions within the sphalerite, of the same density as within anhydrite. In (b), the contact of barite with calcite defines lath-shaped structures with rectilinear terminations (arrowed), interpreted to be pseudomorphs after anhydrite.

Three neptunean dykes of Basal Permian Sands cut the Marl Slate and basal Raisby Formation at this locality. They are very narrow, and a maximum of 80cm in vertical extent. They all lie along joint planes which have a similar strike of 060°-240°, 070°-250° and 073°-253°. Barite cements the sandstone together with iron sulphide. Iron sulphides predate barite, coating silicate grains and, commonly, both the iron sulphide and silicate grains are poikilitically enclosed within coarse plumose barite aggregates, 500μm in diameter. The occurrence of barite-cemented moulds of former quartz grains, outlined by iron sulphide, suggests leaching of silicates prior to/synchronous with barite mineralization.

One bed containing abundant, 10 to 20cm-sized cavities after sulphates, has been heavily mineralized by barite, although in this bed mineralization is restricted to the cavities. The barite is different from other areas of Frenchmans Bay in that it is 'moderate orange-pink' (5 YR 8/4) in colour. Mineralization is complete around cavity margins, and decreases in intensity towards their centre, where it passes into a coarse, zoned calcite cement. The contact of massive barite with zoned calcite is very irregular, commonly describing angular re-entrants of calcite into the barite (Fig. 7.2b). Some of these structures are parallel-sided with rectilinear terminations (Fig. 7.2b). Zonation of the calcite where in contact with barite suggests that it is occluding porosity formed by the dissolution of a former lath shaped mineral, itself replaced by barite.

Barite occurs most extensively at this locality within a coarse debris flow (Fig. 7.3a) which directly underlies, and is truncated by a major slide plane. The barite forms white, millimetre-sized spherulitic aggregates of crystals. It is virtually absent from beds immediately above and below the debris flow. Barite partially or completely occludes cavities formed by the dissolution of dolomite clasts and bioclasts (or a mineral which formerly replaced them, such as gypsum/anhydrite) within the debris flow, and small sub-vertical fractures. It only completely cements the smallest cavities and fractures, larger ones are lined by barite, and the remaining porosity is occluded by calcite.

Small, tens of centimetres long barite-cemented fractures which cut the Marl Slate and Raisby Formation are scattered throughout this section, although restricted to Frenchmans Bay. These fractures are most abundant within the Marl Slate.

7.1.1.3. Man Haven.

Most barite mineralization at this locality is concentrated in the uppermost 20cm of resedimented Raisby Formation below the base of the Z2 collapse breccias. The top surface of the Raisby Formation is heavily encrusted by millimetre-sized, subspherical aggregates of barite. Barite is mainly replacive of Raisby Formation dolostones, although also occurs within calcite cemented cavities formed by the dissolution of tabular clasts in a small, 30cm thick debris flow, whose top is 13cm below the base of the Z2 collapse breccias. No barite mineralization was found within the Z2 collapse breccias during this study, although

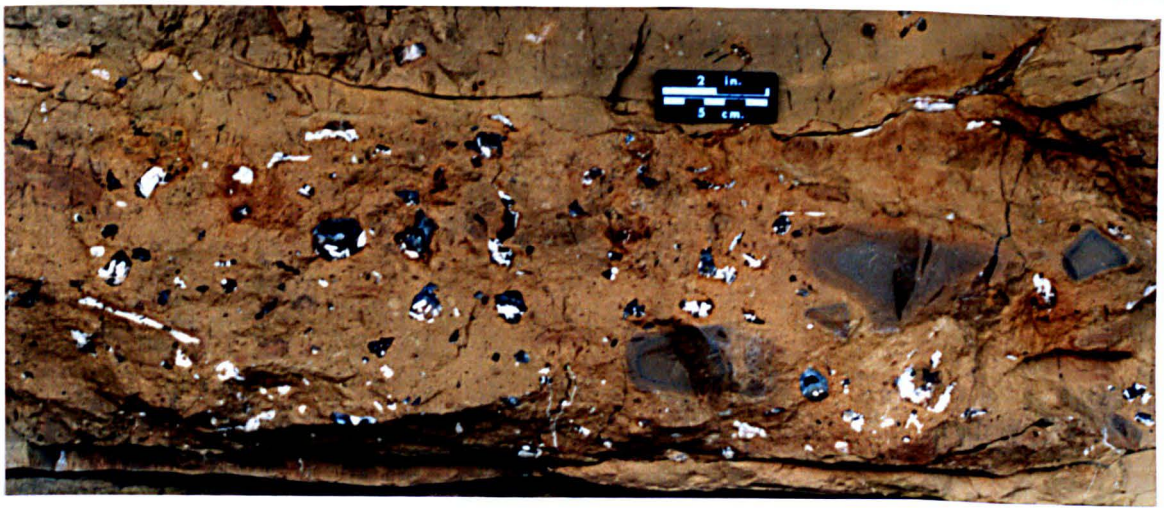

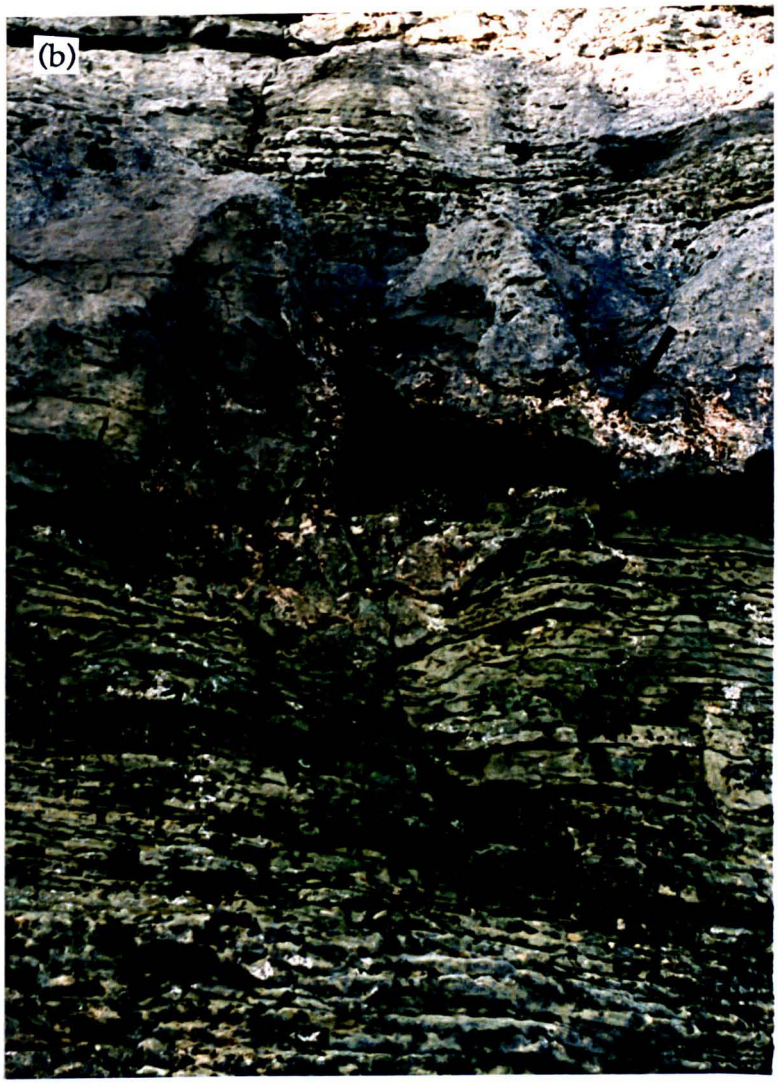

Fig. 7.3. Outcrop photographs of barite mineralization; (a) Frenchmans Bay debris flow conglomerate, (b) Man Haven. In (a), barite occurs within calcite-lined pores. The pores were probably formed by the dissolution of clast-replacive sulphates. Note that the larger clasts are unaltered. By contrast, in (b), barite (arrowed) is replacive of Raisby Formation dolostones, and is joint-controlled. The field of view is approximately 5m vertically.

G.M. Harwood (*pers. comm.*, 1988) has recorded small quantities. A very similar occurrence of barite to that at Man Haven, concentrated beneath the Z2 collapse breccias in a 2ft (0.61m) thick band was recorded replacing the uppermost Raisby Formation by Smythe (1922) (in Dunham, 1934) from Marden Quarry, just north of the Tyne (NZ 355, 709).

Barite also replaces the lower bedded and resedimented upper Raisby Formation dolostones at Man Haven marginal to a 124°-304° striking vertical joint (Fig. 7.3b). Mineralization is not symmetrical about the joint, and is recorded for 2.3m south but only 1.1m north of it. Barite may be parallel to joint margins, or parallel to bedding within the Raisby Formation adjacent to the joint (Fig. 7.3b).

7.1.1.4. Houghton Quarry.

Mineralization is rare in the northern part of the Raisby Formation outcrop around Sunderland (Fig. 7.1). The only locally significant mineralization is at Houghton Quarry, where barite and galena are, in turn, restricted to the northern part of the exposure.

Barite occurs extensively within a debris flow and overlying compaction breccia at this locality. Barite replaces the dolomitic matrix of the debris flow most extensively, whereas dolostone clasts remain intact. The barite occurs as white, 400-500μm sub-spherical plumose aggregates. The overlying compaction breccia contains small quantities of barite, partially cementing interclast porosity, in association with coarse calcite cements. The relationship between calcite and barite is unclear.

Galena is considerably more abundant and widespread than barite. It replaces limestone immediately below the debris flow, the debris flow itself, partially cements interclast porosity within the compaction breccia, and, most abundantly, occurs as a replacive and partially pore-filling phase within the upper autobrecciated dolostone. The galena forms sub-euhedral to euhedral crystals of a few millimetres to few centimetres in size. It has not been recorded in direct association with barite. Galena is most abundant within autobreccia dolostones in the northwest area of the quarry, a few metres either side of a small fault trending 063/70°NW. The throw on the fault is very small (few centimetres). All occurrences of galena and barite were in the same area of the quarry (within a few hundred metres radius) as the fault.

7.1.1.5. Running Waters Quarry.

Large quantities of barite, together with smaller amounts of fluorite have been recorded from this locality. Barite occurs in two distinct petrographic associations; lining large cavities after sulphates and partially replacing calcitized dolostone breccias.

Large, barite-mineralized cavities after sulphates are very abundant, especially in the southeastern part of the quarry, near to the base of the Raisby Formation. The cavities after sulphates are 10-20cm in diameter and hemispherical, with flat bases and convex-upwards

tops. Where the host dolostones are finely laminated, there is evidence for deformation of laminae around the cavities. In any one bed, barite is completely restricted to these cavities. Barite forms large (commonly 1cm-diameter) 'very pale orange' (10 YR 8/2) coloured radiating masses which partly line the cavities (Fig. 7.4), although never completely occlude them. Iron minerals are also very common within the cavities (Fig. 7.4). They may postdate barite (predating calcite) or, rarely, completely occlude the central porosity of the cavity following calcite pore fill cementation (Fig. 7.4). Thus, all iron mineralization postdates barite, although may predate and/or postdate calcite. In thin section, the iron forms 300μm long, rectangular crystals of hematite, although rarely, similar-sized, or slightly smaller crystals of marcasite occur in direct association with the hematite, suggesting that hematite is an oxidation product of marcasite (6.5.5). Along the contact of barite with calcite cement, rare, small (10-20μm), anhedral crystals of fluorite are present; these may have been internally sedimented. Following barite precipitation, the remaining porosity in the cavities has been partially or more commonly completely cemented by coarse calcite. The crystals are zoned bright/dull orange-luminescent and commonly contain internal sediments of hematite and barite. Local dissolution porosity within the cements is occluded by non-luminescent calcite. Geochemically, the calcite cements are very similar to those within other cavities after sulphates within the Raisby Formation (Appendix VII).

Barite associated with calcitized dolomite has a complex petrographic relationship to the diagenesis of the host rocks. Barite selectively replaces calcitized dolomite, which itself occurs within coarse dolostone breccias and as thick veins dissecting the host dolostone. The barite also occurs as a pore filling cement in association with these lithologies. Barite is distinctive, occurring as large (2-3mm long by 300-400μm wide), water-clear laths. The diagenesis of the host rocks is summarized below:

1. Local brecciation (possibly by synsedimentary resedimentation),
2. Precipitation of radiating anhydrite clusters, partially replacing margins of the dolostone clasts and, probably, partly as a pore filling cement. Small dolostone clasts may be almost completely replaced by sulphate, whereas the larger clasts are only replaced around their margins (Fig. 7.6b),
3. Dissolution of sulphates and concurrent calcitization of dolomite (EDR texture). Finely crystalline calcite (70-260μm) poikilitically encloses numerous corroded dolomite crystals 30-40μm in size (Figs. 7.5a & 7.6b). Small dolomite breccia clasts (less than few millimetres in size) are completely calcitized (Fig. 7.6b), whereas only the margins of larger dolostone clasts have been replaced. The replacive calcite is bright orange-luminescent.
4. Barite mineralization. Both partially- and completely-calcitized dolomite is replaced by barite (Fig. 7.5a) which also forms a pore filling cement (Fig. 7.6a). The most anomalous feature of the replacive barite is that it has an identical inclusion density to that of the host replacive calcite, which renders the barite almost invisible in plane light.

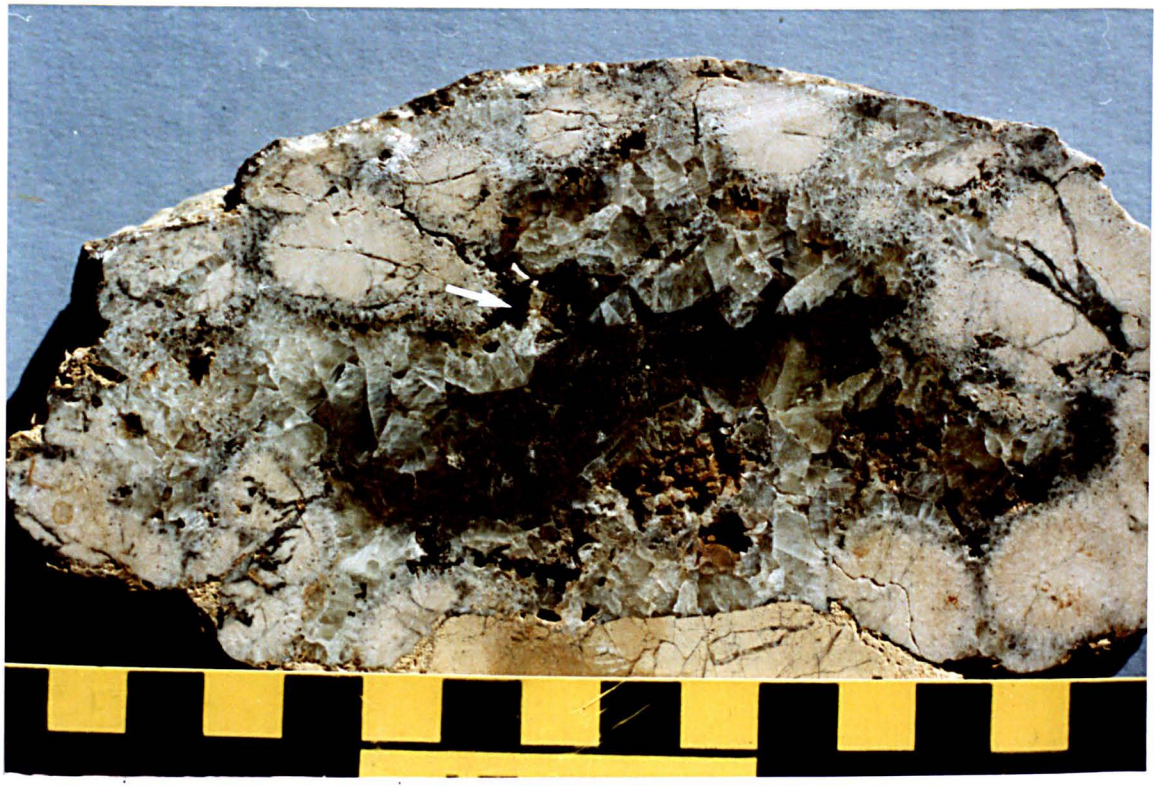

Fig. 7.4. Hand specimen of a large barite-mineralized cavity after sulphate, Running Waters Quarry. Sub-spherical aggregates of barite line the cavity. Barite mineralization was followed by the precipitation of euhedral marcasite (arrowed), calcite cement, and the remaining porosity was occluded by pyrite/marcasite (now hematite). Note the fracturing of one barite aggregate, cemented by iron and calcite. Scale in centimetres.

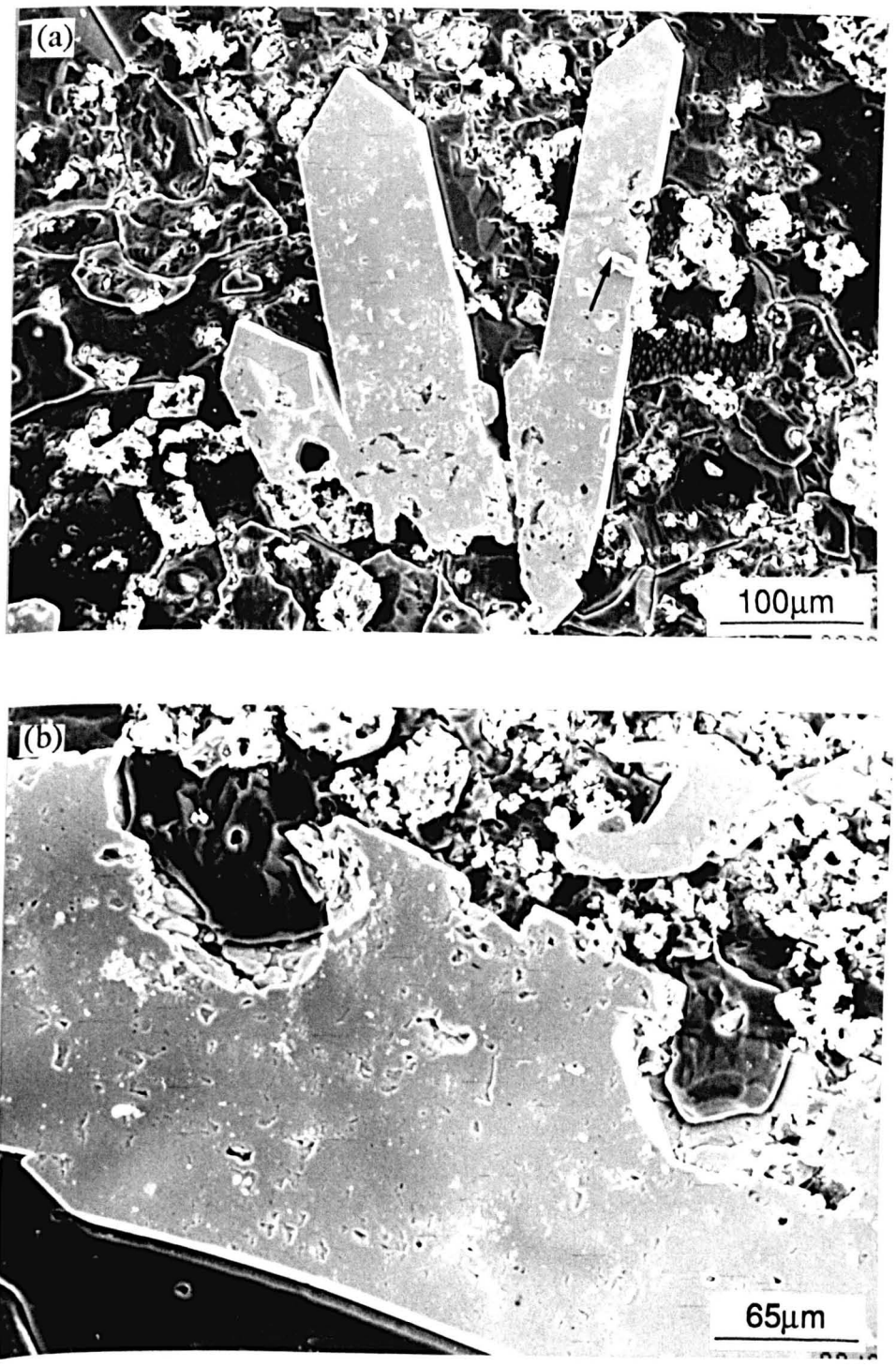

Fig. 7.5. SEM photomicrographs of polished and etched samples of a barite-mineralized calcitized dolostone breccia, Running Waters Quarry. (a) illustrates euhedral barite laths which are replacive of calcitized dolomite. White coloured dolomite relics within the calcite are also enclosed within barite (arrowed). (b) shows detail of the margin of a barite lath, partially replaced on one side by sub-euhedral calcite crystals.

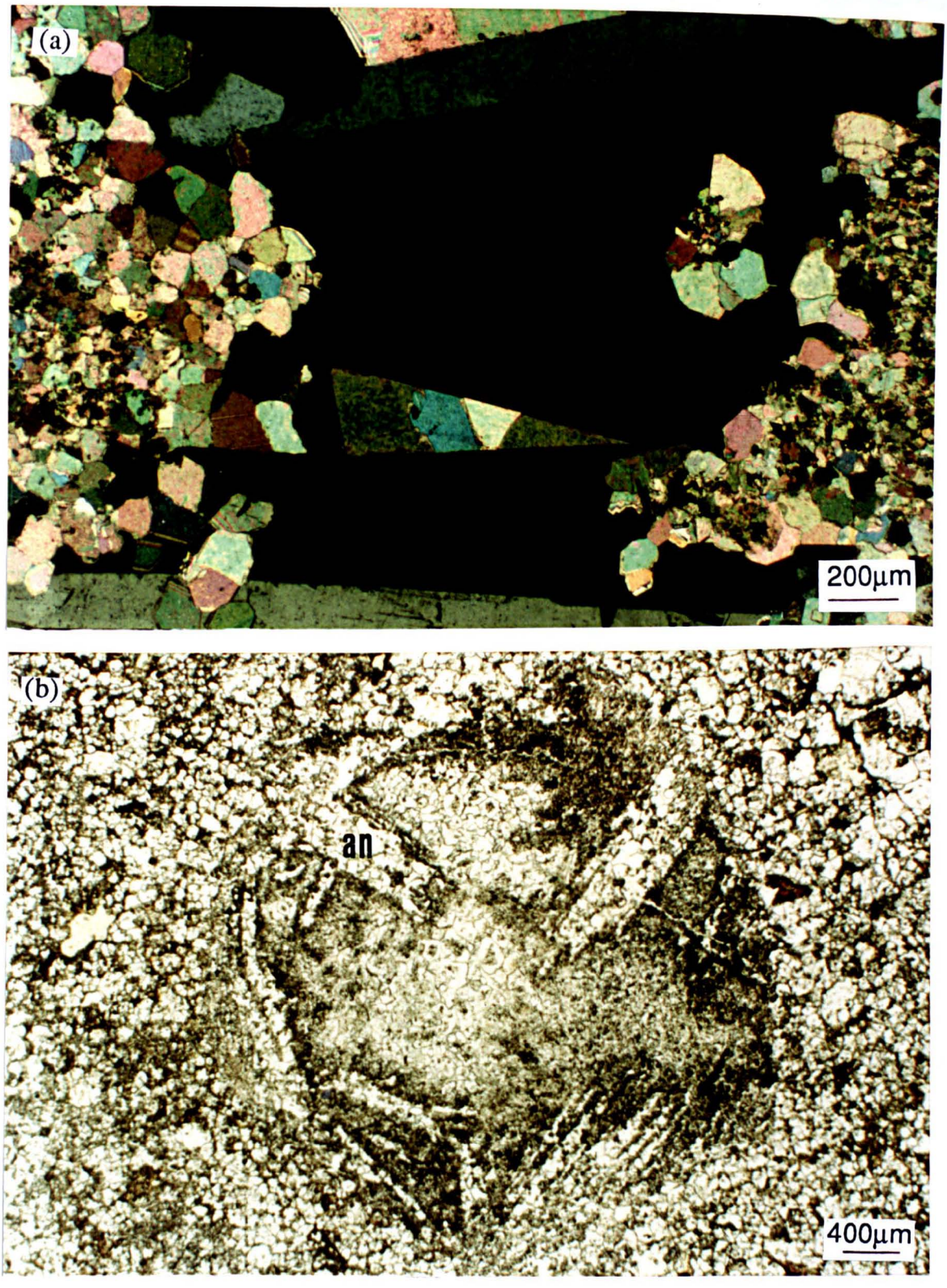

Fig. 7.6. Thin section photomicrographs of barite-mineralized calcitized dolostone breccias, Running Waters Quarry. (a) illustrates euhedral barite laths (in extinction), occluding a pore, later cemented by coarsely crystalline calcite. The laths have been extensively replaced by calcite at their contact with the host calcitized dolostone. (b) is a completely calcitized dolostone clast which was replaced by anhydrite around its margins prior to calcitization. The anhydrite pseudomorphs [an] are occluded by a different generation of calcite to that which replaces dolomite.

5. Calcite cementation. The first phase is finely crystalline (100-300μm) and dull orange-luminescent. This cement occludes inter-breccia clast and evaporite dissolution porosity. The calcite has actively replaced barite laths, presenting sub-euhedral crystal faces into the barite (Figs. 7.5b & 7.6a). Calcite intracrystalline zonation parallels the calcite-barite contact. The second, coarser (500-700μm) cement phase (bright orange-luminescent) is a passive pore filling cement, which does not replace barite (Fig. 7.6a).

The only previous study of barite at this locality was by Hirst and Smith (1974) who obtained fluid inclusion temperature measurements of less than 70°C.

7.1.1.6. Quarrington Quarry.

Lower Raisby Formation dolostones at this locality host very abundant sphalerite, and less common, although still abundant barite mineralization. Sphalerite occurs in a similar stratigraphic position to barite, a few metres above the base of the Raisby Formation, although they have not been recorded together during the present study. However, G.M. Harwood (*pers, comm.*, 1990) has recorded barite and sphalerite together in an old quarry close to the present one.

Some of the sphalerite cements isolated small fractures within dolostones, although most commonly, it occurs as centimetre thick, bed-parallel flats of colloform banded crystals, having a distinct 'dark yellowish brown' (10 YR 4/2) colour. The flats are up to 7cm thick and can be traced for many metres laterally. Colloform banded sphalerite crystals have grown outwards from dolomite nuclei. Angular clasts of brecciated dolomite also occur within the sphalerite. Individual zones of the colloform sphalerite are 200-300μm wide, and defined by abrupt variations in inclusion densities (Fig. 7.7a). Contacts between zones may be irregular, or defined by euhedral crystal faces of sphalerite (Fig. 7.7b). Fractures, which cut the sphalerite may be open, filled by calcite and brecciated dolostone, or cemented by 40-50μm euhedral sphalerite crystals (Fig. 7.7a). M Sweeney (*pers comm.*, 1988) analysed sphalerite from within a vugh in the Marl Slate from this quarry which gave a result of $\delta^{34}S$ -24.1‰ (CDT). It is not known for certain that this is the same phase which occurs within the overlying Raisby Formation, but this is considered likely, especially as calcite and barite from a similar vugh gave oxygen and sulphur isotope results respectively, which are consistent with other data from the Raisby Formation (see below).

Barite at this locality is restricted to calcite cemented cavities after sulphates. It occurs as small, spherical clusters of radiating, plumose crystals. Mineralization predates most, or all calcite cementation. Carbon and oxygen isotope data for one cavity fill cement closely associated with the barite give $\delta^{13}C$ 1.1‰, $\delta^{18}O$ -15.5‰. Sulphur isotope data for barite within a vugh in the Marl Slate at this locality gave a result of $\delta^{34}S$ +11.6‰ (CDT), indicative of Zechstein seawater (Sweeney *et al.*, 1987). As with the sphalerite analysis, the precise paragenesis of Sweeney's sample is uncertain, although carbon and oxygen isotope data for

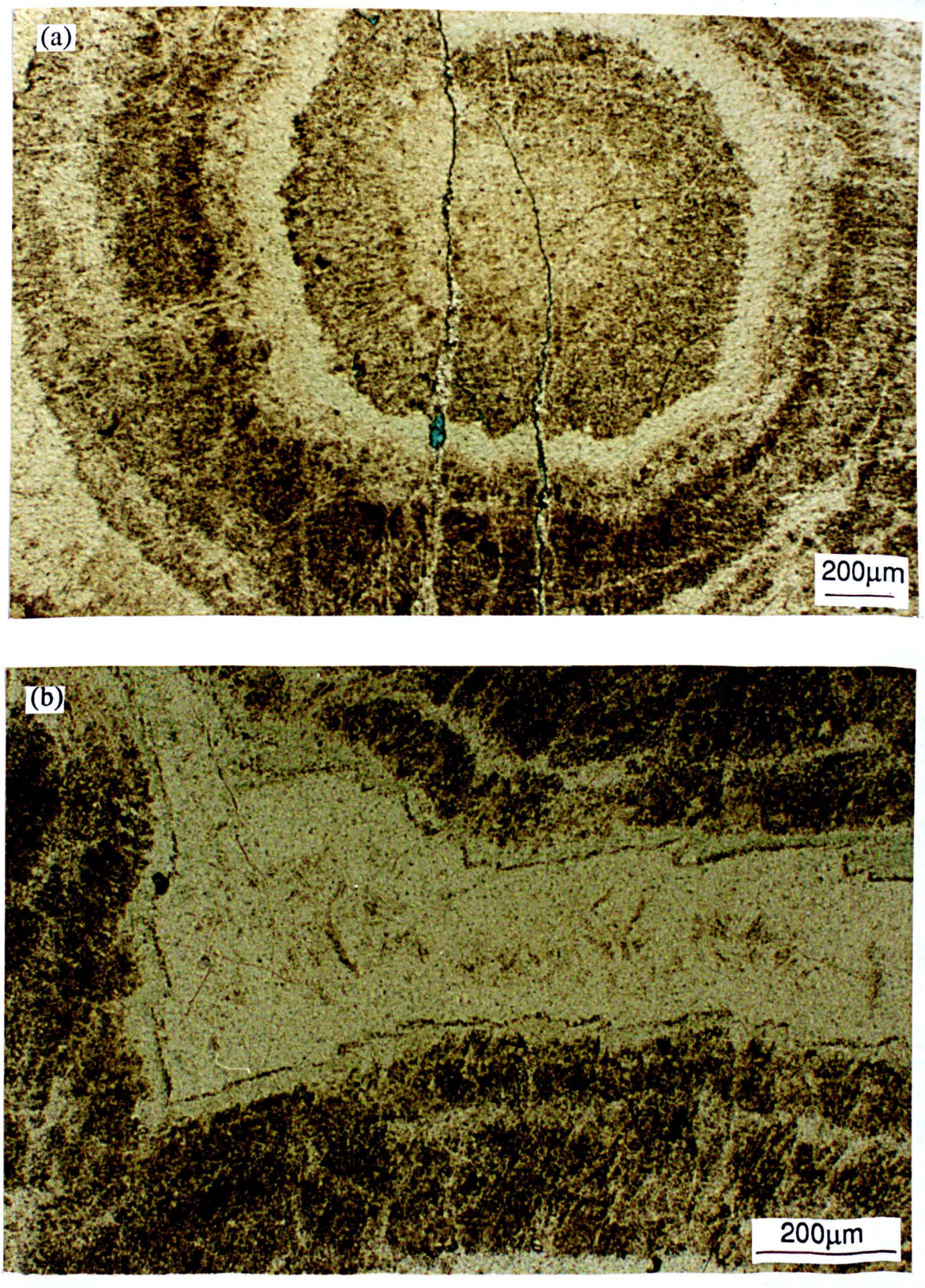

Fig. 7.7. Plane light, thin section photomicrographs of colloform banded sphalerite, Quarrington Quarry. (a) shows the core of a colloform banded structure which has been fractured, and the fractures cemented inclusion-free by sphalerite. (b) illustrates the junction of two adjacent colloform banded structures. Both presented euhedral crystal faces into a central porosity, now filled by inclusion-free sphalerite.

calcite cements from his vugh ($\delta^{13}C$ -3.06 and -2.71‰, $\delta^{18}O$ -10.93‰ and -11.55‰) are very similar to those within cavities after sulphates in the Raisby Formation analysed during this study (6.5.2.3).

7.1.1.7. Raisby Quarry.

This locality is the most commonly cited for mineralization in the Raisby Formation (Appendix XI), although the quantity of mineralization is extremely small. Minor amounts of barite, copper minerals, galena and sphalerite were recorded. Barite occurs as very small (hundreds of microns in diameter) crystals within coarse, luminescent calcites which cement cavities after sulphates within dolostones above the main limestone. Both sphalerite and galena replace the limestone itself, sphalerite cementing small fractures and galena occurring as euhedral replacive crystals.

Copper at this locality is mainly chalcopyrite and associated secondary copper minerals (tennantite, azurite and malachite). Small quantities of chalcopyrite ($CuFeS_2$) with tennantite (CuO) and malachite ($Cu_2(OH)_2CO_3$) were recorded lining calcite-cemented pores within dolostones above the limestone. Tennantite occurs as millimetre-sized anhedral crystals in which small (average 200μm), chalcopyrite inclusions are common. Malachite occurs along the contact of tennantite with calcite cement (Fig. 7.8a). It forms radiating aggregates of small (up to 50μm long), columnar or acicular crystals (Fig. 7.8a). Malachite has also grown along corroded cleavages within the enclosing calcite, commonly for up to 100μm from the tenanite (Fig. 7.8a). Along cleavage planes where malachite is not present, the calcite has been irregularly corroded, with resultant porosity cemented by non-luminescent calcite (Fig. 7.8b). The corroded calcite cleavage planes are lined by iron hydroxides. Where the two are in contact, malachite postdates hydroxide precipitation. Pseudomorphs after anhydrite, similar to those described by Lee and Harwood (1989, figs. 7 & 9) from Raisby Quarry, have been identified within the enclosing calcite by luminescence. Previous work suggests that the copper mineralization at Raisby Quarry occurs in veins (with vein copper also being recorded from Garmondsway nearby (Lebour 1903 [in: Fowler, 1943]), and breccias associated with the Butterknowle Fault (Hirst and Smith, 1974).

7.1.1.8. Rough Furze Quarry.

The Raisby Formation within this quarry is extensively mineralized by barite and fluorite, restricted to calcite lined cavities after sulphates, and immediately adjacent host dolostones.

All fluorite and barite has grown from margins of the cavities into their centers, or occludes small fractures which cut host dolostones immediately adjacent to the cavity fills. Fluorite predates barite, and forms cubic crystals 200μm in size (Fig. 7.9a). Barite occurs as white coloured, millimetre-sized hemispherical aggregates of fine crystals which nucleate

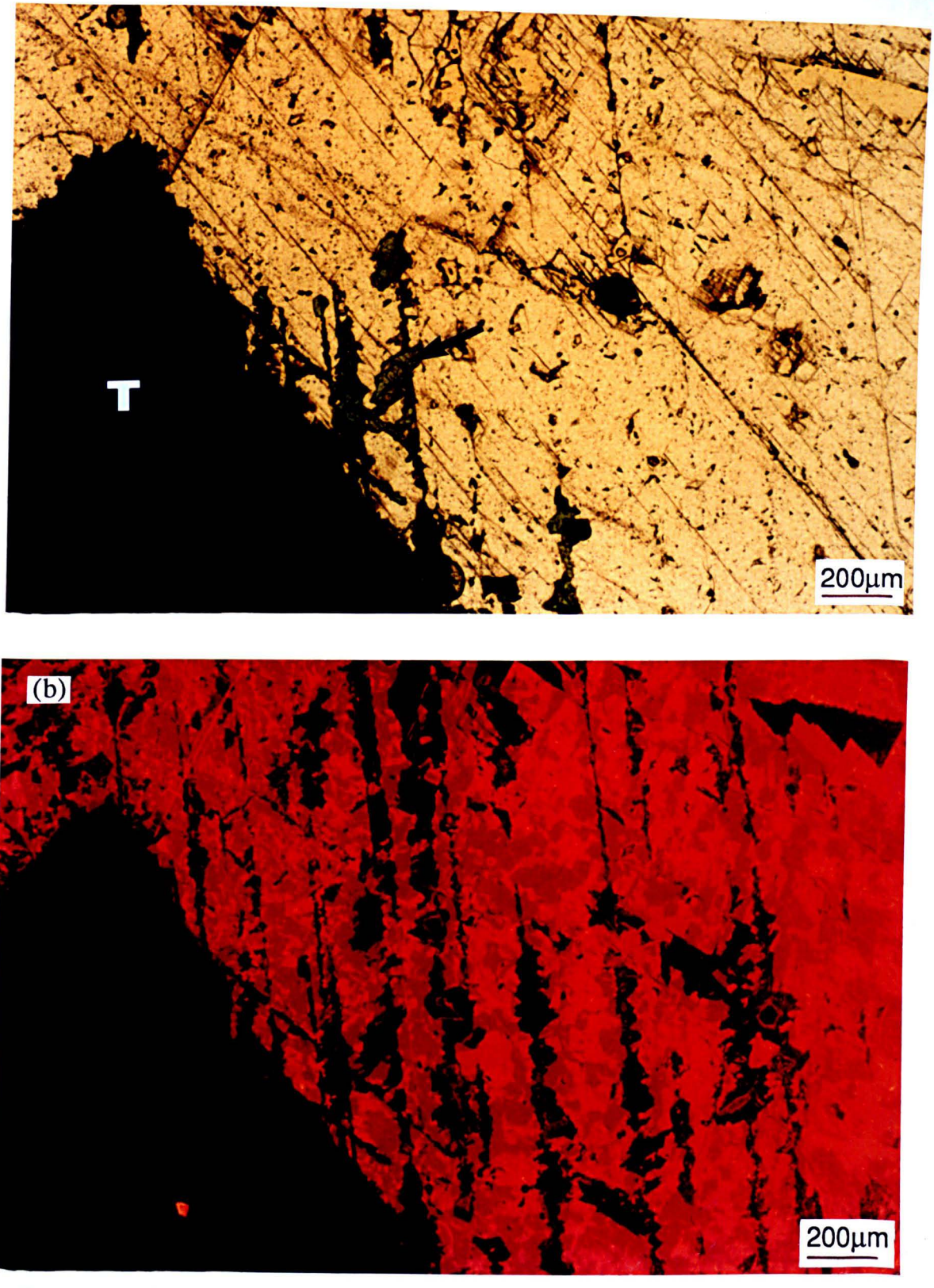

Fig. 7.8. Thin section photomicrographs of the contact of copper with calcite cement, Raisby Quarry; (a) plane light, (b) luminescence. Tennantite(T) has partially altered to malachite (arrowed) which precipitated along corroded cleavages of the enclosing calcite cement. Dissolution porosity which formed in advance of the malachite has been occluded by non-luminescent calcite.

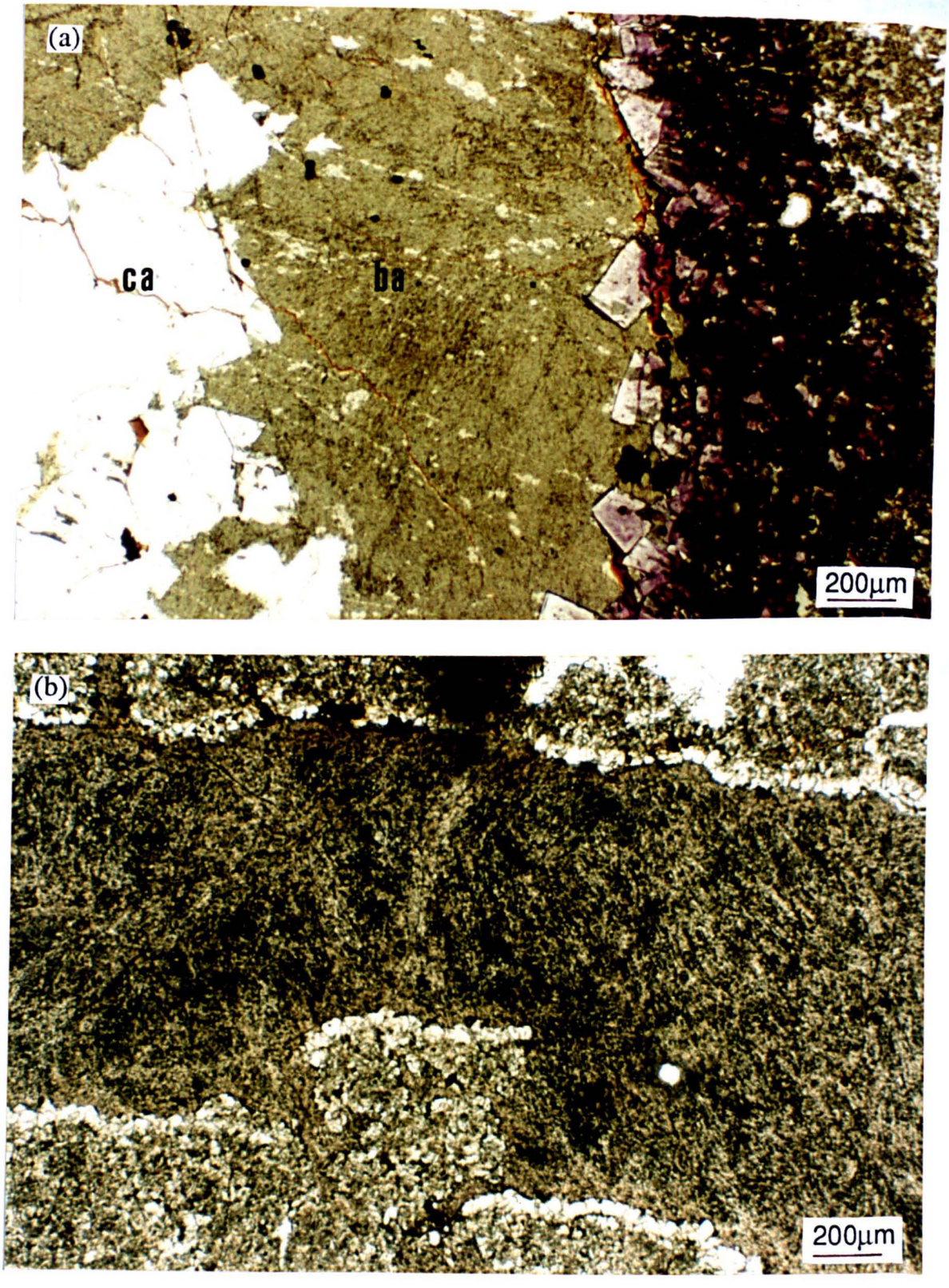

Fig. 7.9. Plane light, thin section photomicrographs of mineralization, Rough Furze Quarry. (a) shows the margin of a mineralized cavity after sulphate which passes from fluorite (purple coloured), into barite (ba) and calcite (ca). The contact of barite with calcite defines anhydrite pseudomorphs. In (b), barite completely fills a fracture lined by stubby dolomite crystals associated with dolomitized anhydrite. Note brecciation of the dolomite-cemented fracture margin prior to mineralization.

from dolostone and fluorite, and only partially occlude porosity (Fig. 7.9). Barite mineralization postdates fracturing and dolomite cementation of the host dolostone, although predates calcite cementation (Fig. 7.9). The contact of barite with calcite commonly defines rectangular re-entrants with square or wedge ends and generally straight, parallel sides a few hundred microns long (Fig. 7.9a). The angular re-entrants are very similar to those within mineralized cavities after sulphates from Frenchmans Bay (Fig. 7.2b), and described by Harwood (1983) from Ferryhill, and Rough Furze Quarry. The succeeding calcite cements are zoned, and the core blotchy orange/non-luminescent zone is possibly replacive of anhydrite (PER calcitized sulphate [6.2.1.1]). The contact of calcite with host dolostone or barite is commonly encrusted by hematite after marcasite.

7.1.1.9. Chilton Quarry.

Along with Raisby Quarry, this locality has been the most commonly cited to host mineralization (Appendix XI). Barite, fluorite and sphalerite were recorded during the present study, in common with previous works (Appendix XI). Barite and fluorite mineralization is concentrated at the N N W end of the quarry, although sphalerite occurs in very small quantities within dolostones throughout. Barite is considerably more abundant than fluorite.

Fluorite occurs as millimetre to centimetre-sized, orange-brown euhedral crystals (Fig. 7.10b). In thin section, the fluorite is colourless and luminesces bright blue (Lee and Harwood, 1989, Emery and Marshall, 1989, fig. 1b). It occurs either partially occluding cavities and small fractures by itself, where it is followed by coarse, zoned calcite cement (Lee and Harwood, 1989, fig. 12a and b), or it is overgrown by barite (Fig. 7.10b). Where in contact with barite, fluorite clearly predates barite mineralization (Fig. 7.10b). There is evidence, in one cavity fill, for internal sedimentation of brecciated fluorite during a hiatus in calcite cementation (Lee and Harwood, 1989, fig.12b).

Barite more commonly occurs alone and completely occludes porosity (Fig. 7.10a). Many of the barite, and barite with fluorite mineralized cavities are considerably larger than unmineralized cavities after sulphates in the Raisby Formation (i.e., figure 5.24a). Enlargement by dissolution and subsequent fracturing is suggested by the occurrence of angular brecciated host dolostone within the barite cavity fills (Fig. 7.10a).

Previous work on mineralization at Chilton by Fowler (1957), suggests that at least some barite is related to a NW-SE striking fault which has "..... quite clearly provided a path for mineralizing solutions" (Fowler, 1957, 258). Fowler (1957) and Hirst and Smith (1974) demonstrate that fluorite predates barite mineralization, and Fowler (1957) further suggests that sphalerite mineralization may have postdated fluorite and barite, although he admits his evidence is inconclusive. Hirst and Smith (1974) estimate that the quantity of barite in the northwest area of the quarry locally approaches 10-20% by volume. Analysis of the barite

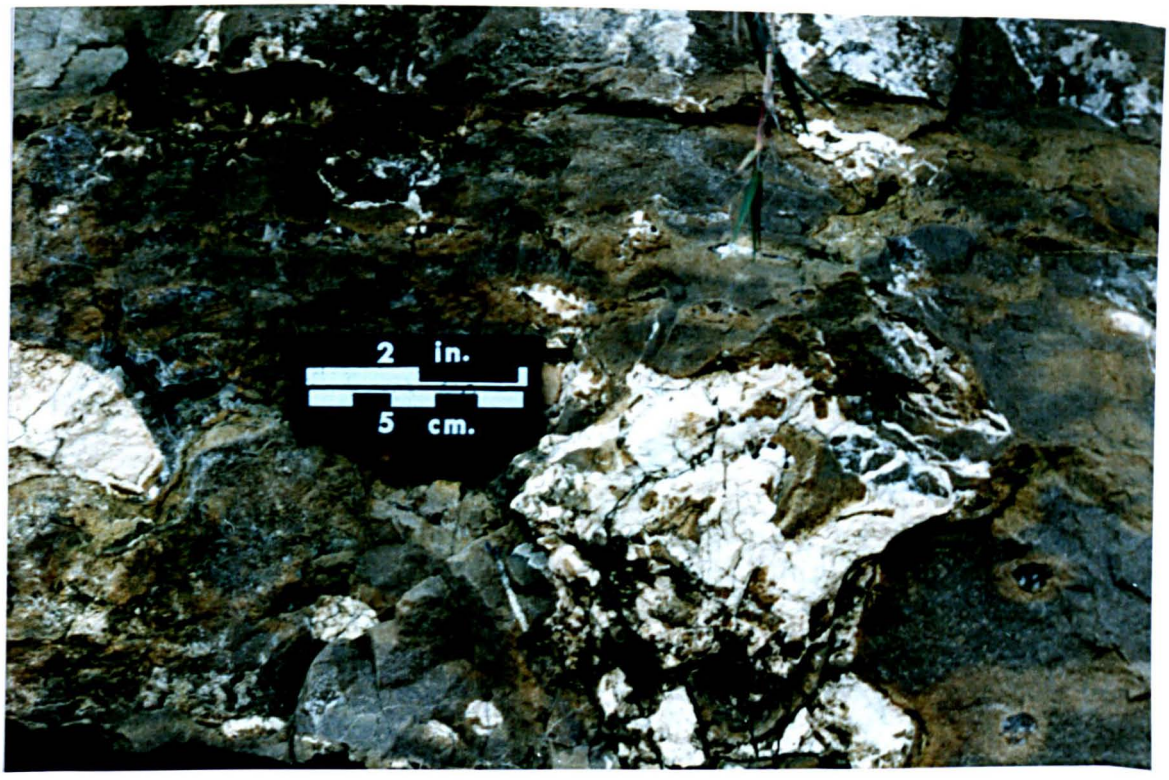

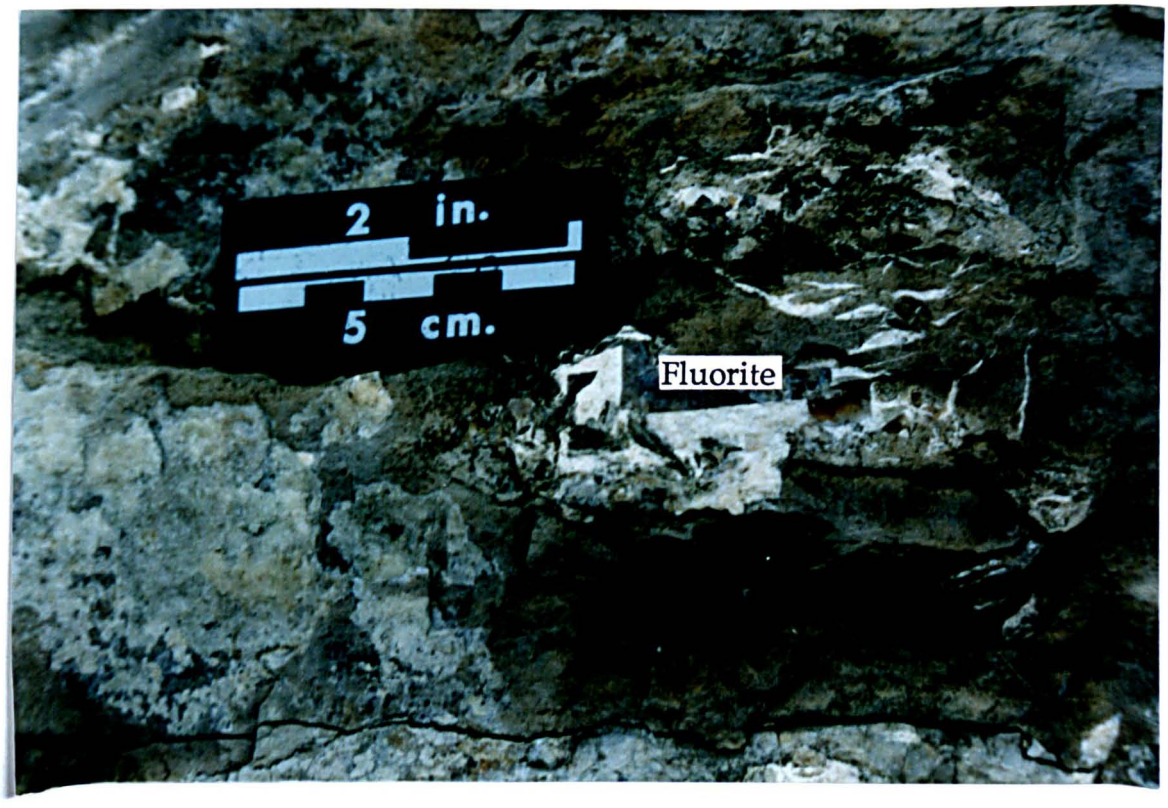

Fig. 7.10. Outcrop photographs of mineralization, Chilton Quarry. (a) illustrates two large barite mineralized cavities after sulphates, one of which experienced brecciation before/during mineralization. (b) shows the juxtaposed cubic fluorite with barite. Fluorite clearly predates barite mineralization.

from this locality by Solomon *et al.*, (1971) gives a $\delta^{34}S$ of +9.3‰(CDT) and $\delta^{18}O$ of +10.0‰(SMOW); fluid inclusions within fluorite from this locality analysed by Hirst and Smith (1974) gives a temperature of 104-108°C and salinity of 22.35% NaCl. Analyses of yttrium contents of fluorites from this locality and Rough Furze Quarry by Hirst and Smith (1974), gave results of 22-53ppm (compared to 120-815ppm for Alston Block fluorites). Moorbath (1962) analysed galena occurring in disseminated aggregates from Chilton Quarry for lead isotopes, which gave a model age of 280±70 Ma, older than the Raisby Formation itself, and so the quality of the analysis is questionable.

7.1.1.10. Thickley Quarry.

Mineralization is scarce at this locality, restricted to large calcite cemented cavities, probably after replacive sulphates. The dominant mineral is sphalerite, with minor chalcopyrite. Sphalerite forms coarse (600-1000μm) sub-euhedral to euhedral pore-lining crystals (Fig. 7.11a). Chalcopyrite occurs as small inclusions within the sphalerite. Mineralization postdates precipitation of coarse saddle dolomite, which also lines the pores (Figs. 6.33 & 6.34). The sphalerite may selectively not replace, or may pseudomorph the saddle dolomite. The remaining porosity is occluded by coarse luminescent calcite cement (Fig. 7.11a). One isotope analysis of this cement gave results of $\delta^{13}C$ 0.6‰ and $\delta^{18}O$ -13.1‰. Very similar cavity fills possibly also associated with sphalerite, were recorded in a nearby quarry at Middridge.

7.1.1.11. Old Towns Quarry.

This exposure is extensively mineralized by barite and galena (Fig. 7.11b), which are concentrated within dolostones of the uppermost part of the quarry. This locality has the most abundant galena mineralization recorded during the present study. The dolostone host rocks to mineralization are commonly brecciated, although all mineralization is concentrated within or in association with cavities after sulphates.

7.1.1.12. Hurworth Place borehole.

Barite, galena and chalcopyrite mineralization have been recorded throughout the Raisby Formation in this borehole, although only in very small quantities. Barite occurs at the base of the section filling the intraskeletal porosity of ?bivalves in a shelly coquina. Galena and chalcopyrite are scattered throughout, occluding small fractures. In one part of the borehole, a ?chalcopyrite mineralized area has been partially dissolved by microstylolites.

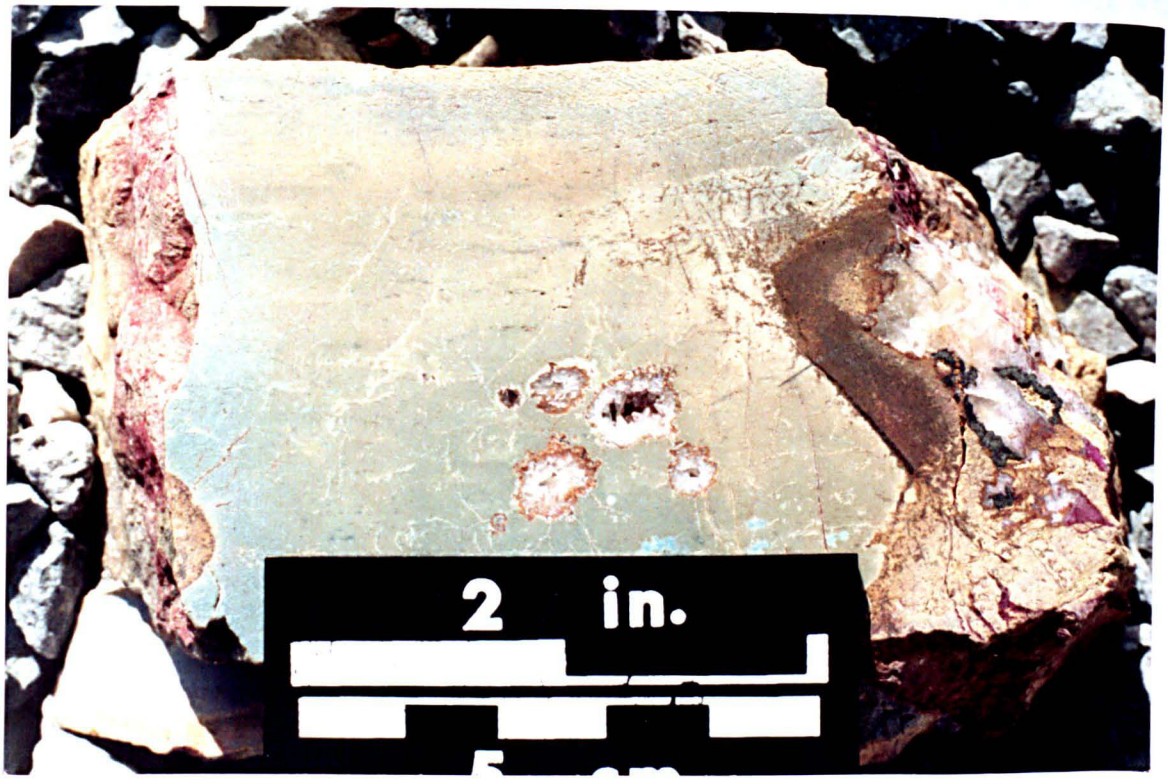

Fig. 7.11. Photographs of hand specimens of mineralization from Thickley Quarry (a), and Old Towns Quarry (b). In (a), sphalerite (arrowed), lines a calcite cemented cavity. Ferroan dolostones for 1cm marginal to the cavity have been altered to goethite (FDA texture). (b) illustrates a barite and galena mineralized dolostone.

7.1.1.13. Other localities

A number of borehole records (unpublished data) identify fault and vein-related barite and galena mineralization (ICI WT/O and Hill House bores) and joint-related galena, pyrite and sphalerite mineralization (OB8) (Appendix XI).

The most extensive recorded mineralization outside the Raisby Formation in the Permian of northeast England is at Black Hall Rocks where galena occurs within a fault breccia. The mineralization was extensive enough to have once been investigated by a trial adit (Smith and Francis, 1967).

7.2.1. Mineralization in the Raisby Formation - Discussion.

Mineralization has been described from selected areas of the Raisby Formation by a number of previous workers, including Winch (1817), Sedgwick (1835), Woolacott (1919b), Fowler (1943 & 1957), Raymond (1962), Smith and Francis (1967), Jones (1969), Jones and Hirst (1972), Hirst and Smith (1974), Mills and Hull (1976), Harwood (1983) and Lee and Harwood (1989), although no comprehensive study has yet been undertaken. Most previous workers have concentrated on the variety of minerals present and their geographical distribution. Only Solomon *et al.*, (1971), Jones and Hirst (1972) and Hirst and Smith (1974) have attempted to relate mineralization to fluid origins and flow paths. Detailed work on barite, fluorite and base metal sulphide mineralization in the Cadeby Formation (Harwood, 1981; Harwood and Coleman, 1983; Harwood and Smith, 1986), identifies both possible sources for mineralizing fluids, and fluid conduits responsible for localizing the mineralization.

Early work suggested that mineralization in Zechstein carbonates of northeast England (mainly the Raisby Formation), was more or less coeval with the nearby extensive Pennine mineralization (Dunham, 1934; Fowler, 1943), and may have been syngenetic, with base metals being precipitated from springs or rivers flowing into the Zechstein Sea from the Pennine uplands (Dunham, 1934; Westoll, 1943). However, later study clearly established that mineralization was epigenetic (Trotter, 1944; Dunham, 1952; Fowler, 1957; Stewart, 1965), and geochemically distinct from that of the Pennine veins (Solomon *et al.*, 1971; Hirst and Smith, 1974). Fowler (1957) relates distinct centres of mineralization around the Butterknowle Fault and Ninety-Fathom Fault to a period of crustal movement and volcanism in the Tertiary. Such structural control on mineralization in the Butterknowle Fault area was also suggested by Hirst and Smith (1974). Jones and Hirst (1972) invoke and altogether different origin for mineralization in the Permian of northeast England, suggesting it was relatively early diagenetic and related to up-dip flowing connate brines from the evaporite basin in the east.

7.2.2. Mineralization in the Raisby Formation - Interpretation; spatial relationships of mineralization.

A considerable amount of information regarding the processes of mineralization may firstly be gained by considering the vertical and lateral distribution of mineralized localities. Mineralization of Zechstein carbonates in northeast England is almost completely restricted to the Raisby Formation. Although second, third and fourth cycle carbonates are not well exposed in northeast England, the Ford Formation is extensively exposed and has been intensively studied, especially in the reef facies (Smith and Francis, 1967; Smith, 1981; Aplin, 1985; Tucker and Hollingworth, 1986; Hollingworth and Tucker, 1987). This is a very suitable host rock for mineralization, but none has been recorded. A similar preponderance of mineralization within the Cadeby Formation has been demonstrated (Harwood and Smith, 1986), although some mineralization does occur within third cycle carbonates of the Yorkshire Province (G.M. Harwood, *pers. comm.*, 1990). Such restriction is taken here to almost guarantee that the mineralizing fluids were sourced, at least in part, from Carboniferous or older Palaeozoic basement rocks underlying the Permian. Furthermore, recorded mineralized localities in the Raisby Formation at outcrop appear to cluster in several distinct geographical areas (Fig. 7.1). A similar distribution pattern has been recorded for mineralization within carbonates of the Cadeby Formation (Harwood, 1981; Harwood and Smith, 1986). However, unlike the Yorkshire Province, in the Raisby Formation this clustering in part reflects a bias of both exposure, and intensity of previous investigation. The Raisby Formation is poorly exposed and is relatively thin in the north around Sunderland, and in the southernmost part of its outcrop. It is best exposed in a central area to the south of Durham, where most of the mineralization localities have been recorded. Furthermore, many previous records of mineralization are from the work of Hirst and Smith (1974) (Appendix XI), who concentrated in the Ferryhill area. However, owing to earlier investigations of the economic potential of the Raisby Formation, most localities with substantial mineralization are considered to have been already described.

7.2.2.1. Northern subarea

The northernmost concentration of mineralized localities includes Marden, Cullercoats, Frenchmans Bay and Man Haven, dominantly barite mineralized. The Raisby Formation immediately to the southwest of this area is poorly exposed, although the restriction of barite mineralization to Frenchmans Bay and Man Haven along the extensive South Shields coastal section does suggest a strong localization of mineralization. In detail, the distribution of barite is controlled by joints (and neptunean dykes within joints), the distribution of replacive evaporites, resedimented units, and the overlying Z2 collapse breccias. The preference of barite for debris flows is due, in turn, to the preference of sulphates to replace debris flow clasts (5.6.3.5). A joint control is the most prominent

determinant on the occurrence of barite, although the Basal Permian Sands exposed in Frenchmans Bay form a small dune which may have additionally localized barium-rich fluids. Hirst and Smith (1974) consider that a much larger dune structure was significant in localizing barite mineralization in the Ferryhill area (Fig. 7.13). To them, the Marl Slate was a potentially significant permeability barrier. The Marl Slate is present in Frenchmans Bay, although the joints and neptunean dykes which cut it would have circumvented such a barrier to fluid movement. The Permian in this area also overlies a faulted anticline in the Carboniferous, which may have further acted as a focussing agent for mineralizing solutions.

Ponding of barite below the Z2 collapse breccias both at Man Haven and Marden implies that a significant permeability barrier existed there, which may have been the Z2 collapse breccias, the clay-rich residue of the Hartlepool Anhydrite Formation, or the Hartlepool Anhydrite Formation itself prior to dissolution. As the dissolution residue is patchy at Man Haven, the Z2 collapse breccias show no unequivocal evidence for barite mineralization, and that former sulphate nodules replaced by barite in Frenchmans Bay demonstrate anhydrite was still present during mineralization (Fig. 7.2b), is taken to indicate that the Hartlepool Anhydrite Formation itself was the barrier. The presence of this permeability barrier helps explain why mineralization is locally intense in this area, as the barium-rich fluids were prevented from diffusing upwards, precipitating widespread, disseminated barite.

Thus, in some parts of the northernmost area, mineralization predated hydration and dissolution of anhydrite (pre-Tertiary?), and was localized by joints, possibly a dune structure in the Basal Permian Sands, a faulted anticline within the Coal Measures, the Hartlepool Anhydrite Formation, and the abundant nuclei for barite precipitation - sulphate evaporites. On a larger scale, the Ninety Fathom Fault may have been very important to mineralization. It cuts the Permian just to the north of Tynemouth (Fig. 7.1), near to Marden Quarry and Cullercoats. In addition to Marden, Land (1974) documents galena, sphalerite and less common barite mineralization in the Coal Measures and Raisby Formation of the Tynemouth area. Winch (1817) describes veins of galena in the Raisby Formation at Whitley (Marden Quarry ?), and Haslehurst (1911 [in: Land, 1974]) describes veins containing galena in the Raisby Formation at Cullercoats. Fault-parallel mineralized veins including sphalerite have been recorded from Coal Measures on St. Mary's Island nearby (NZ 3519, 7541) (Land, 1974). Such fault and fracture localization of mineralization in this area suggests that the Ninety Fathom Fault was a possible conduit for mineralizing solutions, further localized by associated fractures and possibly larger fractures in conjunction with dunes of Basal Permian Sands at Frenchmans Bay. Land (1974) suggests that the originally Hercynian Ninety Fathom Fault was reactivated in the Tertiary. The Ninety Fathom Fault defines, approximately, the southern margin of a major hinge belt in northeast England (Bott, 1961)

(Fig. 7.12). The hinge belt is marked by an abrupt thickening of lower Carboniferous and possibly Devonian sediments to the north, delineating the northern margin of the Alston Block. The hinge belt extends for approximately four miles (6.4km) to the north of the Ninety Fathom Fault (Fig. 7.12). It comprises a monoclinal downwarp, or a series of small en-echelon faults.

No substantial mineralization has been recorded between the South Shields coastal section and Houghton Quarry in the Raisby Formation, or Ford Formation (Fig. 7.1). Also, exposure is good around Houghton Quarry further suggesting that in this area, mineralization is restricted to Houghton Quarry. Mineralization here is clearly fault controlled, more apparent for galena than barite, although both occur close to the fault. Its ENE-WSW strike is very similar to that of faults which cut the Permian in this area (Fig. 7.1). Furthermore, its similarity of orientation to faults in the underlying Coal Measures strongly suggests it may have formed by reactivation of a Hercynian fault, as is probable for most faults in the Permian (Smith and Francis, 1967; Land, 1974; Mills and Hull, 1976) (1.6.1). Such reactivation is commonly considered to be of Tertiary age (Smith and Francis, 1967; Land, 1974; Mills and Hull, 1976) (1.6.1), accompanying uplift, therefore putting a similar age constraint on mineralization. Restriction of galena and barite to one small area of Houghton Quarry suggests both that the quantity of barium and lead in the mineralizing solutions was low, and that precipitation occurred almost immediately on the contact of lead and barium-bearing solutions with the Raisby Formation.

7.2.2.2. Central and southern area

The remaining mineralization within the Raisby Formation is centered on Ferryhill, although widely distributed south and, to a lesser extent, north of that area (Figs. 7.1 & 7.13). Barite mineralization to the north of Ferryhill at Running Waters Quarry, possibly represents the northernmost extension of Ferryhill mineralization, or may represent a separate centre. The great abundance of barite here (possibly more abundant than at Chilton Quarry) supports the idea of a discrete locus of barite mineralization. The Raisby Formation in the area of Running Waters Quarry is cut by a number of small faults which also cut the Carboniferous (Fig. 7.12), and is very close to the subcrop of the Ludworth Dyke (an igneous intrusive), although its bounding faults are not recorded to cut the Permian (Smith and Francis, 1967). However, no unequivocal evidence for fault-control on mineralization can be demonstrated and so the origin of mineralizing fluids remains speculative. Petrographic evidence, especially that barite mineralization postdates evaporite dissolution and calcitization of dolomite suggests relatively late diagenetic mineralization, probably during Tertiary uplift.

It is possible that another subarea of mineralization can be identified in the south of the Raisby Formation outcrop, distinct from the main area around Ferryhill (Fig. 7.1). This

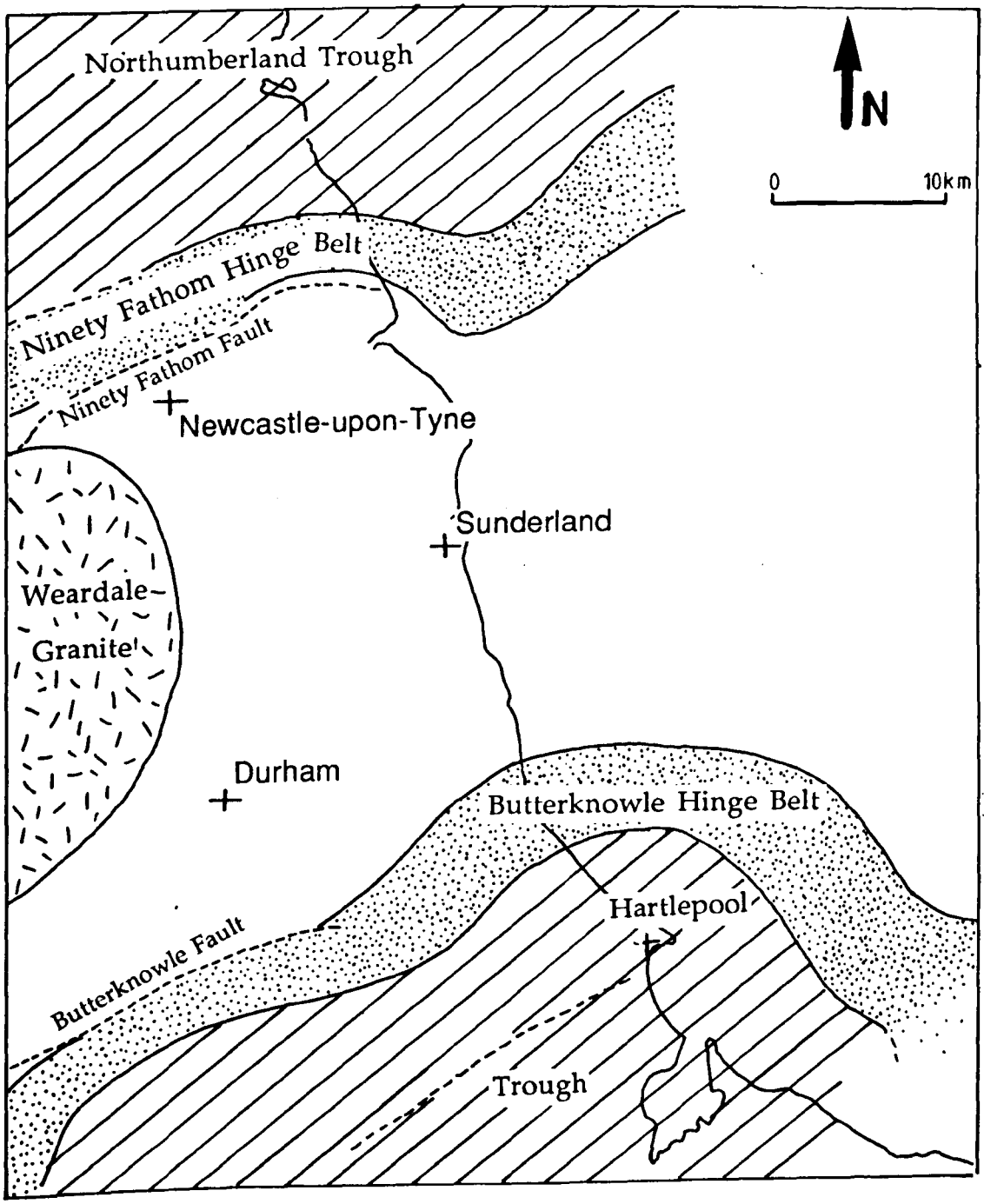

Fig. 7.12. Map showing the location of two large hinge belts (stippled) in northeast England marginal to a central block partially underlain by the Weardale Granite. The hinge belts, identified by gravity anomalies, demarcate an area of thickening of Lower Carboniferous sediments into troughs (diagonal shading). Modified from Bott (1961).

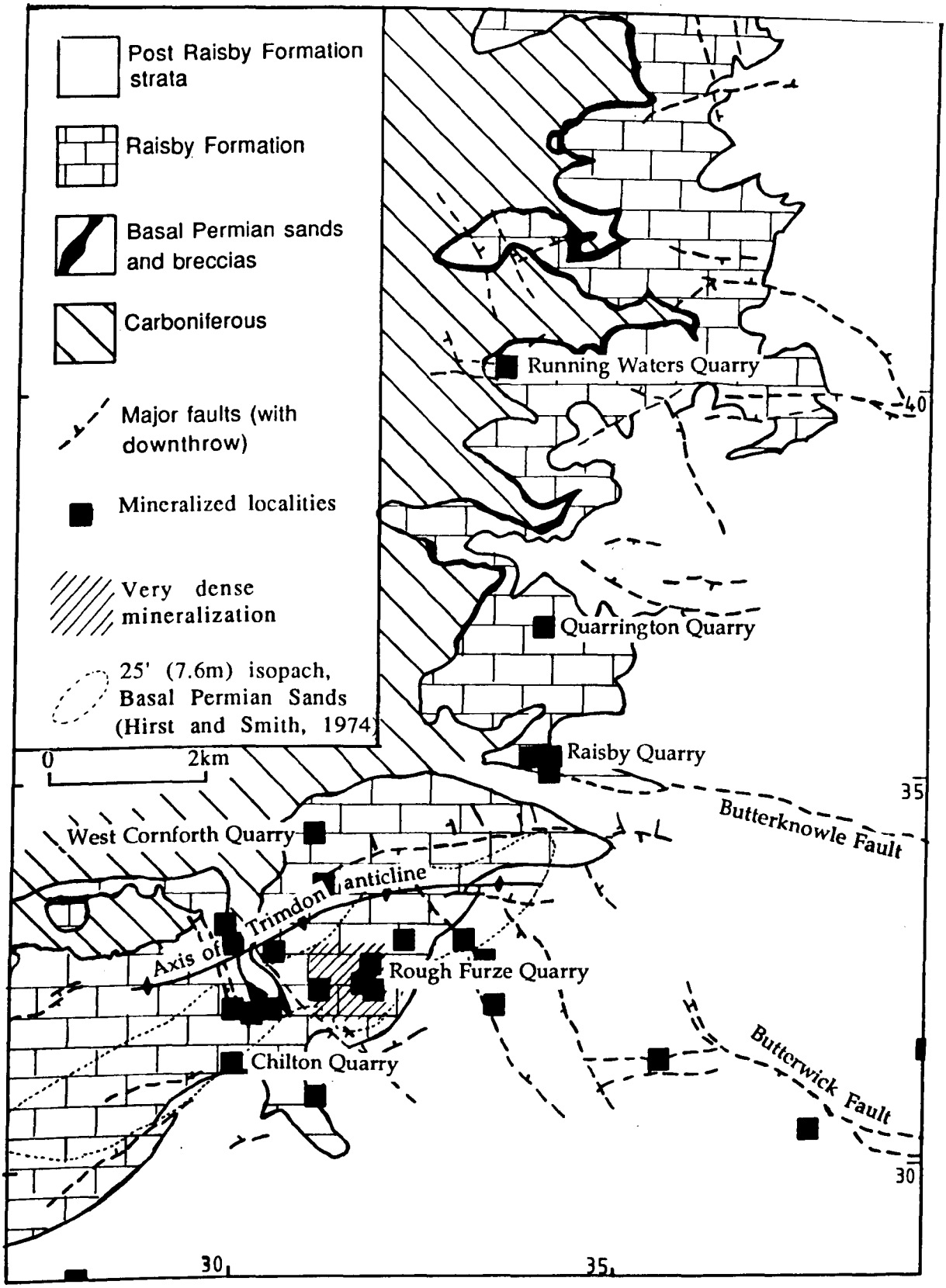

Fig. 7.13. Map showing detail of the relationships between mineralization in the Raisby Formation and structure in the Ferryhill area. Note, most mineralized localities are close to faults, and the most densely mineralized area corresponds to the axis of the Trimdon Anticline and a 'dune' of Basal Permian Sands identified by Smith and Francis (1967) and Hirst and Smith (1974). Base map modified from Smith and Francis, 1967.

subarea includes Thickley, Old Towns and possibly Middridge Quarries. Thickley is the only locality apart from Raisby Quarry where copper mineralization has been recorded, and Old Towns Quarry is the most heavily galena-mineralized locality examined during this study. There is no direct evidence for structural control of mineralization in this area. However, a barite-mineralized dolostone borehole from Cold Sides nearby, lies very close to a small fault, suggested by Fowler (1957) to have been the conduit for mineralizing fluids.

The area immediately adjacent, and to the south of the Butterknowle Fault is the most heavily mineralized region of the Raisby Formation. All minerals recorded elsewhere within the Raisby Formation have been recorded here, along with almost all copper and fluorite. Most mineralization is almost certainly directly related to the Butterknowle Fault, a major tectonic feature within northeast England, cutting both the Carboniferous and Permian (1.6.1). The associated Trimdon anticline and syncline in the Coal Measures lie slightly to the south of the Butterknowle Fault (with axial planes parallel to it) (Smith and Francis, 1967) (Fig. 7.13). The Trimdon anticline itself is complexly faulted, especially along its northern limb around Garmondsway (Smith and Francis, 1967). Furthermore, Smith and Francis (1967) suggest that anticline axes in the Permian directly overlying the Carboniferous in this area are roughly coincident with those in the Coal Measures. Hirst and Smith (1974) identify a large NE-SW trending 'dune' structure within the basal Permian sands of the Ferryhill area (Fig. 7.12), which they suggest further acted to localize mineralization. Therefore, there is abundant evidence for a structural control on mineralization, although its identification is in part due to intensive study of this area owing to the importance of the Butterknowle Fault. The Blackhall Fault (which parallels the Butterknowle Fault to the north [Figs. 7.1 & 7.12]), may have also localized galena mineralization in the Ford Formation at the Blackhall Rocks (Fig. 7.1).

The Raisby Formation has also been recorded to be mineralized from boreholes to the east of the Ferryhill area (Fig. 7.1 & 7.13). The trend of mineralization parallels the Butterknowle Fault, although is considerably offset to the south. These localities lie almost directly along the line of the Butterwick Fault and its eastwards extension, the West Hartlepool Fault (Figs. 7.1 & 7.13). Both faults cut the Permian and Coal Measures, downthrowing to the south, as does the Butterknowle Fault (Smith and Francis, 1967). Cu-Pb-Zn mineralization has been recorded in Coal Measures directly underlying the Whin Houses borehole (Fowler, 1943), which lies along this trend.

Mineralization in the Ferryhill area is therefore directly related to faulting and to a lesser extent folding, in the Coal Measures which has a more subdued expression in the Raisby Formation. Such a tectonic control was first advocated by Hirst and Smith (1974) although they did not recognize the importance of the Blackhall, Butterwick and West Hartlepool Faults. Tectonic influence is also recorded at outcrop, with copper mineralization occurring in fault breccias at Raisby Quarry (Hirst and Smith, 1974) and barite mineralization

in fault breccias at Chilton Quarry (Fowler, 1957). The Butterknowle Fault is approximately coincident with the southern margin of the Alston Block (Dunham, 1948; Bott and Masson-Smith, 1957; Bott, 1961) (Fig. 7.12). This hinge belt, in common with the one delineated by the Ninety Fathom Fault, is probably a monoclinal downwarp or a series of small en-echelon faults (Bott, 1961). Such a location is ideal for the sourcing of mineralizing fluids from Carboniferous or older rocks. Again, the Butterknowle fault is considered to have been reactivated in the Tertiary (Smith and Francis, 1967), thus imposing a constraint on the timing of mineralization.

7.2.3. Origin of the mineralizing fluids

It is most likely that mineralization in the Ferryhill area and most of the rest of the Raisby Formation, was produced by barium, fluorine and base metal-rich fluids moving up along faults and concentrating in major tectonic structures of the Coal Measures and Permian. Gibbons (1978) records elevated reflectivities of organic components within brecciated Marl Slate from core VT8 (NZ 48616, 50946). This is taken by him to indicate the possible passage of hot solutions along a fault plane. Furthermore, Gibbons (1978) also notes base metal sulphide mineralized brecciated Marl Slate and Raisby Formation from boreholes VT1 (NZ 46191, 52051) and B2 (43906, 78584), suggesting that fault planes acted as solution channels. Upward-movement of Coal Measure, or older, fluids may have been driven by a regionally high heat flow, owing to proximity to the Weardale Granite (Fig. 7.12). The region of outcrop of the Zechstein in northeast England lies on the very margin of one of two areas of anomalously high present day heat flow identified in England and Wales by Brown *et al.*, (1980). The mineralized Cadeby Formation of the Yorkshire province lies well within this zone. Brown *et al.*, (1980) suggest that the high surficial heat flow may be directly correlated to the rate of radiogenic heat production from pre-Variscan or Variscan crystalline or low-grade metamorphic rocks in these areas. They suggest that fluid circulation and mineralization may be driven by radiogenic heat production from buried granites long after their emplacement. Such fluid circulation and mineralization may have continued into the Tertiary. However, one problem is with evaluating the precise timing of faulting in the Permian. Most workers assume an early Tertiary age for the faulting and mineralization, although with minimal evidence. The intrusion of the ESE-WNW trending Cleveland Dyke (age 56±1Ma (Eocene) [Green, 1989]), which cuts the Permian, probably followed pre-existing fault lines, although only gives a minimum age for faulting. Movement along major structures such as the Ninety Fathom Fault and the Butterknowle Fault throughout the Mesozoic cannot be discounted.

7.2.4. Controls on the precipitation of base metal sulphides.

The origin of base metal ions for galena, sphalerite, and copper mineralization within the Raisby Formation is very difficult to evaluate. Possible sources include leaching of base metals from the sub-Permian basement (sedimentary or igneous), and the Marl Slate. The local abundance of fluorite indicates an origin by interaction with intrusive igneous rocks, although reworking of fluorite (and base metal sulphides) from buried 'Pennine' mineral veins cannot be discounted, although is unlikely. The large concentrations of barium in solution within the Coal Measures of Durham (Edmunds, 1975), is an attractive barium source, although the same Coal Measures have negligible concentrations of base metals or fluorine (Edmunds, 1975). However, some barite-mineralized localities in the south of the area directly overlie Dinantian limestones (i.e., Hurworth Place borehole), and so the Coal Measures cannot always be invoked as a direct source of barium.

7.2.4.1. Diagenetic environment of mineralization

The very close association of pore-lining saddle dolomite with sphalerite at Thickley Quarry suggests a genetic association. Saddle dolomite is considered to precipitate from fluids of elevated temperatures and salinities (60°-150°C [Radke and Mathis, 1980] or 90° to 215-220°C and 2-6 times seawater salinity [Machel, 1987]). The close association of saddle dolomite with sulphate evaporites, hydrocarbons and base metal (Mississippi valley-type [MVT]) mineralization has been thoroughly documented (Beales and Hardy, 1980; Radke and Mathis, 1980; Anderson and Garven, 1987; Machel, 1987a). The carbonate anions for precipitation of saddle dolomite (which is often strongly depleted in ^{13}C) are commonly considered to be derived from reactions involving hydrocarbons and sulphate; bacterial or thermochemical sulphate reduction. No isotopic data is available for the saddle dolomite at Thickley Quarry, although oxygen isotope values of the enclosing luminescent calcite cement ($\delta^{18}O$ = -13.1‰) implies precipitation from fluids of elevated temperatures (Fig. 6.65b).

The association of sphalerite with saddle dolomite was discussed by Radke and Mathis (1980), who proposed the following expression:

$$CH_4 + ZnCl_2 + SO_4^{2-} + Mg^{2+} + 3CaCO_3 \rightarrow ZnS + CaMg(CO_3)_2 + 2Ca^{2+} + 2Cl^- + H_2O + 2HCO_3^-$$

(after Radke and Mathis, 1980).

Sulphate reduction, utilizing CH_4, is the driving force for the precipitation of both dolomite and sphalerite. This is similar to a reaction proposed by Jones and Hirst (1972) to explain sphalerite mineralization within the Raisby and Ford Formations, which they considered to be associated with the calcitization of anhydrite:

$$CaSO_4 + C + 4H^+ \rightarrow CaCO_3 + H_2S + H_2O$$

$$H_2S + Zn^{2+} \rightarrow ZnS + 2H^+$$

(after Jones and Hirst, 1972).

Such a reaction would produce 6 masses of sphalerite for every 1 mass of hydrocarbon consumed (Shearman, 1971).

In the context of mesogenetic MVT Pb-Zn mineralization, sulphate reduction is commonly considered to be thermochemical (Radke and Mathis, 1980; Machel, 1987a & b). There is some question as to the lower temperature limit of effective thermochemical sulphate reduction (Trudinger *et al.*, 1985; Machel, 1987a & b). It is probably around 135-140°C, although may be as low as 90°C (Krousse *et al.*, 1988).

On the basis of the Thickley example, it is possible that much or all of the base metal mineralization in the Raisby Formation is the direct result of hot, saline, base metal-bearing fluids combining with H_2S produced within the Raisby Formation by reduction (bacterial and/or thermochemical) of autochthonous sulphate evaporites (possibly both processes were operative at different times). Further support for this hypothesis comes from borehole W8, where sphalerite has replaced anhydrite (Fig. 7.2a). This is interpreted to have been a common relationship of much of the base metal sulphide mineralization in the Raisby Formation, prior to sulphate dissolution. Most base metal sulphides at outcrop do occur within large open or calcite-cemented vughs, formerly sites of replacive sulphates. Thus, sulphide is interpreted to have been derived from the reduction of anhydrite, and combined with base metals introduced by solutions, *in situ*.

The occurrence of base metal sulphides within calcitized anhydrite nodules has been described by Harwood (1980) and Harwood and Coleman (1983) from the Cadeby Formation. In this example, sulphur isotopes demonstrate that the sulphides were derived directly from sulphate evaporites by bacterial sulphate reduction accompanying calcitization of anhydrite. Although there is no evidence for calcitization of anhydrite in the W8 borehole, it is possible that acidity produced as a by-product of mineralization prevented carbonate precipitation, in a similar manner to that described by Anderson and Garven (1987) (6.2.2). One possible piece of confirming evidence for sulphate reduction in association with mineralization, is the highly negative sulphur isotope analysis ($\delta^{34}S$ -24.1‰) of vugh-lining sphalerite from the Marl Slate in Quarrington Quarry. Such a low value is typical of an origin for the sulphur by sulphate reduction, and is similar to sphalerite analysed by Harwood and Coleman (1983) from within mineralized, bacterially reduced anhydrites from the Cadeby Formation ($\delta^{34}S$ -21.92‰). This data does not however, differentiate between bacterial and thermochemical sulphate reduction, although that Fe, Pb and Zn sulphides were not precipitated in

equilibrium in the Cadeby Formation (Harwood and Coleman, 1983), suggests that sulphate reduction was not thermochemical in that case.

Carbon isotope analyses show that sulphate reduction took place during calcitization of anhydrite and precipitation of some calcite cements in the Raisby Formation (6.2.3.2). In this context, the source of sulphate was autochthonous, although organic carbon is considered to have been methane derived from the underlying Coal Measures. Natural gas has been recorded within the Zechstein of eastern England in higher cycle carbonates at Eskdale in Yorkshire and Billingham (Jones and Hirst, 1972). It has also been recorded within the Concretionary Limestone/Seaham Formation at Whitby (Smith and Francis, 1967), and small quantities of mineral oil were recorded from within cavities of a dark, bituminous host rock in the base of the Concretionary Limestone Formation of Durham (Trechmann, 1942 [in Smith and Francis, 1967]). It is more than possible that Coal Measure-sourced gas could have been trapped within the Raisby and Ford Formations in structural highs beneath the Hartlepool Anhydrite Formation for an extensive period during the Mesozoic and possibly Tertiary. The average quantity of organic carbon in the 'shelf' facies of the Raisby Formation is 0.51% (Jones and Hirst, 1972), and so probably insufficient to catalyse sulphate reduction. That few bitumen residues have been recorded within the Raisby Formation, also suggests that most hydrocarbon was methane.

Further confirming evidence for sulphate reduction comes from Raymond (1962), who describes native sulphur from first cycle carbonates slightly to the south of the Whitby area. The native sulphur is recorded in vughs associated with calcite, within anhydrite, and as veins cutting both dolostone and anhydrite. These examples are from deep boreholes (1000m+). In another example, calcite and sulphur partly fill a vugh lined by black carbonaceous material (borehole R.H.B.1, 1447m) (Raymond, 1962). Native sulphur has also been recorded within first cycle evaporites and second cycle carbonates in eastern England, again which are very dark coloured and smell strongly of H_2S (Raymond, 1962), and from evaporites in the Eskdale no. 2 borehole of east Yorkshire (Stewart, 1949). Stewart (1949) states that sulphur replaces anhydrite and occurs in association with occasional pyrite. Raymond (1962) suggests that the sulphur has formed by the oxidation of H_2S derived from bacterial reduction of calcium sulphate in the presence of organic matter. Native sulphur is a common by-product of bacterial and thermochemical sulphate reduction (Kirkland and Evans, 1976; Machel 1987a & b) and has been recorded within anhydrite associated with thermochemical sulphate reduction (Krousse *et al.*, 1988) in a similar manner to that described by Raymond (1962). In near-surface environments, sulphur will be rapidly broken down by water to form sulphuric acid, thus possibly explaining its absence in the Raisby Formation at outcrop.

Thus, sulphate reduction was active within the Raisby Formation during burial, providing an attractive mechanism for base metal mineralization. The base of the Raisby

Formation was probably buried to a maximum depth of 2km or slightly more (in the middle/late Cretaceous) (Appendix X), which, with an average geothermal gradient, would not have produced conditions suitable for thermochemical sulphate reduction. However, heat flow may well have been elevated over standard geothermal gradients owing to proximity to the Weardale Granite. Furthermore, it is possible that the elevated temperatures of mineralizing brines themselves (fluorite was precipitated from fluids of approximately 110°C [Hirst and Smith, 1974]) may well have elevated local geothermal gradients adjacent to conduits of mineralizing fluids, thus promoting thermochemical sulphate reduction between resident CH_4 and autochthonous sulphate evaporites.

Although data is limited, it is possible that much of the base metal mineralization within the Raisby Formation formed by the interaction of hot, saline, base metal-bearing fluids with autochthonously produced H_2S. The mineralizing fluids themselves could have triggered thermochemical or bacterial sulphate reduction, or it may have been operative widely, although there is a problem of how to introduce sulphate-reducing bacteria (commonly derived from meteoric groundwaters) at the time when mineralization most likely occurred (?late mesogenetic). The possible configuration of sources for the base metals, organic matter, sulphate and host rocks for mineralization is illustrated in figure 7.14. Organic matter may have been introduced with mineralizing fluids moving up through the Coal Measures, or at a separate time to mineralizing fluids, although utilizing the same lines of structural weakness. Both these reservoir configurations are commonly considered for MVT deposits (Anderson and Garven, 1987).

This model may help explain the common direct association of galena and sphalerite with barite. If sulphur is largely in its reduced form, barium may be transported in solution (Edmunds, 1975). The common evolution in the mineralized localities from galena/sphalerite to barite may suggest a decrease in temperature from a diagenetic environment of relatively elevated temperature undergoing thermochemical sulphate reduction, to one of lower temperature in which sulphate is not reduced. Fluid inclusion evidence suggests that some barite precipitated at relatively low temperatures (less than 70°C) (Hirst and Smith, 1974).

It is possible that some of the calcites cementing cavities after sulphates were precipitated from fluids of relatively elevated temperatures (6.65b) during the waning stages of mineralization. The temperatures calculated (up to approximately 80°C) are lower than fluid inclusion data for fluorites (110°C) and similar to, and less than, fluid inclusion data for barites (less than 70°C) (Fig. 7.15). This is in accordance with the petrographic relation of calcite cements, postdating fluorite and barite mineralization. Precipitation of calcite cement during the waning stages of MVT mineralization, by the interaction of cooling mineralizing solutions with meteoric waters has been described by Spirakis and Heyl (1988). Meteoric-derived fluids were responsible for most telogenetic calcite cementation in the Raisby

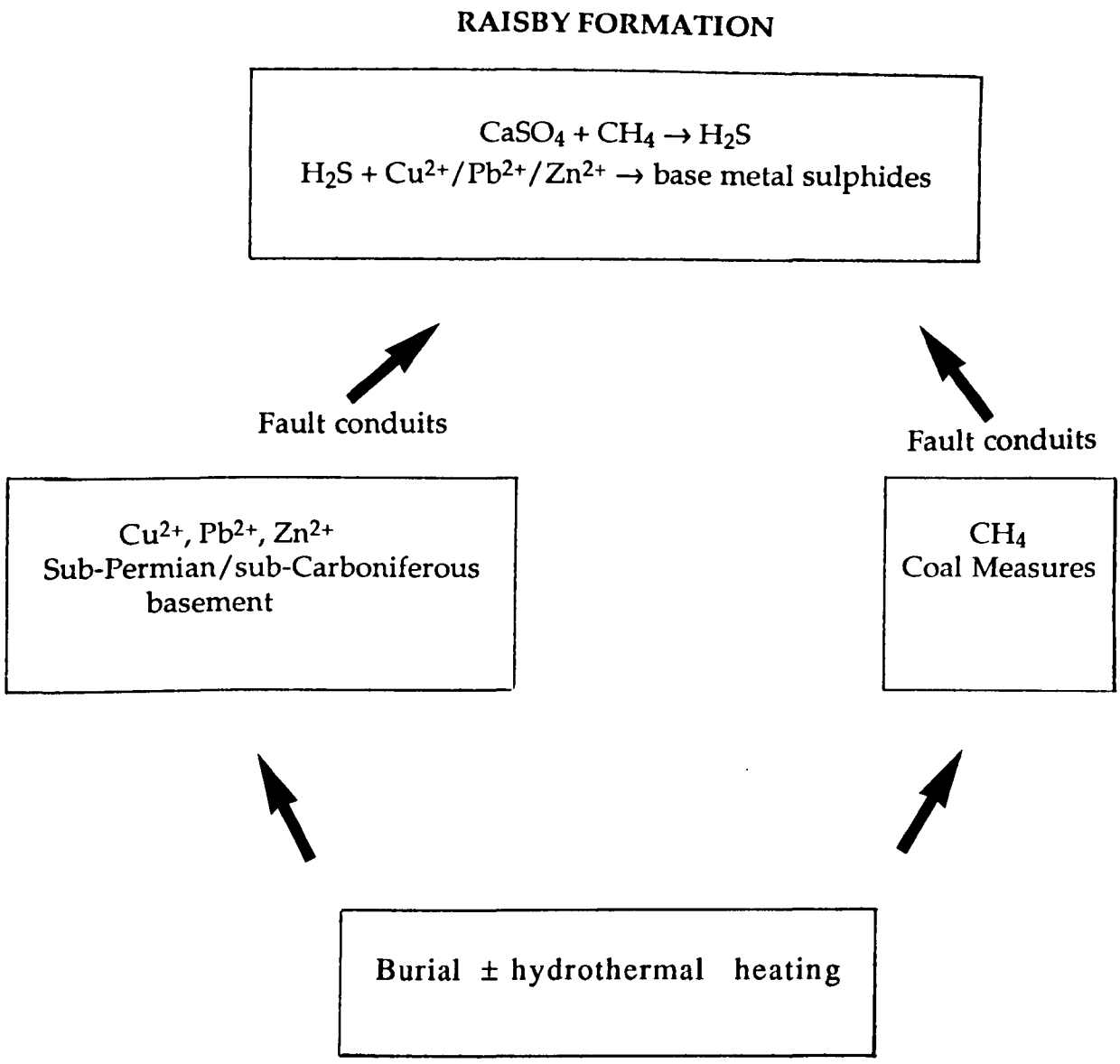

Fig. 7.14. Possible configurations of sources and movement patterns of base metal ions and light hydrocarbons to generate mineralization recorded within the Raisby Formation.

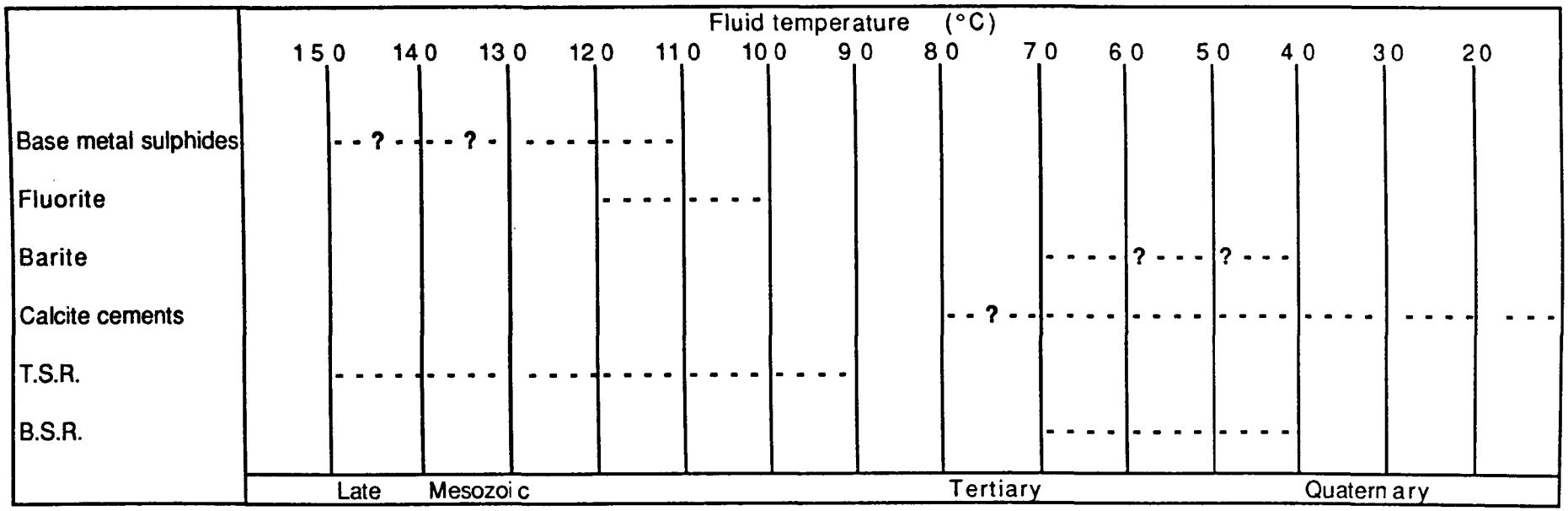

Fig. 7.15. Relative diagenetic timings of mineralization episodes within the Raisby Formation related to the temperature of the precipitating fluids. Temperatures of precipitation of barite and fluorite are based on the work of Hirst and Smith (1974), and of calcite are based on oxygen isotope palaeotemperature determinations in this study. The temperatures of precipitation of base metal sulphides are conjectural.

Formation. If the cements with depleted oxygen isotope values were associated with mineralization, this would further help to establish a relatively late diagenetic (early telogenetic) timing for mineralization.

7.2.5. Selectivity of barite and fluorite mineralization for sulphate evaporites.

At outcrop, barite is commonly contained within cavities after sulphates. This association, together with sulphur isotope data for the barite (very similar to sulphate evaporites), indicates that most barite originated by the interaction of barium-rich fluids with sulphate evaporites. This is further confirmed by the presence of angular re-entrants, now filled by calcite cement within some barites (Figs. 7.2b & 7.9a), interpreted as pseudomorphs after anhydrite (c.f. Harwood, 1983). Raymond (1962) describes barite replacing gypsum (itself hydrating from anhydrite) in the Raisby/Ford Formation from borehole G7, near Gt. Stainton. However, some mineralized cavities after sulphates, notably those at Running Waters Quarry, show no direct evidence for the co-existence of barite with anhydrite, and so barite may be a pore-filling phase. In this case, the cavities after sulphates, being large open pores would have acted as a focus for barite precipitation, possibly aided by input of SO_4^{2-} from still-dissolving sulphate evaporites.

The direct association of barite with cavities after sulphates thus suggests that barium-rich fluids entered the Raisby Formation (along faults/joints) and combined with the first major source of sulphate which they encountered. Prior to sulphate dissolution in the Tertiary, the major sources of sulphates would have been evaporite nodules. The efficiency of the Raisby Formation in precipitating barium moving up from the sub-Permian basement is amply illustrated by the almost complete absence of barite within overlying Zechstein carbonates, which also contained abundant nodular sulphates (i.e., Ford Formation). A significant factor in terminating barite mineralization may have been bacterial sulphate reduction. Many barite-mineralized pores also host pyrite/marcasite. The precipitation of iron sulphides suggests that most sulphate was in a reduced state (and so unable to combine with barium), and that iron (probably sourced intraformationally) was the only base metal ion available in sufficient quantity at this point in the diagenetic history of the Raisby Formation. At two localities (Rough Furze and Running Waters Quarries), marcasite precipitation postdates barite mineralization, suggesting that the onset of sulphate reduction may have terminated barite precipitation on a local, intra-cavity, scale.

The occurrence of small barite euhedra cementing pores formed by the dissolution of replacive sulphates within borehole W8, may suggest, in this case, that much of the barium was derived from dissolution of a barium rich sulphate precursor. Harwood (1980) points out that anhydrite may contain up to 8% Ba^{2+} substituting for Ca^{2+} in the crystal lattice. As barite is very insoluble, local precipitation would be expected.

The evidence thus suggests that barite mineralization in the Raisby Formation was controlled by the spatial and temporal distribution of calcium sulphate, mainly in the form of evaporite nodules. Barite mineralization occurred at three possible times during the diagenetic history of the Raisby Formation:

1. Mesogenetic.

Small quantities of disseminated barite mineralization, probably from the interaction of barium moving up from the Carboniferous/sub-Carboniferous basement with connate Zechstein seawater/related brines. Some predates stylolitization of the host dolostones.

2. Late mesogenetic.

Large quantities of barite mineralization within cavities after sulphates reflecting the main phase of introduction of barium into the Raisby Formation. This possibly postdates Tertiary re-activation of Hercynian faults, although predates hydration of anhydrite to gypsum (which most likely took place within a few hundreds of metres from the surface [5.7.3]),

3. Early telogenetic.

Barite cementing porosity produced by sulphate dissolution and in response to it (calcitized dolomite). Barium may have been derived from the anhydrite/gypsum itself, or possibly from barium rich-brines within the Coal Measures.

Although fluorite and barite are closely spatially associated, Hirst and Smith (1974) suggest that they may represent separate mineralization episodes, supported by fluid inclusion data. Barium and fluorine could have coexisted within the same brine, but during high temperature fluorite mineralization, anhydrite could not dissolve, and so fluorite precipitated by reactions with calcium from calcite or dolomite, whereas as temperatures lowered, anhydrite became more soluble, allowing barite to precipitate (Hirst and Smith, 1974). However, fluorite is never seen apart from barite, and, in at least one sample from Rough Furze Quarry, euhedral fluorite is overlain by barite that replaced anhydrite within the cavity (Fig. 7.9a). Thus, anhydrite was in existence during fluorite mineralization and was most likely replaced by the fluorite. As fluid temperatures were probably high enough during fluorite mineralization to initiate thermochemical sulphate reduction (110°C), upon the breakdown of anhydrite, sulphate would have been converted into sulphide, allowing fluorine to combine with free calcium (from the anhydrite), but inhibiting barite mineralization. Thus, fluorite is considered to be a product of sulphate reduction in conjunction with fluorine rich brines. In the burial diagenetic environment, anhydrite would have been the most ready source of calcium:

$$CH_4 + 2F + CaSO_4 + 2H^+ \rightarrow CaF_2 + H_2S + H_2CO_3 + H_2O$$

Thus, barite is here considered to postdate fluorite mineralization, deposited from cooler fluids in which no sulphate reduction was taking place.

7.2.6. Replacement of barite by calcite.

The replacement of barite by calcite has rarely been described. Barite was recorded being replaced by calcite in borehole G7 (Raisby/Ford Formation) near Gt. Stainton by Raymond (1962). Replacement of barite by calcite was recorded during this study from two localities; within a barite-mineralized calcite-cemented cavity from the North Sands borehole, and within barite-mineralized calcitized dolostone breccias from Running Waters Quarry (Figs. 7.5b & 7.6a). In both examples, the replacement texture is characterized by the growth of calcite within or against barite, calcite crystals showing sub-euhedral faces into the barite (Figs. 7.5b & 7.6a). The replacive calcite from North Sands borehole is an average of 1mm in diameter, and dominantly bright orange-luminescent, whereas that from Running Waters Quarry is finer crystalline (100-300μm), and dominantly dull orange-luminescent.

The replacement of barite by dissolution-reprecipitation, along a thin fluid film within fluids simultaneously undersaturated with respect to barite and supersaturated with respect to calcite is extremely unlikely, given the very low solubility of barite, especially in conditions which would be favorable to the precipitation of calcite. The most likely explanation for the replacement of barite by calcite is by the 'force of crystallization' (Maliva and Siever, 1988). Maliva and Siever (1988) suggest that stresses resulting from the growth of authigenic carbonates against relatively insoluble minerals is sufficient to promote their dissolution. One of the most characteristic textures of this process is "...euhedral authigenic crystal faces in planar contact with unreplaced host phases..." (Maliva and Siever, 1988, 688), very common in Raisby Formation examples. Textures of Raisby Formation replaced barites also fulfill other petrographic criteria for force of crystallization-controlled replacement (cf. Maliva and Siever, 1988).

7.2.7. Diagenesis of copper minerals

Copper minerals in Raisby Quarry have clearly been heavily altered, most likely by oxidation during telogenesis. Oxidation was of great importance with regard to the diagenesis of pyrite/marcasite and the precipitation of iron oxides and hydroxides within the Raisby Formation (6.5.5). Oxidation reactions from chalcopyrite through tenanite into malachite probably proceed thus:

1. Oxidation of chalcopyrite,

$$2CuFeS_2 + 8.5O_2 + 2H_2O \rightarrow Fe_2O_3 + 2Cu^{2+} + 4SO_4^{2-} + 4H^+$$

(chalcopyrite) (hematite)

(after Guilbert and Park, 1986)

(N.B. if the resultant diagenetic environment becomes substantially acidic as suggested by the above reaction, iron may remain in solution and not precipitate as hematite).

2. Precipitation of tenanite,

$$Cu^{2+} + H_2O \rightarrow CuO + 2H^+$$

(tenanite)

3. Precipitation of malachite,

$$2CuO + CO_2 + H_2O \rightarrow Cu_2(OH)_2CO_3$$

Or,

$$2Cu^{2+} + CO_3^{2-} + 2(OH)^- \rightarrow Cu_2(OH)_2CO_3$$

(after Guilbert and Park, 1986).

Thus, cupiferous solutions combine with carbon derived from the dissolution of calcite (or dolomite) to precipitate malachite. Clearly, there is abundant opportunity to dissolve the host carbonate, with acidity being produced during the oxidation of chalcopyrite and cuprite ions. If the stability field for malachite is superimposed on calculated Eh and pH boundaries for luminescent and non-luminescent calcite (Barnaby and Rimstidt, 1989 [Fig. 6.14]), there is an excellent juxtaposition of fields for malachite with those for non-luminescent calcite precipitation, precisely the association which is observed in Raisby Quarry (Fig. 7.8a & b). The stability diagram also shows that the transition from tenanite to malachite must be accompanied by an appreciable decrease in pH, such as by calcite precipitation. Moreover, the stability fields for iron oxide/hydroxides coincide with the malachite stability field, further confirming the association of iron hydroxide-encrusted non-luminescent calcite with malachite. Oxidation of copper minerals contrasts with the oxidation of pyrite/marcasite within calcite cements in the Raisby Formation, where no obvious porosity is created (6.5.5). This may be a factor of contrasts in the openness of the diagenetic system (rate of bulk aquifer advection) during oxidation, or original abundance of base metal sulphides.

7.3.1. Conclusions.

The Raisby Formation is extensively, although patchily mineralized. Barite is the most abundant mineral, followed by fluorite, galena, sphalerite and copper minerals. Most mineralization shows a relationship to sedimentary and/or tectonic structures within the host rocks, which is interpreted to represent selective epigenetic mineralization. In detail, controls on mineralization include the distribution of faults, joints and bedding planes, and sulphate evaporites, the latter being commonly facies-related in their distribution.

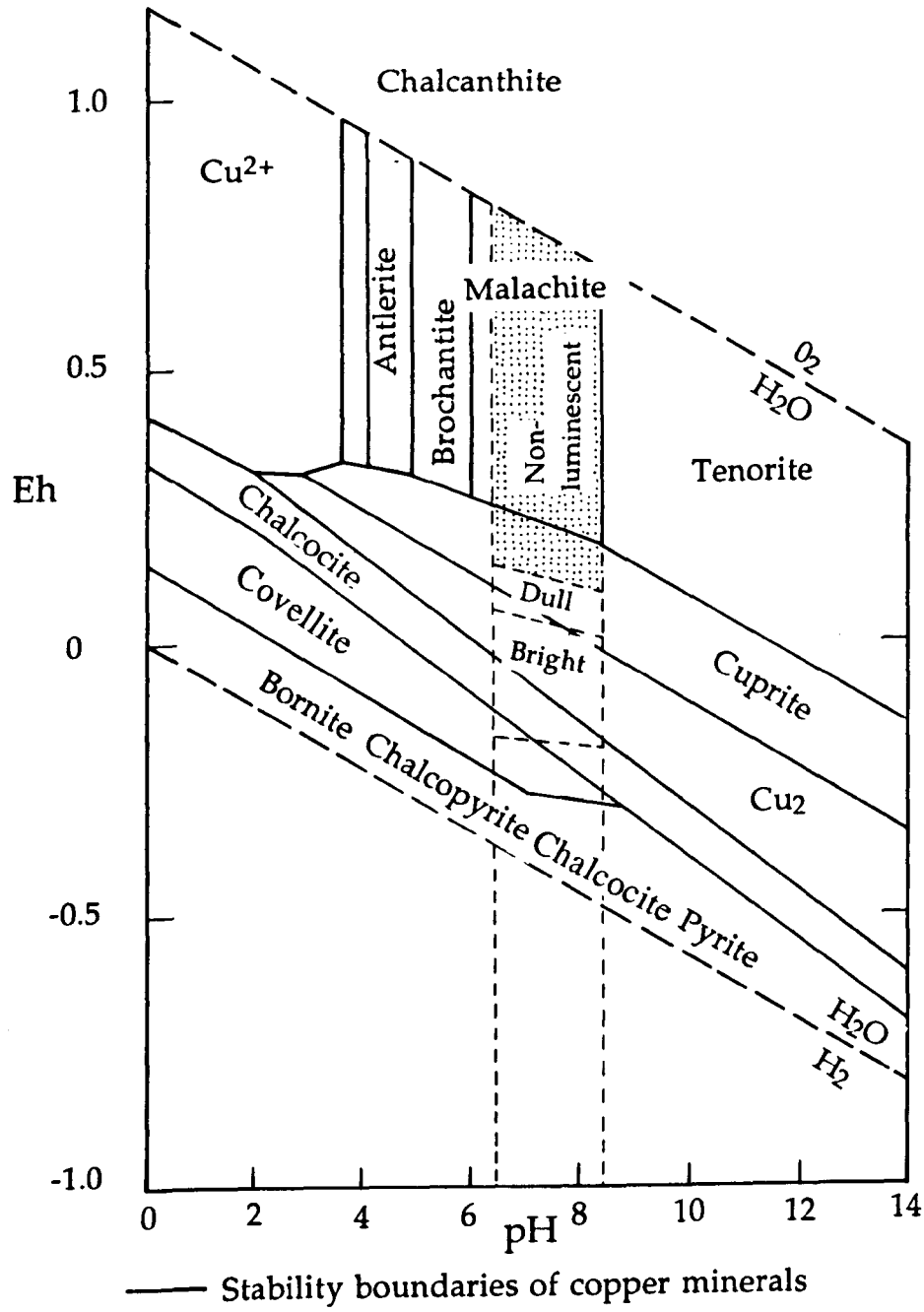

Fig. 7.16. Eh-pH diagram showing the stability ranges of copper minerals (modified from Guilbert and Park, 1986). The Eh - pH fields of precipitation of bright-, dull-, and non-luminescent calcite defined by Barnaby and Rimstidt (1989) have been overlain onto the diagram. Note that the field for malachite almost exactly corresponds with the Eh-pH conditions under which non-luminescent calcite should precipitate (stippled).

The almost complete restriction of mineralization in the Permian of northeast England to the Raisby Formation is interpreted to reflect the sourcing of mineralizing fluids from the sub-Permian basement. Furthermore, the Raisby Formation almost completely filtered out barium, fluorine and base metal ions within upwelling solutions. This was due both to abundant sources of sulphate (and so sulphide) within the Raisby Formation, and input of organic matter (natural gas) directly into the Raisby Formation, sourced from underlying Coal Measures.

The concentration of mineralization in the Ferryhill area and, to a lesser extent, to the north around Tynemouth demonstrates a large scale control on the location of mineralization by the southern and northern margins of the Alston Block and associated tectonic structures. Thus, most base metal deposits within northeast England should occur along these hinge belts. Economically significant accumulations of base metals may lie to the east of the Ferryhill area below a thin Ford Formation cover. The history of mineralization is summarized below:

1. Hercynian fault reactivation (post Raisby Formation, probably post Zechstein, possibly Tertiary),
2. Hydrocarbon input (late Mesozoic, possibly earliest Tertiary),
3. Influx of hot, saline, base metal-rich brines (multiphase),
4. Thermochemical sulphate reduction and mineralization with local saddle dolomite cementation,
5. Local input of fluorine and fluorite mineralization during waning stages of thermochemical sulphate reduction,
6. Widespread input of barium combing with sulphate. No thermochemical sulphate reduction,
7. Widespread sulphate dissolution (Tertiary), pyrite/marcasite precipitation and calcite cementation. Initial calcite cements locally precipitated from fluids of elevated temperatures.

Chapter 8

Summary and conclusions

8.1. Sedimentology.

The results of this thesis have shown that the Raisby Formation, the basal Zechstein carbonate in northeast England, was deposited on the western margin of the Upper Permian Zechstein Sea, in environments ranging from shallow water, through slope, and into basin. In shallow water environments, the lowermost Raisby Formation is diachronous with the Marl Slate Formation. However, in deeper waters, the Raisby Formation was deposited after the Marl Slate, following a eustatic sea level rise, and consequent destruction of a mid-water halocline. The spatial distribution of Raisby Formation lithofacies was largely controlled by the topography of the Permo-Carboniferous unconformity, possibly overprinted by large relic ridges of Basal Permian Sands in the north of the study area. The shallow water lithofacies is poorly exposed, and most of the formation at outcrop and in boreholes was deposited on a carbonate slope. Those shallower water sediments which are seen, grade up from shelly coquinas at the base, to comminuted skeletal wackestones and packstones, attesting to a progressively increasing sea level during deposition of the lower Raisby Formation. The majority of slope sediments were deposited as sparsely fossiliferous carbonate muds, derived from the shelf to the west, and were, at least in part, deposited by energetic, downslope-moving density currents. Coarser clastic horizons formed by the disaggregation of semi-lithified sea floor sediments in response to earthquake shock, or large scale slope failure along listric faults, itself possibly triggered by seismic activity. Early diagenetic lithification of sea floor sediments was a major controlling factor on the stability of the sediment surface, and susceptibility to downslope movement.

Some of the Raisby Formation which was deposited to the east of the Ford Formation reef, at least in the northern part of the study area, was removed by large scale, catastrophic slope failure close to the end of deposition of the Ford Formation reef and lagoonal facies. This episode of slope failure may, in turn, have been related to evaporative drawdown of the Zechstein Sea preceding deposition of the Hartlepool Anhydrite Formation. On the basis of a re-interpretation of the timing of this resedimentation, the Ford Formation should be redefined as a member of the Raisby Formation, as the Ford Formation reef and lagoonal facies are diachronous with the Raisby Formation deposited on lower parts of the slope, and in the basin. The diagenetic history of the Raisby Formation is summarized in figure 8.1.

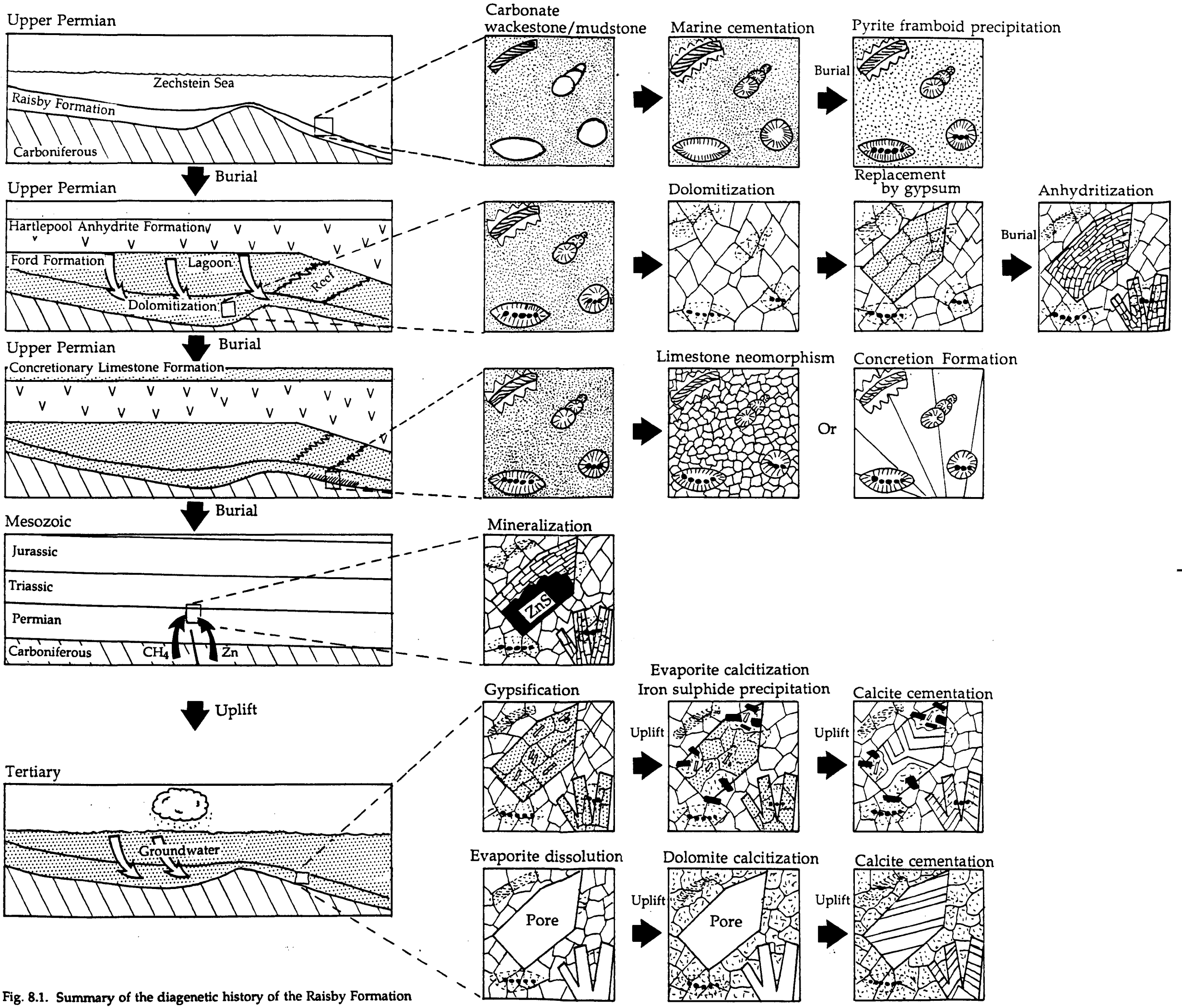

Fig. 8.1. Summary of the diagenetic history of the Raisby Formation

8.2. Eogenesis.

Soon after their deposition, carbonate muds were lithified, and aragonite and high magnesian calcite cements were precipitated within intra-skeletal pores. Lithification of carbonate muds, which started centimetres to decimetres below the sediment-water interface, was probably by add-on growth of authigenic marine cements onto micron-sized detrital carbonate grains. This led to the formation of nodules. The intensity of marine cementation of intra-skeletal porosities was a function of the permeability of the enclosing carbonate muds, and mineralogy and microstructure of the skeletal material. With progressive burial, those pores not already occluded by marine-related cements were partially cemented by non-luminescent calcite, which, in turn, was followed by a phase of bacterial sulphate reduction with concomitant precipitation of framboidal pyrite.

Carbon and oxygen stable isotope data for the Raisby Formation carbonates, helps delineate the primary isotopic composition of first cycle Zechstein seawater. The results show that Zechstein seawater was strongly enriched in ^{13}C, and slightly depleted with respect to ^{16}O relative to present-day seawater. Carbon isotope enrichment was due to the combined effects of large-scale withdrawal of ^{12}C during formation of Permo-Carboniferous coals, and the Marl Slate, which was overprinted by non-equilibrium gas transfer isotope fractionation in evaporating seawater. Enrichment of Zechstein seawater in ^{16}O is part of a trend throughout the Phanerozoic for decreasing $\delta^{18}O$ of seawater, relative to present-day values. In the Zechstein basin, however, this was overprinted by ^{18}O-enrichment of seawater by non-equilibrium gas transfer isotope fractionation, which served to counteract, not amplify, ambient ^{16}O-enrichment.

8.3. Mesogenesis.

During early mesogenesis, the Raisby Formation carbonate muds became diagenetically unstable, and were altered to limestones or dolostones. Limestones, now almost exclusively composed of low-magnesian calcite microspar, formed by the aggrading neomorphism of early-cemented aragonite-dominated carbonate muds, catalysed by elevated temperatures and pressures of burial. The chemistry of the calcite microspar was controlled mainly by the openness of the diagenetic system during neomorphism, an open system being characterized by low-Sr microspars, a more closed system having microspar with a higher concentration of Sr, and, in some instances, preserved relics of aragonite. The openness of the diagenetic system was, in turn, controlled by proximity to the bulk aquifer, which was undersaturated with respect to aragonite and high-magnesian calcite, and supersaturated with respect to low-magnesian calcite. Profiles of decreasing Sr, $\delta^{13}C$, $\delta^{18}O$, and increasing Mn and Fe from the core to margins of limestone bodies on centimetre to metre scales are a result of gradients in the openness of the diagenetic system. These gradients, in turn, were a factor of the interplay between concentration gradients and diffusion

paths, at least in part a function of petrophysical characteristics of the carbonates. These conclusions are borne out by geochemical modelling of the composition of low-magnesian calcite microspar precipitated by the neomorphism of ADP carbonate muds in open and closed diagenetic systems.

Coarsely crystalline calcite concretions occur in direct association with limestones, at two localities in the formation. Their petrography demonstrates that they have formed by neomorphism of carbonate muds, which preserved skeletal material and detrital siliciclastic grains in their original orientations. The trace element and isotopic geochemistry of these concretions is very similar to that of the host limestones, and correlates very well with those limestones which neomorphosed in a more open diagenetic system. Concretion formation postdated sediment compaction and one phase of dolomitization, although predated another episode of fracturing, stylolitization, and dolomite, calcite, and kaolinite cementation. Although it is clear that the concretions are early mesogenetic in origin, the geochemical and mineralogical conditions which cause the growth of coarse, concretionary calcite crystals remains unclear.

Shortly before limestone neomorphism, Raisby Formation carbonates were very extensively dolomitized. Dolomitization of the Raisby Formation was near-complete, apart for originally early-cemented bedded and nodular limestones close to its base. The most widespread phase of dolomitization was texture-destructive. Only ghosts of skeletal material may be defined by variations in inclusion density, although some fossils have had their microstructures preserved by mimic dolomitization. This widespread phase of dolomitization was mediated by Mg-rich brines, refluxing through the formation during deposition of the overlying Hartlepool Anhydrite Formation. The precipitation of replacive gypsum was a by-product of this phase of dolomitization, probably due to calcium liberated during dolomitization,combining with sulphate introduced with the dolomitizing brines. Little can be deduced from the geochemistry of dolomite, owing to the re-setting of its chemical composition by a later phase of dolomite neomorphism, possibly mediated by fluids of elevated temperatures during burial.

Other, volumetrically less-significant episodes of dolomitization accompanied further burial. During stylolitization of limestones, dolomite replaced limestone marginal to the stylolites. This dolomite was derived from the dissolution of earlier replacive dolostones. It also led to some further neomorphism of that calcite microspar which was not previously dolomitized. Ferroan dolomite cements were precipitated in dissolution and fracture pores, although are of very minor volumetric significance. Some cements have a saddle shape, attesting to precipitation from fluids of elevated temperatures, which is supported by oxygen stable isotope data. Most of the ions for this dolomite were again derived by pressure solution of earlier-formed dolostones. Some dolomite also replaced anhydrite, although again it was of little volumetric significance. Carbon isotopes of this

anhydrite-replacive dolomite do not support mediation by sulphate-reducing bacteria, although carbon isotopes could again have been exchanged during later dolomite neomorphism.

Calcium sulphate evaporite minerals are replacive of both dolostones and limestones, although very much more numerous within the dolostones. They were precipitated in two phases; gypsum, which was approximately synchronous with dolomitization, and anhydrite which postdated dolomitization and further burial. Precipitation of replacive anhydrite, which occurs in a number of different habits, was related to burial dewatering and pressure solution of the Hartlepool Anhydrite Formation, and gypsum within the Raisby and Ford Formations. Both gypsum and anhydrite were fabric-selective in their replacement style, preferentially occurring within skeletal carbonates and resedimented horizons.

8.4. Telogenesis.

In offshore boreholes, where sulphates are still preserved, anhydrite has been partially, or completely rehydrated to gypsum. The secondary gypsum occurs as porphyroblasts, commonly with a rosette fabric, or as poorly-crystalline alabastrine gypsum. At outcrop, and in onshore boreholes, gypsum has been near-completely dissolved from within the Raisby Formation. The intensity of gypsum dissolution on a local scale, is a function of the permeability of host Raisby Formation dolostones, itself lithofacies-related, although on a large scale, the contact of Raisby Formation hosting cavities after sulphates with that hosting unaltered gypsum parallels the trend of the present-day outcrop, at approximately 100m depth. However, this profile may be a relic of an originally more extensive groundwater system in the Raisby Formation than at present.

Within dolostones where gypsum has been completely dissolved, calcite cements the resultant secondary porosity. This calcite records a complex history of diagenesis relating to the dissolution of gypsum from within the dolostones. The calcites were precipitated from meteoric-derived fluids within an extensive aquifer. During initial stages of gypsum dissolution, groundwaters were supersaturated with respect to calcite, which led to the calcitization of gypsum, anhydrite, and dolomite. The calcitization of calcium sulphates and some dolomite was closely associated with bacterial sulphate reduction, catalysed by methane derived from underlying Coal Measures and, possibly, fluids of elevated temperatures. Sulphide ions resulting from bacterial sulphate reduction combined with iron in solution to precipitate pyrite and marcasite. During initial stages of sulphate dissolution, barite and fluorite were also precipitated, commonly within the same pore, although from fluids of decreasing temperature. Both barium and fluorine ions were possibly derived from the sub-Permian basement.

Calcite replacive of gypsum, anhydrite, and dolomite, together with calcite cements associated with iron sulphides, is bright orange-luminescent, testifying to very low Eh fluid conditions. However, the calcite precipitated after this initial phase, records a progressive, albeit pulsed, increase in Eh of the groundwaters accompanying uplift of the Raisby Formation, via its luminescence characteristics, with a progression from bright to dull, to bright orange- to non-luminescent calcite. Near-surface groundwaters were oxic, and precipitated non-luminescent calcite in association with iron oxides and hydroxides. Iron sulphides and sparse copper sulphides were also oxidized by these groundwaters. Hematite precipitated as a replacive phase of the iron sulphides, although malachite, which precipitated as a result of chalcopyrite oxidation, occludes calcite dissolution porosity, which was produced in advance of the malachite.

The non-luminescent calcite cements are normally columnar, enriched in Mg, and have carbon and oxygen stable isotopic compositions indicative of precipitation from near-surface groundwaters. The Mg-enrichment of these cements is an intrinsic factor of columnar crystal growth, which elevates the partition coefficient of Mg. Minor calcitization of dolomite by non-luminescent calcite was driven by strongly disparate saturation states between calcite and dolomite in upper aquifer levels, owing to the more rapid attainment of saturation with respect to calcite than dolomite during intense congruent dissolution. Kaolinite and smectite also precipitated in upper levels of the aquifer, probably related to complexing by organic compounds, some of which was also responsible for transportation and precipitation of iron and manganese hydroxides.

8.5. Mineralization.

Patchy Ba-F-Cu-Pb-Zn mineralization within the formation, occurred during late mesogenesis and early telogenesis. Most minerals are directly associated with cavities after gypsum/anhydrite, demonstrating that sulphate evaporites were an important influence on localization of mineralization. This is supported by the occurrence of sphalerite replacing anhydrite within an offshore borehole, and pseudomorphs of anhydrite outlined by replacive barite at outcrop. Spatially, distinct centres of mineralization can be defined, which are directly related to the position of fault conduits along which hot, base metal-rich brines entered the Raisby Formation from the Palaeozoic basement. These fault conduits, in turn, directly correlate with the margins of the Alston Block in northeast England. Methane derived from the maturation of Coal Measures which also utilized these fault conduits, was probably the single most important influence on mineralization, and related carbonate diagenesis.

8.6. Major results of this thesis.

This thesis has built, and expanded upon, sparse previous work on sedimentation of the Raisby Formation, and especially Zechstein carbonate-evaporite diagenesis, the foundations for which have been provided by previous thesis on diagenesis within English Zechstein carbonates (Harwood, 1981 and Aplin, 1985). The most significant results of this thesis are:

1. The first published depositional model for the Raisby Formation,
2. An improved characterization of the isotopic composition of Zechstein seawater,
3. A detailed account of the diagenesis of Raisby Formation limestones, which is directly applicable to other Zechstein limestones, and the first account of calcite concretions within the Raisby Formation, together with an un-surpassed description and interpretation of their petrography and geochemistry,
4. Further characterisation of the petrography and geochemistry of Raisby Formation dolostones,
5. The first in depth description and interpretation of the response of carbonate-evaporite sequences to meteoric diagenesis, and, especially, detailed characterization of the geochemical evolution of pore waters during uplift, and the first account of intimately-related calcitization of dolomite and calcium sulphates. This work is unique and without precedent.
6. The basis of an exploration model for possibly economically significant deposits of barite within the Raisby Formation of Co. Durham.

8.7. Suggestions for further work.

This thesis has given a very thorough, integrated account of the diagenetic history of the Raisby Formation. One area of further work could be to apply other analytical techniques to a further study of the diagenesis of the Raisby Formation. Particularly useful would be strontium isotopes and rare earth element analyses to help with limestone, dolostone, and calcite cement diagenesis, and sulphur isotope data for further investigation of the interrelationships between sulphate evaporites and mineralization, especially with regard to the possible roles of bacterial and thermochemical sulphate reduction. Laser ablation techniques would also greatly help in further delineating the relationships between stable isotope and trace element geochemistry, luminescence, and uplift diagenesis in the Raisby Formation.

Another aspect of further work would be to apply results from the diagenesis of the Raisby Formation to other carbonate-evaporite formations, both within, and outside the Zechstein Basin. Particularly productive would be comparisons with the diagenesis of limestones preserved in other parts of the Zechstein Basin which may have had different

burial histories, and comparison of concretion diagenesis with similar features both at outcrop in northeast England, and from boreholes in the North Sea. A major question still remains as to why calcite concretions form; what factors promote the replacement of carbonate muds by coarsely crystalline, radial splays of calcite. The reasons why concretions grow is one of the main unsolved questions of this thesis, although this study is the first to unequivocally demonstrate that concretions are of neomorphic origin. A comparison of the uplift-related calcite cement sequence in the Raisby Formation with that of other carbonate units now at outcrop, which previously contained evaporites, such as other Zechstein carbonates at outcrop in eastern England, and the Upper Permian reef complex of the Guadalupe Mountains, U.S.A., would be especially productive. Such comparisons may help towards a larger-scale model for the hydrogeochemical evolution of meteoric groundwaters, of particularly significant importance with regard to groundwater resource evaluation.

References

Abbott, P.L., 1974. Calcitization of Edwards Group dolomites in the Balcones fault zone aquifer, south-central Texas. Geology, 2: 359-362.

Adams, J.E. and Rhodes, M.L., 1960. Dolomitization by seepage refluxion. Bull. Am. Assoc. Pet. Geol., 44: 912-920.

Akhurst, M.C., 1988. Deposition and diagenesis of Waulsortian carbonates from Tynagh, Co. Galway, Ireland; their relationship with base metal mineralization. Ph.D. thesis, University of Newcastle-upon-Tyne (unpublished).

Al-Aasm, I.S. and Veizer, J., 1982. Chemical stabilization of low-Mg calcite: An example of brachiopods. J. Sediment Petrol., 52: 1101-1109.

Al-Aasm, I.S. and Veizer, J., 1986a. Diagenetic stabilization of aragonite and low-Mg calcite, I. Trace elements in Rudists. J. Sediment. Petrol., 56: 138-152.

Al-Aasm, I.S. and Veizer, J., 1986b. Diagenetic stabilization of aragonite and low-Mg calcite, II. Stable isotopes in Rudists. J. Sediment. Petrol., 56: 763-770.

Al-Hashimi, W.S. and Hemingway, J.E., 1973. Recent dedolomitization and the origins of the rusty crusts of Northumberland. J. Sediment. Petrol., 43: 82-91.

Al-Rekabi, Y.S., 1982. Petrography, porosity, permeability and geochemistry of the Upper Magnesian Limestone of N.E. England. Ph.D. Thesis, University of Dundee, Dundee (unpublished).

Amieux, P., 1982. Cathodoluminescence: Method of sedimentological study in carbonates. Bull. centres Rech. Explor. Prod. Elf Aquitaine, 6: 437-483.

Anderson, W., 1945. Water supply from underground sources in north-east England. Part III. Supplement-General discussion for new series one-Inch sheets 21 (Sunderland) and 27 (Durham). Geol. Surv. Wartime Pamphlet, 19.

Anderson, T.F. and Arthur, M.A., 1983. Stable isotopes of oxygen and carbon and their application to sedimentologic and paleoenvironmental problems. In: M.A. Arthur, T.F. Anderson, I.R. Kaplan, J.Veizer, and L.S. Land (Editors), Stable isotopes in sedimentary geology. Soc. Econ. Palaeont. Mineral., Short Course 10: 1-1 - 1-151.

Anderson, W. and Dunham, K.C., 1953. Reddened beds in the Coal Measures beneath the Permian of Durham and south Northumberland. Proc. Yorks. Geol. Soc., 29: 21-32.

Anderson, G.M. and Garven, G., 1987. Sulfate-sulfide-carbonate associations in Mississippi valley-type lead-zinc deposits. Economic Geology, 82: 482-488.

Antweiler, R.C. and Drever, J.I., 1983. The weathering of a late Tertiary volcanic ash: importance of organic solutes. Geochim. Cosmochim. Acta, 47: 623-629.

Aplin, G.F., 1981. Diagenesis of the Zechstein Main Reef Complex, N.E. England. Stable Isotope Report 66; Institute of Geological Sciences.

Aplin, G.F., 1985. Diagenesis of the Zechstein main reef complex, N.E.England. Ph.D. Thesis, University of Nottingham, Nottingham (unpublished).

Ayalon, A. and Longstaffe, F.J., 1988. Oxygen isotope studies of diagenesis and pore-water evolution in the western Canada sedimentary basin: Evidence from the Upper Cretaceous Belly River Sandstone, Alberta. J. Sediment. Petrol., 58: 489-505.

Back, W.M., Hanshaw, B.B., Plummer, L.N., Rahn, P.H., Rightmire, C.T. and Rubin, M.,1983. Process and rate of dedolomitization: Mass transfer and ^{14}C dating in a regional carbonate aquifer. Am. Assoc. Pet. Geol. Bull., 94: 1415-1429.

Badiozamani, K., 1973. The dorag dolomitization model-application to the Middle Ordovician of Wisconsin. J. Sediment. Petrol., 43: 965-984.

Baker, P.A. and Kastner, M., 1981. Constraints on the formation of sedimentary dolomite. Science, 213: 214-216.

Barnaby, R.J. and Rimstidt, J.D., 1989. Redox conditions of calcite cementation interpreted from Mn and Fe contents of authigenic calcites. Bull. Geol. Soc. Ame., 101: 795-804.

Bath, A.H., Milodowski, A.E. and Spiro, B., 1987. Diagenesis of carbonate cements in Permo-Triassic sandstones in the Wessex and East Yorkshire-Linconshire basins, UK: a stable isotope study. In: J.D. Marshall (Editor), Diagenesis of Sedimentary Sequences. Geol. Soc. London, Spec. Publ., 36: 173-190.

Bathurst, R.G.C., 1975. Carbonate sediments and their diagenesis. Second Edition, Elsevier, New York, 658pp.

Beauchamp, B., Oldershaw, A.E. and Krouse, R., 1987. Upper Carboniferous to Upper Permian ^{13}C-enriched primary carbonates in the Sverdrup basin, Canadian arctic: comparisons to coeval western North American ocean margins. Chem. Geol., 65: 391-413.

Bein, A. and Land, L.S., 1983. Carbonate sedimentation and diagenesis associated with Mg-Ca-Chloride brines: the Permian San Andres Formation in the Texas panhandle. J. Sediment. Petrol., 53: 243-260.

Bell, J., Holden, J., Pettigrew, T.H. and Sedman, K.W., 1979. The Marl Slate and Basal Permian Breccia at Middridge, Co. Durham. Proc. Yorks. Geol. Soc., 42: 439-460.

Berner, R.A., 1971. Principles of chemical sedimentology. McGraw-Hill, New York, 240pp.

Bjørkum, P.A. and Gjelsvik, N., 1988. An isochemical model for formation of authigenic kaolinite, K-feldspar and illite in sediments. J. Sediment. Petrol., 58: 506-511.

Bott, M.H.P., 1961. A gravity survey off the coast of north-east England. Proc. Yorks. Geol. Soc., 33: 1-20.

Bott, M.H.P. and Masson-Smith, D., 1957. The geological interpretation of a gravity survey of the Alston Block and the Durham coalfield. Q. J. Geol. Soc. London, 133: 93-117.

Braithwaite, C.J.R., 1988. Calcitization and compaction in the upper Permian Concretionary Limestone and Seaham Formations of North-East England. Proc. Yorks. Geol. Soc., 47: 33-45.

Ayalon, A. and Longstaffe, F.J., 1988. Oxygen isotope studies of diagenesis and pore-water evolution in the western Canada sedimentary basin: Evidence from the Upper Cretaceous Belly River Sandstone, Alberta. J. Sediment. Petrol., 58: 489-505.

Back, W.M., Hanshaw, B.B., Plummer, L.N., Rahn, P.H., Rightmire, C.T. and Rubin, M.,1983. Process and rate of dedolomitization: Mass transfer and ^{14}C dating in a regional carbonate aquifer. Am. Assoc. Pet. Geol. Bull., 94: 1415-1429.

Badiozamani, K., 1973. The dorag dolomitization model-application to the Middle Ordovician of Wisconsin. J. Sediment. Petrol., 43: 965-984.

Baker, P.A. and Kastner, M., 1981. Constraints on the formation of sedimentary dolomite. Science, 213: 214-216.

Barnaby, R.J. and Rimstidt, J.D., 1989. Redox conditions of calcite cementation interpreted from Mn and Fe contents of authigenic calcites. Bull. Geol. Soc. Ame., 101: 795-804.

Bath, A.H., Milodowski, A.E. and Spiro, B., 1987. Diagenesis of carbonate cements in Permo-Triassic sandstones in the Wessex and East Yorkshire-Linconshire basins, UK: a stable isotope study. In: J.D. Marshall (Editor), Diagenesis of Sedimentary Sequences. Geol. Soc. London, Spec. Publ., 36: 173-190.

Bathurst, R.G.C., 1975. Carbonate sediments and their diagenesis. Second Edition, Elsevier, New York, 658pp.

Beauchamp, B., Oldershaw, A.E. and Krouse, R., 1987. Upper Carboniferous to Upper Permian ^{13}C-enriched primary carbonates in the Sverdrup basin, Canadian arctic: comparisons to coeval western North American ocean margins. Chem. Geol., 65: 391-413.

Bein, A. and Land, L.S., 1983. Carbonate sedimentation and diagenesis associated with Mg-Ca-Chloride brines: the Permian San Andres Formation in the Texas panhandle. J. Sediment. Petrol., 53: 243-260.

Bell, J., Holden, J., Pettigrew, T.H. and Sedman, K.W., 1979. The Marl Slate and Basal Permian Breccia at Middridge, Co. Durham. Proc. Yorks. Geol. Soc., 42: 439-460.

Berner, R.A., 1971. Principles of chemical sedimentology. McGraw-Hill, New York, 240pp.

Bjørkum, P.A. and Gjelsvik, N., 1988. An isochemical model for formation of authigenic kaolinite, K-feldspar and illite in sediments. J. Sediment. Petrol., 58: 506-511.

Bott, M.H.P., 1961. A gravity survey off the coast of north-east England. Proc. Yorks. Geol. Soc., 33: 1-20.

Bott, M.H.P. and Masson-Smith, D., 1957. The geological interpretation of a gravity survey of the Alston Block and the Durham coalfield. Q. J. Geol. Soc. London, 133: 93-117.

Braithwaite, C.J.R., 1988. Calcitization and compaction in the upper Permian Concretionary Limestone and Seaham Formations of North-East England. Proc. Yorks. Geol. Soc., 47: 33-45.

Brand, U. and Veizer, J., 1980. Chemical diagenesis of a multicomponent carbonate system - 1: trace elements. J. Sediment. Petrol., 50: 1219-1236.

Brand, U. and Veizer, J., 1981. Chemical diagenesis of a multicomponent carbonate system - 2: stable isotopes. J. Sediment. Petrol., 51: 987-997.

Brauer, J.S. and Baker, P.A., 1984. Experimental hydrothermal dedolomitization. Bull. Am. Assoc. Pet. Geol., 68: 457.

Browell, E.J.J. and Kirkby, J.W., 1867. On the chemical composition of various beds of the Magnesian Limestone and associated Permian rocks of Durham. Trans. Nat. Hist. Soc. Northumberland, Durham, and Newcastle upon Tyne, 1: 204-230.

Brown, G.C., Cassidy, J., Oxburgh, E.R., Plant, J., Sabine, P.A. and Watson, J.V., 1980. Basement heat flow and metalliferous mineralization in England and Wales. Nature, 288: 657-659.

Brown, S., 1984. Jurassic. In: K. Glennie (Editor), Introduction to the petroleum geology of the North Sea. Blackwell Oxford, 103-132.

Budai, J.M., Lohmann, K.C. and Owen, R.M., 1984. Burial dedolomite in the Mississippian Madison Limestone, Wyoming and Utah thrust belt. J. Sediment. Petrol., 54: 276-288.

Bullen, S.B. and Sibley, D.F., 1984. Dolomite selectivity and mimic replacement. Geology, 12: 655-658.

Burley, S.D., Kantorowicz, J.D. and Waugh, B., 1985. Clastic diagenesis. In: P.J. Brenchley and B.P.J. Williams (Editors) Sedimentology: recent developments and applied aspects, Blackwell, Oxford, 189-226.

Butler, G.P., 1969. Modern evaporite deposition and geochemistry of coexisting brines, the sabkha, Trucial Coast, Arabian Gulf. J. Sediment. Petrol., 39: 70-89.

Cairney, T., 1972. Hydrological investigation of the Magnesian limestone of south-east Durham, England. J. Hydrology, 16: 323-340.

Carpenter, S.J. and Lohmann, K.C., 1989. $\delta^{18}O$ and $\delta^{13}C$ variations in Late Devonian marine cements from the Golden Spike and Nevis reefs, Alberta, Canada. J. Sediment. Petrol., 59: 792-814.

Carter, R.M., 1975. A discussion and classification of subaqueous mass-transport with particular application to grain-flow, slurry-flow and fluxoturbidites. Earth Science Reviews, 11: 145-177.

Champ, D.R., Gulens, J. and Jackson, R.E., 1979. Oxidation and reduction sequences in groundwater flow systems. Can. J. Earth Sci., 16: 12-23.

Chafetz, H.S., 1972. Surface diagenesis of limestones. J. Sediment. Petrol., 42: 325-329.

Chafetz, H.S., Wilkinson, B.H. and Love, K.M., 1985. Morphology and composition of non-marine carbonate cements in near-surface settings. Soc. Econ. Palaeontol. Mineral., Spec. Publ., 36: 337-347.

Chowns, T.M. and Elkins, J.E., 1974. The origin of quartz geodes and cauliflower cherts through the silicification of anhydrite nodules. J. Sediment. Petrol., 44: 885-903.

Clark, D.N., 1980. The diagenesis of Zechstein carbonate sediments. In: H. Fuchtbauer & T. Peryt (Editors). The Zechstein basin with emphasis on carbonate sequences. Contributions to sedimentology 9, 167-203.

Clark, D.N., 1986. The distribution of porosity in Zechstein carbonates. In: J. Brooks, J.C. Goff and B. van Horn (Editors), Habitat of Palaeozoic Gas in N.W. Europe. Geol. Soc. London, Spec. Publ., 23: 121-149.

Clark, D.N. and Shearman, D.J., 1980. Replacement anhydrite in limestones and the recognition of moulds and pseudomorphs: a review. Revista del Instituto de Investigaciones Geologicas Diputacion Provincial Universidad Barcelona, 34: 161-186.

Clarke, A.M., 1962. Some structural, hydrological and safety aspects of recent developments in south-east Durham. Mining Engineer, 27: 209-231.

Clarke, E.T., Loeppert, R.H. and Ehrman, J.M., 1985. Crystallization of iron oxides on calcite surfaces in static systems. Clays and clay minerals, 33: 152-158.

Coleman, M.L., Walsh, N.J. and Benmore, R.A., 1989. Determination of both chemical and stable isotope composition in milligramme-size carbonate samples. Sed. Geol., 65: 233-238.

Compston, W., 1960. The carbon isotopic compositions of certain marine invertebrates and coals from the Australian Permian. Geochim. et Cosmochim. Acta, 18: 1-22.

Cook, H.E., 1979. Generation of debris flows and turbidity current flows from submarine slides. Am. Assoc. Pet. Geol. Bull., 63: 435.

Cook, H.E., 1983. Ancient carbonate platform margins, slopes and basins. Platform margin and deep water carbonates, Spec. Publ. Soc. Econ. Paleont. Mineral. short course 12: 5-1 - 5-189.

Cook, H.E. and Taylor, M.E., 1977. Comparison of continental slope and shelf environments in the Upper Cambrian and Lowest Ordovician of Nevada. Soc. Econ. Paleont. Minerall., Spec. Publ., 25: 51-81.

Cook, H.E., Taylor, M.E. and Magoon, L.B., 1987. The role of major carbonate debris-flow events in recognising and dating eustatic lowering of sea level-perspectives from pre-Panthalassa ocean-margin terranes. Abstract, Soc. Econ. Paleont. Mineral. conference, Carbonate Gravity Deposits (unpublished).

Cooper, B.S., 1975. Discussion of D.M. Hirst and F.W. Smith, Controls on barite mineralization in the Lower Magnesian Limestone of the Ferryhill area, County Durham. Trans. Instn. Min. Metall., 84: B36.

Cornford, C., 1984. Source rocks and hydrocarbons of the North Sea. In: K. Glennie (Editor), Introduction to the petroleum geology of the North Sea. Blackwell Oxford, 171-204.

Craig, H., 1957. Isotopic standards for carbon and oxygen and correction factors for mass-spectrometric analysis of carbon dioxide. Geochim. Cosmochim. Acta, 12: 133-149.

Craig, J.R. and Vaughan, D.J., 1981. Ore microscopy and ore petrography. John Wiley & Sons, New York, 406pp.

Coplen, T.B., Kendall, C. and Hopple, J., 1983. Comparison of stable isotope reference samples. Nature, 302: 236-238.

Davies, G.R., 1977. Turbidites, debris sheets and truncation structures in the Upper Paleozoic deep water carbonates of the Sverdrup basin, Arctic archipelago. Soc. Econ. Paleont. Minerall., Spec. Publ., 25: 221-247.

De Groot, K., 1967. Experimental dedolomitization. J. Sediment. Petrol., 37: 1216-1220.

Decima, A., McKenzie, J.A. and Schreiber, B.C., 1988. The origin of "evaporative" limestones: An example from the Messinian of Sicily (Italy). J. Sediment. Petrol., 58: 256-272.

Deer, W.A., Howie, R.A. and Zussman, J., 1962. Rock-forming minerals, Vol. 5; Non-silicates. Longmans, London, 371pp.

Degens, E.T. and Stoffers, P., 1980. Environmental events recorded in Quaternary sediments of the Black Sea. J. Geol. Soc. London, 137: 131-138.

Deines, P., 1970. Mass spectrometer correction factors for the determination of small isotopic composition variations of carbon and oxygen. Int. J. Mass Spectrom., Ion Physics, 4: 283.

Dickson, J.A.D. and Coleman, M., 1980. Changes in carbon and oxygen isotopic compositions during limestone diagenesis. Sedimentology, 27: 107-118.

Dixon, J. and Wright, V.P., 1983. Burial diagenesis and crystal diminution. The origin of crystal diminution in some limestones from South Wales. Sedimentology, 30: 537-546.

Doerner, H.A. and Hoskins, W.M., 1925. Coprecipitation of radium and barium sulphates. J. American Chemical Society, 47: 662-675.

Drever, J.I. 1982. The geochemistry of natural waters. Prentice-Hall, Englewood Cliffs, 338pp.

Dunham, K.C., 1934. The genesis of the north Pennine ore deposits. Q. J. Geol. Soc. London, 90: 689-717.

Dunham, K.C., 1948. Geology of the northern Pennine orefield. Volume 1, Tyne to Stainmore (1st edition).

Dunham, K.C., 1952. Fluorospar (4th edition). Mem. Geol. Survey, Special Report Mineral Resources Great Britain, 4.

Dunham, K.C., 1966. The role of juvenile solutions, connate waters and evaporitic brines in the genesis of Pb - Zn- Fluorine - Ba deposits. Trans. Instn. Min. Metall., 75: B226-229.

Dunham, K.C., Claringbull, G.F. and Bannister, F.A., 1948. Dickite and collophane in the Magnesian Limestone of Durham. Min. Mag., 28: 338-342.

Durrance, E.M., Meads, R.E., Ballard, R.R.B. and Walsh, J.N., 1978. Oxidation state of iron in the Littleham Mudstone Formation of the New Red Sandstone Series (Permian-Triassic) of southeast Devon, England. Geol. Soc. Ame. Bull., 89: 1231-1240.

Edmunds, W.M., 1975. Geochemistry of brines in the Coal Measures of north-east England. Trans. Instn. Min. Metall., 84: B39-B52.

Edmunds, W.M., Bath, A.H. and Miles, D.L., 1982. Hydrochemical evolution of the East Midlands Triassic sandstone aquifer, England. Geochim. Cosmochim. Acta, 46: 2069-2081.

Elmore, R.D., Dunn, W. and Peck, C., 1985. Absolute dating of dedolomitization by means of paleomagnetic techniques. Geology, 13: 558-561.

Emery, D. and Marshall, J.D., 1989. Zoned calcite cements: has analysis outpaced interpretation. Sed. Geol., 65: 205-210.

Evamy, B.D., 1963. Application of a chemical staining technique to a study of dedolomitization. Sedimentology, 2: 164-170.

Evamy, B.D., 1967. Dedolomitization and the development of rhombohedral pores in limestones. J. Sediment. Petrol., 37: 1204-1215.

Fanning, K.A., Byrne, R.H., Breland, J.A., Betzer, P.R., Moore, W.S. and Elsinger, R.J., 1981. Geothermal springs of the west Florida continental shelf: evidence for dolomitization and radionuclide enrichment. Earth Planet. Sci. Lett., 52: 345-354.

Fairchild, I.J., 1983. Chemical controls of cathodoluminescence of natural dolomites and calcites: new data and review. Sedimentology, 30: 579-583.

Fairchild, I.J. Hendry, G., Quest, M. and Tucker, M., 1988. Chemical analysis of sedimentary rocks. In: M. Tucker (Editor), Techniques in Sedimentology, Blackwell Scientific Publications, 274-354.

Fisher, I. St. J., 1986. Pyrite replacement of mollusc shells from the Lower Oxford Clay (Jurassic) of England. Sedimentology, 33: 575-585.

Folk, R.L., 1965. Some aspects of recrystallization in ancient limestones. In: L.C. Pray and R.C. Murray (Editors), Dolomitization and limestone diagenesis. Soc. Econ. Paleont. Mineral. Spec. Publ., 13: 14-48.

Folk, R.L., 1974. The natural history of crystalline calcium carbonate: effects of magnesium content and salinity. J. Sediment. Petrol., 44: 40-53.

Folk, R.L. and Land, L.S., 1975. Mg/Ca ratio and salinity: two controls on crystallization of dolomite. Am. Assoc. Petrol. Geol. Bull., 59: 60-68.

Folk, R.L., Chafetz, H.S. and Tiezzi, P.A., 1985. Bizarre forms of depositional and diagenetic calcite in hot-spring travertines, central Italy. In: N. Schneidermann and P.M. Harris (Editors) Carbonate Cements. Soc. Econ. Paleonol. Mineral. Spec. Publ., 36: 349-369.

Folkman, Y., 1969. Diagenetic dedolomitization in the Albian-Cenomanian Yagur dolomite on Mount Carmel (northern Israel). J. Sediment Petrol., 39: 380-385.

Fowler, A. 1943. On fluorite and other minerals in Lower Permian rocks of south Durham. Geol. Mag, 80: 41-51.

Fowler, A., 1957. Minerals in the Permian and Trias of north-east England. Proc. Geol. Ass. 67: 251-265.

Frank, J.R., 1981. Dedolomitization in the Taum Sauk Limestone (Upper Cambrian), southeast Missouri. J. Sediment. Petrol., 51: 7-18.

Frank, J.R., Carpenter, A.B. and Ogelsby, T.W., 1982. Cathodoluminescence and composition of calcite cement in the Taum Sauk Limestone (Upper Cambrian), south-east Missouri. J. Sediment. Petrol., 52: 631-638.

Freeze, R.A. and Cherry, J.A.,1979. Groundwater. Prentice-Hall, Englewood Cliffs, 604pp.

Frey, R.W., and Pemberton, S.G., 1984. Trace fossil facies models. In: R.G. Walker (Editor), Facies models, second edition: 189-207.

Friedman, G.M., 1980. Dolomite is an evaporite mineral: evidence from the rock record and from sea - marginal ponds of the Red Sea. Soc. Econ. Paleontol. Mineral., Spec. Publ., 28: 69-80.

Friedman, I. and O'Neil, J.R., 1977. Compilation of stable isotope fractionation factors of geochemical interest. U.S. geol. Surv. Prof. Paper, 440-KK.

Fusezy, L.M., 1980. Origin of nodular limestones, calcium sulphates and dolomites in the Lower Magnesian Limestone in the neighborhood of Selby, Yorkshire, England. In H. Fuchtbauer & T.M. Peryt (Editors). The Zechstein basin with emphasis on carbonate sequences. Contributions to Sedimentology 9, 35-44.

Gaines, A.M., 1977. Protodolomite redefined. J. Sed. Petrol., 47: 534-546.

Garrels, R.M. and Christ, C.L., 1965. Solutions, minerals and equilibria. Harper and Row, New York.

Garwood, E., 1891. On the origin and mode of formation of the concretions in the Magnesium Limestones of Durham. Geol. Mag., 8: 435-440.

Gawthorpe, R.L., 1987. Burial dolomitization and porosity development in a mixed carbonate-clastic sequence: an example from the Bowland Basin, northern England. Sedimentology, 34: 533-558.

Gawthorpe, R.L. and Clemmey, H., 1985. Geometry of submarine slides in the Bowland Basin (Dinantian) and their relation to debris flows. Q. J. Geol. Soc. London, 142: 555-565.

Gibbons, M.J., 1978. The geochemistry of sabkha and related deposits. Ph.D. thesis, University of Newcastle upon Tyne (unpublished), 407pp.

Given, R.K. and Lohmann, K.C., 1985. Derivation of original isotopic composition of Permian marine cements. J. Sediment. Petrol., 55: 430-439.

Given, R.K. and Wilkinson, B.H., 1985. Kinetic control of morphology, composition, and mineralogy of abiotic sedimentary carbonates. J. Sediment. Petrol., 55: 109-119.

Glennie, K.W., 1982. Early Permian (Rotliegendes) palaeowinds of the North Sea. Sed. Geol. 34: 245-265.

Glennie, K.W., 1984a. The structural framework and the pre-Permian history of the North Sea area. In: K.W. Glennie (Editor), Introduction to the petroleum geology of the North Sea. Oxford, Blackwell: 17-39.

Glennie, K.W., 1984b. Early Permian-Rotliegend. In: K.W. Glennie (Editor), Introduction to the petroleum geology of the North Sea. Oxford, Blackwell: 41-60.

Glennie, K.W., 1986. Development of N.W. Europe's Southern Permian Gas Basin. In: J. Brooks, J.C. Goff and B. van Horn (Editors), Habitat of Palaeozoic Gas in N.W. Europe. Geol. Soc. London Spec. Publ. 23: 3-22.

Glennie, K.W., Mudd, G.C. and Nagtegaal, P.J.C., 1978. Depositional environment and diagenesis of Permian Rotliegendes sandstones in Leman Bank and Sole Pit areas of the UK southern North Sea. Q. J. Geol. Soc. London, 135: 25-34.

Glennie, K.W. and Buller, A.T., 1983. The Permian Weissliegendes of N.W. Europe: the partial deformation of aeolian dune sands caused by the Zechstein transgression. Sediment. Geol., 35: 43-81.

Goldberg, M., 1967. Supratidal dolomitization and dedolomitization in Jurassic rocks of Hamakhtesh Haqatan, Israel. J. Sediment. Petrol., 37: 760-773.

Gonzalez, L.A. and Lohmann, K.C., 1988. Controls on mineralogy and composition of spelean carbonates: Carlsbad Caverns, New Mexico. In: N.P. James and P.W. Choquette (Editors), Paleokarst, Springer-Verlag, New York, 81-101.

Goodall, I.G., 1987. An investigation of the facies and diagenesis of the Edlington Formation (Upper Permian) of Tees-side. Ph.D. Thesis, University of Reading, Reading (Unpublished).

Graber, E.R. and Lohmann, K.C., 1989. Basinal marine dolomicrite from the Pennsylvanian/Wolfcampian Horquilla Formation, New Mexico. J. Sediment. Petrol., 59: 4-12.

Green, P.F., 1986. On the thermo-tectonic evolution of Northern England: evidence from fission track analysis. Geol. Mag., 123: 493-506.

Green, P.F., 1989. Thermal and tectonic history of the East Midlands shelf (onshore UK) and surrounding regions assesed by apatite fission track analysis. J. Geol. Soc. London, 146: 755-773.

Gregg, J.M., 1988. Origins of dolomite in the offshore facies of the Bonneterre Formation (Cambrian), southeast Missouri. In: V.Shukla and P.A. Baker (Editors), Soc. Econ. Paleontol. Mineral, Spec. Publ., 43: 67-83.

Gregg, J.M. and Sibley, D.F., 1984. Epigenetic dolomitization and the origin of xenotopic dolomite texture. J. Sediment. Petrol., 54: 908-931.

Guilbert, J.M. and Park, C.F. Jr., 1986. the geology of ore deposits. W.H. Freeman and Company, New York.

Hampton, M.A. 1972. The role of subaqueous debris flows in generating turbidity currents. J. Sediment. Petrol., 42: 775-793.

Hampton, M.A., 1975. Competence of fine-grained debris flows. J. Sediment. Petrol., 45: 834-844.

Hancock, J.M., 1984. Cretaceous. In: K. Glennie (Editor), Introduction to the petroleum geology of the North Sea. Blackwell Oxford, 133-150.

Hanshaw, B.B., Back, W. and Deike, R.G., 1971. A geochemical hypothesis for dolomitization by groundwater. Economic Geology, 66: 710-724.

Hardie, L.A., 1967. The gypsum-anhydrite equilibrium at one atmosphere pressure. Ame. Mineral., 52: 171-200.

Hardie, L.A., 1987. Dolomitization: A critical review of some current views.J. Sediment. Petrol., 57: 166-183.

Harris, P.M., Kendall, C.G.St.C. and Lerche, I., 1985. Carbonate cementation - a brief review. Soc. Econ. Palaeontol. Mineral., Spec. Publ., 28: 79-95.

Harwood, G.M., 1980. Calcitized anhydrite and associated sulphides in the English Zecstein first cycle carbonate (EZ1 Ca). In: H.Fuchtbauer, and T.M.Peryt (Editors), The Zechstein basin with emphasis on carbonate sequences. Contributions to sedimentology 9: 61-72.

Harwood, G.M. 1981. Controls of mineralization in the Cadeby Formation (Lower Magnesian Limestone). Ph.D. Thesis, Open University (unpublished).

Harwood, G.M., 1983. The application of cathodoluminescence in relative dating of barite mineralization in the Lower Magnesian Limestone (Upper Permian), United Kingdom. Econ. Geol., 78: 1022-1027.

Harwood, G.M., 1986. The diagenetic history of the Cadeby Formation (EZ1 Ca), Upper Permian, eastern England. In: G.M. Harwood and D.B.Smith (Editors), The English Zechstein and related topics. Geol. Soc. London, Spec. Publ., 22, 75-86.

Harwood, G.M. and Coleman, M.L., 1983. Isotopic evidence for UK Upper Permian mineralization by bacterial reduction of evaporites. Nature, 301: 597-599.

Harwood, G.M. and Smith, F.W., 1986. Mineralization in Upper Permian carbonates at outcrop in eastern England. In: G.M.Harwood & D.B.Smith (Editors), The Zechstein basin and related topics. Spec. Publ. Geol. Soc. London, 33: 103-111.

Hawkins, A.B., 1979. Case histories of some effects of solution/dissolution in Keuper rocks of the Severn estuary region. Q. J. Eng. Geol. London, 12: 31-40.

Hemming, N.G., Meyers, W.J. and Grams, J.C., 1989. Cathodoluminescence in diagenetic calcites: The roles of Fe and Mn as deduced from electron probe and spectrophotometric measurements. J. Sediment. Petrol., 59: 404-411.

Hirst, D.M. and Dunham, K.C., 1963. Chemistry and petrography of the Marl Slate of S.E. Durham, England. Economic Geology, 58: 912-940.

Hirst, D.M. and Smith, F.W., 1974. Controls of barite mineralization in the Lower Magnesian Limestone of the Ferryhill area, County Durham. Trans. Instn Min. Metall. (Sect. B: Appl. earth sci.), 83: B49-55.

Hiscott, R.N. and James, N.P., 1985. Carbonate debris flows, Cow Head Group, western Newfoundland. J. Sediment. Petrol., 55: 735-745.

Holail, H., Lohmann, K.C. and Sanderson, I., 1988. Dolomitization and dedolomitization of Upper Cretaceous carbonates: Bahariya Oasis, Egypt. In: V. Holliday, D.W., 1970. The petrology of secondary gypsum rocks: a review. J. Sediment. Petrol., 40: 734-744.

Holliday, D.W. and Shephard-Thorn, E.R., 1974. Basal Purbek evaporites of the Fairlight borehole, Sussex. Rep. Inst. Geol. Sci., 74/4, 14pp.

Hollingworth, N.T.J., 1987. Palaeoecology of the Upper Permian Zechstein Cycle 1 Reef in north-east England. Ph.D. Thesis, University of Durham, Durham (unpublished).

Hollingworth, N.T.J. and Tucker, M.E. 1987. The upper Permian (Zechstein) Tunstall reef of north east England: Palaeoecology and early diagenesis. In: T.M. Peryt (Editor). The Zechstein facies in Europe. Lecture notes in earth sciences 10. Springer-Verlag, Heidelberg, pp 21-50.

Holmes, A., 1931. Concretionary and oolitic structures of the Permian rocks. Proc. Geol. Ass., 42: 255-259.

Howse, R., 1848. A catalogue of the fossils of the Permian system of the counties of Northumberland and Durham. Trans. Tyneside Nat. Field Club 1: 218-264.

Howse, R., 1857. Notes on the Permian system in the counties of Northumberland and Durham. Ann. Mag. Nat. Hist., 19: 33-52, 304-312, 463-473.

Hsu, K.J. and Siegenthaler, C., 1969. Preliminary experiments on hydrodynamic movement induced by evaporation and their bearing on the dolomite problem. Sedimentology, 12: 11-25.

Hudson, J.D., 1975. Carbon isotopes and limestone cementation. Geology, 3: 19-22.

Hudson, J.D., 1977. Stable isotopes and limestone lithification. J. Geol. Soc. London, 133: 637-660.

Hudson, J.D., 1982. Pyrite in ammonite-bearing shales from the Jurassioc of England and Germany. Sedimentology, 29: 639-667.

Hudson, J.D. and Andrews, J.E. 1987. The diagenesis of the Great Estuarine Group, Middle Jurassic, Inner Hebrides, Scotland. In: J.D. Marshall (Editor) Diagenesis of Sedimentary Sequences. Geol. Soc. London, Spec. Publ., 36: 259-276.

Humphrey, J.D. and Quinn, T.M., 1989. Coastal mixing zone dolomite, forward modelling, and massive dolomitization of platform-margin carbonates. J. Sediment. Petrol., 59: 438-454.

Ichikuni, M. and Musha, S., 1978. Partition of strontium between gypsum and solution. Chem. Geol., 21: 359-363.

Illing, L.V., Wells, A.J. and Taylor, J.C.M., 1965. Penecontemporaneous dolomite in the Persian Gulf. In: L.C. Pray and R.C. Murray (Editors), Dolomitization and limestone diagenesis. Soc. Econ. Paleontol. Mineral., Spec. Publ., 13: 89-111.

Irwin, H., Curtis, C. and Coleman, M., 1977. Isotopic evidence for source of diagenetic carbonates formed during burial of organic-rich sediments. Nature, London, 269: 209-213.

James, A.N. and Lupton, A.R.R., 1978. Gypsum and anhydrite in foundations of hydraulic structures. Geotechnique London, 28: 249-272.

Jenkyns, H.C., 1974. Origin of red nodular limestones (Ammonitico Rosso, knollenkalke) in the Mediterranean Jurassic: a diagenetic model. Spec. Publ. Int. Ass. Sediment., 1: 249-271.

Jenyon, M.K., Creswell, P.M. and Taylor, J.C.M., 1984. Nature of the connection between the northern and southern Zechstein basins across the Mid North Sea High. Marine & Petroleum Geol., 1: 355-363.

Jones, K., 1969. Mineralogy and geochemistry of the Lower and Middle Magnesian Limestone of County Durham. Ph.D. Thesis, University of Durham, Durham (unpublished)

Jones, K. and Hirst, D.M., 1972. The distribution of barium, lead and zinc in the Lower and Middle Magnesian Limestone of County Durham, Great Britain. Chem. Geol., 10: 223-236.

Kaldi, J., 1980. The origin of nodular structures in the Lower Magnesian Limestone (Permian) of Yorkshire, England. In: H. Fuchtbauer and T.M. Peryt, (Editors) The Zechstein basin with emphasis on carbonate sequences. Contributions to Sedimentology 9: 45-60.

Kaldi, J., 1986a. Sedimentology of sandwaves in an oolite shoal complex in the Cadeby (Magnesian Limestone) Formation (Upper Permian) of eastern England. In: G.M. Harwood and D.B. Smith (Editors), The English Zechstein and related topics. Geol. Soc. London, Spec. Publ., 22: 63-74.

Kaldi, J., 1986b. Diagenesis of nearshore carbonate rocks in the Sprotbrough Member of the Cadeby (Magnesian Limestone) Formation (Upper Permian) of eastern England. In: G.M.Harwood and D.B.Smith (Editors), the English Zechstein and related topics. Geol. Soc. London, Spec. Publ., 22, 87-102.

Kaldi, J. and Gidman, J., 1982. Early diagenetic dolomite cements: examples from the Permian Lower Magnesian Limestone of England and Pleistocene carbonates of the Bahamas. J. Sediment. Petrol. 52: 1073-1085.

Kaldi, J. and Hartling, A., 1982. Calcitized anhydrite: its significance as an exploration tool in the Mississippian Tilston beds of southeastern Saskatchewan. Summ. Investigations Saskatchewan Geol. Survey, 1982.

Kastner, M., 1982. When does dolomitization occur and what controls it (abstr.). 11th Int. Congress Sedimentology, Hamilton, Ontario, Canada.

Katz, A., 1968. Calcian dolomites and dedolomitization. Nature, 217: 439-440.

Katz, A., 1971. Zoned dolomite crystals. J. Geology, 79: 38-51.

Katz, A., Sass, E., Starinsky, A. and Holland, H.D., 1972. Strontium behaviour in the aragonite-calcite transformation: an experimental study at 40°-90°C. Geochim. Cosmochim. Acta, 36: 481-496.

Keller, W.D., 1976. Scan electron micrographs of kaolins collected from diverse environments of origin - I. Clays and clay minerals, 24: 107-113.

Kendall, A.C., 1975. Anhydrite replacements of gypsum (satin-spar) veins in the Mississippian caprocks of southeastern Saskatchewan. Can. J. Earth Sci., 12: 1190-1195.

Kendall, A.C., 1977. Fascicular-optic calcite: a replacement of bundled acicular carbonate cements. J. Sediment. Petrol., 47: 1056-1062.

Kendall, A.C., 1984. Evaporites. In: R.G. Walker (Editor), Facies models, second edition, 259-296.

Kendall, A.C., 1989. Brine mixing in the Middle Devonian of western Canada and its possible significance to regional dolomitization. Sed. Geol., 64: 271-285.

Kendall, A.C. and Tucker, M.E., 1973. Radiaxial fibrous calcite: a replacement after acicular carbonate. Sedimentology, 20: 365-389.

Kendall, A.C. and Broughton, P.L. 1978. Origin of fabrics in speleothems composed of columnar calcite crystals. J. Sediment. Petrol., 48: 519-538.

Kendall, A.C. and Walters, K.L., 1978. The age of metasomatic anhydrite in Mississippian reservoir carbonates, southeastern Saskatchewan. Can. J. Earth. Sci., 15: 424-430.

King, W., 1850. A monograph of Permian fossils of England. Palaeontographical society of London (monograph).

Kinsman, D.J.J., 1969. Interpretation of Sr^{2+} concentrations in carbonate minerals and rocks. J. Sediment. Petrol., 39: 486-508.

Kirkby, J.W., 1858. On some Permian fossils from Durham. Q. J. Geol. Soc. London, 3: 213-218.

Kirkby, J.W., 1867. On the fossils of the Marl-slate ond Lower Magnesian Limestone. Trans. Nat. Hist. Soc. Newcastle, 1: 184-200.

Kirkland, D.W. and Evans, R., 1976. Origin of limestone buttes, gypsum plain, Culberson County, Texas. Bull. Am. Assoc. Pet. Geol., 60: 2005-2018.

Kitano Y., Kanamori, N. and Oomori, T., 1971. Measurements of distribution coefficients af strontium and barium between carbonate precipitate and solution - Abnormally high values of distribution coefficients measured at early stages of carbonate formation. J. Geochemistry, 4: 183-206.

Kohout, F.A., 1967. Ground water flow and the geothermal regime of the Floridan plateau. Trans. Gulf Coast Assoc. Geol. Soc., 17: 339-354.

Kozur, H., 1981a. The boundaries and subdivisions of the Permian system. In: Proc. Int. Symp. Central European Permian, Warsaw 1978: 401-425.

Kozur, H., 1981b. The correlation of the uppermost Carboniferous and Permian of middle and western Europe with the marine standard scale. In: Proc. Int. Symp. Central European Permian, Warsaw 1978: 426-450.

Krause, F.F. and Oldershaw, A.E., 1979. Submarine carbonate breccia beds - a depositional model for two - layer sediment gravity flows from the Sekwi Formation (Lower Cambrian), Mackenzie Mountains, Northwest Territories, Canada. Canad. J. Earth Sci., 16: 189-199.

Krinsley, D.H. and Smith, D.B., 1981. A selective SEM study of grains from the Permian Yellow Sands of north-east England. Proc. Geol. Ass., 92: 189-196.

Krouse, H.R., Viau, C.A., Eliuk, L.S., Ueda, A. and Halas, S., 1988. Chemical and isotopic evidence of thermochemical sulphate reduction by light hydrocarbon gases in deep carbonate reservoirs. Nature, London, 333: 415-419.

Lahann, R.W., 1978. A chemical model for calcite crystal growth and morphology control. J. Sediment. Petrol., 48: 337-344.

Land,. D.H., 1974. Geology of the Tynemouth district. Mem. Geol. Surv. G.B.

Land, L.S., 1973. Contemporaneous dolomitization of Middle Pleistocene reefs by meteoric water, North Jamacia. Marine Science Bulletin, 23: 64-92.

Land, L.S., 1980. The isotopic and trace element chemistry of dolomite: The state of the art. In: D.H. Zenger, J.G. Dunham and R.L. Ethington (Editors), Concepts and models of dolomitization. Soc. Econ. Paleont. Mineral., Spec. Publ., 28: 87-110.

Land, L.S., 1983. The application of stable isotopes to studies of the origin of dolomite and to problems of diagenesis in clastic sediments. In: M.A. Arthur, T.F. Anderson, I.R. Kaplan, J.Veizer, and L.S. Land (Editors), Stable isotopes in sedimentary geology, Soc. Econ. Paleontol. Mineral., Short Course 10: 4-1 - 4-22.

Land, L.S., 1985. The origin of massive dolomite. J. Geological Education, 33: 112-125.

Land, L.S. and Hoops, G.K., 1973. Sodium in carbonate sediments and rocks: A possible index to the salinity of diagenetic solutions. J. Sediment. Petrol., 43: 614-617.

Land, L.S. and Prezbindowski, D.R., 1981. The origin and evolution of saline formation water, lower Cretaceous carbonates, south-central Texas, USA. J. Hydrology, 54: 51-74.

Lasemi, Z. and Sandberg, P.A., 1984. Transformation of aragonite-dominated lime muds to microcrystalline limestones. Geology, 12: 420-423.

Lebour, G.A., 1905. The Marl-slate and Yellow Sands of Northumberland and Durham. Trans. North England Instn. Min. Met. Eng., 53: 101-122.

Lee, M.R. and Harwood, G.M., 1989. Dolomite calcitization and cement zonation related to uplift of the Raisby Formation (Zechstein carbonate), northeast England. Sed. Geol., 65: 285-305.

Lloyd, R.M., 1966. Oxygen isotope enrichment of sea water by evaporation. Geochim. Cosmochim. acta, 30: 801-814.

Lohmann, K.C., 1988. Geochemical patterns of meteoric diagenetic systems and their application to studies of paleokarst. In: N.P. James and P.W. Choquette (Editors), Paleokarst, Springer-Verlag, New York, 58-80.

Lohmann, K.C. and Meyers, W.J., 1977. Microdolomite inclusions in cloudy prismatic calcites: a proposed criterion for former high - magnesian calcites. J. Sediment. Petrol., 47: 1078-1088.

Lohmann, K.C. and Walker, J.G.C., 1989. The $\delta^{18}O$ record of Phanerozoic abiotic marine calcite cements. Geophys. Res. Lett., 16: 319-322.

Longman, M.W. and Mench, P.A., 1978. Diagenesis of Cretaceous limestones in the Edwards aquifer system of south-central Texas: a scanning electron microscope study. Sed. Geol., 21: 241-276.

Longstaffe, F.J., 1984. The role of meteoric water in diagenesis of shallow sandstones: stable isotope studies of the Milk River aquifer and gas pool, southeastern Alberta. In: D.A. McDonald and R.C. Surdam (Editors), Clastic Diagenesis, Memoir Am. Assoc. Pet. Geol., 37: 81-98.

Loope, D.B. and Watkins, D.K., 1989. Pennsylvanian fossils replaced by red chert: Early oxidation of pyritic precursors. J. Sediment. Petrol., 59: 375-386.

Lorens, R.B., 1981. Sr, Cd, Mn and Co distribution coefficients in calcite as a function of calcite precipitation rate. Geochim. Cosmochim. Acta, 45: 553-562.

Loucks, V. and Elmore, R.D., 1986. Absolute dating of dedolomitization and the origin of magnetization in the Cambrian Morgan Creek Limestone, central Texas. Bull. Geol. Soc. Ame., 97: 486-496.

Lovell, J.P.B., 1984. Cenozoic. In: K. Glennie (Editor), Introduction to the petroleum geology of the North Sea. Blackwell Oxford, 151-170.

Lucia, F.J., 1961. Dedolomitization in the Tansill (Permian) Formation. Bull. Geol. Soc. Ame., 72: 1107-1110.

Lumsden, D.N. and Chimahusky, J.S., 1980. Relationship between dolomite nonstochiometry and carbonate facies parameters. In: D. Zenger and J.B. Dunham (Editors), Concepts and models of dolomitization. Soc. Econ. Paleontol. Mineral., Spec. Publ., 28: 123-137.

Machel, H.G., 1985. Cathodoluminescence in calcite and dolomite and its chemical interpretation. Geosci. Canada 12: 139-147.

Machel, H.G., 1986. Early lithification, dolomitization, and anhydritization of Upper Devonian Nisku buildups, subsurface of Alberta, Canada. In: J.H. Schroeder and B.H. Purser (Editors), Reef Diagenesis. Springer-Verlag, Berlin: 336-356.

Machel, H.G., 1987a. Saddle dolomite as a by-product of chemical compaction and thermochemical sulphate reduction. Geology, 15: 936-940.

Machel, H.G., 1987b. Some aspects of diagenetic sulphate-hydrocarbon redox reactions. In: J.D. Marshall (Editor), Diagenesis of Sedimentary Sequences. Geol. Soc. London, Spec. Publ., 36: 15-28.

Machel, H.G., 1988. Fluid flow direction during dolomite formation as deduced from trace-element trends. In: V. Shukla and P.A. Baker (Editors), Sedimentology and geochemistry of dolostones. Soc. Econ. Paleont. Mineral., Spec. Publ., 43: 115-125.

Machel, H.G. and Mountjoy, E.W., 1986. Chemistry and environments of dolomitization - a reappraisal. Earth. Sci. Review, 23: 175-222.

Machel, H.G. and Mountjoy, E.W., 1987. General contraints on extensive pervasive dolomitization - and their application to the Devonian carbonates of western Canada. Bull. Can. Pet. Geol., 35: 143-158.

Magaritz, M., 1987. A new explanation for cyclic deposition in marine evaporite basins: meteoric water input. Chemical Geology, 62: 239-250.

Magaritz, M. and Schulze, K.H., 1980. Carbon isotope anomoly of the Permian period. In: H. Fuchtbauer & T.M. Peryt (Editors), The Zechstein basin with special emphasis on carbonate sequences. Contributions to Sedimentology 9, 269-277.

Magaritz, M. and Kafri, U., 1981. Stable isotope and Sr^{2+} / Ca^{2+} evidence of diagenetic dedolomitization in a schizohaline environment: Cenomanian of northern Israel. Sed. Geol., 28: 29-41.

Magaritz, M., Turner, P. and Kading, K-C., 1981. Carbon isotope change at the base of the Upper Permian Zechstein sequence. Geol. J., 16: 243-254.

Magaritz, M. and Turner, P., 1982. Carbon cycle changes in the Zechstein Sea: isotopic transition zone in the Marl Slate. Nature, 297: 389-390.

Magraw, D., 1975. Permian of the offshore and coastal region of Durham and Northumberland. J. Geol. Soc. London, 131: 397-414.

Magraw, D., 1978. New boreholes into Permian beds off Northumberland and Durham. Proc. Yorks. Geol. Soc., 42: 157-183.

Magraw, D., Clarke, A.M. and Smith, D.B., 1963. The stratigraphy and structure of part of the south-east Durham coalfield. Proc. Yorks. Geol. Soc., 34: 153-208.

Maliva, R.G., 1987. Quartz geodes: Early diagenetic silicified anhydrite nodules related to dolomitization. J. Sediment. Petrol., 57, 1054-1059.

Maliva, R.G., 1989. displacive calcite syntaxial overgrowths in open marine limestones. J. Sed. Petrol., 59: 397-403.

Maliva, R.G. and Siever, R., 1988. Diagenetic replacement controlled by force of crystallization. Geology, 16: 688-691.

Marshall, D.J., 1988. Cathodoluminescence of geological materials. Allen & Unwin, U.S.A.

Marshall, J.D., 1981. Zoned calcites in Jurassic ammonite chambers: trace elements, isotopes and neomorphic origin. Sedimentology, 28: 867-887.

Martin, G.D., Wilkinson, B.H. and Lohmann, K.C., 1986. The role of skeletal porosity in aragonite neomorphism-*Strombus* and *Montastrea* from the Pleistocene Key Largo Limestone, Florida. J. Sediment. Petrol., 56: 194-203.

Mason, R.A., 1987. Ion microprobe analysis of trace elements in calcite with an application to the cathodoluminescence of limestone cements from the Lower Carboniferous of South Wales. Chem. Geol., 64: 209-224.

Mattes, B.W. and Mountjoy, E.W., 1980. Burial dolomitization of the Upper Devonian Miette buildup, Jasper National Park, Alberta. In: D.H. Zenger, J.B. Dunham and R.L. Ethington (Editors), Concepts and models of dolomitization. Soc. Econ. Paleont. Mineral. Spec. Publ., 28: 259-297.

Mazzullo, S.J., 1980. Calcite pseudospar replacive of marine acicular aragonite and implications for aragonite cement diagenesis. J. Sediment. Petrol., 50: 409-422.

McCrea, J.M., 1950. On the isotopic chemistry of carbonates and a paleotemperature scale. J. Chem. Physics, 18: 849-857.

McIlreath, I.A. and James, N.P., 1984. Carbonate slopes. In: R.G. Walker (Editor), Facies Models, second edition: 245-257.

McIntire, W.L., 1963. Trace element partition coefficients-a review of theory and application to geology. Geochim. Cosmochim. Acta, 27: 1209-1264.

McKenzie, J.A., Hsu, K.J. and Schneider, J.F., 1980. Movement of subsurface waters under the sabkha, Abu Dhabi, UAE, and its relation to evaporative dolomite genesis. In: D.H. Zenger, J.B. Dunham and R.L. Ethington (Editors), Concepts and models of dolomitization. Soc. Econ. Paleont. Mineral. Spec. Publ., 28: 11-30.

McKenzie, J.A., 1985. Stable-isotope mapping in Messinian evaporative carboantes of central Sicily. Geology, 13: 851-854.

Meyers, W.J., 1974. Carbonate cement stratigraphy of the Lake Valley Formation, Mississippian, Sacramento Mountains, New Mexico. J. sed. Petrol., 44: 837-861.

Meyers, W.J. and Lohmann, K.C., 1985. Isotope geochemistry of regionally extensive calcite cement zones and marine components inMississippian limestones, New Mexico. Soc. Econ. Palaeontol. Mineral., Spec. Publ., 36. 223-239.

Middleton, G.V and Hampton, M.A., 1976. Subaqueous sediment transport and deposition by sediment gravity flows. In: D.J. Stanley and D.J.P. Swift (Editors), Marine sediment transport and environmental management, Wiley interscience, New York, 197-218.

Miller, J., 1986. Facies relationships and diagenesis in Waulsortian mudmounds from the lower Carboniferous of Ireland and N.England. In: J.H. Schroeder and B.H. Purser (Editors), Reef diagenesis, Springer-Verlag, Berlin, 311-335.

Miller, J., 1988. Cathodoluminescence microscopy. In: M. Tucker (Editor), Techniques in Sedimentology, Blackwell, Oxford, 174-190.

Milliken, K.L., 1979. The silicified evaporite syndrome - two aspects of the silicification history of former evaporite nodules from southern Kentucky and northern Tennessee. J. Sediment. Petrol., 49: 245-256.

Mills, D.A.C. and Hull, J.H., 1976. Geology of the country around Barnard Castle. Mem. Geol. Surv. G.B., Sheet 32.

Mitterer, R.M. and Cunningham, R., 1985. The interaction of organic matter with grain surfaces: Implications for calcium carbonate precipitation. In: N. Schneidermann and P.M. Harris (Editors) Carbonate cements. Soc. Econ. Paleont. Mineral. Spec. Publ., 36: 17-31.

Moorbath, 1962. Lead isotope abundance studies on mineral ocurrences in the British Isles and their geological significance. Phil Trans. R. Soc. London, A254: 295-360.

Moore, C.H., 1989. Carbonate diagenesis and porosity. Developments in Sedimentology 46, Elsevier, Amsterdam, 338pp.

Morrow, D.W., 1982a. Diagenesis I. Dolomite-part I: The chemistry of dolomitization and dolomite precipitation. Geosci. Canada, 9: 5-13.

Morrow, D.W., 1982b. Diagenesis II. Dolomite-part II: Dolomitization models and ancient dolostones. Geosci. Canada, 9: 95-107.

Morrow, D.W. and Mayers, I.R., 1978. Simulation of limestone diagenesis-a model based on strontium depletion. Can. J. Earth Sci., 15: 376-396.

Morrow, D.W. and Ricketts, B.D., 1986. Chemical controls on the precipitation of mineral analogues of dolomite: The sulfate enigma. Geology, 14: 408-410.

Morrow, D.W. and Ricketts, B.D., 1988. Experimental investigation of sulfate inhibition of dolomite and its mineral analogues. In: V. Shukla and P. A. Baker (Editors), Sedimentology and geochemistry of dolostones. Soc. Econ. Paleontol. Mineral., Spec. Publ., 43: 25-38.

Morse, J.W., Millero, F.J., Cornwell, J.C. and Rickerd, D.T., 1987. The chemistry of the hydrogen sulfide and iron sulfide systems in natural waters. Earth Science Reviews, 24: 1-42.

Moses, C.O., Nordstrom, D.K., Herman, J.S. and Mills, A.L., 1987. Aqueous pyrite oxidation by dissolved oxygen and ferric iron. Geochim. Cosmochim. Acta, 51: 1561-1573.

Moshier, S.O., 1989. Microporosity in micritic limestones: a review. Sed. Geol., 63: 191-213.

Mossop, G.D. and Shearman, D.J., 1973. Origins of secondary gypsum. Trans. Instn. Min. Metall., 82: B147-154.

Mucci, A. and Morse, J.W., 1983. The incorporation of Mg^{2+} and Sr^{2+} into calcite overgrowths: influences of growth rate and solution composition. Geochim. Cosmochim. Acta, 47: 217-223.

Mucci, A., Canuel, R. and Zhong, S., 1989. The solubility of calcite and aragonite in sulfate-free seawater and the seeded growth kinetics and composition of the precipitates at 25°C. Chemical Geology, 74: 309-320.

Mullins, H.T., 1983. Modern carbonate slopes and basins of the Bahamas. Platform margin and deeper water carbonates. Spec. Publ. Soc. Econ. Paleont. Mineral. short course 12: 4-1 - 4-138.

Mullins, H.T., Neumann, A.C., Wilber, R.J. and Boardman, M.R., 1980. Nodular carbonate sediment on Bahamian slopes: possible precursors to nodular limestones. J. Sediment. Petrol., 50: 117-131.

Mullins, H.T. and Cook, H.E., 1986. Carbonate apron models: Alternatives to the submarine fan model for paleoenvironmental analysis and hydrocarbon exploration. Sed. Geol., 48: 37-79.

Murray, R.C., 1964. Origin and diagenesis of gypsum and anhydrite. J. Sediment. Petrol., 34: 512-523.

Napier, E., 1948. The lower anhydrite seams of the Tees area. Proc. Yorks. Geol. Soc., 27: 210-216.

Nickless, E.F.P., Booth, S.J. and Mosley, P.N., 1976. The celestite resources of the area north-east of Bristol. I.G.S. Mineral assesment report 25.

Niemann, J.C. and Read, J.F., 1988. Regional cementation from unconformity-recharged aquifer and burial fluids, Mississippian Newman Limestone, Kentucky. J. sediment. Petrol., 58: 688-705.

Nordstrom, D.K., 1982. Aqueous pyrite oxidation and the consequent formation of secondary iron minerals. Acid sulphate weathering, Soil Science Society of America, 37-56.

Pattison, J., 1970. A review of the marine fossils friom the Upper Permian rocks of Northern Ireland and north-west England. Bull. Geol. Surv. G.B., 32: 123-165.

Pattison, J., Smith, D.B. and Warrington, G., 1973. A review of Late Permian and Early Triassic biostratigraphy in the British Isles. In: A. Logan & L.V. Hills (Editors), The Permian and Triassic systems and their mutual boundaries. Canad. Soc. Pet. Geol., Memoir 2.

Paul, J., 1986a. Environmental analysis of the basin and schwellen facies in the lower Zechstein of Germany. In: G.M. Harwood and D.B. Smith (Editors), The English Zechstein and related topics. Spec. Publ. Geol. Soc. London, 22: 143-148.

Paul, J., 1986b. Stratigraphy of the Lower Werra cycle (Z1) in West Germany (preliminary results). In: G.M. Harwood and D.B. Smith (Editors), The English Zechstein and related topics. Spec. Publ. Geol. Soc. London, 22: 149-156.

Peryt, T.M., 1986. Chronostratigraphical and lithostratigraphical correlations of the Zechstein limestone in central Europe. In: G.M. Harwood and D.B. Smith (Editors), The English Zecghstein and related topics. Spec. Publ. Geol. Soc. London, 22: 203-210.

Pettigrew, T., 1985. A review of the Zechstein paleontology in the Durham provine of northeastern England. Prezeglad Geologiczny, 202-204.

Pierre, C. and Rouchy, J.M., 1988. Carbonate replacements after sulphate evaporites in the middle Miocene of Egypt. J. Sediment. Petrol., 58: 446-456.

Pierson, B.J., 1981. The control of cathodoluminescence in dolomite by iron and manganese. Sedimentology, 28: 601-610.

Pingitore, N.E. Jr., 1976. Vadose and phreatic diagenesis: processes, products and their recognition in corals. J. Sediment. Petrol., 46: 985-1006.

Pingitore, N.E. Jr., 1978. the behaviour of Zn^{2+} and Mn^{2+} during carbonate diagenesis: theory and applications. J. sediment. Petrol., 48: 799-814.

Pingitore, N.E. Jr., 1982. The role of diffusion during carbonate diagenesis. J. Sediment. Petrol., 52: 27-39.

Pingitore, N.E. Jr. and Eastman, M.P., 1984. The experimental partitioning of Ba^{2+} into calcite. Chemical Geology, 45: 113-120.

Pingitore, N.E. Jr. and Eastman, M.P., 1986. The coprecipitation of Sr^{2+} with calcite at 25°C and 1 atm. Geochim. Cosmochim. Acta, 50: 2195-2204.

Plummer, L.N., 1975. Mixing of seawater with calcium carbonate groundwater. Geol. Soc. Ame. Mem., 142: 219-236.

Popp, B.N., Anderson, T.A. and Sandberg, P.A., 1986. Brachiopods as indicators of original isotopic compositions in some Paleozoic limestones. Bull. Geol. Soc. Ame., 97: 1262-1269.

Postma, D. and Brockenhuus-Schack, B.S., 1987. Diagenesis of iron in proglacial sand deposits of late and post-Weichselian age. J. Sed. Petrol., 57: 1040-1053.

Prevot, L. and Lucas, J., 1986. Microstructure of apatite-replacing carbonate in synthesised and natural samples. J. Sediment. Petrol., 56: 153-159.

Pryor, W.A., 1971. Petrology of the Permian Yellow Sands of northeastern England, and their North Sea Basin equivalents. Sediment. Geol., 6: 221-254.

Purser, B.H., 1985. Dedolomite porosity and reservoir properties of middle Jurassic carbonates in the Paris basin, France. In: P.O. Roehl and P.W. Choquette (Editors), Carbonate petroleum reservoirs, Springer-Verlag, New York, 343-355.

Qing, H. and Mountjoy, E.W., 1989. Multistage dolomitization in Rainbow buildups, Middle Devonian Key River Formation, Alberta, Canada. J. Sediment. Petrol., 59: 114-126.

Radke, B.M. and Mathis, R.L., 1980. On the formation and occurence of saddle dolomite. J. Sediment. Petrol., 50: 1149-1168.

Raiswell, R., 1982. Pyrite texture, isotopic composition and the availability of iron. Am. J. Sci., 282: 1244-1263.

Raiswell, R., 1986. Non-steady state microbiological diagenesis and the origin of concretions and nodular limestones. In: J.D. Marshall (Editor), Diagenesis of Sedimentary Sequences, Geol. Soc. London, Spec. Publ., 36: 41-54.

Raven, M.J. and Dickson, J.A.D., 1989. Fir-tree zoning: an indicator of pulsed crystallization in calcite cement crystals. Sed. Geol., 65: 249-259.

Raymond, L.R., 1960. The Pre-Permian floor beneath Billingham, County Durham and structures in overlying Permian sediments. Q. J. Geol. Soc. London, 116: 297-315.

Raymond, L.R., 1962. The petrology of the Lower Magnesian Limestone of north-east Yorkshire and south-east Durham. Q. Jl. Geol. Soc. London, 118: 39-64.

Reeder, R.J. and Prosky, J.L., 1986. Compositional sector zoning in dolomite. J. Sediment. Petrol., 56: 237-247.

Reeder, R.J. and Grams, J.C., 1987. Sector zoning in calcite cement crystals:Implications for trace element distributions in carbonates. Geochim. Cosmochim Acta, 51: 187-194.

Ricken, W., 1987. The carbonate compaction law: a new tool. Sedimentology, 34: 517-584.

Ruppel, S.C. and Cander, H.S., 1988. Dolomitization of shallow-water platform carbonates by sea water ans seawater-derived brines: San Andres Formation (Guadalupian), west Texas. In: V. Shukla and P.A. Baker (Editors), Sedimentology and geochemistry of dolostones. Soc. Econ. Paleontol. Mineral., Spec. Publ., 43: 245-262.

Saller, A.H., 1984. Petrologic and geochemical constraints on the origin of subsurface dolomite, Enewetak atoll: An example of dolomitization by normal seawater. Geology, 12: 217-220.

Sandberg, P.A., 1983. An oscillating trend in Phanerozoic non-skeletal carbonate mineralogy. Nature, London, 305: 19-22.

Sandberg, P., 1985. Aragonite cements and their ocurrence in ancient limestines. In: N. Schneidermann and P.M. Harris (Editors), Carbonate Cements. Soc. Econ. Paleont. Mineral., Spec. Publ., 36: 33-57.

Sandberg, P.A. and Hudson, J.D., 1983. Aragonite relic preservation in Jurassic calcite-replaced bivalves. Sedimentology, 30: 879-892.

Sass, E. and Katz, A., 1982. The origin of platform dolomites: New evidence. American J. Sci., 282: 1184-1213.

Sass, E. and Bein, A., 1988. Dolomites and salinity: A comparative geochemical study. In: V. Shukla and P.A. Baker (Editors) Sedimentology and geochemistry of dolostones. Soc. Econ. Paleont Mineral., Spec. Publ., 43: 223-233.

Schofield, K. and Adams, A.E., 1986. Burial dolomitization in the Woo Dale Limestones Formation (Lower Carboniferous), Derbyshire, England. Sedimentology, 33: 207-219.

Scholle, P.A. and Halley, R.B., 1985. Burial diagenesis: Out of sight, out of mind. In: N. Schneiderm and P.M. Harris (Editors), Carbonate cements. Soc. Econ. Paleont. Mineral., Spec. Publ., 36: 334

Searl, A.M., 1989. Pedogenic columnar calcite from the Oolite Group (Lower Carboniferous), South Wales. Sed. Geol., 62: 47-58.

Sears, S.O. and Lucia, F.J., 1980. Dolomitization of northern Michigan Niagara reefs by brine refluxion and freshwater/seawater mixing. In: D.H. Zenger, J.B. Dunham and R.L. Ethington (Editors), Concepts and models of dolomitization. Soc. Econ. Paleont. Mineral. Spec. Publ., 28: 215-235.

Sedgwick, A., 1835. On the geological relations and internal structure of the Magnesian Limestone, and the lower portions of the New Red Sandstone series in their range from Nottinghamshire, Derbyshire, Yorkshire and Durham, to the southern extremity of Northumberland. Trans. Geol. Soc. London, 3: 37-124.

Shatkay, M. and Magaritz, M., 1987. Dolomitization and sulphate reduction in the mixing zone between brine and meteoric water in the newly exposed shores of the Dead Sea. Geochim. Cosmochim. Acta, 51: 1135-1141.

Shearman, D.J., 1971. Discussion. Trans. Inst. Min. Metall., 80: B50-52.

Shearman, D.J., Khouri, J. and Taha, S., 1961. On the replacement of dolomite by calcite in some Mesozoic limestones from the French Jura. Proc. Geol. Ass., 75: 1-12.

Shearman, D.J. and Fuller, J.G., 1969. Anhydrite diagenesis, calcitization, and organic laminites, Winnipegosis Formation, middle Devonian, Saskatchewan. Can. Pet. Geol. Bull., 17: 496-525.

Shearman, D.J., Mossop, G., Dunsmore, H. and Martin, M., 1972. Origin of gypsum veins by hydraulic fracture. Trans. Instn. Min. Metall., 81: B149-B155.

Sherlock, R.L., 1911. The relationship of the Permian to the Trias in Nottingham. Q. J. Geol. Soc. London, 67: 75-119.

Shukla, V., 1986. Epigenetic dolomitization and the origin of xenotopic dolomite texture - discussion. J. Sediment. Petrol., 56: 733-736.

Sibley, D.F., 1982. The origin of common dolomite fabrics: clues from the Pliocene. J. Sediment. Petrol., 52: 1087-1100.

Sibley, D.F., Dedoes, R.E. and Bartlett, T.R., 1987. Kinetics of dolomitization. Geology, 15: 1112-1114.

Sibley, D.F. and Gregg, J.M., 1987. Classification of dolomite rock textures. J. Sediment. Petrol., 57: 967-975.

Siebert, R.M., Moncure, G.K. and Lahann, R.W., 1984. A theory of framework grain dissolution in sandstones. In: D.A. McDonald and R.C. Surdam (Editors), Clastic diagenesis, Memoir, Am. Assoc. Pet. Geol., 37: 163-175.

Simms, M., 1984. Dolomitization by groundwater-flow systems in carbonate platforms. Trans. Gulf Coasts Association of Geological Societies, 34: 411-420.

Smith, D.B., 1968. The Hampole beds - a significant marker in the Lower Magnesian Limestone of Yorkshire, Derbyshire and Nottinghamshire. Proc. Yorks. Geol. Soc., 36: 463-477.

Smith, D.B., 1970a. Permian and Trias. In: G.A. Hickling (Editor) The geology of Durham county. Trans. Nat. Hist. Soc. Northumberland, 41: 66-91.

Smith, D.B., 1970b. Submarine slumping and sliding in the Lower Magnesian Limestone of Northumberland and Durham. Proc. Yorks. Geol. Soc., 38: 1-36.

Smith, D.B., 1970c. The palaegeography of the English Zechstein. In: L.J. Rau, and L. Dellwig, (Editors), Third Symposium on Salt, Clevelang Geological Society, 1: 20-23.

Smith, D.B., 1971. The stratigraphy of the Upper Magnesian Limestone in Durham - a revision based on the Institute's Seaham Borehole. Report no. 71/3, Inst. Geol. Sci., 12pp.

Smith, D.B., 1972. Foundered strata, collapse-breccias and subsidence features of the English Zechstein. In: G. Richter-Bernburg (Editor) Geology of saline deposits. Proc. Hannover Symp. Unesco, Paris, 255-269.

Smith, D.B., 1979. Rapid marine transgressions and regressions of the Upper Permian Zechstein sea. J. Geol. Soc. London, 136: 155-156.

Smith, D.B., 1980a. Permian and Triassic rocks. In: D.A. Robson (Editor), The geology of north-east England, Nat. Hist. Soc. Northumberland, 36-48.

Smith, D.B., 1980b. The evolution of the English Zechstein basin. In: H. Fuchtbauer and T. Peryt (Editors) the Zechstein basin with emphasis on carbonate sequences. Contributions to sedimentology 9: 7-34.

Smith, D.B., 1981. The Magnesian Limestone (Upper Permian) reef complex of northeast England. Soc. Econ. Palaeontol. Mineral., Spec. Publ., 39: 161-186.

Smith, D.B., 1984. Red basal Permian sands; a new discovery in N.C.B. boreholes off Sunderland, northeast England. Proc. Yorks. Geol. Soc., 44: 497-500.

Smith, D.B., 1985. The evolution of the English Zechstein basin - a summary. Przeglad Geologiczny: 199-202.

Smith, D.B., 1986. The Trow Point Bed - a deposit of Upper Permian marine oncoids, peloids, and columnar stromatolites in the Zechstein of north-east England. In: G.M. Harwood & D.B. Smith (Editors), The English Zechstein and related topics, Geol. Soc. London Spec. Publ., 22: 113-125.

Smith, D.B., 1990. The late Permian palaeogeography of north-east England. Proc. Yorks. Geol. Soc. (in press).

Smith, D.B. (in press). Permo-Triassic strata in Tee-side. Proc. Yorks. Geol. Soc.

Smith, D.B. and Francis, E.A. 1967. Geology of the country between Durham and West Hartlepool. Mem. Geol. Surv. H.M.S.O. London, 354pp.

Smith, D.B. and Moore, P.J., 1973. Deposits of gypsum at Hurworth Place, Darlington. Report Inst. Geol. Sci., 73/16.

Smith, D.B., Brundstrom, R.G.W., Manning, P.I., Simpson, S and Shotton, F.W., 1974. A correlation of Permian rocks in the British Isles. Spec. Rep. Geol. Soc. London, 5: 45pp.

Smith, D.B., Harwood, G.M., Pattison, J. and Pettigrew, T.H., 1986. A revised nomenclature for Upper Permian strata in eastern England. In: G.M. Harwood and D.B. Smith (Editors), The English Zechstein and related topics. Geol. Soc. Lond., Spec. Publ., 22: 9-17.

Smith, D.B. and Taylor, J.C.M., 1990. A 'North-west Passage' to the southern Zechstein basin of the UK North Sea. Proc. Yorks Geol. Soc. (in press).

Sneh, A., 1988. Permian dune patterns in northwestern Europe challenged. J. Sediment. Petrol., 58: 44-51.

Solomon, M., Rafter, T.A. and Dunham, K.C., 1971. Sulphur and oxygen isotope studies in the northern Pennines in relation to ore genesis. Trans. Instn Min. Metall. (Sect. B: Appl. Earth Sci.), 80: B259-75.

Sonnenfeld, P., 1984. Brines and evaporites. Academic Press, Orlando, Fla., 613pp.

Sperber, C.M., Wilkinson, B.H. and Peacor, D.R., 1984. Rock composition, dolomite stoichiometry, and rock - water reactions in dolomitic carbonate rocks. J. Geol., 92: 609-622.

Spirakis, C.S. and Heyl, A.V., 1988. Possible effects of thermal degredation of organic matter on carbonate paragenesis and fluorite precipitation in Mississippi valley-type deposits. Geology, 16: 1117-1120.

Steele, R.P., 1981. Aeolian sands and sandstones. Ph.D. Thesis, University of Durham, Durham (unpublished).

Stemmerik, L., Frykman, P. and Stentoft, N., 1986. Depositional environment, diagenesis and stratigraphy of Zechstein carbonates. Geol. Survey Denmark, Internal report 23, 67pp.

Stewart, F.H., 1949. The petrology of the evaporites of the Eskdale no. 2 boring, east Yorkshire. Part I. The lower evaporite bed. Min. Mag., 28: 621-675.

Stewart, F.H., 1965. The mineralogy of the British Permian evaporites. Min. Mag., 34: 460-470.

Stoessell, R.K., Klimentidis, R.E. and Prezbinidowski, D.R., 1987. Dedolomitization in Na-Ca-Cl brines from 100° to 200°C at 300 bars. Geochim. Cosmochim Acta, 51: 187-194.

Stow, D.A.V., 1986. Deep clastic seas. In: H.G. Reading (Editor), Sedimentary Environments and facies, Blackwell, 339-444.

Surdam, R.C., Boese, S.W. and Crossey, L.J., 1984. The chemistry of secondary porosity. In: D.A. McDonald and R.C. Surdam (Editors), Clastic diagenesis, Memoir Am. Assoc. Pet. Geol., 37: 127-150.

Surlyk, F., Hurst, J.M., Piasecki, S., Rolle, F., Scholle, P.A., Stemmerik. and Thomsen, E., 1986. The Permian of the western margin of the Greenland Sea-A future exploration target. In: M.T. Halbouty (Editor), Future petroleum provinces of the world. Am. Assoc. Pet. Geol. Mem., 40: 629-659.

Sweeney, M., Turner, P. and Vaughan, D.J., 1987. The Marl Slate: a model for the precipitation of calcite, dolomite, and sulphides in a newly-formed anoxic sea. Sedimentology, 34: 31-48.

Swennen, R., Viaene, W., Jacobs, L. and Van Orsmael, J., 1981. Ocurrence of calcite pseudomorphs after gypsum in the Lower Carboniferous of the Vesder region (Belgium). Bull. Soc. Belge de Geol., 90: 231-247.

Swift, A., 1986. The conodont *Merrillina divergens* (Bender & Stoppel) from the upper Permian of England. In: G.M. Harwood and D.B. Smith (Editors), The English Zechstein and related topics. Geol. Soc. London, Spec. Publ., 22: 55-62.

Takano, B., 1985. Geochemical implications of sulfate in sedimentary carbonates. Chem. Geol., 29: 393-403.

Tarr, W.A., 1933. Origin of the concretionary structures of the Magnesian Limestone at Sunderland, England. J. Geol., 41: 268-287.

Taylor, J.C.M., 1980. Origin of the Werraanhydrit in the southern North Sea - a reappraisal. In: H. Fuchtbauer and T.M. Peryt (Editors), The Zechstein Basin with emphasis on carbonate sequences. Contributions to sedimentology 9: 91-113.

Taylor, J.C.M., 1984. Late Permain - Zechstein. In: K.W. Glennie (Editor), Introduction to the petroleum geology of the North Sea. Blackwell, Oxford: 61-83.

Taylor, J.C.M. and Colter, V.S., 1975. Zechstein of the British sector of the southern North Sea Basin. In: A.W. Woodland (Editor), Petroleum Geology of the continental shelf of North-West Europe, 2Vol. 1, (Applied science publishers).

Theriault, F. and Hutcheon, I., 1987. Dolomitization and calcitization of the Devonian Grosmont Formation, northern Alberta. J. Sediment. Petrol., 57: 955-966.

Trechmann, C.T., 1913. On a mass of anhydrite in the Magnesian Limestone at Hartlepool and on the Permian of south-eastern Durham. Q. J. Geol. Soc. London, 69: 184-218.

Trechmann, C.T., 1914. On the lithology and composition of Durham Magnesian Limestones. Q.J. Geol. Soc. London, 70: 232-265.

Trechmann, C.T., 1921. Some remarkably preserved brachiopods from the Lower Magnesian Limestone of Durham. Geol. Mag., 58: 538-543.

Trechmann, C.T., 1925. The Permian Formation in Durham. Proc. Geol. Assoc., 36: 135-145.

Trechmann, C.T., 1931. The Permian. In: Contributions to the geology of Northumberland and Durham. Proc. Geol. Assoc., 42: 246-252.

Trechmann, C.T., 1941. Borings in the Permian and Coal Measures around Hartlepool. Proc. Yorks. Geol. Soc., 24: 313-327.

Trechmann, C.T., 1954. Thrusting and other movements in the Durham Permian. Geol. Mag., 91: 193-208.

Trotter, F.M., 1944. the age of the ore deposits of the Lake District and the Alston Block. Geol. Mag., 81: 223-229.

Trudinger, P.A., Chambers, L.A. and Smith, J.W., 1985. Low-temperature sulphate reduction: biological versus abiological. Can. J. Earth Sci., 22: 1910-1918.

Tucker, M.E., 1976. Quartz replaced anhydrite nodules ('Bristol diamonds') from the Triassic of the Bristol district. Geol. Mag., 113: 569-574.

Tucker, M.E., 1986. Formerly aragonitic limestones associated with tillites in the Late Proterozoic of Death Valley, California. J. sediment. Petrol., 56: 818-830.

Tucker, M.E. and Hollingworth, N.T.J., 1986. The upper Permian reef complex (EZ1) of North East England: Diagenesis in a marine to evaporitic setting. In: J.H. Schroeder and B.H.Purser (Editors), Reef diagenesis. Springer-Verlag Berlin, pp. 270-290.

Turner, P., Vaughan, D.J. and Whitehouse, K.I., 1978. Dolomitization and mineralization of the Marl Slate (N.E. England). Mineral Deposita, 13: 245-258.

Turner, P. and Magaritz, M., 1986. Chemical and isotopic studies of a core of Marl Slate from N.E. England: influence of freshwater influx into the Zechstein Sea. In: G.M. Harwood, and D.B. Smith (Editors), The English Zechstein and related topics. Geol. Soc. London Spec. Publ. 22: 19-29.

Van Eysinga, F.W.B., 1978. Geological time table. Elsevier, Amsterdam.

Van Straaten, L.M.J.U., 1978. Dendrites. Q. J. Geol. Soc. London, 135: 137-151

Vaughan, D.J. and Turner, P. 1980. Diagenesis, magnetization and mineralization of the Marl Slate. In: H. Fuchtbauer and T.M. Peryt (Editors), The Zechstein basin with emphasis on carbonate sequences. Contributions to Sedimentology 9: 73-90.

Veizer, J., 1977. Diagenesis of pre-Quaternary carbonates as indicated by tracer studies. J. Sediment. Petrol., 47: 565-581.

Veizer, J., 1978. Simulation of limestone diagenesis-a model based on strontium depletion: discussion. Can. J. Earth Sci., 15: 1683-1685.

Veizer, J., 1983a. Chemical diagenesis of carbonates: Theory and application of trace element technique. In: Stable isotopes in sedimentary geology. Soc. Econ. Paleont. Mineral., Short Course 10: 3-1 - 3-100.

Veizer, J., 1983b. Trace elements and isotopes in sedimentary carbonates. In: R.J. Reeder (Editor), Carbonates: mineralogy and chemistry, Reviews in Mineralogy 11: 265-299.

Veizer, J. and Hoefs, J., 1976. The nature of O^{18}/O^{16} and C^{13}/C^{12} secular trends in sedimentary carbonate rocks. Geochim. Cosmochim. Acta, 40: 1387-1395.

Veizer, J., Fritz. and Jones, B., 1986. Geochemistry of brachiopods: oxygen and carbon isotopic records of Paleozoic oceans. Geochim. Cosmochim. Acta, 50: 1679-1696.

Walker, J.G.C. and Lohmann, K.C., 1989. Why the oxygen isotopic composition of sea water changes with time. Geophys. Res. Lett., 16: 323-326.

Wanless, H.R., 1979. Limestone response to stress: Pressure solution and dolomitization. J. Sediment. Petrol., 49: 437-462.

Welton, J.E., 1984. SEM petrology atlas. Am. Assoc. Pet. Geol., Methods in exploration series.

West, I.M., 1964. Evaporite diagenesis in the lower Purbek beds of Dorset. Prôc. Yorks. Geol. Soc., 34: 315-330.

Westoll, T.S., 1943. Mineralization of Permian Rocks of South Durham. Geol. Mag., 80: 119-120.

White, A.F., 1978. Sodium co-precipitation in calcite and dolomite. Chemical Geology, 26: 65-72.

Wiggins, W.D., 1986. Geochemical signatures in carbonate matrix and their relation to deposition a diagenesis, Pennsylvanian Marble Falls Limestone, central Texas. J. Sediment. Petrol., 56: 7 783.

Winch, N.J., 1817. Observations on the geology of Northumberland and Durham. Trans. Geol. Soc London, 4: 1-101.

Wolfe, M.J., 1970. Dolomitization and dedolomitization in the Senonian chalk of Northern Ireland. Geol. Mag., 107: 39-50.

Wong, P.K. and Oldershaw, A., 1981. Burial cementation in the Devonian, Kaybob Reef complex, Alberta, Canada. J. Sediment. Petrol., 51: 507-520.

Wood, F.W., 1950. Recent information concerning the evaporites and the pre-Permian floor of S.E. Durham. Q. J. Geol. Soc. London, 419: 327-346.

Wood, W.W., 1985. Origin of caves and other solution openings an the unsaturated (vadose) zone of carbonate rocks: A model for CO_2 generation. Geology, 13: 822-824.

Woolacott, D., 1903. An explanation of the Claxheugh section, Co. Durham. Trans. Nat. Hist. Soc. Northumberland, 14: 211-221.

Woolacott, D., 1905. The Landslip at Claxheugh, Co. Durham. Trans. nat. Hist. Soc. Northumberland, 15?: 434-436.

Woolacott, D., 1909. A case of thrust and crush brecciation in the Magnesian Limestone of County Durham. Proc. Univ. Durham Phil. Soc., Mem. 1.

Woolacott, D., 1912. The stratigraphy and tectonics of the Permian of Durham (northern area). Proc. Univ. Durham Phil. Soc., 4: 241-331.

Woolacott, D., 1914. On sections in the Lower Perman rocks at Claxheugh and Down Hill, Co. Durham. Trans. nat. Hist. Soc. Northumberland, 5: 155-162.

Woolacott, D., 1919a. On borings at Cotefield Close and Sheraton, Co. Durham (Permian and Coal Measures). Geol. Mag., 6: 163-170.

Woolacott, D., 1919b. The Magnesian Limestone of Durham. Geol. Mag., 6: 452-465, 485-498.

Yardley, M.J., 1984. Cross-bedding in the Permian Yellow Sands of County Durham. Proc. Yorks. Geol. Soc., 45: 11-18.

Zenger, D.H., 1973. Syntaxial calcite borders on dolomite crystals, Little Falls Formation (Upper Cambrian), New York. J. Sediment. Petrol., 43: 118-124.

Zenger, D.H. and Dunham, J.B., 1988. Dolomitization of Siluro-Devonian limestones in a deep core (5,350m), southeastern New Mexico. In: V. Shukla and P.A. Baker (Editors), Sedimentology and Geochemistry of Dolostones. Soc. Econ. Paleont. Mineral., Spec. Publ., 43: 161-173.

Ziegler, P.A., 1982. Geological atlas of Western and Central Europe. Elsevier, Amsterdam: 130pp.

Appendix I

Cathodoluminescence

A1.1.1. Cathodoluminescence microscopy - Introduction.

Much of the petrographic work in this thesis involves analysis of calcite and dolomite via cathodoluminescence (CL or luminescence) microscopy. The basis of cathodoluminescence is that individual calcite and dolomite crystals (and distinct areas within those crystals) may have different luminescence characteristics, which are directly related to their trace element composition. Thus, luminescence allows the observer to 'see' geochemical variations within crystals.

A1.1.2. Cathodoluminescence nomenclature.

Standard nomenclature for the reporting of luminescence is followed in this thesis. Luminescence intensity may be classified as bright-, dull-, or non-luminescent, with further possible subdivision of bright and dull-luminescence within any one crystal. Descriptions are thus qualitative, and comparison of luminescence intensity between samples will not be exact. Problems with the subjective description of luminescence intensities and colours are discussed by Miller (1988). Hemming *et al.*, (1989) describe a generally, although not very good agreement between visual description of luminescence intensities and absolute measurements by a spectrophotometer. Calcite and dolomite crystals in cathodoluminescence are commonly composed of one or more concentric zones, whose contacts are normally parallel to each other and which define crystal growth faces. Distinction between concentric zones is on the basis of luminescence intensity. A concentric zone may show internally homogeneous luminescence, or contain two or more narrower concentric subzones. The distinction between a number of narrow concentric zones and a number of wide concentric subzones within one large zone, is made on the basis of size, although the division between a wide subzone and narrow zone is not precise. The contact of zones or subzones with each other may be abrupt, gradational, or irregular. Where irregular the contact is defined by fracturing or corrosion. Numerous calcites in the Raisby Formation also display sector zones, which cross cut concentric zones. These do not define crystal growth faces, and are not internally subzoned. Contact of sector zones with the host calcite are always sharp. Sector zoning is described in appendix II.

A1.1.3. Luminescence in non-carbonate minerals.

Minerals besides calcite and dolomite have been recorded to luminesce in Raisby Formation samples. Most notable are some quartz and fluorite crystals which luminesce bright to dull blue, and barite which luminesces dull blue initially, but that quickly fades within a few seconds of initial observation (Lee and Harwood, 1989). Small, bright green-

luminescing minerals which have been recorded within quartz - rich dolostones and limestones of the Raisby Formation may be sphene.

A1.1.4. Cathodoluminescence operating conditions.

All cathodoluminescence work was conducted on a Technosyn 8200 luminoscope, mounted on a Nikon Labophot microscope. Operating conditions were optimised with a vacuum of 0.05 to 0.065 torr, and an accelerating voltage of 130-190na. Most observation and photography was via a X5 objective. All photography used an Olympus OM-4 camera mounted on the Nikon microscope. Exposure was automatic, and between 20 and 50 seconds depending on the luminescence intensity of the specimen. Luminescence colours were best appreciated with Fuji HR ASA 200 35mm film. Kodak film was found to be inferior for cathodoluminescence work. Subtle textures and structures of crystals in luminescence were bought out considerably better by using black and white Ilford XP-1 ASA 400 35 mm film. Brown discolouration of the viewing port was a significant hindrance to cathodoluminescence work, especially after samples with a lot of exposed mounting medium had been analysed and so it was necessary to clean the viewing port regularly.

Most cathodoluminescence observation was on standard petrographic polished thin sections. Some polished rock chips were used where specific cement phases could be easily isolated.

A1.2.1. Cathodoluminescence activation - Review

Cathodoluminescence is the emission of light produced by the bombardment of a phosphor by electrons. Mn^{2+} is believed to be the main phosphor which produces luminescence in calcite and dolomite. The incident electrons excite an atom or molecule, causing it to jump into a higher energy state. It stays at that level for approximately 10^{-8} seconds and then returns to its former energy level (ground state), emitting visible light (photons) and radiation at other wavelengths (Miller, 1988). Thus, luminescence will only occur in impure crystalline substances where 'foreign' ions (usually divalent) have substituted for calcium and/or magnesium within the crystal lattice. Other less important causes of luminescence include distorted crystal surfaces and cracks, distorted internal structures of crystals, impurities in surface and lattice sites, and charge displacements due to abnormally ionized or sized atoms and/or separated cation/anion pairs (Machel, 1985; Marshall, 1988). Pure carbonates have a dark blue intrinsic luminescence (Amieux, 1982). Apart from activating luminescence, some trace elements may also aid (sensitize) or inhibit (quench) luminescence. Although activators (i.e., Mn^{2+}) promote luminescence, luminescence intensity may decrease above a threshold activator concentration (concentration quenching). Sensitizers promote the luminescence of activators, although cannot induce luminescence by themselves. Quenchers absorb excitation energy by

undergoing energy transitions without emitting radiation (charge transfer adsorption [Fairchild, 1983]). They may lower or completely extinguish luminescence intensity.

The trace elements which control luminescence in carbonates are the source of considerable discussion, and the problem is far from resolved. However, it is generally agreed however that Mn^{2+} is the main activator and Fe^{2+} the main quencher of cathodoluminescence in both calcite and dolomite. These and other possible activators, sensitizers and quenchers are tabulated below:

Calcite

(After Amieux, 1982; Machel, 1985; Marshall, 1988; Hemming *et al.*, 1989).

(Trace elements are not tabulated in any order of importance. REE denotes rare earth elements)

Activators

Mn^{2+}, Pb^{2+}, Cu^{2+}, Zn^{2+}, Ag^{+}, REE (Bi^{2+}, Dy^{3+}, Sm^{3+}, Eu^{3+}, Tb^{3+}) Mg^{2+} (?).

Sensitizers

Pb^{2+}, Ce^{2+}, Ce^{4+}, Tl , REE.

Quenchers

Fe^{2+}, Ni^{2+}, Co^{2+}.

Dolomite

(After Amieux, 1982; Pierson, 1981; Fairchild, 1983; Machel, 1985 and Marshall, 1988).

Activators

Mn^{2+}, Zn^{2+}, REE, Pb^{2+}, Cu^{2+}, Ag^{+}, Bi^{+}.

Sensitizers

Pb^{2+}, Ce^{2+}, Ce^{4+}.

Quenchers

Fe^{2+}, Fe^{3+}, Co^{2+}, Ni^{2+}.

In routine analyses of carbonates by microprobe, in general only the concentrations of Fe, Mg, and Mn can be determined, as most other elements tabulated above are below detection limits. An important goal of many cathodoluminescence studies has to be to determine the concentrations of Mn^{2+} and Fe^{2+} which are necessary to activate and quench luminescence respectively and so allow an approximate quantification of the geochemistry of a particular carbonate mineral without analysing it. The quoted limits for activation and quenching of calcite and for dolomite are tabulated below. Where not quoted so, all published data has been converted to mole% carbonate to allow comparison with the data presented within this thesis (Fig. A1.1).

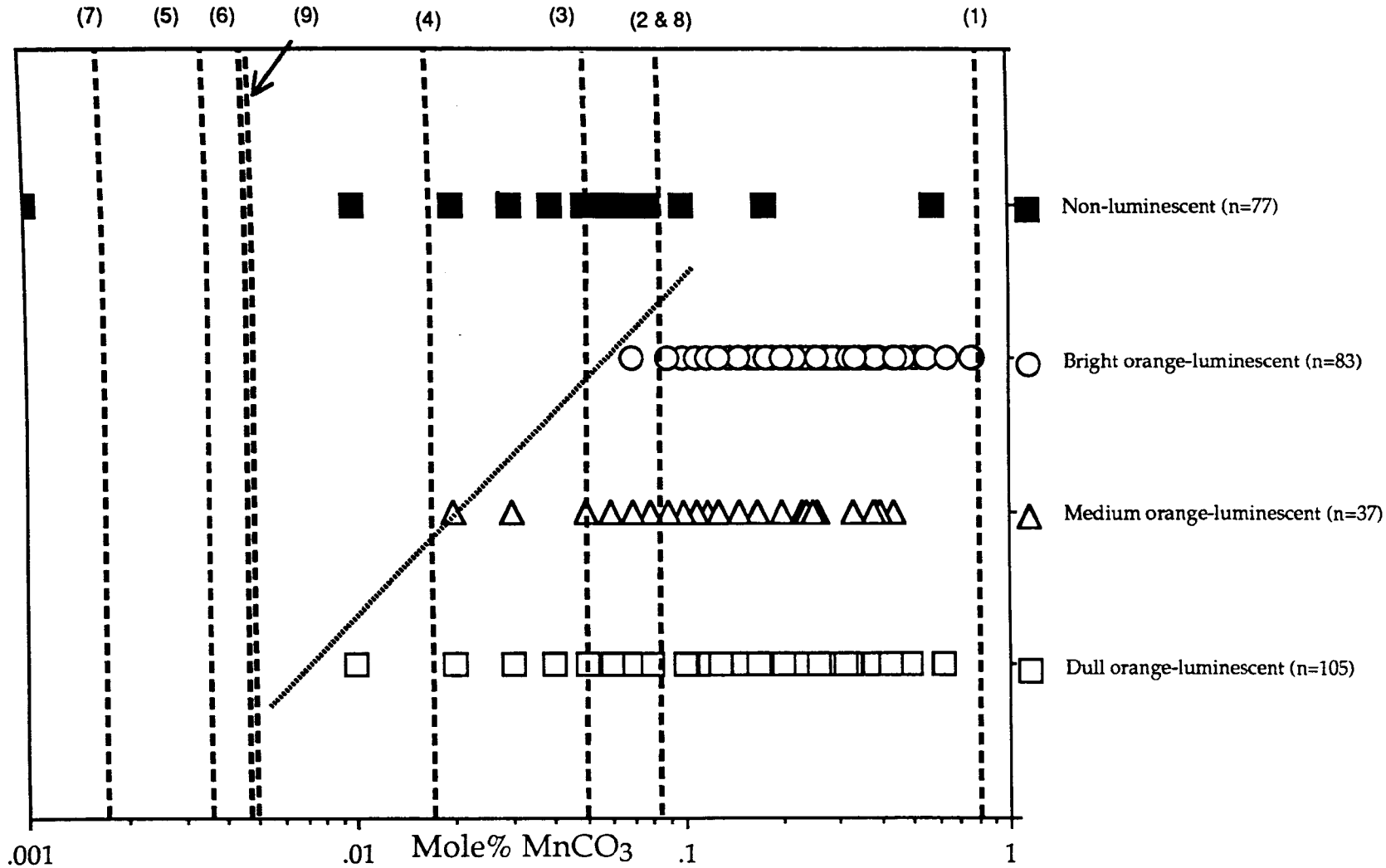

Fig. A1.1. The Mn content of Raisby Formation cements of different luminescence character, plotted against published lower limits for Mn-activated luminescence in calcites. Numbers in brackets refer to the relevant publications in chronological order (listed in the text).

Calcite

Mn^{2+} concentration necessary for activation

1. Greater than 0.182 mole% $MnCO_3$	(Meyers, 1974).
2. Greater than 0.0182 mole% $MnCO_3$	(Pierson, 1981).
3. Greater than 0.05 mole% $MnCO_3$	(Frank *et al.*, 1982).
4. Greater than 0.0174 to 0.0522 mole% $MnCO_3$	(Fairchild, 1983).
5. Greater than 0.0036 to 0.0073 mole% $MnCO_3$	(Machel, 1985).
6. Greater than 0.0046-0.0137 mole% $MnCO_3$	(Mason, 1987).
7. Greater than 0.0018 to 0.0091 mole% $MnCO_3$	(Marshall, 1988).
8. Greater than 0.0182 mole% $MnCO_3$	(Barnaby and Rimstidt, 1989).
9. Greater than 0.0055 to 0.0091 mole% $MnCO_3$	(Hemming *et al.*, 1989).

(Most of these results are in low-Fe calcites).

Mn^{2+} concentration necessary for self-quenching

1. Greater than 17 mole% $MnCO_3$	(Machel, 1985).
2. Between 1.82 and 87 mole% $MnCO_3$	(Mason, 1987).

Fe^{2+} concentration necessary for onset of extinction

1. 0.04 mole% $FeCO_3$	(Machel, 1985).

Fe^{2+} concentration necessary for total extinction

1. Greater than 1.29 mole% $FeCO_3$	(Pierson, 1981).
2. No critical value	(Frank *et al.*, 1982).
3. Greater than 2.01 mole% $FeCO_3$	(Meyers, in Machel, 1985).
4. Greater than 1.27 mole% $FeCO_3$	(Mason, 1987).
5. Greater than 1.82 mole% $FeCO_3$	(Hemming *et al.*,1989).

Dolomite

Mn^{2+} concentration necessary for activation

1. Greater than 0.0146 mole% $MnCO_3$	(Pierson, 1981).
2. 0.007 mole% $MnCO_3$	(Richter and Zinkernagel, 1982, In: Fairchild, 1983).
3. 0.0131 to 0.0261 mole% $MnCO_3$	(Fairchild, 1983).
4. Greater than 0.0036 to 0.0073 mole% $MnCO_3$	(Machel, 1985).
5. Greater than 0.01 mole% $MnCO_3$	(Marshall, 1988).

Mn^{2+} concentration necessary for self-quenching

1. Greater than 17 mole% $MnCO_3$	(Machel, 1985).

Fe^{2+} concentration necessary for onset of quenching

1. Greater than 0.86mole% $FeCO_3$	(Pierson, 1981).
2. 1.73 to 2.59 mole% $FeCO_3$	(Fairchild, 1983).
3. 0.04 mole% $FeCO_3$	(Machel, 1985).

Fe^{2+} concentration necessary for total extinction.

1. Greater than 1.29 mole% $FeCO_3$ (Pierson, 1981).
2. Greater than 3 mole% $FeCO_3$ (Machel, 1985).

Some authors consider that calcites and dolomites will have different controlling limits by trace elements on their luminescence and so must be treated separately (Fairchild, 1983) whereas others consider that both calcite and dolomite have broadly similar controls on their luminescence by trace elements (Machel, 1985).

Despite the work which has been done on determining absolute limits of luminescence intensity control by trace elements, it is now clear that there are no absolute limits of Mn and Fe for every calcite and every dolomite, probably due to the interaction of variable amounts of numerous other activator, quencher and sensitizer trace elements. There are problems also with variable precisions and detection limits of microprobes used, and variable efficiency of the cathodoluminescence units used in the studies. The most recent work on the relationship between luminescence intensity and trace element composition (Hemming *et al.*, 1989) which used a spectrophotometer for absolute intensity measurements, suggests that the luminescence intensity of calcite cements from the Mississippian Lake Valley Formation of New Mexico is controlled both by the Fe^{2+}/Mn^{2+} ratio of the cements and their absolute Fe^{2+} and Mn^{2+} concentrations. In this model, the maximum luminescence intensity is controlled by the (Fe^{2+}/Mn^{2+}) ratio, but below the maximum intensity at a constant (Fe^{2+}/Mn^{2+}) ratio, luminescence intensity is controlled by the absolute Fe^{2+} and Mn^{2+} concentrations of the calcites. At a constant (Fe^{2+}/Mn^{2+}) ratio, luminescence intensity correlates well to Mn^{2+} concentration. Control of calcite luminescence intensity by the Fe^{2+}/Mn^{2+} ratio has previously been described by Frank *et al.*, 1982; Machel, 1985; Mason, 1987 and Barnaby and Rimstidt (1989) and for dolomites by Frank, 1981 and Machel (1985). Frank *et al.*, (1982) calculated that calcites from the Cambrian Taum Sauk limestone, Missouri with a (Fe^{2+}/Mn^{2+}) less than 1 will luminesce brightly whereas those with a (Fe^{2+}/Mn^{2+}) of greater than 1 will have a dull luminescence intensity. Similar conclusions were reached by Barnaby and Rimstidt, (1989). Hemming *et al.*, (1989) agree with the lower intensity limit of Frank *et al.*, (1982), but suggest that calcites have a dull orange luminescence where their (Fe^{2+}/Mn^{2+}) ratio is greater than 2.

The controls on luminescence intensity for dolomite by (Fe^{2+}/Mn^{2+}) ratios appear similar to calcites, with a dolomite having a (Fe^{2+}/Mn^{2+}) ratio of less than 1.5 luminescing brightly whereas one with a (Fe^{2+}/Mn^{2+}) ratio of greater than 7.5 not luminescing (Frank, 1981). Luminescence in dolomites may however be complicated by Mn valency states and Ca or Mg substitution sites for the relevant trace elements (Pierson, 1981; Fairchild, 1983; Machel, 1985). Dolomite luminescence is in general duller than that of calcite due to the generally greater concentrations of Fe^{2+} in dolomite than calcite (Machel, 1985). The peak of

dolomite luminescence is nearer the red end of the visible spectrum (597-690nm) than that of calcite (578-605nm) (Marshall, 1988).

A1.2.2. Cathodoluminescence activation in Raisby Formation calcites

All microprobe analyses of Fe and Mn concentrations from calcite cements within cavities after sulphates from the Raisby Formation were plotted against relative luminescence intensity, in order to determine the controls on luminescence (Figs. A1.2 & A1.3). Only analyses of cements whose luminescence intensity could be determined with a reasonable degree of certainty were plotted. The four intensity divisions - bright orange-, medium orange-, dull orange- and non-luminescent have been defined visually, with no absolute scale or calibration, and so considerable overlap is anticipated.

The Mn concentrations for all four luminescence groups are illustrated in fig. A1.1, along with proposed minimum Mn concentrations for Mn-activated luminescence quoted in previous studies (numbers refer to the previous works listed in the text in chronological order). Where two possible lower limits were quoted (i.e., Fairchild, 1983) only the lower one of the two has been plotted. The dull orange-luminescent calcites from the Raisby Formation in general correlate well with lower limits of Mn-activation quoted in recent publications, although the lower limits for Mn-activated dull orange luminescence are below calculated microprobe detection limits (Appendix V). The lower limits for Mn-activated luminescence will in turn depend on the concentration of Fe, and sensitizer ions within these calcites and the relative efficiency of the cathodoluminescence unit used for this study. These data suggest agreement with the lower limit for Mn-activated luminescence quoted by Fairchild (1983) of 0.174 mole% $MnCO_3$.

The area between 0.02 and 0.08 mole% $MnCO_3$, where appreciable overlap exists between dull and medium orange-luminescent calcites with non-luminescent calcites (Fig. A1.1), most likely represents the lower range of Mn concentrations whereby the presence of appreciable Fe can completely quench Mn-activated luminescence. Thus, a Raisby Formation calcite will luminesce if it has greater than 0.08 mole% $MnCO_3$ regardless of Fe concentration (up to the maximum of 1.2 mole% $FeCO_3$ recorded during this study).

The oblique dotted line on fig. A1.1 represents the variable lower limits of activation for calcites of different luminescence intensities. It clearly illustrates that the brighter the luminescence intensity, the greater the concentration of Mn which is required to produce that intensity. Thus, although a calcite can luminesce dully with 0.02 mole% $MnCO_3$ it will not have bright orange-luminescence with less than 0.08 mole% $MnCO_3$. These results are in accordance with most published works on luminescence activation in calcites.

Nearly all non-luminescent calcites plot in an area of less than 0.1 mole% Fe and $MnCO_3$ (Fig. A1.2a). Outliers at higher values most likely represent contamination by luminescent calcite cement, internally sedimented dolomite and/or internally sedimented

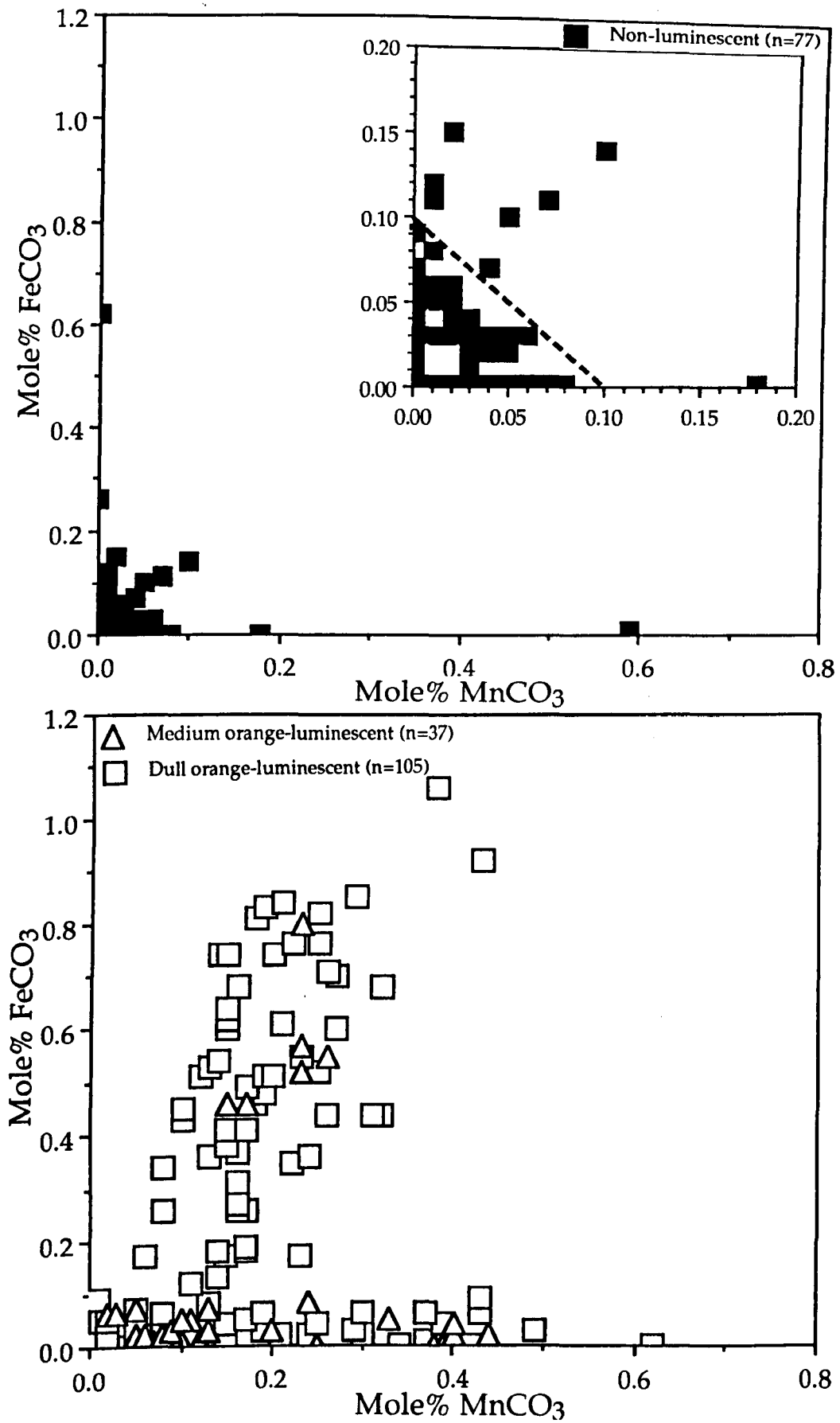

Fig. A1.2. The Fe and Mn compositions of Raisby Formation non-luminescent calcites (A) (inset shows detail of the lower part of the graph), and of medium and dull orange-luminescent calcites (B).

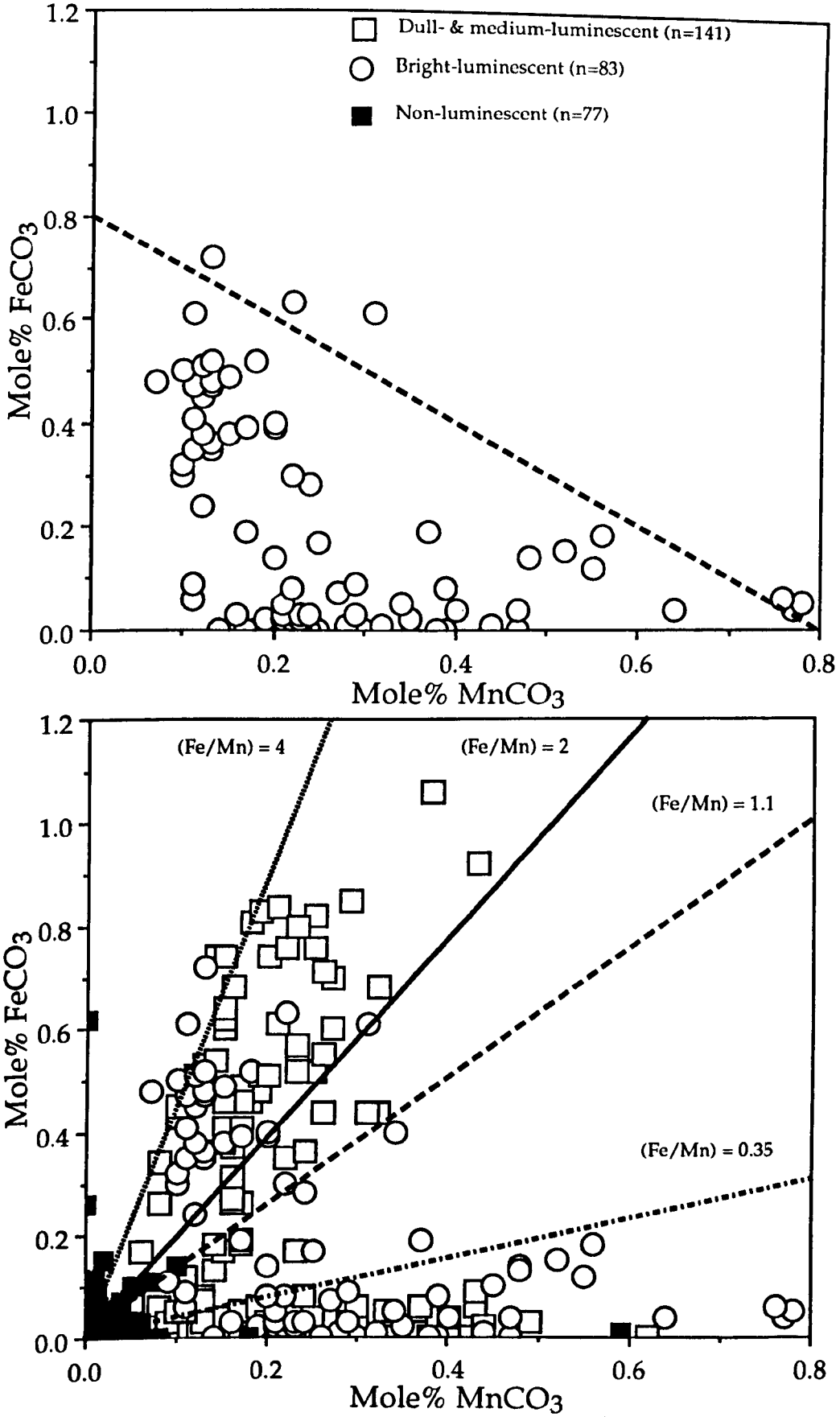

Fig. A1.3. The Fe and Mn compositions of Raisby Formation bright orange-luminescent calcites (A) (the area below the oblique dashed line is where most analyses occur), and the Fe and Mn composition of calcites of all luminescent types, with lines of specific Fe/Mn ratios demarcating the main compositional groups (B). The key in (A) refers to both graphs.

and/or authigenic Mn oxide/hydroxides. Although values of 0.1 mole% Fe and $MnCO_3$ are almost below microprobe detection limits, the consistency of the Mn and Fe data suggests it is reasonably reliable.

A strong overlap exists with regard to plots of Fe versus Mn for dull orange- and medium orange-luminescent calcites, with no clear distinction discernable (Fig. A1.2b). Most points lie in an area of less than 0.3 mole% $MnCO_3$ although variable Fe (Fig. A1.2b). The most well defined field describes an area of variable Fe, although relatively invariant Mn, where all points have a positive Fe/Mn ratio. A smaller number of points lie in an area characterised by strongly negative Fe/Mn ratios (Fig. A1.2b).

The fields defined by bright orange-luminescent calcites overlap with those for dull and medium orange-luminescent calcites, although there are no bright orange luminescent calcites with less than 0.1 mole% $MnCO_3$, or greater than 0.8 mole% $FeCO_3$ (Fig. A1.3a). The maximum $FeCO_3$ concentration of the bright orange-luminescent calcites decreases in a linear manner from 0.8mole% $FeCO_3$ with increasing concentration of Mn (Fig. A1.3a). This is the opposite of the trend which would be expected ($FeCO_3$ concentration of bright orange-luminescent calcites should decrease with decreasing Mn [so that the Fe does not quench luminescence intensity]). However, as for the dull orange- and medium orange-luminescent calcites, on top of the aforementioned trend, two populations may be distinguished - one defined by positive Fe/Mn ratios, the other by strongly negative Fe/Mn ratios (Fig. A1.3a). This may reflect an overlap with medium orange-luminescent calcites; i.e., those 'bright orange-luminescent' calcites with positive Fe/Mn ratios may be closer in luminescence intensity to the medium orange luminescent calcites, or sensitizer trace elements may be influencing luminescence intensity. Likewise the area characterised by negative Fe/Mn ratios may be dominated by bright orange-luminescent calcites, but in some otherwise bright orange-luminescent calcites, quenchers other than Fe (i.e., undetectable) are influencing net luminescence intensity (rendering it duller).

If all luminescence types are plotted along with boundary lines which best describe their area of occurrence, clear trends are apparent (Figs. A1.3b & A1.4):

1. In the area of Fe/Mn ratio greater than 4, very few calcites have been recorded,
2. Between Fe/Mn 4 and Fe/Mn 2 calcites are dominantly dull to medium orange-luminescent,
3. Between Fe/Mn 2 and Fe/Mn 1.1, very few calcites plot, although are dominantly dull to medium orange luminescent,
4. Calcites with Fe/Mn ratios less than 1.1 are dominantly bright orange-luminescent, and especially so with an Fe/Mn less than 0.35.
5. No samples plotted in areas of moderate to high Fe and high Mn.

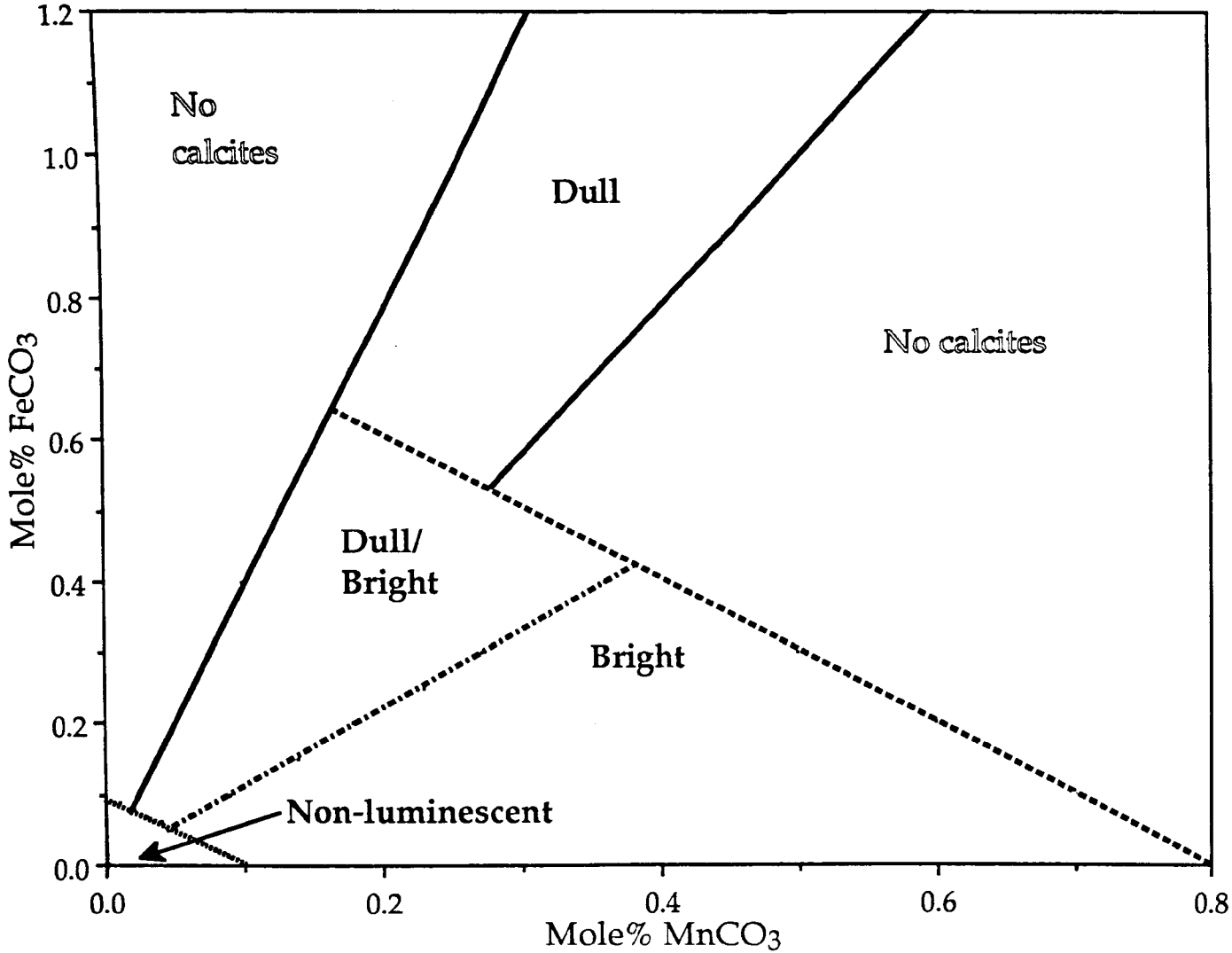

Fig. A1.4. Summary of the Fe and Mn geochemical groupings defined by calcites of different luminescence characteristics.

A1.3.1. Summary:

	This Study	Frank *et al.*, 1982
Medium and dull orange-luminescence	Fe/Mn 2 to 4	Fe/Mn 1 to > 2
Bright orange-luminescence	Fe/Mn < 1.1	Fe/Mn < 1

The relevance of the luminescence fields described is limited to late diagenetic (teolgenetic) cements within the Raisby Formation, and possibly cements precipitated very similar dolomite-evaporite sequences undergoing evaporite dissolution and calcite cementation during uplift diagenesis. The precise position of luminescence fields in relation to Fe and Mn compositions of calcite cements will be controlled to an extent by the supply of Fe and Mn to the growing calcite crystals, in turn a function of the nature of the diagenetic environment. Thus, in the Raisby Formation calcites, supply of Fe^{2+} and Mn^{2+} was limited owing to the very pure nature of the carbonate sequences, which thus limited the range of calcite compositions studied to those of relatively low Fe and Mn. In the model of Frank *et al.*, (1982) calcite compositions ranged from approximately 1 mole% $FeCO_3$ (similar to Raisby Formation) to greater than 2 mole% $MnCO_3$ (2.5 times greater than the Raisby Formation).

The relatively invariant luminescence characteristics of Raisby Formation dolostones analysed within this study mitigates against any meaningful study of their luminescence activation.

Appendix II

Sector zoning in calcite cements

A2.1. Sector zoning in calcites - Introduction.

Concentric zoning is an extremely common feature of calcites within the Raisby Formation. Much less common, although locally significant is compositional sector zoning. This feature of geochemical variation within calcites has only recently become to be widely recognised (Reeder and Prosky, 1986; Reeder and Grams, 1987; Raven and Dickson, 1989).

Concentric zones/subzones within a calcite crystal broadly reflect a temporal variation in the composition of the fluid from which the calcite was precipitating. Each crystal grows by the incorporation of ions onto a number of crystal faces. The portion of a crystal which has formed by ion incorporation onto any one face is known as a growth sector (Reeder and Prosky, 1986). The interface between two adjacent sectors is called the 'growth sector boundary' (GSB). A GSB is demarcated by an abrupt change in the orientation of component zones and subzones across it (Fig. A2.1b). GSBs may be straight, curved or irregular (Reeder and Grams, 1987). Adjacent sectors may be of identical chemical composition, or, more importantly, of a different chemical composition (compositional sector zonation). This is most readily identified by contrasts in luminescence intensity. This difference in intensity between sectors is the cumulative effect of changes in luminescence intensity of all component zones and subzones of the crystal across the GSB.

Any comprehensive study of sector zonation requires detailed geochemical and crystallographic studies, which are beyond the scope of this thesis. However, on a qualitative basis two broad styles of compositional sector zonation have been identified; SZ1 and SZ2. All compositional sector zonation has been identified by cathodoluminescence, and all calcites displaying sector zonation line/fill cavities after sulphates. Sector zoning was not recorded within replacive calcites or dolomite.

A2.1.1. Subtype SZ1 - Description.

This is the most common, and easily recognised style of compositional sector zonation in the Raisby Formation. It occurs within slightly elongate (300-400μm) sub-equant luminescent calcites cementing breccia porosity at Raisby Quarry (Lee and Harwood, 1989, fig. 8) and cementing cavities after sulphates at numerous other localities within the formation. The most pronounced difference in composition occurs within a small, dull orange-luminescent growth sector (commonly the smallest within the crystal) orientated parallel to the C-axis (axis of elongation) of the crystal, which correlates to a small crystal face perpendicular to the C-axis (Fig. A2.1a & b). In most calcites this sector is discontinuous, reflecting orientation of the plane of the thin section at an angle to that of the C-axis of the calcite. The luminescence intensity of the dull orange-luminescent sector is always considerably less than that of the adjacent sectors. If the adjacent sectors are concentrically

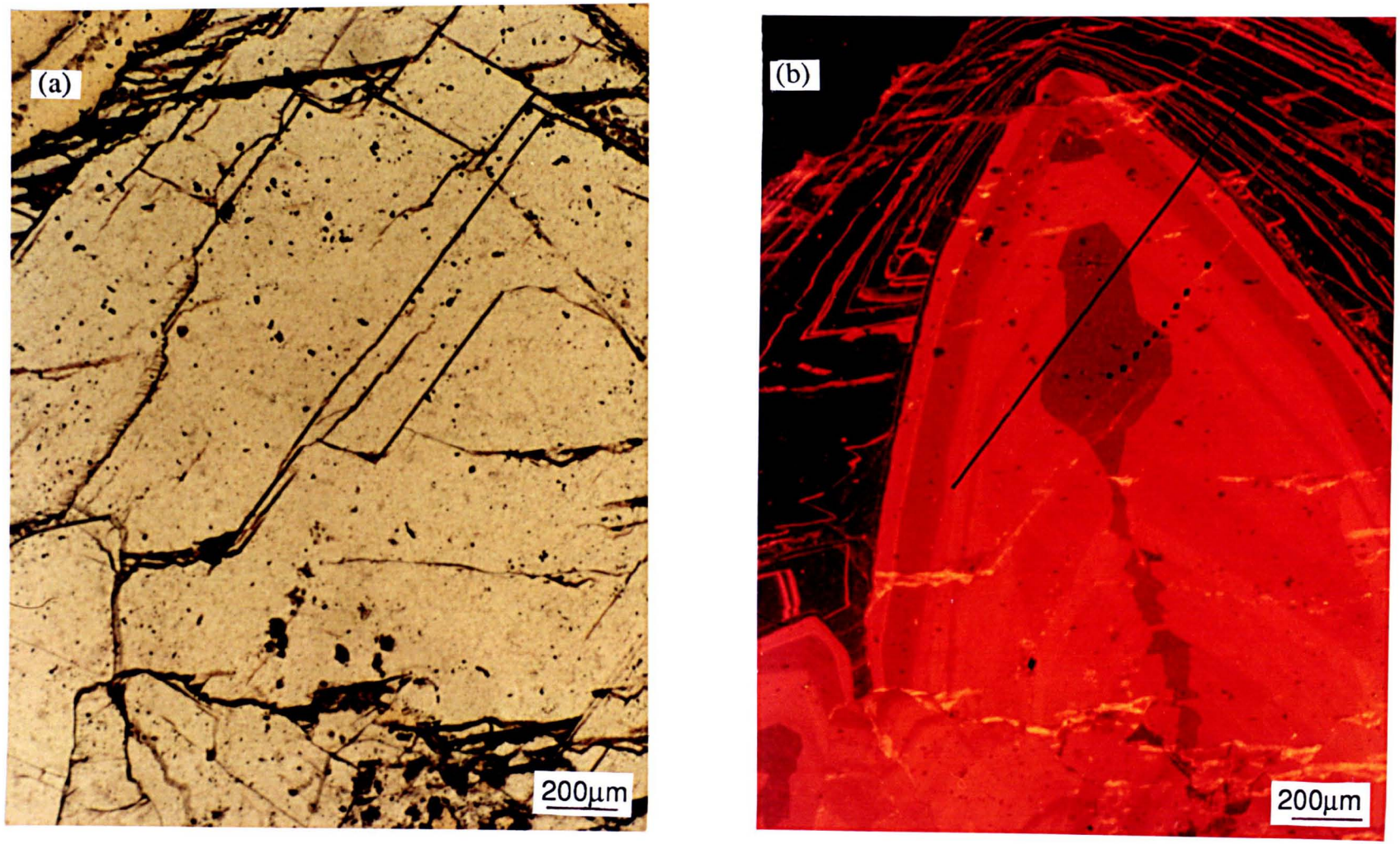

Fig. A2.1. Plane light (a) and luminescence (b) photomicrographs of a calcite crystal from the upper part of a GC cavity after sulphate, Haswell Moor Farm Quarry. A large SZ1 'fir-tree' sector zone in (b) has been analysed by microprobe via both a line traverse (continuous line) and point traverse (small squares) (Fig. A2.3).

zoned, the dull orange-luminescent sector is also concentrically zoned, but each zone is always duller orange-luminescent than in the immediately adjacent sectors. GSBs may be straight, but are more commonly irregular, varying along the length of the sector in question. Where irregular, the GSB is of identical shape along the contact with both adjacent sectors (Fig. A2.1b). variation in the shape of GSBs along the length of the sector zone defines 'fir-tree' structures (Raven and Dickson, 1989) (Fig. A2.1b).

Although the most noticeable difference in composition is between the C-axis parallel sector and adjacent sectors, the adjacent sectors themselves may be compositionally distinct (Fig. A2.1b). In this example, the luminescence intensity of each sector decreases with proximity to the dullest orange luminescent sector (Fig. A2.1b). A variant of the fir-tree sector zone style is of three 'propeller'-like sector zones, 120° apart which radiate out from the center of triangular-shaped crystals (Fig. A2.2b). These are interpreted, after Raven and Dickson (1989) as basal sections of columnar crystals which display fir-tree sector zoning.

Geochemical analyses show that fir-tree sectors are depleted in Mg, Mn and ?Fe in relation to adjacent sectors (Fig. A2.3). Depletion with respect to Fe and Mn is near total.

A2.1.2. Subtype SZ2 - Description

This, less common style of compositional sector zonation was restricted to three localities. At all three, the calcite crystals were relatively small (100-150μm) and equant to barrel-shaped. All crystals contain three to four dull orange-luminescent sectors formed by precipitation on small crystal faces commonly orientated at angles to the axis of elongation of the crystal. This produces a very distinct, X-shaped sector zonation pattern which is commonly incompletely developed in thin section owing to its orientation relative to crystallographic axes of the calcite (Fig. A2.4b). In contrast to SZ1, GSBs are always planar and fine concentric subzones may be clearly traced through the dull orange-luminescent sectors (Fig. A2.4b).

Analyses demonstrate that the dull orange-luminescent sectors are depleted in Mg and Mn relative to adjacent brighter orange-luminescent sectors (Fig. A2.5). The trends for Fe are unclear. These analyses must be treated with caution owing to the small size of concentric subzones within the sector zones, relative to microprobe points (Fig. A2.4b).

Extreme developments of compositional sector zonation occur within some calcites from Haswell Moor Farm and Quarrington Quarries. Within any one calcite, each sector has a different luminescence intensity, and intensities and concentric zoning patterns may even vary within a sector (Fig. A2.6a & b). Microprobe analyses of one of the crystals (from Quarrington Quarry [Fig. A2.6a]) supports these differences (Fig. A2.7 & A2.8). Within some sectors of these calcites, very anomalous structures reminiscent of en echelon tension gashes have been recorded. They are defined by variations in luminescence intensity and their component banding is commonly orientated perpendicular to concentric subzones of the

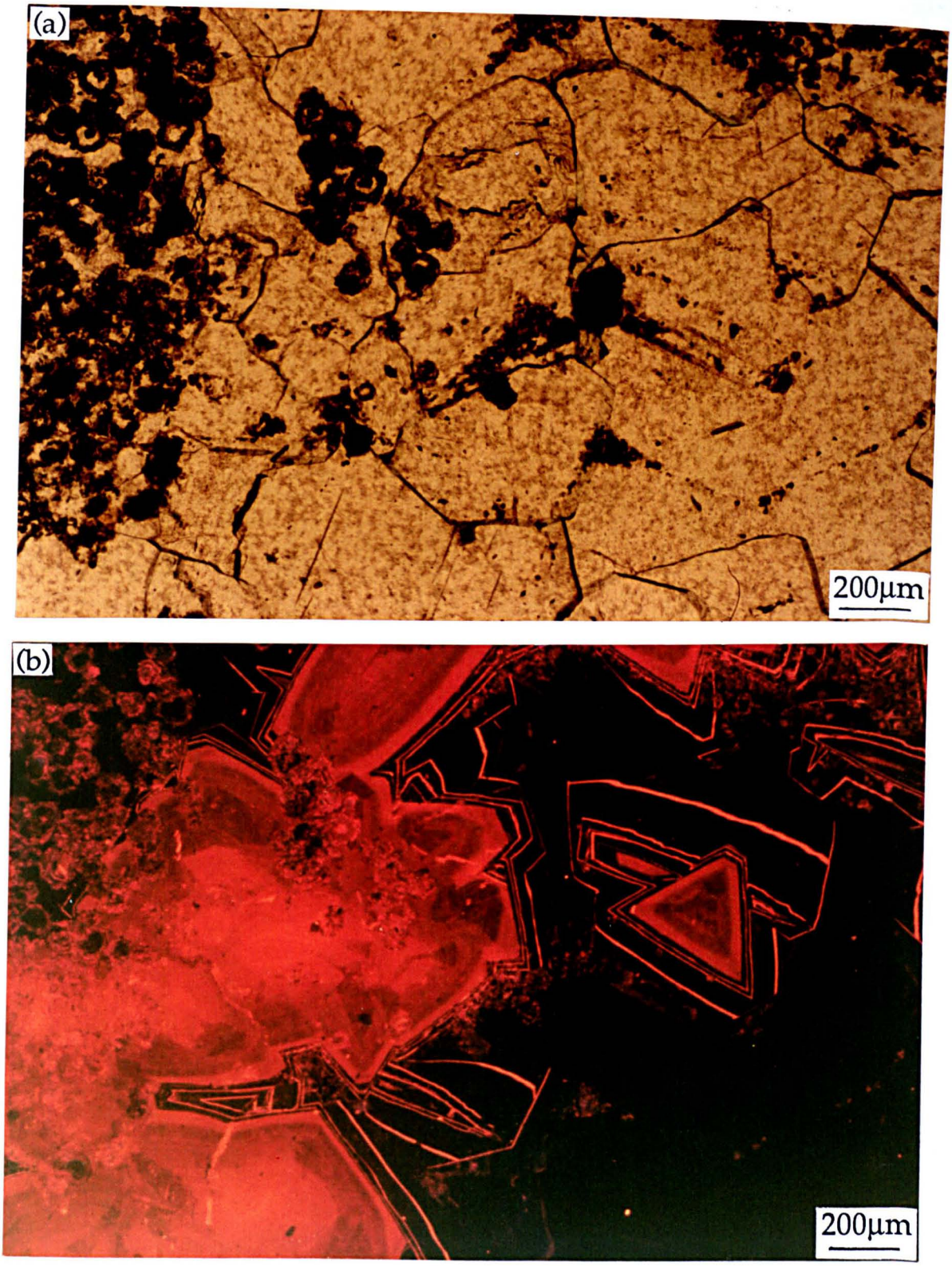

Fig. A2.2. Plane light (a) and luminescence (b) photomicrographs of calcite cementing inter-clast porosity within a small evaporite dissolution collapse breccia near to the top of the Raisby Formation, Raisby Quarry. The small crystal just right of center in (b) shows propellor-like sector zoning.

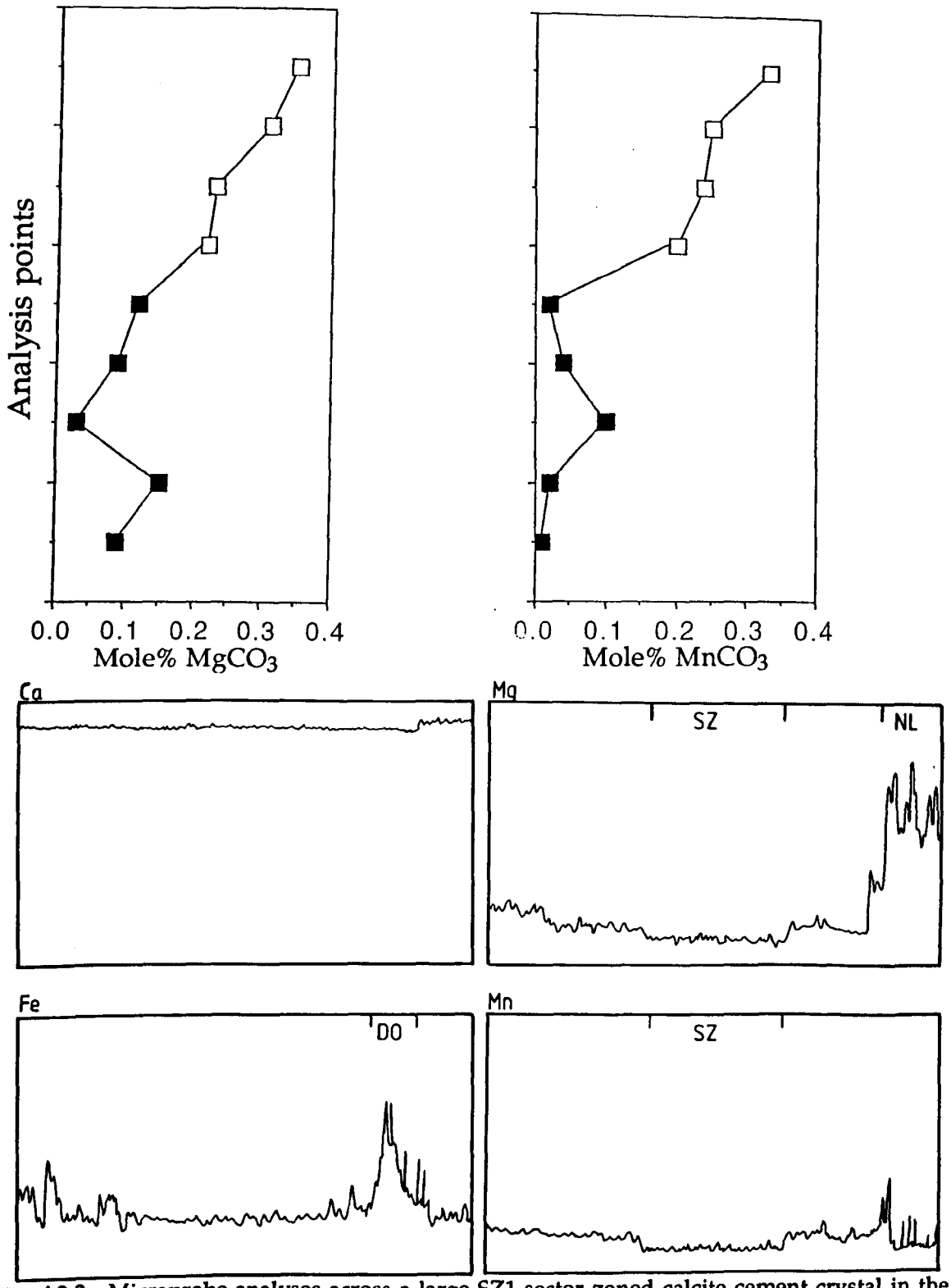

Fig. A2.3. Microprobe analyses across a large SZ1 sector zoned calcite cement crystal in the upper part of a GC cavity after sulphate, Haswell Moor Farm Quarry (Fig. A2.1b). The upper two graphs show the geochemical variation from the dull orange-luminescent sector zone (filled squares) into bright orange-luminescent host calcite (open squares). The lower four graphs illustrate a semi-quantitative line traverse through, from left to right, bright orange-luminescent calcite, a fir-tree SZ1 sector zone (SZ), bright orange-luminescent calcite, a dull orange-luminescent zone (DO) and non-luminescent (NL) calcite (see fig. A2.1b for location of the traverse).

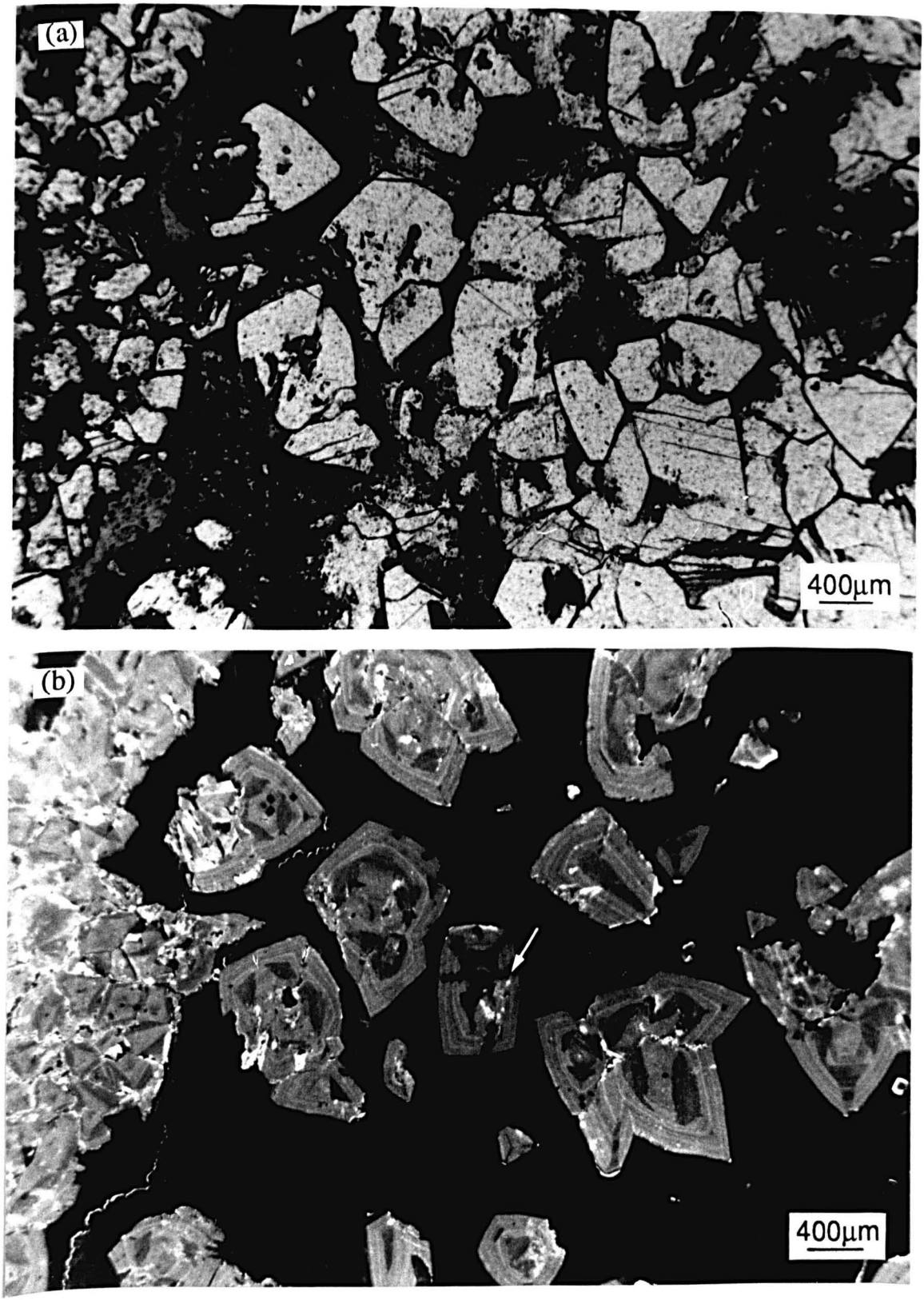

Fig. A2.4. Plane light (a) and luminescence (b) photomicrographs of equant calcite crystals within clay-rich internal sediments from the base of a GC cavity after sulphate, Frenchmans Bay. One SZ2 sector zone within a barrel-shaped calcite crystal in the center of (b) (arrowed) has been analysed by microprobe (fig. A2.5).

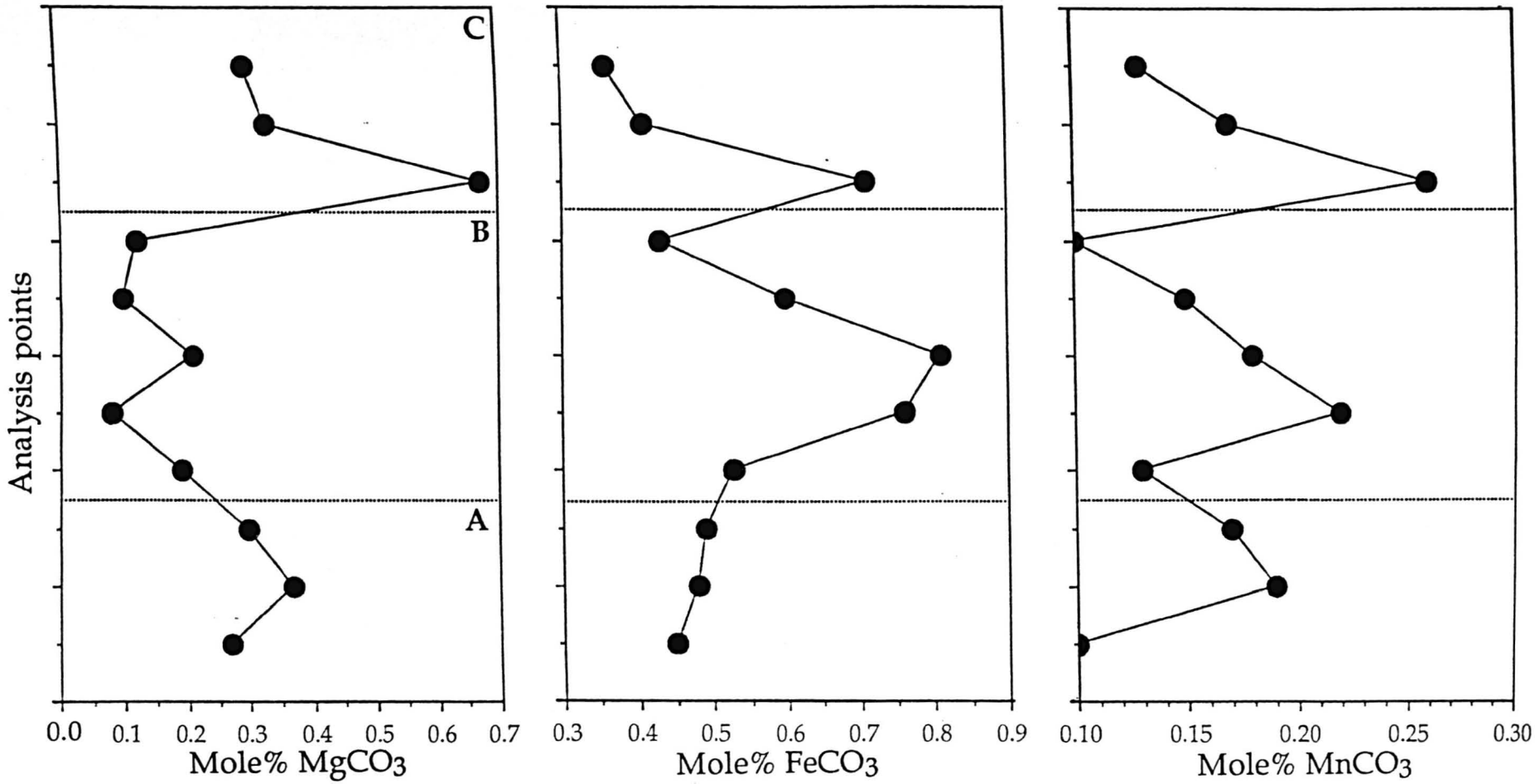

Fig. A2.5. Microprobe analyses across a SZ2 sector zoned calcite crystal from within a type GC cavity after sulphate, Frenchmans Bay (Fig. A2.4b). A and C denote subzoned bright/dull orange-luminescent calcite, B denotes the dull orange-luminescent sector zone.

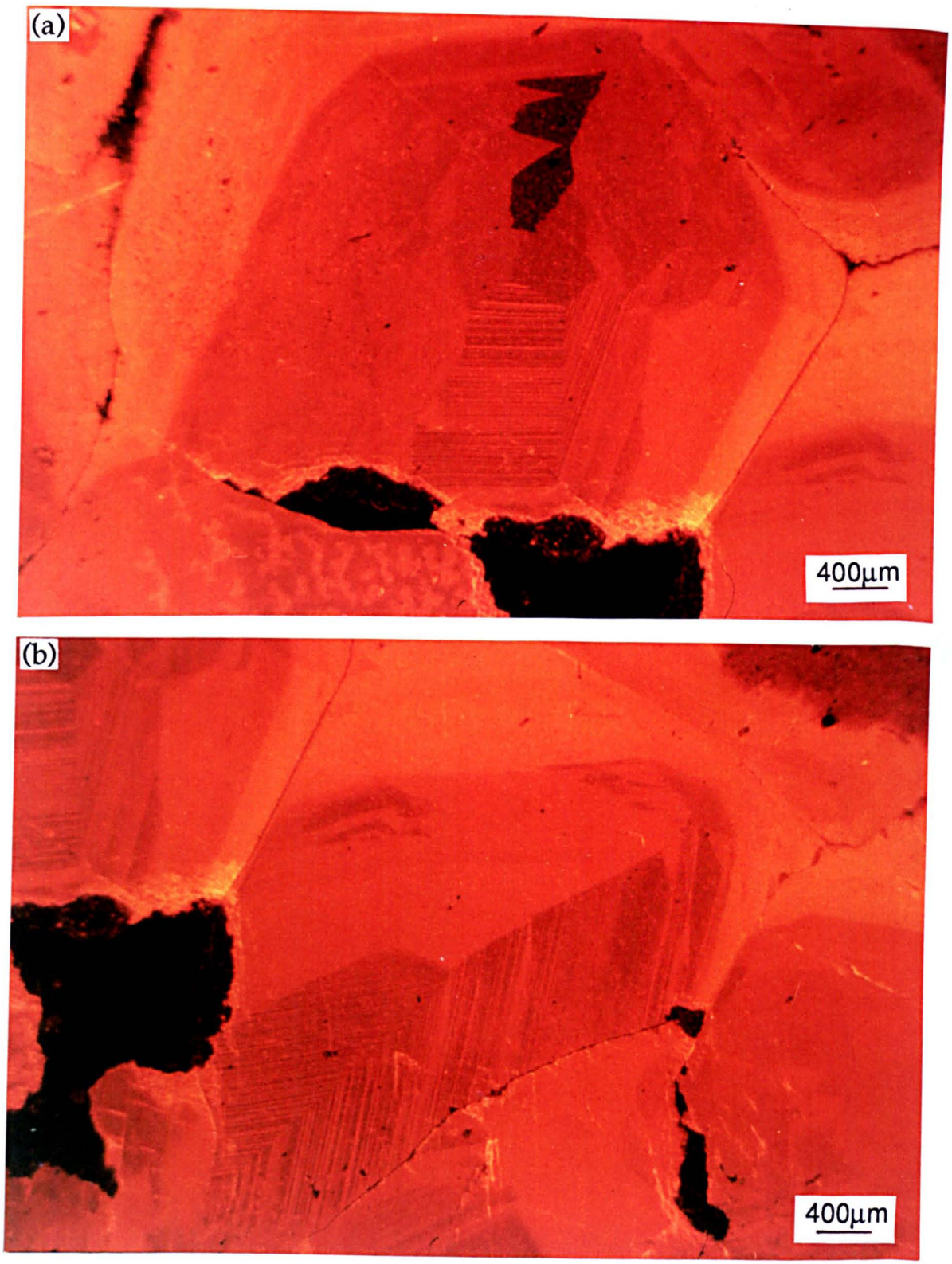

Fig. A2.6. Luminescence photomicrographs of two complex sector zoned calcite crystals from within a barite-mineralized cavity after sulphate, Quarrington Quarry. Microprobe analyses of areas of different luminescence within (a) are given in fig. A2.7, and a transect across the SZ1 dull orange-luminescent sector zone in fig. A2.8. The abrupt junction of zones in (b) may be attributable to twinning.

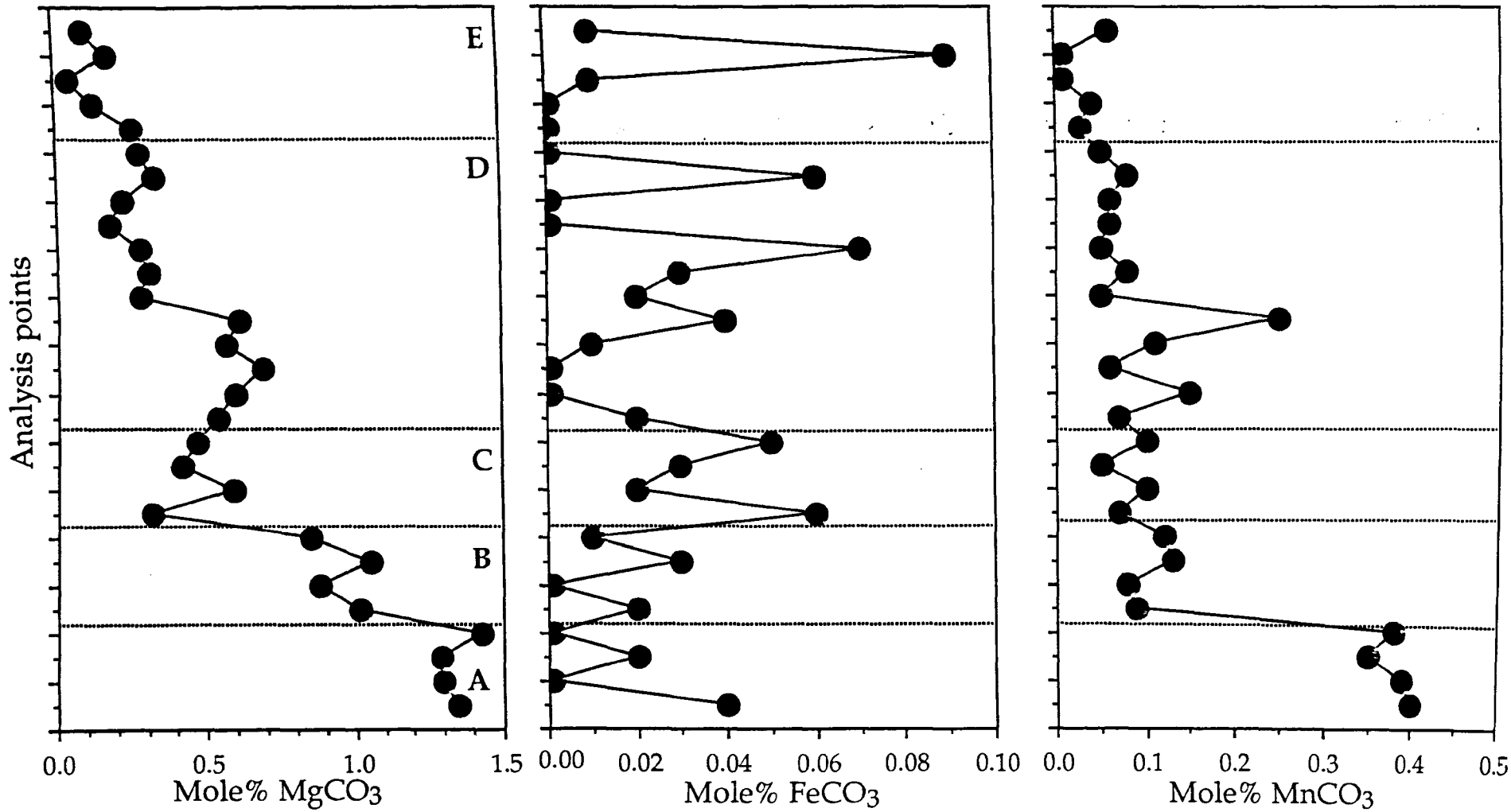

Fig. A2.7. Microprobe analyses of a complex sector zoned calcite crystal within a barite-mineralized cavity after sulphate, Quarrington Quarry (Fig. A2.6a). A = bright orange-luminescent, B = medium orange-luminescent, C = subzoned medium orange-luminescent, D = dull orange-luminescent, E = very dull orange-luminescent calcite.

Fig. A2.9. Luminescence photomicrograph of a very complex sector zoned calcite crystal from within a calcite lined cavity after sulphate, Quarrington Quarry. Tension gash-like structures can be recognised in the upper part of the crystal (arrowed).

same sector (Fig. A2.9). They are however commonly continuous with underlying concentric subzones and restricted to an area parallel to the concentric subzones.

A2.2. Sector zoning in calcites - Interpretation.

All compositional sector zones identified from calcites within the Raisby Formation represent a contrast in the incorporation of trace elements onto different crystal faces. These differences can be recognised by luminescence, as Mn is one of the elements affected. However, other sector zoning styles which do not affect Mn may well be present.

The most common style of compositional sector zonation (SZ1) reflects the limited incorporation of Mg, Mn and ?Fe onto a small crystal face perpendicular to the C-axis of the calcite. The absolute luminescence intensity of this sector is in general comparable between different samples, which suggests that this sector may have an intrinsic limit on the amount of Mn (at least) which can be incorporated, although this value does vary slightly in response to concentric zoning (i.e., changes in bulk pore fluid composition). These sectors are much duller orange-luminescent than the dull orange-luminescent sectors of SZ2, again suggesting that there may be an absolute control on trace element incorporation, dependant on the crystal face developed.

The variation in width of the small, dull orange-luminescent SZ1 sector controls the shape of its GSBs. That the GSBs are symmetrical either side of the dull orange-luminescent sector, demonstrates that variation in shape of the GSBs is due to variation in growth rate of the dull orange-luminescent sector in contrast to that of adjacent growth sectors. This is illustrated in fig. A2.10. A very similar conclusion has been reached by Raven and Dickson (1989), who suggest that fir-tree sector zoning is due to a combination of variation in partition coefficients and growth rates between sectors. Raisby Formation calcites in which fir-tree zoning occurs, are slightly elongate, demonstrating that growth rates were slightly faster parallel to the C-axis (i.e., along the sector concerned) than along side faces. In fig. A2.1b growth rates were approximately twice as fast parallel to the C-axis than on adjacent steeper faces.

Subtype SZ2 form from a different crystal structure than SZ1, whereby the sectors in which Mg, Mn and ?Fe are most depleted are normally not perpendicular to the C-axis. However, in common with SZ1, these sectors are considerably smaller than adjacent ones. That GSBs are generally straight shows that growth rates for all sectors were constant. A proposed structure for an ideal SZ2 crystal is illustrated in fig. A2.11. Note, in this reconstruction, the core of the crystal is dull orange-luminescent as it formed wholly by growth along the depleted sectors whereas the incoming of brighter orange-luminescent calcite is marked by the development of larger faces which eventually controlled crystal form.

Even growth rates
Sector zone increases in width upwards

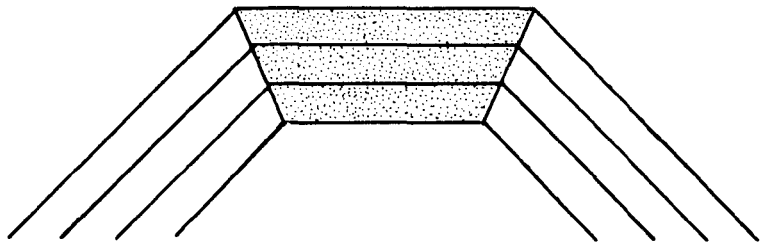

Growth rate of sector zone 2x adjacent sectors
Sector zone decreases in width upwards

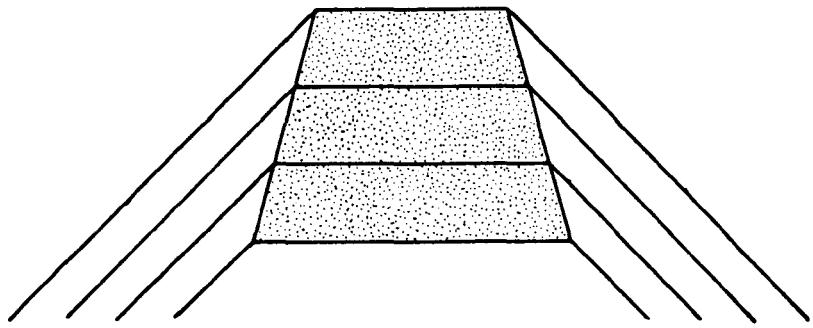

Growth rate of sector zone 0.5x adjacent sectors
Sector zone increases in width upwards

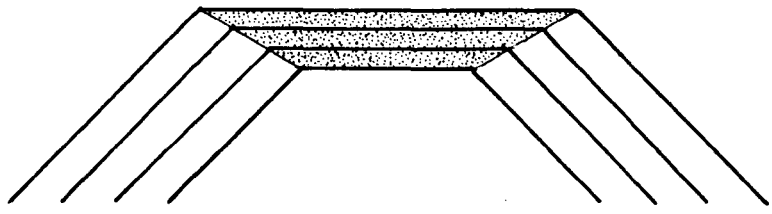

Fig. A2.10. Diagram illustrating how different growth rates between the sector zone (stippled) and adjacent sectors of a SZ1 fir-tree sector zone (shown cut parallel to the c-axis of a calcite crystal) can create the typical fir-tree structure.

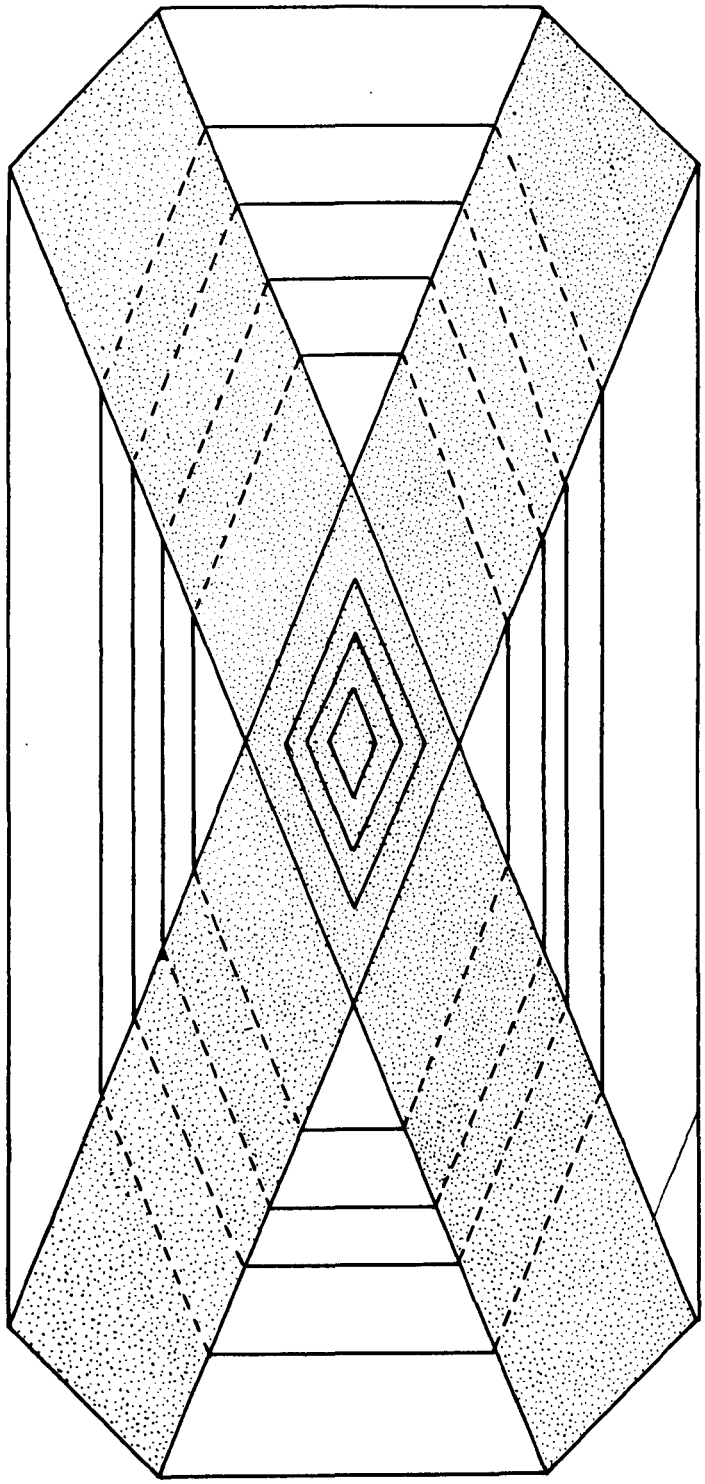

Fig. A2.11. Diagram illustrating the ideal structure of a SZ2 sector zone (stippled) within a concentrically zoned, barrel-shaped calcite crystal (see fig. A2.4b).

The intricate compositional sector zonation in calcites from Haswell Moor Farm and Quarrington Quarries represents a very complex form of differential trace element partitioning, more limited versions of which have been recorded from other localities. At least one of the examples (Fig. A2.6b) is probably attributable to twinning and so is not strictly compositional sector zonation. The bizarre sectorial differences in calcites from Quarrington Quarry may be related to anomalous geochemical conditions during cement precipitation as the calcites do occlude pores associated closely with barite mineralization. The calcites are also nearly completely depleted in Fe, which may also suggest scavenging of iron to form pyrite/marcasite during precipitation.

Limited analytical data shows that, in both SZ1 and SZ2 examples, the small dull orange-luminescent sector is depleted in Mg by 48 to 72% and in Mn by 30 to 85% relative to adjacent bright orange-luminescent sectors (Figs. A2.3, A2.5 & A2.8) This is in excellent agreement with Reeder and Grams (1987) who documented depletions in Mg of 50 to 95% and Mn of 30 to 80% for calcite cements within Mississippian limestones, Iowa. Such depletion within Raisby Formation examples suggests that if, under normal conditions (i.e., large bright orange-luminescent sectors) $K^{Mg}_{Calcite} = 0.023$ and $K^{Mn}_{Calcite} = 15$ (3.1.1), these partition coefficients decrease to between 0.012 and 0.006 for Mg and 10 to 2 for Mn in the small, dull orange-luminescent sectors. Reeder and Grams (1987) demonstrated that depletion of Mg was greater than Mn between any two sectors, although both elements were depleted in the same sectors. These results are again consistent with SZ1 and SZ2 examples. Reeder and Grams (1987) state that the 'top' faces of crystals have less Mg and Mn substitution than 'side' faces. This is in general agreement with SZ1 although not so much with SZ2. This may be because Reeder and Grams (1987) only studied pore filling calcites of a certain habit, nucleating off limestone host into pores (which are very similar to calcites hosting SZ1). Reeder and Grams (1987) do not mention a correlation with sector size which appears to be the most important factor within Raisby Formation examples.

Compositional sector zoning was interpreted by Reeder and Prosky (1986) (for dolomite) and Reeder and Grams (1987) (for calcite) to represent differences in effective partition coefficients of Mg, Mn and ?Fe between the fluid and certain faces of calcite crystals. The effect of precipitation rate on partition coefficients was discounted by them, although clearly, with SZ1, precipitation rate is faster parallel to the C-axis, along the face concerned. However, the magnitude of difference in precipitation rate (approximately two times) is most likely insufficient to cause a substantial variation in partition coefficients (3.1.1.). The model proposed by Reeder and Prosky (1986) and Reeder and Grams (1987) which accords with most of the Raisby Formation observations, is that differential trace element partitioning is a function of the atomic structure of the surface of each face, which is in turn controlled by the orientation of the face relative to internal structure of the calcite crystal. In their 'prosite' model (Reeder and Prosky, 1986; Reeder and Grams, 1987) the quantity of

'foreign' cations (i.e., Mg, Fe, and Mn) incorporated into an incompletely bonded (partially formed) cation site (prosite) is a function of its ability to accommodate imperfectly sized ions. This ability is in turn related to the geometrical orientation of the crystal face concerned. Occupancy of prosites is favoured by small size and high charge of ions which explains the largest partitioning differences being recorded for the smallest ions (Mg) and smallest partitioning differences for Mn (the largest ion). Reeder and Prosky (1987) suggest there may be an overprint in some cases on partitioning by the type of ions already substituted into prosites, in that the abundance of one ion on a face may enhance or diminish the incorporation of another. In the Raisby Formation examples, partitioning of Mg and Mn into surface sites appears to be directly related to surface area of the crystal face concerned. Although large sectors may have compositional differences, they are much more pronounced for the smallest sectors. It may be that smaller faces only occur in specific orientations relative to crystal structure. However, it is more likely that partitioning is controlled by factors which are proportional in their effectiveness to the surface area of the crystal face, although do not affect Ca or CO_3 incorporation and so crystal growth rates.

A2.3. Summary

Compositional sector zonation in Raisby Formation calcites is the product of differences in partition coefficients between the fluid and crystal faces related to the surface area and crystallographic orientation of those faces. Accordingly, certain faces have consistently less trace element substitution than others. In most examples, the faces with least trace element incorporation were the smallest within the crystal and perpendicular or at an angle to the axis of elongation of the calcite. All sector zonation was recorded within calcites cementing cavities after sulphates. Their abundance within the Raisby Formation may just reflect the suitability of coarse pore filling calcites for the illustration of sector zonation, or may be related to a feature of the pore fluids which in turn control the growth of specific calcite crystal forms. Raven and Dickson (1989) suggest that fir-tree sector zoning may be specific to certain hydrogeochemical environments, among which they list the near-surface meteoric environment. In this environment, variations in the properties of advecting fluids can cause abrupt changes in crystal growth rates, necessary for fir-tree zoning. This is in excellent agreement with the diagenetic environment of Raisby Formation sector zoned calcites.

Appendix III

Procedure for stained acetate peels.

Stained acetate peels of polished rock slabs were prepared by using a combined staining technique modified from that developed by J.A.D. Dickson, for distinguishing ferroan and non-ferroan calcite and ferroan and non-ferroan dolomite. The combined stain was prepared from solutions of Alizarin red S (ARS) (sodium alizarinsulphonate) and potassium ferricyanide (PFC) ($K_3Fe(CN)_6$). 4g of PFC was dissolved in 200ml of 0.5% HCl and 0.6g of ARS was dissolved in 300ml of 0.5% HCl. These solutions were mixed in the ratio of three parts ARS to two parts PFC. Polished rock slabs were ultrasonically cleaned, then etched for approximately 15 seconds in 5% HCl before staining for 65-70 seconds. Acetate peels were taken after the stain had fully dried.

Typically, Raisby Formation dolostones did not take the stain, although a few stained blue (between 'dusky blue green' [5 BG 3/2] and 'dusky blue' [5 PB 3/2]) which correlated with an iron rich composition (greater than a few mole% $FeCO_3$). Raisby Formation limestones stained well with a uniformly pinkish colour (most commonly 'dusky red' [5 R 3/4]). Calcite cements either took the stain, with a similar colour to that of the limestones, or did not take the stain at all. These differences correlate well with luminescence characteristics of those cements (pink stain = dull orange-luminescent, no stain = bright orange-luminescent) and trace element composition (those calcite cements containing greater than 0.4-0.5 mole% $FeCO_3$ stained well). Almost no blue-staining ferroan calcites were encountered during this study.

Within some borehole samples, gypsum and anhydrite could be differentiated where relatively coarsely crystalline in the stained peels. Although both were unstained, anhydrite stood out from gypsum, presumably owing to the lower solubility of anhydrite than gypsum at room temperature in dilute HCl.

<u>Summary.</u>

Dolomite

Non-ferroan.....No stain

Ferroan.....Dusky blue green to dusky blue stain

Calcite

Iron poor.....Unstained

(<0.4-0.5 mole% $FeCO_3$)

Iron rich.....Dusky red stain

(>0.4-0.5 mole% $FeCO_3$)

Appendix IV

Scanning electron microscope (S.E.M.) sample preparation and operating conditions.

For most SEM work, a JEOL JSM T20 scanning electron microscope was used, at the department of metallurgy, University of Newcastle-upon-Tyne. Standard operating conditions were 20kv accelerating voltage with an electron probe current of 10^{-11} - 10^{-8} amps., at a working vacuum pressure of $5x10^{-5}$ Torr. All photographs were taken on black and white Ilford FP4 film with a 60-100 second exposure time. Owing to distortion at high magnifications, in general a 7,500 times magnification was the maximum used for photography.

Samples were mounted on 10mm diameter stubs with an acetone-soluble glue. Some of the samples were gold coated, others carbon coated. Carbon coating produced superior results at high magnifications. Sample preparation was variable depending on the textures to be studied. External crystal surfaces and clay minerals were most easily studied on fracture surfaces, whereas internal textural details and interrelations between crystals were best appreciated on polished and etched samples. Most samples were cleaned in an ultrasonic bath for 15 to 20 minutes prior to mounting and coating. For the distinction of calcite from dolomite, the polished samples were etched in 5% hydrochloric acid for 15 to 40 seconds. To distinguish aragonite from calcite the polished samples were either etched in 0.25% formic acid for approximately one minute (after Sandberg and Hudson, 1983) or 0.15% formic acid for 15 to 20 seconds (after Lasemi and Sandberg, 1984). In general, the preparation of Sandberg and Hudson (1983) produced superior results.

For analytical SEM and backscattered electron microscopy, a JEOL JSM 35 scanning electron microscope also in the department of metallurgy, University of Newcastle-upon-Tyne was used. Only carbon coated polished thin sections were analysed. Analytical detection limits were very poor, and so analyses are only quoted on a semi-quantitative basis. Backscattered electron imaging worked well for the differentiation of calcite, dolomite and iron minerals, although not so well for distinguishing compositional zones within calcite and dolomite crystals.

Appendix V

Electron Microprobe analysis

The basis of electron microprobe analysis is that major and minor element chemical determinations may be made of parts of minerals on polished thin sections by bombarding them with a beam of electrons. The electron beam interacts with the specimen in numerous ways, among which is the generation of X-ray photons. The incidence of X-ray photons onto a detector creates electrical pulses, which define the presence, and the concentrations, of various elements.

All electron microprobe analysis was carried out at the Department of Geology, University of Edinburgh, using a Cameca Camebax electron microprobe. All analyses were of carbon-coated standard petrographic polished thin sections. Calcite analyses were optimised by using a 15μm rastered beam, at 8Kv accelerating voltage, and with a 10 nannoamp beam current. Dolomite samples, however, gave better results again with a 15μm rastered beam, but at 20Kv accelerating voltage. The lower accelerating voltage for calcite analyses was necessitated by the relative instability of Raisby Formation calcite cements under the electron beam. Count times, for both calcite and dolomite, were 30 seconds on peak, and 15 seconds on background. Typically, eight elements were analysed in a single analysis run (two separate runs on four spectrometers); Ca, Mg, Fe, Mn, Sr, Ba and Na. Si was also determined in order to ensure overall reliability of the analysis. A non-carbonate analysis package, with a different set of elements was also used for clay minerals and other non-carbonates.

The analytical data was presented by the on-line computer as weight percent oxide, and further recalculated to weight percent carbonate. These data were then recalculated back in Newcastle to 100 mole% Ca, Mg, Fe and Mn carbonate, in order to facilitate direct comparison with AAS and ICP results, and allow a direct expression of dolomite stoichiometry. Sr data was not used in the recalculation, owing to the generally very small amounts of Sr in the samples, and poor detection limits for Sr, which would give misleading results if presented along with the other carbonate elements. Therefore, in the following results tables, all calcite and dolomite analyses are presented as mole % carbonate, normalised to 100 mole% carbonate. Presentation of microprobe data in this form is common in recent carbonate literature (i.e., Gregg, 1988; Carpenter and Lohmann, 1989). As with the normalization of AAS and ICP data, only the Ca values of calcites show any significant change as a result of normalization.

Analytical accuracy.

Detection limits for Ca, Mg, Fe, and Mn were calculated in the form adopted at Edinburgh University. Detection limits for both calcite and dolomite from a number of separate analysis runs gave consistent results, which are comparable with other quoted detection limits:

	Calcite	*Dolomite*
Mole% $CaCO_3$	0.055	0.050
Mole% $MgCO_3$	0.056	0.053
Mole% $FeCO_3$	0.074	0.081
Mole% $MnCO_3$	0.076	0.086
Ca ppm	221	199
Mg ppm	135	131
Fe ppm	405	454
Mn ppm	420	468

The precision of analyses was again calculated in the form adopted at Edinburgh University, from a number of analyses. Calculated precision for Ca in calcites was ±0.46 mole% $CaCO_3$, and in dolomites ±0.64 mole% $CaCO_3$, with precision of Mg being ±0.33 mole% $MgCO_3$ in dolomites. For the range of Fe values within calcites and dolostones, precisions were ±0.27 mole% $FeCO_3$ (for an analysis with 11.4 mole% $FeCO_3$) and ±0.082 mole% $FeCO_3$ (for an analysis with 0.64 mole% $FeCO_3$). Precision of Mn values were calculated at ±0.056 mole% $MnCO_3$ (for an analysis with 0.35 mole% $MnCO_3$) and ±0.048 mole% $MnCO_3$ (for an analysis with 0.16 mole% $MnCO_3$).

Microprobe results, presented in the following tables, are tabulated in order of the chapters to which they refer. All analytical results are presented, even where below detection limits. An analysis where an element gave a zero reading is represented by 'x' on the results tables.

	Sample no.	Mole% $CaCO_3$	Mole% $MgCO_3$	Mole% $FeCO_3$	Mole% $MnCO_3$
Dawsons Plantation					
Unit 5 of debris flow conglomerate					
Non-luminescent area of disarticulated	TS20/17	99.30	0.66	0.02	0.02
Horridonia horrida	18	99.22	0.73	x	0.05
Luminescent area of disarticulated	19	99.39	0.53	0.01	0.07
Horridonia horrida	20	99.12	0.50	0.12	0.26
"	21	99.54	0.44	x	0.02
Brachiopod shell fragment	TS53/1	98.94	0.99	0.01	0.06
"	2	98.91	1.05	0.03	0.01
Acicular altered marine cement	3	98.82	1.08	0.05	0.05
growing off shell fragment	4	95.74	4.18	0.02	0.06
"	5	97.85	2.00	0.09	0.06
"	6	98.33	1.60	0.04	0.03
"	10	96.97	2.63	0.31	0.09
"	11	99.05	0.78	0.10	0.07
"	12	98.02	1.87	0.04	0.07
Orange-luminescent calcite cement	7	98.96	0.39	0.36	0.29
overgrowing altered acicular cement	8	97.91	1.78	0.22	0.09
Non-luminescent cement	9	97.80	2.15	0.04	0.02
overlying orange-luminescent calcite					
High Moorsley Quarry					
Basal nodular limestone					
Shell wall of articulated brachiopod	TS94/1	99.26	0.48	0.17	0.09
"	2	99.26	0.48	0.17	0.09
"	3	99.24	0.50	0.12	0.13
"	4	99.02	0.57	0.20	0.20
Acicular, altered marine cement	TS94/5	98.69	0.87	0.26	0.17
(orange luminescent) growing off	6	98.54	1.24	0.14	0.09
internal shell wall	7	98.58	1.22	0.10	0.10
"	8	98.27	1.59	0.09	0.05
"	9	98.45	1.00	0.23	0.33
"	10	98.75	0.89	0.11	0.23
Non-luminescent cement overlying	11	98.74	1.21	x	0.06
orange-luminescent calcite	12	99.00	0.94	x	0.06
"	13	98.71	1.23	0.05	0.01
"	14	98.93	1.04	0.02	0.01
"	15	99.06	0.91	0.02	x
CL zoned, coarse, blocky, final pore	16	99.15	0.63	0.12	0.10
fill cement.	17	99.03	0.61	0.17	0.19
"	18	97.91	1.00	0.70	0.39
"	19	97.86	1.14	0.70	0.30
"	20	97.96	1.10	0.63	0.31
"	21	97.68	1.12	0.71	0.48
"	22	98.32	0.82	0.61	0.25
"	23	98.04	0.74	0.72	0.50
Ralsby Quarry					
Upper isolated nodular limestone					
Altered blotchy bright- to non-	TS74/6	97.80	2.15	0.03	0.02
luminescent cement occluding	7	97.98	2.00	0.02	x
V-shaped fracture in upper part	8	97.80	2.14	0.04	0.02
of nodule	9	98.55	1.32	0.05	0.08
"	10	98.64	1.24	0.05	0.07
"	11	99.27	0.63	0.03	0.09
"	12	97.96	2.02	0.02	x
"	13	97.85	2.09	0.03	0.03
"	14	97.85	1.98	0.10	0.07
"	15	97.61	2.37	x	0.01

	Sample no.	Mole% $CaCO_3$	Mole% $MgCO_3$	Mole% $FeCO_3$	Mole% $MnCO_3$
Ford Fm. Tunstal Hills					
Reef base coquina					
Non-luminescent cement occluding	TS46/1	98.92	1.00	0.08	x
mollusc shell mould	2	99.26	0.71	0.01	0.02
"	3	99.39	0.61	x	x
Acicular, altered marine cement crust	4	98.26	1.46	0.13	0.15
on inner surface of mollusc shell	5	97.06	2.54	0.24	0.16
"	6	93.77	5.86	0.26	0.11
"	7	98.92	0.82	0.13	0.12
"	8	93.59	6.39	0.02	x
"	9	97.25	2.66	0.02	0.07
Non-luminescent cement overlying	10	98.26	1.74	x	x
altered marine cement crust	11	98.66	1.34	x	x
"	12	98.62	1.29	0.07	0.02
"	13	99.44	0.55	x	0.01
"	14	99.30	0.63	0.07	x
"	15	99.28	0.65	0.05	0.02
Coarse, pore filling, zoned orange-	16	98.42	1.20	0.13	0.25
luminescent cement	17	98.18	0.87	0.48	0.47
"	18	98.39	0.85	0.36	0.40
"	19	98.87	0.82	0.18	0.13
"	20	98.89	0.86	0.07	0.17
"	21	99.07	0.71	0.12	0.10
"	22	98.89	0.87	0.10	0.14
"	23	98.83	0.92	0.07	0.18
"	24	99.48	0.38	0.01	0.13
"	25	99.17	0.31	0.24	0.28
"	26	99.03	0.85	x	0.12
"	27	98.26	0.91	0.44	0.38

	Sample no.	Mole% $CaCO_3$	Mole% $MgCO_3$	Mole% $FeCO_3$	Mole% $MnCO_3$
Dawsons Plantation					
Microspar, clasts within calcirudite	TS20/13	98.63	1.23	0.09	0.04
within debris flow conglomerate	14	98.97	1.03	x	x
"	15	98.42	1.49	0.05	0.04
"	16	98.62	1.26	0.04	0.07
High Moorsley Quarry					
Microspar, within uniform calcite	TS94/24	98.82	0.83	0.16	0.18
mudstone	25	98.68	1.09	0.13	0.09
"	26	98.52	1.16	0.19	0.13
"	32	98.65	0.72	0.33	0.30
"	33	98.49	1.06	0.28	0.17
Faecal (?) pellet within limestone	TS94/29	98.66	0.95	0.22	0.17
	30	98.57	0.92	0.33	0.18
"	31	98.70	0.83	0.27	0.19
Houghton Quarry					
CL zoned microspar, within	TS23/11	99.57	0.07	0.08	0.29
fossiliferous limestone	18	98.91	0.49	0.37	0.23
"	19	98.80	0.68	0.27	0.24
"	20	98.51	0.85	0.35	0.29
"	35	99.02	0.60	0.28	0.27
"	36	99.00	0.68	0.20	0.12
CL zoned, orange-luminescent	TS23/32	98.22	0.98	0.59	0.21
cement nucleating off zoned	33	98.36	0.98	0.46	0.19
microspar, fossiliferous limestone	34	97.62	1.39	0.40	0.59
Ralsby Quarry					
Microspar, isolated limestone	TS74/3	98.28	1.43	0.18	0.11
nodule within partially	4	98.33	1.53	0.07	0.07
dolomitized limestones above the	5	98.05	1.75	0.15	0.05
main limestone	TS74/37	98.45	1.00	0.44	0.11
"	38	98.51	1.05	0.26	0.17
"	39	98.46	1.16	0.21	0.17
"	40	98.40	1.18	0.33	0.09
"	41	98.49	1.28	0.23	x
"	42	98.42	1.31	0.16	0.11
"	43	98.76	0.87	0.26	0.11
Microspar, isolated limestone	TS1/1	98.98	0.78	0.14	0.09
nodule within partially	2	99.06	0.69	0.17	0.08
dolomitized limestones below the	3	98.93	0.89	0.15	0.02
main limestone					

	Sample no.	Mole% $CaCO_3$	Mole% $MgCO_3$	Mole% $FeCO_3$	Mole% $MnCO_3$
Raisby Quarry					
LC concretionary calcite	TS74/52	98.69	1.06	0.13	0.12
"	53	98.19	0.96	0.62	0.23
"	54	98.22	1.09	0.54	0.14
"	44	98.17	1.17	0.49	0.17
"	45	98.59	1.08	0.24	0.09
"	47	98.59	1.11	0.17	0.13
"	48	98.50	1.07	0.27	0.16
"	19	98.00	1.63	0.25	0.12
"	20	98.46	1.28	0.20	0.06
"	21	98.52	1.29	0.12	0.07
"	22	97.87	1.82	0.16	0.15
"	23	98.20	1.44	0.26	0.10
"	24	98.26	1.38	0.24	0.12
Dull orange-luminescent zone of	TS74/26	97.30	1.25	1.06	0.38
scalenohedral calcite, overgrowing	27	98.14	0.86	0.68	0.32
the terminations of LC concretion	28	97.38	1.27	0.92	0.43
calcite crystals	29	99.16	0.10	0.44	0.31
"	30	98.19	1.10	0.51	0.20
Bright orange-luminescent zone of	TS74/31	98.64	1.08	0.08	0.20
scalenohedral calcite overgrowing	32	98.65	1.09	x	0.26
the terminations of LC concretion	33	98.38	1.01	0.13	0.48
calcite	34	98.37	1.08	0.10	0.45
"	35	98.21	1.05	0.40	0.34
"	36	98.86	0.93	0.11	0.09
Orange-luminescent calcite,	TS74/49	99.09	0.77	0.06	0.08
cementing a pore after dissolution	50	98.09	0.97	0.57	0.37
of a foraminifera from within LC	51	97.91	0.72	0.86	0.50
concretionary calcite					
HC dolomite within inter-concretion	TS74/1	54.92	43.83	1.11	0.13
porosity of LC concretions. Some	55	51.60	39.03	8.65	0.72
crystals poikilitically enclosed	56	53.44	44.12	2.29	0.14
within SO dolomite crystals.	58	54.00	45.10	0.76	0.14
"	59	53.24	44.27	2.32	0.17
"	60	55.03	43.60	1.19	0.17
"	61	54.23	42.93	2.60	0.24
SO dolomite, overgrowing corroded	TS74/2	53.35	37.72	8.30	0.63
HC crystals within inter-concretion	62	50.88	39.84	8.70	0.59
porosity of LC concretions	63	52.31	36.94	10.02	0.73
"	64	52.14	40.09	7.09	0.69
"	65	55.54	38.45	5.53	0.58
"	66	55.09	39.47	4.98	0.46
"	67	54.68	38.41	6.39	0.51
HC dolomite crystal enclosed within	TS74/18	51.99	44.43	3.25	0.33
LC concretionary calcite					

	Sample no.	Mole% $CaCO_3$	Mole% $MgCO_3$	Mole% $FeCO_3$	Mole% $MnCO_3$
Finely Crystalline Replacive					
(FCR) dolomite					
FCR dolomite, borehole E3a, 352.70m	11m/14	53.25	40.05	6.12	0.58
"	15a	53.76	35.38	10.14	0.71
"	15b	53.26	31.50	14.21	1.03
"	16	53.29	37.36	8.79	0.57
"	19	54.23	35.98	9.10	0.69
"	20	52.25	46.60	1.02	0.13
"	21	52.26	38.39	8.71	0.64
FCR dolomite, associated with calcitized	AA28/1	52.62	46.81	0.51	0.06
dolomite, borehole W8, 279.45m	9	53.00	46.69	0.20	0.11
"	11	52.17	47.66	0.16	0.02
"	12	54.67	44.59	0.66	0.08
FCR dolomite replacing coated grain,	TS58/14	50.32	48.92	0.70	0.05
Hurworth Place borehole, 148.98m	15	49.83	46.29	3.73	0.15
"	16	51.03	48.34	0.51	0.12
"	17	51.33	47.72	0.60	0.15
"	18	51.73	47.80	0.33	0.14
"	19	50.67	48.46	0.66	0.21
"	21	52.02	47.66	0.14	0.19
"	22	51.81	47.50	0.53	0.16
FCR dolomite, mimic of echinoderm	TS23/3	51.25	46.09	2.37	0.29
fragment, fossiliferous turbidite, Houghton	4	50.82	48.02	1.07	0.09
Houghton Quarry	5	52.29	46.58	1.00	0.14
"	6	51.03	47.72	1.07	0.18
"	7	51.31	47.57	0.94	0.19
"	8	50.99	48.05	0.84	0.12
FCR dolomite, breccia clast, tectonic/	TS7/2	50.81	49.06	0.08	0.05
dissolution breccia above the main	3	49.86	49.92	0.18	0.04
limestone, Raisby Quarry	4	50.03	49.76	0.11	0.10
"	5	49.69	50.12	0.13	0.06
"	6	50.57	49.14	0.21	0.08
"	7	50.54	49.30	0.10	0.06
"	8	49.58	50.12	0.24	0.06
"	9	49.71	50.07	0.17	0.06
"	14	49.90	49.90	0.17	0.03
"	15	49.80	50.00	0.13	0.06
"	17	50.14	49.65	0.20	0.01
"	18	49.91	49.87	0.16	0.06
FCR dolomite, breccia clast, tectonic/	TS8a/1	49.33	50.54	0.08	0.05
dissolution breccia above the main	18	49.88	50.00	0.08	0.04
limestone, Raisby Quarry	19	50.30	49.51	0.13	0.06
"	20	49.69	50.20	0.07	0.04
"	21	50.33	49.20	0.37	0.10
"	29	49.68	50.13	0.12	0.07
"	30a	50.05	49.85	0.10	x
"	30b	48.89	50.83	0.20	0.08
"	31	49.20	50.22	0.47	0.11
"	32	48.55	51.16	0.20	0.09
"	33	49.58	49.99	0.37	0.07
FCR dolomite, breccia clast, tectonic/	TS8b/10	50.17	49.62	0.17	0.04
dissolution breccia above the main	11	49.62	50.15	0.20	0.03
limestone, Raisby Quarry	12	50.11	49.70	0.16	0.02
"	13	49.92	49.90	0.18	x
"	14	51.13	48.75	0.06	0.06
"	15	50.13	49.53	0.26	0.08
"	16	50.74	49.09	0.12	0.05
"	17	50.62	49.31	0.06	0.01
FCR dolomite, associated with calcite	TS74/1	54.92	43.83	1.11	0.13
concretion and ferroan dolomite cements,	55	51.60	39.03	8.65	0.72
Raisby Quarry	56	53.44	44.12	2.29	0.14
"	58	54.00	45.10	0.76	0.14
"	59	53.24	44.27	2.32	0.17
"	60	55.03	43.60	1.19	0.17
"	61	54.23	42.93	2.60	0.24
FCR dolomite, associated with ferroan	TS64/15	49.17	47.86	2.60	0.37
dolomite cements, above the main limestone,	16	51.44	45.53	2.70	0.33
Thickley Quarry	17	51.26	45.66	2.78	0.30
"	18	51.38	45.79	2.52	0.32
"	19	51.08	45.98	2.62	0.32

	Sample no.	Mole% $CaCO_3$	Mole% $MgCO_3$	Mole% $FeCO_3$	Mole% $MnCO_3$
CL zoned FCR dolomite, Tynemouth	TS38/37	48.79	50.76	0.23	0.23
Casle Cliff turbidite sandstone matrix	39	49.13	50.49	0.20	0.17
"	41	49.26	50.25	0.27	0.23
"	43	48.95	50.64	0.23	0.18
"	44	49.03	50.64	0.17	0.17
"	45	49.36	50.20	0.28	0.17
"	49	49.41	50.20	0.44	0.13
Pervasive Pressure Solution (PPS) dolomite					
PPS dolomite, replacing calcitiezd	AA28/3	52.01	47.74	0.26	x
dolomite, W8 borehole, 279.45m	4	51.80	46.20	1.90	0.10
"	5	53.38	44.95	1.51	0.16
"	6	51.30	48.19	0.44	0.07
PPS dolomite, contact of main limestone	TS1/5	51.60	45.06	3.09	0.25
with underlying FCR dolostones,	6	50.82	35.19	12.88	1.11
Raisby Quarry	8	51.74	39.46	8.14	0.66
"	9	50.43	42.78	6.34	0.45
"	10	51.78	44.05	3.76	0.41
"	11	51.03	37.71	10.31	0.95
"	12	51.06	40.41	7.77	0.76
"	14	51.65	44.18	3.85	0.32
"	15	47.88	43.85	7.61	0.66
"	16	50.91	39.96	8.44	0.69
"	17	51.85	39.56	7.93	0.66
"	18	51.60	39.55	8.13	0.72
Ferroan dolomite cements					
Ferroan dolomite cement,	11m/3	52.18	46.58	1.03	0.31
borehole E3a, 352.70m	4	52.44	40.70	6.26	0.60
"	5	52.94	37.29	9.23	0.55
"	6	54.28	36.06	9.08	0.58
"	21	54.98	35.55	8.82	0.65
"	22	52.88	30.19	15.56	1.36
"	23	53.02	35.51	10.62	0.84
"	24	52.48	40.76	6.21	0.55
"	26	52.26	44.28	3.20	0.26
"	27	52.08	45.98	1.76	0.19
"	28	51.32	46.43	1.99	0.26
"	29	51.93	47.13	0.81	0.14
"	31	50.99	47.88	1.03	0.11
"	32	51.44	47.75	0.69	0.12
"	33	50.36	48.65	0.87	0.11
"	34	52.10	45.97	1.70	0.23
"	35	52.42	45.25	2.12	0.21
"	36	50.96	47.96	0.94	0.14
"	37	50.61	45.90	3.19	0.31
"	38	53.01	41.35	5.18	0.46
"	39	53.22	34.10	11.53	1.14
Ferroan dolomite cement syntaxially	TS58/6	50.44	41.82	7.47	0.27
overgrowing an echinoderm	7	50.25	45.64	3.96	0.15
fragment, Hurwoth Place borehole, 148.98m	8	50.01	45.78	4.06	0.15
"	9	50.83	43.83	5.16	0.18
Ferroan dolomite cement associated	TS23/22	51.63	33.28	13.62	1.46
with mimic FCR dolomitized	23	51.87	30.89	15.70	1.54
echinoderm fragments, Houghton Quarry	24	50.34	35.47	12.93	1.25
"	25	51.36	47.46	1.01	0.18
"	26	51.50	47.66	0.71	0.13
"	27	52.23	41.94	5.14	0.69
"	28	51.18	32.98	14.40	1.43
"	29	51.88	28.88	17.54	1.70
"	30	50.41	47.74	1.65	0.20
"	31	50.89	46.77	2.08	0.25
Ferroan dolomite cement associated	TS74/2	53.55	37.72	8.30	0.63
with calcite concretion, Raisby Quarry	62	50.88	39.84	8.70	0.58
"	63	52.31	36.94	10.02	0.73
"	64	52.14	40.09	7.09	0.69
"	65	55.54	38.45	5.53	0.58
"	66	55.09	39.47	4.98	0.46
"	67	54.68	38.41	6.39	0.51
Ferroan dolomite cement (saddle dolomite)	TS64/4	53.30	44.03	2.47	0.21
lining calcite cemented porosity,	5	53.46	43.70	2.60	0.24
Thickley Quarry	6	54.03	43.35	2.39	0.23

	Sample no.	Mole% $CaCO_3$	Mole% $MgCO_3$	Mole% $FeCO_3$	Mole% $MnCO_3$
Dolomitized anhydrite					
Dolomitized anhydrite, debris flow clast,	15m/10	49.85	49.73	0.36	0.06
High Moorsley Quarry	11	49.06	50.04	0.77	0.13
	12	49.05	50.62	0.25	0.08
Dolomite cement associated with	15m/1	49.44	50.40	0.10	0.05
dolomitized anhydrite, debris flow,	2	49.16	50.37	0.39	0.07
High Moorsley Quarry	5	50.05	49.73	0.16	0.05
"	6	50.00	49.75	0.18	0.08
"	7	49.80	49.79	0.30	0.11
"	8	48.72	50.89	0.28	0.10
"	9	48.28	50.91	0.66	0.15
"	14	48.44	51.29	0.17	0.10
"	15	49.60	50.06	0.28	0.06
"	16	49.12	50.70	0.11	0.07
"	17	49.11	50.65	0.22	0.02
"	18	49.73	50.13	0.09	0.05
"	19	50.36	49.56	0.06	0.02
"	20	49.30	50.04	0.63	0.03
"	21	49.43	50.49	0.06	0.03
"	22	49.33	50.55	0.09	0.03
"	23	49.67	50.12	0.17	0.05

Sample description	Mole% $CaCO_3$	Mole% $MgCO_3$	Mole% $FeCO_3$	Mole% $MnCO_3$
Calcitized dolomite				
Embayed dolomite (ED) texture				
W8 borehole				
AA28/2	98.65	1.26	0.05	0.04
7	98.88	1.06	0.04	0.02
8	98.87	0.97	0.12	0.04
13	98.62	1.31	0.02	0.05

Sample description	Mole% CaCO3	Mole% MgCO3	Mole% FeCO3	Mole% MnCO3
Field House Quarry				
Calcite cementing a GC cavity after sulphate				
Luminescent equant calcite cement				
7	98.96	0.62	0.18	0.25
8	99.54	0.36	0.05	0.05
9	99.65	0.17	0.09	0.09
10	99.49	0.38	0.04	0.09
11	99.24	0.45	0.14	0.17
12	98.94	0.28	0.53	0.24
13	99.09	0.31	0.36	0.23
14	99.32	0.46	x	0.22
Non-luminescent columnar calcite cement				
15	97.25	2.15	0.01	0.59
16	98.07	1.88	x	0.05
1	98.27	1.69	x	0.04
2	98.18	1.78	0.04	x
3	98.10	1.86	x	0.05
4	98.02	1.92	0.06	x
5	97.96	2.02	0.02	x
6	97.79	2.20	x	0.01
Frenchmans Bay				
Traverse through a calcite cemented GC cavity after sulphate				
Finely crystalline dull orange-luminescent equant calcite				
TS27/1	98.80	0.36	0.68	0.16
2	98.51	0.54	0.74	0.20
3	98.75	0.47	0.62	0.15
4	99.02	0.30	0.54	0.14
5	98.79	0.32	0.74	0.14
6	98.81	0.40	0.64	0.15
Medium crystalline dull orange-luminescent equant calcite				
TS27/8	98.59	0.39	0.76	0.25
10	98.88	0.22	0.74	0.15
11	98.47	0.39	0.85	0.29
Coarsely crystalline dull orange-luminescent equant calcite				
TS27/12	98.05	0.89	0.84	0.21
16	98.91	0.38	0.51	0.19
18	98.91	0.47	0.51	0.12
19	98.12	0.80	0.82	0.25
20	98.29	0.69	0.83	0.19
21	98.96	0.26	0.52	0.25
22	99.12	0.31	0.41	0.15
23	99.03	0.27	0.44	0.26
24	97.85	1.86	0.21	0.08
25	97.73	2.18	0.05	0.04
26	97.87	1.99	0.03	0.11

Sample description	Mole% $CaCO_3$	Mole% $MgCO_3$	Mole% $FeCO_3$	Mole% $MnCO_3$
Transect through large zoned				
equant cement crystal				
Subzoned bright orange-luminescent				
calcite				
TS26/3	99.18	0.27	0.45	0.10
4	98.96	0.37	0.48	0.19
5	99.04	0.30	0.49	0.17
Dull orange-luminescent				
sector zone				
6	99.14	0.19	0.53	0.13
7	98.94	0.08	0.76	0.22
8	98.79	0.21	0.81	0.18
9	99.15	0.10	0.60	0.15
14	99.35	0.12	0.43	0.10
Subzoned bright orange-luminescent				
calcite				
10	98.36	0.67	0.71	0.26
11	99.09	0.33	0.41	0.17
12	99.21	0.30	0.36	0.13
Zoned bright orange-luminescent				
equant calcite				
TS26/1	98.88	0.27	0.63	0.22
13	99.18	0.29	0.41	0.11
17	99.04	0.31	0.49	0.15
18	99.01	0.37	0.48	0.13
24	99.08	0.34	0.47	0.11
25	99.18	0.28	0.38	0.15
26	99.02	0.35	0.51	0.12
27	99.10	0.25	0.52	0.13
Non-luminescent columnar calcite				
TS26/15	99.04	1.89	0.05	0.02
16	98.28	1.70	0.02	x
28	98.11	1.88	0.01	x
29	97.66	2.31	x	0.03
30	98.28	1.65	0.04	0.03
31	97.87	2.06	0.06	0.01
Frenchmans Bay				
Calcite cementing a GC cavity				
after sulphate				
Medium orange-luminescent				
calcite				
TS15/27	98.81	0.39	0.57	0.23
28	98.99	0.37	0.46	0.17
29	98.88	0.08	0.80	0.23
35	99.08	0.16	0.52	0.23
36	99.31	0.08	0.46	0.15
37	99.00	0.19	0.55	0.26
Subzoned bright orange-luminescent				
calcite				
TS15/31	97.79	1.69	0.28	0.24
32	97.94	1.67	0.09	0.29
33	97.92	1.77	0.08	0.22
34	98.03	1.79	0.06	0.11
38	97.78	1.86	0.24	0.12
39	97.95	1.48	0.19	0.37
40	98.11	1.47	0.17	0.25

Sample description	Mole% CaCO3	Mole% MgCO3	Mole% FeCO3	Mole% MnCO3
Haswell Moor Farm Quarry				
Traverse through calcite cementing				
a GC cavity after sulphate				
Bright orange-luminescent				
evaporite-replacive calcite				
TS108/15	99.31	0.44	x	0.25
16	99.39	0.33	x	0.28
17	99.21	0.45	0.07	0.27
18	99.45	0.34	0.02	0.19
19	99.37	0.38	x	0.25
20	99.42	0.40	x	0.18
Medium orange-luminescent				
calcite cement				
TS108/21	98.66	0.92	0.02	0.40
22	98.62	1.00	x	0.39
23	98.60	0.99	0.01	0.40
24	98.59	0.95	0.02	0.44
25	98.67	0.89	0.04	0.40
26	98.67	0.94	x	0.38
Dull orange-luminescent 'fir-				
tree' sector zone				
TS108/27	99.90	0.09	x	0.01
28	99.78	0.15	0.05	0.02
29	99.87	0.03	x	0.10
30	99.87	0.09	x	0.04
31	99.84	0.12	0.02	0.02
Medium orange luminescent host				
calcite to the sector zone				
TS108/32	99.57	0.20	0.03	0.20
33	99.45	0.23	0.08	0.24
34	99.44	0.31	x	0.25
35	99.27	0.35	0.05	0.33
Dull orange-luminescent calcite				
TS108/12	99.31	0.21	0.31	0.16
13	99.41	0.18	0.17	0.23
14	99.20	0.20	0.36	0.24
Bright orange-luminescent				
calcite				
TS108/1	97.92	1.42	0.15	0.52
2	98.12	1.26	0.14	0.48
3	97.93	1.40	0.12	0.55
4	97.75	1.51	0.18	0.56
Non-luminescent columnar calcite				
TS108/5	97.73	2.21	0.05	0.01
6	97.79	2.16	0.05	x
7	98.03	1.93	0.04	x
8	98.30	1.70	x	x
Bright orange-luminescent				
subzone within non-luminescent				
TS108/9	97.16	2.31	x	0.53
10	97.60	2.15	0.02	0.23

Sample description	SiO2	Al2O3	CaO	MgO	K2O	Fe2O3	Na2O
Frenchmans Bay							
Internal sediment 'rafts'							
within equant calcite cement							
of a GC cavity after sulphate							
TS27/13	43.21	19.41	12.68	2.08	4.90	4.87	0.51
14	32.45	3.19	18.92	2.78	0.60	2.50	0.87
TS26/20	8.27	10.29	9.78	4.09	2.47	3.38	0.34
21	7.09	4.69	18.79	12.52	0.85	4.47	0.09
22	11.27	6.16	12.80	8.74	1.09	6.09	0.18

Sample description	Mole% CaCO3	Mole% MgCO3	Mole% FeCO3	Mole% MnCO3
Chilton Quarry				
Calcite cementing a fluorite-mineralized cavity after sulphate				
Dull orange-luminescent calcite				
TS73/1	99.45	0.35	0.08	0.13
2	99.47	0.33	0.07	0.13
3	99.53	0.24	0.17	0.06
17	99.59	0.18	0.12	0.11
Non-luminescent calcite with bright orange hairline subzones				
TS73/5	96.84	3.09	0.04	0.03
6	96.51	3.10	x	0.40
Non-luminescent calcite				
TS73/7	97.49	2.48	0.03	x
8	97.15	2.79	0.02	0.04
9	97.29	2.67	0.03	0.01
10	97.18	2.81	x	0.01
11	97.62	2.30	0.06	0.02
12	97.12	2.81	0.03	0.04
Bright orange-luminescent subzone within non-luminescent calcite				
TS73/13	96.87	2.32	0.04	0.77
14	96.78	2.39	0.05	0.78
15	96.72	2.60	0.04	0.64
16	96.37	2.81	0.06	0.76
Dawsons Plantation				
Calcite cementing inter-clast porosity within a debris flow conglomerate				
TS20/1	99.41	0.58	0.01	x
2	99.04	0.89	x	0.07
3	98.47	1.53	x	x
4	98.46	1.46	0.08	x
5	98.83	1.16	x	0.01
6	98.93	1.03	0.04	0.01
7	99.05	0.88	0.04	0.03
8	98.86	1.10	0.04	x
9	98.87	1.07	0.01	0.05
10	98.38	1.55	0.06	0.01
11	98.60	1.37	0.02	0.01
12	98.71	1.24	0.05	x
High Moorsley Quarry				
Traverse through a calcite crystal cementing inter-clast sulphate dissolution porosity within a dolomitic debris flow				
Zoned orange-luminescent calcite cement				
15m/32	97.01	2.92	0.02	0.05
33	96.74	3.15	0.01	0.10
34	96.94	2.98	0.01	0.07
35	97.59	2.22	0.07	0.13
36	97.50	2.43	0.02	0.05
37	97.11	2.78	0.01	0.10
38	97.07	2.85	0.02	0.06
39	97.09	2.83	0.06	0.02

Sample description	Mole% $CaCO_3$	Mole% $MgCO_3$	Mole% $FeCO_3$	Mole% $MnCO_3$
High Moorsley Quarry traverse (cont.)				
15m/40	97.25	2.65	0.02	0.08
41	97.37	2.56	x	0.07
42	97.26	2.62	0.07	0.05
43	97.51	2.42	x	0.07
44	97.18	2.66	0.05	0.11
45	97.27	2.64	0.06	0.03
46	97.30	2.55	0.05	0.10
47	97.39	2.55	0.01	0.05
48	97.42	2.46	0.03	0.09
Non-luminescent calcite cement				
15m/24	96.59	3.41	x	x
25	96.69	3.31	x	x
26	96.32	3.68	x	x
27	96.62	3.36	x	0.02
28	96.48	3.44	x	0.08
29	96.21	3.72	0.07	x
30	96.46	3.51	x	0.03
Houghton Quarry				
Traverse through calcite cementing				
a cavity after sulphate				
Non-luminescent calcite				
TS111/1	99.81	0.11	x	0.08
2	99.66	0.25	0.03	0.06
Dull orange-luminescent calcite				
TS111/3	98.80	0.38	0.61	0.21
4	98.92	0.30	0.55	0.23
5	98.90	0.22	0.60	0.27
6	99.07	0.17	0.44	0.32
7	99.25	0.48	0.13	0.14
8	98.92	0.66	x	0.42
Bright orange-luminescent calcite				
TS111/9	98.85	0.91	0.02	0.22
10	98.79	0.91	x	0.30
11	98.86	0.98	x	0.16
12	98.91	0.90	0.03	0.16
23	98.88	0.98	x	0.14
24	98.89	0.94	x	0.17
25	98.33	1.43	0.01	0.23
26	98.16	1.62	x	0.21
27	98.43	1.32	0.02	0.23
28	98.59	1.17	x	0.24
Non-luminescent calcite				
TS111/13	97.93	2.07	x	x
14	97.65	2.26	0.08	0.01
15	97.91	2.09	x	x
16	97.97	2.00	0.03	x
17	98.05	1.90	0.05	x
18	98.02	1.92	0.03	0.03
19	98.23	1.68	0.09	x
20	98.12	1.85	x	0.03
21	98.19	1.69	0.11	0.01
22	98.32	1.65	0.03	x

Sample description	Mole% $CaCO_3$	Mole% $MgCO_3$	Mole% $FeCO_3$	Mole% $MnCO_3$
Quarrington Quarry				
Calcite cementing a barite-mineralized cavity after sulphate				
Bright orange-luminescent calcite				
5	98.21	1.35	0.04	0.40
6	98.31	1.30	x	0.39
7	98.34	1.29	0.02	0.35
8	98.19	1.43	x	0.38
Medium orange-luminescent calcite				
9	98.87	1.02	0.02	0.09
10	99.05	0.88	x	0.08
11	98.79	1.05	0.03	0.13
12	99.02	0.85	0.01	0.12
Subzoned orange-luminescent calcite				
13	99.56	0.32	0.06	0.07
14	99.29	0.59	0.02	0.10
15	99.49	0.42	0.03	0.05
16	99.38	0.47	0.05	0.10
Dull orange-luminescent calcite				
17	99.37	0.54	0.02	0.07
18	99.24	0.60	x	0.15
19	99.24	0.69	x	0.06
20	99.30	0.57	0.01	0.11
21	99.09	0.61	0.04	0.25
22	99.64	0.28	0.02	0.05
23	99.58	0.31	0.03	0.08
24	99.61	0.28	0.07	0.05
28	99.76	0.18	x	0.06
29	99.72	0.22	x	0.06
32	99.53	0.33	0.06	0.08
33	99.67	0.28	x	0.05
Very dull orange-luminescent calcite (sector zone)				
25	99.70	0.26	x	0.03
26	99.83	0.13	x	0.04
27	99.93	0.05	0.01	0.01
30	99.73	0.18	0.09	0.01
31	99.83	0.10	0.01	0.06
Raisby Quarry				
Traverse through calcite cementing a cavity after sulphate				
Equant bright orange-luminescent calcite				
TS56/1	99.10	0.30	0.40	0.20
2	98.74	0.35	0.61	0.31
3	99.15	0.28	0.39	0.17
4	99.20	0.40	0.30	0.10
5	99.05	0.47	0.35	0.13
6	99.17	0.36	0.35	0.11
7	99.23	0.28	0.36	0.13
8	99.01	0.41	0.45	0.12
9	99.08	0.32	0.47	0.13

Sample description	Mole% $CaCO_3$	Mole% $MgCO_3$	Mole% $FeCO_3$	Mole% $MnCO_3$
Raisby Quarry traverse (cont.)				
TS56/10	99.09	0.31	0.50	0.10
11	99.30	0.27	0.32	0.10
12	99.29	0.21	0.38	0.12
13	99.09	0.21	0.52	0.18
14	98.84	0.30	0.72	0.13
15	98.79	0.49	0.61	0.11
16	99.00	0.46	0.48	0.07
Dolomitc internal sediment				
TS56/17	92.40	6.67	0.91	0.01
22	80.11	19.06	0.81	0.02
Non-luminescent columnar calcite				
calcite				
TS56/18	98.98	0.97	0.03	0.02
19	99.01	0.95	0.04	x
20	98.93	1.02	0.05	x
21	98.91	1.06	0.03	x
23	98.65	1.30	0.03	0.02
24	98.72	1.26	x	0.02
25	98.73	1.22	0.05	x
26	98.77	1.16	0.02	0.05
27	98.87	1.07	0.04	0.02
28	99.01	0.96	x	0.03
29	98.94	0.99	x	0.07
30	99.01	0.94	0.02	0.03
31	98.52	1.42	x	0.06
32	98.65	1.31	0.04	x
33	98.40	1.55	0.03	0.02
34	98.60	1.40	x	x
35	99.41	0.53	0.03	0.03
36	99.41	0.54	0.01	0.03
37	99.34	0.61	0.03	0.01
38	99.38	0.62	x	x
39	99.32	0.58	0.10	x
40	99.34	0.62	0.01	0.03
Thickley Quarry				
Calcite cementing a sphalerite-				
mineralized cavity after sulphate				
Non-luminescent fracture-				
filling calcite cement				
1	98.16	1.76	0.08	x
2	98.45	1.53	0.02	x
3	98.28	1.67	0.02	0.03
Bright orange-luminescent				
calcite				
7	98.78	0.90	0.03	0.29
8	98.71	0.91	0.05	0.34
9	99.25	0.30	0.01	0.44
12	98.34	1.34	0.01	0.32
13	98.04	1.45	0.04	0.47
14	98.70	0.83	0.08	0.39
Non-luminescent calcite within				
leached saddle dolomite rhomb				
10	97.91	1.99	0.09	0.01
11	97.56	2.35	0.07	0.02

Sample description	Mole% $CaCO_3$	Mole% $MgCO_3$	Mole% $FeCO_3$	Mole% $MnCO_3$
Tynemouth Castle Cliff				
Calcite cementing dissolution				
porosity within a sandstone				
TS38/46	98.07	1.87	0.03	0.03
47	98.89	1.01	0.09	0.02
48	98.88	1.01	0.07	0.04
50	98.10	1.88	0.02	x
51	98.07	1.89	0.04	x
Raisby Quarry				
Calcite cementing inter-clast				
porosity within a dolostone breccia.				
Traverse through clast-rimming				
luminescent cement crystal				
TS5/3	99.25	0.53	0.01	0.21
4	99.35	0.38	0.05	0.22
5	99.22	0.53	x	0.25
6	97.77	1.92	0.04	0.28
7	99.26	0.28	0.29	0.16
8	99.19	0.26	0.40	0.15
9	99.17	0.24	0.43	0.16
10	99.19	0.43	0.25	0.12
11	99.63	0.35	x	0.02
12	99.51	0.44	0.03	0.02
14	98.85	1.14	0.01	x
Traverse through clast-rimming				
luminescent cement crystal				
TS5/20	95.48	3.91	0.50	0.10
21	99.12	0.29	0.42	0.16
22	99.32	0.08	0.45	0.15
23	99.45	0.14	0.23	0.18
24	99.18	0.23	0.45	0.14
25	99.40	0.19	0.31	0.10
26	99.18	0.37	0.27	0.18
27	99.42	0.29	0.06	0.23
28	99.64	0.35	0.01	x
29	99.27	0.35	0.34	0.05
Traverse through luminescent				
cement crystal				
TS5/30	99.36	0.37	0.01	0.26
31	99.49	0.31	x	0.19
32	99.54	0.26	x	0.19
33	99.50	0.36	x	0.14
34	98.53	1.06	0.03	0.38
35	99.17	0.51	0.01	0.30
36	98.93	0.66	0.03	0.38
38	98.92	0.71	0.04	0.33
39	99.00	0.66	0.03	0.31
40	99.18	0.47	0.02	0.33
41	98.92	0.75	0.03	0.30
42	99.03	0.64	x	0.32
43	99.45	0.39	x	0.16
EDR calcitized dolostone clast				
TS5/15	89.75	9.35	0.77	0.13
17	87.07	6.74	6.06	0.12
18	98.63	0.47	0.76	0.14
19	98.62	0.21	1.04	0.13

Sample description	Mole% $CaCO_3$	Mole% $MgCO_3$	Mole% $FeCO_3$	Mole% $MnCO_3$
Raisby Quarry dolostone breccia (cont.)				
EDR calcitized dolostone clast				
TS7/10	98.51	1.17	0.07	0.25
11	98.20	1.35	0.02	0.43
Traverse through dull orange-luminescent calcite cement crystal				
TS7/12	98.36	1.21	x	0.43
13	99.48	0.30	0.03	0.19
19	98.82	0.79	0.01	0.37
20	99.51	0.27	0.05	0.17
21	98.98	0.65	0.06	0.30
22	99.03	0.68	0.04	0.25
23	98.30	1.27	0.04	0.39
24	97.91	1.47	x	0.62
25	99.43	0.24	0.02	0.30
27	98.44	1.07	0.06	0.43
28	98.72	0.94	x	0.34
EDR calcitized dolostone clast				
TS9/47	79.14	18.89	1.78	0.19
49	88.95	7.17	3.78	0.10
50	87.93	11.29	0.73	0.06
51	96.09	2.64	1.22	0.05
52	99.52	0.27	0.21	x
48	99.28	0.24	0.38	0.10
Traverse through clast-rimming calcite cement sequence				
(Bright orange-luminescent)				
TS9/21	98.86	0.67	x	0.47
22	99.60	0.19	0.09	0.11
23	99.51	0.14	0.14	0.20
25	99.48	0.26	0.05	0.21
(Fir-tree sector zone)				
27	99.75	0.06	0.04	0.15
28	99.92	0.04	0.02	0.02
29	99.89	0.03	0.03	0.05
30	99.38	0.20	0.27	0.16
(Dull orange-luminescent)				
31	99.59	0.08	0.18	0.14
32	99.23	0.24	0.38	0.15
33	99.17	0.26	0.35	0.22
34	99.15	0.51	0.26	0.08
36	99.18	0.40	0.34	0.08
37	98.72	0.31	0.70	0.27
(Non-luminescent)				
38	99.50	0.37	0.12	0.01
39	99.57	0.35	0.03	0.05
(Dolomitic internal sediment)				
53	86.02	13.16	0.82	x
(Non-luminescent columnar calcite)				
54	98.37	1.46	0.15	0.02
55	98.36	1.49	0.10	0.05
56	98.17	1.58	0.26	x
57	97.80	1.58	0.62	x

Sample description	Mole% $CaCO_3$	Mole% $MgCO_3$	Mole% $FeCO_3$	Mole% $MnCO_3$
Raisby Quarry dolostone breccia (cont.)				
(Non-luminescent columnar calcite)				
TS9/58	98.80	1.11	0.09	x
60	98.85	1.14	x	0.01
61	98.62	1.27	0.07	0.04
62	98.55	1.36	0.03	0.06
Traverse through zoned clast-rimming calcite cement				
(Dull orange-luminescent)				
TS9/40	99.15	0.32	0.37	0.16
41	99.19	0.16	0.46	0.18
(Bright orange-luminescent)				
42	98.89	0.52	0.39	0.20
43	98.99	0.49	0.30	0.22
(Non-luminescent)				
46	99.52	0.30	x	0.18
4	98.79	0.96	0.14	0.10
5	98.66	1.16	0.11	0.07
6	98.53	1.41	x	0.06
Calcite cement -filled anhydrite cement pseudomorph (ACP texture)				
TS9/6	99.50	0.42	0.01	0.07
20	99.80	0.13	x	0.07
21	99.62	0.21	0.04	0.13
Host equant luminescent calcite crystal				
TS9/7	99.33	0.63	x	0.04
8	99.51	0.48	x	0.01
9	99.47	0.47	x	0.06

Appendix VI

AAS analysis

Atomic adsorption spectrophotometry (AAS) is a technique which quantifies the concentration of elements in acid solution, by measuring the amount of adsorbed light. The solution to be analysed is atomised by being introduced into a flame (produced by an air-acetylene or nitrous oxide-acetylene mixture), and a light of a specific spectrum is passed through the flame. Only atoms of the selected element will adsorb part of the light of specific wavelength. The amount of light adsorbed depends on the concentration of atoms of the specific element within the flame.

All AAS analyses were conducted using a Varian AA-575 AAS at the Department of Geology, University of Newcastle upon Tyne. Both nitrous oxide-acetylene and air-acetylene flames were used during analysis, depending on the element being analysed for. The steps in sample preparation were as follows:

1. Samples were accurately cut from slabs, and ground up in an agate,
2. Powders were accurately weighed (0.2 or 0.4g),
3. Both calcite and dolomite samples were dissolved in 30ml v/v Aristar® hydrochloric acid. The dolomite samples were gently heated to ensure full acid-digestion,
4. The main solutions were diluted prior to analysis:

Dilutions:

Calcites	x1	K
	x1.25	Ba, Sr
	x 10	Fe, Mg, Mn, Na
	x 200	Ca
Dolomites	x1	K
	x1.25	Ba, Sr
	x10	Fe, Mn, Na
	x 200	Ca, Mg.

For some AAS samples, insoluble residues were weighed by separating out the insoluble residues with filter paper, drying the filter paper, weighing the filter paper plus residue, removing the insoluble residue, and then re-weighing the filter paper. The difference between the two filter paper weights was taken as the weight of insoluble residue. However, this method gave very variable results, most of which are probably significantly inaccurate.

Both acid blanks, international and laboratory standards were analysed with the samples. The below table gives the mean difference of analytical totals between published standard results and analyses of six standards on the Newcastle AAS (B. Jones *pers. comm.*, 1989). These results can be taken as an indication of accuracy of the AAS analyses, for samples containing elements of similar concentrations:

	Mean value	Mean difference
Mole% $CaCO_3$	22.29	1.325
Mole% $MgCO_3$	10.42	0.262
Mole% $FeCO_3$	4.62	0.054
Mn ppm	810	2.4
Sr ppm	193	2
% Al_2O_3	12.92	0.035
% Na_2O	2.41	0.107
% K_2O	2.09	0.434
V ppm	270	23
Si ppm	9104	30

The detection limits for trace elements on the AAS (those expressed as ppm in the analyses) is approximately 5ppm, whereas the detection limits for major elements (expressed as %), is 0.05%. AAS results have been calculated in the same manner as ICP results (Appendix VII).

AAS results are tabulated together with ICP results in appendix VII. The number of AAS analyses is far fewer than ICP results.

Appendix VII

ICP analysis

ICP-OES (Inductively Coupled Plasma-Optical Emission Spectrometry) analysis was carried out at the department of Geology, Royal Holloway and Bedford New College, Egham, Surrey. ICP analysis involves passing a sample, in acid solution, through a plasma (a luminous volume of argon gas with atoms and molecules in an ionised state at a temperature of 6000-10000°K [Fairchild *et al.*, 1988]). As the solution passes through the argon plasma, it is completely atomised. Emission spectra from atomisation of the sample are analysed by a spectrometer to give abundances of the elements required. The principle of the analysis technique is similar to AAS, although ICP has the advantage of analysing many elements at one time.

All ICP and stable isotope samples were obtained by extracting 10-20mg samples of powder from polished slabs of rock with a modified dental drill. The precision of the sampling was a function of the diameter of the drill bits, the smallest allowing sampling down to 0.5-1mm resolution. Stages in the preparation of ICP samples were as follows:

1. Slabs of rock, a few centimeters in thickness were cut, and polished with carborundum powder,
2. The slabs were cleaned ultrasonically for 10-15 minutes,
3. The cleaned slabs were washed in distilled and de-ionised water, dried, and then the samples was extracted,
4. The powder was dried fully (110°C for two hours), and then weighed to 0.01mg.
5. The powders were dissolved in 5ml of 5% Aristar® hydrochloric acid, and then gently heated overnight, to ensure full acid digestion. Both acid blanks and standard samples were prepared at the same time, with the same acids.

After ICP analysis, the remaining few ml of solution was carefully drawn off, leaving a small amount of solution containing any insoluble residues. Vials containing insoluble residues were then fully dried, evaporating off the remnant solution, and then weighed. The insoluble residues were then cleaned out of the vials and the vials were re-weighed. The difference between the two vial weights was taken as the weight of insoluble residue. The detection limit for insoluble residues using this technique was approximately 0.1mg (i.e., 0.5 - 1 wt%). However, analytical accuracy, owing to the very small weights involved, was probably only ±0.3-0.4 mg (i.e., 1.5-4 wt%). This procedure for insoluble residue determination was done for most, although not all analysis runs.

The carbonate analysis programme, which was used for most analysis runs, gave data for 22 elements, expressed either as ppm element or as % oxide. The oxides (Al_2O_3, CaO, Fe_2O_3, K_2O, MgO, Na_2O, P_2O_5) were all quoted to the nearest 0.01%, and down to 0.01%

(i.e., 100ppm [which is thus their effective detection limits]). Trace elements (Ba, Cr, Cu, Li, Mn, Nb, Ni, Sc, Sr, Ti, V, Y, Zn, Zr), were all quoted to the nearest ppm, and down to 1ppm. In practise, many of the elements were unsuitable, probably owing to interference between lines, and gave substantial readings even on acid blank and Specpure® calcite analyses. Thus, these elements (Co, Cr, Cu, Li, Ni, Nb, Sc and Zn) are not quoted. Additionally, P_2O_5 was not detected during any analysis runs. Owing to contamination of the samples by flakes of metal abraded from the dental drill during sampling, Ti and Zn also were unusable. Thus, the analyses of only 11 elements are quoted in this thesis.

Calculation of results.

All results of the eleven elements were firstly calculated as a percentage of the sample weight (10-20mg). In addition, at this stage, it was necessary to correct down some of the calcium totals, as the ICP over-read on Ca, especially with regard to pure calcite and limestone samples. Correction was done by recalculating on the basis of Specpure calcite data, and on one analysis run Specpure dolomite data also. Additionally, the Specpure samples were analysed every twelve analyses to help correct for machine drift during the duration of the analysis run. Machine drift was considerable during some analysis runs, at least with respect to Ca (Fig. A7.1).

One problem with expressing analytical totals as weight %, is that variable amounts of insoluble residues within the samples (whose precise quantity is difficult to determine), make the accurate comparison of analytical totals between samples difficult. This is especially marked in the Raisby Formation when trying to compare the geochemistry of limestones (minimal insoluble residue) and dolostones (commonly significant insoluble residue). To get round this problem, all AAS and ICP data has been normalised to 100 % acid-soluble carbonate. Thus, Ca, Mg, Fe, Mn and Sr are all expressed as a percentage of pure carbonate (calcite or dolomite). These data have further been recalculated to 100 mole% carbonate. This is the most useful way in which to express the carbonate data, as it gives a measurement of the relative abundance of various elements within the carbonate lattice. This is important, as carbonate elements have greatly different atomic weights (Ca=40.08, Mg= 24.305). Expressing the data in this way also allows the stoichiometry of dolomite analyses to be directly calculated. All electron microprobe data has also been normalised to 100 mole% Ca, Mg, Fe and Mn carbonate, to allow direct comparison with AAS and ICP data. In effect, this correction procedure only makes a significant difference to the Ca values of limestone and calcite samples, and the Ca and Mg totals of dolomite analyses.

Non-carbonate minor and trace elements (Ba, Al_2O_3, Na_2O, K_2O, V and Y) are presented as weight %, as they do not occur in significant quantities within the carbonate lattice, and are commonly directly related to the weight of insoluble residues. Abridged details of these correction procedures are outlined in Fairchild *et al.*, (1988).

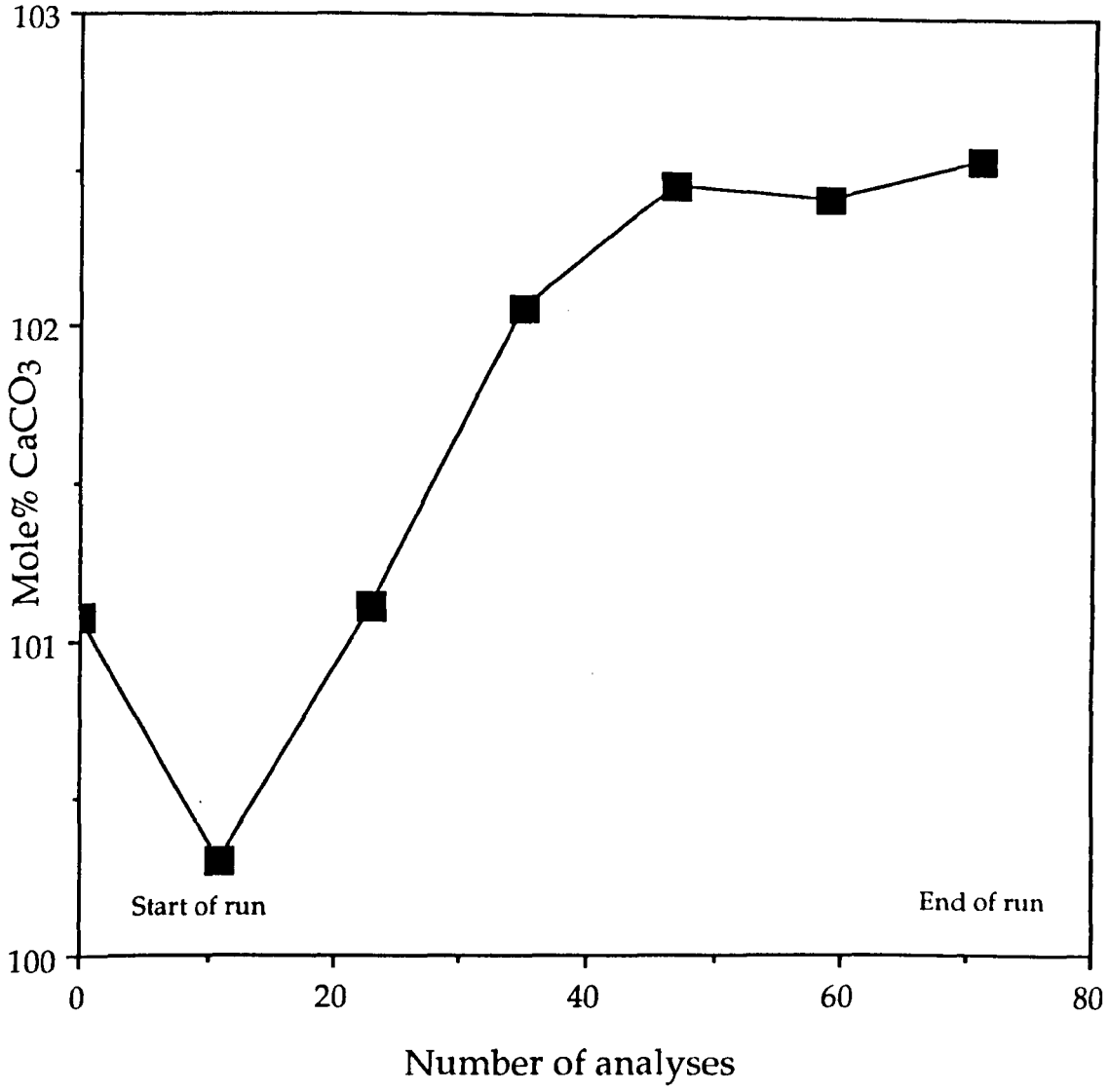

Fig. A7.1. Graph showing the drift in results for a Specpure calcite standard measured at intervals throughout one analysis run.

Standard data and analytical accuracies.

The data below gives the population standard deviation (σn) and mean values for Specpure calcite, Specpure dolomite, and KC11 standard data (a University of London standard), analysed during one ICP run:

	KC11 (n=6)		*Specpure calcite (n=6)*		*Specpure Dolomite (n=6)*	
	Mean	σn	Mean	σn	Mean	σn
Mole% $CaCO_3$	11.897	0.081	101.702	0.808	53.72	0.565
Mole% $MgCO_3$	11.120	0.048			47.13	0.367
Mole% $FeCO_3$	6.410	0.023				
Mn ppm	1080	4.6				
Sr ppm	363	1.6				
Ba ppm	490	2.9				
$\%Al_2O_3$	16.10	0.050				
$\%\ Na_2O$	3.34	0.018				
$\%\ K_2O$	2.20	0.013				
V ppm	210	1.2				
Y ppm	30	0.4				

These data may be taken to represent the precision of ICP analyses for elements within a sample at similar concentrations to those within the standards above. Thus, for calcite data, the precision of Ca values is ± 0.808 Mole%, and dolomites Ca ± 0.565 mole%, Mg ± 0.367 mole%. The KC11 data for the other elements are of similar concentrations of most Raisby Formation samples and so may be taken as representative of their analytical precision. These data in turn are in good agreement with published data on the accuracy of the Egham ICP (after Akhurst, 1988):

Mole%	$CaCO_3$	$MgCO_3$	$FeCO_3$	$MnCO_3$
KH standard	85.24	1.786	0.532	0.1269
ICP result	85.77	1.687	0.501	0.1128
Difference	0.53	0.099	0.031	0.0141
1C standard	89.69	1.0421	0.3444	0.0352
ICP result	88.98	1.0669	0.3319	0.0352
Difference	0.71	0.025	0.013	0.0

Akhurst (1988) quotes the reproducibility for trace element data as ±5ppm (where the value is < 100ppm) and ±5% of the value where > 100ppm. Reproducibility for major elements is quoted as 0.05 weight % where the value is 1% and ±1% where the value is 50%. This is in good agreement with the values derived from Specpure and KC11 standard data. The detection limits for the elements expressed as oxides is 0.25 wt% (250ppm) and for trace elements (the elements expressed in ppm) it is 5ppm.

In the following results tables, the carbonate analyses are shown first (normalised to 100 mole% acid-soluble carbonate), with additionally, Mn and Sr presented both as mole% carbonate and as weight ppm Mn and Sr, again normalised to 100 % acid-soluble carbonate. Where a reading of an element or oxide was not obtained, in the results tables it is signified by x, and where the element or oxide was not analysed for, by -. Carbon and oxygen stable isotope analyses of sub-samples of the ICP samples is also given in the following results tables. Isotope results are given in more detail in appendix IX.

	Sample no.	Wt (mg)	Mole% CaCO3	Mole% MgCO3	Mole% FeCO3	Mole% MnCO3	Mn ppm	Mole% SrCO3	Sr ppm
High Moorsley Quarry									
CL zoned brachiopod intraskeletal	1D	18.7	98.48	0.77	0.39	0.3498	1922	0.0096	84
cement from within nodular limestone.									
Raisby Quarry									
Non-luminescent, brachiopod	7E	20.5	99.07	0.70	0.03	0.0063	35	0.1905	1674
intraskeletal cement from limestone.									
Blotchy bright- and non-luminescent	67D	14.3	98.15	1.59	0.13	0.0772	424	0.0582	511
inclusion rich fracture filling calcite									
from isolated nodular limestone.									
Ford Fm. Tunstall Hills									
Intraskeletal cements from articulated	4D	19.8	98.52	1.06	0.15	0.1698	933	0.1006	884
bivalves and brachiopods, reef base	5D	20.0	98.62	0.72	0.29	0.3328	1828	0.0415	365
coquina.	6D	19.5	98.46	1.17	0.15	0.1917	1053	0.0231	203

	Sample no.	Wt (mg)	Ba ppm	% Al2O3	% K2O	% Na2O	V ppm	Y ppm	% I.R.	$\delta^{13}C$ ‰	$\delta^{18}O$ ‰
High Moorsley Quarry											
CL zoned brachiopod intraskeletal	1D	18.7	13	x	x	0.05	8	13	x	2.4	-9.7
cement from within nodular limestone.											
Raisby Quarry											
Non-luminescent, brachiopod	7E	20.5	27	0.02	x	0.05	x	x	x	5.5	-1.0
intraskeletal cement from limestone.											
Blotchy bright- and non-luminescent	67D	14.3	42	0.04	x	0.04	x	x	x	-	-
inclusion rich fracture filling calcite											
from isolated nodular limestone.											
Ford Fm. Tunstall Hills											
Intraskeletal cements from articulated	4D	19.8	18	x	x	0.04	10	5	x	-	-
bivalves and brachiopods, reef base	5D	20.0	20	x	x	0.04	8	8	x	-	-
coquina.	6D	19.5	51	x	x	x	10	5	x	-	-

		Sample no.	Wt (mg)	Mole% CaCO3	Mole% MgCO3	Mole% FeCO3	Mole% MnCO3	Mn ppm	Mole% SrCO3	Sr ppm
Penshaw Hill Quarry										
Homogenous main limestone		32B	22.00	98.66	1.20	0.06	0.0554	783	0.0291	255
"		33B	20.50	96.68	2.98	0.18	0.1426	484	0.0233	204
Raisby Quarry										
Isolated limestone nodules		AA33	400.60	98.03	1.41	0.36	0.1167	641	0.0869	761
within partially dolomitized		AA73	400.00	98.54	0.77	0.52	0.0851	467	0.0903	791
limestones, directly below		71A	20.00	98.95	0.88	0.03	0.0701	385	0.0697	612
the main limestone unit		72A	21.00	98.88	0.96	0.03	0.0676	371	0.0594	522
"		73A	19.40	98.64	0.89	0.16	0.2722	1496	0.0368	323
"		93A	16.50	99.02	0.75	0.08	0.0855	470	0.0591	519
"		2B	20.70	96.98	2.61	0.22	0.1037	570	0.0827	727
Homogenous limestone, main		AA30	400.40	99.10	0.52	0.13	0.0259	142	0.2221	1946
limestone unit.		AA31	400.20	98.75	0.74	0.29	0.0379	208	0.1799	1576
"		AA32	400.00	98.71	0.98	0.09	0.0243	133	0.2012	1763
"		81A	12.00	97.68	0.53	0.03	1.4624	8034	0.2936	2580
"		82A	20.00	99.04	0.72	0.03	x	x	0.2074	1822
"		83A	9.10	99.06	0.71	0.03	x	x	0.1921	1688
"		6C	18.30	98.53	1.19	0.05	0.0085	47	0.2164	1896
"		33C	19.01	98.97	0.78	0.07	0.0602	331	0.1186	1039
"		34C	19.21	98.99	0.74	0.02	0.0059	33	0.2487	2179
"		35C	20.09	99.01	0.70	0.06	0.0318	175	0.1970	1724
"		36C	15.11	98.95	0.84	0.06	0.0343	188	0.1073	940
"		52C	20.48	98.87	0.92	0.05	0.0352	193	0.1335	1170
"		53C	20.67	99.04	0.69	0.08	0.0659	362	0.1237	1084
"		54C	18.62	98.99	0.81	0.05	0.0426	234	0.1023	896
"		55C	20.38	98.91	0.77	0.08	0.0438	241	0.1851	1622
"		41E	20.00	98.14	1.62	0.08	0.0251	138	0.1373	1206
Isolated limestone nodules		51B	20.00	98.20	1.50	0.13	0.0949	521	0.0720	631
within partially dolomitized		58B	19.20	97.94	1.85	0.08	0.0584	321	0.0625	547
limestones/dolostones above		60B	15.40	98.88	0.89	0.08	0.0512	281	0.0980	859
the main limestone unit.		61B	15.82	97.22	2.59	0.08	0.0755	415	0.0290	254
"		62B	21.74	98.02	1.80	0.10	0.0568	312	0.0270	237
"		65B	15.99	98.67	1.14	0.08	0.0521	286	0.0648	568
"		70B	18.72	98.11	1.70	0.03	0.0149	82	0.1480	1297
"		46C	18.50	98.87	0.97	0.07		190	0.0494	434
"		47C	19.50	98.43	1.38	0.10		211	0.0468	411
"		68D	14.00	98.34	1.27	0.16	0.1423	782	0.0848	734
Transect through colour-		59E	20.60	98.50	1.12	0.06	0.0291	160	0.2948	2583
banded limestone nodule		60E	19.50	98.80	0.80	0.03	0.0107	59	0.3652	3200

		Sample no.	Wt (mg)	Ba ppm	%Al2O3	%K2O	%Na2O	V ppm	Y ppm	Si ppm	% I.R.	$\delta^{13}C$ ‰	$\delta^{18}O$ ‰
Penshaw Hill Quarry													
Homogenous main limestone		32B	22.00	20	0.05	x	0.16	9	5	-	x	-	-
"		33B	20.50	39	0.10	0.02	0.12	12	5	-	2.40	-	-
Raisby Quarry													
Isolated limestone nodules		AA33	400.60	x	0.19	0.02	0.07	19	-	623	1.40	-	-
within partially dolomitized		AA73	400.00	x	0.16	0.02	0.06	x	-	504	1.13	-	-
limestones, directly below		71A	20.00	x	0.05	0.03	0.10	3	8	-	-	-	-
the main limestone unit		72A	21.00	x	0.05	0.02	0.12	3	7	-	-	-	-
"		73A	19.40	46	0.10	0.05	0.11	8	8	-	-	-	-
"		93A	16.50	x	0.12	0.03	0.18	x	9	-	-	-	-
"		2B	20.70	22	0.12	0.02	0.19	15	5	-	x	-	-
Homogenous limestone, main		AA30	400.40	x	0.09	0.01	0.07	19	-	175	2.65	-	-
limestone unit.		AA31	400.20	x	0.15	0.02	0.03	17	-	322	2.93	-	-
"		AA32	400.00	x	0.22	0.02	0.05	17	-	700	1.60	-	-
"		81A	12.00	x	0.08	0.04	0.25	x	4	-	-	-	-
"		82A	20.00	x	0.08	0.03	0.10	3	8	-	-	-	-
"		83A	9.10	x	0.05	x	0.22	x	6	-	-	-	-
"		6C	18.30	18	0.06	x	0.11	8	5	-	1.94	-	
"		33C	19.01	20	0.08	x	0.13	8	5	-	1.64	-	-
"		34C	19.21	14	0.05	x	0.08	8	3	-	x	-	-
"		35C	20.09	16	0.05	x	0.08	10	5	-	0.05	-	-
"		36C	15.11	18	0.03	x	0.06	10	3	-	x	-	-
"		52C	20.48	16	0.05	x	0.29	7	5	-	x	-	-
"		53C	20.67	13	0.10	x	0.08	7	5	-	x	-	-
"		54C	18.62	15	0.05	x	0.05	8	5	-	x	-	-
"		55C	20.38	18	0.22	x	0.20	10	5	-	x	-	-
"		41E	20.00	28	0.20	0.03	0.51	3	5	-	x	-	-
Isolated limestone nodules		51B	20.00	20	0.08	0.03	0.11	15	8	-	x	-	-
within partially dolomitized		58B	19.20	29	0.08	0.03	0.09	13	5	-	x	-	-
limestones/dolostones above		60B	15.40	26	0.10	x	0.09	13	3	-	x	-	-
the main limestone unit.		61B	15.82	27	0.03	x	0.06	6	6	-	2.53	-	-
"		62B	21.74	15	0.09	x	0.07	7	7	-	x	-	-
"		65B	15.99	20	0.06	x	0.06	16	6	-	x	-	-
"		70B	18.72	23	0.16	x	0.13	11	3	-	x	-	-
"		46C	18.50	67	0.16	x	0.08	8	5	-	x	-	-
"		47C	19.50	88	0.13	x	0.05	10	5	-	x	-	-
"		68D	14.00	32	0.07	x	0.04	18	14	-	x	-	-
Transect through colour-		59E	20.60	19	0.05	x	0.07	2	2	-	2.91	-	-
banded limestone nodule		60E	19.50	20	0.05	x	0.05	3	3	-	1.54	-	-

		Sample no.	Wt (mg)	Mole% CaCO3	Mole% MgCO3	Mole% FeCO3	Mole% MnCO3	Mn ppm	Mole% SrCO3	Sr ppm
Raisby Quarry										
"		61E	18.80	98.33	1.37	0.10	0.0756	415	0.1198	1050
"		62E	20.30	98.23	1.46	0.13	0.0849	466	0.0897	786
Transect from lower nodular										
limestone, through main										
limestone, into upper										
nodular limestone										
Lower nodular limestone		1B	19.40	98.93	0.83	0.10	0.0698	383	0.0720	631
Main Limestone		56B	18.90	98.83	0.94	0.07	0.0396	217	0.1222	1071
"		55B	19.20	98.76	1.05	0.07	0.0381	209	0.0821	720
"		54B	19.50	98.66	1.10	0.05	0.0207	114	0.1730	1516
"		57B	17.80	98.59	1.20	0.05	0.0324	178	0.1313	1150
Upper nodular limestone		45C	17.06	98.50	1.31	0.06	0.0816	448	0.0467	409
"		48C	19.21	96.48	3.24	0.14	0.1176	446	0.0281	246
Thickley Quarry										
Main homogenous limestone		63c	16.97	96.51	3.13	0.19	0.0999	549	0.0727	637
"		AA63	400.00	96.26	2.76	0.75	0.1678	922	0.0618	543
W15 borehole										
Limestone nodule 199.87m	Core	42E	19.60	97.07	2.52	0.23	0.0278	153	0.1465	1284
"	|	43E	19.50	97.21	2.49	0.22	0.0256	140	0.0601	527
"	Margin	44E	20.00	97.16	2.59	0.17	0.0332	182	0.0430	377
Transect through homogenous										
limestone										
"	251.23m	36E	20.00	98.19	1.64	0.10	0.0357	196	0.0345	303
"	258.1m	37E	19.20	97.44	2.36	0.12	0.0335	184	0.0402	353
"	266.10m	38E	19.50	98.17	1.67	0.07	0.0400	220	0.0462	406

		Sample no.	Wt (mg)	Ba ppm	%Al2O3	%K2O	%Na2O	V ppm	Y ppm	Si ppm	% I.R.	$\delta^{13}C$ ‰	$\delta^{18}O$ ‰
"		61E	18.80	27	0.05	x	0.05	13	11	-	2.66	-	-
"		62E	20.30	22	0.07	x	0.08	5	7	-	1.00	-	-
Transect from lower nodular													
limestone, through main													
limestone, into upper													
nodular limestone													
Lower nodular limestone		1B	19.40	28	0.10	0.03	0.20	13	5	-	x	5.0	-5.1
Main Limestone		56B	18.90	27	0.05	x	0.09	11	3	-	x	5.7	-3.9
"		55B	19.20	21	0.08	x	0.11	10	5	-	0.05	5.7	-4.5
"		54B	19.50	20	0.08	x	0.09	10	3	-	x	5.6	-3.2
"		57B	17.80	23	0.14	x	0.10	11	6	-	x	5.7	-3.6
Upper nodular limestone		45C	17.06	16	0.12	x	0.09	9	6	-	x	5.0	-5.7
"		48C	19.21	17	0.13	x	0.05	13	8	-	x	4.5	-7.1
Thickley Quarry													
Main homogenous limestone		63c	16.97	128	0.25	x	0.06	10	6	-	x	5.8	-3.1
"		AA63	400.00	x	0.19	0.04	0.06	20	x	574	5.00	-	-
W15 borehole													
Limestone nodule 199.87m	Core	42E	19.60	115	0.26	0.03	0.20	5	3	-	6.12	-	-
"	|	43E	19.50	174	0.31	0.05	0.11	5	5	-	6.15	-	-
"	Margin	44E	20.00	30	0.25	0.03	0.12	5	5	-	x	-	-
Transect through homogenous													
limestone													
"	251.23m	36E	20.00	18	0.10	x	0.30	5	3	-	1.50	6.0	-3.5
"	258.1m	37E	19.20	21	0.21	0.03	0.31	5	5	-	2.60	5.6	-3.1
"	266.10m	38E	19.50	18	0.10	x	0.18	3	3	-	x	5.5	-2.5

		Sample no.	Wt (mg)	Mole% CaCO3	Mole% MgCO3	Mole% FeCO3	Mole% MnCO3	Mn ppm	Mole% SrCO3	Sr ppm
Dawsons Plantation										
Limestone clasts of calcirudite		81D	18.90	98.58	1.20	0.05	0.0237	130	0.1413	1238
within debris flow		83D	19.60	98.56	1.30	0.05	0.0487	267	0.0389	341
"		8E	19.60	98.28	1.52	0.07	0.0297	163	0.1004	879
"		AA60	400.50	97.52	2.01	0.33	0.0965	530	0.0462	405
"		AA61	400.00	98.04	1.73	0.16	0.0420	231	0.0305	267
Host homogenous limestone to		AA62	400.40	95.97	3.39	0.48	0.1480	813	0.0235	206
debris flow conglomerate										
Houghton Quarry										
Homogenous limestone		AA68	400.00	97.34	2.14	0.37	0.1300	714	0.0216	189
"		27B	20.00	98.93	0.58	0.20	0.2715	1492	0.0169	148
"		28B	19.90	98.60	1.07	0.14	0.1711	940	0.0156	136
"		30B	19.20	98.99	0.55	0.18	0.2611	1435	0.0119	151
Transect through limestone	8.9cm	46E	20.20	98.27	1.60	0.09	0.0808	444	0.0252	220
bands alternating with	8.0cm	47E	20.40	97.75	2.01	0.12	0.0922	507	0.0230	201
partially dolomitized	6.3cm	50E	20.40	97.40	2.33	0.13	0.1152	633	0.0232	203
limestones associated with	4.4cm	53E	19.70	96.83	2.84	0.18	0.1258	691	0.0220	192
microstylolites.	3.7cm	54E	19.20	96.71	2.95	0.17	0.1383	760	0.0216	189
"	0.9cm	57E	19.00	98.62	1.21	0.07	0.0780	429	0.0244	214
"	0.0cm	58E	20.40	98.49	1.29	0.09	0.1031	567	0.0225	197
Transect through homogenous	0cm	38B	18.00	95.15	4.38	0.24	0.1938	1065	0.0340	298
limestone	8cm	40B	15.90	98.10	1.55	0.16	0.1555	854	0.0415	365
"	14cm	42B	11.50	97.62	2.08	0.14	0.1147	630	0.0480	422
"	22cm	44B	16.40	96.83	2.78	0.22	0.1145	629	0.0503	442
"	71cm	46B	20.00	98.69	0.97	0.14	0.1380	758	0.0582	511
"	78cm	47B	19.00	98.72	0.94	0.15	0.1313	721	0.0569	500
"	87cm	48B	16.40	98.75	0.93	0.13	0.1450	797	0.0518	455
"	128cm	49B	20.30	98.95	0.71	0.15	0.1722	974	0.0200	176
High Moorsley Quarry										
Homogenous limestone below		2D	19.20	98.72	0.84	0.20	0.2079	1142	0.0428	375
erosion surface		3D	19.70	98.74	0.87	0.15	0.1878	1032	0.0523	458
"		AA46	400.00	98.34	0.93	0.46	0.2138	1175	0.0550	482
Offerton Quarry										
Limestone associated with		AA66	400.00	97.06	2.29	0.46	0.1533	842	0.0332	292
partially dolomitized limestone										

		Sample no.	Wt (mg)	Ba ppm	%Al2O3	%K2O	%Na2O	V ppm	Y ppm	Si ppm	% I.R.	$\delta^{13}C$ ‰	$\delta^{18}O$ ‰
Dawsons Plantation													
Limestone clasts of calcirudite		81D	18.90	21	0.05	x	0.03	8	5	-	x	-	-
within debris flow		83D	19.60	41	0.05	x	0.02	8	5	-	x	-	-
"		8E	19.60	31	0.05	x	0.05	3	X	-	2.55	5.4	-2.0
"		AA60	400.50	45	0.37	0.04	0.05	x	-	1295	2.00	-	-
"		AA61	400.00	61	0.07	0.01	0.01	x	-	210	x	-	-
Host homogenous limestone to		AA62	400.40	41	0.08	0.11	0.06	25	-	147	0.50	-	-
debris flow conglomerate													
Houghton Quarry													
Homogenous limestone		AA68	400.00	56	0.06	0.01	0.04	x	-	210	1.10	-	-
"		27B	20.00	45	0.03	x	0.15	13	10	-	X	-	-
"		28B	19.90	35	0.03	x	0.15	13	8	-	x	-	-
"		30B	19.20	23	0.03	x	0.13	10	8	-	x	-	-
Transect through limestone	8.9cm	46E	20.20	61	0.07	x	0.05	7	5	-	1.94	-	-
bands alternating with	8.0cm	47E	20.40	17	0.05	x	x	2	2	-	x	-	-
partially dolomitized	6.3cm	50E	20.40	17	0.05	x	x	2	2	-	1.96	-	-
limestones associated with	4.4cm	53E	19.70	25	0.08	x	0.10	x	3	-	x	-	-
microstylolites.	3.7cm	54E	19.20	34	0.08	x	0.05	3	3	-	0.52	-	-
"	0.9cm	57E	19.00	16	0.03	x	x	x	3	-	3.16	-	-
"	0.0cm	58E	20.40	25	0.02	0.05		2	2	-	0.49	-	-
Transect through homogenous	0cm	38B	18.00	32	0.07	0.04	0.12	11	4	-	x	-	-
limestone	8cm	40B	15.90	41	0.28	0.09	0.57	13	3	-	x	4.5	-5.2
"	14cm	42B	11.50	52	0.39	0.13	0.78	13	4	-	x	-	-
"	22cm	44B	16.40	46	0.31	0.12	0.61	12	3	-	x	-	-
"	71cm	46B	20.00	20	0.05	x	0.15	10	8	-	0.50	4.2	-5.4
"	78cm	47B	19.00	21	0.08	x	0.16	11	8	-	2.60	-	-
"	87cm	48B	16.40	21	0.03	x	0.18	12	6	-	x	-	-
"	128cm	49B	20.30	20	0.05	0.03	0.15	10	10	-	x	-	-
High Moorsley Quarry													
Homogenous limestone below		2D	19.20	16	0.08	x	0.02	13	16	-	x	-	-
erosion surface		3D	19.70	15	0.08	x	0.02	13	15	-	x	3.3	-5.1
"		AA46	400.00	41	0.10	0.02	0.05	16	-	336	1.10	-	-
Offerton Quarry													
Limestone associated with		AA66	400.00	25	0.07	0.01	0.10	x	-	224	2.20	-	-
partially dolomitized limestone													

		Sample no.	Wt. (mg)	Mole% CaCO3	Mole% MgCO3	Mole% FeCO3	Mole% MnCO3	Mn ppm	Mole% SrCO3	Sr ppm
Houghton Quarry										
Transect through	9.4cm	45E	20.60	84.36	14.64	0.72	0.2703	1485	0.0179	157
microstylolite-associated	7.3cm	48E	19.90	76.35	22.51	1.24	0.6186	3399	0.0134	118
partially dolomitized	6.9cm	49E	20.40	83.45	15.26	0.90	0.3717	2024	0.0168	148
limestone. Height above	5.5cm	51E	20.30	82.11	16.48	0.97	0.4278	2350	0.0143	126
base of sample.	5.1cm	52E	19.50	83.59	15.13	0.91	0.3533	1941	0.0165	145
"	3.1cm	55E	19.60	82.55	16.18	0.85	0.4085	2244	0.0156	137
"	2.4cm	56E	20.60	84.15	14.55	0.90	0.3782	2078	0.0164	144
Microstylolite-associated		AA67	400.00	88.90	9.24	1.63	0.2296	1261	0.0131	115
partially dolomitized		29B	19.40	86.30	11.85	1.22	0.6198	3405	0.0118	104
limestone		39B	20.90	84.06	15.01	0.58	0.3259	1790	0.0245	215
"		41B	18.90	85.66	13.33	0.64	0.3317	1822	0.0314	275
"		43B	16.90	84.08	15.18	0.41	0.2936	1613	0.0345	302
"		45B	19.90	86.30	12.89	0.50	0.2762	1517	0.0352	308
"		50B	21.00	84.09	13.74	1.67	0.4848	2663	0.0154	135
Penshaw Hill Quarry										
Partially dolomitized		35B	17.50	58.04	41.60	0.19	0.1615	887	0.0088	77
limestone										
Raisby Quarry										
Partially dolomitized		AA34	400.00	89.88	7.36	2.44	0.2640	1451	0.0530	464
limestone interbedded		AA74	401.20	75.41	19.00	5.13	0.4386	2410	0.0170	149
with undolomitized		AA75	400.00	82.42	14.57	2.63	0.3420	1879	0.0380	333
nodular limestone, below		91A	18.40	78.93	17.96	2.66	0.4132	2270	0.0273	240
the main limestone unit.		92A	17.40	79.48	19.07	1.42	x	x	0.0291	255
"		3B	20.70	83.80	13.67	2.17	0.3232	1776	0.0372	326
"		4B	20.80	84.40	13.69	1.61	0.2449	1345	0.0462	405
Partially dolomitized		5B	19.90	69.76	27.80	1.91	0.5240	2879	0.0086	75
limestone, interbedded		59B	18.10	89.14	10.45	0.36	0.0654	359	0.0221	193
with un-dolomitized		63B	20.33	82.84	16.32	0.48	0.3391	1863	0.0960	172
nodular limestone, above		66B	20.29	74.86	23.60	0.98	0.5572	3061	0.0088	77
the main limestone unit.		71B	19.70	83.64	15.58	0.52	0.2311	1269	0.0285	250

		Sample no.	Wt. (mg)	Ba ppm	% Al2O3	% K2O	% Na2O	V ppm	Y ppm	Si ppm	% I.R.
Houghton Quarry											
Transect through	9.4cm	45E	20.60	61	0.07	x	0.05	7	5	-	1.94
microstylolite-associated	7.3cm	48E	19.90	141	0.10	x	0.03	13	3	-	4.52
partially dolomitized	6.9cm	49E	20.40	69	0.12	x	0.10	7	2	-	2.94
limestone. Height above	5.5cm	51E	20.30	76	0.12	x	0.02	10	2	-	x
base of sample.	5.1cm	52E	19.50	59	0.13	x	0.03	8	3	-	3.59
"	3.1cm	55E	19.60	79	0.10	x	0.03	8	3	-	3.06
"	2.4cm	56E	20.60	78	0.10	x	0.02	7	2	-	1.94
Microstylolite-associated		AA67	400.00	41	0.28	0.04	0.02	x	-	1015	7.20
partially dolomitized		29B	19.40	299	0.08	x	0.16	31	8	-	8.20
limestone		39B	20.90	72	0.12	0.05	0.10	14	5	-	4.30
"		41B	18.90	77	0.13	x	0.09	16	5	-	2.10
"		43B	16.90	59	0.12	x	0.09	15	3	-	3.60
"		45B	19.90	65	0.13	0.03	0.11	15	5	-	3.50
"		50B	21.00	98	0.14	0.02	0.08	26	7	-	6.20
Penshaw Hill Quarry											
Partially dolomitized		35	17.50	34	0.20	x	0.08	20	3	-	6.90
limestone											
Raisby Quarry											
Partially dolomitized		AA34	400.00	56	0.81	0.10	0.05	36	-	3892	6.20
limestone interbedded		AA74	401.20	56	0.75	0.11	0.05	16	-	4620	2.30
with undolomitized		AA75	400.00	56	0.77	0.12	0.04	17	-	3500	3.33
nodular limestone, below		91A	18.40	22	0.19	0.06	0.11	11	8	-	-
the main limestone unit.		92A	17.40	x	0.17	0.03	0.15	11	9	-	
"		3B	20.70	150	0.22	0.02	0.17	27	7	-	5.00
"		4B	20.80	50	0.22	0.05	0.15	26	7	-	10.00
Partially dolomitized		5B	19.90	55	0.25	0.03	0.18	28	5	-	7.50
limestone, interbedded		59B	18.10	28	0.28	0.06	0.08	17	6	-	5.00
with un-dolomitized		63B	20.33	97	0.17	x	0.05	10	7	-	7.38
nodular limestone, above		66B	20.29	173	0.20	x	0.05	12	7	-	9.86
the main limestone unit.		71B	19.70	65	0.15	x	0.05	15	5	-	11.68

		Sample no.	Wt (mg)	Mole% CaCO3	Mole% MgCO3	Mole% FeCO3	Mole% MnCO3	Mn ppm	Mole% SrCO3	Sr ppm
Raisby Quarry										
Radial transect through an	0.0cm	6C	18.30	98.53	1.19	0.05	0.0085	47	0.2164	1896
LC concretion, from nodular	2.0cm	7C	12.1	97.76	1.79	0.19	0.1797	987	0.0770	677
limestone (0cm) through	3.7cm	8C	12.3	97.74	1.73	0.24	0.2209	1214	0.0631	554
to outer margin of	4.4cm	9C	9.7	97.92	1.51	0.28	0.2435	1338	0.0544	478
concretion (8.35cm)	6.0cm	10C	15.3	98.22	1.19	0.28	0.2709	1488	0.0415	365
"	6.9cm	11C	8.3	98.13	1.35	0.26	0.2334	1282	0.0413	363
"	8.4cm	12C	12.8	98.08	1.49	0.20	0.1827	1003	0.0429	377
All of a small LC concretion		52B	14.8	97.87	1.77	0.20	0.1254	689	0.0359	315
growing off a limestone bed										
Radial profiles through a		13C	19.6	92.92	6.67	0.22	0.1621	890	0.0257	226
large, oblate, UNL		14C	17.6	93.65	6.03	0.20	0.0954	524	0.0265	233
concretion from the upper		15C	17.2	93.04	6.68	0.16	0.0981	539	0.0265	233
nodular limestone of Rasiby		16C	16.4	93.59	6.05	0.23	0.1008	554	0.0262	230
Quarry		17C	17.6	93.73	5.90	0.25	0.0894	491	0.0278	244
"		18C	15.5	93.82	5.76	0.30	0.0896	492	0.0273	240
"		19C	17.1	93.06	6.56	0.27	0.0848	466	0.0282	248
"		20C	15.2	90.94	8.66	0.28	0.0930	511	0.0314	276
"		21C	20.7	93.70	5.89	0.29	0.0875	481	0.0259	228
"		22C	21.8	93.28	6.36	0.19	0.1391	764	0.0306	269
"		23C	16.3	94.61	5.08	0.17	0.1133	623	0.0258	227
"		24C	17.7	93.10	6.56	0.21	0.0973	535	0.0273	240
"		25C	14.5	94.58	5.15	0.17	0.0757	416	0.0257	226
"		26C	20.9	94.00	5.66	0.15	0.1528	840	0.0299	263
"		27C	15.2	94.43	5.28	0.19	0.0711	391	0.0259	228
"		28C	18.2	92.74	6.88	0.25	0.0977	537	0.0258	227
"		29C	20.7	94.32	5.32	0.23	0.1004	552	0.0283	249
"		30C	18.3	93.88	5.76	0.18	0.1556	855	0.0259	228
"		31C	19.9	94.17	5.50	0.22	0.0851	468	0.0259	228
"		32C	18.9	92.46	7.12	0.21	0.1894	1041	0.0255	224

		Sample no.	Wt (mg)	Ba ppm	% Al2O3	% K2O	%Na2O	V ppm	Y ppm	% I.R.	$\delta^{13}C$ ‰	$\delta^{18}O$ ‰	UNL corrected Mn ppm	UNL corrected Sr ppm
Raisby Quarry														
Radial transect through an	0.0cm	6C	18.30	18	0.06	x	0.11	8	5	1.94	-	-	UNL concretion	data, corrected
LC concretion, from nodular	2.0cm	7C	12.1	23	0.08	x	0.08	4	12	2.61	5.2	-5.1	for dolomite	content, assuming
limestone (0cm) through	3.7cm	8C	12.3	22	0.08	x	0.08	8	16	x	-	-	UNL concretion	calcite=1.55
to outer margin of	4.4cm	9C	9.7	28	0.05	x	0.05	5	16	x	-		mole% MgCO3,	98.45 mole%
concretion. (8.35cm)	6.0cm	10C	15.3	21	0.03	x	0.06	7	16	x	4.2	-6.2	CaCO3, and Mn	(Dol.)=330ppm
"	6.9cm	11C	8.3	27	0.06	x	0.06	12	12	1.74	-	-	and Sr(Dol.)=	100ppm.
"	8.4cm	12C	12.8	25	0.08	x	0.08	8	12	x	4.9	-6.4		
All of a small LC concretion		52B	14.8	27	0.14	x	0.1	14	7	4.70	-	-		
growing off a limestone bed														
Radial profiles through a		13C	19.6	37	0.15	x	0.05	10	8	x	-	-	970	245
large, oblate, UNL		14C	17.6	30	0.11	x	0.06	9	9	x	-	-	552	250
concretion from the upper		15C	17.2	28	0.12	x	0.06	9	6	1.56	-	-	573	253
nodular limestone of Rasiby		16C	16.4	32	0.15	x	0.09	9	6	2.55	-	-	586	247
Quarry		17C	17.6	21	0.14	x	0.06	11	6	3.55	-	-	515	262
"		18C	15.5	21	0.19	x	0.06	10	6	8.07	-	-	515	258
"		19C	17.1	22	0.18	x	0.03	9	6	x	-	-	490	269
"		20C	15.2	28	0.23	x	0.03	13	7	x	-	-	551	311
"		21C	20.7	18	0.17	x	0.05	10	7	x	-	-	504	244
"		22C	21.8	45	0.14	x	0.05	9	7	1.47	-	-	824	292
"		23C	16.3	38	0.12	x	0.06	9	6	3.93	-	-	657	241
"		24C	17.7	24	0.17	x	0.06	11	8	x	-	-	568	260
"		25C	14.5	22	0.1	x	0.04	10	7	x	-	-	430	240
"		26C	20.9	42	0.12	x	0.07	10	7	x	-	-	901	283
"		27C	15.2	21	0.13	x	0.06	10	7	0.52	-	-	402	243
"		28C	18.2	26	0.14	x	0.05	11	6	x	-	-	572	246
"		29C	20.7	28	0.12	x	0.08	10	7	4.94	-	-	580	265
"		30C	18.3	42	0.14	x	0.05	8	8	x	-	-	919	244
"		31C	19.9	21	0.13	x	0.05	10	8	3.81	-	-	488	243
"		32C	18.9	49	0.16	x	0.11	11	8	13.33	-	-	1150	244

		Sample no.	Wt (mg)	Mole% CaCO3	Mole% MgCO3	Mole% FeCO3	Mole% MnCO3	Mn ppm	Mole% SrCO3	Sr ppm
Radial transect from nodular										
limestone, through UNL										
concretion, into partially										
dolomitized limestone										
Nodular limestone	0cm	45C	17.1	98.54	1.31	0.06	0.2207	214	0.0467	410
"	1.3cm	46C	18.5	98.87	0.97	0.07	0.1377	190	0.0494	434
"	2.3cm	47C	19.5	98.43	1.38	0.10	0.2289	211	0.0468	411
"	3.6cm	48C	19.2	96.54	3.24	0.14	0.0562	309	0.0280	246
UNL concretion	4.6cm	49C	19.6	80.34	18.76	0.56	0.0384	1257	0.0184	162
"	6.5cm	50C	16.9	77.10	22.27	0.48	0.0346	756	0.0171	150
Partially dolomitized	8.2cm	51C	16.1	65.12	34.04	0.61	0.0390	1212	0.0107	94
limestone										
Inter-LC concretion		5E	19.8	98.67	0.99	0.15	0.1900	1044	0.0132	116
porosity cemented by										
scalenohedral calcite crystals										
HC and SO dolomite intermixed		53B	16.9	67.24	29.04	3.18	0.5740	3153	0.0098	86
with scalenohedral calcite										
inbetween a large LC concretion										
Dolostone surrounding a		35E	17.4	53.53	39.10	6.17	1.1869	6521	0.0085	75
small LC concretion (mainly										
SO dolomite)										

		Sample no.	Wt (mg)	Ba ppm	% Al2O3	% K2O	%Na2O	V ppm	Y ppm	% I.R.	$\delta^{13}C$ ‰	$\delta^{18}O$ ‰	UNL corrected Mn ppm	UNL corrected Sr ppm
Radial transect from nodular limestone, through UNL concretion, into partially dolomitized limestone														
Nodular limestone	0cm	45C	17.1	64	0.12	x	0.09	9	6	x	5.0	-5.7		
"	1.3cm	46C	18.5	67	0.16	x	0.08	8	5	x	-	-		
"	2.3cm	47C	19.5	88	0.13	x	0.05	10	5	x	-	-		
"	3.6cm	48C	19.2	17	0.13	x	0.05	13	8	1.56	4.5	-7.1		
UNL concretion	4.6cm	49C	19.6	19	0.31	x	0.05	15	5	2.55	4.4	-6.0	1785	200
"	6.5cm	50C	16.9	20	0.36	x	0.06	15	6	3.55	4.9	-5.5	1086	170
Partially dolomitized limestone	8.2cm	51C	16.1	16	0.37	x	0.06	19	6	8.07	4.0	-6.1		
Inter-LC concretion porosity cemented by scalenohedral calcite crystals		5E	19.8	23	0.1	x	x	3	8	7.58	2.9	-11.3		
HC and SO dolomite intermixed with scalenohedral calcite inbetween a large LC concretion		53B	16.9	24	0.12	x	0.11	24	9	7.10	-	-		
Dolostone surrounding a small LC concretion (mainly SO dolomite)		35E	17.4	17	0.29	x	x	14	11	x	4.3	-6.3		

Locality	Depth	Sample no.	Wt. (mg)	Mole% CaCO3	Mole% MgCO3	Mole% FeCO3	Mole% MnCO3	Mn ppm	Mole% SrCO3	Sr ppm
FCR Dolostones										
Borehole E3a										
Homogenous FCR Dolostones,	338.0m	11E	20.0	48.54	49.49	1.74	0.2282	1254	0.0082	72
incorporating some ferroan	338.0m	AA54	208.5	50.17	45.30	4.19	0.3366	1849	0.0080	70
dolomite cements	341.5m	AA51	200.8	50.38	45.88	3.47	0.2617	1438	0.0096	84
"	353.6m	10E	19.8	40.22	56.15	3.14	0.4708	2586	0.0109	96
"	357.9m	AA49	201.5	53.69	41.26	4.63	0.4083	2243	0.0102	89
Borehole E4										
Homogenous FCR Dolostones,	472.7m	17E	20.1	48.52	49.86	1.44	0.1774	975	0.0072	63
silty at some depths	472.3m	18E	19.4	48.77	49.74	1.31	0.1701	935	0.0082	72
"	472.2m	19E	19.4	48.84	49.99	1.01	0.1517	833	0.0088	77
"	471.2m	20E	19.1	49.29	48.61	1.83	0.2639	1450	0.0100	87
"	470.2m	21E	19.3	49.56	48.04	2.13	0.2563	1480	0.0119	104
"	469.2m	22E	20.0	49.21	48.83	1.72	0.2288	1257	0.0092	81
"	468.1m	23E	19.7	48.77	49.30	1.70	0.2206	1212	0.0080	70
"	467.1m	24E	20.0	48.86	49.29	1.60	0.2496	1371	0.0099	87
"	466.1m	25E	19.9	49.25	48.81	1.73	0.2077	1141	0.0107	93
"	465.9m	26E	19.0	50.23	47.79	1.73	0.2336	1284	0.0145	128
"	465.1m	27E	18.8	49.81	48.17	1.78	0.2285	1255	0.0150	132
"	464.4m	28E	18.8	49.42	48.74	1.62	0.2126	1168	0.0123	108
Seaham borehole										
Homogenous FCR Dolostones	90.8m	74C	18.7	50.82	48.33	0.70	0.1452	798	0.0065	57
"	95.6m	73C	19.7	54.44	44.72	0.63	0.2004	1101	0.0094	82
"	98.5m	72C	17.3	51.82	47.02	1.00	0.1603	881	0.0075	66
"	102.6m	71C	19.5	51.15	47.78	0.86	0.2058	1131	0.0099	87
"	107.9m	70C	20.6	50.15	49.54	0.25	0.0440	242	0.0164	144
"	110.6m	69C	15.0	51.42	47.97	0.50	0.0983	540	0.0122	107
"	112.5m	68C	19.8	50.93	48.41	0.55	0.1025	563	0.0131	114
"	116.4m	67C	19.7	49.39	49.80	0.67	0.1306	717	0.0081	71

Locality	Depth	Sample no.	Wt.(mg)	Ba ppm	% Al2O3	% K2O	% Na2O	V ppm	Y ppm	Si ppm	% I.R.	$\delta^{13}C$ ‰	$\delta^{18}O$ ‰
FCR Dolostones													
Borehole E3a													
Homogenous FCR Dolostones,	338.0m	11E	20.0	30	0.03	x	0.08	10	x	-	1.50	6.3	-2.8
incorporating some ferroan	338.0m	AA54	208.5	-	-	-	0.11	-	-	-	35.00	-	-
dolomite cements	341.5m	AA51	200.8	-	-	-	0.13	-	-	-	5.00	-	-
"	353.6m	10E	19.8	34	0.07	0.19	1.09	17	5	-	4.83	5.5	-4.35
"	357.9m	AA49	201.5	-	-	-	1.64	-	-	-	9.00	-	-
Borehole E4													
Homogenous FCR Dolostones,	472.7m	17E	20.1	22	0.20	x	0.10	15	2	-	3.48	-	-
silty at some depths	472.3m	18E	19.4	26	0.15	x	0.08	18	3	-	1.55	5.6	-2.3
"	472.2m	19E	19.4	26	0.21	x	0.15	13	3	-	3.61	-	-
"	471.2m	20E	19.1	24	0.29	0.03	0.08	10	3	-	3.66	-	-
"	470.2m	21E	19.3	31	0.47	0.08	0.08	16	5	-	4.15	-	-
"	469.2m	22E	20.0	33	0.33	0.03	0.18	13	3	-	4.00	5.7	-3.1
"	468.1m	23E	19.7	33	0.28	0.03	0.20	13	3	-	2.54	-	-
"	467.1m	24E	20.0	28	0.63	0.13	0.28	13	5	-	9.00	-	-
"	466.1m	25E	19.9	68	0.05	x	0.05	8	3	-	2.01	-	-
"	465.9m	26E	19.0	29	0.16	x	0.05	11	3	-	2.11	-	-
"	465.1m	27E	18.8	32	0.24	x	0.05	13	3	-	3.19	6.1	-2.7
"	464.4m	28E	18.8	27	0.11	x	0.03	11	3	-	2.66	-	-
Seaham borehole													
Homogenous FCR Dolostones	90.8m	74C	18.7	274	0.08	x	0.27	16	3	-	3.74	5.7	-1.2
"	95.6m	73C	19.7	47	x	x	0.20	13	x	-	x	-	-
"	98.5m	72C	17.3	25	0.06	x	0.18	20	6	-	x	-	-
"	102.6m	71C	19.5	32	0.03	x	0.51	13	3	-	2.56	6.1	-1.8
"	107.9m	70C	20.6	13	0.02	x	0.05	10	x	-	x	-	-
"	110.6m	69C	15.0	15	0.03	x	0.07	13	x	-	x	-	-
"	112.5m	68C	19.8	11	0.03	x	0.36	13	4	-	x	-	-
"	116.4m	67C	19.7	11	0.03	x	0.18	15	3	-	x	6.0	-1.4

Locality	Depth	Sample no.	Wt. (mg)	Mole% CaCO3	Mole% MgCO3	Mole% FeCO3	Mole% MnCO3	Mn ppm	Mole% SrCO3	Sr ppm
Borehole W8										
Homogenous, FCR Dolostones	271.0m	14E	20.0	48.87	50.00	1.02	0.0996	547	0.0126	111
"	271.0m	AA37	200.0	51.01	47.46	1.39	0.1088	598	0.0148	130
"	276.6m	15E	20.6	61.09	38.01	0.77	0.1172	644	0.0140	123
"	286.0m	16E	20.2	49.68	49.92	0.32	0.0661	363	0.0177	155
"	284.4m	AA36	200.2	52.19	46.96	0.77	0.0628	345	0.0178	156
"	273.1m	AA27	200.7	56.11	42.63	1.13	0.1117	614	0.0193	169
"	273.2m	AA26	200.5	53.55	45.28	1.05	0.1003	551	0.0131	115
"	280.5m	AA40	200.0	60.95	37.39	1.52	0.1191	654	0.0122	107
"	281.2m	AA23	200.0	53.42	45.62	0.86	0.0823	452	0.0146	128
"	281.3m	AA22	201.7	53.01	45.75	1.14	0.0843	463	0.0235	206
"	281.4m	AA21	202.0	53.55	45.30	1.05	0.0863	474	0.0228	200
"	281.5m	AA20	200.0	53.44	45.12	1.31	0.1061	583	0.0148	130
"	283.0m	AA38	200.3	52.75	45.90	1.24	0.0955	525	0.0148	130
"	283.1m	AA41	200.8	56.58	42.11	1.18	0.1038	570	0.0195	171
"	286.1m	AA43	202.0	52.35	46.66	0.86	0.1108	609	0.0161	141
"	287.5m	AA28	200.6	51.76	46.64	1.46	0.1219	670	0.0164	144
"	287.7m	AA29	200.0	51.42	46.94	1.51	0.1028	565	0.0186	163
High Moorsley Quarry										
Transect through FCR	Margin	41C	17.1	49.88	49.37	0.63	0.1098	603	0.0136	119
dolostone isolated nodule	|	42C	16.5	49.91	49.27	0.67	0.1333	732	0.0090	79
"	|	43C	14.5	50.17	49.02	0.66	0.1400	769	0.0142	124
"	Margin	44C	17.2	50.05	49.13	0.67	0.1429	785	0.0113	99
Houghton Quarry										
Homogenous FCR Dolostones		21B	20.0	50.35	49.39	0.16	0.0907	498	0.0113	99
"		18B	17.1	49.91	49.80	0.21	0.0751	412	0.0064	56
"		17B	19.4	49.67	50.15	0.12	0.0495	272	0.0064	56
"		16B	19.0	49.73	50.09	0.13	0.0508	279	0.0069	61
"		15B	18.5	50.04	49.79	0.11	0.0368	202	0.0083	73
"		20B	21.9	50.01	49.80	0.13	0.0490	269	0.0130	114
"		19B	20.3	49.89	49.90	0.15	0.0455	250	0.0092	81
"		40D	20.5	52.55	44.96	2.04	0.4421	2429	0.0146	128

Locality	Depth	Sample no.	Wt.(mg)	Ba ppm	% Al2O3	% K2O	% Na2O	V ppm	Y ppm	Si ppm	% I.R.	$\delta^{13}C$ ‰	$\delta^{18}O$ ‰
Borehole W8													
Homogenous, FCR Dolostones	271.0m	14E	20.0	36	0.43	0.10	0.46	15	x	-	10.66	5.4	-1.0
"	271.0m	AA37	200.0	-	-	-	0.73	-	-	-	18.00	-	-
"	276.6m	15E	20.6	22	0.20	0.05	0.57	17	2	-	3.98	5.7	-4.1
"	286.0m	16E	20.2	34	0.50	0.11	0.13	11	5	-	3.70	5.7	-0.6
"	284.4m	AA36	200.2	-	-	-	0.40	-	-	-	30.00	-	-
"	273.1m	AA27	200.7	62	-	-	-	-	-	-	-	-	-
"	273.2m	AA26	200.5	31	-	-	-	-	-	-	-	-	-
"	280.5m	AA40	200.0	-	-	-	0.84	-	-	-	8.00	-	-
"	281.2m	AA23	200.0	37	-	-	-	-	-	-	-	-	-
"	281.3m	AA22	201.7	65	-	-	-	-	-	1960	-	-	-
"	281.4m	AA21	202.0	39	-	-	-	-	-	-	-	-	-
"	281.5m	AA20	200.0	x	-	-	-	-	-	-	-	-	-
"	283.0m	AA38	200.3	-	-	-	0.67	-	-	-	29.00	-	-
"	283.1m	AA41	200.8	-	-	-	0.38	-	-	-	5.00	-	-
"	286.1m	AA43	202.0	-	-	-	0.27	-	-	-	13.00	-	-
"	287.5m	AA28	200.6	64	-	-	-	-	-	-	-	-	-
"	287.7m	AA29	200.0	32	-	-	-	-	-	-	-	-	-
High Moorsley Quarry													
Transect through FCR	Margin	41C	17.1	22	0.06	x	0.06	15	6	-	x	5.6	-1.4
dolostone isolated nodule	|	42C	16.5	29	0.06	x	0.06	12	3	-	x	-	-
"	|	43C	14.5	36	0.10	x	0.07	17	3	-	x	-	-
"	Margin	44C	17.2	42	0.12	x	0.06	15	6	-	1.74	5.5	-1.9
Houghton Quarry													
Homogenous FCR Dolostones		21B	20.0	30	0.05	x	0.15	20	3	-	2.50	-	-
"		18B	17.1	32	0.06	x	0.18	18	x	-	x	-	-
"		17B	19.4	31	0.05	x	0.13	18	x	-	2.60	-	-
"		16B	19.0	47	0.08	x	0.16	18	x	-	2.60	-	-
"		15B	18.5	32	0.05	x	0.11	19	x	-	4.30	-	-
"		20B	21.9	39	0.07	x	0.13	16	2	-	1.80	-	-
"		19B	20.3	39	0.15	x	0.12	20	2	-	3.40	-	-
"		40D	20.5	2072	0.10	x	0.02	24	7	-	3.90	-	-

Locality	Depth	Sample no.	Wt.(mg)	Mole% CaCO3	Mole% MgCO3	Mole% FeCO3	Mole% MnCO3	Mn ppm	Mole% SrCO3	Sr ppm
Houghton Quarry		41D	16.7	52.62	44.83	2.13	0.4095	2250	0.0118	103
Homogenous FCR Dolostones		44D	19.6	54.01	43.17	2.31	0.5045	2772	0.0121	106
"		47D	18.7	53.39	44.58	1.61	0.4116	2261	0.0118	103
"		26B	17.5	53.23	45.90	0.64	0.2163	1188	0.0143	125
"		25B	17.0	55.56	43.07	1.09	0.2735	1503	0.0138	121
"		24B	17.3	50.72	48.38	0.70	0.1907	1048	0.0113	99
"		23B	19.7	50.51	48.21	0.86	0.4083	2243	0.0111	98
"		22B	20.3	50.41	48.78	0.67	0.1380	758	0.0107	94
"		72B		52.21	46.98	0.66	0.1424	782	0.0130	114
Penshaw Hill Quarry										
Homogenous FCR Dolostones		32B	20.8	51.10	48.60	0.20	0.0948	521	0.0135	118
"		34B	20.8	52.46	47.27	0.18	0.0831	484	0.0134	117
"		36B	21.0	49.92	49.63	0.31	0.1343	738	0.0068	60
"		37B	18.3	49.50	50.37	0.08	0.0409	225	0.0074	65
Quarrington Quarry										
Homogenous FCR Dolostones		67B	19.5	50.97	48.77	0.18	0.0740	407	0.0107	94
"		68B	17.9	52.00	47.73	0.18	0.0785	431	0.0090	79
Raisby Quarry										
Homogenous FCR Dolostones		13B	20.0	50.57	49.33	0.08	0.0206	113	0.0082	72
"		14B	21.8	49.50	50.40	0.06	0.0199	109	0.0077	67
"		1C	19.8	52.10	47.67	0.16	0.0565	311	0.0075	66
"		4C	20.6	50.77	49.09	0.09	0.0348	191	0.0149	131
"		2C	19.3	50.46	49.15	0.27	0.0376	207	0.0092	81
"		5C	14.4	50.68	49.10	0.14	0.0590	324	0.0144	126
"		18D	19.9	49.72	50.08	0.13	0.0509	280	0.0101	88
"		49D	19.6	48.78	51.02	0.14	0.0409	225	0.0106	93
"		53D	20.0	49.15	50.65	0.13	0.0596	327	0.0102	89
"		58D	20.4	48.63	51.15	0.16	0.0525	288	0.0110	96
"		56C	17.8	56.21	42.13	1.32	0.3306	1816	0.0135	118
"		6B	19.6	51.18	48.56	0.19	0.0546	300	0.0072	63
"		7B	21.0	54.64	44.81	0.39	0.1558	856	0.0120	105

Locality	Depth	Sample no.	Wt.(mg)	Ba ppm	% Al2O3	% K2O	% Na2O	V ppm	Y ppm	Si ppm	% I.R.	$\delta^{13}C$ ‰	$\delta^{18}O$ ‰
Houghton Quarry		41D	16.7	39	0.15	x	0.03	30	6	-	0.60	-	-
Homogenous FCR Dolostones		44D	19.6	839	0.15	x	0.02	23	8	-	3.60	-	-
"		47D	18.7	85	0.05	x	0.03	21	8	-	1.60	-	-
"		26B	17.5	114	0.14	x	0.14	43	6	-	8.00	-	-
"		25B	17.0	206	0.21	x	0.18	59	6	-	8.80	-	-
"		24B	17.3	116	0.12	x	0.12	38	3	-	4.00	-	-
"		23B	19.7	467	0.15	x	0.15	41	3	-	?	-	-
"		22B	20.3	91	0.15	0.02	0.15	27	2	-	x	-	-
"		72B		20	0.13	x	0.06	28	3	-	2.52	-	-
Penshaw Hill Quarry													
Homogenous FCR Dolostones		32B	20.8	26	0.19	0.02	0.15	19	2	-	1.90	6.0	-1.5
"		34B	20.8	34	0.24	0.05	0.07	19	5	-	11.00	-	-
"		36B	21.0	88	0.24	0.02	0.10	21	2	-	7.60	-	-
"		37B	18.3	46	0.08	x	0.06	16	x	-	x	5.9	-1.3
Quarrington Quarry													
Homogenous FCR Dolostones		67B	19.5	45	0.03	x	0.05	15	3	-	3.59	-	-
"		68B	17.9	29	0.06	x	0.08	14	3	-	x	-	-
Raisby Quarry													
Homogenous FCR Dolostones		13B	20.0	20	0.05	x	0.15	15	x	-	x	-	-
"		14B	21.8	18	0.05	x	0.13	14	x	-	x	-	
"		1C	19.8	49	0.03	x	0.05	13	3	-	x	5.2	-1.1
"		4C	20.6	72	0.07	x	0.10	12	2	-	x	-	-
"		2C	19.3	17	0.16	x	0.08	18	3	-	2.49	-	-
"		5C	14.4	26	0.17	x	0.07	14	3	-	x	-	-
"		18D	19.9	30	0.13	x	0.02	18	5	-	2.51	-	-
"		49D	19.6	23	0.10	x	0.02	18	5	-	x	-	-
"		53D	20.0	23	0.10	x	0.03	15	5	-	3.80	-	-
"		58D	20.4	20	0.12	x	0.03	17	5	-	3.90	-	-
"		56C	17.8	18	0.25	x	0.06	17	6	-	3.93	-	-
"		6B	19.6	140	0.05	x	0.20	15	x	-	1.00	-	-
"		7B	21.0	36	0.14	x	0.12	21	5	-	2.40	4.9	-3.3

Locality	Depth	Sample no.	Wt.(mg)	Mole% CaCO3	Mole% MgCO3	Mole% FeCO3	Mole% MnCO3	Mn ppm	Mole% SrCO3	Sr ppm
Raisby Quarry		8B	20.8	53.01	46.45	0.39	0.1392	765	0.0073	64
Homogenous FCR Dolostones		9B	18.7	51.68	48.39	0.33	0.1039	571	0.0122	107
"		124A	10.6	48.26	51.61	0.06	0.0624	343	0.0096	84
"		125A	11.8	48.32	51.63	0.05	x	x	0.0095	83
Thickley Quarry										
Homogenous FCR Dolostones		61C	14.2	52.17	46.95	0.76	0.1089	598	0.0138	121
"		62C	14.2	48.51	50.64	0.73	0.1117	614	0.0134	117
"		37C	15.8	52.15	46.36	1.24	0.2339	1285	0.0154	134
"		38C	17.6	52.16	46.03	1.51	0.2819	1548	0.0150	131
"		59C	18.5	49.92	48.62	1.18	0.2741	1506	0.0115	101
"		60C	19.3	49.22	49.50	1.05	0.2159	1186	0.0113	99
Ferroan dolomite cement										
Raisby Quarry										
Ferroan dolomite cement,		35E	17.4	49.02	35.81	5.65	1.0869	5972	0.0079	69
within inter-concretion										
porosity										
Dolomitized anhydrite										
High Moorsley Quarry										
Dolomitized anhydrite,		12E	19.6	48.50	51.13	0.28	0.0665	365	0.0162	142
pseudomorphing clasts within		13E	19.5	51.15	54.02	0.36	0.0840	437	0.0149	131
debris flow conglomerate										
Carboniferous										
Holy Island										
Dolostone		39C	15.5	53.20	42.93	3,52	0.3462	1902	0.0107	94
"		40C	15.3	53.09	43.09	3.45	0.3571	1962	0.0106	93

Locality	Depth	Sample no.	Wt.(mg)	Ba ppm	% Al2O3	% K2O	% Na2O	V ppm	Y ppm	Si ppm	% I.R.	$\delta^{13}C$ ‰	$\delta^{18}O$ ‰
Raisby Quarry		8B	20.8	34	0.14	x	0.15	22	2	-	6.70	-	-
Homogenous FCR Dolostones		9B	18.7	35	0.13	x	0.16	21	3	-	0.50	-	-
"		124A	10.6	24	0.05	x	0.19	5	5	-	-	-	-
"		125A	11.8	x	0.08	x	0.21	8	4	-	x	-	-
Thickley Quarry													
Homogenous FCR Dolostones		61C	14.2	26	0.53	x	0.08	34	8	-	x	6.1	-1.1
"		62C	14.2	44	0.46	x	0.12	19	4	-	4.94	-	-
"		37C	15.8	46	0.25	x	0.09	25	6	-	x	-	-
"		38C	17.6	30	0.20	x	0.09	23	6	-	x	-	-
"		59C	18.5	126	0.09	x	0.12	14	3	-	x	4.3	-2.3
"		60C	19.3	43	0.06	x	0.14	14	3	-	0.52	-	-
Ferroan dolomite cement													
Raisby Quarry													
Ferroan dolomite cement,		35E	17.4	17	0.29	x	x	14	11	-	x	-	-
within inter-concretion													
porosity													
Dolomitized anhydrite													
High Moorsley Quarry													
Dolomitized anhydrite,		12E	19.6	28	0.08	x	0.05	8	x	-	2.07	-	-
pseudomorphing clasts within		13E	19.5	25	0.05	x	0.05	8	x	-	1.50	-	-
debris flow conglomerate													
Carboniferous													
Holy Island													
Dolostone		39C	15.5	21	0.13	x	0.12	19	3	-	1.94	-	-
"		40C	15.3	25	0.13	x	0.22	20	7	-	2.61	-	-

	Sample no.	Wt(mg)	Mole%CaCO3	Mole%MgCO3	Mole%FeCO3	Mole%MnCO3	Mnppm	Mole% SrCO3	Srppm
Enclosed dolomite relic (EDR) calcitization									
Man Haven									
Calcitized uppermost Raisby	33D	20.10	95.63	3.95	0.25	0.1077	592	0.0674	590
Formation dolostones	34D	19.30	95.74	3.83	0.25	0.1110	610	0.0694	608
Calcitized lowermost Z2 collapse	35D	19.50	98.61	0.97	0.32	0.0887	487	0.0150	132
breccia	36D	20.70	98.42	0.94	0.53	0.0890	489	0.0156	136
Target Rocks, South Shields									
Calcitized bedded Raisby	37D	16.90	98.97	0.65	0.21	0.1517	833	0.0171	150
Formation dolostones	38D	18.90	98.57	0.95	0.30	0.1536	844	0.0156	137
"	39D	19.30	98.54	0.95	0.29	0.2001	1099	0.0164	144
Marsden Bay									
Calcitized Z2 collapse breccia									
Breccia clast	30D	18.50	98.78	1.06	0.05	0.0366	201	0.0630	552
Inter-clast matrix	31D	19.10	88.09	11.62	0.21	0.0703	386	0.0041	36
"	32D	20.20	72.23	27.40	0.28	0.0750	412	0.0062	54
Raisby Quarry									
Calcitized dolostone breccia clasts	11D	20.00	92.60	6.68	0.59	0.1091	599	0.0171	150
"	12D	19.90	94.97	4.32	0.55	0.1503	826	0.0140	123
"	24A	16.60	76.93	22.64	0.26	0.1553	853	0.0106	93
"	25A	20.50	94.18	5.24	0.44	0.1201	660	0.0141	124
"	34A	20.00	94.30	5.31	0.27	0.1025	563	0.0169	148
"	152A	20.70	87.23	12.23	0.40	0.1310	720	0.0105	92

	Sample no.	Wt(mg)	Ba ppm	%Al2O3	%K2O	%Na2O	V ppm	Y ppm	% I.R.	$\delta^{13}C$ ‰	$\delta^{18}O$ ‰
Enclosed dolomite relic (EDR) calcitization											
Man Haven											
Calcitized uppermost Raisby	33D	20.10	20	0.03	x	0.01	10	5	x	-0.1	-6.3
Formation dolostones	34D	19.30	21	0.03	x	x	10	5	x	-	-
Calcitized lowermost Z2 collapse	35D.	19.50	28	0.15	0.03	0.09	15	5	6.20	-0.2	-6.5
breccia	36D	20.70	48	0.24	0.05	0.11	19	5	9.70	-	-
Target Rocks, South Shields											
Calcitized bedded Raisby	37D	16.90	30	0.03	x	0.03	9	6	x	-	-
Formation dolostones	38D	18.90	27	0.08	x	0.11	13	8	4.80	-	-
"	39D	19.30	80	0.10	x	0.11	13	8	4.10	-	-
Marsden Bay											
Calcitized Z2 collapse breccia											
Breccia clast	30D	18.50	38	0.03	x	0.05	16	5	x	-	-
Inter-clast matrix	31D	19.10	42	0.11	x	0.08	16	3	0.50	-	-
"	32D	20.20	27	0.07	x	0.15	17	2	x	-	-
Raisby Quarry											
Calcitized dolostone breccia clasts	11D	20.00	30	0.03	x	x	13	5	3.50	-	-
"	12D	19.90	23	0.03	x	0.02	10	5	4.00	-	-
"	24A	16.60	102	0.03	x	0.12	3	6	-	-	-
"	25A	20.50	2	0.03	0.03	0.15	2	6	-	-	-
"	34A	20.00	65	0.03	0.03	0.12	5	3	-	-	-
"	152A	20.70	10	0.02	x	0.10	5	5	-	-	-

	Sample no.	Wt(mg)	Mole%CaCO3	Mole%MgCO3	Mole%FeCO3	Mole%MnCO3	Mnppm	Mole% SrCO3	Srppm
Crystallographically-selective (CS) calcitization									
Raisby Quarry									
Dolostone breccia clasts, marginally	122A	20.40	66.26	33.29	0.33	0.1057	581	0.0116	102
calcitized in zone-selective (CSa) style	123A	15.70	51.66	48.22	0.06	0.0447	246	0.0109	96
"	131A	20.00	91.63	8.14	0.03	0.1835	1019	0.0157	138
"	134A	20.00	84.16	15.58	0.06	0.1853	1018	0.0141	124
"	13D	20.00	71.38	28.29	0.21	0.1156	635	0.0124	109
"	14D	19.40	66.20	33.52	0.17	0.1022	561	0.0118	103
"	15D	20.00	74.66	25.01	0.18	0.1286	707	0.0132	116
"	16D	20.00	67.87	31.84	0.17	0.1084	596	0.0115	101
"	17D	19.40	56.74	43.06	0.11	0.0756	415	0.0104	91
"	24D	19.50	75.31	24.38	0.18	0.1167	641	0.0330	289
"	25D	12.10	85.01	14.50	0.27	0.2059	1131	0.0132	116
"	50D	19.70	79.29	20.33	0.27	0.1028	565	0.0122	107
"	51D	20.10	81.85	17.82	0.21	0.1138	625	0.0124	109
"	54D	20.00	60.01	39.75	0.16	0.0663	364	0.0110	96
"	59D	18.70	81.22	18.30	0.36	0.1100	604	0.0127	111
"	60D	20.00	87.59	11.97	0.30	0.1324	727	0.0133	117
Embayed dolomite (ED) calcitization									
Borehole W8									
Calcitized dolomite	101A	20.00	98.20	1.62	0.08	0.0704	387	0.0307	269
"	103A	21.00	94.98	4.79	0.13	0.0671	369	0.0306	268
"	29E	20.80	98.15	1.69	0.08	0.0450	247	0.0315	276
"	30E	19.60	97.82	2.03	0.08	0.0438	241	0.0304	266
Leached and cemented (LC) dolomite alteration									
Raisby Quarry									
Basal Ford Formation oolitic grainstones									
Calcite cemented corroded dolostone	73B	20.00	90.16	9.74	0.05	0.0302	166	0.0177	155
"	4E	20.50	83.53	16.26	0.15	0.0501	275	0.0104	91

	Sample no.	Wt(mg)	Ba ppm	%Al2O3	%K2O	%Na2O	V ppm	Y ppm	% I.R.	$\delta^{13}C$ ‰	$\delta^{18}O$ ‰
Crystallographically-selective (CS) calcitization											
Raisby Quarry											
Dolostone breccia clasts, marginally	122A	20.40	40	0.15	0.03	0.15	7	5	-	-	-
calcitized in zone-selective (CSa) style	123A	15.70	32	0.06	x	0.16	10	3	-	-	-
"	131A	20.00	45	0.05	x	0.10	3	5	-	-	-
"	134A	20.00	13	0.05	x	0.10	3	5	-	-	-
"	13D	20.00	35	0.08	x	0.02	15	5	1.00	-	-
"	14D	19.40	23	0.08	x	0.02	15	5	3.60	-	-
"	15D	20.00	43	0.08	x	0.02	13	5	0.50	-	-
"	16D	20.00	23	0.08	x	0.02	15	5	8.00	-	-
"	17D	19.40	44	0.05	x	0.02	15	5	4.00	-	-
"	24D	19.50	28	0.10	x	0.02	18	8	8.70	-	-
"	25D	12.10	479	0.17	x	x	17	12	12.40	-	-
"	50D	19.70	20	0.10	x	0.03	13	5	5.60	-	-
"	51D	20.10	22	0.08	x	x	12	7	6.00	-	-
"	54D	20.00	20	0.08	x	0.03	15	8	4.00	-	-
"	59D	18.70	29	0.13	x	0.03	13	5	8.00	-	-
"	60D	20.00	25	0.10	x	0.03	10	8	9.00	-	-
Embayed dolomite (ED) calcitization											
Borehole W8											
Calcitized dolomite	101A	20.00	x	0.03	0.10	0.40	3	5	-	-	-
"	103A	21.00	x	0.05	0.12	0.30	5	5	-	-	-
"	29E	20.80	19	x	x	0.05	2	2	0.48	5.5	-4.5
"	30E	19.60	26	x	x	0.02	3	3	x	5.5	-4.4
Leached and cemented (LC) dolomite alteration											
Raisby Quarry											
Basal Ford Formation oolitic grainstones											
Calcite cemented corroded dolostone	73B	20.00	24	0.03	x	0.05	5	x	x	-	-
"	4E	20.50	24	0.02	x	0.02	2	2	x	-1.7	-12.5

	Sample no.	Wt(mg)	Mole%CaCO3	Mole%MgCO3	Mole%FeCO3	Mole%MnCO3	Mnppm	Mole% SrCO3	Srppm
Ferroan dolomite alteration (FDA)									
Thickley Quarry									
Altered ferroan dolostone	65C	21.01	76.96	18.66	3.66	0.7148	3927	0.0064	56
"	66C	18.32	75.62	21.30	2.59	0.4812	2644	0.0074	65
Internal sediment infulling a cavity	64C	21.01	69.63	29.97	0.14	0.2471	1358	0.0053	46
within altered ferroan dolostone									

	Sample no.	Wt(mg)	Ba ppm	%Al2O3	%K2O	%Na2O	V ppm	Y ppm	% I.R.	$\delta^{13}C$ ‰	$\delta^{18}O$ ‰
Ferroan dolomite alteration (FDA)											
Thickley Quarry											
Altered ferroan dolostone	65C	21.01	273	0.26	x	0.08	18	8	13.33	-	-
"	66C	18.32	333	0.21	x	0.03	21	9	1.64	-	-
Internal sediment infulling a cavity	64C	21.01	155	0.26	x	0.05	5	x	3.81	-	-
within altered ferroan dolostone											

		Sample no.	Wt(mg)	Mole% CaCO3	Mole% MgCO3	Mole% FeCO3	Mole% MnCO3	Mnppm	Mole% SrCO3	Srppm
ECI calcitized evaporites										
Quarrington Quarry										
Small calcitized evaporite nodule		51A	20.00	98.50	1.32	0.05	0.1295	711	0.0089	78
"		52A	20.70	97.99	1.76	0.05	0.1900	1044	0.0081	71
Raisby Quarry										
Large calcitized evaporite nodule		96D	17.60	93.60	6.14	0.05	0.1876	1031	0.0167	146
"		97D	19.40	94.25	5.47	0.05	0.2077	1141	0.0153	134
"		98D	17.80	96.42	3.29	0.05	0.2230	1225	0.0138	147
"		99D	16.20	97.88	1.77	0.11	0.2343	1287	0.0155	136
"		100D	18.70	95.01	4.81	0.05	0.1016	558	0.0195	171
GC cavities after sulphates										
Field House Quarry	Cm from base									
Calcite cemented cavity after	4.6	74D	19.60	98.00	1.93	0.02	0.0460	253	0.0007	6
sulphate	3.7	75D	20.00	98.55	1.04	0.15	0.2369	1301	0.0259	227
"	2.6	76D	19.60	99.13	0.50	0.12	0.2329	1280	0.0114	100
"	1.7	77D	19.00	99.20	0.44	0.11	0.2388	1312	0.0112	98
"	1.1	78D	20.00	99.17	0.48	0.10	0.2390	1313	0.0111	97
"	0.5	79D	20.00	99.11	0.56	0.09	0.2276	1250	0.0109	96
Frenchmans Bay										
Calcite cemented cavity after	Top	86D	13.80	98.21	1.77	0.02	0.0021	12	0.0017	15
sulphate		87D	20.10	97.95	2.02	0.02	0.0134	74	0.0018	16
"		85D	14.90	97.50	2.43	0.06	0.0076	42	0.0020	18
"		91D	18.30	96.89	2.72	0.27	0.1148	631	0.0052	46
"		90D	19.80	98.34	0.98	0.49	0.1842	1012	0.0082	72
"		89D	20.00	98.48	0.95	0.39	0.1836	1009	0.0077	67
"	Base	88D	20.00	98.24	1.17	0.40	0.1865	1025	0.0078	68
Calcite cemented cavity after	Top	41A	18.30	98.13	1.85	0.02	x	x	0.0015	13
sulphate		42A	20.50	98.90	0.55	0.36	0.1890	1038	0.0102	89
"		43A	20.00	97.93	1.95	0.08	0.0346	190	0.0031	27
"	Base	44A	19.40	98.44	1.07	0.29	0.2006	1102	0.0035	31

		Sample no.	Wt(mg)	Ba ppm	%Al2O3	%K2O	%Na2O	V ppm	Y ppm	% I.R.	$\delta^{13}C$ ‰	$\delta^{18}O$ ‰
ECI calcitized evaporites												
Quarrington Quarry												
Small calcitized evaporite nodule		51A	20.00	25	0.30	x	0.73	2	22	-	-	-
"		52A	20.70	24	0.31	x	0.70	x	21	-	-	-
Raisby Quarry												
Large calcitized evaporite nodule		96D	17.60	23	0.03	x	x	11	6	x	-	-
"		97D	19.40	21	0.03	x	x	8	5	x	-12.1	-12.3
"		98D	17.80	20	0.03	x	x	8	8	x	-	-
"		99D	16.20	19	0.03	x	x	9	6	x	-	-
"		100D	18.70	24	0.03	x	x	8	11	x	-6.1	-13.1
GC cavities after sulphates												
Field House Quarry	Cm from base											
Calcite cemented cavity after	4.6	74D	19.60	46	x	x	x	8	3	x	-	-
sulphate	3.7	75D	20.00	233	0.03	x	0.02	10	8	x	-	-
"	2.6	76D	19.60	20	0.10	x	0.02	8	8	x	-	-
"	1.7	77D	19.00	18	0.08	x	0.02	8	8	x	-	-
"	1.1	78D	20.00	20	0.10	x	x	8	8	x	-	-
"	0.5	79D	20.00	20	0.10	x	0.02	8	13	0.20	-	-
Frenchmans Bay												
Calcite cemented cavity after	Top	86D	13.80	36	x	x	x	7	4	x	-8.0	-5.2
sulphate		87D	20.10	40	x	x	x	7	2	x	-	-
"		85D	14.90	47	x	x	x	10	3	x	-	-
"		91D	18.30	101	0.14	0.03	0.49	11	11	6.60	-	-
"		90D	19.80	40	0.18	0.05	0.61	10	20	5.10	-	-
"		89D	20.00	45	0.13	0.03	0.57	10	18	4.50	-	-
"	Base	88D	20.00	28	0.13	0.03	0.55	10	18	7.50	-	-
Calcite cemented cavity after	Top	41A	18.30	14	0.03	x	0.13	x	3	-	-	-
sulphate		42A	20.50	61	0.22	x	1.49	5	37	-	-	-
"		43A	20.00	25	0.08	x	0.12	x	8	-	-	-
"	Base	44A	19.40	10	0.08	x	0.16	3	13	-	-	-

		Sample no.	Wt(mg)	Mole% CaCO3	Mole% MgCO3	Mole% FeCO3	Mole% MnCO3	Mnppm	Mole% SrCO3	Srppm
Frenchmans Bay										
Calcite cemented cavity after		161A	20.00	97.93	1.98	0.02	0.0678	372	0.0014	12
sulphate		162A	19.40	98.55	0.81	0.44	0.1916	1053	0.0077	67
"		163A	21.00	97.74	1.75	0.39	0.1080	593	0.0060	53
Running Waters Quarry										
Calcite filled cavity after	Top	69D	19.80	97.95	1.72	0.05	0.2679	1472	0.0082	72
sulphate		70D	21.10	98.86	0.83	0.04	0.2458	1350	0.0182	159
"		71D	20.00	99.19	0.47	0.09	0.2311	1270	0.0203	178
"		72D	20.10	99.34	0.36	0.09	0.1943	1067	0.0174	152
"	Base	73D	19.00	99.19	0.53	0.09	0.1755	964	0.0152	133
Sherburn Hill Quarry										
Calcite cemented cavity	Top	101D	19.70	98.38	1.25	0.09	0.2624	1442	0.0112	98
after sulphate		102D	20.10	97.88	1.64	0.19	0.2794	1535	0.0103	90
		103D	19.60	97.74	1.58	0.40	0.2678	1471	0.0100	88
	Base	104D	15.20	98.36	1.35	0.07	0.2135	1173	0.0045	39
Pore filling calcite cements										
High Moorsley Quarry										
Calcite cements within a hematite-		94D	20.00	98.51	0.88	0.05	0.5382	2957	0.0136	119
mineralized dolostone breccia		95D	19.60	98.36	0.90	0.05	0.6840	3758	0.0143	125
Houghton Quarry										
Calcite cements within a		92D	16.70	97.83	1.63	0.09	0.4244	2332	0.0161	141
dolostone compaction breccia		93D	20.00	98.41	1.34	0.05	0.1893	1040	0.0079	69
Hetton le Hill Quarry										
Calcite cemented cavity after		61A	20.00	97.86	1.86	0.03	0.2197	1207	0.0354	310
gypsum		62A	19.40	99.59	0.15	0.03	0.2273	1249	0.0108	95
Quarrington Quarry										
Calcite cemented cavity after		6E	19.80	99.03	0.84	0.03	0.0540	297	0.0484	424
sulphate										

		Sample no.	Wt(mg)	Ba ppm	%Al2O3	%K2O	%Na2O	V ppm	Y ppm	% I.R.	$\delta^{13}C$ ‰	$\delta^{18}O$ ‰
Calcite cemented cavity after		161A	20.00	18	0.03	x	0.12	x	3	-	-	-
sulphate		162A	19.40	18	0.13	x	0.21	3	15	-	-	-
"		163A	21.00	40	0.19	x	0.26	2	9	-	-	-
Running Waters Quarry												
Calcite filled cavity after	Top	69D	19.80	261	x	x	x	8	5	x	-	-
sulphate		70D	21.10	294	0.02	x	x	7	17	x	-	-
"		71D	20.00	1355	0.05	x	0.07	8	18	2.50	-	-
"		72D	20.10	352	0.08	x	x	7	15	8.00	-	-
"	Base	73D	19.00	1281	0.05	x	x	8	16	7.40	-	-
Sherburn Hill Quarry												
Calcite cemented cavity	Top	101D	19.70		0.05	x	0.05	8	10	4.80	-	-
after sulphate		102D	20.10		0.08	x	0.10	7	10	7.50	-	-
		103D	19.60		0.05	x	0.05	10	10	3.60	-	-
	Base	104D	15.20		x	x	x	10	7	x	-	-
Pore filling calcite cements												
High Moorsley Quarry												
Calcite cements within a hematite-		94D	20.00	18	x	x	0.23	13	33	x	-1.1	-10.2
mineralized dolostone breccia		95D	19.60	20	x	x	0.23	13	31	x	-	-
Houghton Quarry												
Calcite cements within a		92D	16.70	63	x	x	x	9	12	x	-0.5	-14.5
dolostone compaction breccia		93D	20.00	25	x	x	0.23	8	8	x	-	-
Hetton le Hill Quarry												
Calcite cemented cavity after		61A	20.00	24	0.37	x	0.17	3	18	-	-	-
gypsum		62A	19.40	x	0.05	x	0.11	x	10	-	-	-
Quarrington Quarry												
Calcite cemented cavity after		6E	19.80	23	x	x	0.02	x	13	x	1.1	-15.5
sulphate												

		Sample no.	Wt(mg)	Mole% CaCO3	Mole% MgCO3	Mole% FeCO3	Mole% MnCO3	Mnppm	Mole% SrCO3	Srppm
Raisby Quarry										
Calcite cemented dolostone breccia										
Non-luminescent cement		8D	12.50	97.23	2.74	0.03	0.0015	8	0.0014	12
"		9D	14.90	97.00	2.98	0.02	0.0014	8	0.0012	11
"		10D	14.70	97.18	2.80	0.02	0.0014	8	0.0021	18
"		34E	18.30	97.38	2.58	0.04	0.0010	5	0.0016	14
"		21A	20.00	98.00	2.00	x	x	x	0.0008	7
"		22A	14.50	98.22	1.76	0.02	x	x	0.0007	6
"		23A	20.90	98.08	1.89	0.03	x	x	0.0007	6
Luminescent cement		7D	14.00	98.87	0.82	0.05	0.2398	1317	0.0245	215
"		31E	20.30	99.04	0.76	0.06	0.1217	669	0.0189	166
"		32E	20.80	99.14	0.66	0.01	0.1621	891	0.0256	224
"		33E	13.60	98.60	1.19	0.02	0.1691	929	0.0176	154
Dolomitic internal sediment		11A	20.00	97.64	2.09	0.28	x	x	0.0005	4
"		31A	19.60	67.36	32.61	0.03	x	x	0.0045	39
"		32A	14.90	75.27	24.69	0.04	x	x	0.0033	29
"		33A	18.00	77.35	22.49	0.15	x	x	0.0032	28
Luminescent cement		19D	19.40	98.84	0.68	0.07	0.1026	2212	0.0065	57
"		20D	20.20	99.10	0.45	0.06	0.3754	2062	0.0080	70
"		26D	13.70	98.96	0.63	0.09	0.3141	1726	0.0080	70
"		27D	20.20	99.06	0.50	0.05	0.3809	2093	0.0095	83
"		28D	18.40	92.38	7.25	0.13	0.2241	1231	0.0163	143
"		29D	13.50	99.07	0.47	0.07	0.3754	2062	0.0091	80
"		21D	19.80	96.56	2.94	0.09	0.3870	2126	0.0211	185
"		22D	20.00	97.05	2.49	0.10	0.3385	1860	0.0201	176
"		52D	19.70	98.89	0.73	0.11	0.2618	1438	0.0138	121
"		55D	14.00	99.00	0.54	0.07	0.3809	2093	0.0070	61
"		56D	19.40	99.18	0.38	0.10	0.3262	1792	0.0071	62
"		57D	18.80	98.98	0.62	0.08	0.0348	1675	0.0080	70
"		61D	20.00	98.88	0.76	0.10	0.2428	1334	0.0127	111
"		62D	12.70	98.82	0.81	0.10	0.2622	1440	0.0134	117
"		141A	20.00	96.81	2.84	0.03	0.2987	1641	0.0193	169
"		142A	18.60	98.46	1.19	0.02	0.3154	1733	0.0159	139
"		143A	18.80	98.90	0.71	0.02	0.3637	1998	0.0105	92
"		121A	20.70	98.67	0.87	0.03	0.4170	2291	0.0088	77

		Sample no.	Wt(mg)	Ba ppm	%Al2O3	%K2O	%Na2O	V ppm	Y ppm	% I.R.	$\delta^{13}C$ ‰	$\delta^{18}O$ ‰
Raisby Quarry												
Calcite cemented dolostone breccia												
Non-luminescent cement		8D	12.50	24	x	x	x	8	4	x	-	-
"		9D	14.90	17	x	x	x	7	3	x	-	-
"		10D	14.70	20	x	x	x	7	3	x	-	-
"		34E	18.30	19	0.03	x	0.08	x	x	x	-7.4	-6.2
"		21A	20.00	3	0.03	0.03	0.12	x	3	-	-	-
"		22A	14.50	x	0.04	x	0.14	x	3	-	-7.3	-6.2
"		23A	20.90	2	0.02	0.02	0.09	x	2	-	-	-
Luminescent cement		7D	14.00	21	0.04	x	0.04	11	18	x	-	-
"		31E	20.30	15	x	x	x	5	12	x	-10.3	-13.6
"		32E	20.80	14	0.02	x	0.07	2	12	x	-10.9	-13.0
"		33E	13.60	15	x	x	x	x	4	x	-7.1	-13.8
Internal sediment		11A	20.00	8	0.04	x	0.17	x	4	-	-	-
"		31A	19.60	5	0.05	0.03	0.10	5	3	-	-	-
"		32A	14.90	10	0.07	x	0.13	3	3	-	-	-
"		33A	18.00	3	0.08	x	0.14	3	3	-	-	-
Luminescent cement		19D	19.40	18	x	x	x	10	15	x	-	-
"		20D	20.20	20	x	x	x	10	15	x	-	-
"		26D	13.70	33	x	x	0.04	11	15	x	-	-
"		27D	20.20	17	x	x	0.02	12	15	x	-	-
"		28D	18.40	76	x	x	x	14	8	6.50	-	-
"		29D	13.50	26	0.04	x	x	11	15	x	-	-
"		21D	19.80	3461	0.05	x	x	10	10	4.50	-	-
"		22D	20.00	2635	0.05	x	0.02	10	8	4.00	-	-
"		52D	19.70	30	0.05	x	0.03	10	13	x	-	-
"		55D	14.00	21	x	x	x	14	18	x	-	-
"		56D	19.40	15	x	x	x	10	15	x	-	-
"		57D	18.80	21	x	x	x	8	11	x	-	-
"		61D	20.00	20	0.08	x	0.03	8	13	x	-	-
"		62D	12.70	24	0.04	x	0.04	12	16	x	-	-
"		141A	20.00	3035	0.03	0.03	0.10	3	8	-	-	-
"		142A	18.60	422	0.03	0.03	0.11	x	8	-	-	-
"		143A	18.80	27	0.03	0.03	0.11	3	16	-	-	-
"		121A	20.70	2	x	x	0.10	2	13	-	-	-

		Sample no.	Wt(mg)	Mole% CaCO3	Mole% MgCO3	Mole% FeCO3	Mole% MnCO3	Mnppm	Mole% SrCO3	Srppm
Rough Furze Quarry										
Non-luminescent calcite cement		9E	20.50	98.92	1.06	0.02	0.0031	17	0.0011	10
within cavity after sulphate										
Running Waters Quarry										
Calcite cemented barite mineralized		63D	20.00	98.81	0.73	0.09	0.3494	1920	0.0236	207
cavity after sulphate		64D	20.80	99.00	0.52	0.05	0.3965	2178	0.0302	265
"		65D	18.80	99.01	0.50	0.08	0.3876	2129	0.0253	222
"		66D	20.20	99.16	0.34	0.15	0.3310	1818	0.0206	180
"		11B	18.60	99.12	0.66	0.02	0.1746	959	0.0217	119
Thickley Quarry										
Calcite cemented sphalerite		12B	22.00	98.99	0.02	0.13	0.2402	1320	0.0202	111
mineralized cavity after sulphate										
Houghton Quarry										
Joint-coating speleothem calcite		2E	19.60	97.32	2.66	0.02	0.0005	3	0.0027	24
"		3E	19.80	97.05	2.93	0.02	0.0005	3	0.0020	18
Sherburn Hill Quarry										
Joint-coating speleothem calcite		1E	20.70	95.85	4.13	0.02	0.0004	2	0.0035	31
"		AA65		96.62	3.33	0.04	x	x	0.0045	39

		Sample no.	Wt(mg)	Ba ppm	%Al2O3	%K2O	%Na2O	V ppm	Y ppm	% I.R.	$\delta^{13}C$ ‰	$\delta^{18}O$ ‰
Rough Furze Quarry												
Non-luminescent calcite cement		9E	20.50	41	x	x	0.02	x	x	x	-8.6	-5.8
within cavity after sulphate												
Running Waters Quarry												
Calcite cemented barite mineralized		63D	20.00	380	0.03	x	x	8	13	x	-0.7	-7.1
cavity after sulphate		64D	20.80	290	0.02	x	x	7	7	x	-	-
"		65D	18.80	218	0.05	x	0.03	5	11	x	-	-
"		66D	20.20	114	0.03	x	x	7	27	x	-0.2	-7.3
"		11B	18.60	191	x	x	0.13	11	30	x	-	-
Thickley Quarry												
Calcite cemented sphalerite		12B	22.00	34	0.02	x	0.15	9	11	x	-	-
mineralized cavity after sulphate												
Houghton Quarry												
Joint-coating speleothem calcite		2E	19.60	84	x	x	0.02	x	x	x	-10.2	-5.9
"		3E	19.80	61	x	x	x	x	x	x	-	-
Sherburn Hill Quarry												
Joint-coating speleothem calcite		1E	20.70	24	x	x	0.02	x	x	x	-8.6	-5.3
"		AA65		88	x	0.06	x	x	x	x	-	-

Appendix VIII

Calculation of the composition of precipitates from the Homogeneous Distribution Law

As an example of the use of the Homogeneous Distribution Law, the calculation of the Sr composition of a calcite, from the Sr/Ca ratio of seawater is illustrated below (N.B., the calculation assumes that equilibrium conditions are attained between precipitate and solution during precipitation) (after Veizer, 1983a):

$$\frac{mSr}{mCa}_{Calcite} = K^{Sr}_{Calcite} \times \frac{mSr}{mCa}_{Sea\ water}$$

$$\frac{\left(\frac{Sr\ (ppm)}{87.62}\right)}{\left(\frac{400{,}000}{40.08}\right)} = 0.13 \times \frac{\left(\frac{8}{87.62}\right)}{\left(\frac{411}{40.08}\right)}$$

$$Sr = \frac{0.13 \times 400{,}000 \times 8}{411} = 1012ppm$$

Where,

87.62	= Atomic weight of Sr
400,000	= Ca ppm in calcite
40.08	= Atomic weight of Ca
8	= Sr ppm in seawater
411	= Ca ppm in seawater

Appendix IX

Stable isotope analysis.

Elements may possess two or more isotopes, which are atoms of the same atomic number, but contrasting mass. The contrasts in mass are due to different numbers of neutrons within the nuclei of the atoms. Carbon has two stable isotopes of different abundances; ^{12}C (98.89%) and ^{13}C (1.11%). Oxygen has three isotopes, again of different abundances; ^{16}O (99.76%), ^{17}O (0.0374%) and ^{18}O (0.204%). Only ^{16}O and ^{18}O are of importance with regard to geology. Stable isotope analysis uses mass spectrometers, which measure ratios of CO_2 with mass 44 ($^{12}C^{16}O_2$), 45 ($^{13}C^{16}O_2$), and 46 ($^{12}C^{18}O^{16}O$). Isotope ratios are derived by ionising introduced CO_2 gas by electrical bombardment. Ions produced are separated according to their mass by passage through a magnetic field, and then the proportions of ions of each mass are measured (Fairchild *et al.*, 1988)

The use of isotopes of carbon and oxygen in carbonate diagenesis studies is that they partially separate, or fractionate in relation to physical and chemical processes. Specific environmental and diagenetic processes are characterised by particular fractionations, and so help identify those processes in the geological record. Fractionation, explicable by quantum theory, basically relates to differences in atomic mass of isotopes. An example is the kinetic isotope fractionation which occurs during evaporation of water. As the process is rapid, insufficient time is available for equilibrium to be reached, and so the lighter isotope (^{16}O) is removed preferentially as it participates more easily in the reaction. At 25°C, water is enriched in ^{18}O by about 0.8‰ compared to co-existing water vapour (Fairchild *et al.*, 1988).

As the analysis of the absolute abundances of isotopes within a sample is imprecise, results are expressed relative to a standard, with the del notation (δ) in parts per mill (‰) (Craig, 1957):

$$\delta^{18}O‰ = 1000 \frac{(^{18}O/^{16}O_s - {}^{18}O/^{16}O_{std})}{(^{18}O/^{16}O_{std})}$$

$$\delta^{13}C‰ = 1000 \frac{(^{13}C/^{12}C_s - {}^{13}C/^{12}C_{std})}{(^{13}C/^{12}C_{std})}$$

Where,

s = sample

std = standard

(after McCrea, 1950).

All isotope analyses were conducted at the BGS Isotope Geology Unit, Grays Inn Road, London. Carbon dioxide gas was collected from calcite and dolomite samples and standards reacted with 100% phosphoric acid (H_3PO_4) *in vacuo*. CO_2 gas, collected by vacuum extraction, was analysed in alternation with a reference gas on a VG Micromass mass spectrometer. Details of the extraction line are shown in fig. A9.1. All Raisby Formation samples were approximately 10mg in size, and in nearly all, no acid-insoluble residue remained after sample digestion. Raisby Formation samples were all extracted from polished slabs using a dental drill, in an identical manner to ICP samples (Appendix VII). Two laboratory standards, MCS (calcite) and TDS (dolomite) were prepared with Raisby Formation samples. Normally, two standard samples were included for every eight Raisby Formation samples analysed. For details of the chemical and isotopic composition of MCS and TDS standards, see Coleman *et al.*, (1989).

All calcite samples were reacted with phosphoric acid in a water bath at 25.2°C. Most dolomite samples were reacted at 55°C in a glycol bath, owing to the slowness of the reaction at 25°C. Two batches of dolomite samples were reacted at 25.2°C over two days, which produced results in agreement with those samples reacted at higher temperature. A 0.05-0.1‰ difference was detected between low and high temperature dolomite runs, although this is within analytical precision.

Data collected was corrected for instrumental and isobaric effects using methods of Craig (1957) and Deines (1970). Kinetic fractionation factors for oxygen isotope fractionation between CO_2 and water during phosphoric acid decomposition was used when calculating the results. The fractionation factor for calcite was taken as 1.01025 (Friedman and O'Neil, 1977), and for dolomite, 1.011.

Reproducibility of standard and duplicate samples was in the order of ±0.1‰, better for calcite than dolomite samples. Thus, all the results in this thesis are quoted to one decimal place, apart for averaged values which are quoted to one or two decimal places. However, results quoted from other authors may be written to two decimal places, or the nearest whole number, depending on that authors preference. Where duplicate samples were run, the mean value of the two results in quoted. All of the carbon and oxygen isotope results in this thesis are expressed relative to the PDB standard (a Cretaceous belemnite from the Peedee Formation, south Carolina). For some water analyses quoted from other published works, results are expressed relative to the SMOW (Standard Mean Ocean Water) scale. The conversion between the two scales is as follows:

$$\delta^{18}O\ SMOW = 1.03091\ \delta^{18}O\ PDB + 30.91$$

$$\delta^{18}O\ PDB = 0.97002\ \delta^{18}O\ SMOW - 29.98$$

(after Coplen *et al.*, 1983).

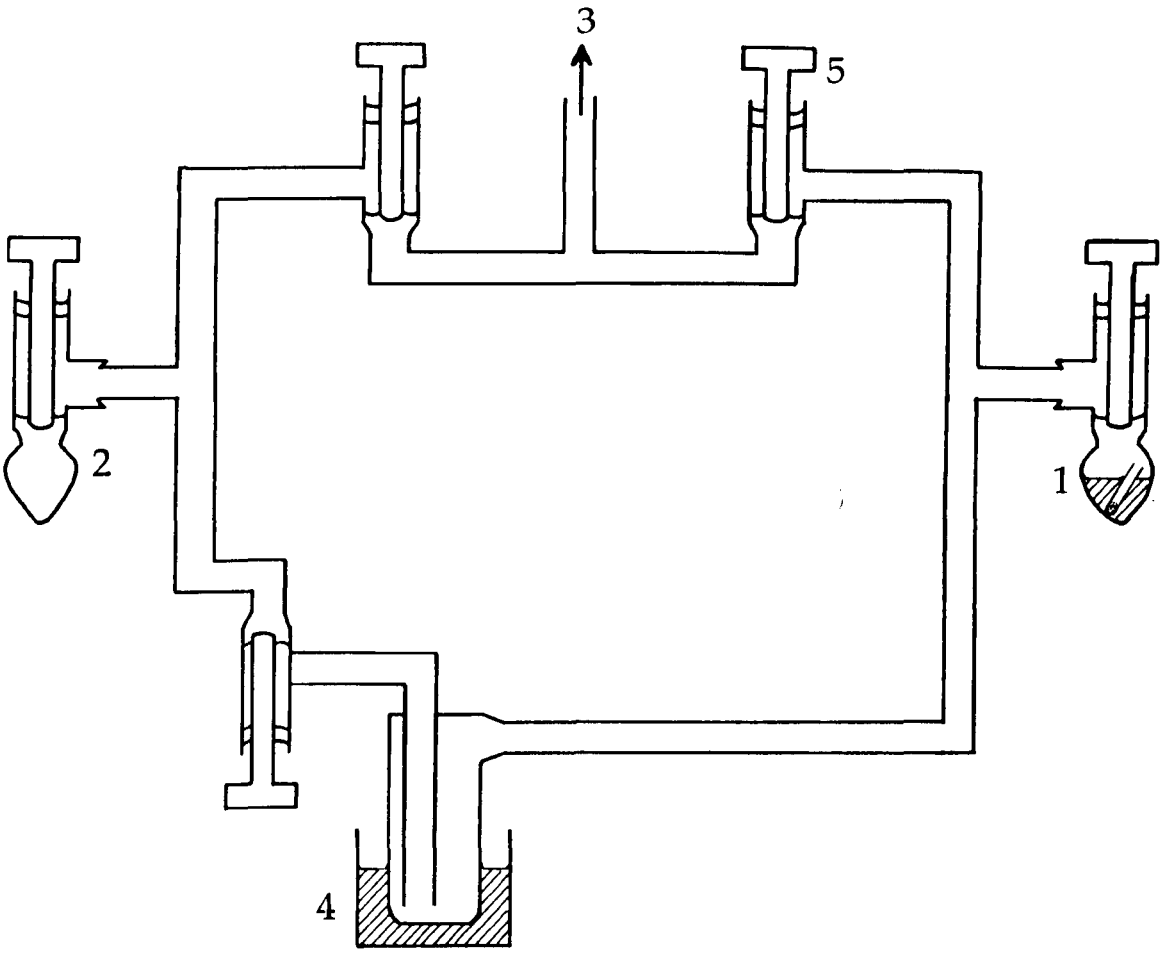

1. Reaction vessel containing 100% phosphoric acid and sample tube
2. Collection vessel
3. To rotary and diffusion pumps
4. Solid CO_2 - acetone trap
5. Stoppers, in closed position

Fig. A9.1. Schematic diagram of the isotope extraction line used.

Sulphur isotope values quoted from other published data is expressed as $\delta^{34}S‰$ relative to the CDT (Canon Diablo Triolite) standard.

One of the most important fractionations of isotopes with regard to geology, is the oxygen isotope fractionation between calcite/dolomite and water. Differences in the temperature of precipitation of carbonate minerals leads to measurable variations in their $^{18}O/^{16}O$ ratios. For calcite and dolomite, polynomial expressions have been derived which express the isotopic composition of calcite and dolomite (with respect to PDB) relative to the isotopic composition of water (with respect to SMOW) and temperature:

For calcite (after Anderson and Arthur, 1983) (Fig. A9.2);

$$T(°C) = 16.0 - 4.14\ (\delta_c - \delta_w) + 0.13\ (\delta_c - \delta_w)^2$$

For dolomite (after Land, 1985);

$$T(°C) = 16.4 - 4.3\ (\delta_c - \delta_w) + 0.14\ (\delta_c - \delta_w)^2$$

Where;

$\delta_c = \delta^{18}O$ of CO_2 liberated by reaction with 100% phosphoric acid at 25°C

$\delta_w = \delta^{18}O$ of CO_2 in equilibrium at 25°C with water

For dolomite, $\delta_c + 3.8 = \delta_{Dolomite}$ (Land, 1985).

Carbon and oxygen isotope results for Raisby Formation samples, together with standard and duplicate analysed are listed in the following tables:

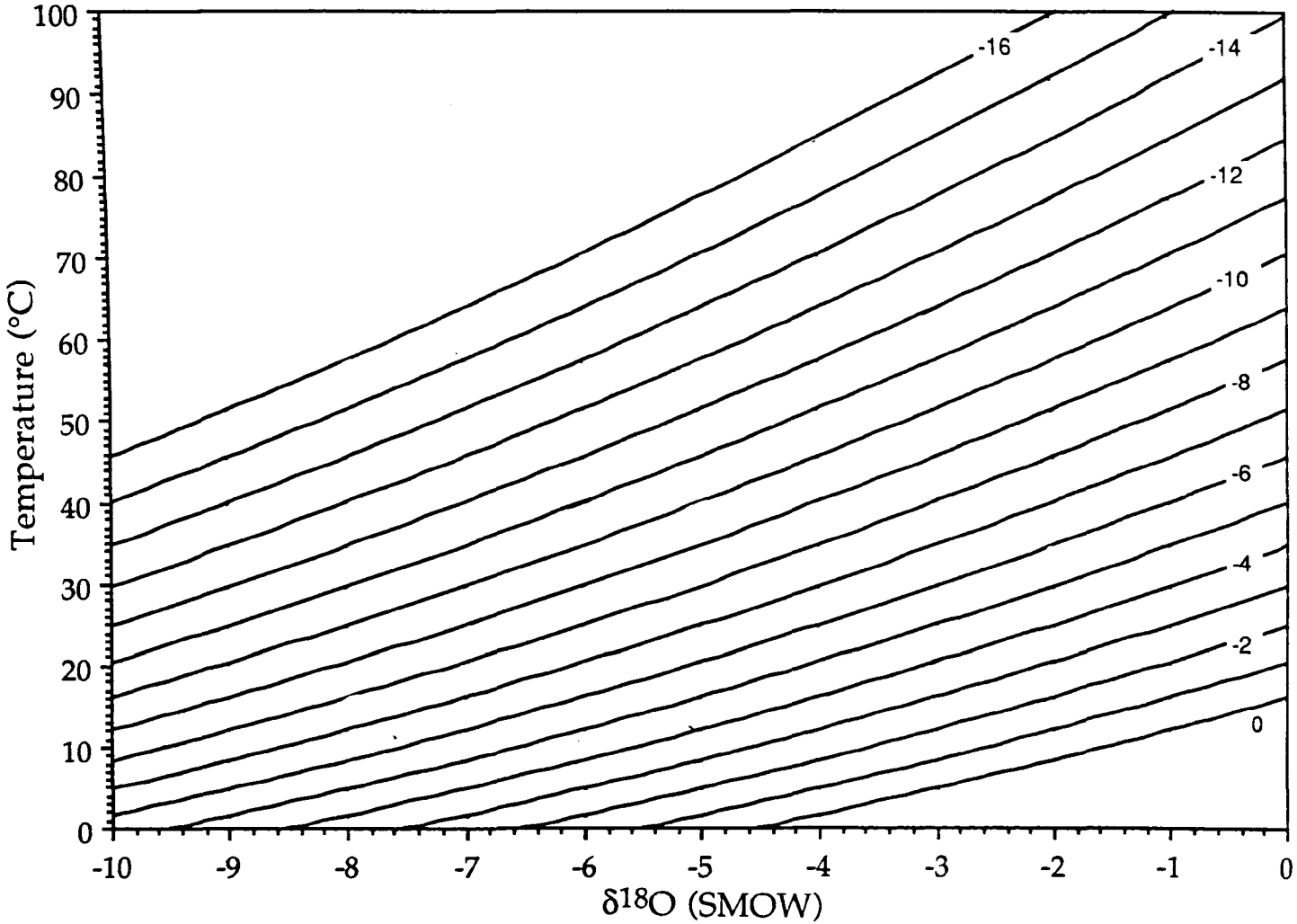

Fig. A9.2. Graph showing the relationship between the oxygen isotopic composition of water (in relation to SMOW), temperature and the isotopic composition of calcite (the lines from 0 to -16). The graph has been derived from the expression $T(°C) = 16.0 - 4.14(\delta_c - \delta_w) + 0.13(\delta_c - \delta_w)^2$

Sample no.	Locality	Depth	National grid reference	Lithology	$\delta^{13}C$ ‰	$\delta^{18}O$ ‰
1	W8 borehole	R.F. 286.00m	NZ 52688 66339	FCR dolostone	5.7	-0.6
2.1	W8 borehole	276.62m	"	"	5.7	-4.1
2.2					5.4	-4.1
3	W8 borehole	271.00m	"	"	5.4	-1.0
4	E4 borehole	465.1m	NZ 5507 5076	"	6.1	-2.7
5	E4 borehole	469.16m	"	"	5.7	-3.1
6	E4 borehole	472.0m	"	"	5.6	-2.3
7	High Moorsley Quarry		NZ 334 455	"	5.5	-1.5
8	"		"	"	5.5	-1.6
9	Raisby Quarry		NZ 338 354-352 352	Brachipod	3.9	-3.1
10	High Moorsley Quarry		NZ 334 455	"	1.8	-5.0
11	"		"	Intraskeletal calcite cement	2.4	-9.7
12	"		"	Limestone	3.3	-5.1
13	Raisby Quarry		NZ 338 354-352 352	Brachiopod	4.1	-3.2
14.1	"		"	Intraskeletal calcite cement	5.4	-1.0
14.2					5.5	-1.0
15.1	Thickley Quarry		NZ 2408 2564	FCR dolostone	4.2	-2.2
15.2					4.3	-2.3
16	"		"	"	6.1	-1.1
17.1	Seaham borehole	115.82m	NZ 4258 5031	FCR dolostone	6.0	-1.3
17.2					5.9	-1.4
18	"	102.11m	"	"	6.1	-1.8
19	"	91.44m	"	"	5.7	-1.2
20	Raisby Quarry		NZ 338 354-352 352	FCR dolostone	4.9	-3.3
21	"		"	"	5.2	-1.1
22.1	Penshaw Hill Quarry		NZ 3365 5460	FCR dolostone	6.0	-1.6
22.2					6.0	-1.4
23	"		"	"	5.9	-1.3
24	Houghton Quarry		NZ 341 506	FCR dolostone	5.9	-1.8
25	"		"	"	5.6	-0.9
26	Raisby Quarry		NZ 338 354-352 352	Calcite concretion (Type LC)	5.2	-5.1
27.1	"		"	"	3.2	-8.6
27.2					4.2	-6.2
28	"		"	"	4.9	-6.4

Sample no.	Locality	Depth	National grid reference	Lithology	$\delta^{13}C$ ‰	$\delta^{18}O$ ‰
29	Thickley Quarry		NZ 2408 2564	Limestone	5.8	-3.1
30	Raisby Quarry		NZ 338 354-352 352	ECI Calcitized evaporite	-6.1	-13.1
31	"		"	"	-12.1	-12.3
32.1	Quarrington Quarry		NZ 327 379	ECI Calcitized evaporite	-0.1	-6.7
32.2					4.1	-3.4
32.3					-0.3	-6.7
33	Thickley Quarry		NZ 2408 2564	Luminescent calcite cement	0.6	-13.1
34	Haswell Moor Farm Quarry		NZ 352 426	Speleothem calcite cement	-8.6	-5.3
35.1	Running Waters Quarry		NZ 334 404	Luminescent calcite cement	-0.8	-7.2
35.2					-0.6	-7.0
36.1	"		"	"	-0.3	-7.5
36.2					-0.1	-7.2
37	Houghton Quarry		NZ 341 506	Luminescent calcite cement	-0.5	-14.5
38	High Moorsley Quarry		NZ 334 455	Luminescent calcite cement	-1.1	-10.2
39	Raisby Quarry		NZ 338 352-352 352	Limestone	5.0	-5.1
40	"		"	"	5.7	-3.9
41	"		"	"	5.7	-4.5
42	"		"	"	5.6	-3.2
43	"		"	"	5.7	-3.6
44	"		"	"	5.0	-5.7
45	"		"	"	4.5	-7.1
46	"		"	Calcite concretion (Type UNL)	4.4	-6.0
47.1	"		"	"	4.8	-5.5
47.2					4.9	-5.5
48.1	"		"	FCR dolostone	3.9	-6.1
48.2					4.1	-6.0
49.1	High Moosley Quarry		NZ 334 455	Dolomitized anhydrite	5.6	-1.4
49.2					5.6	-1.4
50.1	"		"	"	5.6	-1.6
50.2					5.3	-2.2
51	Raisby Quarry		NZ 338 354-352 352	Calcite cement	2.9	-11.3
52	Man Haven	Base EZ2 Ca	NZ 3461 6601	EDR calcitized dolomite	0.2	-6.5
53.1	"	Raisby Fm.	"	"	0.0	-6.3
53.2					-0.1	-6.2

Sample no.	Locality	Depth	National grid reference	Lithology	$\delta^{13}C$ ‰	$\delta^{18}O$ ‰
54.1	Dawsons Plantation		NZ 337 548	Limestone	5.4	-2.0
54.2					5.3	-2.0
55	Raisby Quarry		NZ 338 354-352 352	Ferroan dolomite cement	4.3	-6.3
56	"		"	Luminescent calcite cement	-1.7	-12.5
57	Quarrington Quarry		NZ 327 379	Luminescent calcite cement	1.1	-15.5
58	W15 borehole	251.23m	NZ 4809 7622	Limestone	6.0	-3.5
59	"	258.1m	"	"	5.6	-3.1
60	"	266.1m	"	"	5.5	-2.5
61	Houghton Quarry		NZ 341 506	Speleothem calcite cement	-10.2	-5.9
62.1	W8 borehole		NZ 52688 66339	ED calcitized dolomite	5.4	-4.4
62.2					5.5	-4.3
63	"		"	"	5.5	-4.5
64	Rough Furze Quarry		NZ 318 324	Columnar calcite cement	-8.6	-5.8
65.1	Frenchmans Bay		NZ 3890 6615	Columnar calcite cement	-8.1	-5.1
65.2					-7.9	-5.2
66	Field House Quarry		NZ 354 506	Columnar calcite cement	-7.5	-6.0
67	Raisby Quarry		NZ 338 354-352 352	Luminescent calcite cement	-2.9	-11.4
68	"		"	"	-2.9	-11.4
69.1	"		"	"	-4.0	-11.7
69.2					-3.5	-11.1
70	"		"	"	-10.9	-13.0
71	"		"	"	-10.3	-13.6
72	"		"	"	-7.1	-13.8
73.1	"		"	Columnar calcite cement	-7.5	-6.3
73.2					-7.3	-6.1
74	"		"	"	-7.3	-6.1
75	"		"	"	-7.4	-6.2
76	E3a borehole	338m	NZ 54019 48996	FCR dolostone	6.3	-2.8
77.1	"	353.6m	"	FCR dolostone/Ankerite	5.5	-4.4
77.2					5.5	-4.3
78.1	Houghton Quarry		NZ 341 506	Limestone	4.1	-5.4
78.2					4.2	-5.3
79	"		"	Limestone	4.5	-5.2

.2 denotes duplicate analysis

Standard sample results

Analysis batch no.	Sample No.	$\delta^{13}C$ ‰	$\delta^{18}O$ ‰
T18138	TDS-1/1	1.851	-10.84
T18139	TDS-1/2	1.894	-10.81
C18146	MCS-10/1	-0.904	-10.79
C18147	MCS-10/2	-0.877	-9.74
T18154	TDS-1/1	1.834	-10.80
T18155	TDS-1/2	1.885	-10.79
C18162	MCS-10/1	-0.721	-9.25
C18163	MCS-10/2	-0.687	-9.21
C18170	MCS-10/3	-0.719	-9.51
C18171	MCS-10/4	-0.743	-9.25
C18172	MCS-10/5	-0.932	-9.76
D18173	TDS-1/1	1.804	-10.85
D18174	TDS-1/2	1.756	-10.89
D18175	TDS-1/3	1.789	-10.87
D18176	TDS-1/4	1.780	-10.86
C18181	MCS-10/1	-0.626	-9.26
C18182	MCS-10/2	-0.655	-9.22
C18193	MCS-10/1	-0.712	-9.18
C18194	MCS-10/2	-0.719	-9.25
T18201	TDS-1/1	1.842	-10.83
T18202	TDS-1/2	1.886	-10.85
C18209	MCS-10/1	-0.732	-9.30
C18210	MCS-10/2	-0.988	-9.97
T18217	TDS-1/1	1.838	-10.82
T18218	TDS-1/2	1.891	-10.75
C18225	MCS-10/1	-0.662	-9.14
C18226	MCS-10/2	-0.601	-9.20
C18227	MCS-10/3	-0.675	-9.13
C18241	MCS-10/1	-0.675	-9.43
C18242	MCS-10/2	-0.656	-9.18
T18252	TDS-1/1	1.882	-10.73
C18257	MCS-10/1	-0.598	-9.20
C18258	MCS-10/2	-1.034	-9.86

C denotes calcite sample prepared at 25.2°C

D denotes dolomite sample prepared at 55°C

T denotes dolomite sample prepared at 25.2°C

Analysis batch no.	sample no.	$\delta^{13}C$ ‰	$\delta^{18}O$ ‰
C18237	73.1	-7.462	-6.26
C18238	73.2	-7.349	-6.14
C18243	32.1	-0.086	-6.67
C18244	32.2	4.029	-3.41
	32.3	-0.300	-6.69
C18271	65.1	-8.061	-5.11
C18272	65.2	-7.911	-5.22
	2.1	5.700	-4.10
	2.2	5.880	-4.13
	27.1	3.200	-8.60
	27.2	4.170	-6.23

TDS	$\delta^{13}C$	$\delta^{18}O$
Mean	1.84	-10.82
Standard deviation	0.05	0.05
Preferred value (Coleman *et al.*, 1988)	1.85	-10.78
MCS	$\delta^{13}C$	$\delta^{18}O$
Mean	-0.75	-9.44
Standard deviation	0.129	0.409
Preferred value (Coleman *et al.*, 1988)	-0.71	-9.17

Duplicate sample results

Analysis batch no.	Sample no.	$\delta^{13}C$ ‰	$\delta^{18}O$ ‰
T18140	49.1	5.562	-1.36
T18141	49.2	5.574	-1.36
T18142	50.1	5.551	-1.57
T18143	50.2	5.253	-2.20
T18144	77.1	5.499	-4.39
T18145	77.2	5.531	-4.30
C18148	35.1	-0.813	-7.21
C18149	35.2	-0.583	-7.00
C18150	36.1	-0.342	-7.54
C18151	36.2	-0.058	-7.24
C18152	54.1	5.360	-1.95
C18153	54.2	5.325	-2.01
T18156	15.1	4.234	-2.19
D18177	15.2	4.288	-2.34
T18158	22.1	5.993	-1.56
D18178	22.2	5.960	-1.36
D18179	48.1	3.946	-6.14
D18180	48.2	4.112	-5.99
C18167	62.1	5.434	-4.39
C18185	62.2	5.455	-4.28
C18186	78.1	4.116	-5.43
C18187	78.2	4.154	-5.34
C18196	47.1	4.848	-5.54
C18197	47.2	4.863	-5.47
C18199	53.1	-0.041	-6.27
C18200	53.2	-0.062	-6.19
C18212	14.1	5.441	-1.04
C18213	14.2	5.481	-0.99
T18221	17.1	5.952	-1.28
T18222	17.2	5.893	-1.43
C18232	69.1	-3.962	-11.65
C18233	69.2	-3.536	-11.08

Appendix X

Burial history of the Raisby Formation.

The burial history of the Zechstein sequence in northeast England is very poorly understood, owing to erosion of most post-Permian and all post-Triassic sediments from the study area during Tertiary uplift. The nearest sequence of reasonably well preserved Jurassic and Cretaceous sediments, in east Yorkshire and Linconshire, occupies an area of Mesozoic inversion. Thicknesses recorded in this area will thus not be representative of the Mesozoic overburden on the Permian in northeast England. The prediction of Jurassic and Cretaceous thicknesses is further hampered by probable thinning of both across northeast England towards the Pennines, most likely a positive feature throughout most of the Mesozoic.

In south Durham, the Raisby Formation is overlain by approximately 261m of Zechstein sediments and 442.5m of Triassic continental clastics up to the top of the Mercia Mudstone Group. Data from the Southern North Sea Basin adjacent to northeast England, suggests that the maximum thickness of Rhaetic (uppermost Triassic) sediments would have been approximately 80m and of Jurassic approximately 630m (Brown, 1984). Thicknesses of Cretaceous sediments are extremely difficult to evaluate owing to the strong influence of the east Yorkshire inversion axis on regional isopachs. Total Cretaceous thicknesses were probably in the order of a few hundred metres, with a maximum of approximately 500m (based on southern North Sea data [Hancock, 1984]). A few tens of metres of Paleocene sediments may well have been deposited in northeast England, again by analogy with sequences developed within the Southern North Sea Basin (Lovell, 1984). This is summarised in fig. A10.1, which represents probable maximum burial conditions on the basis of extrapolated sediment thicknesses.

Uplift of northeast England began in the early Tertiary (Paleocene) at approximately 60Ma (± 5Ma) (Green, 1986 & 1989). Green (1986 & 1989) identifies a major phase of regional uplift and cooling at this time in both northern (Green, 1986) and eastern England (Green, 1989) on the basis of fission track data. Green (1989) identifies a further phase of cooling at 20-30Ma (±5Ma) (Oligocene/Miocene) in eastern England.

On the basis of calculated thicknesses, a maximum overburden on top of the Raisby Formation at 60Ma would have been 1954.75m (1.95 km) (Fig. A10.1). This is in good agreement with estimated overburden for the Edlington Formation of Teesside of 2km (Goodall, 1987). If a standard geothermal gradient of 30°C/km and surface temperature of 10°C is assumed, 1.95km burial would have heated the Raisby Formation to 69°C during the period of maximum burial (Fig. A10.1). Scarce paleotemperature data for the Permian in northeast England is in broad agreement with this data. Colour alteration indices of conodonts extracted from the Raisby Formation of 1-1.5 (Swift, 1986), suggest a maximum

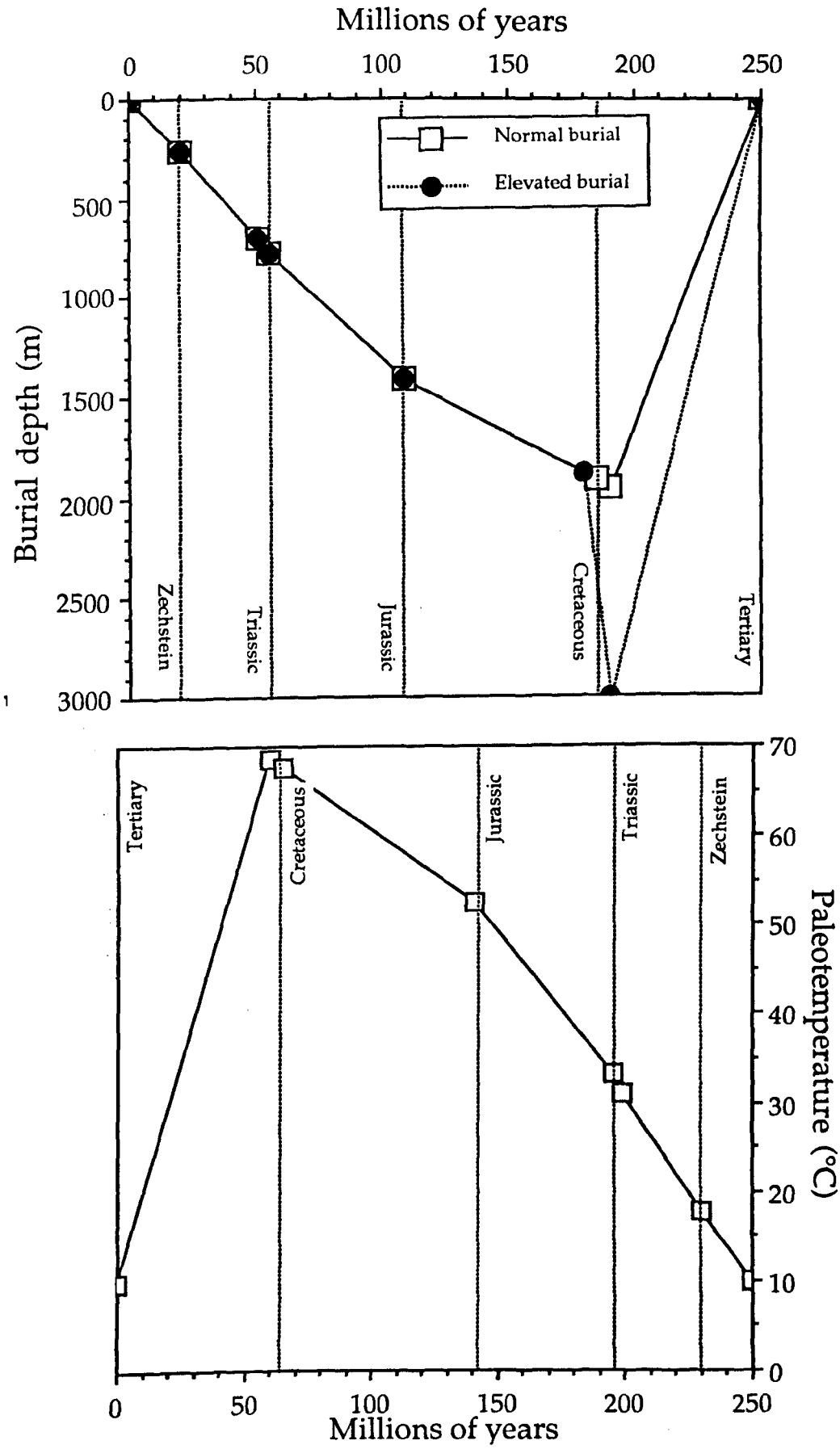

Fig. A10.1. Graphs illustrating the two possible burial curves for the Raisby Formation, and paleotemperatures which would have been reached in the Raisby Formation during normal burial. Key applies to both graphs.

temperature of 90°C. Organic matter within the Marl Slate at outcrop is immature (sub-bituminous coal equivalent rank [Cooper, 1975]) implying maximum temperatures of less than 80°C. Cooper (1975) further suggests, on the basis of reflectance data, that a phase of elevated heat flow (100-110°C) corresponding to barium and fluorite mineralization identified by Hirst and Smith (1974) if present, must have lasted for less than 10Ma.

However, recent work on the thermo-tectonic history of northern and eastern England, based upon fission track studies (Green, 1986 & 1989), suggests that the Permian of northeast England may have been subjected to elevated temperatures during the Mesozoic, either from greater than expected burial under standard geothermal gradients or a regional thermal event. From studies of fission track data from intrusive igneous rocks of the Cheviot and Lake District areas, Green (1986) suggests that northern England may have been buried under a standard geothermal gradient with extensive (kilometre scale) Mesozoic burial followed by uplift and cooling at 60Ma, or it may have undergone a less extensive burial with a short lived thermal pulse (involving temperatures of up to 100°C or more), corresponding to Tertiary igneous activity, widespread in western Scotland and Ireland. In this scenario, both the thermal pulse and uplift are related to a period of widespread crustal instability during the early Tertiary. This is supported by apatite fission track data from samples of Triassic sandstones (Sherwood Sandstone Group) from Croft on Tees (NZ 290, 099 [southernmost part of the study area]) (Green, 1989), which suggest that those sediments reached a maximum temperature of 90-100°C. Green (1989) interprets these data to suggest a combined Jurassic, Cretaceous and early Tertiary overburden of 2.7-3km (geothermal gradient= 30°C/km). This is clearly in excess of calculated Jurassic and Cretaceous overburden in northeast England (Fig. A10.1). Green (1989) invokes up to 1km or more of late Cretaceous and early Tertiary sedimentation to make up the difference. However, the regional elevated geothermal gradients hypothesised by Green (1986) from northern England may also have been operative in this area at this time.

Thus, following the work of Green (1986 & 1989) it is possible that the Permian of northeast England was buried to a greater depth than calculated (possibly 2.5-3km) (Fig. A10.1), and/or that there was an episode of elevated heat flow in the early Tertiary, corresponding to intrusive and extrusive igneous activity. The effects of both processes on paleotemperatures within the Raisby Formation are illustrated in fig. A10.2. These both suggest maximum temperatures of 100°-110°C at around the late Cretaceous/early Tertiary. The Cleveland Dyke (56±1Ma [Green, 1989]) which cuts Zechstein sediments in northeast England is presumed to be allied to the Tertiary igneous centers to the west. It is not suggested that the dyke intrusion elevated geothermal gradients regionally, but it may be a manifestation of a period of regionally high heat flow. This may further help to confine the timing of base metal sulphide mineralization in the Raisby Formation, which is suggestive of an episode of elevated heat flow (Chapter 7).

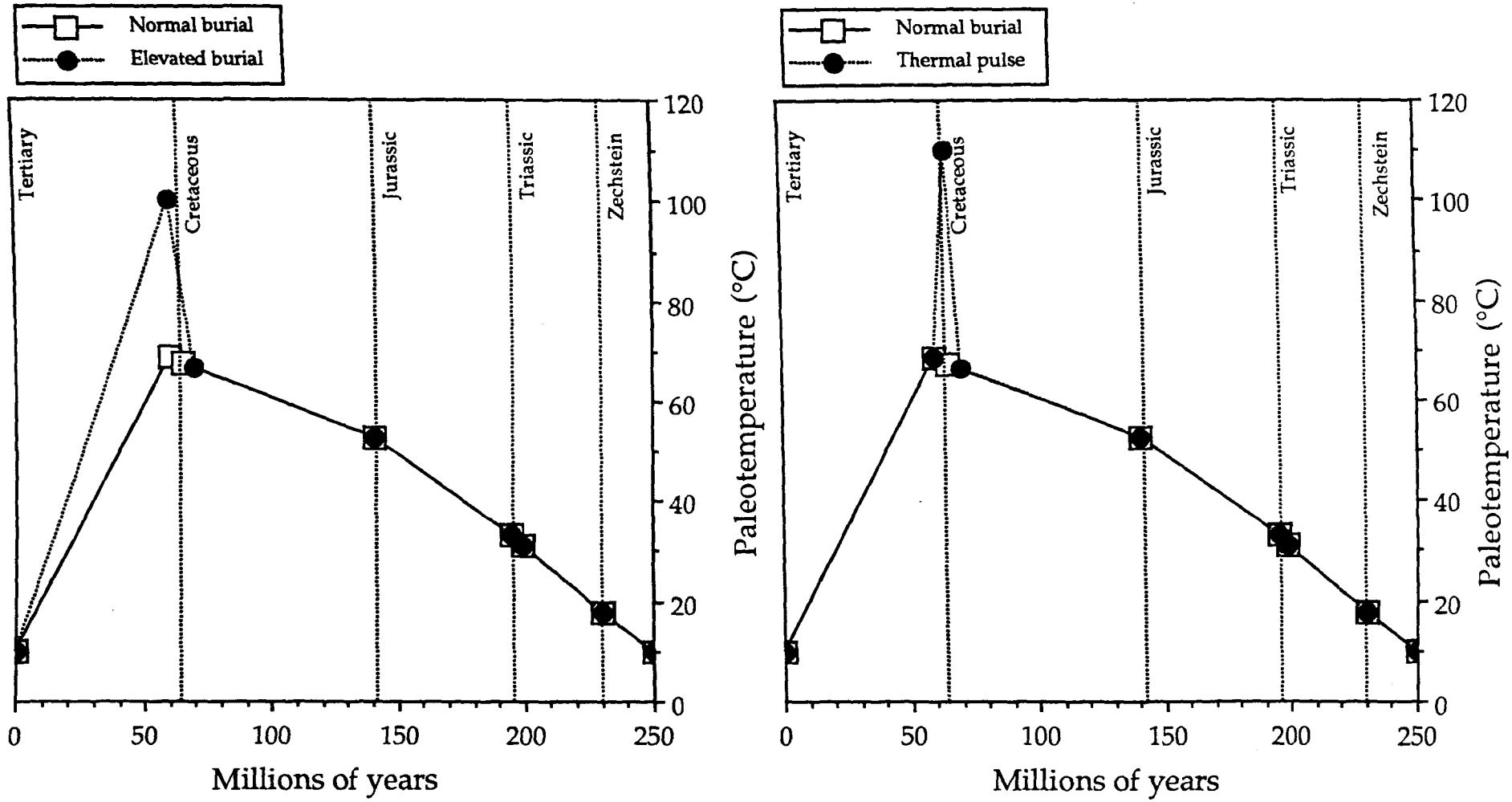

Fig. A10.2. Graphs illustrating the possible thermal evolution of the Raisby Formation superimposed on paleotemperatures achieved during predicted burial on the basis of extrapolated sediment thicknesses.

Appendix XI

Localities of recorded mineralization within the Raisby Formation

Locality	Grid reference	Minerals recorded	Reference
Borehole B2	[NZ 43906, 78584]	Base metal sulphides	Gibbons, 1978
Marden Quarry	[NZ 355, 709]	Barite	Smythe, 1922 (In: Dunham, 1934)
Whitley (Marden Quarry?)	Uncertain	Galena	Winch, 1817 (In: Land, 1974)
Cullercoats	[NZ 367, 711]	Galena	Haslehurst, 1911 (In: Land, 1974)
Borehole W8	[NZ 5268, 6633]	Sphalerite(1), barite(2)	This study
Frenchmans Bay	[NZ 390, 662]	Barite	This study
Man Haven	[NZ 3950, 6605]	Barite	This study
Borehole O.B. 8	[NZ 44829, 56242]	Galena, sphalerite	Unpublished data
Borehole VT1	[NZ 46191, 52051]	Base metal sulphides	Gibbons, 1978
Houghton Quarry	[NZ 341, 506]	Galena(1), barite(2)	This study
Running Waters Quarry	[NZ 335, 405]	Barite	Hirst and Smith, 1974
		Barite(1), marcasite(2), fluorite(3)	This study
Quarrington Quarry	[NZ 340, 370]	Barite, sphalerite	M. Sweeney (*pers. comm.*, 1988)
		Barite, sphalerite	This study

Locality	Grid reference	Minerals recorded	Reference
Raisby Quarry	[NZ 336,355] to [NZ 352,351]	Chalcopyrite, malachite	Dunham, 1934
		Chalcopyrite, malachite	Fowler, 1943
		Chalcopyrite	Fowler, 1957
		Barite, chalcopyrite, copper,	Smith and Francis, 1967
		galena, malachite, sphalerite	"
		Azurite, barite, chalcocite,	Hirst and Smith, 1974
		chalcopyrite, native copper	"
		Barite, chalcopyrite, galena, malachite,	This study
		sphalerite, tenanite	"
North Sands no.2 borehole	[NZ 5023, 3538]	Barite	This study
Garmondsway	[NZ 340, 348] (approx.)	Chalcopyrite, malachite	Lebour, 1903 (In: Fowler, 1957)
West Cornforth	[NZ 318, 345]	Barite	Hirst and Smith, 1974
		Barite	This study
Un-named exposure	[NZ 3120, 3385]	Barite	Hirst and Smith, 1967
Un-named exposure	[NZ 3005, 3325]	Barite, galena	Hirst and Smith, 1974
Un-named exposure	[NZ 3000, 3321]	Barite, galena	Smith and Francis, 1967
Ferryhill Cliff Quarry	[NZ 300, 330]	Barite, galena	Smith and Francis, 1967
		Barite, galena	Hirst and Smith, 1974
Un-named exposure	[NZ 330, 330]	Barite	Hirst and Smith, 1974
Un-named exposure	[NZ 322, 330]	Barite	Hirst and Smith, 1974
Un-named exposure	[NZ 305, 329]	Barite	Hirst and Smith, 1974

Locality	Grid reference	Minerals recorded	Reference
Un-named exposure	[NZ 332, 327]	Barite, galena	Hirst and Smith, 1974
Ferryhill	[NZ 318, 324]	Barite	Harwood, 1983
Rough Furze Quarry	[NZ 317, 325]	Barite	Hirst and Smith, 1974
		Barite(1), fluorite(2), marcasite(3)	This study
Un-named exposure	[NZ 333, 3225]	Barite	Hirst and Smith, 1974
Un-named exposure	[NZ 300, 322]	Barite	Hirst and Smith, 1974
Mainsforth Limeworks	[NZ 305, 321]	Barite	Hirst and Smith, 1974
Rudd Hill	[NZ 303, 321]	Barite	Hirst and Smith, 1974
Un-named exposure	[NZ 312, 321]	Barite	Hirst and Smith, 1974
Un-named exposures	[NZ 310-320, 320-330]	Barite	Hirst and Smith, 1974
Fowler, 1943 BH2	[NZ 355, 315]	Fluorite(1), barite(2)	Fowler, 1943
Fowler, 1943 BH4	[NZ 390, 315]	Fluorite(1), barite(2), galena	Fowler, 1943
Chilton Quarry	[NZ 300, 314]	Barite(1), fluorite (2),	Fowler, 1957
		galena (3), sphalerite (4).	"
		Galena	Moorbath, 1962
		Barite, fluorite, sphalerite	Smith and Francis, 1967
		Barite, fluorite	Solomon et al., 1971
		Barite	Jones and Hirst, 1972
		Barite, fluorite, galena	Hirst and Smith, 1974
		Fluorite	Lee and Harwood, 1989
		Barite(1), fluorite(2), sphalerite(3)	This study

Locality	Grid reference	Minerals recorded	Reference
Thrislington Plantation	[NZ 318, 327] and [NZ 312, 324]	Barite	Hirst and Smith, 1974
Whin Houses bore	[NZ 3988, 3111]	Barite, galena, sphalerite	Fowler, 1943
Thrislington Quarry	[NZ 311, 310]	Barite	Smith and Francis, 1967
		Barite	Hirst and Smith, 1974
Fowler, 1943 BH3	[NZ 375, 305]	Fluorite(1), barite(2)	Fowler, 1943
Ten O'Clock Barn no. 2 borehole	[NZ 3996, 3034]	Barite, fluorite	Fowler, 1957
Fowler, 1943 BH1	[NZ 280, 285] (approx.)	Fluorite(1), barite(2)	Fowler, 1943
NCB Windlestone 'B' borehole	[NZ 2667, 2834]	Barite, ?chalcopyrite	Smith and Francis, 1967
		Barite, ?chalcopyrite	Mills and Hull, 1976
Thickley Quarry	[NZ 246, 257]	Sphalerite(1), chalcopyrite(2)	This study
Middridge Quarry	[NZ 249, 253]	?sphalerite	This study
Borehole ICI WT/O	[NZ 3395, 2541]	Barite, galena	Unpublished data
Old Towns Quarry	[NZ 257, 246]	Barite, sphalerite	Smith and Francis, 1967
		Barite, sphalerite	Mills and Hull, 1976
		Barite(1), galena(2)	This study
Borehole B18	[NZ 4698, 2382]	Fluorite	Raymond, 1962
E.S.E. of Elm Grange	[NZ 2325, 2161]	Barite, magnetite, sphalerite	Smith and Francis, 1967
		Barite, magnetite, sphalerite	Mills and Hull, 1976
Hill House bore	[NZ 2830, 2137]	Barite	Unpublished data

Locality	Grid reference	Minerals recorded	Reference
Borehole W.O.18	[NZ 3121, 2085]	Barite	This study
Cold Sides water bore	[NZ 2536, 1889]	Barite	Fowler, 1957
		Barite	Smith and Francis, 1967
		Barite	Mills and Hull, 1976
Borehole G7	[NZ 3597, 1856]	Barite	Raymond, 1962
Piercebridge	[NZ 210, 160]	Chalcopyrite	Fowler, 1957
Hurworth Place borehole	[NZ 2902, 0953]	Barite, chalcopyrite, galena	This study
Mineralization outside of the	**Raisby Formation**		
Marsden Bay	[NZ 400, 650] (approx.)	Fluorite	G.M. Harwood, *pers. comm.*, 1987
Black Hall Rocks	[NZ 470, 390] (approx.)	Galena	Dunham, 1934
(? Ford Formation)		Galena	Fowler, 1957
		Galena	Smith and Francis, 1967
Middleton Road bore, W.Hartlepool	[NZ 500, 320] (approx.)	Barite, fluorite	Fowler, 1957
(?Ford Formation)			
Villiers St., W.Hartlepool	[NZ 5082, 3233]	Fluorite, sphalerite	Fowler, 1957
(?Ford Formation)			
(1), (2) etc denote relative the			
relative abundance of minerals			
where it could be determined			

Appendix XII

Outcrop and borehole sections

LOCALITY	NATIONAL GRID REFERENCE
OUTCROP	
Claxheugh Rock	NZ 363, 575
Chilton Quarry	NZ 302, 341
Cobblers Quarry	NZ 345, 449
Crime Rigg Quarry	NZ 341, 416
Cullercoats	NZ 3671, 7116
Dawsons Plantation	NZ 337, 548
Down Hill Quarry	NZ 3485, 6012
Eldon Hill Quarry	NZ 242, 272
quarry E.S.E. Elm Grange	NZ 2325, 2161
Field House Quarry	NZ 354, 506
Frenchmans Bay	NZ 3890, 6615
Gilleylaw Plantation Quarry	NZ 376, 537
Haswell Moor farm Quarry	NZ 352, 426
Hetton-le-Hill Quarry	NZ 348, 450
High Moorsley Quarry	NZ 334, 455
Houghton Quarry	NZ 341, 506
Low Moorsley Quarry	NZ 343, 462
(100m north of) Man Haven	NZ 3461, 6601
Middridge Quarry	NZ 249, 252
Morton Limekilns Quarry	NZ 190, 205
Offerton Quarry	NZ 3445, 5540
Old Towns Quarry	NZ 257, 246
Penshaw Hill Quarry	NZ 3365, 5460
Pittington Quarry	NZ 332, 447
Quarrington Quarry	NZ 327, 379
Raisby Quarry	NZ 338, 354 to 352, 352
Rough Furze Quarry	NZ 318, 324
Running Waters Quarry	NZ 334, 404
Summerhouse Quarry	NZ 2100, 1966
Thickley Quarry	NZ 2408, 2564
Trow Point	NZ 384, 667
Tynemouth Castle Cliff	NZ 375, 696
West Cornforth Quarry	NZ 318, 345
BOREHOLE	
E3a	NZ 54019, 48996
E4	NZ 5507, 5076
Hurworth Place	NZ 2902, 0953
North Sands	NZ 5023, 3538
Seaham	NZ 4258, 5031
W.O.10	NZ 3104, 2268
W.O.17	NZ 3253, 2191
W.O.18	NZ 3121, 2085
W8	NZ 52688, 66339
W15	NZ 4809, 7622

The location of these quarries, natural exposures and boreholes is shown in figure A12.1.

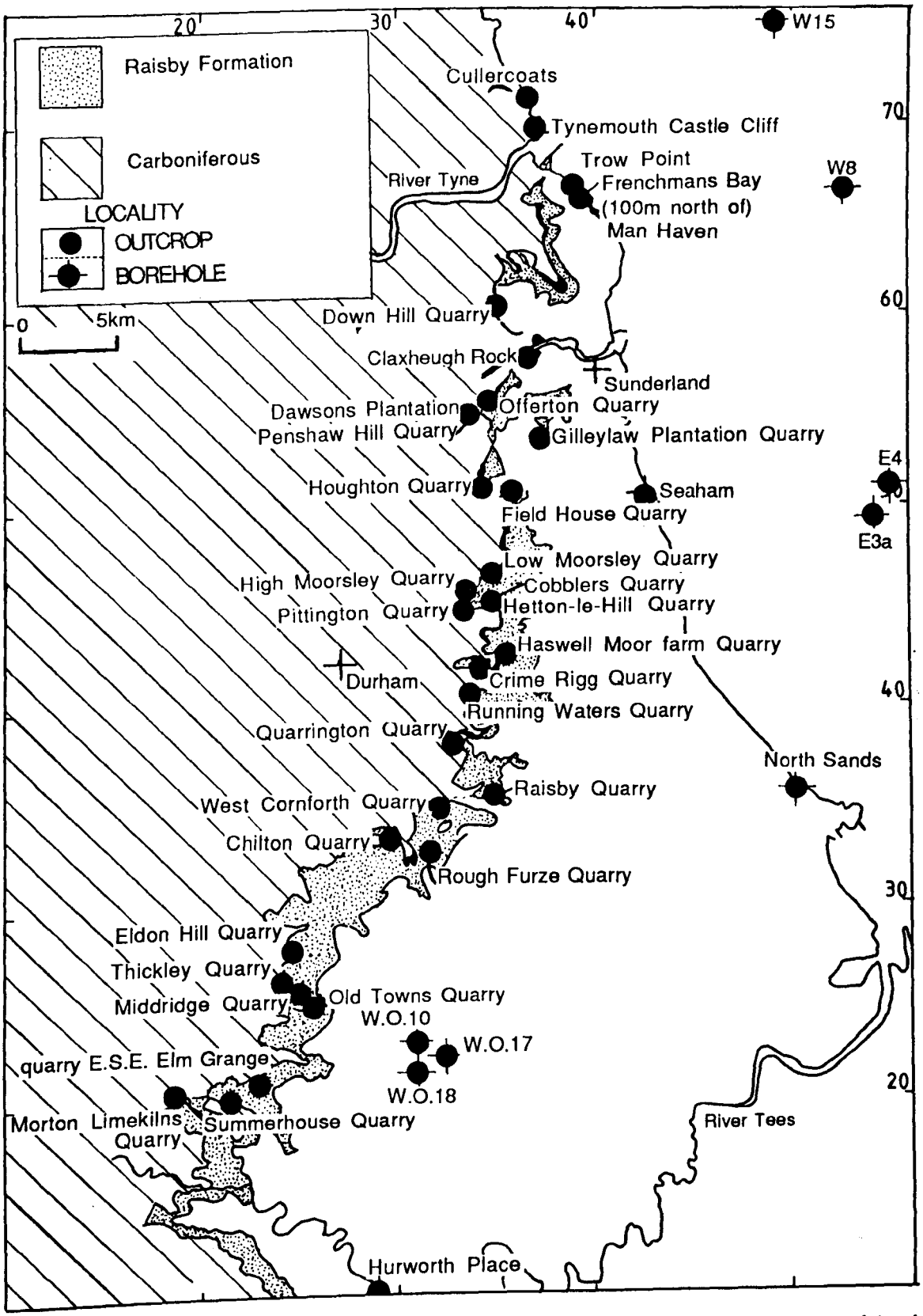

Fig. A12.1. Location of quarry sections, boreholes, and natural exposures mentioned in the text.

Limestone

Dolostone

Gypsum/anhydrite

Sandstone

Sandy limestone/ dolostone

Clay band

MARL SLATE

Sapropel lithotype

Laminite lithotype

Dolostone lithotype

Slump

Nodular bedded

Cross bedded

Breccia

Conglomerate

Ooid

Fossils, broken

Brachiopod

Bryozoan

Burrows

Fracture

Cavity after sulphate

Multiple cavity after sulphate

Euhedral sulphate pseudomorph

Pseudomorph after radiating anhydrite clusters

Gypsum nodule

Anhydrite nodule

Mineralization

Pb Galena

Zn Sphalerite

Ba Barite

F Fluorite

Fe Iron minerals

Cavities after sulphate hosting:

Ⓑ Barite

Ⓕ Fluorite

Ⓟ Galena

Ⓢ Sphalerite

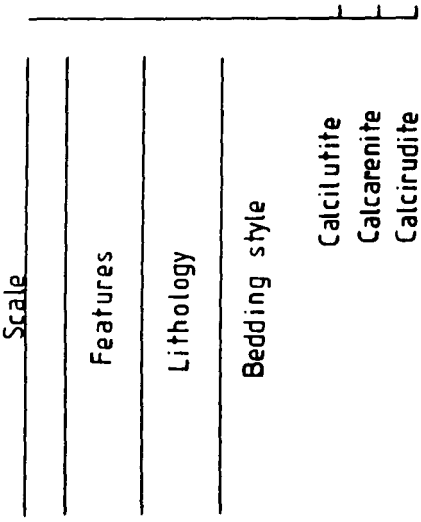

Metre-scale bedding = 3 bed planes per metre

Dm-scale bedding = 5 bed planes per metre

Cm to mm-scale bedding = 10 bed planes per metre

Bed contacts

——— Sharp

~~~ Erosional

Not exposed
~~~

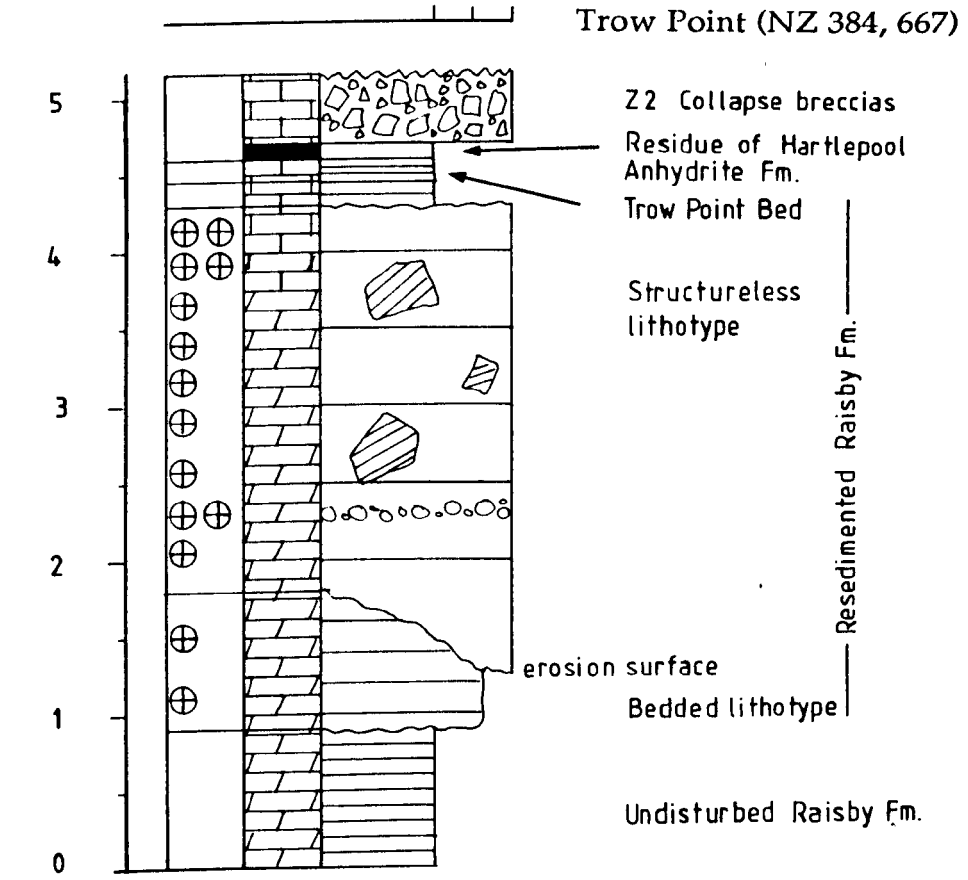
Trow Point (NZ 384, 667)
5
4
3
2
1
0
Z2 Collapse breccias
Residue of Hartlepool Anhydrite Fm.
Trow Point Bed
Structureless lithotype
Resedimented Raisby Fm.
erosion surface
Bedded lithotype
Undisturbed Raisby Fm.

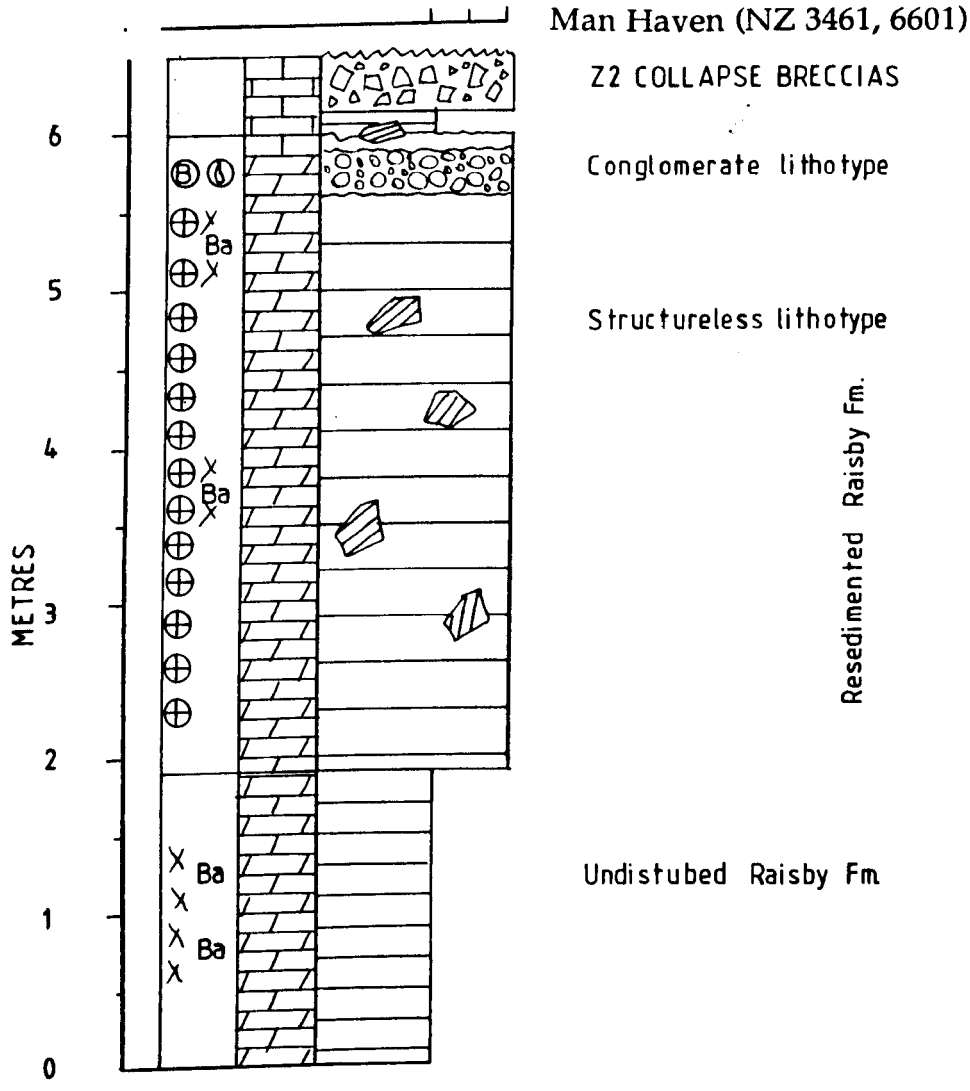
Man Haven (NZ 3461, 6601)
METRES
6
5
4
3
2
1
0
Ba
Ba
Ba
Ba
Z2 COLLAPSE BRECCIAS
Conglomerate lithotype
Structureless lithotype
Resedimented Raisby Fm.
Undistubed Raisby Fm

Claxheugh Rock (NZ 363, 575)

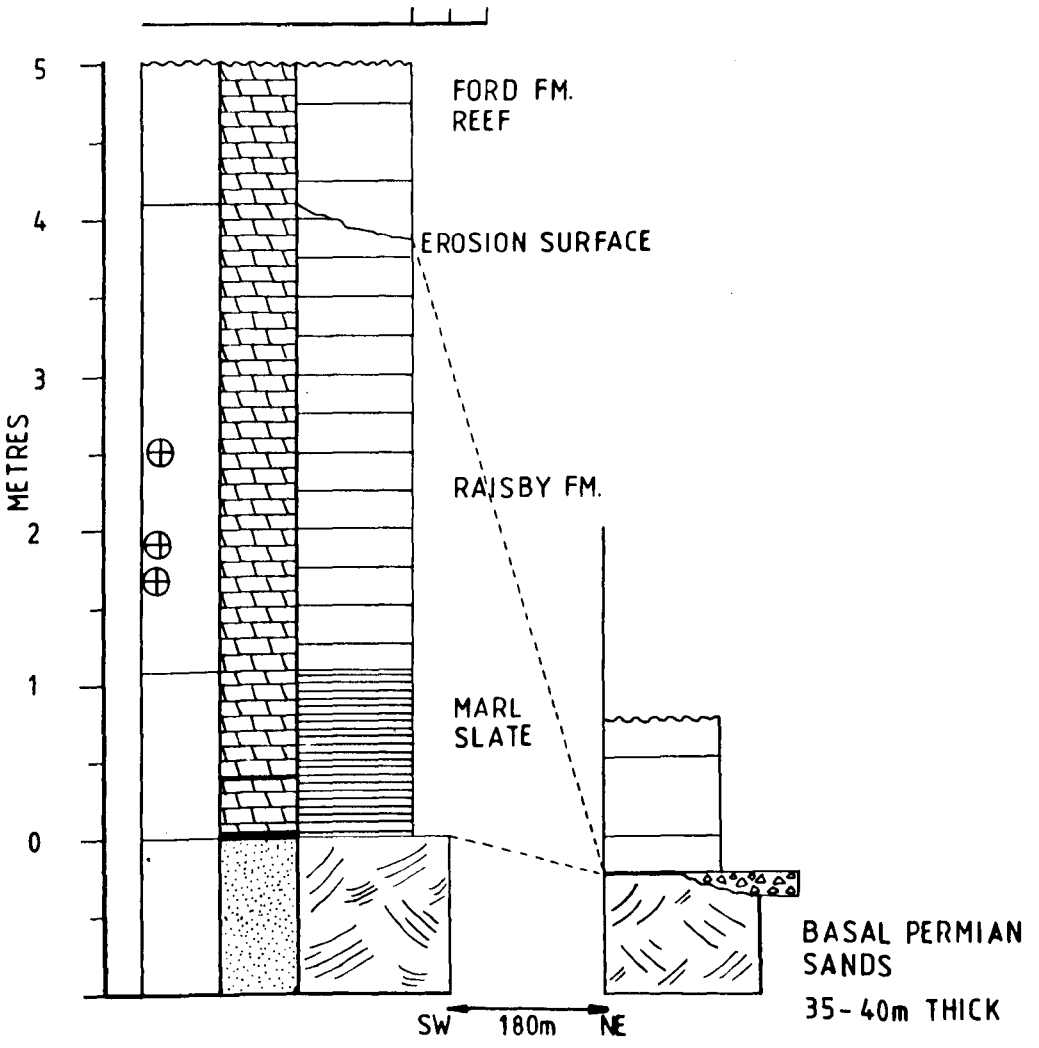

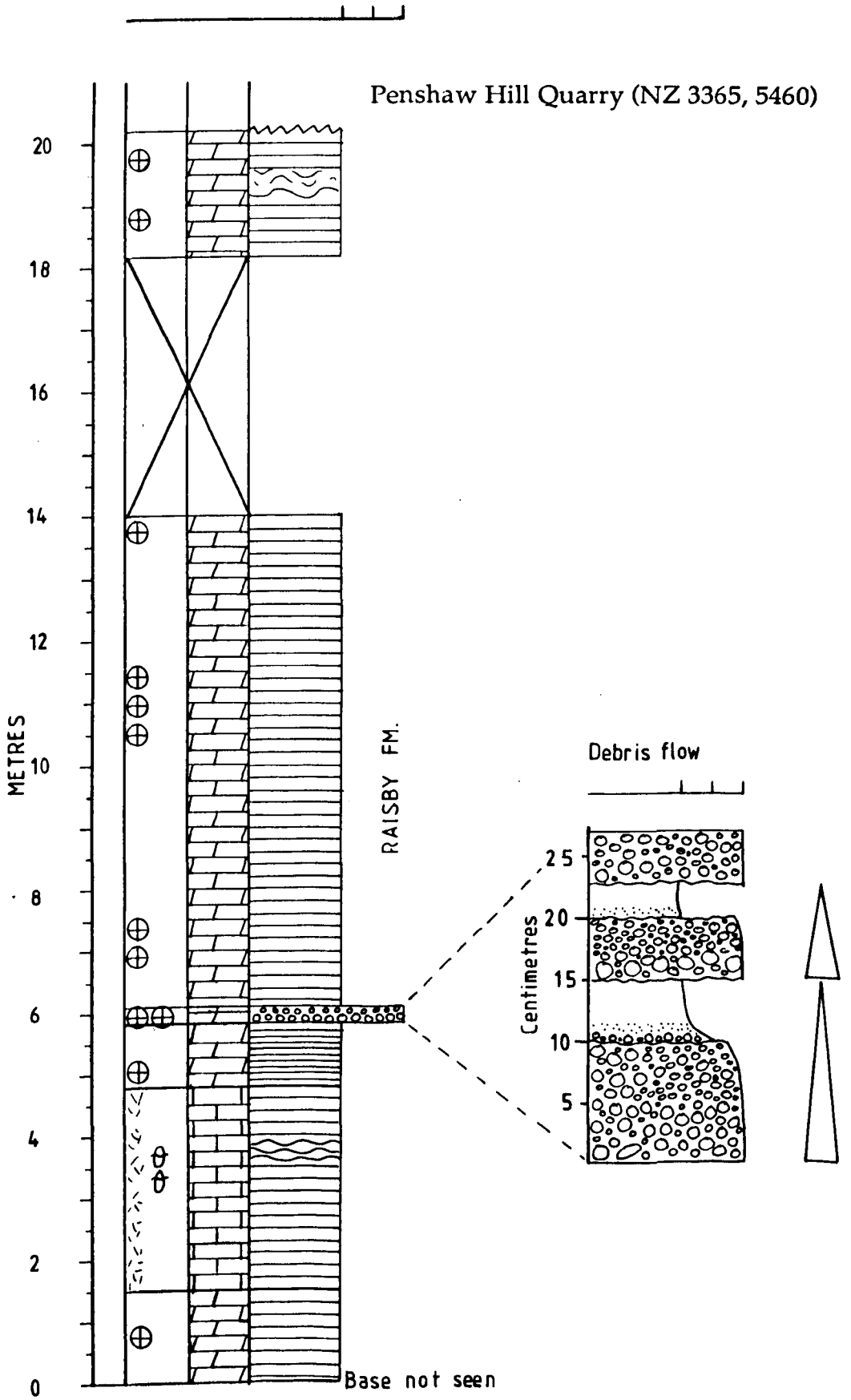
Penshaw Hill Quarry (NZ 3365, 5460)
METRES
20
18
16
14
12
10
8
6
4
2
0
RAISBY FM.
Base not seen
Debris flow
Centimetres
25
20
15
10
5

Houghton Road Cut (NZ 346, 377)

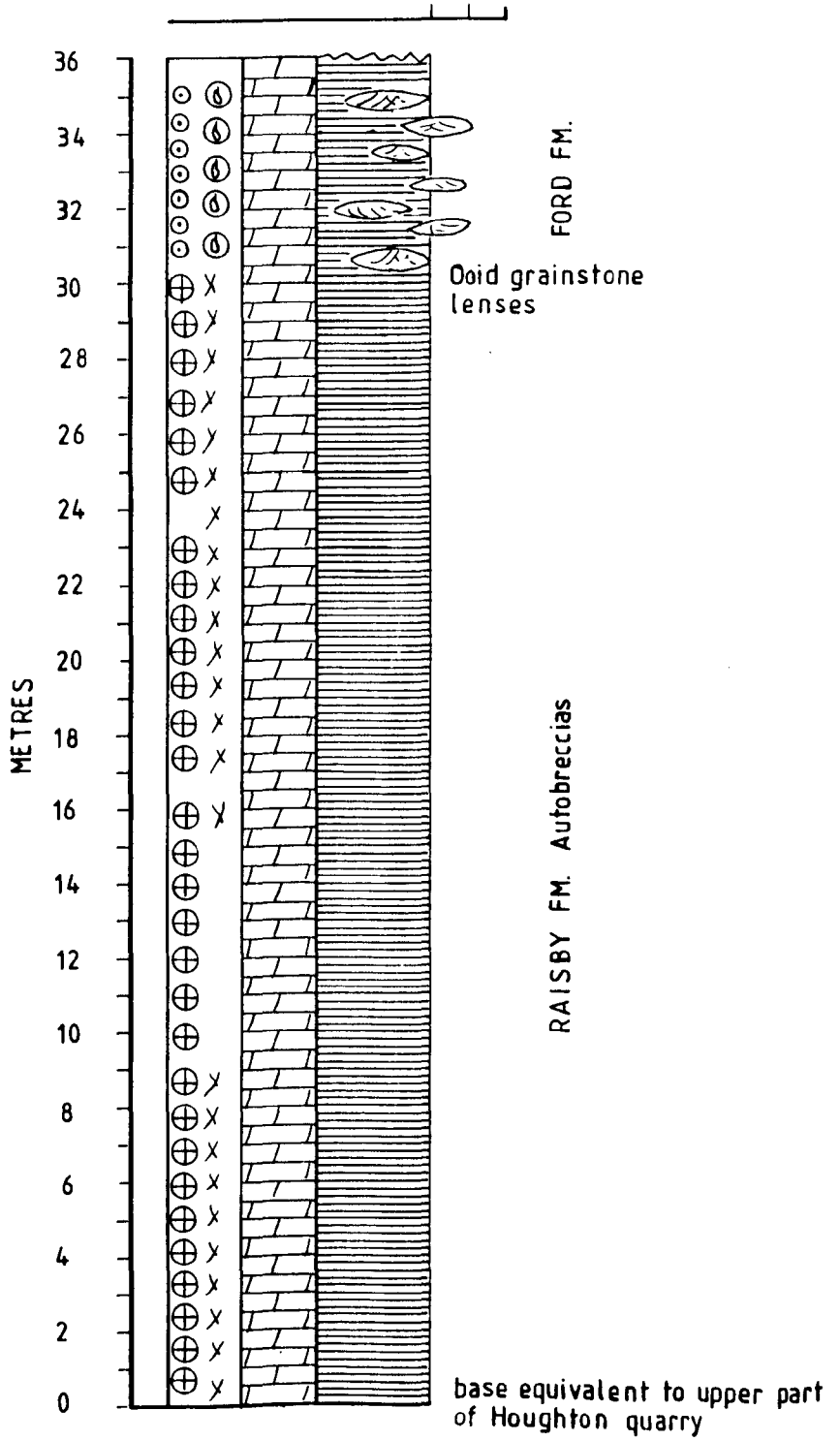

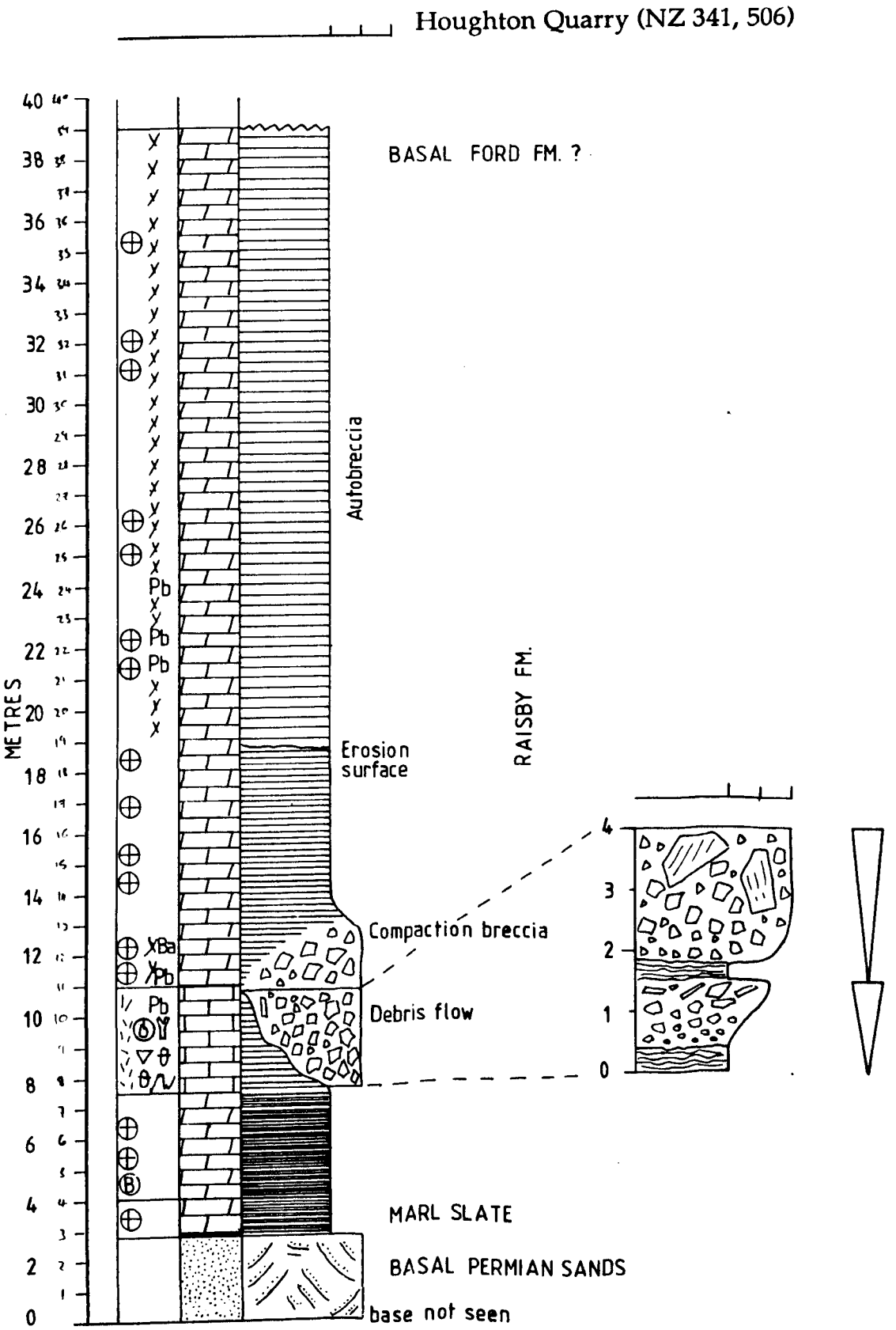
Houghton Quarry (NZ 341, 506)
METRES
BASAL FORD FM. ?
Autobreccia
RAISBY FM.
Erosion surface
Compaction breccia
Debris flow
MARL SLATE
BASAL PERMIAN SANDS
base not seen
Pb
Ba

High Moorsley Quarry (NZ 334, 455)

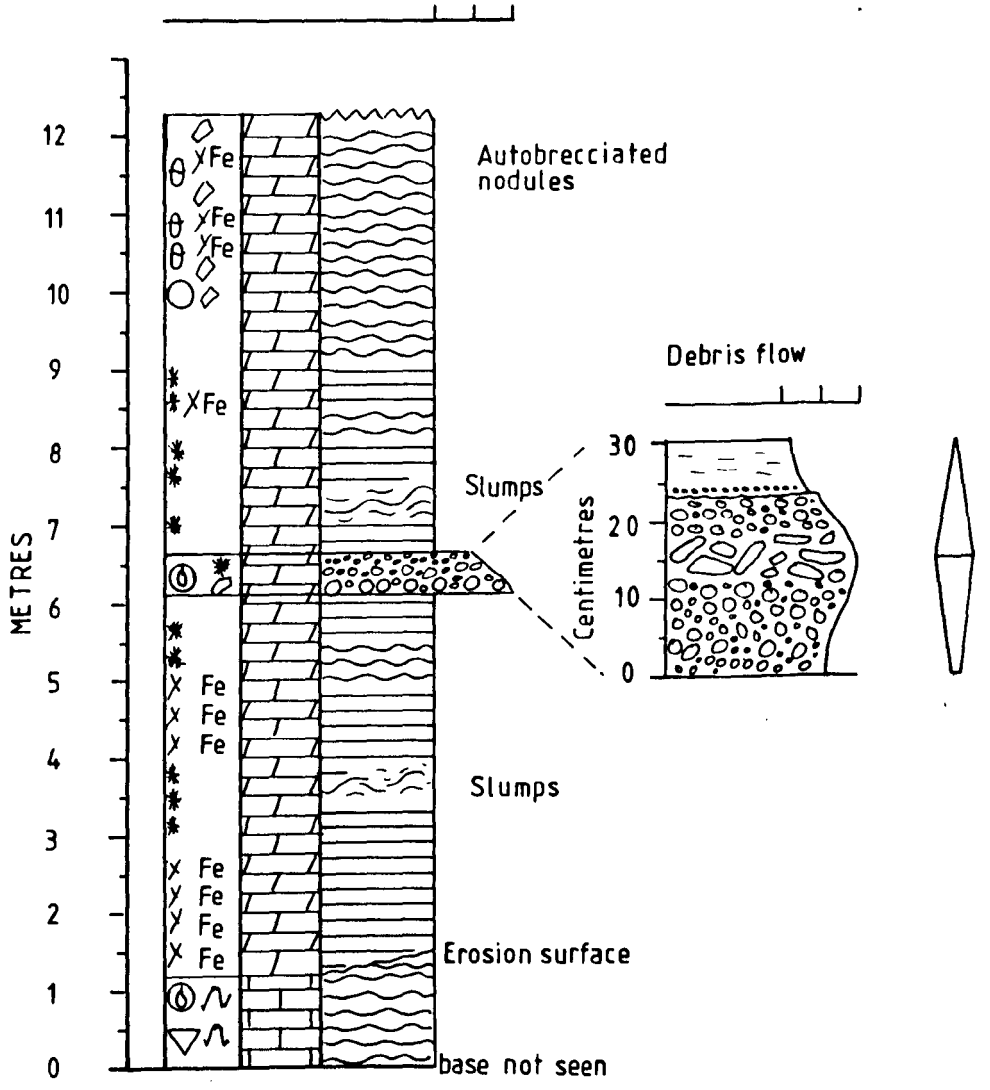

Haswell Moor Farm Quarry (NZ 352, 426)

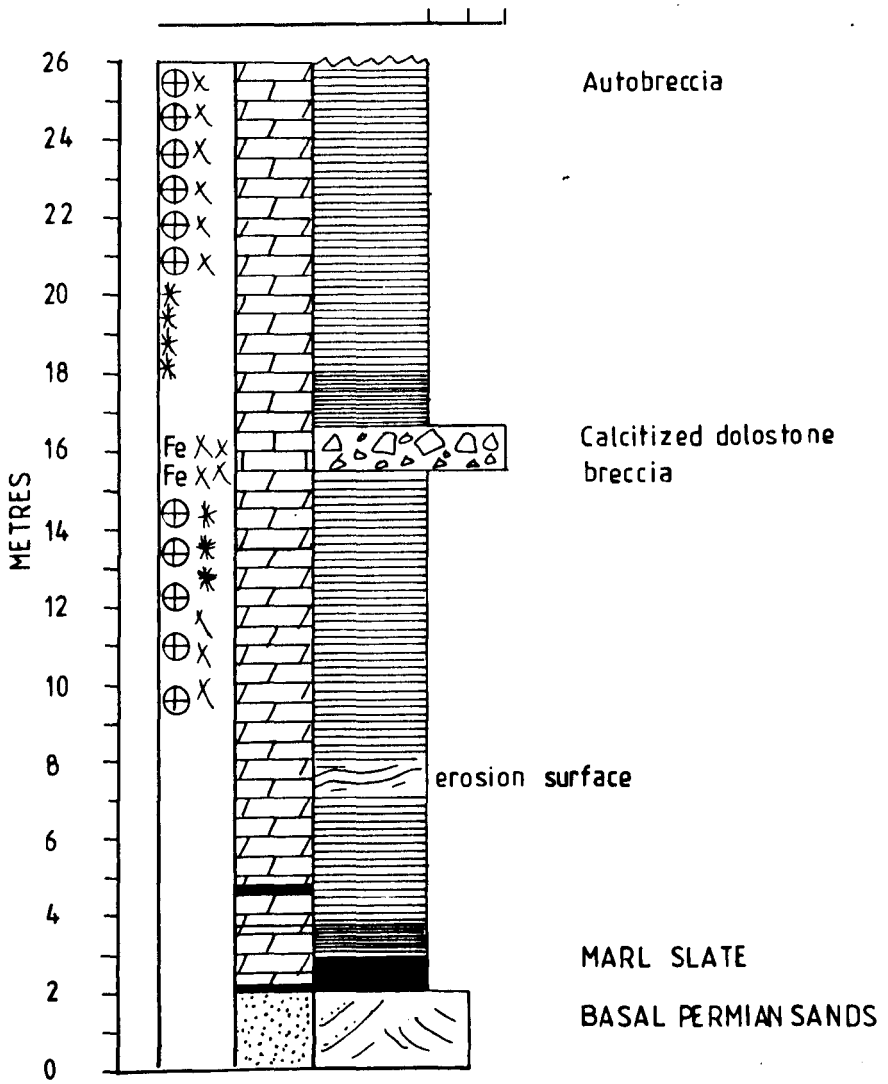

Crime Rigg Quarry (NZ 341, 416)

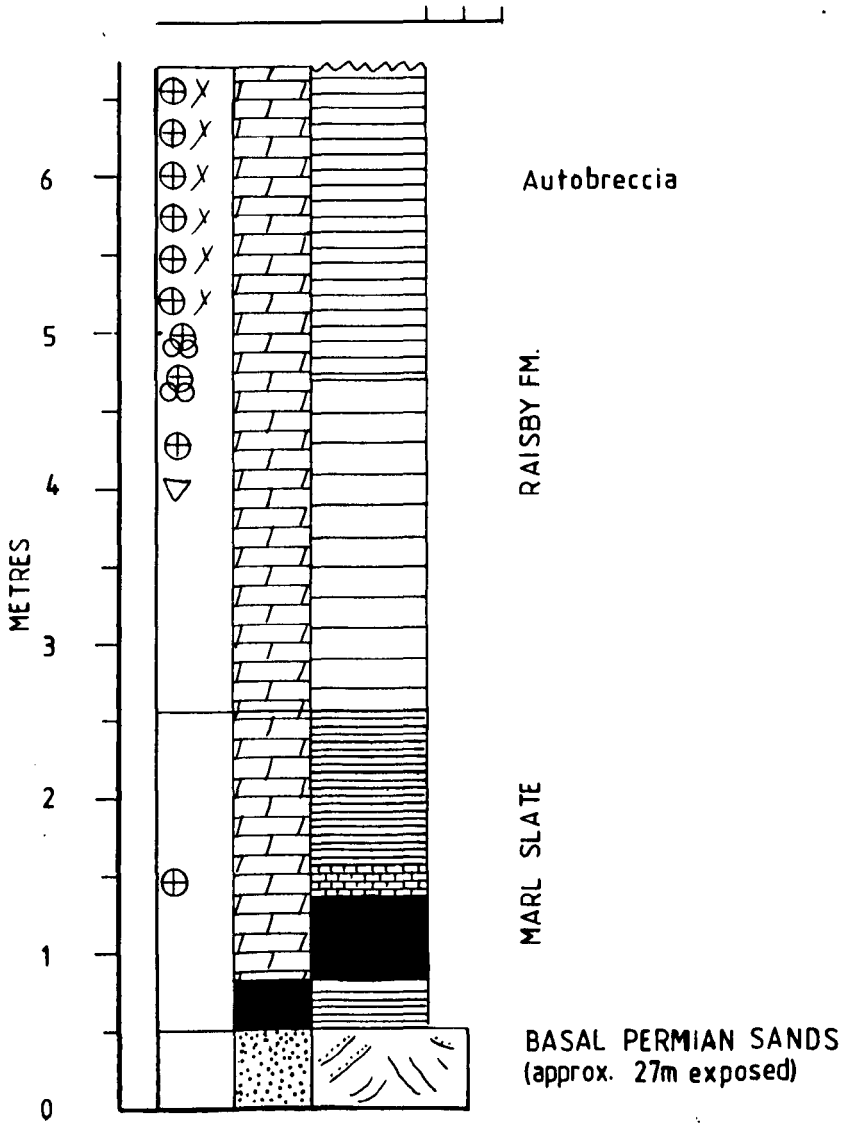

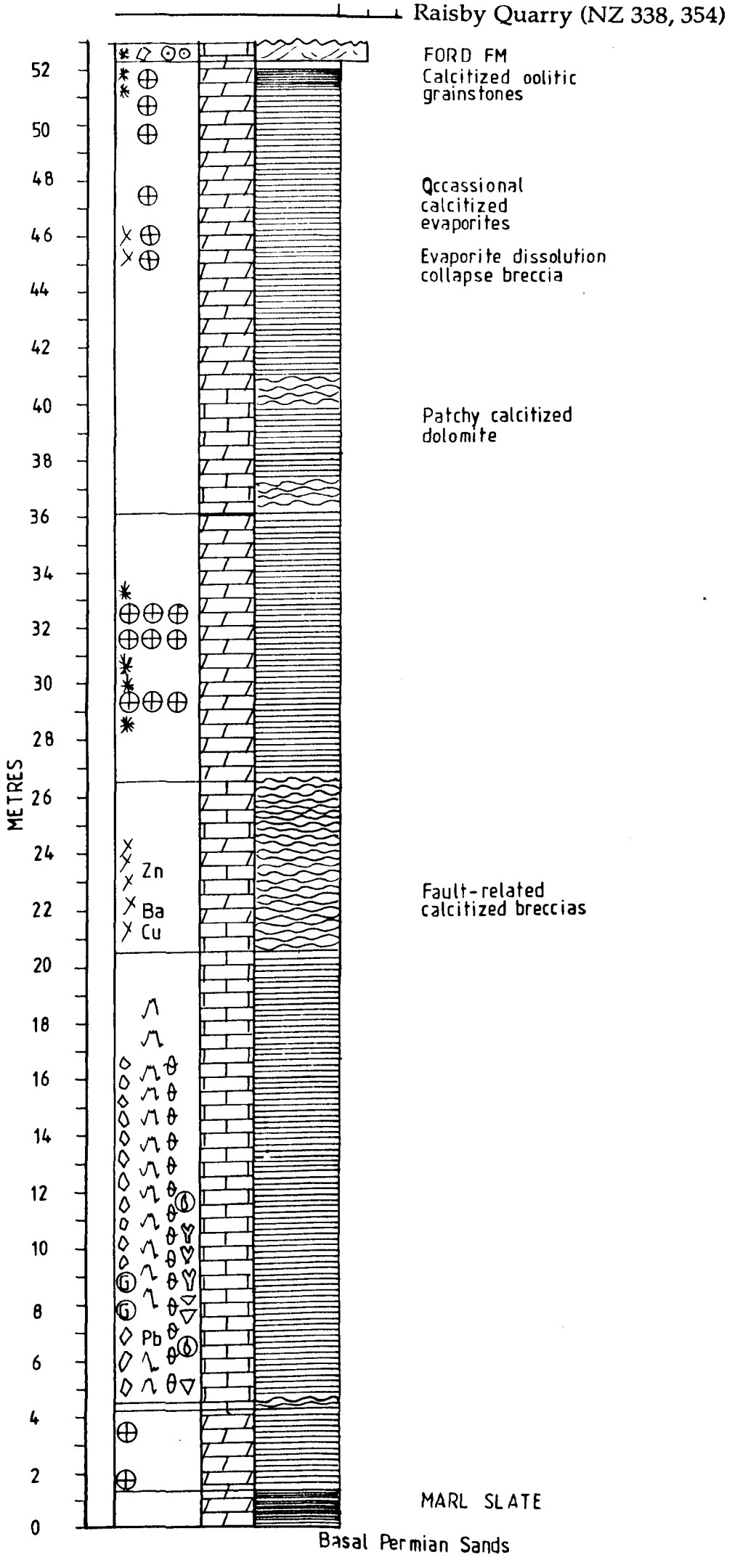
Raisby Quarry (NZ 338, 354)
METRES
52
50
48
46
44
42
40
38
36
34
32
30
28
26
24
22
20
18
16
14
12
10
8
6
4
2
0
FORD FM
Calcitized oolitic grainstones
Occassional calcitized evaporites
Evaporite dissolution collapse breccia
Patchy calcitized dolomite
Zn
Ba
Cu
Fault-related calcitized breccias
Pb
MARL SLATE
Basal Permian Sands

Eldon Hill Quarry (NZ 242, 272)

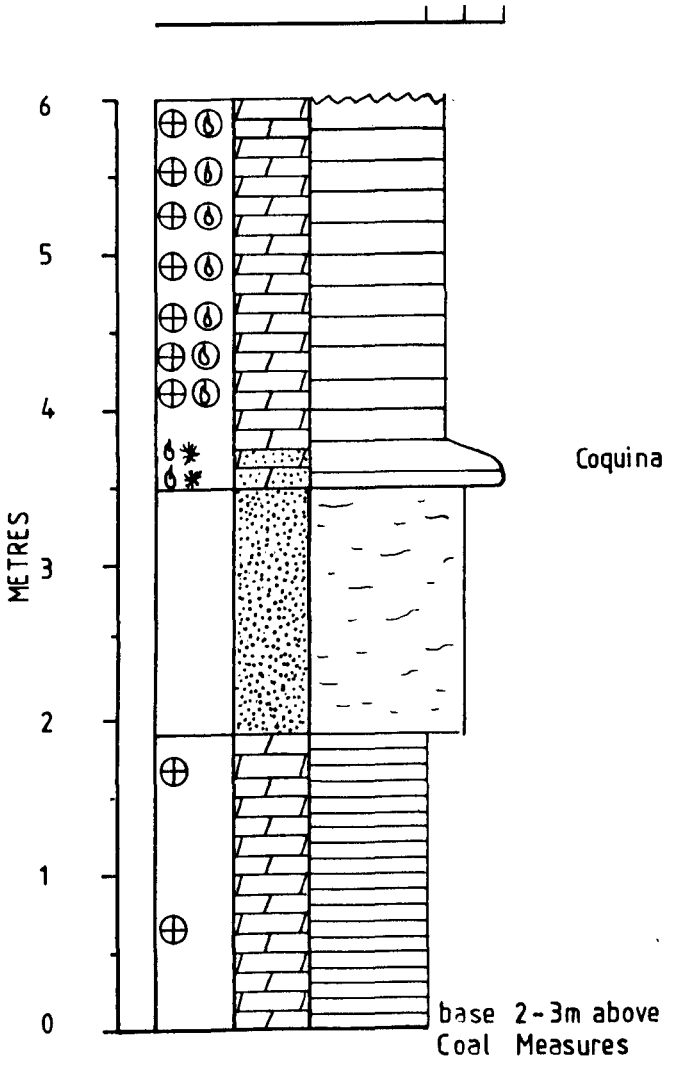

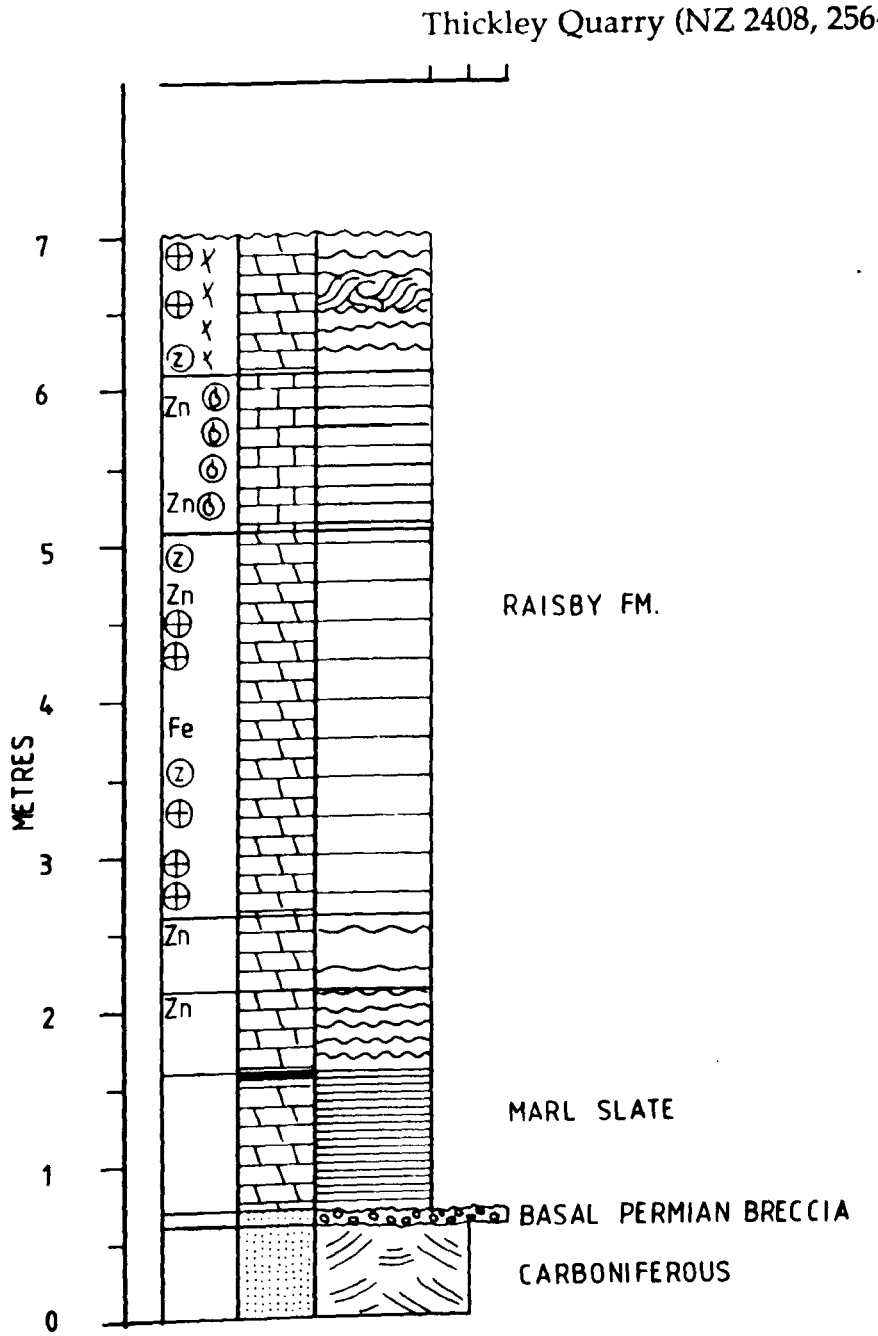
Thickley Quarry (NZ 2408, 2564)
METRES
7
6
5
4
3
2
1
0
Zn
Zn
Fe
Zn
Zn
RAISBY FM.
MARL SLATE
BASAL PERMIAN BRECCIA
CARBONIFEROUS

Old Towns Quarry (NZ 257, 246)

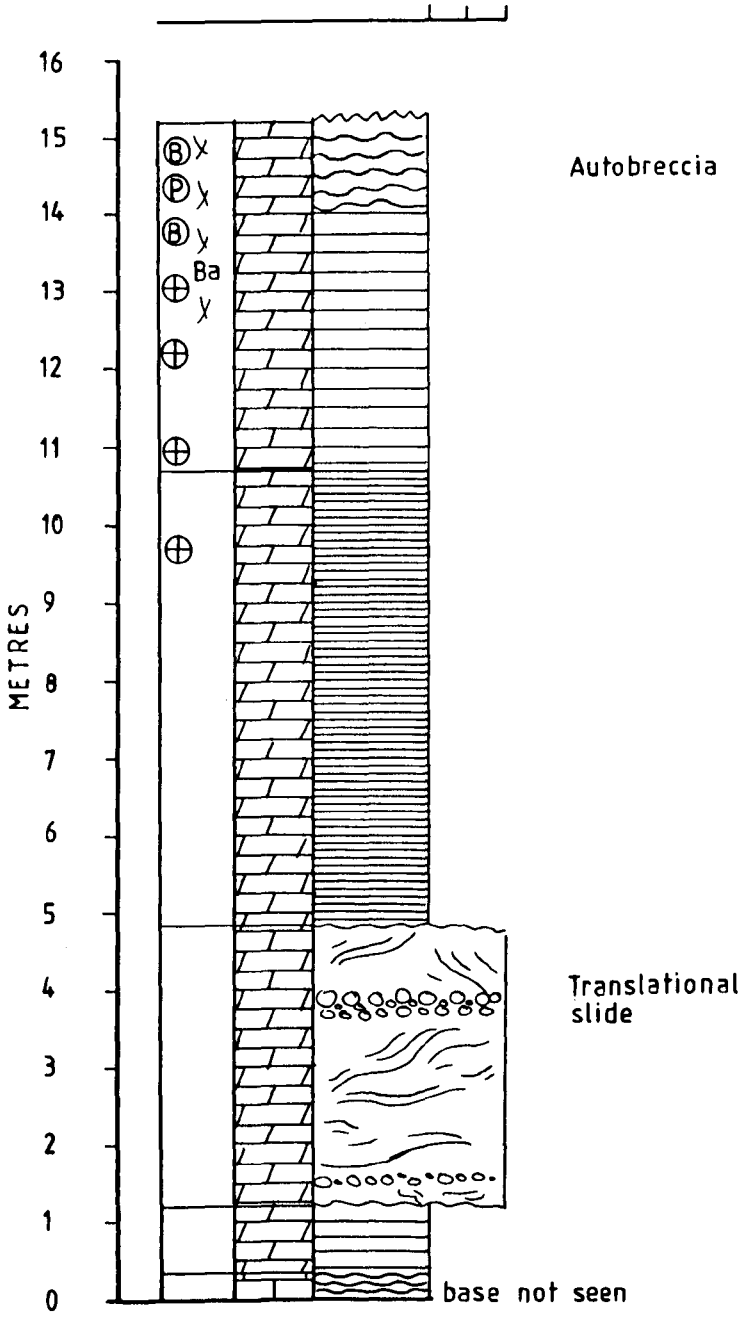

Summerhouse Quarry (NZ 2100, 1966)

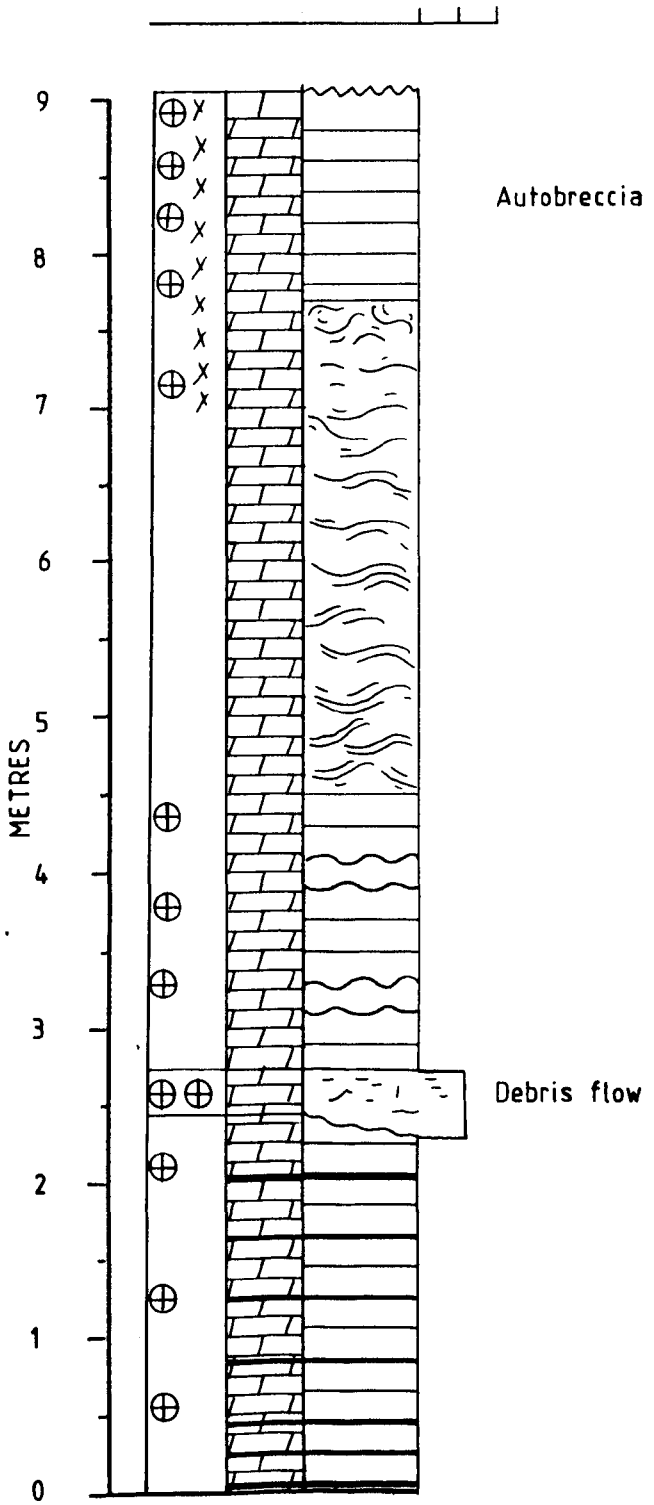

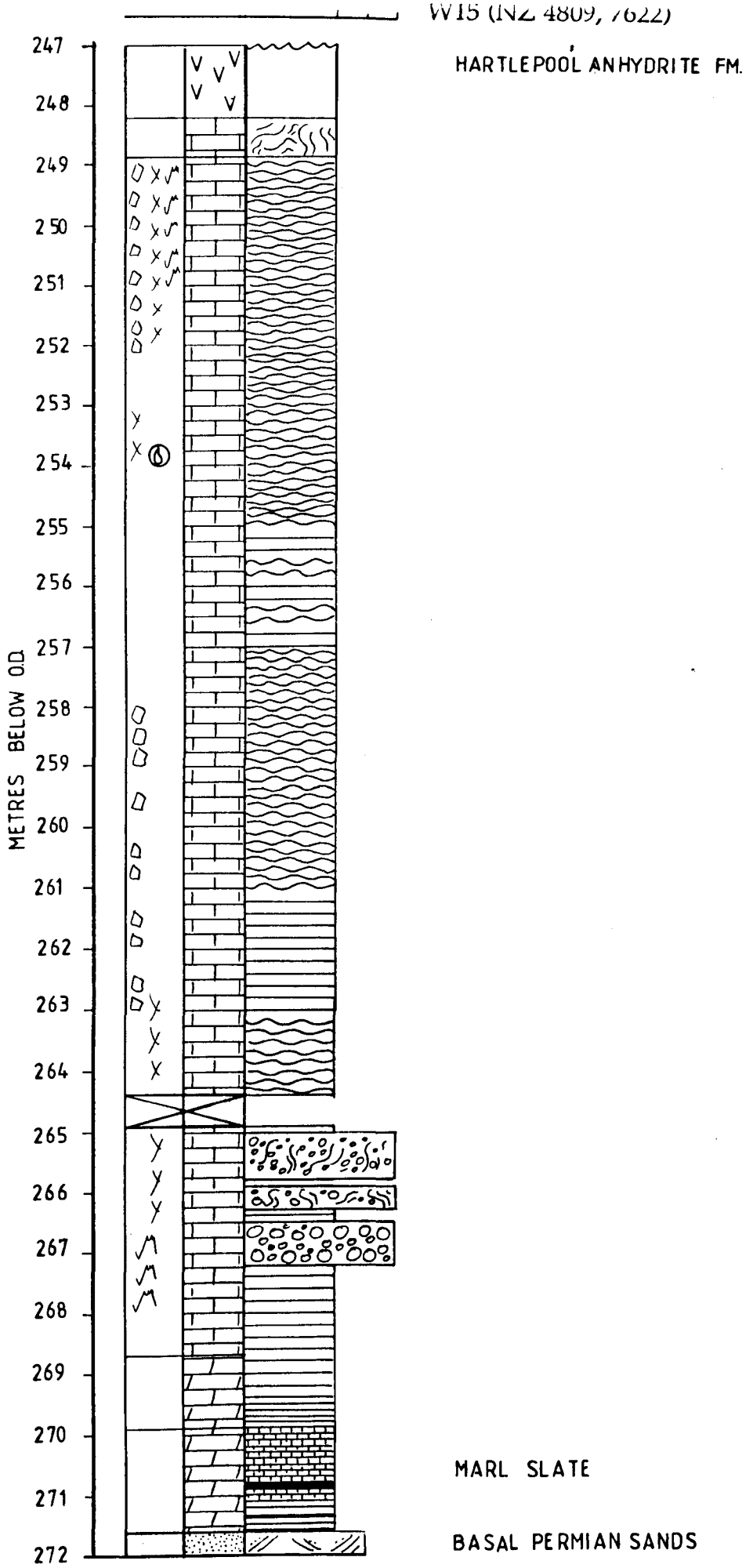
W15 (NZ 4809, 7622)
HARTLEPOOL ANHYDRITE FM.
METRES BELOW O.D.
247
248
249
250
251
252
253
254
255
256
257
258
259
260
261
262
263
264
265
266
267
268
269
270
271
272
MARL SLATE
BASAL PERMIAN SANDS

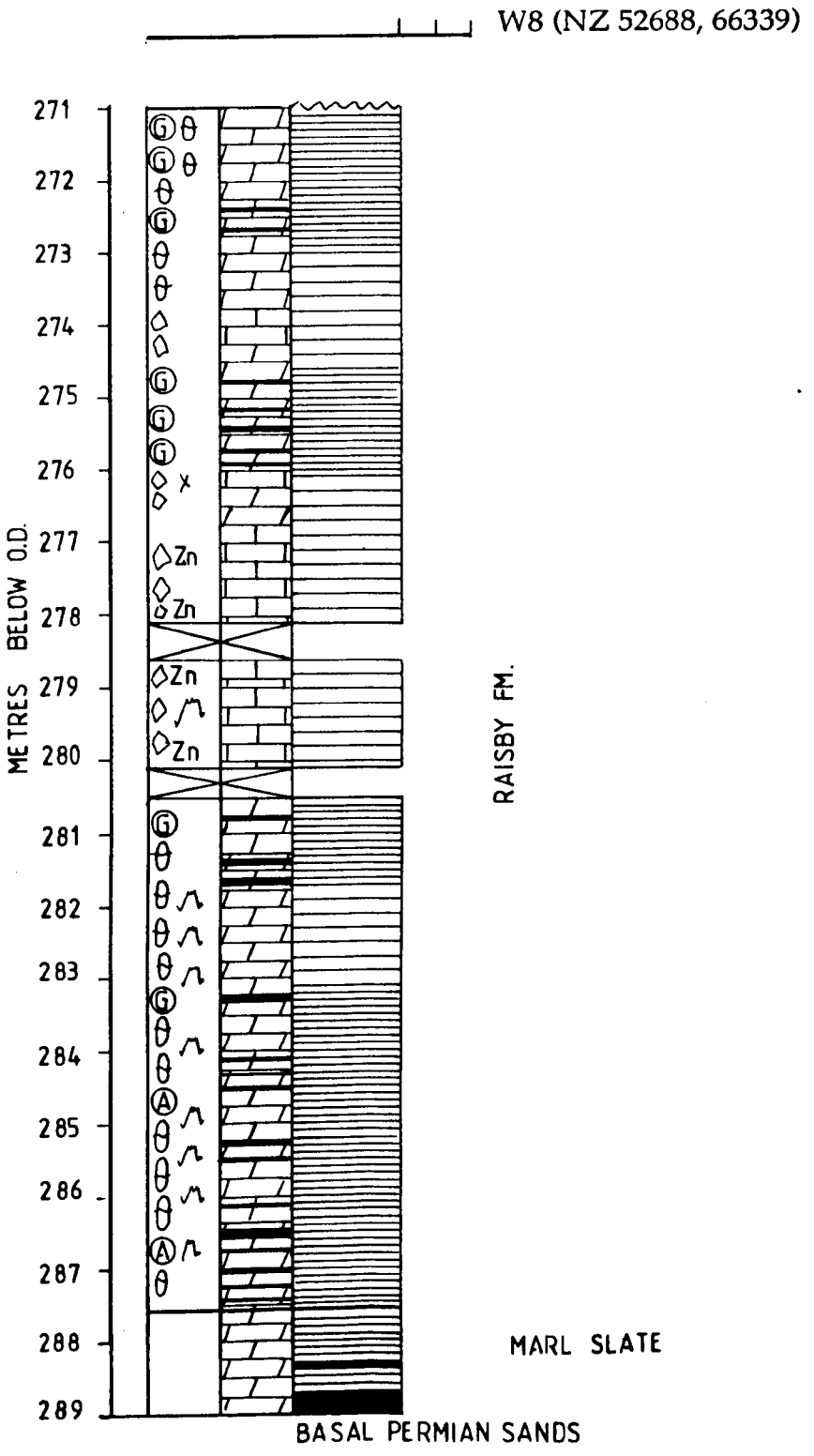
W8 (NZ 52688, 66339)
METRES BELOW O.D.
271
272
273
274
275
276
277
278
279
280
281
282
283
284
285
286
287
288
289
Zn
Zn
Zn
Zn
x
RAISBY FM.
MARL SLATE
BASAL PERMIAN SANDS

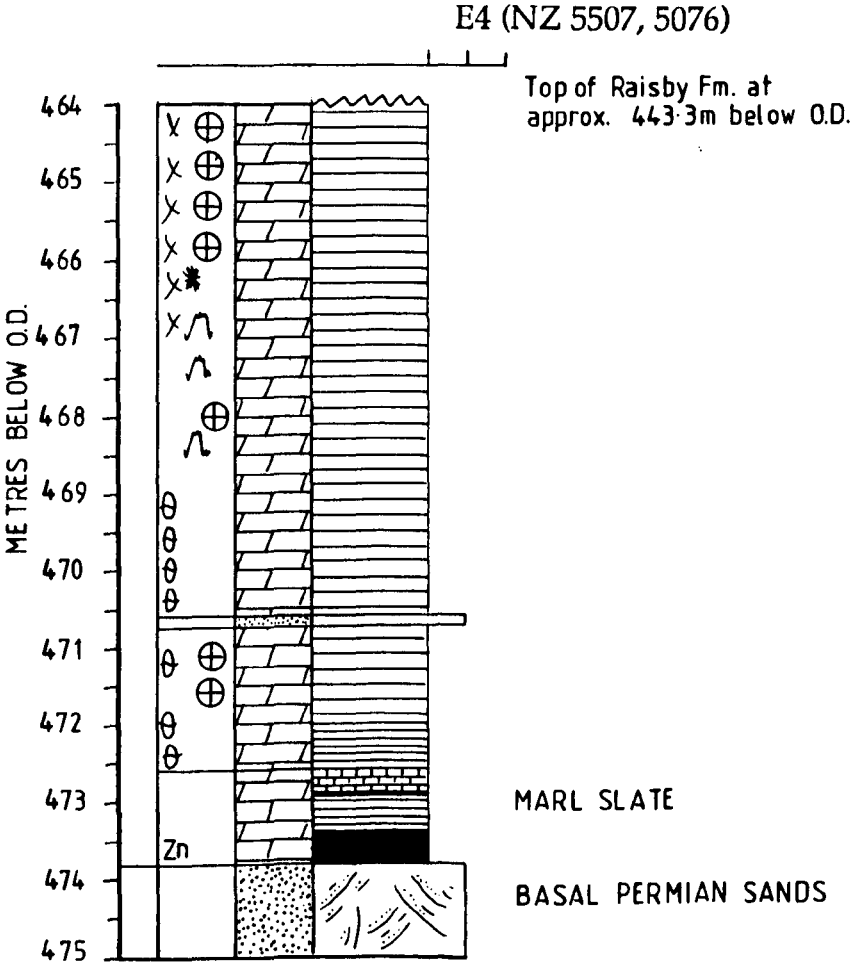
E4 (NZ 5507, 5076)
Top of Raisby Fm. at approx. 443·3m below O.D.
METRES BELOW O.D.
464
465
466
467
468
469
470
471
472
473
474
475
Zn
MARL SLATE
BASAL PERMIAN SANDS

Seaham (NZ 4258, 5031)

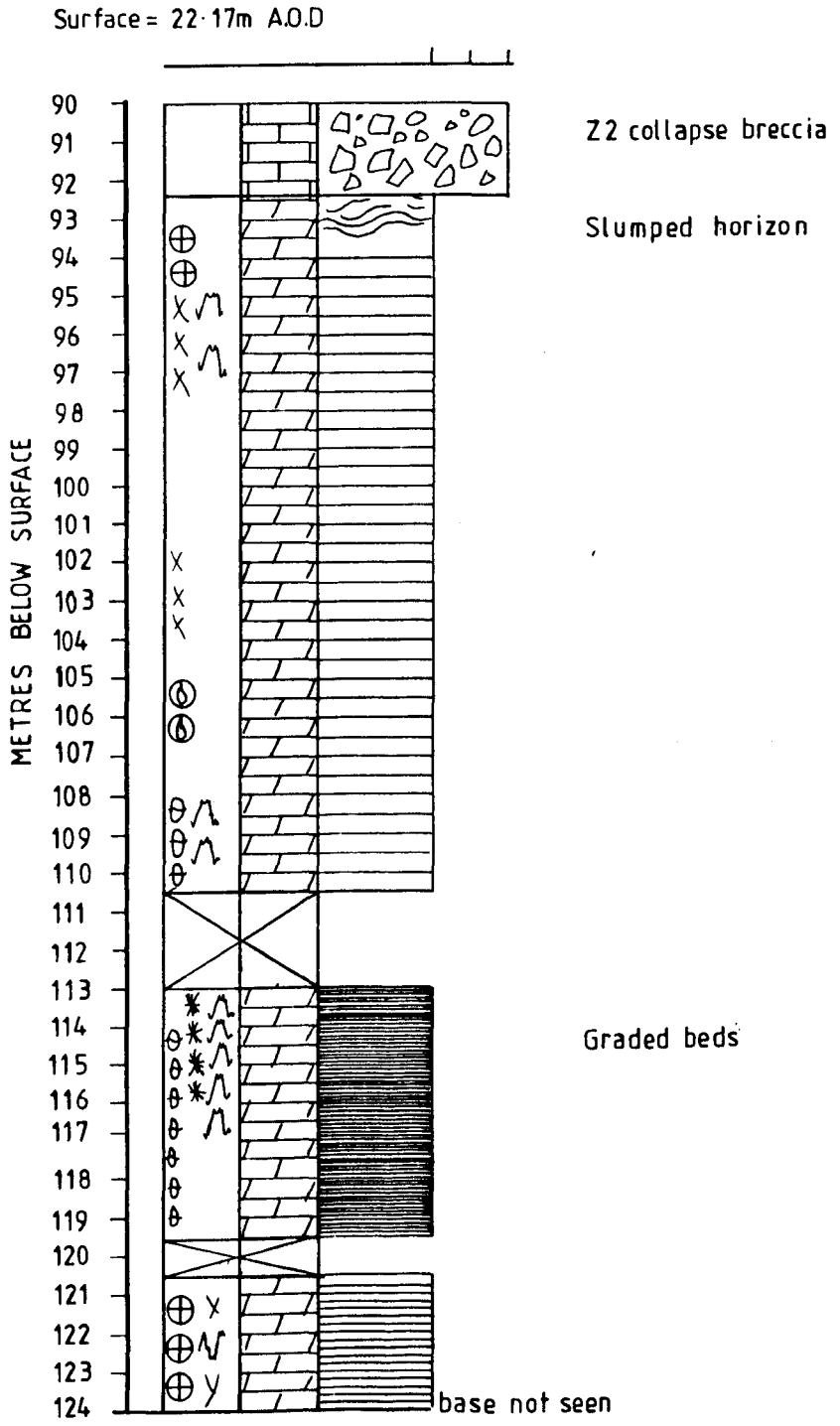

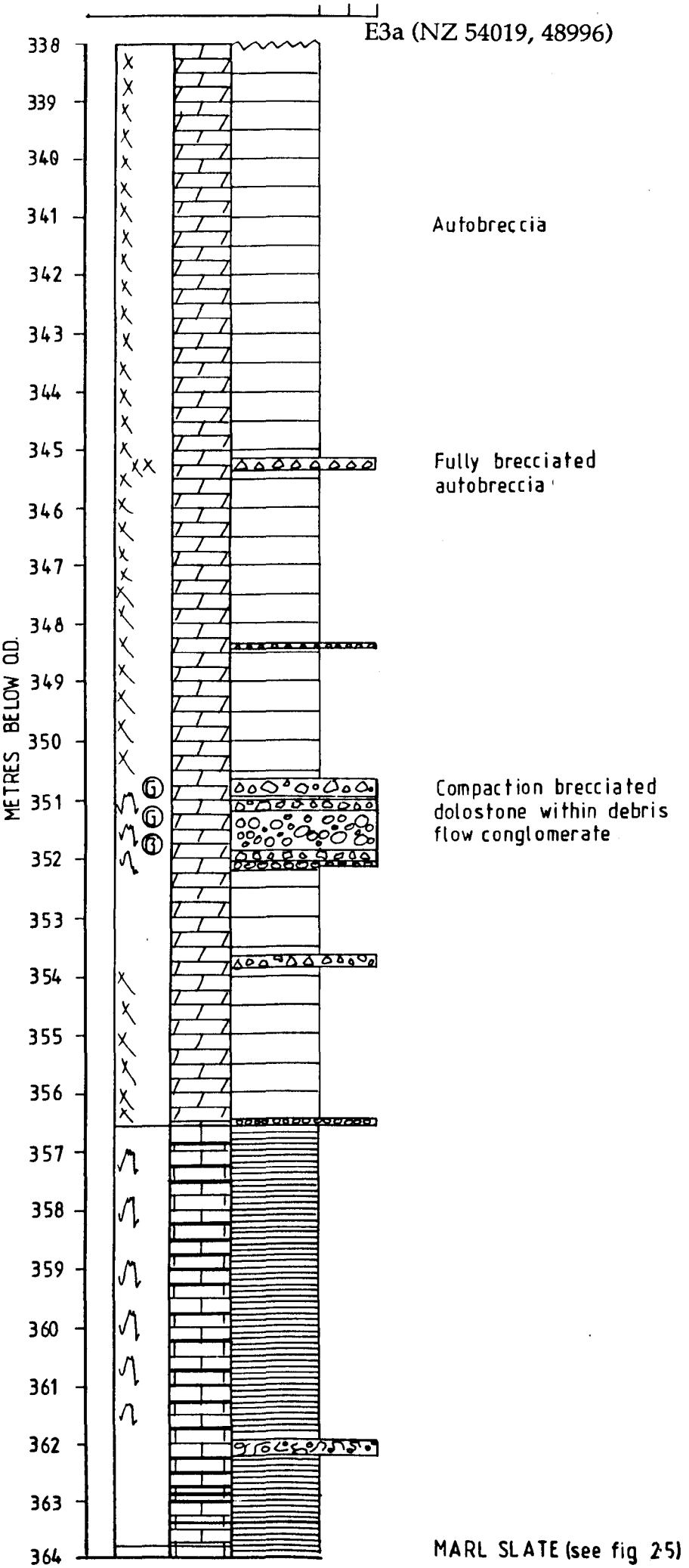
E3a (NZ 54019, 48996)
METRES BELOW O.D.
338
339
340
341
342
343
344
345
346
347
348
349
350
351
352
353
354
355
356
357
358
359
360
361
362
363
364
G
G
G
Autobreccia
Fully brecciated autobreccia
Compaction brecciated dolostone within debris flow conglomerate
MARL SLATE (see fig 2·5)

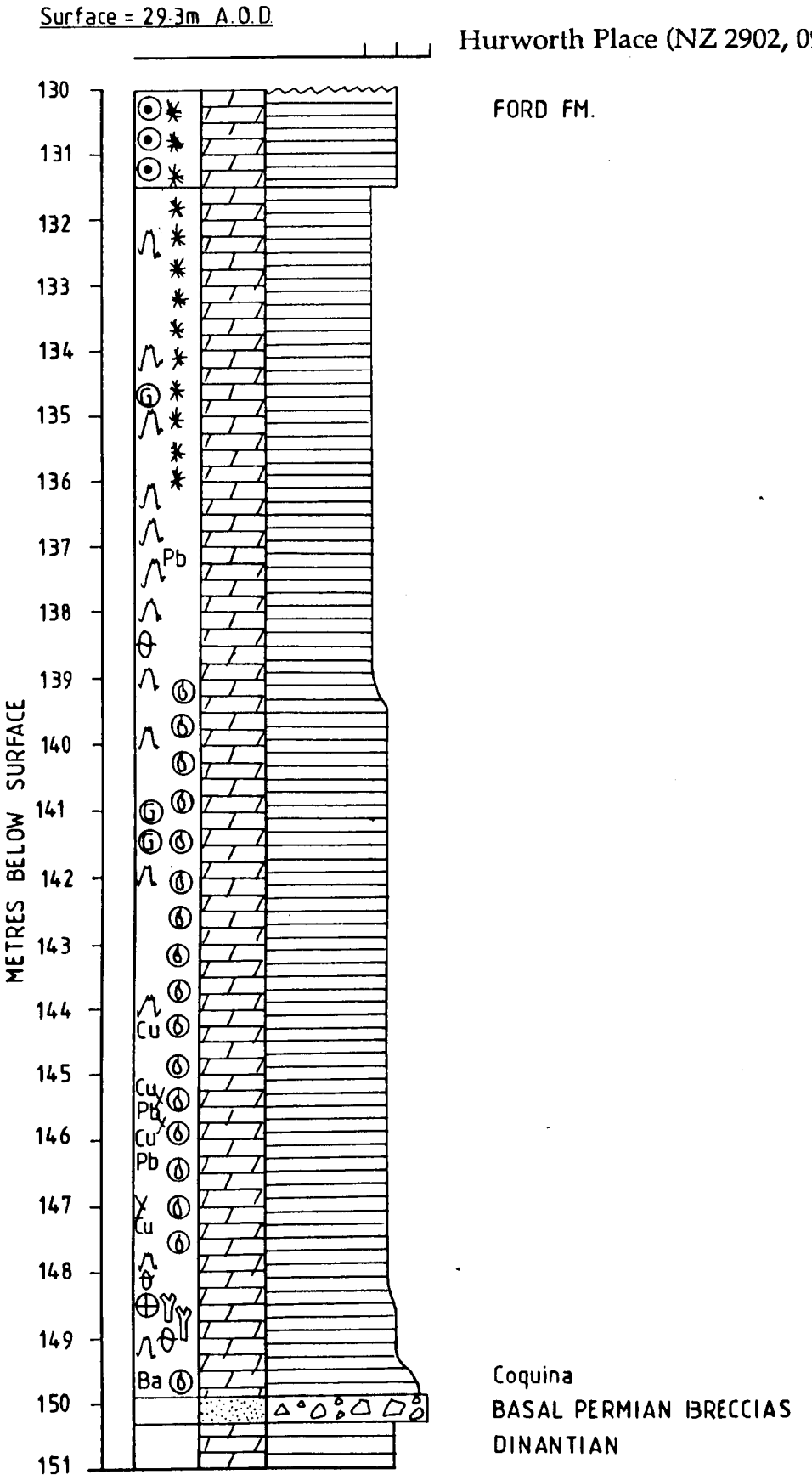
Surface = 29.3m A.O.D.
Hurworth Place (NZ 2902, 0953)
FORD FM.
METRES BELOW SURFACE
130
131
132
133
134
135
136
137
138
139
140
141
142
143
144
145
146
147
148
149
150
151
Pb
Cu
Cu
Pb
Cu
Pb
Cu
Ba
Coquina
BASAL PERMIAN BRECCIAS
DINANTIAN

North Sands borehole (NZ 5023, 3538)

Surface = 7.43m A.O.D.

Raisby Formation = 269.86m to 285.47m below surface

Marl Slate = 285.47 to 285.73m below surface

W.O.17 borehole (NZ 3253, 2191)

Surface = 107.59m A.O.D.

Raisby Formation = 79.86m to 89.31m below surface

W.O. 18 borehole (NZ 3121, 2085)

Surface = 80.77m A.O.D.

Raisby Formation = 103.03m to 119.15m below surface

W.O. 10 borehole (NZ 3104, 2268)

Surface = 92.48m A.O.D.

Raisby Formation = 78.64m to 88.33m below surface

(details from D.B. Smith, *pers. comm.*, 1988).